Handbook of Natural Gas Engineering

McGRAW-HILL SERIES IN CHEMICAL ENGINEERING

SIDNEY D. KIRKPATRICK, *Consulting Editor*

EDITORIAL ADVISORY COMMITTEE

BUILDING FOR THE FUTURE OF A PROFESSION

Fifteen prominent chemical engineers first met in New York more than thirty years ago to plan a continuing literature for their rapidly growing profession. From industry came such pioneer practitioners as Leo H. Baekeland, Arthur D. Little, Charles L. Reese, John V. N. Dorr, M. C. Whitaker, and R. S. McBride. From the universities came such eminent educators as William H. Walker, Alfred H. White, D. D. Jackson, J. H. James, J. F. Norris, Warren K. Lewis, and Harry A. Curtis. H. C. Parmelee, then editor of *Chemical & Metallurgical Engineering*, served as chairman and was joined subsequently by S. D. Kirkpatrick as consulting editor.

After several meetings, this Editorial Advisory Committee submitted its report to the McGraw-Hill Book Company in September, 1925. In it were detailed specifications for a correlated series of more than a dozen text and reference books, including a chemical engineers' handbook and basic textbooks on the elements and principles of chemical engineering, on industrial applications of chemical synthesis, on materials of construction, on plant design, on chemical-engineering economics. Broadly outlined, too, were plans for monographs on unit operations and processes and on other industrial subjects to be developed as the need became apparent.

From this prophetic beginning has since come the McGraw-Hill Series in Chemical Engineering, which now numbers about forty books. More are always in preparation to meet the ever growing needs of chemical engineers in education and in industry. In the aggregate these books represent the work of literally hundreds of authors, editors, and collaborators. But no small measure of credit is due the pioneering members of the original committee and those engineering educators and industrialists who have succeeded them in the task of building a permanent literature for the chemical-engineering profession.

THE SERIES

ARIES AND NEWTON—*Chemical Engineering Cost Estimation*
BADGER AND BANCHERO—*Introduction to Chemical Engineering*
CLARKE—*Manual for Process Engineering Calculations*
COMINGS—*High Pressure Technology*
DODGE—*Chemical Engineering Thermodynamics*
GRISWOLD—*Fuels, Combustion, and Furnaces*
GROGGINS—*Unit Processes in Organic Synthesis*
HENLEY AND BIEBER—*Chemical Engineering Calculations*
HUNTINGTON—*Natural Gas and Natural Gasoline*
JOHNSTONE AND THRING—*Pilot Plants, Models, and Scale-up Methods in Chemical Engineering*
KATZ, CORNELL, KOBAYASHI, POETTMANN, VARY, ELENBAAS, AND WEINAUG—*Handbook of Natural Gas Engineering*
KIRKBRIDE—*Chemical Engineering Fundamentals*
KNUDSEN AND KATZ—*Fluid Dynamics and Heat Transfer*
LEE—*Materials of Construction*
LEVA—*Fluidization*
LEWIS, RADASCH, AND LEWIS—*Industrial Stoichiometry*
MANTELL—*Adsorption*
MANTELL—*Industrial Electrochemistry*
McADAMS—*Heat Transmission*
McCABE AND SMITH, J. C.—*Unit Operations of Chemical Engineering*
MICKLEY, SHERWOOD, AND REED—*Applied Mathematics in Chemical Engineering*
NELSON—*Petroleum Refinery Engineering*
PERRY (EDITOR)—*Chemical Business Handbook*
PERRY (EDITOR)—*Chemical Engineers' Handbook*
PETERS—*Elementary Chemical Engineering*
PETERS—*Plant Design and Economics for Chemical Engineers*
PIERCE—*Chemical Engineering for Production Supervision*
REID AND SHERWOOD—*The Properties of Gases and Liquids*
RHODES, F. H.—*Technical Report Writing*
RHODES, T. J.—*Industrial Instruments for Measurement and Control*
ROBINSON AND GILLILAND—*Elements of Fractional Distillation*
SCHMIDT AND MARLIES—*Principles of High-polymer Theory and Practice*
SCHWEYER—*Process Engineering Economics*
SHERWOOD AND PIGFORD—*Absorption and Extraction*
SHREVE—*The Chemical Process Industries*
SMITH, J. M.—*Chemical Engineering Kinetics*
SMITH, J. M., AND VAN NESS—*Introduction to Chemical Engineering Thermodynamics*
STEPHENSON—*Introduction to Nuclear Engineering*
TREYBAL—*Liquid Extraction*
TREYBAL—*Mass-transfer Operations*
VILBRANDT—*Chemical Engineering Plant Design*
VOLK—*Applied Statistics for Engineers*
WALKER, LEWIS, McADAMS, AND GILLILAND—*Principles of Chemical Engineering*
WILLIAMS AND JOHNSON—*Stoichiometry for Chemical Engineers*
WILSON AND RIES—*Principles of Chemical Engineering Thermodynamics*
WILSON AND WELLS—*Coal, Coke, and Coal Chemicals*
WINDING AND HASCHE—*Plastics, Theory and Practice*

Handbook of Natural Gas Engineering

DONALD L. KATZ

Professor of Chemical Engineering and Chairman
Department of Chemical and Metallurgical Engineering
University of Michigan

DAVID CORNELL

Associate Professor of Petroleum Engineering
Oklahoma State University

RIKI KOBAYASHI

Associate Professor of Chemical Engineering
The Rice Institute

FRED H. POETTMANN

Supervisor, Engineering Department, Research Organization
The Ohio Oil Company

JOHN A. VARY

Chief Reservoir Engineer
Michigan Consolidated Gas Company

JACK R. ELENBAAS

District Engineer, Production and Pipe Line District
Michigan Consolidated Gas Company

CHARLES F. WEINAUG

Professor and Chairman, Department of Petroleum Engineering
University of Kansas

McGRAW-HILL BOOK COMPANY, INC. New York Toronto London 1959

HANDBOOK OF NATURAL GAS ENGINEERING

 Library of Congress Catalog Card Number 58-6686

THE MAPLE PRESS COMPANY, YORK, PA.

Preface

This book has been prepared for engineering students and for graduate engineers who desire to practice in the natural gas industry. It treats natural gas in its various stages from occurrence in the reservoir through production, processing, and transportation to the ultimate consumer. Primary emphasis is given to the properties of the hydrocarbons and the application of these properties in flow and processing operations.

The authors' intention when preparing the manuscript was to present procedures for the conduct of engineering calculations for the design of equipment required to produce and deliver natural gas. Derivations and explanations of engineering principles governing the operations are included to provide background. A considerable amount of quantitative data in the form of charts, tables, and formulas is presented to serve as a basis for design calculations. The Appendix includes the functions of the compressibility factor and several tables from Report 3 of the measurement committee of the American Gas Association. On each subject treated, the authors found it necessary to restrict the material chosen for the manuscript. Enough material is available for most chapters in the book to expand each of them to a full-sized book. The selections made in preparing the manuscript reflect the preferences and experiences of the authors. It is recognized that many alternative procedures and much useful information have been excluded because of the limitations of time and space.

Much of the material in the book is taken from the literature. An effort was made to give the original authors credit for data published or relationships discovered. Appreciation is expressed to the authors and to the owners of the copyright, technical societies or publishers, for permission to reproduce figures. In particular, the *Transactions of the AIME* and the *Journal of Petroleum Technology* provided a large block of the data included. *Industrial and Engineering Chemistry*, the American Petroleum Institute's *Drilling and Production Practice*, the *Transactions of the AIChE*, *Chemical Engineering Progress*, the *Petroleum Refiner*, *The Petroleum Engineer*, *The Oil and Gas Journal*, and *World Oil* all provided basic information and material for reproduction. Several authors were kind enough to provide original copies of figures reproduced from their papers. Conversations and correspondence were carried on with many engineers in industry. Their advice and assistance are appreciated.

The preparation of the manuscript was a joint effort of Dr. Katz and each of the coauthors. The latter prepared drafts of chapters or sections for which they were especially qualified or concerning which they had valuable experience. In some cases the coauthor worked closely with Dr. Katz through the final draft. For example, Dr. Cornell prepared chapters on steady and unsteady flow from reservoirs, on development and operations of gas fields, and on gas measurement; he also participated in the preparation of the final copy. Dr. Kobayashi prepared chapters on water-hydrocarbon systems, field processing and absorption, fractionation, dehydration, and sweetening, as well as material on viscosity and thermal conductivity. Dr. Poettmann prepared a chapter on flow and compression calculations and the section on the drilling of wells. Dr. Weinaug prepared material on the computation of phase behavior and the logging of wells. Mr. Vary and Mr. Elenbaas prepared the chapters on transportation to market and underground storage. The other chapters and the final manuscript were the responsibility of Dr. Katz. The coauthors made contributions throughout the book, in addition to the

chapters or sections for which they have had primary responsibility.

The organizations with which the coauthors are associated provided assistance in the preparation of the manuscript. Mr. Harry F. Cosway, a graduate student in Chemical Engineering at the University of Michigan, prepared many of the figures and tables. Mrs. Ardis Vukas and Mrs. Donna Richards typed the final manuscript. The assistance of everyone who had a part in the preparation of this book is appreciated by the authors.

Donald L. Katz
David Cornell *John A. Vary*
Riki Kobayashi *Jack R. Elenbaas*
Fred H. Poettmann *Charles F. Weinaug*

Contents

CHAPTER 1

Introduction to the Natural Gas Industry

Natural gas has been used commercially as a fuel for over a hundred and thirty years in America and for centuries in China (1-5). The production and distribution of natural gas have become an important segment of our domestic economy (1-25). Engineering methods have been developed for designing facilities to produce the gas from the earth, to separate it from liquid hydrocarbons, and to deliver this superior gaseous fuel to market.

Natural gas is composed primarily of methane (CH_4) with minor amounts of the paraffin hydrocarbon family, ethane (C_2H_6), propane (C_3H_8), and butanes (C_4H_{10}). Nonhydrocarbon constituents include nitrogen, hydrogen sulfide, carbon dioxide, helium, and water vapor. Although natural gas occurs as gas under pressure in porous rock beneath the earth's surface, often it is in solution with crude oil or condensate. Then it may be described as the volatile portion of petroleum.

Important background material for engineers in the natural gas industry includes such subjects as geology and occurrence of natural gas. A knowledge of earth temperatures and pressures is required for predicting the gas content of reservoirs and the rate of delivery therefrom. Typical gas fields are described here in illustration of our gas supplies.

Engineers working in the gas industry are often called upon to compare the costs of fuels. The value of natural gas as a fuel in relation to oil and coal is found from a comparison of heating values and combustion efficiencies and the conversion of prices to a common basis.

THE NATURAL GAS INDUSTRY

Since its discovery, reported to be at Fredonia, N.Y., in 1821 (1-5), natural gas has served as a fuel in geographical areas immediately surrounding the gas fields. Gas was used for lighting, as well as for fuel for homes and industry, in the latter part of the nineteenth century prior to the advent of the electric lamp. Stories are told of gas lights burning in the street all day because it was cheaper to leave the lights on than to pay someone to turn them off and relight them each evening.

In the 1920s and 1930s, a few long pipelines 22 to 24 in. in diameter operating at 400 to 600 pounds per square inch (psi) pressure were installed to bring gas to industrial areas remote from the source. The greatest expansion took place immediately following World War II when several long lines were constructed. By this time, advances in welding and manufacture of pipe permitted pressures up to 1,000 psi and diameters up to 30 in. With the new pipelines now in process of construction, essentially all of the United States and much of Canada will soon be served by natural gas. Figure 1-1 shows a map of gas transmission lines issued by the Federal Power Commission. Table 1-1 indicates the growth in natural gas sales and reserves (1-21, 1-22).

As late as the 1930s, natural gas was blown to the air in large volumes. When gas accompanies crude oil, the gas must find a market or be burned in flares. Prior to rigorous conservation laws on gas flaring, oil gas was often flared. The Oklahoma City and Turner Valley fields each vented approximately a trillion cubic feet of gas from 1930 to 1934. Gas could be purchased in many areas for as little as 1 or 2 cents per 1,000 cubic feet (Mcf), equivalent to 25 to 50 cents per ton of coal or 0.07 to 0.15 cent per gallon of fuel oil. Gas sources at that time were often short-lived because of the waste. A combination of factors, including the low price for a superior fuel, assurance of a continuing supply of gas by conservation and discovery, a gradual rise in the price of competing fuels, and the satisfactory financial returns yielded the pioneering pipelines, all contributed to the mushrooming of the industry in recent years (1-25).

The natural gas industry may be divided into five main subdivisions:

1. *Drilling and discovery of petroleum deposits* in the porous rock of the earth's crust. A knowledge of geology and geophysics is essential to locate and map undrilled or partially drilled traps for petroleum. The drill is a primary tool for exploration. Recent experience shows that, of each 100 wells drilled in the United States, 38 are dry holes, i.e., unproductive, 52

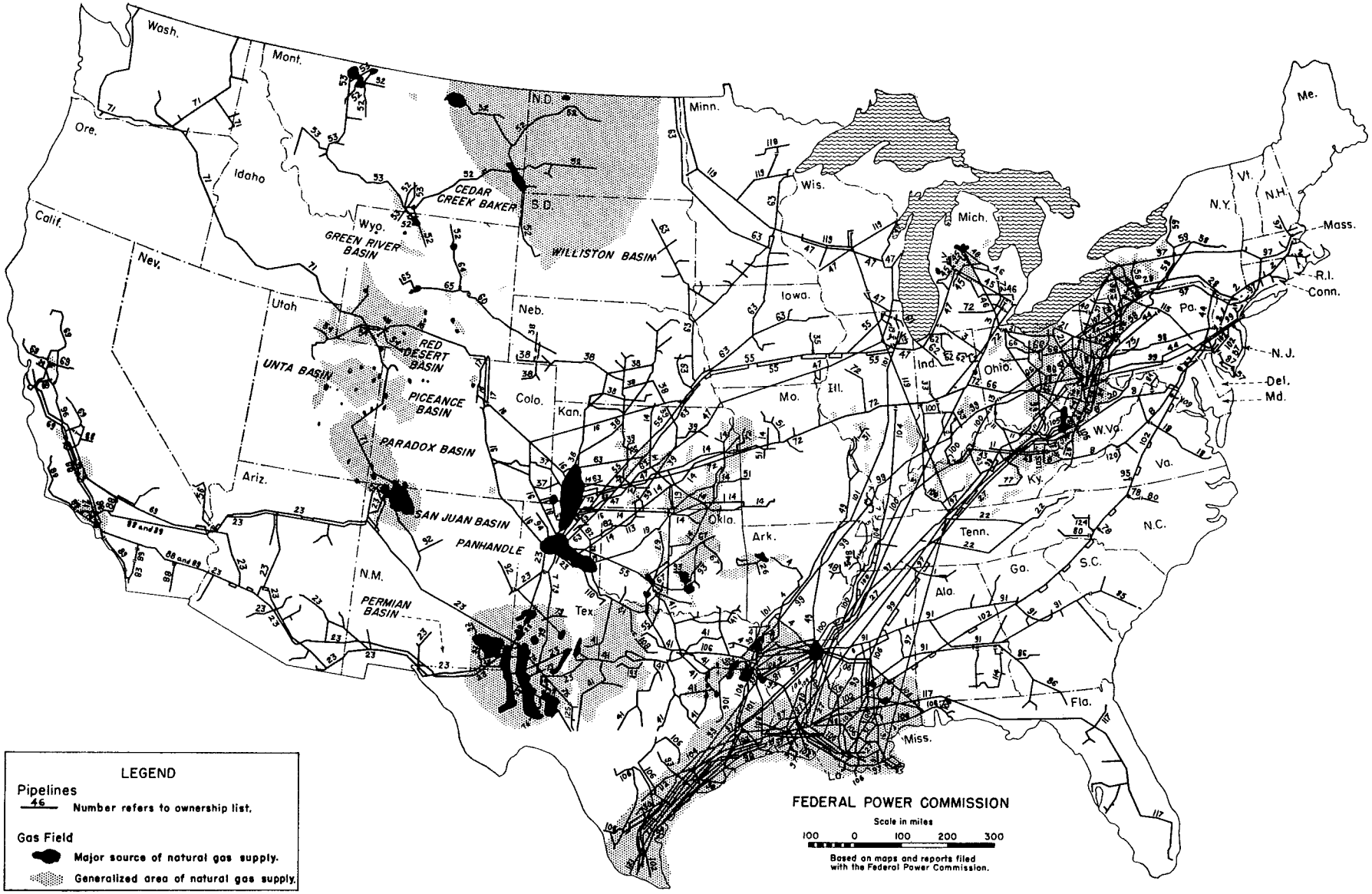

Fig. 1-1. Principal gas transmission lines in the United States. *(Federal Power Commission.)*

Index of Operating Companies in Fig. 1-1

1 Alabama-Tennessee Natural Gas Co.
2 Algonquin Gas Transmission Co.
3 American Louisiana Pipe Line Co.
4 Arkansas-Louisiana Gas Co.
5 Arkansas-Missouri Power Co.
7 Associated Natural Gas Co.
8 Atlantic Seaboard Corp.
11 Central Kentucky Natural Gas Co.
12 Chicago District Pipeline Co.
13 Cincinnati Gas & Electric Co., The
14 Cities Service Gas Co.
16 Colorado Interstate Gas Co.
17 Colorado-Wyoming Gas Co.
18 Commonwealth Natural Gas Corp.
19 Consolidated Gas Utilities Corp.
20 Cumberland & Allegheny Gas Co.
21 East Ohio Gas Co., The
22 East Tennessee Natural Gas Co.
23 El Paso Natural Gas Co.
24 Equitable Gas Co.
26 Fort Smith Gas Corp.
27 Gulf Interstate Gas Co.
28 Home Gas Co.
29 Hope Natural Gas Co.
30 Houston Pipeline Co.
31 Illinois Power Co.
32 Independent Natural Gas Co.
33 Indiana Gas & Water Co., Inc.
35 Iowa-Illinois Gas & Electric Co.
36 Iroquois Gas Corp.
37 Kansas-Colorado Utilities Co.
38 Kansas-Nebraska Natural Gas Co.
39 Kansas Power & Light Co.
40 Lake Shore Pipe Line Co.
41 Lone Star Gas Co.
43 Louisville Gas & Electric Co.
44 Manufacturers Light & Heat Co., The
45 Michigan Consolidated Gas Co.
46 Michigan Gas Storage Co.
47 Michigan-Wisconsin Pipe Line Co.
48 Mid-South Gas Co.
49 Mississippi River Fuel Corp.
51 Missouri Public Service Co.
52 Montana-Dakota Utilities Co.
53 Montana Power Co.
54 Mountain Fuel Supply Co.
55 Natural Gas Pipeline Co. of America
56 Nevada Natural Gas Pipe Line Co.
57 New Jersey Natural Gas Co.
58 New York State Natural Gas Corp.
59 Niagara Mohawk Power Corp.
60 North Central Gas Co.
61 Northern Illinois Gas Co.
62 Northern Indiana Public Service Co.
63 Northern Natural Gas Co.
64 Northern Pipe Line Co.
65 Northern Utilities Co.
66 Ohio Fuel Gas Co., The
67 Oklahoma Natural Gas Co.
68 Olin Gas Transmission Corp.
69 Pacific Gas & Electric Co.
70 Pacific Lighting Gas Supply Co.
71 Pacific Northwest Pipeline Corp.
72 Panhandle Eastern Pipe Line Co.
73 Penn-York Natural Gas Co.
74 Pennsylvania Gas Co.
75 Peoples Natural Gas Co., The
76 Permian Basin Pipeline Co.
77 Petroleum Exploration, Inc.
78 Piedmont Natural Gas Co., Inc.
79 Pioneer Natural Gas Co.
80 Public Service Co. of N.C., Inc.
82 Public Service Corp. of Texas
83 San Diego Gas & Electric Co.
84 Shenandoah Gas Co.
85 South Carolina Natural Gas Co.
86 South Georgia Natural Gas Co.
87 South Jersey Gas Company
88 Southern California Gas Co.
89 Southern Counties Gas Co. of Calif.
90 Southern Gas Lines, Inc.
91 Southern Natural Gas Co.
92 Southern Union Gas Co.
93 Southwest Natural Gas Co.
94 Southwestern Public Service Co.
95 Southwestern Virginia Gas Co.
96 Standard Pacific Gas Lines, Inc.
97 Tennessee Gas Transmission Co.
98 Texas Eastern Penn-Jersey Trans. Corp.
99 Texas Eastern Transmission Corp.
100 Texas Gas Transmission Corp.
101 Texas Illinois Natural Gas Pipe Line Co.
102 Transcontinental Gas Pipe Line Corp.
104 Trunkline Gas Co.
105 United Fuel Gas Co.
106 United Gas Pipe Line Co.
107 United Natural Gas Co.
108 Upham Gas Company
109 Washington Gas Light Co.
110 West Texas Utilities Co.
112 Wilcox Trend Gathering System, Inc.
113 Zenith Gas System, Inc.
114 Southeast Alabama Gas District
115 Trans-Penn Transit Corp.
117 Houston Texas Gas & Oil Corp.
118 Iron Ranges Natural Gas Co.
119 Midwestern Gas Transmission Corp.
120 Roanoke Pipe Line Co.
121 Coastal Transmission Corp.
124 Piedmont Gas Co.
125 Pioneer Gathering System, Inc.

Table 1-1. Statistics on Petroleum Industry in the United States

Year	Natural gas, MMMcf			No. of wells drilled during year	Crude oil and natural gas liquids, MMbbl		
	During year		Reserves at end of year		Production during year		Reserves of both at end of year
	Net prod.	Sales			Crude oil	Nat. gas liquids	
1956	10,908	10,275	237,775	58,664	2,552	346	36,337
1955	10,118	9,405	223,697	56,414	2,419	320	35,450
1954	9,427	8,742	211,711	52,695	2,257	300	34,805
1953	9,239	8,396	211,447	49,966	2,311	302	34,382
1952	8,640	8,013	199,716	47,046	2,256	284	32,957
1951	7,967	7,457	193,811	46,766	2,214	267	32,192
1950	6,893	6,282	185,593	44,058	1,943	227	29,536
1949	6,245	5,419	180,381	39,497	1,818	198	23,378
1948	6,008	5,148	173,869	40,010	2,002	183	26,821
1947	5,630	4,582	165,927	33,798	1,850	160	24,741
1946	4,943	4,030	160,576	30,845	1,726*	...	24,036
1945	4,840	3,918	147,789	27,140	1,736	...	20,826
1944	4,731	3,711	133,500	26,163	1,678	...	20,453
1943	4,336	3,414	110,000	20,820	1,503	...	20,064
1942	3,701	3,053	110,000	22,578	1,385	...	20,082
1941	3,459	2,812	113,800	33,332	1,404	...	19,589
1940	3,331	2,660	85,000	31,149	1,351	...	19,024
1935	2,408	1,916	62,000	24,581	996	...	12,400
1930	.....	1,943	46,000	23,711	898	...	13,600
1925	.....	1,188	23,000	26,412	763	...	8,500
1920	.....	798	15,000	34,029	442	...	7,200

* Includes natural gas liquids.

SOURCE: American Petroleum Institute, American Gas Association, and *World Oil*.

produce crude oil, and 10 produce natural gas or gas-condensate. Knowledge of the properties of reservoir rock that contains the fluids is needed to understand the behavior of wells.

2. *Production from reservoirs* with or without accompanying liquid hydrocarbons. In the exploitation aspect of the industry, the technical problems shift from those of geology to those generally classed as problems in petroleum or reservoir engineering. The prediction of the quantity of natural gas in a given reservoir or the "estimation of reserves" is important. Knowledge of the rates at which the gas can be produced efficiently, or the "deliverability," is necessary for calculating pipeline supplies.

3. *Surface separation or processing plants* to recover liquid hydrocarbons from natural gas and to remove impurities. The design of separators to remove crude oil or condensate at wells, of natural gasoline or cycling plants to extract natural gasoline and LP gas, i.e., propane and butane, of sweetening plants to remove hydrogen sulfide and carbon dioxide, and of dehydration units, embraces most branches of engineering. Chemical engineering deals with the material and energy balances, phase separations, and rate processes of the fluid streams passing through the processing plants.

4. *Transportation and distribution of natural gas to market.* A vast network of transmission lines with associated compressor stations delivers gas from the fields to the centers of population. In many cases, distribution systems in the city previously used for coal gas are enlarged and converted to the distribution of natural gas.

5. *Underground storage of gas near the market.* Natural gas fields often are 1,000 miles or more from the ultimate consumer. Economical delivery of gas requires that the seasonal variations in load for the heating of houses, space heating, be accommodated by removing gas from storage fields near the market rather than by variations in pipeline load.

The Natural Gas Engineer requires data on the behavior of natural gas and associated liquids so that

he can predict the properties, such as density, viscosity, thermal conductivity, and heat capacity, needed in the design of pipelines, gas wells, meters, and processing equipment. Vapor-liquid phase separations among the constituents become complex because of the multicomponent systems involved, and study of these is important background for process design. The flow of gas through porous media governs the recovery of natural gas from reservoirs and controls the capacity of individual wells. Water-hydrocarbon phase relations are specific to the natural gas industry, because natural gas and water may form solid hydrates above 32°F. Knowledge of the behavior of natural gas under pressure is basic to engineering in the five areas just described.

Engineering may be divided into three broad divisions: concepts, basic data, and design procedures. The student or young engineer unfamiliar with the gas industry will find a description of the concepts or methods of describing the behavior of natural gas and processing operations a prerequisite to the conduct of engineering. The highest form of engineering is the conceptual design, which can be made on a rational basis only when a general knowledge of the entire field is part of the engineer's background. The practicing engineer continually uses data in his computations, and the assembly of this information in form suitable for use can be of great service to him. Design procedures are limited by the assumptions made in their derivation. The background for such formulas and examples of their use help to acquaint the engineer with sound practice.

The emphasis given in any writing should be related to the importance of the subject to the reader. In the preparation of such a book as this, much selection takes place, for there is sufficient material available on any phase of natural gas engineering to fill several books. In the sorting process, the writers naturally reflect their experiences and interests. Some subjects, therefore, may be covered in the style of a treatise although other aspects are only touched upon. Geology and related sciences dealing with the earth's surface and the accumulation of petroleum constitute an extensive field treated in separate courses for petroleum or gas engineers. A brief résumé of the geology and occurrence of natural gas is given here for completeness.

GEOLOGY

Study of the nature of the earth's crust and of its ability to accumulate petroleum under pressure constitutes an important background for the engineer in the producing branch of the natural gas industry. Geology treats all phases of the earth's history, including the processes by which reservoirs were created. Man is fortunate that many of the processes which produced the earth's crust are still in evidence to permit a reconstruction of methods by which most reservoirs were formed.

There are several branches of geology and of related earth sciences (1-28, 1-40 to 1-45, 1-50 to 1-52, 1-54). Their nomenclature makes frequent use of such terms as *geo*—earth, *petra*—rock, *lithos*—stone, and suffixes like *logy*—science or discourse, *graphy*—description. *Physical geology* is a study of the processes affecting the earth's surface, such as action of wind, water, ice, and atmosphere. *Historical geology* endeavors to trace the events in the history of the earth, including the processes responsible for the earth's crust. The origin of life and the evolution of plant and animal forms are included. *Structural geology* treats the methods by which the position and shape of the various members of the earth's crust are determined, and studies forces which have brought about both the surface and subsurface structures. *Stratigraphy* covers the character, sequence relationship, distribution, and origin of sedimentary rocks.

Several branches deal with the recognition of rock according to type and age. The study of rocks to determine their character and constitution is termed *lithology*. *Paleontology and micropaleontology* classify information on life in past geologic ages by studies of fossils and microfossils. *Mineralogy, petrography, and petrology* deal with the physical properties, chemical properties, classification, and identification of minerals or rocks and with their genesis.

Sedimentation (1-58) is the process of depositing solids at the bottom of a fluid, and the term is in frequent use to describe methods of depositing particles of rock from bodies of water. *Sedimentary* rocks are rocks that have been deposited by this process. Essentially all petroleum is contained in sedimentary rock. *Geohydrology*, or groundwater geology, combines the principles governing water movement through porous media and the geology of the earth's crust with respect to the ability of the various strata to conduct water.

Geophysics is the application of the principles of physics to problems of the earth (1-54, 1-48). The study of the transmission of shock waves generated either from natural causes, such as earthquakes, or by explosions of dynamite is an example. These principles are utilized in the *seismic* method of searching for structures. The reflection of elastic waves at the interface between layers of rock with different physical properties permits the mapping of the interface.

Other methods of making physical measurements at the earth's surface to find the nature of its subsurface employ the magnetic field, the gravitational field, and the electrical properties of the earth, principally its electric resistivity (1-7). These methods usually depend upon anomalies or irregularities in the earth's crust.

Geochemistry is the application of the principles of chemistry to the study of the earth. The search for petroleum by analyzing soils for hydrocarbons is considered a geochemical method (1-54). The physical chemistry of molten rock and the chemistry of its disintegration and recrystallization are included.

Historical Geology

Historical geology (1-4, 1-6, 1-28, 1-42, 1-50, 1-51) reconstructs the successive events in the history of the earth since it was in a molten condition. Geologic time scales have been devised to indicate the periods of time during which various layers of the earth's surface were formed. The point at which cooling of the earth's surface led to water precipitation is the zero point on a geologic time scale with respect to sedimentary processes. The erosion by rain and wind of the surface that protruded and the covering of the bottom of adjacent shallow water with the eroded material is conceived to be the most active process in the creating of porous rock. The uplifting of areas of the continents to permit erosion while an adjacent area was submerged required movements of the earth's crust now observed only slightly during earthquakes.

Table 1-2 presents the geologic time scale (1-28, 1-50, 1-51) divided into eras, periods, and epochs. The approximately 4,500 million years of the earth's life is difficult of comprehension for persons who individually live less than 100 years and who collectively have a recorded history of approximately 5,000 years in length.

When water condensed on the surface of the earth, the high areas were subjected to rain and the low areas were inundated. The extractive power of water and the ability of streams to carry sediment are primarily responsible for the nature of the immediate surface of the earth's crust. The erosion of mountains and the filling of seas go on continuously. The mountains would all be worn down and the seas all full of sediment if it were not for the changes in elevation (uplifts and submergences) of areas on the earth's surface. It follows that at any point on the earth there may be gaps in the occurrence of sedimentary rocks for some period.

Geologists have mapped the earth to show the present outcrops of sedimentary rock as well as the positions of the seas during geologic periods. Figures 1-2 and 1-3 show the outcrops of Pennsylvanian formation and the extent of the seas that accumulated sediments in that period.

The Pre-Cambrian Eras cover the time span from the formation of the earth up to approximately 500 million years ago. The rocks formed during these eras are of three characters: (1) igneous, products of solidification of molten material; (2) metamorphic, rock that changed its character by solution, heat, and pressure; and (3) sedimentary. Common examples of igneous rock are granite, which has solidified slowly within the earth's crust, and lava, which solidifies rapidly on the surface. Schist and gneiss were formed by metamorphic processes that occur with heat, pressure, and time. Sedimentary rocks include sandstone, limestone, dolomite, and shale. The Canadian Shield, north of the Great Lakes and the St. Lawrence, is an outcrop of Pre-Cambrian formations. Patches also appear in the Appalachian and Rocky Mountains, as well as in the gorge of the Grand Canyon. Many of the world's mineral deposits of iron, nickel, gold, cobalt, and other metals occur largely in rocks of Pre-Cambrian age.

The Cambrian Period is the first in which the sediments can be identified over wide areas by the evidences of life such as marine fossils. Several varieties of Cambrian invertebrates serve as guides to the time of deposition, but few plants remain except lime-secreting seaweeds (calcareous algae, 1-51). The study of life as evidenced by fossil remains, paleontology, may have application in the Cambrian and all younger deposits. Microscopic examination of sediment often shows the evolution of new forms of life. The appearance or disappearance of a given form can be used to correlate ages of rocks at various localities.

The Ordovician Period represents a change in fossils, with the introduction of vertebrates. A great portion of the North American continent was submerged during this period, and an average deposition of 5,000 ft occurred in the Appalachian trough. The Arbuckle Mountains of southern Oklahoma show Ordovician deposits some 10,000 ft thick.

The Silurian, Devonian, Mississippian, Pennsylvanian, and Permian Periods complete the Paleozoic era. The Silurian period is noted for its salt deposits in Michigan and New York. The Devonian period still antedates the formation of the Appalachian and Rocky Mountains. It is characterized by fossil coral reefs and by the appearance of four-legged animals. At the end of each of these periods there was a general recession of the seas, normally accompanied by rapid changes in life before the following submergence corresponding to the next period. The Mississippian and Pennsylvanian periods are often called "car-

Table 1-2. The Geologic Time Scale

Era	Period	Epoch	Formations producing oil and gas (field or area)
Cenozoic 71*	Quaternary	Recent Pleistocene 1	
	Tertiary 70	Pliocene 10	Repetto (Ventura, Calif.)
		Miocene 15	(Krotz Springs, Deep Lake, Erath) (Louisiana) (Kettleman Hills, Coalinga) (California)
		Oligocene 10	
		Eocene 20	Cockfield (Conroe, Texas) Yegua (Katy, Texas)
		Paleocene 15	
Mesozoic 130	Upper Cretaceous 35	Lance Montana Colorado	Woodbine (East Texas) Mesa Verde (San Juan, New Mexico, California)
	Lower Cretaceous 20	Dakota Comanche	Monroe Chalk (Louisiana)
	Jurassic 40	Upper Middle Lower	(Fort St. John, British Columbia)
	Triassic 35	Upper Middle Lower	
Paleozoic 300	Permian 30	Upper Lower	Hugoton Dolomite (Kansas, Oklahoma, Texas) Yates (West Texas, New Mexico) Panhandle Dolomites (Texas)
	Pennsylvanian 30	Virgil Missouri Des Moines Morrow	Reef (Scurry County, Texas) Burbank (Oklahoma)
	Mississippian 30	Chester Valmeyer Kinderhook	Michigan Stray Sands
	Devonian 40	Chautauquan Senecan Erian Ulsterian Oriskanian Helderbergian	Dundee, Traverse (Michigan) Leduc (Alberta) Bradford (Pennsylvania)
	Silurian 30	Cayugan Niagaran Medinan	
	Ordovician 60	Cincinnatian Mohawkian Chazyan Canadian	Simpson (Oklahoma) Viola City Wilcox Bromide Trenton (Michigan)
	Cambrian 80	Ozarkian St. Croixian Acadian Waucoban	Arbuckle Lime (Oklahoma City), (Kansas) Galesville aquifer (Herscher, Illinois)
Proterozoic		Pre-Cambrian 4000	
Archeozoic			

* Approximate duration in millions of years.
SOURCE: (1-28, 1-50, 1-51).

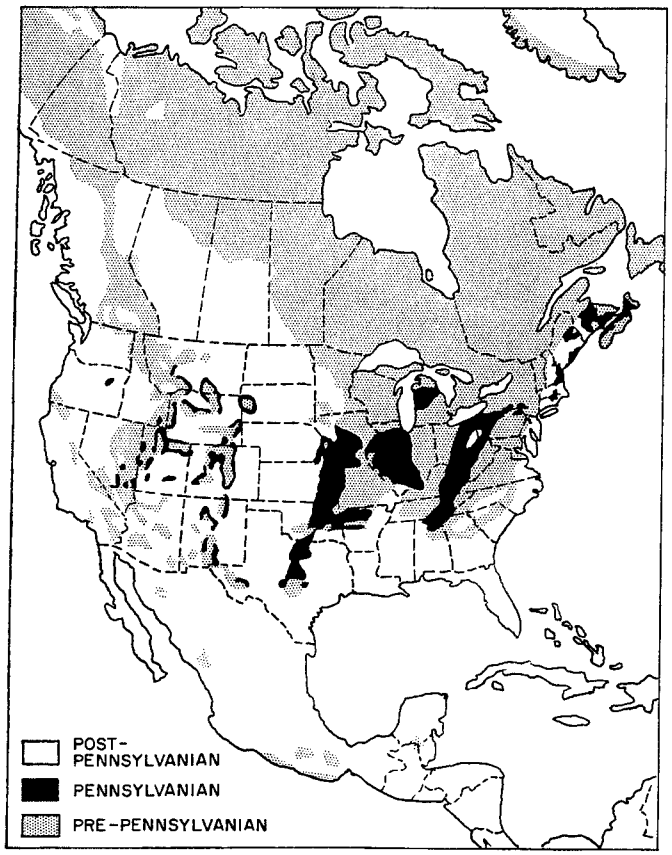

Fig. 1-2. Pennsylvanian outcrops in North America. Except for exposures in easternmost Canada, known deposits of Pennsylvanian age in North America are confined to the United States. The outcrop areas of greatest extent all lie east of the Rocky Mountains. (Moore, 1-51. *Courtesy McGraw-Hill Book Company, Inc.*)

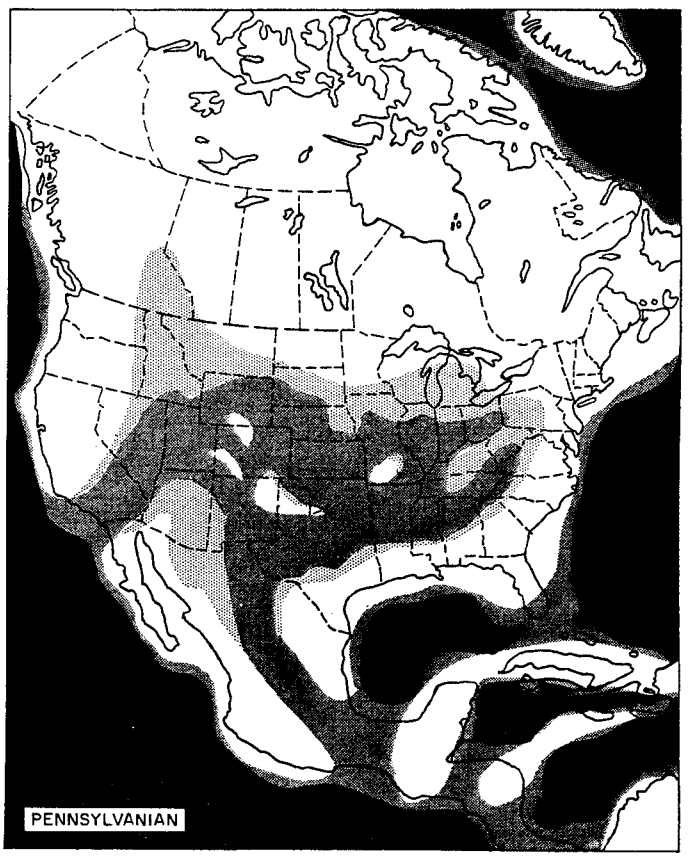

Fig. 1-3. Distribution of Pennsylvanian seas. Oceanic areas are shown in black; the most persistent seaways on the continental platform are represented by dark gray; and areas submerged during only part of the period are indicated by light gray. The shallow seas of Pennsylvanian time were most remarkable from the standpoint of their incessant oscillation. Even the areas represented on the map as persistent seaways were actually emergent many times and then submerged again. Inferred persistent land areas are unshaded. As indicated by distorted outlines of Eastern and Western states, the continent is represented as wider than now, so as to compensate for crustal shortening produced by post-Pennsylvanian mountain building. (Moore, 1-51. *Courtesy McGraw-Hill Book Company, Inc.*)

boniferous," for during them a large proportion of the coal-bearing strata was formed. In the Permian period, thick deposits, left undisturbed, were laid down in a wide area including West Texas, New Mexico, and western Oklahoma. The Appalachian Mountains were formed near the end of the Paleozoic era, and profound changes in life occurred before the Triassic period.

The Mesozoic Era begins with the Triassic period, the Age of Reptiles. During this period, little of the midcontinent and none of the eastern United States received any deposit. Petrified logs in Arizona showed trees to be 7 ft in diameter and 125 ft tall in the Triassic period. Recent gas fields in the Peace River area in British Columbia produce gas from the Triassic.

The Jurassic Period marks the beginning of dinosaurs. During this period there was limited sedimentation in the Rocky Mountain and Plains areas. The Cretaceous seas covered a belt from Texas to Alberta, the geosyncline or trough reaching 700 miles in width with deposits up to 15,000 ft in thickness. It marked the beginning of modern flora, such as elm, oak, maple, and poplar trees, and also the decline of the dinosaur.

The Tertiary Period was very active for the coastlines of the United States. The salt domes of the Gulf Coast came to the surface in the Tertiary period (Fig. 1-4). Oil-shale deposits in the Western states are from this period. Predecessors of the horse and elephant appeared and disappeared in North America. The Rocky Mountains were formed.

The Quaternary Period, recent or pleistocene, is assigned a length of 1 million years. The ice cap appeared on North America. The melting of this

ice left glacial drift over the northern half of the continent. The Great Lakes were formed in the process.

The Thickness of Sedimentary Rock varies from zero to an estimated 40,000 ft and more. The outcrop of igneous rock in eastern Canada and in mountainous areas indicates that either such areas were never submerged or else any sedimentary rocks have been completely eroded away. Figure 1-5, prepared by the U.S. Geological Survey, divides the United States into areas favorable, unfavorable, and impossible with respect to the discovery of oil and gas. The following statement, to accompany Fig. 1-5, is made by the U.S. Geological Survey:

The accompanying map shows the known oil and gas fields in the United States and unproductive areas classified as to their relative likelihood of yielding commercial quantities of oil and gas. This classification, developed by David White, was first published in 1934, and has been revised slightly in successive editions of the map on the basis of additional discoveries of oil and gas, more detailed geologic mapping, and additional knowledge about the occurrence of oil and gas.

In this present classification, the oil and gas possibilities of the United States are divided into four categories: favorable, favorable and unfavorable undifferentiated, unfavorable, and impossible. The possibilities of the continental shelf have not been classified, but in general are considered to be the same as those of the adjacent land area.

Favorable Areas

The unpatterned land areas on the map are those in parts of which oil and gas fields (shown by the black patches or dots) have been found, and in which most of the future discoveries of commercial quantities of oil and gas will probably be made. The relative prospects of the unpatterned areas, which at present are unproductive, vary greatly from region to region and from one locality to another. Oil and gas will be found only in those areas where suitable geologic conditions have combined to form and trap them. In many small parts of the unpatterned areas oil and gas possibilities appear to be unfavorable for such reasons as the nonexistence of suitable structures for traps or the lack of reservoir and source rocks; in other small areas included in this category oil and gas did not reach a trap, or escaped from it because of later earth movements, or were destroyed by later metamorphism. In general, however, most of the unpatterned areas on the map are considered to be favorable for the search for commercial quantities of oil and gas.

Favorable and Unfavorable Areas Undifferentiated

This category includes a large part of the western United States that is covered by extensive lava flows or recent sedimentary deposits concealing rocks that may contain oil and gas, as well as a large area in which the complexity of the geology and present information do not justify classification into many small individual favorable or unfavorable areas. Small areas in which production of oil or gas have been found in this region are left unpatterned.

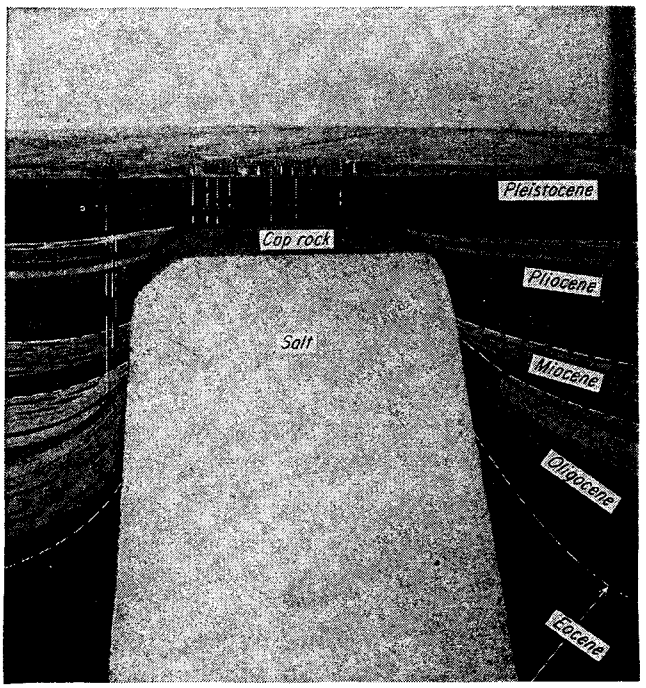

Fig. 1-4. Diorama of Spindletop oil field, Jefferson County, Tex. View northwest toward an east-west section through the center of the salt dome. This typical salt dome, located at the south edge of Beaumont, Tex., has a cylindrical core of salt about a mile in diameter. Its nearly flat top is covered by hard caprock, mainly composed of dolomite and anhydrite that is encountered in wells at a depth of slightly more than 1,000 ft. The Tertiary formations surrounding the salt plug have been turned upward around it by vertical thrust of the rising salt mass. More than 130 million bbl of petroleum has been produced from the flanks and cap rock of this dome. (*Courtesy Texas Memorial Museum, Austin, Tex.*)

Unfavorable Areas

Many regions throughout the United States are considered unpromising for the future production of oil and gas in significant quantities. Among the reasons that lead to this classification are the degree to which the rocks have been altered by heat and pressure (metamorphism), the thinness of strata that could contain oil or gas, and the probable absence of source rocks. Small quantities of oil or gas may at some future time be found in those areas, but, on the basis of present knowledge, it is unlikely that commercial amounts will be found.

Impossible Areas

The areas where oil and gas production in commercial quantities is considered to be impossible generally contain either igneous or metamorphic rocks or both. With the exception of lava flows, these are usually referred to as basement rocks, and constitute almost all the pre-Cambrian rocks in the United States. Granites (intrusive) and basalts

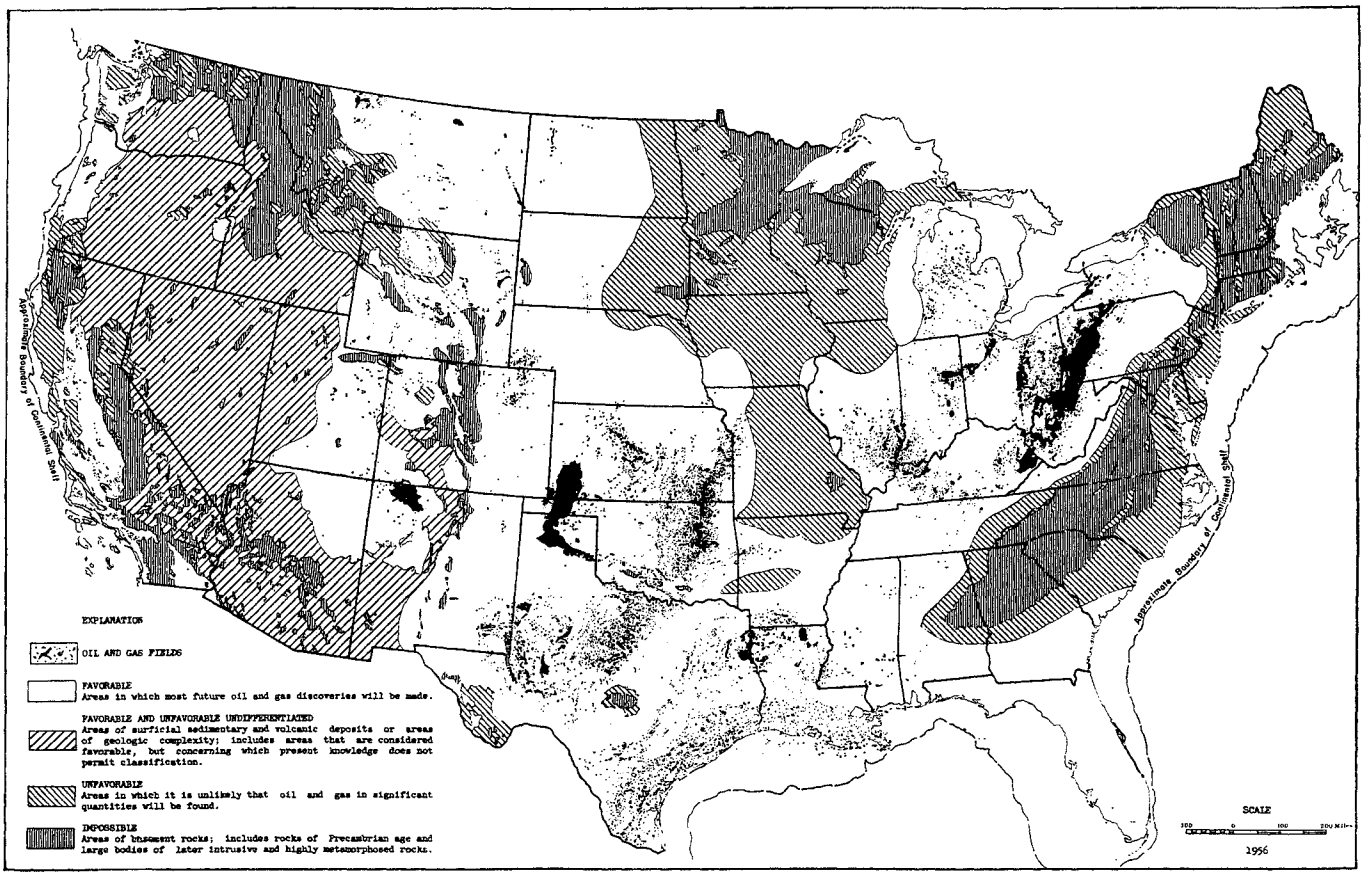

Fig. 1-5. Map of the United States showing favorable and unfavorable areas for oil and gas production. (*United States Geological Survey.*)

(extrusive), which are of igneous origin, are solidified from a molten state either under or on the surface of the earth, and are generally impervious and hard. Schists, gneisses, and marbles, which are metamorphic rock types, are formed by the action of heat and pressure on igneous, sedimentary, or other metamorphic rocks at great depths beneath the surface of the earth. Oil and gas are not usually found in igneous or metamorphic rocks, as both are so non-porous that oil and gas cannot accumulate in or be extracted from them. In the few fields that do produce from such rocks, the oil and gas have seeped from neighboring sedimentary formations into cracks and joints in the igneous and metamorphic rocks.

The deeper sedimentary rocks lie at the center of basins. On the Gulf Coast the Richardson and Bass well at 21,741 ft is the deepest producer. It is located in Plaquemines Parish, La., and was completed in the Miocene formation. The Ohio Oil Company deep test in Kern County, Calif., was in lower Miocene at 21,482 ft (1-30).

Structural Geology—The Formation of Traps for Oil and Gas (1-44, 1-52)

Oil and gas are less dense than water and accumulate in porous rock underneath an impervious cap rock. Generally water underlies the oil or gas, confining it underneath the cap rock. Various geological processes have been responsible for the formation of these traps. Earth movements, erosion, and sedimentary processes have created structures favorable to the accumulation of petroleum. In some instances, known as *stratigraphic* traps, the accumulation is in the porous portion of a stratum and the accumulation is not due to structure. Recent studies (1-34, 1-35, 1-32) show that hydrodynamic conditions as well as structure may determine the type of accumulation.

The *anticline* is a common structure, caused by an uplifting of the rock (Fig. 1-6*a*). Fluids traveling updip through the porous media eventually reach the dome, and are retained by the cap rock when present. The *syncline*, or trough portion of a fold, is often mentioned as a trap for oil, but it provides no trap unless associated with some other feature.

Porous rock pierced by a fault plane often is sealed at the fault to form a trap on one or both sides of the fault (Fig. 1-6*b*). An uplifted surface may be truncated by erosion, submerged, and overlaid with an impervious cap rock (Fig. 1-6*c*) known as an *unconformity*. Likewise, the overlap on protruding basement rock may be sealed (Fig. 1-6*d*). In such cases, the granite may have been eroded prior to the sedi-

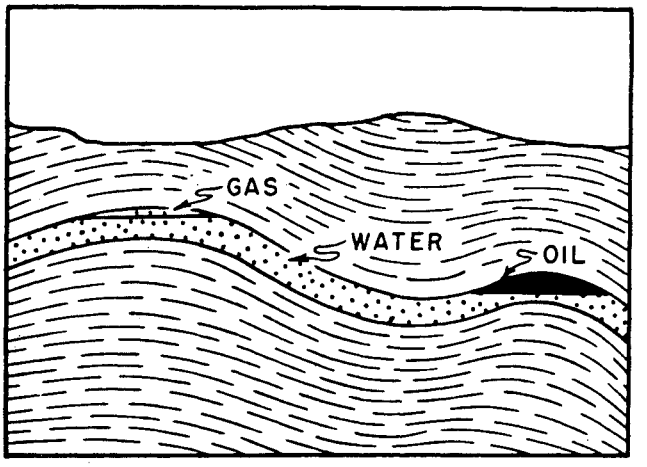

a

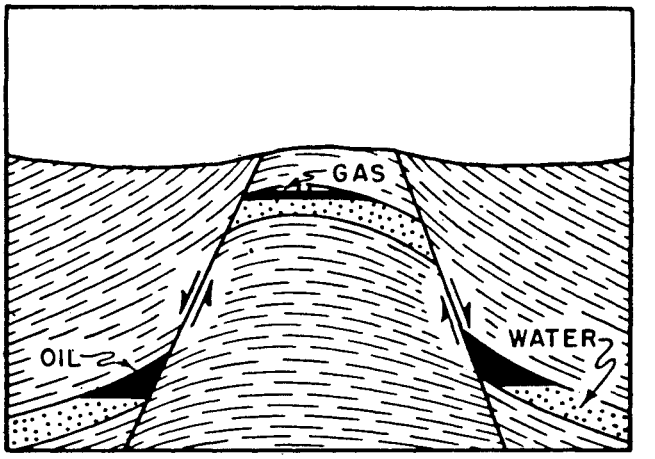

b

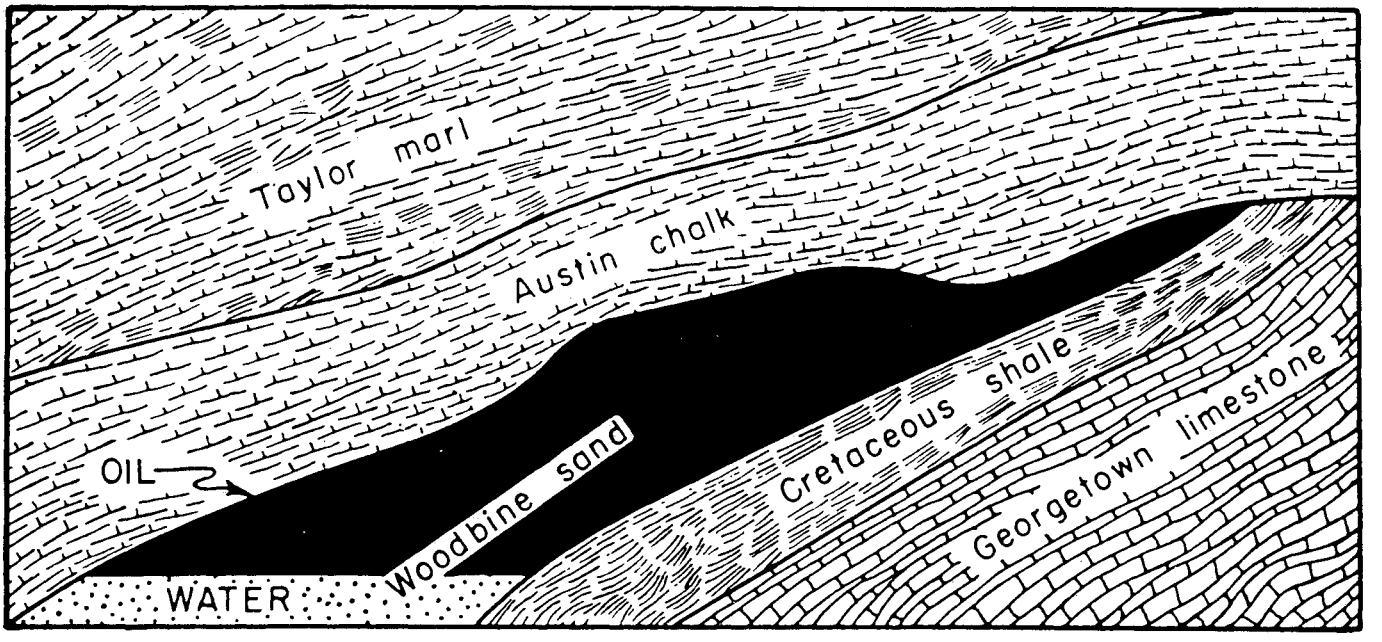

c

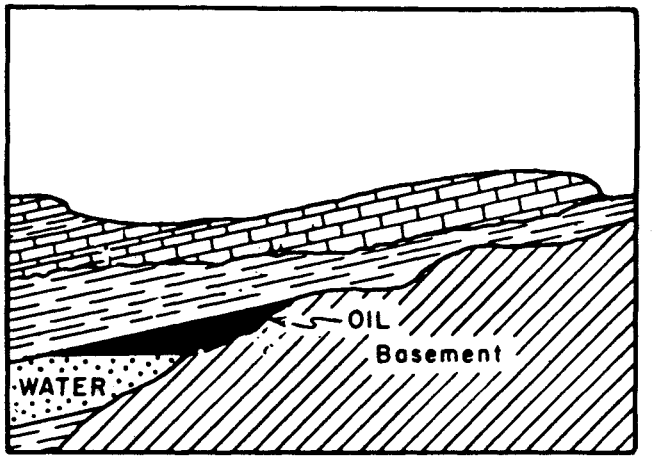

d

Fig. 1-6*a* to *d*. Major types of reservoir traps. (*a*) Simple anticlines. (*b*) Fault traps. (*c*) Truncation trap—east-west cross section of East Texas Reservoir. (*d*) Overlap on beds that flank basement rock. (*LeRoy*, 1-44; *Carson et al.*, 1-4. *Courtesy Colorado School of Mines.*)

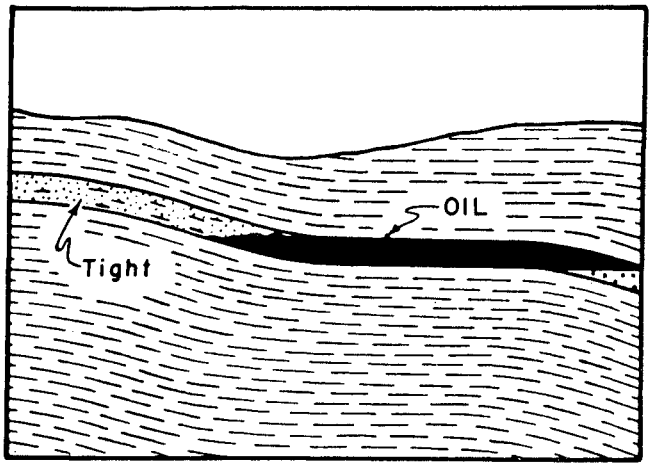

e

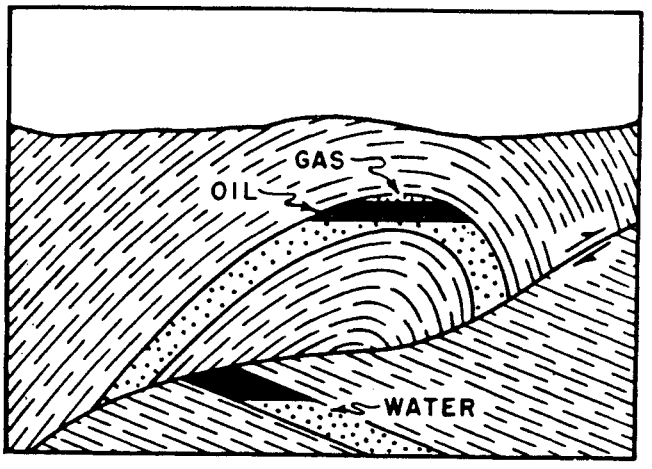

g

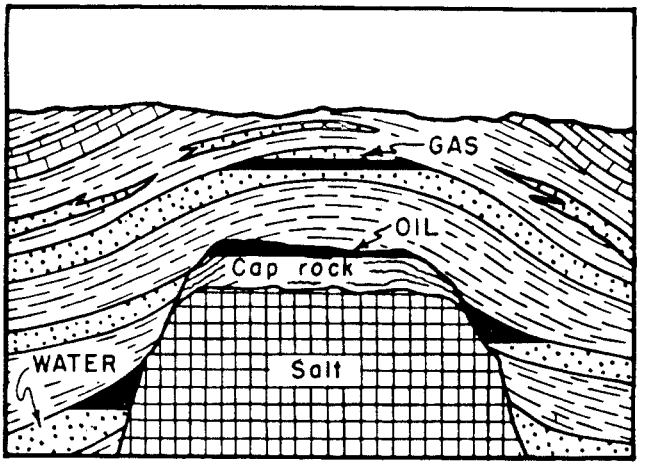

f

Fig. 1-6e to g. Major types of reservoir traps. (e) Loss in porosity and permeability in tight sand forms reservoir's upper boundary. (f) Reservoirs on a salt dome. (g) Anticline broken up into traps by fault. (*LeRoy*, 1-44; *Carson et al.*, 1-4. *Courtesy Colorado School of Mines.*)

mentary action, and petroleum may be found both in the sedimentary rock and in the eroded granite known as *granite wash.*

A stratigraphic trap occurs in a single stratum without any particular structure when the porosity and permeability are reduced in one portion and are sufficiently high in another portion to permit the accumulation of oil and gas (Fig. 1-6*e*). Sands often lose porosity and permeability in the presence of shale. The salt dome is a common occurrence on the Gulf Coast (Fig. 1-6*f*). Many complex structures are formed by severe folding or faulting (Fig. 1-6*g*). In such areas it is not uncommon for the drill to pass through the same layer several times, even in reverse order from top to bottom.

Types of Rock Encountered in Wells (1-6, 1-7, 1-14)

Rocks may be classified as *clastic* or *nonclastic.* Clastic rocks are those made up of particles derived from some preexisting rock. Nonclastic sedimentary rocks such as limestone or dolomite are formed by chemical precipitation.

Important clastic rocks include sands and sandstones, silt and siltstones, conglomerates, arkoses, oölites, and shales. The sands and sandstones are composed of individual quartz grains. Sands may be unconsolidated to the extent that the grains are produced along with oil or gas. Sandstones are bonded sands, with silica, calcite or lime, and iron oxide as typical bonding agents. Sand grains have a maximum dimension of $\frac{1}{16}$ to 2 mm. Aggregates having particles smaller than this range are described as silts or, if bonded, as siltstones. Larger particles are described as gravel. Shale is composed of particles finer than silt, and generally consists of aluminum silicate or clay. Shales may be soft with a high water content, or hard and consolidated. Shales seldom contain oil and gas in commercial quantities, and are good cap rocks because of their low permeability and relative flexibility. The large deposits of oil shales in the Western plateau should be noted. Recovery of this oil will not be through wells, but by mining methods. Sediments containing a portion of the particles larger than sands are conglomerates or breccias. Pebbles and larger fragments may be composed of quartz, limestone, and igneous or metamorphic rocks. The finer particles are normally sand. Arkoses are often referred to as granite wash. Oölites are rocks composed of small, round particles of limestone.

The nonclastic sediments are chiefly limestone, dolomite, and chalk. Limestone in its pure form is calcium carbonate, or calcite. Dolomite is the double carbonate of calcium and magnesium. Limestones and dolomites are likely to have low porosities and permeabilities within the matrix, and they may have

been subjected to solution processes which developed channels, cavities, vugs, and even caverns, which provide the more prolific reservoirs for petroleum. Chalk is a form of limestone that is soft, low in permeability, and high in porosity. Salt, anhydrite, and gypsum are common nonclastic rocks.

Many rocks are mixtures or combinations of the types described. "Shaly sand" or "sandy shale" are terms to denote the mixing of shale in sand or of sand in shale. Limestone and dolomite occur in a range of compositions, often as dolomitic limestones.

The Origin and Accumulation of Petroleum

Most books on the geology of petroleum (1-4 to 1-6, 1-41, 1-45, 1-47, 1-54, 1-56) and many articles (1-32, 1-34, 1-35, 1-55, 1-57) give theories on the origin of petroleum. However, no complete and satisfactory theory is available. There is fair agreement about certain parts of the total process.

Marine sediments sampled in the Gulf Coast contain organic matter which has been shown to include many of the petroleum hydrocarbons (1-55). These studies give a petroleum content of 3 to 7 million bbl of oil per cubic mile of sediment, but do not give a complete story of the paraffin hydrocarbon family including natural gas. Microscopic plant and animal life over the geologic ages in shallow seas no doubt deposited large quantities of similar organic matter which served as the starting point for the formation of petroleum. Bacterial action can convert such material into hydrocarbons (1-62) and may have been the actual process. Other possible processes include slow conversions catalyzed by rock surfaces. Steps in the conversion may be revealed by examining the kerogens found in oil shales or the tars of the Athabaska sands.

Many writers ascribe different origins to natural gas and crude oil. Examination of the gases dissolved in crude oils as well as of heavier liquid hydrocarbons found in gas fields convinces the writer that oil and gas are continuous members of the same family and have the same origin. Differences in accumulation can occur for gaseous and liquid phases, so that gases and liquids formed together can accumulate in different traps.

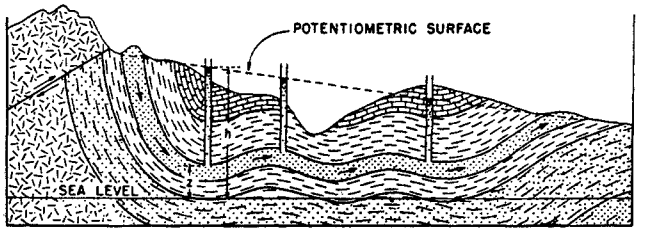

Fig. 1-7. Regional flow of water through sand from higher to lower outcrop. (*Hubbert*, 1-34. *Courtesy AAPG.*)

The migration of oil and gas to the traps created by structure or by porosity and permeability barriers within a stratum is relatively easy to imagine (1-32, 1-34, 1-35). Petroleum generated in the source beds (1-57, 1-58), including shales, could gravitate upstructure until a barrier or ceiling is imposed by the cap rock or low-permeability section. It is easier to understand the accumulation process if one follows the description of the mechanism of entrapment of petroleum under hydrodynamic conditions set forth by Hubbert (1-34).

Hubbert shows that water movement, in most sedimentary strata even today, takes place from one outcrop to another at a different elevation (Fig. 1-7). Such a process in earlier configurations of the earth's crust or with present structures could provide the vehicle by which the oil and gas were conveyed from the source beds to traps. Hubbert shows, further, how such dynamic processes can create traps and will result in tilted interfaces between water and oil or gas (Fig. 1-8). It is possible to find oil on a sloping surface containing small folds when water movement is downstructure (Fig. 1-9).

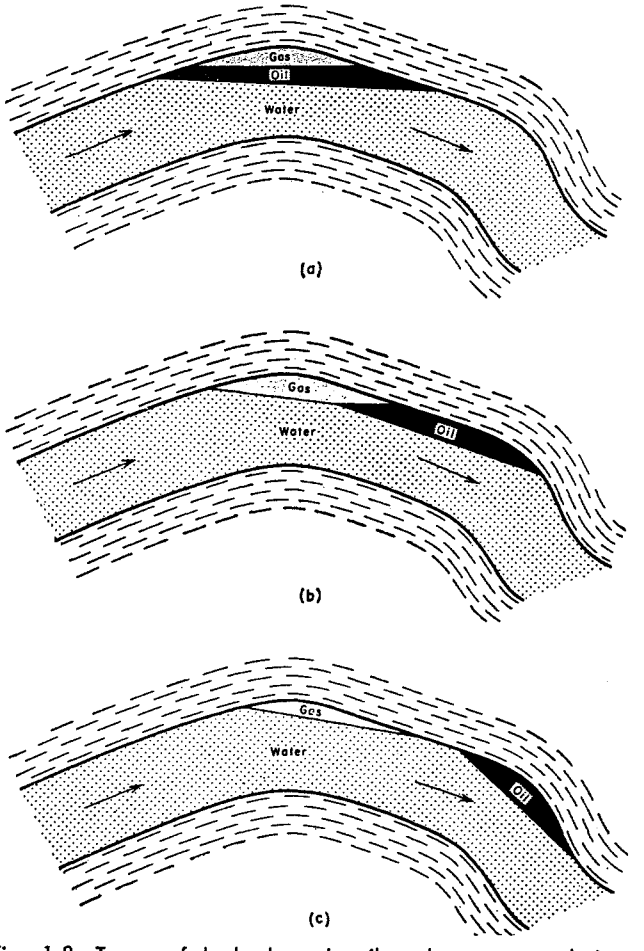

Fig. 1-8. Types of hydrodynamic oil and gas accumulations. (*Hubbert*, 1-34. *Courtesy AAPG.*)

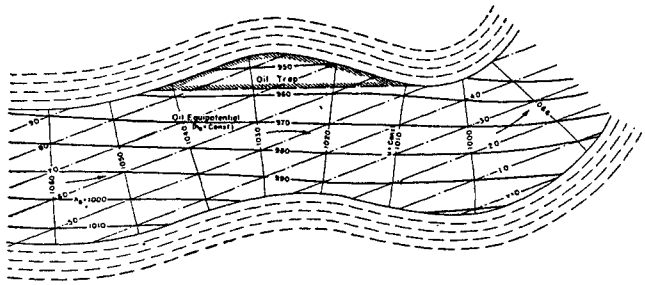

Fig. 1-9. Oil accumulation with hydrodynamic trap. (*Hubbert*, 1-34. *Courtesy AAPG.*)

Methods of Presenting Geological Data

Maps, well logs, isometric views, and cross sections are methods used to convey information about the shape and position of the porous rock containing a petroleum deposit. Surface maps showing section lines, well locations, roads, rivers, etc., are basic to the description of any gas field (Fig. 1-10). Structural contour maps are made on the top of producing strata (Fig. 1-11) or, in some cases, on a definite geological marker just above the pay zone. Isopachous maps contain lines of equal thickness for sands or the oil-bearing portion thereof (Fig. 1-12).

Many types of well logs are prepared when wells are drilled. The drill cuttings and cores of rock formations from a well are examined by the geologist and recorded in sample or core logs (Fig. 1-13). Drilling time versus depth often makes a valuable log to indicate the thickness of various strata. After a section of the well has been completed but before the casing is set, electrical logs and micrologs are determined by lowering electrodes into the well bore and recording electrical potentials at the surface. Gamma-ray or neutron logs are run either before or after setting of the casing. Figure 1-14 shows a schematic electrical log, and Fig. 1-15 shows a comparison of the microlog with other information. Further information will be given when we describe gas wells and typical gas reservoirs.

OCCURRENCE OF NATURAL GAS

In the early days of the petroleum industry (1-5), natural gas and crude oil were described as separate and distinct substances. This concept resulted from the circumstance that the shallow wells then in production either delivered natural gas or produced oil

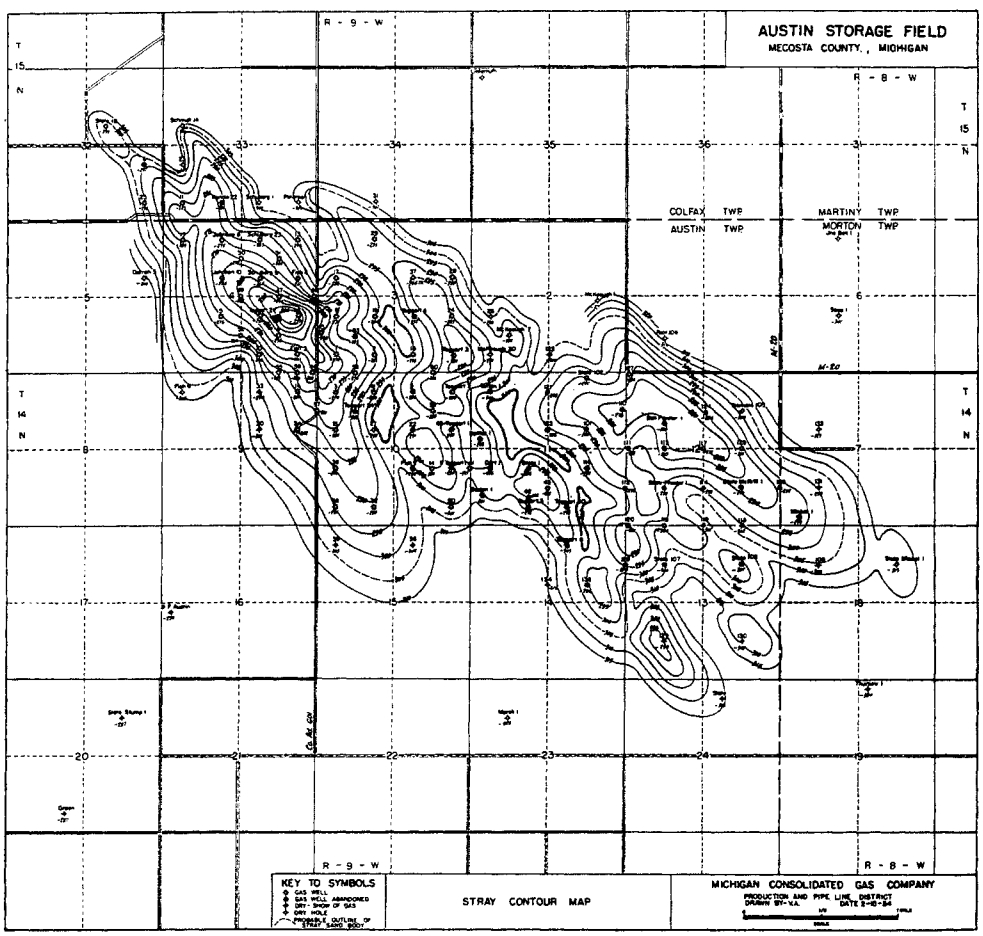

Fig. 1-10. Surface map for Austin storage field. Contours on top of stray sand. (*Courtesy Michigan Consolidated Gas Company.*)

by pumps. As the depth at which oil and gas were found increased, natural gas usually accompanied crude oil and hydrocarbon liquids were found to condense from natural gases. The development of methods to analyze oils and gases brought out the fact that natural gas and most crude oils are of the paraffin hydrocarbon family. "Petroleum" is a generic term covering the naturally occurring hydrocarbons, whether oil or gas. Table 1-4 lists some constituents of petroleum and indicates the products of commerce.

The depths at which oil and gas were discovered in America and the discovery dates are plotted in Fig. 1-16 (1-38). Figures 1-17 and 1-18 show conditions typical of the early shallow fields, when natural gas and crude oil production were essentially distinct operations. By about 1925, the discovery depth had reached 4,000 ft or more and the pressure in these reservoirs reached 1,800 pounds per square inch absolute (psia) or higher. At this pressure, sufficient natural gas was dissolved in the crude oil so that oil-gas separators at the wellhead were necessary to conserve the volatile liquids in the crude oil (Fig. 1-19). By this time the natural gasoline industry was actively recovering the butane, pentane, hexanes, heptanes, and heavier constituents from natural gases in oil-absorption plants, and the separator gases were gathered for this purpose.

By the late 1920s, high-pressure wells producing natural gas predominantly were observed to produce a "water white" distillate in small quantities along with the gas at Big Lake, Tex. (1-39), Turner Valley, Alberta, Kettleman Hills, Calif., and Oklahoma City, Okla. This naphtha or condensate was gradually accepted as a condensate from the gas phase, and the term "retrograde condensation" (1-37) became a common term. Figure 1-20 shows the separation of natural gas from condensate. Today, most discoveries of petroleum include both oil and gas, and the producing industry makes little distinction between the two with respect to exploration or drilling. Production practices are different, and governmental regulations divide wells into oil wells and gas wells. Wells producing both oil and gas are divided arbitrarily on some fixed gas-oil ratio.

The geologic processes—submerging of areas and deposition of sedimentary rock—resulted in the development of fairly large areas with similar geological histories. These areas are often referred to as *basins*. Figure 1-21 and Table 1-3 by Moulton (1-49) show the basins in the United States that are either productive of gas or believed capable of production. Ball (1-23), Denison (1-26), and Levorsen (1-46) describe future prospects for finding oil and gas in North America. Information will be given on a few

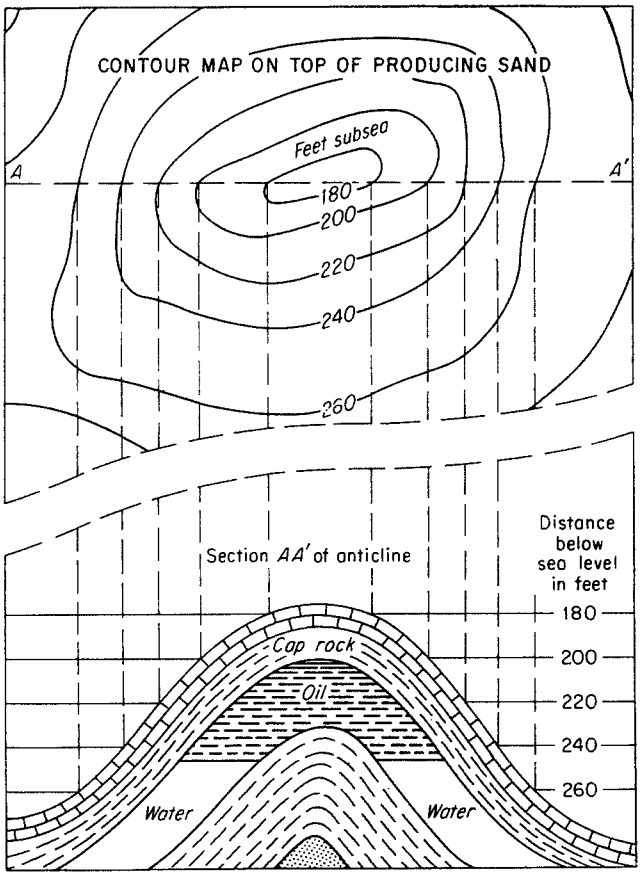

Fig. 1-11. Contour–cross-section map.

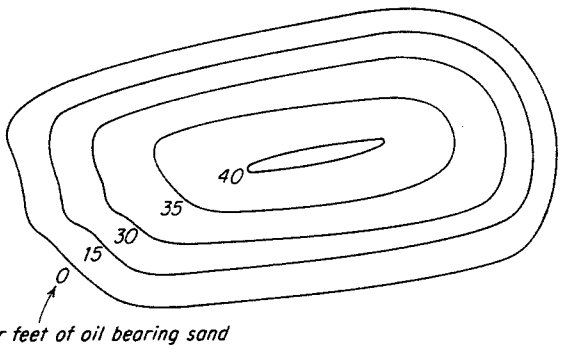

Fig. 1-12. Isopachous map for oil zone of structure in Fig. 1-11.

typical fields producing gas either alone or with hydrocarbon liquid.

The Austin Gas Field, a stray sand field in central Michigan, is typical of the shallow gas fields that do not produce hydrocarbon liquid. Figure 1-22 shows a section of the Michigan basin (1-59), and Fig. 1-10 is a surface map showing well locations. The Michigan stray sand of Mississippian age lies on top of the Marshall sand, also of Mississippian age. The sand contains some shale, has a porosity estimated at 22 per cent, and has a high productivity or perme-

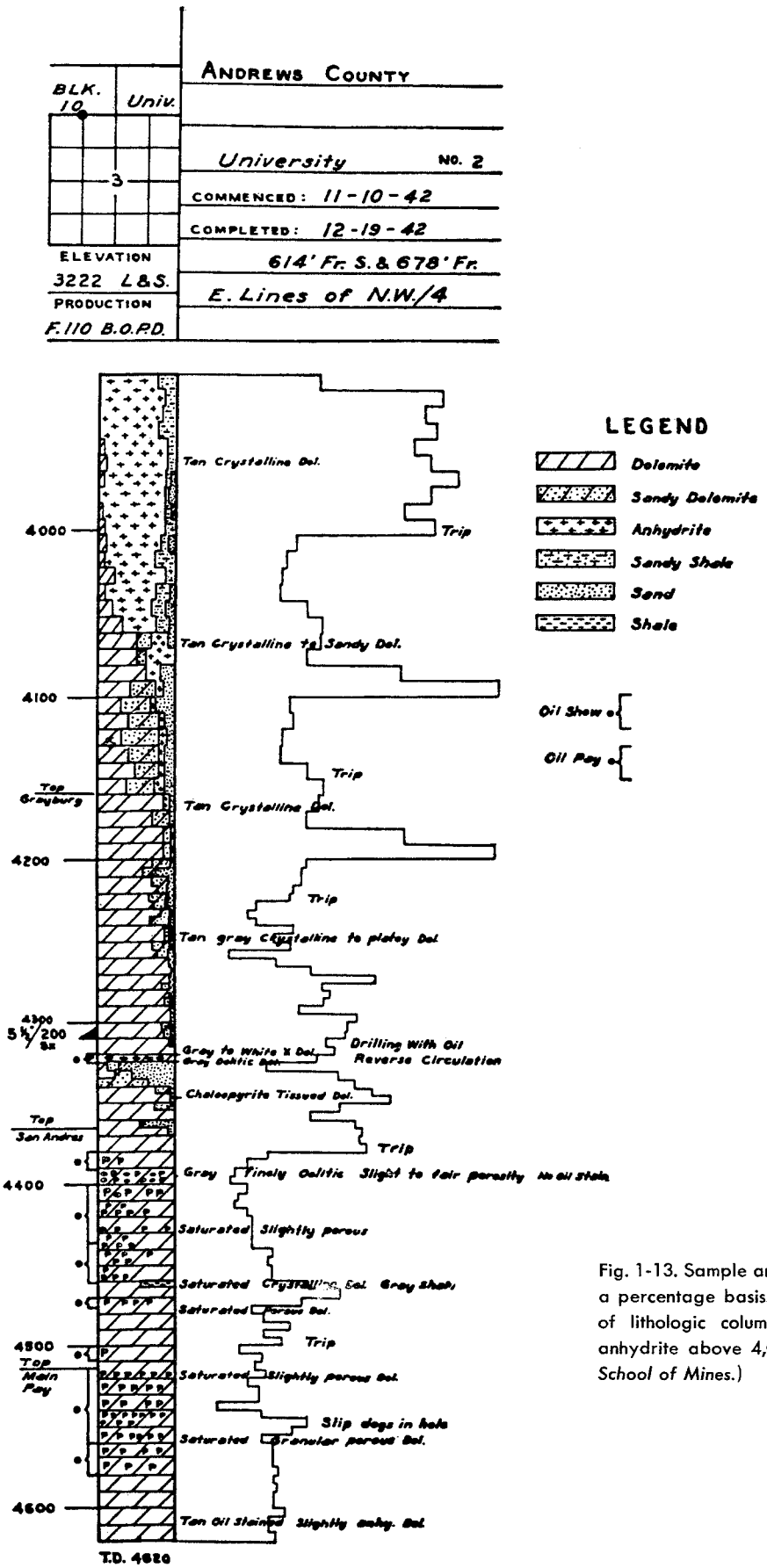

Fig. 1-13. Sample and drilling-time log. Lithology is plotted on a percentage basis. Drilling-time data are recorded to right of lithologic column. Note slow penetration rate through anhydrite above 4,000 ft. (LeRoy, 1-44. *Courtesy Colorado School of Mines.*)

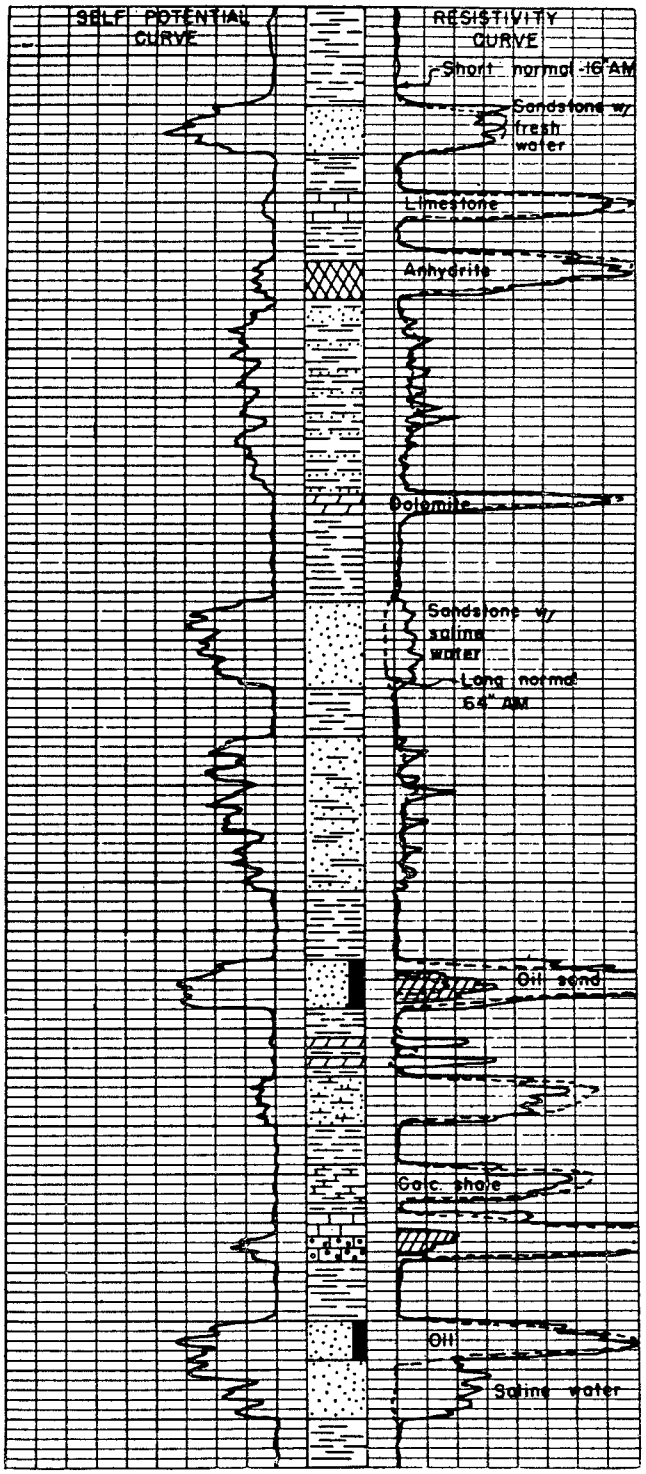

Fig. 1-14. Schematic electrical log showing relationship between electrical characteristics and various lithologic types. (*LeRoy*, 1-44. *Courtesy Colorado School of Mines.*)

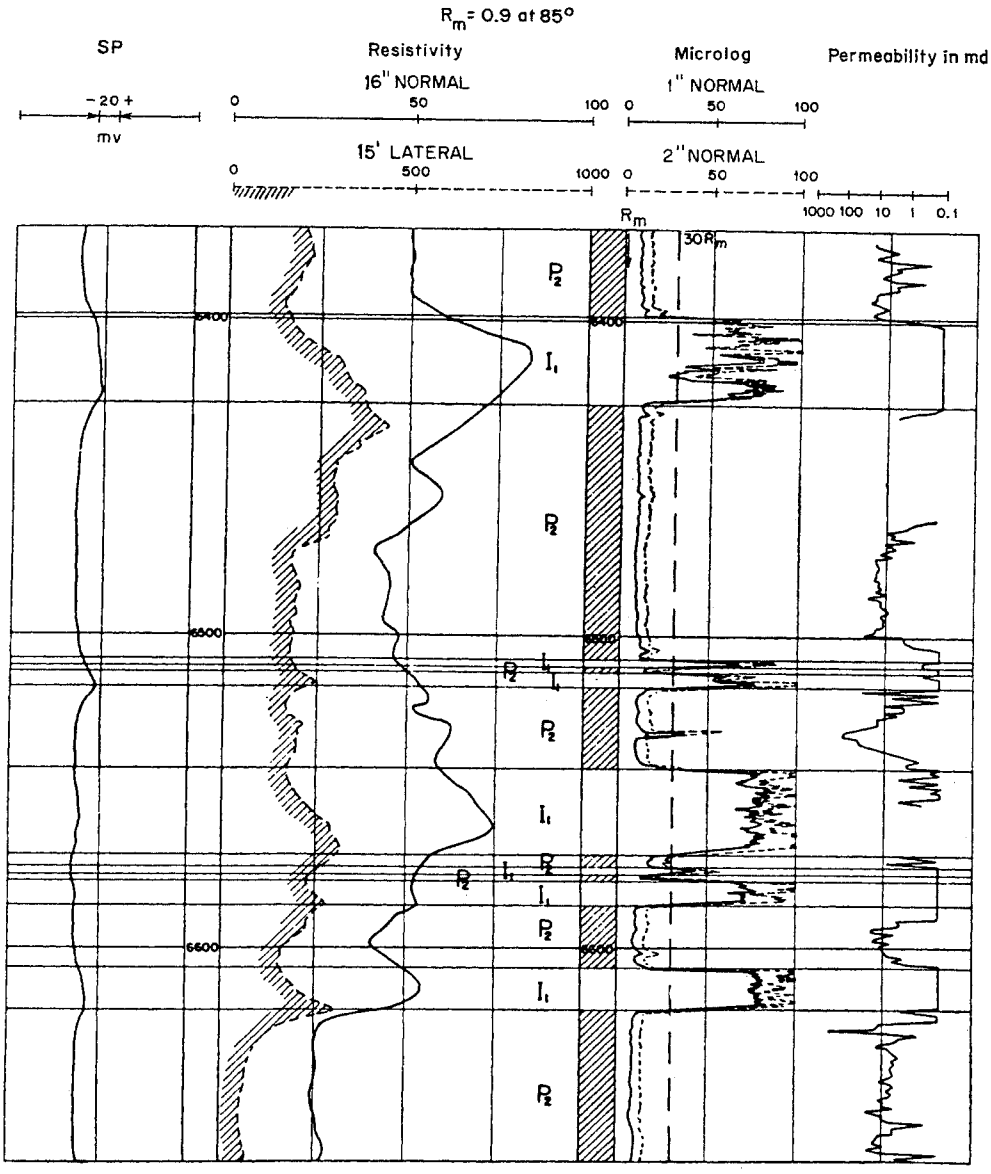

Fig. 1-15. Example of microlog. (*LeRoy, 1-44. Courtesy Colorado School of Mines.*)

ability in the west portion of the field. The reservoir was originally at a pressure of 520 pounds per square inch gauge (psig) wellhead and at 63°F. Figure 1-17 gives the composition of the gas, considered as dry gas. The field produced 6.4 billion cubic feet (MMMcf) of natural gas by primary production and reached a pressure of 284 psig wellhead when it was converted to a gas-storage field.

The Hugoton and Panhandle Gas Fields extend from the Texas Panhandle, through the Oklahoma Panhandle, and some 85 miles into Kansas. They are in the Anadarko basin of Fig. 1-21. Figure 1-23 shows the geographical area covered by these extensive gas fields. Gas is produced from a dolomite of Permian age. Figure 1-24 shows a well log for a Hugoton well made in connection with a study of the porosity of the dolomite (1-36). The gas composition is given in Table 1-5 for the area indicated on Fig. 1-23. The nitrogen content increases in the north end of the field.

The Leduc Field in the province of Alberta is a reef structure of Devonian age. The producing zones D-2 and D-3 both contain crude oil with dissolved gas, as shown in Fig. 1-19, and the D-3 zone has a gas cap as well. Figures 1-25 to 1-28 from Waring and Layer (1-60) give pertinent data on the field. Figure 1-27 shows the wells that penetrated the D-3 zone in the Leduc-Woodbend field. The proved area is somewhat more than 22,000 acres. Closure from the oil-water line (3,020 ft subsea), indicated by the hachured line,

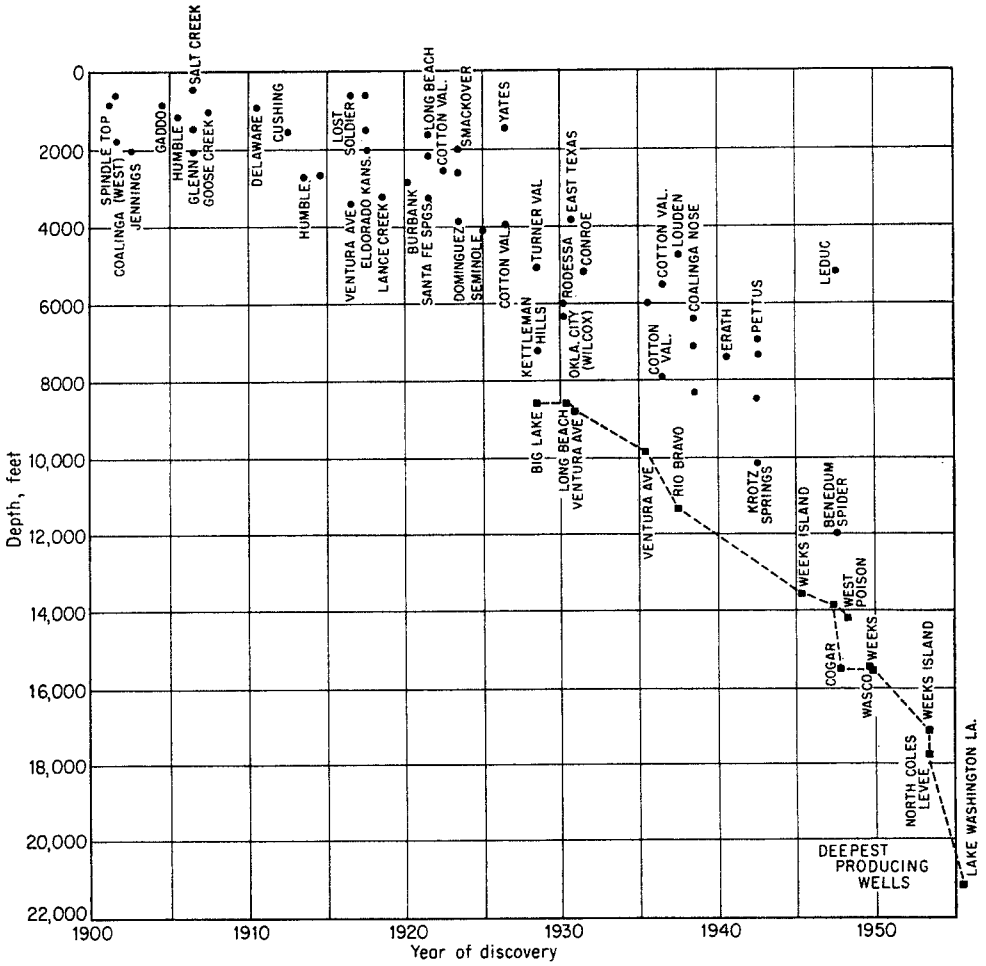

Fig. 1-16. Increase in depth of discovery with time. (*After Katz and Williams*, 1-38.)

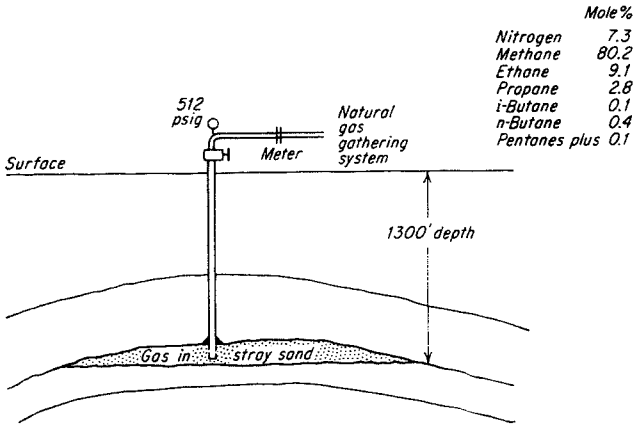

Fig. 1-17. Shallow natural gas field, Austin.

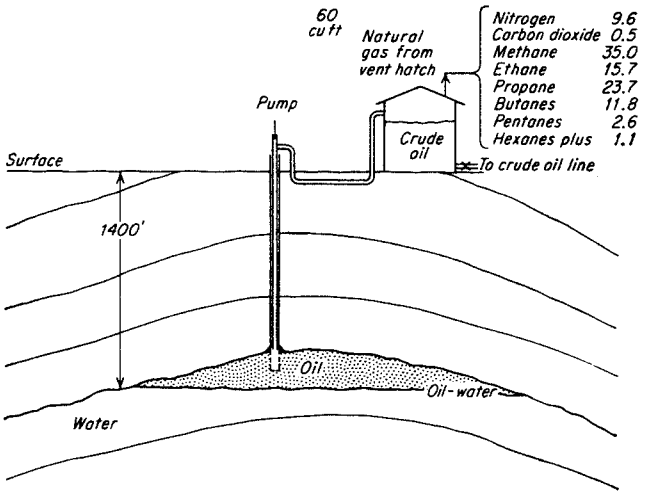

Fig. 1-18. Shallow crude oil production.

Composition of streams - molecular percentages

Component	Well effluent	Separator gas	Vented gas	Stock tank oil
Methane	30.3	75.69	15.31	0.05
Ethane	13.1	17.76	35.54	1.35
Propane	9.4	5.19	30.67	5.03
Iso-butane	1.8	0.27	4.15	2.15
Normal butane	4.9	0.82	8.75	6.72
Pentanes	4.5	0.27	3.81	8.07
Hexanes plus	36.0	0.00	1.77	76.63
Totals	100.0	100.0	100.0	100.0

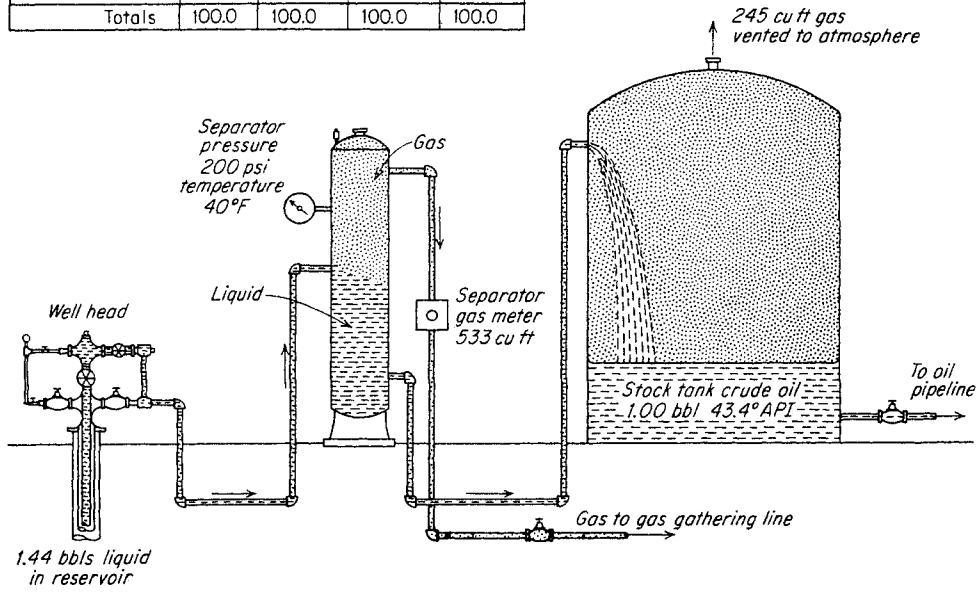

Fig. 1-19. Operation of separator on well producing crude oil with dissolved natural gas. (*Katz and Williams*, 1-38. Courtesy AAPG.)

Molecular percentages

Constituent	Well stream	Separator gas	Separator liquid	Vent gas
Methane	74.4	84.8	18.9	33.4
Ethane	8.3	7.9	11.0	18.2
Propane	4.7	4.2	8.0	22.4
Iso-butane	0.9	0.5	3.0	5.6
Normal butane	1.9	1.1	6.9	10.5
Pentanes	1.4	0.3	7.3	5.7
Hexanes and heavier	7.7	0.3	44.9	3.0
Carbon dioxide	0.7	0.8	—	1.2
Totals	100.0	100.0	100.0	100.0

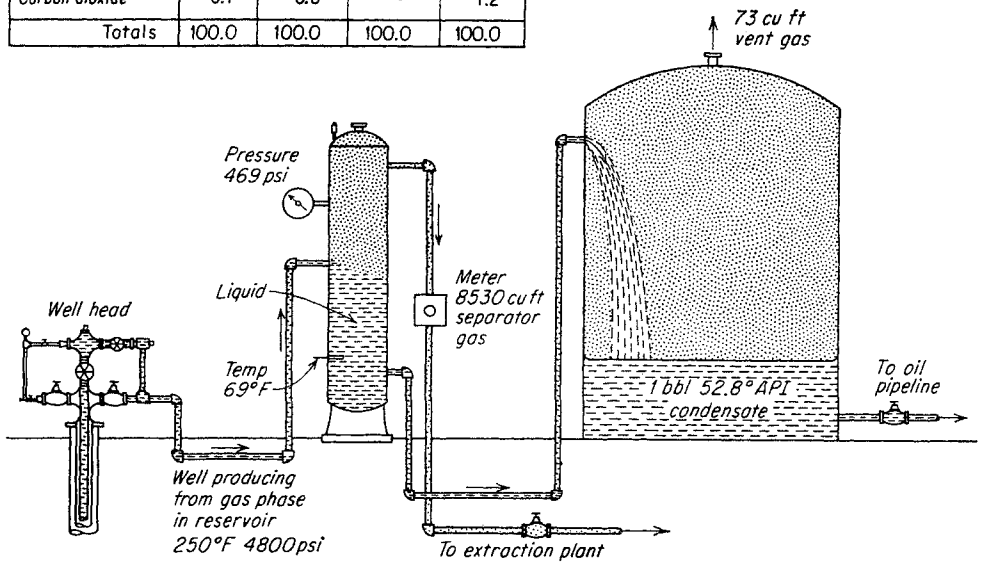

Fig. 1-20. Separation for a condensate well. (*Katz and Williams*, 1-38. Courtesy AAPG.)

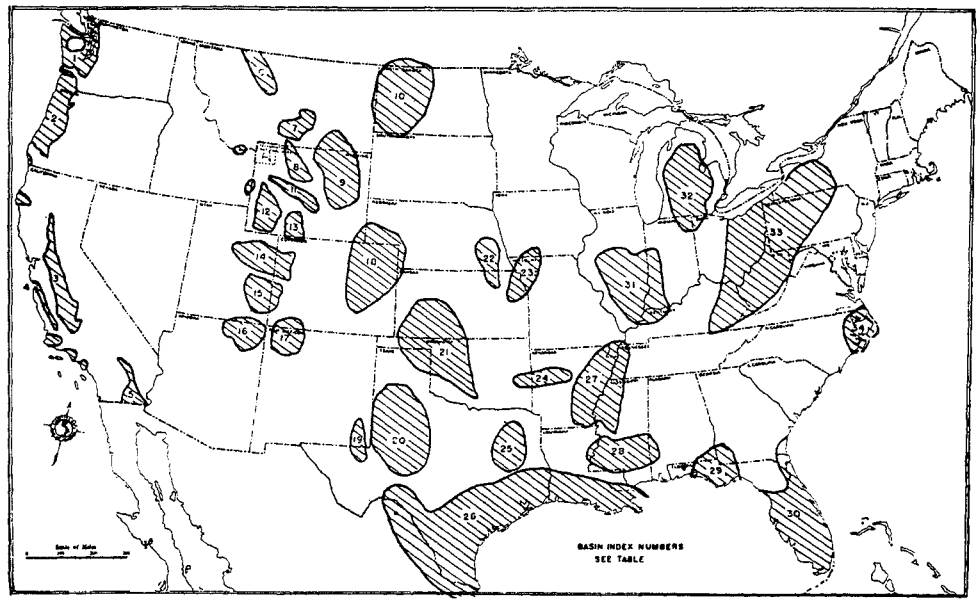

Fig. 1-21. Index map of important sedimentary basins. (*Moulton*, 1-49. *Courtesy AAPG.*)

Table 1-3. Data on Oil and Gas Discovery Prospects of Sedimentary Basins in United States

No. on Fig. 1-21	Basin name	Area, sq miles	Total sediments, cu miles	Prospect classification
1	Puget Sound	21,000	35,000	C-2
2	West Oregon	22,000	35,000	C-3
3	Sacramento	22,000	50,000	A-3
4	Salinas	3,000	4,000	C-3
5	Imperial Valley	5,000	6,000	C-3
6	North Montana–Mountain Front	1,900	3,800	C-2
7	South Central Montana	2,000	4,000	C-2
8	Big Horn	3,000	9,600	A-2
9	Powder River	32,000	96,000	B-2
10	Williston	34,000	42,000	C-3
11	Wind River	2,500	6,000	B-1
12	Bridger	10,000	20,000	B-1
13	Washakie	7,000	14,000	B-1
14	Uinta	13,000	18,000	B-1
15	Colorado River	19,000	25,000	C-1
16	Black Mesa	12,000	18,000	C-1
17	San Juan	12,000	16,000	B-1
18	Denver	36,000	70,000	C-2
19	Delaware	8,000	15,000	C-2
20	Midland	43,000	75,000	A-1
21	Anadarko	45,000	90,000	A-1
22 23	Salina Forest City	60,000	36,000	C-3
24	McAlester	12,000	18,000	B-2
25	East Texas	14,000	21,000	B-1
26	Gulf Embayment	135,000	400,000	A-1
27	Mississippi Valley	33,000	30,000	C-3
28	Mississippi Salt Dome	21,000	42,000	B-1
29	Southwest Georgia	12,000	18,000	C-2
30	Florida	38,000	75,000	C-2
31	Illinois	37,000	25,000	B-3
32	Michigan	28,000	25,000	B-3
33	Appalachian	94,000	210,000	B-2
34	Hatteras	9,000	18,000	C-2

SOURCE: Moulton (1-49).

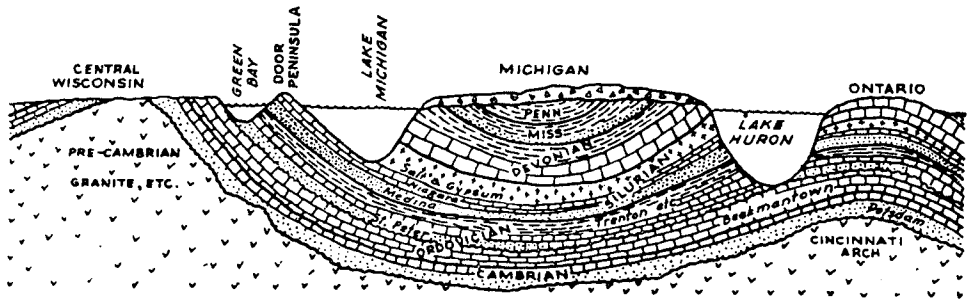

Fig. 1-22. Cross section of the lower peninsula of Michigan. (*Ver Wiebe, 1-59.*)

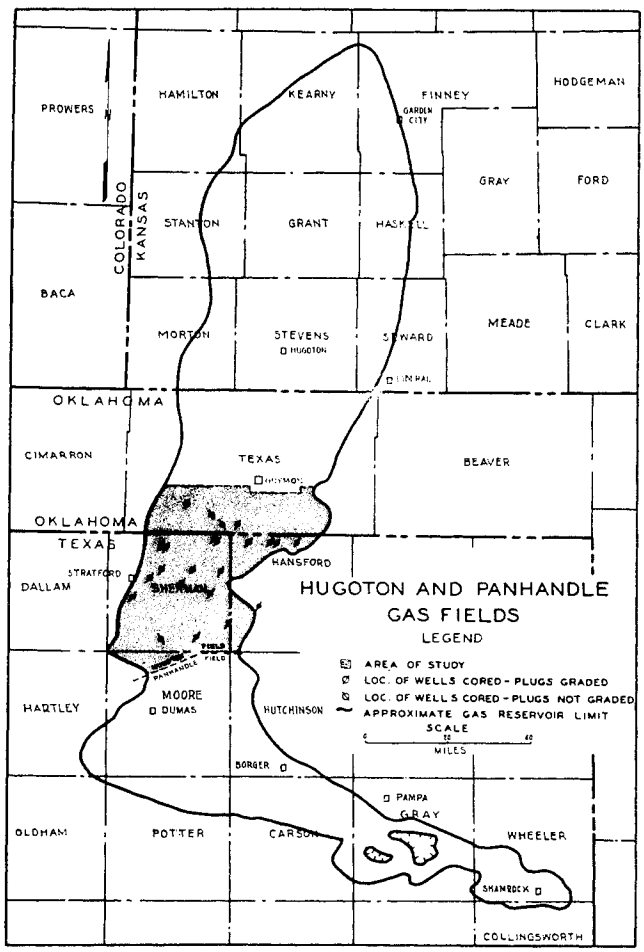

Fig. 1-23. Surface area of Hugoton and Panhandle gas fields. (*Katz et al., 1-36.*)

to the highest point of the gas cap is 233 ft. The thickness of the oil zone is 38 ft. The main porosity is in vugs interconnected by cracks or crevices in the dolomitized reef material. The reservoir pressure in the D-3 zone at 5,300 ft was 1,894 psig at discovery, temperature 153°F. The pressure in the D-2 zone was 1,760 psig at 5,000 ft, temperature 149°F. The separated crude oil has a gravity of 38°API. The composition of gas-cap gas from the D-3 zone is given in Table 1-5, and the composition of the reservoir crude oils in Table 1-8.

The Deep Lake Field on the Gulf Coast of Louisiana has 13 or more sands productive of natural gas. A deep-seated salt dome is believed responsible for the structure. The field has one sand at 6,950 ft that produces by gas expansion; the other sands, all below 9,000 ft, are under water drive. The pressures range from 3,180 to 5,542 psia, and the temperatures range from 130 to 213°F. Table 1-9 gives pertinent data on sand No. 44, and Figs. 1-29 and 1-30 present structural and isopachous maps for the No. 44 sand (1-56).

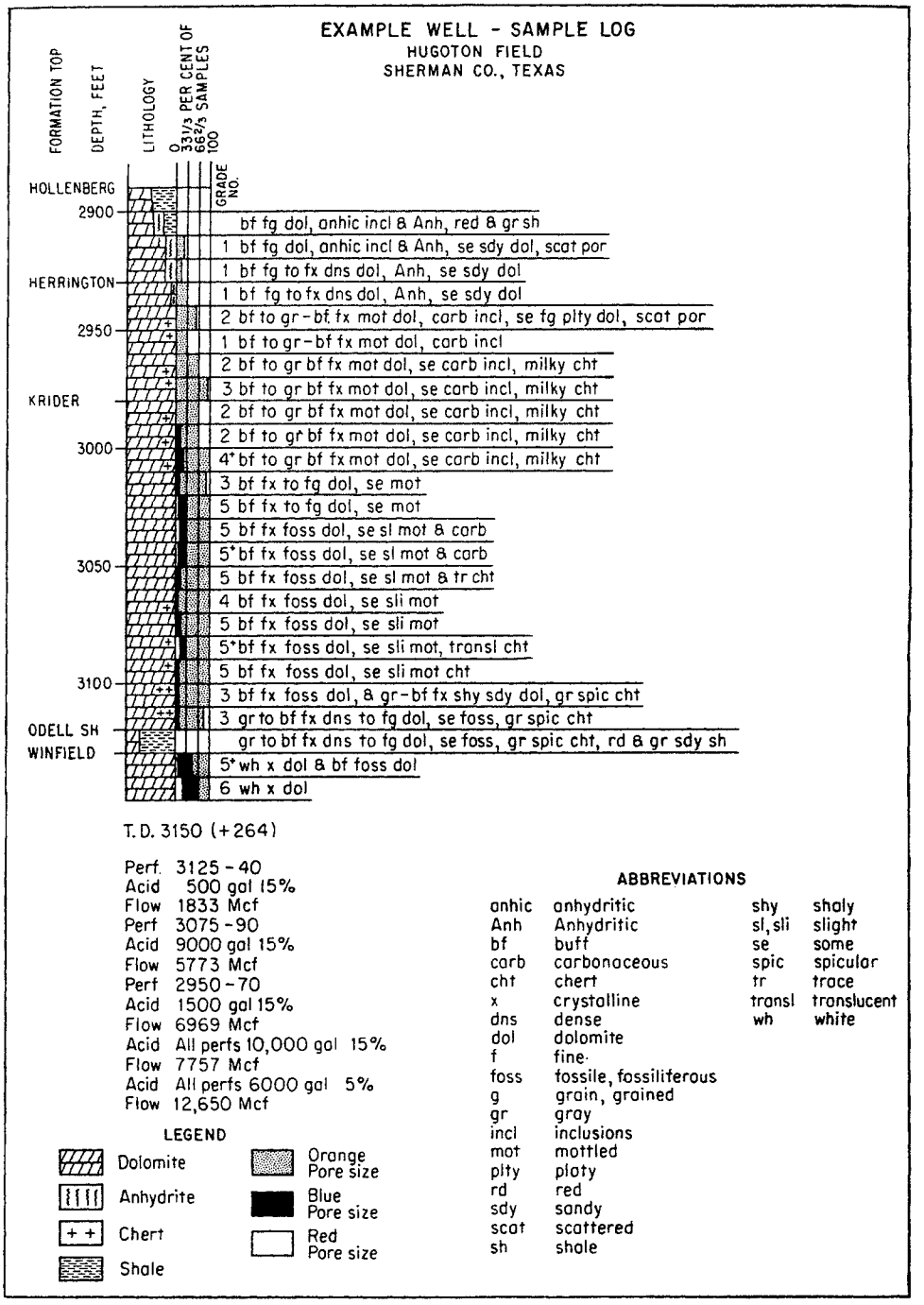

Fig. 1-24. Well log of Hugoton gas well. (Katz et al., 1-36. Courtesy AIME.)

The Miocene sands are of a relatively recent geologic age. They are soft and of high porosity and permeability. The geological work is based mostly on electrical logs of newly drilled wells. Gas compositions are given in Table 1-5. The field recently started production to serve the American Louisiana pipeline.

Compositions of Natural Gases which contain condensate are given in Table 1-6 and compositions of gases separated from crude oil or condensate in Table 1-7. Table 1-8 gives the compositions of crude oils with dissolved-gas contents.

EARTH TEMPERATURES

The temperature of the earth increases with depth at the rate of from 6 to some 30°F per 1,000 ft of depth. The temperature near the surface, usually

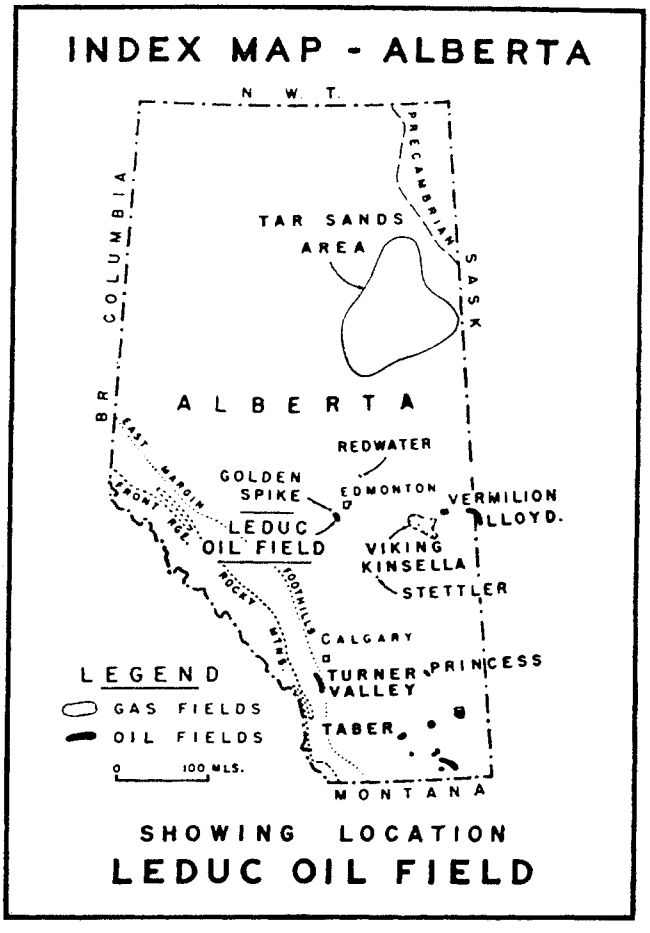

Fig. 1-25. Index map, Alberta. (*Waring and Layer*, 1-60. *Courtesy AAPG.*)

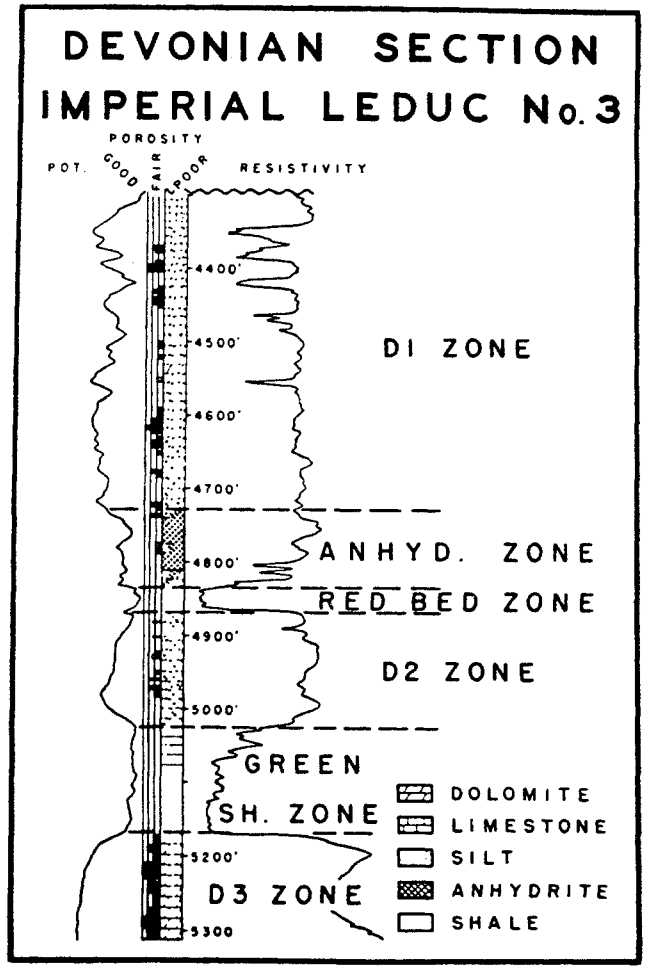

Fig. 1-26. Devonian section, Leduc. (*Waring and Layer*, 1-60. *Courtesy AAPG.*)

taken at 100 ft, approximates the mean annual atmospheric temperature. Since the earth is cooling, the temperature at 100 ft should exceed the mean average atmospheric temperature, and is observed to so exceed it by from 2 to 10°F. At Norman Wells in the Northwest Territory, where permafrost occurs, the ground temperature is 32°F or below; in the Gulf Coast area of Texas the ground temperature reaches 73°F. Table 1-10 gives some ground temperatures in values at 100 ft.

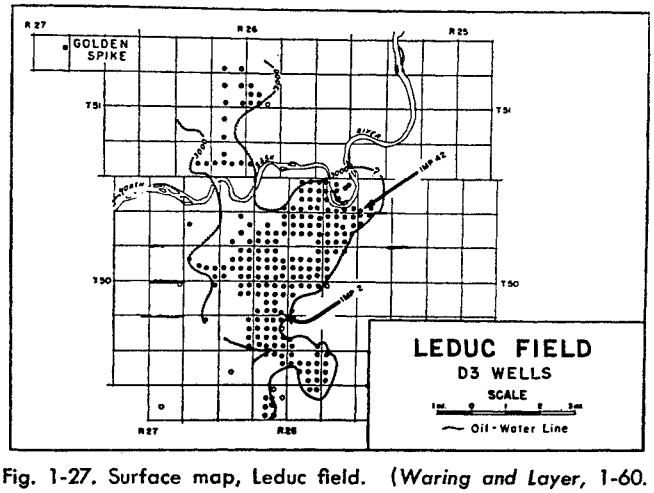

Fig. 1-27. Surface map, Leduc field. (*Waring and Layer*, 1-60. *Courtesy AAPG.*)

Temperature measurements can be made by maximum-indicating mercury-in-glass thermometers enclosed in pressureproof containers, such as bottom-hole pressure gauges. Recording temperature gauges are available for running on a wire line. Van Orstrand (1-61, 1-33) used a resistance thermometer on a cable. Today, thermistors are used on cables of the type used for electrical logging of wells.

The equilibrium earth temperature is of interest since it is representative of reservoir temperatures. By injecting gas or water into a reservoir at a temperature below the reservoir temperature, it is possible to change the formation temperature from the equilibrium earth gradient. For primary production of oil and gas, the reservoir temperature is not likely to change by more than 2 or 3°F at most. In cycling

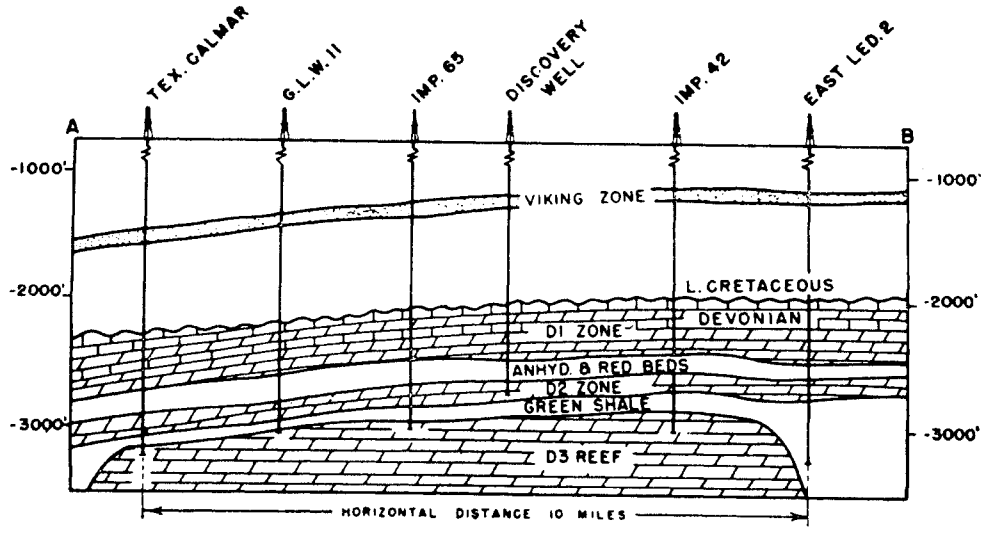

Fig. 1-28. Section across the Leduc field. (*Waring and Layer*, 1-60. *Courtesy AAPG.*)

Table 1-4. Constituents of Petroleum

Name	Formula	Normal boiling point, °F	Product of commerce containing constituent	General range of constituents in field stream
Methane	CH_4	−259	Natural gas	
Ethane	C_2H_6	−128	Natural gas	
Propane	C_3H_8	−44	Natural gas, propane	
Isobutane	i-C_4H_{10}	+11	Natural gasoline, butane	
n-Butane	n-C_4H_{10}	31	Natural gasoline, motor fuel, butane	
Pentanes	C_5H_{12}	90	Natural gasoline, motor fuel	
Hexanes	C_6H_{14}	145	Natural gasoline, motor fuel	
Heptanes	C_7H_{16}	195	Natural gasoline, motor fuel	
Octanes	C_8H_{18}	245	Natural gasoline, motor fuel	
Decanes	$C_{10}H_{22}$	345	Motor fuel	
Tetradecane	$C_{14}H_{30}$	490	Kerosene, light furnace oil	
Hexadecane	$C_{16}H_{34}$	549	Mineral seal oil, furnace oil	
Triacontane	$C_{30}H_{62}$	855	Light lubricating oil, heavy fuel oil	
Tetracontane	$C_{40}H_{82}$	1,012	Lubricating oil, heavy fuel oil	
Asphaltene	$C_{80}H_{162}+$	1,200+	Asphalt, road oil, bunker fuel oil	

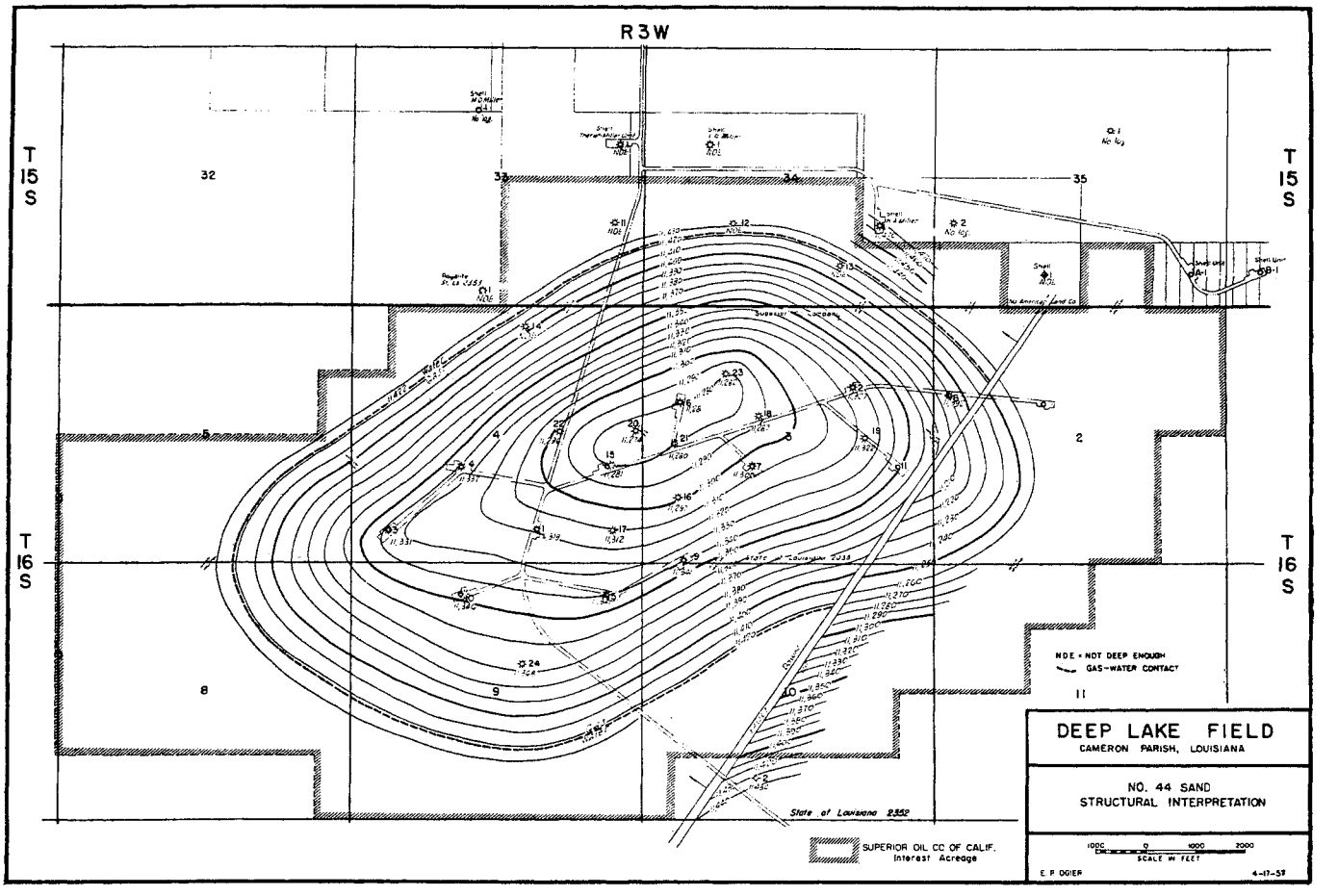

Fig. 1-29. Structural map, No. 44 sand, Deep Lake field. (*Spooner and Ogier*, 1-56.)

operations at Katy, Tex., a reservoir was cooled some 30°F by the injected gas.

The circulation of drilling mud during drilling or the producing of oil and gas up the well bore will upset the equilibrium earth gradient. Figure 1-31 shows the relative position of temperature gradients between the static or equilibrium curve, the temperature in the well bore during drilling, and the temperature while flowing. Eilerts and Schellhardt (1-29) reported data on a gas well in northeast Texas producing from the Trinity formation. The well apparently had been flowing prior to the test period, and was closed in 26 hr, before the first static gradient was measured. Figure 1-32 shows the measured temperatures along with an estimated equilibrium earth temperature for the region. The well-bore temperatures near the surface, and hence the well effluent temperatures, rise with increasing flow rates and with time at a given flow rate. At the highest flow rate, the temperature at the bottom of the well dropped, apparently because of the high pressure drop at the well face.

Typical earth-temperature curves for California fields from French (1-31) are given in Figs. 1-33 and 1-34. Miscellaneous curves are given in Fig. 1-35. Nichols (1-53) reported temperature gradients for areas in Texas, Louisiana, and Oklahoma. He stated that the Gulf Coast has a temperature curve starting from 74°F at the surface, a few degrees above the mean atmospheric temperature, and rising at rates of from 12 to 22° per 1,000 ft of depth. Figure 1-36 is a plot of these gradients. In the Permian basin of West Texas and southeastern New Mexico, the gradients were contoured at 4 to 8°F per 1,000 ft. Table 1-11 lists reservoir temperatures and gradients for several oil and gas fields.

EARTH-PRESSURE GRADIENTS

A great many oil and gas reservoirs are in contact with blanket-water sands which eventually outcrop to the surface of the earth. Such reservoirs have an initial pressure equal to the hydraulic gradient from the outcrop elevation to the reservoir, minus the flowing pressure drop (Fig. 1-7). Even many reservoirs that do not have known direct communication with the surface have pressures that conform to this

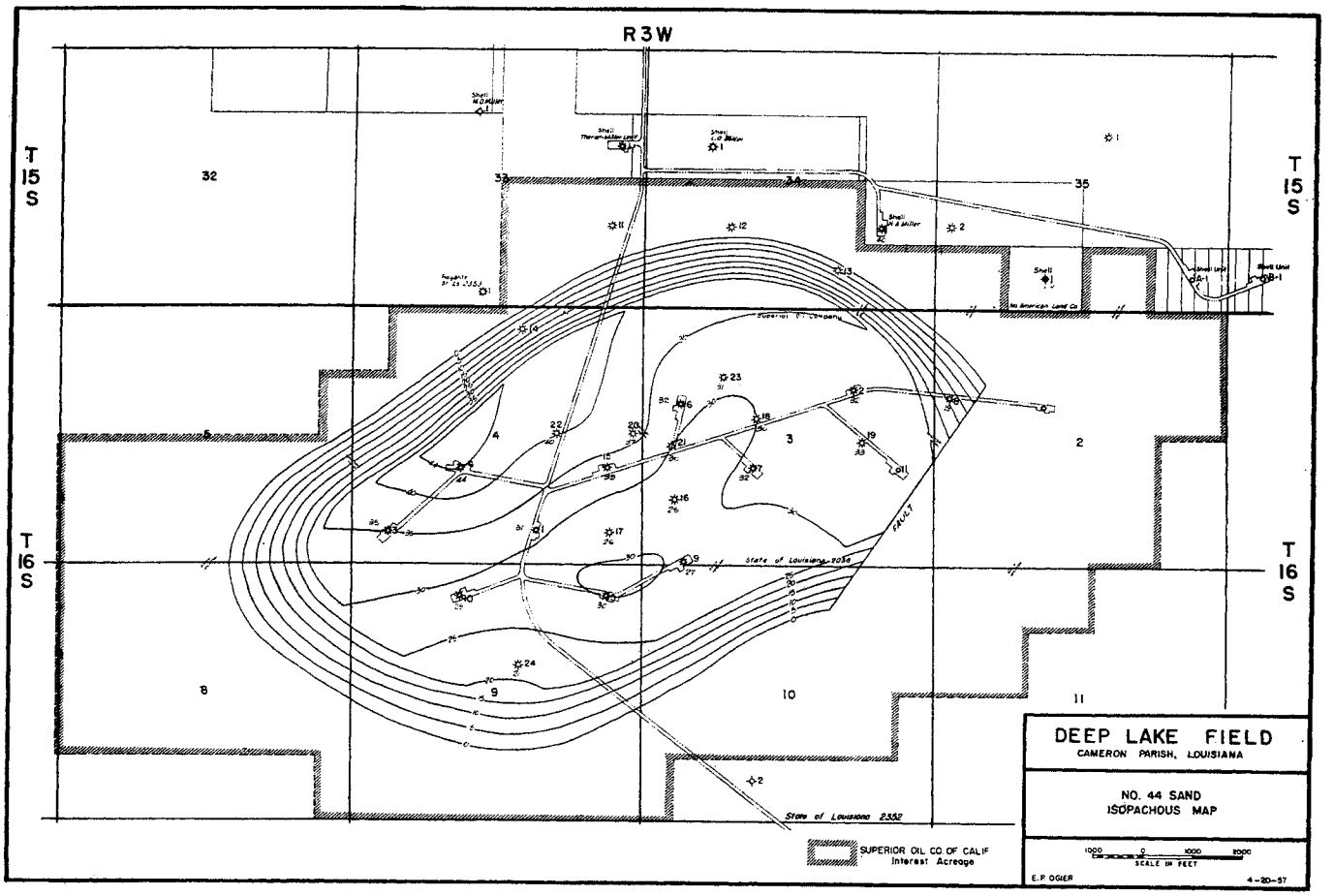

Fig. 1-30. Isopachous map, No. 44 sand, Deep Lake field. (*Spooner and Ogier, 1-56.*)

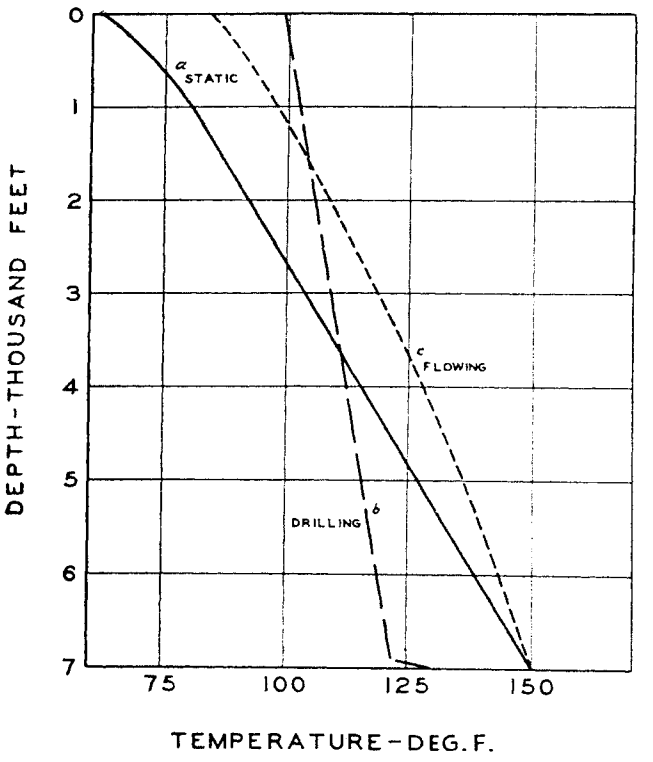

Fig. 1-31. Temperature-gradient distortion by drilling or flowing well. (*French, 1-31. Courtesy API Drill. Prod. Practice.*)

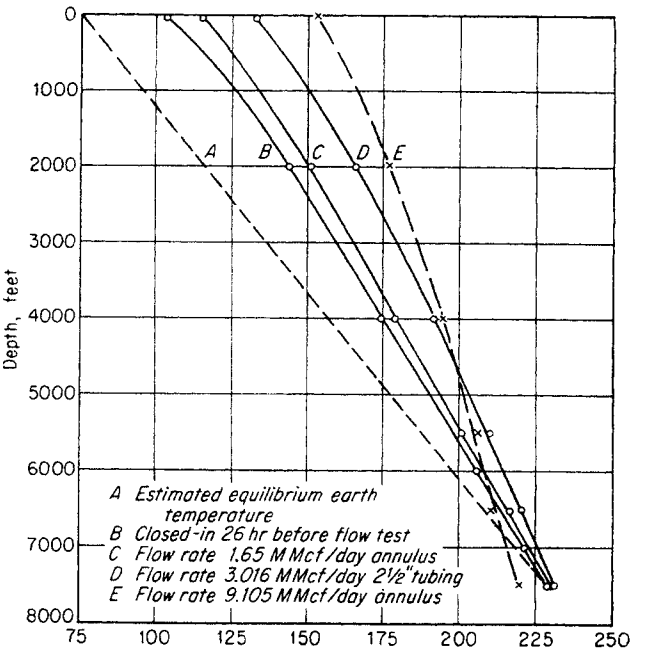

Fig. 1-32. Temperature gradients in gas well. (*After Eilerts and Schellhardt, 1-29.*)

Table 1-5. Composition of Natural Gases

Field	Hugoton	Austin	Leduc Gas Cap D-3	Viking, Kinsella	West Cameron, Blk 149	Deep Lake
State	Oklahoma, Texas*	Michigan	Alberta	Alberta	Louisiana (Gulf)	Louisiana
Formation	Permian dolomite	Stray sand	Devonian	Cretaceous sand	Miocene sand	Miocene sand
Depth, ft	3,000	1,200	5,000	.....	7,150	6,950
Mole percentage:						
Nitrogen	15.5	7.3	7.41	0.24		
Carbon dioxide	.....	.....	0.72	2.26	0.30	0.30
Hydrogen sulfide						
Helium	0.58	0.4				
Methane	71.51	79.74	72.88	88.76	96.65	98.50
Ethane	7.0	9.1	9.97	4.76	2.05	0.87
Propane	4.4	2.8	5.09	2.67	0.47	0.17
Isobutane	0.29	0.1	0.72	0.42	0.08	0.04
n-Butane	0.70	0.4	1.76	0.21	0.09	0.02
Isopentane	0.02	0.1	0.99	0.38	0.03	0.01
n-Pentane	.....				0.02	0.01
Hexanes	.....	0.05	0.46	0.30	0.31	0.08
Heptane+	.....	0.01				
	100.00	100.00	100.00	100.00	100.00	100.00

* Pipeline.

gradient. Variations in the depth-pressure gradient are caused by salinity of the water and temperature. Figure 1-37 gives pressure gradients corresponding to the density for pure water at 63°F (43.3 lb per 100 ft). The curves for 48 and 53 lb per 100 ft are for 1.11 and 1.22 specific gravity brines without any temperature effects. Recognizing that the temperature rises with depth, the 48- and 53-lb gradients correspond to 1.11 to 1.16 and 1.22 to 1.27 specific gravity liquid columns. respectively.

Abnormal pressures are found on both the high and the low sides of these pressure-gradient curves. The Hugoton gas field is an example of an underpressured reservoir (485 psia at 3,325 ft). Numerous Gulf Coast fields, in a belt about 50 miles wide along the coast from the Rio Grande to the Mississippi, have one or more strata with abnormally high pressures (1-27, 1-24). The overburden pressure gradient and the values for several fields are plotted in Fig. 1-37. These abnormal gradients can be due to a tall col-

Table 1-6. Compositions of Condensate Well Fluids

Field	Erath	Erath	Paloma	Chocolate Bayou	Krotz Springs	Deep Lake, No. 51 sand	North Pettus	Frio formation
State	Louisiana	Louisiana	California	Texas	Louisiana	Louisiana	Texas	Texas
Reservoir depth, ft	10,150	11,560	10,600	9,675	8,400	12,060	6,950	6,760
Pressure, psia	4,700	5,431	4,400	4,465	3,893	5,500	3,056	3,836
Temperature, °F	205	212	256	235	188	211	221	201
Mole percentage:								
Nitrogen	.....	.....	.....	.....	.....	.....	0.24	
Carbon dioxide	.....	0.31	0.68	1.76	0.27	1.48	1.97	
Methane	80.95	91.32	74.55	85.11	84.35	91.36	86.27	90.74
Ethane	4.47	3.42	8.28	5.04	5.62	3.50	6.30	4.35
Propane	3.13	1.34	4.74	2.44	3.49	1.31	2.31	1.69
Isobutane	1.55	0.48	0.89	0.67	0.89	0.59	0.32	0.36
n-Butane	1.77	0.41	1.93	0.73	1.19	0.34	0.62	0.54
Isopentane	1.49	0.42	0.75	0.32	0.44	0.23	0.35	0.20
n-Pentane	.....		0.63	0.38	0.54	0.11	0.25	0.21
Hexanes	1.3	0.36	1.25	0.61	0.70	1.08	0.29	0.42
Heptane+	5.62	1.96	6.30	2.94	2.51		1.08	1.49
Specific gravity as liquid, heptanes+	0.7768	0.7967	0.7999	0.7906	.....	0.7695	0.799	0.760
Molecular weight, heptanes+	147	158	132	146	.....	159.0	121	120

Table 1-7. Natural Gases Separated from Crude Oils or Condensates

Field State	Oklahoma City Oklahoma	Osage County Oklahoma	Hobbs New Mexico	Cleveland County Oklahoma	Katy Texas	McKamie Arkansas
Separator:						
Pressure, psia	96	19.0	.....	1,274	764	260
Temperature, °F	67	105	.....	84	63	65
Mole percentage:						
Nitrogen	.....	2.7	2.1	.....	.....	11.11
Carbon dioxide	.....	.....	4.2	.....	0.60	
Hydrogen sulfide	.....	.....	2.4	.....	.....	6.80
Methane	83.9	48.7	55.0	80.36	92.25	68.32
Ethane	9.7	15.6	7.5	11.88	4.14	7.19
Propane	3.9	14.1	14.0	5.19	1.85	3.33
Isobutane	1.7	3.3	2.6	0.34	0.38	0.94
n-Butane		6.5	7.4	1.32	0.41	1.23
Isopentane	0.5	2.1	4.8	0.10	0.16	0.73
n-Pentane		3.0		0.44	0.11	
Hexanes	0.3	2.6	.....	0.37	0.07	0.25
Heptanes+	.....	1.4	.....	.....	0.03	0.10
	100.0	100.0	100.0	100.00	100.00	100.00

Field State	Carthage Texas	Erath Louisiana	Kettleman Hills California	Rodessa Louisiana	Cowden West Texas	Paloma California
Separator:						
Pressure, psia	357	2,200	510	29	27	470
Temperature, °F	76	101	148	93	71	69
Mole percentage:						
Nitrogen	1.83					
Carbon dioxide	0.70	0.41	.....	.....	.....	0.80
Hydrogen sulfide						
Methane	90.06	92.76	83.19	79.4	59.4	84.81
Ethane	4.05	3.03	8.48	8.4	15.7	7.94
Propane	1.51	1.36	4.37	4.6	15.6	4.18
Isobutane	0.40	0.42	0.76	1.9	3.0	0.53
n-Butane	0.71	0.38	1.68	2.0	3.6	1.07
Isopentane	0.18	0.23	0.57	3.7	2.7	0.19
n-Pentane	0.27	0.16	0.32			0.15
Hexanes	0.18	0.26	0.63	.....	.....	0.18
Heptanes+	0.11	0.99	.....	.....	.....	0.15
	100.00	100.00	100.00	100.0	100.0	100.00

umn of natural gas but are believed to be due to the compaction of shales surrounding the strata containing petroleum. Abnormal pressures indicate that the reservoir fluids are not in communication with outcrop formations.

VALUE OF NATURAL GAS AS FUEL

The rapid increase in sales of natural gas (Table 1-1), especially for domestic use, is due both to the convenience of the fuel and to its price. In many areas, natural gas is the cheapest domestic fuel. Since in convenience and cleanliness natural gas surpasses other fuels, conversion to it is rapid.

Comparisons can be made of the relative value of natural gas, fuel oil, and coal on the basis of heating value and unit cost. This has been done for the representative heating values indicated in Fig. 1-38, by the lines labeled "gas efficiency same as oil" or "gas efficiency same as coal." The combustion efficiency in domestic furnaces will be much higher for natural gas than for coal, and may be higher than for oil. Lines are drawn for several comparative combustion efficiencies. Figure 1-38 shows that, when natural gas of 1000 Btu/cu ft heating value costs 80 cents per Mcf (1,000 cu ft), fuel oil at more than 11.2 cents per gallon of 140,000 Btu/gal heating value is more expensive than gas when burned at the

Table 1-8. Analysis of Reservoir Crude Oils Containing Dissolved Gases

Field	Leduc D-2	Leduc D-3	Paloma	Oklahoma City, Wilcox	Rodessa	Keokuk	Schuler (Jones sand)
State or province	Alberta	Alberta	California	Oklahoma	Louisiana	Oklahoma	Arkansas
Reservoir:							
Depth, ft	5,000	5,300	10,600	6,200	5,950	4,026	7,600
Pressure, psia	1,774	1,908	4,663	2,630	2,600	1,455	3,520
Temperature, °F	149	153	255	132	192	130	198
Mole percentage:							
Nitrogen	.....	.....	.....	.....	.....	.....	1.00
Carbon dioxide	.....	.....	.....	.....	.....	.....	0.80
Methane	28.6	30.3	55.8	37.7	40.88	25.60	42.85
Ethane	10.9	13.1	5.81	8.7	4.53	8.88	6.60
Propane	9.4	9.4	6.42	6.3	2.60	12.41	4.10
Isobutane	2.5	1.8	1.31	1.4	1.25	1.93	3.64
n-Butane	4.4	4.9	3.97	3.0	1.82	7.56	
Pentanes	4.8	4.5	3.67	3.3	3.48	5.53	3.10
Hexanes	39.4	36.0	2.61	39.6	4.43	38.09	3.83
Heptanes+	.....	.....	20.41	.....	41.01		34.08
	100.0	100.0	100.00	100.0	100.00	100.00	100.00
Molecular weight, heptanes+	201	193	237	225	220	195	243
Specific gravity as liquid, heptanes+	0.840	0.840	0.891	0.840	0.824	0.839	0.8759

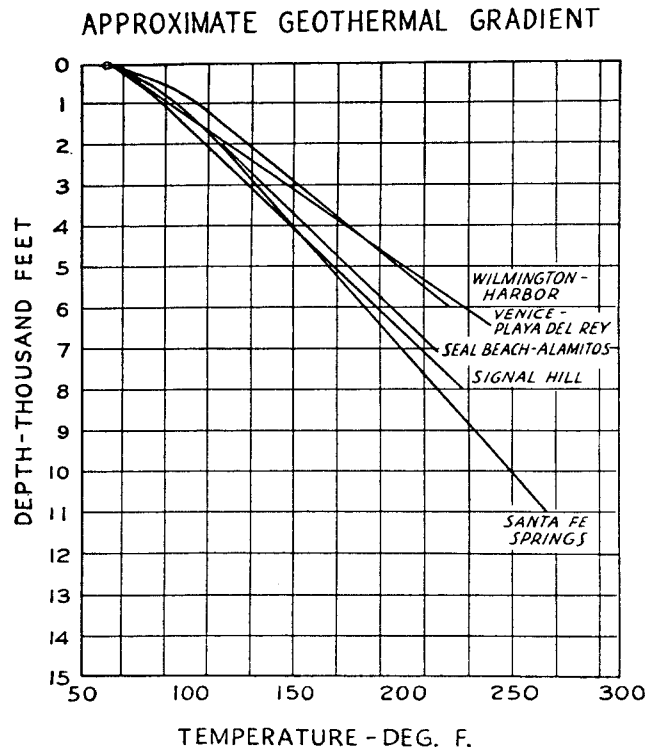

Fig. 1-33. Geothermal gradients for Los Angeles basin fields. (*French*, 1-31. *Courtesy API Drill. Prod. Practice.*)

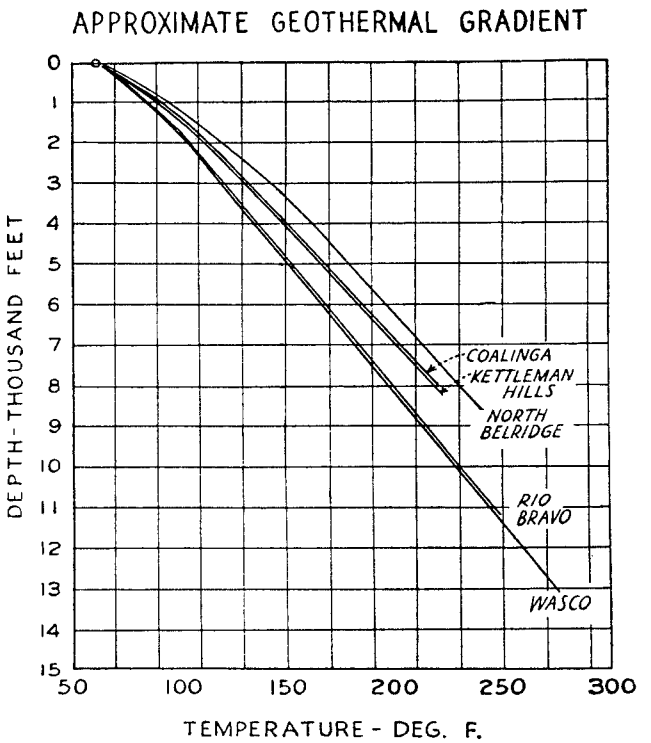

Fig. 1-34. Geothermal gradients for San Joaquin Valley fields. (*French*, 1-31. *Courtesy API Drill. Prod. Practice.*)

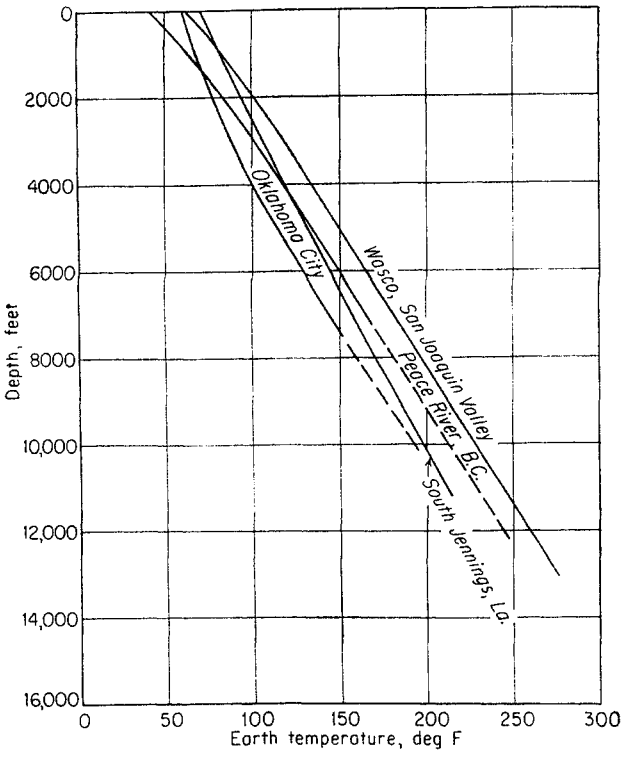

Fig. 1-35. Miscellaneous earth-temperature gradients.

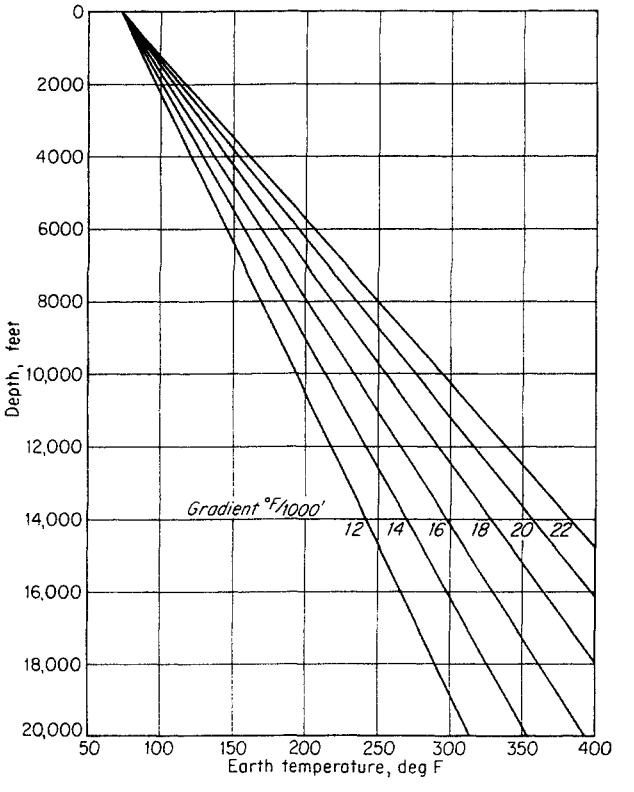

Fig. 1-36. Earth-temperature gradients on the Gulf Coast. (*Nichols*, 1-53.)

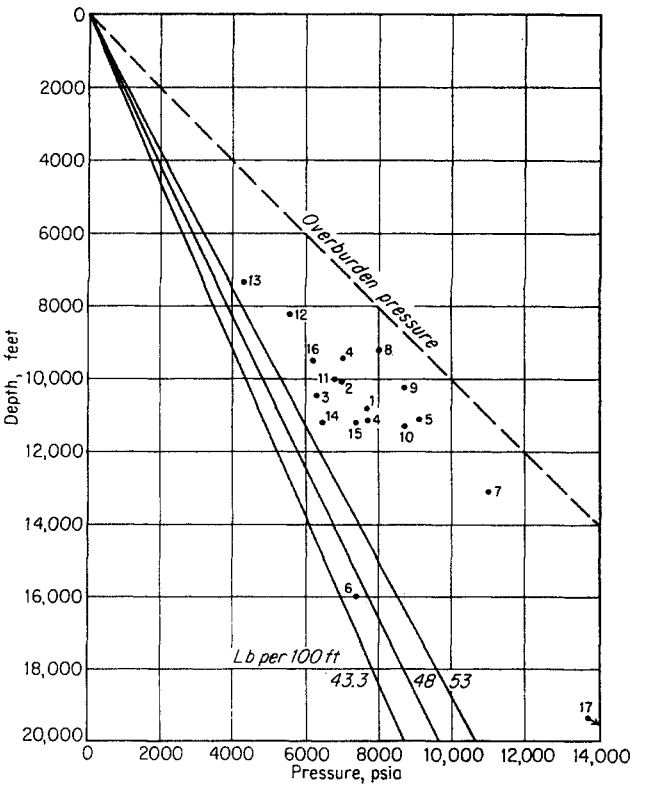

Fig. 1-37. Hydraulic-pressure gradients. 1, Krotz Springs; 2, South Jennings; 3, Savoy Field; 4, Iowa; 5, Cameron; 6, Queen Bess Island (normal); 7, Manila Village; 8, Johnson's Bayou; 9, West Lake Verret; 10, St. Gabriel; 11, Chalkley; 12, East Hackberry; 13, Bel; 14, North Jeanerette; 15, St. Gabriel; 16, South Crowley; 17, Lake Washington, Richardson and Bass deep well, estimated 17,500 psi at 20,741 ft.

same efficiency. On the basis of fuel value alone, coal at $20 per ton is equivalent to 80-cent gas. Should the efficiency of the stoker be 50 per cent when the gas furnace has an efficiency of 85 per cent, 80-cent gas would be equivalent to $11.70 stoker coal.

Table 1-9. Data on Sand No. 44, Deep Lake Field, Cameron Parish, Louisiana

Average depth, ft	11,330
Gas-water contact, ft	11,420
Gas gravity	0.653
Heating value, Btu/cu ft	1,050
Reservoir pressure, psia	5,164
Reservoir temperature, °F	197
Compressibility factor of gas	0.987
Average porosity, per cent	28
Connate water, per cent	25
Gas content, Mcf/(acre)(ft)	2,572
Estimated productive area, acres	2,282
Average sand thickness (Miocene), ft	26.23
Reservoir volume, acre-ft	59,861
Gas content, MMMcf	153.9

SOURCE: (1-56).

Table 1-10. Representative Earth Temperatures at 100 Feet

Field	*°F*
Norman Wells, Northwest Territories	32
Fort St. John, British Columbia	40
Austin Field, central Michigan	47
Kankakee, Illinois	52
Oklahoma City, Oklahoma	60
Lea County, New Mexico	66.7
New Orleans, Louisiana	69.6
Texas:	
Navarro County	67.8
Reagon County	67.2
Van Zandt County	69.2
Brownsville	73.1
Houston	69.2
Los Angeles, California	72.3

Table 1-11. Reservoir Temperatures and Earth Geothermal Gradients

Field	State or province	Depth, ft	Temperature, °F	Gradient, °F/1,000 ft
East Texas Woodbine	Texas	3,600	146	22
Burbank	Oklahoma	2,800	122	22
Panhandle	Texas	3,000	81	7
Monument, Lea County	New Mexico	3,900	90	6
Leduc	Alberta	5,300	153	21
Paloma–San Joaquin	California	10,600	256	17.3
Deep Lake	Louisiana	12,060	211	11.5
Oklahoma City	Oklahoma	6,300	132	11.4
Carthage	Texas-Louisiana	5,920	206	23.6
Hugoton	Oklahoma	3,325	90	8.4
North Pettus, Bee County	Texas	6,950	221	21.7
South Jennings	Louisiana	10,100	211	14
Fort St. John	British Columbia	6,400	156	18.1

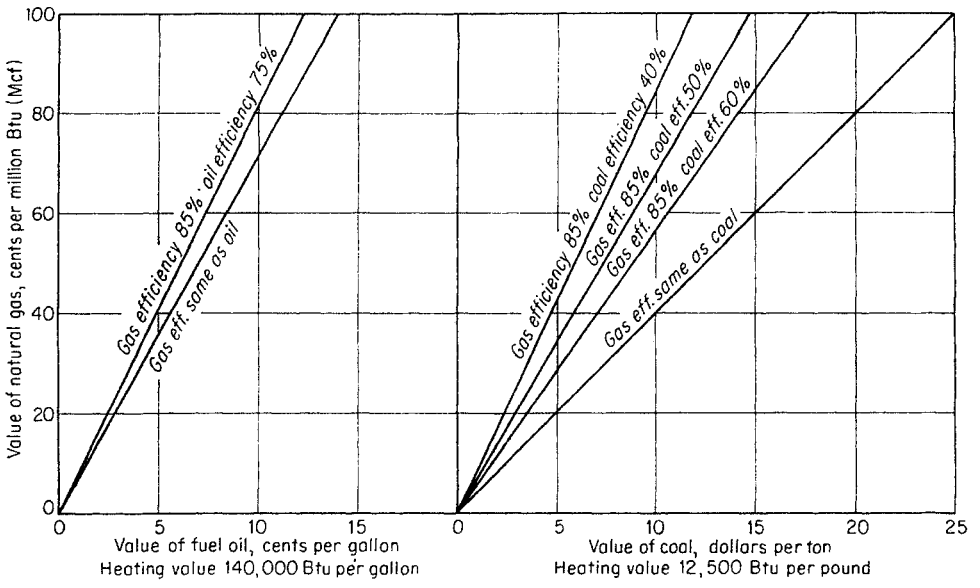

Fig. 1-38. Equivalent values for natural gas, fuel oil, and coal.

CHAPTER 2

Properties of Reservoir Rock

The nature of the reservoir rock bearing petroleum determines the fluid content and the ability of the fluids to move through the rock. Oil and gas are contained in the pores and fractures of sandstones, dolomite, limestones, chert, chalk, and other porous media. The fraction of the total volume of the rock which the interstices occupy is the porosity of the rock. The ability of the rock to serve as a conduit for the flow of fluids is its permeability. Other properties include retaining capacity for water under capillary equilibrium and the tortuous nature of the interstices.

Water is believed to have been present when the petroleum accumulated in most reservoirs. In the accumulation, the oil or gas did not completely replace the water adjacent to the solid surface. This interstitial water found with petroleum in rock is called *connate water*. Knowledge of the fraction of the pore space filled with water, as well as of porosity, is necessary to obtain the reserve of oil or gas per unit volume of rock.

Cores and cuttings taken during the drilling of wells are analyzed in the laboratory to determine porosity and permeability, and sometimes oil content, water content, and other properties. The connate-water content may be estimated by determining the water content as a function of capillary pressure. Electrical logs of wells reveal the properties of the surrounding rock.

Nature of Interstices of Rocks

Many rocks, such as sandstones, are composed of discrete particles held together by compression and cementing material. Most reservoirs composed of granular rocks are of sandstone in which most of the grains range in size from about 0.06 to 2.0 mm. In many reservoirs, either larger or smaller material is mixed with the sandstone of the reservoir rock. The amount of finer material, such as clay, has a marked effect on the porosity and permeability of the reservoir rock. A starting point in understanding the porosity of granular materials, such as sandstones, is consideration of the porosity of rocks composed of spherical particles of similar size and different packing arrangements. Table 2-1 and Fig. 2-1 give seven packing arrangements for uniform spheres with bed porosities varying from 25.95 to 47.6 per cent.

In consolidated porous media, the particles may fit more closely together than indicated in Table 2-1, even without cementing material. Outcrop Wilcox sand (Ordovician) from the Arbuckle Mountains in Oklahoma has a porosity of 15 per cent (permeability 400 to 900 millidarcys). When a piece of this sand is dropped on a hard surface, it disintegrates completely, revealing no evidence of cementing material. Repacking of these sand grains gives a bed with a porosity of 32.5 to 34.0 per cent; this indicates that there is a specific arrangement of the particles in the consolidated sand associated with a porosity of 15 per cent. The sand grains are well rounded and have various shapes including some resembling dumbbells. The nature of the individual particles, sedimentation processes, and earth pressures evidently have brought about this low porosity for a noncemented but consolidated sand. Considerable variation in porosity occurs for media composed of particles having a range of sizes and shapes.

The nature of the interstices of formations producing petroleum is revealed in part by the appearance of the surface of cores cut while drilling wells. Figure 2-2 shows the appearance of cores taken from typical producing formations. The appearance of the surface of Hugoton dolomites of varying porosities is shown in Fig. 2-3 (1-36).

Table 2-1. Porosity of Beds of Stacked Spheres

Stacking arrangement	Fractional porosity	Number of tangent neighbors	Distance between layers
Cubic	0.476	6	D*
Orthorhombic	0.3954	8	$0.866D$
Rhombohedral	0.2595	12	$0.707D$
Orthorhombic	0.3954	8	D
Tetragonal sphenoidal	0.3019	10	$0.866D$
Rhombohedral	0.2595	12	$0.816D$

* D = diameter of spheres.
SOURCE: (2-49).

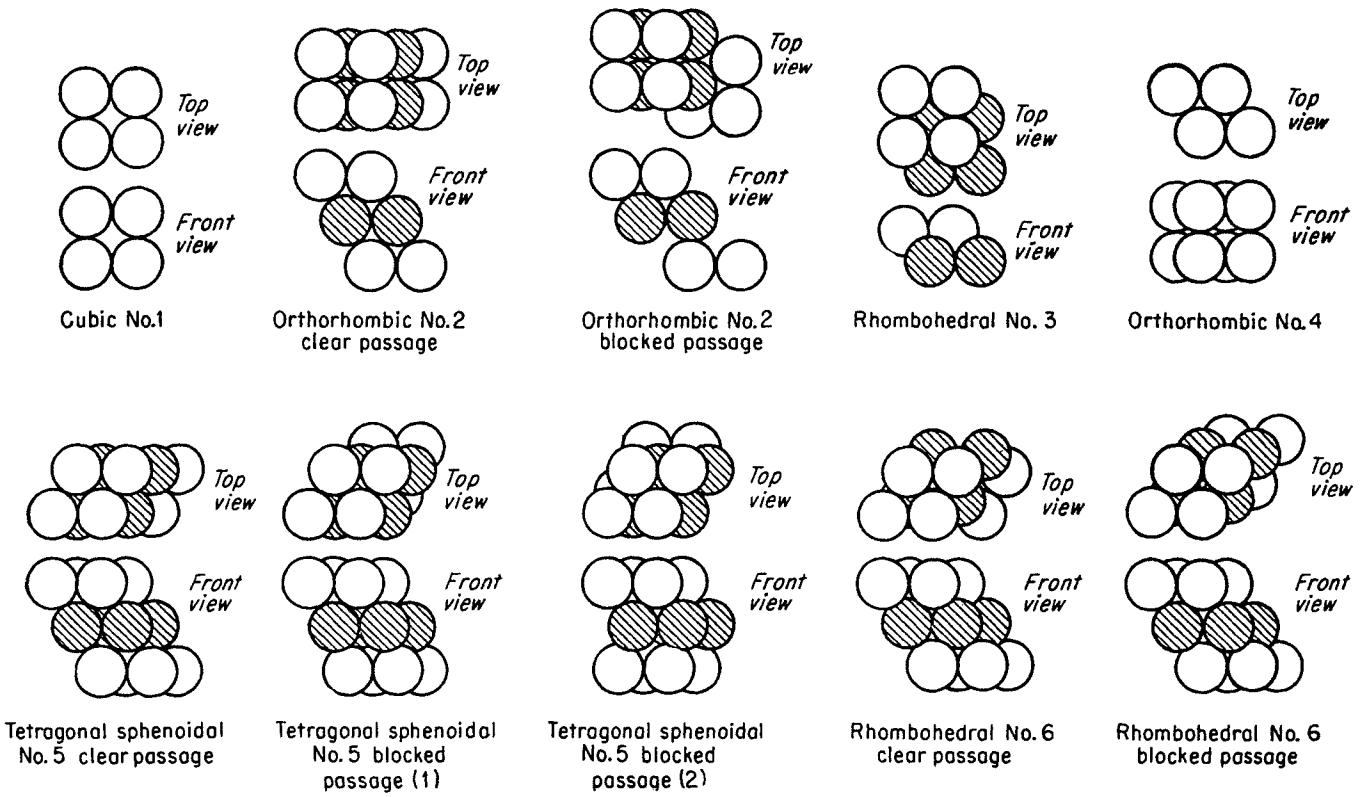

Fig. 2-1. Arrangements in beds of stacked spheres. (*Martin, McCabe, and Monrad, 2-49. Courtesy Chem. Eng. Progr.*)

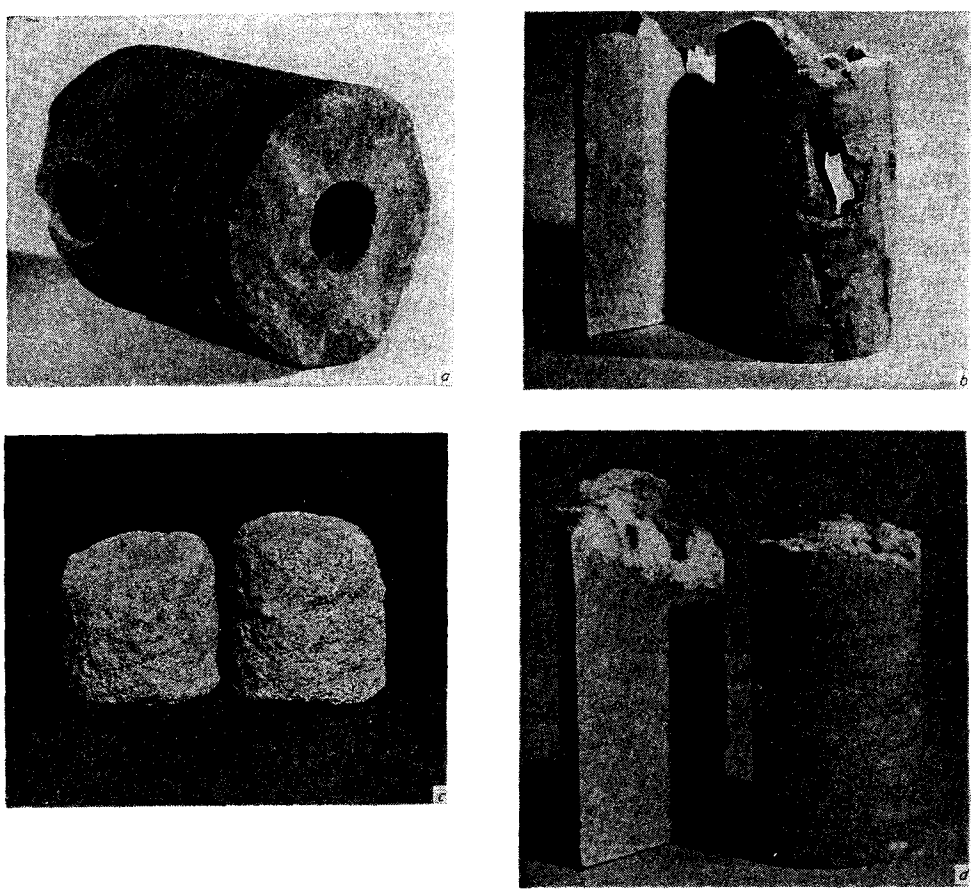

Fig. 2-2a to d. Cores from wells. (a) Bartlesville sand, Cleveland County, Okla., 7,350 ft. (b) Devonian, Lea County, N.Mex., 12,154 ft. (c) Lower Frio, Nueces County, Tex., 7,100 ft. (d) Ellenburger, Upton County, Tex., 13,000 ft. (*Courtesy Core Laboratories, Inc.*)

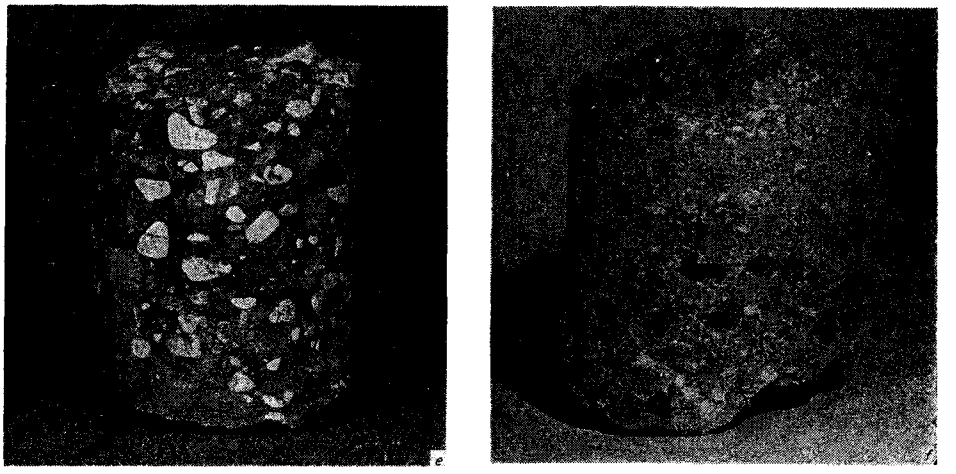

Fig. 2-2e and f. Cores from wells. (e) Wolfcamp conglomerate, Crocket County, Tex., 6,055 ft. (f) Lower Miocene, Kern County, Calif., 16,860 ft. (*Courtesy Core Laboratories, Inc.*)

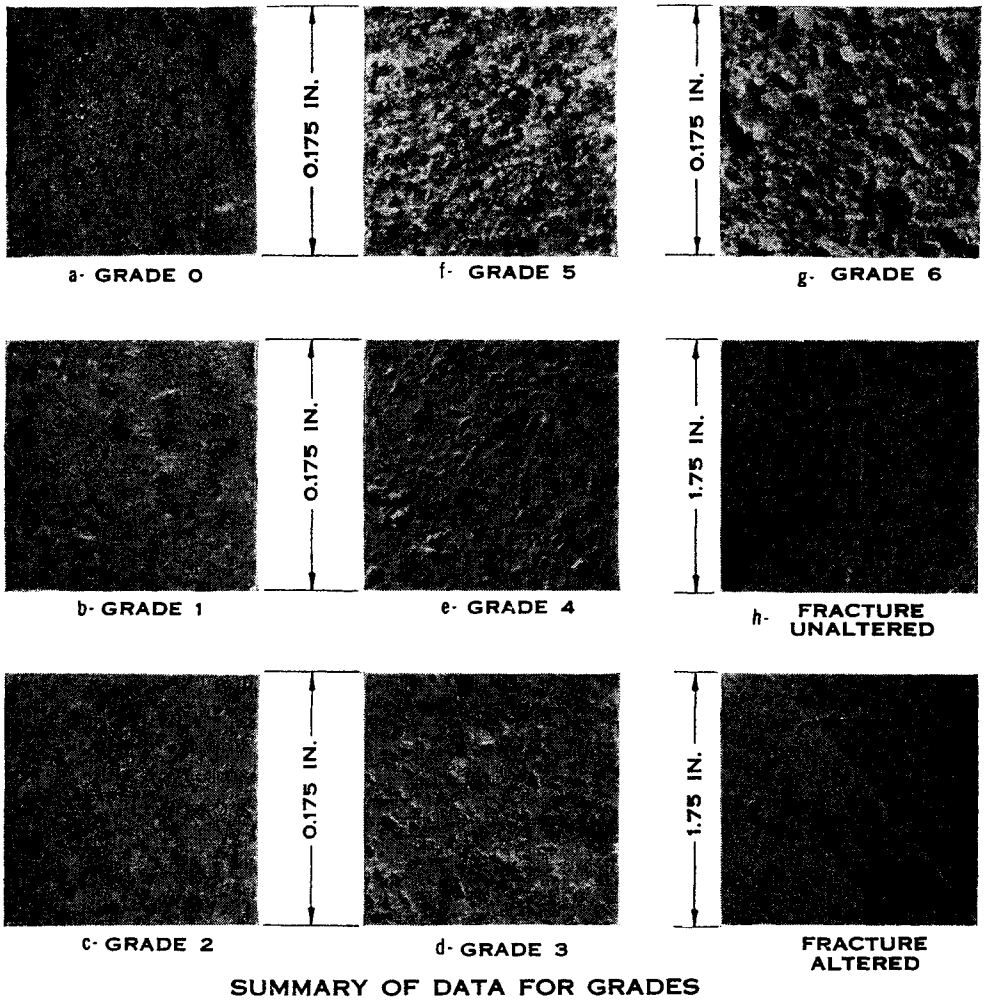

Fig. 2-3. Photographs of Hugoton dolomite. (*Katz, Turner, Grimm, Elenbaas, and Vary,* 1-36. *Courtesy AIME.*)

SUMMARY OF DATA FOR GRADES

EXPOSURE	a	b	c	d	e	f	g
GRADE NO.	0	1	2	3	4	5	6
POROSITY, %	6.49	7.27	9.67	10.35	13.29	16.6	23.6
PERMEABILITY, md	.073	.025	.645	1.17	13.62	168.0	634.0
CONNATE WATER, %	85.0	64.0	17.8	28.5	25.4	11.4	12.8

Cores can be impregnated with wax, plastic, or low-melting metals and the material in the interstices solidified. Removal of the core material by acids leaves the impregnated material in the form of the interstices. Figure 2-4 shows the appearance of the pores in typical rocks. The following description is given of the photographs:

a. This photograph is a reproduction of pore space of a sample of Arbuckle limestone taken, at a depth of between 3,421 and 3,425 ft, from a well in the Silica field, Kansas. Plastic appears as the darkest black in the black-and-white prints. The void space represents the volume formerly occupied by the calcareous material. Attention is called to the weblike structure of some of the pore spaces. The white discolorations, which are present in considerable quantity, have been analyzed and found to be gypsum and silica. In several instances, it will be noted that this material is surrounded by a layer of plastic; this suggests that it is present throughout the sample and partially fills the pore space. It will be noted that one of the largest weblike pore structures does not contain the gypsum and silica.

b. This photograph is a reproduction of the pore space of a sample of Arbuckle limestone from the Silica field. This sample was obtained at a depth of 3,280 to 3,285 ft. The volume previously occupied by calcareous material has been removed by acid and is represented by the dark area in the photograph. Porosity as shown on this particular photograph is very definitely a honeycomblike structure; however, this pattern of development is not considered typical of the Arbuckle limestone. Particular attention is called to the white threadlike pores, for it is believed that a great many more of these fine pores existed but were destroyed in the leaching process.

c. This photograph is a reproduction of the pore space of East Texas field, Woodbine sand. The light color is the plastic and is indicative of the shape and construction of the pore space of the original core. The dark color in contrast represents the shape and portion formerly occupied by the sand grains which were leached out with hydrofluoric acid. It is evident that the distribution of porosity is far more uniform in this sample than in the limestone samples previously discussed. Although core data are not available for the sample shown in the photograph, typical permeability and porosity values would be in the neighborhood of 2,100 millidarcys and 25 per cent, respectively.

d. This is a reproduction of the pore space of the Clearfork formation of the N. Monahans field in West Texas. The light colored area is the plastic which was formerly the pore space of the sample. The very dark area was formerly occupied by calcareous material. The distinguishing characteristic of this sample is the ribbonlike structure of its pore space. This core had a relatively low porosity; and several samples from this formation were found to have no effective porosity.

e. This photograph is a reproduction of the Devonian "pay" taken from a well in the Fullerton field at a depth of 8,557 ft. Effective porosity of the section at this depth is 11.2 per cent, and the permeability is 2,890 millidarcys. This is a rather high value for limestone; however, by close observation of the photograph, it will be noted that a high degree of interconnection of pores exists.

Determination of Porosity

The per cent porosity of an extracted dry rock or core specimen is 100 times the void volume divided by the bulk volume. Most references to porosity measurement emphasize the difference between the effective porosity, defined as the ratio (in per cent) of connected pore volume to total volume, and the absolute porosity, defined as the ratio of total void volume to bulk volume. The difference between absolute and effective porosity in reservoir rocks has been overemphasized; in limestone or highly cemented rocks some voids may be unconnected, but experience with core analyses indicates that generally there is little or no difference between effective and absolute porosity.

Since the same sample is often used for determining porosity and permeability, its preparation usually consists of cutting a plug ¾ to 1 in. in diameter and 1 to 1½ in. in length from a well core, using a diamond drill. The ends of the specimen may be squared by cutting or fracture. To remove oil and water, this specimen is extracted with an organic solvent in a soxhlet extractor and dried in an oven.

The problem is to determine the volume of the rock solids and of the bulk volume. The volume of rock solids may be determined by (1) weighing the dry core plug; (2) placing the plug in a vessel to evacuate the air; (3) admitting a liquid of known density (tetrachlorethane) to submerge the plug and returning atmospheric pressure to the vessel; and (4) weighing the saturated plug, taking care to remove liquid draining from outside the plug when removing it from the liquid. The bulk volume may be determined by finding the liquid displaced in a pycnometer with mercury, water, or a heavy organic liquid such as tetrachlorethane.

The porosity is calculated as follows:

$$\text{Porosity, } \% = \frac{(\text{volume of pores}) \times 100}{\text{volume of core}}$$

$$= \frac{(\text{weight of liquid in pores}) \times 100}{(\text{density of liquid})(\text{volume of core})}$$

Example Determination

Weight of dry core = 19.810 grams
Weight of core saturated with tetrachlorethane = 22.413 grams
Weight of liquid in pores = 2.603 grams
Density of tetrachlorethane = 1.600 grams/cu cm
Volume of core specimen = 9.05 cu cm

$$\text{Porosity} = \frac{2.603 \times 100}{1.600 \times 9.05} = 17.96\%$$

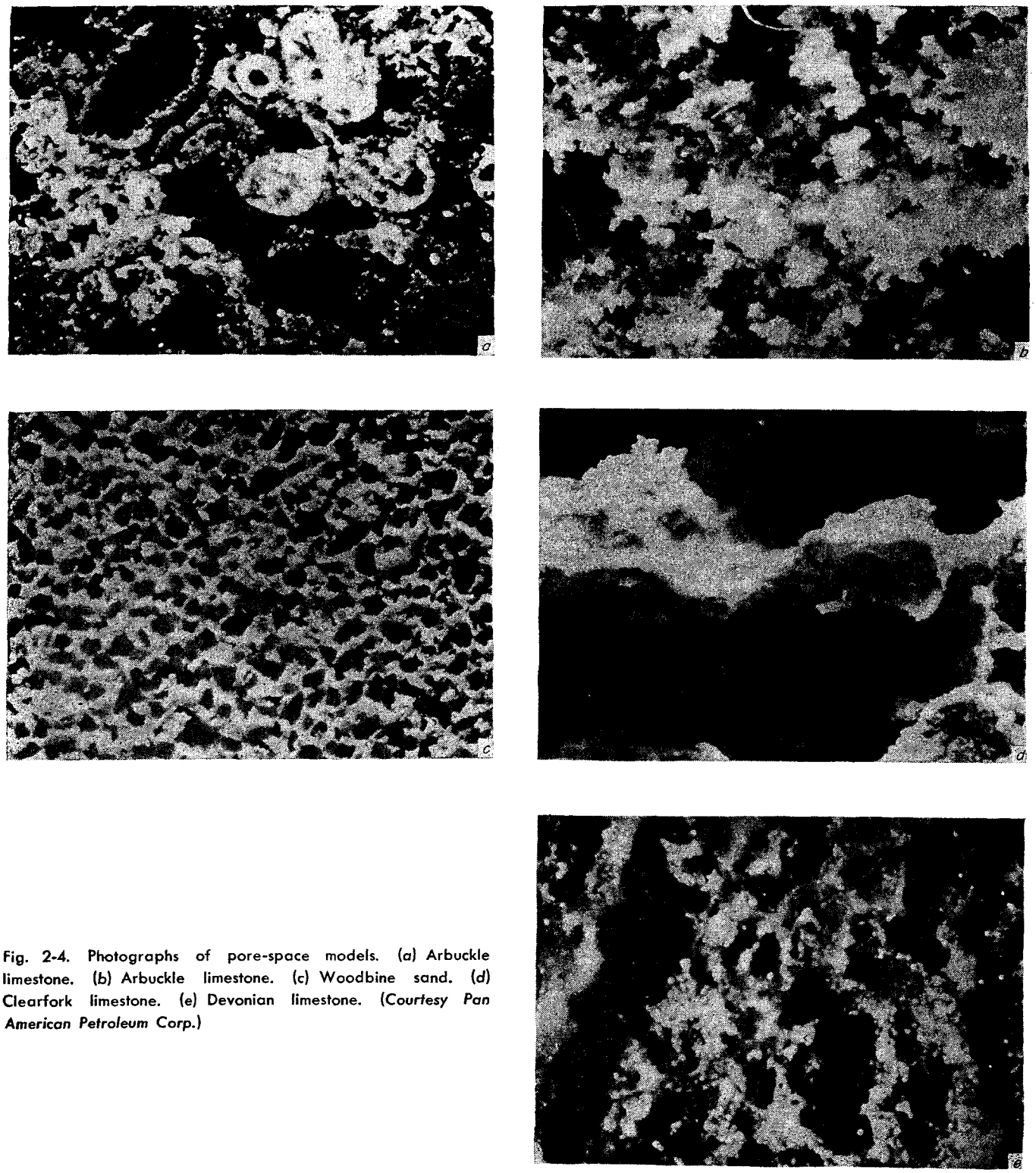

Fig. 2-4. Photographs of pore-space models. (*a*) Arbuckle limestone. (*b*) Arbuckle limestone. (*c*) Woodbine sand. (*d*) Clearfork limestone. (*e*) Devonian limestone. (*Courtesy Pan American Petroleum Corp.*)

Data taken by this method give the density of the total specimen and of the solids or nonpore volume. Typical density data on Oklahoma cores are plotted in Fig. 2-5. It may be seen that a density of 2.67 grams/cu cm applies for the solids and that the bulk density extrapolates to this value at zero porosity. This plot is the basis for the statement that the effective and absolute porosities are normally synonymous.

The above procedure is tedious and time-consuming, but can be conducted in a laboratory without special equipment. There is need for a quick and accurate method suitable for routine measurements. Many methods have been developed for analyzing cores (2-4). The most common method of determining porosity is by use of gases to measure the volume of the solids. The original Washburn-Bunting method has been modified many times, using such equipment as the Bureau of Mines Boyle's law air porosimeter (2-67) and the Kobe porosimeter (2-5).

In the Bureau of Mines method (Fig. 2-6), the volume of the solids is determined by measuring the difference between the volumes of air contained in a pressure bomb with and without the core specimen. The volume of the apparatus is calibrated between the valves C and B, and the amount of air contained therein at a pressure such as 200 psia is measured at atmospheric pressure in the burette. If there are temperature differences between the pressure cell and the measuring burette, corrections are required. The volume of the solids is obtained by measuring the gas released when the core specimen is placed in the bomb. When no temperature correction is required, the fractional reduction in released gas with the core present times the volume of the pressure bomb gives the volume of the solids. The bulk volume of the total-core specimen is obtained by placing the core in a mercury pycnometer. The porosity is found from the ratio of the difference between the two volumes to the bulk volume.

The Kobe porosimeter, shown in Fig. 2-7 (2-55, 2-5), measures both bulk volume and solids volume in the same apparatus. The bulk volume is determined from the volumes of mercury indicated by the micrometer when the mercury level is brought to the sight window, with and without the core specimen. This operation is conducted at atmospheric pressure.

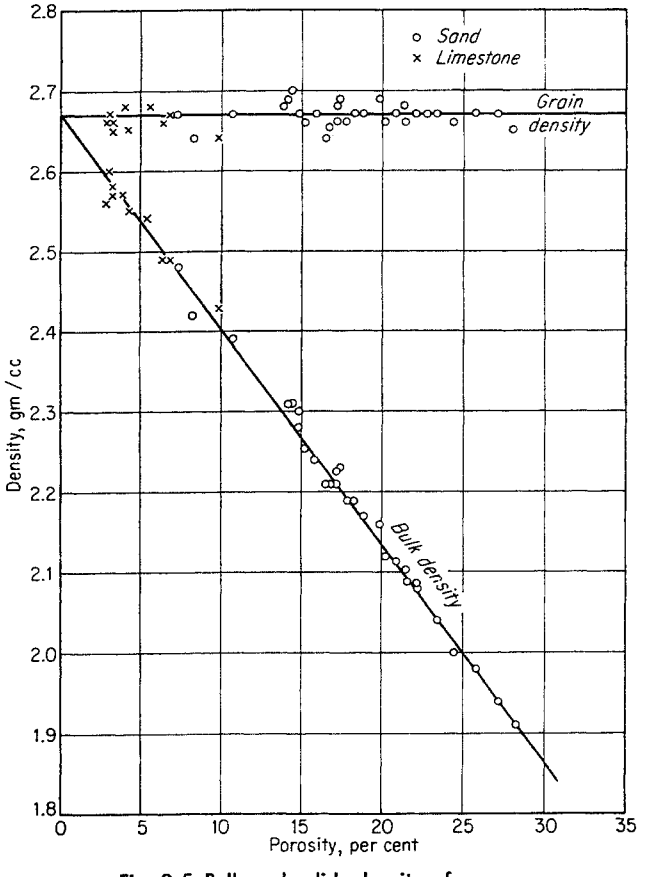

Fig. 2-5. Bulk and solids density of cores.

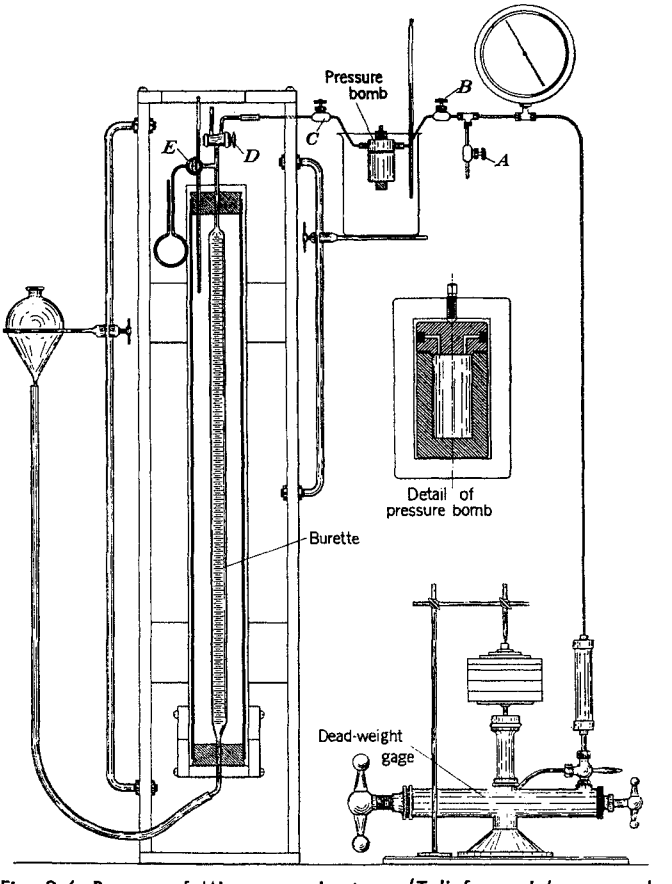

Fig. 2-6. Bureau of Mines porosimeter. (*Taliaferro, Johnson, and Dewees, 2-67.*)

The solids volume is determined by compressing air in the specimen chamber from atmospheric pressure to some pressure predetermined by the floating of the deadweight gauge, with and without the core specimen. The difference in the volume of mercury, as indicated by the micrometer, used to compress the air to the upper pressure for the two cases, along with the volume of the gas chamber at the zero reading of the micrometer, provides sufficient information to compute the volume of the solids in the core specimen. The porosity is calculated by dividing the difference between solids volume and bulk volume by the bulk volume.

Some differences have been observed in porosities obtained by gas porosimeters, depending upon the gas used. It is known that gases are adsorbed on solid surfaces in varying degrees depending upon the temperature, pressure, and nature of the solid. This difference in porosity has been attributed to adsorption of air or nitrogen. Helium is preferred as the gas to use in gas porosimeters because it is nonadsorbing and because it has a minimum deviation from ideal gases.

A mercury-injection method has been developed to measure porosity of both normal-core specimens and drill cuttings or chips. The method is only approximate, at least for low-permeability cores, since mercury will not completely fill the fine pores at pressures up to 1,500 psi or higher. An apparatus similar to that shown in Fig. 2-7 is used. The sample consisting of cuttings or core plug is placed in the place indicated, and evacuated. Mercury is introduced into the chamber until it reaches the sight level, and the

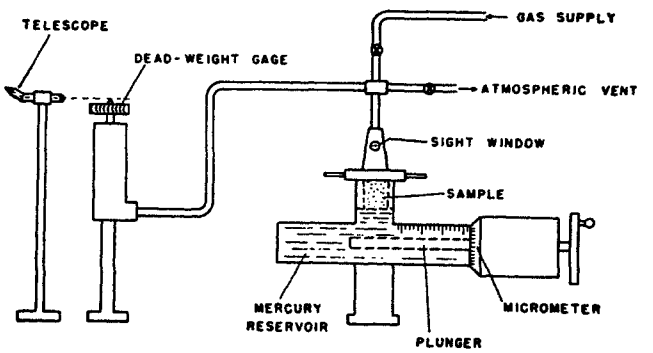

Fig. 2-7. Kobe porosimeter. (*Pollard and Reichertz, 2-55. Courtesy AAPG.*)

micrometer is read. Gas pressure is then introduced above the mercury, and the micrometer screw is turned to bring the mercury level back to the sight point. The amount of mercury introduced into the pores produces the difference between the two micrometer readings. The bulk volume is the difference between the micrometer readings with and without the core plug under vacuum. Table 2-2 gives the results of mercury injection at 1,500 psi to determine the porosity as reported by Burdine, Gournay, and Reichertz (2-15). It would follow that the porosity determined by this method will be low unless a correction is made.

A method of obtaining porosities based on the grain densities is to weigh the extracted and dried cores and measure the bulk volume. A computation of the solids volume is made by dividing the weight of solids in grams by 2.67. Some variations in the density of

Table 2-2. Per Cent Pore Volume Filled during Mercury Imbibition to 1,500 Psia

Sample No.	Measured (gas) permeability, millidarcys	Pore volume filled at 1,500 psia, %	Sample No.	Measured (gas) permeability, millidarcys	Pore volume filled at 1,500 psia, %
171*C*	17	76	190*A*	93	80
164*C*	86	69	174*B*	36	71
171*B*	2.6	85	173*C*	20	78
261*A*	0.5	56	311*B*	52	68
174*C*	38	75	192*A*	1,440	82
164*B*	41	78	169*B*	30	55
311*A*	67	53	171*D*	22	85
161*B*	7	72	295*A*	20	84
173*D*	16	77	261*B*	<0.01	60
163*A*	29	78	686	46	57
681	81	61	867	88	77
866	88	73	683	16	62
680	38	61	696	75	61
682	20	59	14564	112	80
826*A*	440	85	13302	5	68

SOURCE: Burdine, Gournay, and Reichertz (2-15).

the grains or solids may occur according to locality, and, for best results, it is necessary to determine the value occasionally.

Five laboratories each made careful porosity determinations on a group of synthetic and core samples (2-22). Figure 2-8 is a comparison of the results on a sandstone of 20-millidarcy permeability.

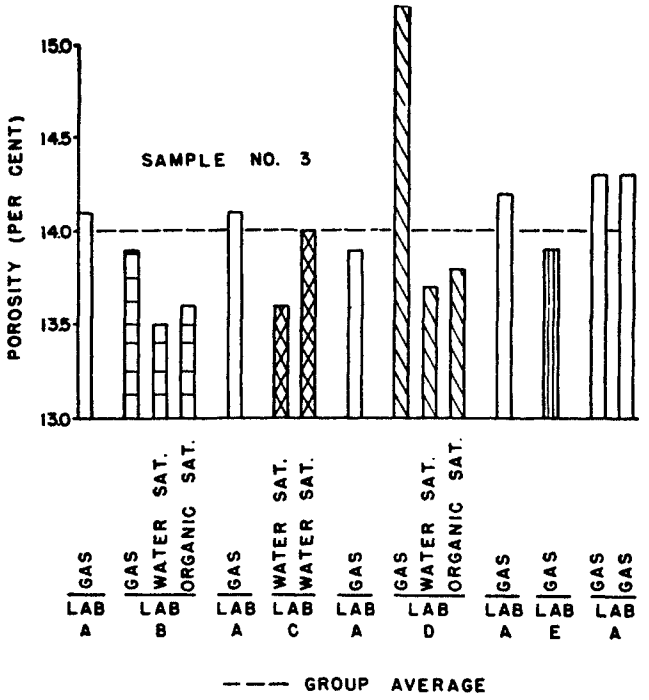

Fig. 2-8. Comparison of porosity measurements by five laboratories. (*Dotson et al., 2-22. Courtesy AIME.*)

Permeability and Its Measurement

The ability of porous media to conduct fluids through their interstices is known as permeability. The definition used in the petroleum industry was adopted in 1935 by the American Petroleum Institute (API) (2-1). The unit of permeability is called a *darcy;* 0.001 darcy is termed a *millidarcy.*

Permeability K is defined by Eq. (2-1):

$$\frac{q}{A} = \frac{K}{\mu}\frac{-dP}{dL} \tag{2-1}$$

where q = volume flow rate, cu cm/sec
A = cross-sectional area, sq cm
μ = fluid viscosity, centipoises
$\frac{-dP}{dL}$ = pressure drop per unit length, atm/cm
K = permeability, darcys

A cube of a porous medium (Fig. 2-9) 1 cm on edge ($\sqrt{A}$, L) will have a permeability of 1 *darcy* if water flows between the front and back faces at a rate q of 1 cu cm/sec under a pressure drop of 1 atm at a temperature of 68°F, where the viscosity is 1 centipoise.

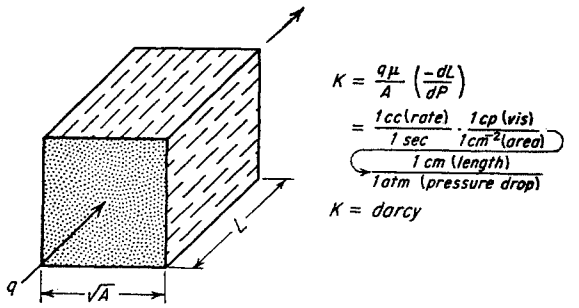

Fig. 2-9. The unit of permeability—a darcy.

Permeability is measured by passing a fluid of known viscosity through a core plug of measured dimensions and then measuring flow rate and pressure drop (Fig. 2-10). A rubber stopper with a hole to hold the core plug snugly prevents air from bypassing the porous medium. The pressure drop is measured by a manometer, and the flow rate either by a calibrated orifice or, with very slow rates, by the rate of movement of a soap bubble in a calibrated glass tube.

Equation (2-1) is written in differential form, and must be integrated to find a suitable equation to use in computing permeability. The volumetric flow rate q is a constant for liquids, because the density does not change significantly during flow through the core plug. Accordingly, Eq. (2-1) becomes (2-2) for liquids flowing through porous media when q, A, μ, and K are constant.

$$q = \frac{KA}{\mu}\frac{P_1 - P_2}{L} \tag{2-2}$$

For gases, the volumetric flow rate q varies with pressure, and either the value for q at the average pressure in the core must be used in Eq. (2-2) or Eq. (2-1) must be integrated, recognizing that the volumetric flow rate q varies with pressure P. Both methods give the same final equation when gases follow ideal-gas behavior.

To convert gas volumes at the mean pressures to gas volumes at 1 atm, the term Q is introduced for gas flows in cubic centimeters at pressure P_b, in accordance with Eq. (2-3).

$$Q = q\frac{P_1 + P_2}{2P_b} \tag{2-3}$$

Substituting in Eq. (2-2),

$$Q = \frac{KA}{2L\mu P_b}(P_1^2 - P_2^2) \tag{2-4}$$

or
$$K = \frac{2QL\mu P_b}{A(P_1^2 - P_2^2)} \quad \text{darcys}$$

or
$$K = \frac{2{,}000QL\mu P_b}{A(P_1^2 - P_2^2)} \quad \text{millidarcys} \tag{2-5}$$

where K = permeability, millidarcys
Q = gas flow rate, cu cm/sec

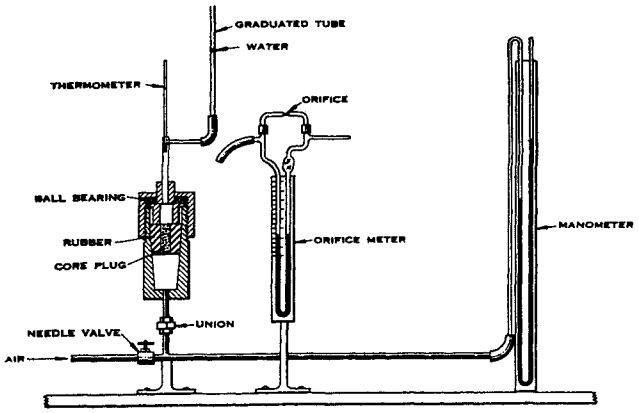

Fig. 2-10. Measurement of permeability.

L = length of core, cm
μ = gas viscosity, centipoises
A = area of core, sq cm
P = absolute pressure, atm
Subscript 1 = upstream core
2 = downstream core
b = base pressure of gas measurement

Table 2-3 gives data taken on a sand core of 18.2 per cent porosity. The permeability values for the four measurements should be the same. Normally no more than two values are taken, but in preliminary work it is advisable to take several points to show that the values give a constant permeability. Should the flow rates be too high, the permeability will decrease, for the flow process will no longer follow Darcy's law.

Several commercial devices are available for measuring permeability with a minimum of readings and calculations (Fig. 2-11).

In measuring permeability, core plugs are cut both horizontally and vertically, since there may be a distinct difference in the two values (Fig. 2-2*a*). Paper-thin bedding planes may contain clay, which reduces the vertical permeability to a fraction of the value found in the horizontal direction. Typical data are given in Table 2-4.

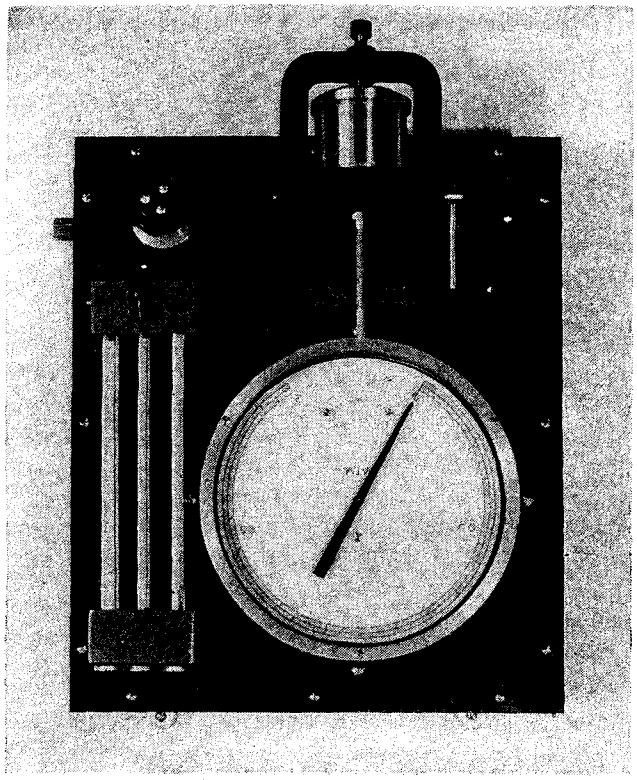

Fig. 2-11. Gas permeameter. (*Courtesy Ruska Instrument Corporation.*)

In field cores of limestone or dolomite (Fig. 2-2*b*), much of the porosity may be in the form of vugs, or solution cavities which could not be included in the usual core plug because of their size. In these cases, it is advantageous to determine the porosity and permeability of the full core. The Hassler type of

Table 2-3. Example of Permeability Data

Core plug, 2.36 cm long, 1.81 cm diameter, 2.58 sq cm area
Barometer, 763 mm Hg Temperature, 68°F μ_{air}, 0.0181 centipoise

Trial No.	P_1, mm Hg	Air flow rate		Pressure drop				$(P_1^2 - P_2^2) \times 10^{-3}$	K, md
		Orifice used	Orifice differential, mm H_2O	Q, cu cm/sec	P_2, mm Hg	P_2, mm Hg abs	P_1, mm Hg abs		
1	782	*A*	17	0.88	1.2	764	1,545	1,805	9.36
2	729	*A*	15	0.80	1.1	764	1,492	1,642	9.35
3	276	*B*	87	0.24	6.25	769	1,039	488	9.44
4	180	*B*	54	0.15	3.95	767	943	301	9.57

$$K = C\frac{Q}{P_1^2 - P_2^2} \quad \text{where } C = \frac{2{,}000 \times 2.36 \times 0.0181 \times 760^2}{2.58} \times \frac{763}{760} = 19.20 \times 10^6$$

P_1 and P_2 in mm Hg abs

Table 2-4. Typical Porosity and Permeability Data

Formation rock	Porosity, %	Permeability, millidarcys	Formation rock	Porosity, %	Permeability, millidarcys
Bartlesville, Okla. (sand)	14.7	6.7	Rodessa oölitic sandstone, La	28.0	14.3
	19.4	48.7		30.5	207
	17.3	41.5		30.2	328
	15.8	18.2		30.2	220
	12.9	21.5		33.9	470
				33.6	595
Benoist, Ill. (sand)	16.7	87.5		28.9	344
	14.2	15.7		24.9	261
	15.3	58.0			
	12.5	20	Tensleep sand, Wyo	11.8	86
	15.1	323		18.0	53
				14.0	189
Cromwell, Okla. (sand)	13.9	171		12.9	119
	14.2	174		11.3	128
	16.3	366		9.3	9.7
	10.8	51			
			Third Los Angeles sand, Calif	19.1	99.5
Cypress, Ill. (sand)	13.7	30		21.2	67
	16.4	249		22.1	84
	20	74		25.6	119
Elenberger dolomite, Tex	5.4	1,285	Wilcox sand, Okla	19.8	242
				23.6	1,650
Frio sand, Tex	22.4	1,475		23.7	2,150
	18.1	42.2		13.1	356
	25.1	860		19.2	456
Gatchell sand, Calif	13.9	965	Wilcox	18.1	155
	14.1	425		16.9	388
				13.4	67
Glenn sand, Okla	16.6	9.5		21.9	1,030
	16.3	10		19.1	786
	17.3	105		15.2	560
	20	302			
			Woodbine sand, Tex	26.8	2,110
Miocene sand, La	36.1	578		25.3	276
	33.2	1,455		23.8	111
	39.4	745		22.1	3,390
	37.3	810		27.7	859
	37.8	360		29.0	341
	34.2	980			
	32.2	1,040	Bradford sand, Pa	10.4	0.77
				12.6	1.67
				14.8	16.8
				14.2	2.7
				16.7	55.8

SOURCE: (2-35, 2-26, 2-41).

permeameter for full well cores is shown in Figs. 2-12 and 2-13 (2-43).

The presence of argillaceous material in cores causes complications in permeability measurements. Drying of the core may shrink the clay, especially bentonite, and the air permeability of the dried core will be higher than would be obtained on the core with water. Fresh water on a core may cause the clay to swell as compared with salt water and thereby reduce the permeability. Permeability data on California cores that have this type of problem are given in Table 2-5 from Johnston and Beeson (2-39).

Slip Phenomenon

Permeability is usually measured by means of air flow, and, therefore, the behavior of gases during flow

at low pressures and in fine capillaries is of interest. When the size of the capillary approaches the mean free path of the molecules, gases flow through it more rapidly than would be predicted by Poiseuille's or Darcy's law. Laminar-flow theory assumes zero fluid velocity at the solid wall, with shear taking place in the fluid. With gases, the individual molecules are in motion and contribute a velocity effect whenever the mean free path approaches the dimensions of the flow conduit.

Using a glass capillary as a model, Klinkenberg (2-44) derived an expression for correcting the gas permeability to that for a fluid of high density for which the mean free path is extremely small.

$$K_g = K_l\left(1 + \frac{4c\lambda}{r}\right) \qquad (2\text{-}6)$$

where K_g = permeability to gas
K_l = permeability to liquid or high-density gas
λ = mean free path of gas molecules under mean pressure at which K_g was measured
c = proportionality factor, approximately equal to unity
r = radius of capillary

Table 2-5. Typical Well Data

Well *A*, Consolidated				Well *B*, Loose				Well *C*, Consolidated				Well *D*, Loose			
Permeability, millidarcys			Fresh-water index,* %	Permeability, millidarcys			Fresh-water index,* %	Permeability, millidarcys			Fresh-water index,* %	Permeability, millidarcys			Fresh-water index,* %
Air	Salt water	Fresh water		Air	Salt water	Fresh water		Air	Salt water	Fresh water		Air	Salt water	Fresh water	
285	62	2.2	3.6	660	354	17	4.8	368	41	27	66	350	165	115	70
481	228	11	4.8	655	340	26	7.6	445	70	62	89	455	110	105	95
123	82	5.9	7.2	680	342	38	11	221	28	8.3	29	625	85	25	29
113	43	1.9	4.4	296	198	40	20	302	58	54	93	975	540	36	6.7
61	6.8	1.2	18	374	279	63	23	73	2.5	0.8	32	1,550	1,140	200	18
36	0.4	0.1	25	1,030	485	22	4.5	33	4.5	5.0	111	565	505	210	42
159	1.6	0.4	25	192	98	21	22	266	69	50	72	6,890	5,510	330	6.0
72	2.3	0.7	30	211†	65	48	74	616	230	168	73	5,000	2,980	155	5.2
310	5.0	1.5	30	625†	242	170	70	262	25	35	140	875	495	28	5.7
328	57	51	90	420	216	22	10	191	57	50	88	420	415	101	24
42	23	6.4	28	236	112	17	15	283	41	42	102	4,250	2,510	34	1.4
24	24	16	67	260	129	56	43	130	34	33	97	3,510	2,460	84	3.4
51	16	5.6	35	322	168	29	17	304	21	15	72	3,140	2,100	40	1.9
42	29	4.1	14	330	58	8	14	66	32	20	63	3,120	1,950	150	7.7
35	17	2.7	16	560	240	56	23	61	17	15	89	1,120	540	135	25
41	15	5.1	34	214	63	7	11	10	3	4	133	1,870	1,090	355	33
22	14	4.0	29	715	437	15	3.4	52	20	20	100	3,810	3,410	1,170	34
46	16	5.7	35	470	305	27	8.8	50	22	5.4	25	1,530	875	125	14
92	89	12	13	535	267	11	4.1	117	37	26	70				
178	40	6.4	16	405	217	14	6.4	230	134	70	52				
20	12	2.9	24	325	186	14	7.5	14	9	5	55				
14	5.9	1.8	31	270	101	34	34								
9.8	6.1	2.8	46	470	240	59	25								
25	13	3.5	27												
14	9.9	3.5	35												
36	22	3.5	16												
104	6.7	2.1	31												
88	11	2.3	21												
438	360	4.9	1.4												

* Ratio of fresh-water to salt-water permeability, per cent. † Consolidated samples.
SOURCE: Johnston and Beeson (2-39).

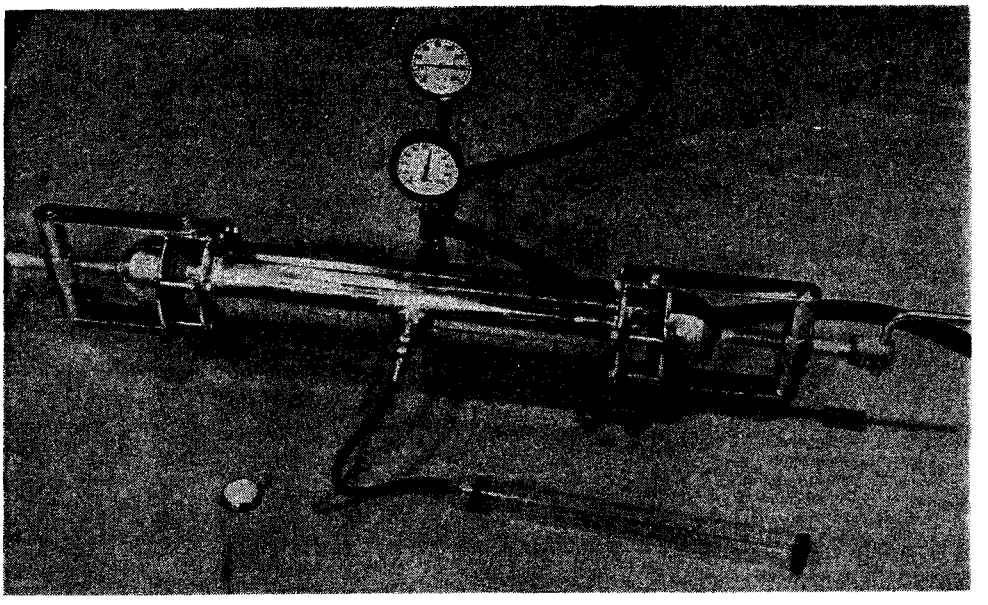

Fig. 2-12. Device for measuring permeability of full-well cores, Hassler type. (*Kelton*, 2-43. *Courtesy AIME.*)

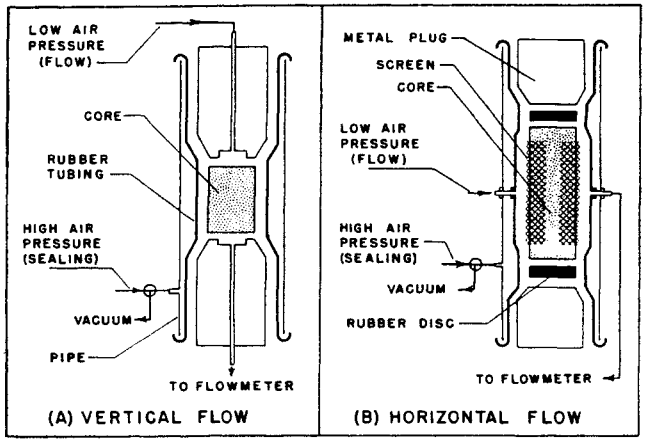

Fig. 2-13. Hassler-type permeameter. (*Kelton*, 2-43. *Courtesy AIME.*)

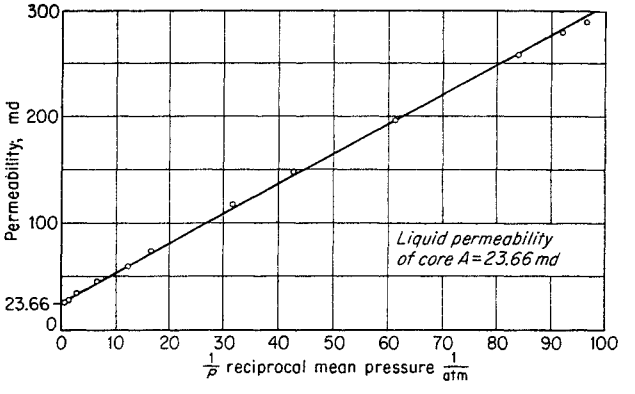

Fig. 2-14. Permeability of core sample *A* to air at various pressures. (*After Klinkenberg*, 2-44.)

Since the mean free path for ideal gases is inversely proportional to pressure and since r is fixed for a given porous medium,

$$K_g = K_l\left(1 + \frac{b}{P_m}\right) \tag{2-7}$$

where b = constant for a gas-solid system
P_m = mean pressure on gas flowing through porous medium

It follows that a graph of permeability K_g measured with a gas at a series of pressures should become a straight line when it is plotted versus the reciprocal of pressure P. Figure 2-14 is a plot of data reported by Klinkenberg on core sample A with a liquid permeability of 23.66 millidarcys. The curve shows clearly that gas pressure has an important effect on permeability, and substantiates the theory that slip is due to the approach of the mean free path of molecules to the pore diameter. It should be noted that all the points on Fig. 2-14 are below 1 atm, an unusual condition for measurement of permeability. Table 2-6 gives some of the points on Fig. 2-14 and also many that cannot be plotted on the scales chosen.

Calhoun and Yuster (2-17) investigated slip effect and presented results for different gases, including methane, ethane, and propane (Figs. 2-15 and 2-16). The pyrex-glass filter used had a permeability to naphtha of 2.70 millidarcys, and the extrapolated values on Figs. 2-15 and 2-16 are 2.75 millidarcys.

Since permeability data are used for predicting flow at conditions other than those prevailing in measuring the permeability, it is advisable to bring permeabilities to values for liquids or gases at high pressure. The reduction in mean free path for the gas molecules re-

Table 2-6. Permeability of Core Sample A to Air at Different Pressures

Permeability to liquid, 23.66 millidarcys

Mean pressure, atm	Reciprocal pressure, atm	Permeability, millidarcys
0.01036	96.56	290
0.01633	61.20	197
0.05921	16.89	75.6
0.1464	6.829	46.6
0.799	1.251	28.6
1.57	0.636	26.79
2.657	0.3764	25.22
5.10	0.1961	24.62
9.19	0.1088	23.93
20.01	0.0499	23.65

SOURCE: Klinkenberg (2-44).

sulting from the increase in gas pressure from the permeability determination at 1 atm to the reservoir at pressures of several atmospheres means that gas flow under the higher pressure will be less than that predicted from permeability measurements at atmospheric pressure. It should be recognized that at low pressures the effective permeability including slip is greater for gases than for liquids.

Yuster and associates (2-35) studied slip phenomena for a group of cores for which porosity, liquid (naphtha) permeability, and air permeability were determined. Figure 2-17 is their plot of the factor b in Eq. (2-7) against liquid permeability, with the straight line represented by Eq. (2-8):

$$b = 0.77K_l^{-0.39} \qquad (2\text{-}8)$$

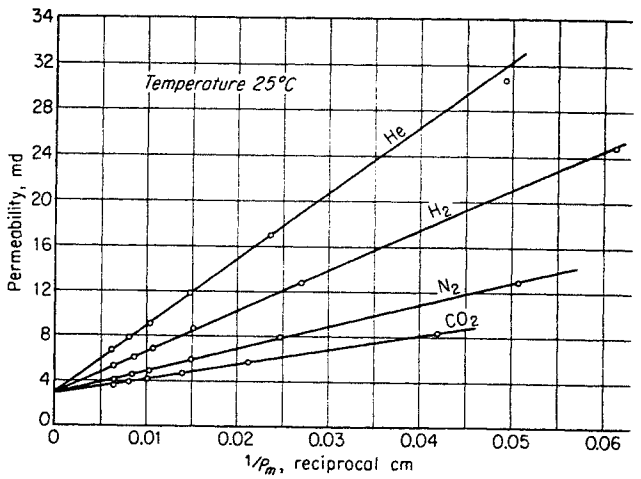

Fig. 2-15. Effect of pressure on permeability for various gases. (*Calhoun and Yuster*, 2-17. *Courtesy API Drill. Prod. Practice.*)

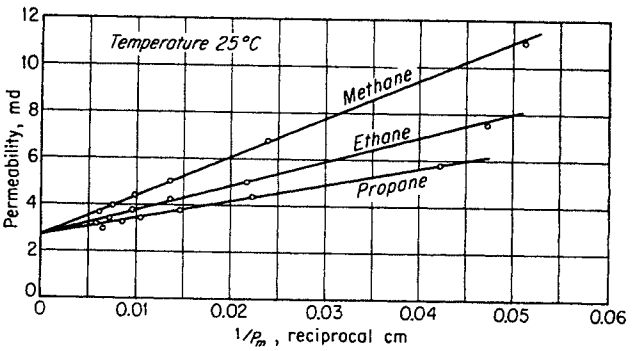

Fig. 2-16. Effect of pressure on permeability for methane, ethane, and propane. (*Calhoun and Yuster*, 2-17. *Courtesy API Drill. Prod. Practice.*)

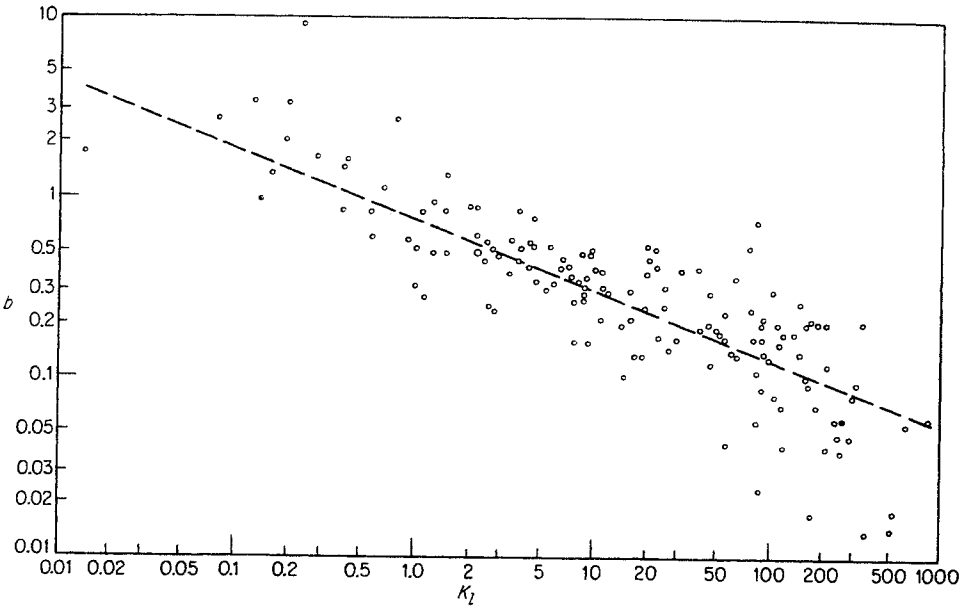

Fig. 2-17. Plot of b factor against extrapolated Klinkenberg permeability. (*Heid, McMahon, Nielsen, and Yuster*, 2-35. *Courtesy API Drill. Prod. Practice.*)

The usual measurement of permeability is made with air at mean pressures just above 1 atm. By using the values of b from Fig. 2-17 and mean air pressures P_m of 1, 1.5, 2.0, 2.5, and 3 atm for the air flowing through the core, correction factors are found that can be applied to air permeabilities to find K_l, the liquid permeability or the permeability to gas at high pressure as shown in Fig. 2-18. For example, at a K_l of 0.1 millidarcy, $b = 1.91$. At 1 atm pressure for air passing through the core,

$$\frac{K_l}{K_g} = m = \frac{1}{1 + 1.91/1.0} = \frac{1}{2.9} = 0.343$$

The K_g is 0.291 millidarcy, and the liquid permeability K_l is $0.343 \times 0.291 = 0.1$ millidarcy. The curves on Fig. 2-18 may be labeled ΔP in atmospheres for 1 atm downstream pressure.

Inspection of Fig. 2-17 reveals a wide scatter in the points, which indicates that permeability is only a moderately successful correlating variable. The mean pore diameter, such as obtained from capillary-pressure measurements, no doubt would have been a better variable to use if its value had been measured in routine core analyses. Permeability measurements, especially on low-permeability cores, can well employ at least two mean-pressure levels for air flowing through the core to evaluate the slip phenomenon. In the absence of such data, Fig. 2-18 will give an average correction but, for any particular porous medium, the actual correction may be either greater or less, as indicated by the scatter of points on Fig. 2-17.

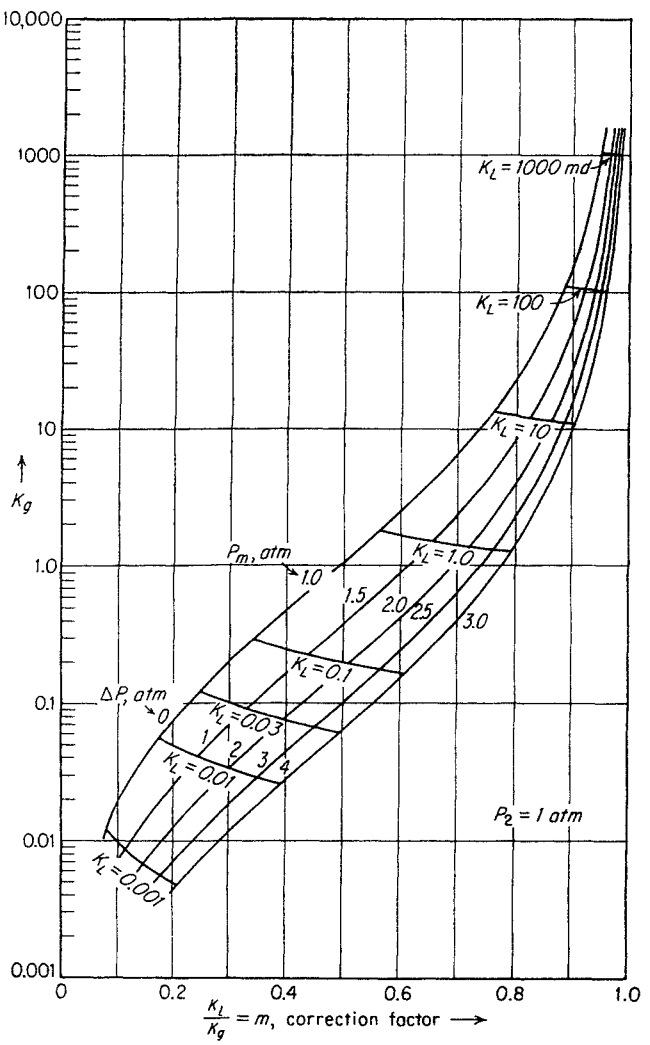

Fig. 2-18. Correction of air permeability for slip.

Values of b can be used to compute the effective permeability to air at other mean pressures. Values of b for gases other than air can be computed from Eq. (2-9).

$$\frac{b_{air}}{b_{gas}} = \frac{\lambda_{air}}{\lambda_{gas}} \tag{2-9}$$

where λ = mean free path.

The mean free paths for air and the gas under consideration must be taken at the same pressure.

The phenomenon of slip is sometimes described as Knudsen flow or molecular streaming. In one sense, the gas is in part diffusing through the medium. At lower pressures, the gas diffuses to a greater extent than at high pressures and thereby contributes more to the total gas passing through porous medium. Wallick and Aronofsky have studied the effect of slip on unsteady-state flow (2-69).

Turbulent Flow

In the flow of a fluid through a porous medium, the flow rate increases proportionally with the increased pressure drop for a range of flows. At some flow rate, it is found that the increased flow rate no longer matches the increased pressure drop for liquids or the difference in squares of pressures for gases (Fig. 2-19). This phenomenon was observed by Osborne Reynolds in 1901 for flow in pipes. He conducted his classical experiments of injecting dye into water flowing in glass tubes, and found that streamline flow held for the velocities where pressure drop was proportional to flow rate. At the juncture in the pressure-drop curve where pressure drop rises more rapidly than flow rate, Reynolds observed turbulence in the flowing stream. For flow in pipes, the terms "streamline," "laminar," and "viscous" flow are used interchangeably for the regime where the velocity is proportional to pressure drop. The term "turbulent flow" is used for the regime where pressure drop is more than proportional to flow rate and where turbulence is observed in tubes.

Fancher and Lewis (2-26) reported flow data for porous media and adopted the same terminology of viscous and turbulent flow. Their data are plotted as

friction factors and Reynolds numbers in Fig. 2-21. The deviation from a 45° line at high velocities indicates the onset of turbulence.

Turbulence has been observed for fluids flowing in porous beds of particles large enough to permit observation of phenomena similar to those in pipes. However, for consolidated porous solids with very small pores and very low permeabilities, it is difficult to visualize eddies or turbulence in the interstices of the media even though the same pressure-drop–flow-rate relations exist for such media. Various explanations are offered for the behavior in the high-velocity-flow regime (2-3, 2-30).

The extra pressure drop is associated with the inertia effects of the fluid passing through narrow passages. In the viscous-flow condition (Fig. 2-20*a*) the kinetic energy of the fluid going from 1 to 2 to 3 is reversibly exchanged with pressure energy. At high velocities (Fig. 2-20*c*) the conversion of kinetic energy at 2 to pressure energy at 3 is interrupted by extra fluid motion over that in the viscous case. This loss of energy creates by force of inertia a greater pressure drop on the solid particle at 2. Some workers reserve the term "turbulence" for completely random motion with time at a given point. By this definition, the flow in Fig. 2-20*c* would not be called turbulent. If one includes extra motion of the fluid to consume the extra pressure loss, then the term "turbulent flow" here is justified. An intermediate case (Fig. 2-20*b*) may be visualized in which the shear planes are lengthened at higher velocities without any eddy motion, accounting for extra energy consumption. In accordance with common usage, the term "turbulent flow" will be used hereafter to describe the condition of velocity such that increases in pressure for liquids or difference of squares of pressures for gases are more than proportional to increases in flow rates.

For expressing flow under both viscous or laminar and turbulent conditions, the Darcy equation (2-1) is no longer adequate. The quadratic equation suggested by Forscheimer (2-3) appears to be suitable for expressing the relationship between pressure drop and velocity:

$$\frac{-dP}{dL} = \frac{\mu v}{K} + \beta\rho v^2 \qquad (2\text{-}10)$$

where P = pressure, atm
L = length, cm
μ = viscosity, centipoises
v = velocity, cm/sec
K = permeability, darcys [= sq cm–centipoises/(atm)(sec)]
ρ = density, grams/cu cm
β = turbulence factor, atm-sec²/gram

For gases, the equation is best expressed in terms of

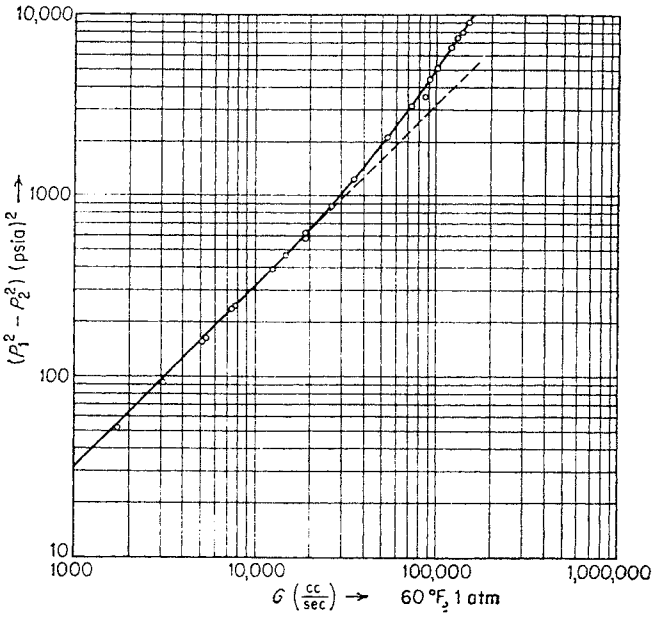

Fig. 2-19. Pressure-drop data for air flowing through a Wilcox sand. (*Cornell*, 2-20.)

mass velocity $W/A = \rho v$, because the mass velocity is a constant when the cross section is constant, permitting integration of the equation. Here

W = mass flow rate, grams/sec
A = flow area, sq cm

$$\rho\frac{-dP}{dL} = \frac{\rho v\mu}{K} + \beta\rho^2 v^2 = \frac{\mu W}{KA} + \beta\left(\frac{W}{A}\right)^2 \qquad (2\text{-}11)$$

Since
$$\rho = \frac{MP}{zRT} \qquad (2\text{-}12)$$

$$-\frac{M}{zRT}\int_1^2 P\,dP = \left[\frac{\mu W}{KA} + \beta\left(\frac{W}{A}\right)^2\right]\int_1^2 dL \qquad (2\text{-}13)$$

where M = molecular weight
z = compressibility factor
R = gas constant
T = absolute temperature

Integrating between points 1 and 2 in the flow path, one obtains

$$\frac{M(P_1^2 - P_2^2)}{2zRT\mu L(W/A)} = \frac{W}{A}\frac{\beta}{\mu} + \frac{1}{K} \qquad (2\text{-}14)$$

Flow data for a core specimen plotted in accordance with this equation are shown in Fig. 2-22. The intercept of the resulting straight line is $1/K$, and the slope is the turbulence factor β. Table 2-7 sum-

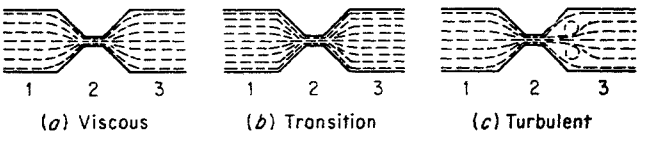

Fig. 2-20. Flow through restriction in porous medium.

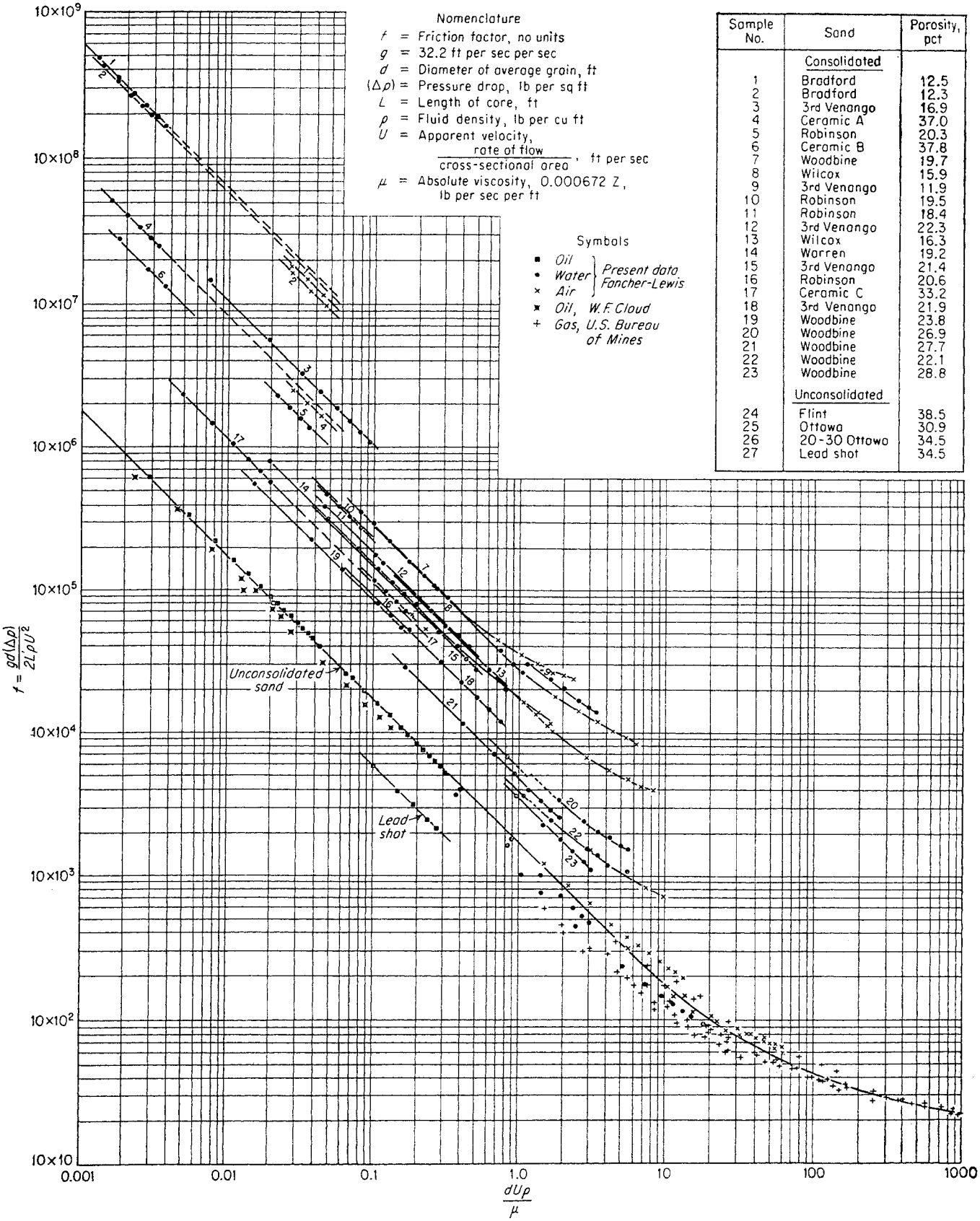

Sample No.	Sand	Porosity, pct
	Consolidated	
1	Bradford	12.5
2	Bradford	12.3
3	3rd Venango	16.9
4	Ceramic A	37.0
5	Robinson	20.3
6	Ceramic B	37.8
7	Woodbine	19.7
8	Wilcox	15.9
9	3rd Venango	11.9
10	Robinson	19.5
11	Robinson	18.4
12	3rd Venango	22.3
13	Wilcox	16.3
14	Warren	19.2
15	3rd Venango	21.4
16	Robinson	20.6
17	Ceramic C	33.2
18	3rd Venango	21.9
19	Woodbine	23.8
20	Woodbine	26.9
21	Woodbine	27.7
22	Woodbine	22.1
23	Woodbine	28.8
	Unconsolidated	
24	Flint	38.5
25	Ottawa	30.9
26	20-30 Ottawa	34.5
27	Lead shot	34.5

Fig. 2-21. Flow through porous media. (*Fancher, Lewis, and Barnes, 2-26. Courtesy Ind. Eng. Chem.*)

marizes values of the turbulence factors obtained in this way for a number of core samples (2-21). The turbulence factors are plotted against permeability in Fig. 2-23 (2-42). Janicek and Katz (2-37) presented a correlation of turbulence factors with permeability and porosity. Their constant-porosity lines are superimposed on Fig. 2-23.

To compare flow data for porous media with veloci-

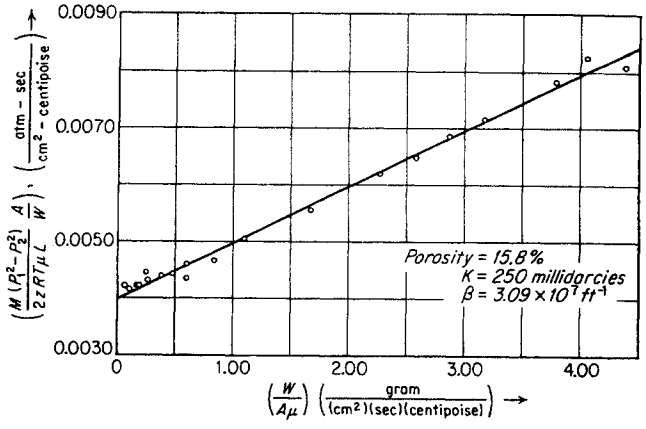

Fig. 2-22. Evaluation of permeability K and turbulence factor β for a Wilcox sand. (Cornell, 2-20.)

Table 2-7. Summarized Characteristics of the Consolidated Samples Studied

$$\alpha = \frac{9.41 \times 10^{13}}{K} \qquad k_2 = \frac{32F^{3/2}}{\beta D_E \phi^{1/2}}$$

Sample type	Resistivity factor F	Fractional porosity ϕ	α, ft^{-2}	β, ft^{-1}	Permeability K, millidarcys	D_E, ft ($k_1 = 0.5$)	L_E/L	k_2
Wilcox*	15.5	0.175	4.90×10^{11}	8.23×10^{7}	192	4.50×10^{-5}	1.64	1.26
	17.4	0.158	3.77×10^{11}	3.09×10^{7}	250	5.42×10^{-5}	1.66	3.48
	16.6	0.160	6.35×10^{11}	9.95×10^{7}	148	4.08×10^{-5}	1.63	1.33
Bromide*	36.2	0.110	4.60×10^{13}	2.80×10^{9}	2.0	7.10×10^{-6}	1.99	1.05
	36.2	0.110	3.92×10^{13}	1.99×10^{9}	2.4	7.68×10^{-6}	1.99	1.38
	62.5	0.030	1.015×10^{15}	9.00×10^{12}	0.093	1.98×10^{-6}	1.36	0.00512
	86.8	0.022	1.97×10^{15}	1.96×10^{12}	0.048	1.68×10^{-6}	1.38	0.053
	30.0	0.123	6.30×10^{12}	4.40×10^{8}	15.0	1.74×10^{-5}	1.92	1.95
Burbank*	39.1	0.150	8.60×10^{12}	1.31×10^{9}	11.0	1.70×10^{-5}	2.41	0.901
	34.8	0.163	2.65×10^{12}	3.47×10^{8}	35.5	2.90×10^{-5}	2.38	1.62
Spraberry*	53.8	0.080	9.75×10^{14}	2.00×10^{11}	0.097	1.88×10^{-6}	2.07	0.119
	60.3	0.084	8.53×10^{15}	1.74×10^{13}	0.011	6.71×10^{-7}	2.25	0.00441
Outcrop*	14.4	0.206	3.00×10^{12}	7.10×10^{8}	31.3	1.75×10^{-5}	1.72	0.310
	14.4	0.206	4.50×10^{12}	8.20×10^{8}	20.9	1.43×10^{-5}	1.72	0.328
Torpedo*	12.1	0.227	2.22×10^{11}	5.90×10^{6}	424	5.90×10^{-5}	1.66	8.11
	13.4	0.228	1.850×10^{11}	4.80×10^{6}	508	6.80×10^{-5}	1.74	10.0
Brown dolomite	49.8	0.143	2.00×10^{12}	6.25×10^{8}	47.0	3.99×10^{-5}	2.66	1.19
	.....	0.160	2.40×10^{12}	1.55×10^{8}	39.2			
	.....	0.125	1.75×10^{13}	3.22×10^{9}	5.4			
	64.7	0.095	9.20×10^{13}	7.25×10^{10}	1.02	6.70×10^{-6}	2.48	0.111
	70.2	0.095	1.25×10^{13}	8.24×10^{9}	7.5	1.90×10^{-5}	2.58	0.390
	68.5	0.094	4.56×10^{14}	2.66×10^{11}	0.207	3.10×10^{-6}	2.54	0.0714
Canyon Reef limestone	142.5	0.051	7.70×10^{14}	1.033×10^{12}	0.122	3.44×10^{-6}	2.69	0.0677
	123.0	0.087	9.10×10^{13}	9.05×10^{10}	1.03	9.30×10^{-6}	3.26	0.176

* Sandstone samples.

SOURCE: Cornell and Katz (2-21).

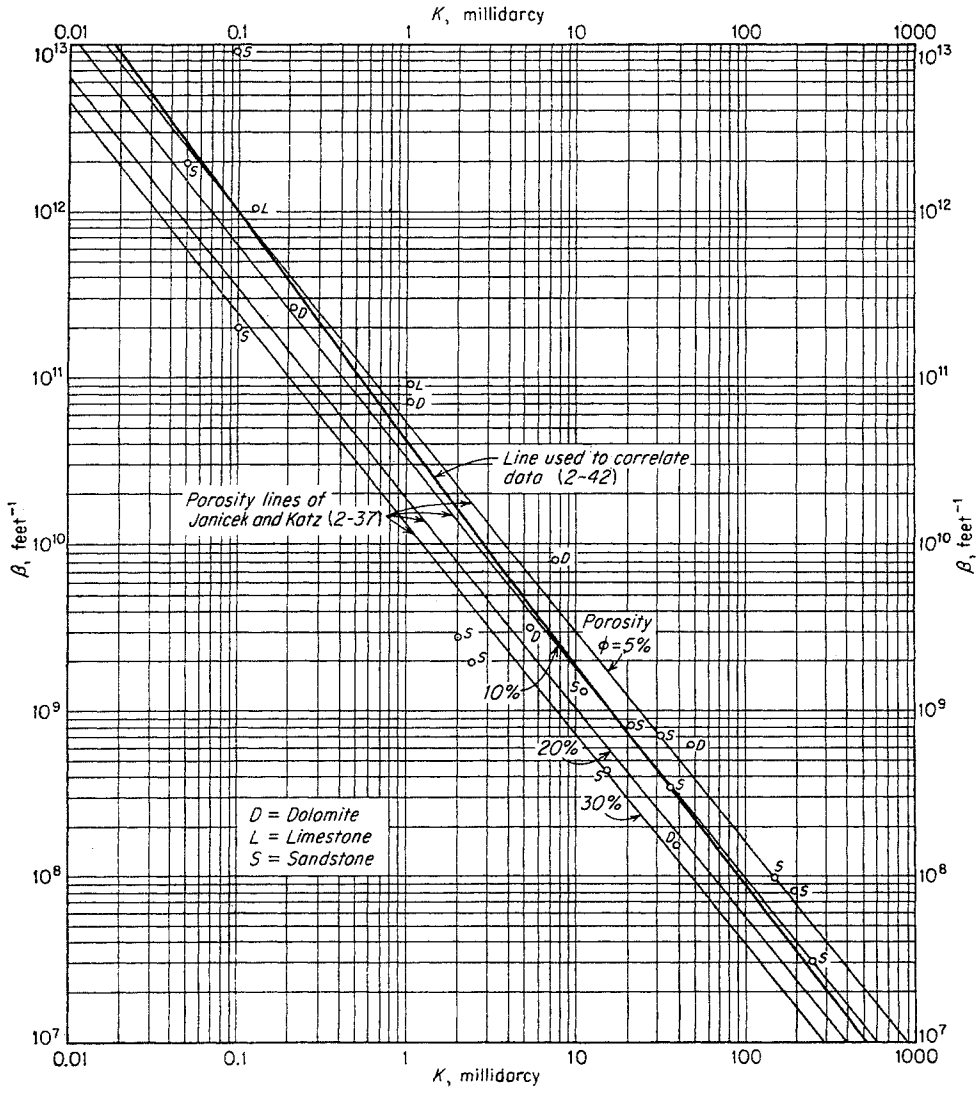

Fig. 2-23. Correlation of turbulence factor β with permeability. (2-37, 2-42.)

ties into the turbulent regime, they may be plotted as friction factor vs. Reynolds number, as in Fig. 2-24 (2-21). The friction factor is defined by Eq. (2-15).

$$f = \frac{64 g_c \rho (P_1 - P_2) A^2}{\beta L W^2} \qquad (2\text{-}15)$$

where f = friction factor, dimensionless
g_c = 32.17 conversion factor, lb mass-ft/(lb force)(sec^2)
ρ = fluid density, lb mass/cu ft
P = pressure, lb force/sq ft
A = area of flow, sq ft
β = turbulence factor, ft^{-1}
L = length of flow, ft
W = mass flow rate, lb mass/sec

The Reynolds number is given by Eq. (2-16).

$$\mathrm{Re} = \frac{\beta W K}{6.33 \times 10^{10} A \mu} \qquad (2\text{-}16)$$

where K = permeability, millidarcys
μ = fluid viscosity, centipoises

Illustrative Problem

Given a sand core 0.725 in. in diameter and 0.730 in. long, porosity 15.8 per cent and permeability 250 millidarcys; compute flow rate for air at upstream pressure of 100 psia and downstream pressure of 14.7 psia. Air temperature = 75°F.

Solution Using Eq. (2-14)

The value of β from Fig. 2-23 is about 2.5×10^7 ft^{-1}. The viscosity of air is 0.020 centipoise, and the compressibility factor may be taken as 1.0. In laboratory units the variables become

M = 29 grams/gram mole
$P_1^2 - P_2^2$ = 45.28 atm^2
μ = 0.020 centipoise
z = 1.0
R = 82.06 cu cm-atm/(gram mole)(°K)
T = 297.2°K
L = 1.85 cm
W = grams/sec

$$\beta = \frac{2.5 \times 10^7}{2.54 \times 12 \times 1{,}013{,}420} = 0.8096 \text{ atm-sec}^2/\text{gram}$$

$$A = \frac{\pi \times 0.725^2 \times 2.54^2}{4} = 2.66 \text{ sq cm}$$

The conversion factor 1,013,420 is the value of g_c in gram-cm/(atm/sq cm)(sec^2).

$$\frac{29 \times 45.28 \times 2.66}{2 \times 1.0 \times 82.06 \times 297.2 \times 0.020 \times W \times 1.85} = \frac{0.8096 \times W}{2.66 \times 0.020} + \frac{1}{0.25}$$

$$15.218W^2 + 4W - 1.935 = 0$$

$$W^2 + 0.2628W - 0.1272 = 0$$

$$W = 0.25 \text{ gram/sec}$$

Alternative Solution Using Fig. 2-24

$\beta = 2.5 \times 10^7$ ft^{-1}
$W =$ lb/sec
$K = 250$ millidarcys
$A = 2.87 \times 10^{-3}$ sq ft
$\mu = 0.020$ centipoise

$$\text{Re} = \frac{2.5 \times 10^7 \times W \times 250}{6.33 \times 10^{10} \times 2.87 \times 10^{-3} \times 0.020} = 1{,}722W$$

$$\bar{\rho} = \frac{57.4 \times 29}{10.731 \times 535} = 0.290 \text{ lb/cu ft}$$

$$P_1 - P_2 = 100 - 14.7 = 85.3 \text{ psi or } 85.3 \times 144 = 12{,}283 \text{ lb/sq ft}$$

$$L = \frac{0.730}{12} = 0.0608 \text{ ft}$$

$$f = \frac{64 \times 32.17 \times 0.29 \times 12{,}283 \times 2.87^2 \times 10^{-6}}{2.5 \times 10^7 \times 0.0608 \times W^2} = \frac{3.97 \times 10^{-5}}{W^2}$$

Assume $W = 7.5 \times 10^{-4}$ lb/sec
Re = 1.29
$f = 70.6$
Re = 1.0 is more nearly correct (Fig. 2-24).

$$W = \frac{1.0}{1{,}722} = 5.81 \times 10^{-4} \text{ lb/sec or } 0.26 \text{ gram/sec}$$

The observed flow rate in this experiment was 0.23 gram/sec. The experimental value of β was 3.09×10^7, as compared with 2.5×10^7 read from Fig. 2-23.

Compressibility of Reservoir Rock

Reservoir rock in underground reservoirs is under considerable compressive stress and fluid pressure, as compared with core specimens examined in the laboratory. Any compressibility effects on porosity and permeability would be of interest in converting laboratory data to field use.

Measurements of rock compressibility and the influence of compressibility on porosity and permeability have been made (2-19, 2-31, 2-27). In the apparatus shown in Fig. 2-25 (2-31), two types of rock-compressibility measurements may be made. The first is to find the rock compaction that occurs when the external pressure on the sheath is increased and atmospheric pressure is kept on the fluid in the core. The liquid "squeezed" out of the core by external pressure is indicated directly by the liquid rise in the glass tube. Data of this type were reported by Carpenter and Spencer (2-19), as shown in Fig. 2-26. A slight hysteresis effect was noted, but other-

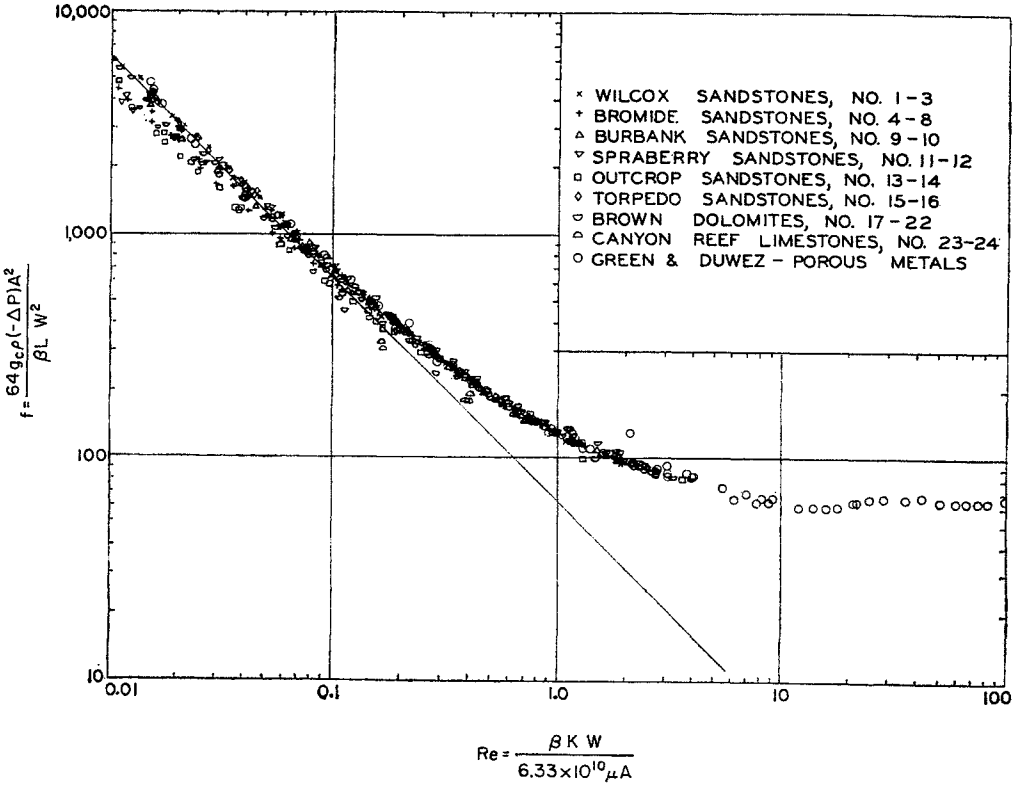

Fig. 2-24. Friction-factor plot for consolidated porous media. (*Cornell and Katz*, 2-21. *Courtesy Ind. Eng. Chem.*)

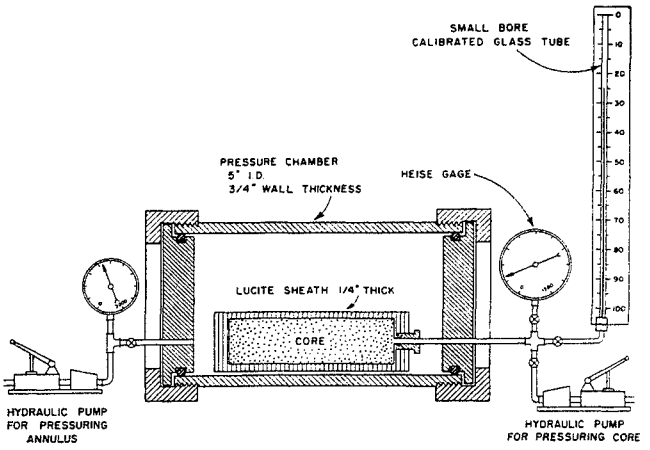

Fig. 2-25. Diagram of equipment used for rock-compressibility tests. (*Hall*, 2-31. *Courtesy AIME.*)

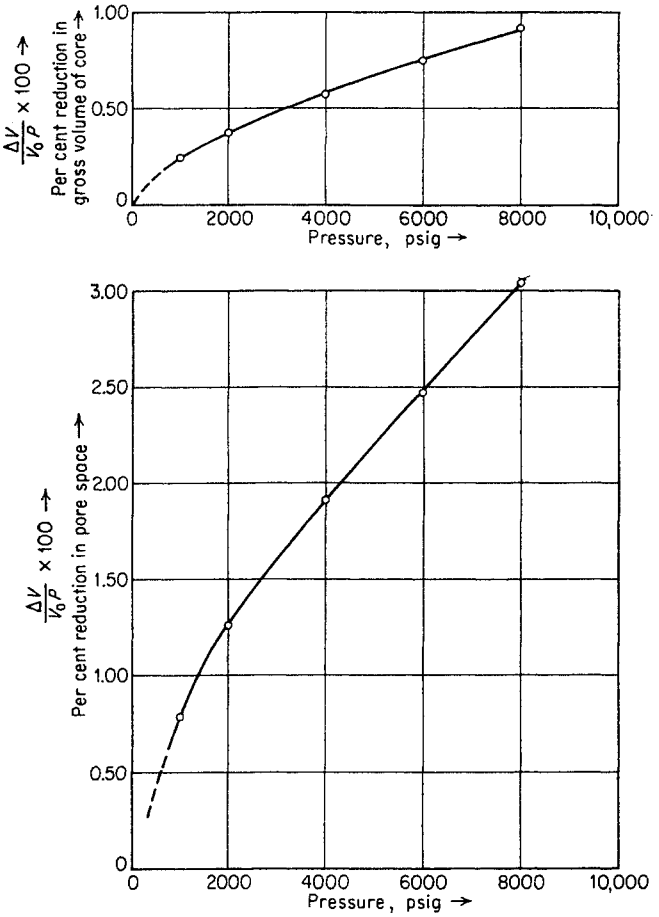

Fig. 2-26. Compaction of Woodbine sand at 146°F. (*After Carpenter and Spencer*, 2-19.)

wise the sand was elastic. No significant effect of temperature was observed from 91 to 146°F. Hall (2-31) also made compaction measurements, and has reported such data in the form of change in pore volume per unit pore volume per psi (Fig. 2-27).

The second type of measurement made by Hall on the apparatus of Fig. 2-25 was to maintain the external pressure on the core (3,000 psi) and find the difference in the liquid actually produced when lowering the pressure on the liquid in the core 1,500 to 2,000 psi from that which would be produced from a constant-volume container. The liquid that would have been produced from the pore space had it remained constant can be computed from the compressibility of the liquid with corrections for the liquid in the system external to the core. The reduction in pore space per unit pore space per psi change between the external and internal pressures is plotted in Fig. 2-28 from Hall.

The effects of external pressure on the permeability of cores was investigated by Fatt and Davis (2-27). Nitrogen at atmospheric pressure was passed through dry cores surrounded by a sheath and subjected to external pressure in apparatus much like that shown in Fig. 2-25. The results in Fig. 2-29 show significant reductions in permeability with increases in external pressure.

Electrical-resistivity Factor of Rocks

The resistivity factor F provides a useful and convenient evaluation of the nature of the pore structure of reservoir rocks. This factor was defined by Archie (2-2) as the ratio of the electrical resistance R_0 of a sample saturated with a conducting brine to the resistance R_w of a volume of the same brine having the same size and shape as the over-all dimensions of the sample.

$$F = \frac{R_0}{R_w} \tag{2-17}$$

Since the flow of electricity is analogous to the flow of a fluid of zero viscosity, pore diameters are not a factor, as, for example, in Poiseuille's law for viscous flow. Accordingly, the resistivity factor depends only on the pore length and porosity and not on permeability. As a result, knowledge of the electrical-resistivity factor permits calculation of pore lengths in rock samples.

The value of the resistivity factor F depends upon the available cross-sectional void area of the sample and upon the increased distance due to the irregular path. Referring to Fig. 2-30, we see that the resistivity depends both upon the area of the pore relative to the total cross section and upon the length of the pore relative to the length of the specimen. The resistivity is inversely proportional to the cross-sectional area of the pore and directly proportional to the ratio of the length of the pore to the core length.

The area of the pore normal to the flow path is

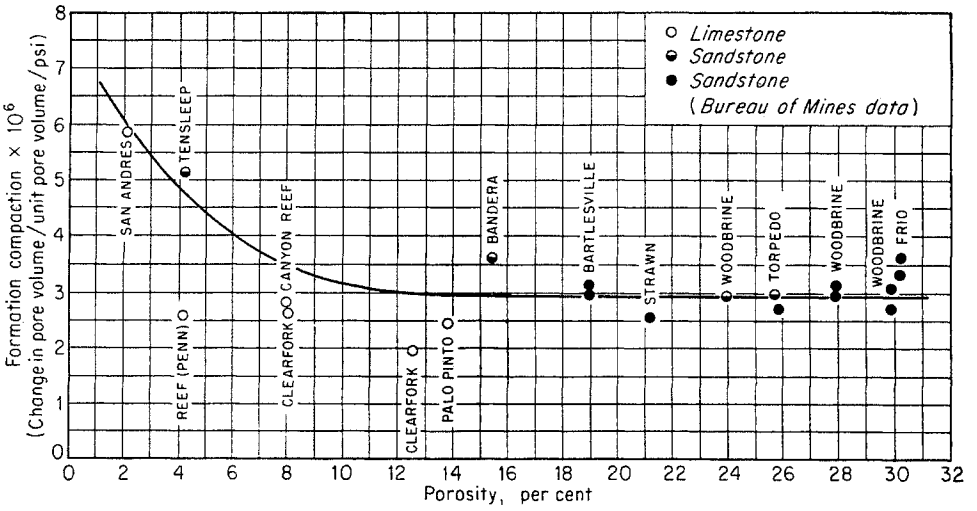

Fig. 2-27. Formation compaction component of total-rock compressibility. (*Hall*, 2-31. *Courtesy AIME.*)

$a \cos \theta = aL/L_e$. Since the porosity $\phi = a/1.0$, the area normal to flow becomes $\phi L/L_e$. Therefore, the resistivity becomes

$$F = \frac{L_e}{\phi L}\frac{L_e}{L} = \frac{L_e^2}{\phi L^2} \qquad (2\text{-}18)$$

This equation was developed independently by Winsauer et al. (2-72) and Cornell (2-20). An alternative equation was presented by Wyllie and Spangler (2-73), based on the concept of a cross-sectional area proportional to the porosity rather than to $\phi L/L_e$.

Measured values of the formation resistivity factor F and the porosity ϕ may be used to calculate tortuosity ratios L_e/L of core samples. Typical data for reservoir materials are included in Table 2-7. Knowledge of the tortuosity ratio is important in

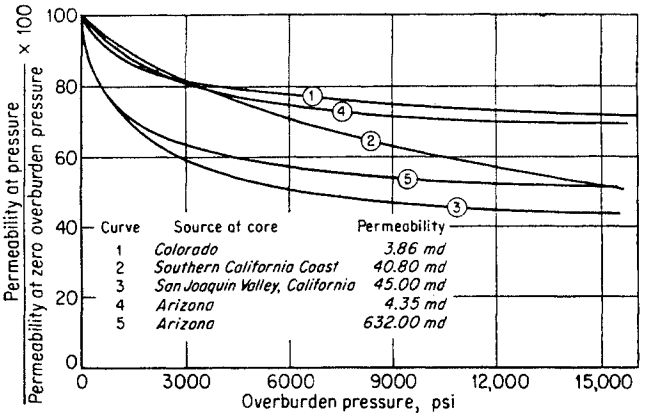

Fig. 2-29. Change in permeability with overburden pressure. (*Fatt and Davis*, 2-27. *Courtesy AIME.*)

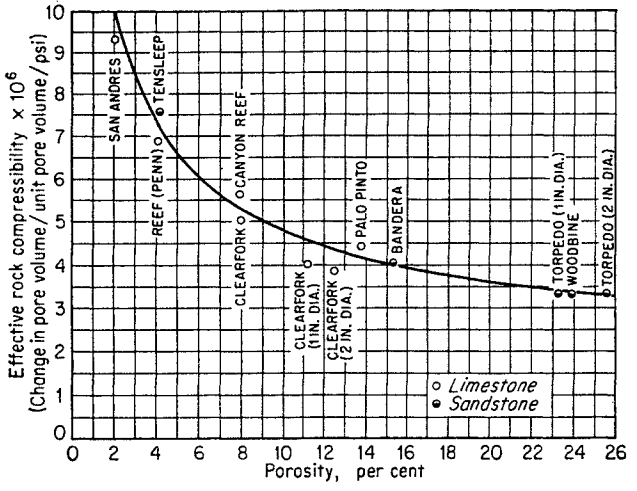

Fig. 2-28. Effective reservoir-rock compressibilities. (*Hall*, 2-31. *Courtesy AIME.*)

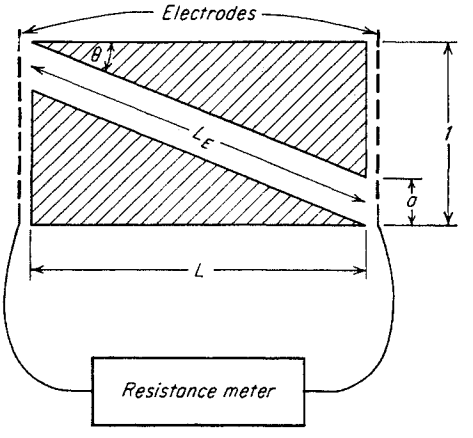

Fig. 2-30. Derivation of electrical-resistivity factor.

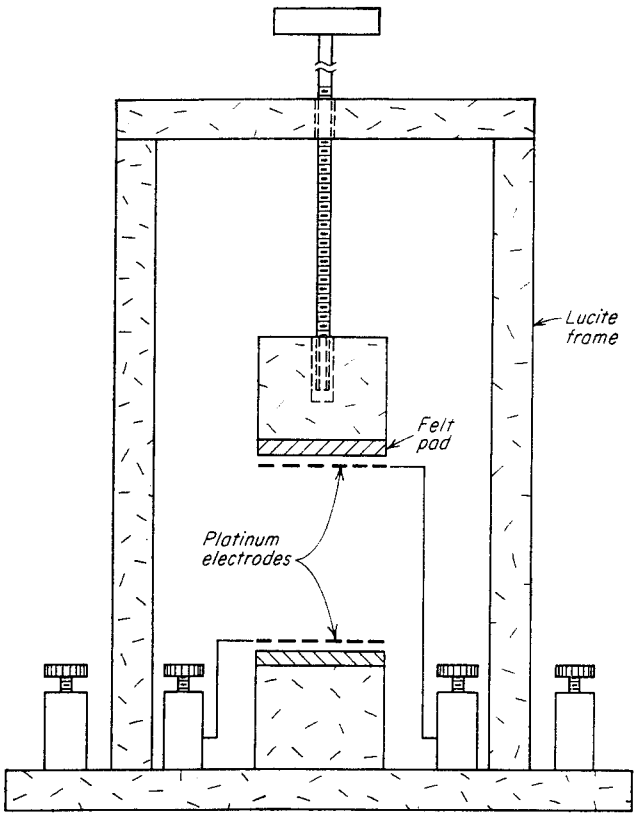

Fig. 2-31. Apparatus for measuring electrical resistivity of cores. (*Cornell*, 2-20.)

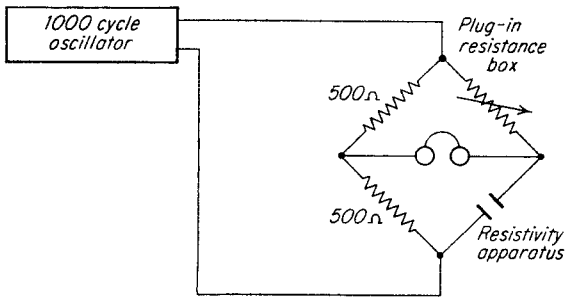

Fig. 2-32. Electric circuit for resistivity measurement. (*Cornell*, 2-20.)

understanding flow through the pore structure of rocks.

To measure the electrical resistivity of a core plug, the plug is extracted, dried, and saturated with 0.100 N KCl solution prepared with freshly boiled water. An apparatus to hold the plug (Fig. 2-31) provides contacts with the solution in the core. The electric circuit (Fig. 2-32) provides that an audio-frequency oscillator and a Wheatstone bridge circuit be used to measure the resistivity of the core. The resistivity factor is computed as the ratio of the resistance of the core specimen to the known resistance of an equal volume of 0.100 N KCl solution.

Illustrative Problem

A core specimen 0.724 in. in diameter and 0.65 in. long has a resistance of 715 ohms at 27.3°C when saturated with 0.1 N KCl solution. What is the resistivity factor for the specimen?

Solution

From the resistivity of KCl solutions, 0.1 N KCl has a resistance of 74.3 ohm-cm at 27.3°C.

$$\text{Resistivity factor } F = \frac{715 \times 3.1416 \times (0.724 \times 2.54)^2}{0.65 \times 2.54 \times 4 \times 74.3} = 15.5$$

The formation resistivity factor becomes of great importance when interpreting resistivity data obtained in the electrical logging of wells. Data on sands in the Gulf Coast by Archie (2-2) are given in Fig. 2-33. The influence of cementation and porosity on the resistivity factor is given in Fig. 2-34 (1-14).

Connate Water in Cores

Many petroleum deposits occur in beds originally containing water. In the accumulation process, water was retained in the porous rock and remains there along with oil or gas. Such water is called *connate water*. The fraction of the pore space containing connate water is of interest, since only the remainder can contain petroleum.

It is possible to obtain cores with oil-base muds and find their water content. Early works on connate

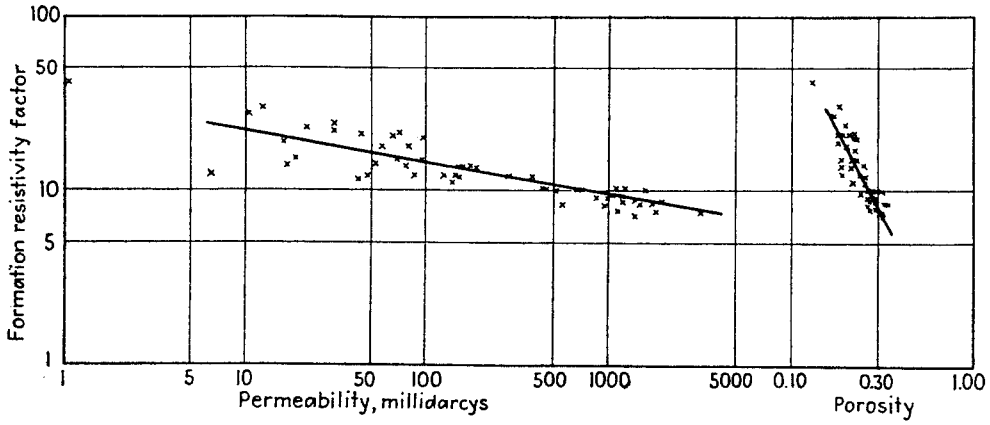

Fig. 2-33. Relation of porosity and permeability to formation resistivity factor for Gulf Coast consolidated sandstone cores. (*Archie*, 2-2. *Courtesy AIME.*)

water include Pyle and Jones (2-57) and Schilthuis (2-63), whose results on connate-water contents of cores are shown in Fig. 2-35, where water content is plotted against dry permeability.

The need for understanding rock properties and interfacial relationships that control connate-water content becomes immediately evident. After the nature of wetting is discussed, methods of measuring the water content of a core by capillary-pressure measurements will be given.

Wettability of Solids

A person driving a car in the rain becomes conscious of the wettability of the windshield by water and of the influence of oil or other substances on the spreading of a smooth film of water over the glass. Water placed on a hot metal surface will form spherical drops, which roll and bounce on the surface without covering or wetting it. Complete wetting or complete absence of wetting is relatively easy to describe;

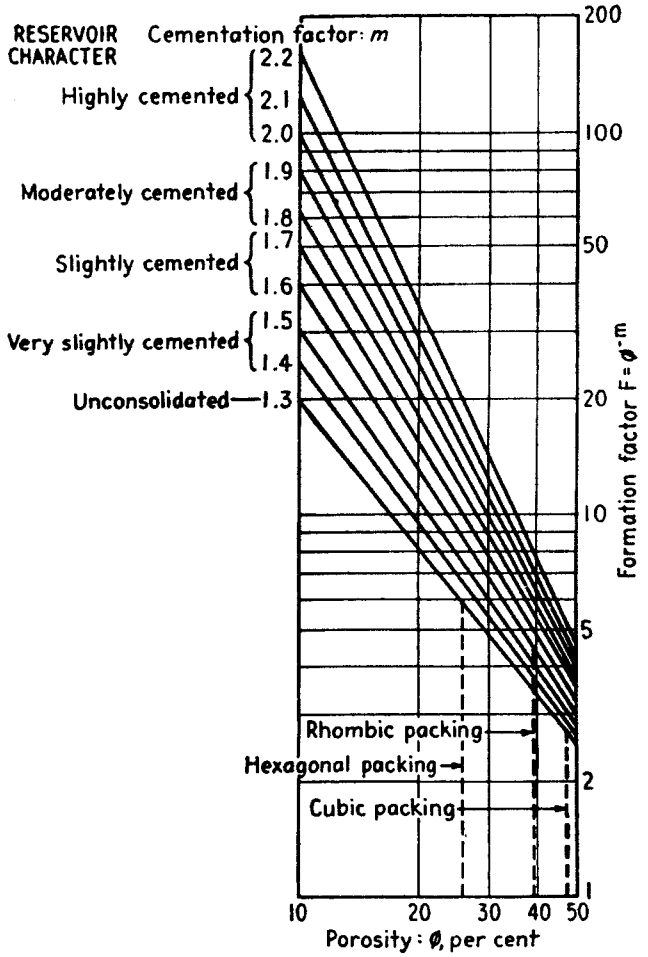

Fig. 2-34. Formation resistivity factor F as a function of porosity for various cementations. (*Pirson*, 1-14. *Courtesy McGraw-Hill Book Company, Inc.*)

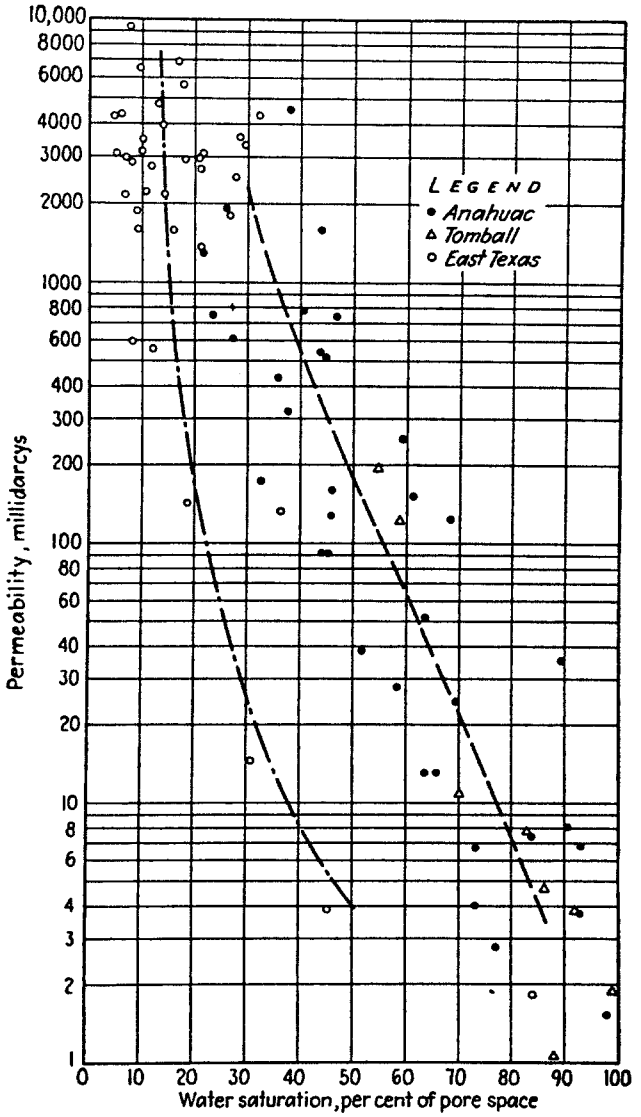

Fig. 2-35. Relation between permeability of cores and connate-water saturation. (*Schilthuis*, 2-63. *Courtesy AIME.*)

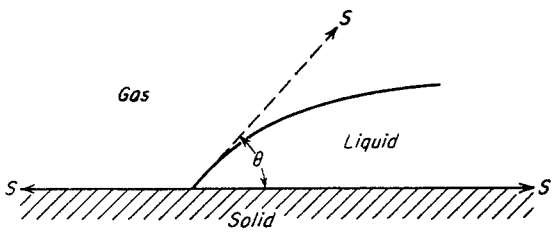

Fig. 2-36. Contact angle between two fluids in contact with a solid, as a measure of wetting.

it is the intermediate values that require more refinement. The contact angle between two fluids in contact with a surface is an accepted measure of the degree of wettability (2-6, 2-29, Fig. 2-36). The interfacial tensions are in balance, according to Eq. (2-19).

$$S_{g,s} = S_{l,s} + S_{g,l} \cos \theta \qquad (2\text{-}19)$$

where S = interfacial tension
g = gas
s = solid
l = liquid
θ = contact angle

The contact angle becomes a method of expressing the degree of wetting, with contact angles of 0° through the wetting fluid for high degree of wetting and angles of 180° through wetting fluid for no wetting. Figure 2-37 illustrates results by Benner and Bartell (2-6, 2-7), showing that it is physically possible to observe the various degrees of wetting with intermediate contact angles from 0 to 180°. Surfaces wet by water are called *hydrophilic* and those not wet, *hydrophobic.*

The fact that water wets silica and calcite is a reason that most petroleum reservoirs have retained connate water. The deposition of complex organic substances such as asphalt on the surface of sand changes its wettability (2-40), and some oil fields may have little or no connate water when the rock surface is altered by the presence of such substances in crude oils. It should be recognized that water can be retained by porous media in the accumulation process because of the configuration of the interstices of the rock regardless of surface phenomena. Gas sands would be expected to be wet by water and to contain connate water. Hough, Rzasa, and Wood (2-36) found that, under some conditions, water no longer wets the stainless-steel tip they used to measure the interfacial tension between methane and water at reservoir temperatures and pressures. It is possible that water does not completely wet sand in contact with gases under certain conditions.

Slobad and Blum (2-64) presented a method of determining wettability of reservoir rocks, consisting of making two displacement experiments. The first is the displacement of water by oil and the second is the displacement of oil by air. The threshold (initial desaturation) pressures for these two tests together with the interfacial tensions oil to water and oil to air are used to define a wettability number, W.

$$W = \frac{\cos \theta_{o,w}}{\cos \theta_{a,o}} = \frac{P_{o,w}\sigma_{a,o}}{P_{a,o}\sigma_{o,w}} \qquad (2\text{-}20)$$

where o = oil
w = water
a = air
$P_{o,w}$ = threshold displacement pressure, oil displacing water
σ = interfacial tension

The apparent contact angle $\theta_{o,w}$ of the water phase can be computed from Eq. (2-21), assuming that $\cos \theta_{a,o}$ is unity.

$$\cos \theta_{o,w} = W \qquad (2\text{-}21)$$

For complete wetting by water, the contact angle $\theta = 0°$ and the wettability number $W = 1.0$; for nonwetting, $\theta = 90°$ and $W = 0$. Table 2-8 gives data obtained by measurements of the type described. Slobad and Blum also found that treatment of cores in the laboratory could change the wettability significantly.

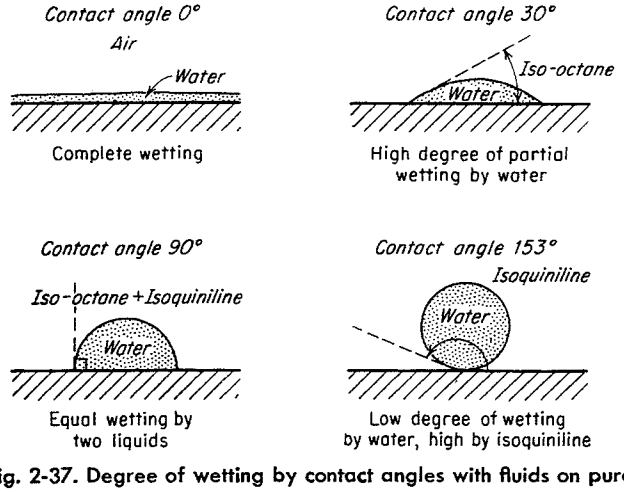

Fig. 2-37. Degree of wetting by contact angles with fluids on pure silica. (*After Benner and Bartell,* 2-6.)

Capillary Pressure

To understand liquid retention by porous solids, the interfacial tensions between liquids or between a liquid and a gas must be considered. The surface tension of a liquid in the presence of gas is measured by the capillary rise in fine-bored glass tubes (Fig. 2-38). When the liquid wets the surface of the glass capillary, it pulls the liquid up the tube. The surface tension around the periphery of the tube is balanced by the downward force due to the column of liquid that has risen above the free surface. The equation expressing this balance is

$$\cos \theta \, \sigma(2\pi r) = \pi r^2 h(\rho_L - \rho_V)g \qquad (2\text{-}22)$$

where σ = surface tension, dynes/cm
r = radius of tube, cm
h = capillary rise, cm
ρ_L = density of liquid, grams/cu cm
ρ_V = density of vapor, grams/cu cm
g = acceleration due to gravity, 980.6 cm/sec²
θ = contact angle between liquid and solid; $\cos \theta = 1$ when $\theta = 180°$, for complete wetting

It is possible to apply pressure above the liquid in the capillary sufficient to lower the meniscus to the

Table 2-8. Comparison of Wettability of Core Samples of Different Origins*

Core no.	Description	Initial desaturation pressure, psi		Wettability number†	Apparent contact angle
		Air-oil	Oil-water		
BTL	Devonian limestone	6.5	6.1	0.84	33°
BTN		6.8	6.2	0.81	36
BTO		6.25	6.0	0.85	31
BTP		6.4	3.9	0.54	57
1588	Yates sandstone	0.86	0.32	0.33	71
1589		0.85	0.3	0.31	71
1590		0.85	0.31	0.32	71
1591		1.00	0.4	0.36	69
1542	Alundum (RA 1139)	0.70	0.25	0.32	72
1543		0.70	0.28	0.36	69
1544		0.68	0.4	0.52	59
1545	Synthetic	0.67	0.28	0.37	68
1592	Clearfork	0.72	0.24	0.30	73
1593		0.54	0.32	0.53	58
1594	Limestone	1.58	0.32	0.18	80
1595		2.90	0.45	0.14	82
1620	Tensleep sand	0.86	0.21	0.22	78
1621		0.86	0.21	0.22	78
1622		0.68	0.12	0.16	81
1623		0.86	0.27	0.28	74

* Routine extraction with chloroform preceded wettability tests except for alundum, which had been regenerated at 1400°F for 3 hr.

† Air-oil surface tension, 24.9 dynes/cm. Oil-water interfacial tension, 28.0.

SOURCE: Slobad and Blum (2-64).

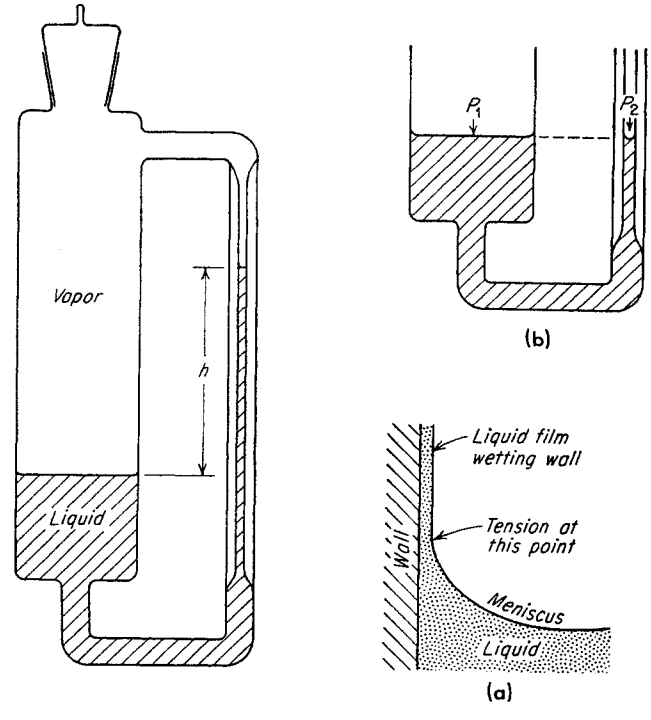

Fig. 2-38. Surface tension by capillary rise.

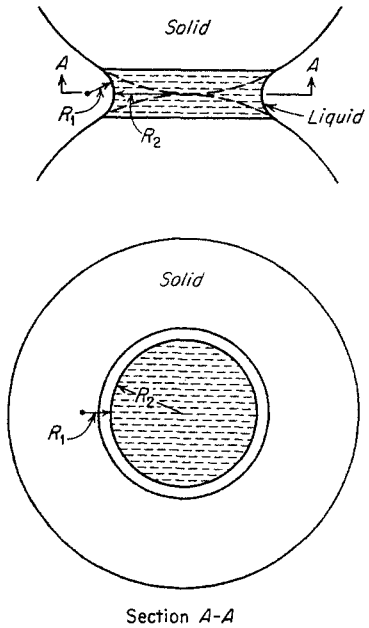

Fig. 2-39. Radii of curvature between particles. (Leverett, 2-47. Courtesy AIME.)

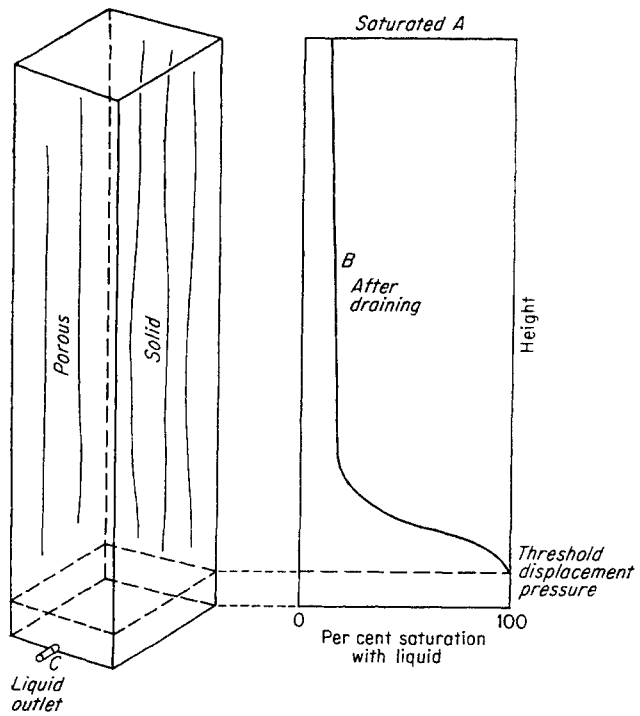

Fig. 2-40. Saturation after draining liquid from porous medium.

level of the bulk liquid. This pressure is computed from Eq. (2-23).

$$2\pi r\sigma = \pi r^2 hg(\rho_L - \rho_V) = \pi r^2(P_2 - P_1)g_c \quad (2\text{-}23)$$

where P = pressure, grams force/sq cm
g_c = conversion factor = 980.6 (grams mass/gram force)(cm/sec^2)

Solving for an equation between pressure difference and surface tension,

$$P_c = P_2 - P_1 = \frac{2\sigma}{rg_c} \quad (2\text{-}24)$$

The pressure difference $P_2 - P_1$ is called the capillary pressure P_c. When the contact angle of liquid is not 0°,

$$P_c = \frac{2\sigma \cos\theta}{rg_c} \quad (2\text{-}25)$$

A pressure difference of P_c occurs across the meniscus in the capillary, when pressure is used to depress the capillary rise completely.

For a capillary or a space between particles that has a shape other than cylindrical, the capillary pressure is related to the curvature of the meniscus by Eq. (2-26).

$$P_c = \frac{\sigma}{g_c}\left(\frac{1}{R_1} + \frac{1}{R_2}\right) \quad (2\text{-}26)$$

where R_1 and R_2 are principal radii of curvature of the menisci, as shown in Fig. 2-39 (2-47).

Consider the case of a porous medium saturated with a liquid (Fig. 2-40), the concentration of liquid shown by line A. Allow the liquid to drain through opening C. At equilibrium, the liquid saturation will take the form shown by curve B. The liquid saturation is 100 per cent at and below C. Some large pores hold the liquid only a small distance above C, and, therefore, with a variation in pore sizes, the curve takes the shape shown. The vertical section can represent either very fine continuous pores sufficiently small to hold the liquid to the heights shown or individual volumes of liquid retained in the spaces with the smaller radii of curvature.

Many studies have been made to determine the connate-water content of cores by capillary-pressure measurements (2-47, 2-68, 2-33, 2-9, 2-70, 2-51, 2-34, 2-62, 2-16). Since the process of displacing the water is akin to that which occurred in the reservoir during gas accumulation, this is sometimes described as the restored-state method. A typical device for obtaining the effect of drainage of water from cores is the capillary-pressure cell (Fig. 2-41). Core plugs saturated with water are placed in contact with a wet, fine, porous plate. Air or gas pressure is admitted over the cores, and water drains out of the plugs. At a given gas pressure, the water content is allowed to come to equilibrium and then measured by weighing; the plug is returned to the cell, and the gas pressure is increased. Gas pressure forces water out of the pores in the core down to the level of the porous plate, just as gas pressure reduced the capillary rise in Fig.

2-38*b*. The porous plate must have such fine pores that gas will not displace the liquid from it at the highest gas pressure used. Figure 2-42 shows typical miscellaneous curves of saturation versus air pressure, and Fig. 2-43 and Table 2-9 give results of cores from Louisiana Miocene, well *A* (2-68). In general the higher-permeability cores have lower water saturations than low-permeability cores.

Raising the air pressure on the cell or the capillary pressure on the core reduces the water content in much the same way as raising the elevation of the core position above the gas-water interface in a reservoir. In the laboratory, water and air are used to determine capillary pressure; in the reservoir, gas under pressure is in contact with the reservoir water. The relationship of these pressures and interfacial tensions is given by Eqs. (2-27).

$$\frac{P_{c,res}}{P_{c,lab}} = \frac{c\sigma_{res} \cos \theta_{res}}{c\sigma_{lab} \cos \theta_{lab}}$$

$$P_{c,res} = P_{c,lab} \frac{\sigma_{res} \cos \theta_{res}}{\sigma_{lab} \cos \theta_{lab}} \qquad (2\text{-}27)$$

$$= \frac{h}{144} \frac{(\rho_l - \rho_g)_{res} g}{g_c}$$

where P_c = capillary pressure difference, psia
h = height of core above water level, ft
ρ_l = density of liquid, lb/cu ft
ρ_g = density of gas, lb/cu ft
res = reservoir
lab = laboratory
g/g_c = lb force/lb mass = 1.0

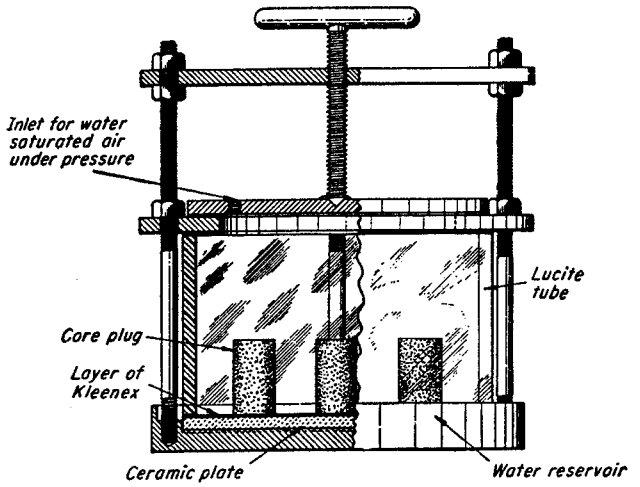

Fig. 2-41. Apparatus for determining connate water by capillary pressure. (2-41.)

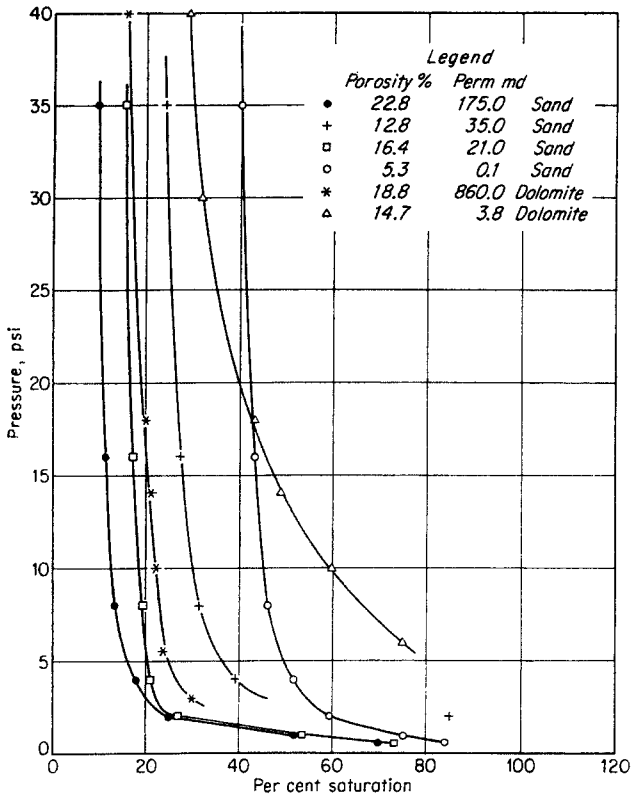

Fig. 2-42. Miscellaneous capillary pressure–saturation curves.

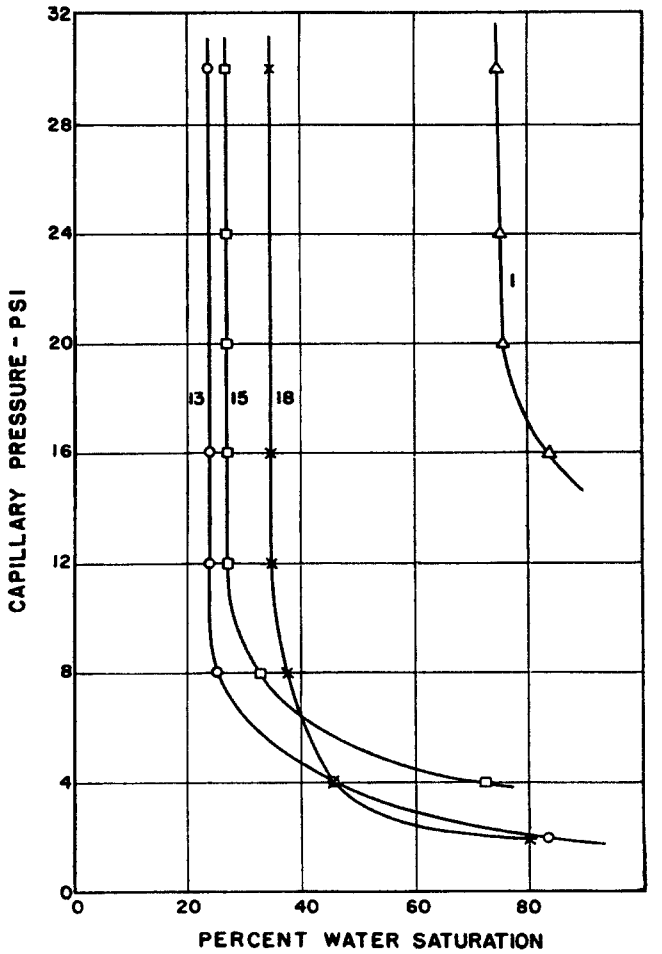

Fig. 2-43. Pressure-saturation curves—well A. (*Thornton and Marshall, 2-68. Courtesy AIME.*)

Table 2-9. Water Saturation, Well *A*

Sample no.	Permeability, md	Porosity, %	Distance above water level, ft	Laboratory pressure, psi	Interstitial water saturation, % of porosity			
					(1) By distillation	(2) From salinity	(3) Capillary method	(4) (3) − (2) Difference
1	29	17.0	78	59	89	71	74	+3
2	312	29.3	74	56	28	23	23	0
3	382	22.3	70	53	52	37	37	0
4	518	28.1	66	50	29	34	33	−1
5	250	23.0	61	47	53	36	38	+2
6	63	16.0	54	41	73	61	61	0
7	2,556	27.2	51	39	36	28	28	0
8	23	20.0	48	37	82	59	59	0
9	319	25.7	43	33	44	32	27	−5
10	1,830	31.1	40	31	19	20	19	−1
11	550	27.1	37	29	47	44	40	−4
12	1,490	27.2	35	27	44	38	38	0
13	1,118	31.0	33	26	30	25	24	−1
14	1,730	32.6	32	25	27	23	24	+1
15	540	27.9	31	24	35	29	27	−2
16	1,048	28.6	30	24	36	34	25	−9
17	410	27.5	29	23	38	37	35	−2
18	1,960	27.4	28	23	33	34	34	0
19	2,238	29.8	24	20	36	34	26	−8
20	1,120	30.9	22	19	32	28	30	+2
Average.....	.....	....	...	...	43	36	35	−1.3

SOURCE: Thornton and Marshall (2-68).

For example, a core taken 20 ft from the gas-water interface in a gas reservoir would require a capillary pressure of 8.05 psi,

$$\Delta P = \frac{20 \times 58}{144} = 8.05 \text{ psi}$$

to bring it to the restored state for this position. Thornton and Marshall (2-68) computed the corresponding laboratory pressure for each position of the cores in Table 2-9, assuming that the density of water was 67.4 lb/cu ft, that the density of oil was 31.8 lb/cu ft, and that the pressure at the water level was 1.5 psi.

The connate-water content of cores depends in a general way upon permeability, but the nature of the interstices is also important. Figure 2-44 shows variations in connate water with capillary pressure for dolomite cores which have a combination of solution and matrix porosity. The clay content of sands has a marked effect on connate water.

Figure 2-45 gives typical curves of connate water for various reservoir media. It should be appreciated that each curve is an average of several points. Although the scatter of points for the several curves is not likely to be so great as the scatter shown in Fig. 2-44, similar effects are observed for all natural rock. Richardson, Perkins, and Osoba (2-59) have shown the effects of aging on the surface characteristics of cores.

Use of Centrifuge

The centrifuge has been shown to be a useful device for measuring capillary pressure (2-34, 2-65, 2-50), using the centrifugal force on the liquid as a substitute for gas pressure. Figure 2-46 (2-65) shows a core holder, and Fig. 2-47 gives the effect of time for a speed corresponding to a static air pressure of 35 psi. In the usual operation, the core is rotated at a series of selected speeds of increasing value long enough to obtain equilibrium as judged by the constancy of the liquid displaced. A comparison (Fig. 2-48) of the results from the centrifuge and from static tests in apparatus similar to that of Fig. 2-41 is taken from Slobad, Chambers, and Prehn (2-65). In some cases, oil or other hydrocarbons are used instead of air as the displacing fluid.

Marx (2-50) has presented a method for predicting the centrifuge speed to give fluid removal in the laboratory equivalent to that in the reservoir. The

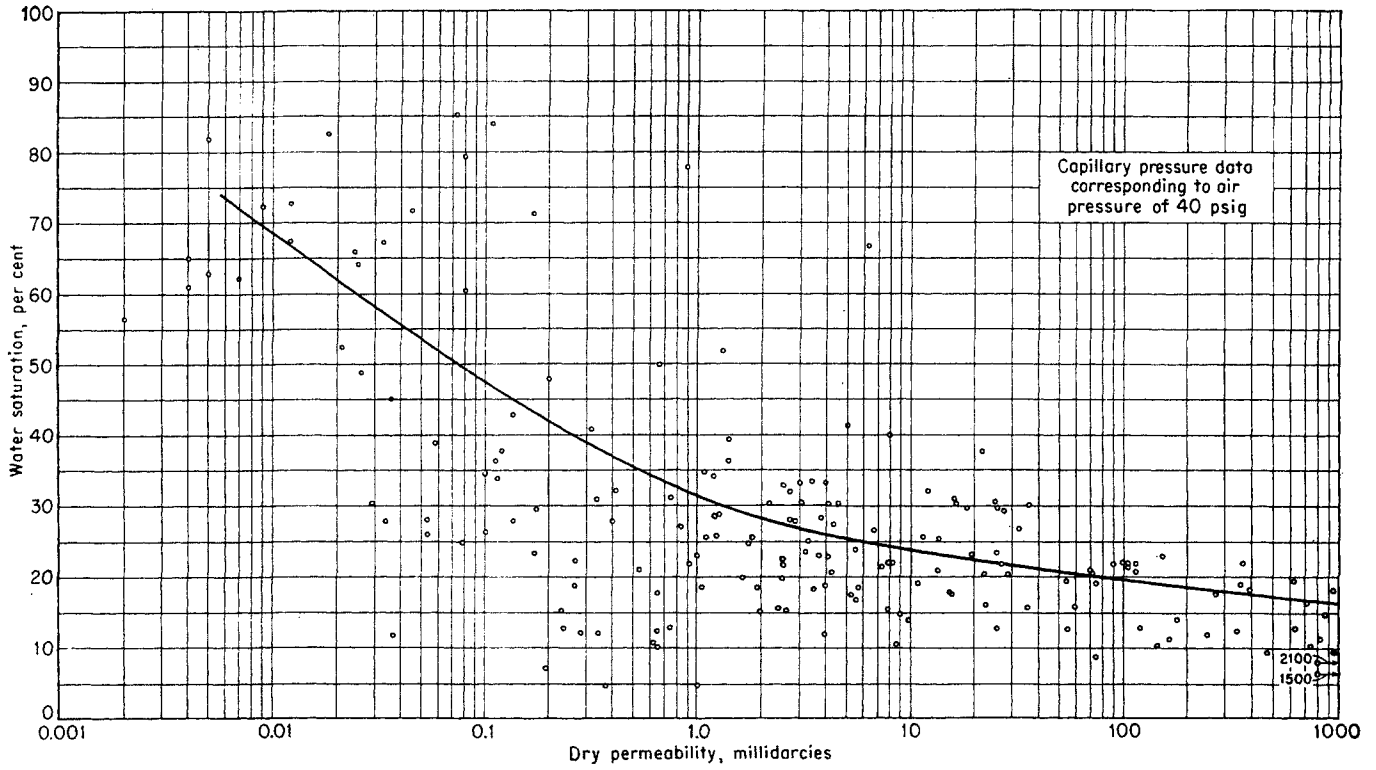

Fig. 2-44. Permeability vs. connate water by capillary pressure. (*Katz, Turner, Grimm, Elenbaas, and Vary, 1-36. Courtesy AIME.*)

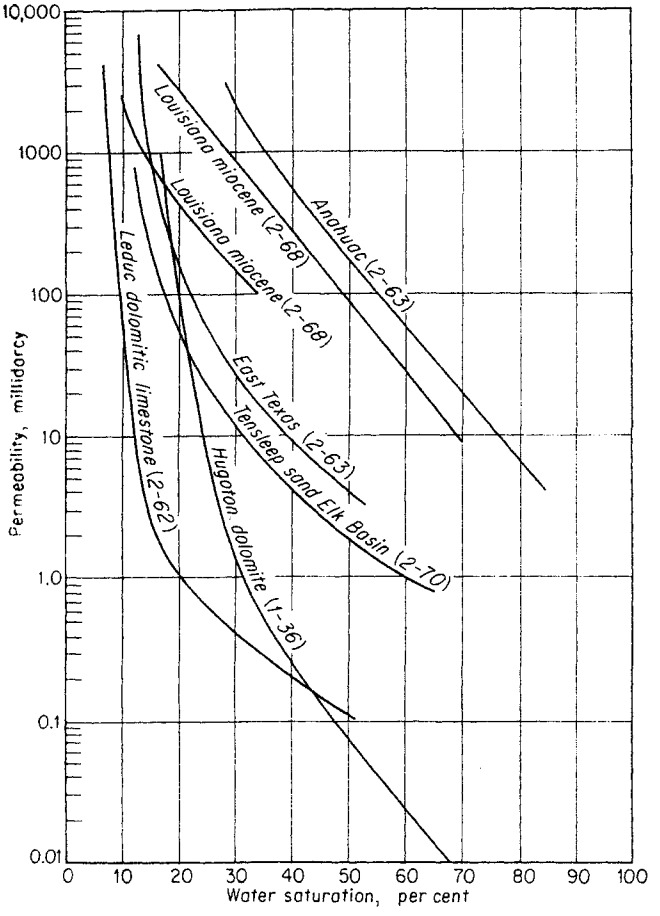

Fig. 2-45. Typical connate-water curves.

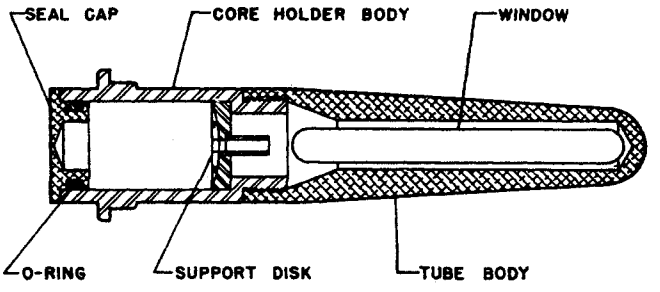

Fig. 2-46. Core holder for capillary-pressure determination in centrifuge. (*Slobod, Chambers, and Prehn, 2-65. Courtesy AIME.*)

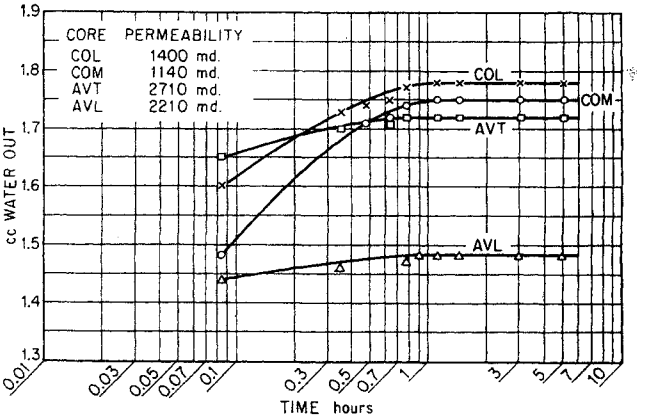

Fig 2-47. Interstitial water saturation in core centrifuged at 2,300 rpm using water-air system. (*Slobad, Chambers, and Prehn, 2-65. Courtesy AIME.*)

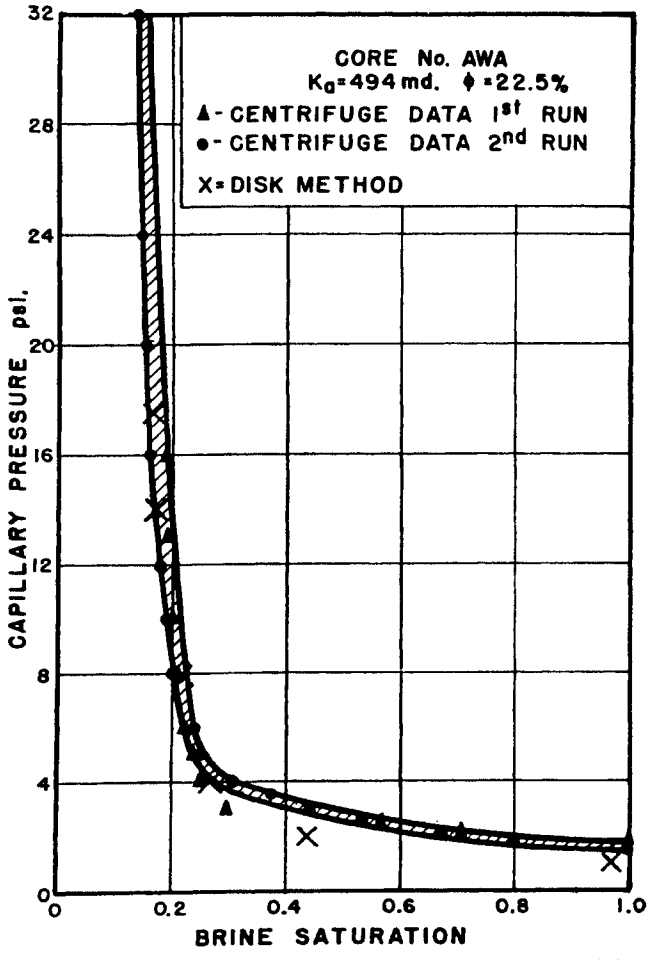

Fig. 2-48. Capillary-pressure curve showing reproducibility. (*Slobod, Chambers, and Prehn, 2-65. Courtesy AIME.*)

capillary end effects in the model and reservoir are the same when

$$h = \frac{a}{g} h_m \tag{2-28}$$

where h_m = height of centrifuge specimen
h = height of model or reservoir
a = acceleration
g = gravity

When end effects are important, the relation between time t for the reservoir or model and time t_m for the centrifuge specimen is obtained from Eq. (2-29).

$$t = \left(\frac{a}{g}\right)^2 t_m \tag{2-29}$$

Marx showed that a centrifuge specimen 2.92 cm long when centrifuged at 525 revolutions per minute (rpm) in a centrifuge at 16.8 cm with times related by Eq. (2-29) gave the same drainage percentages as a model 154 cm high. The ratio of times is found by Eqs. (2-28) and (2-29). It is

$$\frac{t}{t_m} = \left(\frac{a}{g}\right)^2 = \left(\frac{h}{h_m}\right)^2 = \left(\frac{154}{2.92}\right)^2 = 2{,}790$$

The centrifuge takes 1/2,790 as much time as the column 154 cm tall. The centrifuge speed is computed by

$$\frac{a}{g} = 1.118 \times 10^{-5} N^2 r \tag{2-30}$$

where N = speed of centrifuge, rpm
r = mean radius of centrifuge, cm

$$N = \frac{154}{2.92} \frac{1}{16.8 \times 1.118 \times 10^{-5}} = 525 \text{ rpm}$$

Capillary Pressure and Pore-size Distribution

Purcell (2-56) presented a method of measuring capillary pressure by mercury injection, using apparatus similar to that of Fig. 2-7. The relationship between mercury-air and water-air capillary pressures is given by Eq. (2-31).

$$\frac{\text{Mercury-air capillary pressure}}{\text{Water-air capillary pressure}} = \frac{-480 \cos 140°}{70 \cos 0°} \approx 5 \tag{2-31}$$

Thus, the saturations can be compared when the mercury pressure is 5 times the air pressure in the air-water measurement, as in Fig. 2-49 (2-56). The method has the advantages of speed and the use of high pressures. Also, it can be used on chips or small pieces of core. The permeability of the core can be calculated from the mercury-injection curve by

$$K = 0.66 C \phi \int_{S=0}^{S=100} \frac{dS}{P_c^2} \tag{2-32}$$

where K = permeability, millidarcys
C = conversion factor required to make equality true (0.216 on Paluxy and upper Wilcox sands)
ϕ = porosity, per cent
S = saturation, per cent
P_c = capillary pressure by mercury injection, atm

The factor C can be determined on a standard core specimen and then used for small pieces of similar rock.

Relationship between the Formation Resistivity Factor, Capillary Pressure, and Permeability

Since the formation resistivity factor, the capillary-pressure characteristics, and the permeability of reservoir-rock materials are all determined by the size and shape of the pore structure, one would expect to find a relationship existing between these quantities. The formation resistivity is a measure of the effective pore length, and the capillary pressure is a measure

of the effective pore-diameter distribution. These values can, therefore, be used to determine the permeability, which is fixed by the pore lengths and diameters. Such a relationship would be very useful when permeability data are lacking, as when only small fragments of the reservoir rock are available.

Poiseuille's law for viscous flow through capillaries is given in Eq. (2-33).

$$v_e = \frac{g_c D_e^2(-\Delta P_f)}{32 L_e \mu} \tag{2-33}$$

where v_e = effective pore velocity
D_e = effective pore diameter
$-\Delta P_f$ = pressure drop
L_e = effective pore length
μ = viscosity

The effective area for flow is the same as the effective area for the electric resistance determined previously. The effective pore velocity v_e, accordingly, is given by Carman (2-18) as follows:

$$v_e = \frac{vL_e}{\phi L} \tag{2-34}$$

where v is the measured superficial velocity based on the over-all dimensions of the rock sample. It is to be noted that a less accurate formula for effective velocity has found widespread use both before and after the appearance of the work by Carman; this is the Dupuit assumption that $v_e = v/\phi$ (2-18). The use of the Dupuit assumption is to be avoided.

By means of the formation-resistivity-factor Eq. (2-18), the effective-velocity Eq. (2-34), and the capillary-pressure Eq. (2-25), the unknown quantities D_e, v_e, and L_e can be eliminated from Poiseuille's law.

$$v = \frac{(\sigma \cos\theta)^2(-\Delta P_f)}{2\mu F L g_c P_c^2} \tag{2-35}$$

Thus the flow velocity through all pores of such size that capillary pressure is P_c is given by Eq. (2-35). In general, there will be a fraction $d\phi$ of all the pores, having this particular pore size. The volume rate of flow of fluid through this fraction of the porosity is

$$dQ = vA\, d\phi = \frac{(\sigma \cos\theta)^2(-\Delta P_f)A}{2\mu F L P_c^2 g_c}\, d\phi \tag{2-36}$$

where A is the sample cross-sectional area.

The total flow rate through all of the pores is found by integrating Eq. (2-36), remembering that P_c varies with saturation or with ϕ, according to the capillary-pressure curve.

$$Q = \frac{(\sigma \cos\theta)^2(-\Delta P_f)A}{2\mu F L g_c} \int_0^{\phi} \frac{d\phi}{P_c^2} \tag{2-37}$$

Ordinarily, a graphical integration of $d\phi/P_c^2$ will be required.

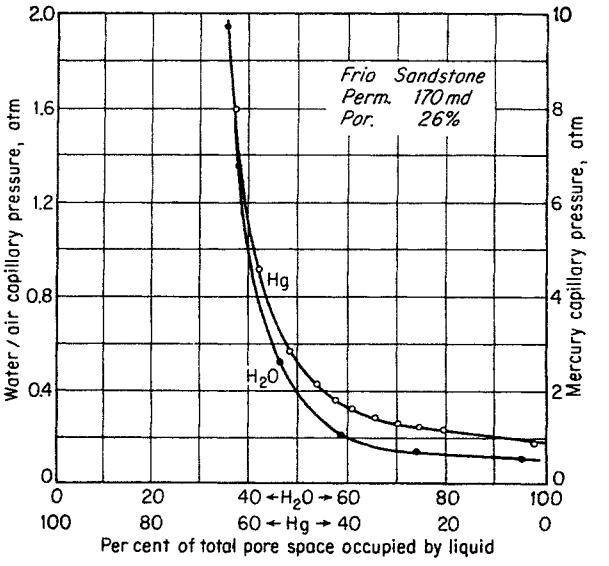

Fig. 2-49. Comparison of capillary-pressure results with mercury and air-water. (*Purcell*, 2-56. *Courtesy AIME.*)

Since the total flow is that given by Darcy's law, Eq. (2-2), the permeability may next be found.

$$K = \frac{(\sigma \cos\theta)^2}{2Fg_c} \int_0^{\phi} \frac{d\phi}{P_c^2} \tag{2-38}$$

When K is expressed in millidarcys, σ in dynes per centimeter, porosity in decimals, and pressure in atmospheres, the permeability equation becomes

$$K = \frac{0.0494(\sigma \cos\theta)^2}{F} \int_0^{\phi} \frac{d\phi}{P_c^2} \tag{2-39}$$

Flow of Two Phases—Relative Permeability

Recovery of crude oil involves the simultaneous flow of oil and gas through porous media. In the production of gas fields, condensate and water movement accompanying gas flow involves the flow of two phases. The simplest way to handle two-phase flow is to consider the flow of a given phase relative to the flow that would take place if that phase only were present in the porous medium. This ratio of the permeability of a phase in two-phase flow to the single-phase permeability is called *relative permeability*.

Many investigators have contributed to the study of simultaneous flow of two or more phases, including (2-8, 2-11, 2-12, 2-32, 2-45, 2-46, 2-48, 2-52 to 2-54, 2-58, 2-61, 2-74). Only a brief discussion of the subject is given here. Consider two phases flowing simultaneously through a porous plug (Fig. 2-50). The permeability of the porous medium is measured for a single-phase liquid to obtain K_l. With the simultaneous flow of a gas and of a liquid such as oil or water, the flow rates for each phase are used to compute the permeability of the medium to that phase.

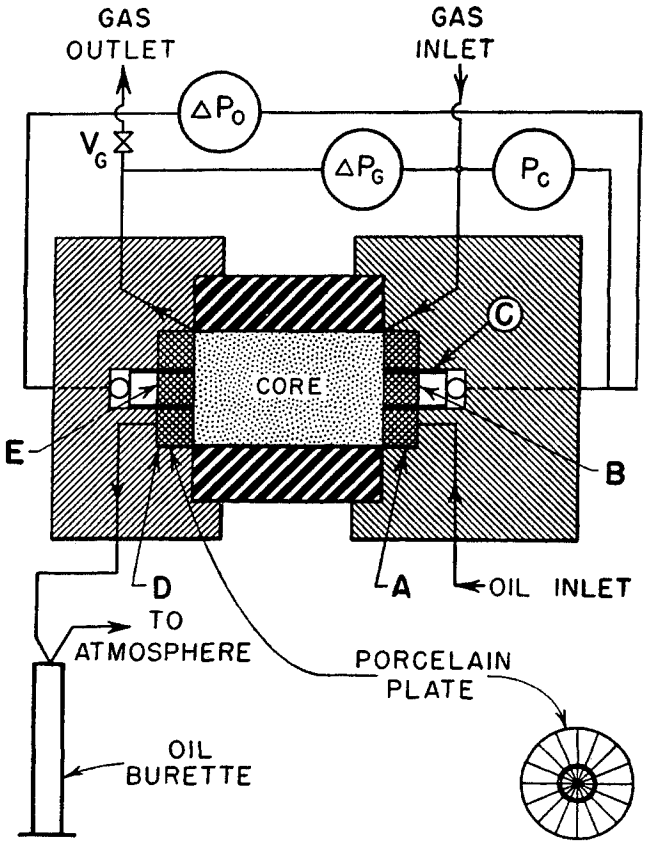

Fig. 2-50. Apparatus for two-phase flow. (*Osoba, 2-54. Courtesy AIME.*)

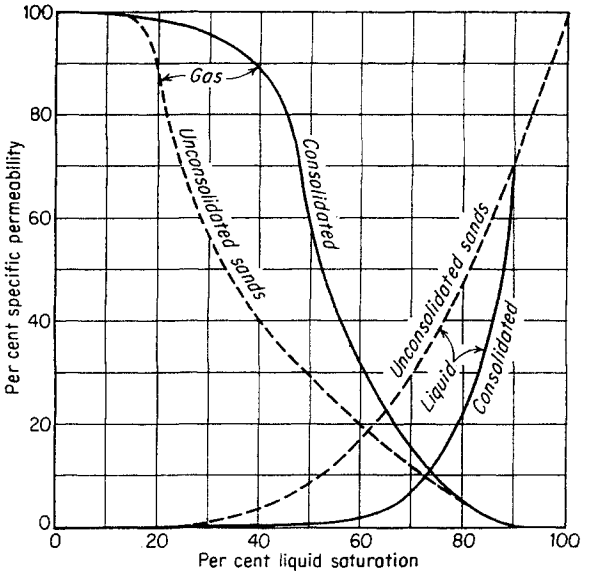

Fig. 2-51. Relative permeability for consolidated and unconsolidated sands. (*After Botset, 2-8.*)

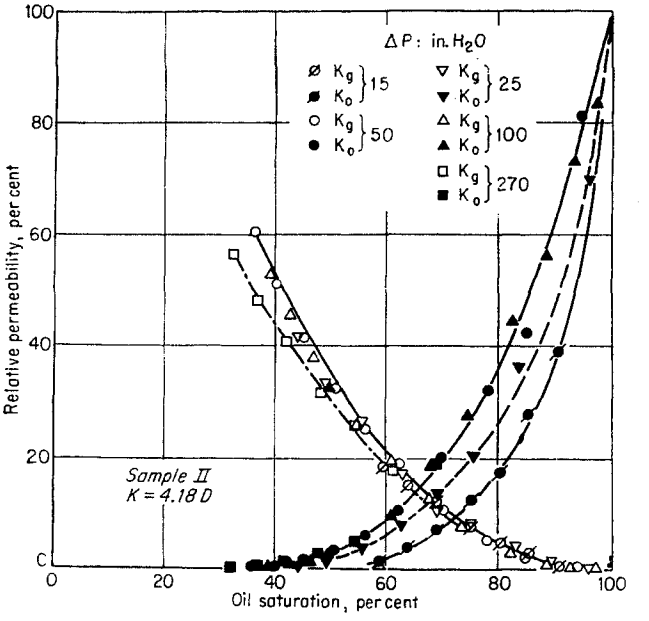

Fig. 2-52. Gas-drive relative permeability with varying pressure differential. (*Osoba et al., 2-54. Courtesy AIME.*)

This permeability divided by the K_l above gives the relative permeability.

The prime variable in relative-permeability measurement is the percentage saturation of the pore space by the flowing phases. Figure 2-51 shows typical relative-permeability curves for gas and liquid flowing simultaneously through consolidated and unconsolidated sands. The curves show that gas will not flow until the gas saturation reaches some value from 10 to 15 per cent and that liquid will not flow when the saturation reaches some value from 30 to 45 per cent. Usually the sum of the relative permeabilities at a given saturation is considerably less than 100 per cent.

There are several variables of considerable importance in relative permeabilities, such as character of the porous medium, phases under consideration, and pressure gradient. Figure 2-52 shows that a greater pressure differential causes the liquid saturation to be reduced. An independent method of handling flow of two phases was advanced by Brownell and Katz, which clearly recognizes the influence of pressure differential on the residual saturation of liquid in a porous medium (2-10). The influence of a third phase is shown by Fig. 2-53 (2-48).

Fatt (2-28) has postulated a network model of interconnected tubes having a spectrum of radii. From this model he is able to predict the nature of capillary-pressure curves and of relative-permeability phenomena.

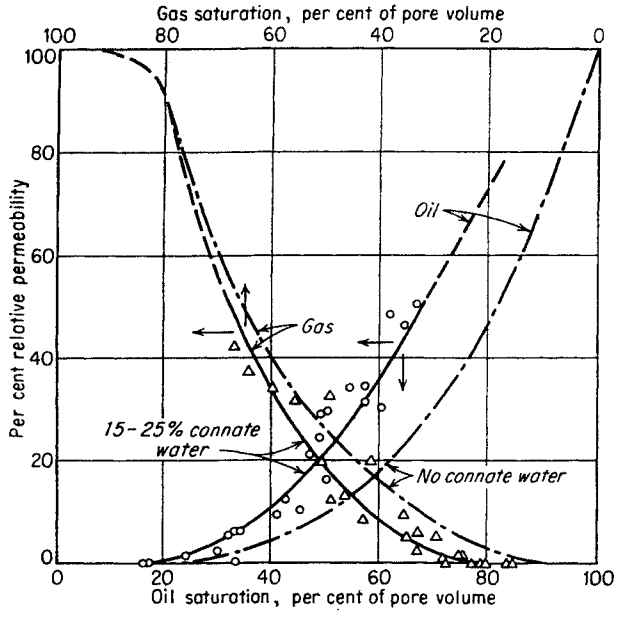

Fig. 2-53. Permeability to oil and gas with and without connate water. (*Leverett and Lewis*, 2-48. *Courtesy AIME.*)

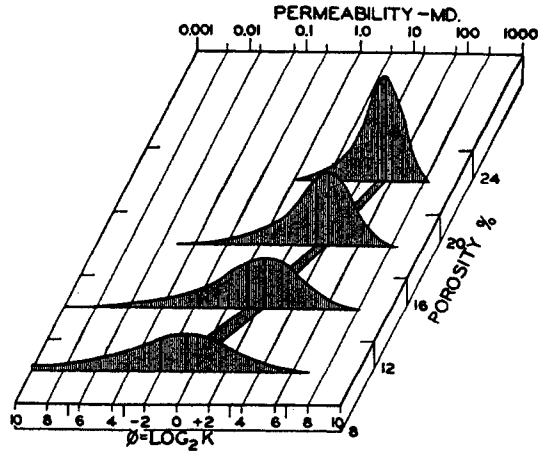

Fig. 2-54. Permeability distribution as a function of porosity—Wasson cores. (*Bulnes*, 2-13. *Courtesy AIME.*)

Porosity and Permeability Distribution

Bulnes (2-13) applied statistical methods to core-analysis data on dolomitic limestone at Fullerton. For any porosity range, the permeabilities took a probability-type distribution, as shown in Fig. 2-54. The per cent of the cores whose permeabilities exceed 1 millidarcy for Fullerton dolomitic limestone is shown in Fig. 2-55. These methods of analyzing core data yield a better estimate of the productive pore space of a reservoir.

A method of evaluating the porosities of cuttings by an examination of both cuttings and core specimen was developed by Katz, Turner, Grimm, Elenbaas, and Vary (1-36). The work encompassed sev-

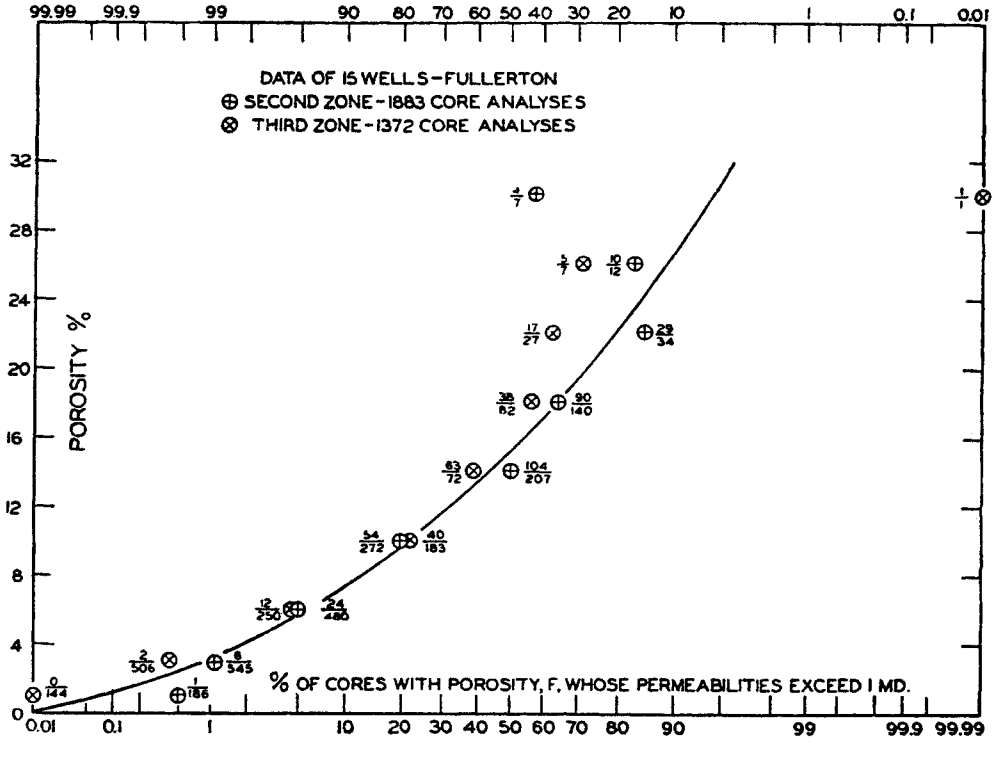

Fig. 2-55. Porosity—probability of permeability relationship. (*Bulnes*, 2-13. *Courtesy AIME.*)

Table 2-10. Chemical Analyses of Frio Waters

Well	Owner	Field	Depth, ft	Top of Frio, ft	Depth below top of Frio, ft	Analysis, ppm						Sample no.
						Na	Ca	Mg	Cl	SO_4	HCO_3	
Starr County												
No. 5, McKinney	Sun Oil Co.	Sun	4,128–4,133	2,550±	1,583	13,802	1,656	73	24,244	18	214	1
No. 1, Requenez	Sun Oil Co.	N. Sun	4,650–4,657	3,400±	1,257	13,819	2,444	58	25,896	53	116	2
No. 2, Vela	Sun Oil Co.	Boyle	2,579–2,590	1,600±	990	11,921	344	90	18,764	None	842	3
No. 1, Hall State	Sun Oil Co.	No. Rincon	3,481–3,485	2,300±	1,185	7,395	1,268	50	12,696	1,400	110	4
No. 1, Hall State	Sun Oil Co.	No. Rincon	4,615–4,619	2,300±	2,319	10,707	933	78	17,923	445	78	5
No. 1, L. Speer	Sun Oil Co.	Wildcat	5,406–5,436	2,750±	2,686	14,249	1,842	82	25,049	130	561	6
Kleberg County												
No. 1, Mark	Humble	Wildcat	5,222–5,243	3,795	1,523	13,756	2,400	24	25,300	160	201	7
No. 3, King Ranch Cabeza	Humble	Seeligson	4,695	4,010	685	8,257	738	35	14,000	111	128	8
No. 7, Cabeza	Humble	Seeligson	5,692–5,697	4,023	1,676	10,634	1,590	10	19,000	54	384	9
No. 31, King Ranch Paso Ancho	Humble	Stratton	6,669	4,217	2,452	5,809	195	18	8,750	None	1,068	10
No. 1, King Ranch Arroyo	Humble	Stratton	6,176–6,221	4,274	1,947	25,551	8,168	234	54,500	None	201	11
Nueces County												
No. 1, Isensee	Texas Conservative	Wildcat	5,968–5,984	4,640	1,344	19,481	2,148	91	34,050	30	140	12
No. 1, Webb	Humble	Flour Bluff	6,680	6,440	440	25,716	1,026	241	41,700	20	805	13
San Patricio County												
No. 2, W. E. Kirk	Shell	E. White Point	5,663–5,673	5,150±	523	29,282	2,925	589	51,783	None	148	14
Refugio County												
No. 1, O'Conner	Humble	O'Conner	4,720	3,706±	1,014	24,402	2,345	410	42,900	None	110	15
No. 2, O'Conner	Humble	O'Conner	4,486–4,489	3,706±	783	24,812	2,022	253	42,500	Tr.	122	16
No. 2, O'Conner	Humble	O'Conner	4,995–5,013	3,706±	1,309	25,900	1,034	115	42,000	None	256	17
No. A-4, T. O'Conner	Quintana	T. O'Conner	5,015	4,850±	165	25,217	1,454	218	42,000	None	244	18
No. 2, F. Heard	Humble	Greta	5,459	4,475	984	27,758	626	195	44,000	None	519	19
Calhoun County												
Welder "A" Tank Battery	Humble	Heyser	5,450	5,198	252	24,154	984	225	39,500	None	311	20
Jackson County												
No. 1, Issacson	Humble	Wildcat	4,598–4,604	4,555	33	21,271	1,832	93	36,200	None	262	21
No. 1, Issacson	Humble	Wildcat	5,450–5,453	4,555	898	18,229	1,052	68	30,000	6	344	22
No. 4, M. Branch	Humble	Ganado	6,632–6,635	5,046	1,589	23,319	652	123	37,250	None	442	23
No. 1, Spacek	Pure	W. Ganado	5,471–5,494	4,974	520	23,290	934	232	38,000	15	488	24
No. 2, Edwards	Humble	Maurbro	5,222–5,232	5,205	37	23,616	1,314	307	39,500	None	305	25
No. B-1, Four Way Ranch	Humble	N. La Ward	5,228	5,210	18	21,598	1,680	119	38,000	None	183	26
No. A-20, L. Ranch	Humble	Lolita	6,397–6,399	5,255	1,144	25,643	900	170	41,500	12	293	27
Wharton County												
No. 5, Cockburn	Humble	Magnet	5,535	5,489	46	30,583	2,352	376	52,000	Tr.	817	28
No. 1, Miller	Pure Oil Co.	Louise	5,808–6,820	5,145	1,685	19,957	870	109	32,400	Tr.	390	29
No. 1, Tank Battery	Texas Co.	Picket Ridge	5,500–	5,300±	200±	23,100	2,660	220	41,000	None	290	30
Matagorda County												
No. 1, Schmidt	Smith & McDannald	Hamman	8,207	8,124	83	34,965	4,350	450	62,800	101	98	31
No. 1, Unit	United North & South	Buckeye	7,926	7,706	220±	19,780	896	174	31,636	50	1,647	32
	Stanolind wellhead while swabbing	Lucky	8,556–8,561	7,900	661	16,968	244	59	26,053	51	1,198	33
	Stanolind from separator	Lucky	8,937–8,940	7,900	1,037	4,616	64	28	6,560	112	1,159	34
	Stanolind W.C. 1 mile north of field, taken while swabbing	Lucky	9,400–9,404	7,900	1,300	6,424	52	51	9,042	66	1,824	35
Brazoria County												
No. 1, J. O. Evans	Shell	Old Ocean	10,104–10,122	8,800±	1,322	.....	.....	...	14,600	.....	.....	36
No. 1, McKinney	Shell	Old Ocean	10,122–10,138	.....	1,338	.....	.....	...	18,100	.....	.....	37
No. 1, J. W. Reynolds	Shell possibly Tretolite contaminated	Old Ocean	10,103–10,124	.....	1,324	10,750	333	21	16,450	Tr.	1,348	38
	Stanolind sample from treater dump	Old Ocean	9,721–9,732	8,800±	932	10,779	98	21	15,769	60	1,815	39
	Stanolind from heating treater	Old Ocean	10,132–10,142	.....	1,342	14,155	137	64	21,276	151	1,507	40
	Stanolind from heating treater	Old Ocean	10,056–10,145	.....	1,345	7,180	24	17	9,928	256	1,808	41
No. 1, Andrau	Phillips	Chocolate Bayou	11,407	8,850	2,557	29,170	2,244	360	49,951	37	580	42
No. C-1, Blakley	Humble	Danbury	6,610–6,625	6,522±	102±	16,625	638	112	26,500	75	976	43
No. B-1, Moller	Humble	Danbury	5,670	5,600±	70±	27,400	1,104	29	43,800	None	921	44
No. 1, Mettler	Humble	Angleton	10,578–10,585	8,905±	1,580	17,581	1,688	68	29,800	None	854	45
No. 16, C. Brown	Humble	Hastings	6,118	5,762	356	38,852	1,804	322	64,000	None	183	46
No. 1, M. McFarland	Humble	Pledger	6,800±	6,557	150±	6,890	253	72	10,900	None	665	47
	Stanolind separator sample	Sandy Point	6,496–6,498	6,464	34	36,262	1,808	338	59,927	69	244	48
	Stanolind Bleeder on Xmas tree	Sandy Point	6,489–6,500	6,464	36	38,899	2,005	368	64,537	37	104	49

SOURCE: Jessen and Polshausen (2-38).

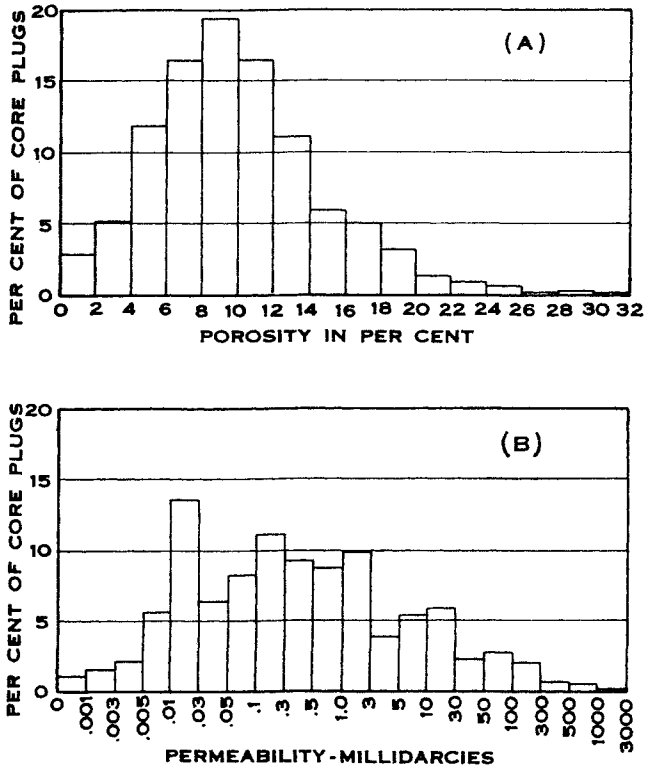

Fig. 2-56. Distribution of porosity and permeability of dolomite cores. (*Katz*, 2-41.)

eral hundred wells of Hugoton dolomite. The cores were separated into six grades by the geologists, and each core was given a rating of per cent of grade. The cores were all analyzed for porosity and permeability, with the distribution shown in Fig. 2-56. The porosity distribution by grades for all cores given a rating of 81 to 100 per cent of grade is shown in Fig. 2-57. A lower productive limit of 0.03 millidarcy was set, and the porosity by grades was similarly determined to find the productive porosity for each grade. The analysis of the core data permitted the assignment of a porosity to the cuttings as examined and graded.

Studies of pore-size distribution (2-12, 2-14) throw some light on the nature of the pores and their ability to produce commercially. The interpretation of core analyses for predicting oil production includes saturation determinations as well as determination of porosities and permeabilities (2-24).

Waters Associated with Rocks

Water containing variable amounts of dissolved solids is present in most porous rocks, whether or not

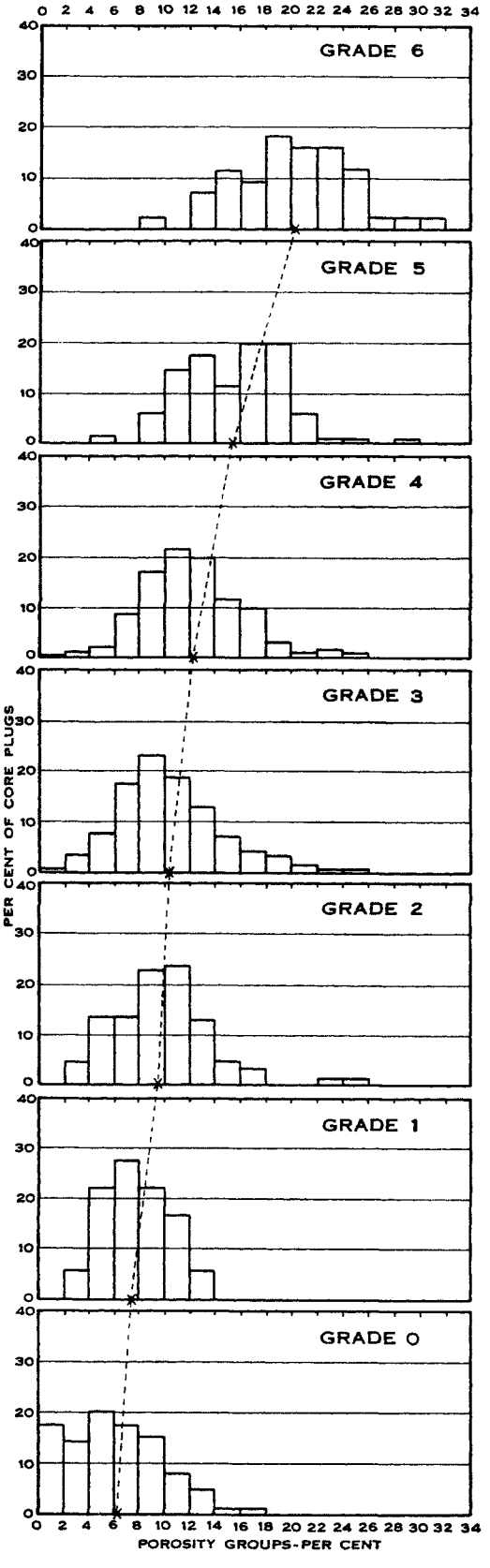

Fig. 2-57. Porosity distribution of core plugs by grades. (*Katz, Turner, Grimm, Elenbaas, and Vary*, 1-36. *Courtesy AIME.*)

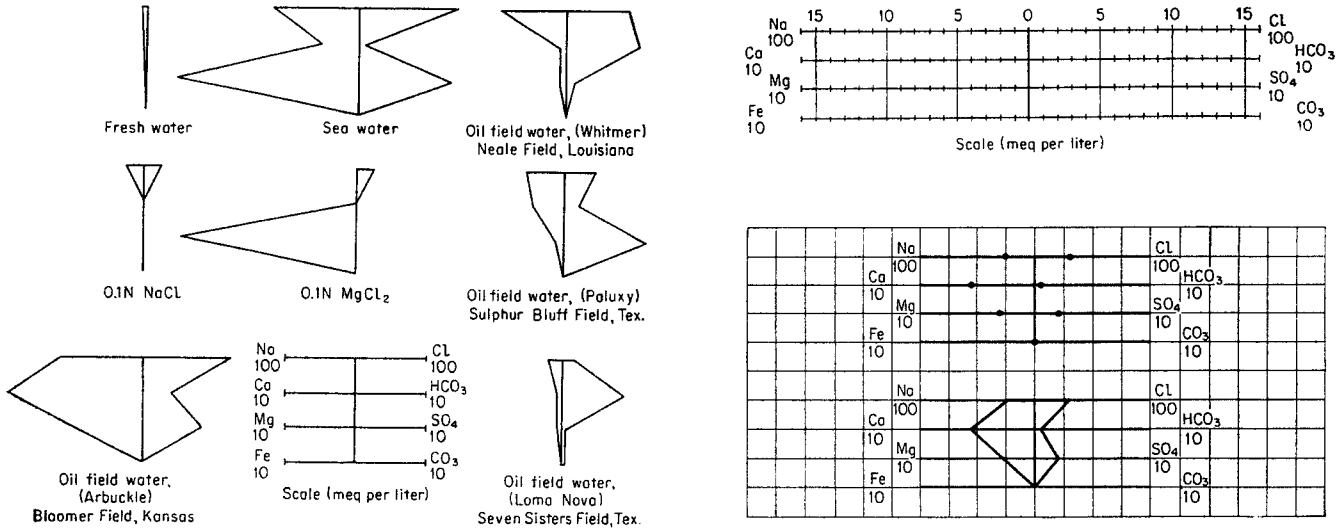

Fig. 2-58. Patterns to represent water analysis. (*Stiff, 2-66. Courtesy AIME.*)

oil and gas are present. The most common constituent dissolved in the water is sodium chloride, for the rocks were deposited in ocean water. The composition of the original connate water in the rocks commonly is changed subsequent to deposition by groundwater circulation. Formations having direct connection to an outcrop may contain fresh water. Concentrated brine is found when solutions have had an opportunity to contact adjacent layers of saline materials (2-66, 2-38). Table 2-10 gives some of the analyses of Frio waters reported by Jessen and Polshausen (2-38).

Stiff has presented a pattern for comparing water analyses (2-66). It consists of plotting milliequivalents on the principal ions, positive ions to left and negative ions to right, as illustrated in Fig. 2-58. Similar waters will have diagrams of similar appearance, for easy recognition.

CHAPTER 3

Phase Behavior of Natural Gas Systems

The phase behavior of pure substances and the phase behavior of mixtures were studied actively and jointly by physicists and chemists from about 1820 to about 1910. During that period, when the laws governing phase behavior were being developed, natural gas and its constituents—methane, ethane, propane, carbon dioxide, and nitrogen—received some attention as example substances. By 1925, however, textbooks of chemistry and physics usually discussed the phase behavior of pure substances only, and omitted the behavior of mixtures. Renewed interest in mixtures arose around 1930 when phase relationships in oil and gas reservoirs became the subject of inquiry and when processing operations reached pressures of 500 psi or more. Project 37, sponsored by the American Petroleum Institute at the California Institute of Technology under the direction of Dr. W. N. Lacey and Dr. B. H. Sage, contributed much to our knowledge of the behavior of hydrocarbon systems involving natural gas constituents (1-16). The earlier work before 1910 was gradually brought to the attention of investigators in specific fields; and a bibliography of this work was compiled in 1946 by Rzasa and Katz (1-9).

The term "natural gas" is used to denote either a mixture of volatile hydrocarbons or a gas phase. When one speaks of "liquefied natural gas," the term "natural gas" refers to the constituents in the mixture; when one speaks of a "gas" cap in a reservoir, the reference is to a gas phase. In this gas phase, under high pressure, there may be several constituents which, as pure substances, occur as high-boiling liquids.

The process of vaporizing liquids by gas pressure is a phenomenon common in the petroleum industry but uncommon elsewhere. An understanding of the phase behavior of hydrocarbon mixtures is necessary for the treating of natural gas–liquid systems. The goal is to predict, when the composition of the mixture is known, the quantities and compositions of the phases that occur at equilibrium for any pressure and temperature. An understanding of the behavior and nomenclature for pure substances is helpful in introducing the properties of single-phase fluids. Knowledge of the nature of simple mixtures provides a background for studying the behavior of naturally occurring natural gas systems.

PURE SUBSTANCES—VAPOR PRESSURE

Pure substances may occur in vapor, liquid, and solid phases depending upon the temperature and pressure. When a substance is in a single phase, its temperature T and pressure P define the volume V of the component. Figure 3-1 (3-66) in three dimensions is a plot of these three variables (P, V, T) for a pure substance. The phase behavior is represented by the surface exposed in the cutaway view. Since three-dimensional figures are more difficult to use than two, pressure-temperature projections of the intersections of the surfaces (Fig. 3-2) and pressure-volume sections at constant temperature (Fig. 3-3) are more commonly employed. Diagrams such as these are used to portray the phase behavior of natural gas constituents.

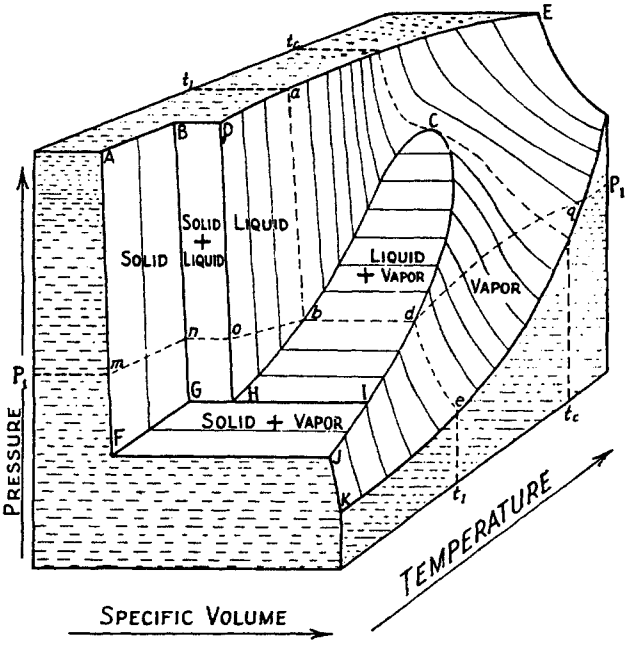

Fig. 3-1. Pressure-volume-temperature diagram for a pure substance. (*After Sherborne*, 3-66.)

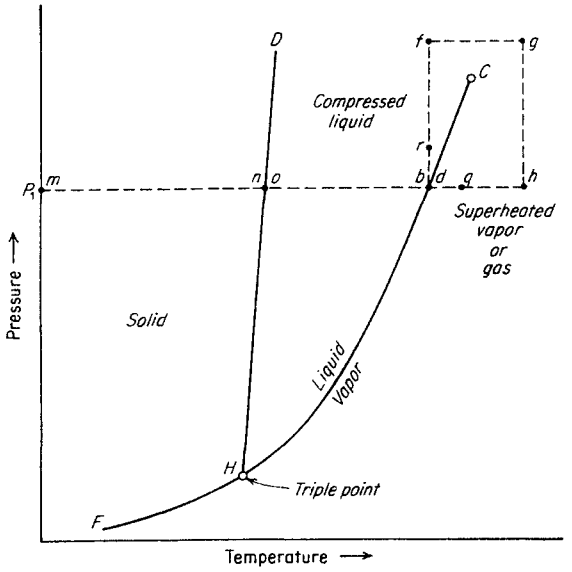

Fig. 3-2. Pressure-temperature diagram.

The conditions at which vapor and liquid may coexist are represented in Fig. 3-1 as the area *HbCdI*. The surface is "ruled"; that is, the lines generating the surface are all parallel to the base of the figure. The projection of *CbH* or *CdI* on a pressure-temperature plane becomes a single curve (*HC* of Fig. 3-2) known as the vapor-pressure curve. The two-phase surface *BDHG* for solid and liquid is ruled likewise, and projects as curve *HD* in Fig. 3-2. The solid-vapor surface projects as *HF*. Consider methane in the solid state at *m*, and increase its temperature at constant pressure P_1. At *n*, liquid begins to form and, upon the addition of heat at constant temperature and pressure, the methane will become all liquid at *o*. Further temperature rise is accompanied by the formation of a less dense fluid phase at *b*, called vapor. Vaporization takes place at constant temperature until at *d* it is completed. Temperature rise beyond *d* to *q* simply causes the volume to increase without any phase change.

At the triple point *H* all three phases coexist; only at this single temperature and pressure can one have three phases together at equilibrium for a pure compound.

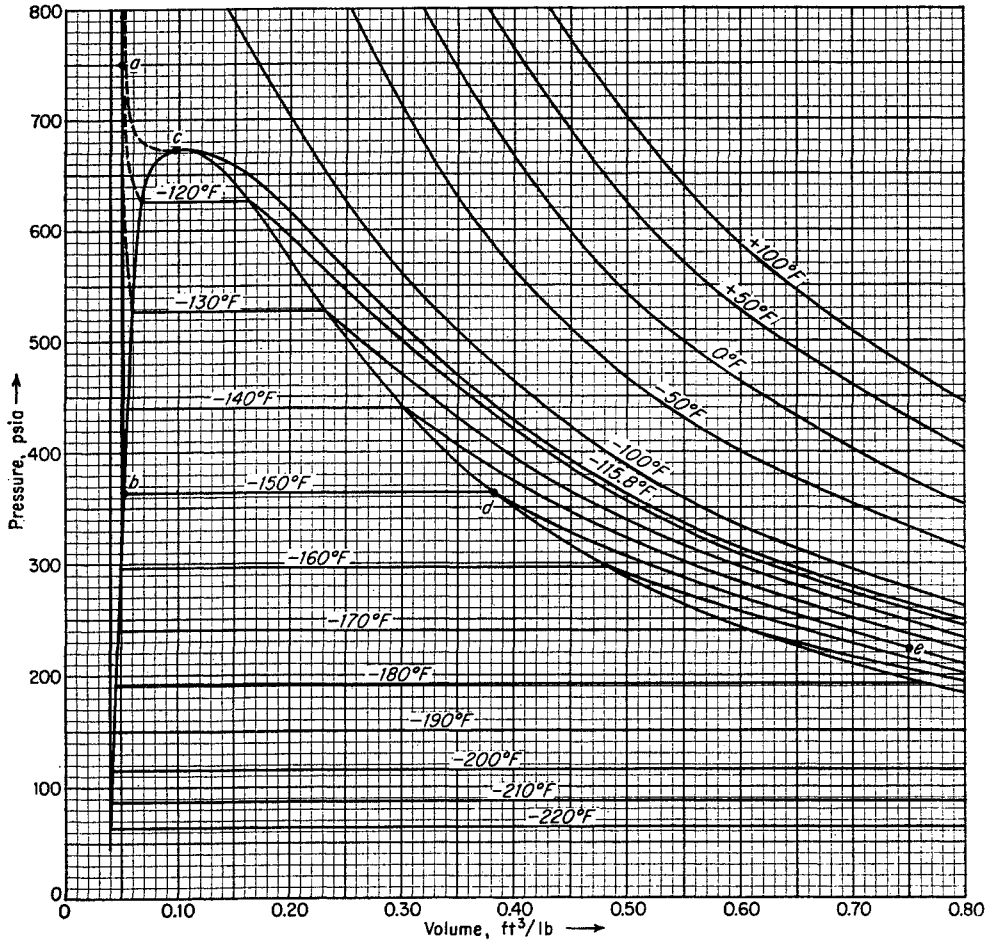

Fig. 3-3. Pressure-volume diagram for methane. (*Data from Matthews and Hurd*, 3-42.)

The specific-volume sections at constant temperature (such as *abde* of Fig. 3-1) may be plotted as isotherms (Fig. 3-3). The densities, reciprocal to the specific volumes, of the saturated phases are plotted in Fig. 3-4. It should be noted that, for increasing temperature, the specific volume of the liquid is rising (density lowering) while the volume of the vapor is decreasing (density rising). At the critical point C, the specific volumes and densities of vapor and liquid merge. At this critical temperature and pressure, all other properties of the phases merge.

A line drawn through the mean values of the vapor and liquid densities intersects the density curve at the critical density. This principle is known as the law of rectilinear diameters; the procedure was proposed by Cailletet and Mathias in 1886 (3-12). Measurements of critical phenomena and data on hydrocarbons are reviewed by Kobe and Lynn (3-38).

The vapor-pressure curve giving the boiling point at various pressures is a most important property of pure substances. Pure hydrocarbons are encountered in processing operations or in the laboratory, and vapor-pressure curves become very useful in handling them. Figures 3-5 to 3-7 give the vapor pressure of the volatile hydrocarbons encountered in the gas industry.

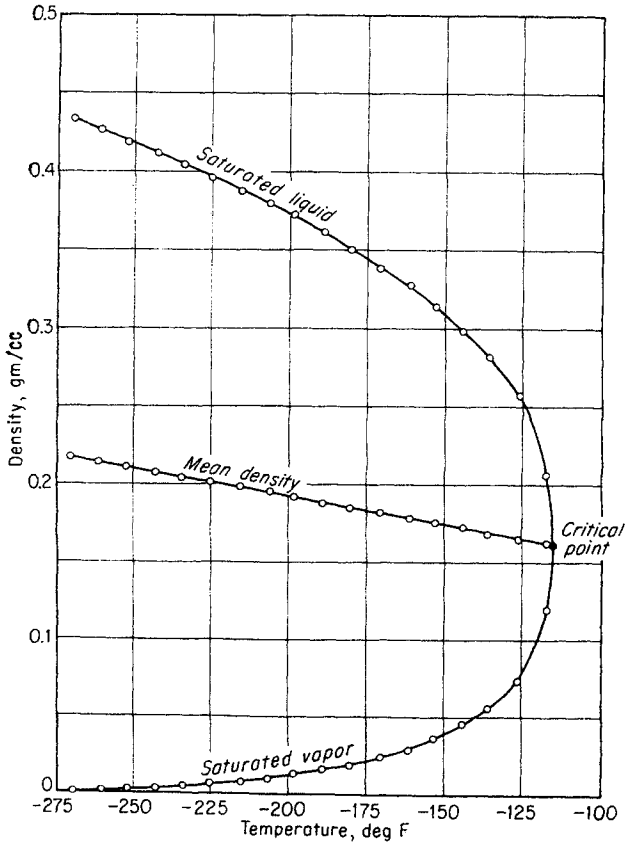

Fig. 3-4. Orthobaric density of methane. *(After Keyes, Taylor, and Smith, 3-37.)*

THE PHASE RULE

The phase rule, first enunciated by J. Willard Gibbs in 1876 (3-14, 3-21), is a most important tool in studying phase behavior. The rule applies for systems at equilibrium. The state of equilibrium between phases can be reached by isolating a system at constant temperature and pressure for long periods of time or by intimate mixing of the parts of a system. At equilibrium, the composition of each phase is uniform throughout, and no net transfer of components occurs between phases when they are permitted to remain in contact over long periods of time. Many natural gas–liquid systems in industry approach equilibrium, but, even for systems that are not in a state of equilibrium, the laws governing equilibrium impose limiting conditions. When phases are in equilibrium with each other, they are said to be saturated.

The phase rule is commonly expressed by Eq. (3-1).

$$C + 2 - P = F \qquad (3\text{-}1)$$

where C = number of independent components
P = number of phases
F = number of variables required to determine the state of the system at equilibrium, or number of degrees of freedom

Case (3-14) states that "the phase rule represents simply the application to certain chemical and physical problems of the familiar rule of algebra that the number of independent equations in a set of simultaneous equations must be equal to the number of variables involved in order that the values of the variables shall be fixed." The degrees of freedom for a system include the temperature, the pressure, and the composition of phases. The concentration of a component in a system of two or more phases is not a phase-rule variable, although the concentration in a given phase is a phase-rule variable.

A pure substance in three phases has zero degrees of freedom; this is represented by the invariant triple point. A pure substance in two phases such as vapor and liquid has one degree of freedom. Along the vapor-pressure curve (Fig. 3-2), specifying either pressure or temperature completely defines the state of the system. For example, at 100°F, propane in two equilibrium phases is at 189 psia, the density of liquid is 0.477 gram/cu cm, and the density of the vapor is 0.027 gram/cu cm. The surface tension is 5.5 dynes/cm. All properties of the phases are fixed by specifying the temperature and the condition that the system is in two phases. It should be noted that

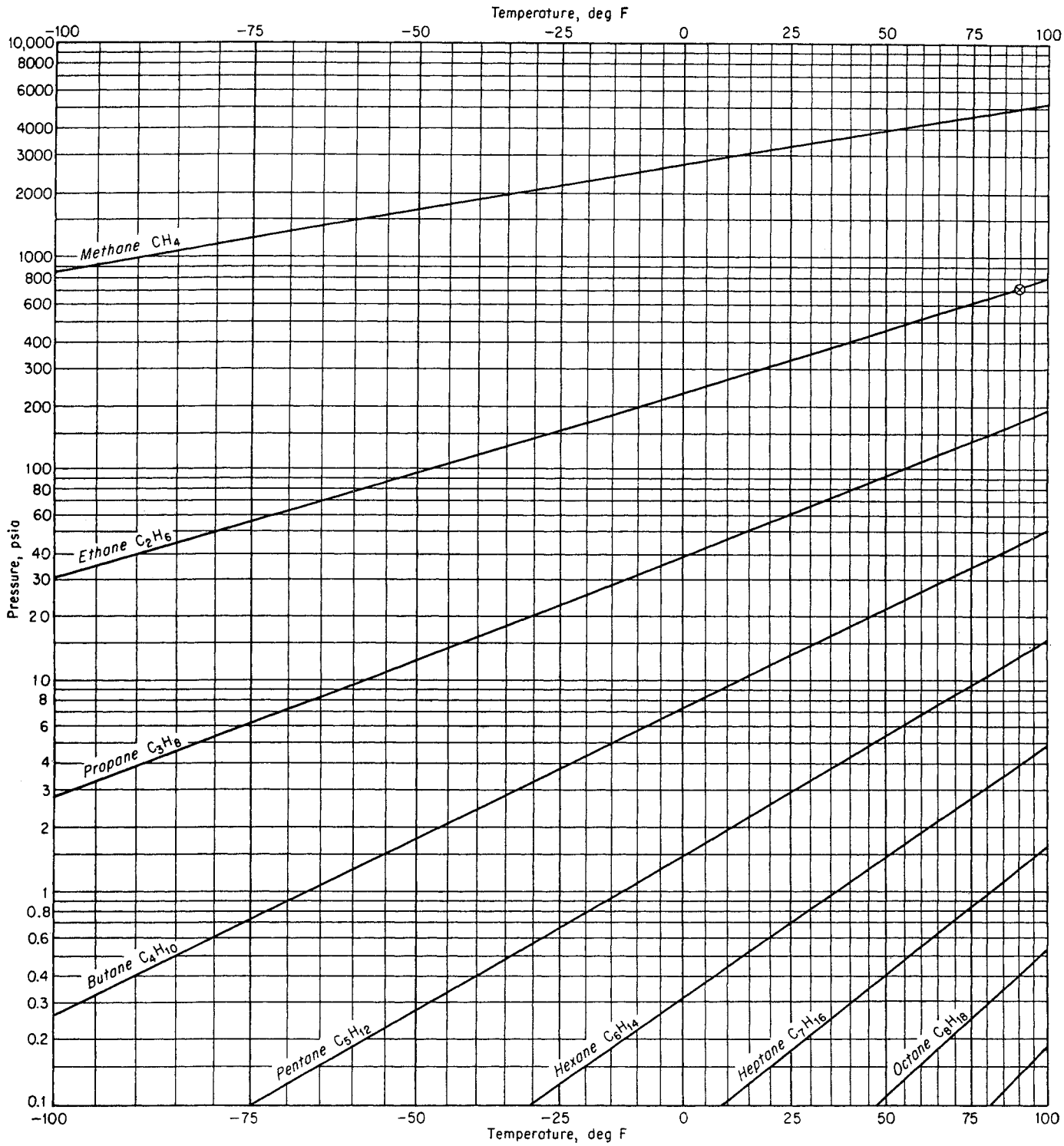

Fig. 3-5. Vapor pressure of normal paraffins.

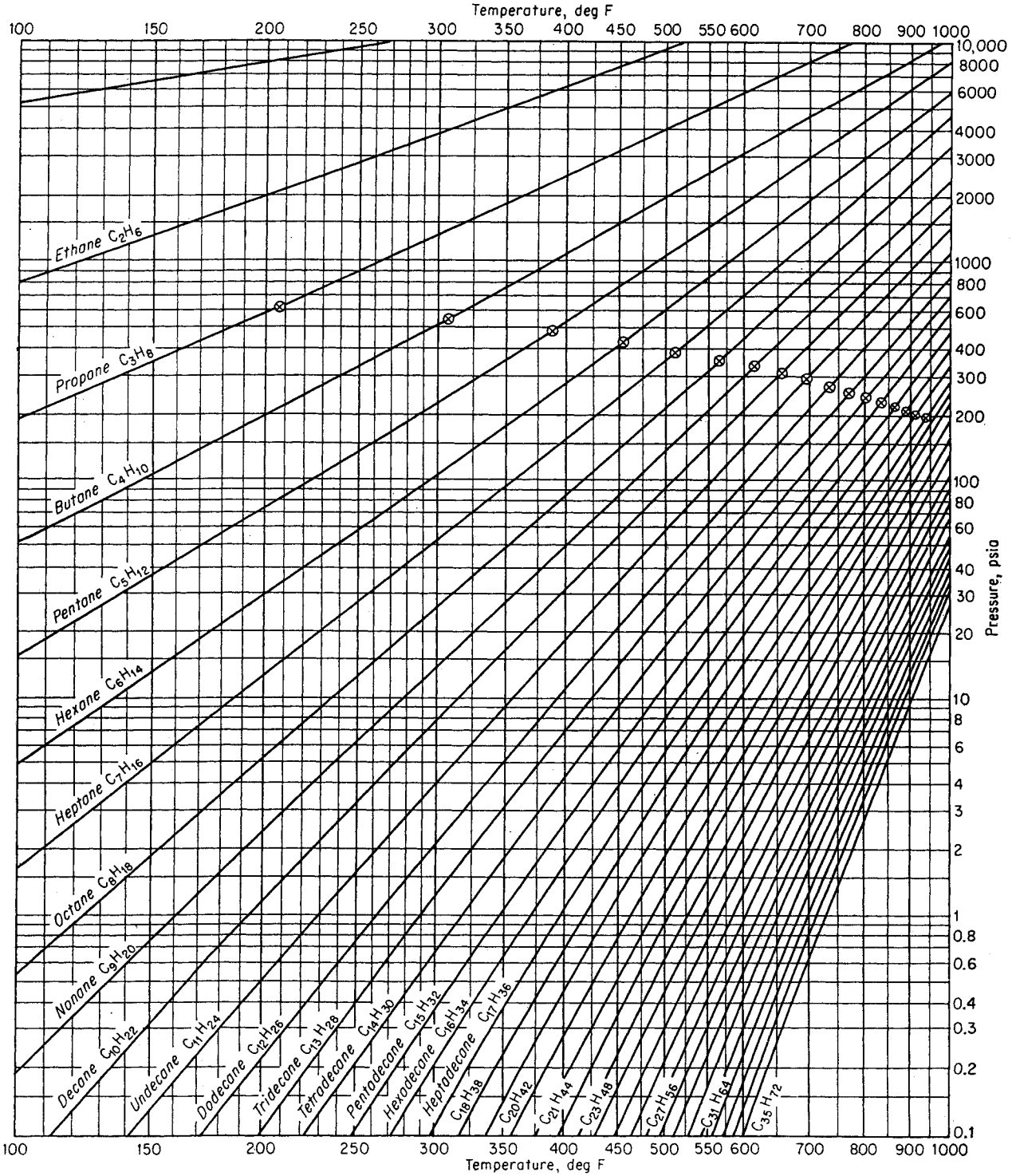

(Data collected by the M. W. Kellogg Company.)

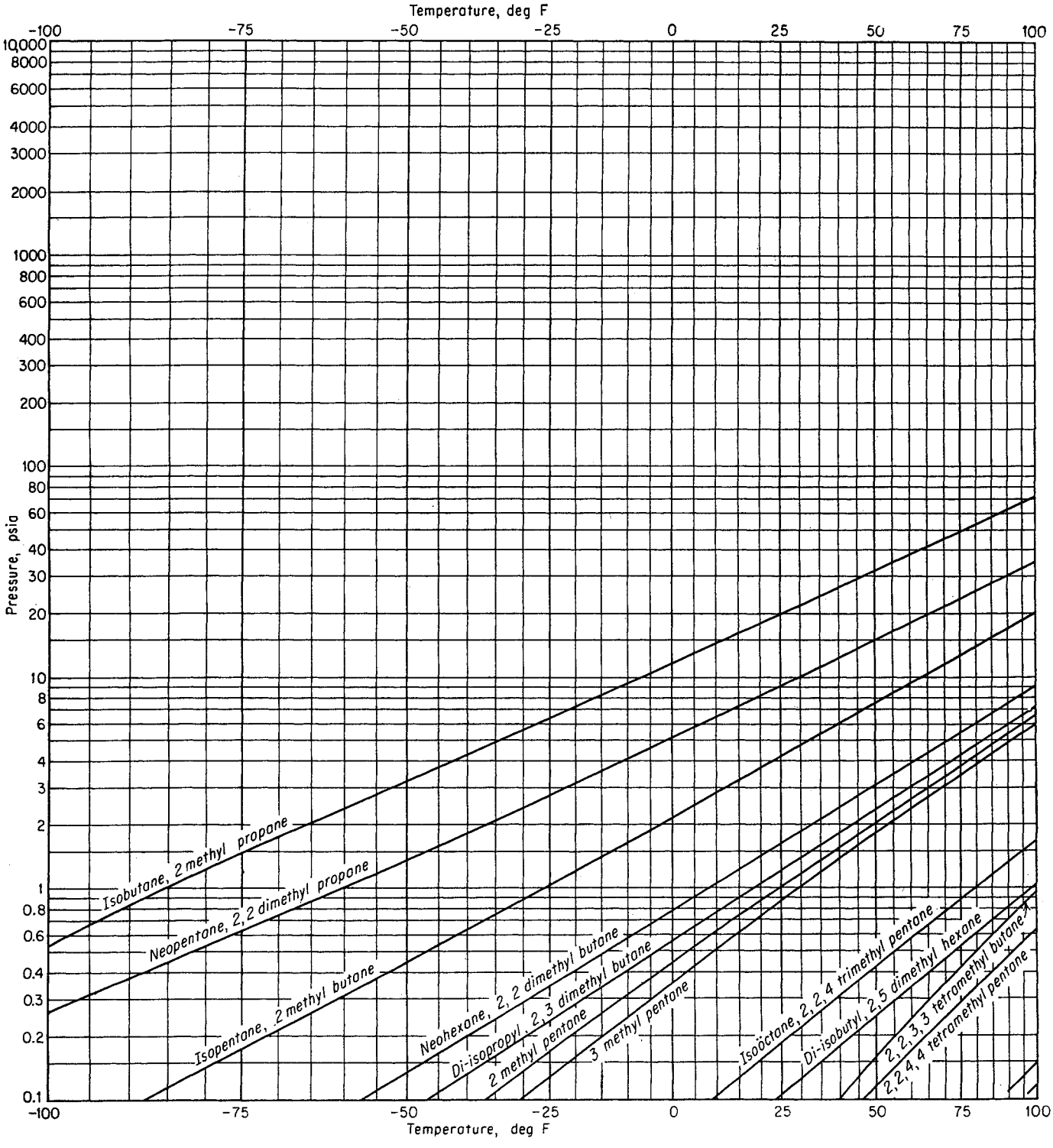

Fig. 3-6. Vapor pressure of isomeric paraffins.

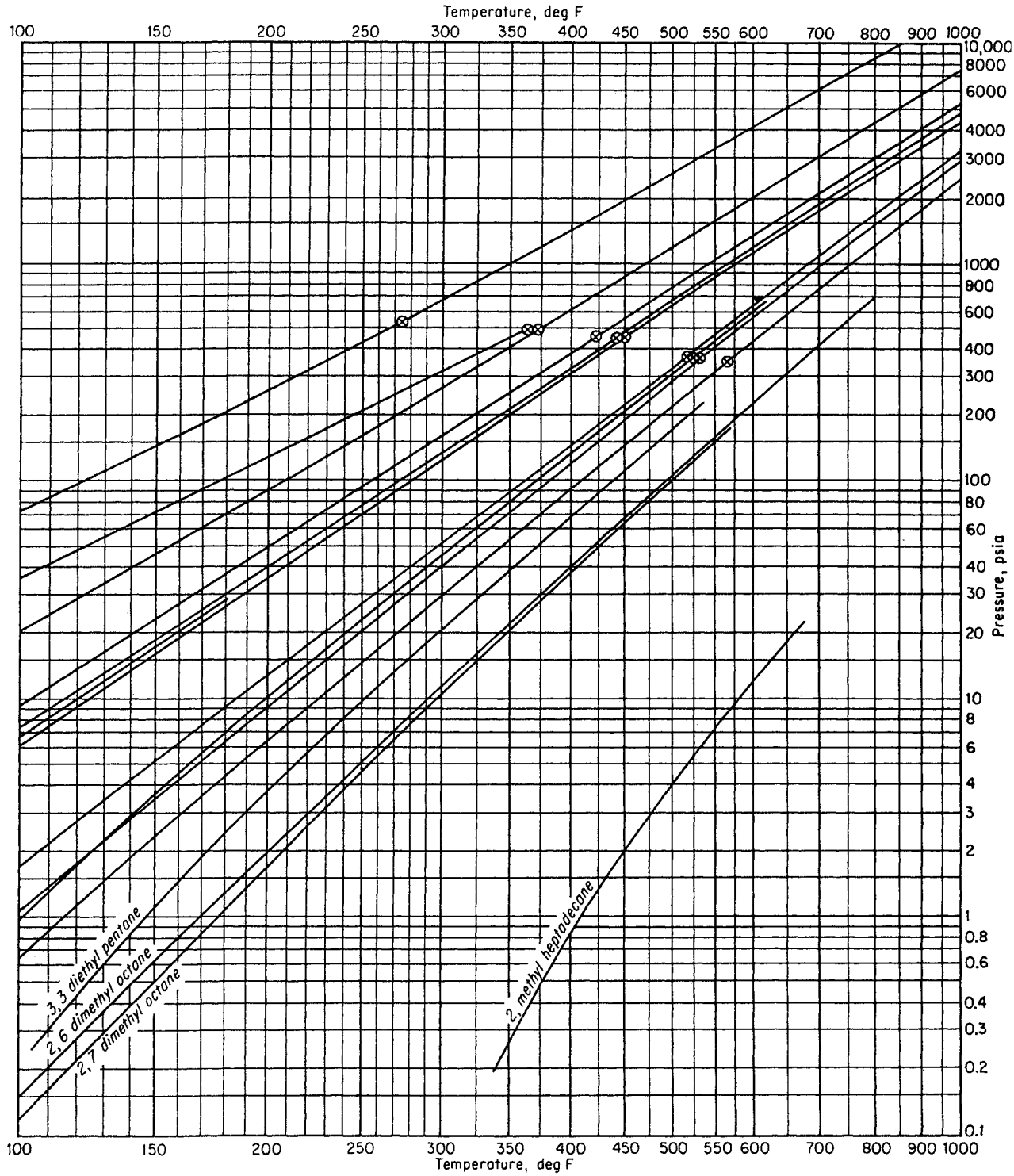

(Data collected by the M. W. Kellogg Company.)

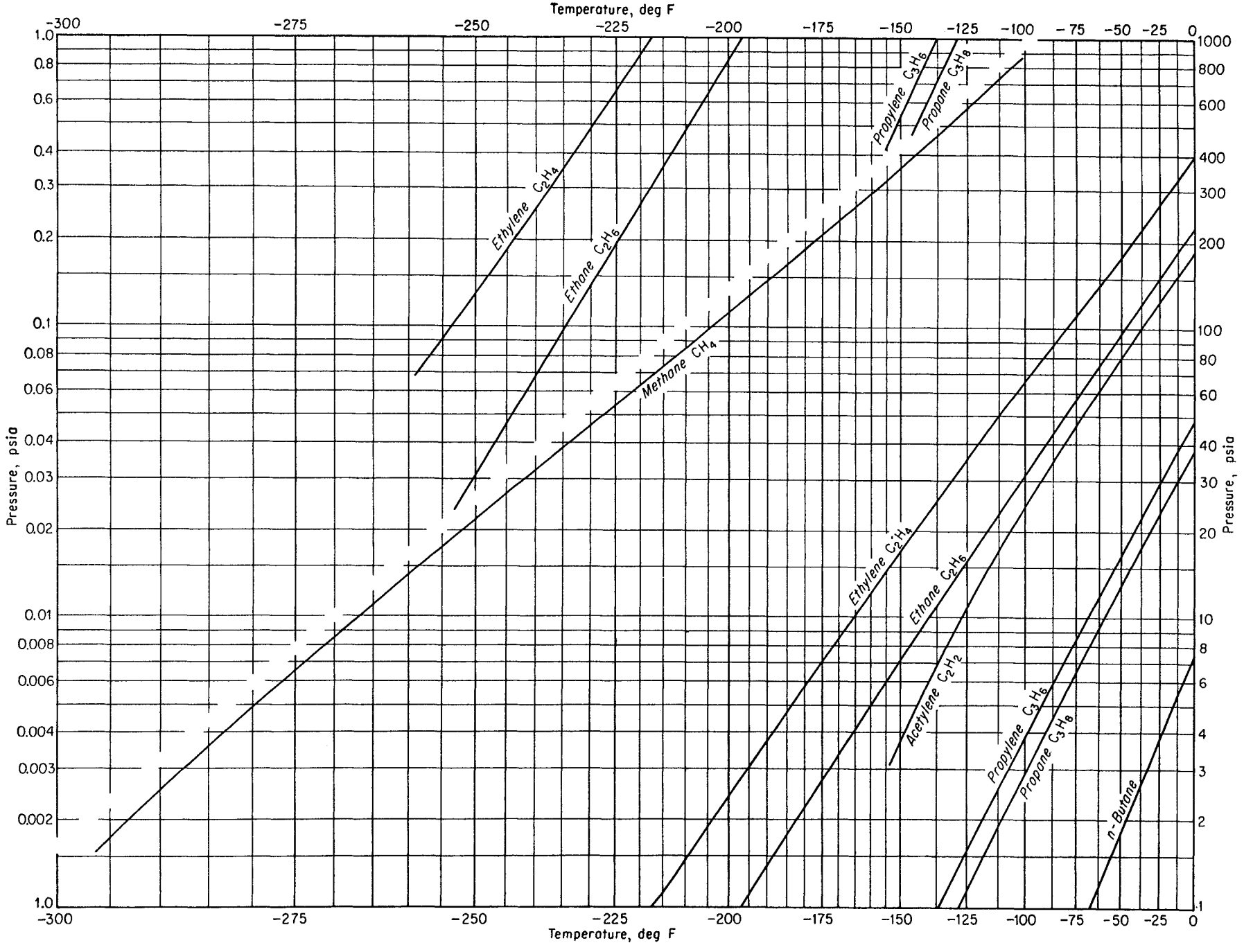

Fig. 3-6a. Vapor pressures of gases at low temperatures. *(Data collected by the M. W. Kellogg Company.)*

the phase rule is concerned only with the nature of the phases, not their extent.

A two-component system in two phases has two degrees of freedom. Temperature and pressure will define the state of such a system. For a three-component system in two phases, temperature, pressure, and a composition variable must be specified. The latter can be the concentration of one constituent in a phase but more often is the ratio of the concentration of one constituent to that of another constituent. For a natural gas with seven constituents in two phases, seven variables are required to fix the system, such as temperature, pressure, and five concentrations. Since five concentrations would not be known for such a mixture and only temperature and pressure would be known, it follows that the prediction from temperature and pressure of phase relationships for complex mixtures depends upon the assumption that the mixtures obey ideal laws for solutions and not upon the more exacting phase rule.

CONTINUITY OF VAPOR AND LIQUID PHASES

The terms "vapor" and "liquid" are useful to designate the less dense and the more dense phases, respectively. However, these vapor and liquid phases merge and lose their identity at the critical point.

In 1869, Thomas Andrews (3-3) gave a lecture "on the continuity of the gaseous and liquid states of matter" in which he pointed out that "the ordinary gaseous and ordinary liquid state are, in short, only widely separated forms of the same condition of matter, and may be made to pass into one another by a series of gradations so gentle that the passage shall nowhere present any interruption or breach of continuity."

In support of Andrews's concept, consider the behavior of methane (Fig. 3-2). Along line *HC*, vapor and liquid coexist. When one removes heat on a mixture of vapor and liquid at *bd*, the amount of liquid present increases and, when it has all become liquid, the temperature drops. It is quite natural to label the area above and to the left of curve *HC* as "liquid." The region on the other side of *HC* is entered when the system is all vapor; hence it is customary to label it "vapor." To illustrate that the terms "vapor" and "liquid" are, strictly, intended to denote the less dense and the more dense fluid phases when two phases are present and not to describe a single phase, consider a liquid at *b* and its behavior in the path *brfghqd*. At *b* the fluid is a liquid. Along the path *brfghqd*, no phase change occurs in the fluid. Is the substance at *d* in the vapor state? If so, how did it change from liquid at *b* into vapor at *d* without a phase change?

To emphasize the continuity of the vapor and liquid regions, Fig. 3-8 was prepared by shading the pressure-temperature (*P-T*) diagram in accordance with the phase density (3-28). Only along the vapor-pressure curve is there any discontinuity, and it disappears at the critical point.

It is better usage to call a pure substance at high pressures a single-phase fluid when it is not along the vapor-pressure curve, since the use of the term "vapor" or "liquid" with any intention of connoting density or other properties may be misleading. In the region of Fig. 3-2 labeled "liquid," one may call the fluid a compressed liquid and, at temperatures above the vapor-pressure curve, one may refer to the fluid as superheated vapor. However, as the critical temperature and pressure are approached, these terms become less definitive. The terms "gas" and "vapor" are generally interchangeable. "Vapor" may have the connotation of proximity to liquid, and "gas" may indicate that the conditions for liquid formation are somewhat distant. A nomenclature used by some is to reserve "gas" for substances when they are above their critical temperature and to use "vapor" for substances when they are below their critical temperature and they can be compressed to form liquids.

MIXTURES—RETROGRADE PHENOMENA

One of the first phase studies for fluid mixtures in the critical region was conducted by J. P. Kuenen in 1892 (3-39, 3-28) using the carbon dioxide–methyl chloride system. Unusual phase changes occur for mixtures which do not occur for pure substances, and Kuenen called these abnormal phenomena "retrograde" (3-28). The behavior of a hydrocarbon mixture is illustrated by Fig. 3-9.

The *P-T* diagram of Fig. 3-9 will be used to illustrate the language used in describing the behavior of a mixture. Inside the curve *ABCDIE*, the mixture is in two phases, vapor and liquid. Outside the border curve, only one phase occurs. The mixture at *K* is in one phase, and it remains in a single phase with a pressure reduction at constant temperature until point *B* is reached. Here, a bubble of vapor appears at equilibrium; point *B* is called a bubble point. Further reduction in pressure causes more vapor to form and, at *F*, 20 vol % is in the vapor state. Points along the curve *ABC* are bubble points for the mixture.

The mixture at *J* is in a single phase, and it continues as such with pressure increase until point *E* is reached. Here, a droplet of liquid or dew appears at equilibrium; the name "dew point" is given to this condition. As further pressure increase occurs from point *E*, more liquid is condensed as indicated. Like-

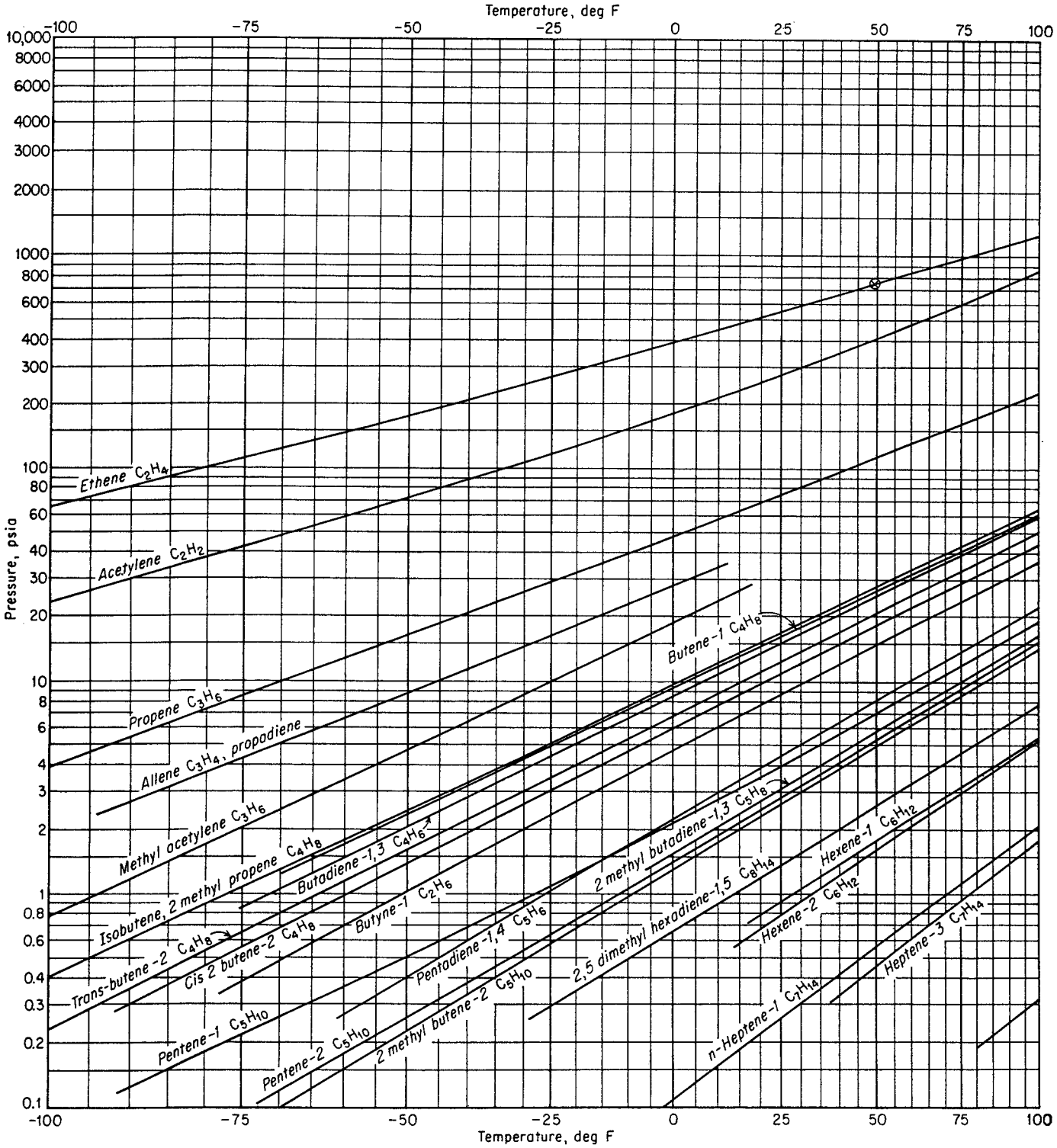

Fig. 3-7. Vapor pressures of unsaturated hydrocarbons.

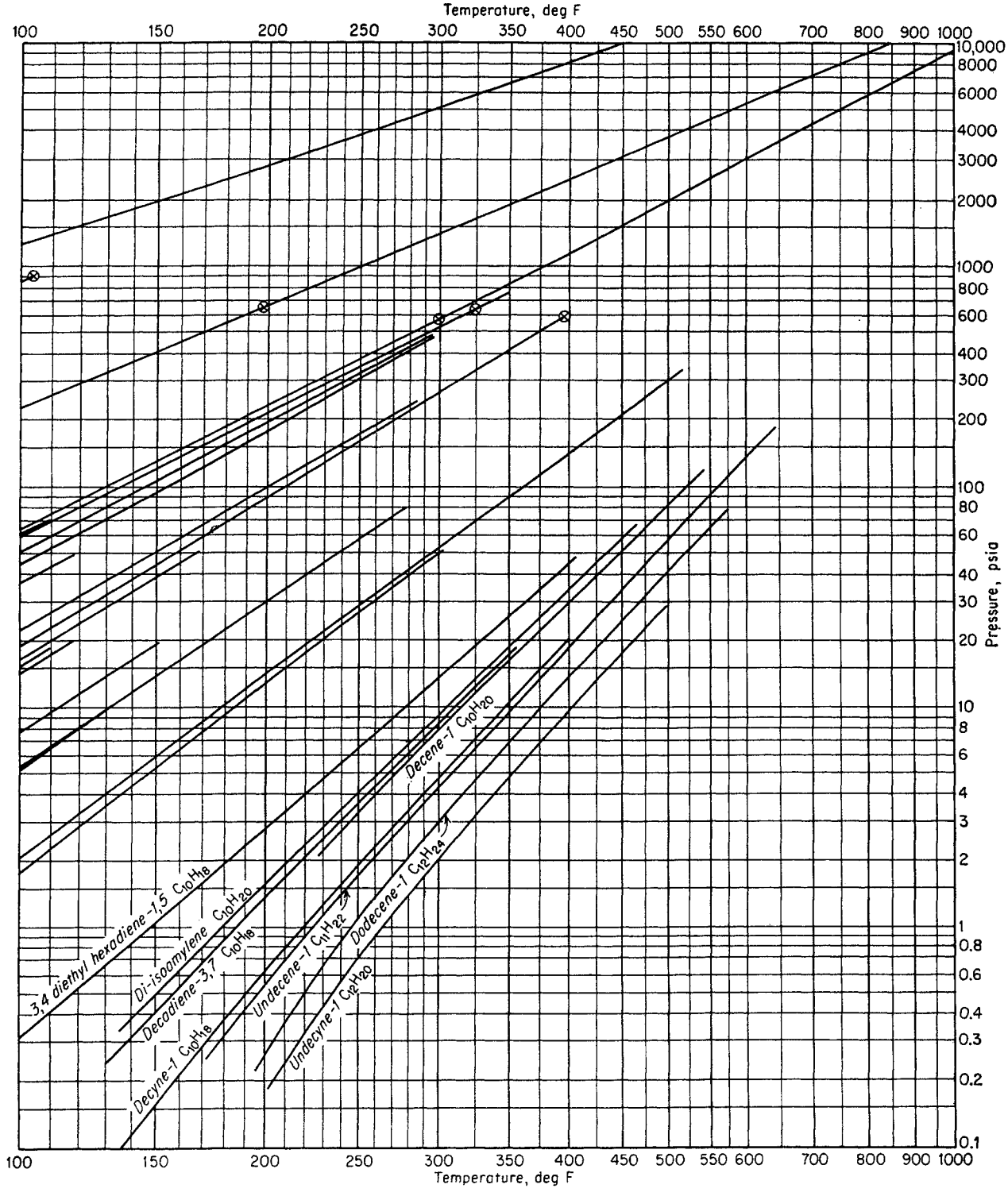

(Data collected by the M. W. Kellogg Company.)

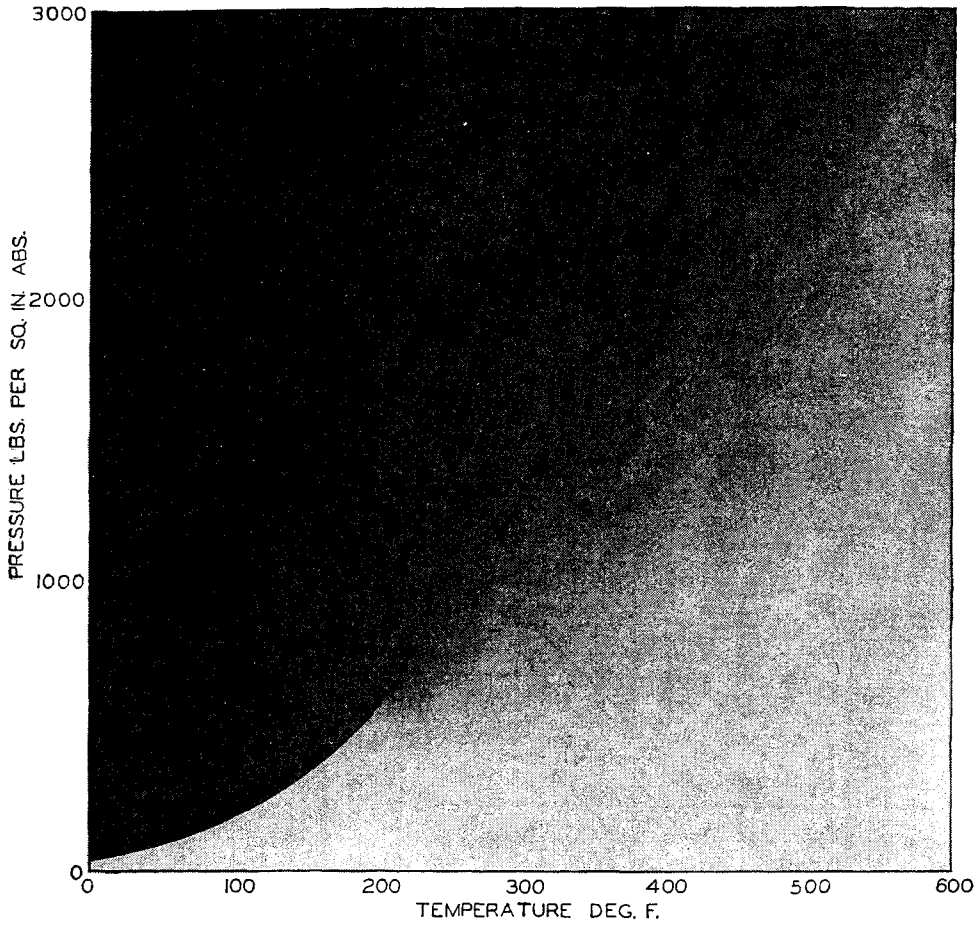

Fig. 3-8. Continuity of vapor and liquid states. (*Katz and Kurata*, 3-28. *Courtesy Ind. Eng. Chem.*)

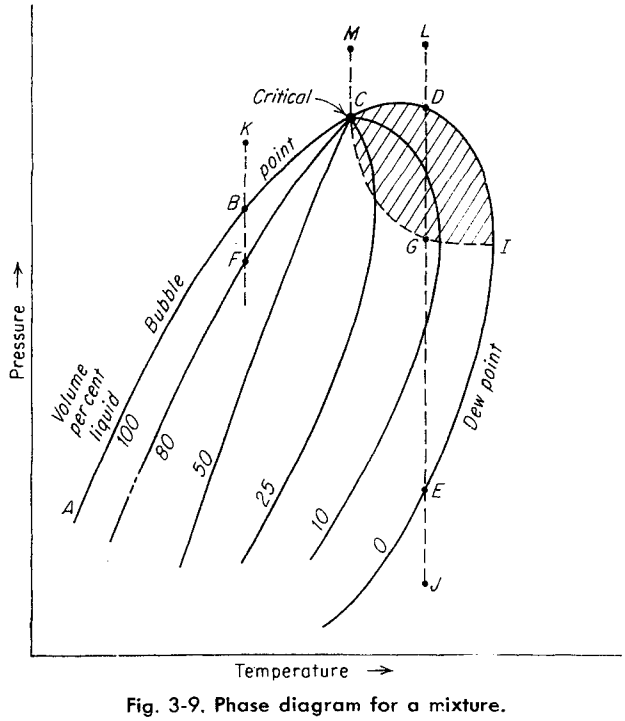

Fig. 3-9. Phase diagram for a mixture.

wise, a pressure reduction from L to D will cause dew to form.

A pressure reduction on the fluid from M to C causes the single-phase fluid to change abruptly to approximately 50 per cent vapor and 50 per cent liquid at C. It so happens that the properties of the vapor along the dew-point curve and those of the liquid along the bubble-point curve merge at C, and this is the critical point for the mixture. Physically, the critical point is very difficult to identify, and the point is more readily determined by plotting the bubble point, the dew point, and per cent liquid lines, and then finding the common point C.

Compressing pure substances in the vapor state to the vapor-pressure curve will cause dew to form; therefore, the behavior from J to E is to be expected. However, anyone unfamiliar with the type of phase behavior from L to D to G—the formation of liquid by pressure reduction on a gas—would be surprised, for this behavior is unlike that of pure substances. The phenomenon of liquid formation by isothermal expansion of a single-phase fluid is *retrograde condensation* (3-28). The expansion from D toward G yields

a maximum percentage of liquid at G, and the liquid vaporizes in a normal manner as the pressure is reduced still further from G to E. Since liquid is vaporized when the mixture at G is compressed to D at constant temperature, this process is called *retrograde vaporization*. The term applies to the vaporization of a liquid by the compression of a vapor in contact with the liquid. The terms "retrograde condensation" and "retrograde vaporization" may also be applied to isobaric phenomena when the phase change occurring is opposite to that which would occur if the same change in conditions were applied to a pure substance. The area represented by $CDIGC$ in Fig. 3-9 is the only part of the diagram where retrograde phenomena occur.

In the fluid near the critical point there occur color changes known as critical opalescence (3-70). Apparently molecular aggregations, though insufficient to cause a separation of phases, are of such a nature that light is scattered. Pressure reduction from the single phase to the border curve near the critical point causes the fluid to take on a reddish brown color with transmitted light or a bluish white color with reflected light. Color persists with time and in both phases for a short pressure range. It is more intense for mixtures containing higher-boiling hydrocarbons. The intensity is greatest at the critical temperature but may still be observed some ± 30 to 40°F from the critical temperature.

SOLUBILITY OF GASES IN LIQUIDS

In some cases the solution of a gaseous constituent in a liquid is measured and reported as solubility data. In these measurements, the vaporization of the liquid is neglected. It has been learned that the volatility of the liquid can seldom be ignored at high pressures, and so the compositions of both phases are generally considered. Before 1896 Villard (3-72) conducted unique experiments in which he observed the vaporization of bromine, iodine, and paraffin wax by methane pressure to 4,000 psi and described his experiments as showing solubility of solids and liquids in gases. Markham and Kobe give references to solubility of gases in liquids at low pressure (3-41a).

The work of Dow and Calkin (3-18) showed the solubility of natural gas in crude oil. The early work of Sage and Lacey included the solubility of methane in various hydrocarbon liquids (3-59). Frolich and coworkers reported the solubility of methane, hydrogen, and nitrogen in miscellaneous liquids (3-20). Schoch and coworkers found the influence of the chemical nature of the solvent on methane solubility (3-65).

BINARY MIXTURES

The behavior of all possible mixtures of two substances is illustrated for the methane-ethane system by Fig. 3-10 from Bloomer, Gami, and Parent (3-8); for the methane-propane system by Fig. 3-11 from Sage, Lacey, and Schaafsma (3-58) and Akers, Burns, and Fairchild (3-1); and for the ethane-heptane system by Fig. 3-12 from Kay (3-30). The critical temperatures of the two pure substances are connected by the critical points of the mixtures of the two components. The vapor-pressure curves and the critical locus enclose the two-phase region for all possible fluid mixtures of the two substances.

It should be noted that a mixture with relatively small amounts of one constituent may have a relatively narrow border curve but that the border curve

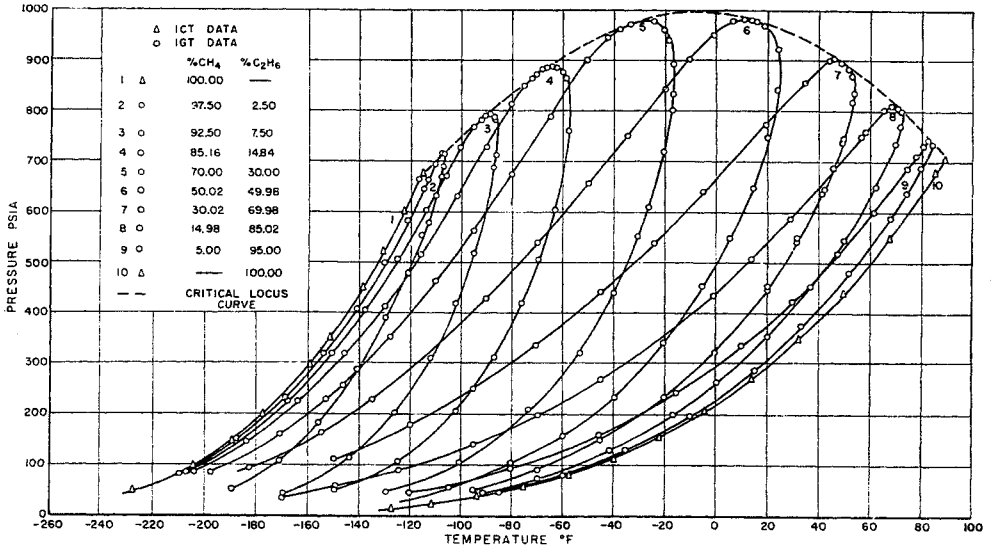

Fig. 3-10. Phase diagram of methane-ethane mixtures. (*By permission from "Physical-Chemical Properties of Methane-Ethane Mixtures," by O. T. Bloomer, D. C. Gami, and J. D. Parent. Copyright 1953, Institute of Gas Technology.* 3-8.)

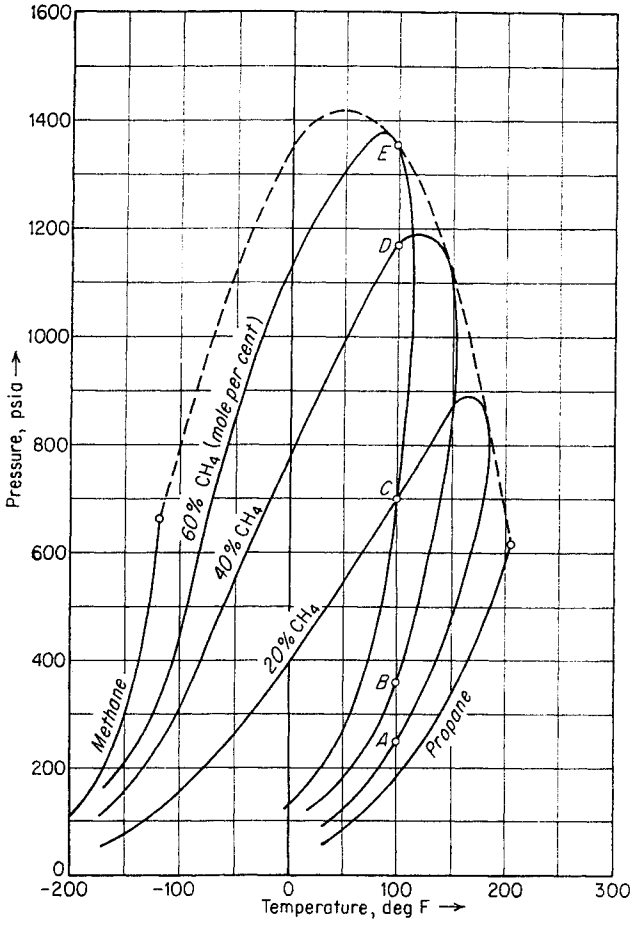

Fig. 3-11. Phase behavior of methane-propane system. (*Sage, Lacey, Akers, et al.*, 3-58, 3-1, 3-53.)

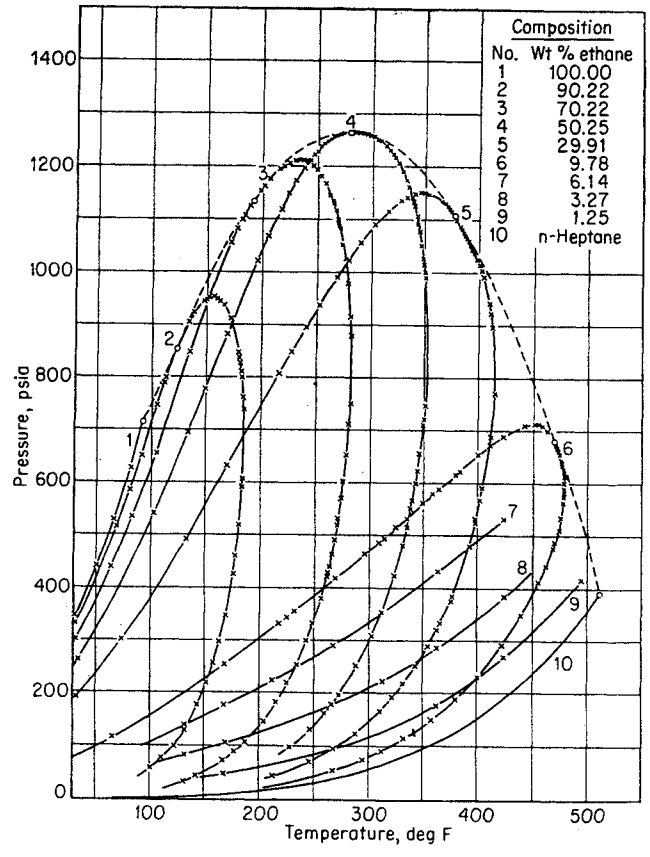

Fig. 3-12. Phase behavior of ethane-heptane system. (*Kay*, 3-30 *Courtesy Ind. Eng. Chem.*)

for a mixture with nearly equal amounts of the two constituents enlarges noticeably. The extent of the diagram for a particular mixture is greater if the constituents have widely different boiling points. Methane systems may have large regions of temperature or pressure between the bubble and dew points.

The critical pressure for a mixture rises above the critical pressure for either of its pure substances. Figure 3-13 gives the loci for binary systems with methane. The greater the difference in boiling point of the two substances, the higher the critical pressure will rise between the two critical pressures of the components. Methane-decane mixtures (3-60) will be in two phases at pressures up to 5,000 psia. Data on methane and a fraction boiling at 567 to 589°F (mol. wt 247) by Rzasa and Katz (3-57) showed that the two-phase regions could exceed 10,000 psia. Critical loci for various systems are given in Fig. 3-14.

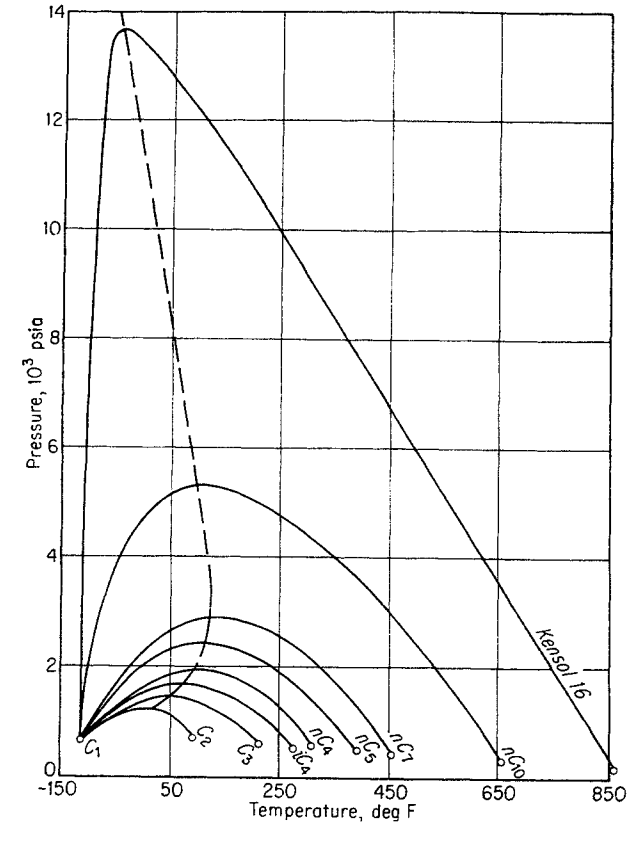

Fig. 3-13. Critical loci of binary methane systems. (*Rzasa and Katz*, 3-57. *Courtesy AIME.*)

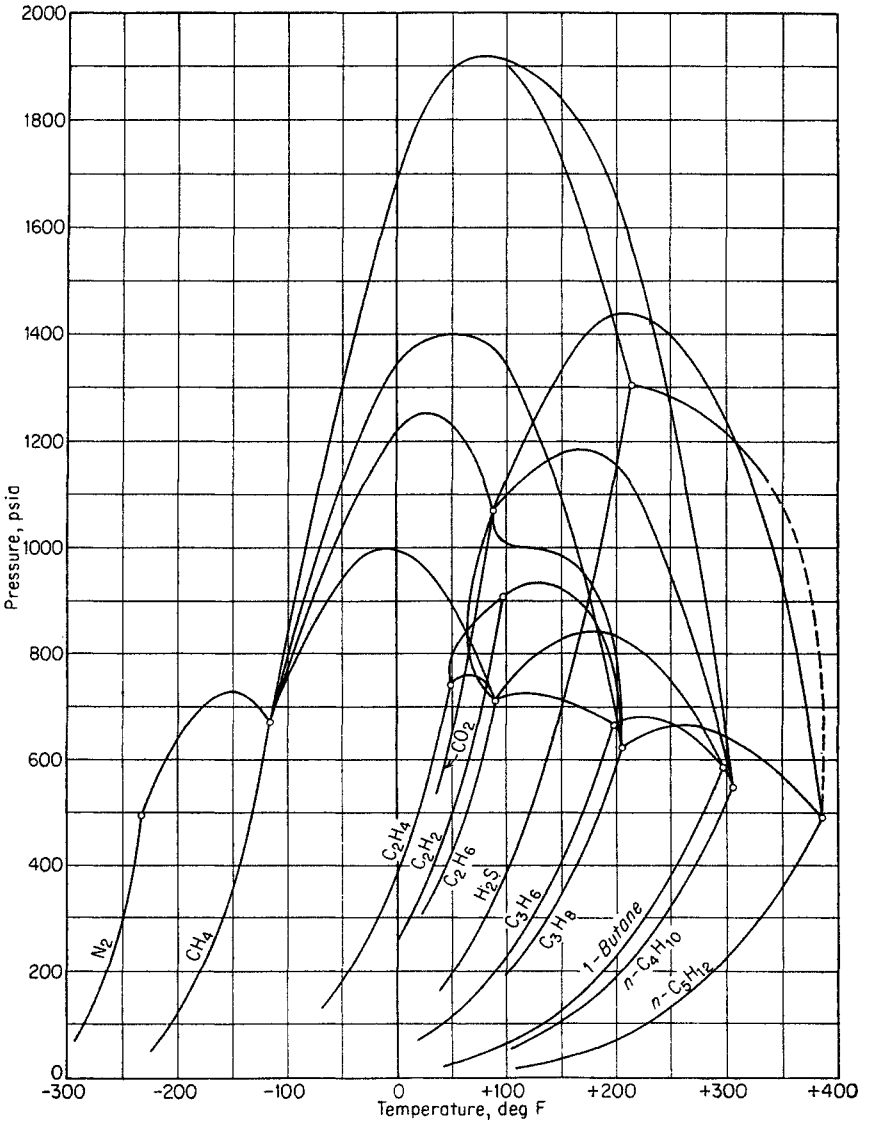

Fig. 3-14. Critical loci for various systems. (1-16, 1-17, 1-9, 3-62, 1-2, 3-17, 3-7, 3-8, 3-48, 3-43.)

It is customary to plot phase data at constant temperature or at constant pressure with composition as a variable. This has been done for binary systems in Figs. 3-15 to 3-17. The density of the saturated vapors and liquids for the ethane-heptane system by Kay (3-30) is given in Fig. 3-18.

TERNARY AND COMPLEX SYSTEMS

Ternary systems illustrate the addition of an intermediate constituent to a binary system and introduce some of the complexities exhibited by systems with numerous components. Of greatest interest are the methane-propane-pentane (3-13) and methane-butane-decane systems (3-51, 3-52) studied by Sage, Lacey, and coworkers. It is convenient to plot phase-boundary conditions at constant pressure and temperature on triangular diagrams. Figure 3-19 gives the diagrams for three pressures, showing the shrinkage of the two-phase region with increased pressure. The critical loci for the various systems described by a parameter of a constant ratio of propane concentration to propane-plus-pentane concentration are shown in Fig. 3-20. The pressure-composition diagram is given in Fig. 3-21.

The methane-butane-decane system investigated by Reamer, Sage, and Lacey (3-52) reaches pressures and temperatures similar to high-pressure gas reservoirs. The behavior of this system is given in Figs. 3-22 to 3-24.

Phase diagrams for few complex mixtures have been determined for most data are in the form of compositions of equilibrium-bubble-point liquids and dew-point vapors. The phase diagram determined by Katz, Vink, and David using visual observation in a glass-windowed cell for a natural gas–natural gasoline mixture is given in Fig. 3-25 and the composition in Table 3-1 (3-29, 1-37). The phase behavior of a gas

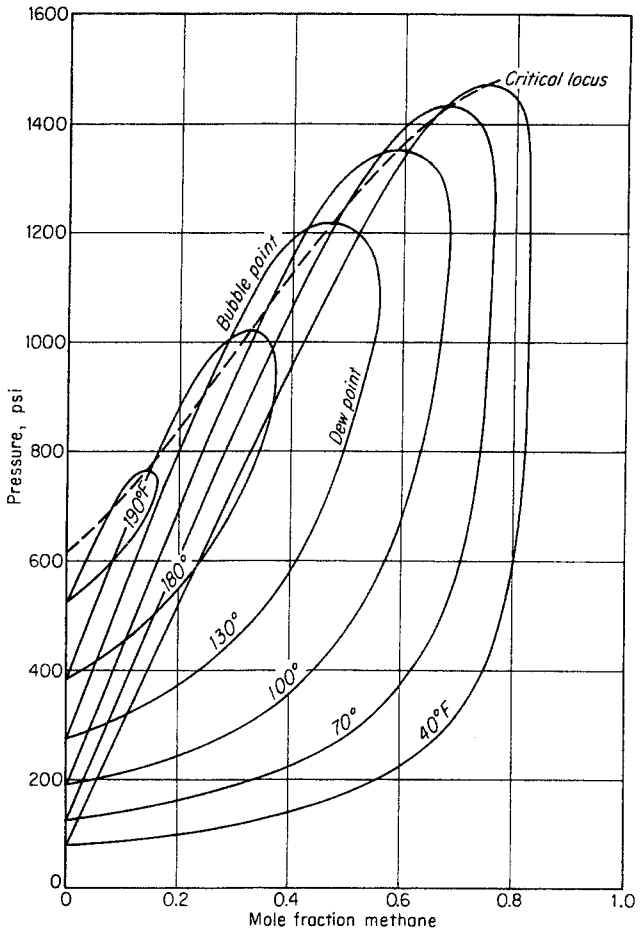

Fig. 3-15. Pressure-composition diagram, methane-propane system. (*Reamer, Sage, and Lacey, 3-53. Courtesy Ind. Eng. Chem.*)

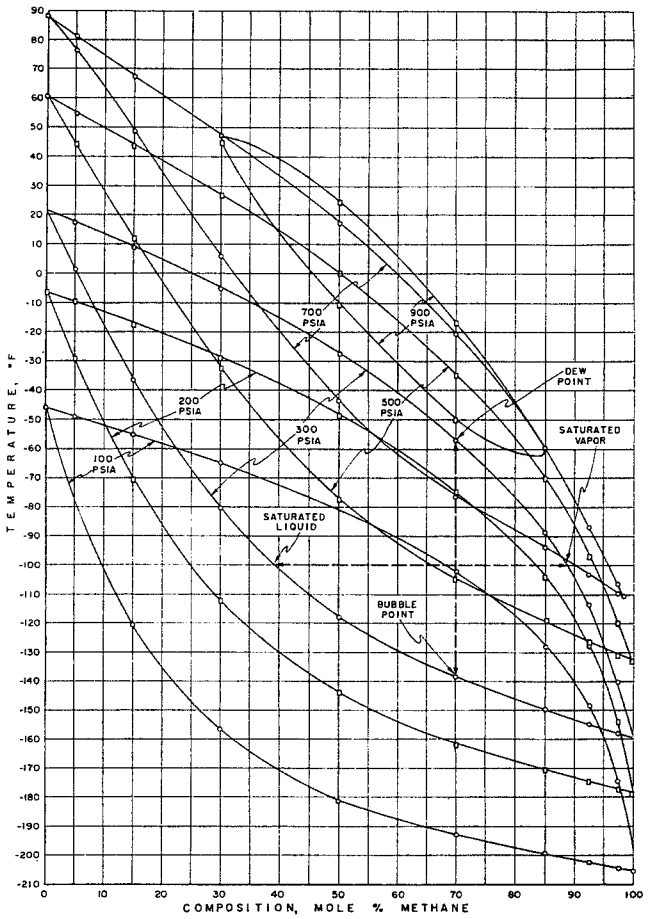

Fig. 3-16. Temperature-composition diagram, methane-ethane system. (*By permission from "Physical-Chemical Properties of Methane-Ethane Mixtures," by O. T. Bloomer, D. C. Gami, and J. D. Parent. Copyright 1953, Institute of Gas Technology.*)

well stream was determined by Buckley and Lightfoot (3-11) by means of a separator and is plotted in terms of the yield of liquid in Fig. 3-26. Studies of reservoir samples of condensate and crude oil will be discussed later.

NONIDEAL SYSTEMS

Certain mixtures of substances do not follow the typical pattern of phase behavior. They may form two liquid phases or they may have liquids that evolve vapor of a composition equal to that of the liquid and, therefore, boil at a constant temperature. These latter mixtures are described as *azeotropic* (minimum or maximum boiling). Water-hydrocarbons and water-ethyl alcohol provide the classical examples of these phenomena.

Such systems as ethane–carbon dioxide (3-40) and acetylene-ethane or acetylene-ethylene (3-43) exhibit nonideal behavior. Figure 3-27 shows binary and ternary data for the ethane-ethylene-acetylene system at 40°F with two binaries having azeotropes.

Crude oil is separated into two liquid phases by propane in deasphaltizing operations (1-13). Katz and coworkers (3-73) formed two liquid phases in a natural gas–crude oil system by propane addition. Botkin, Reamer, Sage, and Lacey (3-10) studied the phase behavior of two California crude oils which produced multiple condensed phases.

Weinaug and Bradley (3-75) observed unusual phase behavior of a naturally occurring reservoir mixture (Fig. 3-28). At a constant temperature below the critical, such as 160°F, the quantity of the liquid phase decreases, then increases in an abnormal manner, and thereafter decreases normally. Weinaug and Bradley called the abnormal phenomenon *renascent* condensation or vaporization. The composition of the system (Table 3-1) shows a high concentration of propane and ethane. A possible explanation is that the formation of a second liquid phase is imminent.

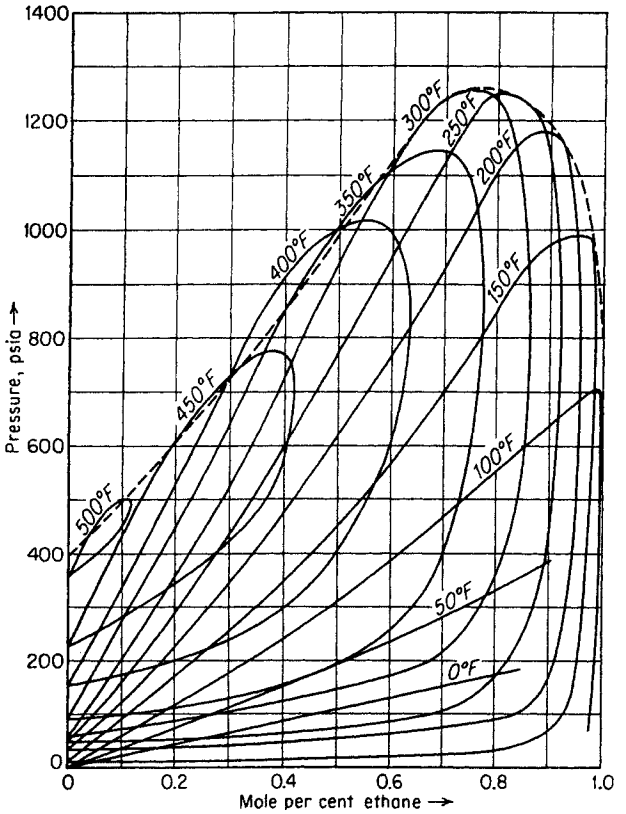

Fig. 3-17. Pressure-composition diagram, ethane-heptane system. (*After Kay*, 3-30.)

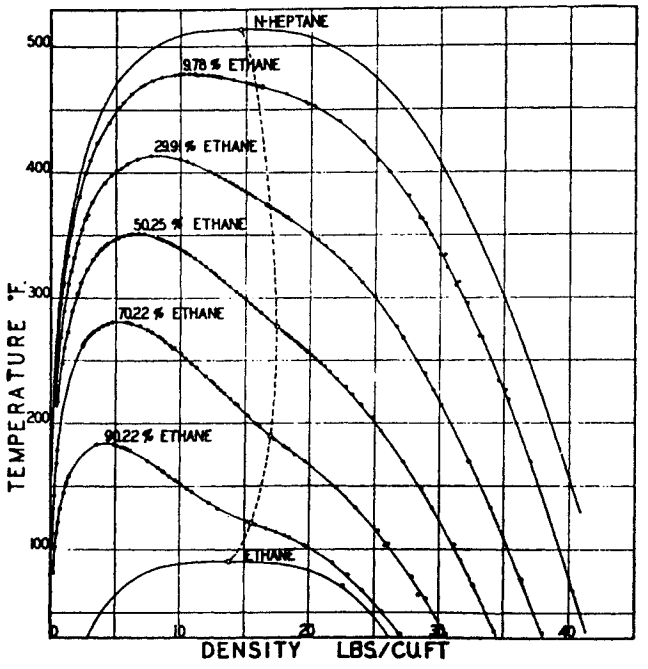

Fig. 3-18. Phase densities of ethane-heptane system. (*Kay*, 3-30. *Courtesy Ind. Eng. Chem.*)

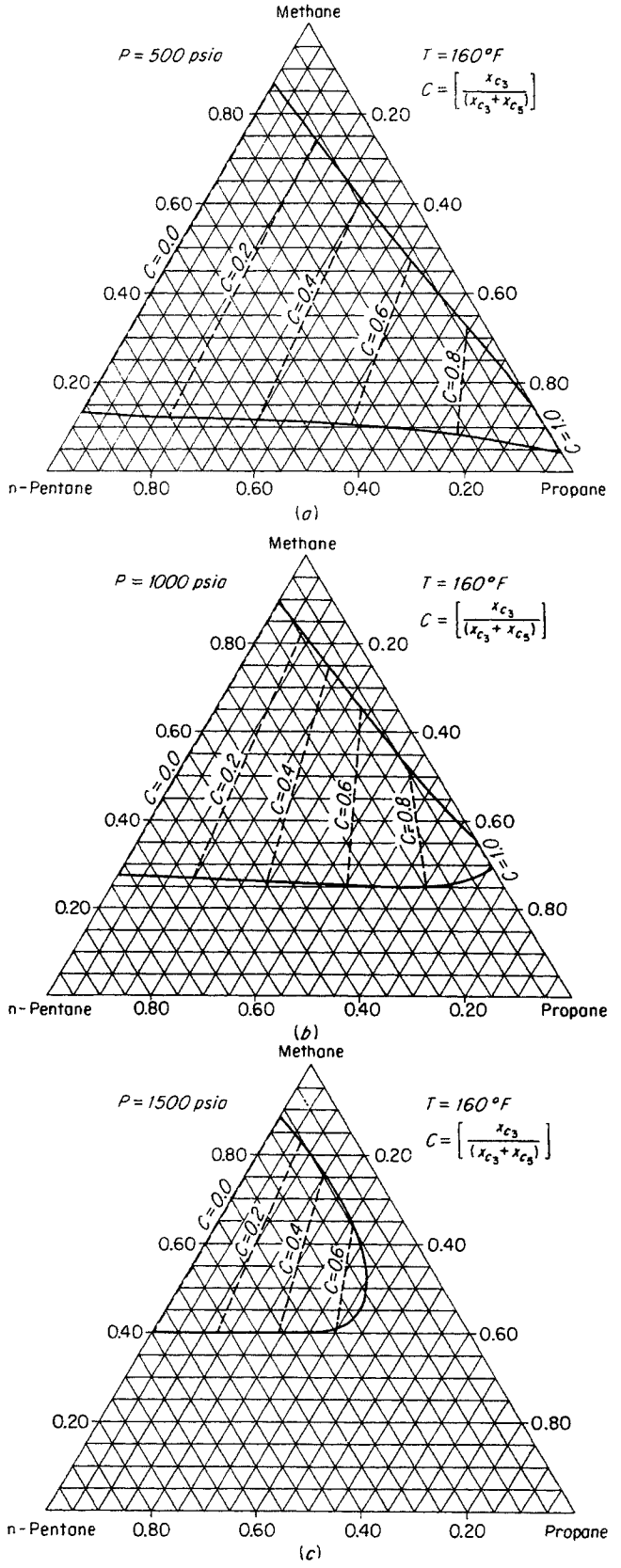

Fig. 3-19. Methane-propane-pentane system at 160°F. (*After Dourson, Sage, and Lacey*, 3-17.)

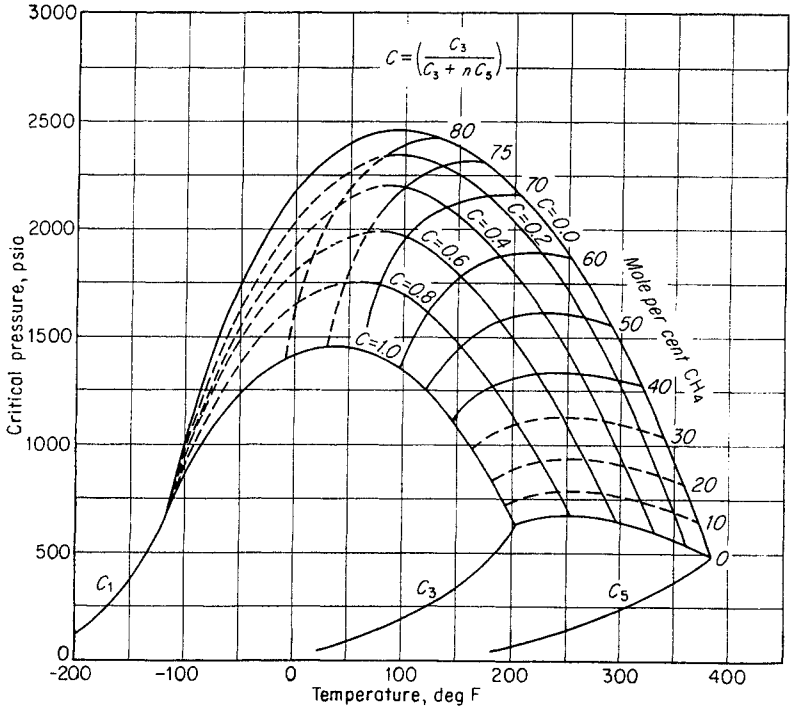

Fig. 3-20. Critical loci for methane-propane-pentane system. (*Data of Sage and Lacey, 3-13, 3-17.*)

Eilerts and coworkers (3-19) at the U.S. Bureau of Mines, Bartlesville, Okla., observed the formation of a second liquid phase at −65°F for the mixture given in Table 3-1. The mixture was below its critical temperature at pressures of 1,100 to 1,250 psia.

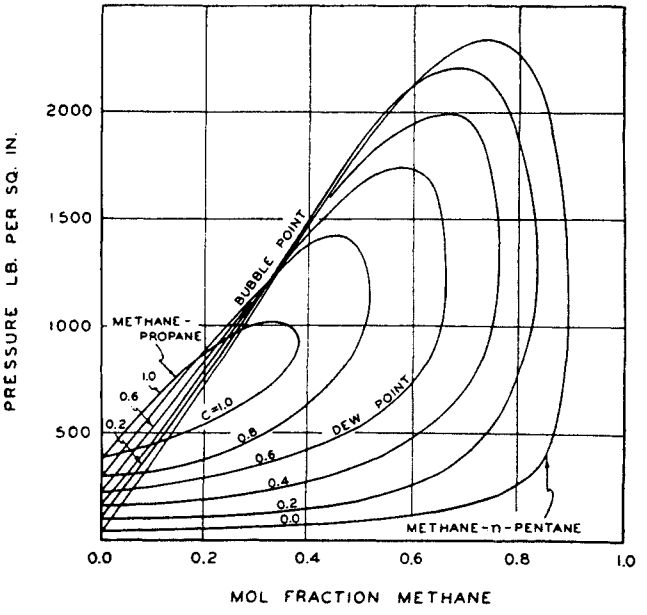

Fig. 3-21. Pressure-concentration diagram for methane-propane-pentane system. (*Dourson, Sage, and Lacey, 3-17. Courtesy AIME.*)

VAPORIZATION-EQUILIBRIUM CONSTANTS

The computation of the phase behavior of hydrocarbon mixtures is normally carried out by means of vapor-liquid equilibrium constants. The constant is defined as

$$K = \frac{y}{x} \tag{3-2}$$

where y = mole fraction of a constituent in the vapor phase
x = mole fraction of the constituent in the equilibrium liquid phase
K = equilibrium constant

The equilibrium constant applies for a given pressure and temperature. In many mixtures the equilibrium constants for most constituents are independent of phase composition at pressures considerably below the critical pressure.

Since the equilibrium constants vary with temperature, pressure, and, in some areas, with composition, they are often referred to as equilibrium ratios. However, the name used here has been accepted by the petroleum industry, and the fact that the y/x ratio does not vary with composition over a wide range of conditions is significant. The use of equilibrium constants started with Brown, Souders, and associates at the University of Michigan in 1931 (3-67). Lewis and Luke presented a method of using fugacities for predicting vapor-liquid equilibria (3-41).

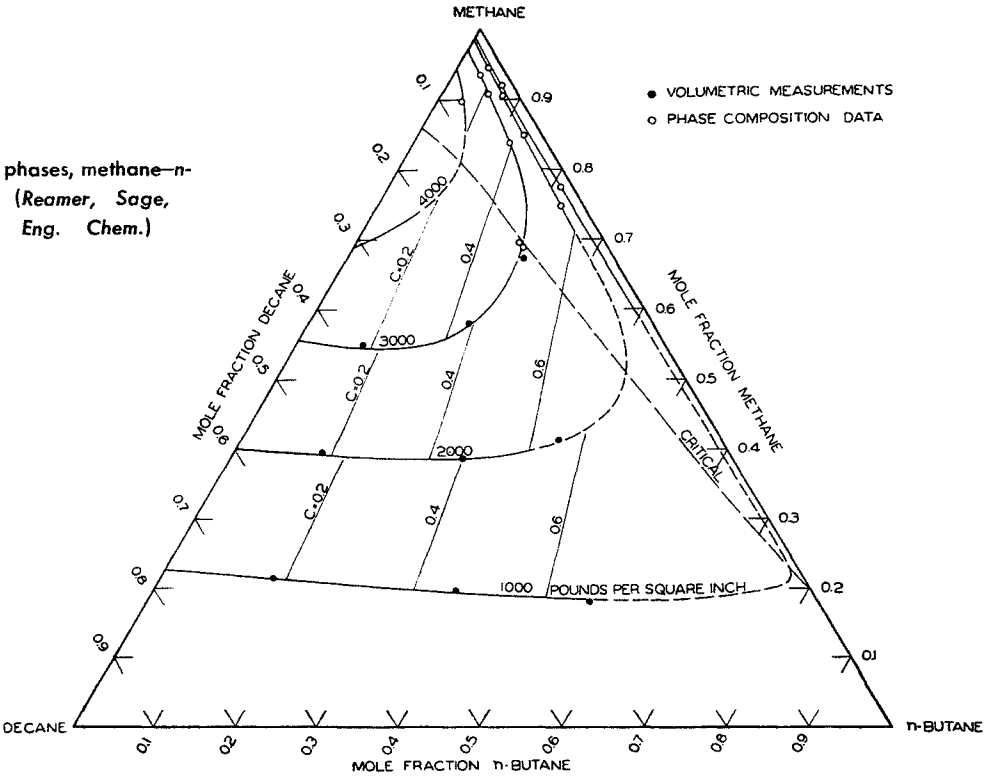

Fig. 3-22. Compositions of coexisting phases, methane–*n*-butane–decane system at 280°F. (*Reamer, Sage, and Lacey,* 3-52. *Courtesy Ind. Eng. Chem.*)

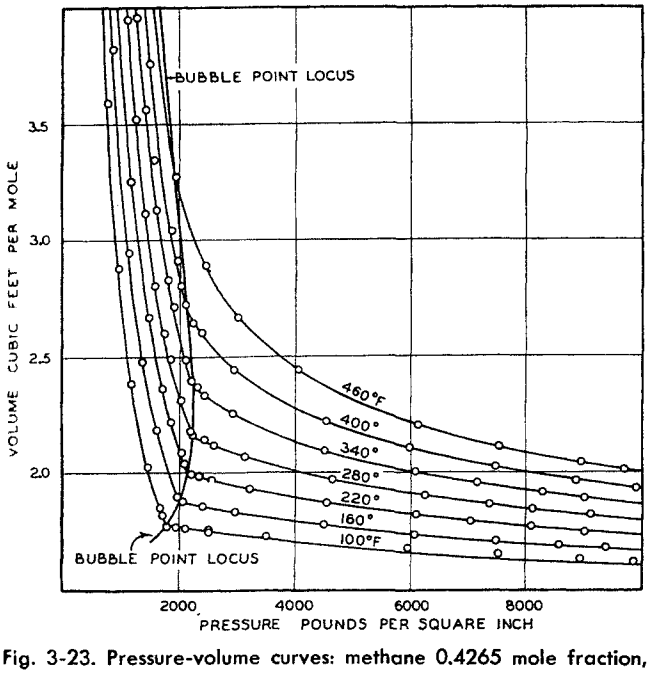

Fig. 3-23. Pressure-volume curves: methane 0.4265 mole fraction, *n*-butane 0.249, and decane 0.288; c = 0.463. (*Reamer, Sage, and Lacey,* 3-52. *Courtesy Ind. Eng. Chem.*)

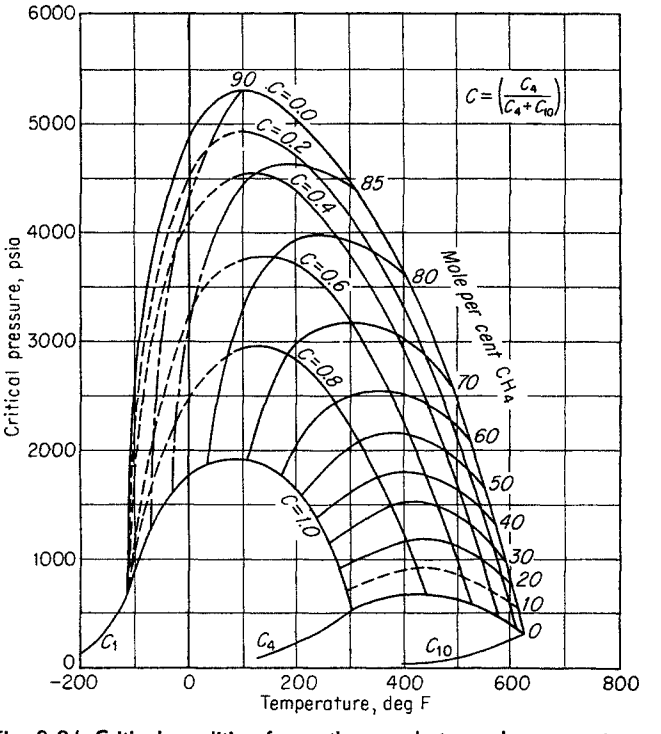

Fig. 3-24. Critical condition for methane–*n*-butane–decane system. (*Data of Sage and Lacey,* 1-17, 3-52, 3-60.)

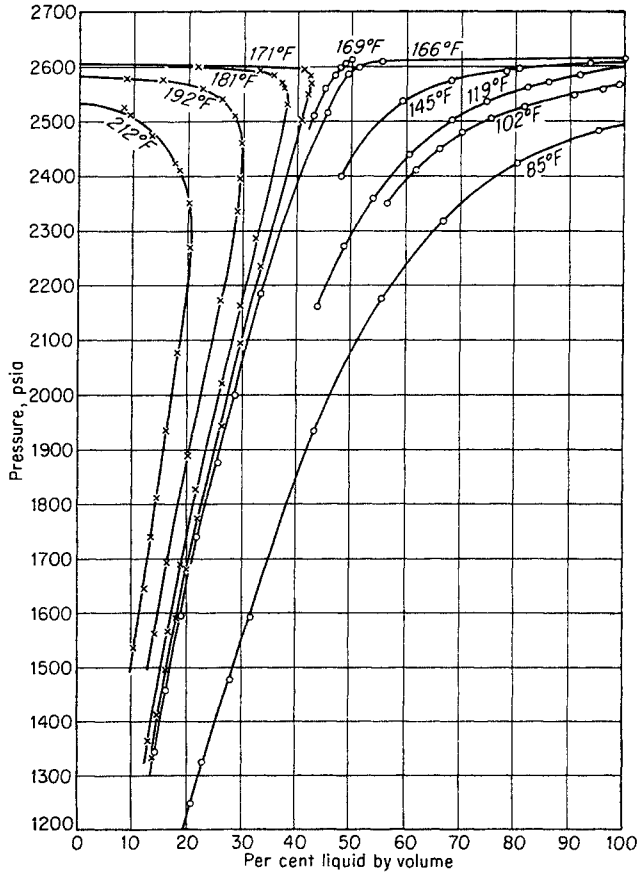

Fig. 3-25. Phase diagrams for a mixture of natural gas and natural gasoline. (*Katz, Vink, and David*, 3-29. *Courtesy AIME.*)

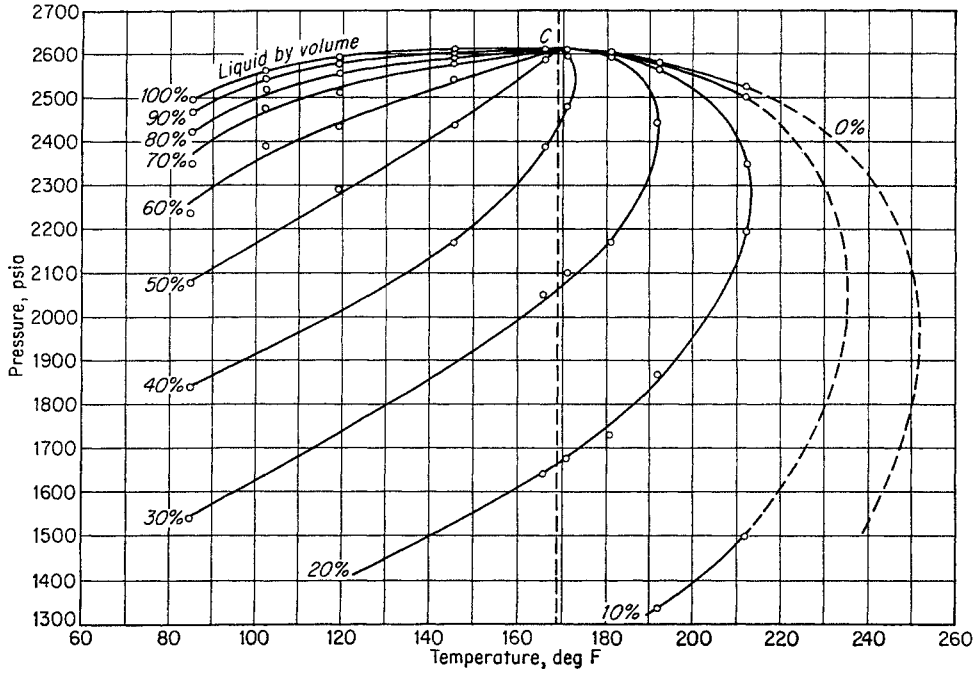

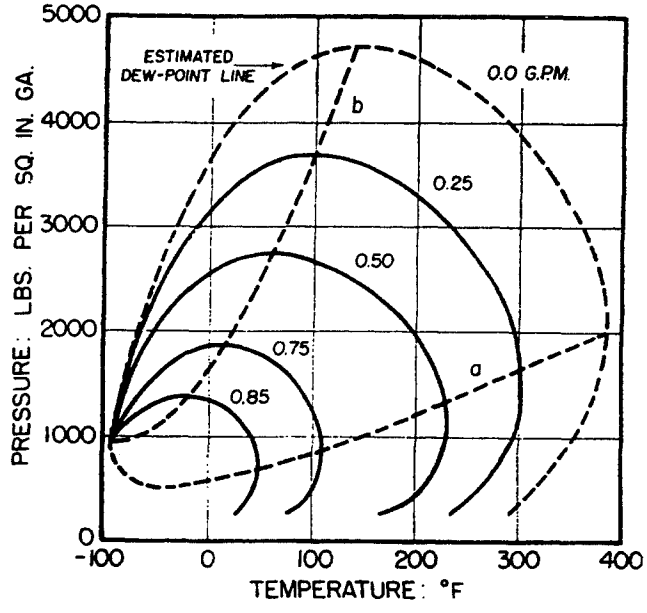

Fig. 3-26. Phase diagram for a natural gas. (*Buckley and Lightfoot*, 3-11. *Courtesy AIME.*)

Table 3-1. Composition of Natural Hydrocarbon Systems

	Investigators			
	Katz, Vink, and David	Buckley and Lightfoot	Weinaug and Bradley	Eilerts et al.
Mole %:				
Carbon dioxide	.....	.....	0.13	0.74
Nitrogen	.....	.....	0.76	1.38
Methane	59.7	94.11	53.91	76.48
Ethane	8.9	2.67	14.20	7.92
Propane	5.0	0.89	9.64	4.30
Isobutane	4.9	0.21	1.25	1.20
n-Butane		0.34	4.29	1.86
Isopentane	9.3	0.20	1.12	0.94
n-Pentane		0.10	1.87	0.78
Hexanes	.....	0.29	2.72	1.41
Hexanes+	12.2			
Heptanes+	.....	1.19	10.11	2.99*
	100.0	100.00	100.00	100.00
Molecular weight:				
Heptanes+	.....	.....	178.5	

* Fractional analysis given.

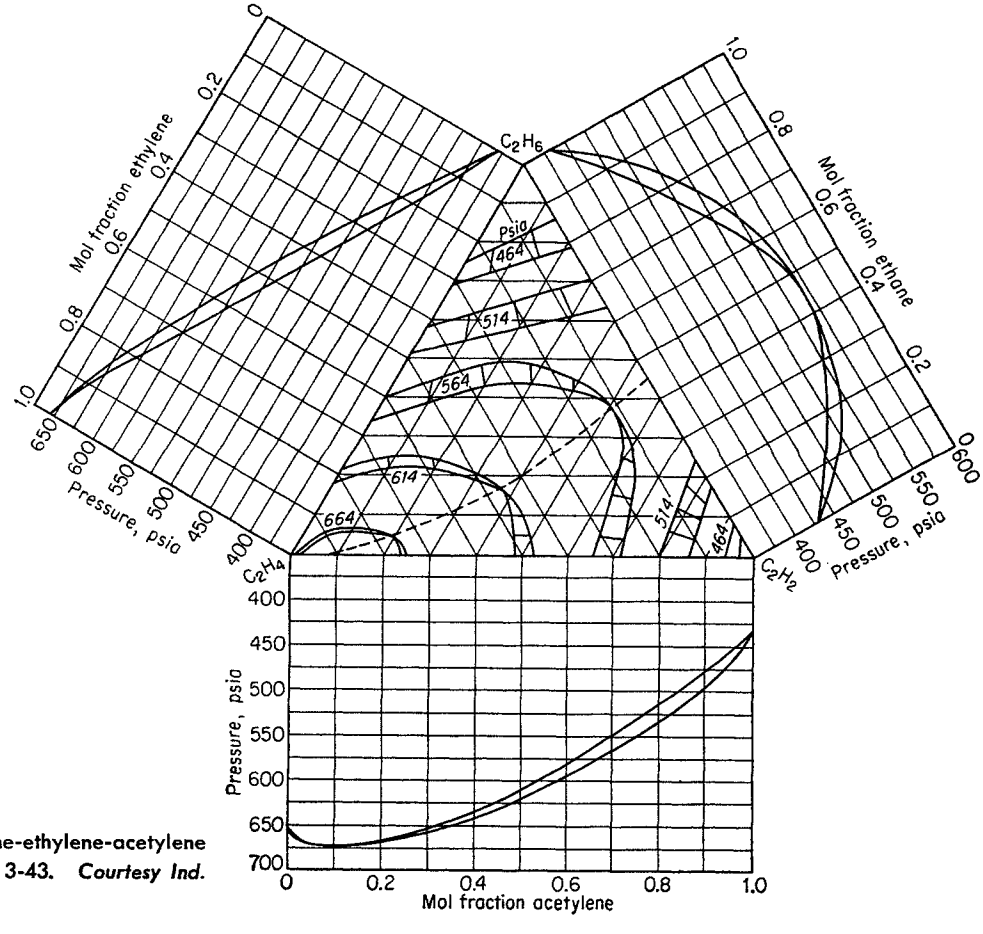

Fig. 3-27. Phase equilibria for ethane-ethylene-acetylene system at 40°F. (*McCurdy and Katz*, 3-43. *Courtesy Ind. Eng. Chem.*)

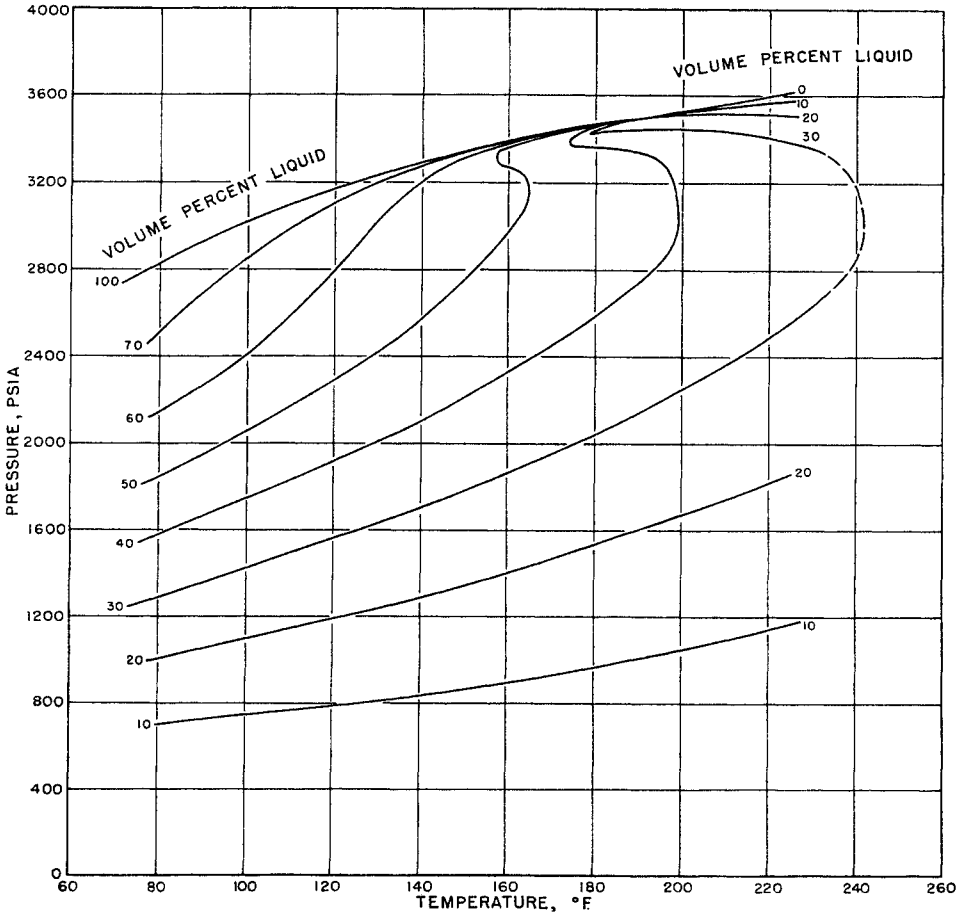

Fig. 3-28. Phase diagram for a naturally occurring hydrocarbon mixture. (*Weinaug and Bradley, 3-75. Courtesy AIME.*)

Raoult's and Dalton's laws are used to predict the phase behavior of fluid mixtures that are found to obey the laws. For a given constituent in a two-phase fluid system at constant temperature and pressure,

$$yP = xp \tag{3-3}$$

where P = total pressure
p = vapor pressure of constituent

Rearranging Eq. (3-3) gives the law in terms of the equilibrium constant,

$$\frac{y}{x} = \frac{p}{P} = K \tag{3-4}$$

There are two shortcomings of Raoult's law: (1) Some fluid mixtures deviate seriously from the law because of their chemical nature. (2) If the law is to hold, all constituents in a mixture must be at temperatures below their critical temperatures so that the vapor pressure may be known. Since the critical temperature of methane is −116°F, Raoult's law has little application for natural gas mixtures containing methane. Mixtures of propane, butanes, pentanes, etc., follow Raoult's law fairly well at temperatures up to 150°F and pressures up to 100 psia.

Instead of Raoult's law, ideal solutions may be assumed, by replacing the pressures of Eq. (3-3) by fugacities.

$$xf_L = yf_V \tag{3-5}$$

where f_L = fugacity of pure component as liquid at equilibrium temperature and pressure
f_V = fugacity of pure component as vapor at equilibrium temperature and pressure

Ideal equilibrium constants were devised (3-67) based on

$$K = \frac{y}{x} = \frac{f_L}{f_V} \tag{3-6}$$

It was found that fugacities could be extrapolated into regions above the critical temperature. The fugacities are found from P-V-T data by the following formulas of thermodynamics.

Definition of fugacity:

$$\ln f = \ln P - \frac{1}{RT}\int_0^P \left(\frac{RT}{P} - V\right) dP \tag{3-7}$$

where R = gas constant
T = absolute temperature
V = specific volume

This is equivalent to

$$RT\,d(\ln f) = V\,dP \tag{3-8}$$

At constant temperature, when energy other than heat and compression is negligible, the fugacity is related to the free-energy term F.

$$dF = V\,dP = RT\,d(\ln f) \tag{3-9}$$

Equation (3-7) or (3-8) converted to the form of Eq. (3-10) is convenient for computing the fugacity of a liquid or gaseous fluid by graphical means.

$$\ln f = \ln P - \int_0^P \frac{1 - z}{P}\,dP \tag{3-10}$$

where z = compressibility factor.

A generalized fugacity chart for natural gases based on reduced temperatures and pressures is given in Fig. 3-29 in terms of f/P, the activity coefficient (3-25). These fugacities served to provide ideal equilibrium constants (3-67).

Equilibrium constants based on experimental determination of vapor and liquid compositions superseded ideal constants, once the data became available. The reports on constants published in 1937 by Katz and Hachmuth for natural gas–crude oil systems (3-26) have been followed by several investigations on complex systems involving natural gases.

A comparison of Raoult's law with experimental equilibrium constants is shown in Fig. 3-30. The natural gas–crude oil data at 120°F are plotted; the methane-propane binary system from Sage and Lacey and the ethane-heptane system of Kay are traced. On log-log paper, Raoult's law gives a straight line of slope -1, drawn through the pressure equal to the vapor pressure at the temperature prevailing. At pressures below the vapor pressure, the experimental constants differ from Raoult's law for propane and the butanes. At higher pressures than the vapor pressures, the experimental constants go to a convergence point at unity. Thus, propane in methane at 1,000 psia and 120°F has an actual constant of 0.6 although Raoult's law gives 0.24. This effect of pressure is the

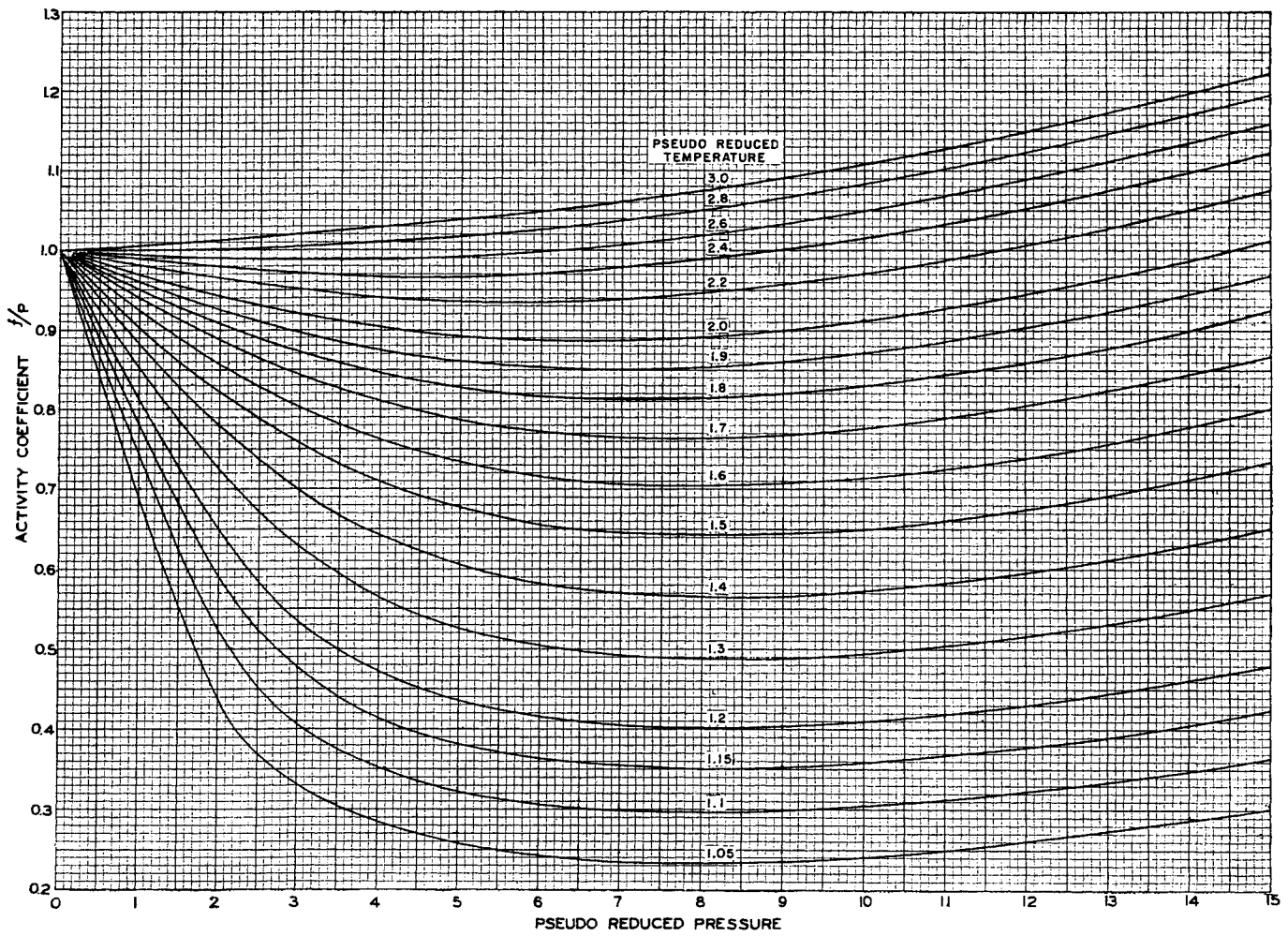

Fig. 3-29. Fugacity of natural gases. (*Brown*, 4-16, 3-25. *Courtesy AIME.*)

Table 3-2. References for Some Binary and Ternary Hydrocarbon Systems

System	Year	Reference	Investigator
Methane-ethane	1953	3-8	Bloomer, Gami, and Parent
	1939	3-56	Ruhemann
Methane-propane	1934, 1950	3-58, 3-53	Sage, Lacey, et al.
	1954	3-1	Akers, Burns, Fairchild
Methane–*n*-butane	1940	3-62, 3-63	Sage, Lacey, et al.
Methane-isobutane	1942	3-47	Olds, Sage, and Lacey
Methane–*n*-pentane	1939, 1942	3-69, 3-64	Sage, Lacey, et al.
	1938	3-9	Boomer, Johnson, Piercey
Methane-isopentane	1952	3-2	Amick, Johnson, and Dodge
Methane-hexanes	1938	3-9	Boomer, Johnson, Piercey
Methane–*n*-heptane	1938	3-9	Boomer, Johnson, Piercey
	1956	3-55	Reamer, Sage, and Lacey
Methane-decane	1942	3-49	Sage, Lacey, et al.
Ethane-butane	1940	3-31	Kay
Ethane-cyclohexane	1956	3-36	Kay and Albert
Ethane-heptane	1938	3-30	Kay
Propane–*n*-butane	1940	3-46	Nysewander, Sage, and Lacey
Propane–isopentane	1942	3-71	Vaughan and Collins
Propane–*n*-pentane	1940	3-61	Sage and Lacey
Methane-nitrogen	1952	3-7	Bloomer and Parent
	1953	3-15	Cines, Roach, Hogan, and Roland
Methane-ethylene	1940	3-23	Guter, Newitt, and Ruhemann
	1940	3-74	Volona
Ethane–hydrogen sulfide	1953	3-35	Kay and Brice
Propane–hydrogen sulfide	1953	3-34	Kay and Rambosek
Carbon dioxide–propane, butane, pentane	1945	3-48	Poettmann and Katz
Propane-propene	1951	3-54	Reamer and Sage
Ethylene-ethane	1953	3-24	Hanson, Hogan, Ruehlen, and Cines
Ethane-propylene	1951	3-45	McKay, Reamer, Sage, and Lacey
Ethylene-propane	1939	3-4	Atack, Evans, and MacCormack
Ethylene–*n*-butane	1947	3-76	Williams
Propane-acetylene	1945	3-44	McCurdy and Katz
Propane-isobutylene	1939	3-22	Gilliland, Lukes, and Scheeline
Methane-butane-decane	1947	3-50	Sage, Lacey, and Reamer
	1949	3-51	Sage, Reamer, and Fiskin
	1947	3-52	Sage, Lacey, and Reamer
Methane-propane-pentane	1941	3-13	Sage, Carter, and Lacey
	1943	3-17	Dourson, Sage, and Lacey
Methane-ethane-pentane	1948	3-6	Billman, Sage, and Lacey
Methane-ethylene-isobutane	1945	3-5	Benedict, Solomon, and Rubin

reason that the constants vary with composition of the phase and deviate seriously from Raoult's law. Methane and ethane are above their critical temperatures at 120°F. The extrapolated vapor pressures used to give the lines labeled "Raoult's law" are rather unreliable at any pressure.

A binary system may be used to understand critical phenomena and phase behavior. Figure 3-31 is a plot of the constants for the methane-propane system at 100°F. Referring to Fig. 3-11, the methane-propane system may be studied at 100°F using mixture *B*. The compositions of vapors and liquids can be used to obtain the equilibrium constants from plots similar to Fig. 3-15 or 3-16. With mixture *B*, the bubble point is reached at the indicated pressure and the *K* curves of Fig. 3-31 would terminate here. Using mixture *C* permits observation of vapor-liquid phenomena until pressure *C* is reached; so the constants in Fig. 3-31 may be extended to *C*. Extension of this process to the critical locus requires that mixture *E* be chosen eventually; *E* is the mixture that has its critical temperature at the equilibrium temperature. The convergence point *E* in Fig. 3-31 is the critical pressure for the binary mixture that has its critical temperature at the equilibrium temperature. The critical locus for binary systems is synonymous with the convergence pressure-temperature locus. A binary system in two phases has two degrees of free-

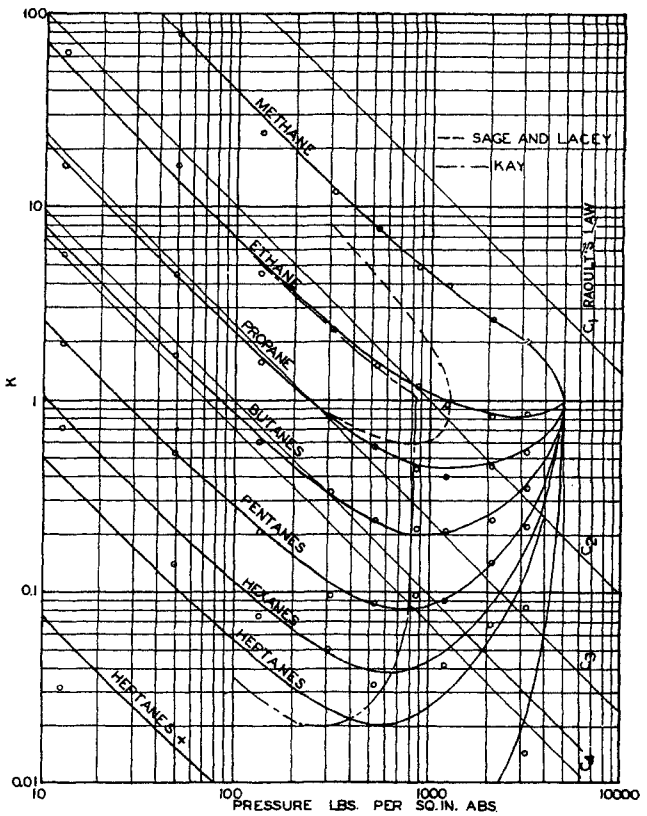

Fig. 3-30. Comparison of Raoult's law with measured equilibrium constants at 120°F. (*Katz, 3-27. Courtesy AIME.*)

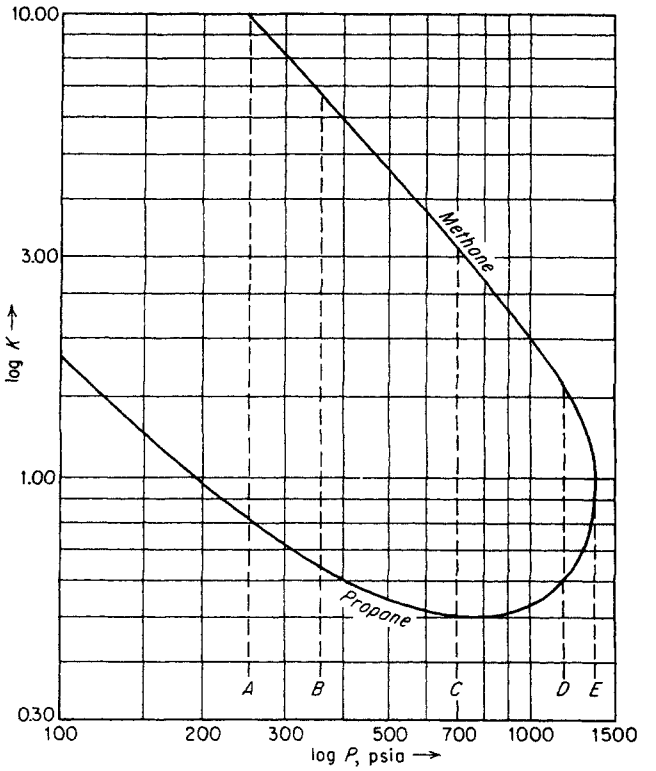

Fig. 3-31. Equilibrium constants for methane-propane at 100°F. (*Data of Sage, Lacey, and Schaafsma, 3-58.*)

dom, and specification of temperature and pressure defines the composition of the phases throughout the two-phase area.

For ternary systems, pressure, temperature, and a third variable are required to define phase compositions. A parameter of composition ratio may be used, and the convergence pressures may be given as shown in Fig. 3-20 or 3-24.

Many simple hydrocarbon systems containing methane have been investigated, and may provide the data required for a problem. Table 3-2 lists references for binary and ternary volatile systems. For complex systems, much can be learned from the behavior of these binary and ternary systems. Data on complex systems and methods of estimating equilibrium constants will be discussed in Chap. 6.

CHAPTER 4

Properties of Natural Gases and Volatile Hydrocarbon Liquids

The behavior of natural gas, whether pure methane or a mixture of volatile hydrocarbons and the nonhydrocarbons nitrogen, carbon dioxide, and hydrogen sulfide, must be understood by the engineer designing and operating equipment for its production, processing, and transportation. The constituents of natural gas are most likely to be found in the gaseous state but can occur as liquids or solids. A knowledge of the state or phase in which the constituents occur is of prime importance. The properties of natural gases and of the constituents therein that are of interest are:

Diffusion coefficients
Compressibility factor for gases
Density of gases and liquids
Surface tension
Thermodynamic properties
  Heat capacity
  Latent heat
  Enthalpy of mixtures
Heating value
Limits of flammability
Critical properties
Viscosity
Thermal conductivity

Natural gas compositions have been given in Tables 1-5 and 1-7. Methods of analysis are discussed in connection with vapor-liquid equilibria (Chap. 6). Natural gases are similar in composition in that the ratios of the concentrations of the constituents do not vary over a wide range for most gases. The use of gas gravity as a characterizing parameter depends upon this similarity of compositions. Legatski, Tooke, and Grundy (4-57) presented a chart on which the composition of all gases lie on a straight line (Fig. 4-1).

The physical constants for the pure hydrocarbons are given in Table A-1.

MOLECULAR THEORY OF GASES AND LIQUIDS

Gases and liquids are made up of molecules and may be treated on a molecular basis. The nature of the molecules and of the forces existing between them controls the properties of the fluid. The kinetic theory of gases developed in the nineteenth century by such people as Joule, Clausius, Boltzmann, and Maxwell treats a gas as "a crowd of molecules, each moving on its own independent path, entirely uncontrolled by forces from the other molecules, although its path may be abruptly altered as regards both speed and direction, whenever it collides with another molecule or strikes the boundary of the containing vessel" (4-45). In its simplest state, a gas may be considered as composed of particles that have no volume and between which there are no forces. The general behavior of gases at low pressure was found to comply with the theories developed from this simple concept, but gradually disparities between theory and observed behavior caused modification of the theory to include molecular volumes and forces between the molecules. More recently the statistical-mechanics theories evolved from the quantum theory of molecules have provided means for relating the bulk properties of gases to intermolecular forces (4-41).

In the theory of matter, the concept of a *mole* has been used to relate the quantity of one substance to that of another. The mass of one atom of oxygen was arbitrarily fixed at 16 (a mole of oxygen O_2 at 32) and the relative mass of other elements or molecules was determined as their atomic or molecular weights. Avogadro's rule states that equal volumes of gas, at any given temperature and pressure, contain an equal number of molecules. This number is 6.02×10^{23} molecules for 1 gram mole of a substance (32 grams of O_2) at 0°C and 1 atm (22,415 cu cm). A pound mole (lb mole) of oxygen is 32 lb, with

$$453 \times 6.02 \times 10^{23} = 2.7 \times 10^{26}$$

molecules in 359 cu ft at 32°F and 1 atm, or 379 cu ft at 60°F and 14.7 psia.

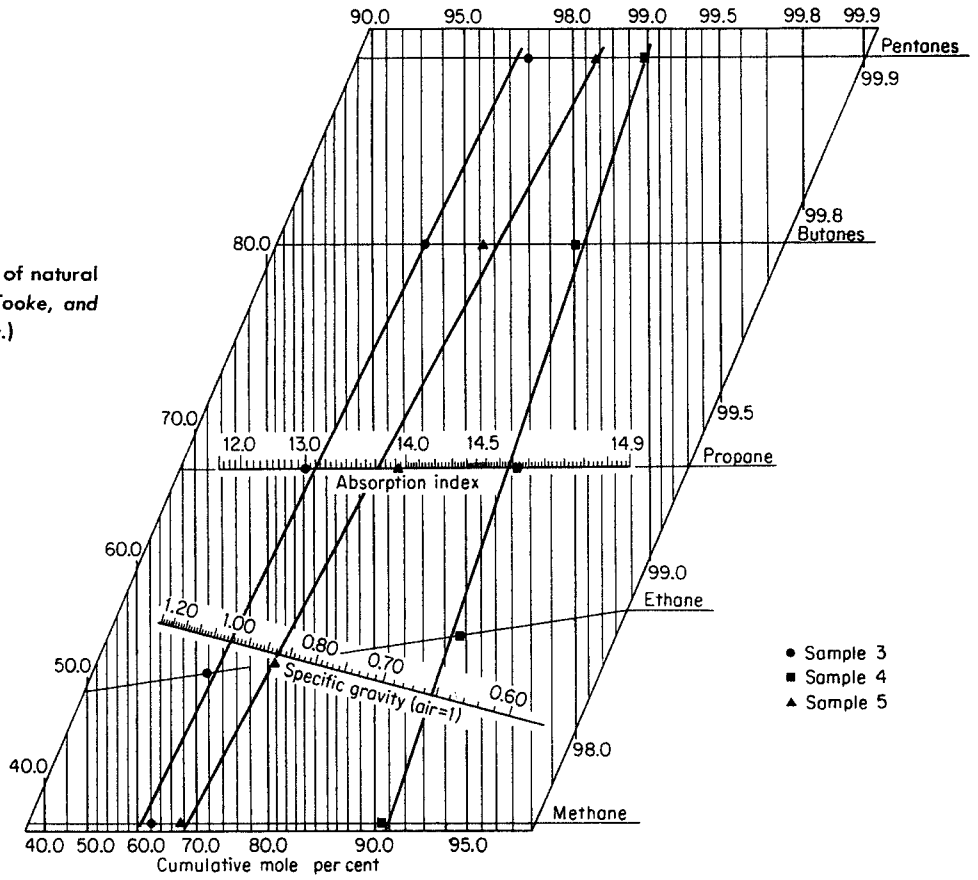

Fig. 4-1. Chart for plotting composition of natural gases as a straight line. *(Legatski, Tooke, and Grundy, 4-57. Courtesy Petrol. Refiner.)*

Equation of State—the Gas Law

The gas law relating pressure, temperature, and volume for a gas with molecules of zero size and without intermolecular forces is known as the ideal- or perfect-gas law,

$$PV = nRT \qquad (4\text{-}1)$$

where P = pressure
V = volume
n = number of moles
R = gas constant
T = absolute temperature

The values of R for various units of temperature, pressure, and volume are given in Table 4-1. Gases near atmospheric pressure follow the ideal-gas law; so pressure or volume can be predicted from temperature and mass within 5 per cent or better. If more precise prediction becomes necessary or if gases at high pressure are to be treated, the ideal-gas equation becomes inadequate. Voluminous data are available on P-V-T relations of pure substances and of mixtures of natural gases, from which the deviations from ideal-gas laws may be noted. (Bibliographies are given in Refs. 4-61, 4-80, 1-2, 1-9.)

There are two common methods of correcting this equation to obtain the P-V-T behavior of real gases.

Table 4-1. Gas-law Constants

$PV = nRT$

Values of R for Various Units

Unit of pressure P	Unit of temperature T	Unit of volume V	R for n = 1 mole
atm	°K (°C + 273.16)	liter	0.082055
psia	°R (°F + 460)	cu ft	10.73
lb/sq ft abs	°R (°F + 460)	cu ft	1,545.0
R for Air when n = 1 lb			
lb/sq ft	°R (°F + 460)	cu ft	53.2

Volume of 1 Mole of Ideal Gas for Various Units

Pressure	Temperature	Molecular volume
1 atm	0°C	22.414 liters/gram mole
14.7 psia	32°F	359 cu ft/lb mole
14.7 psia	60°F	379 cu ft/lb mole

One is to insert a variable correction factor, *the compressibility factor z*, into the ideal-gas equation.

$$PV = znRT \tag{4-2}$$

This gas law is general, and z may be either a graphical or a mathematical function of temperature, pressure, and the composition of the gas. Methods of predicting the compressibility factor from graphical correlations will be given in detail in a subsequent section, for this method of handling gas behavior is commonly used in engineering practice.

The second method of predicting the P-V-T behavior more accurately is to use an enlarged or expanded equation, commonly called *the equation of state*. Van der Waals gave the first such equation, in which constants were added to Eq. (4-1) to represent the volume b occupied by the molecules and the attractive forces a between the molecules.

$$\left(P + \frac{a}{V^2}\right)(V - b) = RT \tag{4-3}$$

The van der Waals constants a and b are given in Table 4-2.

Many equations of state have been proposed, and the required constants determined from experimental data. The Beattie-Bridgeman equation (4-7, 4-90) has been used considerably and has good precision up to two-thirds of the critical densities. This is

$$P = \frac{RT}{V^2}\left(1 - \frac{c}{VT^3}\right)\left[V + B_0\left(1 - \frac{b}{V}\right)\right] - \frac{A_0(1 - a/V)}{V^2} \tag{4-4}$$

where a, b, c, A_0, and B_0 are constants for a given constituent, as shown in Table 4-2.

An equation employing eight constants was applied to the light hydrocarbons by Benedict, Webb, and Rubin (4-10). This equation is

$$P = RTd + \left(B_0RT - A_0 - \frac{C_0}{T^2}\right)d^2 + (bRT - a)d^3 + a\alpha d^6 + \frac{cd^3}{T^2}[(1 + \gamma d^2)e^{-\gamma d^2}] \tag{4-5}$$

where d = molal density and where the parameters B_0, A_0, C_0, a, b, c, α, and γ are numerical constants for pure compounds and functions of compositions for mixtures.

These constants for pure compounds are given in Table 4-2. The constants for pure compounds, with the mole fractions x of the constituents in a given phase, are used to obtain the parameter for a mixture according to the following relationships:

$$B_0 = \Sigma x_i B_{o,i} \tag{4-6}$$
$$A_0 = (\Sigma x_i A_{o,i}^{1/2})^2 \tag{4-7}$$
$$C_0 = (\Sigma x_i C_{o,i}^{1/2})^2 \tag{4-8}$$
$$b = (\Sigma x_i b_i^{1/3})^3 \tag{4-9}$$
$$a = (\Sigma x_i a_i^{1/3})^3 \tag{4-10}$$
$$c = (\Sigma x_i c_i^{1/3})^3 \tag{4-11}$$
$$\alpha = (\Sigma x_i \alpha_i^{1/3})^3 \tag{4-12}$$
$$\gamma = (\Sigma x_i \gamma_i^{1/2})^2 \tag{4-13}$$

Using these summations of the products of the mole fractions of the several constituents and the constants for the pure constituents may not be the best method of obtaining the equations for mixtures when more data are available.

Table 4-2. Constants in Equations of State*

Substance	Van der Waals constants		Beattie-Bridgeman constants					Benedict-Webb-Rubin constants							
	a†	b‡	$A_0 \times 10^{-3}$	a	B_0	b	$c \times 10^{-6}$	A_0	B_0	$C_0 \times 10^{-6}$	a	b	$c \times 10^{-6}$	$\alpha \times 10^3$	$\gamma \times 10^2$
Methane	2.253	0.04278	8.5863	0.2972	0.8950	−0.2542	11.986	6,995.25	0.682401	275.763	2,984.12	0.867325	498.106	511.172	153.961
Ethane	5.489	0.06380	22.174	0.9389	1.506	+0.3068	84.08	15,670.7	1.00554	2,194.27	20,850.2	2.85393	6,413.14	1,000.44	302.790
Propane	8.664	0.08445	44.951	1.173	2.899	+0.6877	112.10	25,915.4	1.55884	6,209.93	57,248.0	5.77355	25,247.8	2,495.77	564.524
Isobutane	12.87	0.1142	62.614	1.7895	3.771	+1.233	280.27	38,587.4	2.20329	10,384.7	117,047	10.8890	55,977.7	4,414.96	872.447
n-Butane	14.47	0.1226	67.102	1.9481	3.944	+1.509	326.98	38,029.6	1.99211	12,130.5	113,705	10.2636	61,925.6	4,526.93	872.447
Isopentane	18.05	0.1417	.....	.....	.....	.....	.....	4,825.36	2.56386	21,336.7	226,902	17.1441	136,025	6,987.77	1,188.07
n-Pentane	19.01	0.1460	106.570	2.4187	6.311	+2.236	373.70	45,928.8	2.51096	25,917.2	246,148	17.1441	161,306	7,439.92	1,218.86
n-Hexane	24.39	0.1735	.....	.....	.....	.....	.....	5,443.4	2.84835	40,556.2	429,901	28.0032	296,077	11,553.9	1,711.15
n-Heptane	31.51	0.2654	205.600	3.2144	11.344	+3.072	373.70	66,070.6	3.18782	57,984.0	626,106	38.9917	483,427	17,905.6	2,309.42
Nitrogen	1.390	0.03913	5.0702	0.4192	0.8083	−0.1107	3.92								
Carbon dioxide	3.592	0.04267	18.880	1.1425	1.6781	+1.1590	61.66								
Hydrogen sulfide	4.431	0.04287													
Helium	0.03412	0.02370	0.08146	0.9586	0.2243	0	0.0037								
Water	5.464	0.03049													
Hydrogen	0.2444	0.02661	0.7448	−0.0811	0.3358	−0.6983	0.0471								
Ethylene	4.471	0.05714	23.200	0.7952	1.9473	+0.5762	21.19	12,593.6	0.891980	1,602.28	15,645.5	2.20678	4,133.60	731.661	236.844
Propylene	8.379	0.08272	.....	.....	.....	.....	.....	23,049.2	1.36263	5,365.97	46,758.6	4.79997	20,083.0	1,873.12	469.325

* T in °R (°F + 459.63); d in lb moles/cu ft; P in psia. R = 10.7335 psia-cu ft/(lb mole)(°R). † a in liters²-atm/mole². ‡ b in liters/mole.

Martin and Hou (4-59) have developed a complicated but promising equation for pure substances, which involves ten constants and which can be evaluated from the critical P-V-T data and from the slope of the vapor-pressure curve at the critical point.

These equations of state are methods of extending experimental behavior and predicting deviations from ideal-gas laws. They have the advantage of providing a mathematical basis for predicting thermodynamic properties that depend upon P-V-T data.

Equations of state have been developed from statistical mechanical theory (4-41, 4-12), in which it is assumed that the forces between the molecules are the basis for the deviation from ideal behavior. The virial equation of state, Eq. (4-14), in effect reports the compressibility factor in terms of a power series.

$$\frac{PV}{RT} = z = 1 + \frac{B}{V} + \frac{C}{V^2} + \frac{D}{V^3} \qquad (4\text{-}14)$$

where the term B is called the second virial coefficient, C the third virial coefficient, and D the fourth. The virial coefficients are functions of temperature only, and depend primarily on interaction of groups of two, three, and four molecules, respectively. The prediction of virial coefficients and compressibility factors is more reliable for simple molecules such as oxygen and nitrogen (4-36) and has not been extended to natural gas systems as yet. The methods of statistical mechanics are useful for determining such properties as viscosity and thermal conductivity as well as density.

Molecular Velocity—Mean Free Path

At steady state, individual gas molecules have a wide range of linear velocities and move in all directions. The distribution of molecular velocities is given by Maxwell's law (4-45, 4-89) and is shown qualitatively in Fig. 4-2. The molecules will travel greater or lesser distances before collision with other molecules, depending upon the concentration or density of the gas. Just as there is a velocity-distribution curve, there is a relationship between number of molecules and distance traveled for specified conditions. The mean distance traveled between collisions is usually referred to as the *mean free path.*

Chapman and Cowling (4-24) give the following formula for computing the length of the mean free path of smooth, rigid, elastic, spherical molecules:

$$\lambda = \frac{1}{N\pi\sigma^2\sqrt{2}} = \frac{0.225}{N\sigma^2} \qquad (4\text{-}15)$$

where λ = mean free path of molecules, cm
N = number of molecules per cu cm
σ = collision diameter of molecule, cm

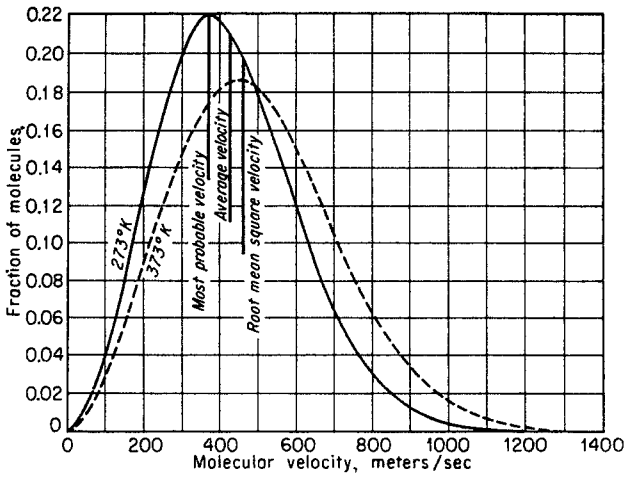

Fig. 4-2. Velocity distribution for molecules. *(After Taylor and Taylor, 4-89.)*

For hydrogen, Chapman and Cowling give a collision diameter found from viscosity studies as 2.73×10^{-8} cm. The number of molecules at 32°F and 1 atm in 1 cu cm of volume is 6.02×10^{23} divided by 22,414 cu cm/mole or 2.68×10^{19} molecules. The mean free path at 1 atm becomes

$$\lambda = \frac{0.225}{2.68 \times 10^{19} \times 2.73^2 \times 10^{-16}} = 1.12 \times 10^{-5} \text{ cm} \qquad (4\text{-}16)$$

For hydrogen, the number of collisions per second is 2.05×10^{29}, the collision frequency is 1.5×10^{10}/sec, and the time between collisions is 6.6×10^{-11} sec, all at 32°F and 1 atm (4-24). The length of the mean free path does not depend upon the mass of the mole-

Table 4-3. Molecular Diameters and Mean Free Paths

Substance	Collision diameter σ, A*	Mean free path λ, cm $\times 10^5$	
		Computed† at 32°F and 1 atm	From flow data
Methane	3.35–3.88	0.75 –0.56	0.64
Ethane	3.54–3.81	0.67 –0.58	0.40
Propane	4.21–4.42	0.473–0.430	0.28
n-Butane	4.5 –4.82	0.415–0.362	
Ethylene	3.70–3.35	0.614–0.749	
Propylene	4.02–4.32	0.52 –0.45	
Hydrogen	2.57–2.73	1.27 –1.125	1.45
Nitrogen	3.36–3.68	0.74 –0.62	0.83
Helium	1.90	2.33	2.33
Carbon dioxide	3.996	0.53	0.53

* 1 angstrom (A) = 10^{-8} cm. σ, A = σ, cm $\times 10^8$.

† $\lambda = 0.225/(N \times \sigma^2) = 0.225 \times 10^{16}/(2.68 \times 10^{19} \times \sigma^2) = 8.4 \times 10^{-5}/\sigma^2$ for λ in centimeters and σ_0 in angstroms (cm $\times 10^8$).

cule nor upon the temperature unless temperature affects the diameter of the molecule. Thus, the mean free path of all gases at 1 atm is of the order of 10^{-5} cm. This distance is from 200 to 400 times the diameter of the molecule (Table 4-3) and is the basis of the assumption of molecular chaos made in deriving Eq. (4-15). The mean free path depends upon the number of molecules in a given volume and, for ideal gases, is inversely proportional to the pressure. At 100 atm, the mean free path calculated by Eq. (4-15) approaches molecular diameters and the equation is no longer valid; at pressures of 0.01 mm Hg, the mean free path reaches values of 1 cm.

The collision diameter is not known accurately for hydrocarbon molecules, which are more complex than hydrogen molecules, since calculation of these diameters from different measurements gives a range of values. The diameters are given in Table 4-3, along with the range of mean free paths computed for the diameters shown. The mean free path at pressures other than 1 atm can be found by dividing the mean free path at 1 atm by the absolute pressure in atmospheres.

Figure 2-16 shows the difference in the permeability of a porous solid to various gases. The experiments on which Fig. 2-16 is based indicate a more definite relationship between the mean free paths than that given by Table 4-3. By computing b in Eq. (2-7) for the several gases in Fig. 2-16, one can relate the mean free paths by the following equation:

$$\frac{b_1}{b_2} = \frac{\lambda_1}{\lambda_2} \tag{4-17}$$

With the value for helium used as a standard, the rest of the mean free paths are computed from flow data (2-17) by Eq. (4-17), and are given in Table 4-3. In general, the agreement between these values of mean free path and those found from molecular-collision diameters is reasonable.

Diffusion of Gases

With individual gas molecules in rapid motion, contact of a gas composed of molecules A with gas composed of molecules B will cause diffusion of A into B and of B into A. Diffusion is the process by which a gas body becomes of uniform composition.

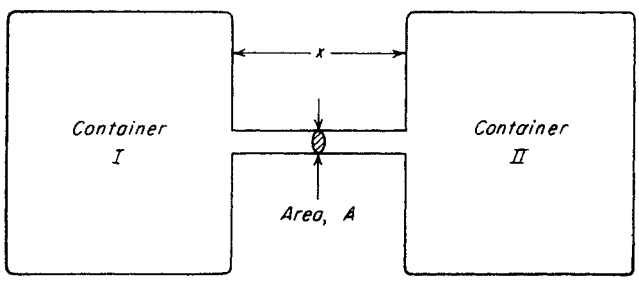

Fig. 4-3. Diffusion process.

Diffusion becomes significant in several operations in the gas industry. In such simple operations as mixing gases under pressure in a cylinder in the laboratory, how long must one wait after admitting a second gas before the content of the cylinder becomes uniform in composition through interdiffusion? When constituents are transferred preferentially between gas and liquid phases, diffusion rates of the extracted constituent in either the gaseous or the liquid phase may control the extraction process. When gases are displaced from porous media by other gases, molecular diffusion can cause mixing at the interface between the two gases. When gas is passed through a porous solid wet with liquid, the rate of attaining equilibrium between the gas and the liquid phase depends upon diffusion processes.

Diffusion coefficients can be measured in apparatus shown symbolically in Fig. 4-3. Container I may contain pure hydrogen gas and container II a mixture of hydrogen and carbon dioxide. The carbon dioxide molecules in constant motion in container II would find their way through the passage between the containers. If the containers were large in proportion to the passage and if the contents of the containers were agitated to keep them of uniform composition at the entrance and exit of the passage, then the diffusion of carbon dioxide would be a steady-state process. Fick's law for such a diffusion process is given by Eq. (4-18).

$$\frac{dn}{dt} = -DA\frac{dc}{dx} \tag{4-18}$$

where n = number of molecules of gas constituent diffusing
t = time
A = area
c = concentration of diffusing constituent
x = distance through which diffusion takes place
D = diffusion coefficient

Illustrative Problem

The diffusion coefficient for $C^{14}O_2$ in hydrogen at 100°C is 0.341 sq cm/sec (4-25). Compute the diffusion rate of 100°C through a conduit 2 mm × 2 mm and 2.0 cm long, when hydrogen with 0.1 mole per cent $C^{14}O_2$ is in container I and hydrogen with 1.0 per cent $C^{14}O_2$ is in container II.

$$\frac{dn}{dt} = -DA\frac{dc}{dx} \tag{4-18}$$

$$= \left(0.341\ \frac{\text{sq cm}}{\text{sec}}\right)\left(\frac{0.2 \times 0.2\ \text{sq cm}}{2.0\ \text{cm}}\right)\left(\frac{0.009 \times 273\ \text{gram moles}}{22{,}414 \times 373\ \text{cu cm}}\right)$$

$$= 2.0 \times 10^{-10}\ \text{gram mole/sec}$$

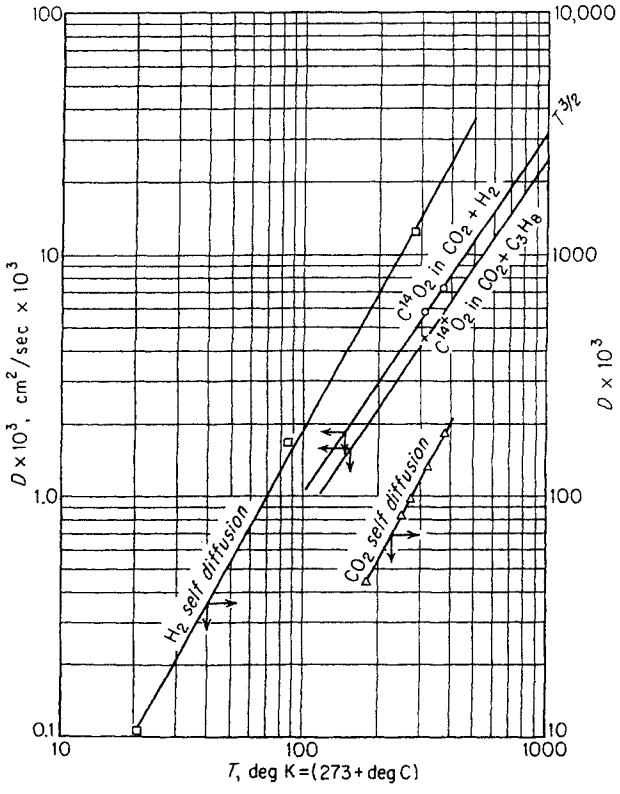

Fig. 4-4. Effect of temperature on diffusion coefficient at 1 atm.

In case the diffusion takes place rapidly, an unsteady state can occur since the inlet and outlet concentrations are changing continuously. Then Fick's second law for unsteady state applies, Eq. (4-19).

$$\frac{dn}{dt} = D\frac{\partial^2 c}{\partial x^2} \tag{4-19}$$

Diffusion coefficients may be predicted from the behavior of molecules (4-5, 4-24, 4-39). Gilliland (4-34) has correlated diffusion coefficients for gases at 1 atm pressure by the following equation:

$$D = \frac{0.0043T^{3/2}\left(\frac{1}{M_A} + \frac{1}{M_B}\right)^{1/2}}{(V_A^{1/3} - V_B^{1/3})^2 P} \tag{4-20}$$

where T = absolute temperature, °K (273 + °C)
M_A = molecular weight of gas A
M_B = molecular weight of gas B
V = molal volume at normal boiling point, cu cm/mole
P = total pressure, atm
D = diffusion coefficient of gas, sq cm/sec

The diffusion coefficient is inversely proportional to pressure; that is, the diffusion coefficient times the density gives a constant value. The power on the absolute temperature depends upon the type of molecule involved; the 3/2 power used above applies for elastic spheres, and other values apply for different models.

Chou and Martin (4-25) studied the diffusion of carbon dioxide containing C^{14} into mixtures of carbon dioxide with hydrogen and into mixtures of carbon dioxide with propane. Their data at 1 atm are plotted as a function of temperature in Fig. 4-4, as well as self-diffusion data for hydrogen (4-39). Table 4-4 presents diffusion coefficients for a few gases at atmospheric pressure. Plots of Chou and Martin's data (4-25) are given in Fig. 4-5, demonstrating that the product of the diffusion coefficient and the density is essentially a constant; and in Fig. 4-6, giving the effect of composition in a binary system on the diffusion coefficient. Other data of interest include the work of Jeffries and Drickamer (4-46) on the methane-

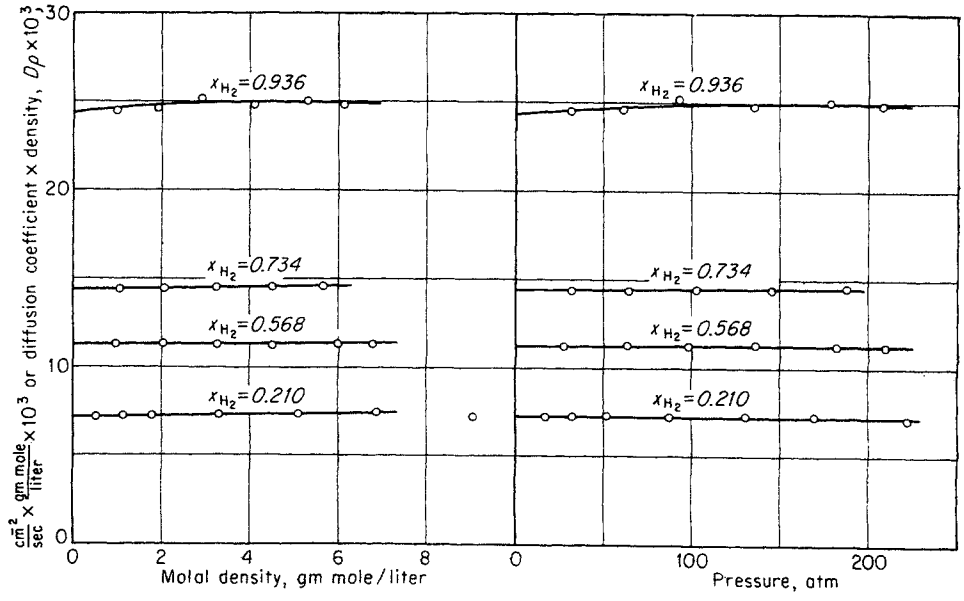

Fig. 4-5. Diffusion coefficients of $C^{14}O_2$ in $C^{12}O_2$-H_2 system at 100°C. (*Chou and Martin, 4-25. Courtesy Ind. Eng. Chem.*)

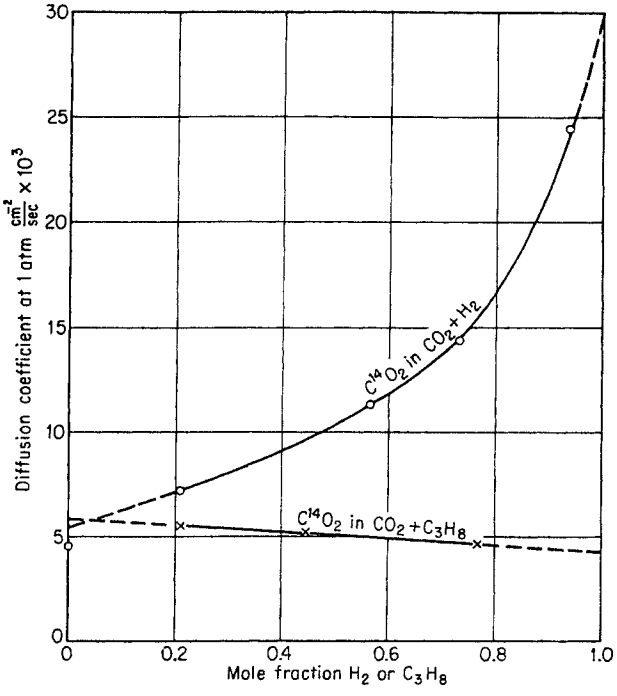

Fig. 4-6. Effect of concentration on diffusion coefficient. (*Chou and Martin, 4-25. Courtesy Ind. Eng. Chem.*)

TCH_3 (methane with tritium replacing one H) system (Fig. 4-7) and data of O'Hern and Martin (4-62) and of Timmerhaus and Drickamer (4-92).

Sage, Lacey, and coworkers have measured diffusion coefficients of *n*-hexane and heptane in vapors of methane, ethane, and propane (4-21 to 4-23). Figure 4-8 shows that diffusion coefficients for methane in *n*-hexane vary as a straight-line function of concentration. Table 4-5 lists the diffusion coefficients for hydrocarbon gases from Carmichael, Sage, and Lacey (4-22).

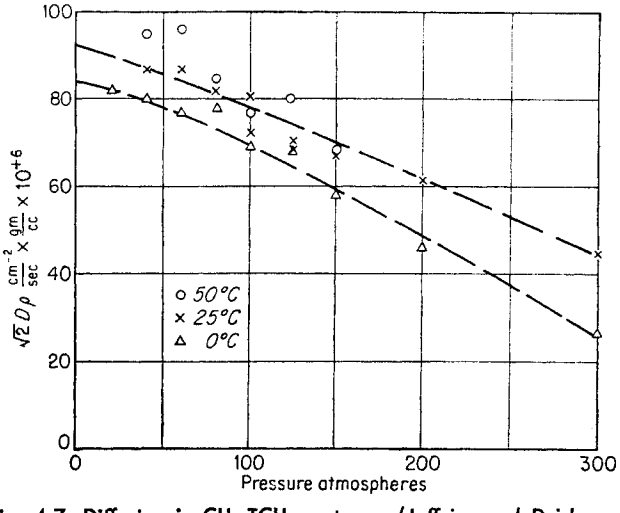

Fig. 4-7. Diffusion in CH_4-TCH_3 system. (*Jeffries and Drickamer, 4-46. Courtesy J. Chem. Phys.*)

In predicting the diffusion coefficient for a constituent in a multicomponent mixture, the equation of Wilke (4-96) can be used. This is

$$D'_A = \frac{1 - y_A}{y_B/D_{AB} + y_C/D_{AC} + y_D/D_{AD} + \cdots} \quad (4\text{-}21)$$

where D'_A = effective average diffusion coefficient for A in complex mixture
D_{AB} = diffusion coefficient of A in system AB
D_{AC} = diffusion coefficient of A in system AC
y = mole fractions

and where subscripts A, B, C, etc., represent constituents A, B, C, etc.

Mixing in Cylinders

The mixing of gases in cylinders under pressure was studied by Smith (4-84). He calculated diffusion between the top and bottom halves of cylinders, using a procedure developed by Loschmidt. Figure 4-9 shows the difference in composition between a constituent's mole fraction F_L in the lower half and F_U in the upper half of the cylinder as a function of pressure. The calculations are for a standard gas cylinder 32 in. tall. The coefficients used were 0.564 sq cm/sec for helium in methane and 0.081 sq cm/sec for butane in air. When the gas-concentration gradient has disappeared, $F_L - F_U = 0$. It will be seen that long mixing times for large molecules of hydrocarbon gases are required

Table 4-4. Diffusion Coefficients of Gases at Atmospheric Pressure

System	Temperature, °C	Fick diffusion coefficient D, sq cm/sec
Hydrogen in air	25	0.410
Hydrogen in hydrogen	0	1.29
Carbon dioxide in air	25	0.164
Carbon dioxide in methane	0	0.147
Methane in air	0	0.196
Hydrogen in carbon dioxide	0	0.53
Hydrogen in methane	0	0.63
Hydrogen in ethane	0	0.46
Octane in air	25	0.060
Benzene in air	25	0.088
$C^{14}O_2$ in $C^{12}O_2 + C_3H_8$:		
Mole % of C_3H_8: 20.3	100	0.0054
44.1	100	0.0051
77	100	0.0047
$C^{14}O_2$ in $C^{12}O_2 + H_2$:		
Mole % of H_2: 21	100	0.0073
56.8	100	0.0113
73.4	100	0.0144
93.6	100	0.0244
Methane in methane	19	0.214

SOURCE: (4-5, 4-25, 4-121a).

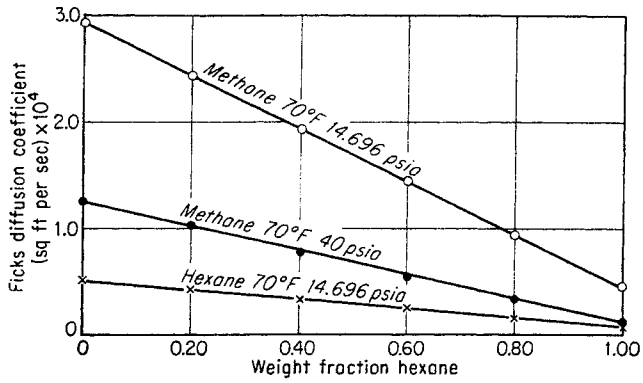

Fig. 4-8. Diffusion coefficients in methane–*n*-hexane system. (*Data of Carmichael, Sage, and Lacey*, 4-22.)

to attain complete homogeneity when halves of the cylinder are filled initially with different gases. In actual practice, the injection of the second constituent would cause considerable mixing and thermal, natural convection currents would assist in the mixing. Nevertheless, precautions, such as heating the bottom of the cylinder, should be taken under circumstances when complete mixing of gases under high pressure is desired quickly.

Diffusion through Porous Solids

Diffusion through the interstices of porous solids has been mentioned in connection with slip phenomena. Diffusion is less in a porous solid than in open space because of the restriction imposed by the solid network. O'Hern (4-62) calibrated a porous metal plug (porosity 0.398) with diffusion of carbon dioxide and computed a diffusivity factor:

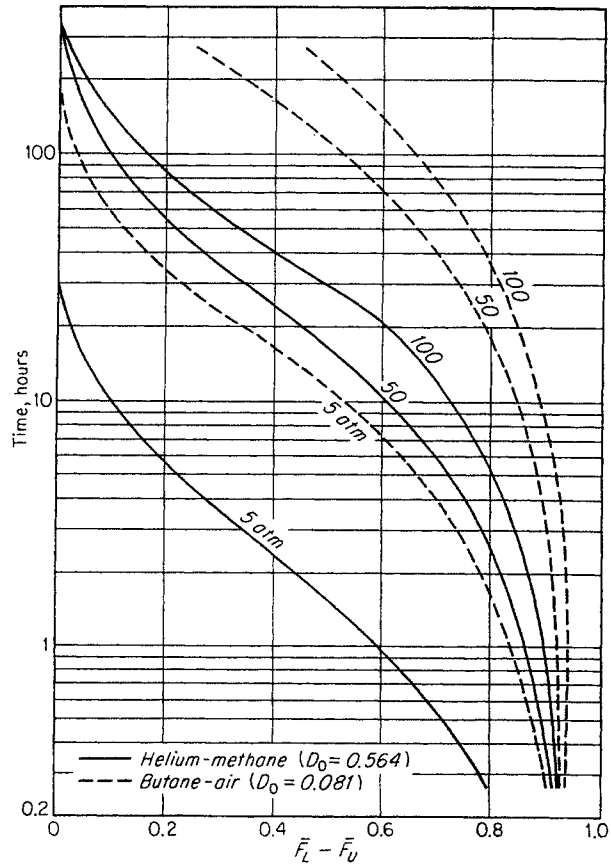

Fig. 4-9. Mixing of gases in cylinders by diffusion only. (*Smith*, 4-84. *Courtesy Ind. Eng. Chem.*)

$$\frac{\text{Diffusion coefficient of empty space}}{\text{Diffusion coefficient of porous solid}}$$

similar to the electrical-resistivity factor. For this

Table 4-5. Fick's Diffusion Coefficients for Hydrocarbon Gases

	Diffusion coefficient, sq ft/sec × 10^4							
Temperature	70°F		100°F		160°F		220°F	
Weight fraction	0	1.00	0	1.0	0	1.0	0	1.0
Pressure, 14.696 psia								
Methane in *n*-hexane	0.449	2.933	0.615	3.842				
n-Hexane in methane	0.512	0.078	0.681	0.109				
Ethane in *n*-hexane	0.344	1.180	0.462	1.508				
n-Hexane in ethane	0.388	0.113	0.503	0.154				
Propane in *n*-hexane	0.174	0.397	0.292	0.639				
n-Hexane in propane	0.193	0.085	0.315	0.144				
Pressure, 60 psia								
Methane in *n*-hexane	0.047	0.952	0.097	1.151	0.190	1.567	0.277	1.936
n-Hexane in methane	0.114	0.006	0.164	0.014	0.253	0.031	0.331	0.048
Ethane in *n*-hexane	0.029	0.291	0.059	0.355	0.097	0.488	0.175	0.623
n-Hexane in ethane	0.067	0.007	0.097	0.016	0.150	0.030	0.202	0.057
Propane in *n*-hexane	0.015	0.089	0.037	0.138	0.084	0.223	0.136	0.310
n-Hexane in propane	0.031	0.005	0.057	0.015	0.103	0.039	0.310	0.136

SOURCE: Carmichael, Sage, and Lacey (4-22).

sintered metal of relatively high permeability, a diffusivity factor of 3.94 was found at atmospheric pressure. Since the interference with diffusion by the porous solid is related to the mean free path and size of the pores of the solid, one would expect the diffusivity factor to go down with increased pressure.

Diffusion Coefficients for Liquids

Wilke (4-95) correlated diffusion coefficients for liquids with a group:

$$\frac{T}{D\mu} = \text{°K-sec/(sq cm)(centipoise)}$$

as a function of molal volume with a solvent factor as parameter. Liquid diffusion coefficients are less by a factor of 10^4 to 10^5 than gaseous coefficients at 1 atm. The rule that the product of the diffusion coefficient and the density of the fluid medium is essentially constant may be an acceptable rule of thumb for converting from gaseous to condensed systems. For example, for hydrogen at 25°C and 1 atm,

$$D\rho = \frac{1.4 \times 2 \times 273}{22{,}400 \times 298} = 0.000012 \text{ gram/(sec)(cm)}$$

but, for hydrogen in liquid water at 25°C,

$$D\rho = 0.0000099$$

The diffusion coefficients for a group of organic substances in benzene and in methyl alcohol at 15°C all were in the range of 0.78 to 2.64 $\times$ 10^{-5} sq cm/sec.

Lacey and coworkers (4-38, 4-69) have measured the diffusion coefficients for methane and propane in liquid hydrocarbons. Figure 4-10 shows the diffusion coefficients for propane in kerosene, and Table 4-6 lists the coefficients for methane in various liquids. A correlation between diffusion coefficient for methane and the ratio of the viscosity of the liquid to $(t - 60)^{0.3}$, where t is measured in degrees Fahrenheit, is shown as Fig. 4-11. Sage and coworkers (4-74) recently studied systems of methane with decane, pentane, and white oil over a range of temperature, pressure, and methane concentration, with values at 1,000 psia (Fig. 4-12).

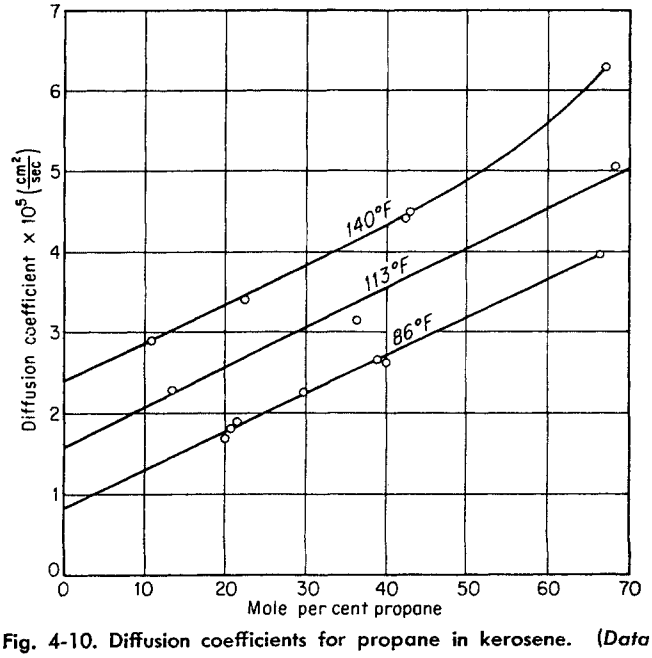

Fig. 4-10. Diffusion coefficients for propane in kerosene. *(Data of Hill and Lacey, 4-38.)*

COMPRESSIBILITY OF NATURAL GASES

Early work on the P-V-T behavior of gases at pressures up to 200 atm or more was conducted by such men as Andrews and Amagat around 1870 (1-9). The measurement of the specific volumes of saturated vapors by Sidney Young on 30 pure substances was in part to determine the variations in the PV/T ratio (4-97). The work by Amagat on ethylene (4-4) published in 1892 and the work by Sidney Young on isopentane (4-75) were important contributions of the early physicists and physical chemists to the compressibility of hydrocarbon gases. Burrell and Robertson made measurements on the compressibility of natural gases at moderate pressures in 1916 (4-18). Around 1930 an interest in the behavior of petroleum substances was revived, with studies of compressibility of gases by Cope, Lewis, and Weber (4-28) and by Brown, Souders, and Smith (4-15). During the 1930s Berwald and Johnson (4-11) reported the deviation of natural gas from Boyle's law; and Sage and Lacey, on API Project 37, measured the volumetric behavior of pure hydrocarbons (1-16, 1-17, 4-76) and

Table 4-6. Diffusion Coefficients for Methane in Liquid Hydrocarbons

Solvent liquid	Temperature, °F	Mole fraction methane in liquid	Increase in volume of liquid, %	Diffusion coefficient, (sq cm/sec) $\times 10^5$
Isopentane	86	0.1068	6.15	13.3
n-Pentane	86	0.1016	5.43	13.2
n-Hexane	86	0.1098	4.45	10.2
Cyclohexane	86	0.0638	3.14	4.7
n-Heptane	86	0.0960	3.74	8.36
Benzene	86	0.0403	2.26	5.47
Kerosene, 44.2°API	86	0.0956	2.15	3.33
	140	0.0760	1.91	5.38
Crude oils:				
Bartlesville, 32.7°API	86	0.0895	1.6	1.71
Sugarland, 26.9°API	86	0.0856	1.5	1.11
Smackover, 20°API	86	0.0886	1.2	0.71
Bradford, 44.5°API	86	0.0883	2.11	3.03
	140	0.0777	1.68	4.83

SOURCE: Hill and Lacey (4-38).

mixtures such as the methane-ethane system (4-77) from 70 to 460°F and to 10,000 psia. A correlation of the deviations of natural gases from ideal-gas laws by Brown, Holcomb, Standing, and Katz (4-14, 4-60, 4-87) was accepted as a tentative standard by the Natural Gasoline Association of America (NGAA) in 1942 (4-60). The behavior of hydrocarbon gases on the basis of residual partial volumes has been presented by Sage, Lacey, and coworkers (1-16, 1-17, 4-76).

Theorem of Corresponding States

J. D. van der Waals proposed the *theorem of corresponding states* as part of this theoretical treatment of fluid behavior, beginning with his thesis in 1873. The theorem states that two substances should have similar properties at corresponding conditions with reference to some basic property such as the critical temperature and pressure. For example, at a temperature equal to twice the critical temperature and a pressure equal to four times the critical pressure, methane and ethane should have the same deviation z from ideal-gas laws. This comparison is made in Table 4-7, showing a difference in compressibility of 0.3 per cent. The ratio of the temperature to the critical temperature, 2:1 in this case, is the *reduced temperature*. Likewise, the ratio of the pressure to the critical pressure is the *reduced pressure*. By the theorem of corresponding states, one would expect that, at the same reduced temperatures and reduced pressures, the compressibility factors of the hydrocarbons would be the same.

Figure 4-13 is a comparison of the compressibility factors for the volatile paraffinic hydrocarbons. Although there is general agreement between the pure constituents, the differences represent more than experimental error. For accurate work, with pure compounds, one must rely upon experimental data, equations of state, or use a more refined correlation. Figure 4-14 gives the compressibility factor for pure methane (1-2).

Natural Gases

Natural gases are composed primarily of methane with varying amounts of ethane, propane, butanes, etc. The work of Kay (4-54) makes possible the use of the theorem of corresponding states for mixtures. He suggested the use of molal-average critical pressures and temperatures for mixtures in place of the critical pressures and temperatures used for pure compounds. These molal-average properties are the *pseudocritical temperatures* and *pseudocritical pressures* for mixtures, and they may be used like true criticals for purposes of comparing corresponding states. The

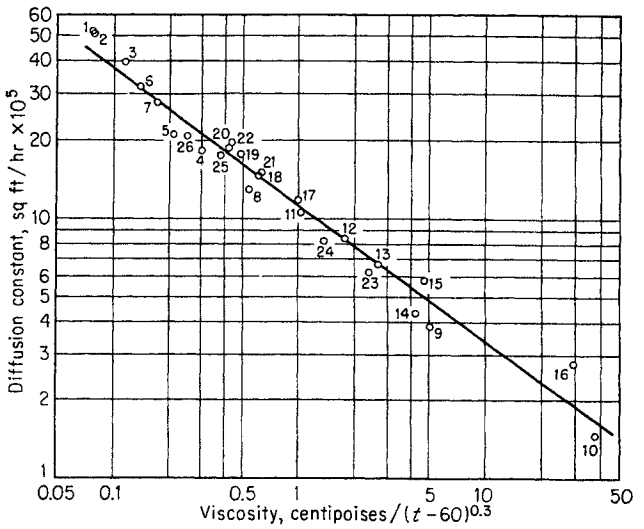

Fig. 4-11. Relation between diffusion coefficient of methane, viscosity of liquid, and temperature. (*Hill and Lacey, 4-38. Courtesy Ind. Eng. Chem.*)

pseudocritical point has no physical significance, but it approximates the point of convergence of constant-volume lines on a present-temperature diagram. The fact that these isochors are straight is significant. Figure 4-15 illustrates the degree to which the pseudocritical point for a 70 mole % methane–30 mole % butane mixture fits the above criterion. It also shows

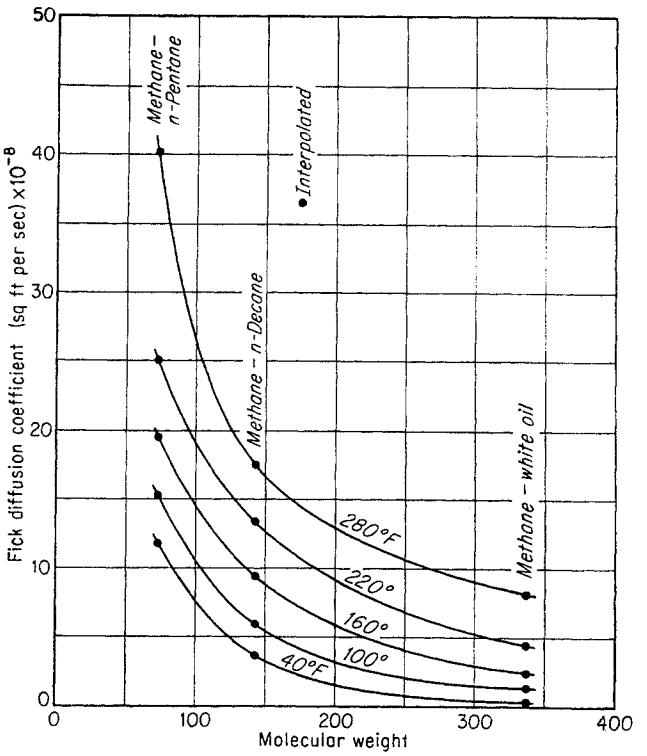

Fig. 4-12. Influence of molecular weight of less volatile component on diffusion coefficient for methane in liquid phases at 1,000 psia. (*Reamer, Duffy, and Sage, 4-74. Courtesy Ind. Eng. Chem.*)

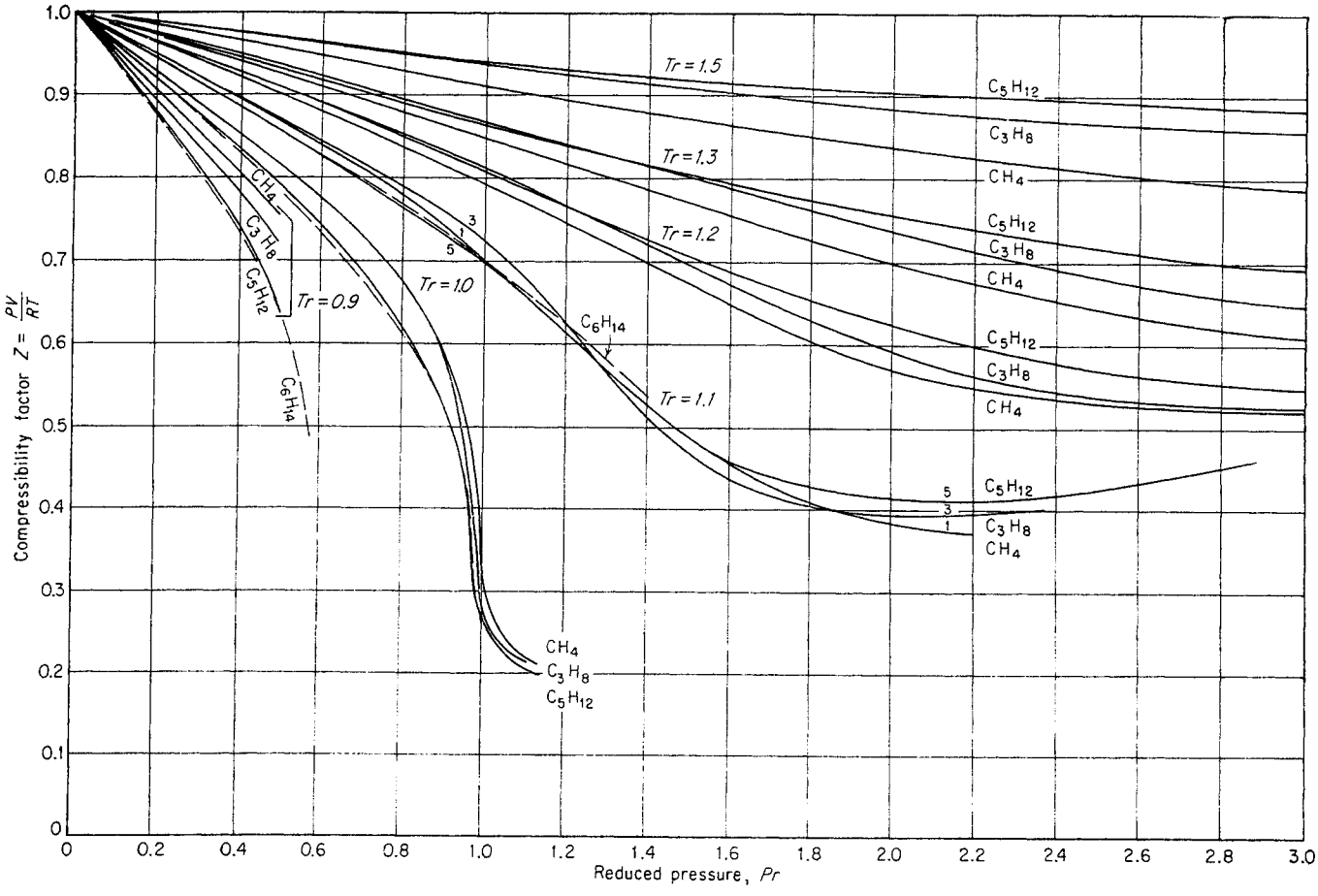

Fig. 4-13. Deviation from law of ideal gases.

Table 4-7. Corresponding States for Methane and Ethane

Factor	Methane	Ethane
Critical temperature, °R	343.2	549.7
Twice the critical temperature, °R	686.4	1,099.4
Twice the critical temperature, °F	226.7	639.7
Critical pressure, psia	673.1	708.3
4 × critical pressure, psia	2,692.4	2,833.2
Compressibility factor z at twice critical temperature and 4 × critical pressure	0.959	0.962

the relation to the true critical point for the mixture.

A comparison of the compressibility factors of methane on a reduced-temperature and reduced-pressure basis with those of natural gases and the methane-ethane system (4-77) indicated that curves below those of methane would apply better to natural gases. Using the data available in 1941, a series of charts were drawn, culminating in Fig. 4-16 (4-87). This chart was compared with further data (4-60) and found to be valid to within ±1.2 per cent. The method of computing a density of natural gas, using the compressibility factor found from the composition of the gases and from Fig. 4-16, is illustrated in Table 4-8. Figure 4-16 is based on data up to 10,000 psia for gas mixtures. The methane data by Kvalnes and Gaddy (4-53), which go to 1,000 atm, have been used to extend the range of pressure in Fig. 4-16*a*. The critical properties of some natural gas constituents are given in Table 4-9 for convenience.

In handling hydrocarbon gases near atmospheric pressure, the deviations from ideal-gas laws are significant for close volumetric measurements. Figure 4-17 is an enlarged chart for predicting the deviations from ideal behavior near atmospheric pressure (4-83a). For very accurate work with pure constituents Fig. 4-18 from McKetta, Silberberg, and Kuo (4-83) should be used. For mixtures at pressures below 800 mm Hg, additive volumes may be assumed.

Influence of Nonhydrocarbon Constituents

Natural gases frequently contain carbon dioxide, nitrogen, and hydrogen sulfide in sufficient quantities so that the influence of the nonhydrocarbon on the

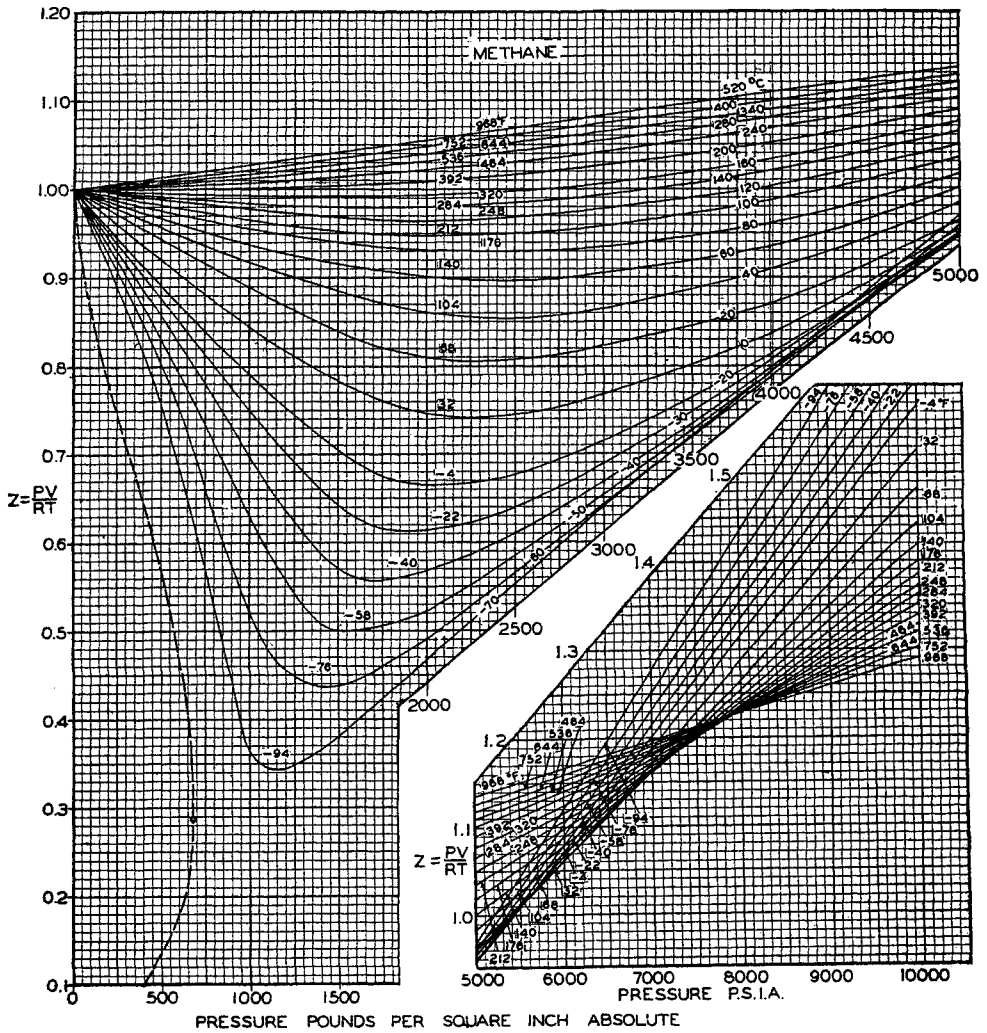

Fig. 4-14. Compressibility factor for methane. (*Brown, Katz, Oberfell, and Alden*, 1-2.)

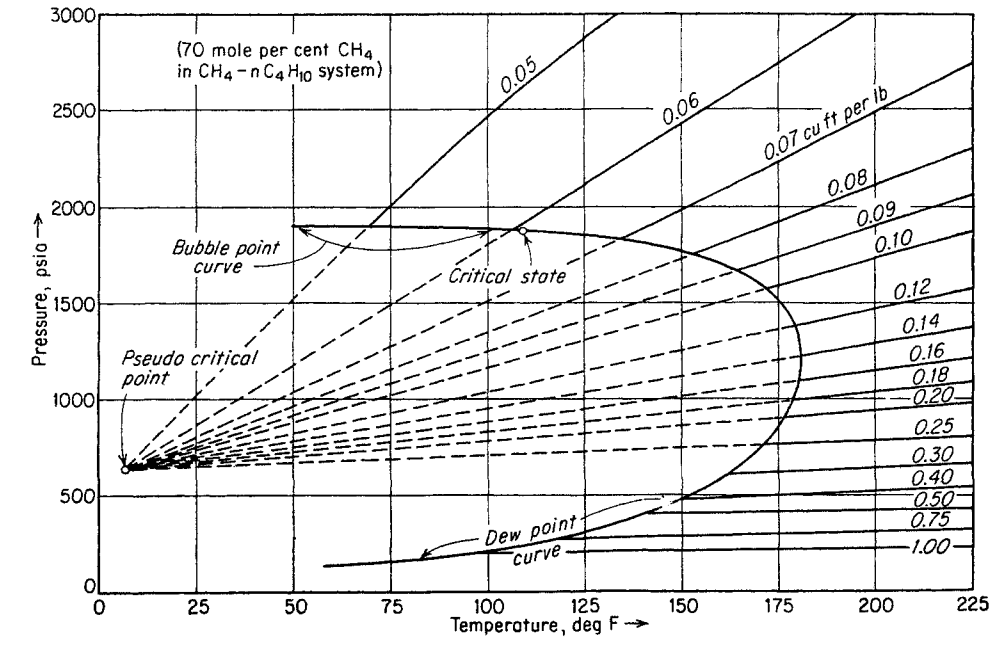

Fig. 4-15. Pressure-temperature diagram illustrating pseudocritical point of 0.4 weight fraction CH_4 in CH_4-C_4H_{10} system. (*Data of Sage and Lacey*, 3-62, 3-63.)

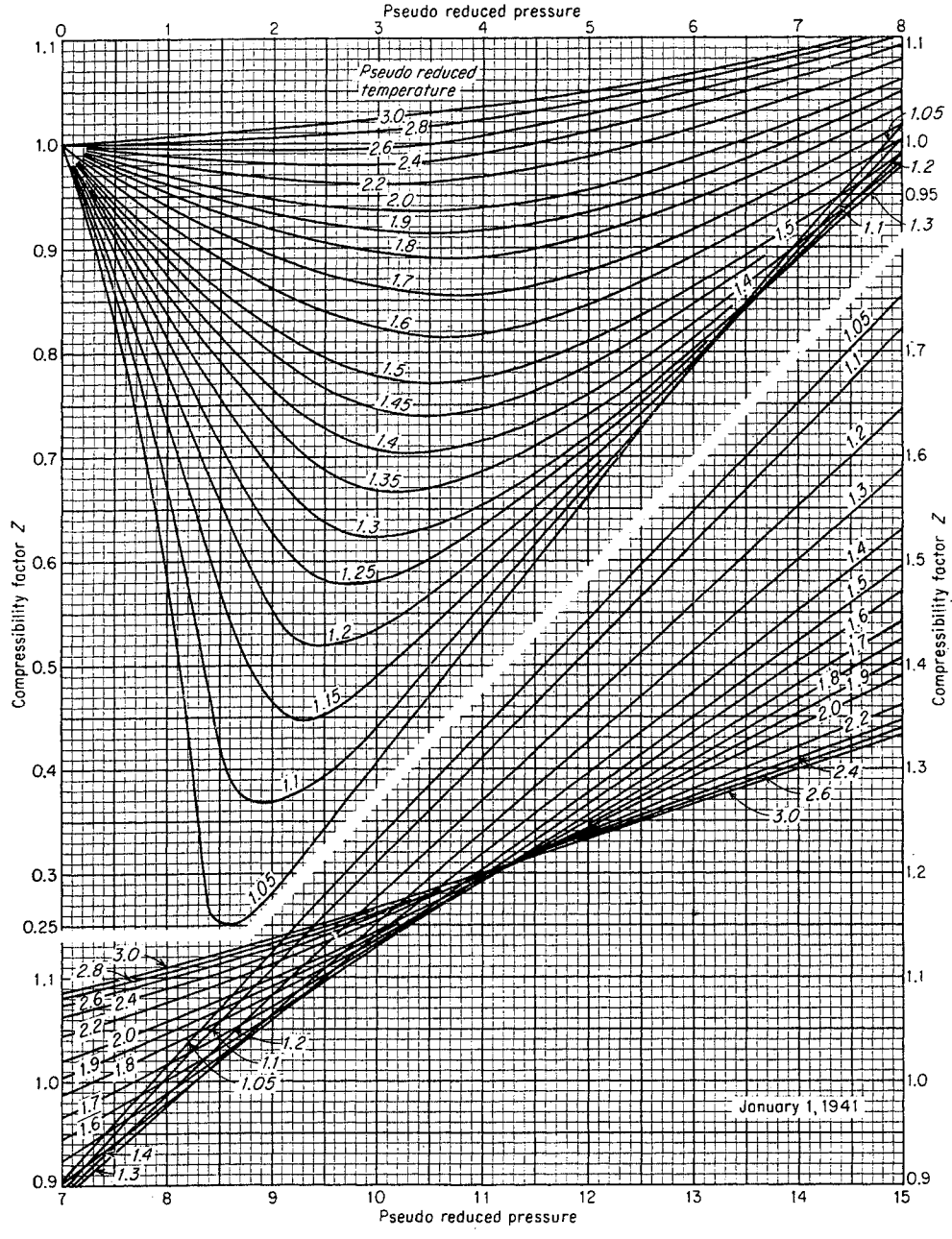

Fig. 4-16. Compressibility factor for natural gases. (*Standing and Katz, 4-87. Courtesy AIME.*)

degree of conformity to the theorem of corresponding states must be considered.

The *P-V-T* relations for methane-nitrogen mixtures were determined by Keyes and Burks (4-55) and for a natural gas containing 8.5 and 18.8 mole % nitrogen by Eilerts, Carlson, and Mullens (4-30). Table 4-10 gives the analyses of the natural gases, and Table 4-11 gives a comparison of the compressibility factors computed from Fig. 4-16 and the reduced temperature and pressure, with the experimental values for these compressibility factors. The calculated compressibility factors are lower than the measured values by about 2 per cent at the higher temperatures and intermediate pressures. The factors for the gases with nitrogen are lower on the average over the full range of temperature.

Reamer, Olds, Sage, and Lacey (4-72) have measured the compressibility of four mixtures of methane and carbon dioxide from 100 to 460°F and up to 10,000 psia, with data at 100 and 280°F reproduced in Table 4-12. For gases with 1 or 2 mole % carbon dioxide, the pseudocritical chart is reliable but, for higher percentages, a correction may be necessary as indicated by comparing computed compressibilities with the measured compressibilities in Table 4-12.

Likewise, for methane–hydrogen sulfide mixtures,

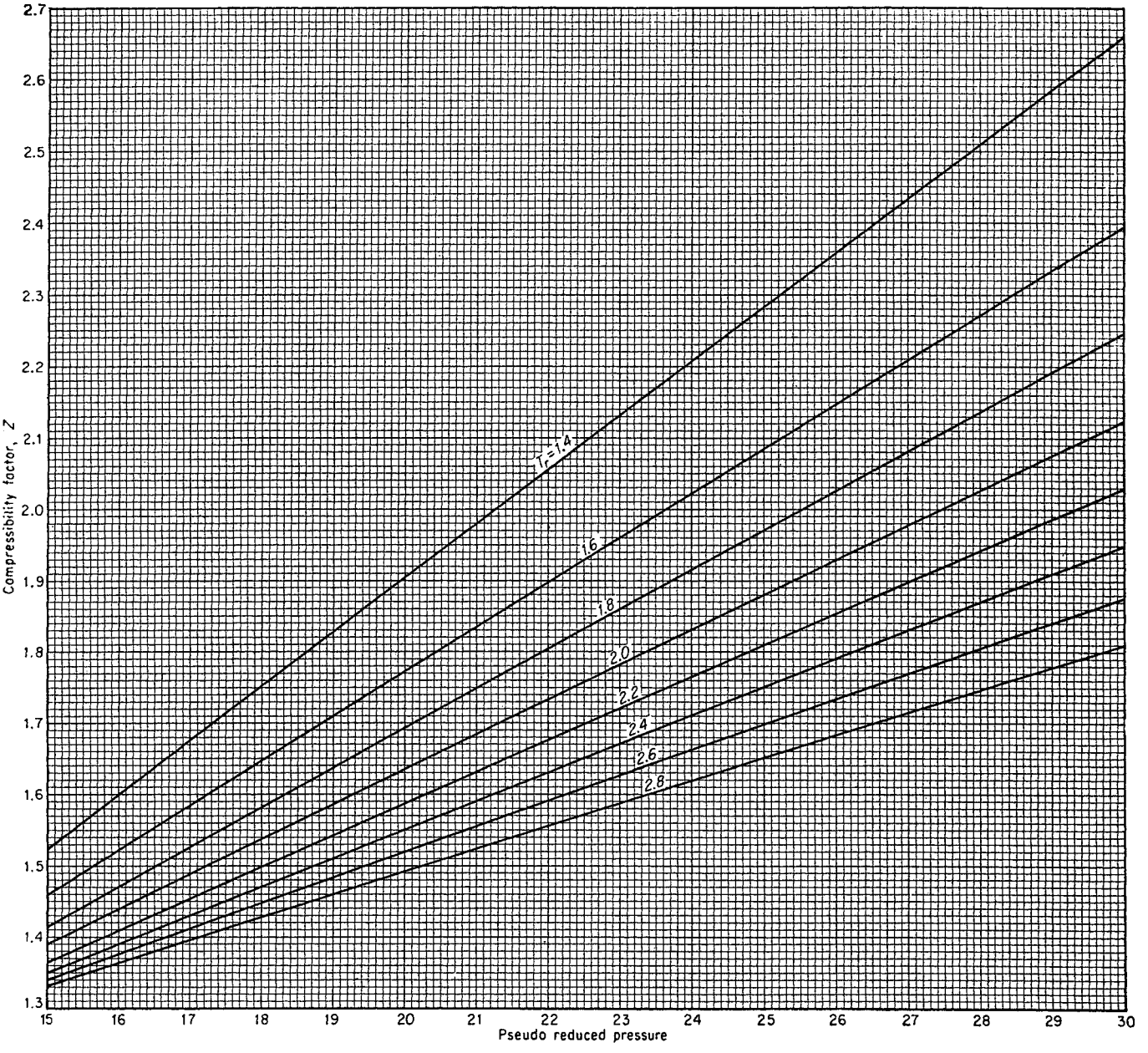

Fig. 4-16a. Compressibility factors for natural gases at pressures of 10,000 to 20,000 psia.

Reamer, Sage, and Lacey (4-73) have reported the specific volumes (Table 4-13) and the compressibility factors (Fig. 4-19) for high methane concentrations.

Pseudocriticals for Heptanes and Heavier Constituents

The hexanes, heptanes, and heavier constituents of natural gas contain several hydrocarbon compounds as well as the normal and isomeric paraffins. In fractional analyses, these individual constituents are difficult to identify, and often they are collected as a liquid with the molecular weight and specific gravity determined thereon. Kay (4-54) devised a method of obtaining pseudocriticals for liquids, which was revised by Smith and Watson (4-86) and in which the slope of the boiling-point curve, the molecular weight, and the specific gravity were required. A group of microdistillations was available on heptane and heavier fractions for condensates, and this was used, along with Smith and Watson's charts, to predict the relationship of pseudocritical conditions to molecular weight and specific gravity (Fig. 4-20). For constituents pentanes and heavier, hexanes and heavier, or heptanes and heavier, when specific gravity and molecular weight of the liquid are known, the chart is believed to be satisfactory. It was used in comparing

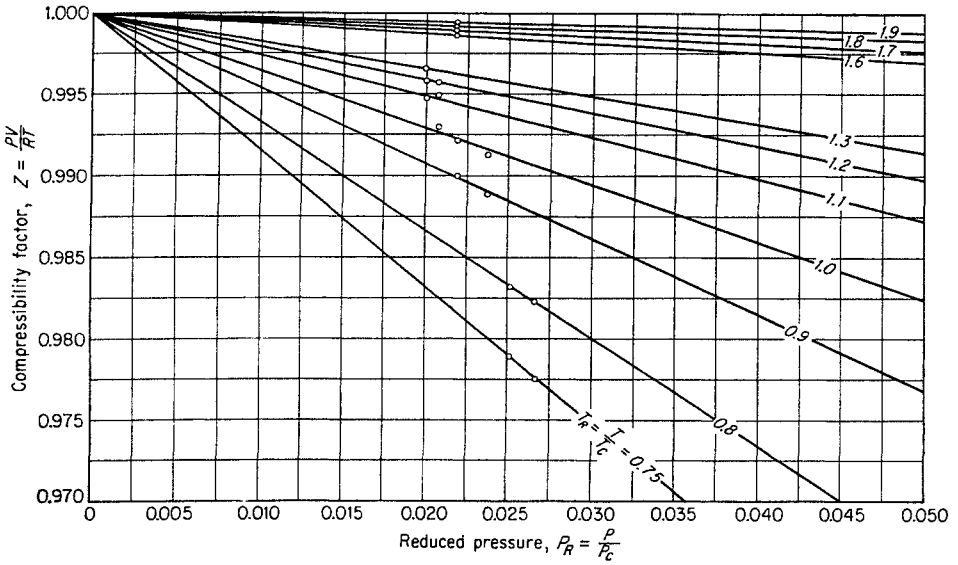

Fig. 4-17. Compressibility factors for natural gas near atmospheric pressure. (*McKetta et al.*, 4-83a.)

Table 4-8. Computation of the Density of a Natural Gas from the Gas-composition and Compressibility-factor Chart

Compute the density of gas D with the composition shown at 1,000 psia and 90°F.

Constituent	Computation of pseudocritical point						
	Mole fraction y	Mol wt	Lb/mole	Crit temp, °R		Crit pressure, psia	
				T_c	yT_c	P_c	yP_c
Carbon dioxide	0.0040	44	0.17	548	2.1	1,073	4.3
Methane	0.9432	16	15.09	343	323.5	673	634.7
Ethane	0.0390	30	1.17	550	21.4	708	27.6
Propane	0.0117	44	0.51	666	7.8	617	7.2
Isobutane	0.0008	58	0.04	735	0.6	528	0.4
n-Butane	0.0013	58	0.07	766	1.0	551	0.7
	1.0000		17.05		356.4		674.9

Reduced temperature $T/T_c = (90 + 460)/356.4 = 1.54$

Reduced pressure $P/P_c = 1{,}000/674.9 = 1.48$

Gas gravity $= 17.05/29.0 = 0.588$

From Fig. 4-16, at $T_r = 1.54$ and $P_r = 1.48$, compressibility factor $z = 0.872$.

The compressibility factor reported at these conditions by Stevens and Freidman (4-60) is 0.875.

$$\text{Density of natural gas} = \frac{17.05 \times 1{,}000 \times 520}{379 \times 14.7 \times 550 \times 0.872} = 3.31 \text{ lb/cu ft}$$

Alternative calculation:

$$\rho = \frac{1}{V} = \frac{P}{znRT} = \frac{1{,}000}{0.872}\frac{17.05}{1}\frac{1}{10.73}\frac{1}{550} = 3.31 \text{ lb/cu ft}$$

Table 4-9. Critical Properties of Natural Gas Constituents

Constituent	Molecular weight	Critical temperature, °R	Critical pressure, psia
Methane	16.04	343.3	673.1
Ethane	30.07	549.8	708.3
Propane	44.09	666.0	617.4
Isobutane	58.12	734.7	529.1
n-Butane	58.12	765.3	550.7
Isopentane	72.15	829.8	483
n-Pentane	72.15	845.6	489.5
Isohexane, 121*	72.15	880.9	450.5
Isohexane, 140*	84.16	896.5	440.1
n-Hexane, 155*	84.16	914.1	439.7
Isoheptane, 174*	98.18	937.6	417
Isoheptane, 194	98.18	955.9	400
n-Heptane, 209	98.18	972.3	396.9
Isooctane, 229	114.22	999	379
Isooctane, 240	118.22	1019	391
n-Octane, 258	114.22	1024.9	362.1
n-Nonane	128.25	1071	331
n-Decane	142.28	1114	306
Helium	4.0	9.4	33.2
Air	29.0	238.4	547
Nitrogen	28.02	226.9	492
Oxygen	32.0	277.9	730
Carbon dioxide	44.01	547.7	1073
Hydrogen sulfide	34.08	672.4	1306

* Number indicates boiling point in degrees Fahrenheit.

SOURCE: (1-15).

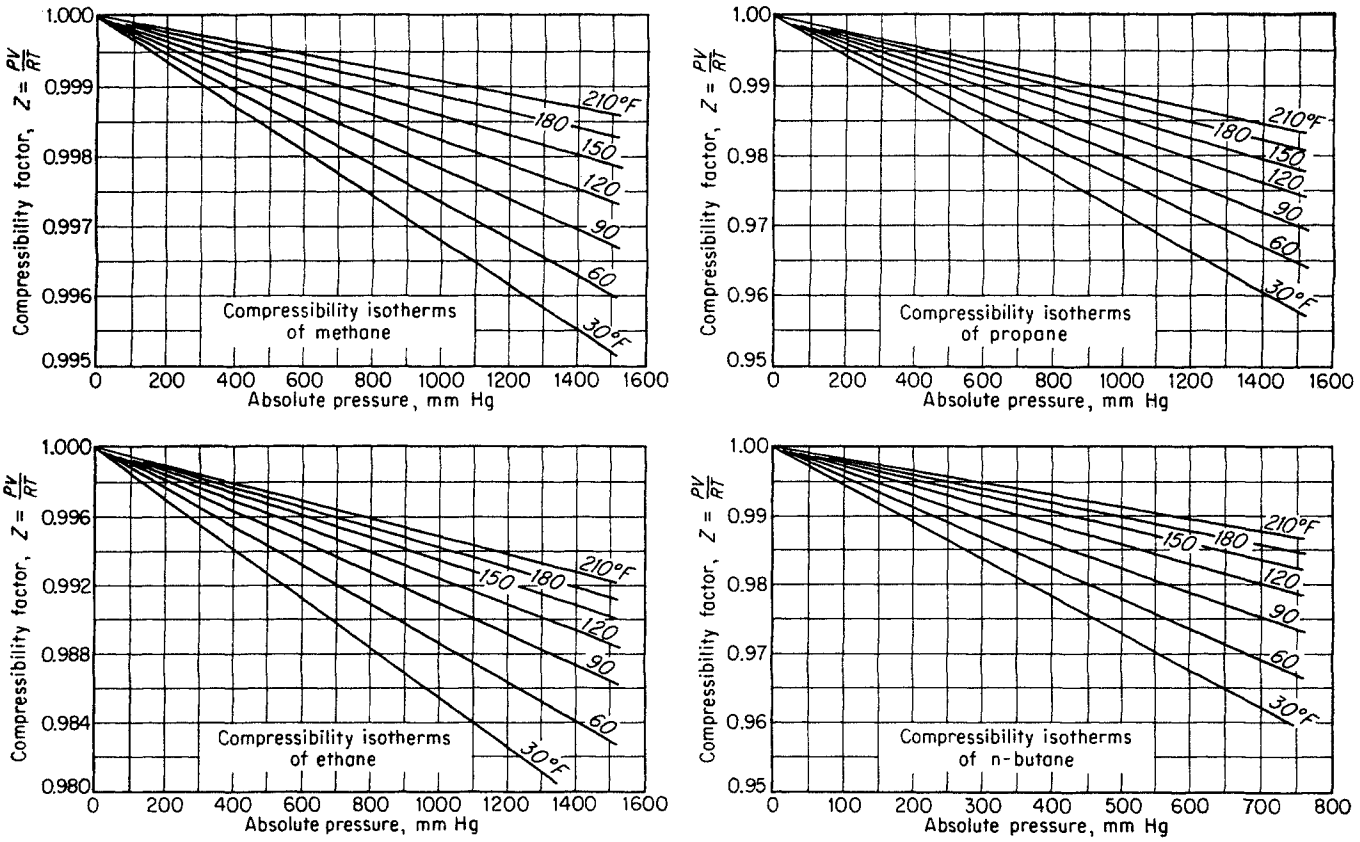

Fig. 4-18. Compressibility factors for pure hydrocarbons near atmospheric pressure. *(Silberberg, Kuo, and McKetta, 4-83. Courtesy Petrol. Engr.)*

Table 4-10. Compositions of Natural Gases Containing Nitrogen

	Gas 1	Gas 2	Gas 3
Gravity	0.649	0.675	0.706
Pseudocritical:			
Temperature, °R	375.3	363.5	348.2
Pressure, psia	669.4	655.3	636.9
Mole fraction:			
Nitrogen	0.0069	0.0855	0.1884
Methane	0.8771	0.8077	0.7169
Ethane	0.0649	0.0598	0.0530
Propane	0.0322	0.0297	0.0263
Isobutane	0.0076	0.0070	0.0062
n-Butane	0.0058	0.0053	0.0047
Isopentane	0.0021	0.0019	0.0017
n-Pentane	0.0012	0.0111	0.00099
Hexanes, 135–56*	0.00070	0.00063	0.00058
Hexanes, 56–35	0.00036	0.00033	0.00029
Heptanes, 35–17	0.00034	0.00031	0.00028
Heptanes, 17–11	0.00012	0.00011	0.00010
Octanes +	0.00068	0.00062	0.00056

* Vapor pressure, mm Hg, at 0°C.
SOURCE: (4-30).

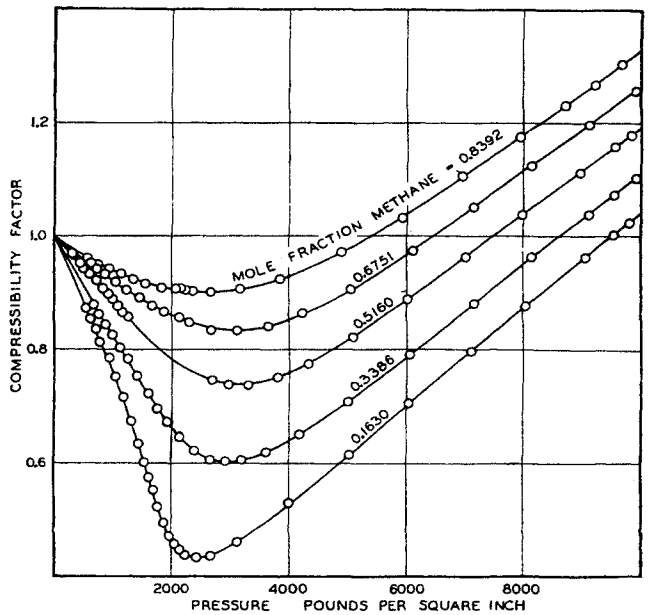

Fig. 4-19. Compressibility factors for mixtures of hydrogen sulfide in methane. *(Reamer, Sage, and Lacey, 4-73. Courtesy Ind. Eng. Chem.)*

Table 4-11. Comparison of Calculated and Experimental* Compressibility Factors for Natural Gases with Nitrogen

Pressure, psia	Compressibility factor z					
	Gas 1, 0.7% N_2		Gas 2, 8.5% N_2		Gas 3, 18.8% N_2	
	Calc	Exp	Calc	Exp	Calc	Exp
Temperature, 32°F						
1,400	0.685	0.6885	0.715	0.7270	0.748	0.7747
1,600	0.658	0.6593	0.692	0.7024	0.736	0.7557
1,800	0.640	0.6433	0.676	0.6871	0.720	0.7410
2,000	0.634	0.6369	0.668	0.6797	0.713	0.7343
3,000	0.687	0.6981	0.717	0.7258	0.750	0.7720
4,000	0.802	0.8103	0.822	0.8287	0.853	0.8660
5,000	0.932	0.9333	0.942	0.9443	0.970	0.9736
Temperature, 100°F						
1,400	0.812	0.8213	0.832	0.8443	0.855	0.8706
1,600	0.797	0.8044	0.816	0.8299	0.843	0.8596
1,800	0.782	0.7896	0.805	0.8188	0.832	0.8518
2,000	0.773	0.7805	0.795	0.8102	0.825	0.8461
3,000	0.785	0.7901	0.810	0.8210	0.838	0.8584
4,000	0.858	0.8600	0.880	0.8864	0.910	0.9193
5,000	0.952	0.9516	0.960	0.9750	0.996	1.0031
Temperature, 190°F						
1,400	0.896	0.9097	0.911	0.9234	0.922	0.9401
1,600	0.888	0.9009	0.903	0.9171	0.917	0.9362
1,800	0.872	0.8943	0.898	0.9125	0.912	0.9333
2,000	0.875	0.8899	0.892	0.9097	0.910	0.9317
3,000	0.876	0.8932	0.899	0.9164	0.918	0.9437
4,000	0.927	0.9356	0.947	0.9577	0.970	0.9849
5,000	0.998	1.005	1.012	1.0196	1.033	1.0459
Temperature, 280°F						
1,400	0.941	0.9557	0.952	0.9640		
1,600	0.938	0.9516	0.946	0.9625		
1,800	0.935	0.9486	0.948	0.9615	0.952	0.9748
2,000	0.932	0.9472	0.945	0.9612	0.952	0.9761
3,000	0.939	0.9571	0.953	0.9733	0.970	0.9928
4,000	0.980	0.9890	0.998	1.0058	1.012	1.0269
5,000	1.022	1.0384	1.050	1.0547	1.064	1.0754

* Experimental data (4-30).

compressibility factors for the saturated vapors of Standing and Katz (4-87), which included molecular weights of heptanes and heavier as high as 157.

These pseudocriticals are used in computing pseudocriticals for a natural gas mixture just as critical temperatures and pressures are used for pure constituents.

Use of Gas Gravity to Predict Pseudocritical Conditions

The compositions of natural gases are known to be related to one another (4-57), and it is to be expected

Table 4-12. Compressibility Factors for Mixtures of Methane and Carbon Dioxide

Pressure, psia	Compressibility factor with weight fraction methane as follows:				
	0	0.0852	0.19912	0.3583	0.6685
Temperature, 100°F					
0	1.000	1.0000	1.0000	1.0000	1.0000
200	0.941	0.9512	0.9606	0.9685	0.9760
400	0.875	0.8995	0.9202	0.9372	0.9525
600	0.798	0.8437	0.8788	0.9063	0.9296
800	0.704	0.7830	0.8360	0.8754	0.9075
1,000	0.580	0.7160	0.7920	0.8451	0.8869
1,250	0.315	0.6262	0.7350	0.8084	0.8634
1,500	0.255	0.5388	0.6830	0.7738	0.8428
1,750	0.272	0.4715	0.6402	0.7460	0.8259
2,000	0.299	0.4438	0.6100	0.7243	0.8131
2,500	0.355	0.4565	0.5890	0.7041	0.8027
3,000	0.411	0.4958	0.6055	0.7103	0.8081
3,500	0.465	0.5247	0.6400	0.7335	0.8260
4,000	0.519	0.5921	0.6820	0.7702	0.8565
4,500	0.572	0.6433	0.7276	0.8130	0.8937
5,000	0.624	0.6947	0.7755	0.8584	0.9363
6,000	0.727	0.7976	0.8752	0.9531	0.0291
7,000	0.828	0.8982	0.9745	0.0502	1.1240
8,000	0.926	0.9995	1.0745	1.1469	1.2187
9,000	1.023	1.1012	1.1752	1.2448	1.3130
10,000	1.116	1.2035	1.2785	1.3414	1.4078
Temperature, 280°F					
0	1.000	1.0000	1.0000	1.0000	1.0000
200	0.979	0.9834	0.9872	0.9901	0.9931
400	0.957	0.9668	0.9747	0.9805	0.9866
600	0.934	0.9503	0.9625	0.9713	0.9805
800	0.912	0.9339	0.9507	0.9627	0.9749
1,000	0.889	0.9179	0.9397	0.9545	0.9699
1,250	0.862	0.8987	0.9263	0.9453	0.9649
1,500	0.835	0.8810	0.9145	0.9379	0.9608
1,750	0.810	0.8643	0.9040	0.9313	0.9583
2,000	0.787	0.8487	0.8950	0.9267	0.9572
2,500	0.750	0.8247	0.8820	0.9217	0.9588
3,000	0.729	0.8125	0.8763	0.9226	0.9650
3,500	0.720	0.8100	0.8778	0.9289	0.9759
4,000	0.724	0.8154	0.8865	0.9404	0.9914
4,500	0.737	0.8290	0.9020	0.9571	0.0109
5,000	0.759	0.8483	0.9223	0.9788	1.0337
6,000	0.818	0.8992	0.9721	1.0306	1.0848
7,000	0.883	0.9592	1.0310	0.0877	1.1423
8,000	0.952	1.0243	1.0955	1.1495	1.2030
9,000	1.023	1.0921	1.1610	1.2148	1.2672
10,000	1.091	1.1605	1.2268	1.2817	1.3350

SOURCE: Sage and Lacey (4-72).

Table 4-13. Molal Volumes of Mixtures of Methane–Hydrogen Sulfide

Pressure, psia	Molal volume of mixture, cu ft/lb mole							
	At 40°F		At 100°F		At 160°F		At 280°F	
	Mole fraction of methane							
	0.8	0.9	0.8	0.9	0.8	0.9	0.8	0.9
200	25.69	25.85	29.19	29.31	32.65	32.74	39.37	39.41
400	12.28	12.43	14.18	14.30	16.03	16.13	19.53	19.59
600	7.80	7.96	9.11	9.31	10.48	10.59	12.92	12.99
800	5.54	5.73	6.69	6.89	7.71	7.83	9.63	9.69
1,000	4.18	4.40	5.20	5.33	6.05	6.24	7.65	7.72
1,250	3.08	3.35	4.00	4.15	4.73	4.86	6.07	6.14
1,500	2.389	2.696	3.21	3.36	3.86	3.99	5.02	5.10
1,750	1.942	2.191	2.662	2.817	3.25	3.38	4.28	4.35
2,000	1.646	1.870	2.270	2.423	2.802	2.924	3.72	3.80
2,250	1.452	1.647	1.985	2.134	2.459	2.582	3.30	3.37
2,500	1.326	1.489	1.773	1.917	2.195	2.317	2.959	3.03
2,750	1.235	1.373	1.613	1.745	1.990	2.108	2.685	2.762
3,000	1.168	1.285	1.495	1.610	1.830	1.939	2.464	2.542
3,500	1.070	1.160	1.329	1.423	1.601	1.687	2.131	2.203
4,000	1.004	1.074	1.208	1.289	1.436	1.516	1.893	1.963
4,500	0.9558	1.014	1.125	1.194	1.318	1.388	1.710	1.776
5,000	0.9195	0.9702	1.065	1.125	1.231	1.290	1.573	1.631
6,000	0.8678	0.9072	0.9829	1.029	1.109	1.157	1.382	1.430
7,000	0.8307	0.8628	0.9250	0.9610	1.026	1.066	1.251	1.291
8,000	0.8022	0.8300	0.8819	0.9127	0.9695	1.002	1.157	1.191
9,000	0.7787	0.8030	0.8479	0.8755	0.9625	0.9538	1.083	1.116
10,000	0.7590	0.7808	0.8210	0.8450	0.8865	0.9125	1.206	1.056

SOURCE: Reamer, Sage, and Lacey (4-73).

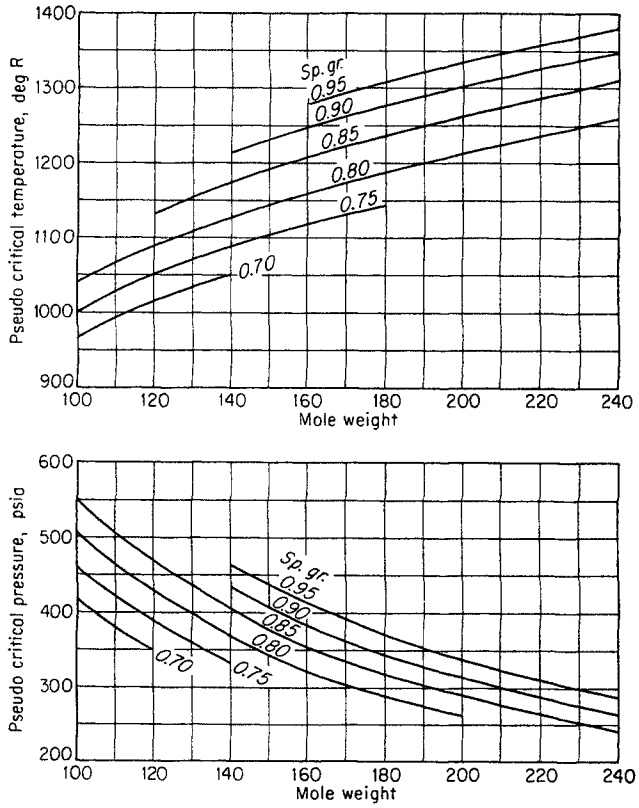

Fig. 4-20. Pseudocritical temperatures and pressures for heptanes and heavier. (*Matthews, Roland, and Katz*, 4-60.)

that natural gases, at least from a single field, would have such compositions that their pseudocritical temperatures and pressures would be a function of gas gravity. Figure 4-21 (4-60), accordingly, plots pseudocritical properties versus gravity for field and plant gases in the Oklahoma City field. It was found that gases containing less than 2 or 3 per cent of nonhydrocarbons from fields all over the country also fit a single curve (1-2, 4-60, 4-87). Condensate-bearing gases containing enough high-molecular compounds to increase their gravity were found to have curves separate from dry gases (1-2). The California Natural Gasoline Association (4-3) adopted a relationship between gas gravity and pseudocriticals. These three curves are presented in Fig. 4-22.

For gases that comply with such a curve as those shown in Fig. 4-22, the compressibility factor or density becomes a function of gas gravity, temperature, and pressure. Charts giving the density of natural gases as a function of temperature, pressure, and gravity are given in Fig. 4-23, the pseudocriticals for

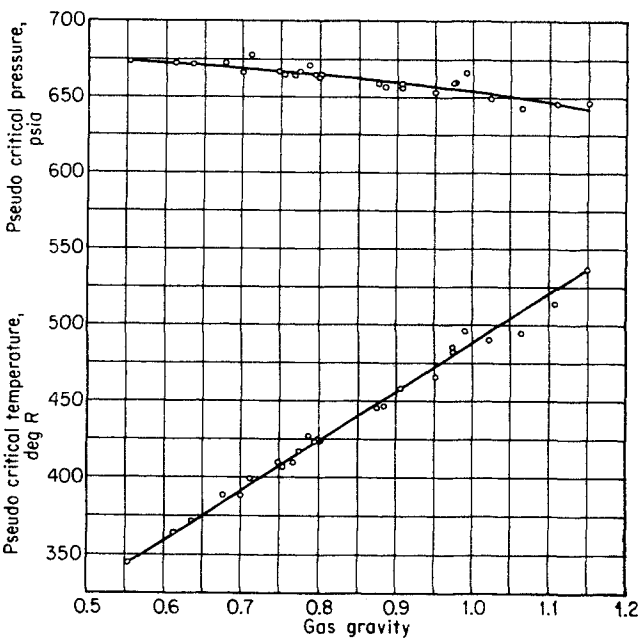

Fig. 4-21. Pseudocritical properties of Oklahoma City gases. (*Matthews, Roland, and Katz*, 4-60.)

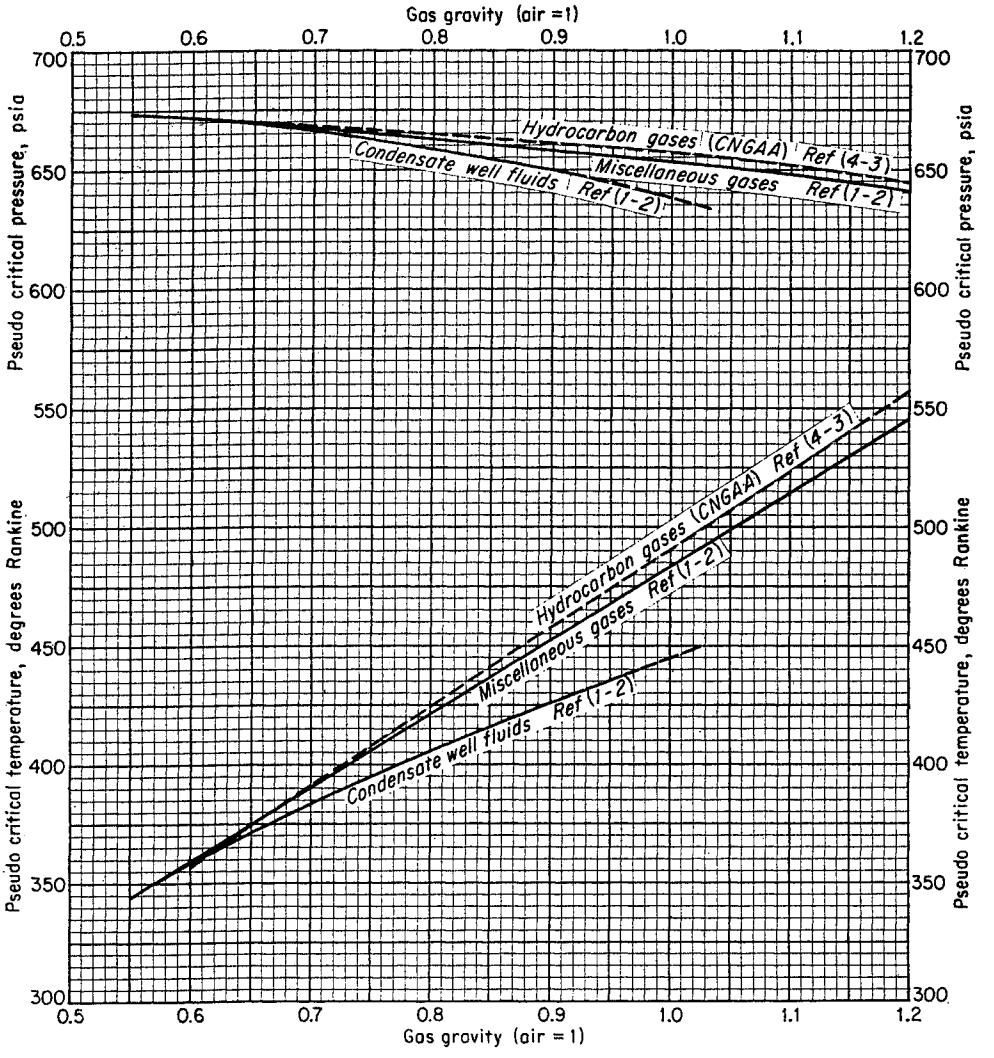

Fig. 4-22. Pseudocritical properties of natural gases. (*Brown, Katz, Oberfell, and Alden*, 1-2.)

the 0.7 and 0.8 gravity gases corresponding to the condensate well fluids.

Effect of Liquid Phase

It was found that certain natural gases entered the two-phase region during P-V-T studies and that the compressibility factor for the entire mixture was similar to that for a single phase. To study the use of the compressibility factor for density calculations in the high-pressure two-phase region, data on a natural gas–natural gasoline mixture were used. The phase diagram for the mixture is given by Fig. 4-24 and includes the regions likely to be encountered in high-pressure gases. The effect of a small amount of liquefaction on the over-all density is of especial interest in meter calculations.

Table 4-14 gives the comparison between experimental and calculated densities for the natural gas–natural gasoline mixture. The calculations were made assuming that the system density could be computed from Eq. (4-2), including the compressibility factor. The observed volume percentages of liquid were taken from the phase diagram (Fig. 4-24). Table 4-14 demonstrates that the compressibility-factor method can be used to compute the density of a mixture in the single-phase region above the bubble-point curve, a short way into the two-phase region below the bubble-point curve, and completely through the two-phase region at high temperatures where a small volume percentage of liquid is present. The region in which these calculations may be made is limited to T_R of 1.05 or higher.

A study of the methane-butane system also indicated that the over-all density of a system existing as a small proportion of liquid and the remainder gas can be computed at high pressure by assuming that the system is a single phase. The explanation of this remarkable behavior lies in the relatively small change in partial molal volume between the vapor and liquid phases at these conditions. Hence, it matters little

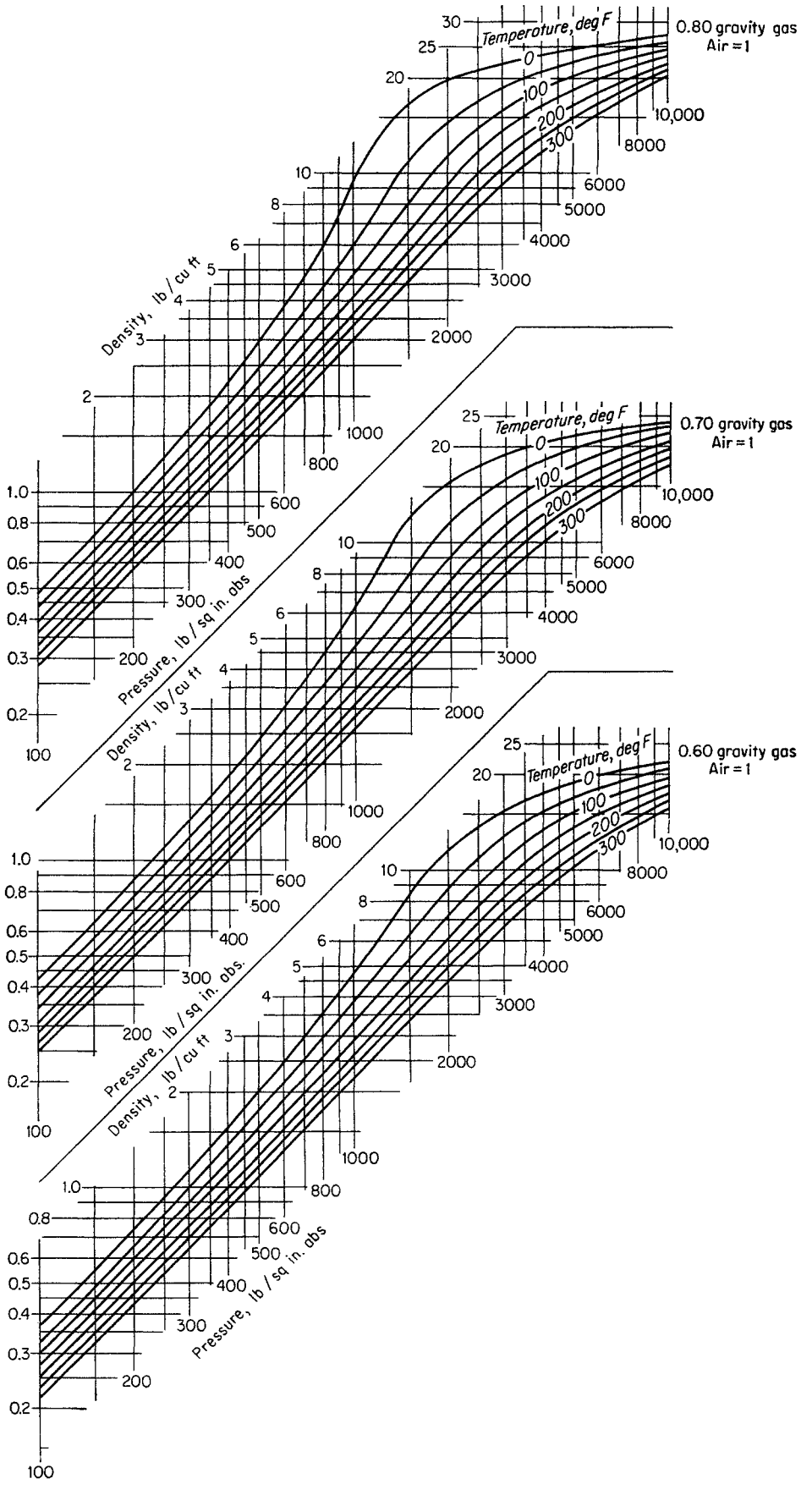

Fig. 4-23. Density of natural gases. (*Standing and Katz*, 4-87. Courtesy *AIME*.)

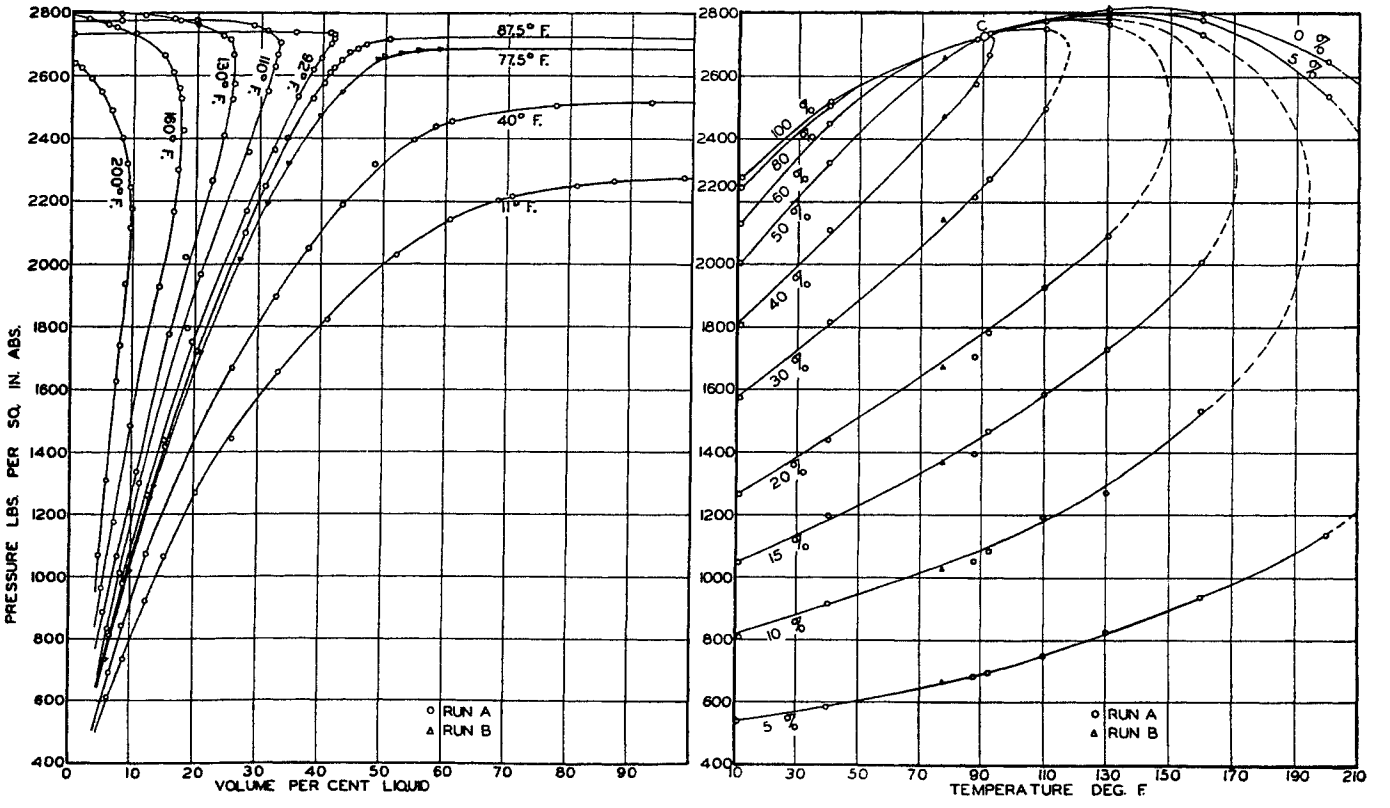

Fig. 4-24. Phase diagram for a natural gas–gasoline mixture. (*Kurata and Katz, 3-28. Courtesy Ind. Eng. Chem.*)

for the over-all density if a portion of the system is in the liquid phase. Caution must be exercised in applying this assumption generally without regard to position on the phase diagram. However, at pressures above 1,000 lb, at temperatures above the critical temperature of the mixture, and at volume percentages of liquid under 10, the presence of the liquid phase is not likely to interfere with the calculation of the average density of the mixture by the compressibility-factor method.

Negative Apparent Volumes for Liquid Constituents

Negative apparent volumes for liquids dissolved in high-pressure gas phases become evident from a study of compressibility-factor data (4-52). One of the authors, in the course of preparing a cylinder of natural gas for use in the laboratory, observed some unusual behavior. The cylinder of natural gas, free from liquid at 75°F and 2,005 psi, was cooled at 32°F; about a pint of liquid was drained from the cylinder; and the temperature of the cylinder was brought back to 75°F. The pressure on the cylinder had risen to 2,060 psi. It would follow that if the liquid, which had been removed, were reinjected into the cylinder the pressure would drop.

An experiment was conducted with a gas-windowed cell containing 0.859 gram mole of methane at 100°F and 2,000 psia. Butane to the extent of 0.141 mole was pumped into the cell maintained at 100°F. The pressure on the cell at the end of the butane injection was 1,913 psia and the methane-butane mixture was in a single phase. Figure 4-25 was constructed from data by Sage, Hicks, and Lacey (3-62) on the methane-butane system (4-52). In area 1, butane has a negative apparent volume; that is, methane alone would occupy more space at the same temperature and pressure. The presence of the butane influences the forces between the methane molecules and makes them approach each other more easily. In area 2, the apparent volumes of the butane are between zero and that of pure liquid butane; and, in area 3, the apparent volumes in the gas phase exceed that of the liquid. At or near atmospheric pressure, such constituents have close to their ideal-gas volume in the gas phase.

Effect of Molecular Nature on Compressibility

The deviation of gases from the theory of corresponding states and the above case of negative apparent volumes for liquefiable constituents injected into methane indicate that the fundamental forces between the molecules govern their behavior and that

Table 4-14. Comparison of Calculated and Experimental Densities of Fluid in Single- and Two-phase Regions

Pressure, psia	Calculated		Experimental	
	z	Density, grams/cu cm	Density, grams/cu cm	Volume % liquid
Temperature = 40°F Pseudoreduced Temperature = 1.13 True Reduced Temperature = 0.91				
2,890	0.628	0.380	0.376	Single phase
2,524	0.569	0.367	0.366	Single phase
2,452	0.556	0.364	0.361	60.5
2,187	0.511	0.353	0.320	43.2
1,493	0.43	0.287	0.204	20.7
687	0.680	0.083	0.082	6.6
Temperature = 87.5°F Pseudoreduced Temperature = 1.21 True Reduced Temperature = 0.995				
2,901	0.658	0.339	0.334	Single phase
2,720	0.633	0.330	0.326	Single phase
2,700	0.631	0.328	0.323	46.7
2,623	0.662	0.324	0.314	41.7
2,524	0.609	0.319	0.300	38.3
2,098	0.558	0.289	0.246	28.0
1,412	0.542	0.200	0.157	15.2
980	0.660	0.114	0.103	8.9
Temperature = 160°F Pseudoreduced Temperature = 1.40 True Reduced Temperature = 1.13				
2,798	0.728	0.256	0.263	Single phase
2,775	0.727	0.254	0.263	3.9
2,612	0.718	0.242	0.246	16.1
2,300	0.705	0.217	0.216	16.7
1,923	0.706	0.181	0.176	14.1
1,482	0.738	0.13	0.132	9.9
962	0.815	0.079	0.082	5.1
Temperature = 200°F Pseudoreduced Temperature = 1.49 True Reduced Temperature = 1.20				
2,955	0.788	0.235	0.243	Single phase
2,628	0.774	0.213	0.221	1.4
2,250	0.769	0.208	0.215	4.5
2,245	0.764	0.184	0.188	9.4
1,937	0.769	0.158	0.159	8.7
1,624	0.787	0.129	0.130	7.4
1,305	0.814	0.100	0.102	5.9
1,070	0.842	0.079	0.082	4.7

SOURCE: (4-60).

more must be known before a completely reliable prediction of volumetric behavior can be made.

Pitzer (4-68), on API Research Project 50, presented an imperfection parameter n to classify molecules on the basis of their deviation from behavior as perfect liquids. This parameter is a function of the vapor pressure p_s at a reduced temperature of 0.7 and of the critical pressure P_c as follows:

$$n = \log \frac{P_c}{p_s} - 1 \qquad (4\text{-}22)$$

The compressibility factor at a reduced pressure of 1.6 is plotted at various reduced temperatures against the imperfection parameter (Fig. 4-26).

Functions of the Compressibility Factor

In thermodynamic calculations, several functions of the compressibility factor with pressure and temperature are required. The values given in Table A-2 were calculated by first reading and computing z from the large-scale plot in Fig. 4-16. In the Appendix the following functions are given both in tabular and in graphical form:

Table A-2. Compressibility Factors for Natural Gases

Table A-3. $\int_{0.2}^{P_r} z\, dP_r$

Table A-4. $\int_{0.2}^{P_r} \frac{z}{P_r}\, dP_r$

Table A-5. $\int_{P_r}^{0.2} z\, dP_r$ and $\int_{P_r}^{0.2} \frac{z}{P_r}\, dP_r$

Table A-6. $\int_{0}^{P_r} \frac{P_r}{z}\, dP_r$

Table A-7. $\int_{0}^{P_r} \left(\frac{P_r}{z}\right)^2 dP_r$

Table A-8. $\left[0.5 + \int_{P_r}^{3} \frac{z/P_r}{1 + B(z/P_r)^2}\, dP_r\right]_{T_r}$

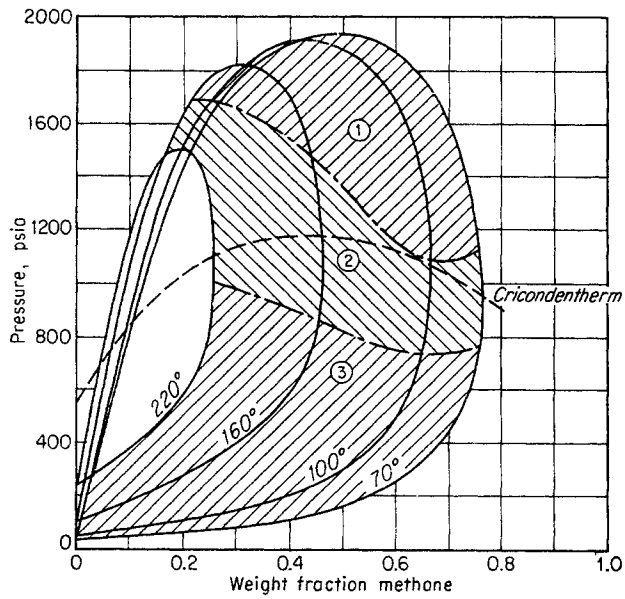

Fig. 4-25. Apparent volumes of butane in saturated methane-butane mixtures. (*Katz and Sliepcevich*, 3-62, 3-63, 4-52. Courtesy *Oil Weekly*.)

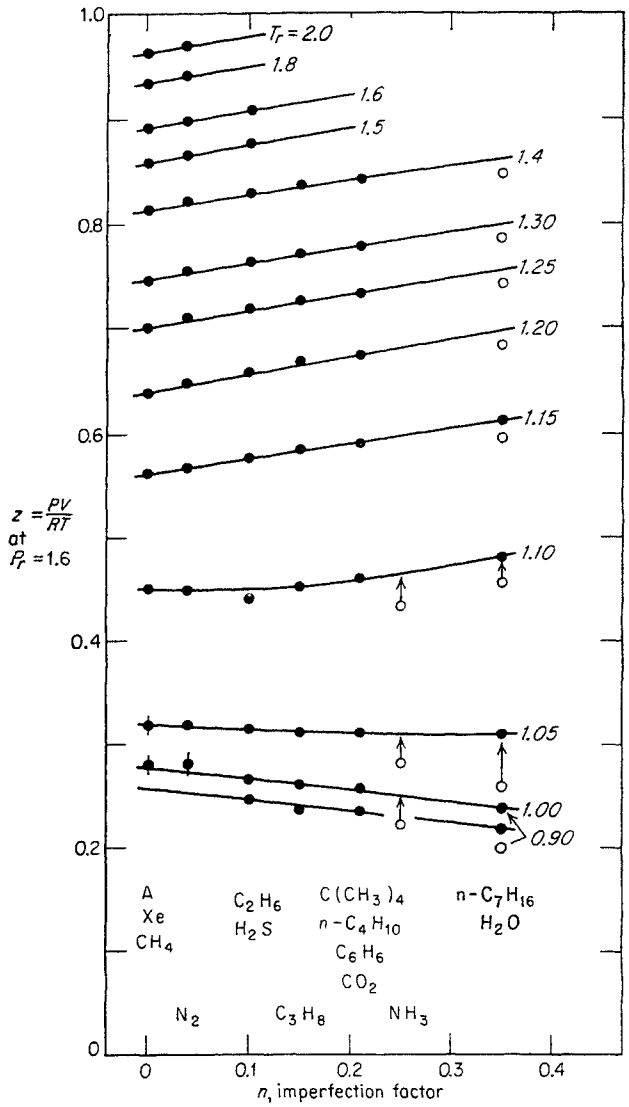

Fig. 4-26. Variation of compressibility factor with imperfection factor at $P_r = 1.6$. (*Pitzer, Pimentel, and Brattain, 4-68. Courtesy API.*)

Compressibility Chart for Natural Gases

Certain equations require that the compressibility of natural gases be written in the form normally used for liquids. The coefficient of compressibility is written as follows:

$$C_g = -\frac{\partial V}{V\,\partial P} \qquad (4\text{-}23)$$

Trube (4-93) has defined a pseudoreduced compressibility C_r as $C_g P_c$, a dimensionless quantity. He computed the C_r from the compressibility factors for natural gases (Fig. 4-16) on the basis of the following relationship:

$$C_r = C_g P_c = \frac{1}{P_r} - \frac{\partial z}{z\,\partial P_r} \qquad (4\text{-}24)$$

Figures 4-27 and 4-28 show pseudoreduced compressibility as a function of reduced temperature and reduced pressure.

Illustrative Problem

Find the compressibility of a natural gas with a gravity of 0.65 at 1,483 psia and 156°F.

The 0.65 gravity gas has a T_c of 374°R and a P_c of 669 psia (Fig. 4-22).

$$T_r = \frac{616}{374} = 1.65 \qquad P_r = \frac{1{,}483}{669} = 2.22$$

From Fig. 4-27

$$C_r = 0.51$$

$$C_g = \frac{0.51}{669} = 0.000763 \text{ vol/(vol)(psia)}$$

or

$$C_g = \frac{0.51 \times 14.7}{669} = 0.0112 \text{ vol/(vol)(atm)}$$

Density of Liquids

The density of liquids for pure substances decreases with increasing temperature and reaches the density of the vapor at the critical temperature (Fig. 4-29). Liquid mixtures have a change in density with temperature similar to that for pure compounds as given by tables of corrections (4-1). The density of a pure constituent is illustrated for propane in Fig. 4-30 (1-2).

The density of a liquid can be determined in the laboratory by the use of hydrometers or pycrometers. Corrections of density for temperature to some standard temperature such as 60°F are made by using standard measurement tables (4-1). Pure hydrocarbon liquids such as pentane and hexane have nearly additive volumes at room temperature and pressure.

The density of hydrocarbon liquids can be computed from the composition of the liquids and the density of their components (4-88, 1-19, 1-2). Constituents propane and heavier at 60°F are assumed to have additive volumes. Given the densities of liquid mixtures of methane and heavier hydrocarbons at 60°F and 1 atm, it is possible to compute the apparent density of the dissolved methane. Figure 4-31 gives the apparent density of methane and ethane in hydrocarbon liquids with weight per cent of concentration and density of the solvent as variables. Table 4-15 gives an example of computation of a liquid density from its composition. The apparent density of dissolved nitrogen is 0.48 gram/cu cm for a solvent having a density of 0.68 gram/cu cm.

The effect of pressure on the density of a liquid varies with the liquid density, the higher compressibilities occurring for low-density liquids or those approaching the critical temperature. Figure 4-32 gives a correction for pressure at 60°F based on the density of the liquid. Trube (4-93a) has devised charts for predicting the compressibility of hydrocarbon-reservoir liquids. Figures 4-32*a* and 4-32*b* give

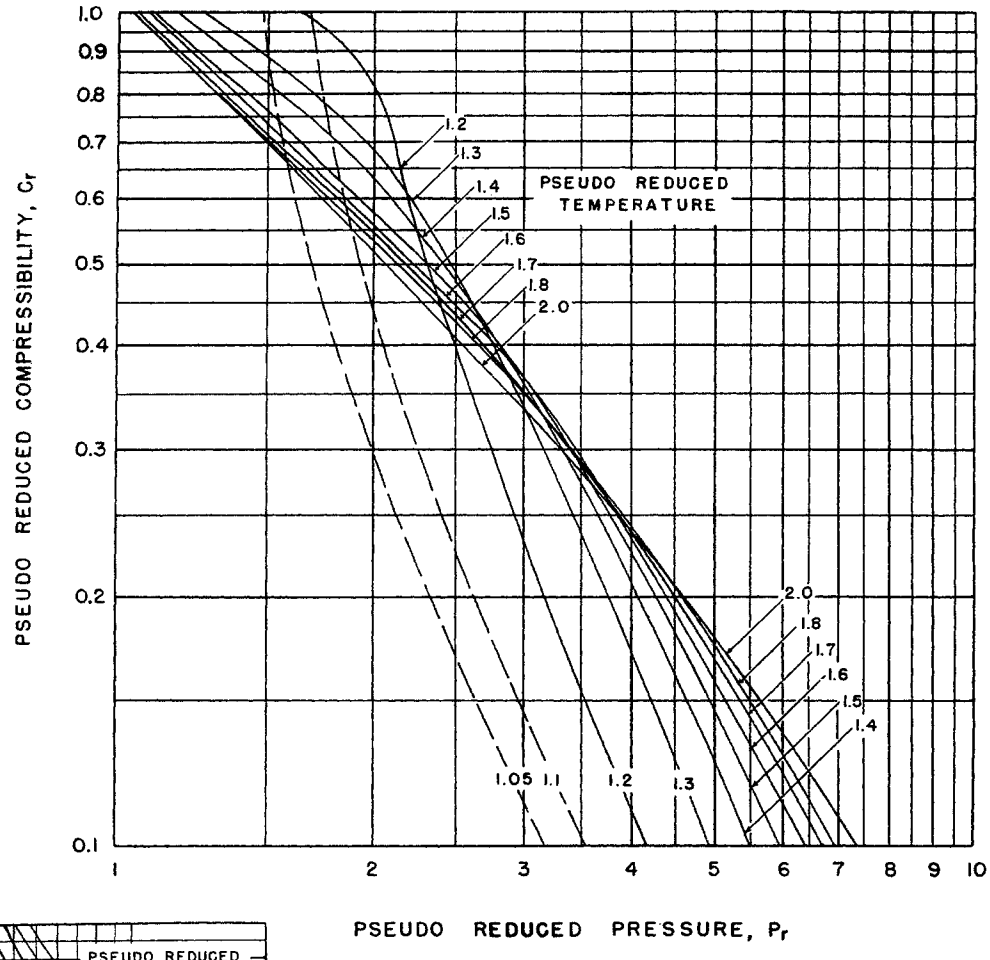

Fig. 4-27. Compressibility of natural gases. (*Trube*, 4-93. *Courtesy J. Petrol. Technol., AIME.*)

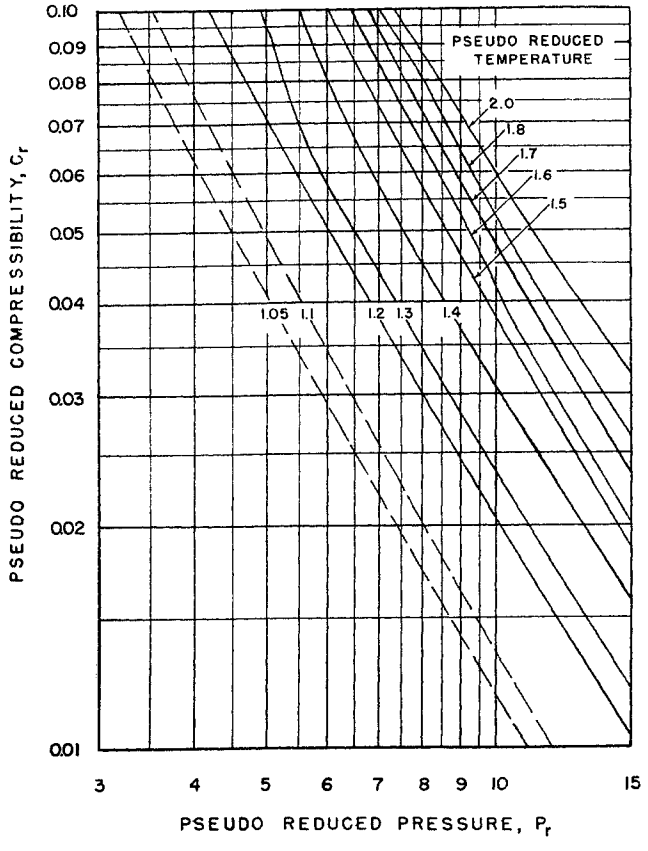

Fig. 4-28. Compressibility of natural gases. (*Trube*, 4-93. *Courtesy J. Petrol. Technol., AIME.*)

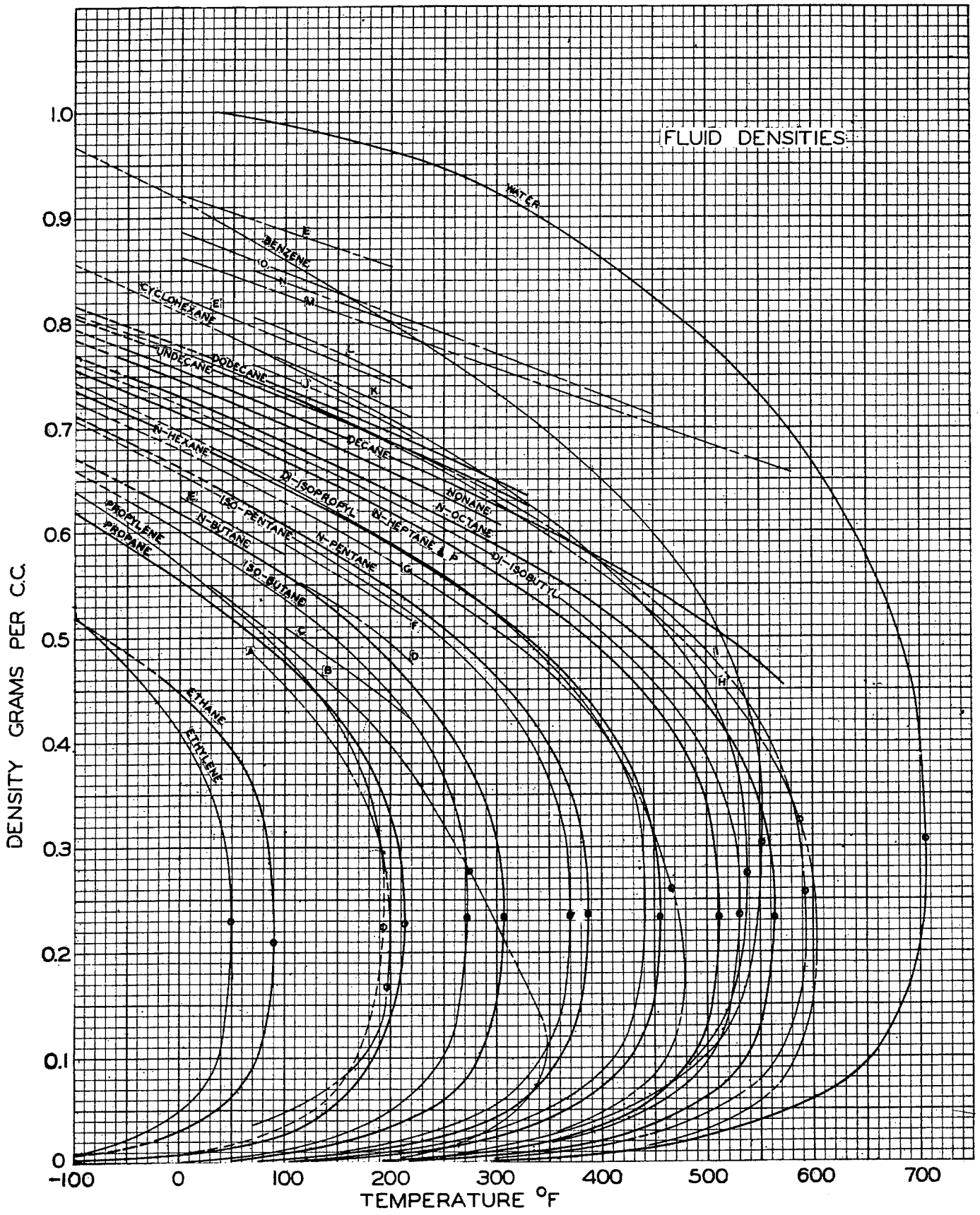
FLUID DENSITIES
DENSITY GRAMS PER C.C.
TEMPERATURE °F
1.0
0.9
0.8
0.7
0.6
0.5
0.4
0.3
0.2
0.1
0
-100
0
100
200
300
400
500
600
700
WATER
BENZENE
CYCLOHEXANE
UNDECANE
DODECANE
N-HEXANE
DECANE
NONANE
N-OCTANE
DI-ISOPROPYL
DI-HEPTANE
DI-ISOBUTYL
ISO-PENTANE
N-PENTANE
PROPYLENE
PROPANE
N-BUTANE
ISO-BUTANE
ETHANE
ETHYLENE

Fig. 4-29. *(Left)* Orthobaric density of liquids and vapors. *A*, 8 mole % CH_4–92 mole % C_3H_8 (370–739 lb); *B*, 50.25 wt % C_2H_6–49.75 wt % *n*-C_7H_{16}; *C*, 19.2 wt % CH_4–80.8 wt % C_6H_{14} (2,412–2,506 lb); *D*, 7.15 wt % CH_4–92.85 wt % *n*-C_5H_{12} (854–1,043 lb); *E*, National Standard Petroleum Oil Tables; *F*, 7.15 wt % CH_4–92.85 wt % *n*-C_5H_{12} (at 3,000 lb); *G*, 9.78 wt % C_2H_6–90.22 wt % *n*-C_7H_{16}; *H*, gasoline; *I*, naphtha; *J*, Conroe Crude, saturated liquid, changing composition (1,642–2,079 lb); *K*, 8 wt % gas in Dominguez crude oil (2,459–3,096 lb); *L*, 5.11 wt % gas in Santa Fe Springs crude oil (2,118–2,575 lb); *M*, Pennsylvania Spindle oil at atmospheric pressure; *N*, 4 wt % CH_4 in crystal oil (1,945–2,433 lb); *O*, Oklahoma lubricating oil at atmospheric pressure; *P*, Kettleman Hills condensate (543–829 lb). *(Brown, Katz, Oberfell, and Alden,* 1-2.)

procedures for finding the pseudocriticals for reservoir fluids, and Fig. 4-32*c* gives the compressibility.

Partial Volumes

The partial volume of a constituent is defined as the change in volume of a system when a unit mass of the constituent is added. It varies with temperature, pressure, and composition of the phase (4-78). When data are available on the partial volumes of constituents for several compositions of a mixture, correlations of partial volumes can be very helpful (4-78). Olds, Sage, and Lacey (4-65) have presented the partial volume of butane and decane at 280°F as a function of

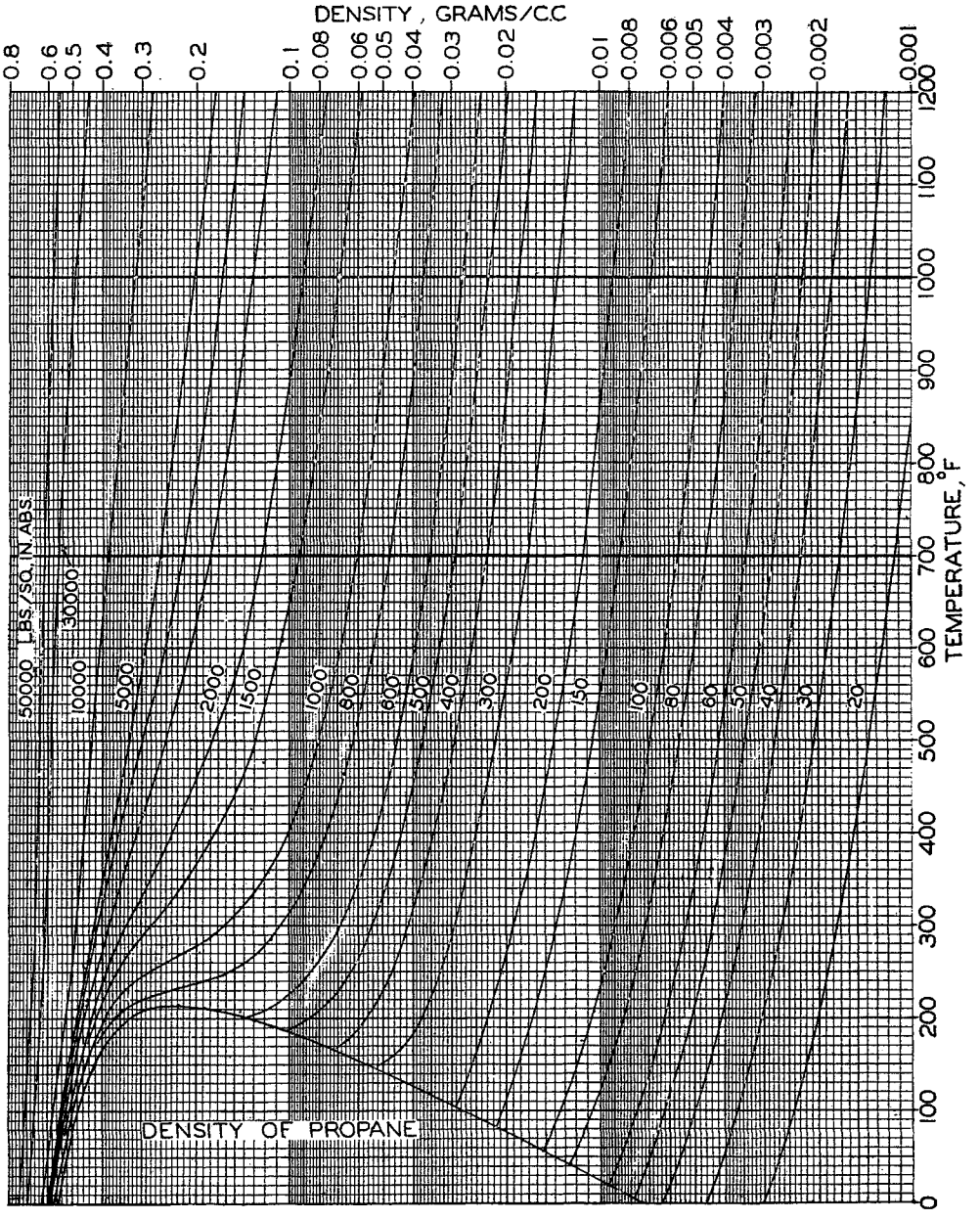

Fig. 4-30. Density of propane. *(Brown, Katz, Oberfell, and Alden,* 1-2.)

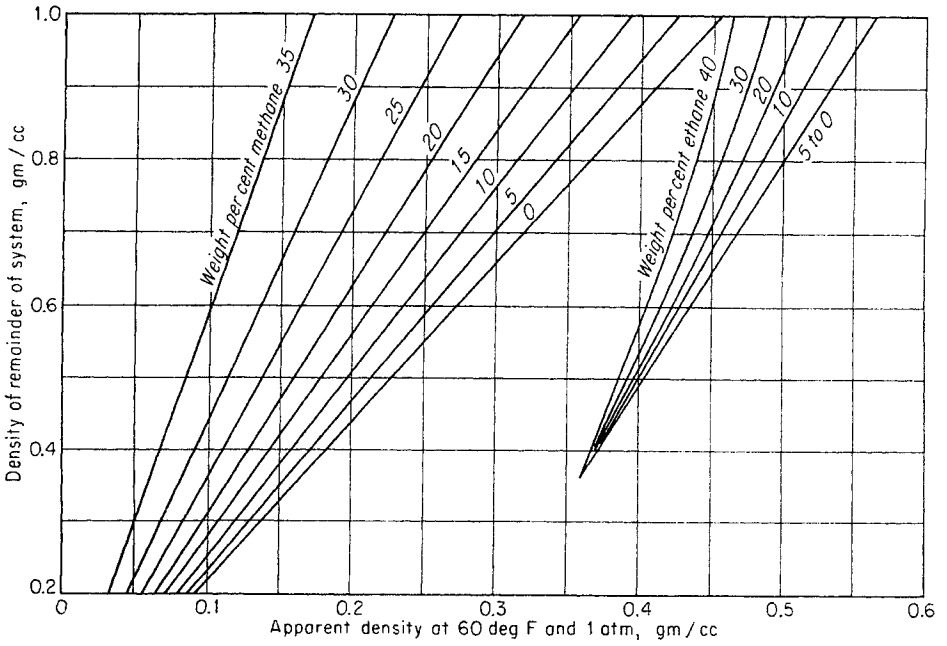

Fig. 4-31. Apparent density of methane and ethane. (*Standing and Katz*, 4-88; 1-2.)

pressure and concentration of butane in the binary system (Figs. 4-33 and 4-34). These charts permit computation of the liquid-phase density at 280°F directly.

Illustrative Problem

Compute the density of a liquid composed of 0.463 mole fraction butane and 0.537 mole fraction decane at 4,000 psi and 280°F. (Olds, Sage, and Lacey report 2.623 cu ft/lb mole as the experimental density.)

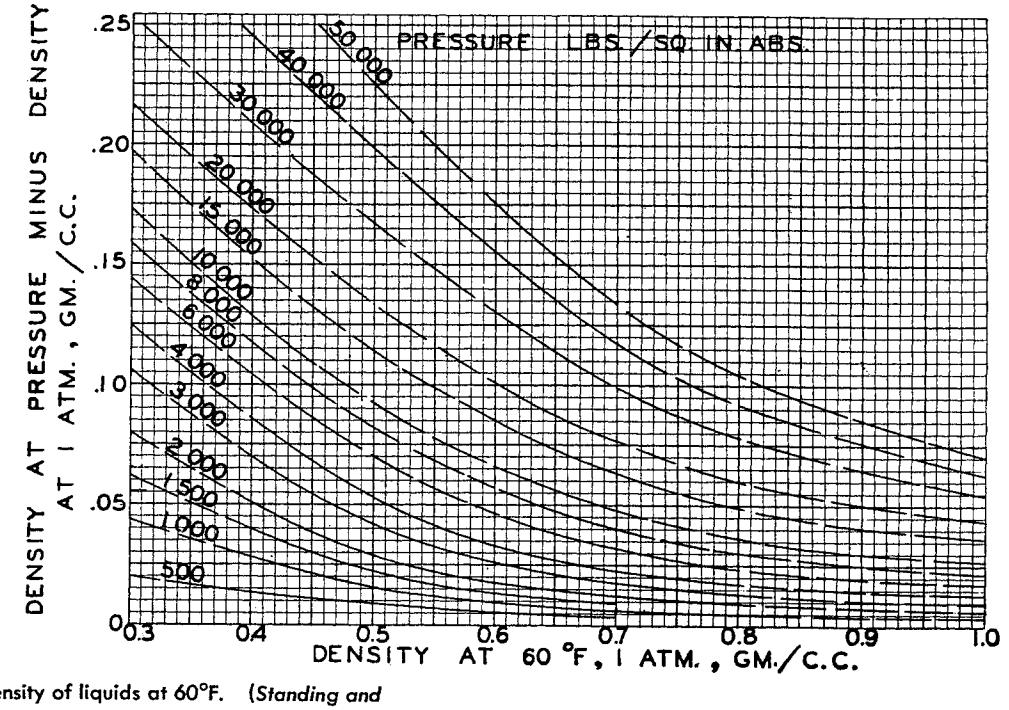

Fig. 4-32. Effect of pressure on the density of liquids at 60°F. (*Standing and Katz*, 1-2; 4-88.)

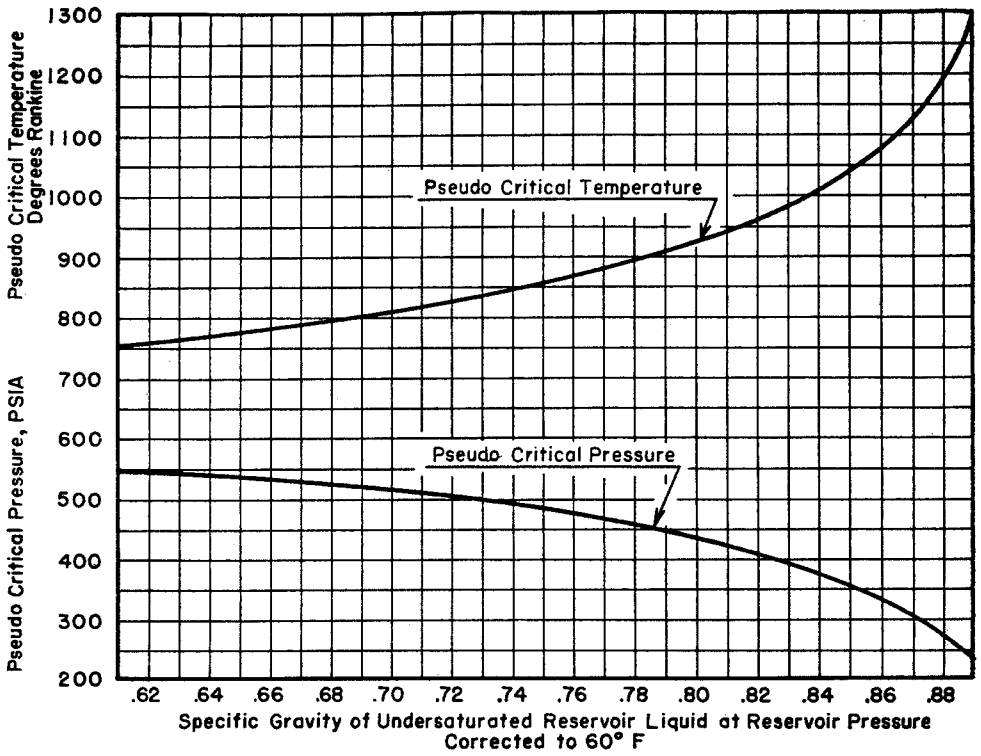

Fig. 4-32a. Pseudocritical conditions for undersaturated reservoir liquids. (*Trube*, 4-93a.)

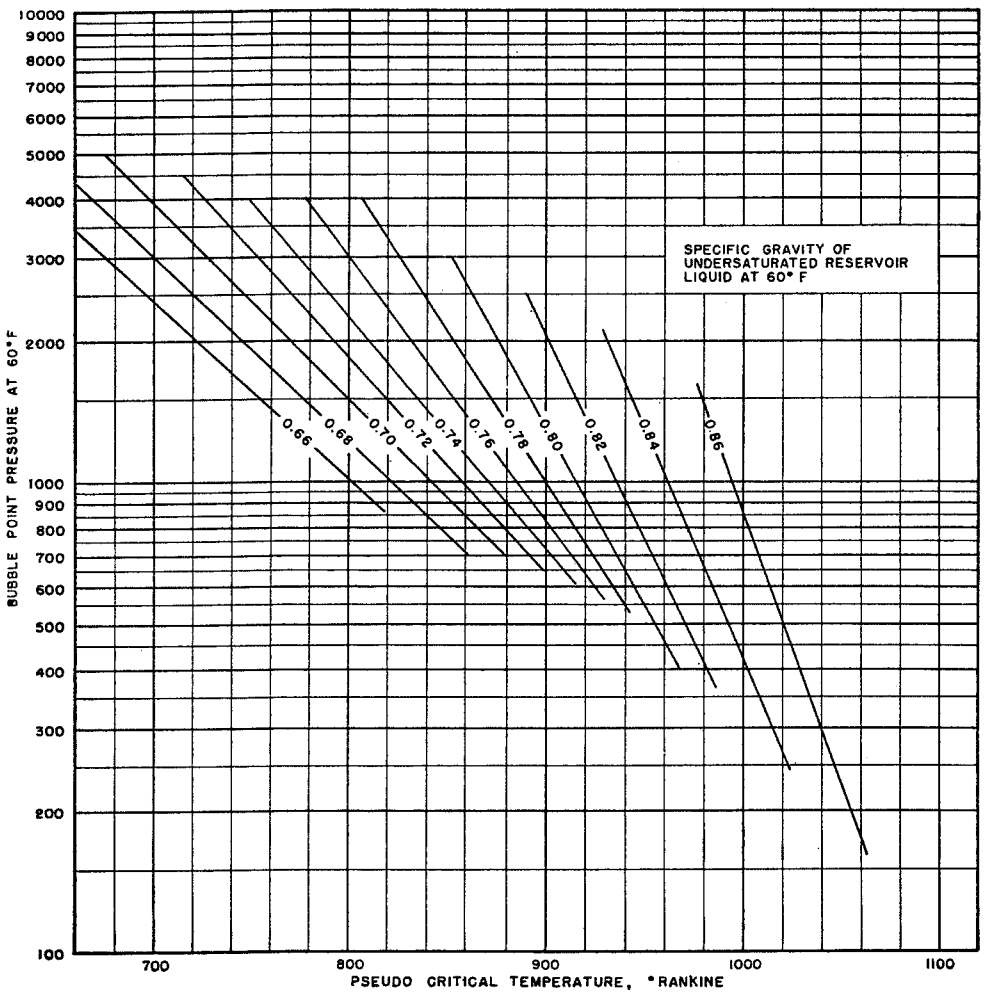

Fig. 4-32b. Variation of pseudocritical temperature with specific gravity and bubble point of liquid. (*Trube*, 4-93a.)

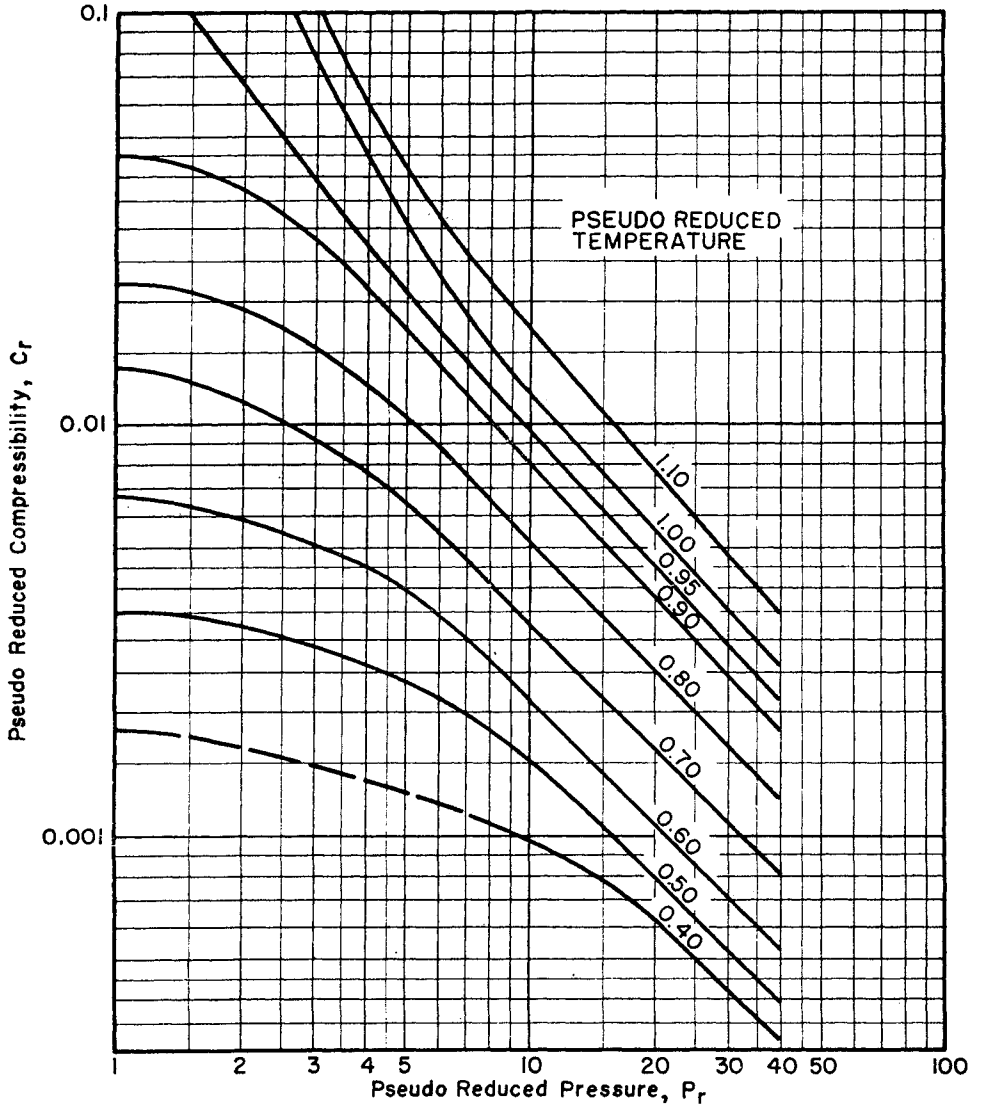

Fig. 4-32c. Reduced compressibility for undersaturated reservoir fluids. (*Trube*, 4-93a.)

Solution

Using partial volumes (Figs. 4-33 and 4-34),

	Mole fraction	Partial vol at 4,000 psia, 280°F, cu ft/lb mole	Product
n-Butane	0.463	1.80	0.834
Decane	0.537	3.33	1.785
			2.619

The value 2.619 cu ft/lb mole agrees closely with experimental value. Using apparent densities of pure constituents with temperature and pressure corrections for mixture,

	Mole fraction	Molecular weight	Grams/mole	Density at 60°F, grams/cu cm	Cu cm/mole
Butane	0.463	58	31.2	0.5844	53.5
Decane	0.537	144	77.4	0.7341	105.4
			108.6		158.9

At 60°F, 1 atm, density $\frac{108.6}{158.9}$ = 0.684 gram/cu cm

Correction for pressure (Fig. 4-32) = 0.024

Density at 60°F, 4,000 psia = 0.708 gram/cu cm

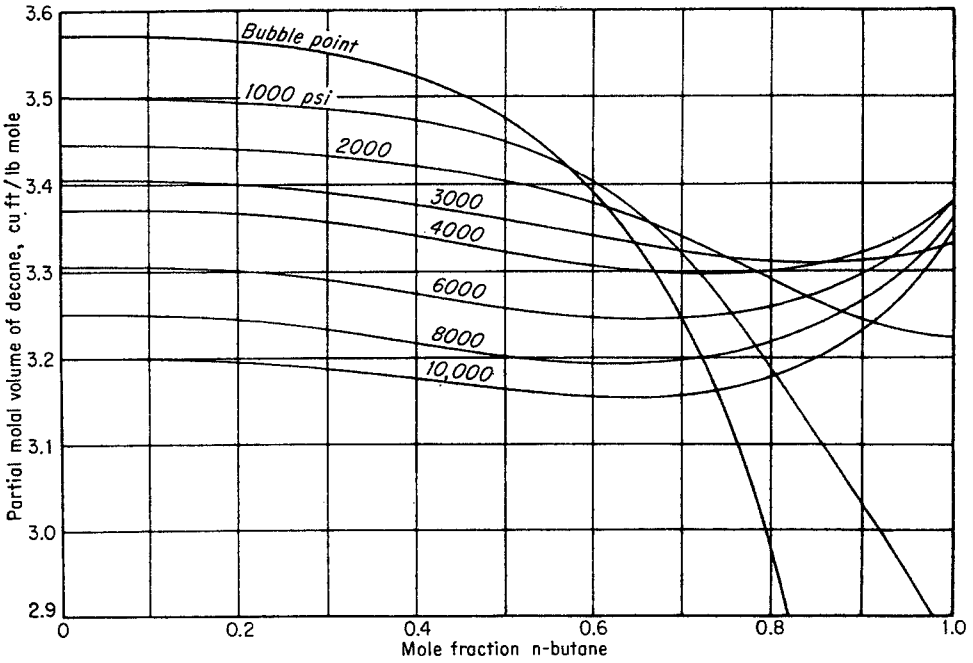

Fig. 4-33. Partial volume of decane at 280°F. *(Olds, Sage, and Lacey, 4-65. Courtesy API.)*

Correction to 280°F (Fig. 4-29): 0.708 at 60°F goes to 0.600 gram/cu cm at 280°F.

0.600 × 62.43 = 37.4 lb/cu ft.

2.623 cu ft/lb mole corresponds to 108.6/2.623 = 41.4 lb/cu ft.

The liquid density computed in this case is 10 per cent too low.

Table 4-15. Computation of Liquid Density at 1,600 Psia and 120°F from Composition

Constituent	Liquid mole fraction	Mol. wt	Grams/ mole	Liquid density, grams/ cu cm	Cu cm/ mole
Carbon dioxide.	0.0029	44	0.13	(0.420)	0.31
Methane.....	0.2943	16	4.73	(0.320)	(14.77)
Ethane.....	0.0510	30	1.53	(0.485)	(3.16)
Propane.....	0.0356	44	1.57	0.5072	3.09
Isobutane.....	0.0167	58	0.97	0.5625	1.72
n-Butane.....	0.0275	58	1.60	0.5836	2.75
Pentanes.....	0.1463	72	10.55	0.6270	16.80
Hexanes.....	0.1283	86	11.05	0.6630	16.70
Heptanes+....	0.2974	196	58.30	0.8500	68.50
C_1+.....	.....	...	90.43	.....	127.80
C_2+.....	.....	...	85.70	.....	113.03
C_3+.....	.....	...	84.17	.....	109.87

Density C_1+ = 90.43/127.8 = 0.708 gram/cu cm

Density C_3+ = 84.17/109.87 = 0.768 gram/cu cm

Density C_2+ = 85.7/113.03 = 0.757 gram/cu cm

Density at 60°F and 1 atm = 0.708 gram/cu cm

By density correction for pressure of 1,600 psia (Fig. 4-32), +0.010, density 0.708 goes to 0.718.

By density correction for temperature of 120°F [Fig. 4-29 or tables (4-1)], density 0.718 goes to 0.691.

Density at 120°F and 1,600 psia = 0.691 gram/cu cm.

SOURCE: (4-50).

Characterization Factor of Hydrocarbons

The hydrocarbons in the gaseous range for naturally occurring systems are paraffinic, but, when boiling points above about 150°F are reached, compounds from the aromatic, naphthenic, and cycloparaffins are often present. The usual analysis for such hydrocarbon liquids includes boiling range, specific gravity, and sometimes molecular weight. Smith and Watson

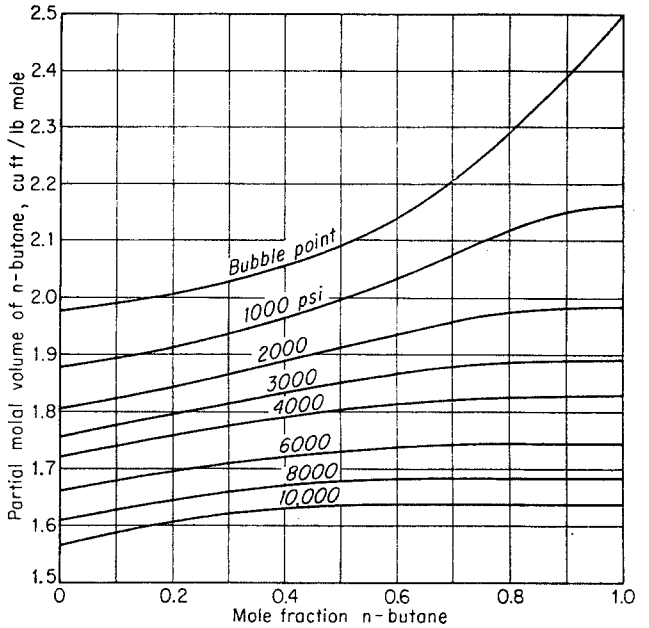

Fig. 4-34. Partial volume of butane at 280°F. *(Olds, Sage, and Lacey, 4-65. Courtesy API.)*

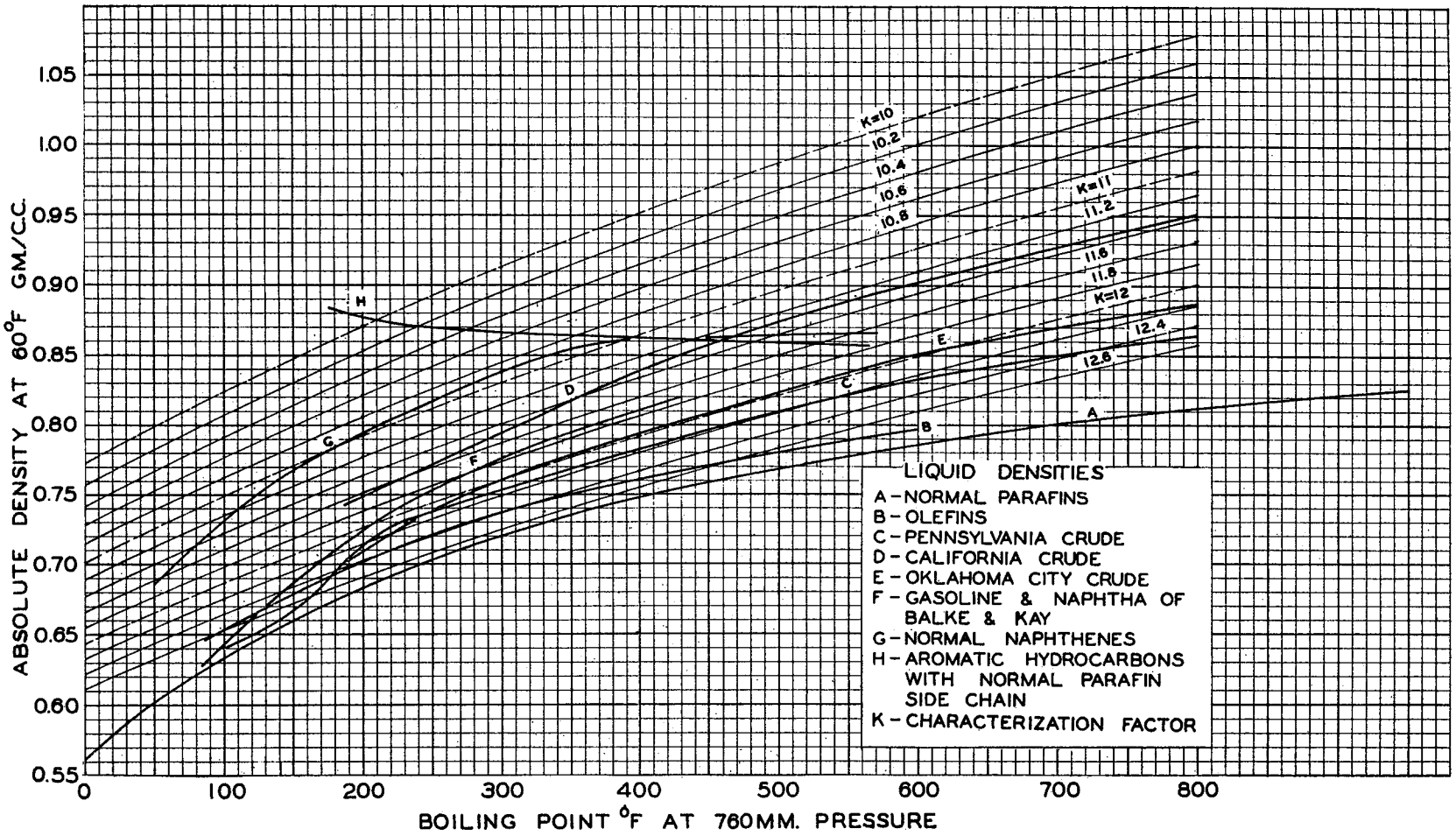

Fig. 4-35. Densities of liquids at 60°F as a function of normal boiling point. (*Brown, Katz, Oberfell, and Alden*, 1-2.)

(4-86) redefined a characterization factor for a hydrocarbon fraction as follows:

$$K = \frac{T^{1/3}}{\text{sp gr}} \qquad (4\text{-}25)$$

where K = characterization factor
T = cubic average boiling point, °R (460 + °F)
sp gr = specific gravity of liquid at 60°F with reference to water at 60°F, or grams/cu cm

Figure 4-35 (1-2) shows the relationship between density and boiling point for various liquids and also the lines of constant characterization factor K. Figure 4-36 (1-2) gives the relationships among n-boiling point, molecular weight, specific gravity, and characterization factor.

SURFACE TENSION

Surface tension is the property that causes coffee to be imbibed into a lump of sugar when the corner touches the liquid. Capillary forces are responsible for retaining liquids in porous solids, as shown in the section on capillary pressures. Surface tension has to do with foams and the nature of bubbles when vapor and liquids are in intimate contact, for instance, in fractionating columns.

Surface tension is the stress at the surface between a liquid and a vapor caused by differences between the molecular forces in the vapor and those in the liquid and by the imbalance of these forces at the interface. Early work on the surface tension of crude oils containing dissolved gases was done by Beecher and Parkhurst (4-8). Figure 4-37 shows one method of measuring surface tension. In this measurement, the force on the ring required to break the liquid-vapor interface is divided by twice the circumference of the ring, one surface on each side of the ring, to give the tension in dynes per centimeter. The capillary method is illustrated in Fig. 2-38, and Eq. (2-22) shows how it is measured from capillary rise.

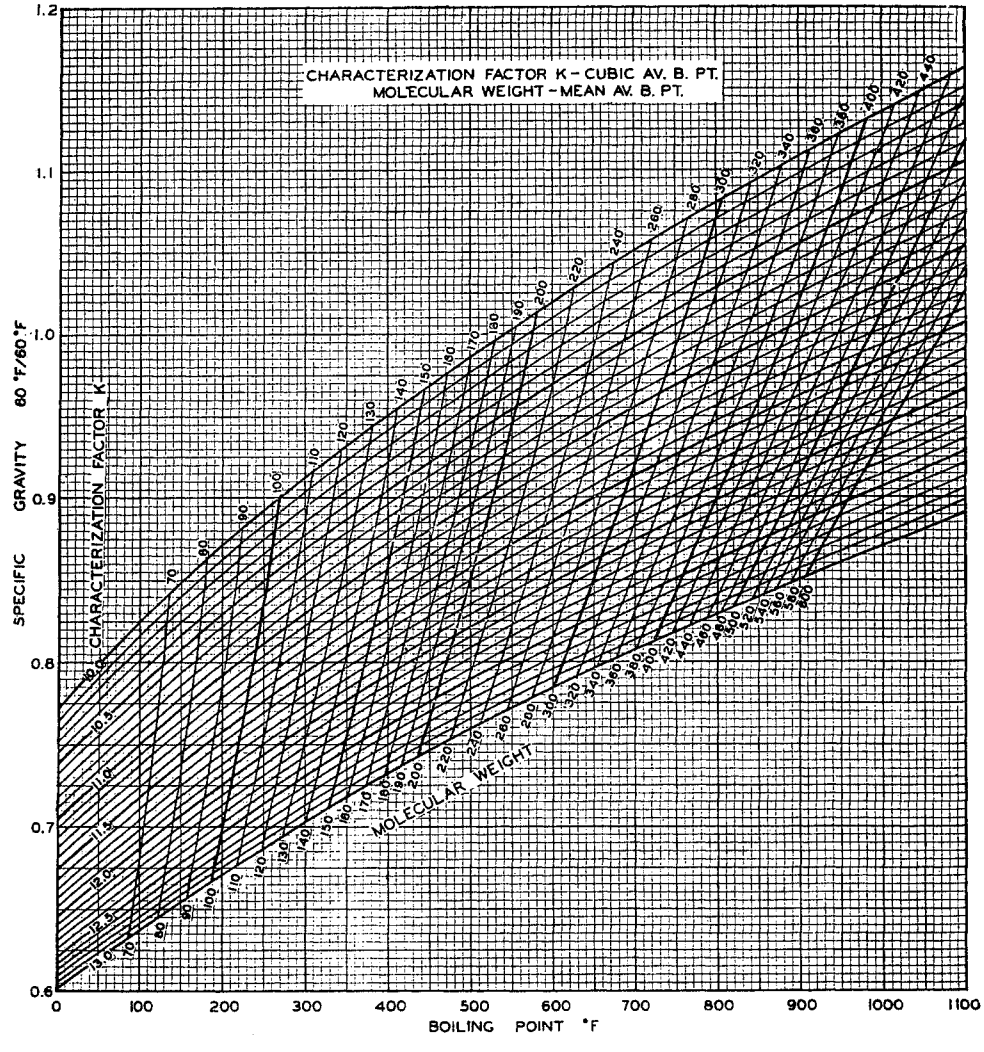

Fig. 4-36. Relationship between molecular weight, characterization factor, density, and boiling points. (*Brown, Katz, Oberfell, and Alden*, 4-86, 1-2.)

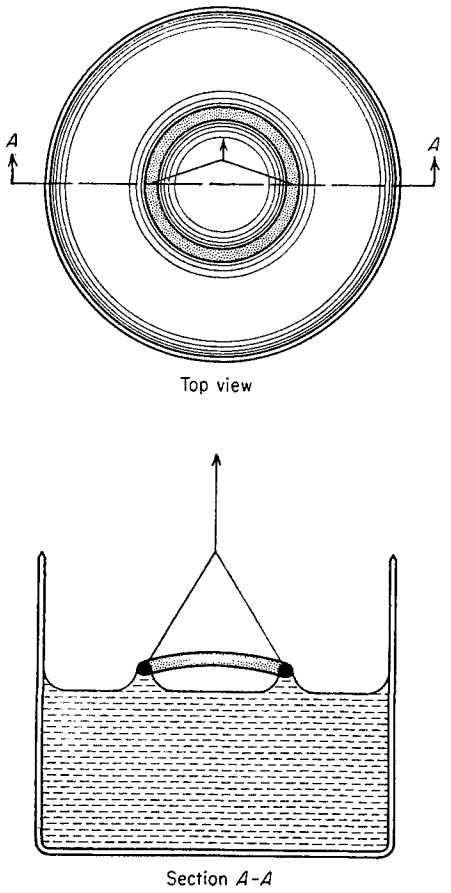

Fig. 4-37. Surface tension by ring method.

The capillary-rise method of measuring surface tension (Fig. 2-38) depends upon the contact angle between the liquid and the capillary wall. When the liquid completely wets the glass capillary, cos θ is unity and the measurement is direct and reliable. The *pendant-drop* method of measuring surface tension has found favor because it depends only on the density of the fluids and the dimensions of the drop. This method eliminates any uncertainty due to contact angle between the fluid and a solid.

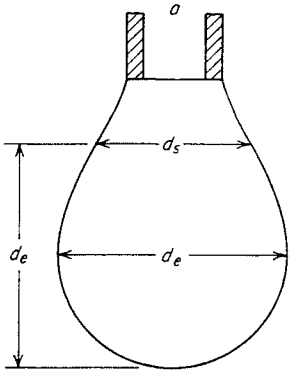

Fig. 4-38. Surface tension by pendant drop.

Figure 4-38 shows a pendant drop hanging on tip *a*. The entire equipment may be housed in pressure apparatus (2-36, 4-44). The formula for the surface or interfacial tension between the liquid in the drop and the surrounding fluid is Eq. (4-26).

$$\sigma = \frac{g d_e^2}{H} (\rho_L - \rho_V) \tag{4-26}$$

where σ = surface tension
d_e = maximum diameter of droplet (Fig. 4-38)
g = acceleration due to gravity
H = constant, a function of d_s/d_e, where d_s is measured as in Fig. 4-38

Fordham worked out values of H as a function of d_s/d_e and presented the results as a table (4-33).

The surface tension of a pure substance decreases with temperature and reaches zero at the critical temperature [Figs. 4-39 and 4-40 (4-49)]. A plot of surface tension for pure substances against reduced temperature gives a single curve for each family of compounds [Fig. 4-41 (4-49)].

Weinaug and Katz (4-94) reported the surface tension of methane-propane mixtures under pressure (Fig. 4-42). The surface-tension parameters are superimposed on a pressure-temperature diagram, starting with zero surface tension at the critical locus (Fig. 4-43). Methane-propane mixtures have surface tensions less than 0.5 dyne/cm over the last 200 psi of pressure below the critical locus. The surface tensions of methane-propane mixtures were correlated by Weinaug and Katz (4-94) by the use of parachors for the pure constituents and Eq. (4-27).

$$\sigma^{1/4} = P_1\left(x_1 \frac{d_L}{M_L} - y_1 \frac{d_V}{M_V}\right) + P_2\left(x_2 \frac{d_L}{M_L} - y_2 \frac{d_V}{M_V}\right) + \cdots \tag{4-27}$$

where P = parachor for any constituent or mixture
x = mole fraction in liquid phase
d_L = density of liquid phase, grams/cu cm
M_L = molecular weight, liquid phase
y = mole fraction in vapor phase
d_V = density of vapor phase, grams/cu cm
M_V = molecular weight, vapor phase
σ = surface tension, dynes/cm

Subscripts 1, 2, 3, . . . , refer to individual constituents in mixture.

It should be noted that the densities and molecular weights are for the entire liquid and vapor phases. Parachors are predicted from the structure of the molecules or can be computed for pure substances and mixtures from a surface-tension measurement taken under atmospheric conditions. The parachors for pure substances are given in Table 4-16. Measure-

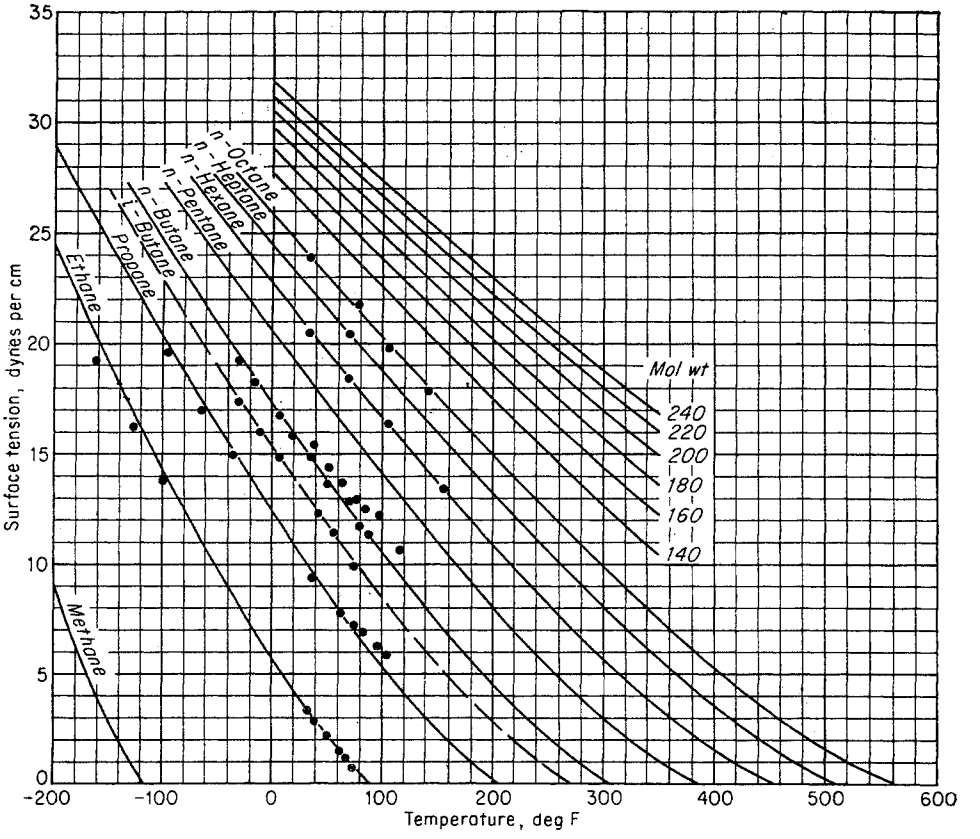

Fig. 4-39. Surface tension of hydrocarbons. (*Katz et al.*, 4-49, 4-48. *Courtesy AIME.*)

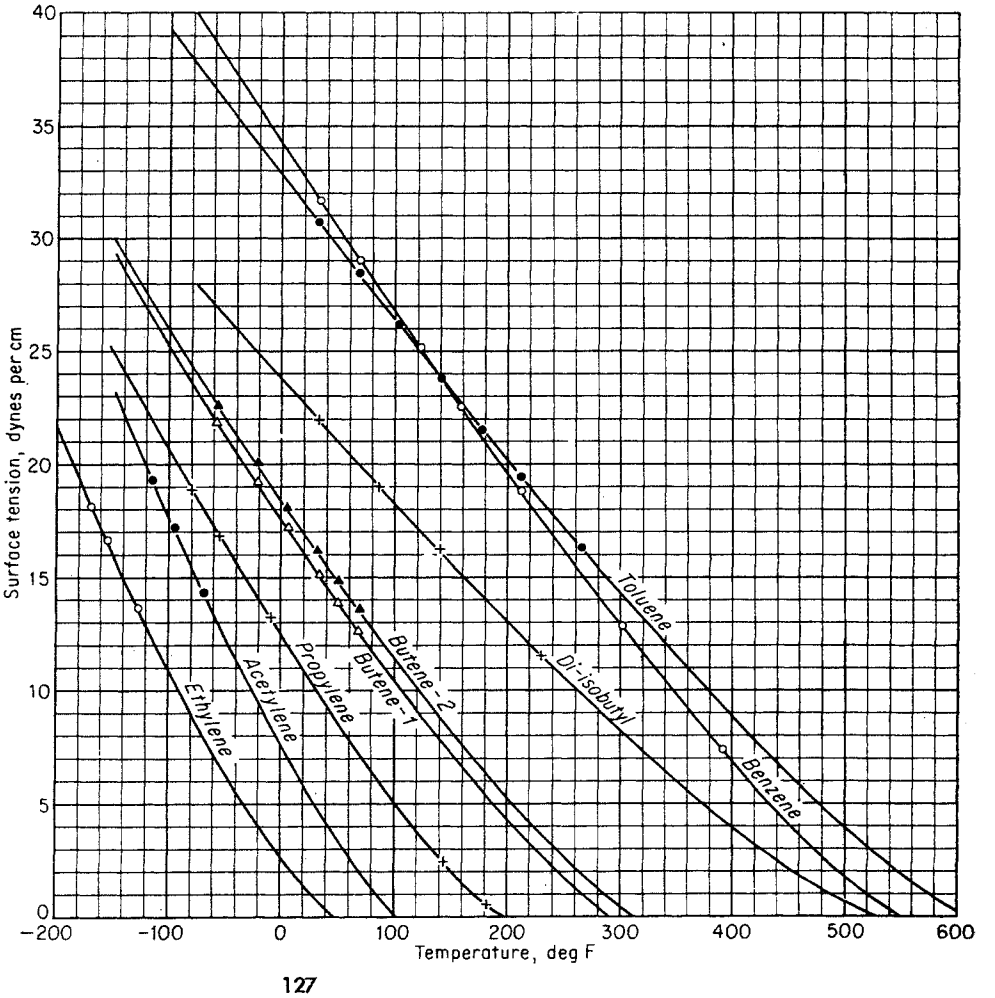

Fig. 4-40. Surface tension of hydrocarbons.

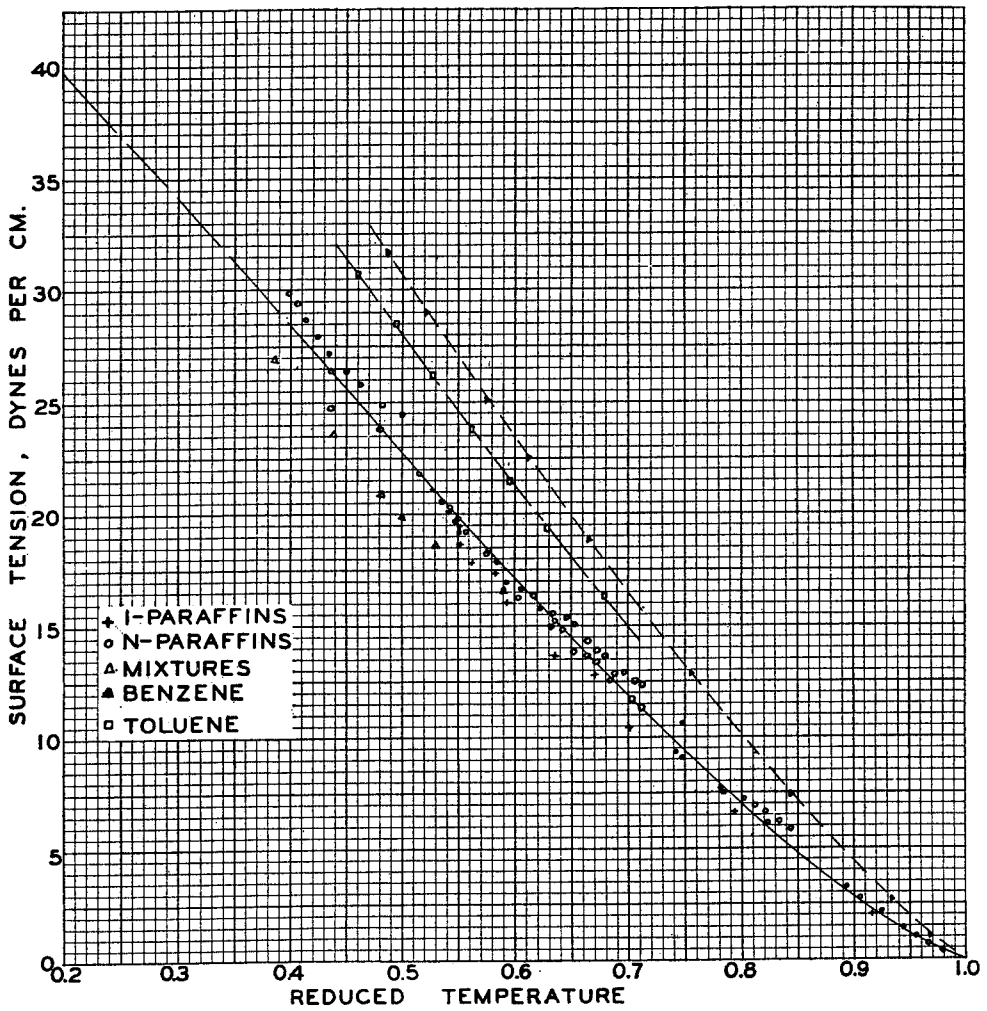

Fig. 4-41. Surface tension as a function of reduced temperature. (*After Katz and Saltman, 4-49.*)

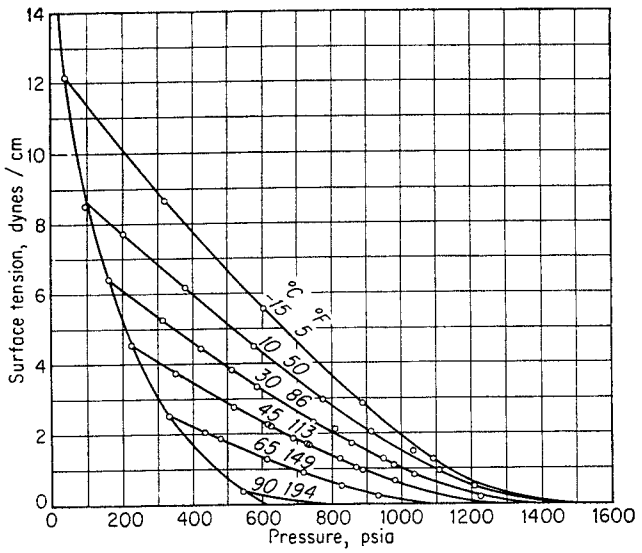

Fig. 4-42. Surface tension of methane-propane system. (*Weinaug and Katz, 4-94. Courtesy Ind. Eng. Chem.*)

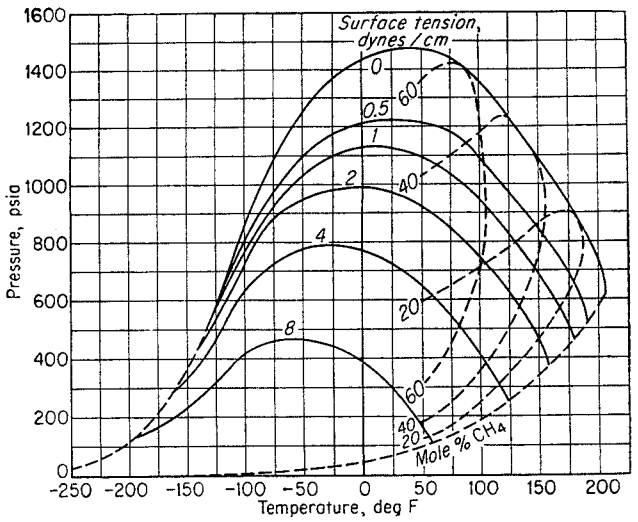

Fig. 4-43. Surface tension of methane-propane system. (*Weinaug and Katz, 4-94. Courtesy Ind. Eng. Chem.*)

Table 4-16. Parachors for Computing Surface Tension

Constituent	*Parachor*	
Methane	77.0	
Ethane	108.0	
Propane	150.3	
Isobutane	181.5	
n-Butane	189.9	
Isopentane	225.0	
n-Pentane	231.5	
n-Hexane	271.0	
n-Heptane	312.5	
n-Octane	351.5	
Ethylene	100.1	
Acetylene	88.6	
Propylene	139.9	
Hydrogen	34	(approx)
Nitrogen	41	(approx)

SOURCE: (4-94).

ments were made on the heptane and heavier fractions of a crude oil to obtain parachors. These values, with those for pure substances, are plotted in Fig. 4-44.

The method of computing surface tension was applied to equilibrium mixtures of crude oil and natural gas. The results, along with data from Schwartz (4-81) and Jones (4-47), are given in Fig. 4-45 (4-48). Later, a comparison between the calculated and the measured surface tensions of a crude oil showed the measured value at 115°F and 2,700 psia to be 1.1 dynes/cm and the computed value to be 0.85 dyne/cm (4-50). In general, one can be fairly sure that a hydrocarbon liquid, condensate, or crude oil, saturated with natural gas in the reservoir at pressures of 3,000 psia or more, will have a surface tension of 2 dynes/cm or less. Table 4-17 gives an example computation of surface tension from parachors.

The surface tensions of pure substances are given in the API tables (1-15). The surface tensions of miscellaneous substances were correlated with reduced surface tension (4-13).

The surface tension of water in equilibrium with natural gas was investigated by Hocott (4-42) and by Hough, Rzasa, and Wood (2-36). Their data are plotted in Fig. 4-46.

Interfacial Tension between Liquids

Interfacial tension exists between two liquid phases such as water and crude oil or condensate. Hassan, Nielsen, and Calhoun (4-37) measured the interfacial tension between pure hydrocarbons and water as a function of temperature and pressure. A plot of their data at 120°F is given in Fig. 4-47. Increased pressure reduces the interfacial tension. Hocott (4-42) measured the interfacial tension between water and

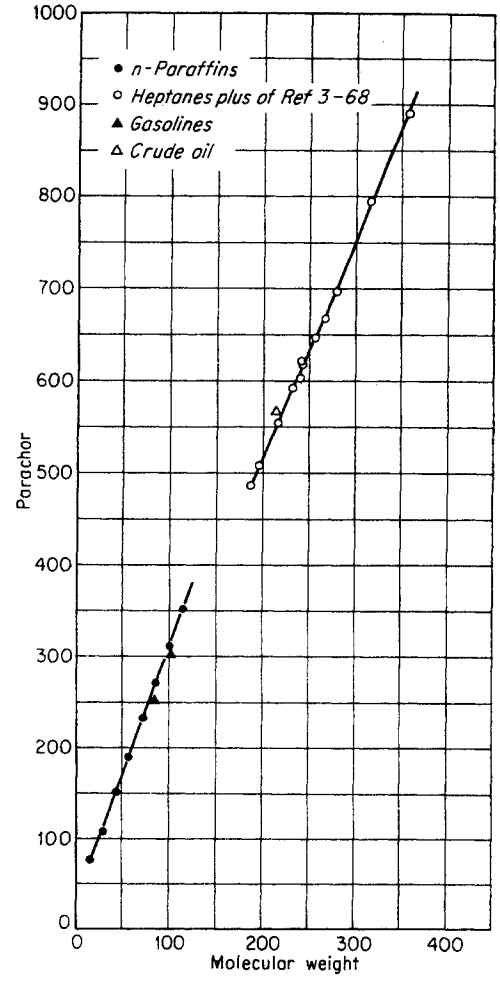

Fig. 4-44. Parachors for hydrocarbons. (*Katz, Monroe, and Trainer, 4-48. Courtesy AIME.*)

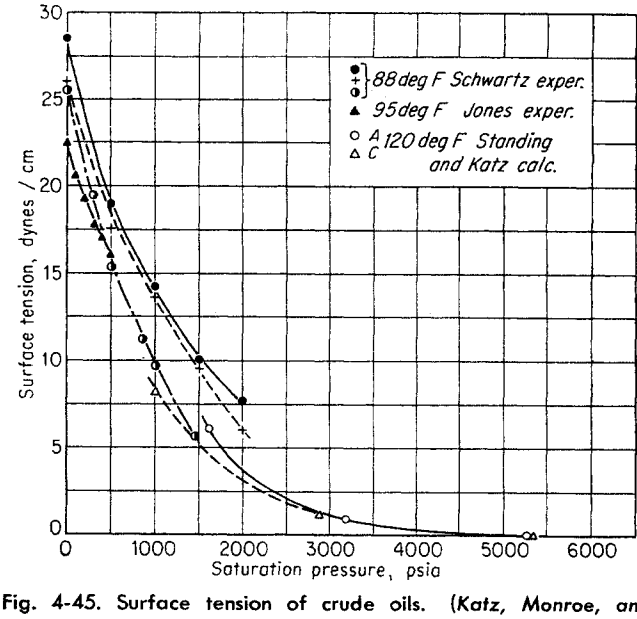

Fig. 4-45. Surface tension of crude oils. (*Katz, Monroe, and Trainer, 4-48.*)

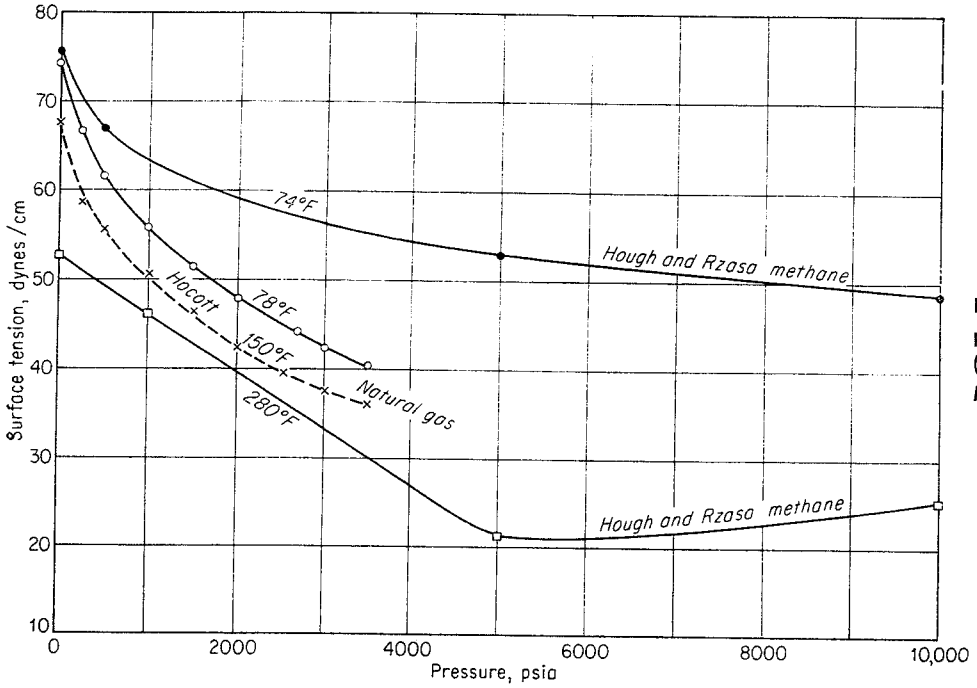

Fig. 4-46. Surface tension of water under pressure with methane and natural gas. (*Hough, Rzasa, and Wood,* 2-36; *Hocott,* 4-42.)

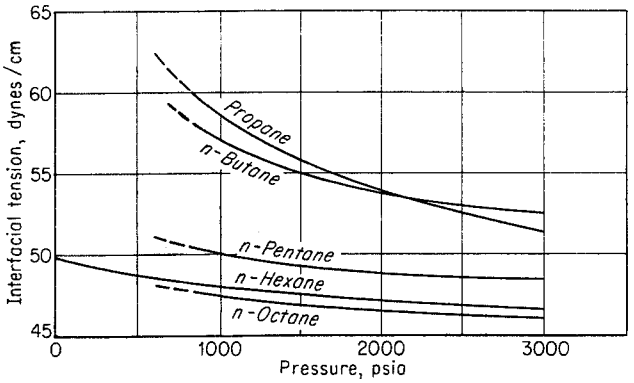

Fig. 4-47. Interfacial tension between pure hydrocarbons and water at 120°F. (*Data of Hassan, Nielsen, and Calhoun,* 4-37.)

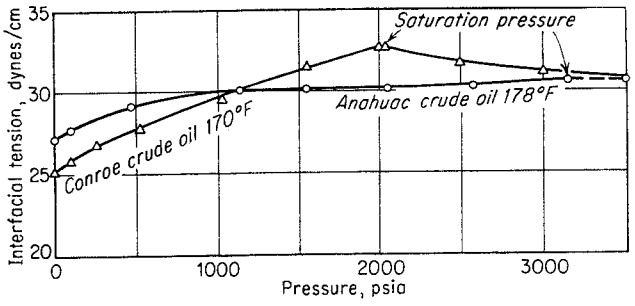

Fig. 4-48. Interfacial tension between crude oils saturated with natural gas and water. (*Data of Hocott,* 4-42.)

crude oils saturated with natural gas (Fig. 4-48). As might be expected, the effect of increased concentration of dissolved gas is to increase the interfacial tension by adding lower-molecular-weight hydrocarbons. When the saturation pressure is reached, further increases in pressure cause the interfacial tension to decrease.

Table 4-17. Calculation of Surface Tension from Composition

At 808 psia and 86°F, methane-propane mixtures have the following phase properties:

Property	Liquid	Vapor
Mole fraction methane	0.255	0.672
Mole fraction propane	0.745	0.328
Molecular weight	36.9	25.2
Density, grams/cu cm	0.4200	0.0807

The parachor for methane is 77 and for propane is 150.3. Compute the surface tension at 808 psia and 86°F.

$$\sigma^{1/4} = 77\left(\frac{0.42}{36.9}\times 0.255 - \frac{0.0807}{25.2}\times 0.672\right) + 150.3\left(\frac{0.42}{36.9}\times 0.745 - \frac{0.0807}{25.2}\times 0.328\right)$$

$$= 1.176$$

$$\sigma = 1.91 \text{ dynes/cm}$$

The experimental value was 2.14 dynes/cm at this condition (4-94).

SOURCE: (4-50).

THERMODYNAMIC PROPERTIES

The principles of thermodynamics find wide application in correlating and predicting the properties of hydrocarbons. For example, the effect of pressure on the enthalpy of a gas can be computed from pressure-volume-temperature data. Latent heats can be computed from the slopes of vapor-pressure curves. The properties of greatest interest are specific heats of gases and liquids, heats of vaporization, and the effects of pressure on the enthalpies of compressible fluids. Enthalpy-entropy charts for natural gases permit prediction of temperature change when expanding gases or the reversible work of compression.

Heat Capacity

The property of a fluid which denotes the heat required to raise or lower its temperature is its enthalpy H. Changes in enthalpy with changes in temperature T and pressure P for a single-phase fluid are given by the equation

$$H_2 - H_1 = \int_1^2 C_p \, dT + \int_1^2 \left(\frac{\partial H}{\partial P}\right)_T dP \quad (4\text{-}28)$$

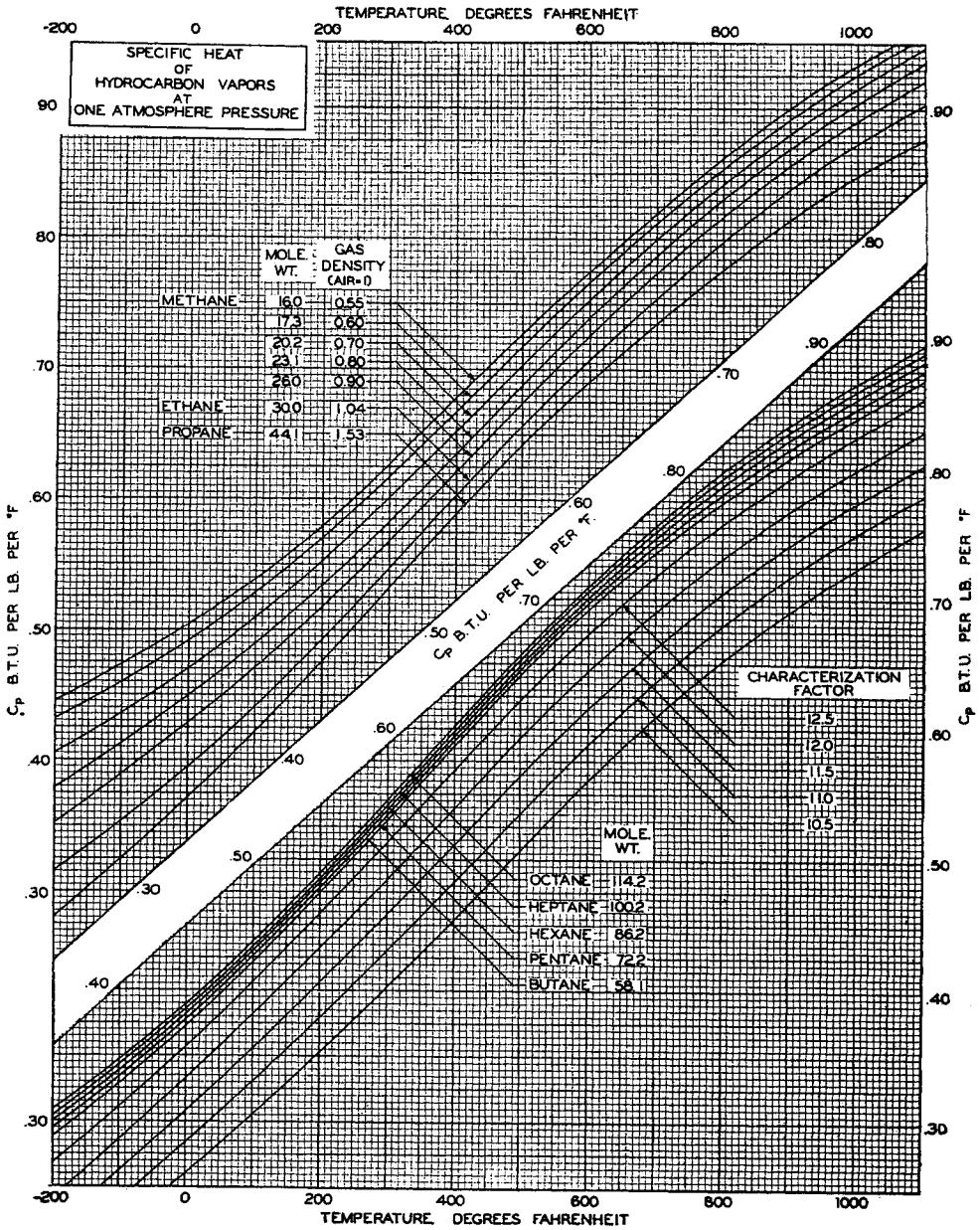

Fig. 4-49. Specific heat of hydrocarbon gases. (*Brown*, 4-16. *Courtesy AIME.*)

The effect of temperature alone on enthalpy is the specific heat C_p at constant pressure.

$$C_p = \left(\frac{\partial H}{\partial T}\right)_P \tag{4-29}$$

The effects of pressure alone are given by Eq. (4-30).

$$\left(\frac{\partial H}{\partial P}\right)_T = V - T\left(\frac{\partial V}{\partial T}\right)_P \tag{4-30}$$

where V = volume. For ideal gases, $(\partial H/\partial P)_T = 0$. An alternative equation, in which changes in enthalpy with pressure are related to the compressibility factor z, is Eq. (4-31).

$$\left(\frac{\partial H}{\partial P}\right)_T = \frac{-RT^2}{P}\left(\frac{\partial z}{\partial T}\right)_P \tag{4-31}$$

The specific heats of gases and liquids are determined experimentally in a calorimeter, usually at 1 atm. The specific heat of simple molecules can be predicted from spectroscopic data. For natural gases, the specific heat at 1 atm pressure is a function of temperature and of gas gravity or molecular weight. Figures 4-49 and 4-50 are plots of specific heats of gases and liquids by Brown and Holcomb (3-25, 4-14, 4-16). The gravity of a natural gas is used to identify the specific heat line for vapors. For high-boiling liquids, only the characterization factor is required to obtain the vapor specific heat (1-8). For liquids, the compound name or the specific gravity of the liquid identifies the hydrocarbon in finding the specific heat from Fig. 4-50.

Effect of Pressure on Enthalpy and Specific Heat

The law of corresponding states has found application in correlating the effects of pressure on enthalpy. Also, it has been convenient to use the expression $-\Delta H/T$, since the effects of pressure are found at constant temperature. Figure 4-51 by Brown (4-16) is a plot of $-\Delta H/T$ versus reduced pressure, with lines of constant temperature. The chart is for natural gases and is based on the compressibility factors of Fig. 4-16. The enthalpy of a gas decreases upon compression or increases upon expansion when $(\partial z/\partial T)_P$ is positive, for pressures up to about 5,000 psia [P_r = 8 to 10, Eq. (4-31)]. Therefore, positive values of $\Delta H/T$ are the enthalpies absorbed when expanding a gas, since $\Delta H = H_2 - H_1$. The pseudocritical pressure and temperature are used for gaseous mixtures when obtaining the reduced conditions. When the $\partial z/\partial T$ is negative for gases at high pressure (Fig. 4-16), the temperature rises upon expansion.

Edmister (4-29) has presented a similar but different plot of this function. Figure 4-52 uses the pseudocritical temperature instead of the actual temperature when dividing $-\Delta H$ to find the $-\Delta H/T_c$ function.

The Joule-Thomson coefficient μ (4-91) is

$$\mu = \left(\frac{\partial T}{\partial P}\right)_H$$

The change in temperature upon expansion, which occurs without heat transfer or work, includes the

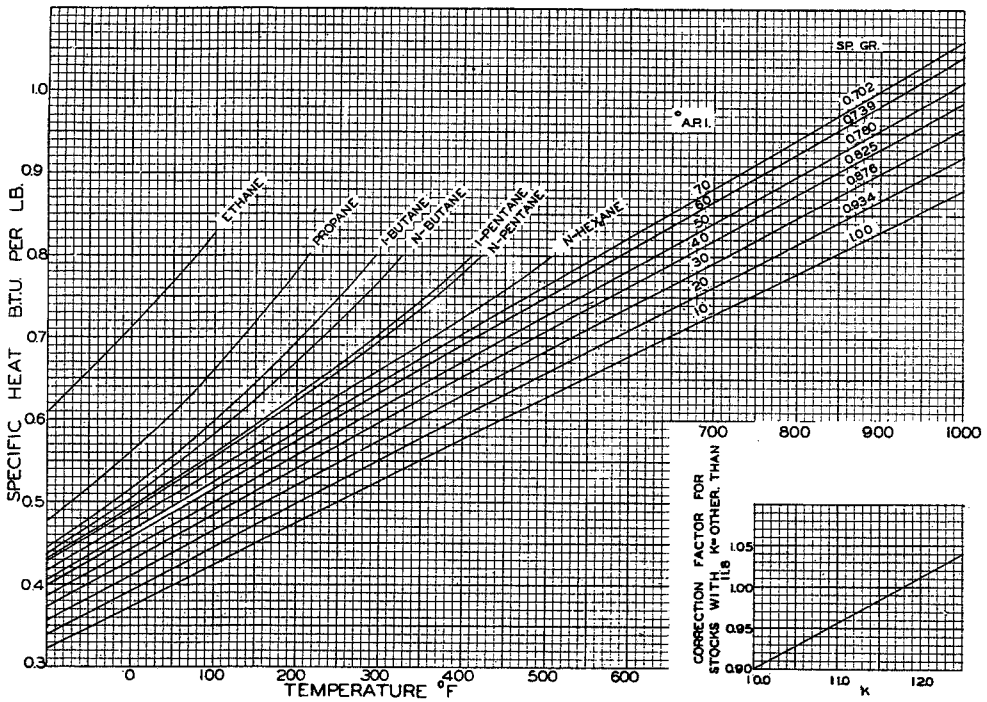

Fig. 4-50. Specific heats of hydrocarbon liquids. (*Holcomb and Brown, 3-25. Courtesy Ind. Eng. Chem.*)

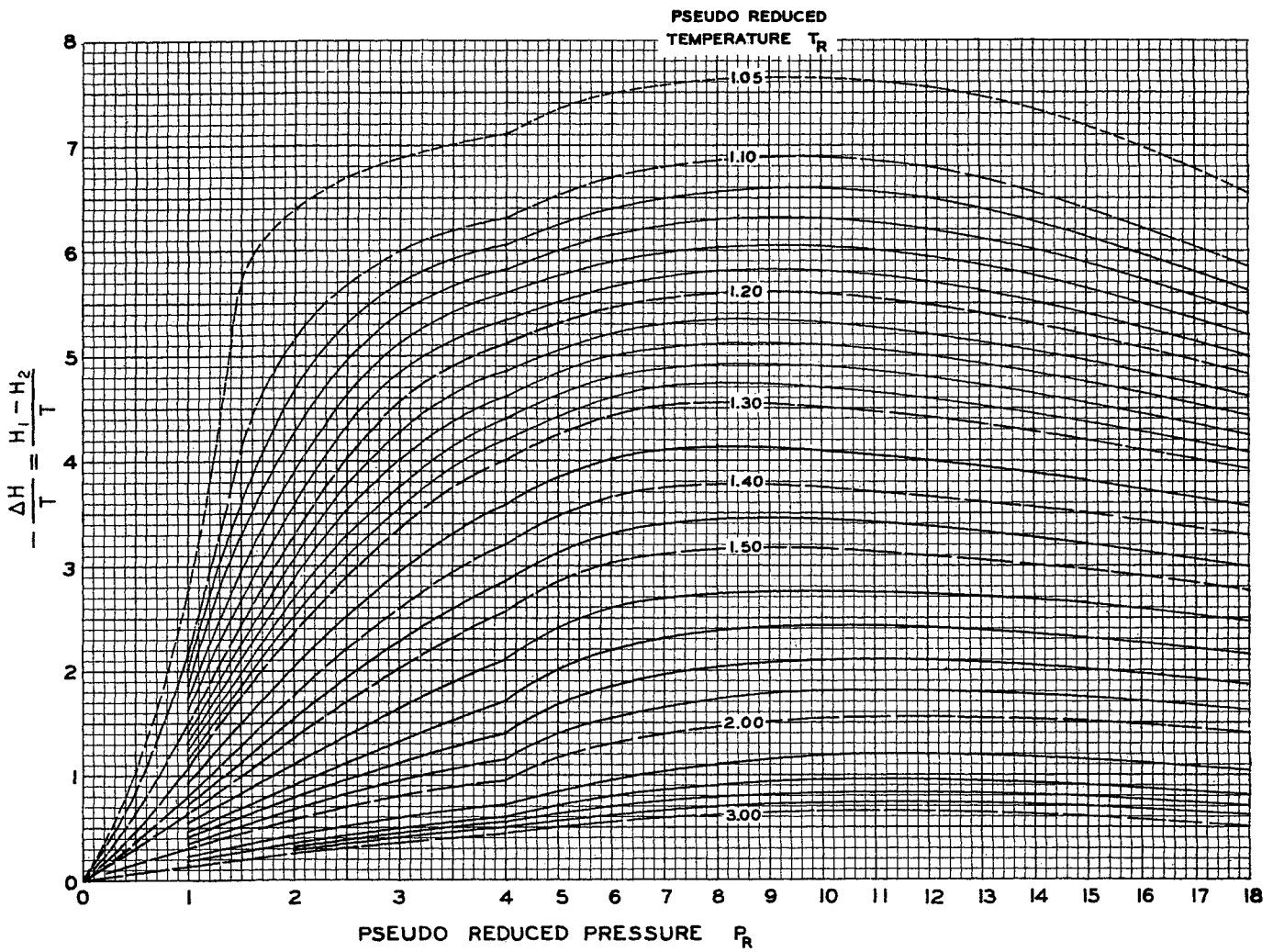

Fig. 4-51. Effect of pressure on enthalpy for natural gases. (*Brown*, 4-16. *Courtesy AIME.*)

effect of pressure on the enthalpy and the specific heat of the fluid:

$$\mu = \frac{T(\partial V/\partial T)_p - V}{C_p} \qquad (4\text{-}32)$$

Edmister (4-29) has developed a generalized chart for predicting the Joule-Thomson coefficient. Sage and Lacey have measured Joule-Thomson coefficients for several hydrocarbons. Budenholzer, Botkin, Sage, and Lacey (4-17) reported the Joule-Thomson coefficients for methane-propane mixtures. Figure 4-53 shows their data for one mixture.

The isobaric heat capacity or specific heat is a function of pressure for real gases. Figure 4-54 is a plot of the heat capacity for an 85.4 mole % methane–14.6 mole % propane mixture (4-17). To avoid preparing many plots such as these, all of them different, for gases of different gravity, the increase in specific heat ΔC_P over the atmospheric-pressure value can be used, where $\Delta C_P = C_P$ at reference pressure minus C_P at atmospheric pressure. Figure 4-55 is such a plot, prepared by Edmister, on a reduced temperature–reduced pressure basis (4-29).

The specific heat at constant volume C_v is related to specific heat at constant pressure for ideal gases as follows:

$$C_p = C_v + R = C_v + 1.99 \text{ Btu/(lb mole)(°F)}$$

The ratio $k = C_p/C_v$ of the specific heats has usefulness in computing the adiabatic compression of gases, for which ideal gases follow the relationship

$$PV^k = \text{constant}$$

Figure 4-56 gives the specific-heat ratio for hydrocarbon vapors from Edmister, and Table A-1 gives rhe atmospheric-pressure values for pure compounds.

Latent Heat

The latent heat, or enthalpy of vaporization, for pure substances is the energy necessary to vaporize a

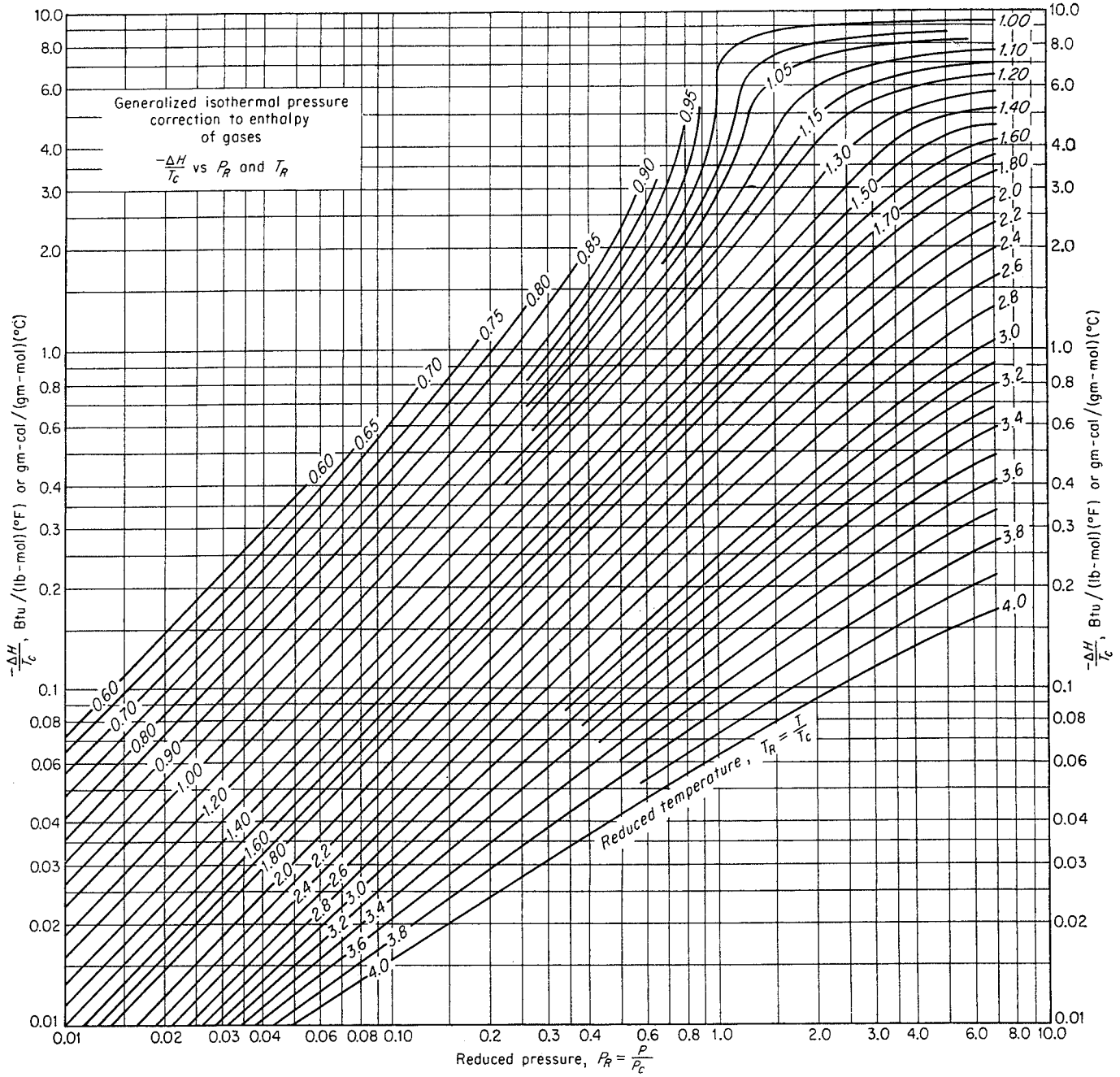

Fig. 4-52. Effect of pressure on enthalpy for natural gases. (*Edmister, 4-29. Courtesy Petrol. Engr.*)

unit of the substance at constant temperature and pressure. It is related to the vapor-pressure curve by the Clausius-Clapeyron equation:

$$\frac{dP}{dT} = \frac{\Delta H}{T\,\Delta V} = \frac{\Delta S}{\Delta V} \tag{4-33}$$

where dP/dT = slope of vapor-pressure curve
ΔH = latent heat, enthalpy increase for phase change
T = absolute temperature
ΔV = volume increase upon vaporization
ΔS = entropy increase upon vaporization

Young (4-97) computed the latent heat for the thirty pure substances for which he obtained vapor pressure and phase densities.

The increase in enthalpy when heat is added to a pure substance is illustrated by Fig. 4-57. Defining T_1 as the datum temperature, the enthalpy above the datum at constant pressure is shown as $ABCD$. Line AB represents the sensible heat of the liquid; BC, the latent heat of vaporization; and CD, the sensible heat of the vapor. The sensible-heat increases for the single phases are found from appropriate specific-heat data. The latent heat corresponds to the temperature

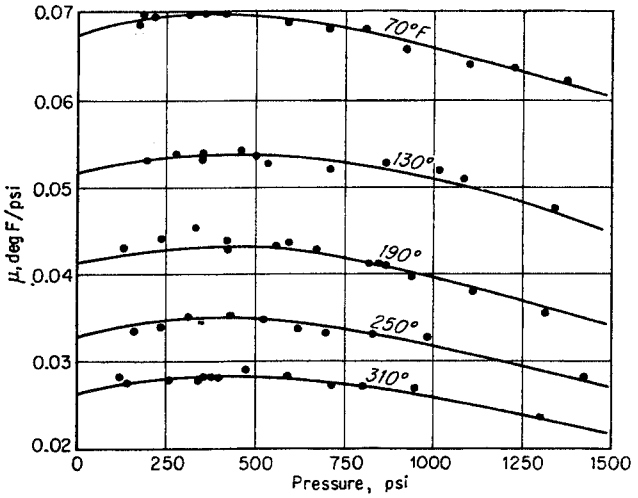

Fig. 4-53. Joule-Thomson coefficients for a methane-propane mixture containing 0.7552 weight fraction (85.4 mole fraction) methane. (*Budenholzer, Botkin, Sage, and Lacey*, 4-17. *Courtesy Ind. Eng. Chem.*)

or to the vapor pressure at T_2. At the critical point, the latent heat diminishes to zero, since there is no longer a phase change for higher temperatures. Figure 4-58 from Konz and Brown (4-56) shows the $\Delta H/T$ plot for pentane, indicating that the decrease in latent heat to zero is accompanied by a sharp change in $\Delta H/T$ for the single-phase fluid, essentially offsetting the absence of latent heat. Plotting $\Delta H/T$ for latent heat is equivalent to plotting ΔS, the entropy change upon vaporization.

For mixtures, vaporization does not take place at constant temperature and pressure (Fig. 4-57). The temperature rise from T_2 to T_3 represents the boiling range, and the change in enthalpy from F to G represents not only the latent heat but also a temperature rise on the fluid. Under such conditions it is very difficult to obtain a satisfactory correlation of latent heats. It should be noted that liquid can occur at temperatures above the critical temperature T_4 for a mixture.

Figure 4-59 is a plot of latent heats for pure hydrocarbons (3-25). The molal entropy of vaporization for pure substances (Fig. 4-60) has been correlated on the basis of reduced temperature (4-29).

Enthalpy Diagrams

Plots of enthalpy as a function of entropy, pressure, or temperature are very useful. The Mollier diagram for steam, enthalpy-entropy, has demonstrated its usefulness in flow problems. Free expansion of a fluid, for example, through a throttle or valve, takes place at constant enthalpy, $\Delta H = 0$. Adiabatic and reversible expansion or compression occurs at constant entropy, $\Delta S = 0$.

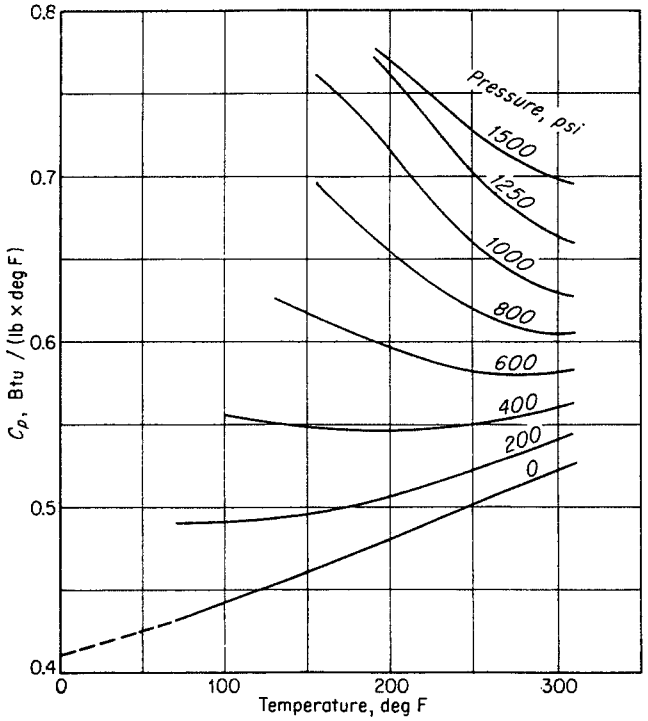

Fig. 4-54. Isobaric heat capacity for mixture containing 85.4 mole % methane–14.6 mole % propane. (*Data of Budenholzer, Botkin, Sage, and Lacey*, 4-17.)

Brown (4-16) has prepared enthalpy-entropy diagrams for natural gases using the specific heats from Fig. 4-49, the $\Delta H/T$ relationship of Fig. 4-51, and the f/P relationship of Fig. 3-29. The pressure-volume-temperature relations are those of Fig. 4-16. The isothermal ΔS relationship is that of Fig. 4-61. The enthalpy-entropy diagrams for natural gases of 0.6, 0.7, and 0.8 gravity are given in Figs. 4-62, 4-63, and 4-64, respectively. The pseudocritical temperatures and pressures used are given on the charts and correspond essentially to hydrocarbon gases. The datum for each chart is 32°F, 1 atm. A chart for a gas of 0.7 gravity but containing 10 mole % nitrogen is given by Fig. 4-65. The pseudocritical conditions were used as indicated, but the $\Delta H/T$ and ΔS charts for hydrocarbon gases were used in the construction of Fig. 4-65. These charts are useful in finding the temperature change upon expanding or compressing gases and for finding the reversible work of compression or expansion.

Illustrative Problem

Thirty-six MMcf/day (60°F, 14.7 psia) of natural gas at 140°F, 0.6 gravity, is flowing freely through an expansion valve with the pressure dropping from 800 to 400 psia.

(*a*) What is the temperature change across the valve?

(*b*) What is the maximum work that could be derived from this expanding gas stream without the use of heat?

(*c*) What would be the temperature change on the gas when expanding through an adiabatic and reversible engine?

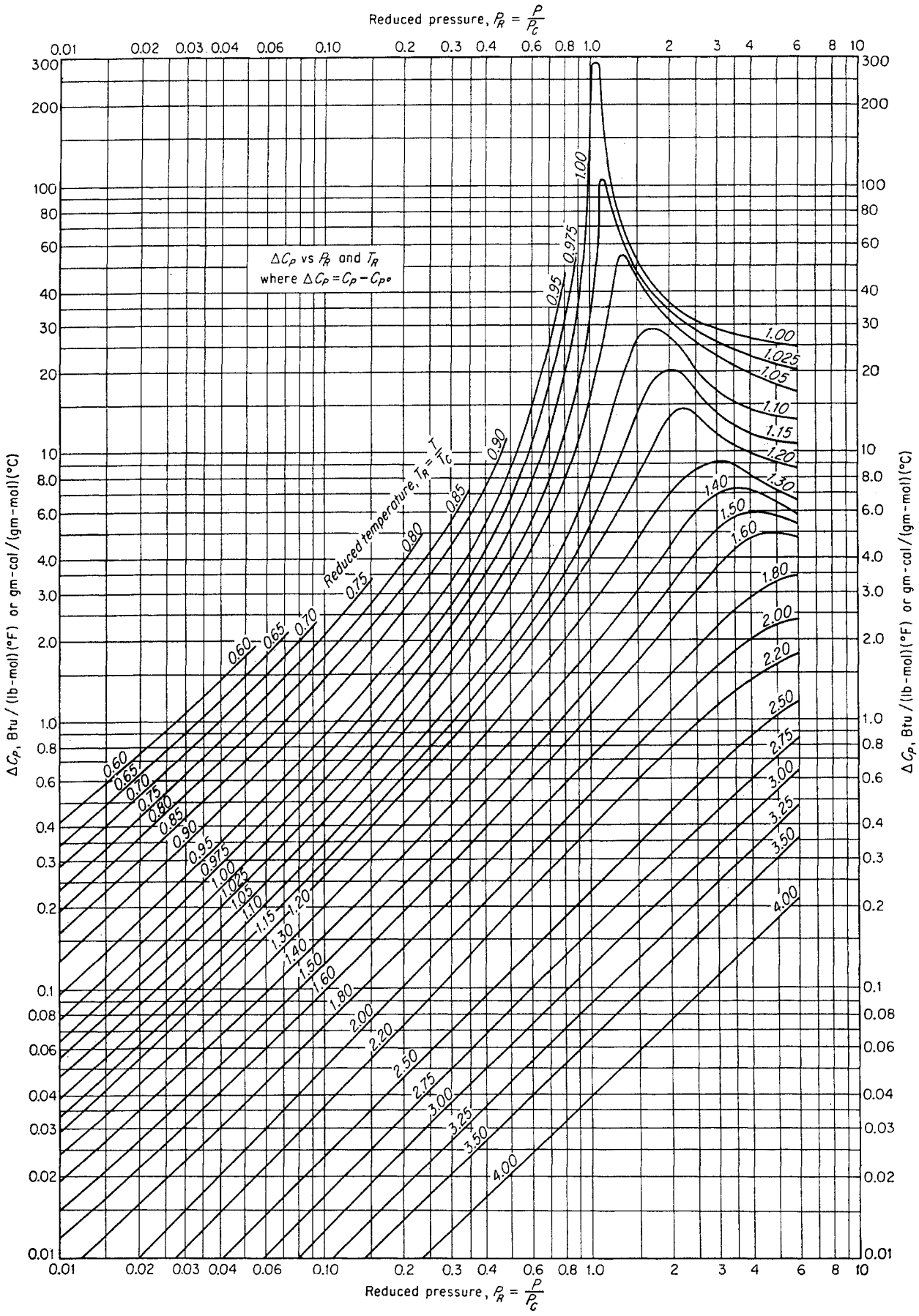

Fig. 4-55. Isothermal pressure correction to heat capacity of vapors. (*Edmister, 4-29. Courtesy Petrol. Engr.*)

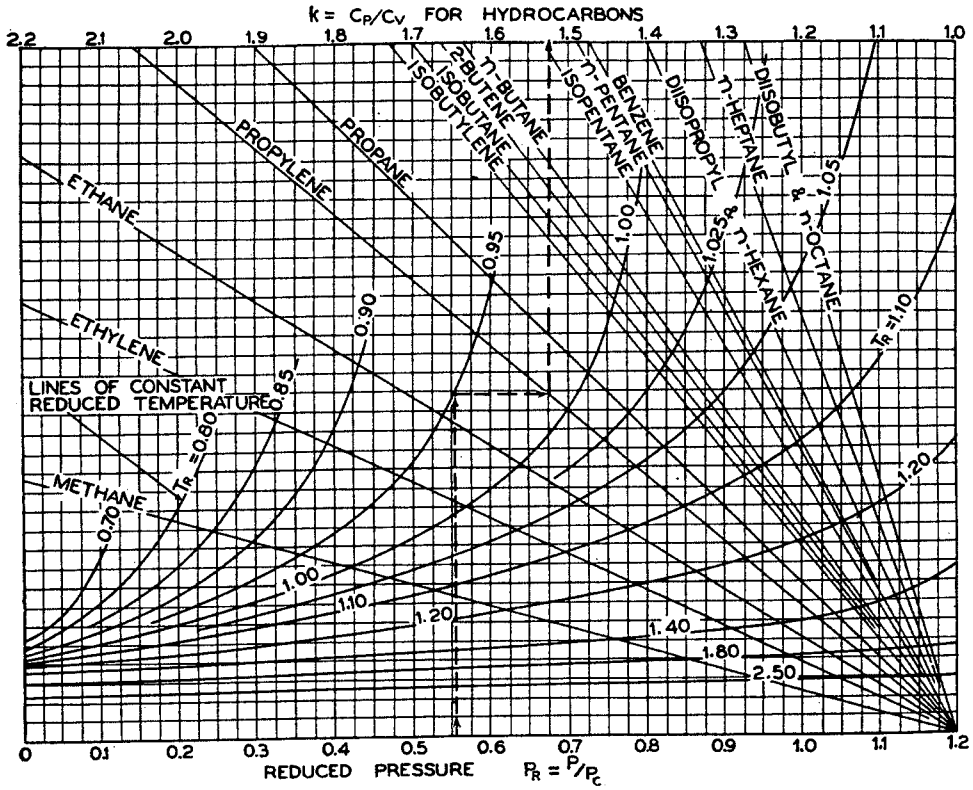

Fig. 4-56. Specific-heat ratios for hydrocarbon vapors. (*Edmister, 4-29. Courtesy Petrol. Engr.*)

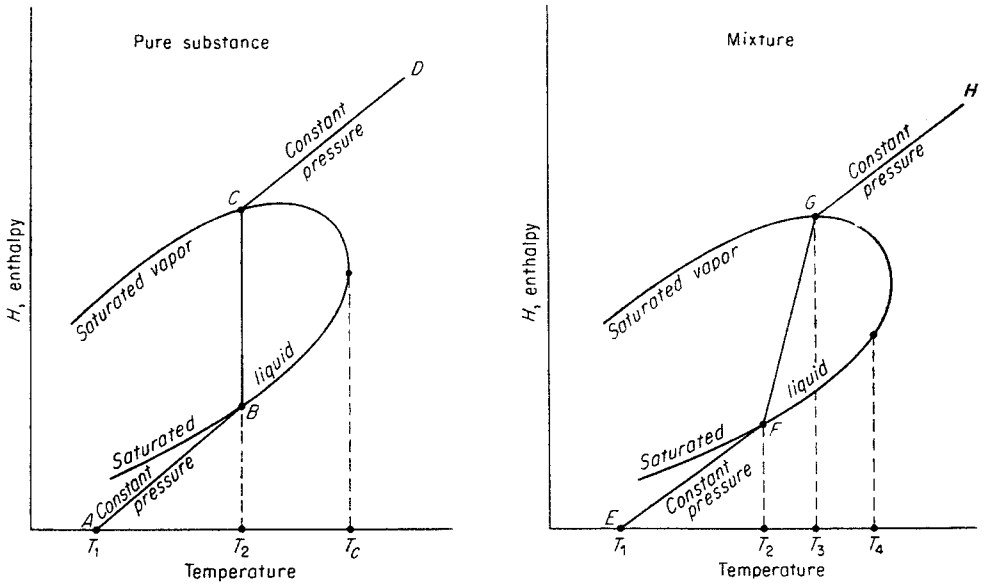

Fig. 4-57. Illustration of enthalpy increase during vaporization.

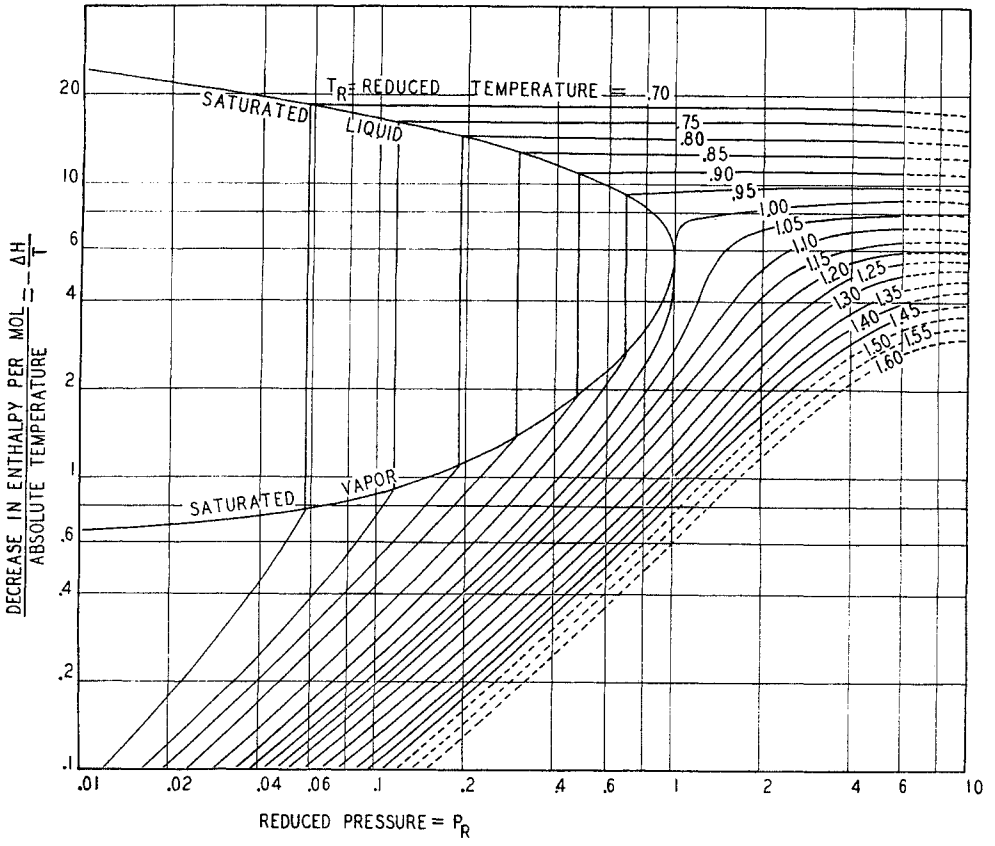

Fig. 4-58. Effect of temperature and pressure on enthalpy of pentane. (Konz and Brown, 4-56. Courtesy Ind. Eng. Chem.)

Solution

Referring to Fig. 4-62,
(*a*) At 800 psia and 140°F,

$$H = 620$$

At 400 psia and $H = 620$,

$$\text{Temperature} = 120°\text{F}$$

(*b*) and (*c*) At 800 psia and 140°F,

$$S = -6.55$$

At 400 psia and $S = -6.55$,

$$\text{Temperature} = 50°\text{F}$$

$$H = -80 \text{ Btu}$$

$$-\Delta H = H_1 - H_2 = 620 - (-80) = 700 \text{ Btu}$$

$$\text{Work} = -\Delta H = 700 \text{ Btu/lb mole}$$

$$1 \text{ horsepower (hp)} = \frac{33{,}000 \times 60}{778} = 2545 \text{ Btu/hr}$$

$$\text{hp} = \frac{36{,}000{,}000 \times 700}{379 \times 24 \times 2{,}545} = 1{,}089$$

Charts showing temperature change upon expansion are given as Figs. 5-48 to 5-50 in connection with the prediction of conditions for hydrate formation.

Pressure-enthalpy diagrams (Figs. 4-66 to 4-69) for pure substances have been prepared for methane by Matthews and Hurd (3-42); for ethane by Barkelew, Valentine, and Hurd (4-6); for propane by Shell Development Company; and for butane by Prengle, Greenhaus, and York (4-71). The datum for each chart is indicated; they are not the same. Lines of constant entropy S, volume V, and temperature are indicated. Flow problems at constant H or constant S can be solved readily by using these charts.

Enthalpy-temperature diagrams have been prepared for pure substances by Edmister (4-29), Maxwell (1-10), and others. These diagrams give the enthalpy-temperature-pressure relations for pure substances and are useful also for handling mixtures containing the substances.

Illustrative Problem

One std MMcf/hr of methane at 1,000 psia and 100°F is to be converted to a saturated liquid at 25 psia. How much heat must be removed?

Solution

From Fig. 4-66, at 1,000 psia and 100°F $H = 395$ Btu/lb.
At 25 psia, temperature = −247°F and $H = 25$ Btu/lb.
Heat removed = $-\Delta H = -q = 395 - 25 = 370$ Btu/lb.

$$\frac{1{,}000{,}000}{379} \times 16 \times 370 = 15{,}600{,}000 \text{ Btu/hr}$$

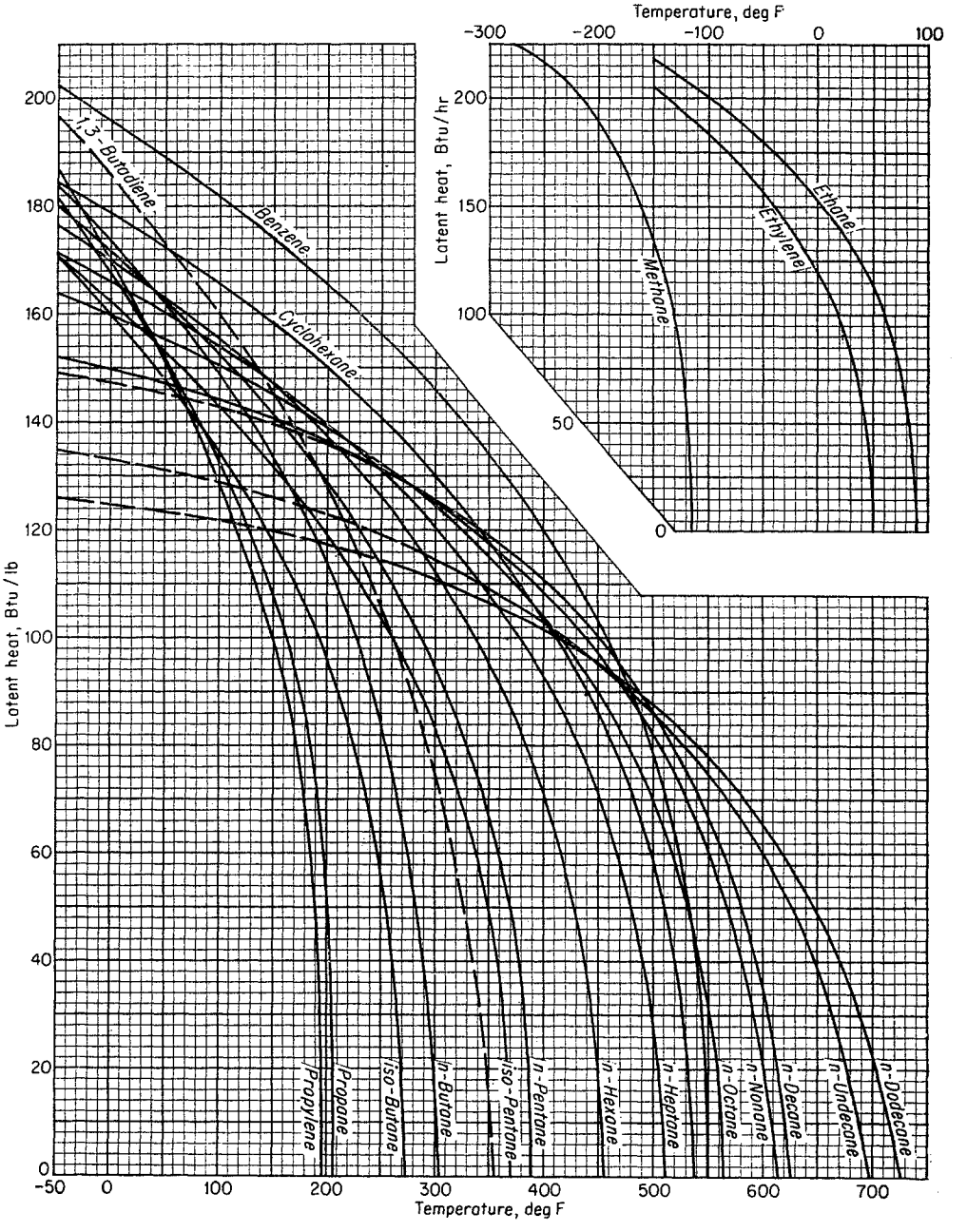

Fig. 4-59. Latent heat of pure compounds. (*Holcomb and Brown, 3-25. Courtesy Ind. Eng. Chem.*)

Enthalpy of Mixtures

Figure 4-57 illustrates the problem of finding the latent heat of a mixture, where the temperature is changing during the vaporization. Figure 4-70 shows data obtained by Fekula and Brown on a 65°API naphtha-gasoline mixture. A second problem lies in the fact that liquids often contain dissolved gases at temperatures above their critical temperatures as pure substances. A third complication is that the enthalpy of a component depends upon the remainder of the system and its concentration. Only approximate methods for handling enthalpies of mixtures are available (4-51).

The partial enthalpy $\bar{H}_1$ of substance 1 is defined as the change in enthalpy of a system as a unit of substance 1 is added.

$$\bar{H}_1 = \frac{\partial H_S}{\partial n_1} \tag{4-34}$$

where $\bar{H}_1$ = partial enthalpy of substance 1 in this system
n_1 = concentration of substance 1
H_S = enthalpy of system

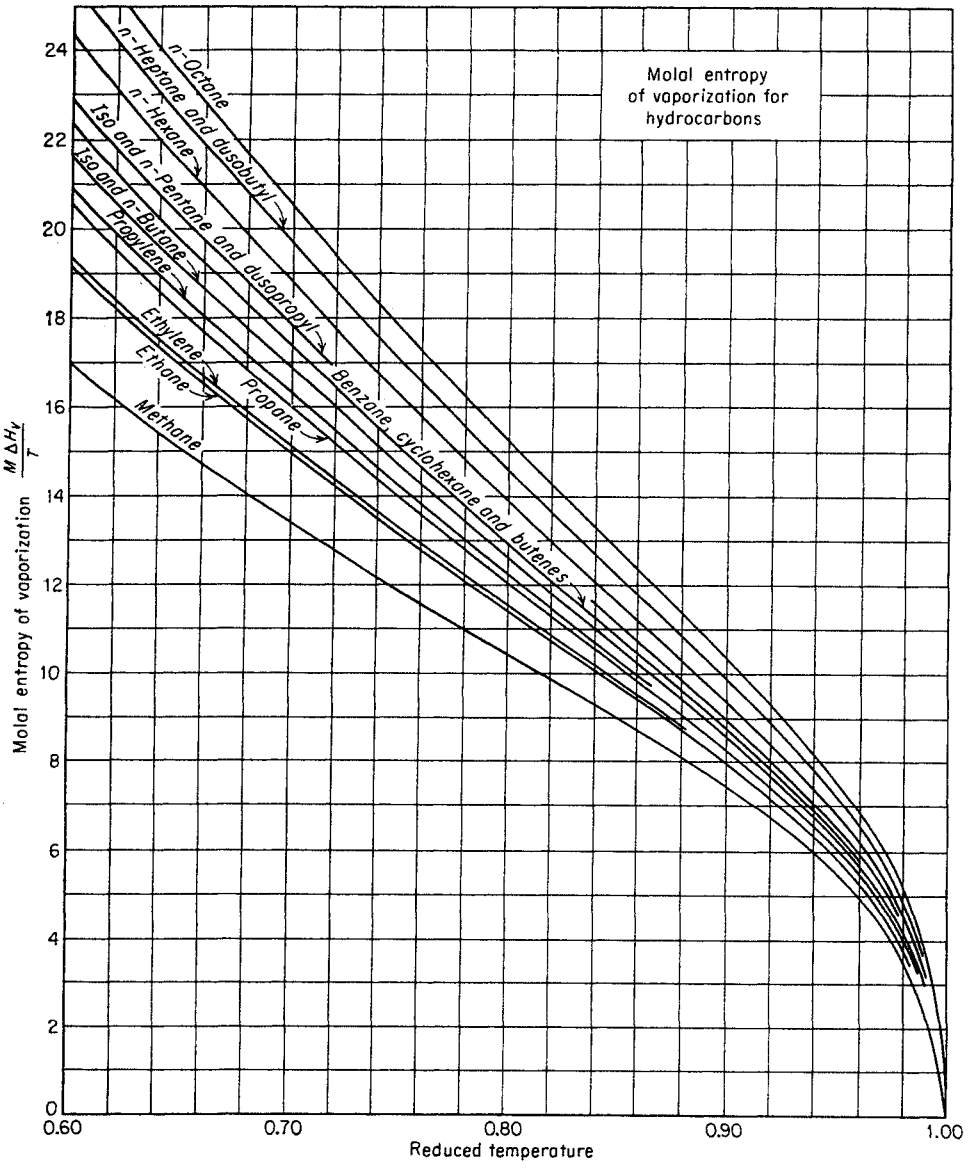

Fig. 4-60. Molal entropy of vaporization. (*Edmister*, 4-29. *Courtesy Petrol. Engr.*)

Figure 4-70*a* is a plot of the partial enthalpy of methane in three systems from Sage, Olds, and Lacey (4-79), illustrating the influence of concentration and systems of the partial enthalpy.

Miller measured the heat of solution of butane in a solvent at temperatures above and below the critical temperature of butane (Fig. 4-71). The heat of solution depends upon the concentration and presents a smooth curve through the critical temperature of butane when it is plotted against temperature at constant concentration.

Efforts have been made to compute the partial enthalpies (4-19, 4-70) of the light hydrocarbons, but no complete system of handling enthalpies is available. More data on energy relationships during phase transitions would be helpful.

Two methods of handling the enthalpies of mixtures will be given. The first is that of Holcomb and Brown (3-25) in which the effects of concentration are neglected. The second method uses charts by Peters (4-67) and Maxwell (1-10) for the enthalpies of pure constituents as they occur in mixtures and calculates the enthalpy of the mixture from the enthalpies of the constituents.

Holcomb and Brown chose a datum point of zero pressure and 32°F. The enthalpies of liquids above this temperature at zero pressure are shown in Fig. 4-72. The chart is based on specific heats (Fig. 4-50) and a cross plot of enthalpies against atmospheric boiling points (3-25). The enthalpy of a mixture is found by adding the enthalpies of the constituents in proportion to their concentration. The correction of

enthalpy for pressure is found from the specific gravity of the liquid, the temperature, and the pressure, using Fig. 4-73.

For gases, the basic relationship required is the enthalpy of gases at 32°F and atmospheric pressure above that of liquid at 32°F and zero pressure (Fig. 4-74). This chart is based on ΔH for vaporization computed from equilibrium constants by the van't Hoff equation

$$\frac{d\ (\ln K)}{dT} = \frac{\Delta H}{RT^2} \qquad (4\text{-}35)$$

The specific heat of a vapor (Fig. 4-49) is used to raise its temperature, and the $-\Delta H/T$ plot to find the effects of pressure (Fig. 4-51).

Illustrative Problem

One hundred pound moles of a mixture composed of 63.7 mole % methane and 36.3 mole % *n*-butane is flowing as a single phase at 250°F and 2,000 psia. The mixture is passed through a heat exchanger and is flashed into a separator at 70°F and 400 psia, where 67 moles of vapor (88.3 mole % methane) and 33 moles of liquid (13.8 mole % methane) are removed. Compute the heat extracted in the exchanger.

Solution

Using Holcomb and Brown's charts based on liquid at 32°F and zero pressure as datum, find the enthalpy of the initial

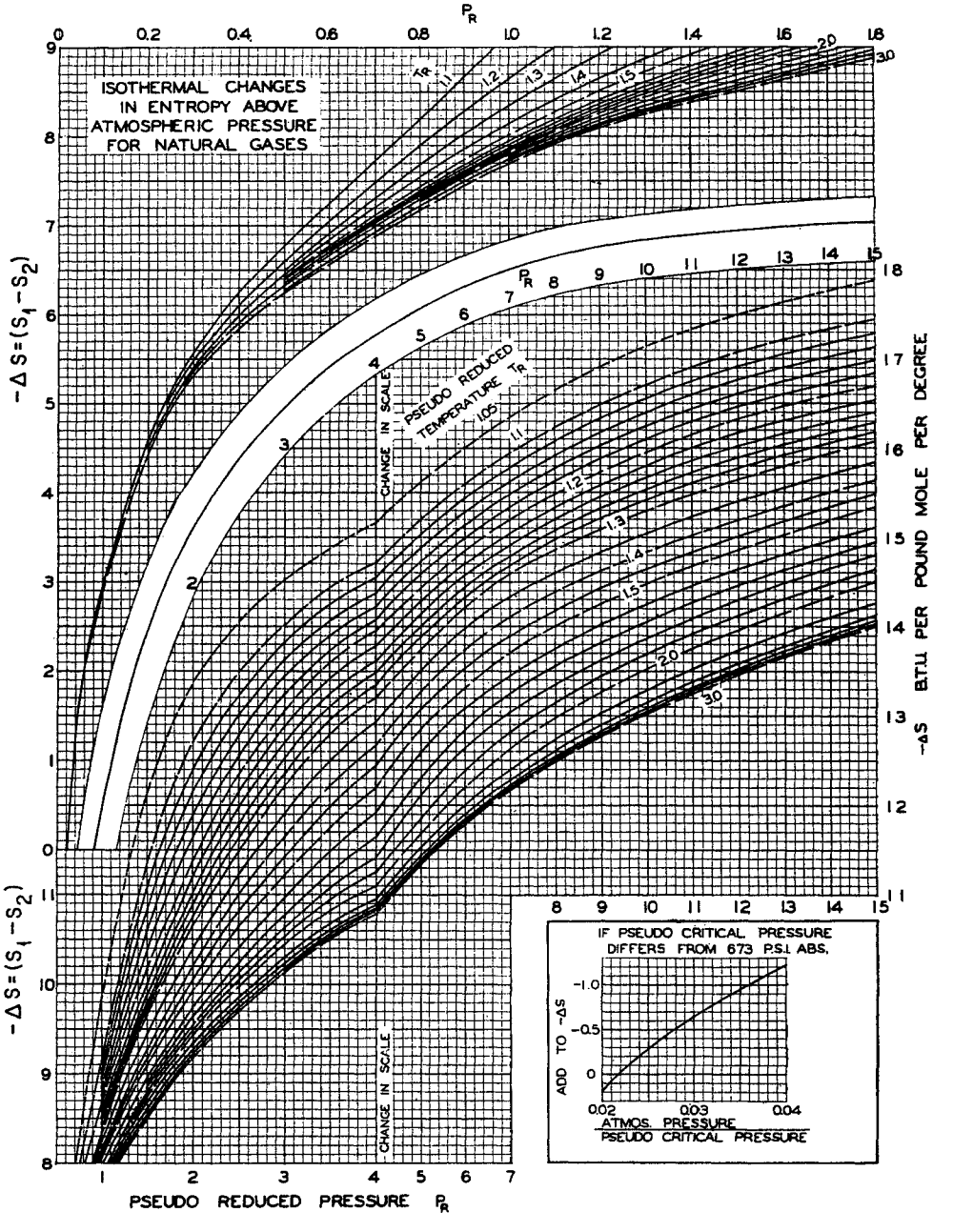

Fig. 4-61. Isothermal entropy change for natural gases. (*Brown*, 4-16. *Courtesy AIME.*)

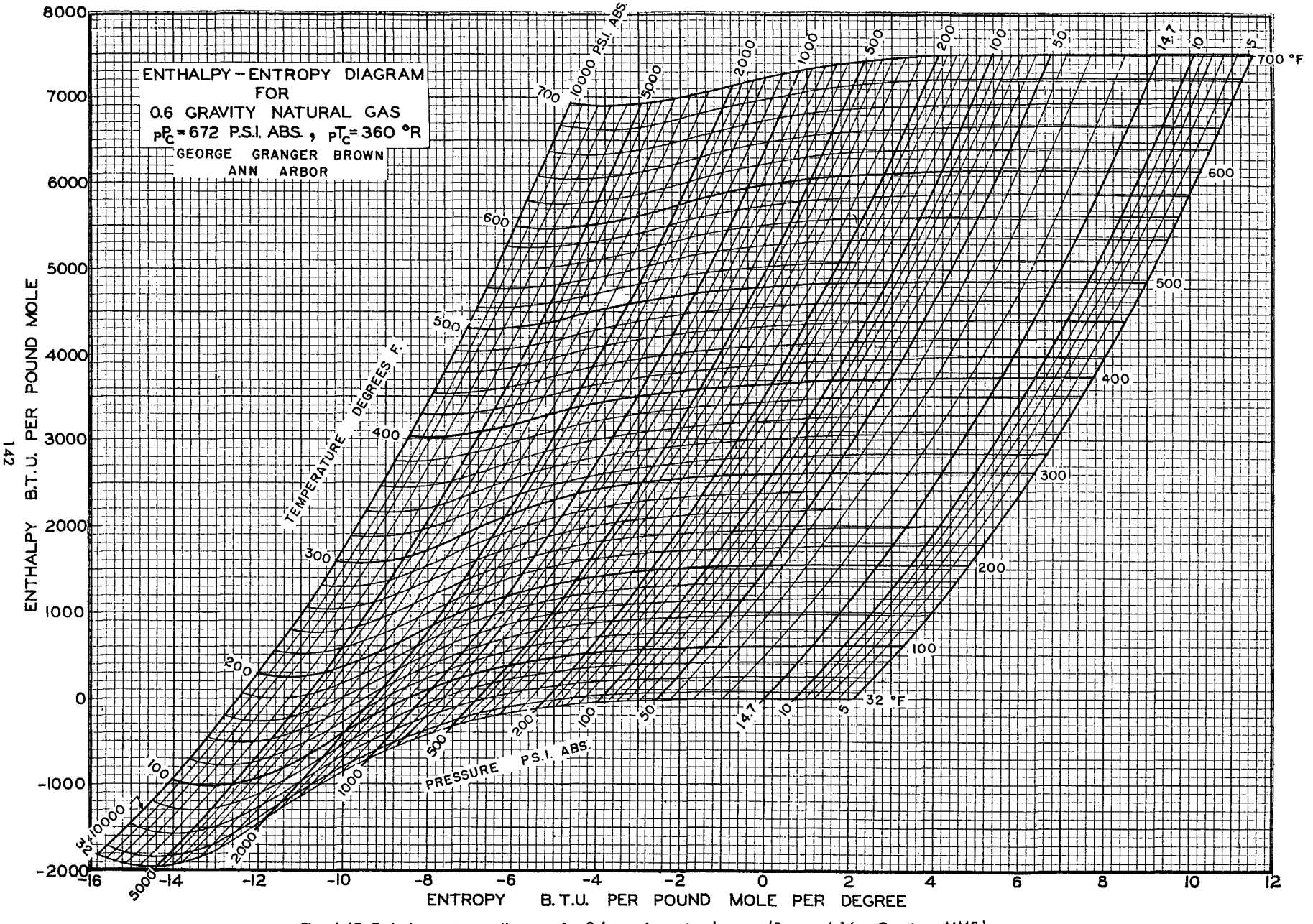

Fig. 4-62. Enthalpy-entropy diagram for 0.6 gravity natural gas. (*Brown, 4-16. Courtesy AIME.*)

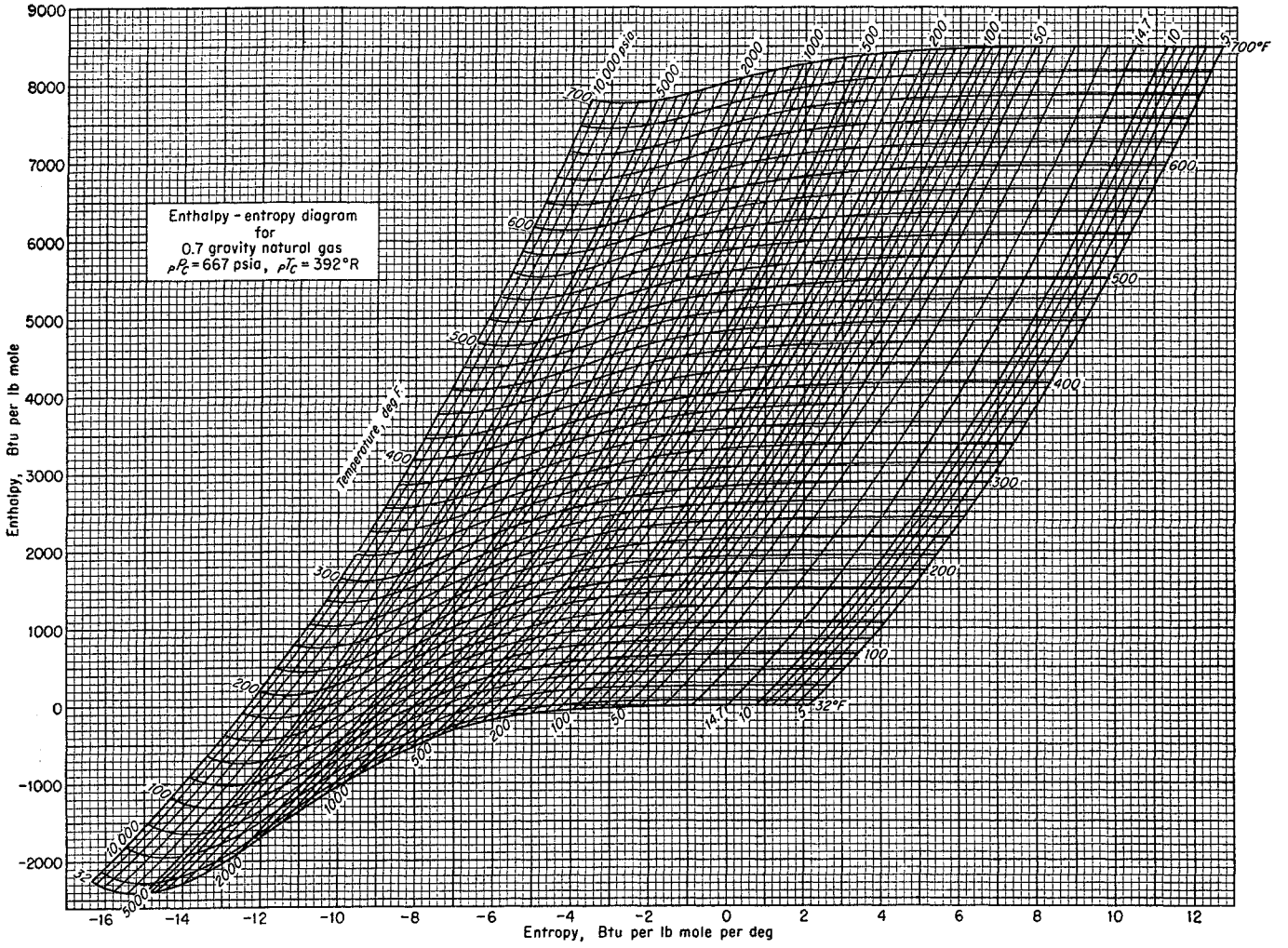

Fig. 4-63. Enthalpy-entropy diagram for 0.7 gravity natural gas. (*Brown, 4-16. Courtesy AIME.*)

stream at 250°F and 2,000 psia and of the vapor and liquid from the separator at 70°F and 400 psia. The difference in enthalpy was extracted in the heat exchanger.

Compute pseudocritical properties of initial and vapor streams and density of hydrocarbon liquid.

	T_c, °R	P_c, psia	Initial stream			Separator vapor		
			Mole fraction	pT_c	pP_c	Mole fraction	pT_c	pP_c
Methane.....	343.2	673.1	63.7	218.5	429	88.3	303	595
n-Butane.....	765.3	550.7	36.3	278	200	11.7	89.5	64.5
				496.5	629		392.5	659.5

Reduced temperature and pressure:
Initial stream:

$$\frac{710}{496.5} = 1.43 = T_R \qquad \frac{2{,}000}{629} = 3.18 = P_r$$

Separator vapor:

$$\frac{530}{392.5} = 1.35 = T_R \qquad \frac{400}{659.5} = 0.607 = P_r$$

Separator liquid:

	Grams/ cu cm	Mole %	Grams/ mole	Cu cm/ mole
Methane.....	0.25*	13.8	2.21	8.84
Butane.....	0.584	86.2	50.1	86.0
			52.31	94.84

* From Fig. 4-31, 52.31/94.84 = 0.552 gram/cu cm.

Initial vapor. Enthalpy above datum: 32°F, liquid at zero pressure (Fig. 4-74):

63.7 moles × 3,900 = 248,500 Btu
36.9 moles × 15,400 = 569,000
817,500 Btu

Effect of pressure (from Fig. 4-51):

$$-\frac{\Delta H}{T} = 2.5$$

$-\Delta H = 2.5 \times 710 = 1775$ Btu/mole

817,500 Btu at zero pressure, 250°F
−177,500 Btu at 250°F, 0 to 2,000 psia
640,000 Btu for 100 moles

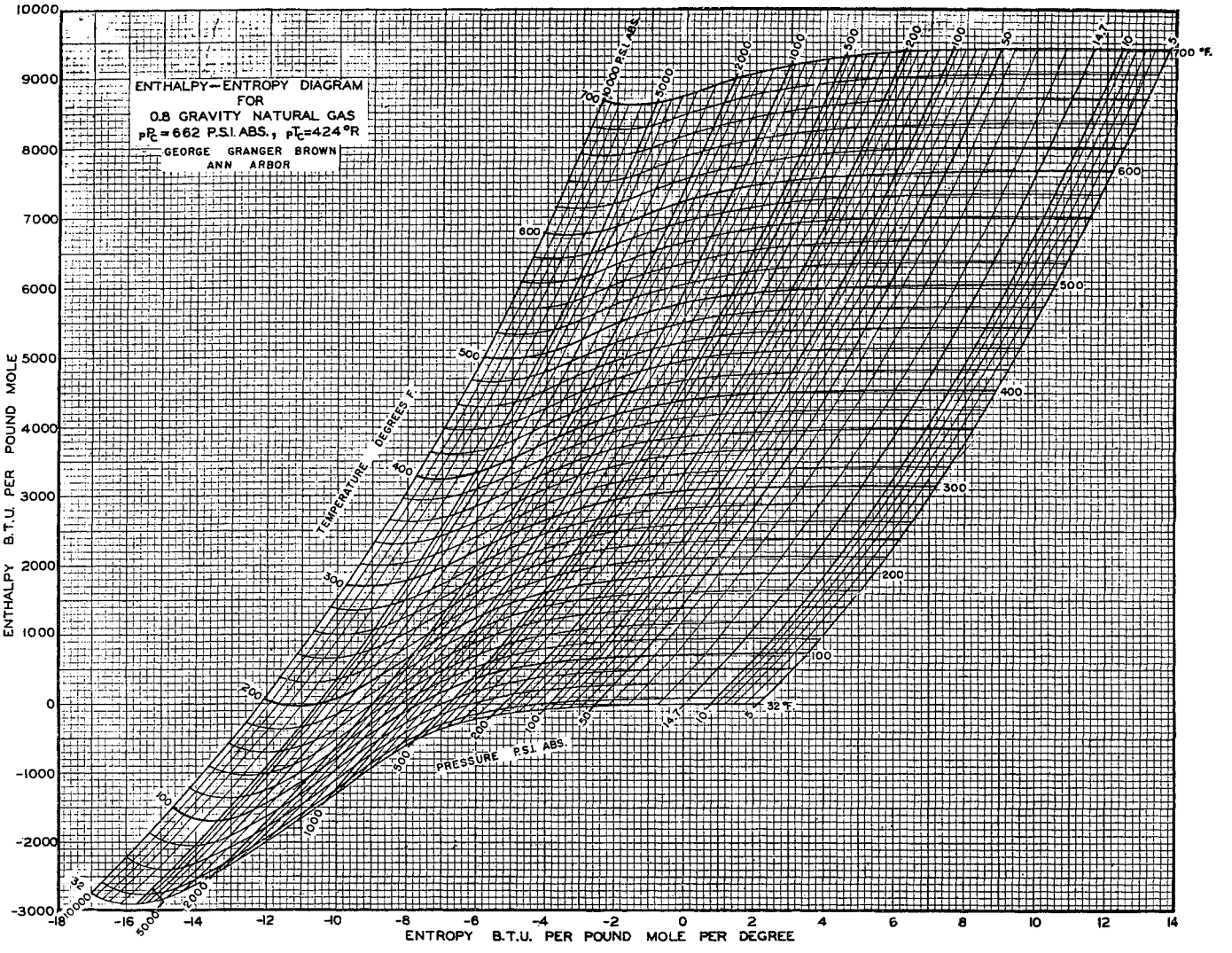

Fig. 4-64. Enthalpy-entropy diagram for 0.8 gravity natural gas. (*Brown*, 4-16. *Courtesy AIME.*)

Separator vapor at zero pressure (Fig. 4-74):

$$0.883 \times 67 \times 2{,}800 = 136{,}000 \text{ Btu}$$
$$0.117 \times 67 \times 10{,}630 = \underline{83{,}500}$$
$$219{,}500 \text{ Btu}$$

Effect of pressure:

$$-\frac{\Delta H}{T} = 0.58$$
$$-\Delta H = 0.58 \times 530 = 307 \text{ Btu}$$
$$-307 \times 67 = -20{,}600 \text{ Btu/lb mole}$$
$$219{,}500 \text{ Btu}$$
$$\underline{-20{,}600}$$
$$198{,}900 \text{ Btu}$$

Separator liquid, 70°F at zero pressure (Fig. 4-72):
Methane:

$$0.138 \times 33 \times 540 = 2{,}460 \text{ Btu} \qquad 73 \text{ lb}$$

Butane:

$$0.862 \times 33 \times 1200 = \underline{34{,}100} \qquad \underline{1{,}650}$$
$$36{,}560 \text{ Btu} \qquad 1{,}723 \text{ lb}$$

Effect of pressure (Fig. 4-73):

$$h_{3{,}000} - h_0 = 5.9$$
$$h_p - h_0 = 0.58 \text{ Btu/lb}$$
$$h_p - h_0 = 0.38 \times 1{,}723 = 1000 \text{ Btu}$$
$$\text{Enthalpy of liquid} = 36{,}560 + 1000 = 36{,}560 \text{ Btu}$$

Initial stream − separator vapor − separator liquid
= Btu extracted in heat exchanger

$$640{,}000 - 198{,}900 - 37{,}560 = 403{,}540 \text{ Btu}$$

Maxwell has presented charts giving enthalpy of individual constituents as a function of temperature and pressure (Fig. 4-75). The enthalpies of individual constituents of a mixture are additive for liquids. For vapors, the enthalpies are additive at 0 to 1 atm pressure rather than at the pressure. The change in enthalpy of the entire vapor with pressure is found by interpolating between charts for the average molecular weight of the mixture. When a constituent is in the liquid phase although temperature

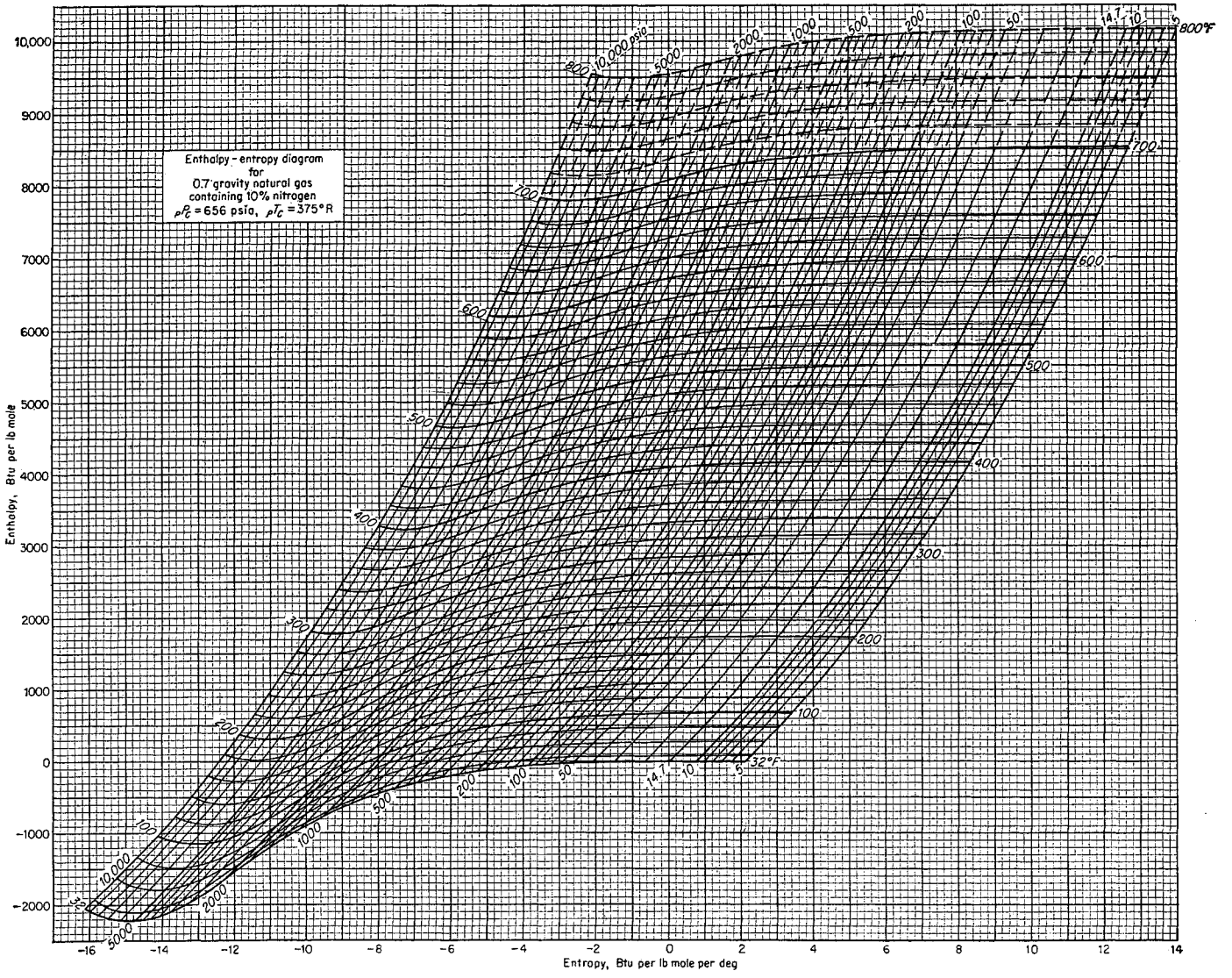

Fig. 4-65. Enthalpy-entropy diagram for 0.7 gravity gas containing 10 per cent nitrogen. (Brown, 4-16.)

and pressure indicate two phases, use the saturated-liquid line at the temperature to find the liquid enthalpy.

Illustrative Problem

Solve the above problem using Maxwell's charts. Datum: liquid at −200°F.

	Initial stream at 250°F, 136 atm				Separator vapor at 70°F, 27 atm				Separator liquid at 70°F			
	Moles	Lb	Btu/lb	Btu	Moles	Lb	Btu/lb	Btu	Moles	Lb	Btu/lb	Btu
Methane	63.7	1,020	445	454,000	59.2	946	342	324,000	4.5	74	255	18,900
Butane	36.3	2,110	382	806,000	7.8	455	300	136,500	28.5	1,655	142	235,000
	100.0	3,130	...	1,260,000	67.0	1,401	...	460,500	33.0	1,729	...	253,900

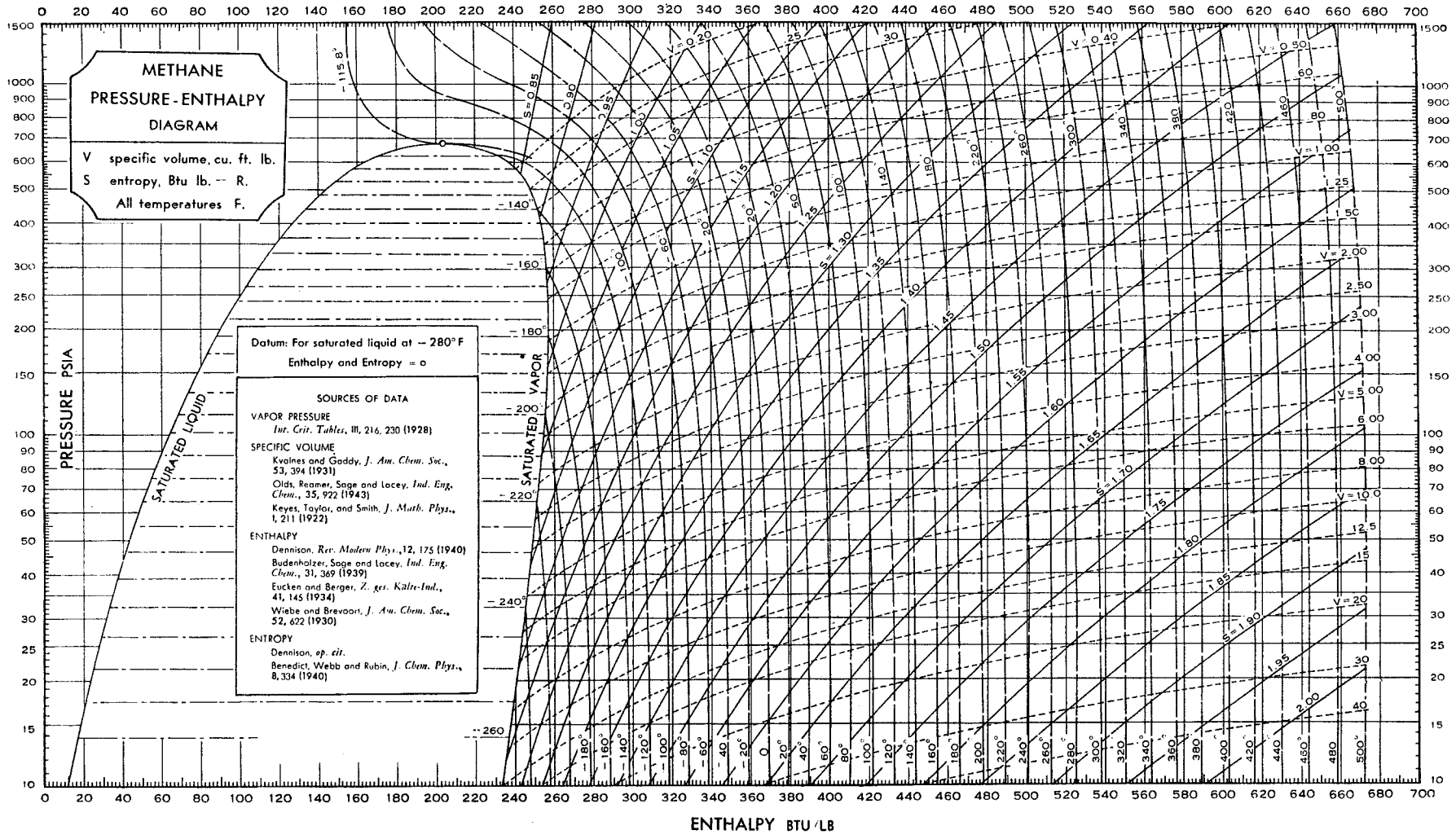

Fig. 4-66. Pressure-enthalpy diagram for methane. *(Matthews and Hurd, 3-42. Copyright 1945 by Shell Development Company.)*

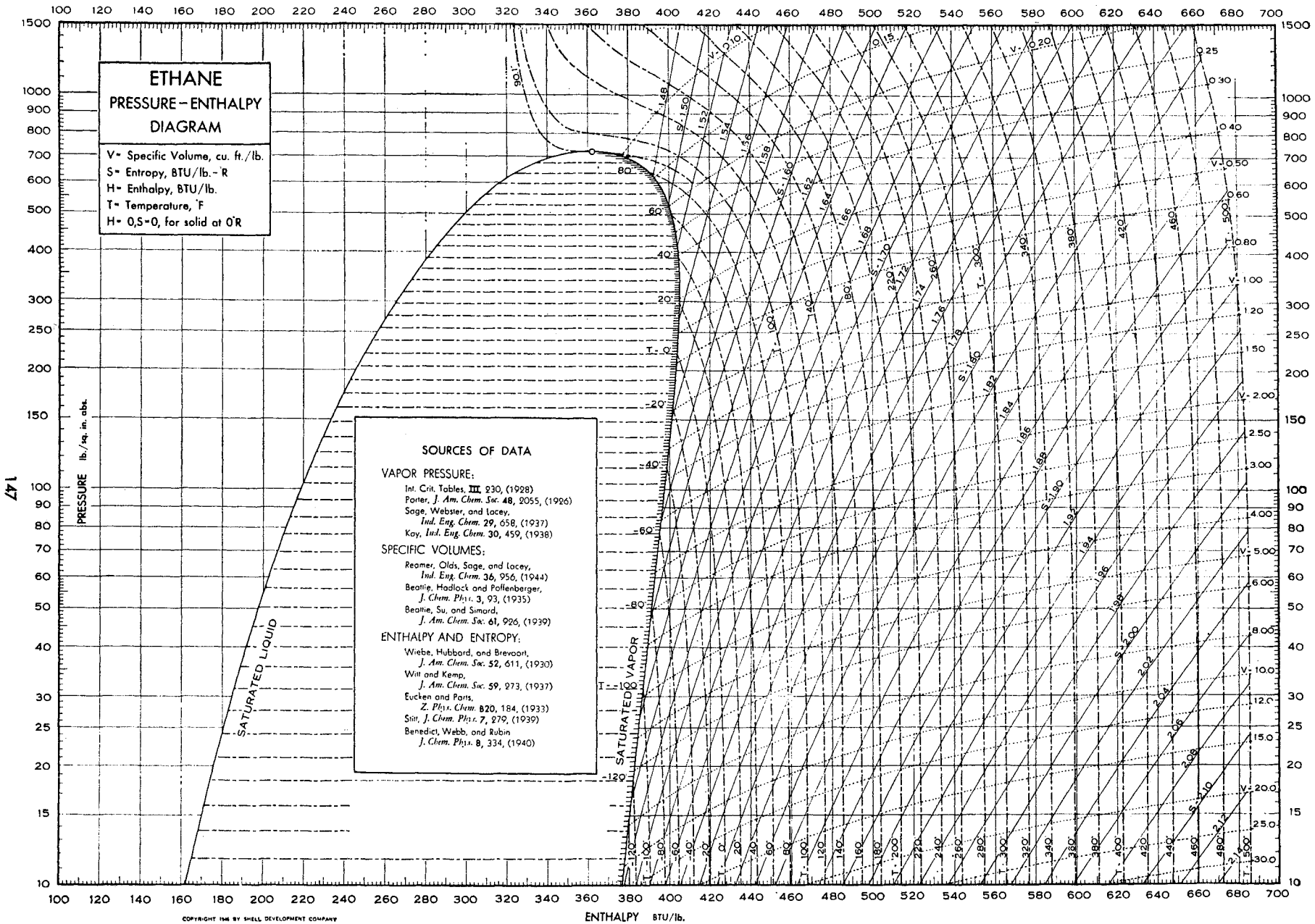

Trans. Am. Inst. Chem. Engrs., 43, 25, (1947)

Fig. 4-67. Pressure-enthalpy diagram for ethane. (*Barkelew, Valentine, and Hurd, 4-6. Copyright 1946 by Shell Development Company.*)

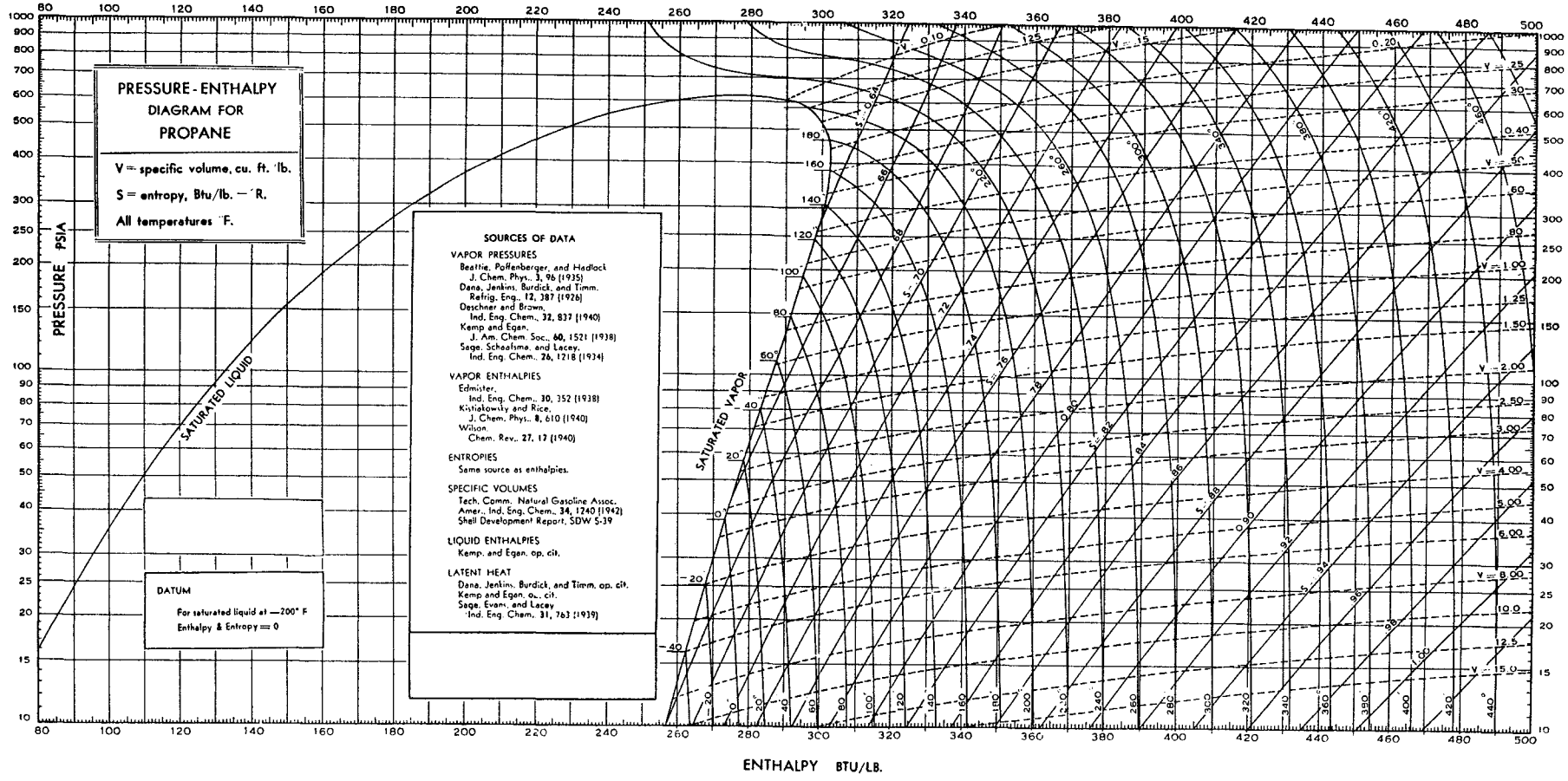

Fig. 4-68. Pressure-enthalpy diagram for propane. *(Shell Development Company, private communication.)*

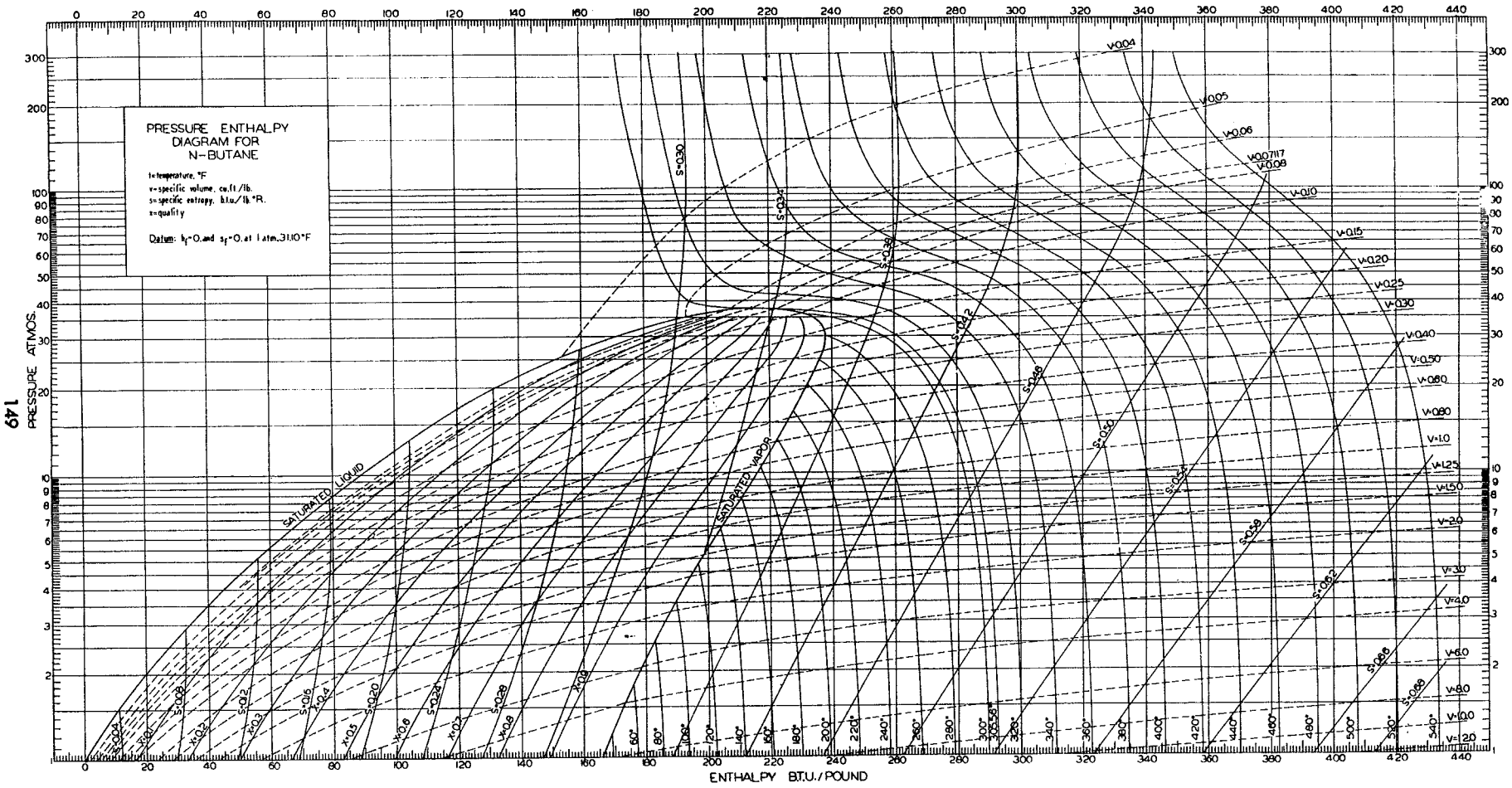

Fig. 4-69. Pressure-enthalpy diagram for *n*-butane. (*Prengle, Greenhaus, and York*, 4-71. *Courtesy AIChE.*)

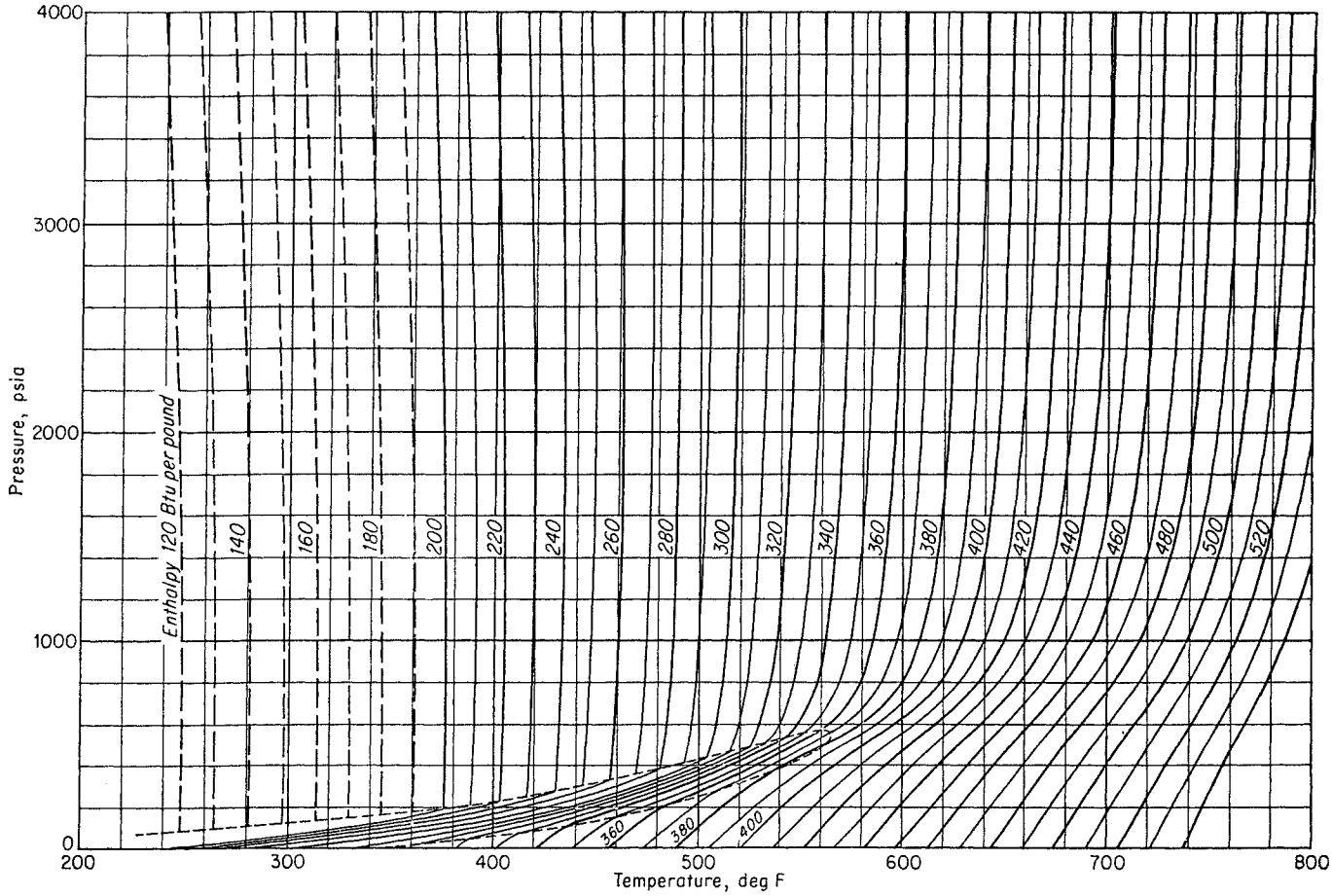

Fig. 4-70. Enthalpy referred to 32°F and 1 atm of a 65.2°API gasoline-kerosene mixture. (*Fekula and Brown, 4-32.*)

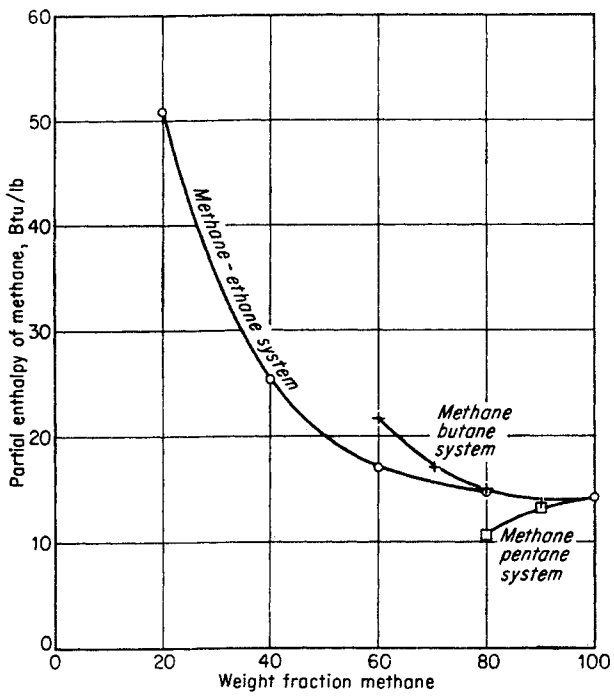

Fig. 4-70a. Partial enthalpy of methane in gaseous fluids. (*Data of Sage, Olds, and Lacey, 4-79.*)

Average molecular weight of initial stream, 31.3; of separator vapor, 20.9.

Initial Stream. Interpolate effect of pressure between ethane and propane.

Pressure, atm	H, Btu	
	Ethane	Propane
0	408	388
136	330	265
	78	123

$$\frac{1.3}{14.0} \times (123 - 78) + 78 = 82.8$$

$$3{,}130 \times 82.8 = 259{,}000 \text{ Btu less at 136 atm}$$

$$1{,}260{,}000 - 259{,}000 = 1{,}001{,}000 \text{ Btu at 250°F, 2,000 psia}$$

Separator Vapor. Interpolate effect of pressure between methane and ethane.

Pressure, atm	H, Btu	
	Methane	Ethane
0	341	324
37	327	295
	14	29

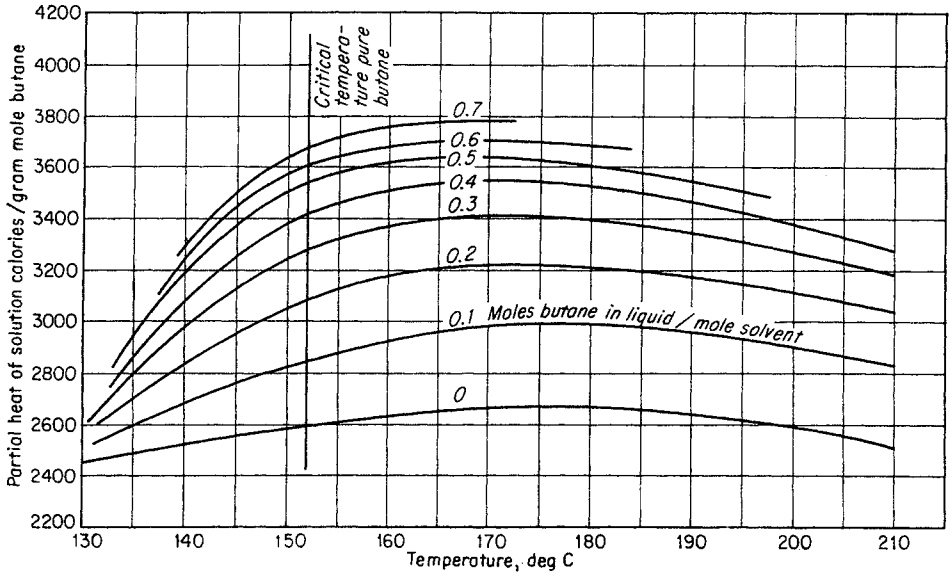

Fig. 4-71. Partial heat of solution of *n*-butane in 145 molecular weight solvent at 400 psia. (*Data of Miller, in Katz et al.*, 4-51.)

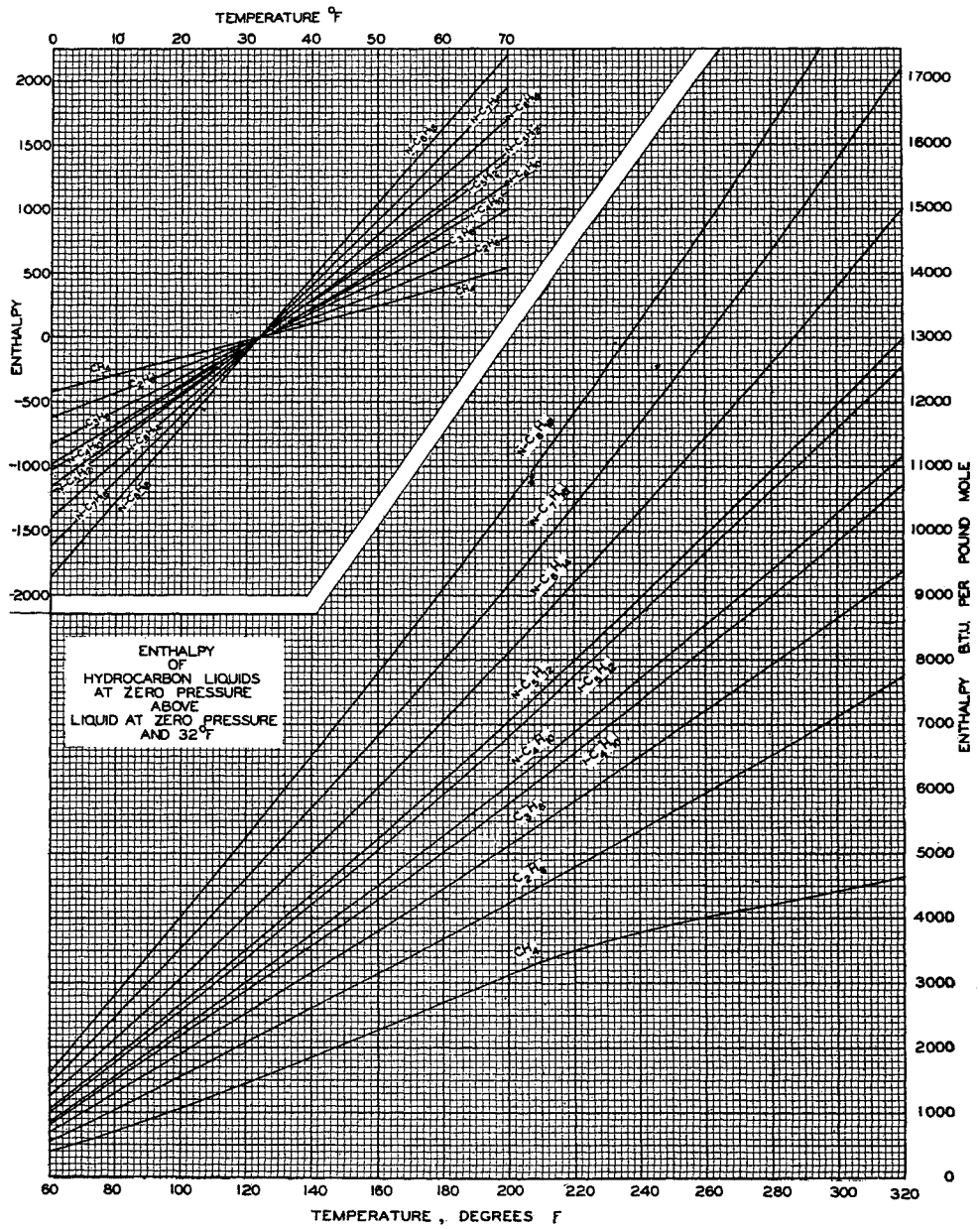

Fig. 4-72. Enthalpy of liquid hydrocarbons at zero pressure above liquid at zero pressure and 32°F. (*Holcomb and Brown*, 3-25. *Courtesy Ind. Eng. Chem.*)

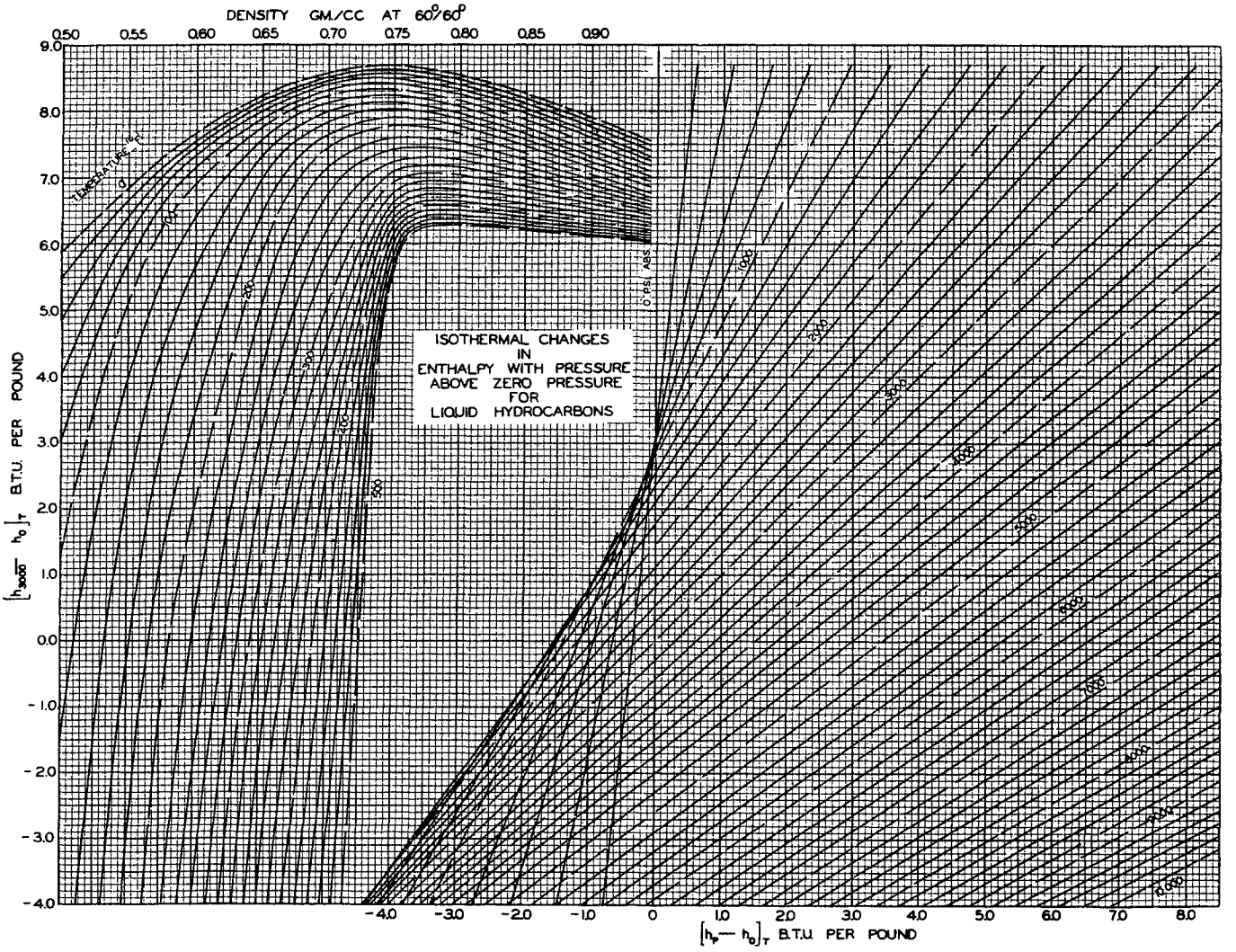

Fig. 4-73. Isothermal changes in enthalpy with pressure above zero pressure for

$$\frac{4.9}{14} \times 15 + 14 = 19.2$$

$$19.02 \times 1{,}401 = 26{,}700 \text{ Btu less at 37 atm}$$

$$460{,}500 - 26{,}700 = 433{,}800 \text{ Btu at 70°F, 400 psia}$$

$$1{,}001{,}000 - 433{,}800 - 253{,}900 = 313{,}300 \text{ Btu removed by exchanger}$$

Peters (4-67) has presented partial-enthalpy diagrams for constituents methane to propane when present in mixtures (Figs. 4-76 to 4-80). The enthalpy of a mixture is equal to the sum of the partial enthalpies. To find the enthalpy of a mixture above a datum of liquid at −200°F, simply multiply the pounds of each constituent by the enthalpy read from the charts, using molecular weight or molal-average boiling point to identify the quality of the liquid.

HEATING VALUE

The heating value of natural gas is the heat liberated when a unit of fuel is burned under specified conditions. Methane has a heating value of 1012 Btu per actual cu ft of gas at 60°F and 14.7 psia, when burned with air. This heating value is obtained by cooling the products of combustion to 60°F and condensing the moisture formed, and it is known as the *total* or *gross* heating value. Other hydrocarbon constituents of natural gas have higher heating values, as indicated in Table A-1.

The chemical reaction for combustion of 1 lb mole of methane is as follows:

$$CH_4\ (g) + 2O_2\ (g) \rightarrow CO_2\ (g) + 2H_2O\ (l) + 382{,}778 \text{ Btu} \quad (4\text{-}36)$$

Since the latent heat of water at 60°F and 1 atm is 1060 Btu/lb, or $18 \times 2 \times 1060 = 38{,}160$ Btu for 2 lb moles of water,

$$2H_2O\ (l) \rightarrow 2H_2O\ (g) - 38{,}160 \text{ Btu} \quad (4\text{-}37)$$

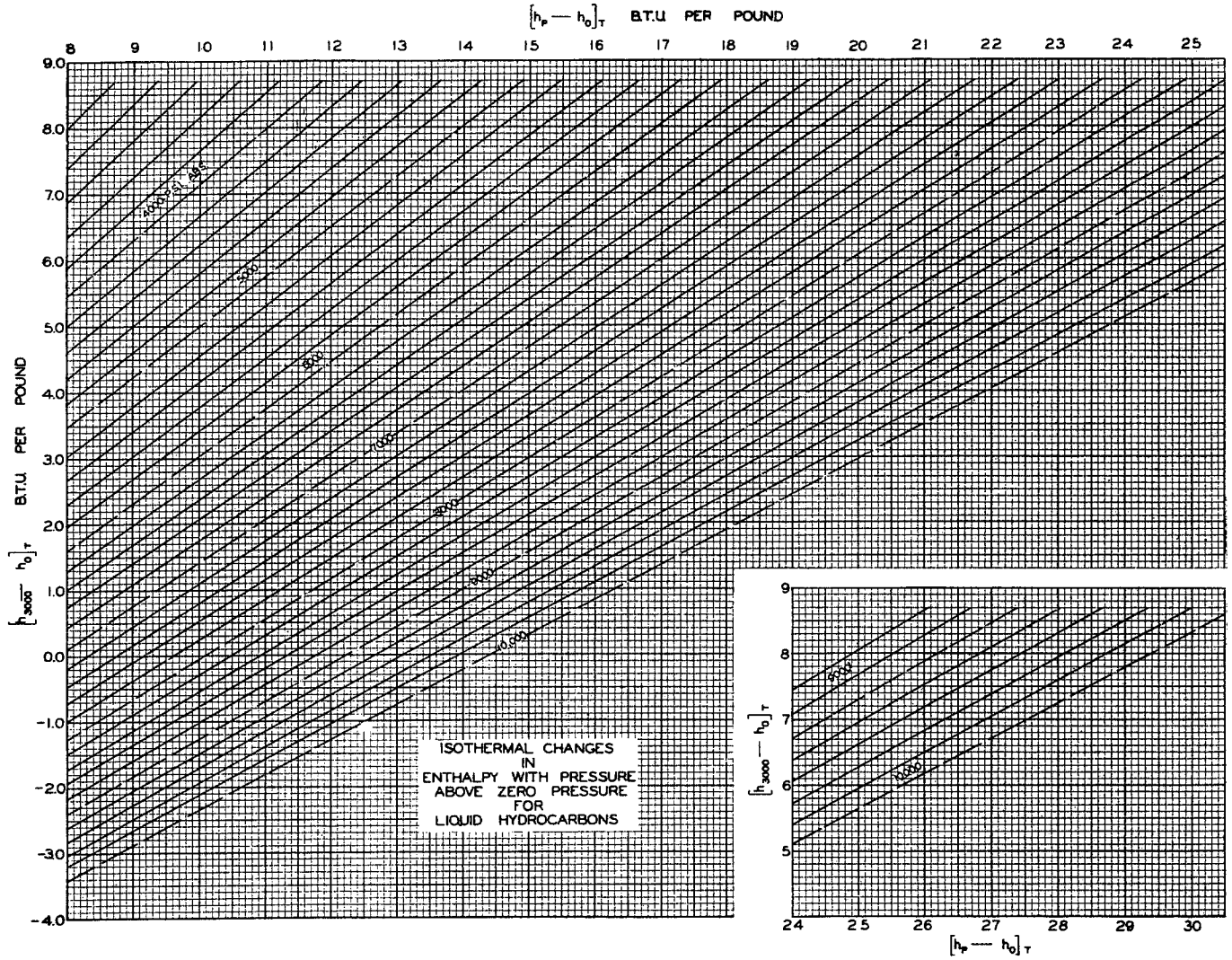

liquid hydrocarbons. (*Holcomb and Brown, 3-25. Courtesy Ind. Eng. Chem.*)

Adding Eq. (4-36) to (4-37) gives the *net* heat of combustion when water leaves as a vapor.

$$CH_4\ (g) + 2O_2\ (g) \rightarrow CO_2\ (g) + 2H_2O\ (g) + 344{,}618\ \text{Btu} \quad (4\text{-}38)$$

The computation of the heating value per cubic foot of methane at 60°F and 14.7 psia is found for ideal-gas-law conditions by dividing 382,778 Btu by 379 cu ft/lb mole for ideal gases or 1010 Btu/cu ft of ideal volume. Methane has a compressibility factor of 0.998 at 60°F and 14.7 psia (Fig. 4-18), and the gross heating value per actual cubic foot becomes

$$\frac{1010}{0.998} = 1012\ \text{Btu/cu ft}$$

ASTM procedure D900-55 (4-2) outlines the test procedure in detail and describes equipment for measuring the heating value of natural gas. Figure 4-81 is a sketch of a water-flow calorimeter. Gas is burned at a measured rate, and the heat evolved is found by the temperature rise on water flowing through the calorimeter. The water-flow rate is determined by weighing the flow for a measured time. The condensed water is collected in a graduate. The air used in excess of that theoretically required for combustion is 40 per cent. Calculation of heating values includes corrections for humidity in air and in flue gas to find the total heating value when all moisture formed is condensed to liquid.

Continuous-recording calorimeters are used for measuring the heating value of pipeline gases, but such instruments are calibrated by the above ASTM procedure.

The heating value may be computed from the gas analysis and the heating values of constituents (Table A-1), assuming either the ideal-gas law or additive volumes. Table 4-18 presents such calculations, assuming additive volumes for the constituents.

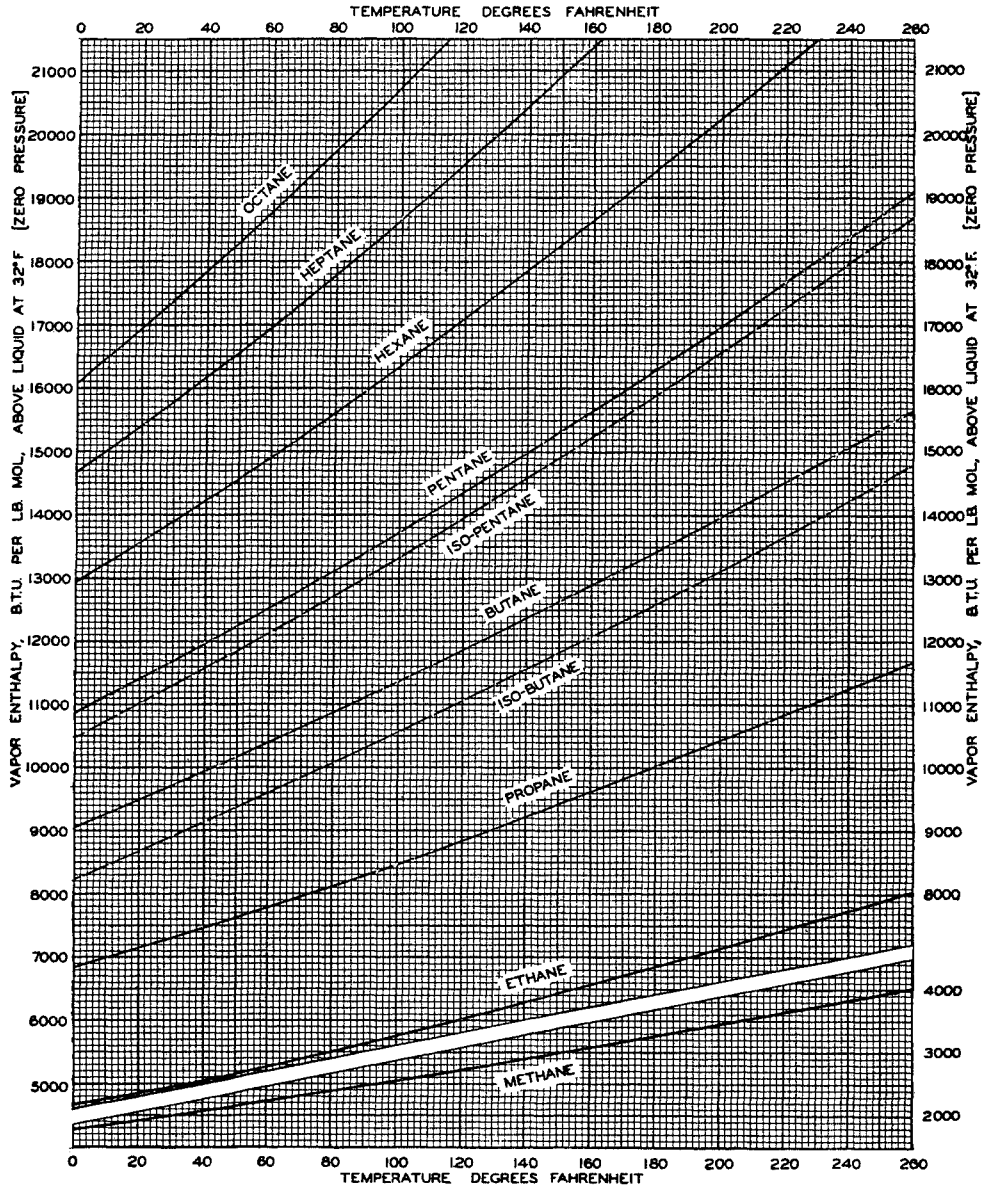

Fig. 4-74. Enthalpy of hydrocarbon above liquid at zero pressure and (*Courtesy Ind. Eng. Chem.*)

Zapffe (4-98) has presented a chart of heating value as a function of specific gravity with lines of inert gas such as nitrogen (Fig. 4-82). This chart gives a quick conversion between gravity, heating value, and per cent of inerts.

Limits of Flammability

Air and natural gas in the proper proportions will ignite, liberating heat, which is absorbed primarily by the products of combustion. The temperature rise of the gases causes an increase in pressure and, under confinement, can result in an explosion. It is important that everyone connected with the natural gas industry understand flammability limits and the nature of combustion (4-35, 4-58, 4-27, 4-82).

Equation (4-36) for combustion of methane does not reveal the mechanism of the chemical reaction. Methane and air in the proper proportions do not react until some ignition source initiates the process. Possible steps in the chemical reaction are given by Lewis and Von Elbe (4-58, 4-35), as follows:

$$HCHO + O_2 \rightarrow \text{free radicals} \rightarrow OH \quad (4\text{-}39)$$

$$OH + CH_4 \rightarrow H_2O + CH_3 \quad (4\text{-}40)$$

$$CH_3 + O_2 \rightarrow OH + HCHO \quad (4\text{-}41)$$

$$OH + HCHO \rightarrow H_2O + CHO \quad (4\text{-}42)$$

$$CHO + O_2 \rightarrow CO + HO_2 \quad (4\text{-}43)$$

$$CHO + O_2 + M \rightarrow CHO_3 + M \quad (4\text{-}44)$$

$$CHO_3 + HCHO \rightarrow 2CO + H_2O + OH \quad (4\text{-}45)$$

To start the combustion process, the ignition source

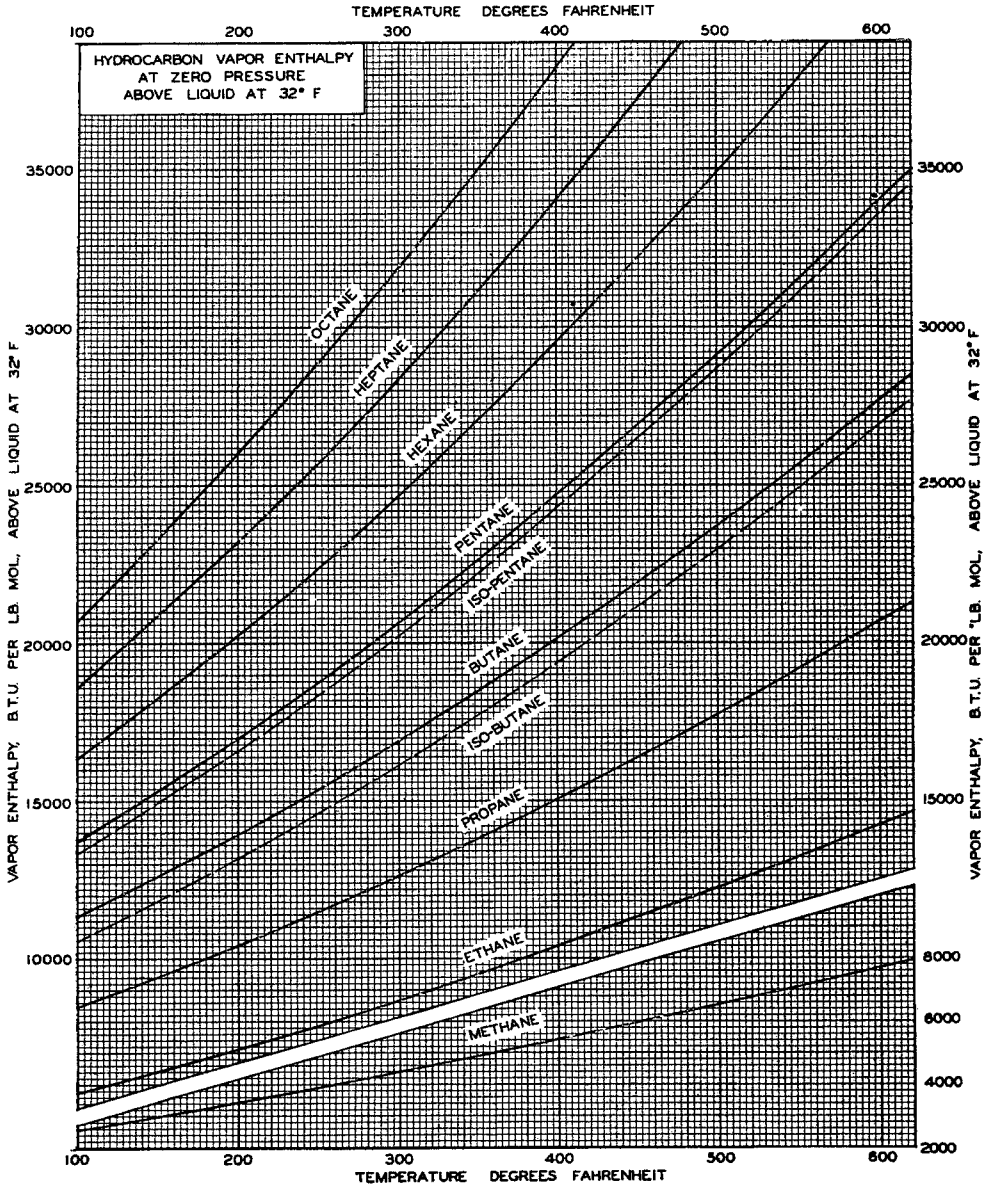

vapors at atmospheric pressure 32°F. (*Holcomb and Brown*, 3-25.

converts some methane (CH_4) into free radicals, which in turn are oxidized to formaldehyde (HCHO) and OH. The OH radical reacts with methane, by Eq. (4-40), and is regenerated, by Eq. (4-45), in a chain reaction. Similar reactions account for the combustion of other hydrocarbons. Conditions under which combustion does not proceed include those which destroy the OH radicals before they can react with CH_4. Solid surfaces often destroy the OH radical.

The rate of chemical reaction must be considered in the light of the molecular velocities and number of collisions mentioned earlier. Reaction rates are measurable, but, under certain conditions, time scales expanded to microseconds (1/1,000,000 sec) are required. The rates rise rapidly with increasing temperature. A rule of thumb is that reaction rates double for each 27°F of temperature rise.

There are two composition limits of flammability for air and a gaseous fuel under specified conditions. The lower limit corresponds to the minimum concentration of combustible gas that will support combustion, the higher limit to the maximum concentration. Table A-1 lists lower and higher limits for pure hydrocarbons in air. For methane in air, the flammable range is from 5 to 15 mole or vol %. For propane, the range is 2.4 to 9.5 mole or vol %.

The lower limits of gaseous mixtures can be predicted from the limits of the pure constituents by a simple formula (4-27),

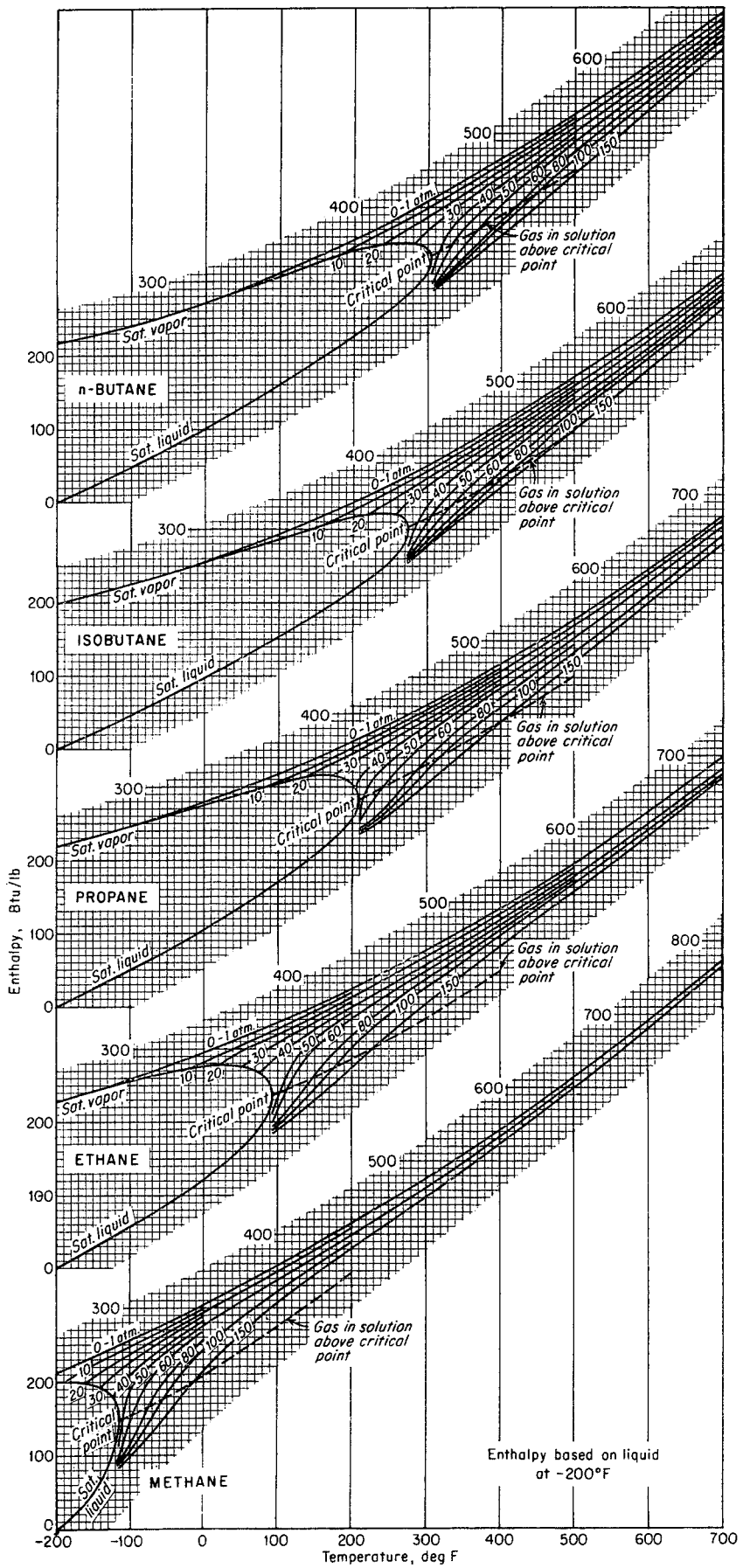

Fig. 4-75. Enthalpy of hydrocarbons. (*After* pany, Inc.)

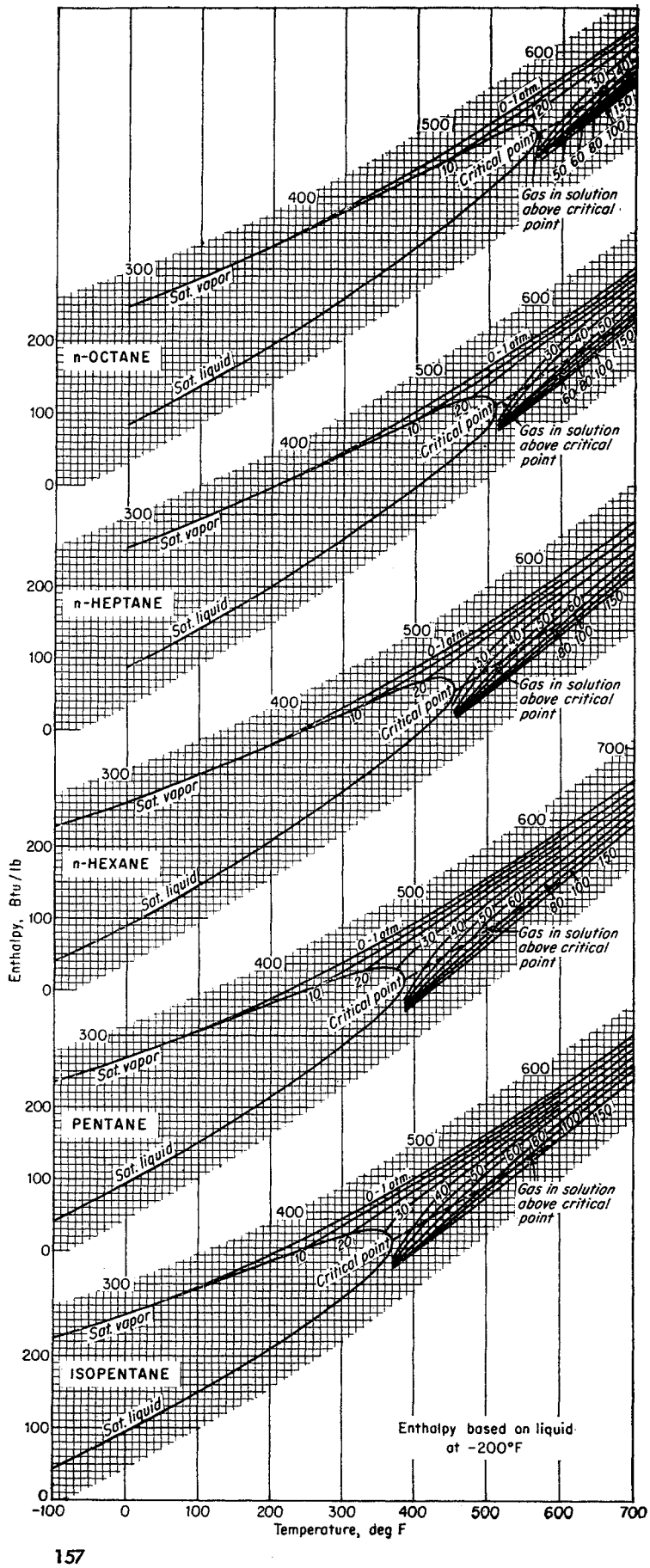

Maxwell, 1-10. *Courtesy D. Van Nostrand Com-*

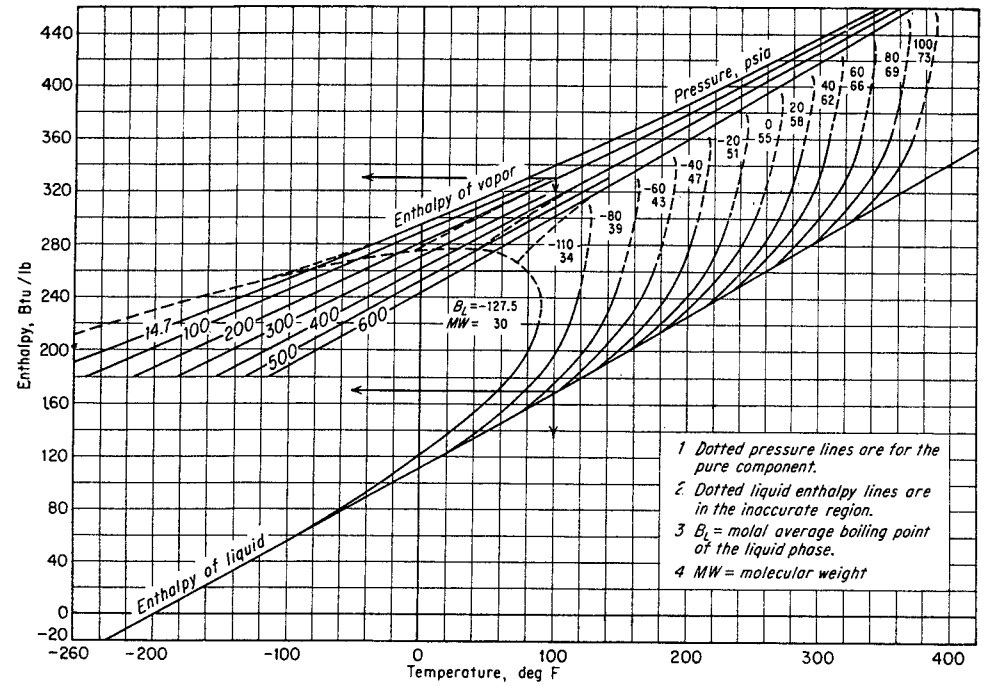

Fig. 4-76. Enthalpy of methane. (*Peters, 4-67. Courtesy Petrol. Refiner.*)

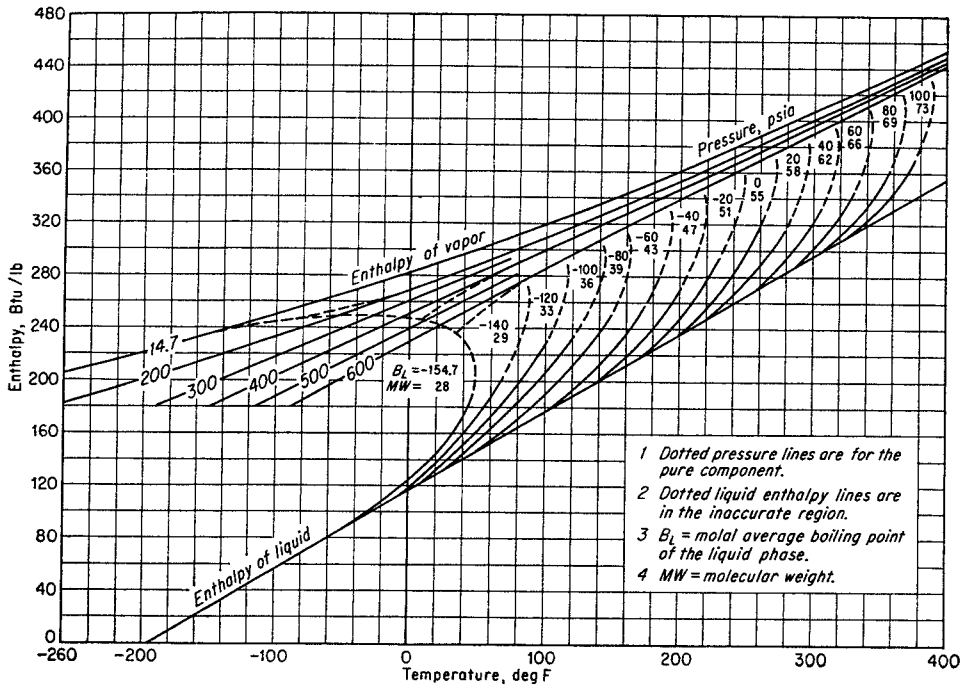

Fig. 4-77. Enthalpy of ethylene. (*Peters, 4-67. Courtesy Petrol. Refiner.*)

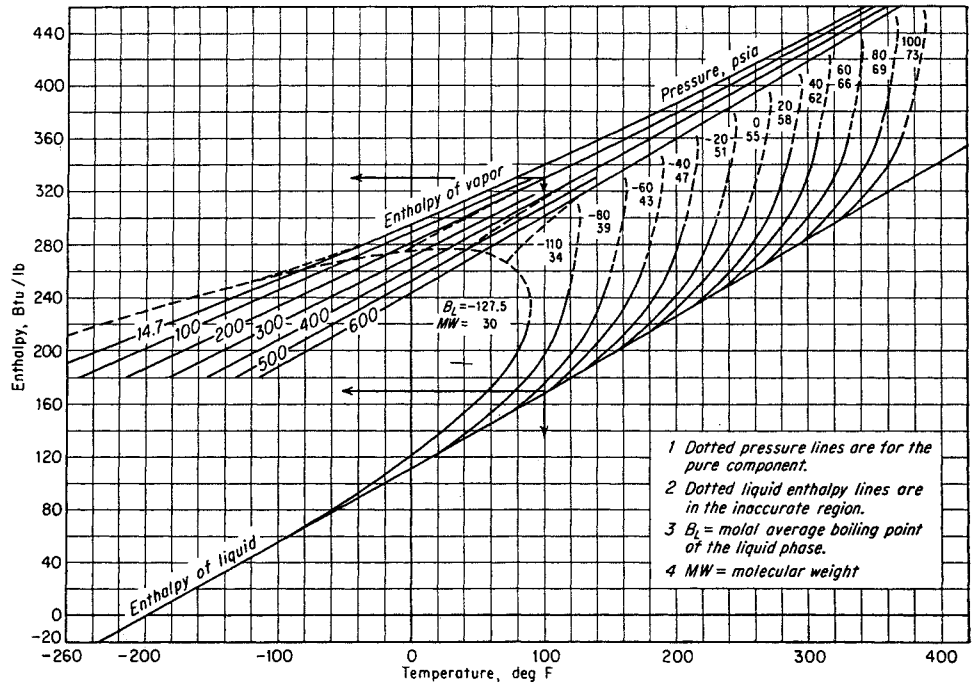

Fig. 4-78. Enthalpy of ethane. (*Peters, 4-67. Courtesy Petrol. Refiner.*)

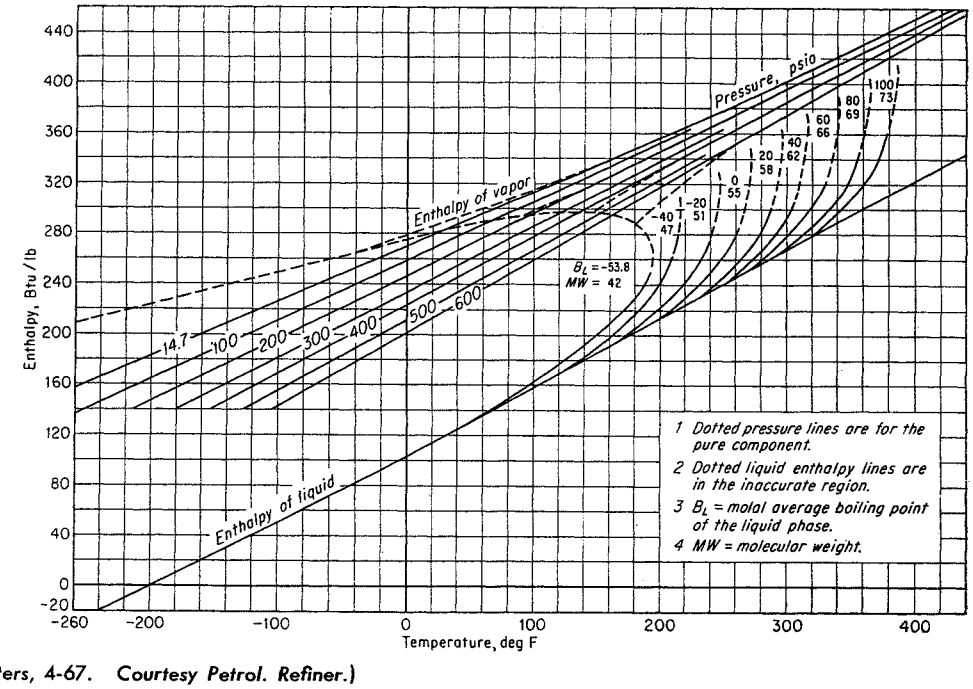

Fig. 4-79. Enthalpy of propylene. (*Peters, 4-67. Courtesy Petrol. Refiner.*)

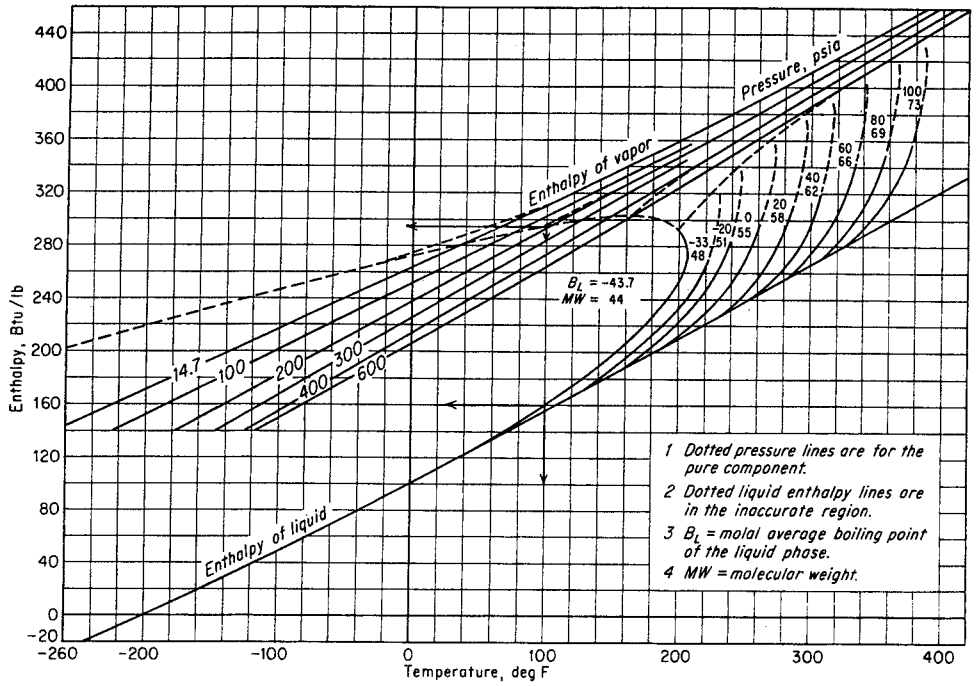

Fig. 4-80. Enthalpy of propane. (*Peters, 4-67. Courtesy Petrol. Refiner.*)

$$\frac{n_1}{N_1} + \frac{n_2}{N_2} + \frac{n_3}{N_3} = 1 \qquad (4\text{-}46)$$

where subscripts 1, 2, 3 refer to constituents 1, 2, 3

n = proportion of each constituent in the total mixture at lower limit, mole or vol %

N = lower limit for each constituent as a pure constituent, mole or vol %

Illustrative Problem

Compute the lower flammability limit for a natural gas composed of 92 vol % CH_4, 5.5 vol % C_2H_6, and 2.5 vol % C_3H_8.

Solution

Let x = vol % of gas in mixture of air and gas

$$\frac{92.0x}{5.0} + \frac{5.5x}{3.22} + \frac{2.5x}{2.37} = 1$$

$$18.5x + 1.71x + 1.05x = 1$$

$$x = \frac{1}{21.26} = 4.7 \text{ vol \% of gas in mixture of air and gas}$$

The influence of pressure on the flammability limits is given by Figs. 4-83 and 4-84. At low pressures, 50 mm Hg, natural gas–air mixtures are not combustible. At high pressures, the upper limit rises rapidly. A 40 mole % propane–60 mole % air mixture reacted in a commercial flow system when hot air from a compressor was mixed with propane at 600 psia, causing the pipes to become cherry red but without causing any violence. The diluting of a fuel-air mixture with inert constituents such as nitrogen and carbon dioxide changes the limits of flammability, as shown by Figs. 4-85 and 4-86. Both the lower and higher limits of flammability are raised by addition of the diluent, an effect due in part to the lowered oxygen concentration.

Table 4-18. Computation of Heating Value from Gas Analysis

Component	Mole or vol fraction	Heating value of component at 14.7 psia and 60°F, Btu/cu ft	Total heating value of gas, Btu/cu ft
Nitrogen	0.023	0	0
Methane	0.887	1012	897.6
Ethane	0.056	1783	99.9
Propane	0.021	2578	54.0
Isobutane	0.003	3354	10.0
n-Butane	0.006	3369	20.2
Pentanes	0.004	4001	16.0
	1.000		1097.7

Dry-basis heating value at 14.696 psia and 60°F = 1097.7 Btu/cu ft. At 14.65 psia, 60°F, the heating value is 14.65/14.696 × 1097.7 = 1094.2 Btu/cu ft. Sometimes natural gas is saturated with water vapor at 60°F and 30 in. Hg; convert the above value to this basis.

$$1097.7 \times \frac{30.00}{29.92} \times \frac{30.0 - 0.522}{30.00} = 1081.5 \text{ Btu/cu ft}$$

If the gas contains 9 lb (0.5 lb mole) of water per MMcf, compute the total heating value with this moisture content at 14.65 psia and 60°F.

$$1094.2 \times \frac{1{,}000{,}000}{1{,}000{,}000 + (0.5 \times 379)} = 1094.0 \text{ Btu/cu ft}$$

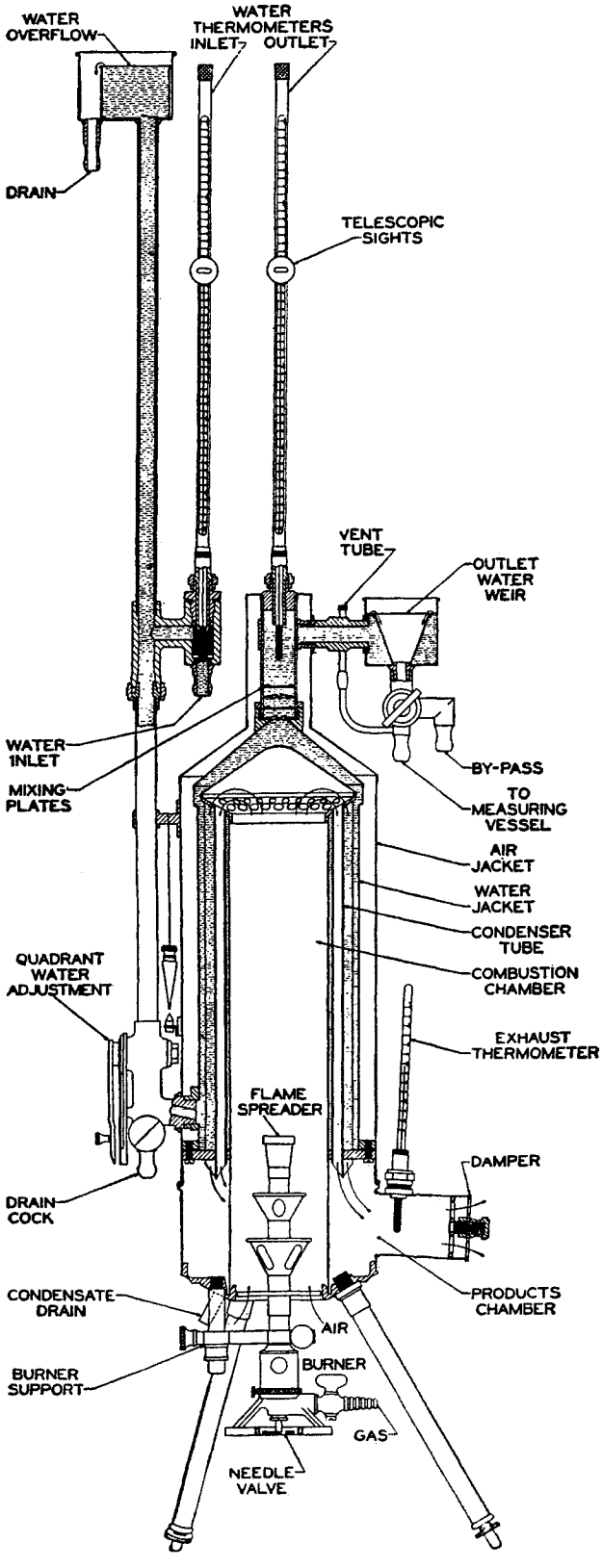

Fig. 4-81. American flow-calorimeter assembly. (*ASTM*, 4-2.)

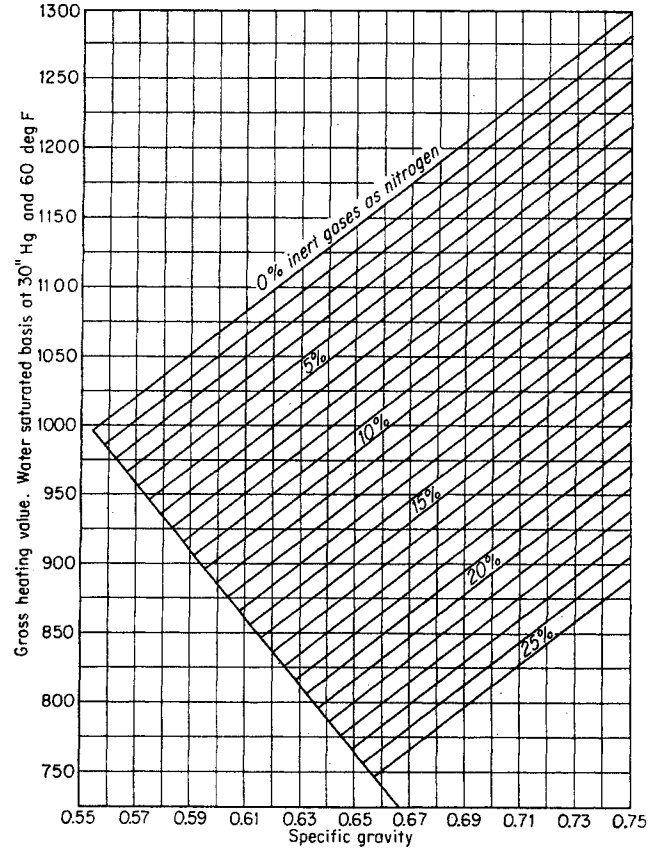

Fig. 4-82. Conversion between heating value, gravity, and percentage of inerts. (*Zapffe*, 4-98. *Courtesy Petrol. Refiner.*)

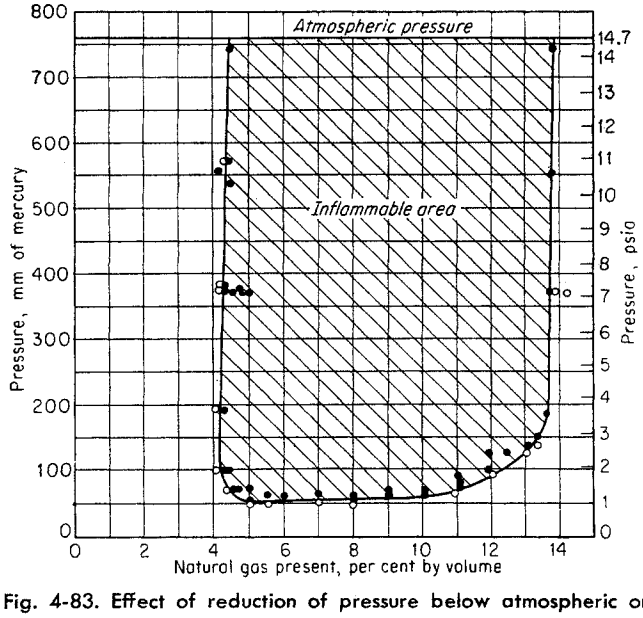

Fig. 4-83. Effect of reduction of pressure below atmospheric on limits of flammability of natural gas–air mixtures. (*Lewis and Von Elbe*, 4-58. *Courtesy Academic Press, Inc.*)

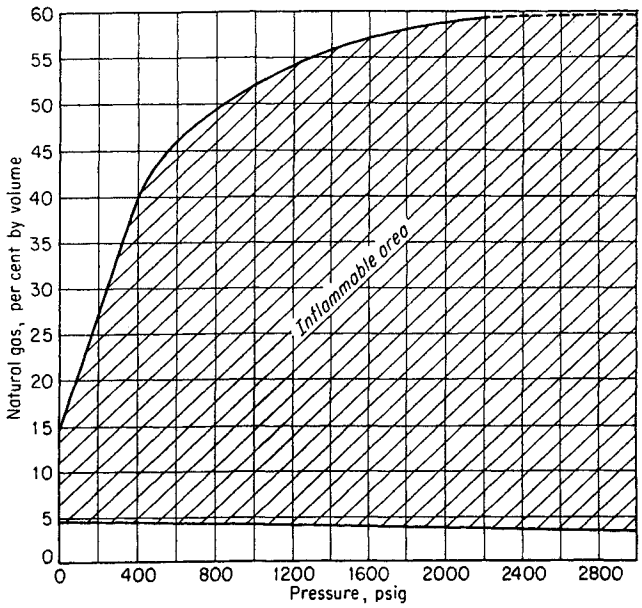

Fig. 4-84. Effect of pressure rise above atmospheric on limits of flammability of natural gas–air mixtures. (*Lewis and Von Elbe, 4-58. Courtesy Academic Press, Inc.*)

The combustion process may take place in a relatively slow *combustion wave* or in a rapid *detonation wave* (4-58). The combustion wave propagates by heat transfer and diffusion between the burning mixture and the unburned fuel. Detonation waves are shock waves that are sustained by the energy released during the chemical reaction. Flame velocities at atmospheric pressure are of the order of 1 to 8 ft/sec, with the hydrocarbons in natural gas at the low end of the range and with hydrogen at the high end. These velocities are slow enough for a person to observe visually the combustion wave of flame propagation.

In certain combustion processes, the combustion wave started by an ignition accelerates rapidly to a detonation wave whose velocity remains relatively constant. The velocities of detonation waves are of the order of 3,000 to 10,000 ft/sec, several times the velocity of sound in air at room temperature. Figure 4-87 illustrates the development of a combustion wave into a shock wave. The unburned fuel-air mixture is compressed just ahead of the burning zone, as indicated in Fig. 4-87*a*. This compression raises the temperature, which in turn increases the reaction rate. The increase in the reaction rate with distance traveled causes a build-up of the wavefront (Fig. 4-87*b*), until it reaches the condition (Fig. 4-87*c*) known as a *shock front.* This shock front or detonation wave moves at a high, but constant, velocity as long as it is supported by the energy of a chemical reaction. For many fuel-air mixtures, combustion waves do not reach velocities high enough to become detonation waves. Limits of detonability are given in Table 4-19.

Sufficient pressure to cause considerable damage may be generated by combustion of an air-gas mixture in a room, without reaching detonation velocities. More severe damage will result when a combustion wave grows into a detonation wave and develops a shock front.

Predicting Critical Pressure and Temperature

In determining the phase behavior of a mixture, the true critical temperature and critical pressure may be desired. Methods of predicting these critical properties were presented by Smith and Watson (4-86), Kurata and Katz (1-2, 4-52a), and Organick (4-66). The method of Organick is presented here. It consists of computing the molal-average boiling point $\bar{B}$ and the weight-average molecular weight W_m of the mixture and then reading the critical conditions from

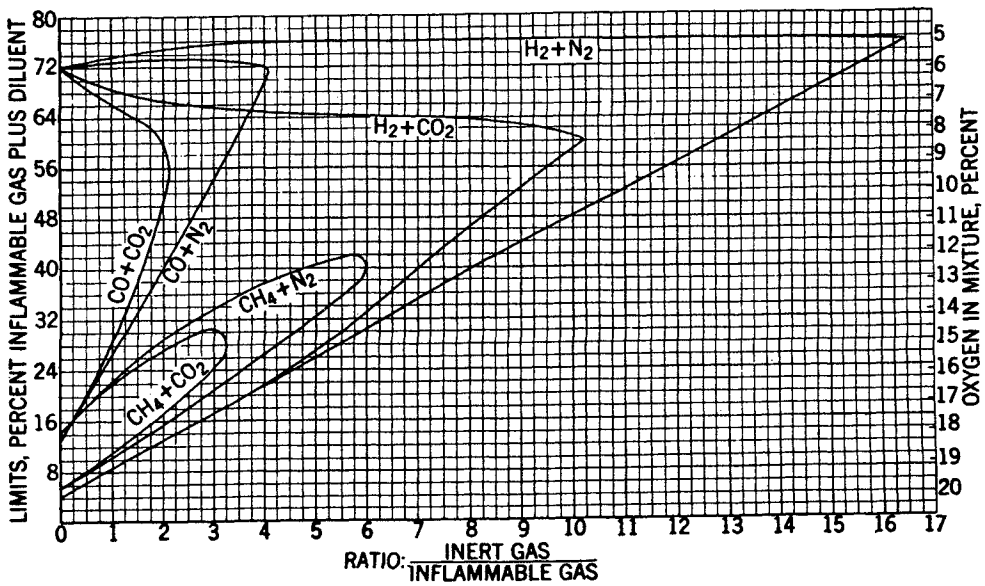

Fig. 4-85. Limits of flammability of fuel gas–air mixtures when diluted with various proportions of nitrogen and carbon dioxide. (*Lewis and Von Elbe, 4-58. Courtesy Academic Press, Inc.*)

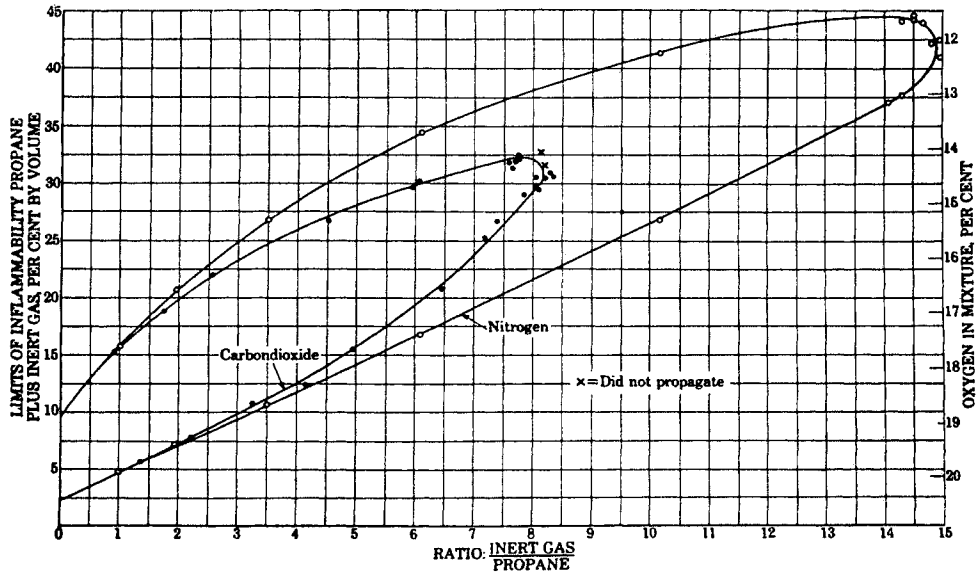

Fig. 4-86. Limits of flammability of propane-air mixtures when diluted with various proportions of nitrogen and carbon dioxide. (*Lewis and Von Elbe, 4-58. Courtesy Academic Press, Inc.*)

Table 4-19. Limits of Detonability

Mixture	Volume % fuel	
	Lower limit	Upper limit
H_2-air	18.3	59
H_2-O_2	15.0	90
C_3H_8-O_2	3.2	37
i-C_4H_{10}-O_2	2.8	31
C_2H_2-O_2	3.5	92
C_2H_2-air	4.2	50
NH_3-O_2	25.4	75

SOURCE: Lewis and Von Elbe (4-58).

Fig. 4-88. It may require the use of Fig. 4-89, a correction to the volumetric-average boiling points, and the use of Fig. 4-36.

Illustrative Problem (4-66)

Given the following stream composition from a well, compute the critical temperature and pressure for the mixture.

Well-stream Composition

Component	Separator gas, wt fraction	Separator liquid, wt fraction	Well stream, wt fraction
CO_2	0.0229	.....	0.0145
C_1	0.6383	0.0173	0.4106
C_2	0.1187	0.0136	0.0802
C_3	0.0972	0.0338	0.0739
i-C_4	0.0199	0.0210	0.0203
n-C_4	0.0398	0.0460	0.0421
i-C_5	0.0136	0.0336	0.0209
n-C_5	0.0136	0.0382	0.0226
C_6's	0.0116	0.1026	0.0450
C_7+ (separator gas)	0.0244	.....	0.0155
C_7+ (separator liquid)	.....	0.6939	0.2544

ASTM Distillation of C_7+ from Separator Liquid
Gravity at 60°F: 49.8° API; 0.7805 gram/cu cm

Distillation		Cut	Density, grams/cu cm
IBP	175°F	1	0.7425
10%	196	2	0.7436
20%	212	3	0.7503
30%	230	4	0.7572
40%	250	5	0.7678
50%	278	6	0.7796
60%	310	7	0.7910
70%	350	8	0.8054
80%	400	Residue	0.8423

Remarks: 10–90 per cent slope = 3.3. Volumetric-average boiling point = 303°F.

Solution (reproduced from Organick, 4-66)

Step 1. Calculation of Molal- and Weight-average Properties of the Heavy Ends. In order to compute $\bar{B}$ and W_m for the well-stream composition, it is desirable first to determine these properties for the C_7+ fraction in the separator-gas and separator-liquid streams. The C_7+ fraction from the separator gas may be assumed to have the properties of normal octane: $\bar{B}$ = 718°R and W_m = 114. Two methods are recommended for computing $\bar{B}$ and W_m for the C_7+ in the separator liquid.

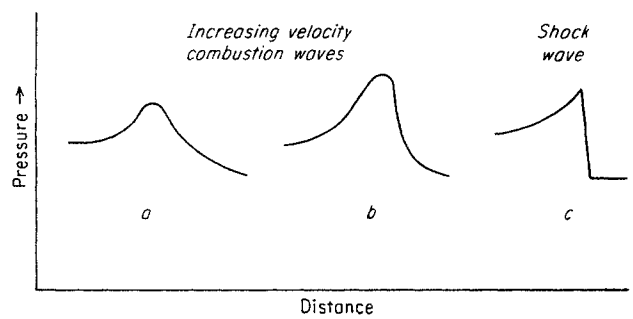

Fig. 4-87. Simplified representation of development of shock wave (*Hirschfelder, 4-40.*)

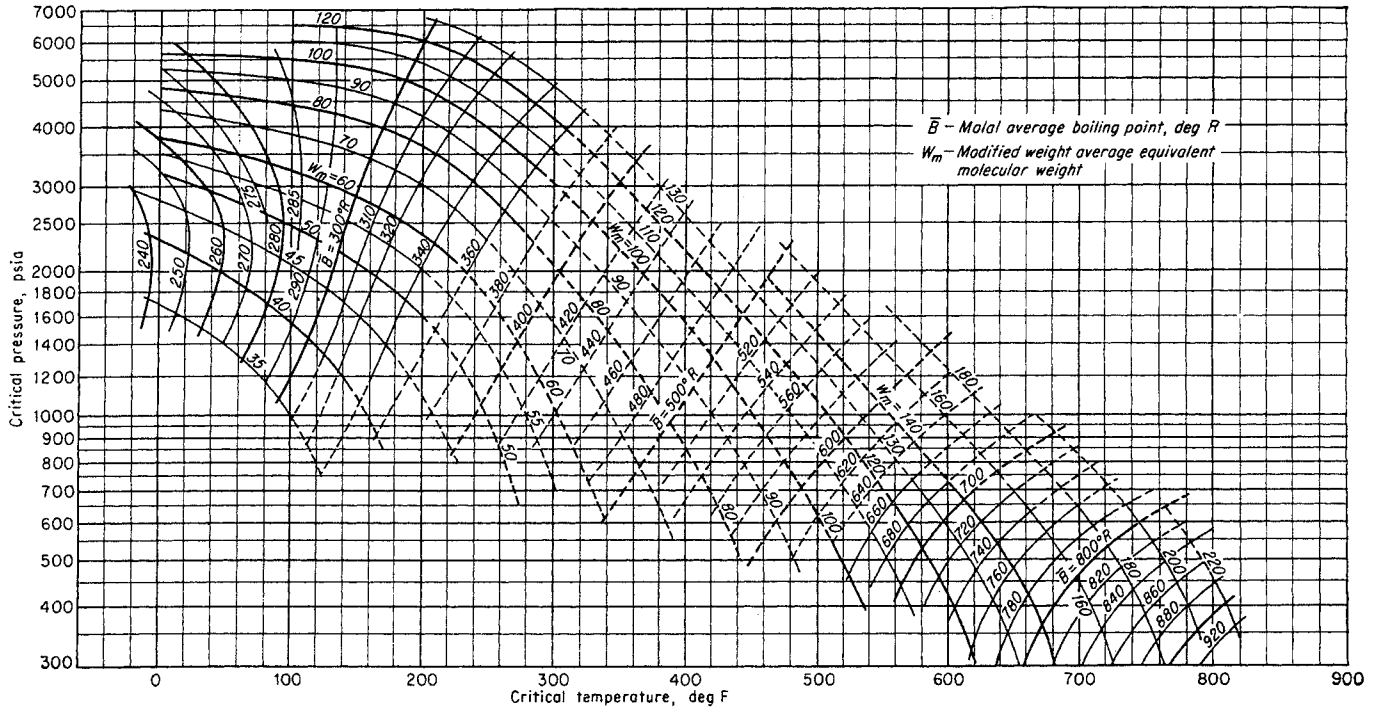

Fig. 4-88. Correlation for predicting critical temperatures and critical pressures of complex mixtures. (*Organick*, 4-66. Courtesy *AIChE*.)

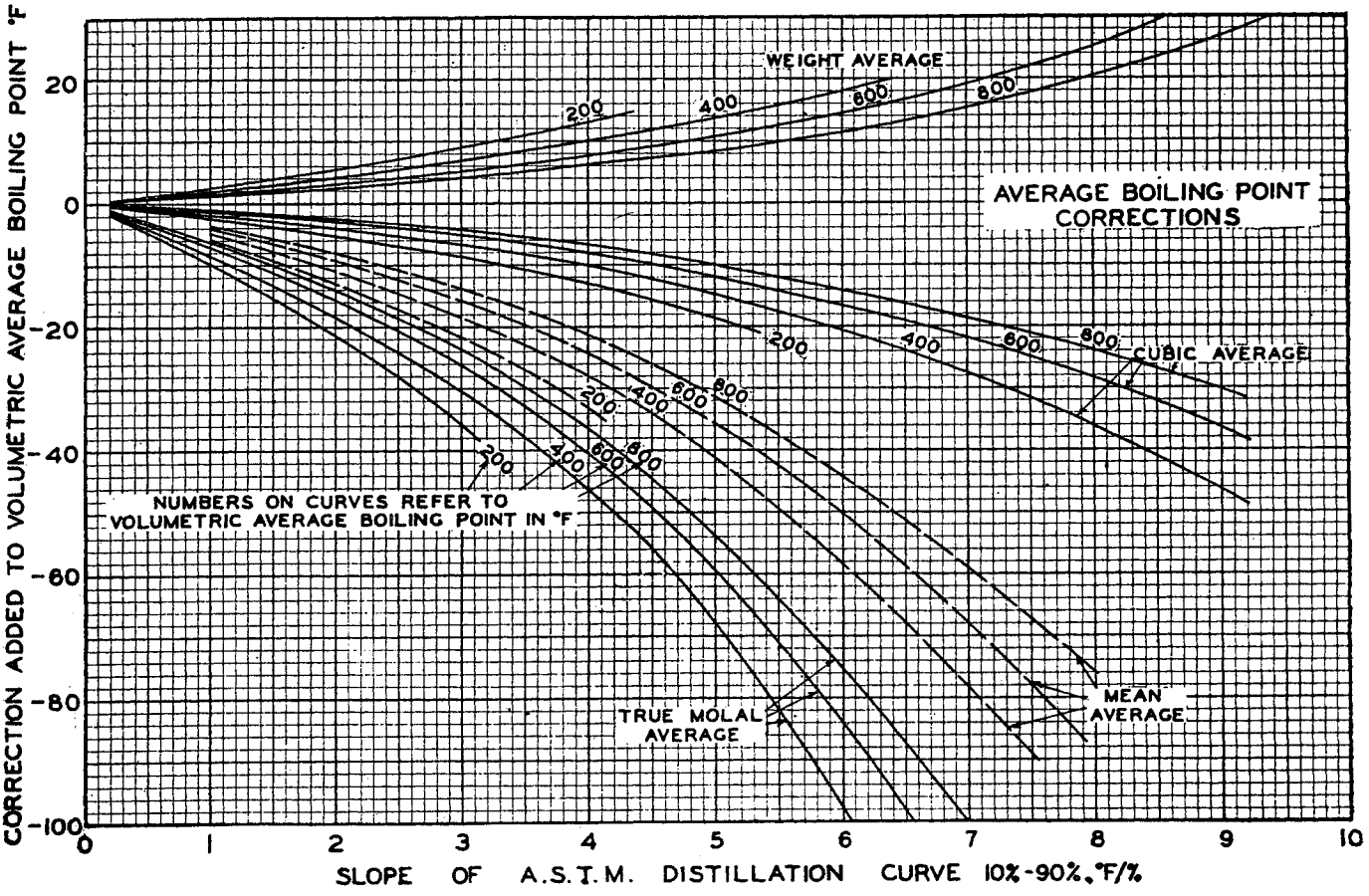

Fig. 4-89. Correction to volumetric-average boiling points. (*Smith and Watson*, 4-86; 1-2.)

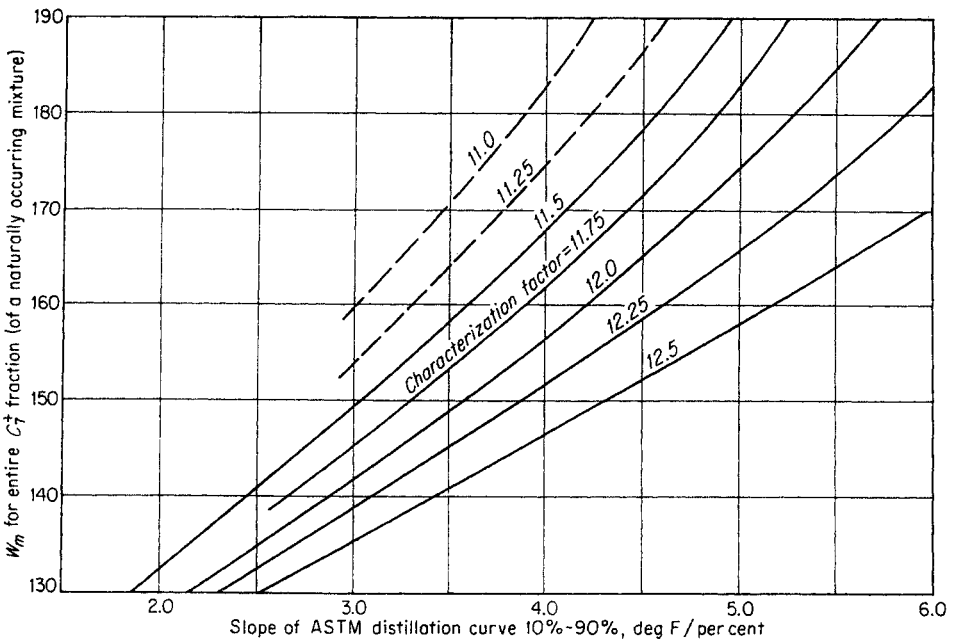

Fig. 4-90. Weight-average molecular weight of petroleum fractions (C_7+). (*Organick*, 4-66. Courtesy AIChE.)

The first method is a short-cut procedure designed for quick estimates of these properties. For more accurate calculation, the second, somewhat more involved, method is recommended.

The first method, the short-cut procedure, assumes that $\bar{B}$ is approximately equal to the mean average boiling point and that W_m for a C_7+ fraction in a naturally occurring mixture may be obtained directly from the ASTM slope and the average characterization factor.

The mean average boiling point is obtained from Fig. 4-89:

ASTM 10 to 90 per cent slope = 3.3	
Volumetric-average boiling point	303°F
Correction to volumetric-average boiling point	−23°F
Mean average boiling point	280°F

B, therefore, is 280 + 460 = 740°R.

W_m is obtained from the ASTM slope and the average characterization factor. The latter may be read from Fig. 4-36, knowing the density (0.7805 gram/mole) and the cubic average boiling point. Figure 4-89 is used to obtain the cubic average boiling point:

Volumetric-average boiling point	303°F
Correction to volumetric-average boiling point	−9°F
Cubic average boiling point	294°F

From Fig. 4-36 the average characterization factor is 11.7. W_m can now be read directly from a chart such as that shown in Fig. 4-90, which is a plot of W_m versus ASTM slope with lines of constant characterization factor. (This chart is applicable to C_7+ fractions in naturally occurring condensate gas and volatile crude oils but should not be used for C_8+, C_9+ fractions, etc.) From Fig. 4-90, W_m is 151.

The second method is a more precise calculation, because the heavy ends are broken up into a number of arbitrarily selected cuts. The properties of each cut are ascertained and summed to obtain the properties of the entire fraction. Table 4-20 summarizes this calculation. Columns 3 and 4 list the midboiling points of ten selected cuts as read from the ASTM distillation curve.

The characterization factors of the individual cuts (column 6) are read from Fig. 4-36, using the experimental densities and the midboiling points. Because these characterization factors are approximately constant at 11.7, the same value is assumed for the equiweight cuts, cuts 9 and 10 of the residue. The weight of each cut (column 7) may be expressed as a weight fraction of the entire separator liquid (column 8) by multiplying the weight of each cut by the ratio 0.6939/78.05, the ratio of the weight fraction of C_7+ to the total weight of C_7+. These weight fractions are expressed as cumulative weight fractions of the separator liquid (column 9).

A plot of log absolute midboiling point (column 4) versus average cumulative weight % (column 10) is constructed (Fig. 4-92). A best straight line through all the points in Fig. 4.92 is extrapolated to 100 cumulative per cent, and the average boiling points of the residue cuts 9 and 10 are obtained from the extrapolated portion of the line. These values, 857° and 890°R, respectively, are used to determine the densities, molecular weights, and equivalent molecular weights of these cuts.

The equivalent molecular weight of each cut (column 1) is a function of the average boiling point and the characterization factor, and may be read from Fig. 4-91. The modified weight-average equivalent molecular weight for the entire C_7+ fraction is then computed to be 135.5, the summation in column 12 divided by the total weight of sample found in column 7. The molal-average boiling point for the C_7+ fraction is shown as the summation of column 15 divided by the summation of column 14, and is 745°R.

Step 2. Calculation of $\bar{B}$ and W_m for the Well-stream Composition. Once the properties of the C_7+ materials have been determined, it is possible to compute the values of $\bar{B}$ and W_m for the well-stream composition, as shown in Table 4-21.

Columns 1 and 5 express the well-stream composition in weight and mole fractions. The latter is derived from the former, using the molecular weights shown in column 4. Column 2 represents equivalent molecular weights of the hydrocarbons, including the lumped values for the C_7+ fraction as computed in Table 4-20. W_m for the well stream is the summation in column 3, or 60.1. $\bar{B}$ is the summation in column 7, or 279°R.

Step 3. Reading the Critical Pressure and Critical Tem-

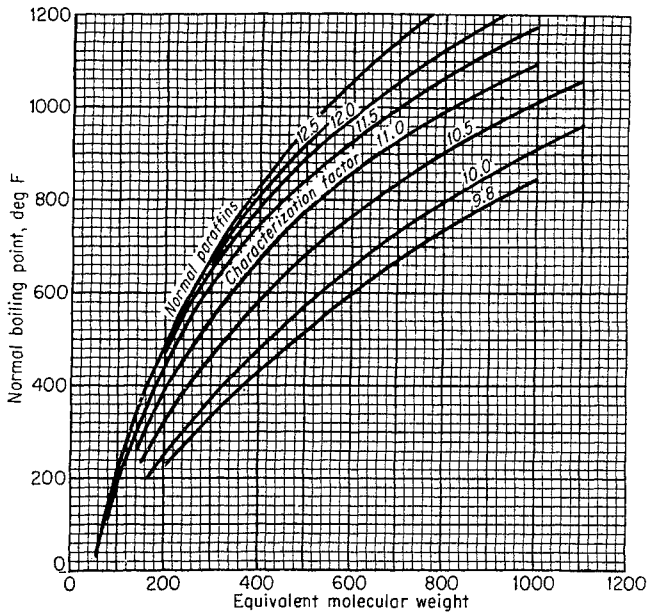

Fig. 4-91. Equivalent molecular weights of petroleum fractions and gas constituents. (*Organick, 4-66. Courtesy AIChE.*)

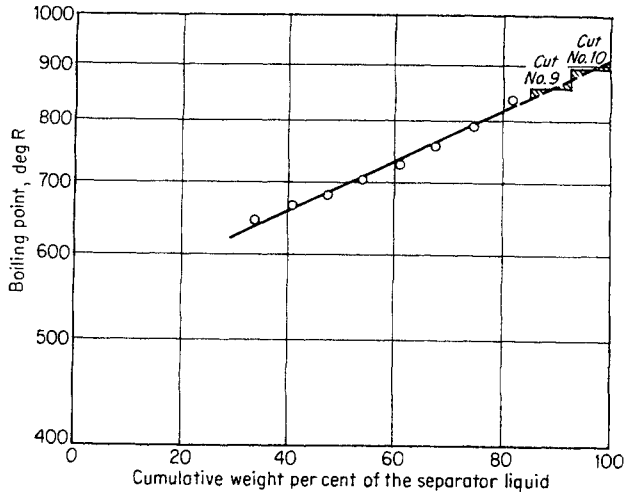

Fig. 4-92. ASTM distillation of the C_7+ fraction in the separator liquid (semilog plot). (*Organick, 4-66. Courtesy AIChE.*)

perature from Fig. 4-88, the Working Chart. The values of $\bar{B}$ and W_m just computed define a point in Fig. 4-88 representing the predicted values of the critical pressure and temperature of the mixture.

From Fig. 4-88, at $W_m = 60.1$ and $\bar{B} = 279°R$,

$$\text{Critical pressure } P_c = 3{,}350 \text{ psia}$$
$$\text{Critical temperature } T_c = 80°F$$

The critical pressure, estimated from incomplete experimental phase-behavior data for this mixture, lies between 3,000 and 3,200 psia; the critical temperature is 50 to 75°F.

If the short-cut procedure were used, agreement between predicted and observed values of critical pressure would not be satisfactory, although agreement between predicted and observed critical temperature would be quite good. W_m by the short-cut method is 64, and $\bar{B}$ is again 279°R. For these values of the composition parameters, $P_c = 3{,}680$ psia and $T_c = 70°F$.

For a mixture consisting of compounds such as methane, ethane, etc., without any C_7+, the procedure is simplified considerably.

VISCOSITY

A knowledge of the viscosity of hydrocarbon fluids is essential for a study of the dynamic or flow behavior of these fluids through pipes, porous media, or, more generally, wherever transport of momentum occurs in fluid motion. The influence of fluid viscosity on

Table 4-20. Calculation of Molal- and Weight-average Properties of the Heptanes-and-heavier Fraction of the Separator Liquid

Cut	Mole %	Mid-boiling point, °F	Mid-boiling point, °R	Experimental density, grams/mole	Characterization factor	Weight, grams	Wt fraction of separation liquid, grams × 0.6939/78.05	Cumulative wt fraction of separator liquid	Av cumulative wt fraction of separator liquid	Equiv. mol. wt	Grams × equiv. mol. wt	Actual mol. wt	Moles = grams/mol. wt	Moles × mid-boiling point, °R
(1)	(2)	(3)	(4)	(5)	(6)	(7)	(8)	(9)	(10)	(11)	(12)	(13)	(14)	(15)
1.....	10	186	646	0.7525	11.65	7.425	0.0659	0.3061	0.3390	95	705	90	0.00825	5.33
2.....	10	205	665	0.7436	11.74	7.436	0.066	0.3720	0.4050	100	746	96	0.00774	5.15
3.....	10	220	680	0.7503	11.70	7.503	0.0666	0.4380	0.4713	110	825	100	0.00750	5.26
4.....	10	242	702	0.7572	11.75	7.572	0.0672	0.5046	0.5382	113	855	107	0.00709	4.96
5.....	10	267	727	0.7678	11.72	7.678	0.0681	0.5718	0.6058	125	960	114	0.00673	4.90
6.....	10	293	753	0.7796	11.68	7.796	0.0691	0.6399	0.6744	133	1,037	122	0.00639	4.81
7.....	10	329	789	0.7910	11.69	7.910	0.0702	0.7090	0.7441	145	1,148	133.5	0.00594	4.67
8.....	10	378	838	0.8054	11.70	8.054	0.0715	0.7792	0.8150	162	1,303	151	0.00534	4.47
9 (residue)..	.....	(397)	(857)*	(0.8110)	(11.70)	(8.340)	(0.0646)	0.8507	0.8896	170	1,418	159	0.00555	4.76
10 (residue)..	.....	(430)	(890)*	(0.8220)	(11.70)	(8.340)	(0.0746)	(0.9253)	0.9642	190	1,581	172	0.00485	4.31
								(1.0000)						
Total.....	(100)	.....	.....	.....	.....	78.05	.....	.....	.....	...	10,578	.....	0.06538	48.62

$$W_m = \frac{10{,}578}{78.05} = 135.5 \qquad \bar{B} = \frac{48.62}{0.0654} = 745°R$$

* Extrapolated from Fig. 4-92.

Table 4-21. Calculation of $\overline{B}$ and W_m for the Well-stream Composition

Component	Wt fraction (1)	Equiv. mol. wt (2)	Wt fraction × equiv. mol. wt (3)	Actual mol. wt (4)	Mole fraction (5)	Boiling point, °R (6)	Mole fraction × boiling point, °R (7)
CO_2	0.0145	44	0.64	44	0.0095	350	3.3
C_1	0.4106	16.04	6.60	16.04	0.7371	201	148.2
C_2	0.0802	30.1	2.42	30.1	0.0766	332	25.4
C_3	0.0739	44.1	3.26	44.1	0.0482	416	20.0
i-C_4	0.0203	54.5	1.11	58.1	0.0101	471	4.8
n-C_4	0.0421	58.1	2.45	58.1	0.0209	491	10.3
i-C_5	0.0209	69	1.44	72.2	0.0084	542	4.6
n-C_5	0.0226	72.2	1.63	72.2	0.0090	557	5.0
C_6's	0.0450	85	3.82	86.2	0.0150	660	9.0
C_7+ sep. gas	0.0155	114	2.23	114	0.0039	718	2.8
C_7+ sep. liquid	0.2544	135.5*	34.5	119.5	0.0613	745*	45.6
Total	1.0000	.....	W_m = 60.1†	.....	1.0000	....	$\overline{B}$ = 279°R†

* Computed in Table 4-20.

† If short-cut method were used, values obtained would be W_m = 64, $\overline{B}$ = 279°R.

flow is especially important in petroleum reservoirs, since the flow is predominantly in the laminar-flow region where the pressure drop is proportional to the viscosity. In the laminar or viscous region, viscosity is defined by the relationship

$$\omega = \frac{\mu}{g_c}\frac{du}{dy} \qquad (4\text{-}47)$$

where μ = coefficient of viscosity, or absolute viscosity, grams mass/(cm)(sec)

ω = shear stress per unit area in the shear plane parallel to the direction of flow, grams force/sq cm

du/dy = velocity gradient perpendicular to the plane of shear, cm/(sec)(cm)

g_c = conversion factor (gram mass/gram force) (cm/sec²)

The concept of viscosity was first postulated by Sir Isaac Newton and later verified experimentally for the flow of fluids through capillaries by Poiseuille (4-123). The importance of viscosity will become evident in subsequent treatments of the flow of fluids.

The unit of absolute viscosity is the gram mass/(cm)(sec), or the *poise*. Other units are the centipoise, or 0.01 poise; the millipoise, or 0.001 poise; and the micropoise, or 0.000001 poise. Water at 68.4°F has a viscosity of 1.0 centipoise.

The kinematic viscosity is the ratio of the absolute viscosity to the density.

$$\frac{\mu}{\rho} = \frac{\text{centipoises}}{\text{grams/cu cm}} = \text{centistokes} \qquad (4\text{-}48)$$

Viscosity measurements on liquids flowing through capillaries under the driving force of the head of liquid yield kinematic viscosities (4-2).

The rolling-ball viscosimeter is used for measuring viscosity, with the ball forcing the fluid through the crescent between the ball and the tube wall (Fig. 4-93). Comings, Mayland, and Egly (4-108) have shown that the rolling-ball viscosimeter can give erroneous results when used with low-density fluids, because of the turbulent flow through the crescent. The preferred instrument for gases is the Rankine viscosimeter (Fig. 4-94) in which the pressure gradient for the fluid flowing through the capillary can be very small. The glass viscosimeter is enclosed in a pressure vessel and can be operated by rotation. The rolling-ball viscosimeter (Fig. 4-95) finds application for liquids at high pressure, such as for subsurface samples (4-112).

The nature of the viscosity change with pressure and temperature is shown for ethane in Fig. 4-96. At atmospheric pressure, gaseous ethane increases in viscosity with increase in temperature. On the other hand, liquid ethane decreases in viscosity with temperature rise; at conditions above the critical tem-

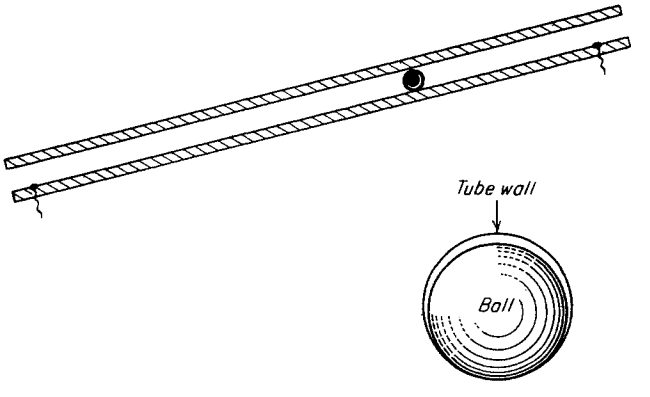

Fig. 4-93. Principle of rolling-ball viscosimeter.

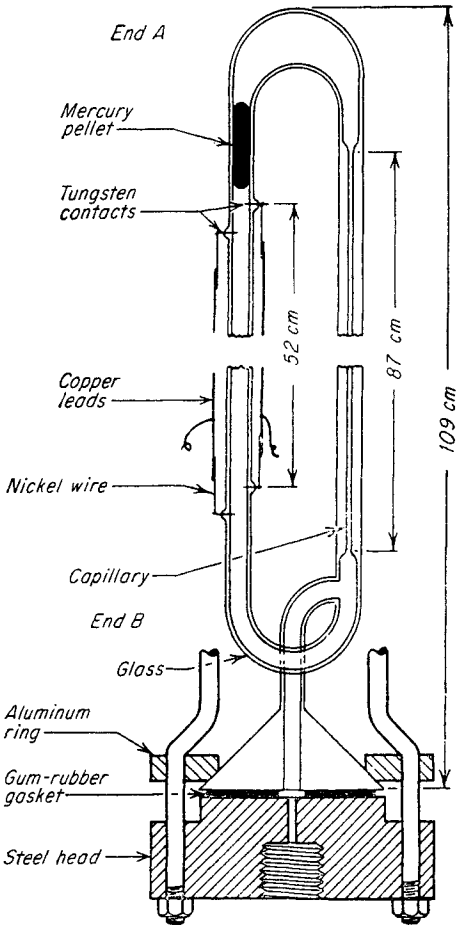

Fig. 4-94. Rankine viscosimeter of Comings, Mayland, and Egly. (4-108.)

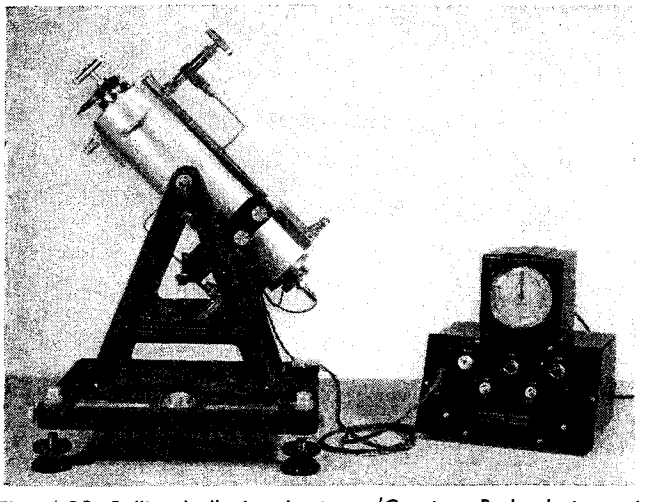

Fig. 4-95. Rolling-ball viscosimeter. (*Courtesy Ruska Instrument Corporation.*)

perature, a gradual merging of the vapor and liquid properties takes place. At high pressure, increases in temperature cause a decrease in viscosity even at temperatures far above the critical. The variation in viscosity with molecular weight of vapors at atmospheric pressure is opposite to the variation for liquids, for viscosity decreases with increase in molecular weight of vapors. The increased size of the gas molecules influences their behavior to decrease the shear stress between layers in motion.

A summary of the references for viscosities of pure gases at atmospheric pressure is given in Table 4-22. These data, together with the viscosity values computed by the method of Hirschfelder, Bird, and Spotz (4-39), have been used to prepare Fig. 4-97. It should be noted that the curve for the viscosity of isobutane lies slightly above the curve for *n*-butane over the entire temperature range, although the experimental data of Titani (4-132) indicate that the viscosities of isobutane and *n*-butane become identical for temperatures above 212°F. Recent studies indicate that the viscosities of the *n*-paraffins are from 0 to 5 per cent lower than those of the corresponding branched isomers (4-136) over the temperature range of Fig. 4-97. The similarity in viscosity of the isomers lends support to the conclusion that "the molecules of the *n*-paraffins must, on average, be highly coiled in the gas phase" (4-136).

Correlation of Low-pressure Viscosities

Bicher and Katz (4-101) presented a plot of the viscosity of paraffin gases at 1 atm as a function of molecular weight. This plot was revised slightly by Carr, Kobayashi, and Burrows (Fig. 4-98).

Table 4-22. References for Experimental Viscosity Data at 1 Atm

Gas	Investigator	Reference
Helium	Onnes and Weber	4-121
Air	Johnston and McCloskey	4-114
Nitrogen	Johnston and McCloskey	4-114
Carbon dioxide	Johnston and McCloskey	4-114
Hydrogen sulfide	Rankine and Smith	4-124
Methane	Trautz and Sorg	4-133
Ethylene	Trautz and Stauf	4-135
Ethane	Trautz and Sorg	4-133
Propane	Trautz and Kurz	4-134
	Titani	4-132
Isobutane	Titani	4-132
n-Butane	Titani	4-132
n-Pentane	Titani	4-132
n-Hexane	Titani	4-132
n-Heptane	Melaven and Mack	4-116a
n-Octane	Melaven and Mack	4-116a
n-Nonane	Melaven and Mack	4-116a

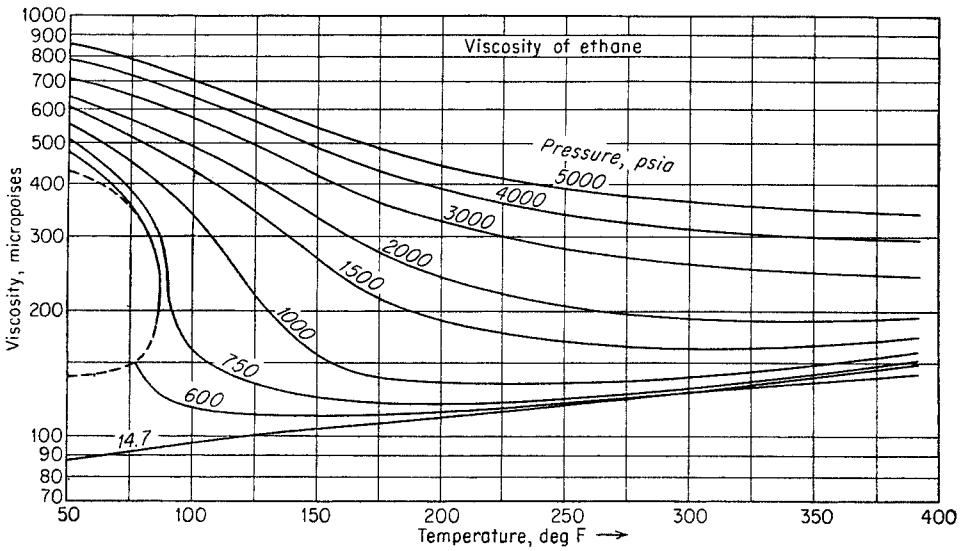

Fig. 4-96. Viscosity of ethane. (*Data of Smith and Brown*, 4-130.)

The prediction of the viscosities of complex hydrocarbon mixtures under pressure is dependent on the prediction of the viscosities of mixtures at 1 atm. Methods of predicting the viscosities of gaseous mixtures at 1 atm that apply to hydrocarbons have been presented by Bicher and Katz (4-101), Herning and Zipperer (4-111), and by Hirschfelder et al. (4-39). The last is based on the theoretical work of Chapman and Cowling (4-24). The calculations are quite involved and not generally suited to routine engineering calculations for mixtures. The computational methods of Hirschfelder et al. have been adapted to graphical and nomographical solutions by Bromley and Wilke (4-103).

Herning and Zipperer (4-111) proposed the following rule to calculate the viscosity of a mixture of gaseous components:

$$\mu_m = \frac{\sum_{i=1}^{n} \mu_i x_i \sqrt{M_i}}{\sum_{i=1}^{n} x_i \sqrt{M_i}} \qquad (4\text{-}49)$$

where μ_m = viscosity of mixture
μ_i = viscosity of component i
x_i = mole fraction of i
M_i = molecular weight of component i

Equation (4-49) affords a simple and reliable means for calculating the viscosity of natural gas mixtures whose analyses are known. The application of Eq. (4-49) to both binary and complex mixtures encountered in natural gases has been verified by Carr (4-104, 4-105) and by Carr, Burrows, and Kobayashi (4-106). Figure 4-98 is recommended for predicting the viscosity of gases *composed primarily of hydrocarbons*. It provides a rapid and reliable method for obtaining the viscosity of gases at 1 atm pressure from a knowledge of the gas gravity and temperature alone. Insert plots on Fig. 4-98 show corrections to the hydrocarbon-viscosity value which may be applied to take into account the presence of low concentrations of hydrogen sulfide, nitrogen, and carbon dioxide. The effect of the presence of each of the nonhydro-

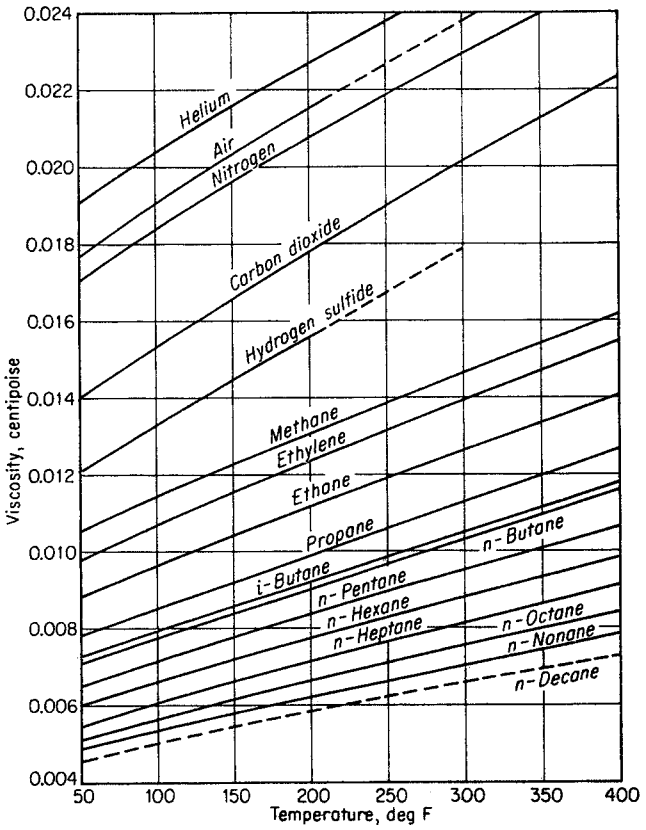

Fig. 4-97. Viscosity of gases at atmospheric pressure. (*Carr, Kobayashi, and Burrows*, 4-106. *Courtesy AIME.*)

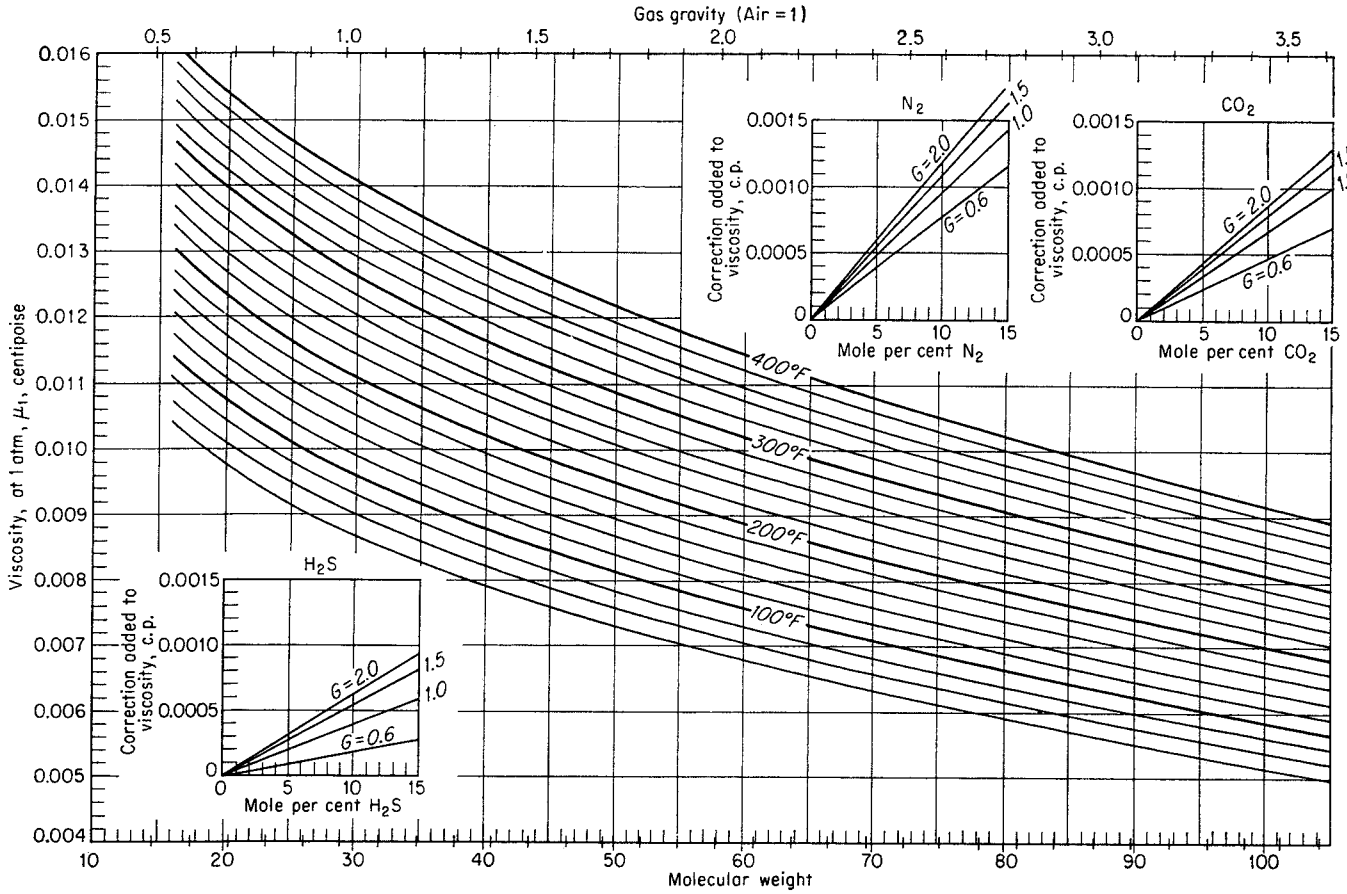

Fig. 4-98. Viscosity of gases at 1 atm pressure. (*Carr, Kobayashi, and Burrows, 4-106. Courtesy AIME.*)

carbons is to increase the viscosity of the hydrocarbon mixture.

Viscosity of Gases under Pressure

The references for viscosities of gases under pressure are given in Table 4-23. The work of Comings, Mayland, and Egly (4-107, 4-108) and of Carr (4-104, 4-105a) shows that the rolling-ball viscosimeter may give viscosities as much as 30 per cent too high. The available data have been correlated, with preference for the data taken on the Rankine viscosimeter (4-124), to give the viscosity of methane (Fig. 4-99) and of propane (Fig. 4-100). Figure 4-101 gives the data of Comings, Mayland, and Egly for ethylene (4-108).

As early as 1894, Onnes and deHaas (4-120, 4-121) recognized that the viscosities of homologues under corresponding states could be correlated. The theorem of corresponding states has been further developed and applied to nonpolar gases by several authors (4-130, 4-108, 4-106, 4-100, 4-107, 4-137). Only one of these correlations will be presented here.

Figures 4-102 and 4-103 present the gas-viscosity correlation of Carr (4-104, 4-105) based on the original correlation of Comings, Mayland, and Egly (4-108) for pure, nonpolar gases. Carr et al. extended the correlation of Comings et al. to higher pressures and to complex mixtures of nonpolar gases (4-104, 4-105, 4-105a). The ratio μ/μ_1 of the viscosity at high pressure to the viscosity at 1 atm is shown as a function of the reduced pressure P_R and of the reduced temperature T_R.

Here $T_R = \dfrac{\text{temperature, absolute scale}}{\text{critical temperature, absolute scale}}$

$P_R = \dfrac{\text{pressure, absolute scale}}{\text{critical pressure, absolute scale}}$

μ = viscosity of gas at reduced temperature T_R and reduced pressure P_R

μ_1 = viscosity of gas at temperature T_R and atmospheric pressure

When mixtures are involved, the pseudocritical pressures and temperatures of typical natural gases may be estimated from gas gravity alone from Fig. 4-22, which is based on typical natural gases.

The correlation of Uyehara and Watson (4-137) relates the reduced viscosity $\mu_R = \mu/\mu_c$ by graphical means, using the reduced pressure and reduced temperature as variables. A method is provided for predicting the critical viscosity μ_c for pure components, and a combination rule for mixtures is suggested.

Grunberg and Nissam (4-110) have developed a similar correlation, which is designed specifically to predict viscosities of pure substances in the critical region. Smith and Brown (4-130) and Bicher and Katz (4-100) show the absolute viscosity as a function of reduced pressure, reduced temperature, and molecular weight.

The viscosity ratio μ/μ_1 has been successfully calculated by the application of the Beattie-Bridgeman (4-7) and the Benedict-Webb-Rubin (4-10) equations of state to the "kinetic pressure" analogy (4-102, 4-104). This analogy states that

$$\frac{\mu}{\mu_1} = \frac{P_k}{P_i} \tag{4-50}$$

where P_k = kinetic pressure, or the time rate of transfer of momentum across an imaginary plane-unit surface in the interior of the gas

P_i = ideal-gas pressure corresponding to the ideal-gas volume

Figure 4-104 gives a comparison of the experimental viscosities with those computed by application of the kinetic-pressure terms of the Benedict-Webb-Rubin equation to calculate P_k in Eq. (4-50).

Carr (4-105) reported the viscosity of three natural gases to 10,000 psia at two temperatures (Fig. 4-105). Table 4-24 gives the compositions of the gases.

Correlations of the viscosity for natural gases are given in Fig. 4-106 at temperatures of 60, 100, 200, 300, and 400°F for gases of different gravity. The viscosities as a function of tenperature and pressure for gases of 0.6, 0.7, 0.8, and 1.0 gravity are given in Fig. 4-107. Both of these figures are based on Figs. 4-102 and 4-103. These figures may be used for gases with the pseudocritical–gas gravity relationships of Fig. 4-22, miscellaneous gases.

For gases with appreciable concentrations of nitrogen, carbon dioxide, or hydrogen sulfide, the pseudocritical conditions may be computed from compositions and viscosities obtained from Figs. 4-102 and 4-103. When gas gravity and concentration of the nonhydrocarbon constituent are known, the corrections to pseudocritical pressures and temperatures, as read from Fig. 4-22, can be made, using Fig. 4-108 (4-106), before using Fig. 4-102 or 4-103.

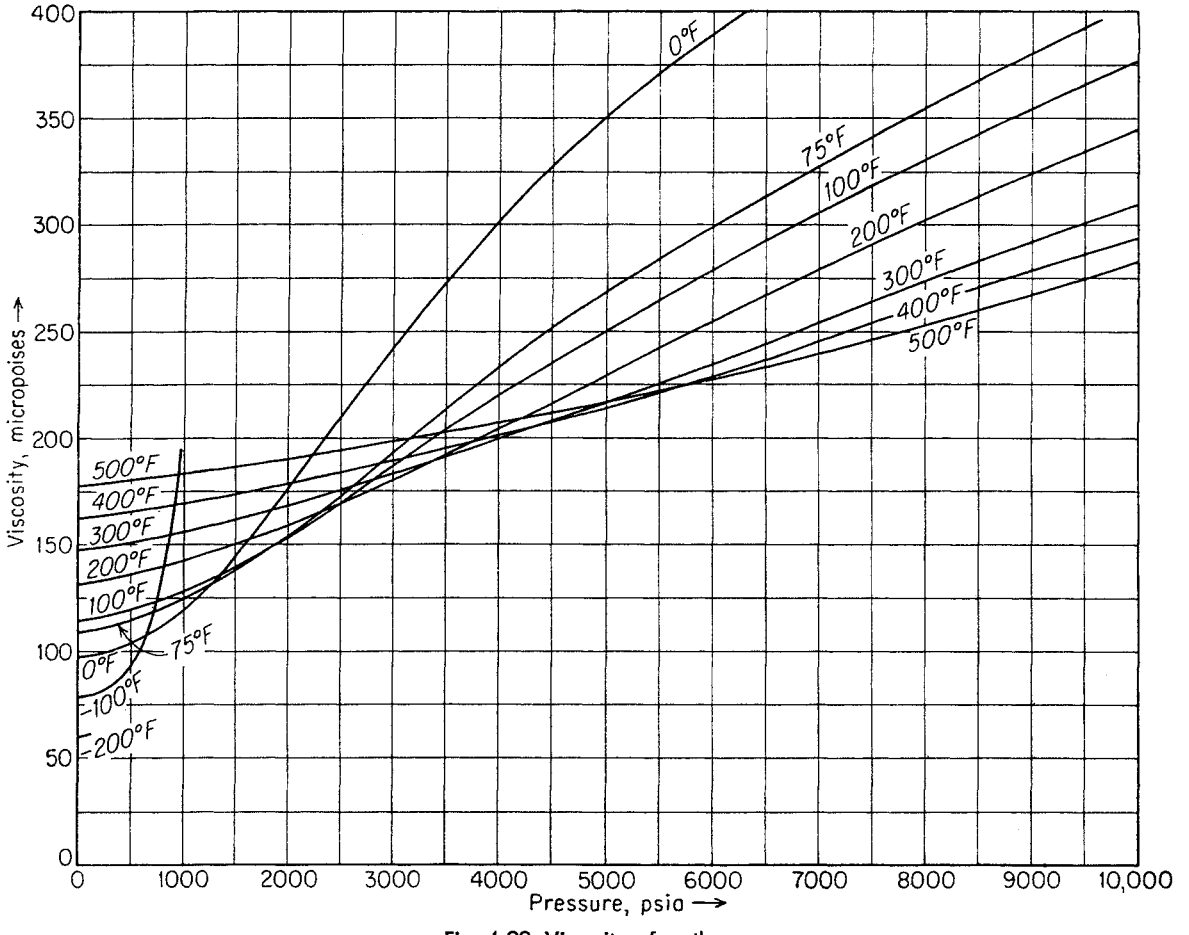

Fig. 4-99. Viscosity of methane.

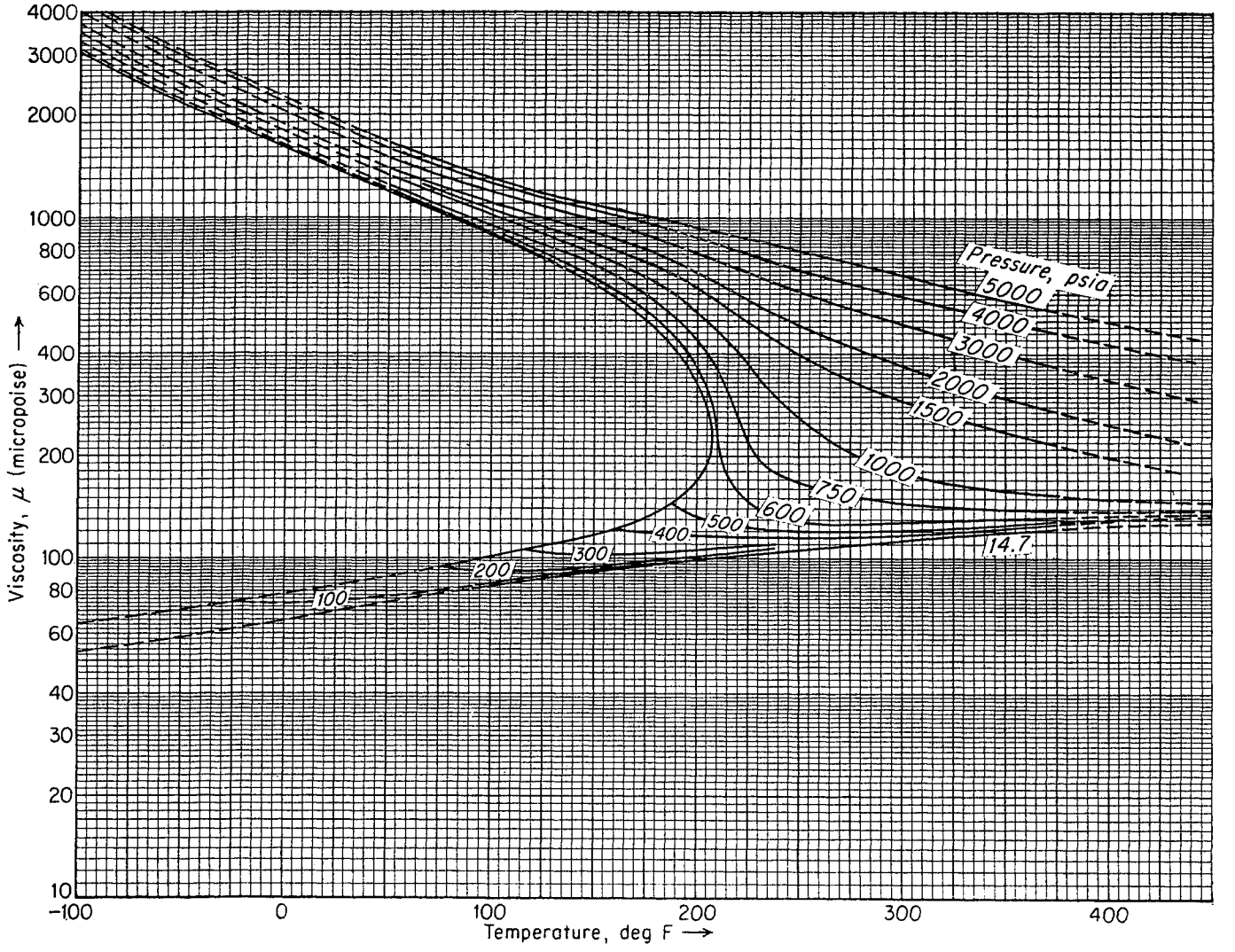

Fig. 4-100. Viscosity of propane.

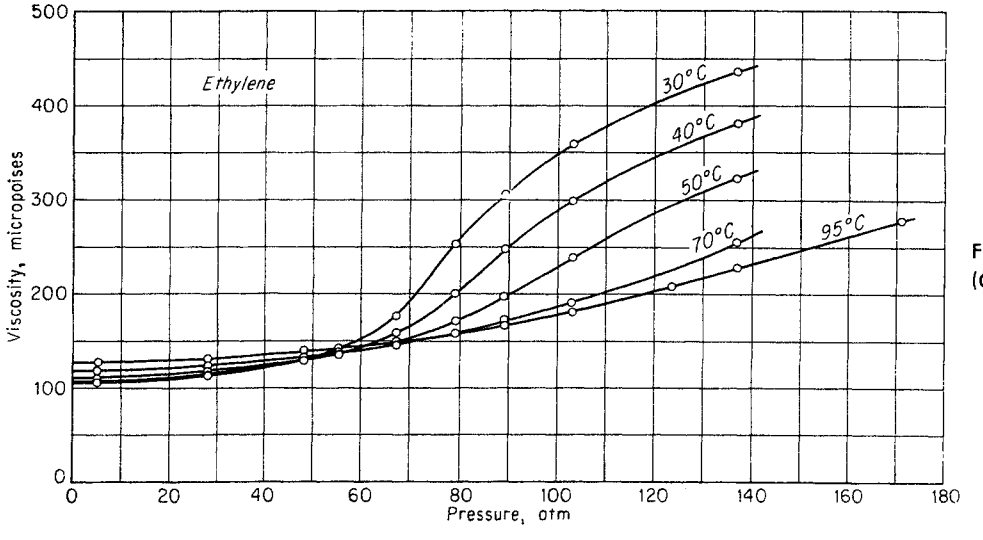

Fig. 4-101. Viscosity of ethylene. (*Comings, Mayland, and Egly*, 4-108.)

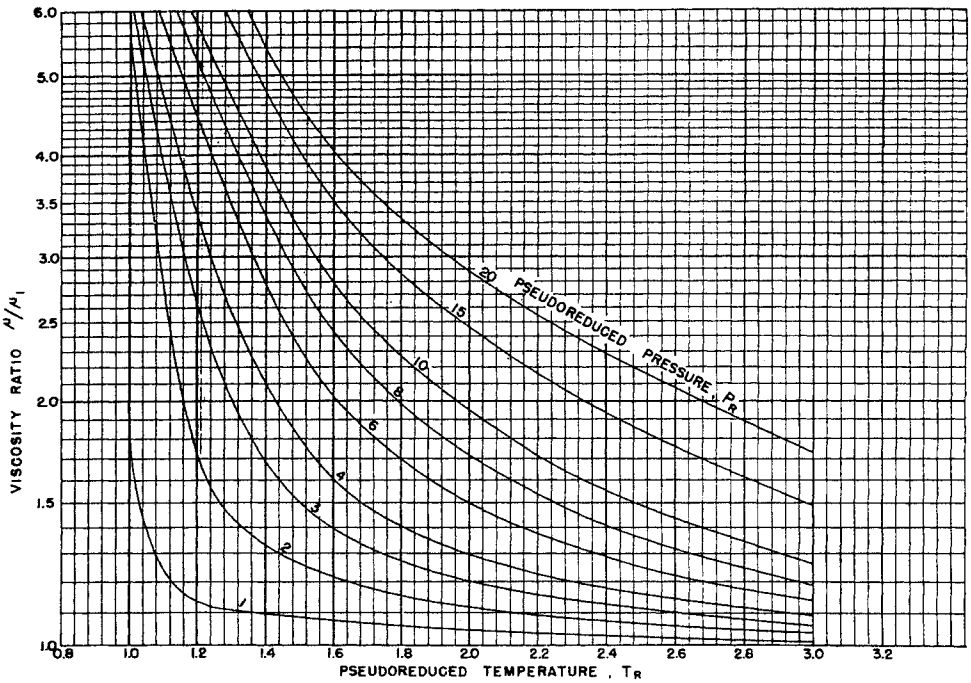

Fig. 4-102. Correlation of viscosity ratio with reduced temperature. (*Carr*, 4-106. *Courtesy AIME.*)

Table 4-23. References for Experimental Viscosity Data on Gases at High Pressure

Gas	Investigator	Method used	Reference
Nitrogen	Boyd	Capillary	4-102
	Michels and Gibson*	Capillary	4-117
Carbon dioxide	Phillips*	Capillary	4-122
	Stakelbeck*	Falling body	4-131
	Schroer and Becker	Falling body	4-129
	Naldrett and Maass	Oscillating disk	4-118
	Comings, Mayland, and Egly*	Capillary	4-108
Methane	Sage and Lacey	Rolling ball	4-127
	Bicher and Katz	Rolling ball	4-100
	Comings, Mayland, and Egly*	Capillary	4-108
	Carr*	Capillary	4-105
Ethylene	Mason and Maass	Oscillating disk	4-116
	Comings, Mayland, and Egly*	Capillary	4-108
Ethane	Smith and Brown	Rolling ball	4-130
Propane	Sage and Lacey	Rolling ball	4-128
	Smith and Brown	Rolling ball	4-130
	Bicher and Katz	Rolling ball	4-100
	Comings, Mayland, and Egly*	Capillary	4-108
Isobutane	Sage, Yale, and Lacey	Rolling ball	4-126
n-Butane	Sage, Yale, and Lacey	Rolling ball	4-126
Methane-propane	Bicher and Katz	Rolling ball	4-100
Natural gas	Sage and Lacey	Rolling ball	4-127
High-nitrogen-content natural gas	Carr*	Capillary	4-105
Low-ethane-content natural gas	Carr*	Capillary	4-105
High-ethane-content natural gas	Carr*	Capillary	4-105

* Data used in generalized correlation (Figs. 4-102, 4-103).

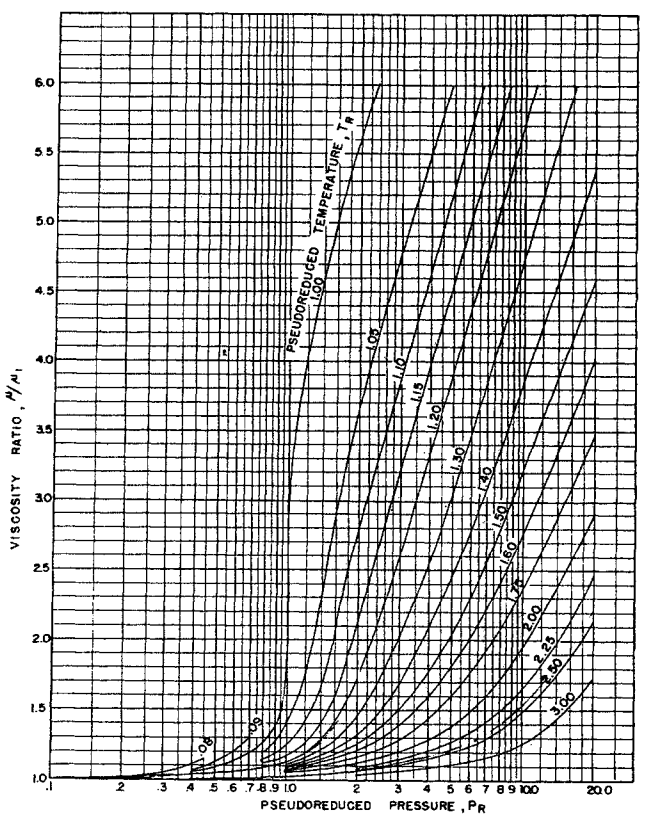

Fig. 4-103. Correlation of viscosity ratio with reduced pressure. (*Carr, Kobayashi, and Burrows*, 4-106. *Courtesy AIME.*)

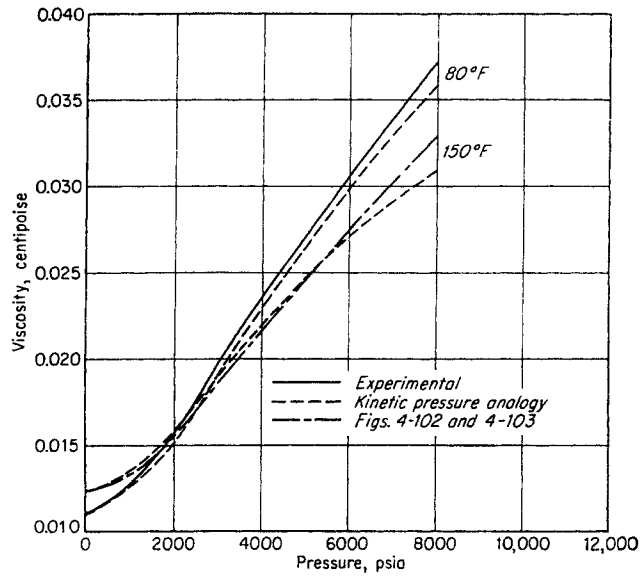

Fig. 4-104. Comparison of experimental viscosities of methane with kinetic-theory calculations. (Carr, Kobayashi, and Burrows, 4-106. Courtesy AIME.)

Illustrative Problem

Find the viscosity of a natural gas of 0.702 gravity at 195°F and 1,815 psia.

Solution

Using pseudocritical properties from Fig. 4-22,

Pseudocritical pressure = 667 psia

$$P_R = {}^{1815}\!/_{667} = 2.72$$

Pseudocritical temperature = 390°R

$$T_R = \frac{460 + 195}{390} = 1.68$$

From Fig. 4-103,

$$\mu/\mu_1 = 1.28$$

From Fig. 4-97,

For 0.702 gravity $\mu_1 = 0.0122$ centipoise

At 195°F and 1,815 psia, $\mu = 0.0122 \times 1.28 = 0.0156$ centipoise.

From Fig. 4-107,

Chart reads directly 0.0155 centipoise for 0.7 gravity gas.

From Fig. 4-106,

At 200°F and 1,815 psia, $\mu = 0.0157$.

At 100°F and 1,815 psia, $\mu = 0.0163$.

By interpolation,

At 195°F and 1,815 psia, $\mu = 0.0158$ centipoise.

Viscosity of Liquids

Liquids decrease in viscosity with increased temperature and increase in viscosity with increased pressure. Figure 4-109 shows the viscosities of pure con-

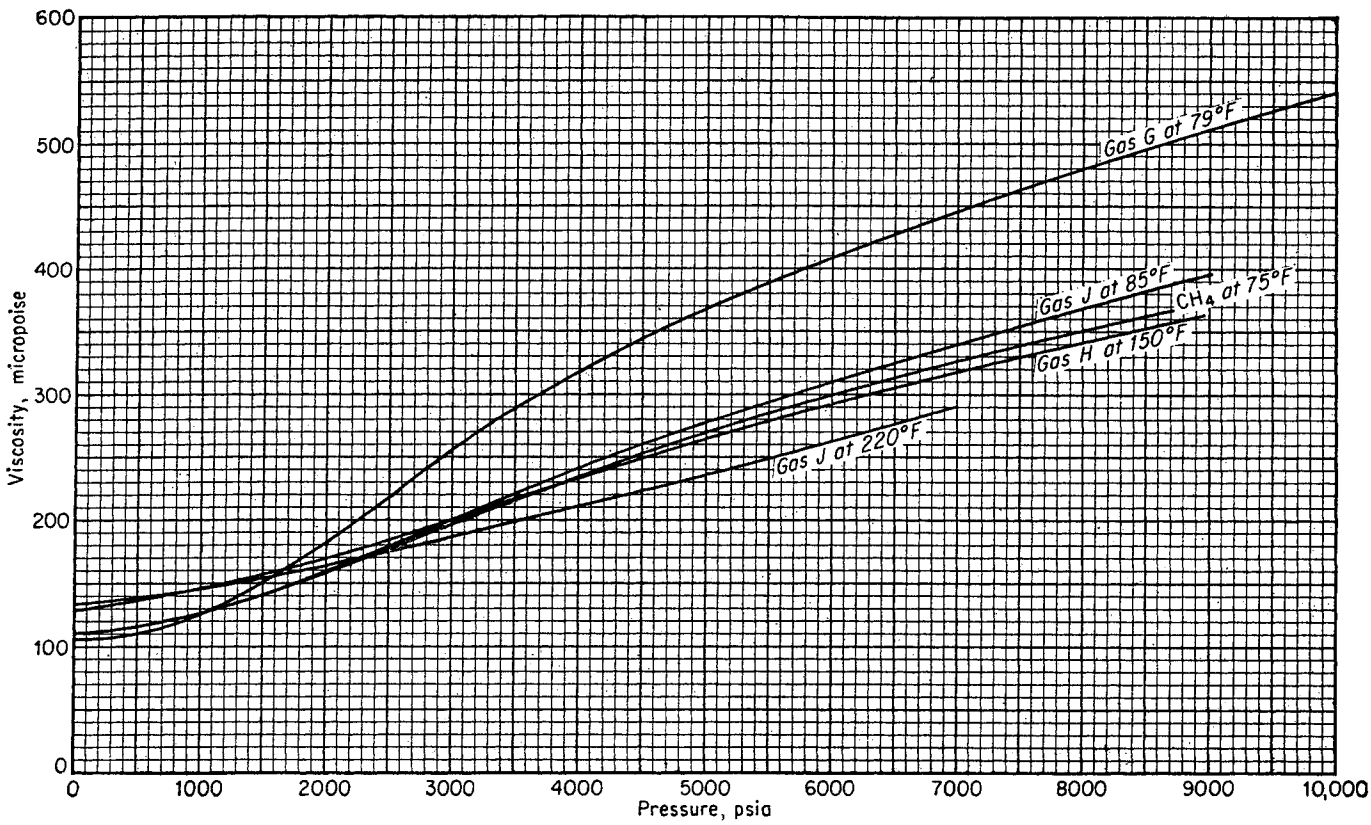

Fig. 4-105. Viscosity data on natural gases. (Data of Carr, 4-105.)

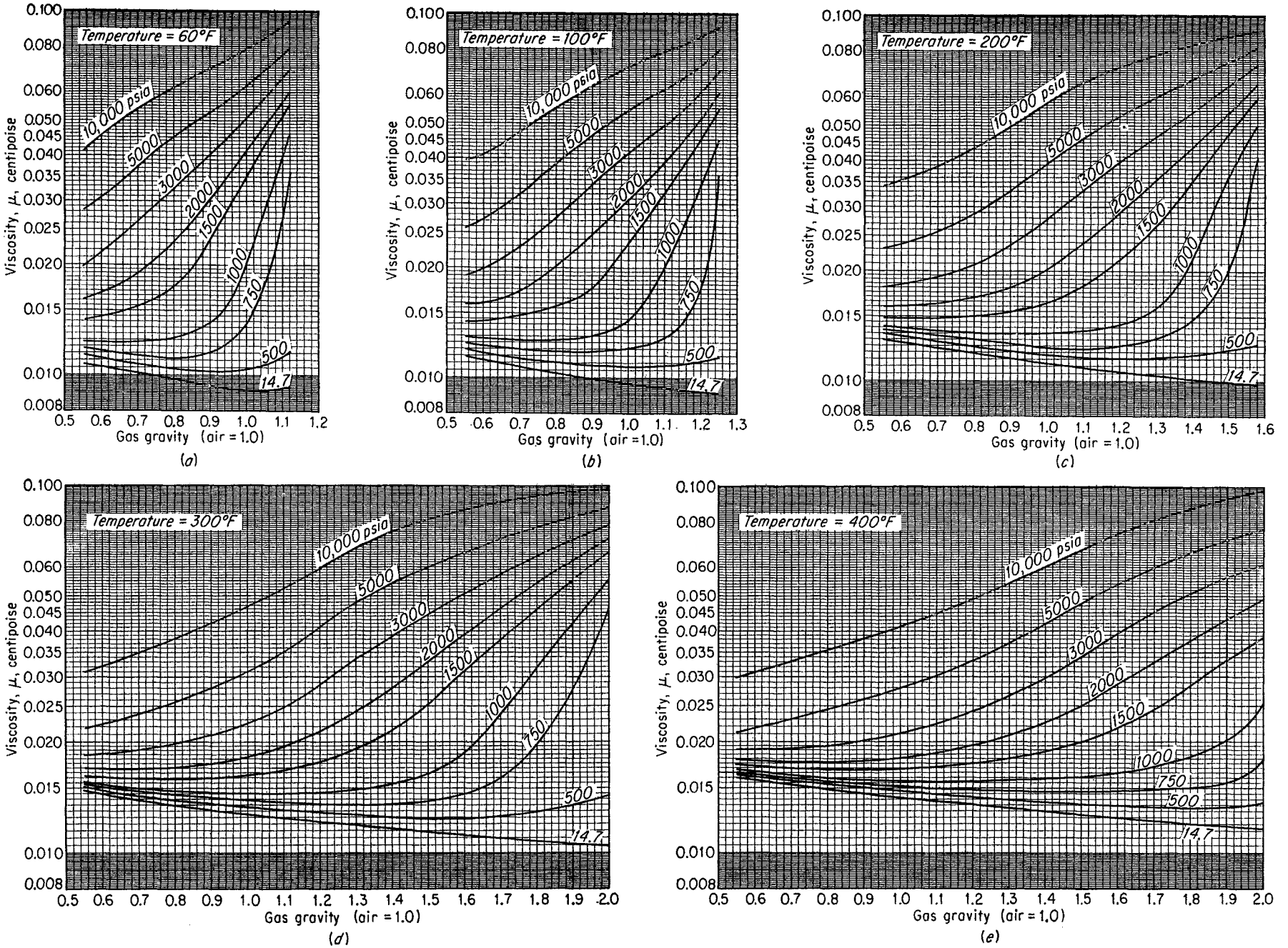

Fig. 4-106. Viscosity of natural gases. (a) 60°F. (b) 100°F. (c) 200°F. (d) 300°F. (e) 400°F.

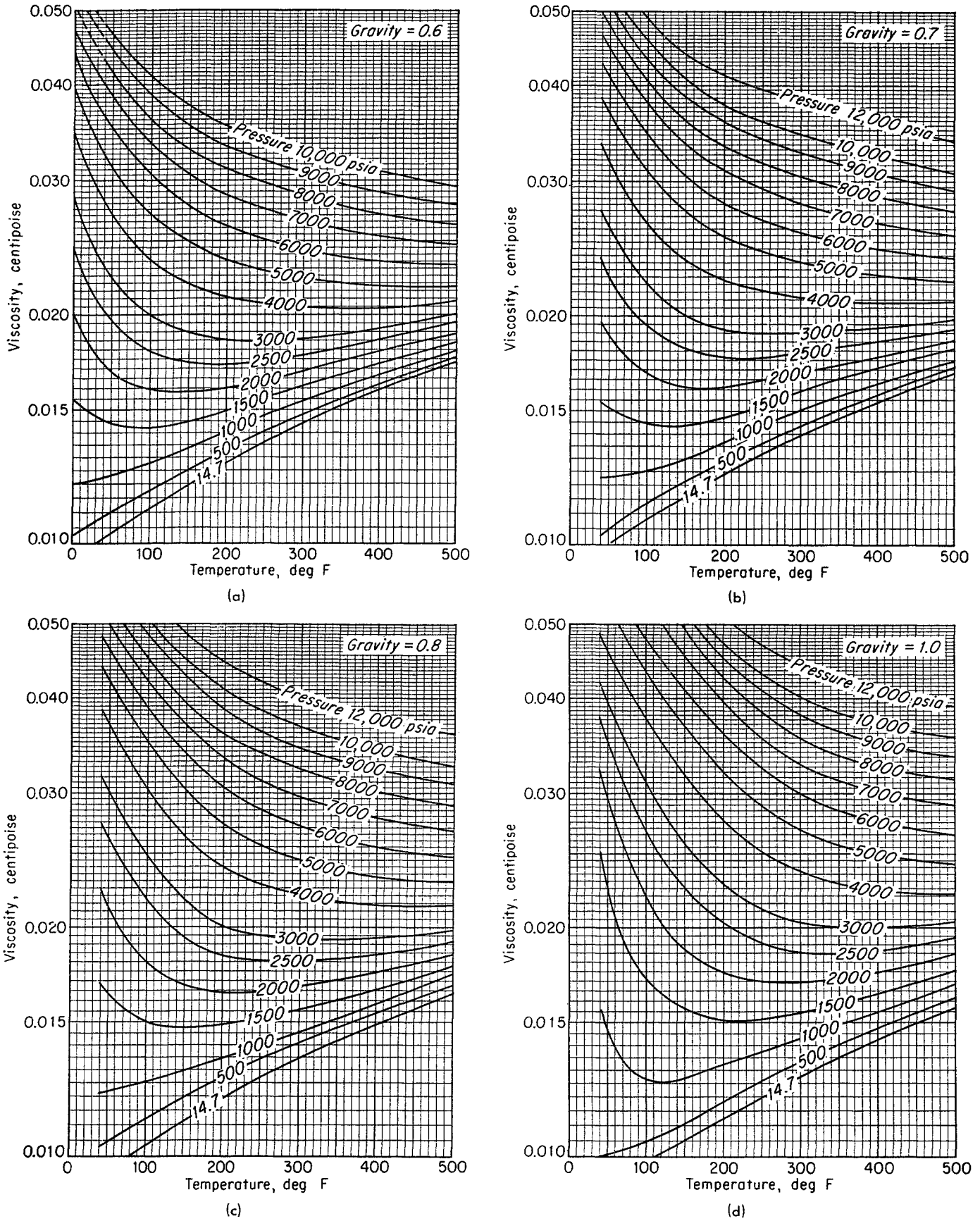

Fig. 4-107. Viscosity of natural gases. (a) 0.6 gravity. (b) 0.7 gravity. (c) 0.8 gravity. (d) 1.0 gravity. (2-42.)

Table 4-24. Composition of Natural Gases Used for Viscosity Measurements of Fig. 4-105

Natural Gas *G*		Natural Gas *H*		Natural Gas *J*	
Gas	*Mole %*	*Gas*	*Mole %*	*Gas*	*Mole %*
Methane	73.5	Methane	73.1	Methane	95.6
Ethane	25.7	Ethane	6.1	Ethane	3.6
Nitrogen	0.6	Nitrogen	15.8	Nitrogen	0.3
Propane	0.2	Propane	3.4	Propane	0.5
		Helium	0.8		
		n-Butane	0.6		
		Isobutane	0.2		

SOURCE: Carr (4-105).

stituents plotted from the values correlated by the API (1-15). Hocott and Buckley (4-112) presented measurements of the viscosity of crude oils containing dissolved gases (Fig. 4-110). The analyses of the four saturated oils are given in Table 4-25. Sage and Lacey (4-125, 4-126, 4-128) and others (4-138a) have measured the viscosity of liquids under pressure.

Beal presented correlations of viscosity data on crude oils. Figure 4-111 is a plot of viscosity of gas-free crude oils against gravity, and Fig. 4-112 shows the influence of dissolved gas on viscosity. When pressure is increased on the reservoir oil into the undersaturated zone, Fig. 4-113 gives the increase in viscosity of the constant-composition liquid per 1,000 psia of pressure increase.

Sometimes viscosities of oils are given as Saybolt seconds at a given temperature. These viscosities are kinematic values and may be converted to centistokes using Table 4-26 (4-2). The kinematic viscosity in centistokes times the density in grams per cubic centimeter gives the viscosity in centipoises.

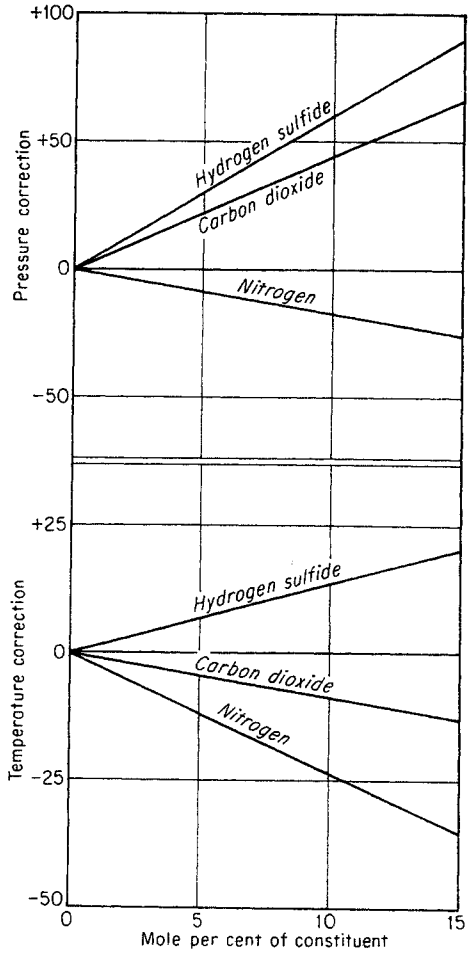

Fig. 4-108. Corrections to pseudocritical conditions as read from Fig. 4-22, to be used when finding viscosity of gases containing N_2, CO_2, and H_2S.

Table 4-25. Hydrocarbon Analyses of Subsurface Oil Samples

Component	Viscosity curve *D*			Viscosity curve *C*			Viscosity curve *B*			Viscosity curve *A*		
	Wt %	Sp gr	Mol. wt	Wt %	Sp gr	Mol. wt	Wt %	Sp gr	Mol. wt	Wt %	Sp gr	Mol. wt
Methane	7.93	.....	...	1.50	.....	...	4.38	.....	...	0.83		
Ethane	1.65	.....	...	0.93	.....	...	1.05	.....	...	1.41		
Propane	1.80	.....	...	3.42	.....	...	0.35	.....	...	0.71		
Isobutane	0.84	.....	...	0.83	.....	...	0.11	.....	...	0.47		
n-Butane	1.42	.....	...	3.51	.....	...	.....	.....	...	0.92		
Isopentane	1.07	.....	...	1.40	.....	...	0.05	.....	...	1.17		
n-Pentane	1.23	.....	...	2.24	.....	...	.....	.....	...	0.28		
Hexanes	3.64	.....	...	4.02	.....	...	0.34	.....	...	1.64		
Heavier fraction	80.42	0.8076	147	82.15	0.8418	215	93.72	0.8974	250	92.57	0.8896	229
	100.00	.....	...	100.00	.....	...	100.00	.....	...	100.00		
	Viscosity oil at 0 psig, 158°F = 0.950 centipoise			Viscosity oil at 0 psig, 128°F = 1.84 centipoises			Viscosity oil at 0 psig, 164°F = 5.4 centipoises			Viscosity oil at 0 psig, 100°F = 8.25 centipoises		

SOURCE: Hocott and Buckley.

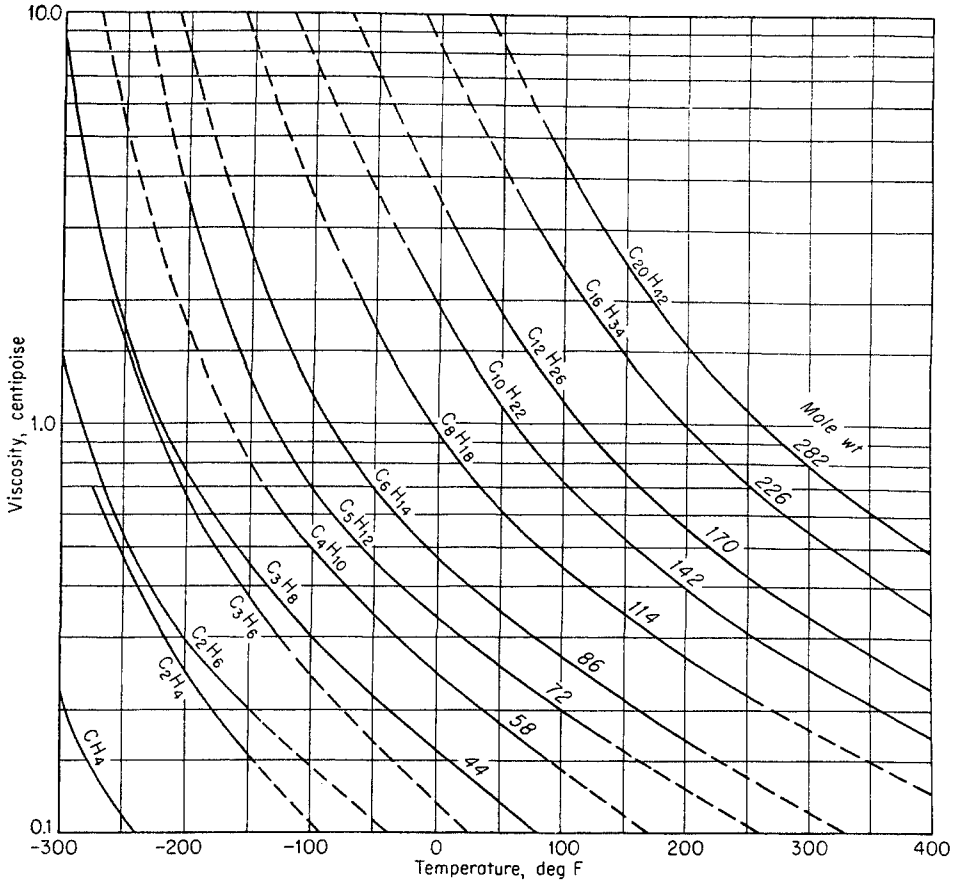

Fig. 4-109. Viscosity of hydrocarbon liquids. (*Data of Rossini et al.*, 1-15.)

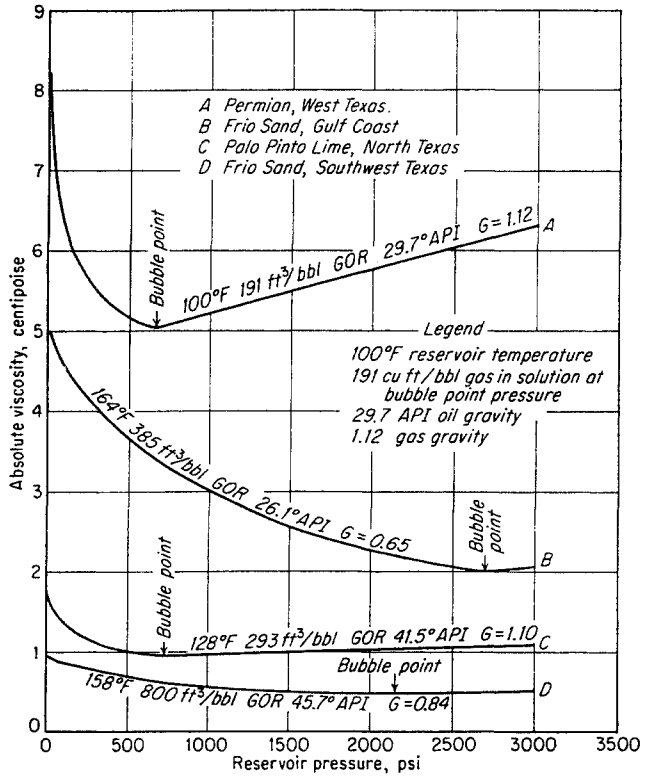

Fig. 4-110. Viscosity of subsurface samples of crude oil. (*Hocott and Buckley*, 4-112. *After Beal*, 4-99. *Courtesy AIME.*)

Table 4-26. Conversion of Saybolt Universal Viscosity to Kinematic Viscosity

Kinematic viscosity, centistokes	Equivalent Saybolt universal viscosity, sec	
	At 100°F	At 210°F
2	32.6	32.9
3	36.0	36.3
4	39.1	39.4
5	42.4	42.7
6	45.6	45.9
7	48.8	49.1
8	52.1	52.5
9	55.5	55.9
10	58.9	59.3
15	77.4	77.9
20	97.8	98.5
25	119.3	120.1
30	141.3	142.3
35	163.7	164.9
40	186.3	187.6
45	209.1	210.5
50	232.1	233.8

SOURCE: ASTM D 446-53 (Abridged).

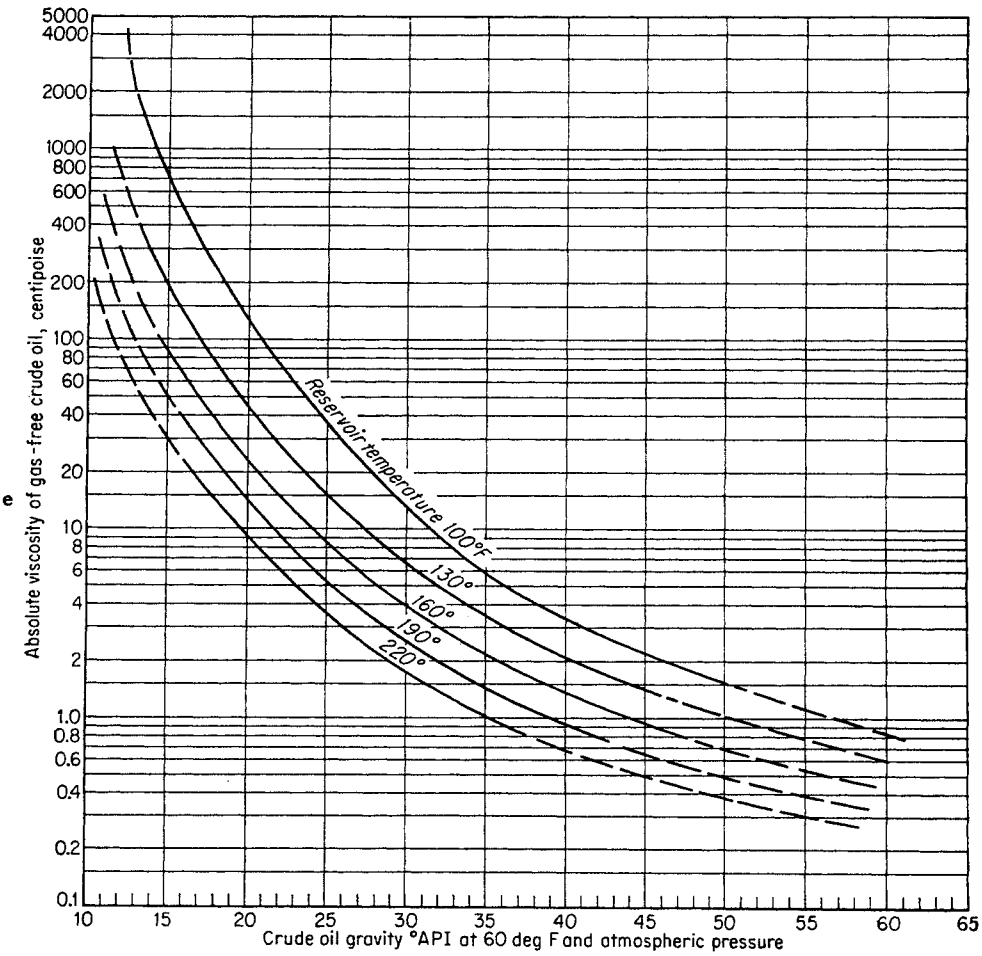

Fig. 4-111. Viscosity of gas-free crude oils. (*Beal*, 4-99. *Courtesy AIME.*)

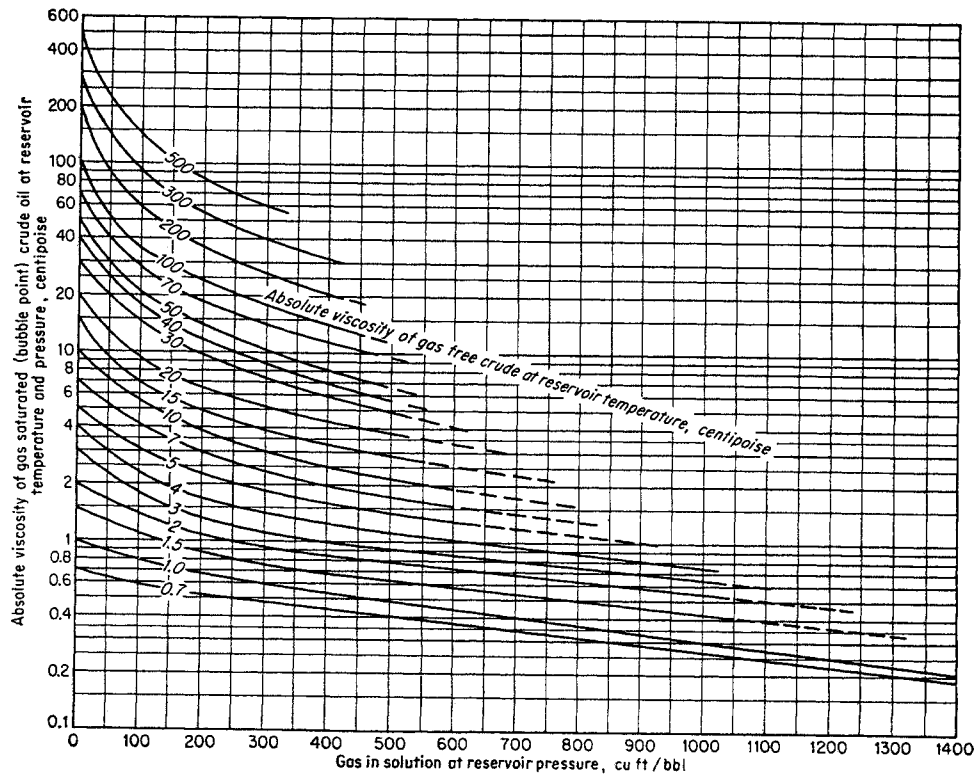

Fig. 4-112. Effect of dissolved gas on reservoir-oil viscosity. (*Beal*, 4-99. *Courtesy AIME.*)

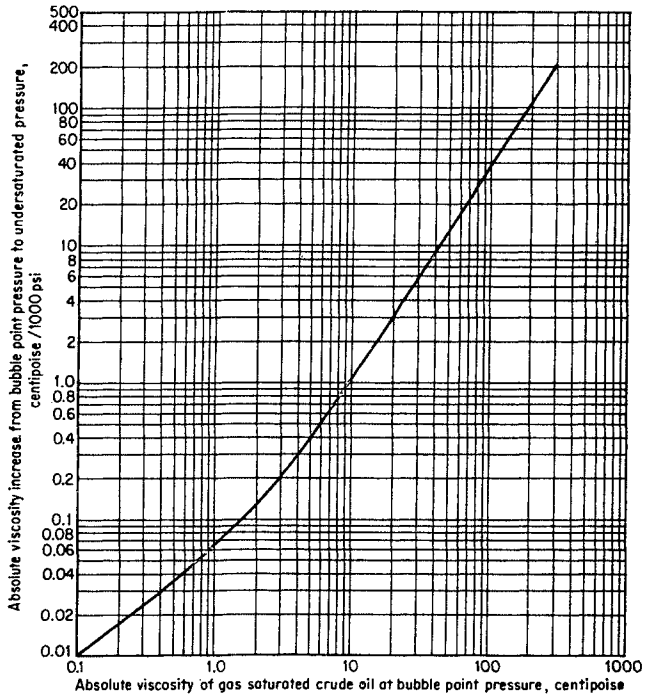

Fig. 4-113. Effect of pressure on viscosity for reservoir oils at constant composition and temperature. (*Beal*, 4-99. *Courtesy AIME.*)

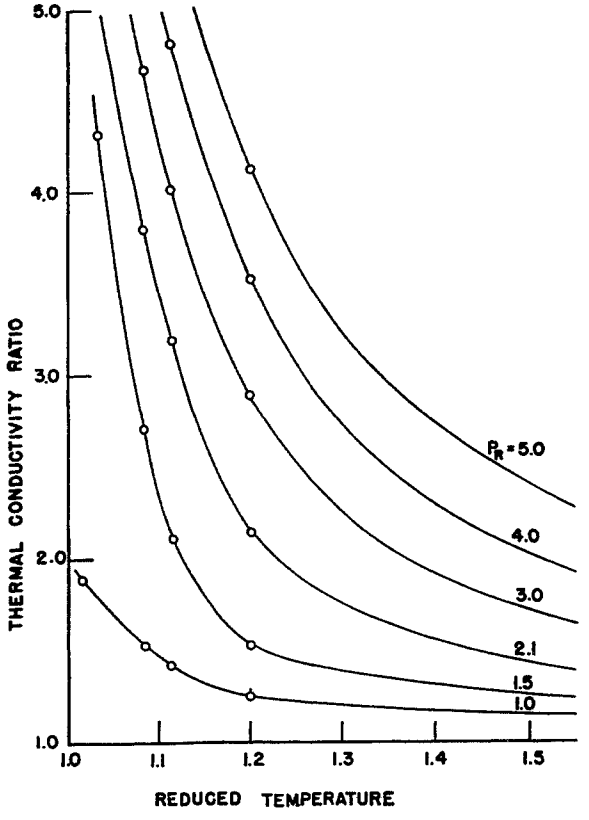

Fig. 4-114. Thermal-conductivity ratio vs. reduced temperature. (*Lenoir, Junk, and Comings*, 4-167. *Courtesy AIChE.*)

THERMAL CONDUCTIVITY OF GASES

Thermal conductivity is the fundamental property of substances that governs the rate of transfer of heat by conduction. Thermal conductivity is defined by Fourier's relation, which was first formulated for solids:

$$\frac{dQ}{dt} = -kA\frac{dT}{dx} \qquad (4\text{-}51)$$

where k = thermal conductivity of the substance, Btu/(hr)(sq ft)(°F/ft)
A = area at right angles to the direction of heat flow, sq ft
x = distance, ft
dQ/dt = heat transferred by the mechanism of conduction alone, Btu/hr
T = temperature, °F

This section presents correlations for the prediction of the effect of pressure and temperature on the thermal conductivity of pure gases. Tentative correlations are recommended for predicting the thermal conductivity of mixtures, although no experimental data on natural gas mixtures are available to substantiate the correlations. Only limited experimental thermal-conductivity data for pure components commonly found in natural gases are available.

Experimental Data

Experimental determinations of thermal conductivities involve measurements of heat flux, lengths, and temperatures, and the application of some form of Eq. (4-51). The most common procedure is the Schleiermacher "hot-wire method" (4-175) in which a measured quantity of heat energy is generated by the passage of electric current through a wire stretched along the axis of a cylindrical tube. The gas whose thermal conductivity is to be measured is placed in the annulus between the wire and the inside walls of the confining tube.

Table 4-27 gives a list of references for thermal conductivity of pure hydrocarbons, nitrogen, carbon dioxide, and ethylene at 1 atm. Table 4-28 gives references for data on the same gases at high pressures.

Thermal Conductivity of Compressed Gases

The effect of pressure on the thermal conductivity of gases has been predicted by Enskog (4-145). Comings and Nathan (4-140) computed the thermal conductivity of pure gases at high pressures by applying known gas-viscosity and density data to the Enskog relations. Later Lenoir, Junk, and Comings (4-167) measured and correlated the effect of pressure and temperature on the thermal conductivity of pure non-

polar gases. The correlation of thermal-conductivity ratio and its cross plot are presented in Figs. 4-114 and 4-115. The experimental data used in the correlation are essentially those corresponding to the references of Table 4-28. The thermal-conductivity ratio is defined as the ratio of the thermal conductivity for a given temperature at high pressure to the thermal conductivity for the same temperature at 1 atm.

Gamson (4-149) plotted the reduced thermal conductivity for the gas state as a function of reduced temperature and reduced pressure. The reduced thermal conductivity is defined as the ratio of the thermal conductivity at a particular pressure and temperature to the thermal conductivity at the critical conditions. For mixtures, the molal-average values of critical pressures, temperatures, and thermal conductivities of the components comprising the mixture are used.

Some work has been done on the thermal conductivity of mixtures at high pressures. Figures 4-116 and 4-117 present the thermal conductivity of nitrogen-ethylene and carbon dioxide–ethylene systems at 107.7°F for various pressures (4-157). These data, compared with the values from the general correlation, indicate that the thermal conductivity of mixtures cannot be predicted with the same degree of accuracy as gas viscosity. Lenoir, Junk, and Comings (4-167) found that the correlation presented in Figs. 4-114 and 4-115 predicted the thermal conductivity of nitrogen-ethylene mixtures with an average deviation of 5 per cent, but resulted in an average deviation of 36 per cent for the carbon dioxide–ethylene mixtures.

Another discrepancy of the correlation presented should be mentioned. Experimental thermal-conductivity ratios for ethane reported by Lenoir, Junk, and Comings (4-167) are found to be about 30 per cent lower than the correlation. On the other hand, the thermal conductivity of ethylene correlates with other gases cited in Table 4-28.

Possible reasons for the inadequacy of reduced pressure and temperature as correlating parameters are discussed from the standpoint of kinetic theory by Lenoir, Junk, and Comings (4-167), Pidduck (4-172), and Eucken (4-147). Although the correlation presented here and the correlation of Gamson (4-149) have not succeeded in correlating all nonpolar gases (viz., ethane) and gas mixtures (viz., carbon dioxide–ethylene), they provide the only practical means of predicting the effect of pressure on the thermal conductivity of dense gases at the present time.

The reduced-pressure and reduced-temperature parameters are computed in accordance with the definitions provided in the previous section on gas viscosities.

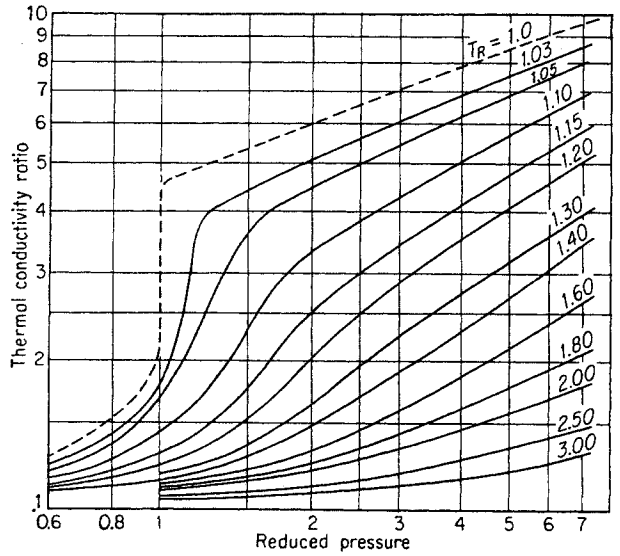

Fig. 4-115. Correlation of thermal-conductivity ratio. (*Lenoir, Junk, and Comings, 4-167. Courtesy AIChE.*)

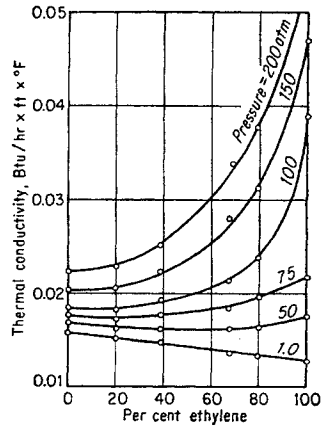

Fig. 4-116. Thermal conductivity of N_2-C_2H_4 mixtures. (*Junk and Comings, 4-157. Courtesy AIChE.*)

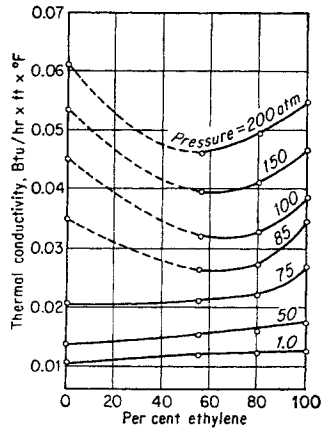

Fig. 4-117. Thermal conductivity of CO_2-C_2H_4 mixtures. (*Junk and Comings, 4-157. Courtesy AIChE.*)

Table 4-27. References for Experimental Data on Thermal Conductivity of Gases at 1 Atm

Gas	Investigator and year	Experimental temperature, °F	k_0* × 10^5	Reference
Methane	Stefan (1875)	32	.....	4-181
	Winkelmann (1875)	32	6.89	4-191
	Winkelmann (1891)	45	.....	4-192
	Ziegler (1904)	32 to 212	7.493	4-194
	Eucken (1913)	−295, −104, and +32	7.145	4-147
	Moser (1913)	32	7.145	4-171
	Weber (1917)	32	7.200	4-189
	Mann and Dickins (1932)	32 to 50	7.210	4-169
	Trautz and Zündel (1933)	32	7.205	4-186
	Johnston and Grilly (1946)	−285 to +230	7.336	4-156
	Lenoir and Comings (1951)	106	.....	4-166
	Schottky (1952)	212 to 932	.....	4-176
	Lenoir, Junk, and Comings (1953)	127	.....	4-167
	Keyes (1954)	122, 302, 482, and 572	.....	4-161
Ethane	Ziegler (1904)	32 to 212	4.981	4-194
	Eucken (1913)	−95, −36, and +32	4.260	4-147
	Moser (1913)	32 and 212	4.306	4-171
	Mann and Dickins (1932)	32 to 50	4.360	4-169
	Lenoir, Junk, and Comings (1953)	107, 134, and 153	.....	4-167
	Keyes (1954)	125	.....	4-161
Propane	Mann and Dickins (1932)	32 to 50	3.600	4-169
	Trautz and Zündel (1933)	32	3.549	4-186
n-Butane	Mann and Dickins (1932)	32 to 50	3.220	4-169
n-Pentane	Moser (1913)	32 and 68	2.933	4-171
	Mann and Dickins (1932)	32	3.120	4-169
n-Hexane	Moser (1913)	32 and 68	2.604	4-171
	Mann and Dickins (1932)	32	2.96	4-169
n-Heptane	Moser (1913)	212	.....	4-171
Isobutane	Mann and Dickins (1932)	32 to 50	3.32	4-169
Isopentane	Moser (1913)	32 to 363	2.912	4-171
Ethylene	Stefan (1875)	32	.....	4-181
	Winkelmann (1875)	32	4.53	4-191
	Wüllner (1878)	32 to 212	.....	4-193
	Eickhorn (1890)	32	.....	4-144
	Krey (1912)	32	4.02	4-163
	Eucken (1913)	−95, −35, and +32	4.07	4-147
	Moser (1913)	32	4.07	4-171
	Lenoir and Comings (1951)	106 and 153	.....	4-166
	Keyes (1954)	162 and 306	.....	4-161
Carbon dioxide	Stefan (1875)	32	.....	4-181
	Kundt and Warburg (1875)	32	.....	4-164
	Winkelmann (1875)	32	3.55	4-191
	Wüllner (1878)	32	.....	4-193
	Graetz (1881)	32	3.091	4-150
	Schleiermacher (1888)	32 to 212	3.27	4-174
	Eickhorn (1890)	32	.....	4-144
	Winkelmann (1891)	32	3.07	4-192
	Echerlein (1900)	−109 to +32	3.434	4-143
	Todd (1910)	131	.....	4-184
	Stafford (1911)	72 to 1015	.....	4-180
	Eucken (1911)	−109, +32, and 212	3.37	4-146
	Moser (1913)	32	3.34	4-171
	Weber (1917)	32	3.393	4-189
	Gregory and Marshall (1927)	32 to 55	3.604	4-151
	Weber (1927)	32	3.44	4-190
	Trautz and Zündel (1933)	32 to 55	3.375	4-186
	Kannuluik and Martin (1934)	32	3.43	4-158
	Archer (1935)	32 to 608	3.47	4-139

Table 4-27. References for Experimental Data on Thermal Conductivity of Gases at 1 Atm (*Continued*)

Gas	Investigator and year	Experimental temperature, °F	k_0* × 10^5	Reference
	Johnston and Grilly (1946)	−125 to +230	3.485	4-156
	Vargaftik and Oleshchuk (1946)	32 to 1112	3.50	4-188
	Stops (1949)	32 to 1832	3.57	4-183
	Lenoir and Comings (1951)	106, 134, and 153	.....	4-166
	Lenoir (1952)	90 to 150	.....	4-165
	Rothman and Bromley (1955)	32 to 1,430	3.50	4-173
Helium.....	Schwarze (1903)	32	33.86	4-177
	Eucken (1913)	−422 to +212	33.60	4-147
	Moser (1913)	32	33.60	4-171
	Weber (1917)	32	34.38	4-189
	Gallo (1921)	32	.....	4-148
	Curie and Lepape (1931)	32	.....	4-141
	Johnston and Grilly (1946)	−315 to +230	33.90	4-156
	Lenoir and Comings (1951)	109	.....	4-166
Nitrogen.....	Winkelmann (1891)	46	.....	4-192
	Günther (1906)	32	5.694	4-153
	Todd (1910)	131	.....	4-184
	Eucken (1911)	−312 to +212	5.68	4-146
	Moser (1913)	32	5.68	4-171
	Weber (1917)	32	5.66	4-189
	Gregory and Marshall (1928)	41 to 55	5.80	4-152
	Dickins (1934)	32	5.81	4-142
	Vargaftik and Oleshchuk (1946)	32 to 112	5.72	4-188
	Stops (1949)	32 to 1832	5.77	4-183
	Keyes and Sandell (1950)	32 to 752	5.816	4-162
	Lenoir and Comings (1951)	106	.....	4-166
	Keyes (1951)	32, 122, and 302	5.74	4-160
	Schottky (1952)	212 to 392	.....	4-176
	Lenoir (1952)	90 to 150	.....	4-165
	Lenoir, Junk, and Comings (1953)	127	.....	4-167
	Rothman and Bromley (1955)	32 to 1430	5.76	4-173

* k_0 = thermal conductivity in cal/(sq cm)(sec)(°C/cm). Thermal conductivity in cal/(sq cm)(sec)(°C/cm) × 242 = Btu/(sq ft)(hr)(°F/ft).

Thermal Conductivity at Low Pressures

Thermal conductivity at low pressures is thermal conductivity in the neighborhood of 1 atm pressure. Only a limited amount of experimental data for pure gases and their mixtures commonly found in natural gases is available. It has, therefore, been necessary to resort to the use of theoretical equations applicable to nonpolar gases. These equations have been inferred to apply to the paraffin hydrocarbon series.

The thermal conductivity of simple gases has been related to the viscosity and to the specific heat at constant volume by Chapman and Cowling (4-24) and by Eucken (4-147). The relation of Chapman and Cowling, which applies to rigid spherical molecules, is

$$k = f\mu C_v \qquad (4\text{-}52)$$

where k = thermal conductivity
f = a pure number, equal to 2.5 for smooth, spherically symmetrical molecules and to 2.522 for rigid elastic spheres
μ = viscosity
C_v = specific heat at constant volume

Equation (4-52) has been applied with fair success to predict the thermal conductivities of simple molecules from gas-viscosity and specific-heat data.

The Eucken equation relating thermal conductivity to viscosity and specific heat (4-155), in its modified form (4-154), is

$$k = \frac{H}{V}\frac{\mu}{M}\left(C_v + \frac{9}{4}R\right) \qquad (4\text{-}53)$$

where k = thermal conductivity, Btu/(hr)(sq ft)(°F/ft)
H, V are complex interaction coefficients between pairs of molecules
R = gas constant, Btu/(°F)(lb mole)
M = molecular weight
μ = viscosity, lb mass/(hr)(ft)
C_v = molal specific heat at constant volume, Btu/(lb mole)(°F)

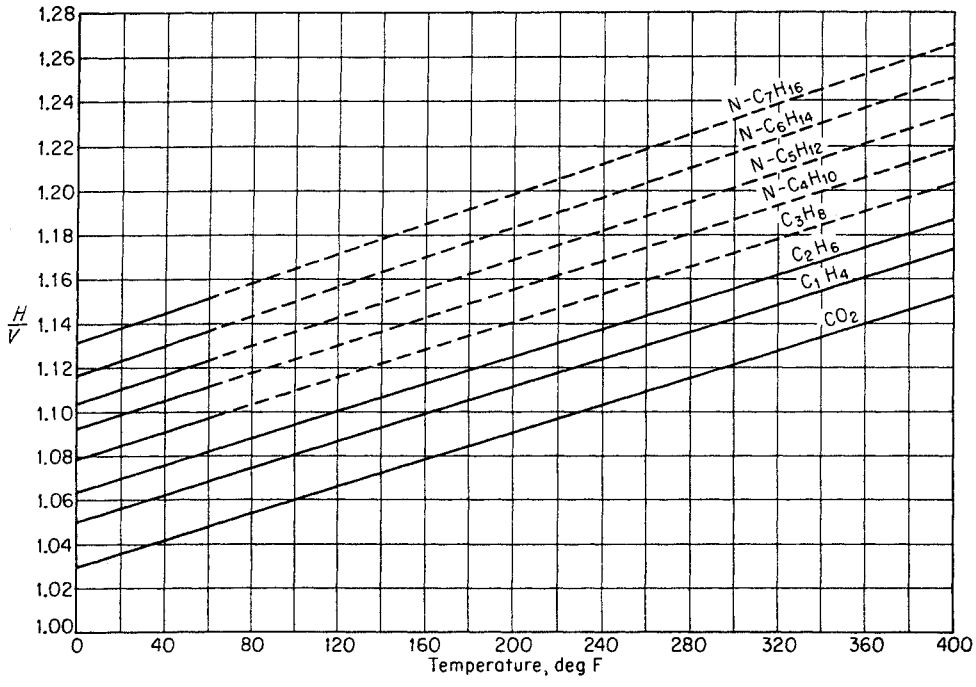

Fig. 4-118. Ratio of interaction coefficients in the Eucken equation relating thermal conductivities to specific heat.

If the relation $C_p - C_v = R$ is assumed to hold, Eq. (4-53) reduces to

$$k = \frac{H}{V}\mu\left(C_p + \frac{5R}{4M}\right) \qquad (4\text{-}54)$$

where C_p = specific heat at constant pressure, Btu/(lb)(°F). The values of H/V were calculated from Eq. (4-54) by means of experimental thermal-conductivity data. The values of H/V calculated in this manner do not agree with those based on molecular theory (4-154). The computed values of H/V vary with temperature and with the gas for carbon dioxide, methane, and ethylene. The calculated value of H/V for nitrogen always falls in the vicinity of 1.0, over the temperature range from −100 to 400°F. The final values for H/V used in calculating the temperature dependence of the thermal conductivity of gases are presented in Fig. 4-118. Since thermal-conductivity data for propane and higher-molecular-weight hydrocarbons are available over a limited temperature range, the H/V values are extrapolated linearly from the values calculated in the region from 32 to 50°F. The slope of the H/V-versus-temperature lines was assumed to be the same as that slope for pure methane and for carbon dioxide.*

The specific-heat values used to compute the thermal conductivities were taken from a summary of the work performed under API Research Project 44 (1-15). The viscosity values chosen are those presented in the previous section on gas viscosity. The final pure-component thermal-conductivity values are plotted in Fig. 4-119. Figure 4-120 is essentially a cross plot of Fig. 4-119, giving the thermal conductivity of pure components as a function of molecular weight for various temperatures.

Analytical relations which may be used to compute the thermal conductivities of mixtures from pure-component values have been proposed by several authors (4-24, 4-41, 4-159, 4-168). The relation developed and studied by Lindsay and Bromley (4-168) has been applied successfully to compute the thermal conductivity of gas mixtures. The relation gives the thermal conductivity of mixtures as a function of the thermal conductivity, viscosity, molecular weight, and Sutherland constant of the pure component, the gas composition, and the temperature.

The thermal conductivity of a gas mixture is given by Eqs. (4-55) and (4-56). It is necessary to compute values of A by Eq. (4-56) to insert in Eq. (4-55) to obtain the thermal conductivity of mixture k_m:

---

* Since the calculations discussed above were made, the thermal conductivity of light hydrocarbon gases has been correlated by the relation

$$\frac{Mk}{\mu} = 1.04 + 1.29C_p$$

where M = molecular weight, grams
k = thermal conductivity, cal/(sq cm)(sec)(°C/cm)
μ = viscosity, grams/(cm)(sec)
C_p = heat capacity, cal/(mole)(°C)

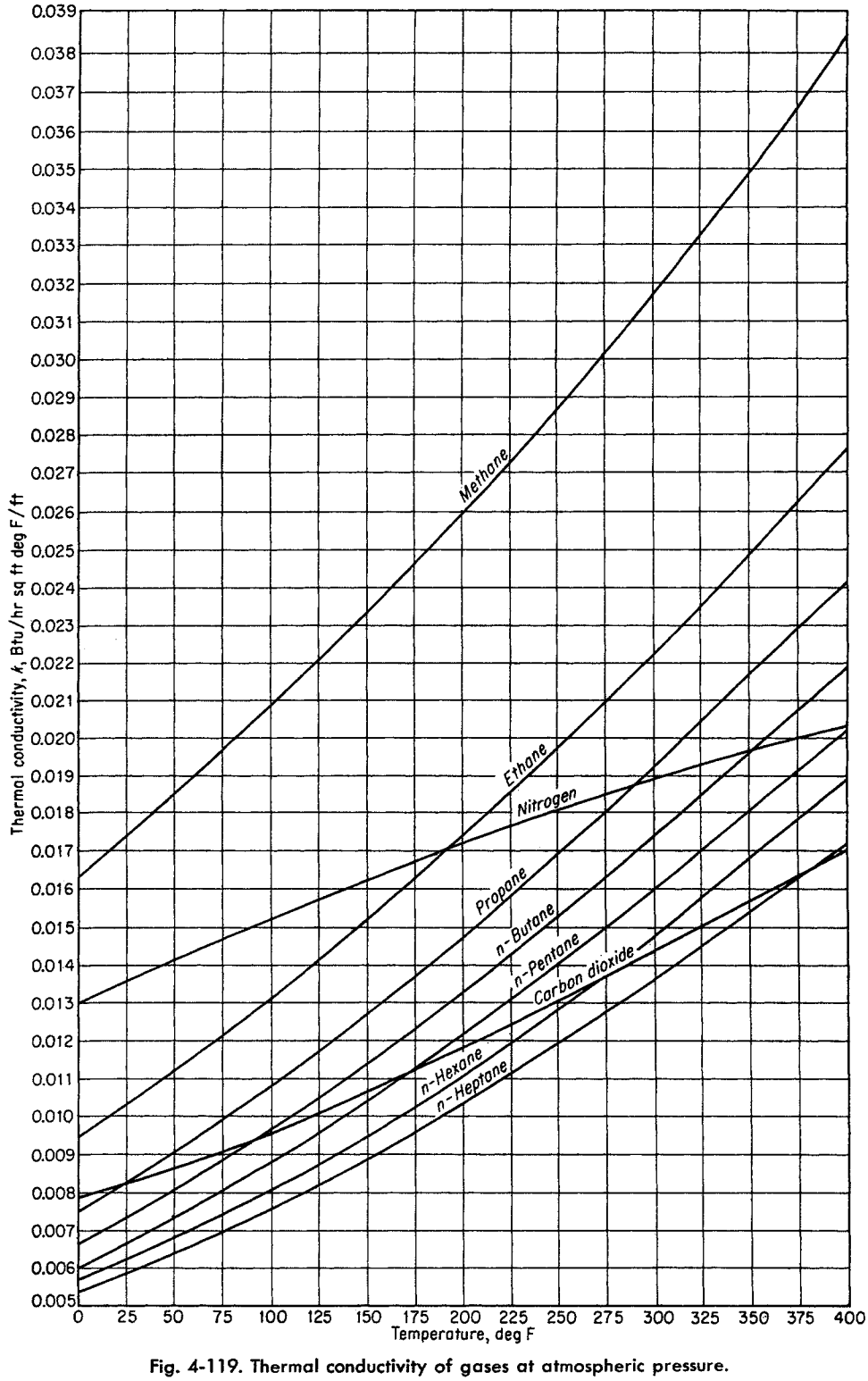

Fig. 4-119. Thermal conductivity of gases at atmospheric pressure.

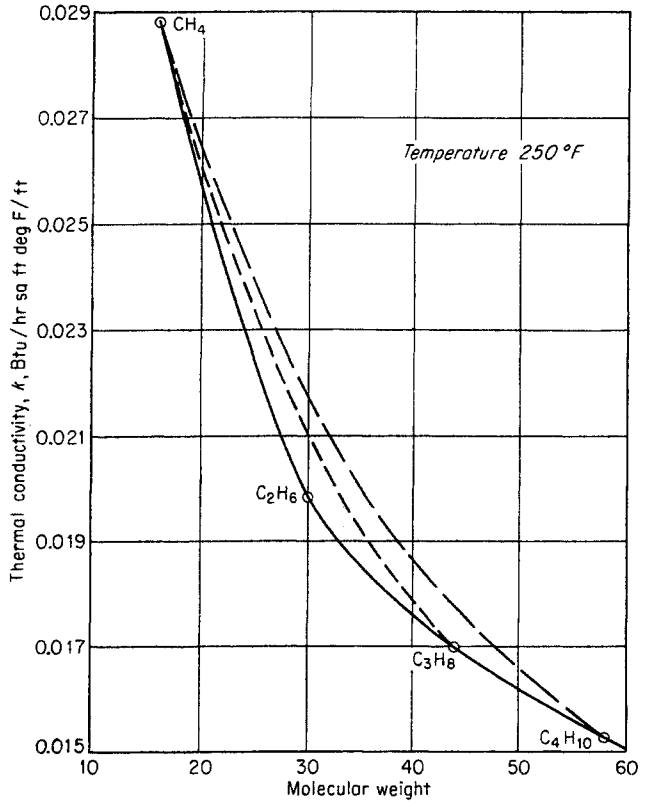

Fig. 4-120. Computed thermal conductivity of binary gas mixtures at 250°F.

$$k_m = \frac{k_1}{1 + A_{1,2}\frac{x_2}{x_1} + A_{1,3}\frac{x_3}{x_1} + A_{1,4}\frac{x_4}{x_1} + \cdots} + \frac{k_2}{1 + A_{2,1}\frac{x_1}{x_2} + A_{2,3}\frac{x_3}{x_2} + A_{2,4}\frac{x_4}{x_2} + \cdots} + \frac{k_3}{1 + A_{3,1}\frac{x_1}{x_3} + A_{3,2}\frac{x_2}{x_3} + A_{3,4}\frac{x_4}{x_3} + \cdots} + \cdots \quad (4\text{-}55)$$

where k_1, k_2, . . . are thermal conductivities of the pure components and where x_1, x_2, . . . are compositions in mole fractions. When $A_{i,j} = A_{1,2}$

$$A_{1,2} = \frac{1}{4}\left\{1 + \left[\frac{\mu_1}{\mu_2}\left(\frac{M_2}{M_1}\right)^{3/4}\frac{1 + S_1/T}{1 + S_2/T}\right]^{1/2}\right\}^2 \frac{1 + S_{1,2}/T}{1 + S_1/T} \quad (4\text{-}56)$$

where μ = viscosity
M = molecular weight
S = Sutherland constant (Table 4-29)
$S_{1,2} = (S_1 S_2)^{1/2}$
T = absolute temperature, °K

The thermal conductivity of synthetic mixtures was calculated by means of Eq. (4-55). In making the computations it was assumed that the Sutherland constants were independent of temperature although in fact they show variation with temperature for real gases. It was found that relatively large variations in the Sutherland constants produce only slight variations in the computed thermal conductivities.

The calculated thermal-conductivity values for several binary hydrocarbon mixtures at 250°F have been plotted in Fig. 4-120. Portions of Fig. 4-121 superimposed on Fig. 4-120 indicate the degree of approximation introduced through the direct application of molecular weight to determine the thermal conductivity of complex mixtures.

Calculations indicate that natural gas mixtures containing up to 35 per cent nitrogen and/or carbon dioxide are represented by the curves given in Fig. 4-121. In general, the application of Fig. 4-121 to natural hydrocarbon mixtures will yield conservative values of the thermal conductivity. Equation (4-55) or (4-56) may be applied to the thermal-con-

Table 4-28. References for Experimental Data on Thermal Conductivity of Gases at High Pressures

Gas	Investigator and year	Reference
Methane	Stoyarov, Ipat'ev, and Teodorovich (1950)	4-182
	Lenoir and Comings (1951)	4-166
	Lenoir, Junk, and Comings (1953)	4-167
	Keyes (1954)	4-161
Ethane	Lenoir, Junk, and Comings (1953)	4-167
	Keyes (1954)	4-161
Ethylene	Lenoir and Comings (1951)	4-166
	Keyes (1954)	4-161
Carbon dioxide	Sellschopp (1934)	4-178
	Stoyarov, Ipat'ev, and Teodorovich (1950)	4-182
	Lenoir and Comings (1951)	4-166
	Keyes (1951)	4-160
	Junk and Comings (1953)	4-157
Helium	Lenoir and Comings (1951)	4-166
Argon	Lenoir and Comings (1951)	4-166
	Lenoir, Junk, and Comings (1953)	4-167
Nitrogen	Vargaftik (1937)	4-187
	Stoyarov, Ipat'ev, and Teodorovich (1950)	4-182
	Keyes and Sandell (1950)	4-162
	Lenoir and Comings (1951)	4-166
	Keyes (1951)	4-160
	Junk and Comings (1953)	4-157
	Michels and Botzen (1953)	4-170
	Lenoir, Junk, and Comings (1953)	4-167

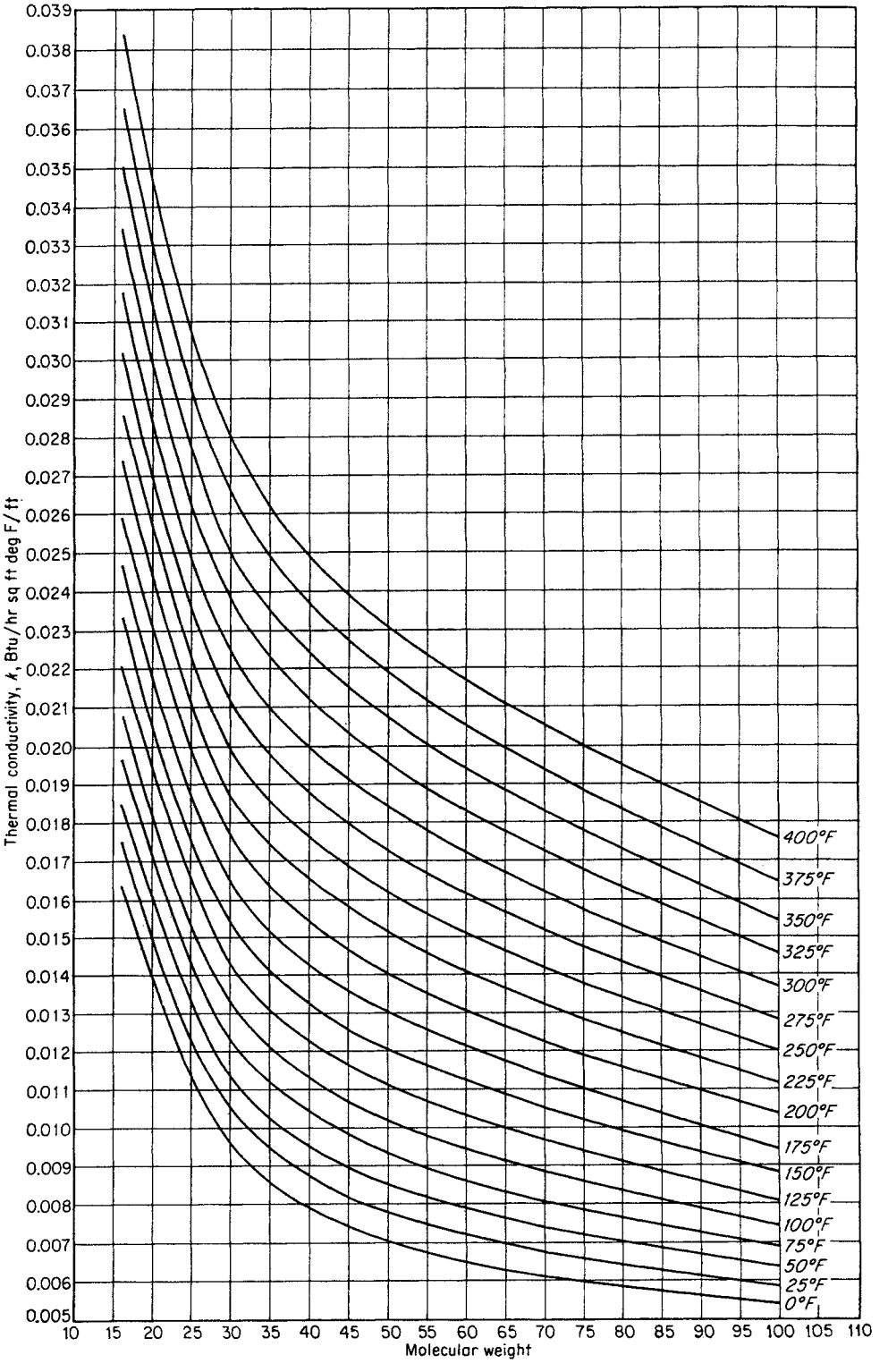

Fig. 4-121. Effect of molecular weight on the thermal conductivity of gases.

Table 4-29. Sutherland Constants for Gases

Gas	*S*, °K	Investigator	Reference
Methane	198	Rankine and Smith	4-124
Ethane	287	Titani	4-132
Propane	341	Titani	4-132
n-Butane	377	Titani	4-132
n-Pentane	382.8	Titani	4-132
n-Hexane	436.1	Titani	4-132
Nitrogen	102.7	Trautz and Baumann	4-185
Carbon dioxide	274	Smith	4-179

ductivity ratios obtained from Fig. 4-114 or Fig. 4-115 to obtain the absolute thermal conductivity of compressed gases.

The thermal conductivity of liquids is not covered here. Some values are tabulated for hydrocarbons in Table 4-30.

Table 4-30. Thermal Conductivity of Liquids

Liquid	Temperature, °F	Thermal conductivity, Btu/(hr)(sq ft)(°F/ft)
Water	32	0.343
	100	0.363
	200	0.393
	300	0.395
n-Pentane	86	0.078
	167	0.074
n-Heptane	86	0.081
	140	0.079
Nonane	86	0.084
	140	0.082
Gasoline	86	0.078
Kerosene	68	0.086
	167	0.081
Ethylene glycol	32	0.153

SOURCE: Perry (4-121a).

CHAPTER 5

Water-Hydrocarbon Systems

Water is a conspicuous component of natural gas in all steps of gas handling from its initial production until its ultimate consumption. The presence of water in compressed natural gas is especially troublesome, because the solubility of water in the gas is diminished by increased pressure and decreased temperature. Pressure favors the combination of water with natural gases to form solid gas hydrates, even though the temperature is above the freezing point of water. The formation of gas hydrates, which resemble wet snow, is to be avoided since they plug pipe lines and valves, interrupting the steady flow of gas.

Information of concern to the engineer includes the equilibrium water content of natural gases for various temperatures and pressures and also the conditions at which hydrates form when liquid water is present. The water content of natural gases determines the amount of water that must be removed when the gases are dehydrated, so that they will not reach a water dew point at specified pipeline conditions. Since the small quantities of water that dissolve in propane, butane, and other light hydrocarbon liquids must be removed before distribution, their concentrations are also of interest.

An understanding of the physicochemical relationships governing the behavior of hydrocarbon-water systems assists the engineer in handling the problems involved in controlling moisture content of natural gas and light hydrocarbon liquids. Quantitative data on the water content of gases and liquids are available for most problems that arise. Information on the nature of gas hydrates and the equilibrium conditions at which they form when water is present will permit the engineer to select temperatures and pressures for wet gases at which hydrates will not form. Since the measurement of water dew points and of absolute water contents of natural gas is important, methods of performing these measurements are discussed.

References to the large amount of work in this field are given by Katz and Rzasa (1-9) and Deaton and Frost (5-21).

GENERAL PHASE RELATIONS FOR HYDROCARBON-WATER SYSTEMS

Binary systems of water and one pure hydrocarbon represent the simplest phase relations to be expected in hydrocarbon-water systems. These systems at temperatures above 32°F will be described before complex behavior is presented.

Figure 5-1 gives the phase behavior of the propane-water system above 32°F. In this temperature range, propane as a pure substance may occur as a vapor at low pressure, as a liquid at high pressure, or as an equilibrium mixture of vapor and liquid along the vapor-pressure curve BC_1. Terms used to represent phases in hydrocarbon-water systems are:

G = gas
L_1 = water-rich liquid
L_2 = hydrocarbon-rich liquid
H = hydrate
I = ice
M = solid methane
P = solid propane
X = concentration of component

The phase rule, Eq. (3-1), governs the degree of freedom as follows:

Number of components	Number of phases	Representation on P-T diagram
2	2	Area
2	3	Line
2	4	Point
3	3	Area
3	4	Line

Thus, the phase relations of propane and water with vapor V, liquid-water L_1, and liquid-propane L_2 phases are represented by the curve EBC_2, sometimes called a three-phase vapor-pressure curve. This curve is the P-T projection of the intersection in a P-T-X diagram of a surface representing the two liquids and one representing gas and water-rich liquid, as indicated

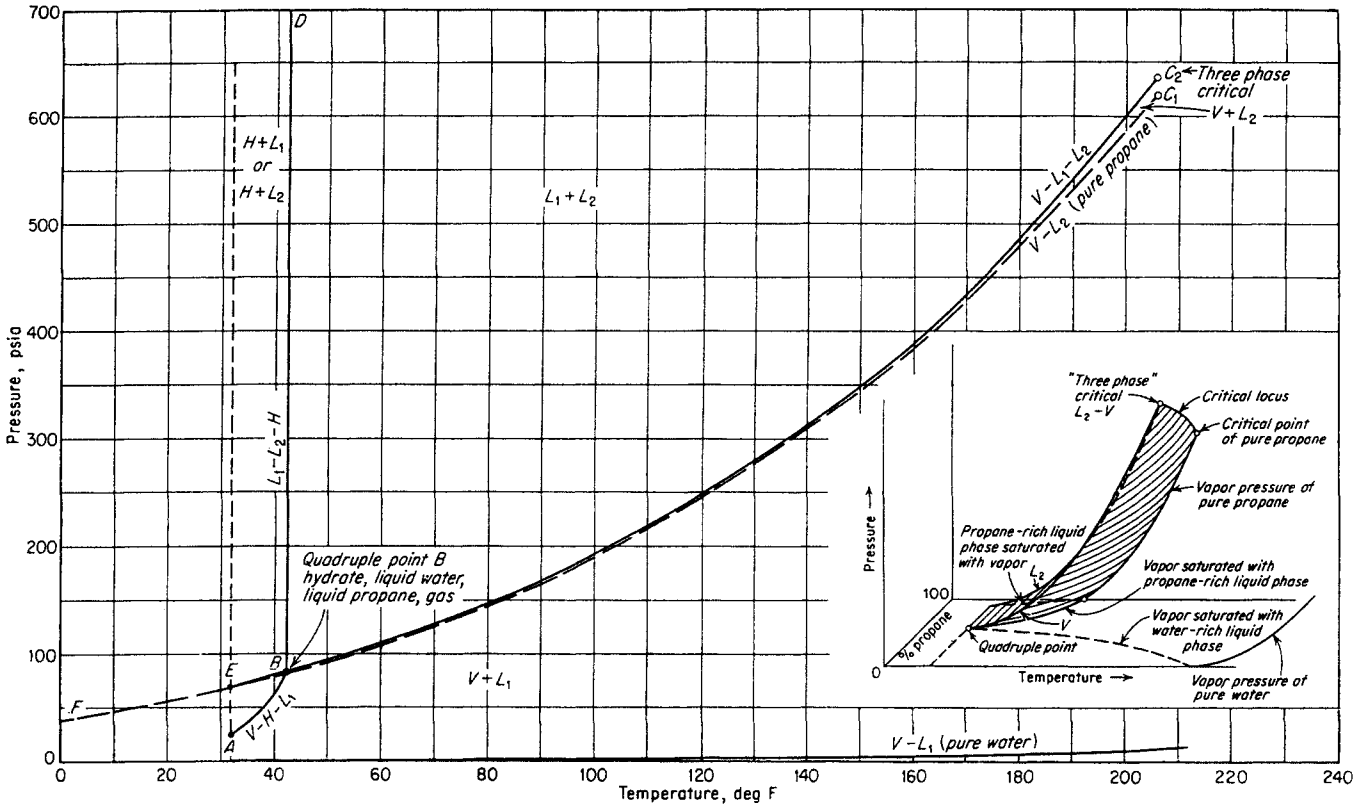

Fig. 5-1. Phase behavior of propane-water system above 32°F.

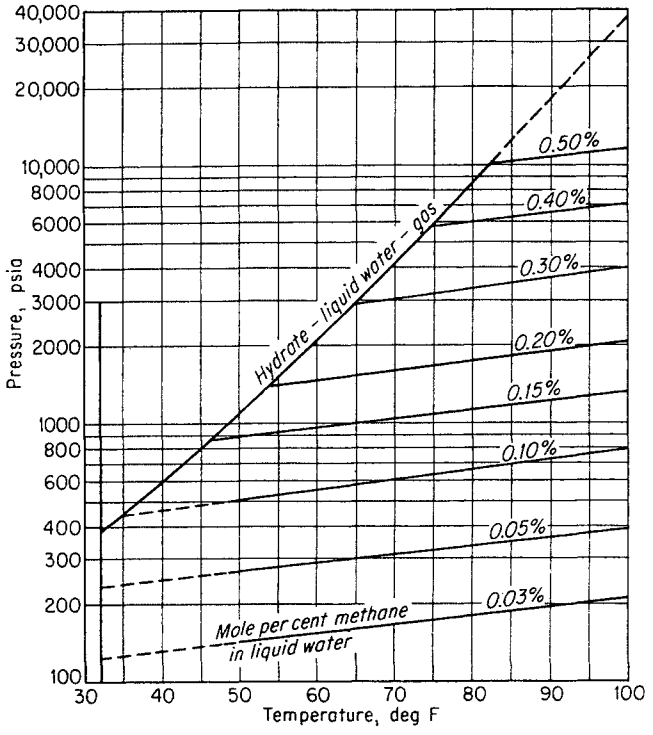

Fig. 5-2. Phase behavior of methane-water system above 32°F.

in the insert of Fig. 5-1. The vapor-pressure curve FC_1 terminates in the critical point for pure propane at C_1, and the three-phase vapor-pressure curve EBC_2 terminates in point C_2, the critical point between gas and propane-rich liquid.

Propane vapor and liquid water form hydrate at 32°F and 23.5 psia. As the pressure increases, the temperature for hydrate formation also increases, until the curve intersects the V-L_1-L_2 curve. At this quadruple point, the system is invariant because four phases are present. Liquid propane and liquid water form hydrate at pressures above the three-phase vapor-pressure curve and at temperatures below the quadruple point, as indicated. In any particular system, hydrate, liquid water, and liquid propane are in equilibrium along the indicated nearly vertical line. In the region at temperatures below DBE, either hydrate and water-rich liquid L_1 or hydrate and propane-rich liquid L_2 occur, depending upon which component is in excess.

The phase relations for methane and water in the region above 32°F may be shown in the form of a P-T curve representing the conditions at which hydrate, liquid water, and gas are in equilibrium (Fig. 5-2).

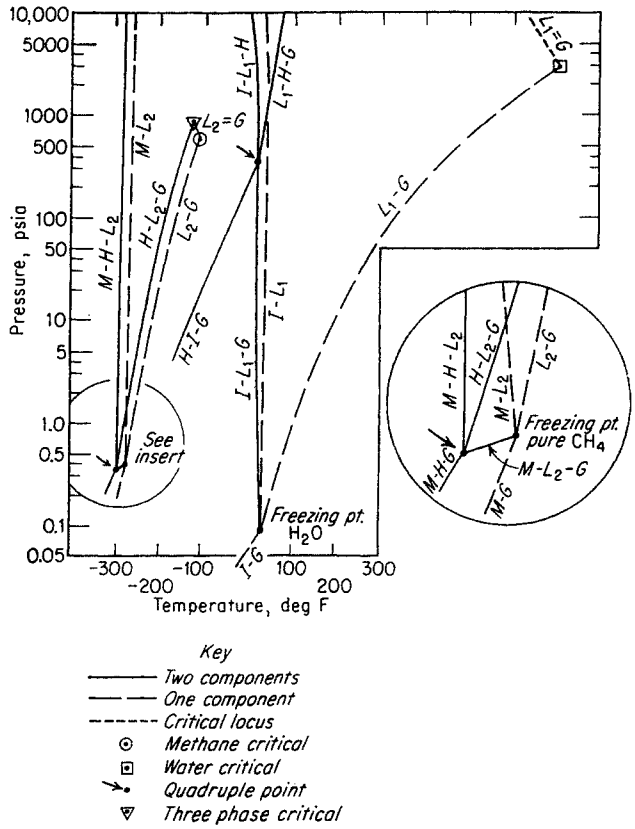

Fig. 5-3. Pressure-temperature projection for the condition of univariant heterogeneous equilibrium in methane-water system. (5-42.)

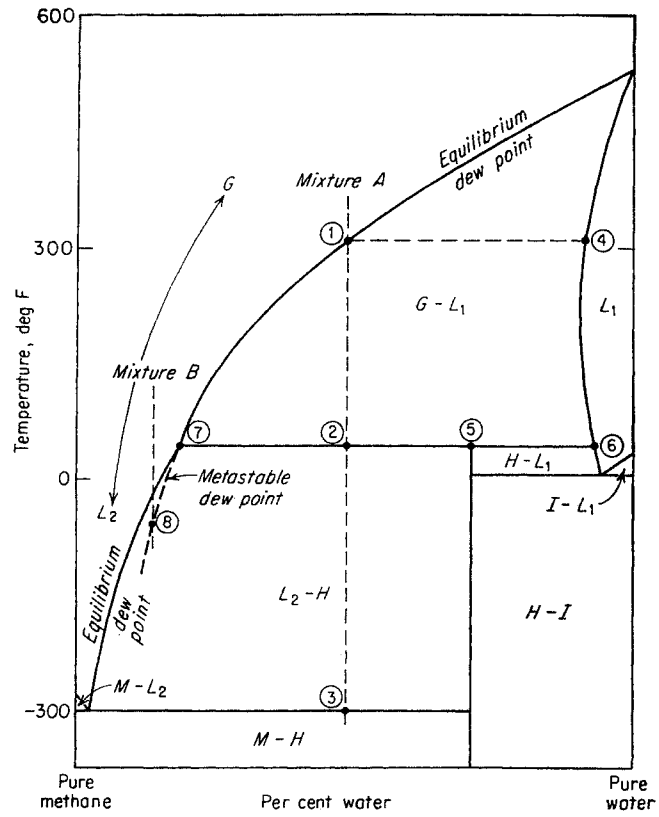

Fig. 5-4. Phase diagram of the methane-water system at a pressure greater than the critical pressure of methane. (5-42.)

The study of a methane-water system by Villard in 1888 (5-85) showed that methane formed hydrate at pressures up to 4,000 psia. However, because ethane and propane had an abrupt stoppage of hydrate formation with increasing temperatures at the quadruple point, Villard expected a critical temperature for hydrate formation for methane and named 70.7°F as this critical point. Kobayashi and Katz (5-42) showed that the methane-hydrate curve extends to high pressure by measurements up to 11,800 psia. The bubble-point curves for water containing dissolved methane indicate the concentration of gas in the water forming the hydrate.

The complex nature of the phase relations of natural gas–water systems can be inferred from Figs. 5-3 and 5-4 for the entire methane-water system and from Figs. 5-5 and 5-6 for the propane-water system. Figures 5-3 and 5-5 are the pressure-temperature projections of the univariant and invariant equilibrium conditions that occur in the two systems. These conditions represent values obtained by measurements or through postulates made according to the restrictions of the phase rule. The measured values have been followed as closely as possible, but exaggerations have been introduced when necessary to show each feature distinctly.

The information provided by Figs. 5-3 and 5-5 can be combined with information on the relative concentrations of the coexisting phases to develop the phase diagrams shown in Figs. 5-4 and 5-6 at specific pressures. Since the mutual solubilities of hydrocarbon and water are generally very low, no attempt has been made to draw Figs. 5-4 and 5-6 to scale. Figure 5-4 is a schematic temperature-composition diagram for the methane-water system taken at a pressure just exceeding the critical pressure of pure methane, a feasible pipeline pressure. A similar diagram (Fig. 5-6) has been constructed for the propane-water system, somewhat below the critical pressure of pure propane. This pressure was chosen to illustrate a condition where two liquid phases and a gas phase coexist. The open areas are labeled to indicate the phase or phases formed by any mixture falling within the area by virtue of its composition and the imposed temperature and pressure.

In the single-phase regions, the phase composition and the mixture composition are identical and, hence, represented at the same value. In the two-phase region, to fix two variables, such as pressure and

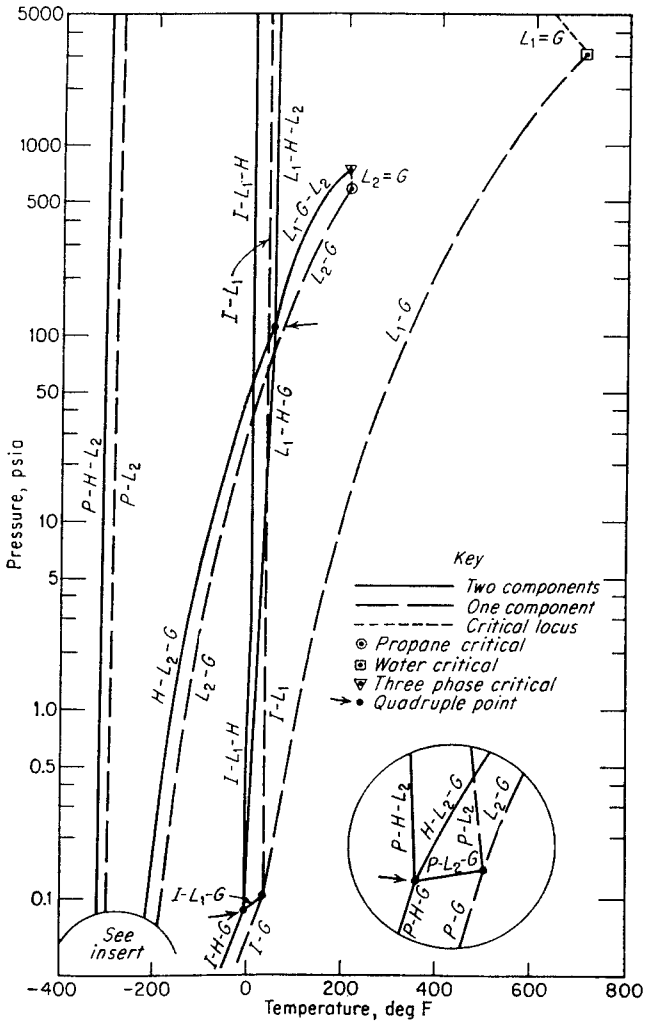

Fig. 5-5. Pressure-temperature projection for the condition of univariant heterogeneous equilibrium in propane-water system. (5-39.)

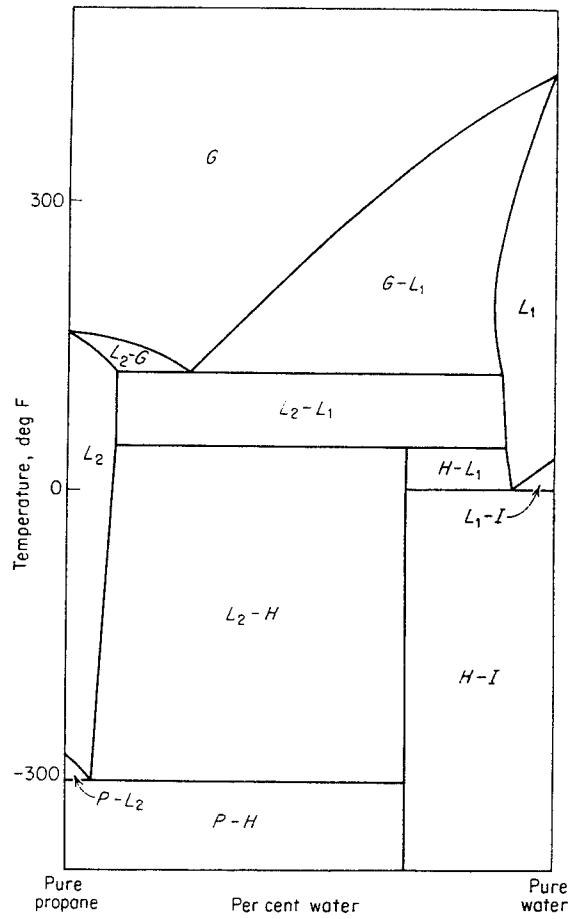

Fig. 5-6. Phase diagram of the propane-water system at a pressure less than the critical pressure of propane. (5-39.)

temperature, establishes the two-phase compositions. All heavy lines in Figs. 5-4 and 5-6 that are not horizontal represent loci of these compositions. Since the independent variables for the coexistence of three phases are reduced to one, on a constant-pressure (or constant-temperature) diagram the three phases that are in equilibrium must fall at a fixed temperature (or pressure). Points of intersection of the loci of two-phase compositions in the adjoining areas with the horizontal three-phase line define the individual three-phase compositions. For a quadruple point with four phases present, the values of the pressure and temperature and the compositions of the four coexisting phases are, accordingly, fixed by nature. All these features are evident in the practical region of interest for a binary hydrocarbon-water system.

Figure 5-4 for the methane-water system may be used to illustrate the transitions to be expected when mixture A is cooled at constant pressure. The mixture exists as a single-phase gas until point 1 is reached. The *phase boundary* on which 1 is located is the *dew point*, at which the water-rich liquid 4 initially condenses on cooling. Further cooling of the gas-liquid mixture to point 2 causes the formation of an additional phase, $CH_4 \cdot 5\frac{3}{4}H_2O$ (5-14). Continued removal of heat at a fixed temperature leads to gradual disappearance of the liquid-water phase 6, leaving vapor 7 in equilibrium with hydrate 5. At a very low temperature, the equilibrium M-L_2-H may be expected to occur at point 3.

A methane-water mixture of another composition will produce phase transitions under different conditions or, conceivably, even different phase transitions. Although such a phase diagram cannot represent the natural gas–water system consistently, substantially the same features do exist in natural gas–water behavior. In the latter, three-phase conditions occur over a range of temperatures, but, for a given gas at a

given pressure, discrete temperatures for the inception of two-phase vapor-liquid conditions can be determined (5-21). Similarly, the three-phase border conditions for the occurrence of vapor-liquid-solid equilibria can be established for a given gas (5-21, 5-90).

SOLUBILITY OF WATER IN HYDROCARBON PHASES AND OF HYDROCARBONS IN WATER

Quantitative information on the mutual solubilities of water and hydrocarbons is presented. This involves three types of solubilities: water in gas, water in liquid hydrocarbon, and hydrocarbon in water. The references for experimental data on water-hydrocarbon systems are presented in Table 5-1. Thermodynamic continuity of the behavior in different phases should be recognized even though the three solubilities are treated separately. The measurement of water content of gases is a delicate measurement and will be treated first.

Measurement of the Water Content of Natural Gas

Many methods of measuring the amount of water in natural gases have been developed to fit various applications. No single method of analysis can be utilized under all conditions. Table 5-2 gives a summary of some of the methods that have been used, their references, and their applications. This choice is somewhat arbitrary, but it represents the three commonest methods of measuring water in natural gas. Of the methods listed in Table 5-2, the following will be discussed:

1. Bureau of Mines dew-point tester
2. Solid chemical absorbents
3. Absorption by liquid and subsequent titration by Karl Fischer reagent

Table 5-1. References for Hydrocarbon-Water Phase-equilibrium Data

System	Phase studied	Pressure range, psia	Temperature range, °F	Reference
Hydrogen-water	Water-rich liquid	370–14,700	32–212	5-88
	Water-rich liquid	740–2,200	77	3-20
Methane-water	Water-rich liquid	200–10,000	77–340	5-18
	Water-rich liquid	590–6,800	80–300	5-53
	Water-rich liquid	590–1,700	77	3-20
	Water-rich liquid	526–9,680	77	5-16
	Hydrocarbon-rich gas	200–10,000	100–460	5-56
	Hydrate region	250–700	10–45	5-28
	Hydrate region	240–1,570	7–56	5-69
	Hydrate region	440–4,400	30–70	5-85
Ethane-water	Water-rich liquid	100–10,000	100–340	5-17
	Hydrocarbon-rich gas	200–10,000	100–460	5-62
	Hydrate region	40–150	10–45	5-28
	Hydrate region	40–1,000	10–60	5-69
	Hydrate region	90–410	30–55	5-85
Ethylene-water	Water-rich liquid	110–7,500	95–212	5-6
	Three-phase region	450–1,500	60–78	5-23, 5-24
Propane-water	Water-rich liquid	100–2,800	100–300	5-40
	Hydrocarbon-rich liquid	100–2,800	100–300	5-40
	Three-phase region	80–640	40–205	5-40
	Hydrate region	117–887	41–43	5-90
	Three-phase region	100–400	60–187	5-60
n-Butane–water	Water-rich liquid	1,000–10,000	100–220	5-8
	Water-rich liquid	1–10,000	100–460	5-64
	Hydrocarbon-rich liquid	1,000–10,000	100–220	5-8
	Hydrocarbon-rich liquid	1–10,000	100–460	5-64
	Three-phase region	50–623	100–300	5-63
1-Butene–water	Water-rich liquid	63–10,000	100–310	5-46
	Hydrocarbon-rich liquid	63–10,000	100–310	5-46
	Three-phase region	50–1,000	100–280	5-9
n-Butane–methane–water	Two-phase region	200–3,000	100–280	5-51
	Three-phase region	200–3,000	100–280	5-51
Hexane-water	Three-phase region	.....	.....	5-75

The Bureau of Mines Dew-point Apparatus has found wide usage in the determination of dew points since its development in 1938 (5-22). It permits the visual determination of the temperature at which water will condense from a gas onto a silvered mirror (Fig. 5-7), which is significant because it represents the actual equilibrium saturation temperature of the gas for temperatures above the hydrate-formation value. And, at temperatures below the equilibrium hydrate-formation conditions, it measures a reproducible metastable equilibrium condition between gas and liquid water.

Figure 5-7 presents a sectional view of the apparatus without lead lines and refrigerant source. Gas entering the apparatus through valve *A* is deflected by nozzle *B* so as to strike the cooled mirror *C*. The mirror is cooled through the copper cooling rod *F* by the evaporation of a refrigerant, such as propane, carbon dioxide, or some liquefied gas, in chiller *G*. Pressure gauges and a bulb thermometer are used to record the pressure and temperature conditions for the inception of condensation or fog formation on the silvered mirror.

In the absence of interfering substances, the accuracy of the determinations, given an experienced operator, is reported to be ± 0.2°F down to 32°F, and ± 0.5°F from 32 to 0°F. "ASTM Standards" (4-2) provides a detailed description of the apparatus and procedures for operating it. The apparatus is recommended for use up to pressures of 2,500 psi, and has been operated as low as -60°F through the use of a dry ice–acetone mixture as the refrigerant (5-78).

Deaton and Frost determined the dew point of several natural gases with the dew-point apparatus up to 600 psi and at temperatures as low as -10°F (5-21).

Table 5-2. Methods of Measuring Water in Natural Gases

Method	Application	Remarks	References
Visual observation of dew point	Laboratory and field	Operable under pressure down to -50°F	5-21 5-22, 5-78
Absorption by solid desiccants	Laboratory	Must be presaturated with hydrocarbons	5-51, 5-80
Absorption and subsequent titration by Karl Fischer reagent	Laboratory	Possible field application	5-7
Freezing and weighing	Laboratory	The extremely low-boiling-point gases	5-56
Spectroscopic	Laboratory	Portable instrument designed, but complex	5-83
Spectroscopic	Laboratory	Reference (5-29) applies to propane-water system	5-29, 5-83
Electric hygrometer	Field	Used in stratospheric measurements	5-26, 5-86

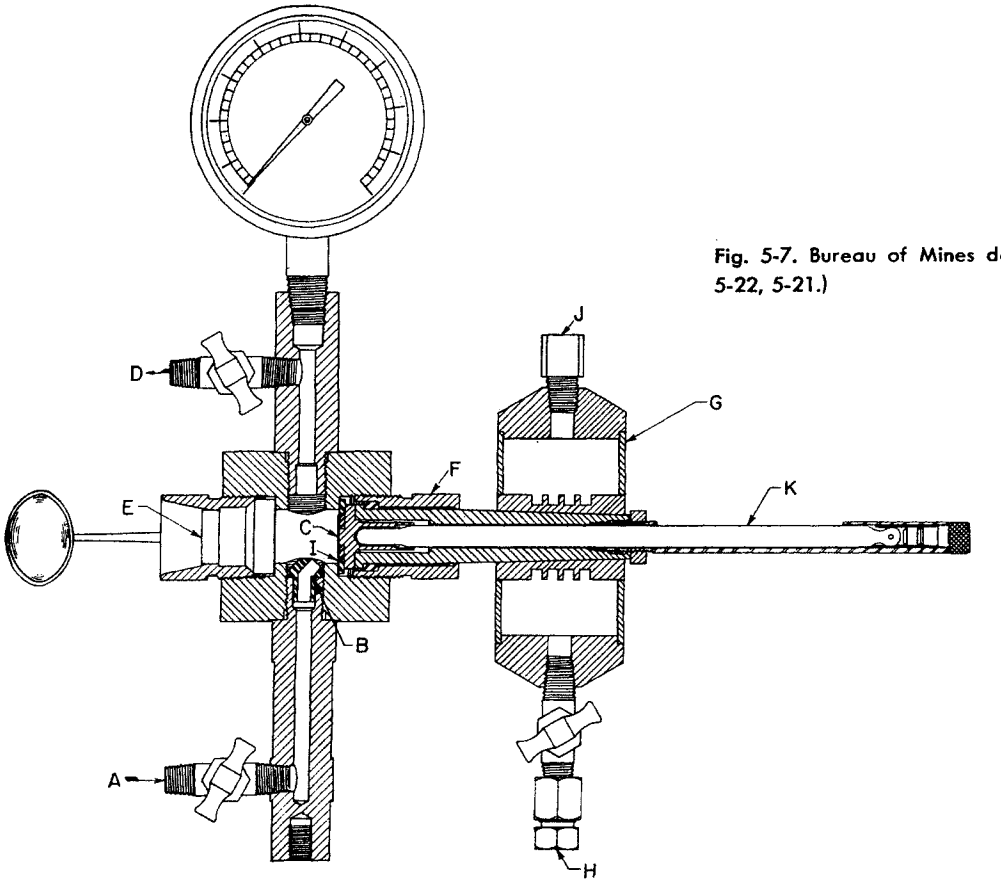

Fig. 5-7. Bureau of Mines dew-point tester. (*Deaton and Frost*, 5-22, 5-21.)

Photographs of the mirror in the neighborhood of the dew point are given, and the formation of liquid droplets and ice crystals is described. The dew-point content of the gas is plotted versus temperature (using a $1/T$ scale) for lines of constant pressure. The absence of a break in these curves at or near 32°F indicates that the condensation of dew under 32°F occurs under nonequilibrium or metastable equilibrium conditions. In fact, the dew point observed by the Bureau of Mines instrument corresponds to the vapor pressure exerted by metastable or subcooled water. In calculating the amount of water in gas at temperatures below 32°F at moderate pressures, it is recommended that the vapor pressure of subcooled water rather than of ice be used (4-2). If conditions for water drop-out exist below 32°F, eventual ice or solid-hydrate formation may be expected.

Figure 5-4 may be used to illustrate the operational significance of a dew-point determination. Gas generally exists in the single-phase region G in which it is undersaturated with respect to water. Slowly lowering the temperature of mixture A causes an additional liquid phase to appear at point 1. The visual determination of the dew point, through the use of such instruments as the Bureau of Mines dew-point tester (5-22), is the establishment of such an initial point of condensation. Further cooling causes additional separation of water, but only the initial point of condensation is needed to determine the amount of water in the gas. Mixture B, containing a smaller amount of water, does not reveal a dew point by this procedure until the temperature reaches the metastable extension of the dew-point curve at point 8. This, apparently, is the dew point determined at temperatures below the hydrate-formation temperatures (5-41).

Riesenfeld and Frazier (5-68) studied the dew-point determination of gases dehydrated by diethylene glycol–water solution and by diethylene glycol–monoethanolamine–water solution, and concluded that the Bureau of Mines apparatus was not suited for such determinations. They presented a method for determining the absolute water content of the gas when glycol is present.

Campbell and Laurence made material-balance measurements of inlet and outlet streams of several full-scale triethylene glycol dehydrators (5-11). The average absolute deviation of the value for water removal calculated from dew-point measurements and that calculated from the glycol streams was 6.6 per cent. The maximum deviation for seven plants was 18.9 per cent. An effective scrubber placed before the gas-inlet valve to the apparatus is frequently used to reduce interfering hydrocarbon liquids.

Cooling of natural gases often brings them to a hydrocarbon dew point, which must be distinguished from a water dew point.

Solid Chemical Absorbents have been used to obtain most of the experimental data on the water content of pure volatile hydrocarbons and their synthetic mixtures (5-40, 5-45, 5-51, 5-64). Solid chemical absorbents, magnesium perchlorate or Dehydrite (5-80), permit accurate gravimetric determination of water corresponding to a measured amount of gas. Precautions such as presaturation and postsaturation of the absorbent train with hydrocarbons, buoyancy correction, and diffusion of water through semipermeable connections must be carefully observed. Solid desiccants may be used for low-pressure natural gas containing substantial amounts of water. However, their application to high-pressure streams of natural gases containing even small amounts of high-molecular-weight hydrocarbon or liquid desiccants such as diethylene glycol may be misleading.

The Karl Fischer Reagent used to determine water content is a methanol solution of iodine, pyridine, and sulfur dioxide. The main reaction for the Karl Fischer reagent in which water participates appears to be

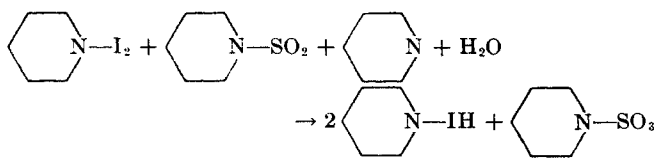

Mitchell and Smith (5-79) have devoted an entire book to the titrimetric determination of water using the Karl Fischer reagent. Peters and Jungnickel (5-59) found that the stability of the Karl Fischer reagent could be improved by the substitution of methyl cellosolve for methanol in the reagent.

Brickell (5-7) adapted the Karl Fischer method to the determination of water in hydrocarbon gases. The water is quantitatively absorbed for a measured quantity of gas by diethylene glycol at either low or high pressures. The glycol-water solution is then titrated to yield the water absorbed from the gas stream. A study of the effect of interfering compounds such as hydrogen sulfide, mercaptans, and amines is given. The over-all precision of Brickell's procedure is reported as 0.60 lb of water per MMcf of gas. The method can undoubtedly be refined to produce even greater accuracy.

Water-content Chart for Natural Gases

Several charts have been prepared to show the equilibrium moisture content of natural gases (5-21, 5-78, 5-52, 5-50). Figure 5-8 is a plot of the dew-point water-vapor content of a lean nitrogen-free natural gas in equilibrium with liquid water. It has been pre-

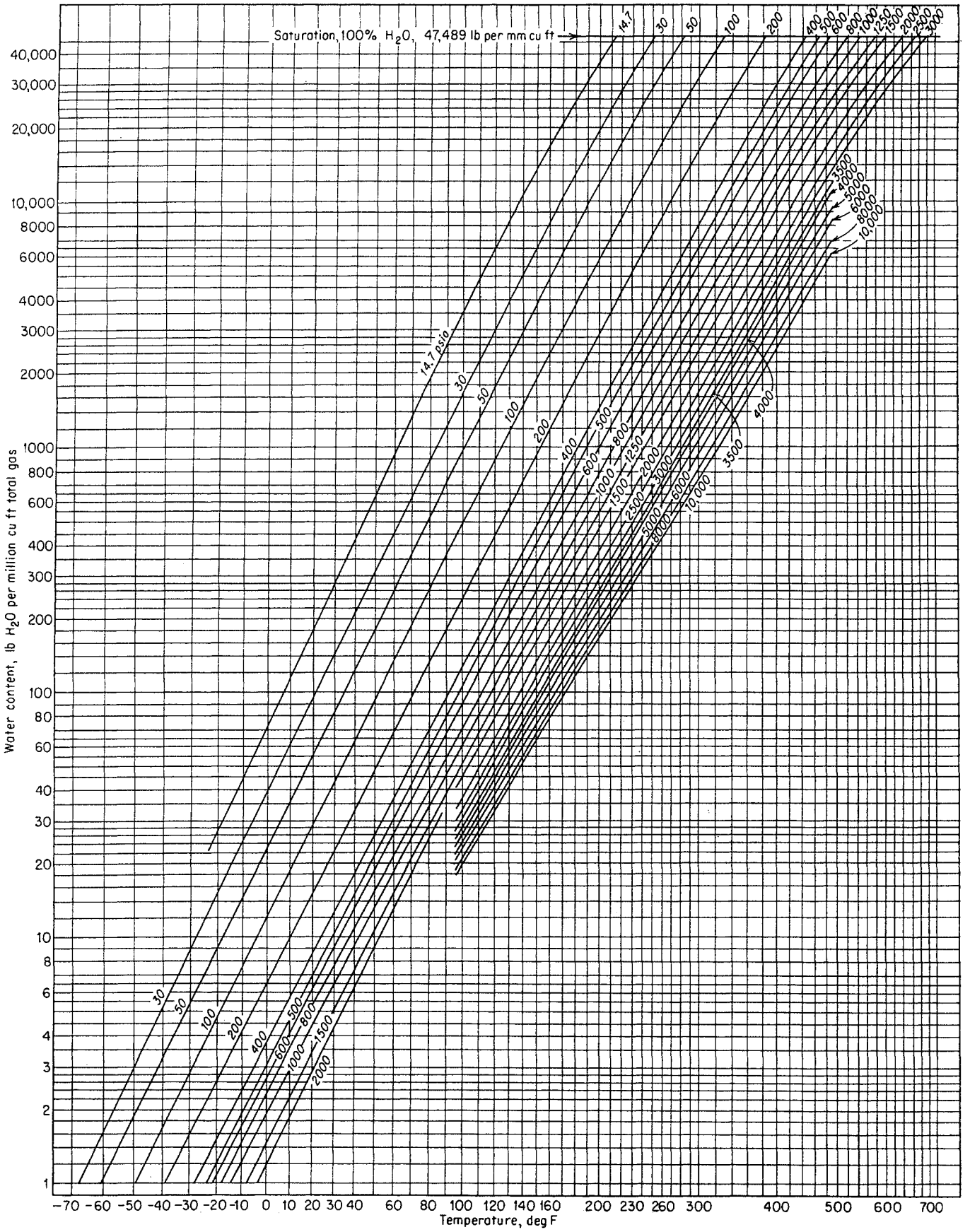

Fig. 5-8. Water content of natural gas in equilibrium with liquid water.

pared from experimental measurements by several investigators (5-21, 5-22, 5-56, 5-78, 5-25). Above the hydrate region it is in substantial agreement with charts published by McKetta and Katz (5-52) and by McCarthy, Boyd, and Reid (5-50). Below the hydrate-formation temperature, the water content represents the condition under which initial dew formation takes place under metastable-equilibrium conditions. The isobars have been drawn as smooth dotted extensions of the stable gas–liquid water equilibria into the metastable region, as shown in Fig. 5-8.

Figure 5-8 is based on pounds of water per MMcf of total gas at 14.7 psia and 60°F. At water contents below 50 lb, the difference between pounds per MMcf of total gas and pounds per MMcf of dry gas is less than 0.1 per cent.

The disparity between the 1,500- and 2,000-lb lines from the low-temperature data of Skinner (5-78) and the corresponding lines from the high-temperature data of Dodson and Standing (5-25) and of Olds, Sage, and Lacey (5-56) cannot be explained. Skinner's data on a 0.7 gravity gas at 1,500 psia was taken by measuring dew points; the high-temperature data were measured water contents of equilibrium phases.

The measured dew point of gases that have been brought into equilibrium with gas hydrates, for example in low-temperature separators (Fig. 13-10), will be lower than the equilibrium temperature (5-33, 5-66). Figure 5-10 from Records and Seely shows such a deviation. This decrease in the dew point below the temperature of contact with the hydrate is explained by the fact that measured dew points are metastable equilibria (5-41). In Fig. 5-4, it may be seen that the metastable dew point is lower than the equilibrium dew or hydrate point. The data in Fig. 5-10 have been plotted in Fig. 5-11, showing depression of dew point as a function of the difference between the temperature at which the gas would form hydrate initially and the actual temperature of hydrate formation. Thus, at 900 psi, the gas in Fig. 5-11 initially formed hydrate at 61°F. At an equilibrium temperature of 15°F, the dew point is observed at 0°F. The difference between the initial temperature, 61°F, and the equilibrium temperature, 15°F, is plotted as a function of the depression, 15 − 0°.

When metastability occurs in the gas-ice region, Fig. 5-9 may be used to correct the dew-point charts to actual equilibrium conditions.

The presence of dissolved solids in water lowers the partial pressure of water in the gas phase in equilibrium with the aqueous solution. Dodson and Standing (5-25) estimated the effect of brines on the water content of natural gases up to 30,000 parts per million (ppm) of dissolved solids. The lowering of the vapor

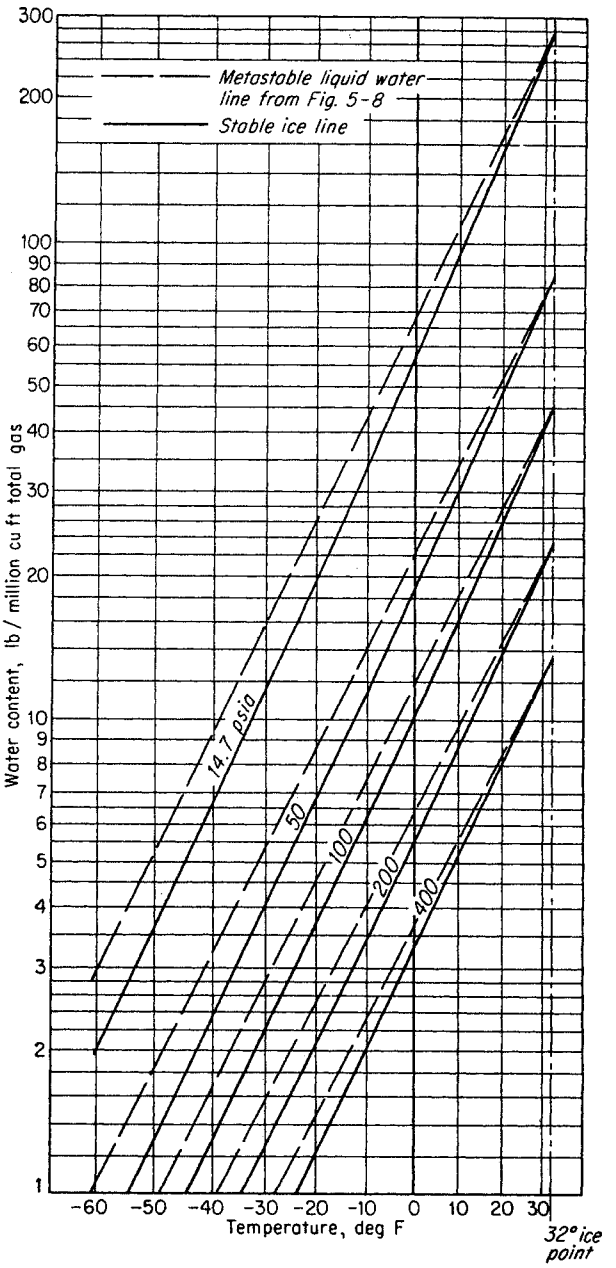

Fig. 5-9. Correction of water content for natural gas in equilibrium with ice.

pressure of water at atmospheric pressure over such salt solutions as sodium chloride, magnesium chloride, calcium chloride, and sodium bicarbonate gives a correction curve which may approximate the effect for brines with high contents of dissolved solids (Fig. 5-12).

Effect of Gas Composition on Water Content

The content of water in a gas phase may be computed at low pressures by assuming that water exerts

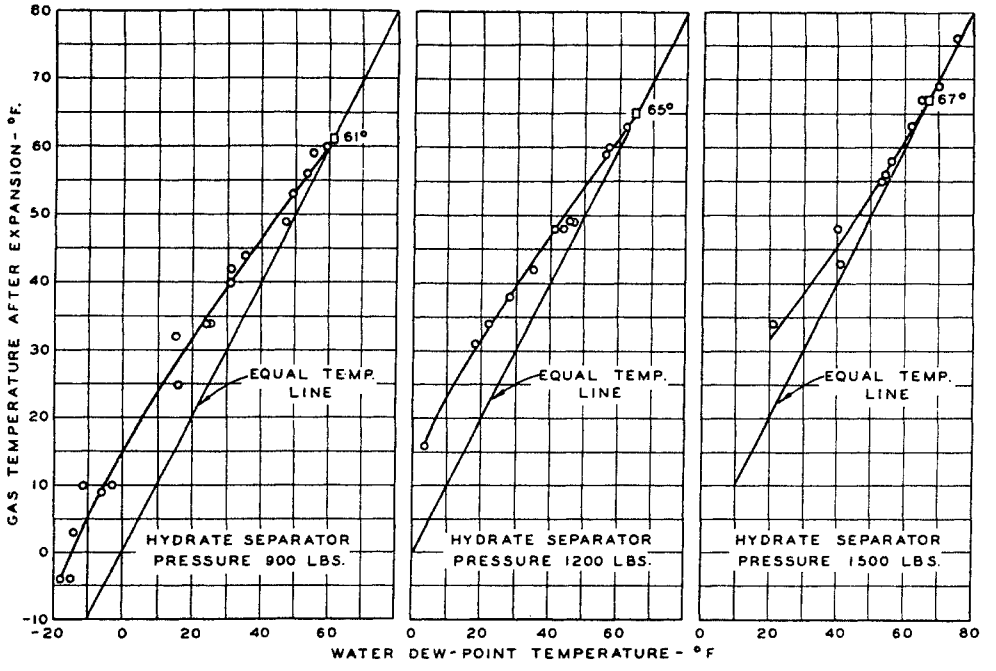

Fig. 5-10. Water dew-point temperature vs. hydrate-separator temperature. (*Records and Seely, 5-66. Courtesy AIME.*)

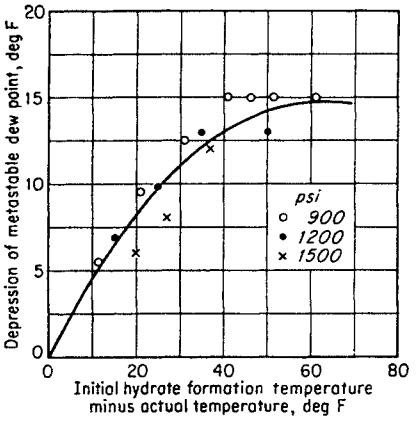

Fig. 5-11. Depression of metastable dew point below hydrate temperature.

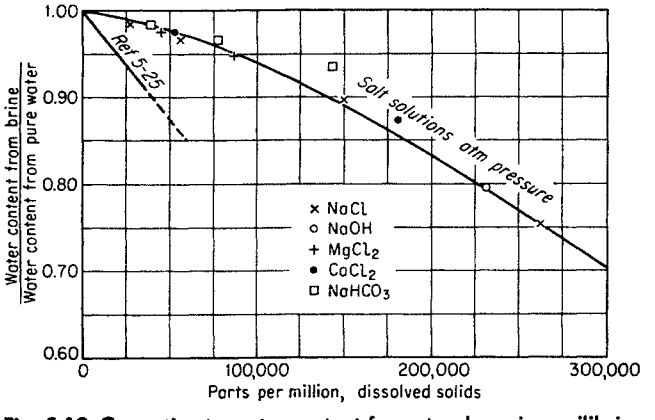

Fig. 5-12. Correction to water content for natural gas in equilibrium with brines.

Table 5-3. Water Content of Nitrogen and Hydrogen Gases

Temp, °F	Pressure, psia	Compressibility factor z	Mole % water in gas	
			Exp	Calc*
Water-Hydrogen System				
122	1,470	1.06	0.139	0.129
	2,939	1.117	0.0785	0.068
	5,878	1.250	0.0468	0.038
	8,817	1.370	0.0363	0.0268
	14,696	1.615	0.0284	0.0197
Water-Nitrogen System				
122	1,470	1.006	0.156	0.122
	2,939	1.058	0.0979	0.0644
	5,878	1.251	0.0695	0.0381
	8,817	1.476	0.0585	0.0299
	14,969	1.940	0.0405	0.0236
3 Hydrogen–1 Nitrogen–Water System				
77	1,470	1.058	0.0440	0.033
	2,939	1.118	0.0285	0.0174
	5,878	1.266	0.0208	0.0099
	8,817	1.424	0.0199	0.0074
	14,969	1.738	0.0197	0.0054
122	1,470	1.053	0.151	0.128
	2,939	1.112	0.094	0.067
	5,878	1.251	0.064	0.038
	8,817	1.398	0.059	0.0283
	14,969	1.697	0.055	0.0207

* Compressibility factor of gas times vapor pressure of water at given temperature divided by total pressure.

SOURCE: Data of Bartlett (5-4).

its vapor pressure at the given temperature. The vapor pressure divided by the total pressure will give the mole fraction of water for ideal gases. When the gases deviate from ideal, the mole fraction of water will be obtained by multiplying the compressibility factor of the gas by the ratio of the vapor pressure to the total pressure. Table 5-3 shows a comparison between experimental and calculated water contents of nitrogen, hydrogen, and mixtures of hydrogen and nitrogen. The data show that, at high pressure, the water content depends upon the gas and that water is more volatile than the above rule indicates.

Poynting (5-47) reasoned that external pressure should increase the vapor pressure of liquids or solids. Application of Poynting's correction to the solubility of water in gases accounts for only a fraction of the increase in the solubility of water in hydrocarbon gases with pressure (5-4, 5-56). From the standpoint of a binary system, water must become very volatile as the critical pressure is reached and an upturn in concentration would be expected at the pressure in Table 5-3. Gases with the greatest solubility in water would approach critical conditions at the lower pressures; hence, at a given pressure such as 1,000 psi, these gases should contain more water.

Binary data on the solubility of water in carbon dioxide (5-88) and in hydrogen sulfide (5-77) indicate that the solubility of water in natural gases should be increased by the presence of appreciable quantities of these substances.

The data of Deaton and Frost (Fig. 5-13) indicate that the saturated water content of natural gases containing substantial amounts of nitrogen is lower than that of nitrogen-free gases (5-21). Figure 5-14 shows the effect of pressure on the deviation from ideal-gas behavior for several natural gases, some of which contain appreciable quantities of nitrogen. Their compositions are listed in Table 5-4. Nitrogen in natural gas tends to decrease the solubility of water in the gas, because it decreases the deviation from ideal-gas behavior and is less soluble in water. The data of Fig. 5-13, when converted to a mole-fraction basis, show that the nature of the gas, its solubility in water, etc., in addition to the deviation from ideal

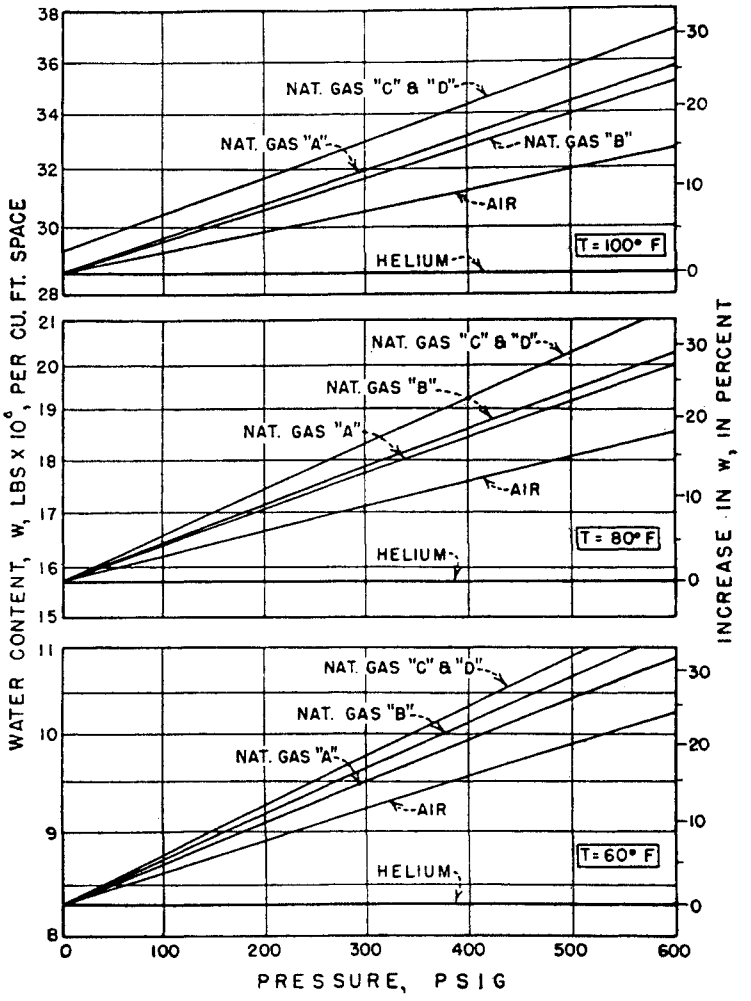

Fig. 5-13. Water content per cubic foot of space occupied by the gas under pressure when saturated with water at the indicated pressure and temperature. *(Deaton and Frost, 5-21.)*

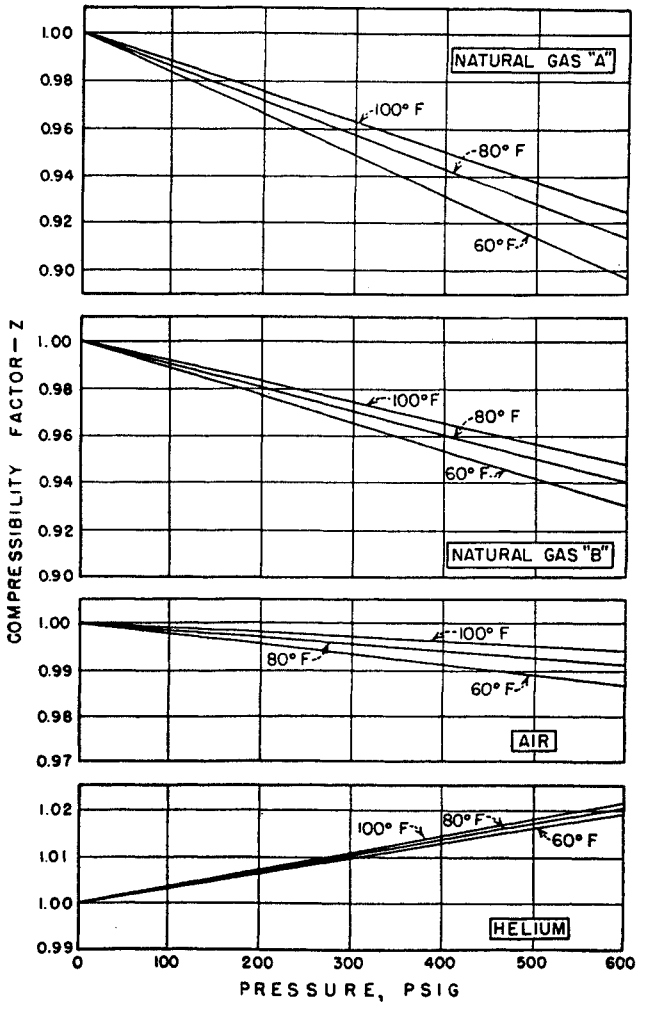

Fig. 5-14. Compressibility factor for gases in Fig. 5-13. (*Deaton and Frost, 5-21.*)

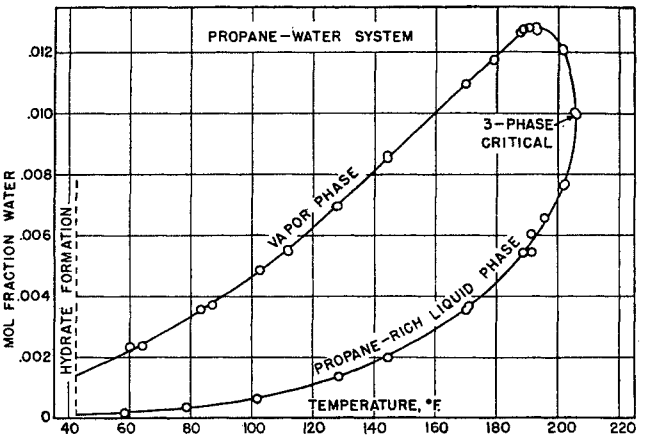

Fig. 5-16. Concentration of water in the propane-rich phases in the three-phase region. (*Kobayashi and Katz, 5-40. Courtesy Ind. Eng. Chem.*)

Table 5-4. Analysis of Gases in Fig. 5-13

Constituent	Mole %					
	Natural gas				Air	Helium
	A	*B*	*C*	*D*		
Air	.....	.....	.....	.....	100.0	
Carbon dioxide	0.3	0.8	0.2	0.60		
Nitrogen	9.4	25.0	1.1	1.00	.....	2.0
Helium	.....	.....	.....	.....	.....	98.0
Methane	79.4	67.4	87.9	94.36		
Ethane	5.9	3.7	4.4	2.64		
Propane	3.3	1.9	4.9	0.96		
Butane+	1.7	1.2	1.5	0.44		
	100.0	100.0	100.0	100.0	100.0	100.0

SOURCE: (5-21).

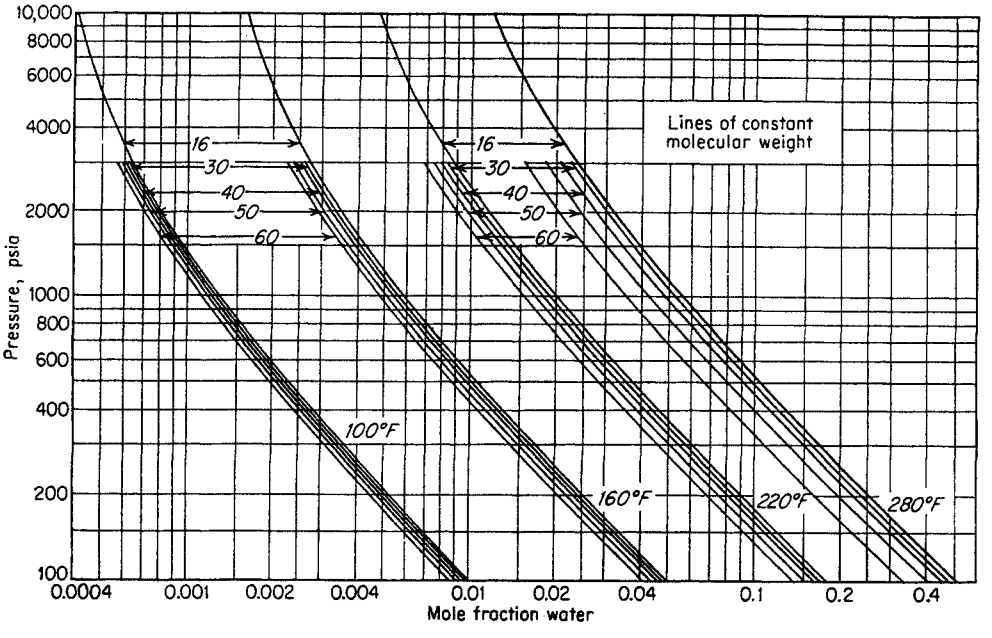

Fig. 5-15. Effect of molecular weight on the water content of the methane-butane-water system. (*McKetta and Katz, 5-52. Courtesy AIME.*)

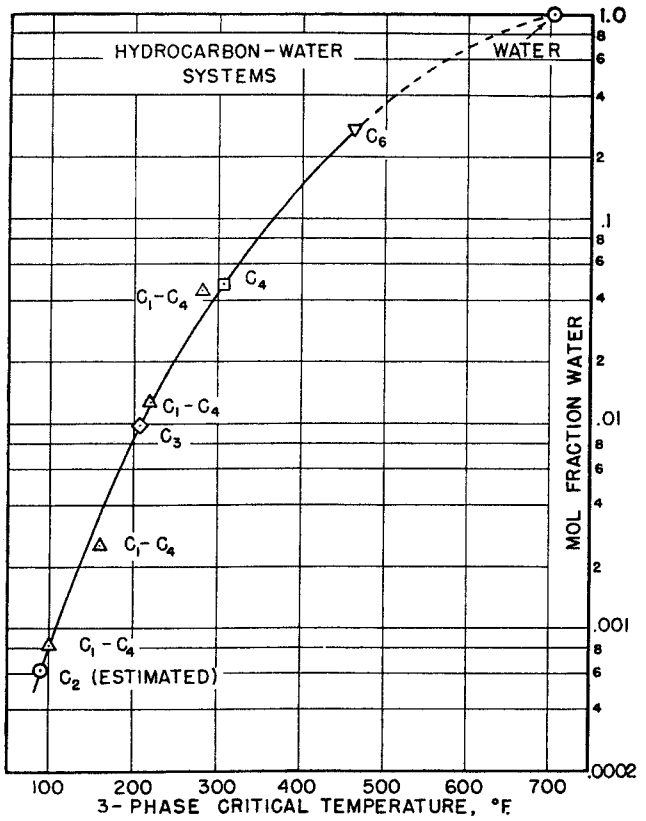

Fig. 5-17. Composition of hydrocarbon-rich phase at three-phase critical conditions. (*Kobayashi and Katz, 5-40. Courtesy Ind. Eng. Chem.*)

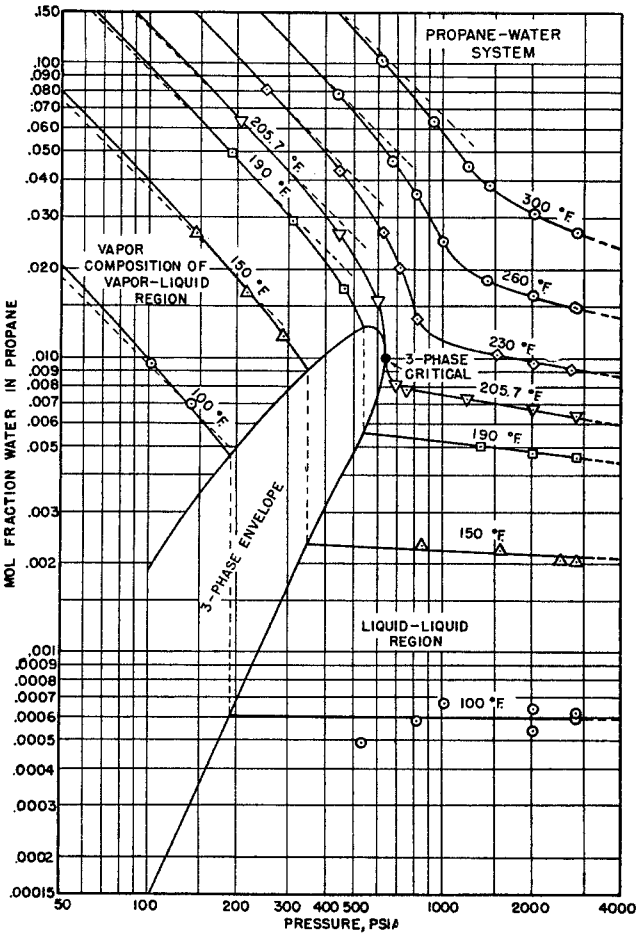

Fig. 5-18. Concentration of water in propane-rich phases in two-phase region. (*Kobayashi and Katz, 5-40. Courtesy Ind. Eng. Chem.*)

gases, affect the mole fraction of water in an equilibrium gas phase.

McKetta and Katz (5-51, 5-52) measured the water content of equilibrium vapors in the methane-butane-water system. The influence of adding the butane to methane is shown in Fig. 5-15. The effect of molecular weight increases with increased temperature. All natural gases from methane to 1.0 gravity gases have molecular weights between 16 and 30. Based on the methane-butane data, one would expect a small but negligible decrease in water content with increase in gas gravity.

Solubility of Water in Hydrocarbon-rich Liquids

Kobayashi and Katz (5-39, 5-40) reported data on the water content of propane in the propane-water system. Figure 5-16 shows the water content of vapor and liquid in the three-phase region and merging at the three-phase critical. Figure 5-17 gives the water content at the three-phase criticals for other hydrocarbon-water systems.

In the two-phase region, Fig. 5-18 gives the water content of the propane phase. At high pressures, the system may be considered as liquid (propane)–liquid (water) equilibria while at low pressures and high temperatures it may be considered as vapor (propane)–liquid (water) equilibria. The transition in the neighborhood of the three-phase critical is rapid but smooth.

Figure 5-19 has been prepared to show the solubility of water in hydrocarbon liquids with references as shown.

Figures 5-20*a* and 5-20*b*, prepared from information by Kobayashi and Katz (5-40), show the continuity in the solubility of water in gas and in liquid hydrocarbons. The concentration of water is plotted as a function of temperature, phase molal volume, and molecular weight. This plot has considerable generality and may be applied to the hydrocarbon-rich liquid phase as well as to the gas phase. The phase molal volume, expressed in cubic centimeters per gram mole, may be calculated from the compressibility factors or density charts.

The equilibrium constants for water

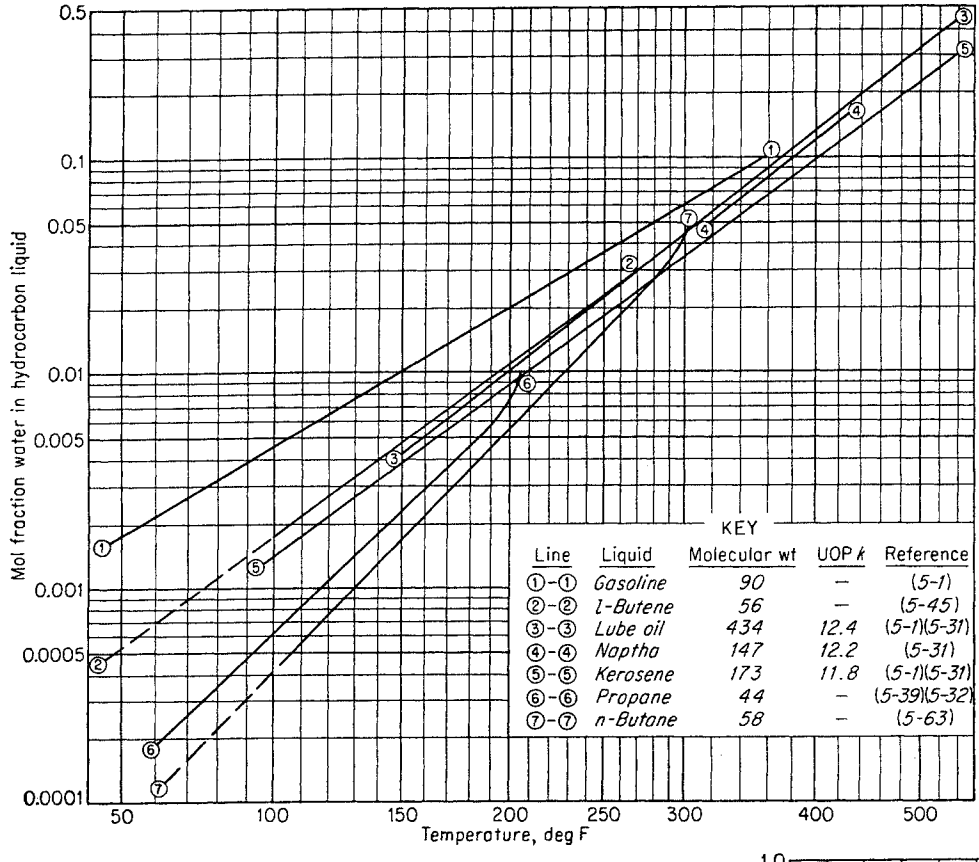

Fig. 5-19. Solubility of water in liquid hydrocarbons.

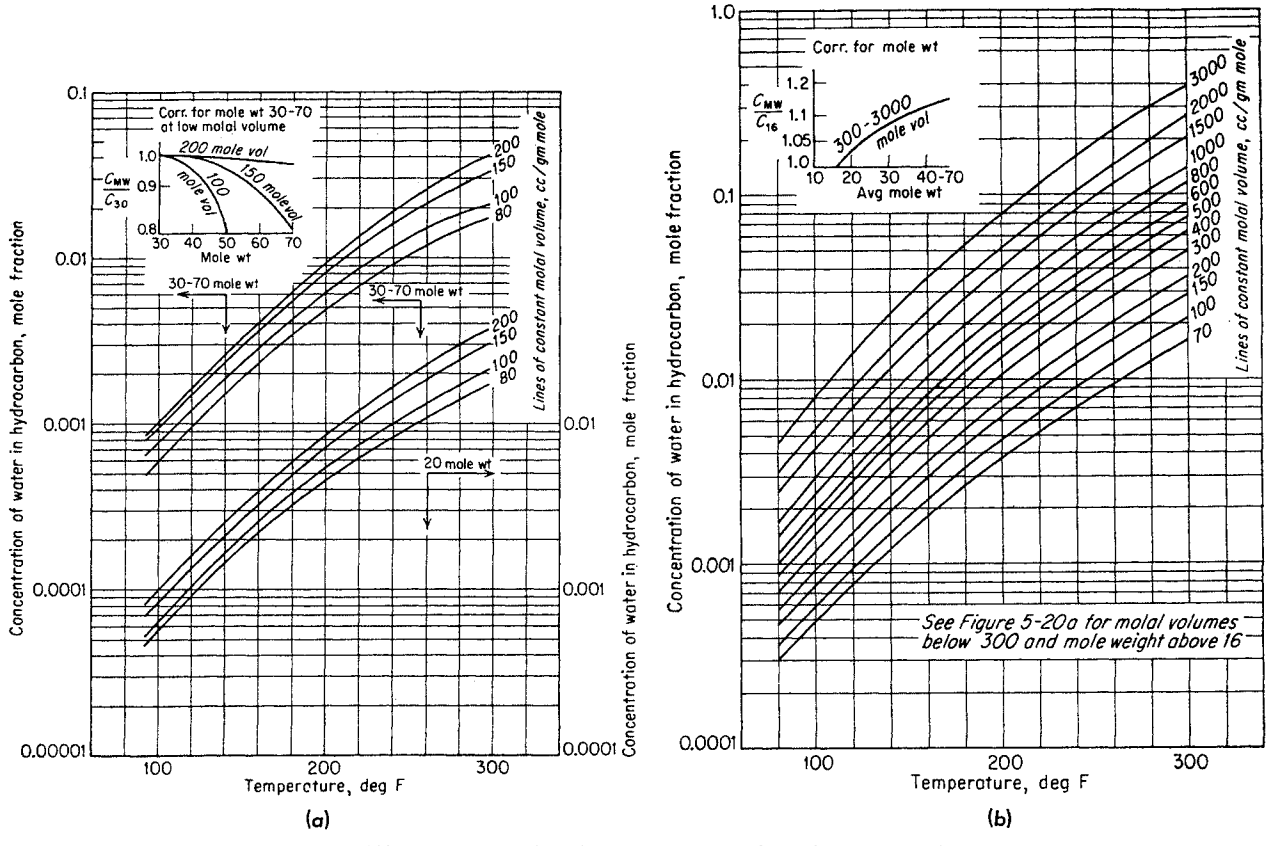

Fig. 5-20. Water content of hydrocarbon phases based on phase density.

$$K = \frac{\text{mole fraction of water in vapor}}{\text{mole fraction of water in hydrocarbon liquid}}$$

may be obtained for hydrocarbon-water systems along the three-phase L_1-L_2-G conditions. Figure 5-21 shows equilibrium constants which may be used to compute the distribution of water between the gas phase and the hydrocarbon-rich liquid phase, composed of natural gas–natural gasoline mixtures. The chart is based on the methane-butane-water system studied by McKetta and Katz (5-51). When water is present at temperatures above 200°F, the hydrocarbon vapor-liquid equilibrium constants may be appreciably different from those for the corresponding anhydrous mixtures (5-51). Poettmann and Dean (5-60) and Gentry and Gunther (5-32) report equilibrium constants for propane and propylene.

Leland (5-45) has calculated the solubility of water in various pure hydrocarbons by applying the intermolecular-potential-energy concepts of Scatchard (5-72) and Hildebrand and Scott (5-37). The procedure is based on molecular models for which the following assumptions are made:

1. The mutual energy of two molecules depends upon the distance between them and is independent of other molecules in the neighborhood and of temperature.
2. The distribution of the molecules in position and in orientation is random.
3. The change in volume on mixing at constant pressure is zero.

Leland further assumed an empirical method for combining the virial coefficients of the pure gases. Table 5-5 gives values comparing calculated and experimental solubilities of the hydrocarbon-rich phase in the 1-butene–water system.

Robin and Vodar (5-70) have applied the 6-12 Lennard-Jones potential to the solubility of methanol, water, and xenon in compressed gases. Their computations assume that the solution of liquids (or solids) in compressed gases results from the occurrence of two phenomena:

1. An increase in the vapor pressure of the liquid as a result of pressure
2. An interaction between the molecules of the liquid and of the compressed gas, tending generally to increase the quantity of liquid contained in the gaseous phase

Table 5-5. Solubility of Water in 1-Butene

Temp, °F	Pressure, psia	Solubility, mole fraction of water	
		Calc	Exp
100	1,000	0.00179	0.00173
	6,000	0.00159	0.00162
	10,000	0.00158	0.00158
160	1,000	0.00571	0.00554
	6,000	0.00431	0.00493
	10,000	0.00398	0.00455
220	1,000	0.01272	0.01445
	6,000	0.01005	0.01180
	10,000	0.00915	0.01085
280	1,000	0.0294	0.0322
	6,000	0.0211	0.0260
	10,000	0.0190	0.0229

SOURCE: (5-46).

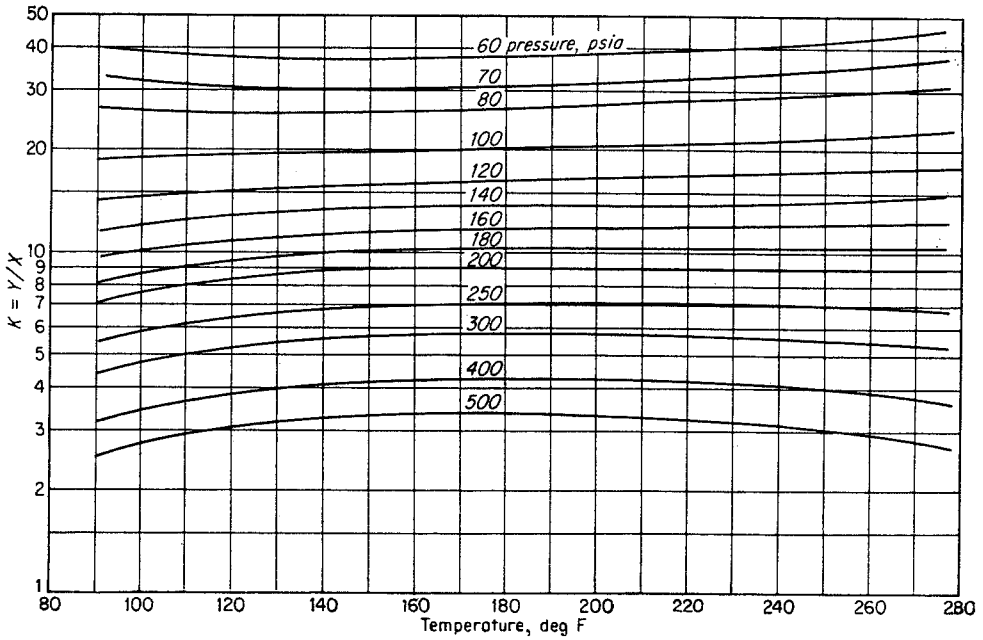

Fig. 5-21. Equilibrium constants for water between gas phase and hydrocarbon-rich liquid phase, natural gasoline systems.

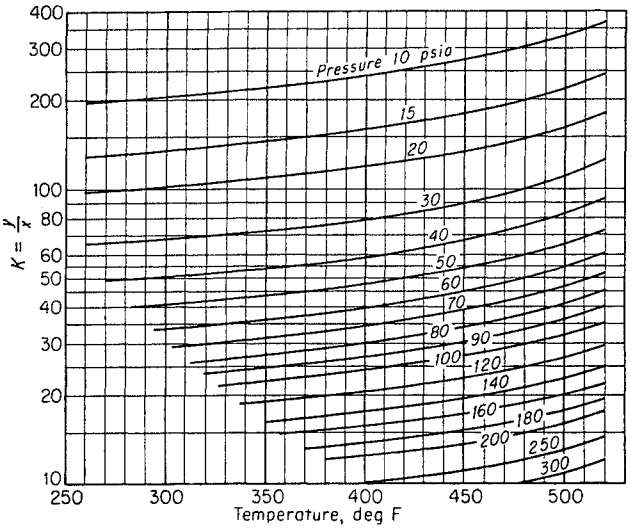

Fig. 5-22. Equilibrium constants for water between gas phase and hydrocarbon-rich liquid phase, 170 molecular weight absorber oil.

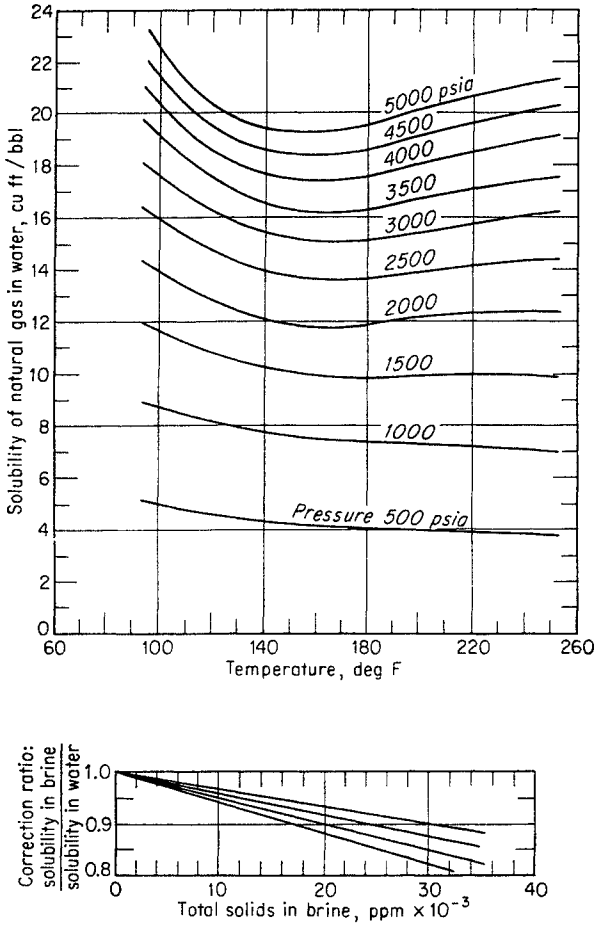

Fig. 5-23. Solubility of natural gas in water. (*Dodson and Standing, 5-25. Courtesy API.*)

Phenomenon 1 is demonstrated by Poynting's effect, with corrections for non-ideal-gas behavior. The agreement between experimental and calculated values is good up to pressures of 100 to 200 atm, but the discrepancies become serious thereafter. Although these calculations based on molecular models do not provide us with immediate explanations for the solubility of water and other slightly volatile liquids in gases, they do yield understanding of the probable forces that comprise the solvent effects of gases on liquids. Refinement of these calculations is necessary to provide a general explanation for the solubility of water in gases such as methane and the light hydrocarbons, which are considered to be nonpolar.

Leland (5-45) and Hibbard and Schalla (5-36) recommend the following equation in plotting the solubility of water in liquid hydrocarbons:

$$\ln x_1 = \frac{H_1^{\infty} - H_1^{0}}{RT} + C \qquad (5\text{-}1)$$

where x_1 = mole fraction of water
H_1^{∞} = partial molar enthalpy of the solute at infinite dilution
H_1^{0} = molar enthalpy of pure liquid solute
R = gas-law constant
T = temperature, degrees absolute
C = integration constant

The supposition that the difference $H_1^{\infty} - H_1^{0}$ is independent of temperature holds remarkably well for the solubility of water in hydrocarbon liquids except in the vicinity of the critical temperature of the hydrocarbon solvent (5-40, 5-45).

The solubility of water in various hydrocarbon liquids along the three-phase L_1-L_2-G conditions is presented in Fig. 5-19 in the form suggested by Eq. (5-1). At low and moderate pressures, these solubility values may be used to compute equilibrium ratios of the concentration of water in the gas phase to concentration of water in the hydrocarbon-rich liquid phase, by combining Dalton's and Henry's laws (5-30) to give

$$K = \frac{y_{H_2O}}{x_{H_2O}} = \frac{p}{x_s P} \qquad (5\text{-}2)$$

where K = equilibrium constant at total pressure P and at temperature T
y = mole fraction of water in the gas phase
x = mole fraction of water in hydrocarbon-rich liquid phase
p = vapor pressure of water at temperature T
x_s = mole fraction of water at saturation
P = total pressure of the system

Figure 5-19 may be used to obtain the values of x_s using the appropriate molecular weight hydrocarbon. The total pressure of the system may be taken as the

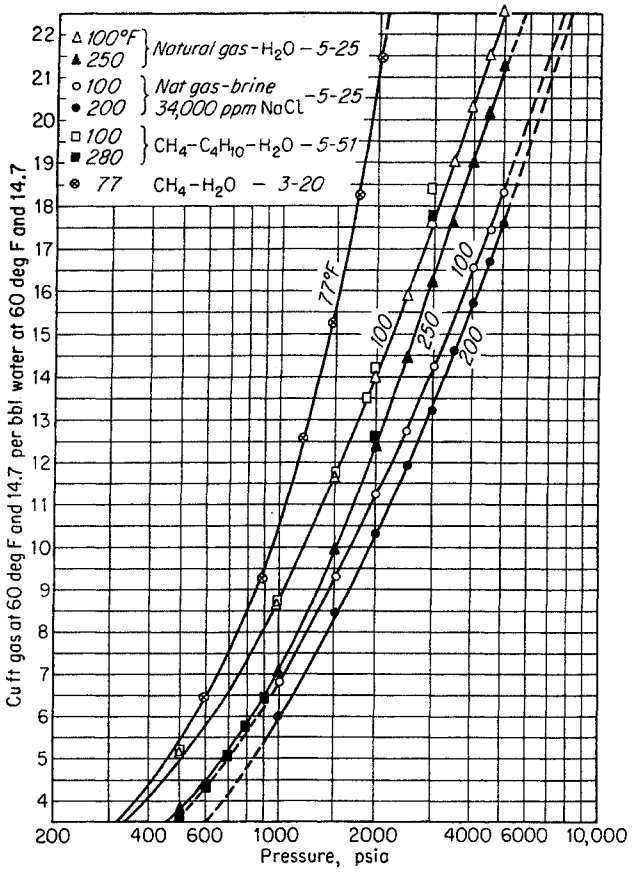

Fig. 5-24. Solubility of natural gases in water and brine. (*McKetta and Katz, 5-52. Courtesy AIME.*)

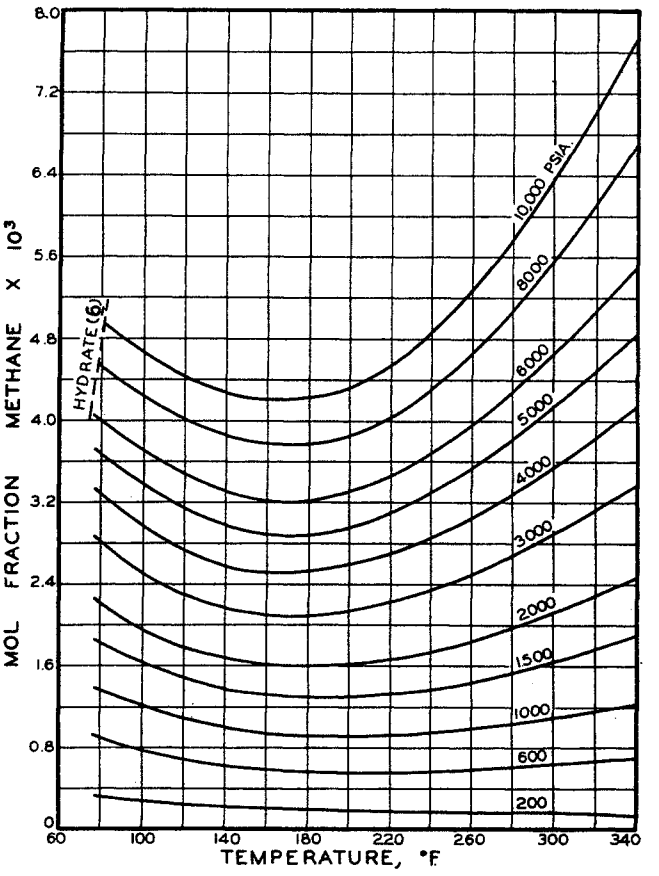

Fig. 5-25. Solubility of methane in water. (*Culberson and McKetta, 5-18. Courtesy AIME.*)

sum of the vapor pressures of hydrocarbon and of water without involving appreciable error until the solubility in oil reaches several mole per cent. The actual system pressure P will be somewhat higher than the sum of the vapor pressures of oil and water because the solutions of hydrocarbon and water behave nonideally (5-75).

Equation (5-2) has been applied to a 170 average molecular weight hydrocarbon to compute the K values for water presented in Fig. 5-22.

Solubility of Hydrocarbons in Water

The solubility of pure hydrocarbons and natural gas in water has been studied rather extensively (5-9, 5-16 to 5-19, 5-25, 5-40, 5-46). The paraffin hydrocarbons are very slightly soluble in water even at high pressures. The appearance of hydrogen unsaturation tends to increase the solubility of hydrocarbon in water (5-46).

Dodson and Standing (5-25) determined the solubility of a natural gas in water and found substantially the same features that are exhibited by the solubility of methane in water. Figure 5-23 gives the solubility of natural gas in water up to 5,000 psi and 260°F. Minimum isobaric solubility exhibited by many slightly soluble gases is indicated for all pressures above 1,500 psi. The solubility of natural gas in water is somewhat diminished by the presence of dissolved solids in the liquid phase. Figure 5-24 compares the solubility of methane in water, natural gas in water, and natural gas in brine. It is interesting to note that this solubility (approximately 0.003 mole fraction of gas in liquid water) produces an increase of about 18 per cent in the compressibility of the saturated liquid phase (5-25).

Culberson and McKetta have presented data on the solubility of methane and ethane in water at pressures to 10,000 psia [Fig. 5-25 and Fig. 5-26 (5-17, 5-18)]. Kobayashi and Katz reported the solubility of propane as shown in Fig. 5-27.

Calculations for the solubility of hydrocarbon in water may be made by the use of Henry's law for dilute solutions:

$$\bar{p}_1 = Hx_1 \quad \text{where the gas behaves ideally} \qquad (5\text{-}3)$$

or

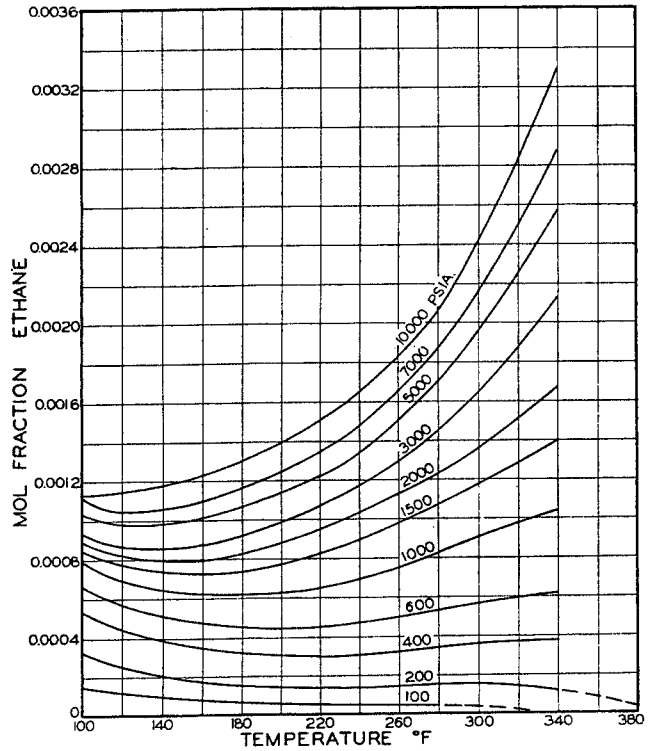

Fig. 5-26. Solubility of ethane in water. (*Culberson and McKetta, 5-17. Courtesy AIME.*)

$$\bar{f}_1 = Hx_1 \quad \text{where the gas behaves nonideally} \qquad (5\text{-}4)$$

where $\bar{p}_1$ = partial pressure of component 1
x_1 = concentration of component 1 in solution
H = Henry's law constant
$\bar{f}_1$ = partial fugacity of component 1

For a given substance the Henry's law constant is a function of temperature only, since it is evaluated at low pressures under ideal-gas conditions for infinitely dilute solutions. Figure 5-28 is a plot of Henry's law constants for common constituents of natural gases. Each gas shows a characteristic maximum in the constant at some temperature.

A more rigorous approach to the solubility of nonpolar gases in liquids has been suggested by Krichevsky and Kasarnovsky (5-44) and by Wiebe and Gaddy (5-88). The equation given by Krichevsky and Kasarnovsky has been rederived by Leland (5-45) to give

$$\ln \frac{\bar{f}_2}{x_2} = \ln H + \frac{\bar{v}_2}{RT}(p - p_s) \qquad (5\text{-}5)$$

where $\bar{f}_2$ = partial fugacity of solute gas
x_2 = mole fraction of dissolved solute
$\bar{v}_2$ = partial molal volume of gas dissolved in water (assumed to be a function of temperature only)

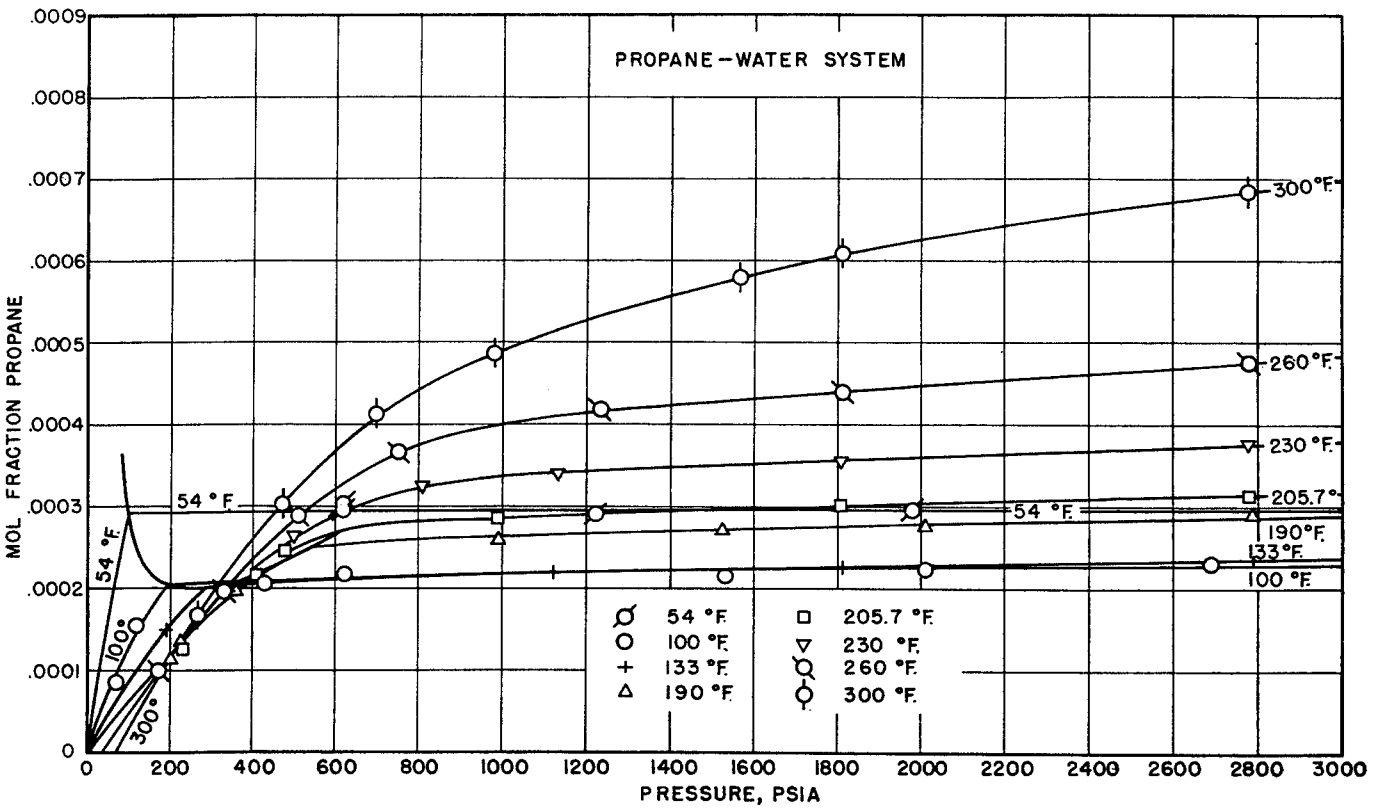

Fig. 5-27. Solubility of propane in water. (*Kobayashi and Katz, 5-40. Courtesy Ind. Eng. Chem.*)

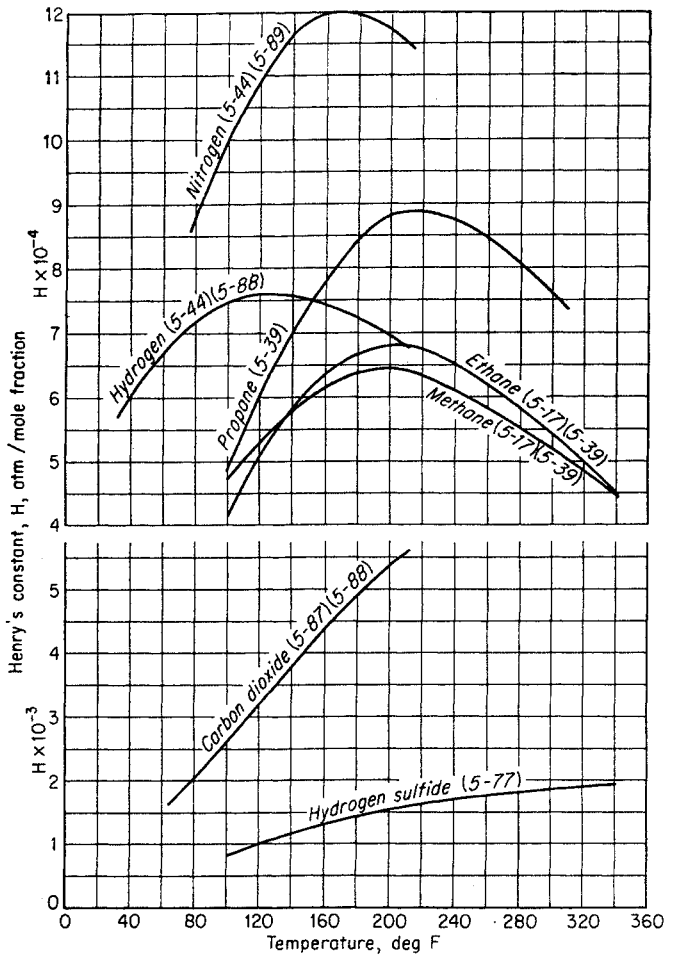

Fig. 5-28. Henry's law constants for solubility of hydrocarbons in water. (5-40.)

p_s = saturation pressure of pure water
T = absolute temperature
H = Henry's law constant evaluated at $p = p_s$

Kobayashi and Katz (5-40) applied this relationship to the water-rich phase of hydrocarbon-water binaries to determine values of $\bar{v}_2$ and to represent the data thermodynamically (Figs. 5-29 and 5-30). Leland, McKetta, and Kobe (5-46) have applied the equation to both liquid phases for the 1-butene–water system. Near the hydrocarbon criticals, deviation of isothermal plots of ln $(\bar{f}_2/x_2)$ versus $p - p_s$ indicates that $\bar{v}_2$ cannot be assumed to be independent of pressure. More general application of Eq. (5-5) has been hampered by the lack of partial-fugacity and partial-volume data for mixtures. Equation (5-5) may be used most profitably at the present time in the extrapolation of intermediate-pressure data to higher pressures.

GAS HYDRATES

Hammerschmidt (5-33) called the natural gas industry's attention to the fact that the freezing of gas lines was due to gas hydrates. Much early work had been done by scientists in Europe who were exploring the nature of substances (1-9). Faraday was the first to discover gas hydrates in his investigation of the hydrates of chlorine (5-27). Early work on normally gaseous substances such as methane, ethane, and carbon dioxide was carried out during the period of theoretical studies by Villard, De Forcrand, and others, as reviewed by Schroeder (5-76). Hammerschmidt's report on the problems of hydrate formation in the natural gas industry gave the hydrate-formation conditions for a natural gas. Since the problem of

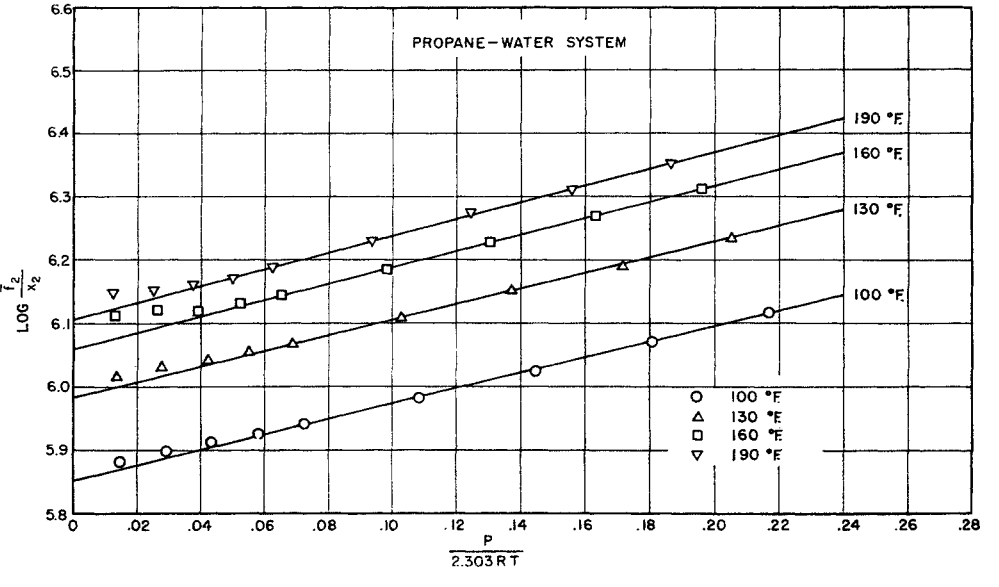

Fig. 5-29. Plot of solubility of propane in water to determine partial volume and Henry's law constant. (*Kobayashi and Katz, 5-40. Courtesy Ind. Eng. Chem.*)

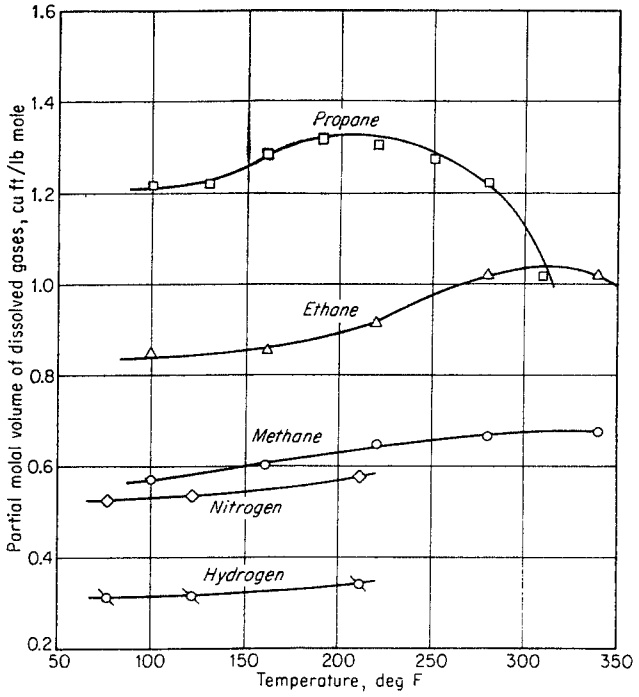

Fig. 5-30. Partial molal volumes of pure hydrocarbons, H_2, and N_2 dissolved in water. (*Kobayashi and Katz, 5-40. Courtesy Ind. Eng. Chem.*)

hydrate formation has gained practical significance, many studies by Deaton and Frost (5-21, 5-28), Katz and coworkers (5-12, 5-90, 5-43, 5-38, 5-42, 5-55, 5-84), and others (5-77, 5-49, 5-65, 5-69, 5-2, 5-3, 5-48) have been conducted in the hydrate region for binary and multicomponent mixtures of hydrocarbons and water. More recently, fundamental work on the crystal structure of hydrocarbon-type hydrates has pointed to theoretical hydrate structures (5-14, 5-57, 5-81) that have been confirmed by X-ray studies (5-15, 5-82).

Nature of Gas Hydrates

Gas hydrates have some of the properties that are ascribed to chemical compounds, but in other respects they behave as solutions of gases in crystalline solids. As a result of experimental measurements and thermodynamic analyses, various formulas have been assigned to the hydrates. The instability of the hydrates at low pressures has contributed to the uncertainties of the experimental measurements.

The experimental determination of hydrate formation is normally conducted in glass-windowed equipment. Figure 5-31 shows a diagram of a glass-windowed cell used to determine hydrate formation for the methane-propane-water system (5-12). In this case, quadruple points were determined by lowering the temperature on a mixture of gas, hydrocarbon-rich liquid, and water-rich liquid until hydrate formed. Often hydrates are difficult to form; an appreciable degree of subcooling is required. Hydrates are not known to form unless liquid water is present. Once seed crystals are formed, positive and negative temperature changes along the equilibrium curve will cause crystals to reappear and melt rather readily. Sudden withdrawal of a small amount of gas phase is used to give the cooling required to initiate crystallization.

Hydrate crystals resemble ice or wet snow in appearance. When the pressure is relieved on hydrates to cause decomposition, the crystals do not change in appearance. Crystals that have just been released from pressure give off a low crackling sound when held to the ear, indicating rupture of the crystal.

Natural gas hydrate crystals, like ice, float on water and have a density of 0.88 to 0.90 gram/cu cm.

The fundamental X-ray investigations of hydrate crystals previously cited indicate that two types of lattice are in evidence: the diamond pentagonal dodecahedron and the pentagonal dodecahedron body-centered type. Physical data on the lattices are presented in Table 5-6.

The fundamental hypotheses used by Claussen (5-13) are:

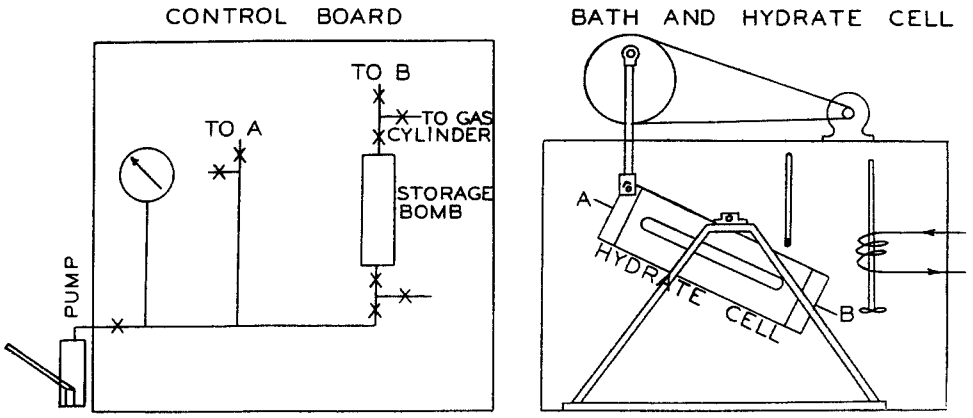

Fig. 5-31. Apparatus for forming hydrates.

1. That the main framework of the hydrate must be water molecules, with the hydrocarbon or inert molecules occupying void spaces in the water network without forming any chemically strong bonds with water

2. That this water framework is icelike because of comparable heats of formation (5-21, 5-76) but somewhat different from ice, since the ice lattice provides no void space or receptacle for even the smallest hydrocarbon molecule

Of the paraffin-hydrocarbon hydrates, the structure of propane hydrate only has been studied (5-82). A chart (Fig. 5-32) showing molecular sizes and ratio of water molecules to gases, prepared from the combined works of Stackelberg (5-81) and Claussen (5-13, 5-14), indicates that larger molecules cannot enter the structure so frequently as small molecules. Presumably, two argon molecules fit into the large holes to give a theoretical hydrate formula of $A \cdot 4\frac{1}{4}H_2O$ (5-20). The propane molecules fit only the larger voids of the diamond-type lattice, giving propane a theoretical hydrate number of $C_3H_8 \cdot 17H_2O$. One of the largest hydrocarbon molecules that is reported to form hydrates is cyclopentane (5-48). Isopentane and methyl cyclopentane are not hydrate formers (5-48). Small concentrations of ethane or propane in methane drastically lower the pressure required for hydrate formation [Figs. 5-33 and 5-34 (5-21)]. From studies involving the molecular models of the hydrocarbons and the crystal structure of the hydrates, it appears that the molecules are free to rotate in the voids (5-20, 5-81). Substances such as hydrochloric acid, which are highly soluble in water, form no hydrates of this type even though their molecular sizes are of the right order. The number of water molecules associated with each gas molecule is indicated in Fig. 5-32. Experiments verify the order of magnitude but not the exact numbers shown. Liquid normal butane

Table 5-6. Physical Data on Hydrate Lattices

Factor	Diamond type	Body-centered type
Cell constant, A	17	12
Number of water molecules per unit cell	136	46
Number of small voids	16	2
Number of medium voids	0	6
Number of large voids	8	0
Hypothetical hydrating numbers:		
Filling all voids	$5\frac{2}{3}$*	$5\frac{3}{4}$
Filling only larger voids	17	$7\frac{2}{3}$

* Never observed and probably unstable.
SOURCE: (5-13).

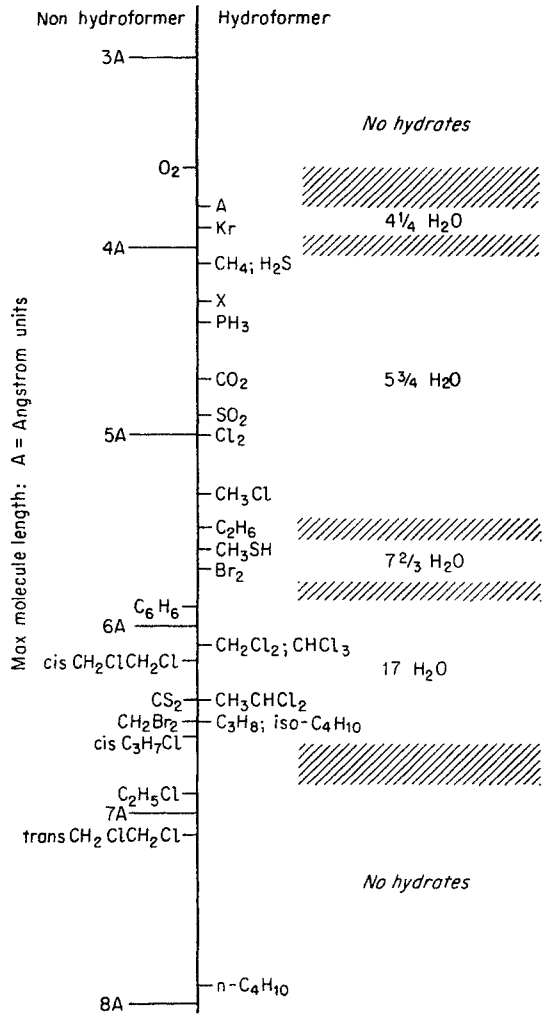

Fig. 5-32. Size of hydrate molecules. (5-13, 5-14, 5-81.)

was shown to form hydrate at 33.8°F (5-90), indicating only a small range of temperature above 32°F for pure butane vapor to form hydrate. However, in the presence of other gases, butane vapor enters the hydrate form at higher temperatures.

Hydrates appear to be solid solutions. The study of the methane-propane-water system showed the quadruple point to have one degree of freedom (Fig. 5-35) which corresponds to a single solid phase. The hydrocarbon compositions of gas hydrates were measured and indicate a smooth change in composition with temperature (Fig. 5-36).

Conditions for the Formation of Gas Hydrates

For a given gas, initial conditions for the formation of solid hydrates may be represented by lines on the pressure-temperature plane. The conditions for the formation of hydrates for binary systems of paraffinic hydrocarbons when water is present are given in

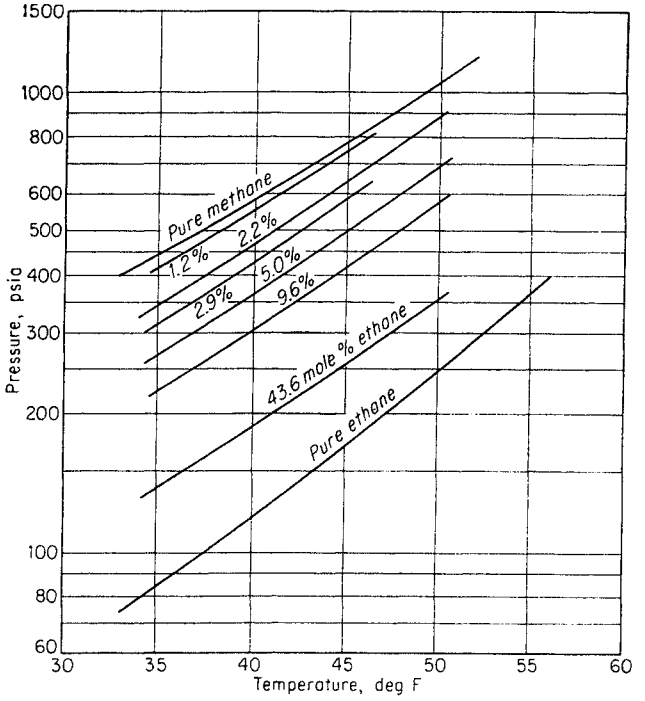

Fig. 5-33. Hydrate-formation conditions of methane-ethane mixtures. (*Deaton and Frost*, 5-21.)

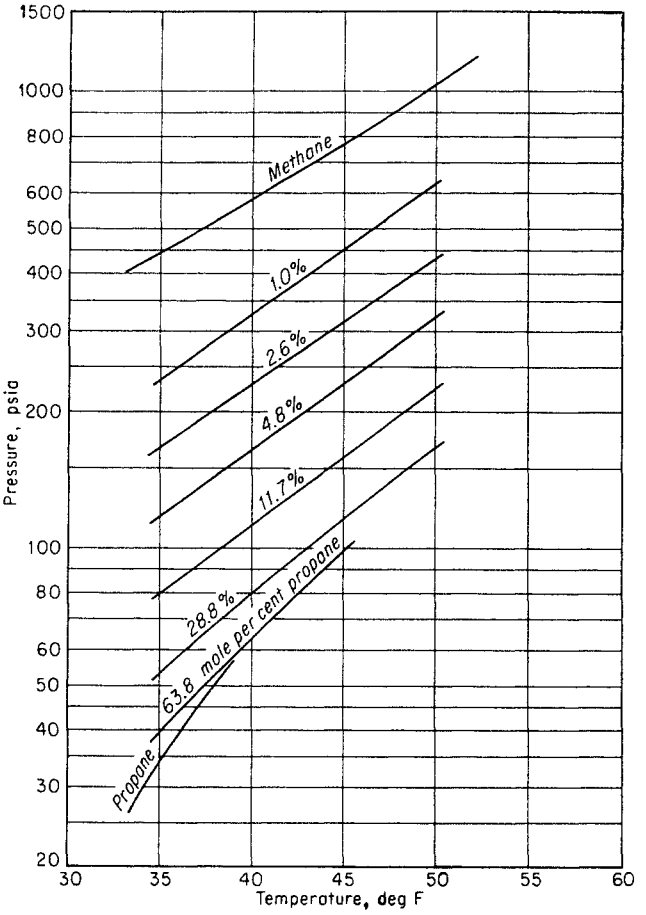

Fig. 5-34. Hydrate-formation conditions of methane-propane mixtures. (*Deaton and Frost*, 5-21.)

Fig. 5-37, from data in the literature (5-12, 5-21, 5-42, 5-69, 5-76, 5-85, 5-90, 1-9). Pentane and hexane are not known to form hydrates. If they did form hydrates, from Fig. 5-37 it might be presumed that they would do so only at temperatures below 32°F. Other gases form hydrates as shown in Fig. 5-38, the vapor–water-rich liquid–hydrate curve intersecting the V-L_1-L_2 curve at a quadruple point. The hydrate-liquid curve extends nearly vertically from this quadruple point. Figures 5-33 and 5-34 show the effect of varying the concentration of ethane and propane in the gas phase on hydrate-forming conditions for the methane-ethane-water and the methane-propane-water systems (5-21). Small changes in the concentration of ethane or propane in the gas phase cause relatively large changes in the gas-hydrate equilibrium curves.

Conditions for gas–liquid water equilibrium accompanied by a trace of solid hydrates, representing the initial conditions for hydrate formation, have been determined for several natural gases [Fig. 5-39 (5-21, 5-90)]. The equilibrium conditions are quite sensitive to nitrogen concentration (5-21) as well as to hydrocarbon composition. The gas gravity (air = 1.0) of the equilibrium gas has been utilized as a correlating parameter in preparing Fig. 5-40. Figure 5-41 has more gravity lines and gives the effect of small concentrations of nitrogen on the hydrate-formation conditions of natural gases.

Prediction of Hydrate-formation Conditions by Vapor-Solid Equilibrium Calculations

In the previous discussion it was indicated that solid gas hydrates behave to some extent as solutions of gases in crystalline solids. Gases evolved from the decomposition of natural gas hydrates (5-12, 5-90) gradually increase in density and, in this respect, resemble solid solutions. By analogy with liquid-vapor equilibria, Wilcox, Carson, and Katz (5-90) postulated that hydrate-formation conditions could be calculated from empirically determined vapor-solid equilibrium constants.

$$K_{v-s} = \frac{y}{x_s} \tag{5-6}$$

where y = mole fraction of hydrocarbon in the gas on a water-free basis

x_s = mole fraction of hydrocarbon in the solid on a water-free basis

Carson and Katz present equilibrium constants for methane, ethane, propane, and isobutane. In later

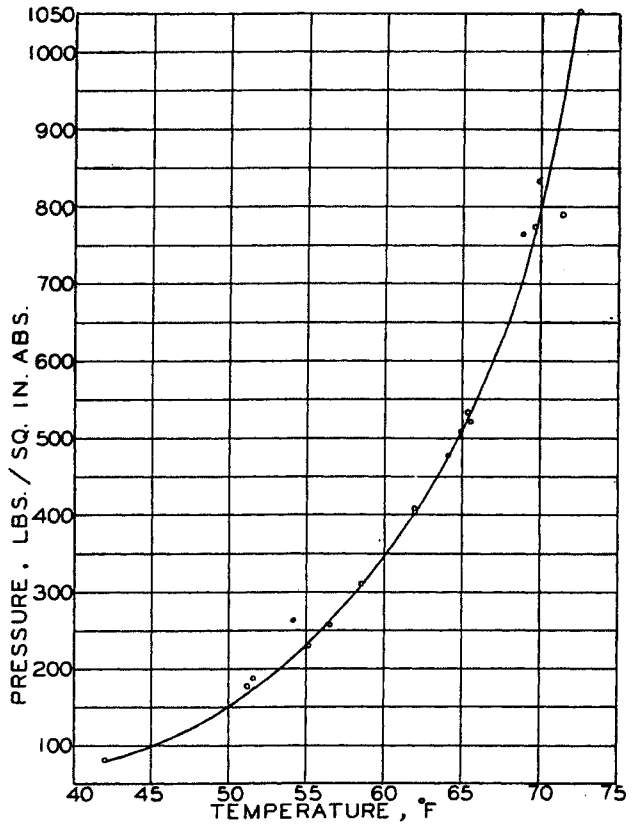

Fig. 5-35. Locus of quadruple point for methane-propane-water system. (*Carson and Katz, 5-12. Courtesy AIME.*)

researches vapor-solid equilibrium constants have been determined for ternary mixtures of methane, carbon dioxide, and water (5-84) and of methane, hydrogen sulfide, and water (5-55). These equilibrium constants are presented in Figs. 5-42 to 5-47. In the presence of lighter hydrocarbons, the equilibrium constants for *n*-butane, for low concentrations of *n*-butane, may be taken as those of ethane. For nitrogen and hydrocarbons heavier than butane, the equilibrium constants are taken as infinity, since they form mixed hydrates with difficulty. The equilibrium constants are assumed to be functions of pressure and temperature only, but actually they should show variation with hydrocarbon composition. The conditions for initial formation are obtained by satisfying the relationship

$$\sum \frac{y}{K_{v-s}} = 1.0 \qquad (5\text{-}7)$$

a procedure analogous to the dew-point calculation for complex gaseous mixtures. Table 5-7 gives the hydrate-formation calculation for a natural gas at 50°F. The calculated pressure of 337 psia agrees satisfactorily with the observed pressure of 325 psia. It should be noted that the y/K terms each equal x_s, the hydrate composition on an anhydrous basis.

Table 5-8 demonstrates the agreement between the calculated and experimental hydrate-formation conditions at several pressures. In view of the experimental difficulties of working with a solid phase, the calculations seem to support the hypothesis that the complex hydrates behave as solid solutions.

Katz and coworkers (5-38) have combined calculated and observed hydrate-formation conditions (Fig. 5-40) for natural gases with thermodynamic enthalpy-entropy data (5-10) to obtain Figs. 5-48 to 5-50. These figures may be employed to predict the maximum free expansion ($\Delta H = 0$) of natural gases without hydrate formation when liquid water is

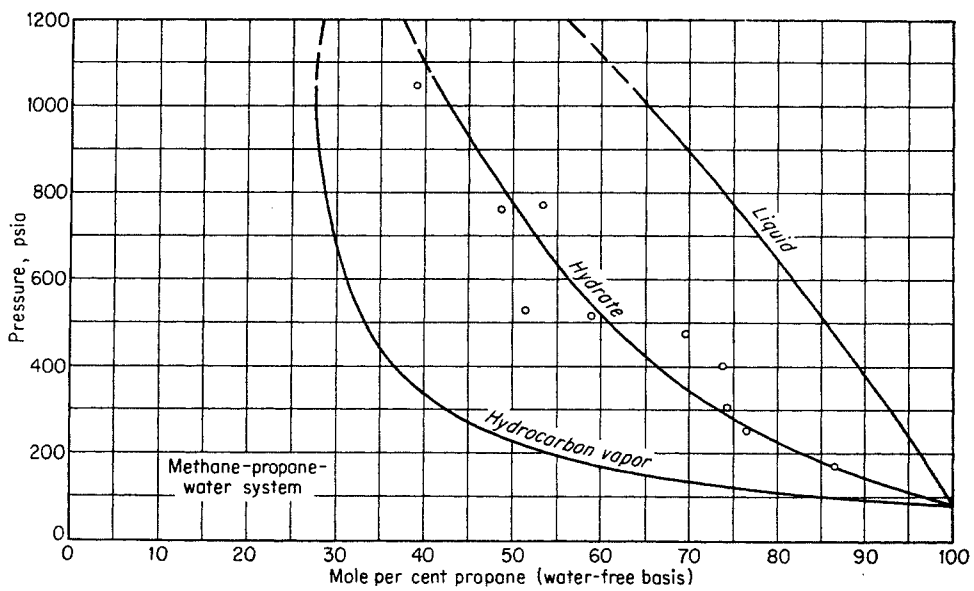

Fig. 5-36. Phase compositions in methane-propane-water system. (*Carson and Katz, 5-12. Courtesy AIME.*)

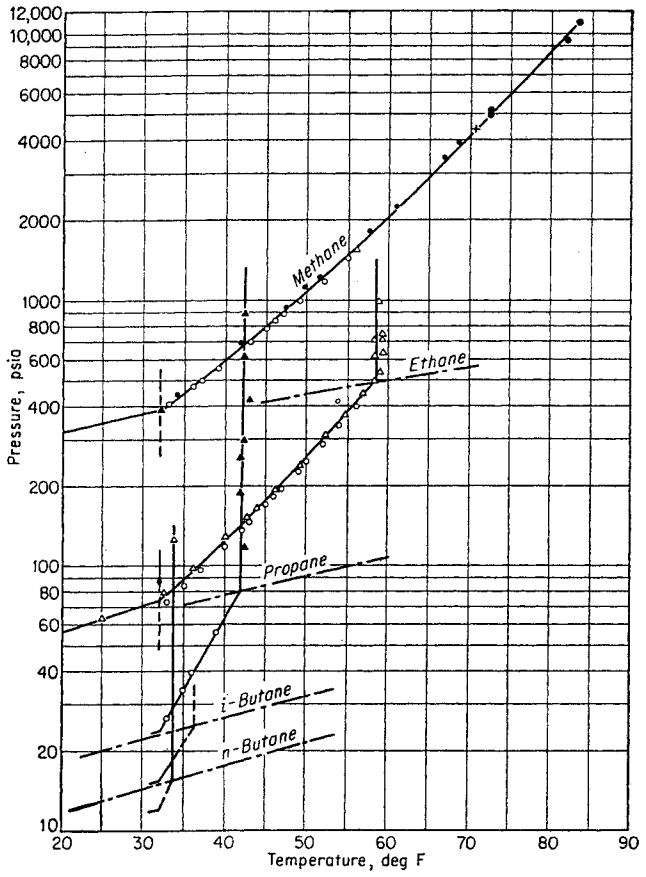

Fig. 5-37. Hydrate-forming conditions for paraffin hydrocarbons.

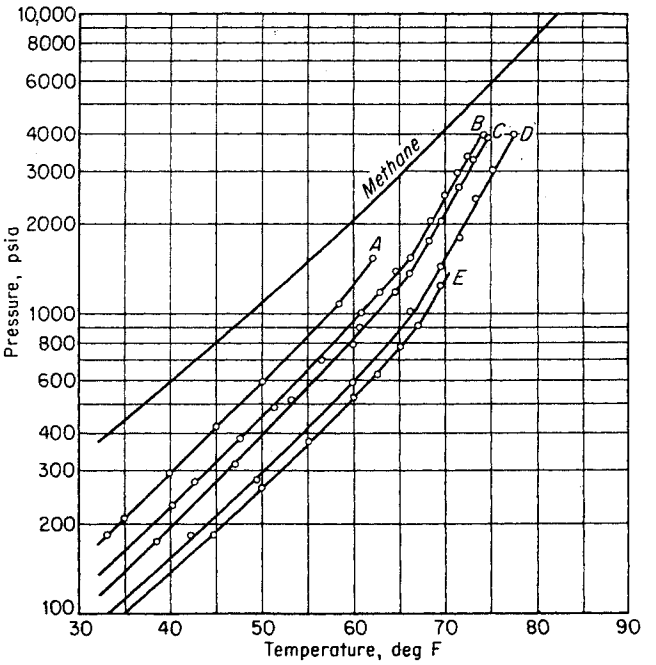

Fig. 5-39. Hydrate-forming conditions for natural gases. (*Data of Refs. 5-21, 5-90, 5-42.*)

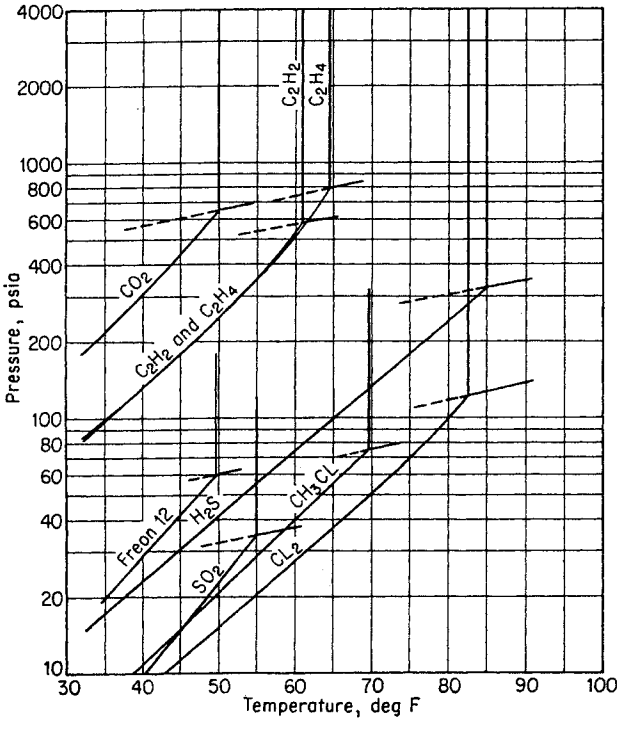

Fig. 5-38. Hydrate-forming conditions for miscellaneous substances.

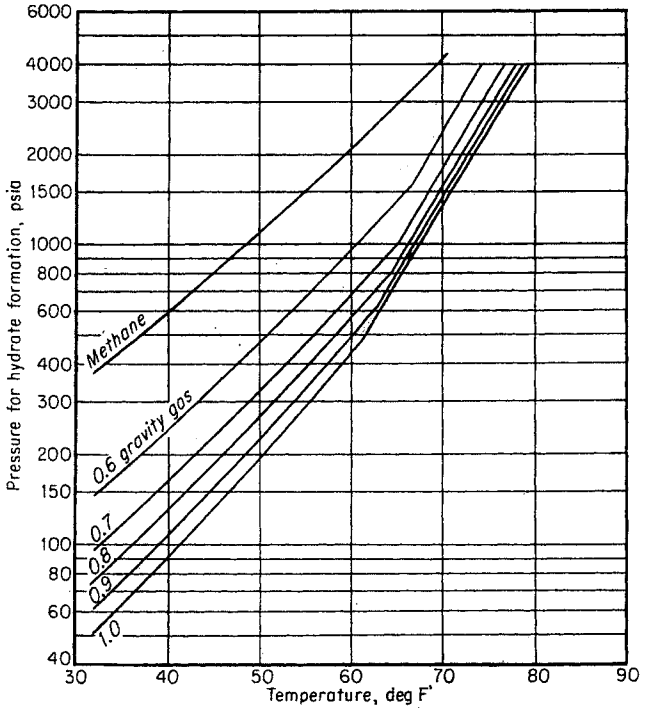

Fig. 5-40. Hydrate-forming conditions for natural gases with various gravities. (*Katz, 5-38. Courtesy AIME.*)

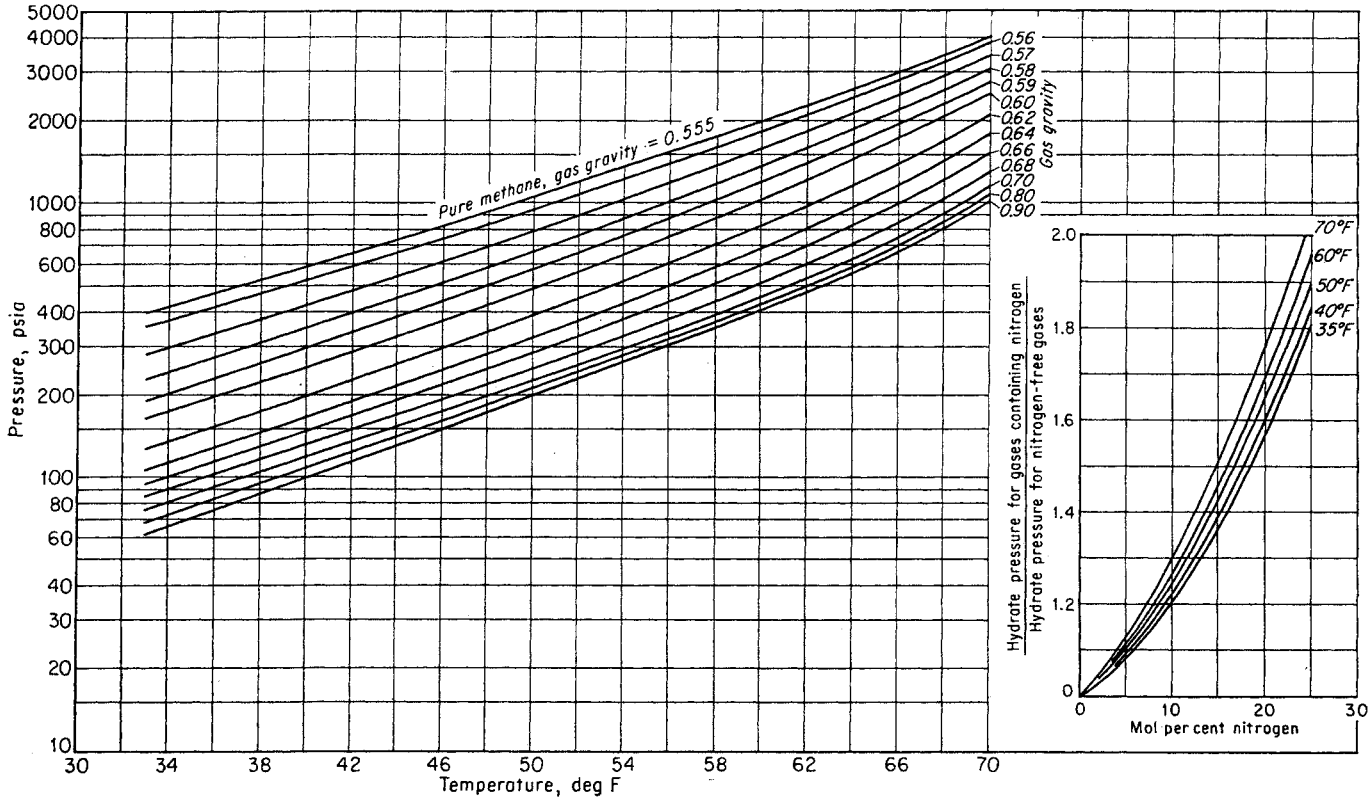

Fig. 5-41. Hydrate-formation conditions for natural gases, including effects of nitrogen.

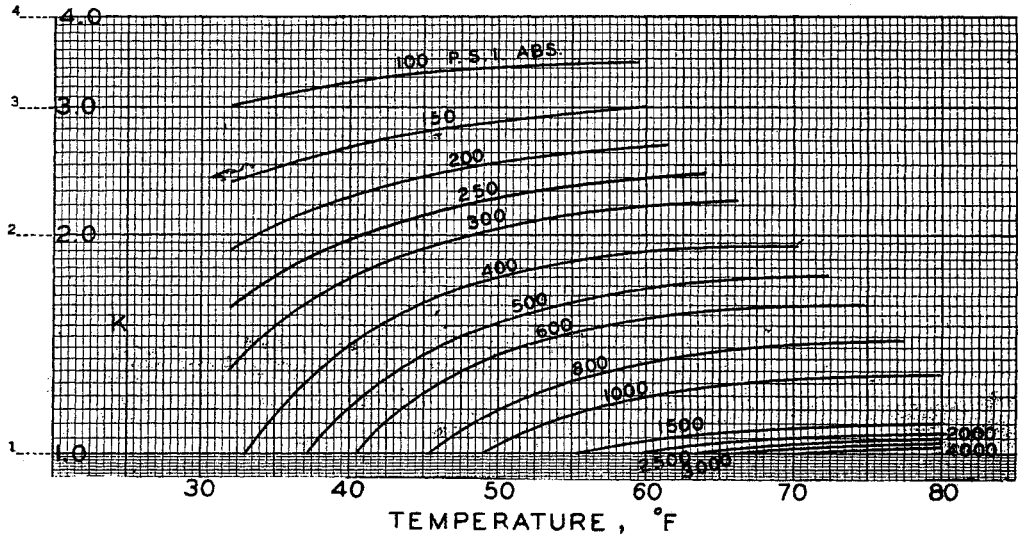

Fig. 5-42. Vapor-solid equilibrium constants for methane. (*Carson and Katz, 5-12. Courtesy AIME.*)

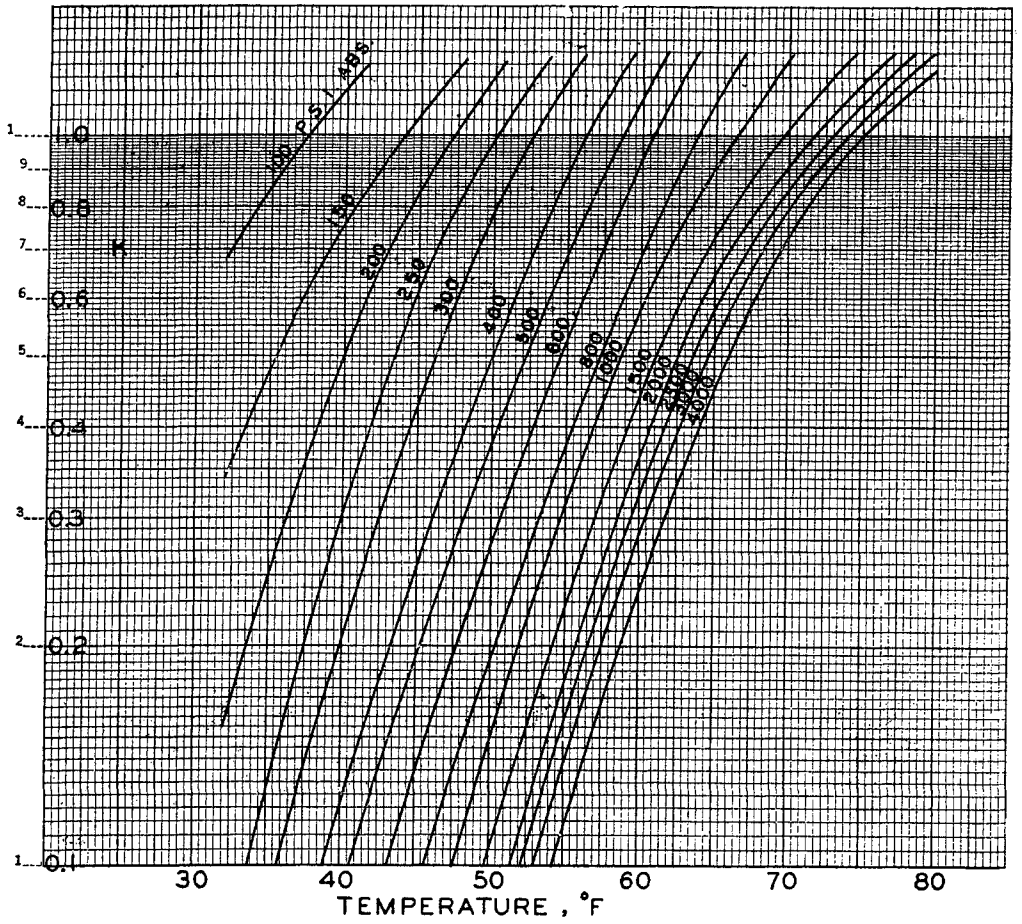

Fig. 5-43. Vapor-solid equilibrium constants for ethane. (*Carson and Katz, 5-12. Courtesy AIME.*)

Table 5-7. Calculation of Pressure for Hydrate Formation at 50°F

Component	Mole fraction in gas	At 300 psia		At 350 psia	
		K	y/K	K	y/K
Methane	0.784	2.04	0.3841	1.90	0.4126
Ethane	0.060	0.79	0.0759	0.63	0.0952
Propane	0.036	0.113	0.3185	0.086	0.4186
Isobutane	0.005	0.0725	0.0689	0.058	0.0862
n-Butane	0.019	0.79	0.0240	0.63	0.0301
Nitrogen	0.094	Infinity	0.0000	Infinity	0.0000
Carbon dioxide	0.002	3.0	0.0007	2.3	0.0008
Total	1.000	.....	0.8721	.....	1.0435

Interpolating linearly, $y/K = 1.0$ at 337 psia.

The experimentally observed hydrate-formation pressure at 50°F was 325 psia.

SOURCE: (5-12).

present. The charts also give the temperature change upon expansion.

Prevention of Hydrate Formation

Hydrates form only when liquid water is present with the gas. The addition of a substance to the water can change its "freezing point." Methanol is a common substance used in industry. Much work has been done on hydrate prevention (5-5, 5-21, 5-34, 5-35, 5-43, 5-91).

Water-soluble substances inhibit or suppress hydrate formation; the hydrogen dipole may attack the water structure (5-81) or the solute may decrease the activity of the water (5-43). Ammonia inhibits the formation of hydrates by the first mechanism; salts such as sodium chloride reduce the activity of the water.

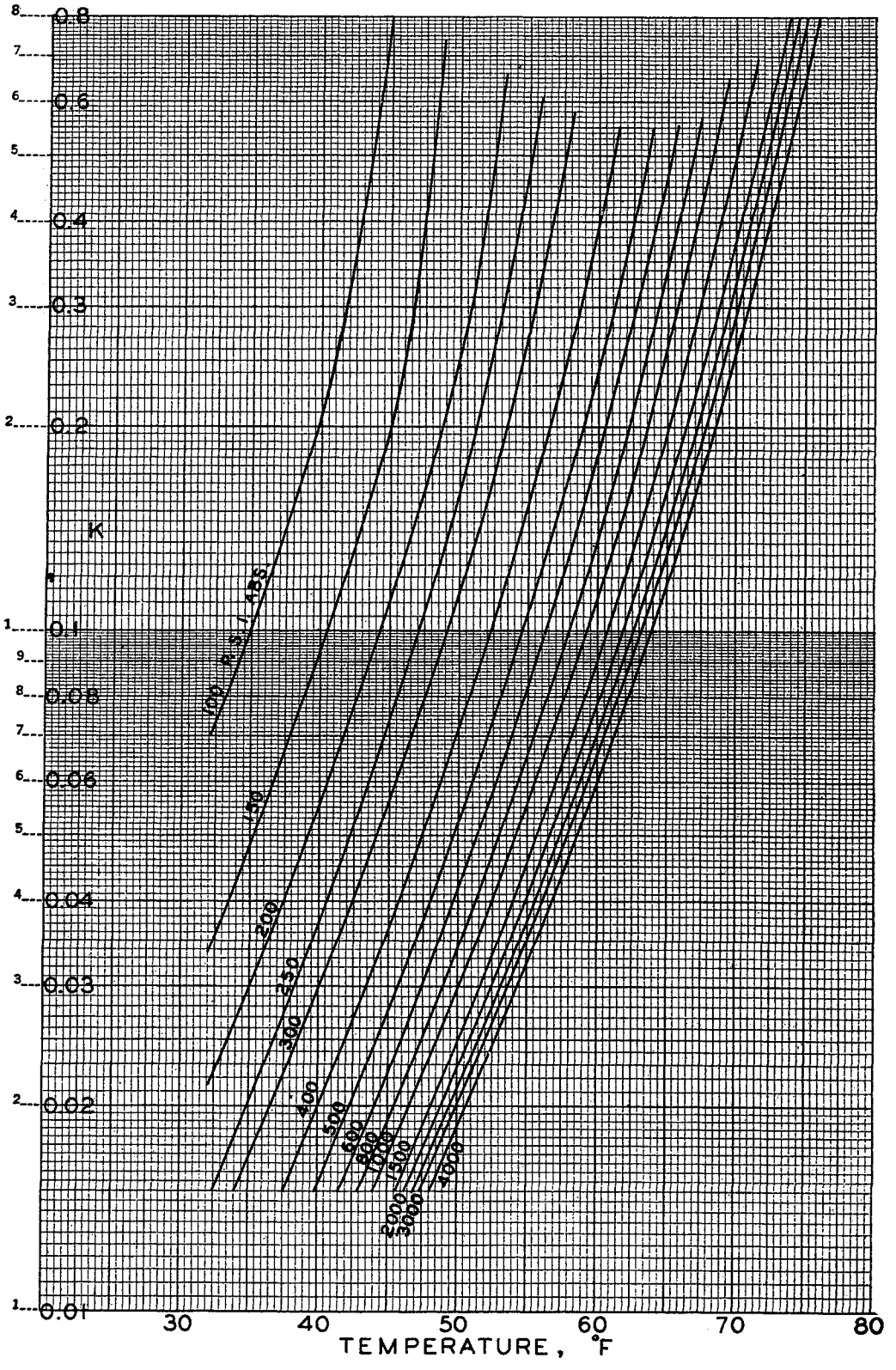

Fig. 5-44. Vapor-solid equilibrium constants for propane. (*Carson and Katz,* 5-12. *Courtesy AIME.*)

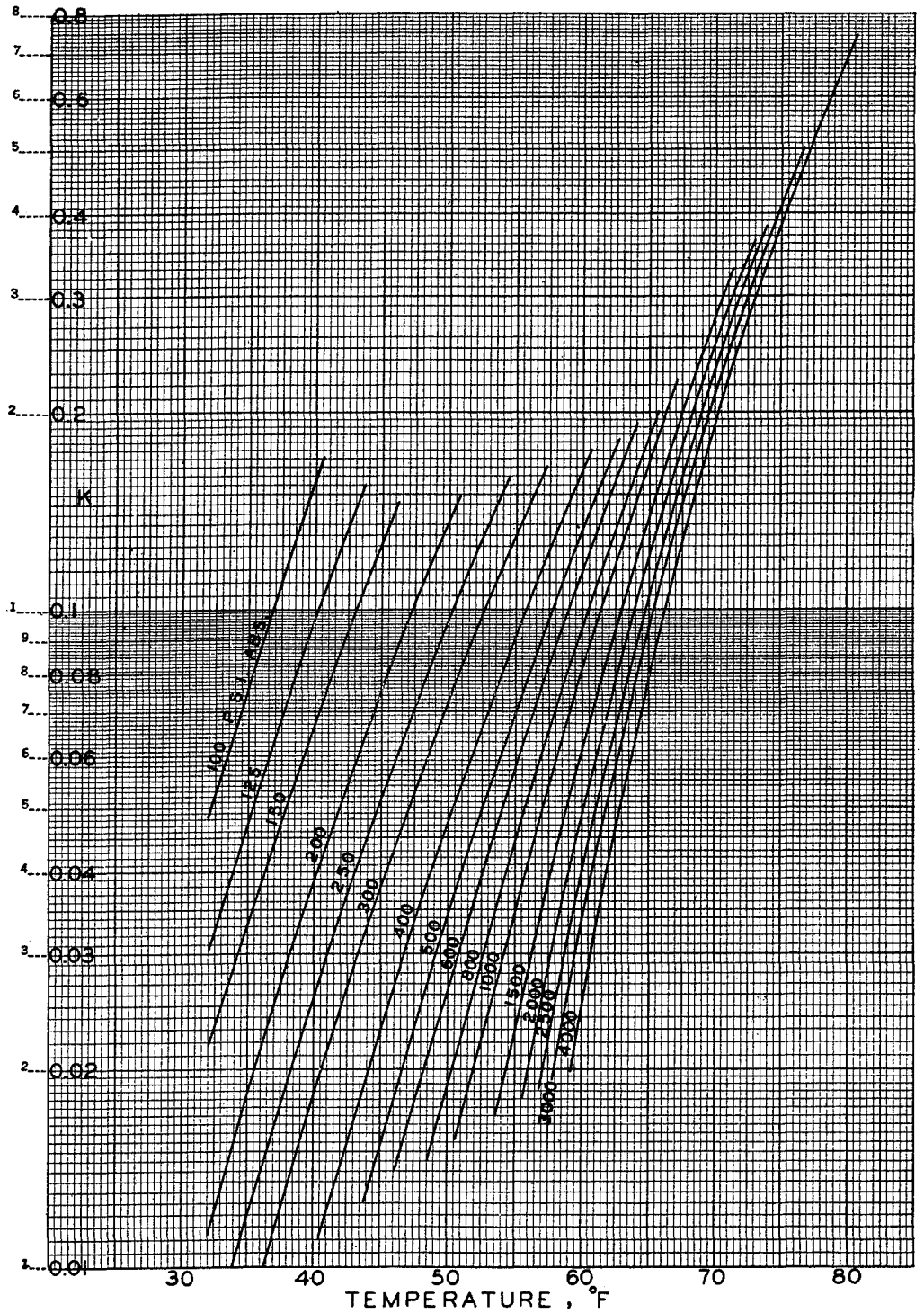

Fig. 5-45. Vapor-solid equilibrium constants for isobutane. (*Carson and Katz, 5-12. Courtesy AIME.*)

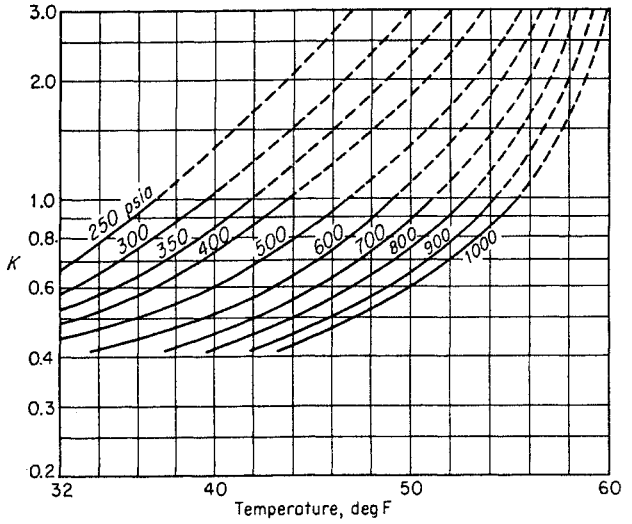

Fig. 5-46. Vapor-solid equilibrium constants for carbon dioxide. (*Unruh and Katz, 5-84. Courtesy AIME.*)

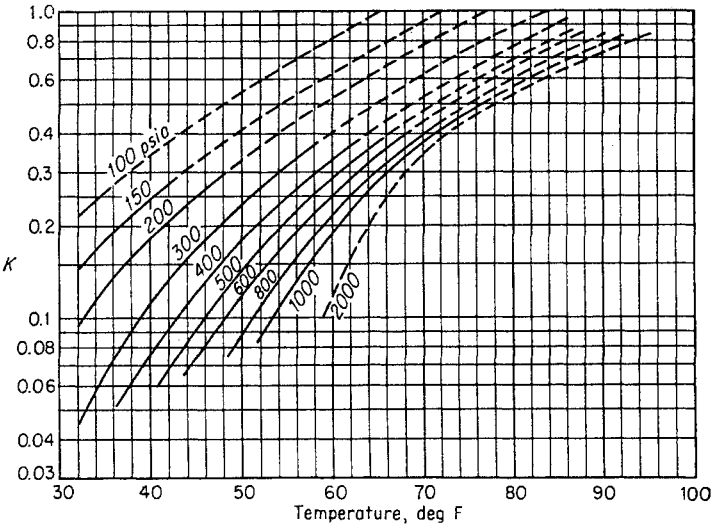

Fig. 5-47. Vapor-solid equilibrium constants for hydrogen sulfide. (*Noaker and Katz, 5-55. Courtesy AIME.*)

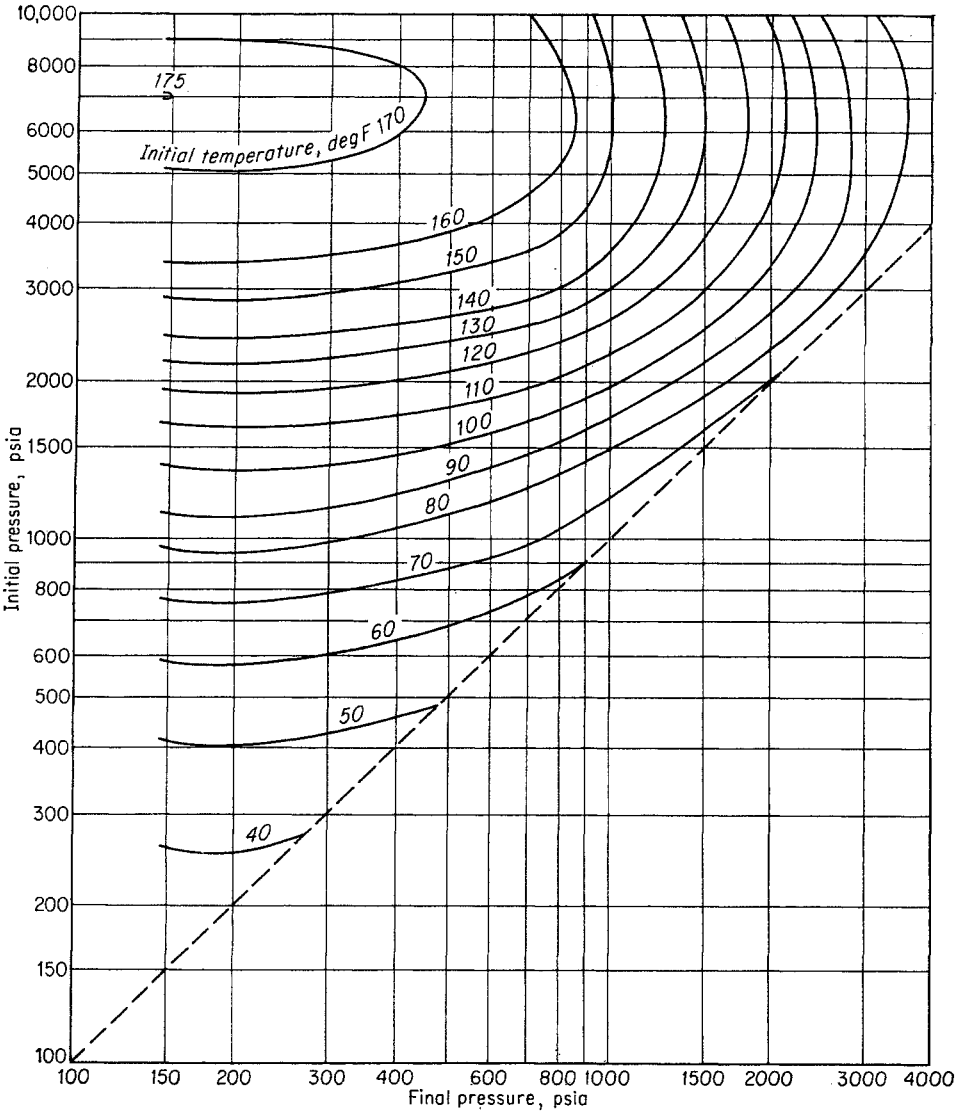

Fig. 5-48. Permissible expansion of 0.6 gravity gas without hydrate formation. (*Katz, 5-38. Courtesy AIME.*)

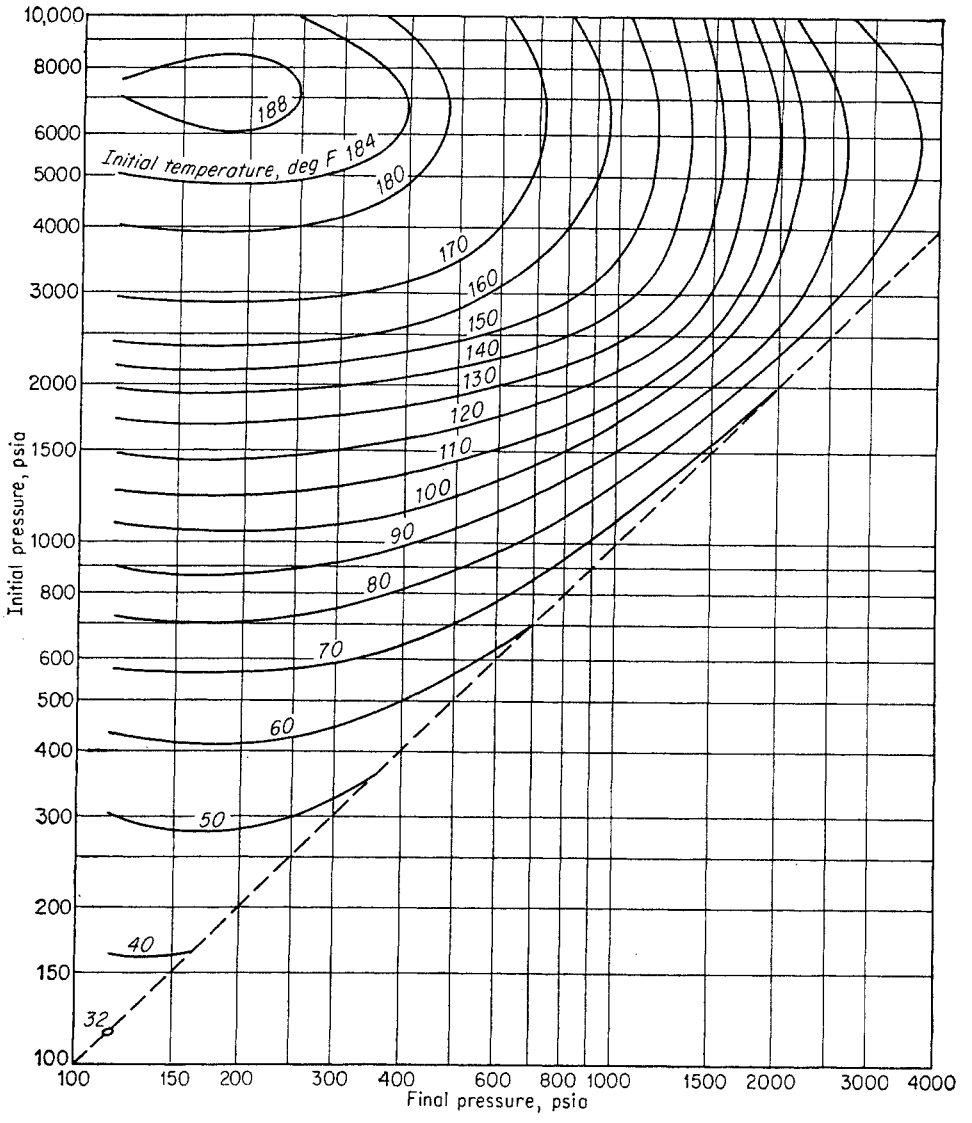

Fig. 5-49. Permissible expansion of 0.7 gravity gas without hydrate formation. (*Katz, 5-38. Courtesy AIME.*)

The suppression of hydrate formation by 10 wt % aqueous solutions of several inhibitors is shown in Fig. 5-51. The effectiveness of alcohols in preventing hydrate formation is in the order of their volatility: methanol, ethanol, then isopropanol. The effect of the concentration of various solvents on the hydrate-formation temperatures of a natural gas is plotted in Fig. 5-52, which neglects the slight dependence of the depression on pressure. The concentration shown is the actual concentration of the liquid in equilibrium with the natural gas. The effect of sodium chloride on propane hydrate is given in Fig. 5-53. The total amount of a volatile inhibitor required to produce a given depression is the sum of the amount required to produce a given liquid-phase composition and the amount that has volatilized into the gas phase (5-34). For nonvolatile inhibitors, it may be possible to compute the effect of concentration on the extent to which the hydrate-formation temperature is depressed (5-43).

Di- and triethylene glycol are used for the inhibition of hydrate formation as well as in the dehydration of natural gases. Figure 5-54 gives the depression effect produced by various concentrations of diethylene glycol on a 0.595 gravity natural gas (5-73). The presence of oil with the glycol solution further depresses the hydrate-formation conditions, but the over-all depression is less than the sum of the depressions produced by the two solutions independently (5-73).

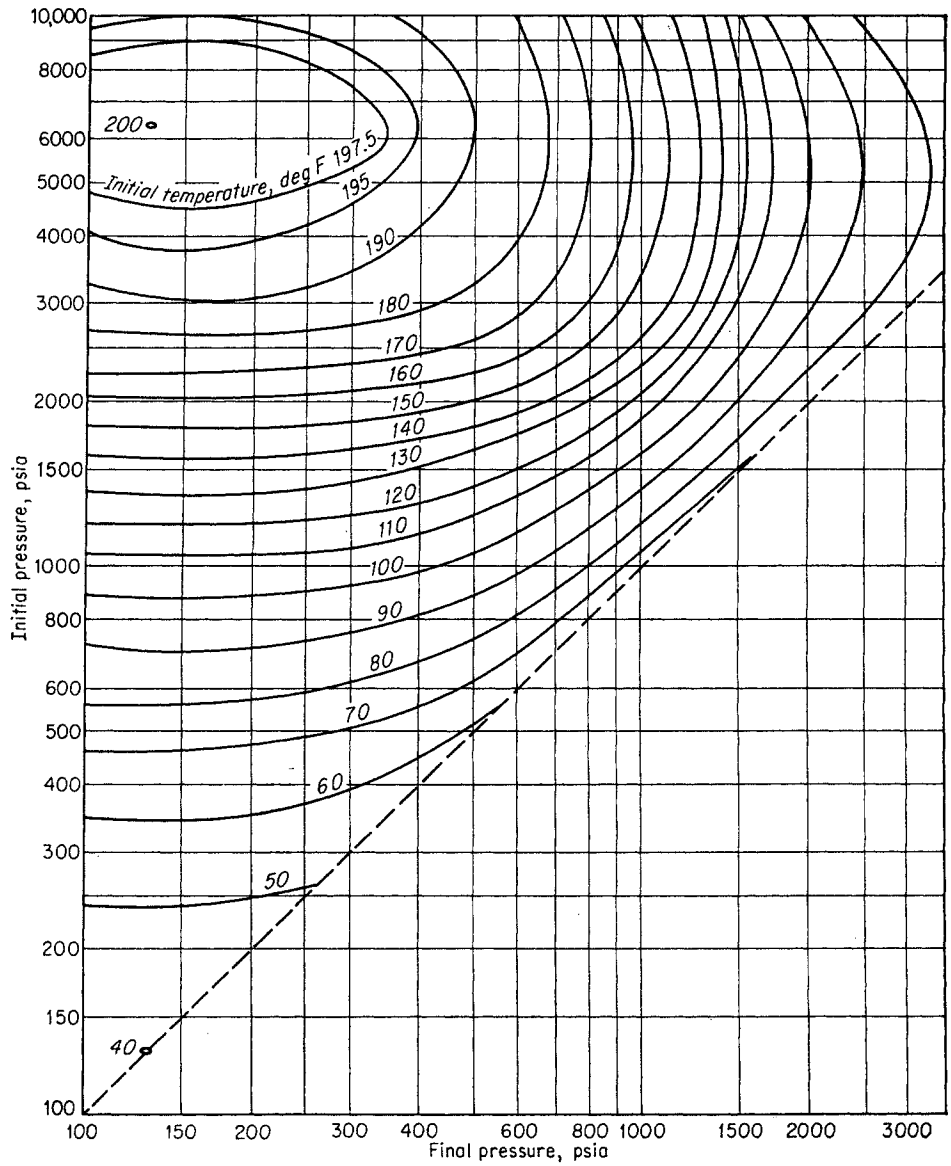

Fig. 5-50. Permissible expansion of 0.8 gravity gas without hydrate formation. (*Katz, 5-38. Courtesy AIME.*)

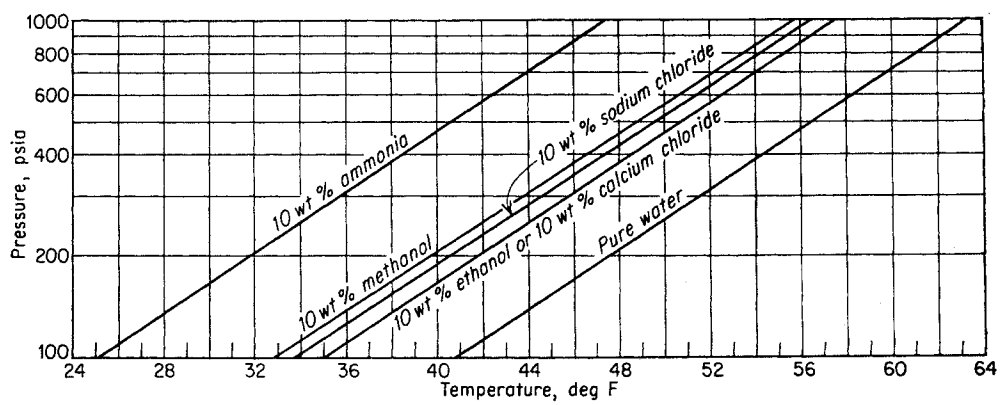

Fig. 5-51. Effect of dissolved substances in water on hydrate-formation conditions. (5-21.)

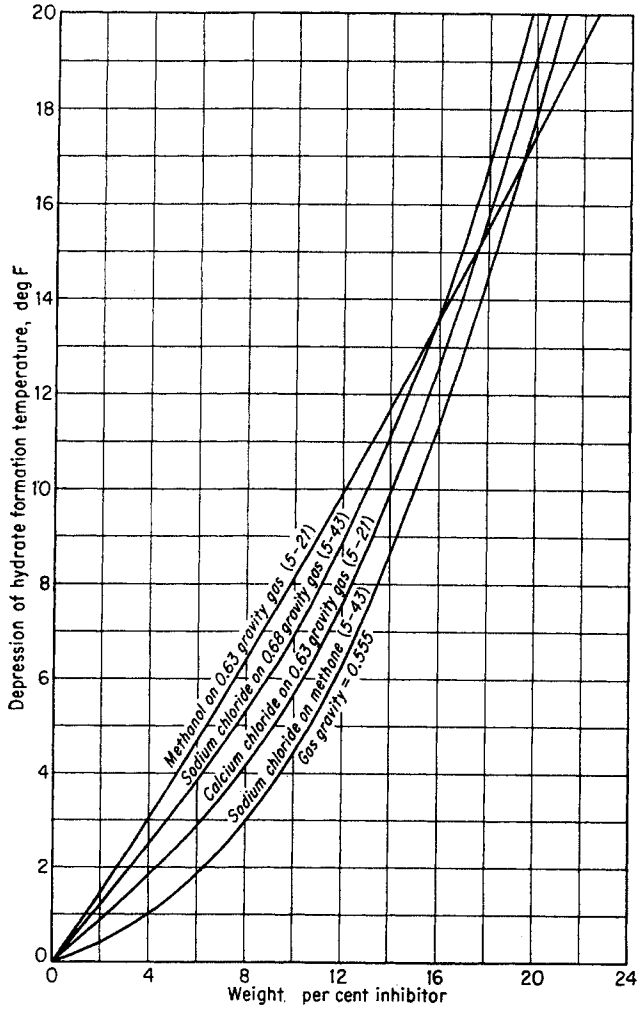

Fig. 5-52. Depression of hydrate-formation temperatures by inhibitors.

The formation of gas hydrates for a 0.595 gravity gas and for a natural brine have been studied independently and in the presence of varying amounts of a 46.8°API gravity separator oil (5-73, 5-74). Figure 5-55 shows that the conditions for the formation of gas hydrates are affected by the ratio of gas to oil, although computations seem to indicate that the gas-phase composition is almost independent of the ratio of gas to oil. The mechanism responsible for the depression of the hydrate-formation conditions is not understood.

Studies of the storage of gas as hydrate have been made by Miller and Strong (5-54) and by Parent (5-58). Figure 5-36 shows that gas hydrate would remove propane preferentially over methane.

Table 5-8. Comparison of Calculated with Experimental Conditions for Hydrate Formation

A. Gas Analysis, Mole Fraction

Component	D	B	C	4-H	5	6-K	7-A
Methane	0.8641	0.9320	0.8800	0.7516	0.8250	0.674	0.9497
Ethane	0.0647	0.0425	0.0682	0.0595	0.0599	0.037	0.0296
Propane	0.0357	0.0161	0.0254	0.0333	0.0326	0.019	0.0081
Isobutane	0.0099	.....	0.0038	0.0050	0.0030	0.006	0.0020
n-Butane	0.0114	.....	0.0089	0.0005	0.0049	0.006	0.0036
Pentane	0.0078	.....	0.0101	0.0051	0.0007	.....	0.0028
Carbon dioxide	.....	0.0051	.....	0.002	0.002	0.008	0.0042
Nitrogen	0.0064	0.0043	0.0036	0.143	0.0719	0.250	
Reference	5-90	5-90	5-20	5-21	5-33	5-21	5-73

B. Hydrate Data

Gas	Pressure, psia	Temp at which hydrate formed, °F	
		Exp	Calc
D	200	44.0	43.8
	400	54.9	53.3
	800	63.5	61.7
	1,500	70.0	69.2
	4,000	77.0	75.4
B	250	41.0	40.6
	500	51.6	50.7
	1,000	60.7	59.9
	2,500	70.0	70.3
	4,000	73.5	73.8
C	200	40.2	41.2
	500	53.1	54.3
	1,000	62.4	62.5
	1,500	66.8	67.8
	3,000	72.5	73.1
4-H	150	37.1	35.4
	250	44.8	45.1
	400	52.0	51.4
5	250	42.8	44.5
	400	49.4	51.4
	800	59.8	59.8
6-K	200	37.7	38.8
	300	43.7	44.5
	400	47.9	48.3
7-A	300	37.6	41.2
	400	42.7	45.4
	500	46.4	48.6
	600	49.4	51.2
	800	54.0	55.0
	1,000	57.4	57.9

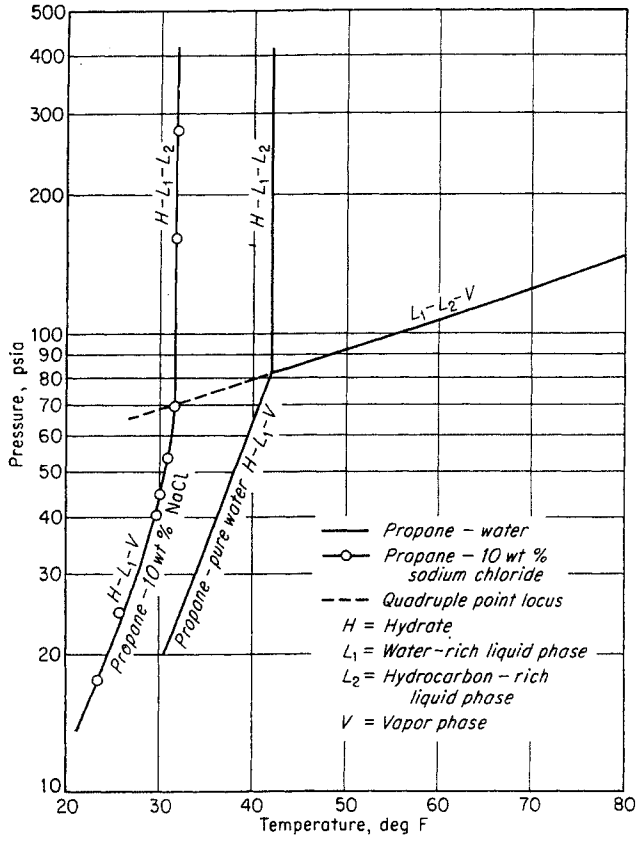

Fig. 5-53. Effect of NaCl on formation of propane hydrate. (*Kobayashi, Withrow, Williams, and Katz, 5-43.*)

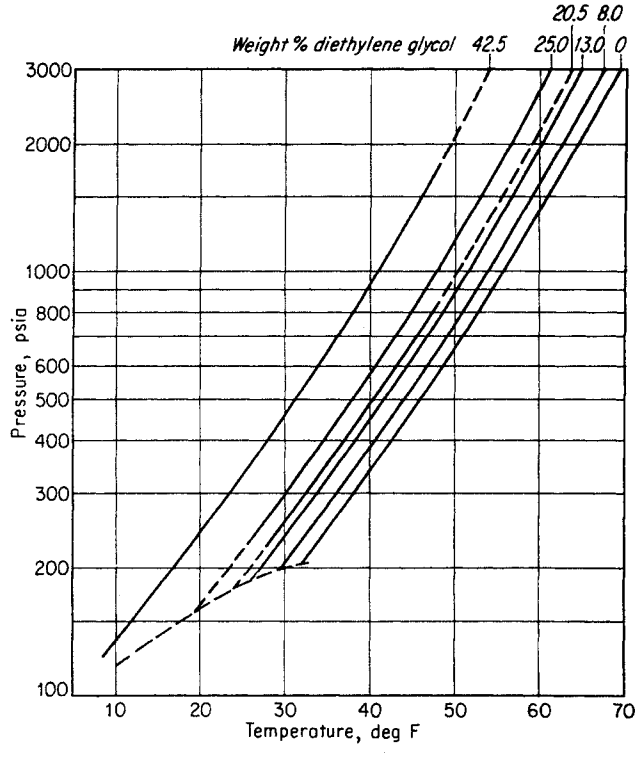

Fig. 5-54. Effect of diethylene glycol on conditions for hydrate formations. (*Scauzillo et al., 5-73, 5-74.*)

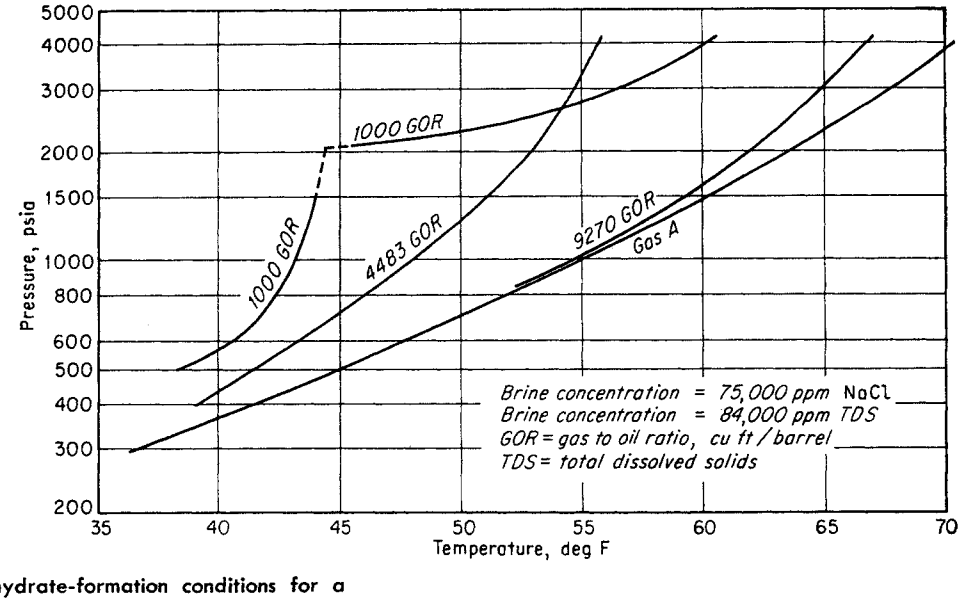

Fig. 5-55. Effect of gas-oil ratio on hydrate-formation conditions for a 46.8°API oil in presence of excess field brine. (*Scauzillo, 5-74. Courtesy AIChE.*)

CHAPTER 6

Measurement and Computation of Vapor-Liquid Equilibria for Complex Mixtures

Measurement of vapor-liquid equilibria for complex systems of natural gas and crude oil requires the analysis of complex mixtures similar to natural gases. Methods of analysis for the phases and equipment used for obtaining equilibrium will be here described.

Once data on phase compositions of given systems are available, equilibrium constants $K = y/x$ can be plotted for predicting constants for new systems. Methods of correlating equilibrium constants will be discussed, and charts for predicting constants for some systems will be presented.

A combination of equilibrium constants with definitions of *dew point* and *bubble point* yields methods for predicting phase boundaries for hydrocarbon mixtures. Combination of equilibrium constants with the material balance for a flash vaporization yields an expression for predicting, from the composition of an over-all mixture and from the K's, the quantity and composition of the equilibrium phases. Calculation of vapor-liquid equilibria on card-program high-speed calculators has become commonplace in the petroleum industry, and a method of programming will be discussed.

GAS ANALYSES

The first prerequisite of vapor-liquid equilibrium measurements on complex systems is a reliable procedure for analyzing gases and liquids. Four types of equipment are in common use for analyzing natural gases and volatile hydrocarbon mixtures:

1. Low-temperature fractionation
2. Analytical mass spectrometer
3. Infrared absorption spectrometer
4. Gas chromatography

A brief description of methods used for determining the composition of a hydrocarbon gas or liquid will be given.

Common methods of gas analysis by absorption of a constituent in a solution are described in physicochemical texts and handbooks (6-58) and in ASTM procedures such as method D 1136 (6-6). Gas density may be taken by weighing given volumes (6-6, D 1070-52). The measurement of gas density is a satisfactory method for analyzing binary mixtures, but deviations from ideal gases should not be neglected (4-83). The thermal-conductivity cell, as well as equipment for measuring other properties (6-9), has found application to analyses for streams in continuous flow.

Low-temperature Fractionation

Prior to the late 1920s, the composition of natural gases could not be determined in the laboratory on a routine basis. After a combustion analysis was run, in which the shrinkage resulting from combustion and the carbon dioxide content of the combustion gases were measured, the constituents in a natural gas were reported as methane and ethane equivalent. W. J. Podbielniak, working for the Phillips Petroleum Company at Bartlesville and studying for his doctorate at the University of Michigan under Dr. G. G. Brown, designed and operated a low-temperature fractionating column using liquid air or nitrogen as cooling agent to generate reflux (6-41).

The type of glass low-temperature fractionating equipment used in the early days is illustrated by Fig. 6-1. Columns were insulated by evacuated and silvered jackets to permit methane liquid to be refluxed in the column. A thermocouple at the top of the column gave the boiling point. The pressure rise on an evacuated bottle, measured by a manometer, was used to measure the volume of gas distilled. Methane, ethane, propane, isobutane, n-butane, etc., are distilled in turn. When the boiling point reaches room temperature (isopentane has a normal boiling of

86°F) it becomes necessary to operate the column at reduced pressure to prevent condensation of overhead vapors in the connecting lines. The several isomeric hexanes have boiling points relatively close together and they are, therefore, grouped as a hexane fraction. Beyond hexanes, a heptane-and-heavier residue may be vaporized if it is small in quantity and of sufficiently low boiling range. More often, the heptane-and-heavier residue is collected and measured as a liquid, its density determined by weighing a known volume in a pycnometer, and its molecular weight determined by its influence on the freezing point of benzene. The gas analysis when a liquid residue is present requires the conversion of gas volumes for each constituent and of liquid-residue volume to moles to find the mole fractions. Carbon dioxide and hydrogen sulfide are normally removed from the charged gas by caustic pellets, since these compounds will form solids in the fractionating column. They are determined on a separate sample by absorption in caustic solution, or hydrogen sulfide may be determined with iodine solution (6-2).

Many improvements have been made in low-temperature fractionation equipment (6-44) since the early days, including such items as better column packing, automatic recording of volume of gas distilled and corresponding temperature, automatic control of cooling for reflux and of rate of distillation (Figs. 6-2 and 6-3). The measurement of thermal conductivity of the overhead vapor as a means of identifying cut points (6-43) was a step forward. The Natural Gasoline Association of America (NGAA) carries on tests to determine the accuracy of low-temperature fractional analyses, for these are frequently used as a basis for contracts (6-35). The sample size for low-temperature analysis is normally measured in liters and the time for analysis in hours.

A complex liquid mixture containing constituents from methane to hydrocarbons with boiling points at 250°F or more may be analyzed by low-temperature distillation in two stages. The gases to pentanes are analyzed as for a natural gas, and then the rest of the sample is fractionated in a distillation column which condenses the overhead product. A distillation curve may be provided for the liquid portion, or it may be represented by a series of close-boiling fractions or cuts identified by boiling range, molecular weight, and density. On occasion, the cut temperatures used correspond to intermediate temperatures between normal paraffin hydrocarbons, and the fractions are labeled octanes, nonanes, decanes, etc. Table 6-1 gives a reservoir-fluid analysis in which the combined method of analysis was employed (6-27).

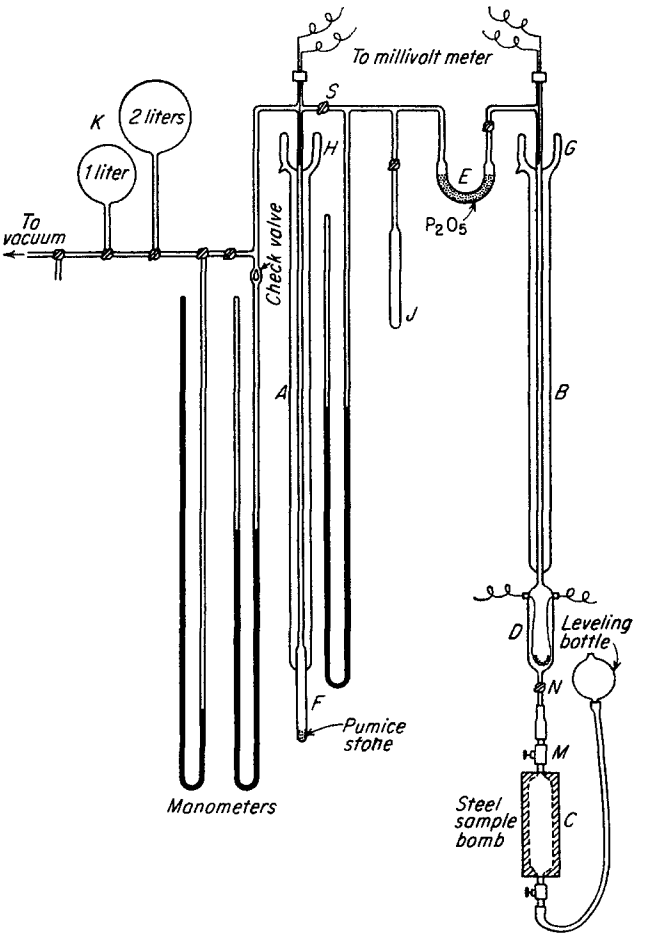

Fig. 6-1. Early low-temperature fractionating columns for analyzing natural gases *A* and volatile liquids *B* plus *A*.

Mass Spectrometer

A mass spectrometer ionizes gas molecules at low pressure and sorts the molecules or fragments according to their mass (6-12, 6-1, 6-6, 6-63). Figure 6-4 is a flow diagram of such an analytical instrument. The gas to be analyzed is expanded into a low-pressure supply chamber which holds about $\frac{1}{5}$ cu cm of gas at 1 atm pressure. Arrangements may be made to vaporize liquids and convert them into a low-pressure vapor sample.

A small stream of molecules is allowed to leak from the supply chamber through the analytical system. In the ionizing chamber some of the molecules are not only ionized but fragmented or cracked as well. The ionized particles are accelerated by a high voltage and passed through a slit to a magnetic field. These particles are deflected by the magnetic field according to their mass, and a given mass can be focused on the collector slit. The charged particles striking the col-

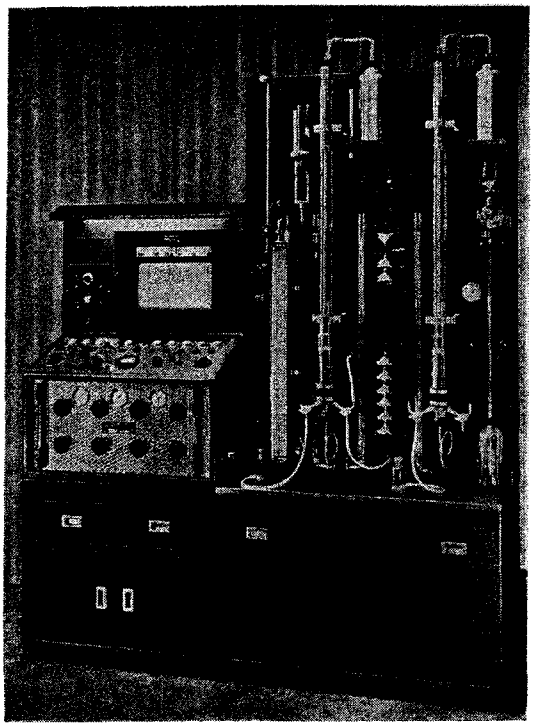

(a)

lector plate activate the amplifier, which provides signals for the photographic recorder.

Figure 6-5 is a photograph of an analytical mass spectrometer (Consolidated Engineering Corporation). The system is maintained continuously under vacuum and is calibrated almost daily by standard reference samples. Once the sample is in the supply container, a scan of the abundance of charged particles of mass from 1 to 250 or more is made in a matter of minutes by changing the accelerating voltage on the ions. The decreasing velocities lower the centrifugal force for a constant magnetic field, passing the ions with increasing mass in turn through the exit slit. The recorder plots peak heights (Fig. 6-6) versus mass-charge ratio. The relationship between the peak height in scale units and the micron pressure of the sample in the inlet volume at a given mass is constant, and is expressed as a *sensitivity*. The relative heights of the peaks, as compared to any one peak selected as reference, constitute the *cracking pattern*. Different molecules of the same molecular weight can be distinguished by their cracking patterns. The analytical instrument is designed to maintain constant cracking

Fig. 6-2. Modern low-temperature distillation apparatus. (a) Exterior view; (b) flow diagram. (*Courtesy Podbielniak, Inc.*)

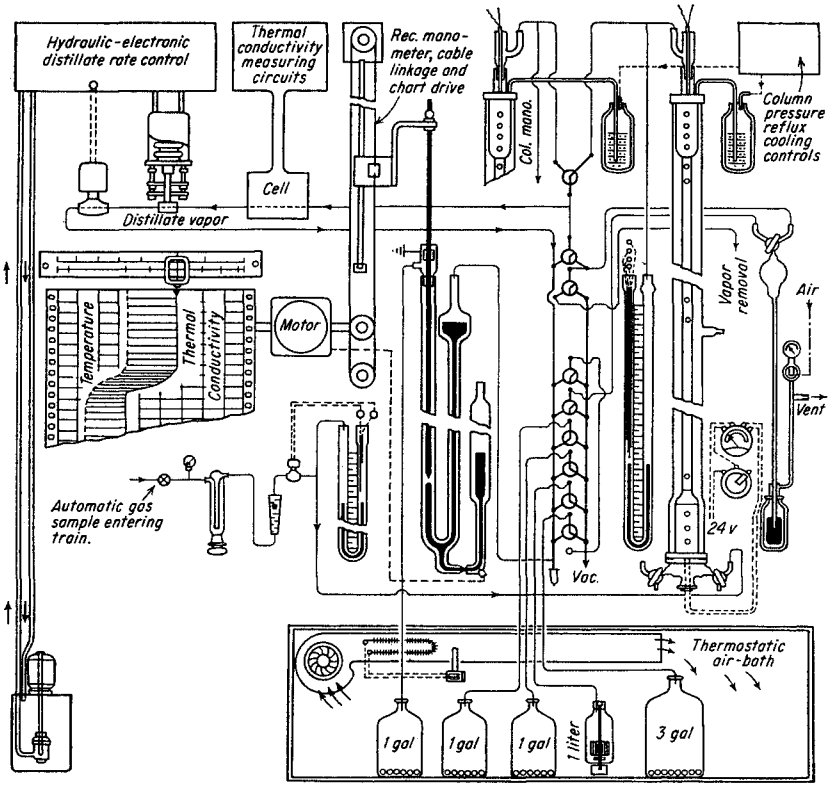

(b)

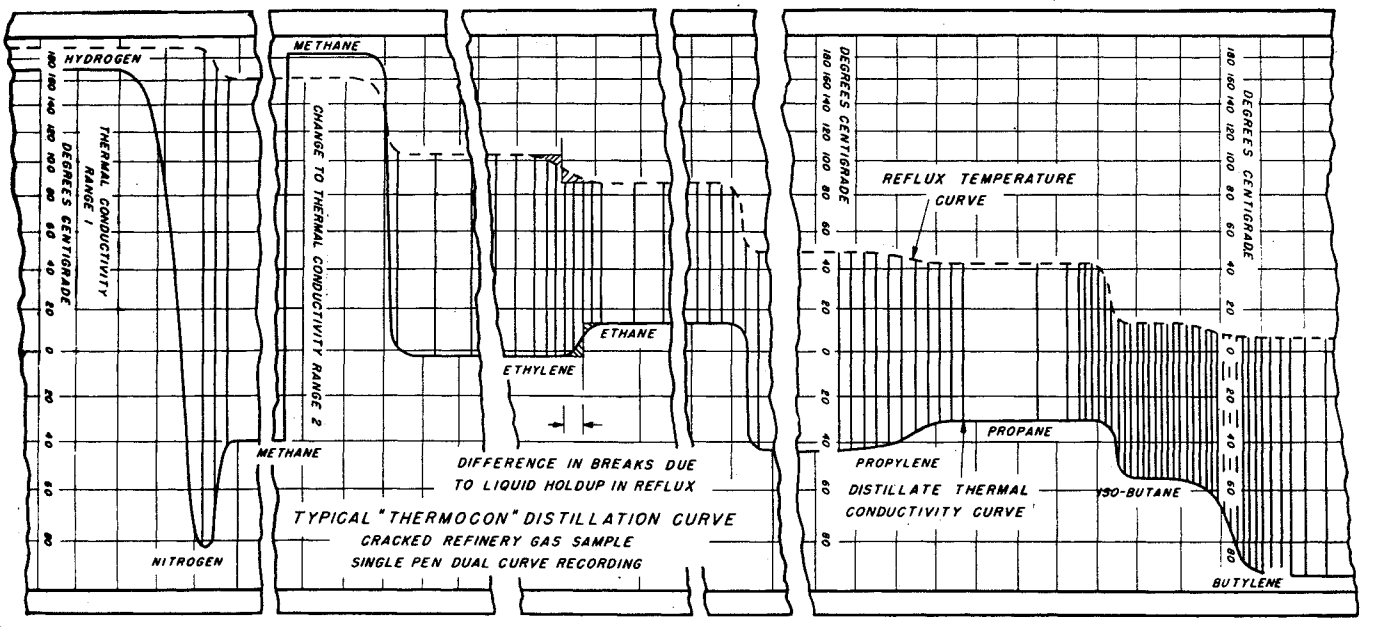

Fig. 6-3. Chart showing components by low-temperature distillation. (*Courtesy Podbielniak, Inc.*)

patterns and sensitivity for each molecular species independent of time and of the partial pressure of other molecular species. The American Petroleum Institute (API) has tabulated cracking patterns and sensitivity for an extensive list of hydrocarbons (6-1). By using the sensitivity and cracking pattern for each component in a mixture, as determined from standard samples of the individual components, the analysis of the mixture can be calculated by solving a set of linear equations equal in number to the number of components. Electronic computers are often used to solve the equations. It is possible to analyze multicomponent mixtures containing twenty or more components. In addition, traces of material at the level of parts per million can be detected by the instrument under favorable circumstances. Table 6-2 gives

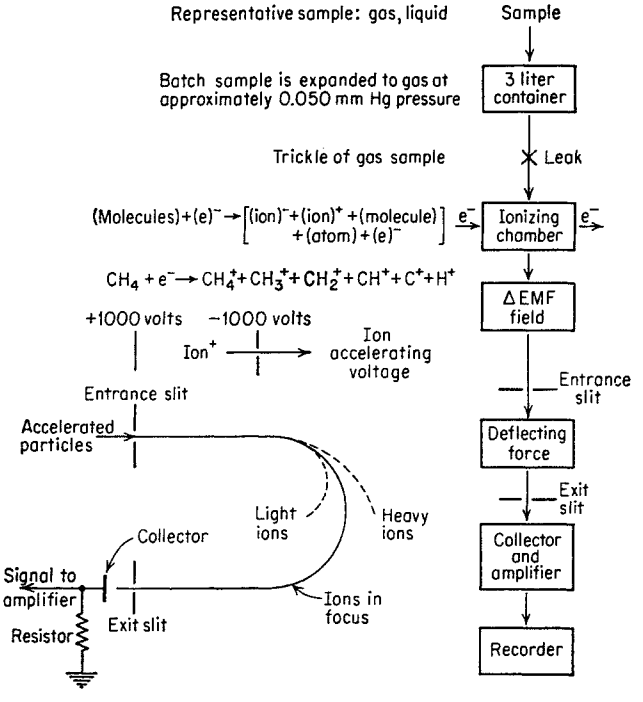

Fig. 6-4. Flow diagram for mass spectrometer.

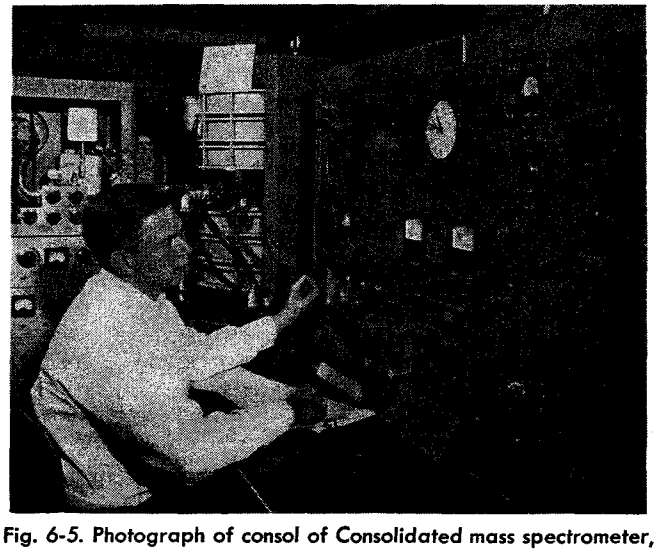

Fig. 6-5. Photograph of consol of Consolidated mass spectrometer, model 21-103B.

comparative analyses with group *A* made as repeat runs on a synthetic sample over a period of 6 months and with group *B* made on samples taken from a gas cylinder and shipped to a laboratory as unknowns along with other routine samples.

Table 6-1. Analysis of Hydrocarbons Containing Both Gases and High-boiling Constituents

Analysis of Reservoir Fluids in Equilibrium at 3,840 Psia and 210°F

Component	Reservoir oil			Reservoir gas		
	Mole %	Liquid density at 60°F, grams/cu cm	Mol. wt	Mole %	Liquid density at 60°F, grams/cu cm	Mol. wt
Methane	52.00	.....	...	91.35		
Ethane	3.81	.....	...	4.03		
Propane	2.37	.....	...	1.53		
Isobutane	0.76	.....	...	0.39		
n-Butane	0.96	.....	...	0.43		
Isopentane	0.69	.....	...	0.15		
n-Pentane	0.51	.....	...	0.19		
Hexanes	2.06	.....	...	0.39		
Fraction 7*	2.63	0.749	99	0.361	0.745	100
Fraction 8	2.34	0.758	110	0.285	0.753	114
Fraction 9	2.35	0.779	121	0.222	0.773	128
Fraction 10	2.240	0.786	132	0.158	0.779	142
Fraction 11	2.412	0.798	145	0.121	0.793	156
Fraction 12	2.457	0.812	158	0.097	0.804	170
Fraction 13	2.657	0.826	172	0.083	0.816	184
Fraction 14	3.262	0.846	186	0.069	0.836	198
Fraction 15	3.631	0.854	203	0.050	0.840	212
Fraction 16	2.294	0.852	222	0.034	0.839	226
Fraction 17	1.714	0.838	238	0.023	0.835	240
Fraction 18	1.427	0.846	252	0.015	0.850	254
Fraction 19	1.303	0.851	266	0.010	0.865	268
Fraction 20	1.078	0.871	279	0.006	0.873	282
Fraction 21	0.871	0.878	290	0.004	0.876	296
Fraction 22	0.715	0.884	301	0.002	0.878	310
Fraction 23	0.575	0.889	315			
Fraction 24	0.481	0.893	329			
Fraction 25	0.394	0.897	343			
Fraction 26	0.335	0.900	357			
Fraction 27	0.280	0.903	371			
Fraction 28	0.250	0.906	385			
Fraction 29	0.232	0.908	399			
Fraction 30	0.195	0.910	413			
Fraction 31	0.170	0.912	427			
Fraction 32	0.156	0.914	441			
Fraction 33	0.143	0.916	455			
Fraction 34	0.130	0.917	469			
Fraction 35	0.118	0.918	483			
Total	100.000	.....	...	100.000		

* The boiling range of a fraction corresponds to the range of boiling points of *n*-paraffin hydrocarbons with number of carbon atoms equal to fraction number.

SOURCE: Hoffman, Crump, and Hocott (6-27).

Table 6-2. Duplicate Analyses of Natural Gases by Mass Spectrometer

Analyses Made on Synthetic Sample over a Period of 6 Months

Component	Mole fraction				
	Synthetic mixture	Analysis no. 1	Analysis no. 2	Analysis no. 3	Analysis no. 4
Helium	0.83	0.82	0.73	0.80	0.79
Nitrogen	15.7	15.5	15.6	15.5	15.0
Methane	70.0	70.0	69.8	70.0	70.1
Ethane	7.3	7.4	7.4	7.3	7.8
Propane	3.5	3.4	3.6	3.5	3.5
Isobutane	1.0	1.2	1.1	1.2	1.1
n-Butane	1.7	1.7	1.8	1.7	1.7

Analyses Made on Successive Samples Taken from Gas Cylinder and Sent to Laboratory as Unknowns

Component	Mole fraction		
	Analysis no. 1	Analysis no. 2	Analysis no. 3
Helium	0.66	0.69	0.58
Nitrogen	15.6	15.5	15.5
Methane	73.0	72.5	71.5
Ethane	6.2	6.8	7.0
Propane	3.7	3.6	4.4
Isobutane	0.20	0.25	0.29
n-Butane	0.54	0.57	0.70
Pentanes+	0.07	0.07	0.02

The larger hydrocarbon molecules (six or more carbon atoms) are more difficult to analyze because of the more complicated cracking patterns and the possible presence of many isomers. It is necessary to perform a calibration of the cracking pattern for each compound determined in an analysis, although patterns are similar enough to group several isomers.

Infrared Spectroscopy

The infrared-absorption spectrometer obtains a spectrum of the infrared energy absorbed by a sample of gas or liquid (6-22). Different molecules cause absorption at different frequencies, permitting a determination of the quantities of each species present. Figure 6-7 gives the optical system for an infrared instrument.

Infrared is most useful in distinguishing between unsaturated molecules and paraffins, for example among the four carbon molecules containing normal and isomeric butanes, butylenes, and butadiene.

Gases, liquids, transparent solids, or substances in solvents may be analyzed by infrared spectroscopy,

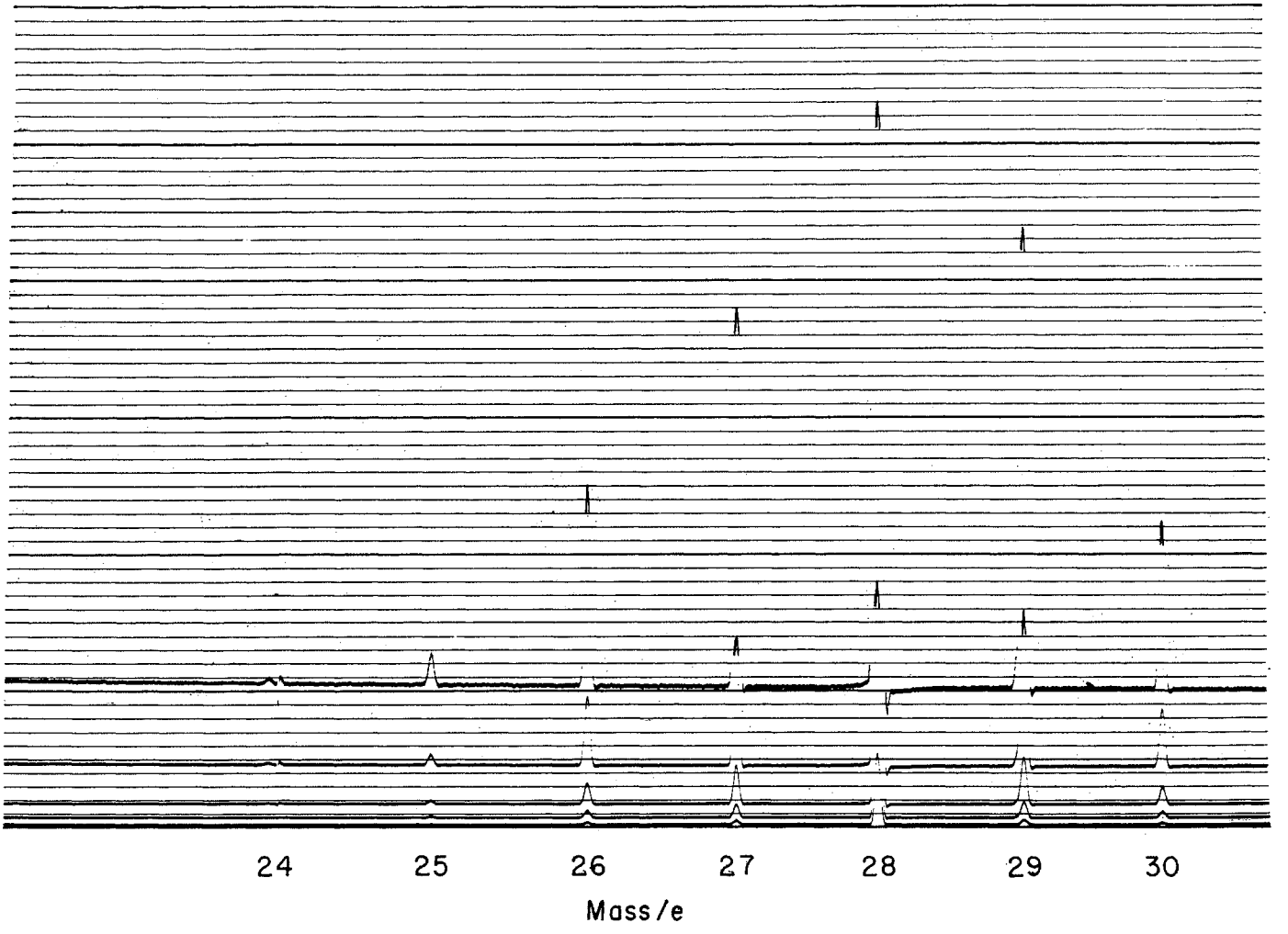

Fig. 6-6. Chart for Consolidated mass spectrometer.

employing samples of 1 to 2 cu cm of liquid or less and 200 cu cm of gas or less. The absorption of energy at various wavelengths is recorded for comparison with standard absorptions made from calibrations of the instrument or published in the literature (6-1).

Gas Chromatography

Gas chromatography is a relatively new analytical tool. Its name comes from the change in color that adsorbents exhibit when adsorbing certain compounds. The analysis is made by separating a mixture into individual components by adsorbing them on the surface of a solid and desorbing them one at a time with a carrier gas stream (6-42, 6-18, 6-43, 6-8, 6-17). The thermal conductivity of the exit-gas stream gives the amount of each constituent present.

Chromatography consists of depositing the sample as an adsorbed or absorbed vapor on the surface of the porous solid. A carrier gas moves the individual compounds forward in the bed, sorting them according to

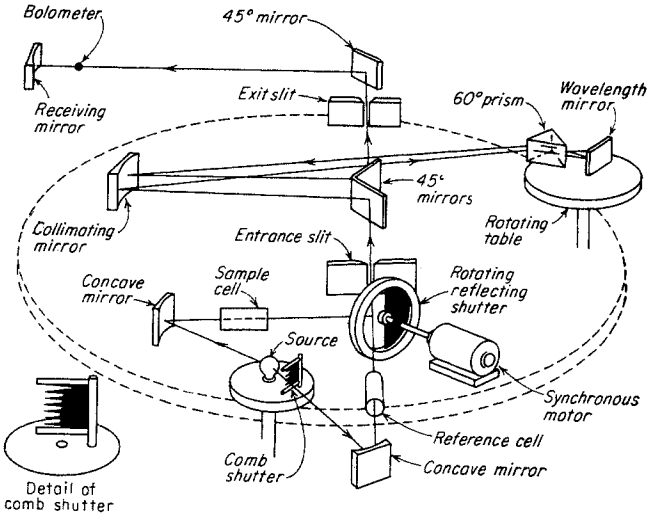

Fig. 6-7. Schematic representation of the optical system of an infrared spectrometer. (Ewing, 6-22. Courtesy Baird Associates, Inc., Cambridge, Mass.)

the varying degrees of adsorption. By the time the end of the column is reached, the compounds are separated, and they follow one another to the conductivity cell. Figure 6-8 illustrates the essential equipment required for separation and analysis. The elutriating column may be a tube ¼ in. in diameter and from 4 to 6 ft long. It is packed with a granulated solid, such as ground firebrick, which has had its surface covered with a nonvolatile absorbent such as tri-isobutylene, dioctyl phthalate, or silicone. Thermal-conductivity cells indicate the concentration of the compounds in the exit-carrier-gas stream. Care must be exercised to inject the sample in a short period of time and to allow no space between the exit of the absorbent bed and the entrance to the thermal-conductivity cell for longitudinal mixing of gases separated in the column. Variables in chromatography are column packing, column size, temperature, carrier gas, carrier-gas flow rate, and sample size. The proper combination is selected for the type of analysis under consideration, and the apparatus is calibrated with known samples.

The procedure for an analysis is as follows:

1. Stabilize the column at constant temperature with a stream of carrier gas such as helium.
2. Introduce the sample into the inlet helium stream.
3. Record the changes in thermal conductivity with time.

Figure 6-9 is a chart for an analysis. The time for an analysis depends upon the length and content of the elutriating column, the carrier-gas flow rate, and the size of the sample. The compound is identified by the time it takes to traverse the bed and the concentration is determined by the area under the thermal-conductivity peak.

Developments are taking place very rapidly in improvement of this analytical technique, especially in methods for finding the correct absorbent column for a given analysis. A typical commercial unit is shown in Fig. 6-10.

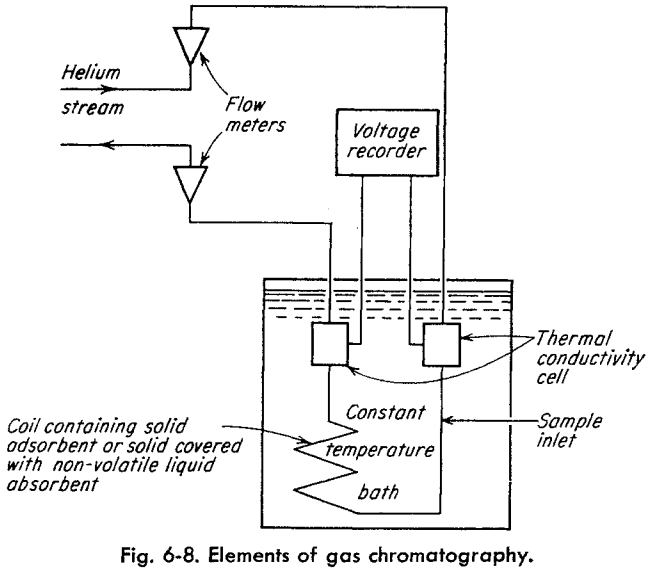

Fig. 6-8. Elements of gas chromatography.

Helium

Knowledge of the helium content of natural gases is often desired for tracer work or in finding a source of helium. The mass spectrometer gives a good analysis for helium. The Bureau of Mines (6-3) has developed a method of analysis, specific for helium, which is accepted as a standard. It consists of adsorbing all other gases on activated charcoal at liquid-nitrogen temperatures and observing the gas pressure due to helium.

Hydrogen Sulfide

The Tutweiler method has been widely used for measuring the hydrogen sulfide content of natural gas (6-2). The hydrogen sulfide is dissolved in water and reacted with standard iodine solution, using starch as an indicator. The method of reporting is usually in

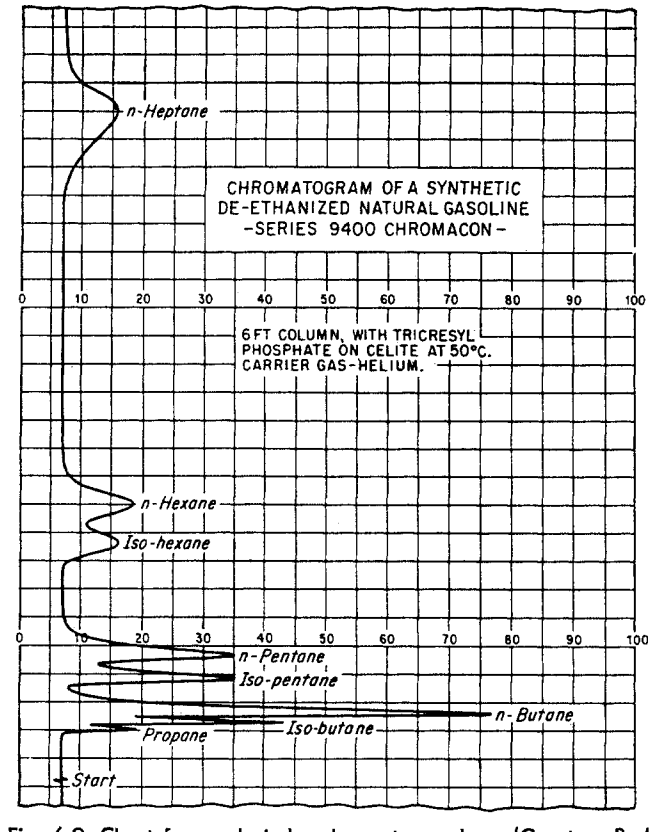

Fig. 6-9. Chart for analysis by chromatography. (Courtesy Podbielniak, Inc.)

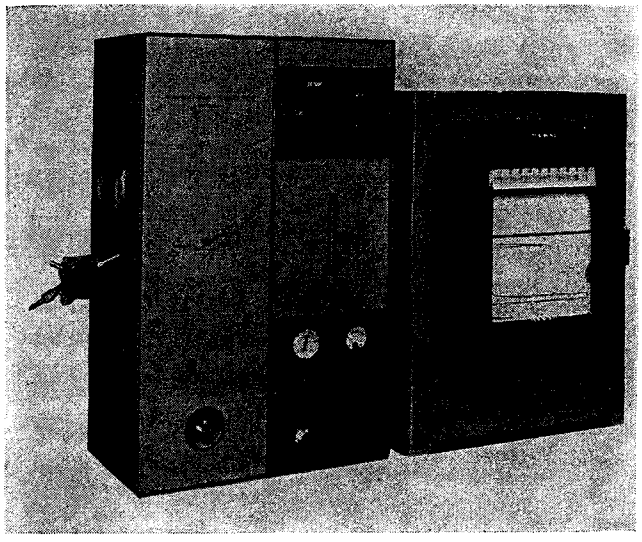

Fig. 6-10. Photograph of chromatography apparatus. (*Courtesy Perkin-Elmer Corp.*)

grains of sulfur per 100 cu ft of gas; 590 grains of sulfur per 100 cu ft = 1 vol % (1 × 32 × 7,000/379 = 590 grains per 100 cu ft at 60°F and 14.7 psia).

MEASUREMENT OF VAPOR-LIQUID EQUILIBRIA

Many types of apparatus have been devised to obtain equilibrium between vapor and liquids. The experiment may consist of a measurement of vapor pressure on a pure substance or of bubble points and dew points for binary mixtures. Complex mixtures of natural gas and crude oil may be brought into equilibrium and samples taken from the equilibrium phases for analysis. In the field, a flowing stream may be separated into vapor and liquid, for example in oil-gas separators.

The apparatus used by Sidney Young (6-68) for determining the vapor pressures and densities of the saturated phases for thirty pure substances is shown in Fig. 6-11. The substance is confined by mercury in glass tubes surrounded by constant-temperature vapor jackets with visual observation of bubble and dew points. Kay (3-30) used similar equipment for his studies of binary systems (Fig. 3-12). He inserted a small steel ball in the glass capillary and stirred the fluid by means of a solenoid placed outside the heating jacket.

Several types of equipment have been used to bring complex mixtures into equilibrium under pressures of 5,000 psi or more. Thick-walled steel cells holding 500 to 1,000 cu cm can be equipped with an internal stirrer (3-26), as shown in Fig. 6-12, placed on a trunnion, and agitated by rocking (3-68), or can have

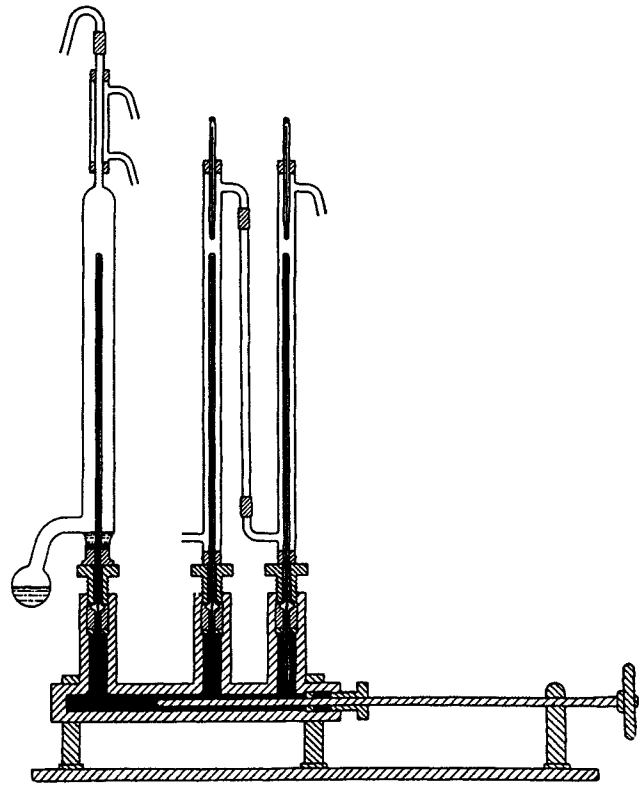

Fig. 6-11. Sidney Young apparatus for determining vapor-liquid properties.

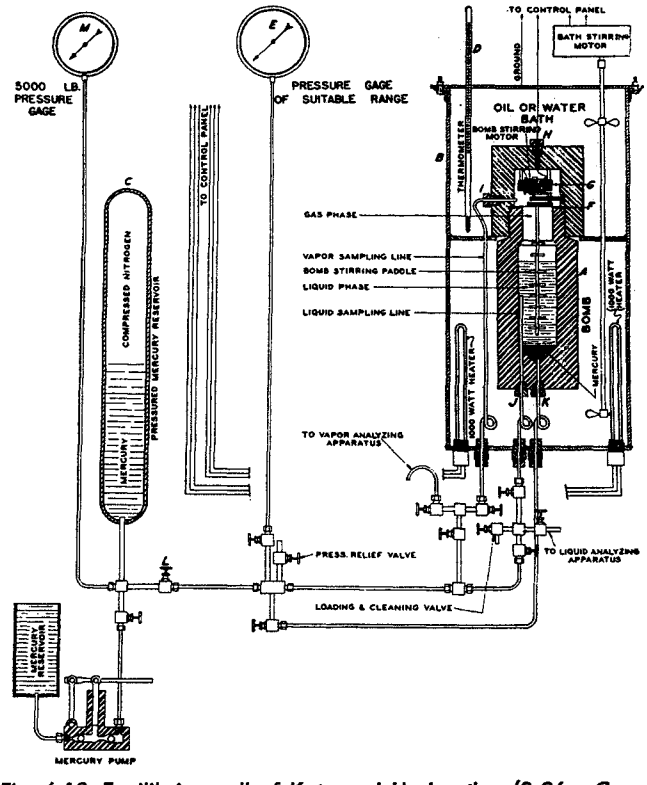

Fig. 6-12. Equilibrium cell of Katz and Hachmuth. (3-26. *Courtesy Ind. Eng. Chem.*)

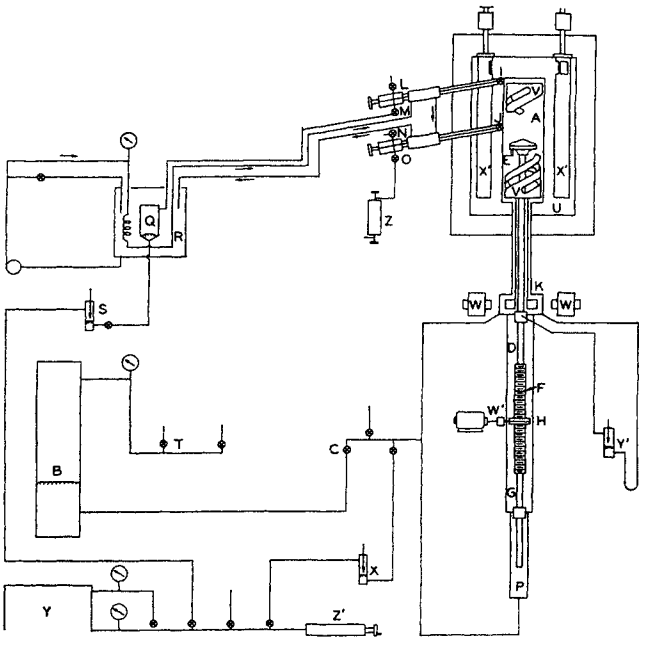

Fig. 6-13. Volumetric and phase-behavior apparatus of Sage and Lacey. (6-55. *Courtesy AIME.*)

the vapor circulated through the liquid (6-11) to obtain equilibrium. This type of equipment provides equilibrium samples of vapor and liquid for analysis.

Sage, Lacey, and coworkers have developed equipment for combined measurements of volumetric properties and vapor-liquid equilibria (6-55).

The general arrangement of the apparatus is shown in Fig. 6-13. The equilibrium cell A is immersed in an agitated oil bath, the temperature of which is controlled by equipment similar to that described elsewhere. Mercury can be added to the cell from the reservoir B through the valve C, or withdrawn through the same connections. A vertical rod D entering through the lower part of the cell carries at its upper end a mercury-level indicator E consisting of an electric contact point extending downward. The point and the electric lead wire which extends from it through the rod are insulated from the rod and the cell. Thus by connecting the metal of the cell to the other side of an indicating circuit, a signal is given when the point is lowered until it makes contact with the mercury surface. The rod D leaves the mercury-filled part of the cell through a gland in the lower wall of the chamber K. This gland allows vertical movement of the rod without permitting more than very slight leakage of mercury from the equilibrium cell. The rod below the gland is connected to an accurately machined lead screw F which is driven by an electric motor through a worm engaging a gear attached to the nut on the lead screw. These parts are sufficiently carefully constructed so that a revolution counter W' on the worm shaft H, after suitable calibration, gives the location of the contact point E with an uncertainty of less than 0.002 in.

In order to avoid changes in the total volume of the cell

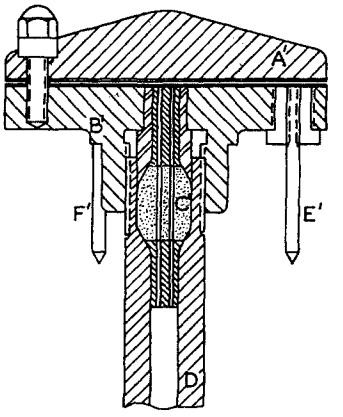

Fig. 6-14. Details of level indicator. (*Sage and Lacey, 6-55. Courtesy AIME.*)

system as the rod D is raised or lowered, a rod G of the same diameter as the rod D is attached to the lower end of the lead screw and passes through a gland into the chamber P which is filled with mercury and is connected to the equilibrium cell. Not only does this compensating device eliminate any effect of movement of the rod on the total volume of the fluid-filled system but it also serves to avoid appreciable movement of the level indicator point E as a result of change in pressure within the cell since on increase of pressure the only significant deformations are those of elastic compression in the screw F and of elastic extension in the housing surrounding it.

Two valves are built into the equilibrium cell wall, valve I at the top of the cell and valve J at approximately half the maximum working volume. The former connects to a vacuum pump through valve L or to apparatus for adding or withdrawing samples through valve J by way of valve N or O. Valve N permits evacuation of the lower manifold independently of the equilibrium cell.

Attainment of equilibrium within the cell is hastened by means of a spiral agitator V, which is designed so that the free cross section within the cell is the same at each elevation, except near the top and bottom of the cell, where measurements of mercury-hydrocarbon or hydrocarbon liquid-gas interfaces are avoided. This spiral agitator is driven by means of a tubular shaft to which is attached a soft iron armature within the case K. The case is constructed of stainless steel of relatively low permeability. Close outside the case is a revolving electromagnet W of sufficient flux to induce the necessary torque in the shaft to drive the spiral agitator at a speed of approximately 100 rpm, despite the presence of the case K which must withstand the maximum working pressure of the equilibrium cell.

The details of the construction of the level indicator are given in Fig. 6-14, and those of the equilibrium cell in Fig. 6-15. A pressure balance Y is used for the determination of pressure. The range of pressure is to 10,000 psia, and that of the temperature bath around the equilibrium cell is 30 to 460 $\pm$ 0.1°F.

The volumetric and phase measurements are made on a weighed quantity of material, gases from reservoir Q through valve M and liquids from vessel Z through valve O. The total volume of the hydrocarbons in the equilibrium cell is determined by the mercury-level indicator E', and the liquid-hydrocarbon level by a hot-wire indicator attached to F'. The volume of the hydrocarbon system is controlled by mercury displacement through valve C.

Figures 6-16 and 6-17 illustrate data obtained on the above equipment for mixtures given in Table 6-3.

Methods of determining vapor-liquid equilibria at low temperatures are reviewed by Bloomer and Parent (3-7).

A stream of two phases flowing through a pipe to a separator operating at constant temperature and pressure usually will give phases closely approximating equilibrium. Sampling of these phases followed by analysis of the samples will give equilibrium data. Table 6-4 gives analyses for the two phases sampled from field separators.

Table 6-3. Composition of Hydrocarbon Mixtures

Component	Composition of mixture for Fig. 6-16		Composition of mixture for Fig. 6-17	
	Weight fraction	Mole fraction	Weight fraction	Mole fraction
Methane	0.0520	0.2632	0.3548	0.7155
Ethane	0.0191	0.0517	0.0768	0.0826
Propane	0.0424	0.0782	0.0717	0.0526
Isobutane	0.0181	0.0254	0.0197	0.0110
n-Butane	0.0439	0.0615	0.0400	0.0222
Isopentane	0.0252	0.0283	0.0182	0.0081
n-Pentane	0.0304	0.0343	0.0190	0.0085
Hexanes+*	0.7678	0.4553	0.3894	0.0919
Carbon dioxide	0.0011	0.0020	0.0104	0.0076

* Average molecular weight, 137.1.

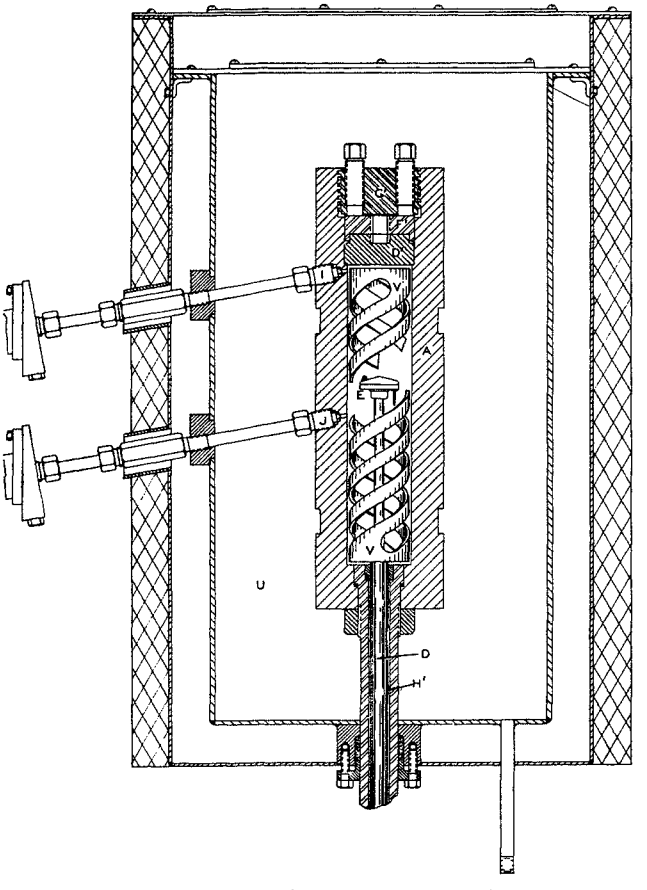

Fig. 6-15. Equilibrium cell. (*Sage and Lacey, 6-55. Courtesy AIME.*)

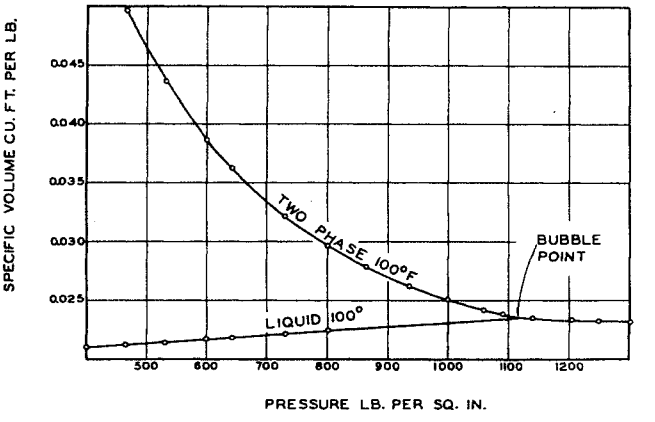

Fig. 6-16. Volumetric behavior of natural gas–oil mixture. (*Sage and Lacey, 6-55. Courtesy AIME.*)

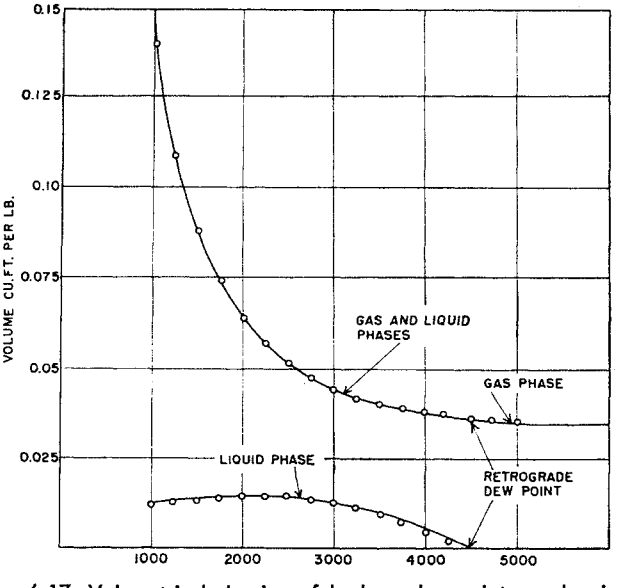

Fig. 6-17. Volumetric behavior of hydrocarbon mixture, showing retrograde dew point. (*Sage and Lacey, 6-55. Courtesy AIME.*)

Table 6-4. Composition of Field Separator Samples

	Erath, La., condensate at 2,200 psia and 101°F		Oklahoma condensate at 1,274 psia and 84°F		Carthage, Tex., condensate at 364 psia and 79°F		Kettleman Hills, Calif.,* at 510 psia and 148°F	
	Vapor	Liquid	Vapor	Liquid	Vapor	Liquid	Vapor	Liquid
Mole fractions:								
Nitrogen	.....	.....	.....	.....	0.0173			
Carbon dioxide	0.0041	.....	.....	.....	0.0060			
Methane	0.9276	0.3406	0.8053	0.2732	0.9012	0.1110	0.8319	0.1000
Ethane	0.0303	0.0415	0.1188	0.1544	0.0403	0.0302	0.0848	0.0613
Propane	0.0136	0.0297	0.0519	0.1519	0.0152	0.0338	0.0437	0.0533
Isobutane	0.0042	0.0152	0.0034	0.0095	0.0036	0.0193	0.0076	0.0224
n-Butane	0.0038	0.0167	0.0132	0.0941	0.0073	0.0519	0.0168	0.0666
Isopentane	0.0023	0.0142	0.0011	0.0189	0.0016	0.0386	0.0057	0.0384
n-Pentane	0.0016	0.0132	0.0044	0.0590	0.0034	0.0615	0.0032	0.0430
Hexanes	0.0026	0.0463	0.0037	0.0542	0.0016	0.1568	0.0063	0.6150
Heptanes	0.0029	0.4826	.....	0.1878	0.0025	0.4969		
Specific gravity:								
Heptanes+	.....	0.7994	.....	0.761	.....	0.686		
Molecular weight:								
Heptanes+	.....	159.5	.....	131	.....	126.5	.....	107.5

* Lacey and Sage (6-52).

EQUILIBRIUM CONSTANTS FOR COMPLEX MIXTURES

The first charts for predicting equilibrium constants were based on an extrapolation of fugacities and their ratios (3-67, 3-41, 6-30). Such charts were called charts of *ideal equilibrium constants*, since they depended upon the hydrocarbon mixtures following the laws of ideal solutions. Figures 6-18 to 6-20 give ideal equilibrium constants calculated by Brown and Holcomb (4-14) for propane, isobutane, and *n*-butane. After vapor-liquid equilibrium data became available, the correlations of such data were used, especially for high pressure.

Table 6-5 lists references and conditions at which measurements were made of equilibrium phase compositions for complex systems including natural gas constituents. One method of predicting the equilibrium constants is simply to plot the data for a given

Table 6-5. References for Vapor-Liquid Equilibrium Data on Complex Hydrocarbon Mixtures

System	Reference	Temperature, °F	Pressure, psia	Year	Investigators
Natural gas–crude oil	3-26	40,120,200	14–3,300	1937	Katz and Hachmuth
Natural gas–absorber oil	6-64	33–180	100–5,000	1941	Webber
Natural gas–distillate	6-49	40–200	200–4,000	1941	Roland, Smith, and Kaveler
Gas-distillate	6-65	575–820	118–650	1942	White and Brown
Gas–absorber oil	6-31	64–94	124–3,200	1943	Kirkbride and Bertetti
Natural gas–crude oil	3-68	35–250	1,000–8,200	1944	Standing and Katz
Natural gas–hexane	6-26	100	500–1,800	1945	Hanson and G. G. Brown
Natural gas–crude oil	6-50	120–200	1,000–9,300	1945	Roland
Carbon dioxide–natural gas–condensate	6-45	100–250	500–2,800	1946	Poettmann and Katz
Natural gas	6-61	130–240	100	1949	Stutzman and G. M. Brown
Carbon dioxide–natural gas–crude oil	6-47	38–202	600–8,500	1951	Poettmann
Gas–absorber oils	6-59	100–220	500–1,000	1952	Soloman
Carbon dioxide, hydrogen sulfide, natural gas, crude and absorber oils	6-29	100–200	200–5,000	1952	Jacoby and Rzasa
Gas condensate	6-27	201	500–3,000	1953	Hoffman, Crump, and Hocott
Hydrogen sulfide–natural gas–crude oil	6-62	154	700–2,500	1954	Vagtborg
Natural gas–crude oil	6-21	190	1,000–6,000	1956	Evans and Harris

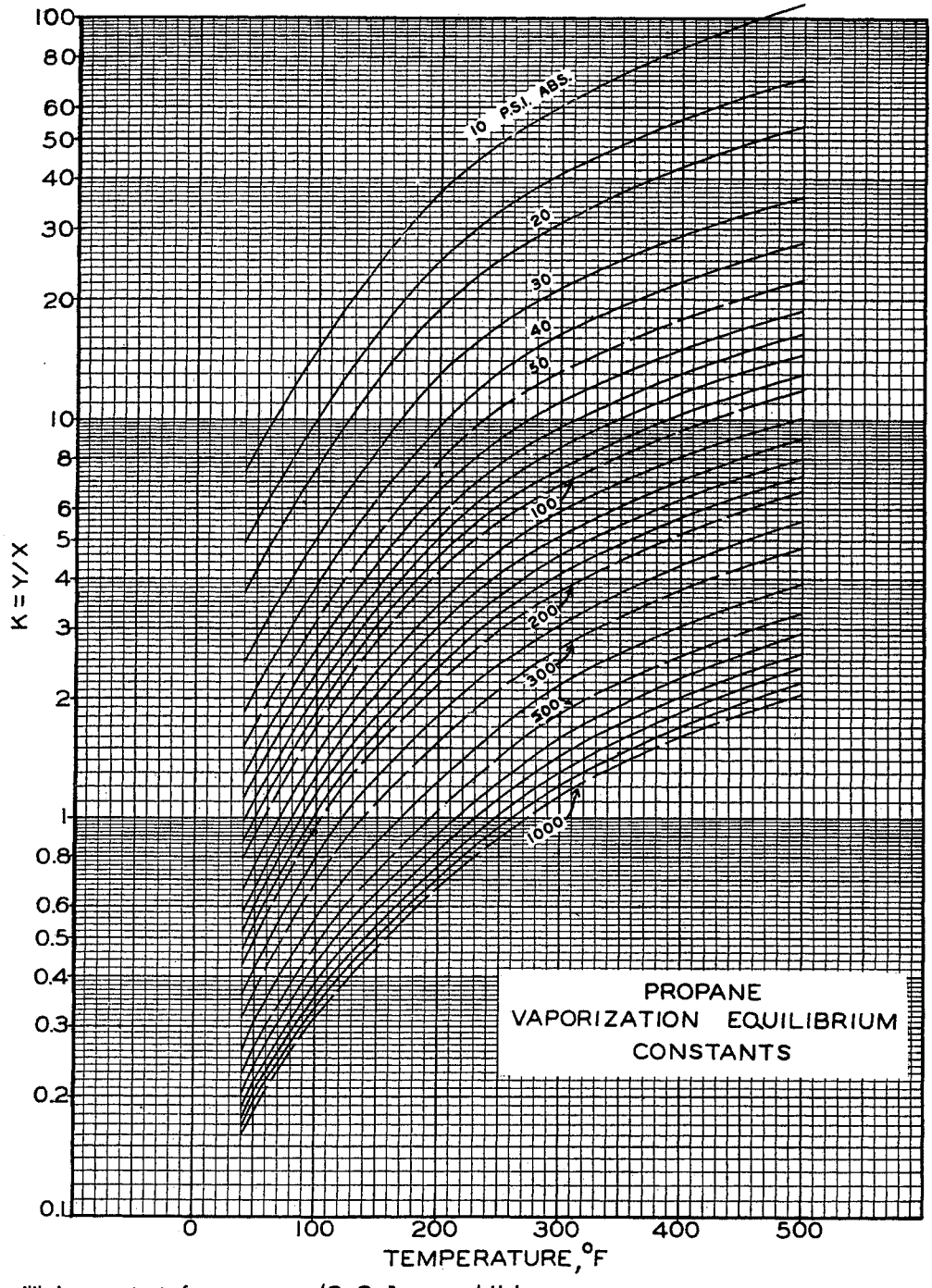

Fig. 6-18. Ideal equilibrium constants for propane. (G. G. *Brown and Holcomb*, 4-14. *Courtesy Petrol. Engr.*)

kind of mixture as a function of temperature and pressure. This was done for the Oklahoma City crude oil–natural gas mixtures by Katz and Hachmuth (3-26). These charts (Fig. 6-21 to 6-29*a*) are suitable for many mid-continent crude oils. The charts for isobutane, *n*-butane, isopentane, and *n*-pentane were drawn in 1953 by R. F. Hinds and D. B. Burrows while they were attending a phase-behavior course at the University of Michigan.

A factor of 0.15 times the equilibrium constant for heptane will give a reasonably close approximation to the value of the constant for heptanes and heavier

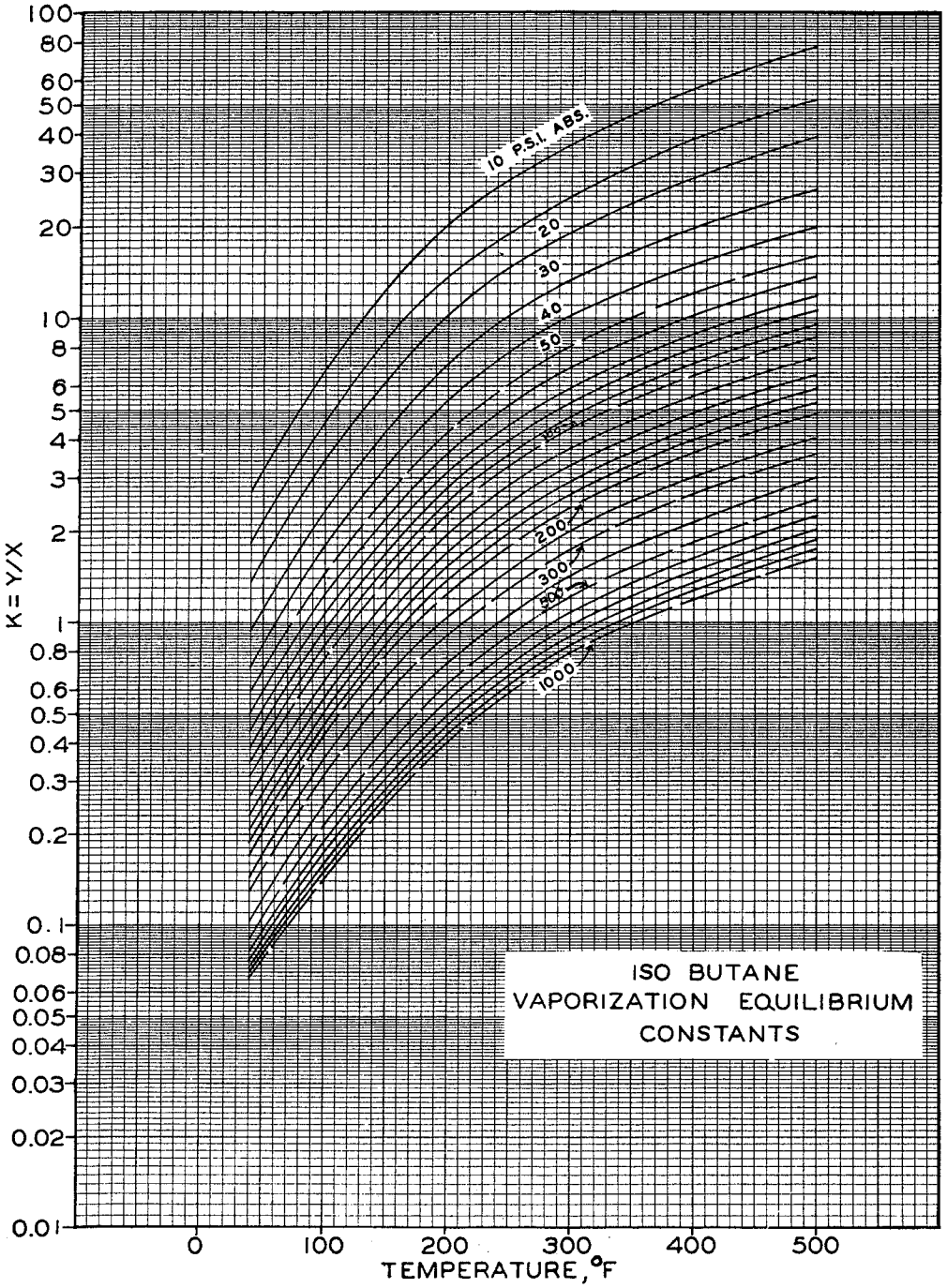

Fig. 6-19. Ideal equilibrium constants for isobutane. (*G. G. Brown and Holcomb, 4-14. Courtesy Petrol. Engr.*)

in Oklahoma City crude oil. Some modification may be required for methane (6-53) and for the heptane-and-heavier constituent when the charts for crude oil–natural gas systems are used. The work of Standing and Katz (3-68) indicates a significant effect of oil composition for high pressures. Constants based on crude oil such as Oklahoma City apply reasonably well to oil absorbers. The data by Roland, Smith, and Kaveler (6-49) can be reduced to charts for predicting vapor-liquid separation of natural gas distillate.

The nonhydrocarbon constituents, carbon dioxide,

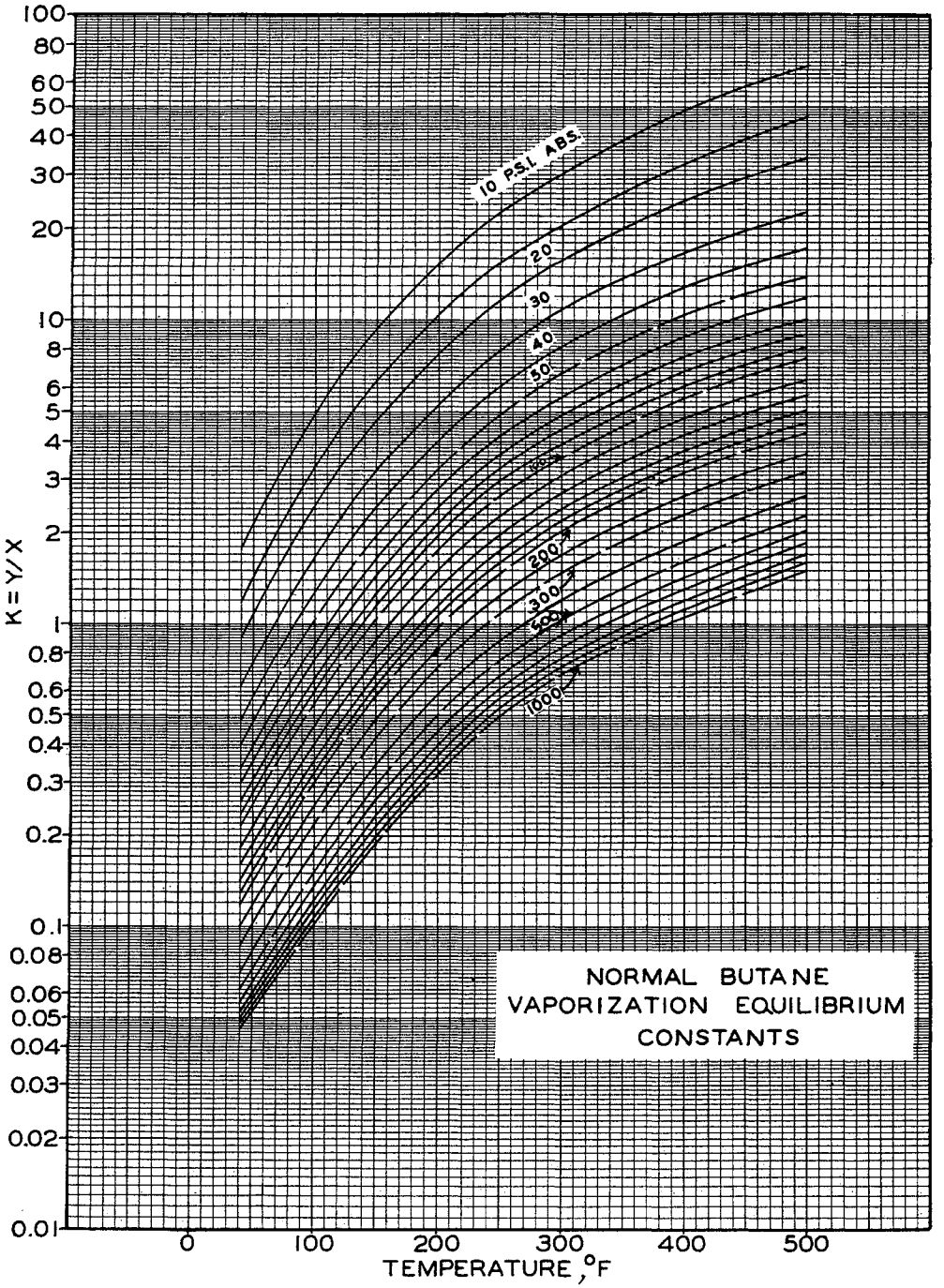

Fig. 6-20. Ideal equilibrium constants for *n*-butane. (*G. G. Brown and Holcomb*, 4-14. *Courtesy Petrol. Engr.*)

nitrogen, and hydrogen sulfide, have been investigated as indicated in Table 6-5. A chart by Poettmann for carbon dioxide in crude oil is given in Fig. 6-30 (6-47). Poettmann's measurements were for 6 to 11 mole % carbon dioxide in the vapor phase. Carbon dioxide was more soluble in the Billings crude oil than in the Erath condensate (6-45). Jacoby and Rzasa (6-29) measured the phase compositions for a crude oil–natural gas system (molecular weight of C_7+, 227; specific gravity, 0.894) (C-6) in which nitrogen, carbon dioxide, and hydrogen sulfide were included each at 5 mole %. Figures 6-31 to 6-33 give a comparison

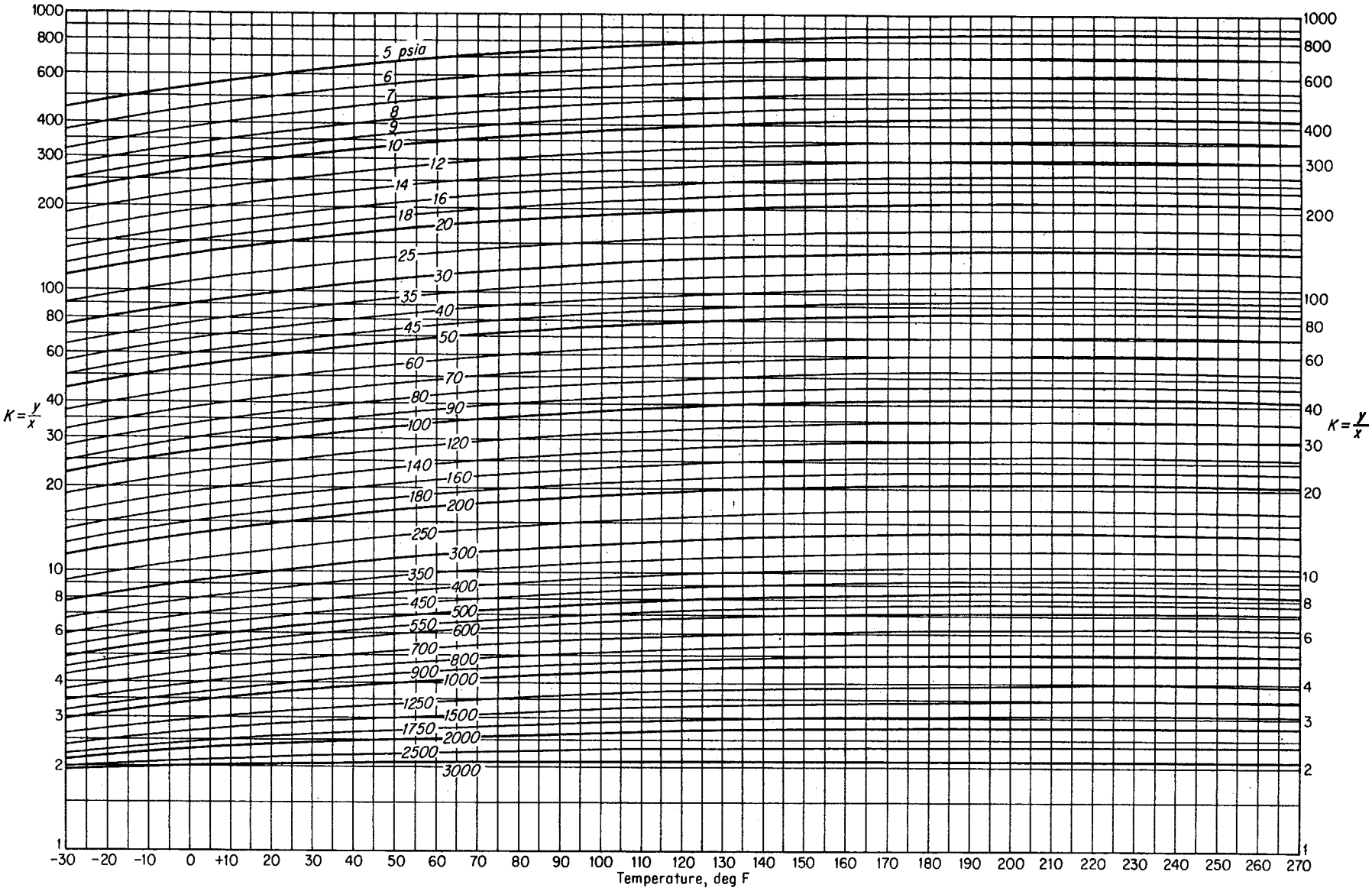

Fig. 6-21. Equilibrium constants for methane in Oklahoma City crude oil. (*Katz and Hachmuth*, 3-26.)

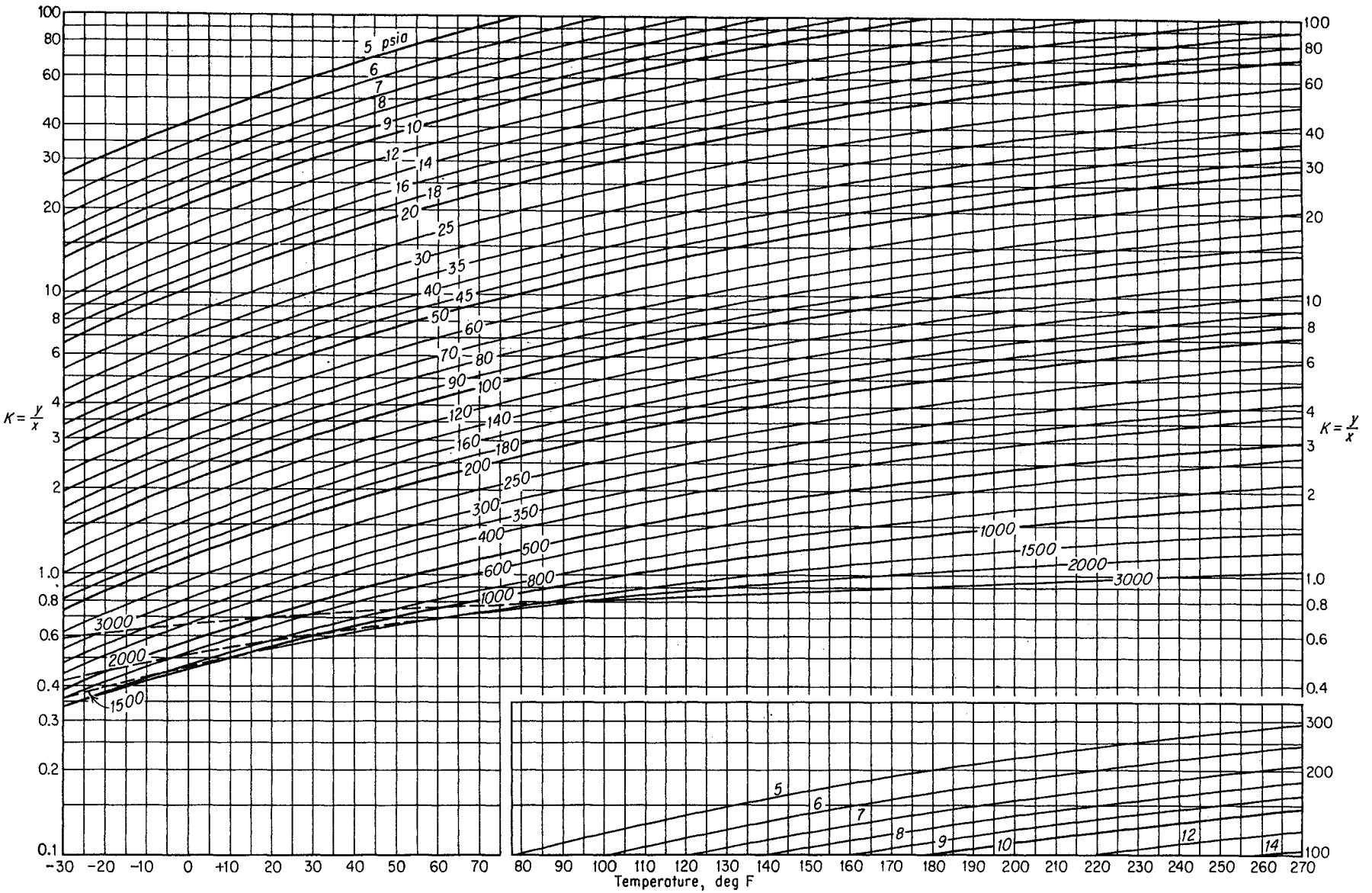

Fig. 6-22. Equilibrium constants for ethane in Oklahoma City crude oil. (*Katz and Hachmuth*, 3-26.)

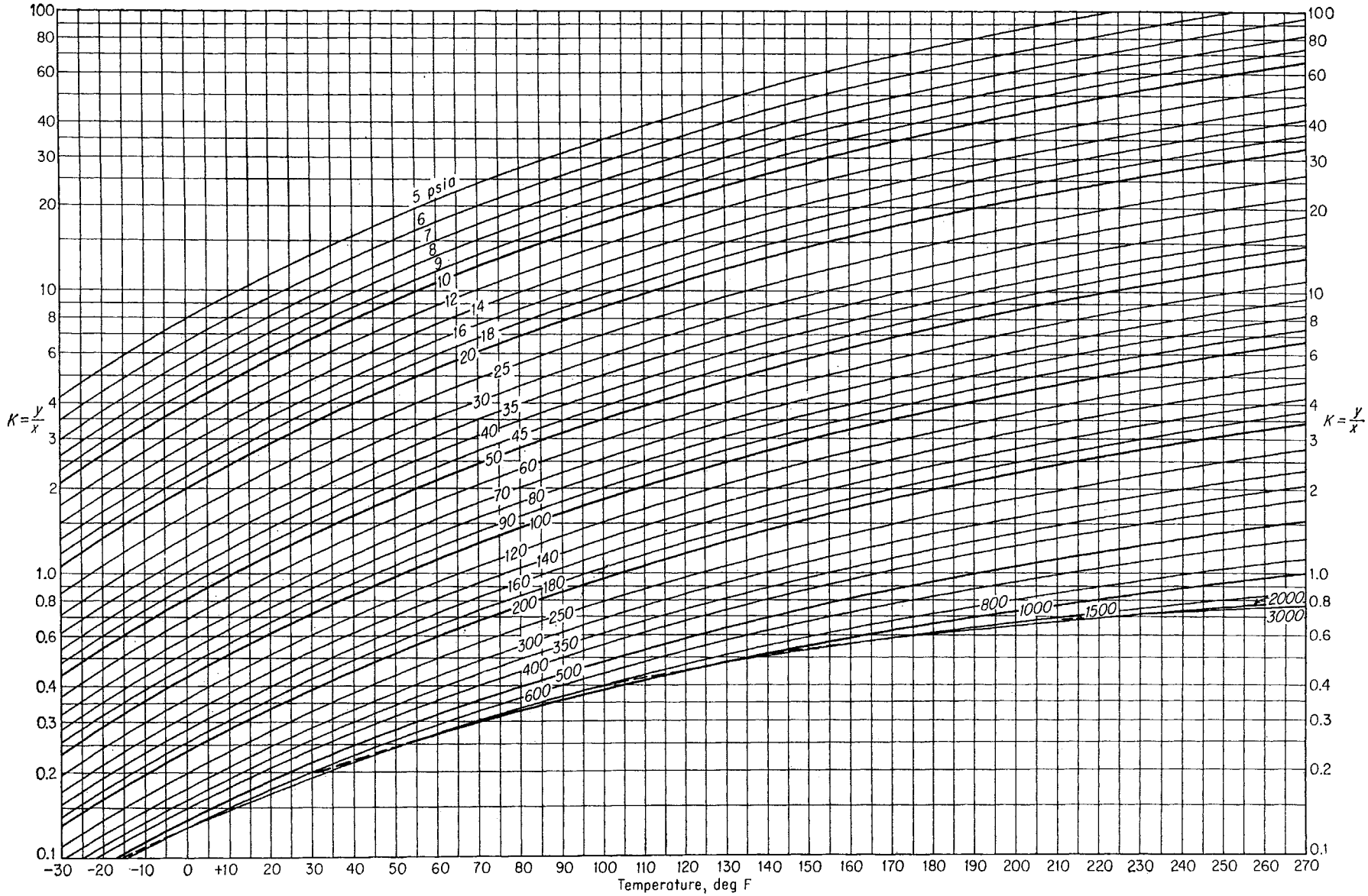

Fig. 6-23. Equilibrium constants for propane in Oklahoma city crude oil. (*Katz and Hachmuth*, 3-26.)

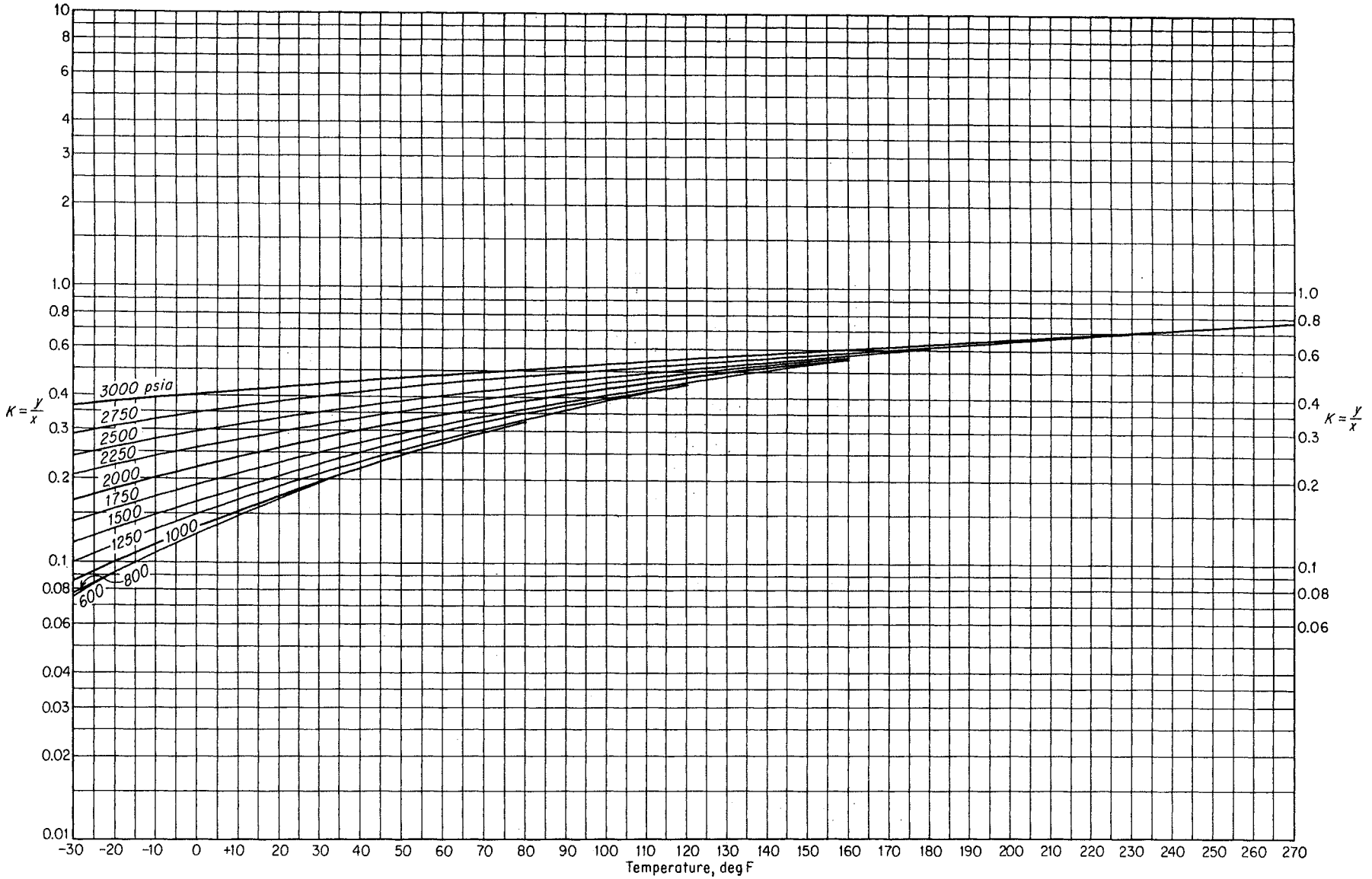

Fig. 6-23*a*. Equilibrium constants for propane in Oklahoma City crude oil. (*Katz and Hachmuth*, 3-26.)

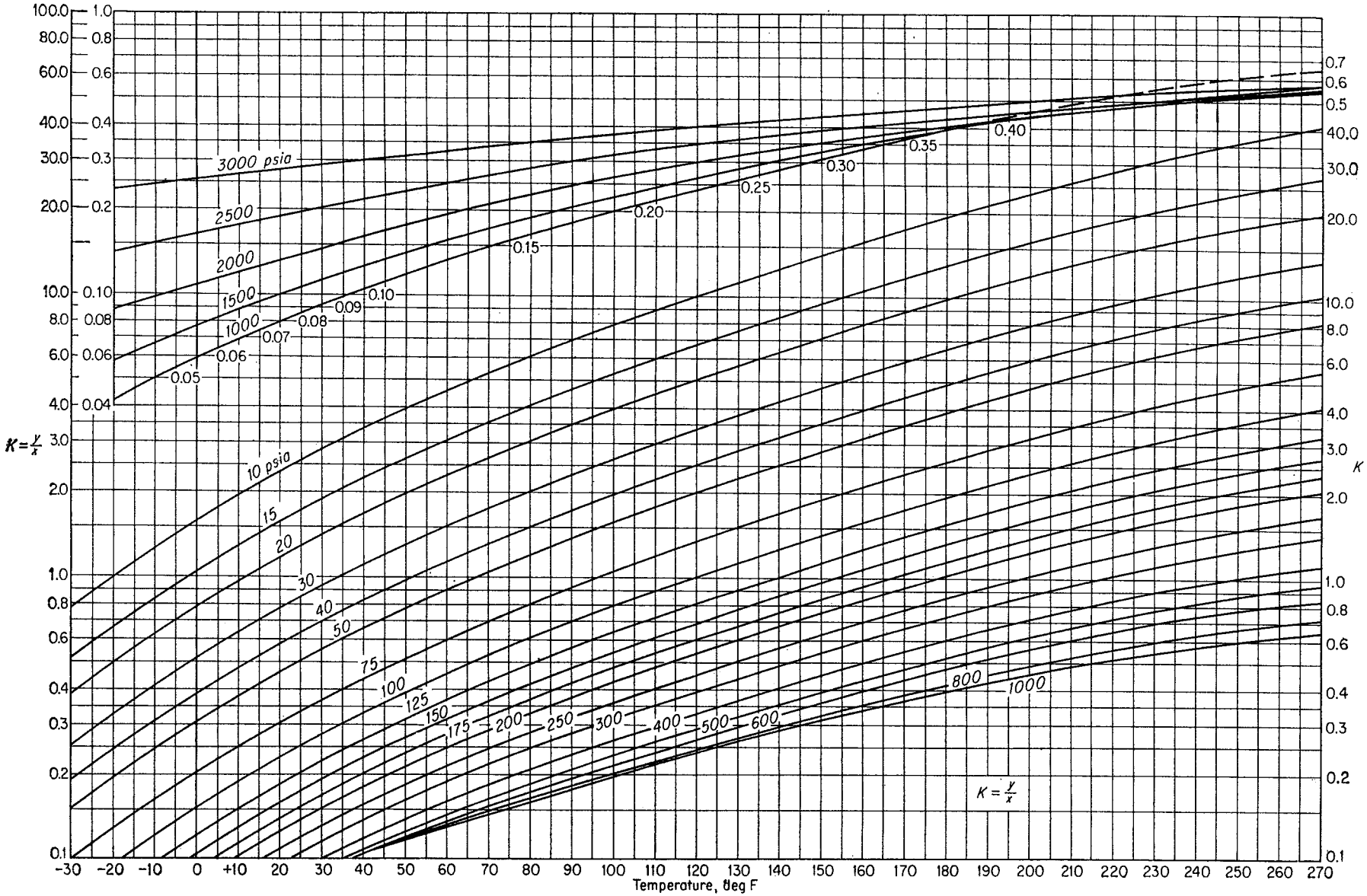

Fig. 6-24. Equilibrium constants for isobutane in Oklahoma City crude oil. (*Katz and Hachmuth*, 3-26.)

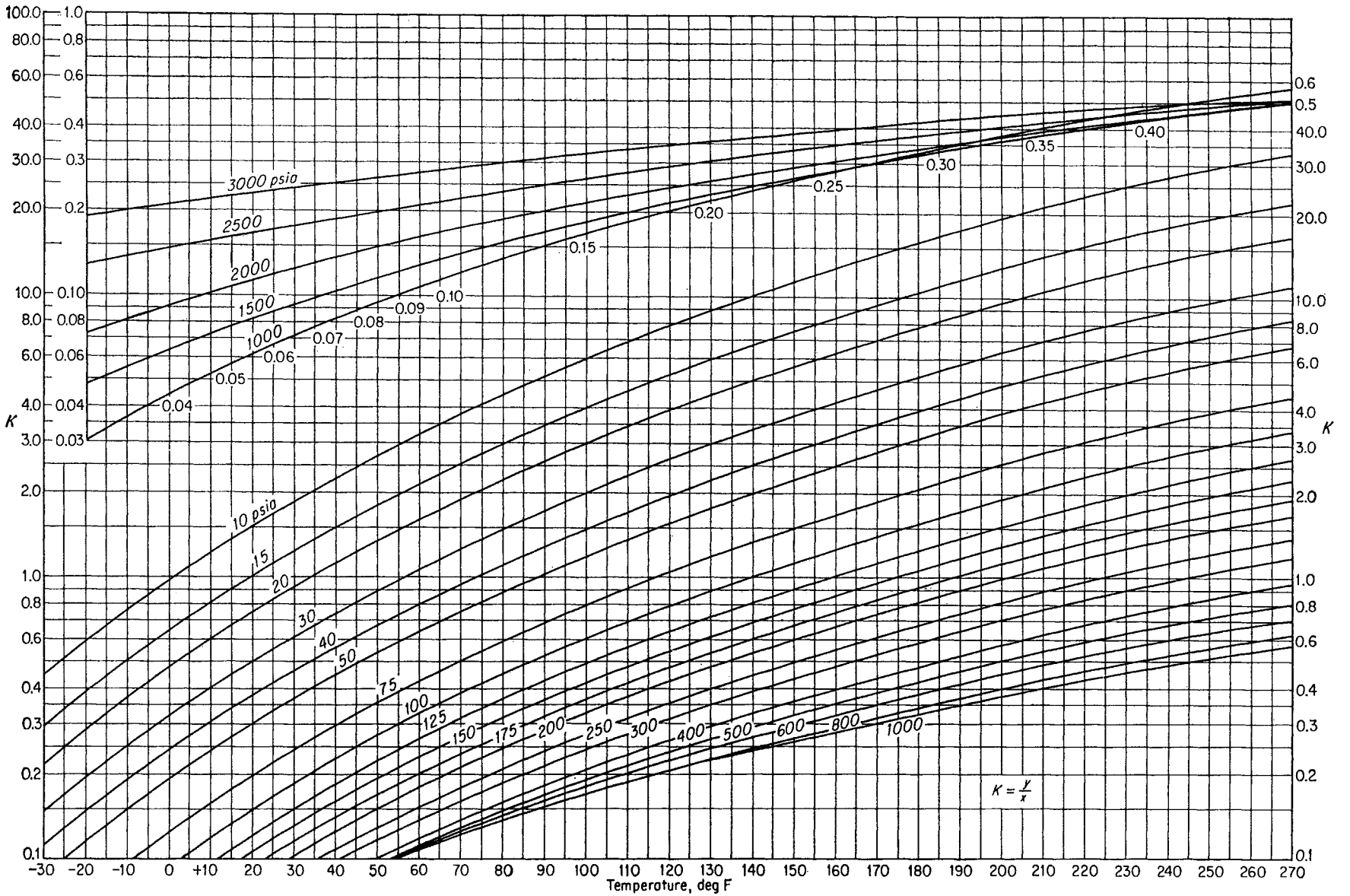

Fig. 6-25. Equilibrium constants for *n*-butane in Oklahoma City crude oil. (*Katz and Hachmuth*, 3-26.)

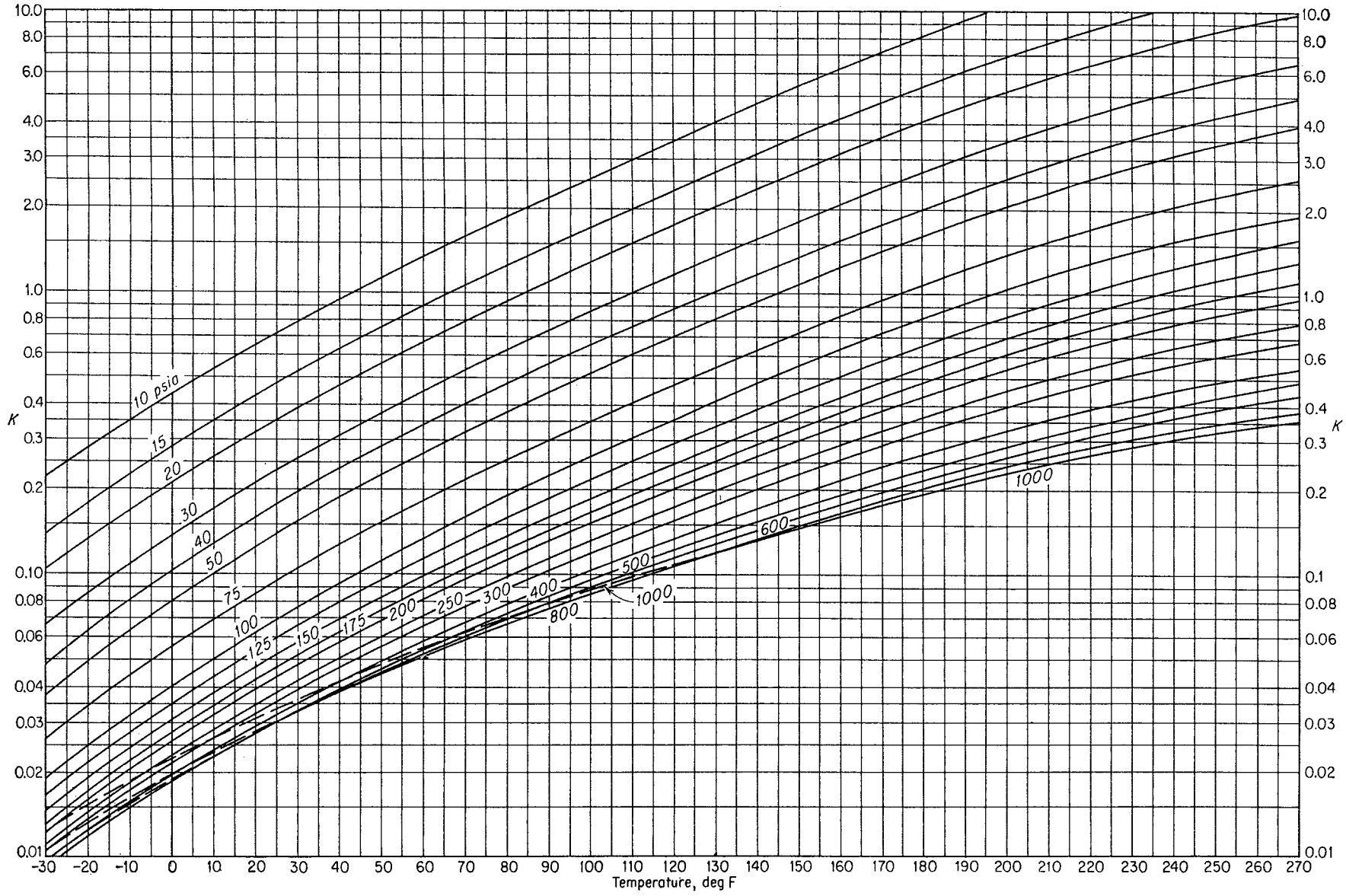

Fig. 6-26. Equilibrium constants for isopentane in Oklahoma City crude oil. (*Katz and Hachmuth*, 3-26.)

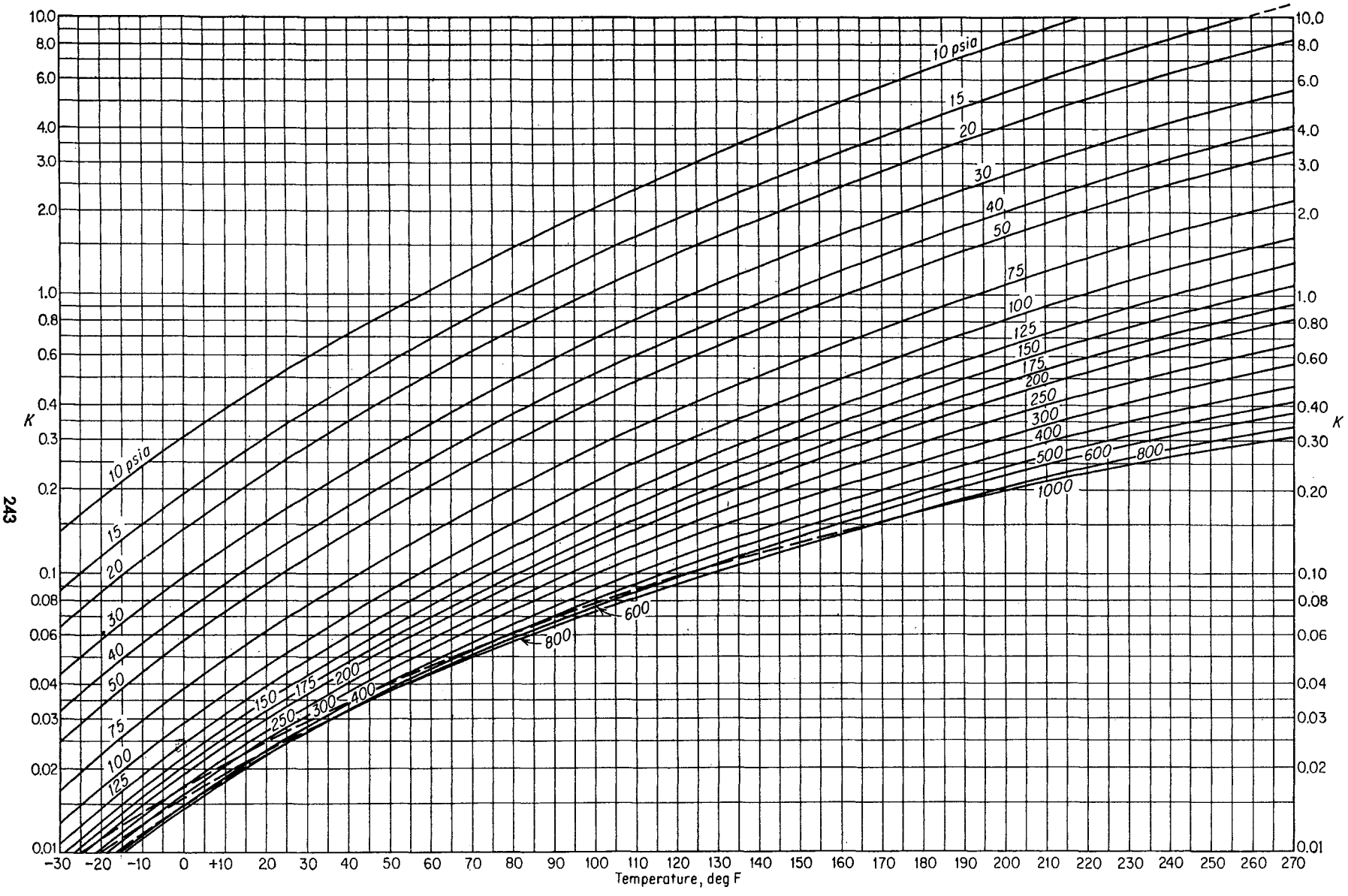

Fig. 6-27. Equilibrium constants for *n*-pentane in Oklahoma City crude oil. (*Katz and Hachmuth*, 3-26.)

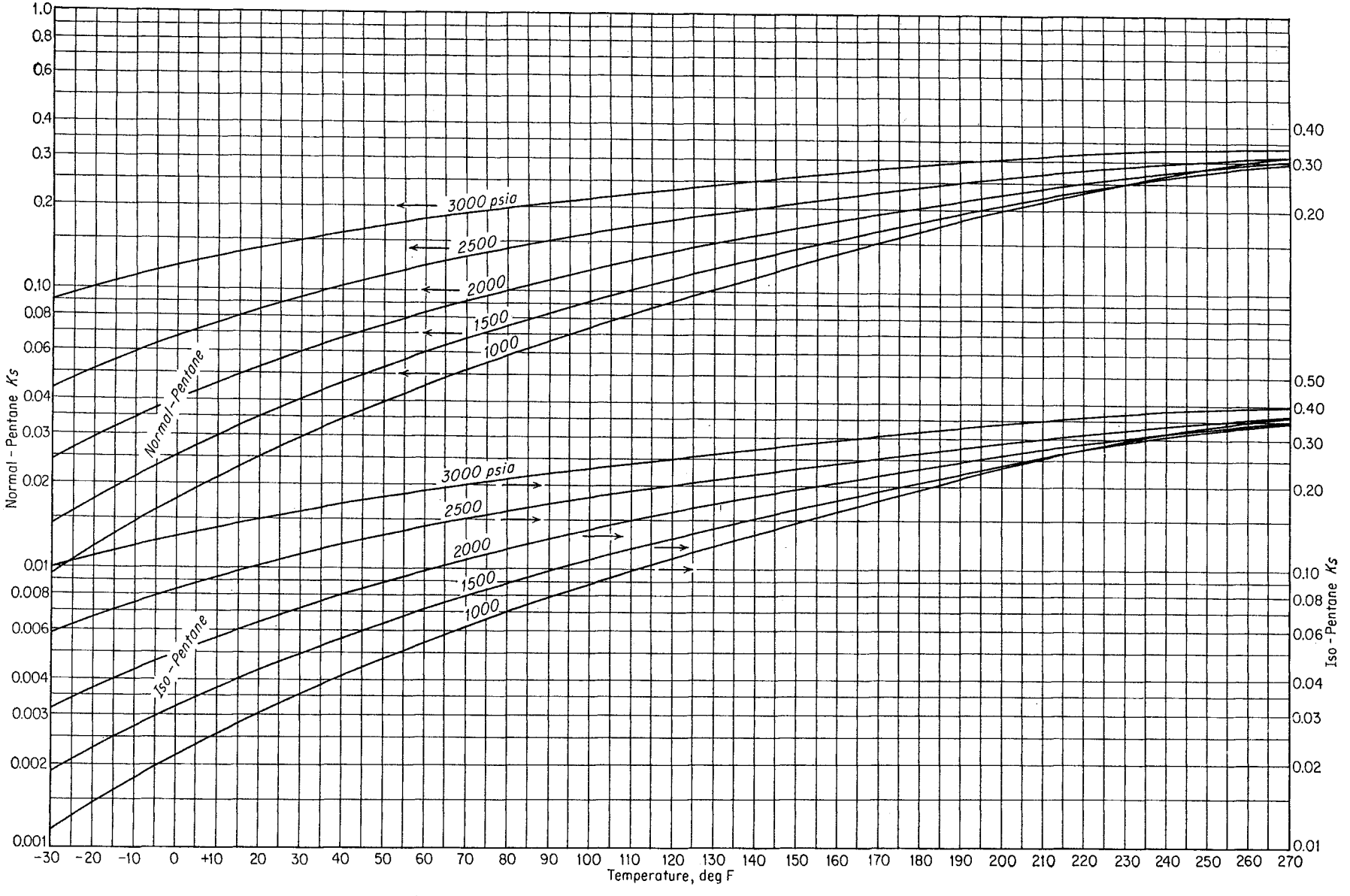

Fig. 6-27*a*. Equilibrium constants for isopentane and *n*-pentane at high pressures.

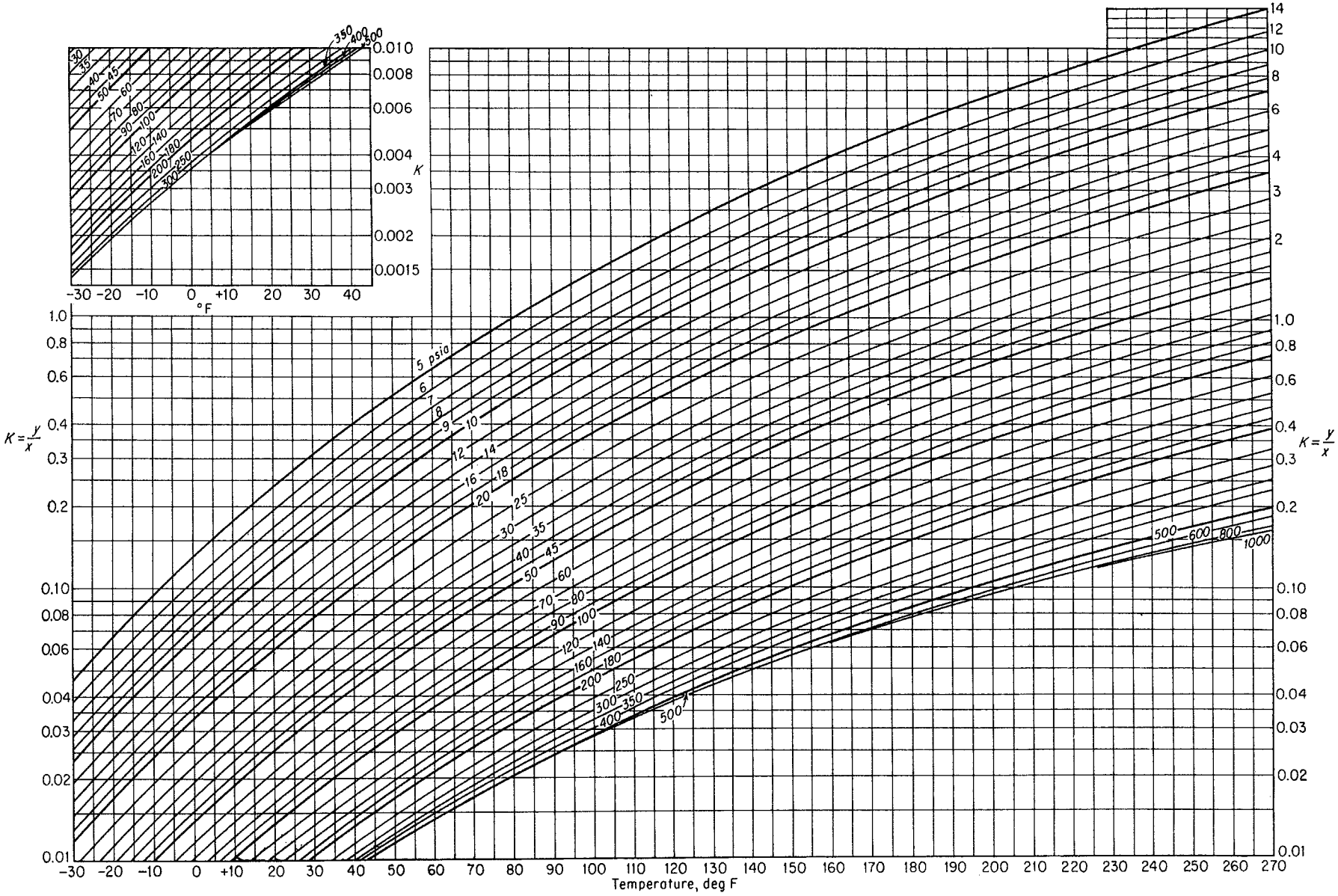

Fig. 6-28. Equilibrium constants for hexanes in Oklahoma City crude oil. (*Katz and Hachmuth*, 3-26.)

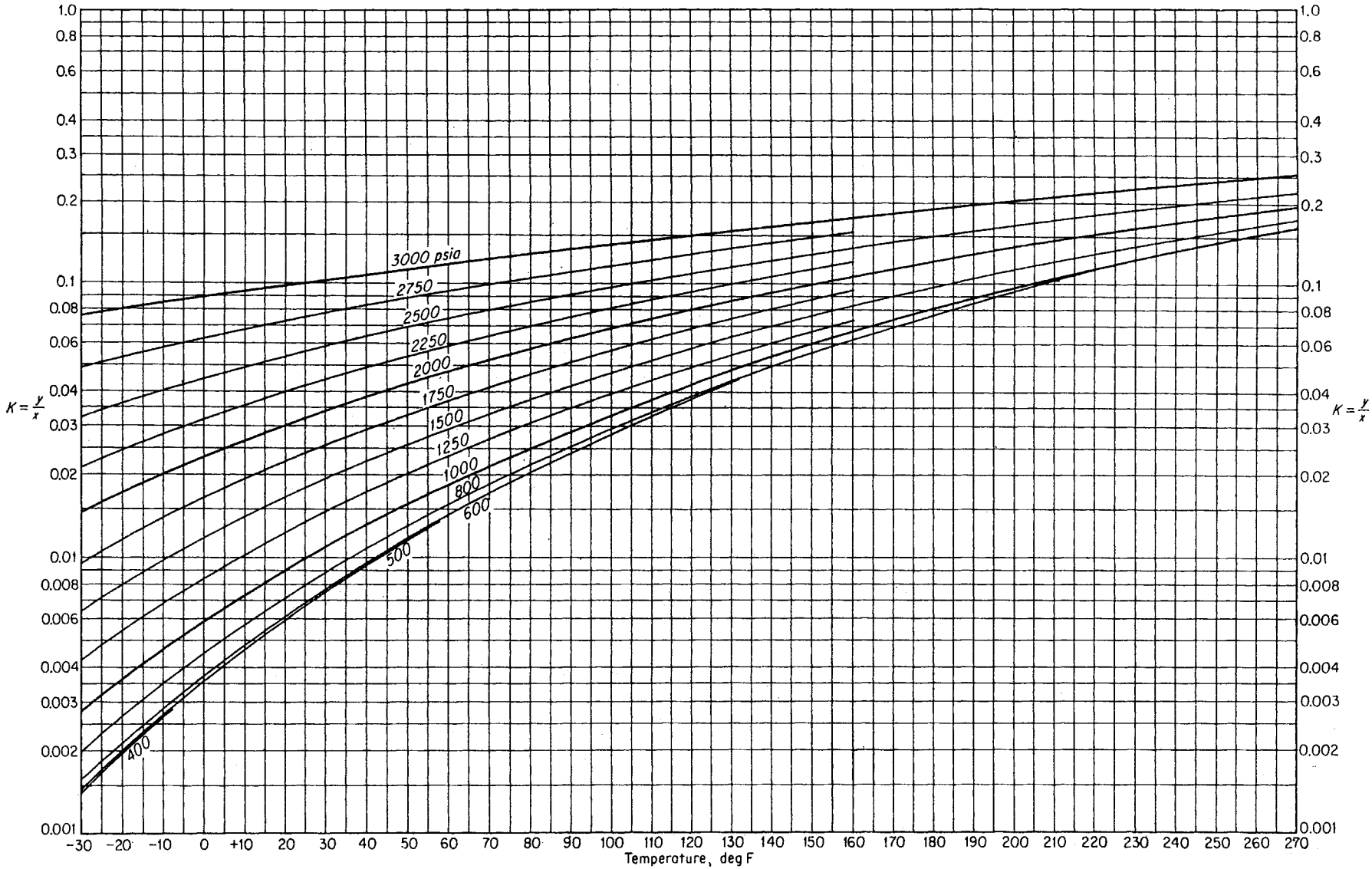

Fig. 6-28a. Equilibrium constants for hexanes in Oklahoma City crude oil. *(Katz and Hachmuth, 3-26.)*

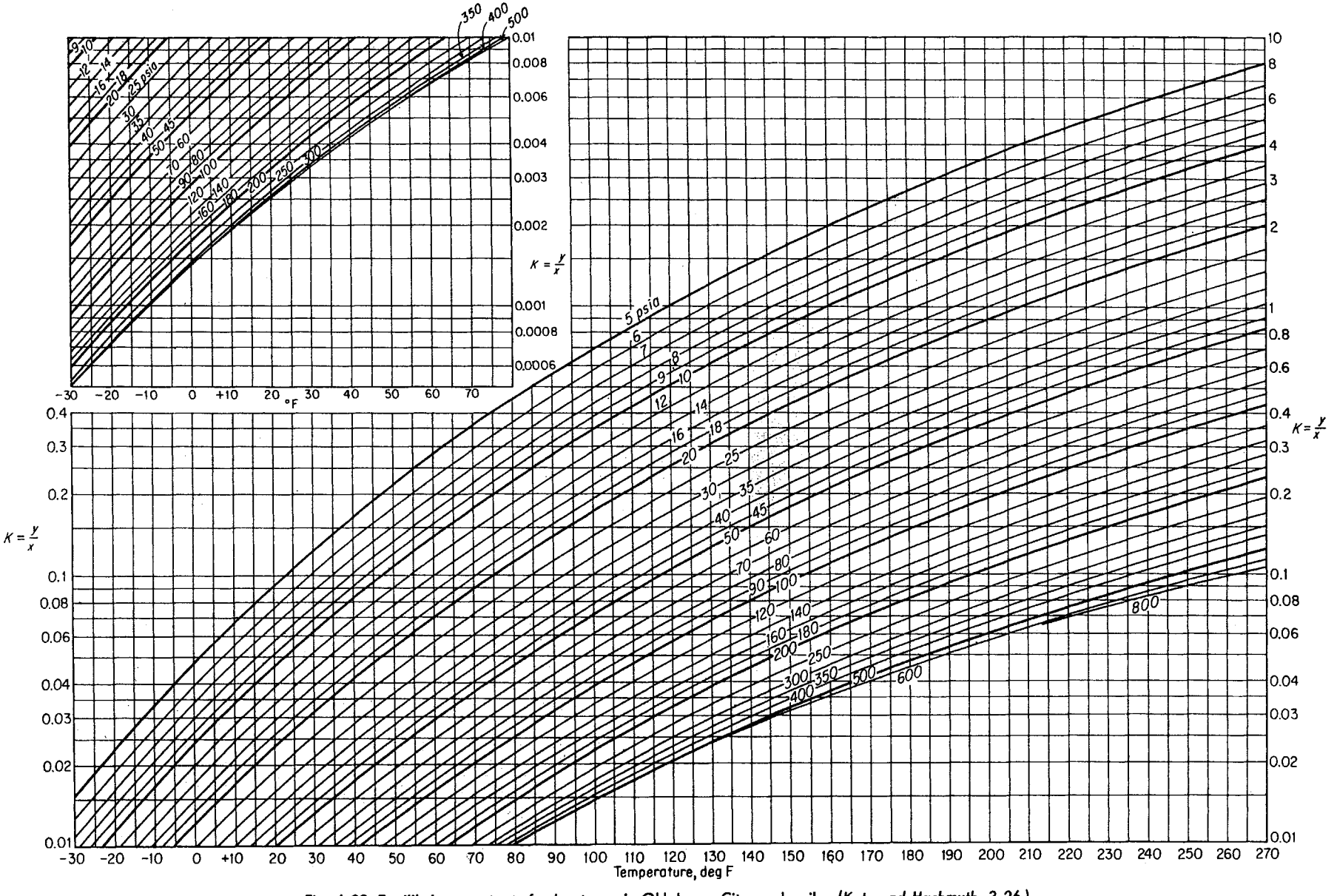

Fig. 6-29. Equilibrium constants for heptanes in Oklahoma City crude oil. (*Katz and Hachmuth*, 3-26.)

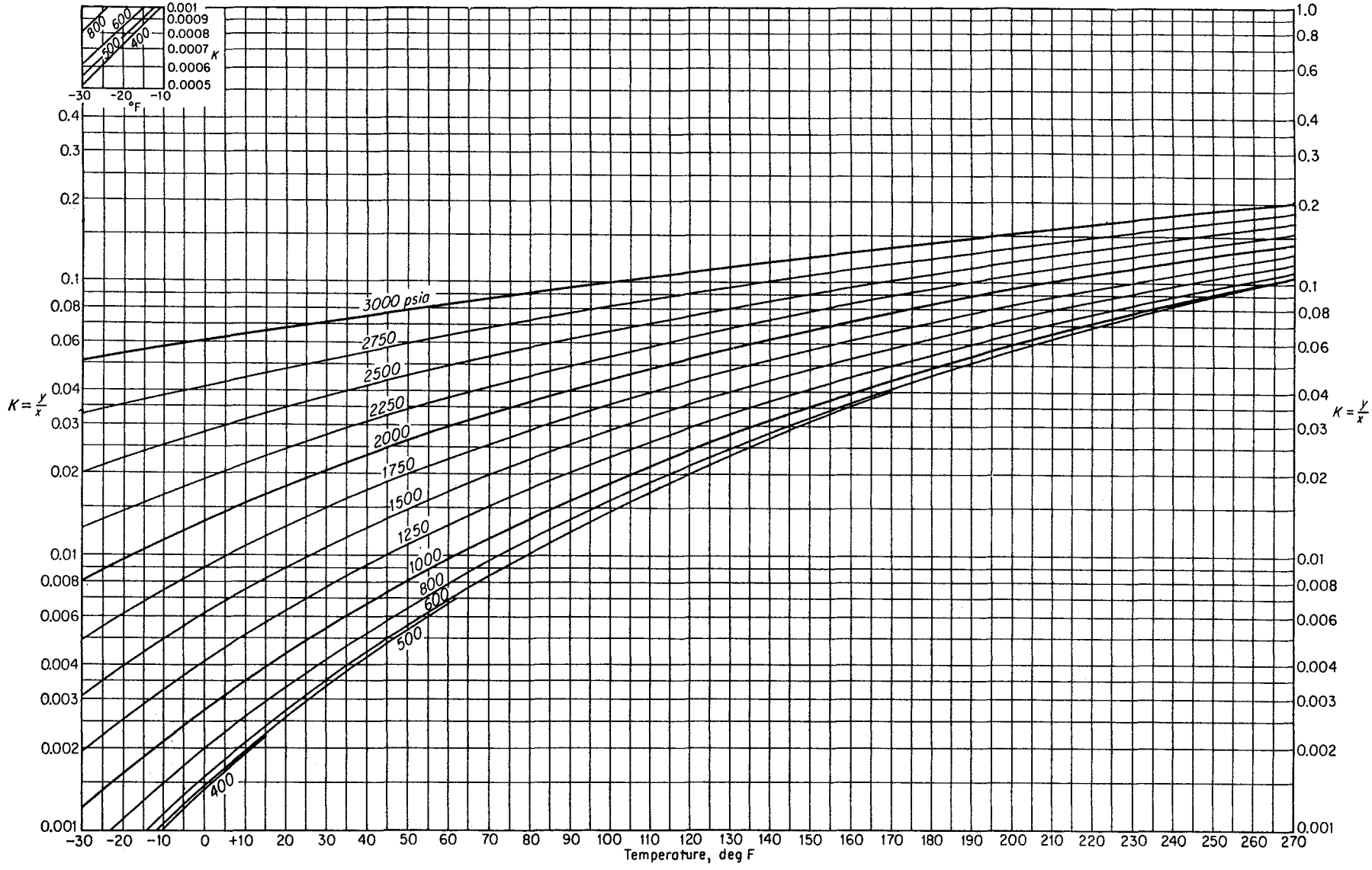

Fig. 6-29a. Equilibrium constants for heptanes in Oklahoma City crude oil. (*Katz and Hachmuth*, 3-26.)

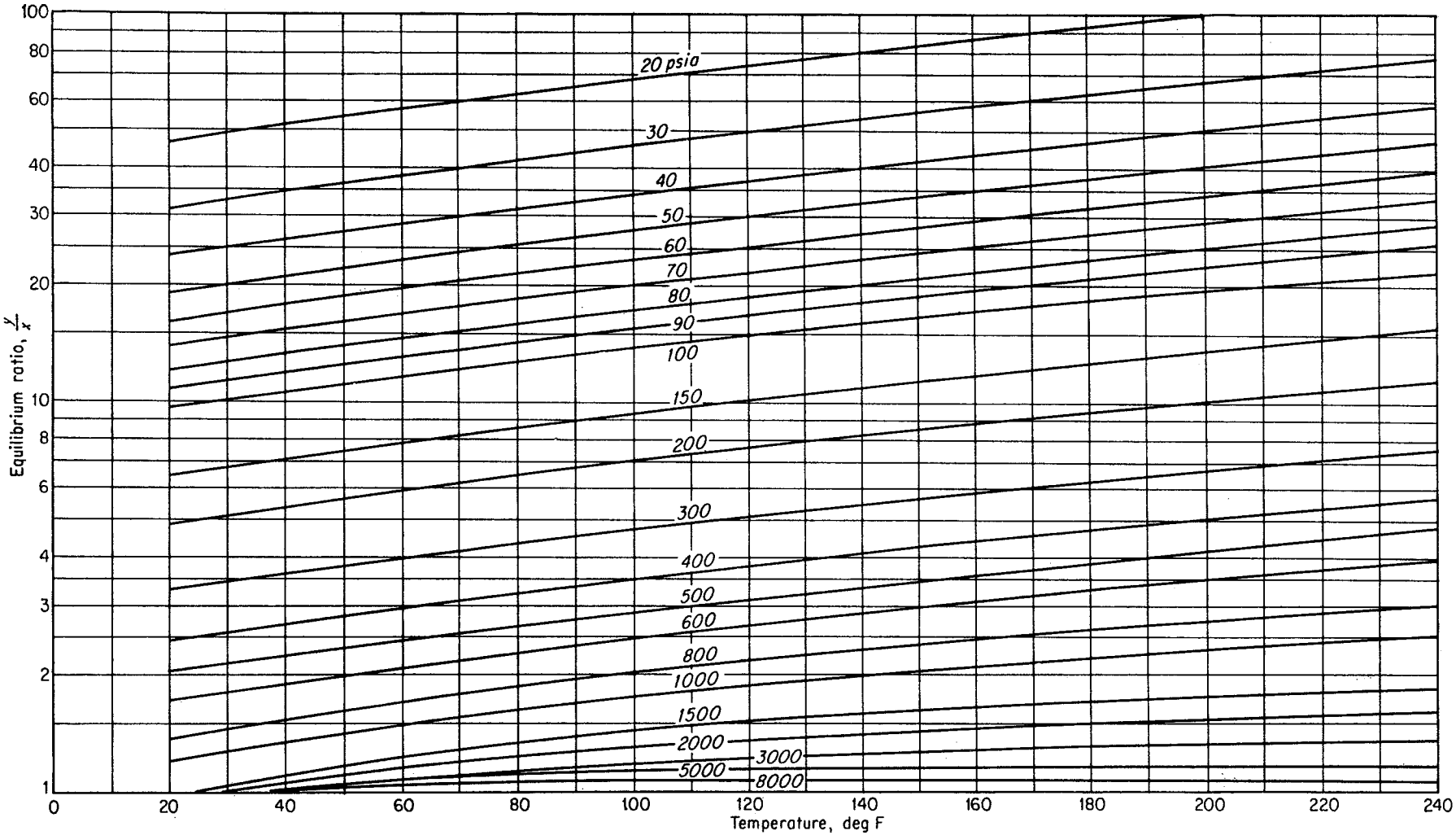

Fig. 6-30. Equilibrium constants for carbon dioxide in Billings crude oil. (*Poettmann, 6-47. Courtesy AIME.*)

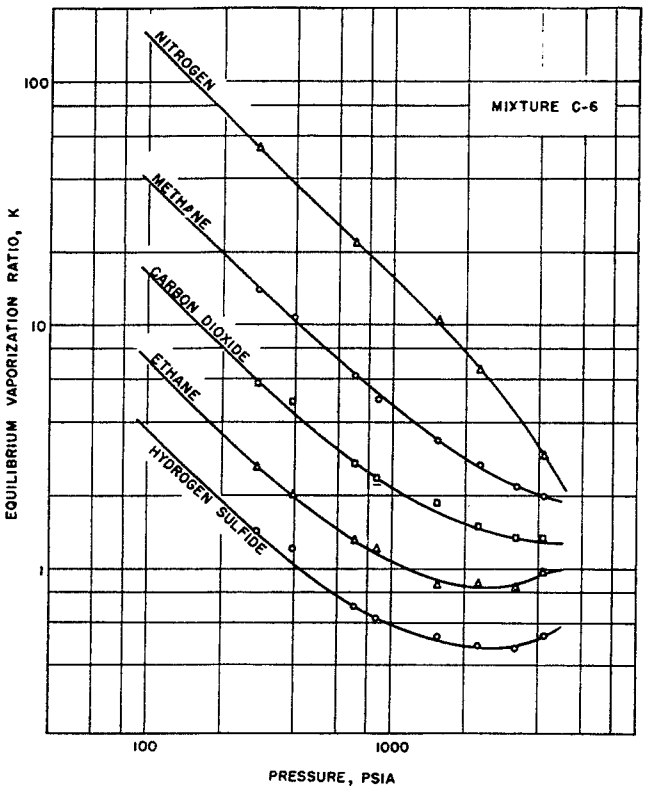

Fig. 6-31. Equilibrium constants in crude oil mixture at 100°F. (*Jacoby and Rzasa, 6-29. Courtesy AIME.*)

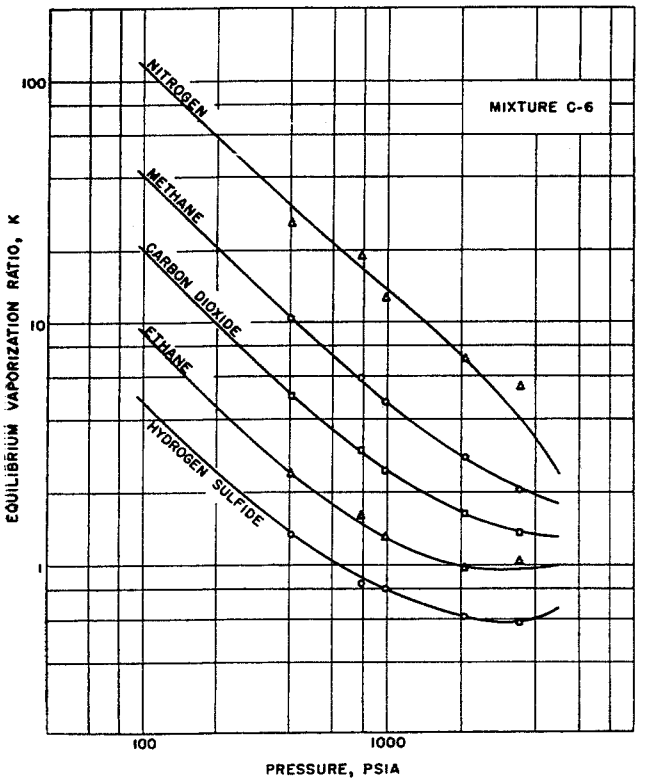

Fig. 6-32. Equilibrium constants in crude oil mixture at 150°F. (*Jacoby and Rzasa, 6-29. Courtesy AIME.*)

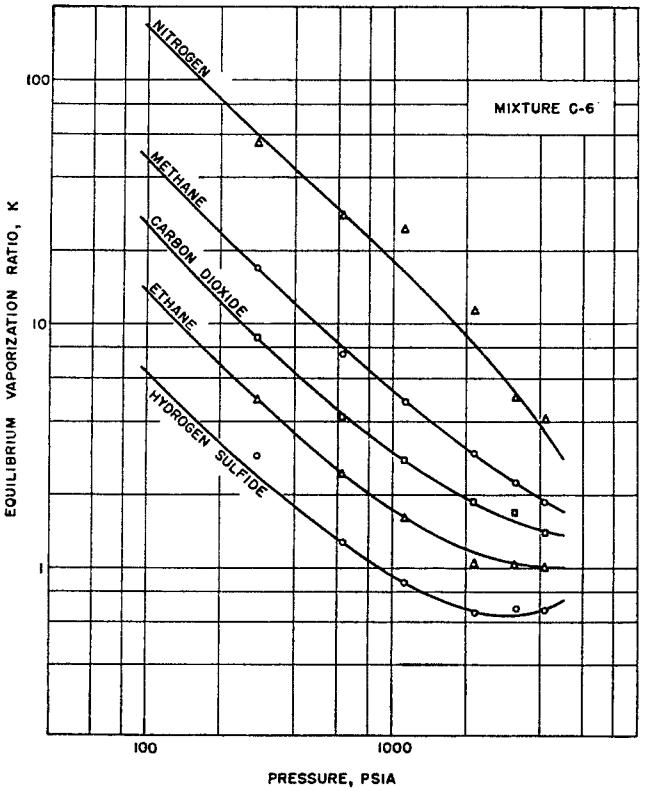

Fig. 6-33. Equilibrium constants in crude oil mixture at 200°F. (*Jacoby and Rzasa, 6-29. Courtesy AIME.*)

of the K's for these constituents with those of methane and ethane. Charts for nitrogen and hydrogen sulfide in this system are given in Figs. 6-34 and 6-35. Vagtborg (6-62) studied a naturally occurring crude oil–natural gas system that contained large amounts of hydrogen sulfide and small amounts of carbon dioxide and nitrogen. He made a differential vaporization of the crude oil saturated at 2,500 psia and 154°F. Table 6-7 gives the smoothed differential compositions of the phases and Table 6-8 gives the equilibrium constants, all at 154°F.

Correlations of Equilibrium Constants

From the phase rule, a ten-component system in two phases at constant temperature and pressure requires specification of eight phase concentrations for rigorous system definition. It follows that correlations of equilibrium constants for complex systems using two variables other than temperature and pressure depend in good measure upon the similarity of hydrocarbon systems. The behavior of the hydrocarbons as a family of substances has been demonstrated in the successful use of gas gravity to represent the composition of a natural gas; this family uniformity of behavior is useful again in relation to vapor-liquid equilibria.

Table 6-6. References for Correlations of Vapor-Liquid Equilibrium Constants

Systems	Reference	Year	Investigators
Light paraffins	6-57	1932	Souders, Selheimer, Smith, and G. G. Brown
Light paraffins	3-41	1932	Lewis and Luke
Light paraffins	6-54	1938	Sage, Hicks, and Lacey
Methane in mixtures	6-53	1938	Sage and Lacey
	4-29	1948	Edmister
Complex systems	6-24	1948	Hadden
High-boiling components	6-46	1949	Poettmann and Mayland
Light hydrocarbons	6-13	1950	Benedict, Webb, Rubin, and L. Friend
Methane in light hydrocarbons	6-10	1952	Arnold
Complex systems	6-51	1952	Rzasa, Glass, and Opfell
Complex systems	6-37	1952	Organick and G. G. Brown
Complex systems	6-67	1952	Winn
Complex systems	6-33	1953	Lenoir and White
Complex systems	6-25	1953	Hadden
Light hydrocarbons	6-19	1953	De Priester
Complex systems	6-40	1955	Organick, NGAA

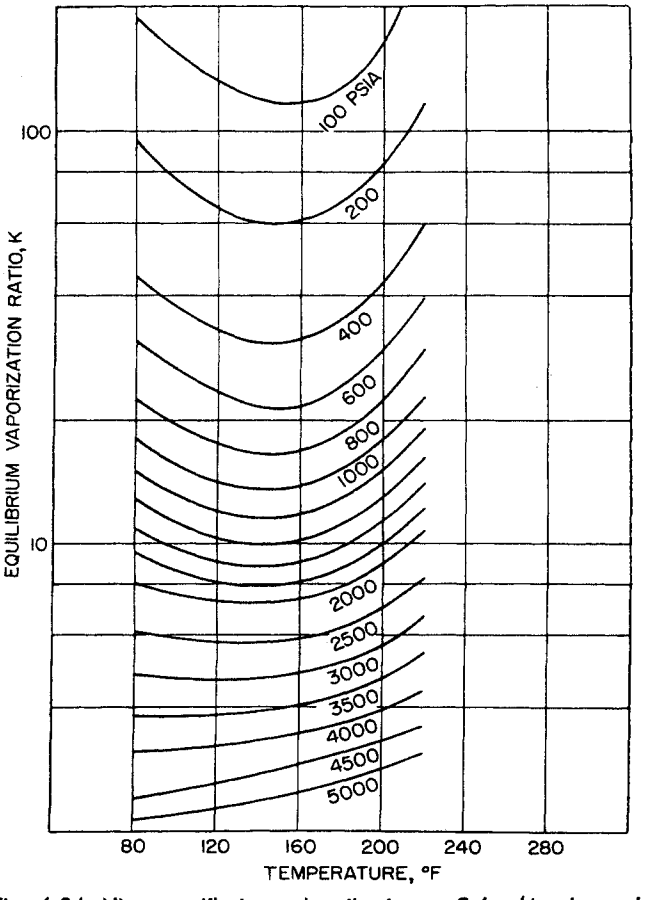

Fig. 6-34. Nitrogen *K*'s in crude oil mixture C-6. (*Jacoby and Rzasa, 6-29. Courtesy AIME.*)

According to Fig. 4-19, the convergence pressures for different systems vary. Hanson and Brown in connection with their studies (6-26) have compared several systems at 120°F (Fig. 6-36). They showed that the equilibrium constants for a given constituent would be the same when the convergence pressure was the same, even though the composition of the mixture were different. An early method for predicting equilibrium constants of systems with volatility intermediate between those measured was to interpolate on charts like Fig. 6-36. White and Brown (6-65) pre-

Table 6-7. Vapor-Liquid Composition during Liberation of Dissolved Gas from Reservoir Fluid
In mole %, at 154°F

Component	1 atm*		726 psia		1,111 psia		1,554 psia		2,043 psia		2,500 psia†
	Liquid	Vapor	Liquid	Vapor	Liquid	Vapor	Liquid	Vapor	Liquid	Vapor	Liquid
C_1	0.00	13.80	7.787	37.58	12.10	45.86	16.843	53.23	21.723	56.73	26.121
C_2	0.00	9.50	5.361	10.15	6.05	10.49	6.677	9.94	7.127	8.08	7.247
C_3	1.37	4.00	2.854	2.06	2.74	2.04	2.641	1.60	2.497	1.45	2.366
C_4	2.00	3.45	2.818	1.71	2.66	1.34	2.473	1.00	2.270	0.84	2.090
C_5	3.63	1.70	2.541	0.88	2.30	0.74	2.081	0.68	1.888	1.04	1.782
C_6+	92.23	0.87	40.677	0.44	34.86	0.48	30.023	0.64	25.971	0.83	22.812
H_2S	0.77	64.55	36.761	43.28	37.70	34.60	37.267	29.06	36.135	25.72	34.827
CO_2	0.00	1.45	0.818	2.27	1.03	2.36	1.216	2.36	1.374	2.33	1.494
N_2	0.00	0.68	0.383	1.63	0.56	2.09	0.779	2.49	1.015	2.98	1.261

* Atmospheric liquid compositions determined experimentally. Vapor compositions are smoothed data.
† Bubble-point liquid (2,500 psia) composition determined by extrapolation.
SOURCE: Vagtborg (6-62).

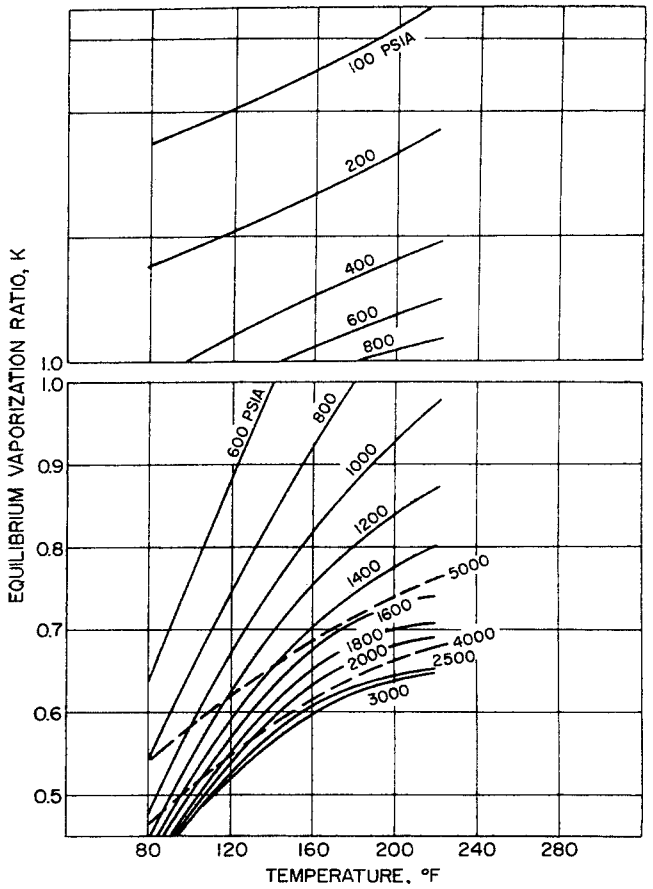

Fig. 6-35. Hydrogen sulfide K's in crude oil mixture C-6. (*Jacoby and Rzasa, 6-29. Courtesy AIME.*)

sented a simple concept for predicting equilibrium constants when the apparent convergence pressure was known. On a log K–log pressure graph, the ideal equilibrium constant was plotted. Charts provided values for the minimum equilibrium constant and the pressure for the minimum K as a function of convergence pressure and vapor pressure of the constituent. The equilibrium-constant curve was drawn in graphically, as shown in Fig. 6-37.

Convergence pressures or critical loci for binary systems are shown in Fig. 3-14. Qualitatively, in complex systems, increases in convergence pressure are caused by adding high-volatility substances like nitrogen or hydrogen to the system or by reducing the concentration of intermediate constituents. Higher convergence pressures cause the K's of the less volatile components to rise more slowly and the K's for the more volatile components to fall more slowly at pressures where they no longer follow ideal behavior.

Hadden (6-24) has presented a correlation of equilibrium constants based on convergence pressure and methods of approximating the convergence pressure (6-25). Winn (6-67) has presented a nomograph (Fig. 6-38) for obtaining equilibrium constants when the convergence pressure is 5,000 psi. A straight line between the pressure-temperature point on the grid and the component point intersects the vertical scale at the equilibrium constant. For other convergence pressures, Fig. 6-39 gives a grid pressure to be used in connection with Fig. 6-38 as follows:

1. Locate on the grid of Fig. 6-38 the system pressure-temperature point. Draw a straight line between this point and $K = 1.0$.
2. Locate the point of intersection of the line in (1) with the grid-pressure curve corresponding to the grid pressure of Fig. 6-39.
3. Using this point of intersection and the component point, by a straight line find the K.

For components boiling above 210°F (heptane C_7), the following equation will give the constants:

$$K_h = \frac{K_7}{(K_2/K_7)^b} \qquad (6\text{-}1)$$

where K_h = K value of petroleum fraction or high-boiling compound
K_2 = K value of ethane at the temperature, pressure, and convergence pressure of the system
K_7 = K value of n-heptane at the temperature, pressure, and convergence pressure of the system
b = volatility exponent from Fig. 6-40

For the convergence pressure, Winn takes the values from the binary loci shown in Fig. 6-41. For ternary and complex systems, Winn gives the following procedure:

Refer to Fig. 6-41 and, at the temperature of the system, read the pressures of the two critical-locus curves connecting the lightest component to the intermediate and heavy

Table 6-8. Equilibrium Vaporization Ratios for Reservoir Fluid at 154°F

Component	At 726 psia	At 1,111 psia	At 1,554 psia	At 2,043 psia
C_1	4.826	3.790	3.101	2.612
C_2	1.893	1.734	1.489	1.133
C_3	0.722	0.745	0.606	0.581
C_4	0.607	0.504	0.404	0.370
C_5	0.346	0.322	0.327	0.551
C_6+	0.011	0.014	0.021	0.032
H_2S	1.177	0.918	0.780	0.712
CO_2	2.775	2.291	1.941	1.696
N_2	4.256	3.732	3.196	2.936

SOURCE: Vagtborg (6-62).

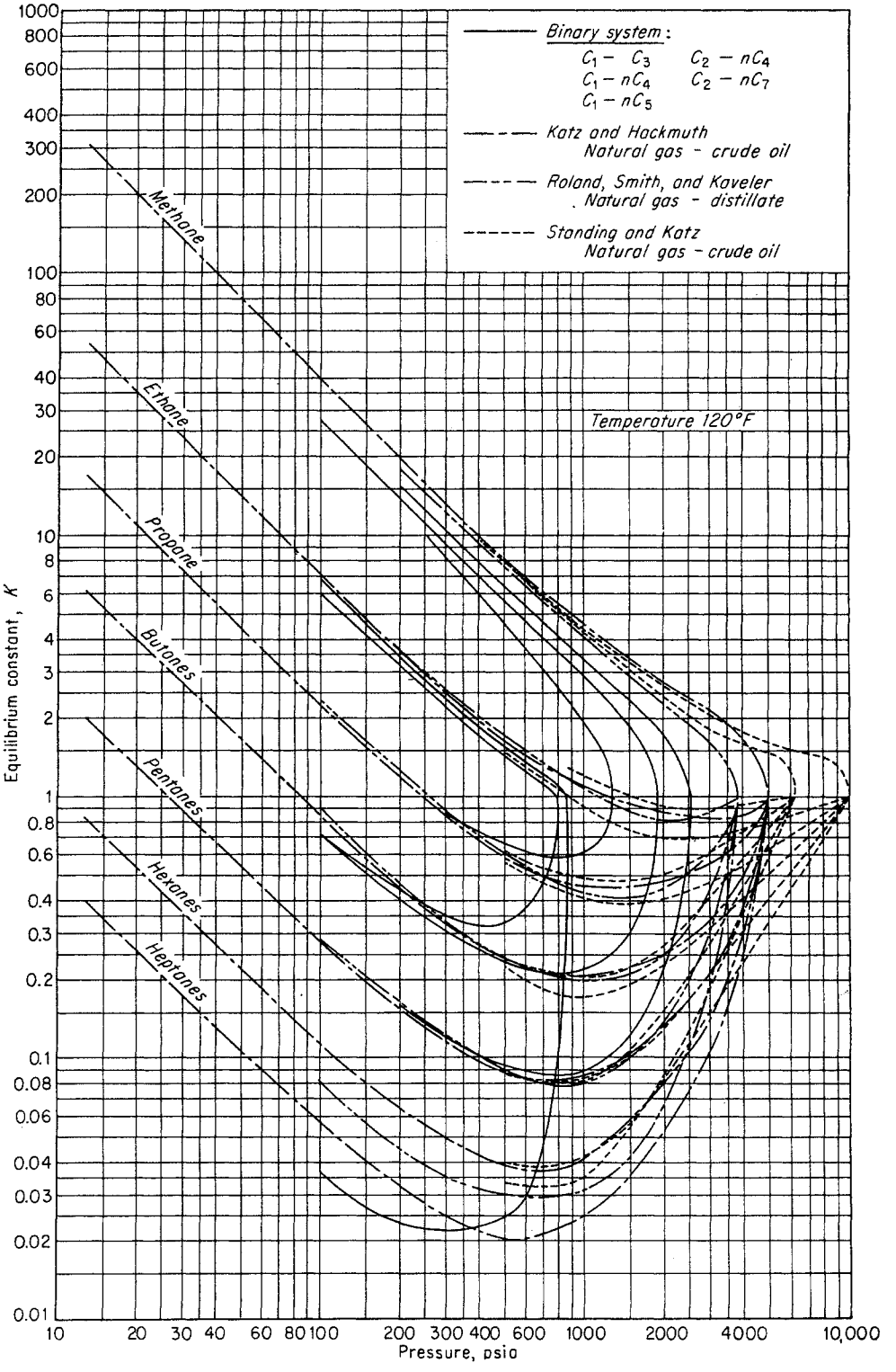

Fig. 6-36. Equilibrium-constant data at 120°F. ***(Hanson and Brown.)***

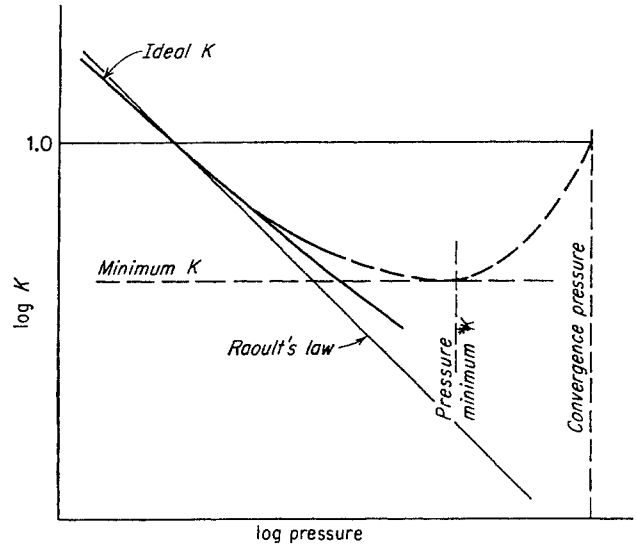

Fig. 6-37. Prediction of K's from convergence pressure.

components. If the system temperature is above the critical temperature of the intermediate component read the critical pressure of that component. Multiply these two pressures by the respective weight fractions of the intermediate and heavy components in the liquid phase, add the results, and divide by the sum of the weight fractions of the intermediate and heavy components in the liquid base.

Multicomponent Systems. Follow a procedure similar to that given for ternary systems, i.e.:

$$P_{c,v} = \frac{(P_{c,v})_2 W_2 + (P_{c,v})_3 W_3 + \cdots}{W_2 + W_3 + \cdots}$$

where $P_{c,v}$ = the convergence pressure of the system, psia
$(P_{c,v})_1$ = the pressure on the critical-locus curve of the lightest component and the component identified by subscript at the temperature of the system or, if the system temperature exceeds the critical temperature of the subscript component, the critical pressure of the subscript component
W_1 = the weight fraction in the liquid phase of the component identified by the subscript

Subscripts 1, 2, 3, . . . identify the components, 1 being the lightest, 2 the next heavier, etc.

Rzasa, Glass, and Opfell (6-51) presented a correlation of K's for complex oil-field systems in which the convergence pressure is predicted from temperature and from the product of molecular weight and specific gravity of heptanes-and-heavier fraction (Fig. 6-42). Equilibrium constants at the various convergence pressures at 260°F are given in Fig. 6-43.

The Kellogg fugacity charts (6-13) have found wide application for predicting equilibria of natural gas liquids. The equilibrium constant is found by Eq. (6-2).

$$K = \frac{f/x}{f/y} = \frac{y}{x} \qquad (6\text{-}2)$$

where f/x = fugacity of component divided by mole fraction in liquid
f/y = fugacity of component divided by mole fraction in vapor

The fugacity–mole fraction ratio is dependent upon the molal-average boiling point (MABP) of the phase and is given by a series of charts, one for each component at a given pressure. The use of the charts (Fig. 6-44 is an example for methane) requires a trial-and-error procedure, but it uses four variables to find K's: temperature, pressure, MABP of liquid, and MABP of vapor.

References for other correlations are given in Table 6-6.

Organick-Brown Correlation—NGAA Charts

Organick and Brown (6-37) have prepared a correlation of equilibrium constants in which the apparent convergence pressure is computed from the MABP of the vapor and the weight-average equivalent molecular weight of the liquid. Charts of K are available as a function of temperature, pressure, and convergence pressure.

The correlation that provides the convergence pressure consists of two charts, Figs. 6-45 and 6-46. For a given equilibrium at a temperature and pressure, the MABP of the vapor $(\text{MABP})_V$ and the weight-average molecular weight W of the liquid are determined. A convergence pressure or correlating pressure P_K is assumed and the ratio P/P_K is found. From Fig. 6-45, the exponent n in $(100/W)^n$ is found, using the $(\text{MABP})_V$ parameter. In Fig. 6-46, the ordinate $P_K(100/W)^n$ is determined for comparison with the value calculated from the assumed P_K and W. This trial-and-error process, coupled with the trial-and-error calculations of vapor-liquid equilibria, becomes involved and tedious. However, the method is completely rigorous for finding K's at any convergence pressure.

It is convenient to plot the equilibrium constant as a function of the normal boiling point of the constituent at constant temperature and pressure. In Figs. 6-47 to 6-49, this has been done at 200°F for several pressures at three convergence pressures, using the constants of Organick and Brown.

When treating constituents other than normal paraffin hydrocarbons, Organick and Brown recommend the use of an equivalent molecular weight (Fig. 6-50). This molecular weight is used throughout the vaporization calculations. Kirkbride and Bertetti give data on the effect of solvent for aromatic and naphthenic absorber oils (6-31).

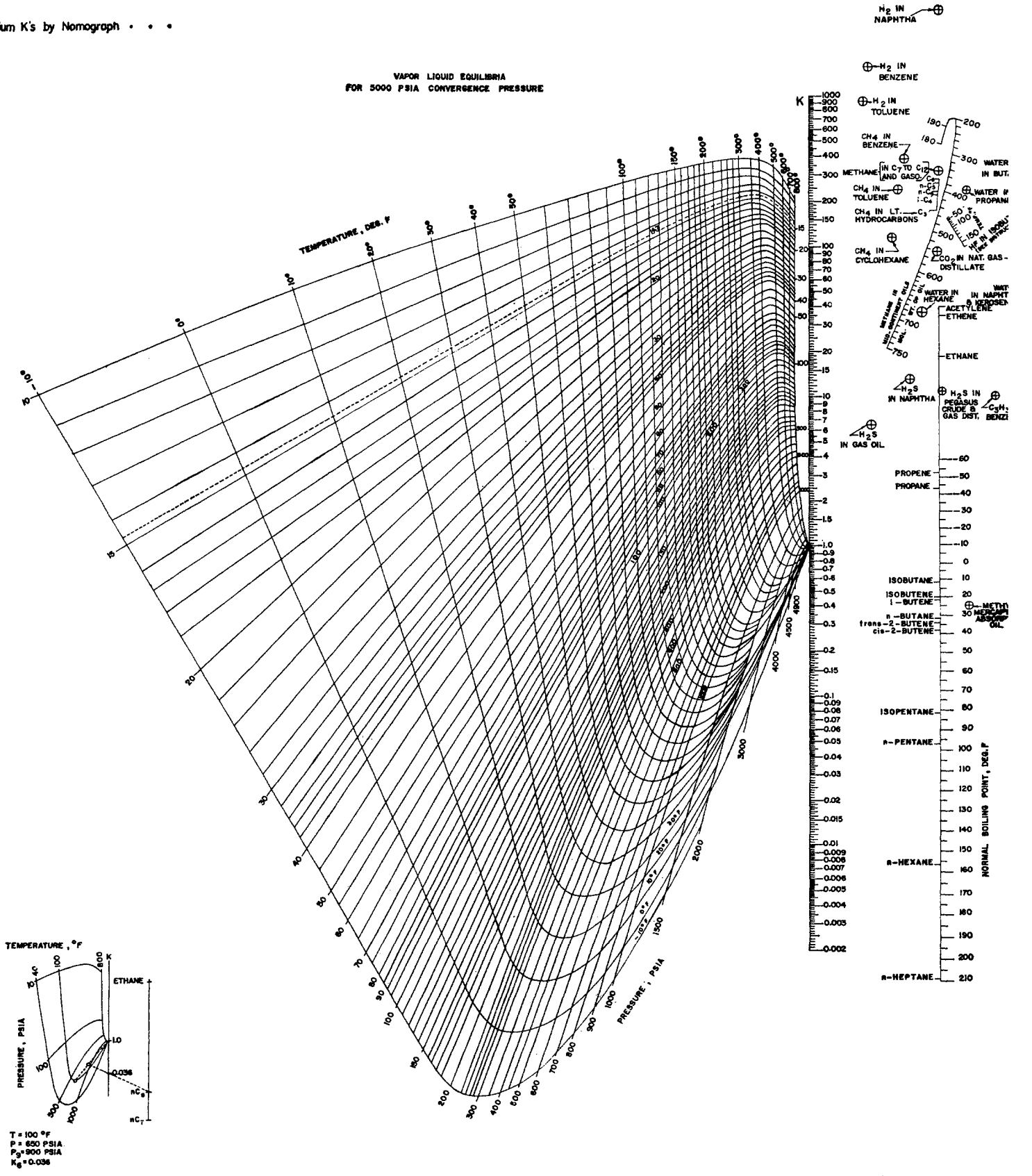

Fig. 6-38. Vapor-liquid equilibrium constants for 5,000 psia convergence pressure. (*Winn, 6-67. Courtesy AIChE.*)

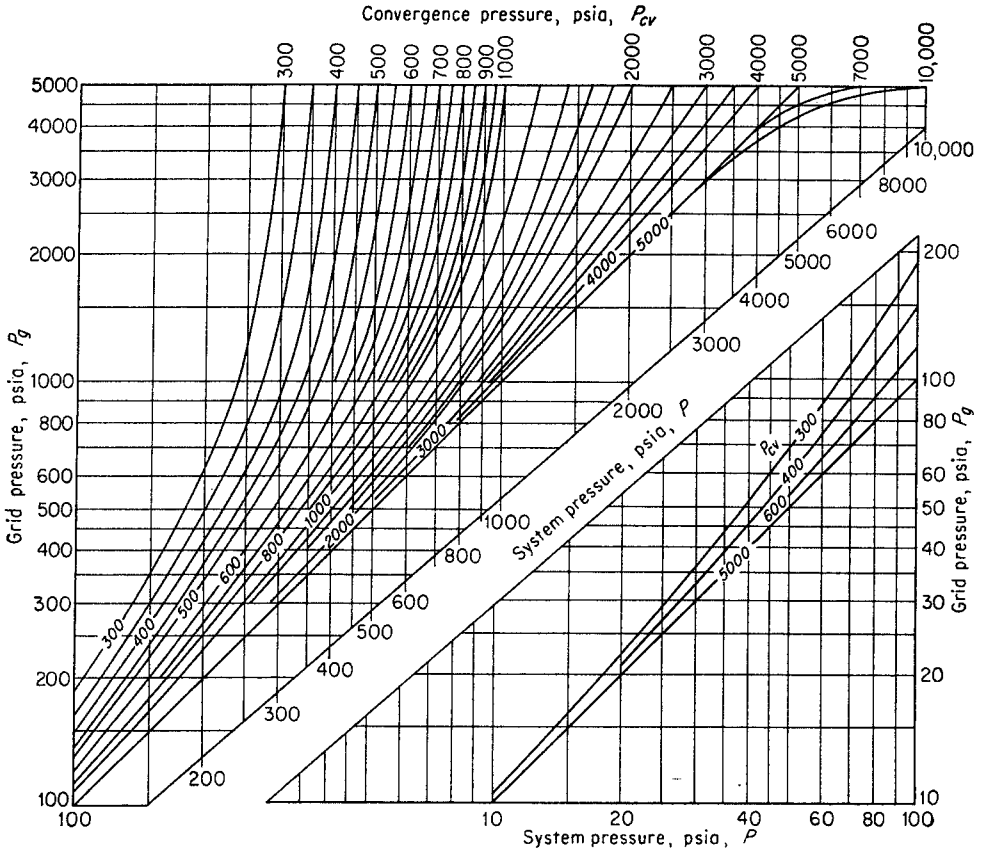

Fig. 6-39. Chart for determining grid pressure when convergence pressure is other than 5,000 psia. (*Winn, 6-67. Courtesy AIChE.*)

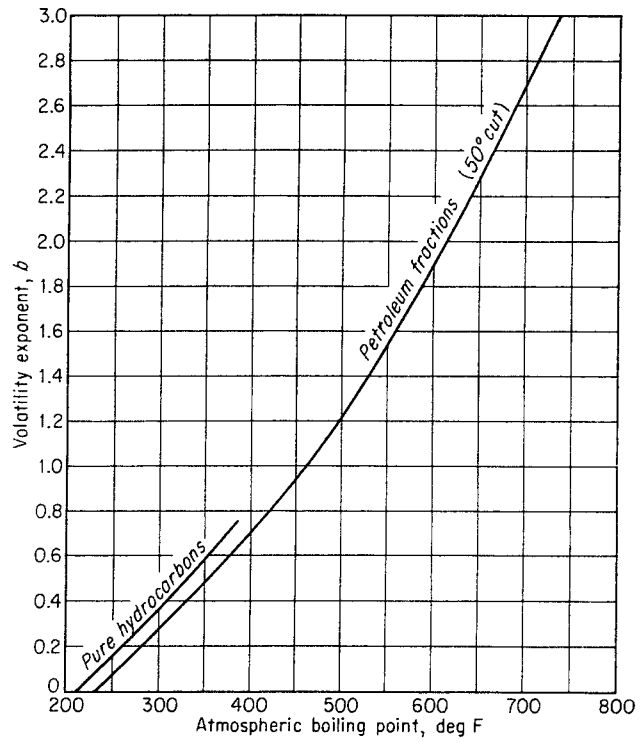

Fig. 6-40. Volatility exponent for Eq. (6-1). (*Winn, 6-67. Courtesy AIChE.*)

The calculation of the convergence pressure is to be avoided unless there is no other procedure. The NGAA has prepared a book of equilibrium-constant charts and curves of convergence pressure of typical mixtures (Figs. 6-51 to 6-53). Charts of K's for the convergence pressure of 2,000 psia for the several natural gas constituents are included as Figs. 6-54 to 6-66. Charts are available at convergence pressures of 600, 800, 1,000, 3,000, 4,000, 5,000, 10,000, and 20,000, as well as at 2,000 psia (5-1).

Approach to Convergence Pressure

"Convergence pressure" and "critical pressure" are synonymous for binary mixtures. Also, for a complex mixture, equilibrium constants at the critical temperature of the over-all mixture will converge at the critical pressure. The problems lie in handling complex mixtures that approach a dew point as the pressure is raised at constant temperature. The data of Roland (6-50; Fig. 6-67) show that the constants may not converge as the dew point is approached. This phenomenon may be related to the presence of asphalt in the oil. A dew point in the presence of asphalt becomes indefinite, for the plastic solid asphaltic phase remains. It follows that the term

"apparent convergence pressure" or "correlating pressure" is more appropriate than "convergence pressure" for complex systems of natural gas and crude oil.

High-boiling Constituents

In high-pressure reservoirs, high-boiling constituents are volatile at reservoir temperature. Hoffman, Crump, and Hocott (6-27) give limited data for these high-boiling constituents at reservoir conditions. Webber reported the volatility of absorber oils for some of the equilibria (6-64).

Poettmann and Mayland correlated the equilibrium constants for high-boiling constituents (6-46) based on a fugacity chart prepared by Kirkbride. Figure 6-68 gives the chart for components with a normal boiling point of 500°F. The components are listed separately since the character of the component affects the convergence pressure. The data of Hoffman, Crump, and Hocott (6-27) were combined with the charts of Poettmann and Mayland by students in the phase-behavior course at the University of Michigan in 1953 (Figs. 6-69 to 6-71).

CALCULATION OF VAPOR-LIQUID EQUILIBRIA

For a mixture of known composition, it is possible to compute from equilibrium constants the temperature and pressure of bubble points and of dew points as well as the distribution of the mixture into two phases at given conditions. The quantity and composition of each phase are found by a trial-and-error calculation (6-30, 3-27).

The Bubble Point is the condition at which the liquid is just ready to evolve a vapor phase or boil, and is expressed as the temperature and pressure at which the sum of the Kx terms equals unity.

$$\Sigma Kx = \Sigma y = 1 \qquad \text{at bubble point} \qquad (6\text{-}3)$$

where K = equilibrium constant
x = mole fraction in liquid
y = mole fraction in vapor

Table 6-9 is a bubble-point calculation for a natural gasoline. It can be seen that the Kx values are the mole fractions for the first bubble of vapor that forms at equilibrium before its formation changes the composition of the liquid.

The Dew Point is the condition at which the first droplet of liquid or dew is about to form, and it is computed as the temperature and pressure at which the sum of the y/K terms equals unity.

$$\Sigma y/K = \Sigma x = 1.0 \qquad \text{at dew point} \qquad (6\text{-}4)$$

The example calculation of the dew point (Table 6-10) shows the y/K terms to be the mole fractions of the initial liquid droplet.

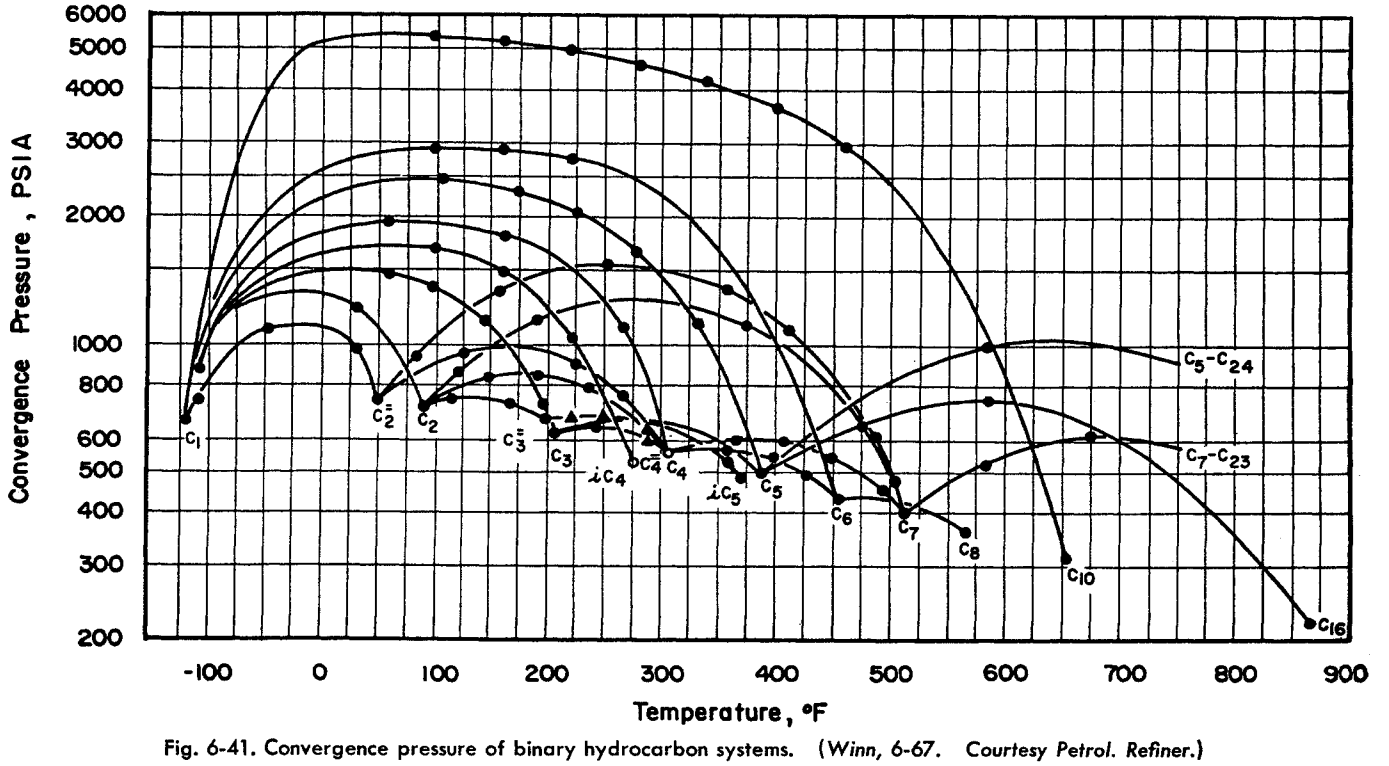

Fig. 6-41. Convergence pressure of binary hydrocarbon systems. (*Winn, 6-67. Courtesy Petrol. Refiner.*)

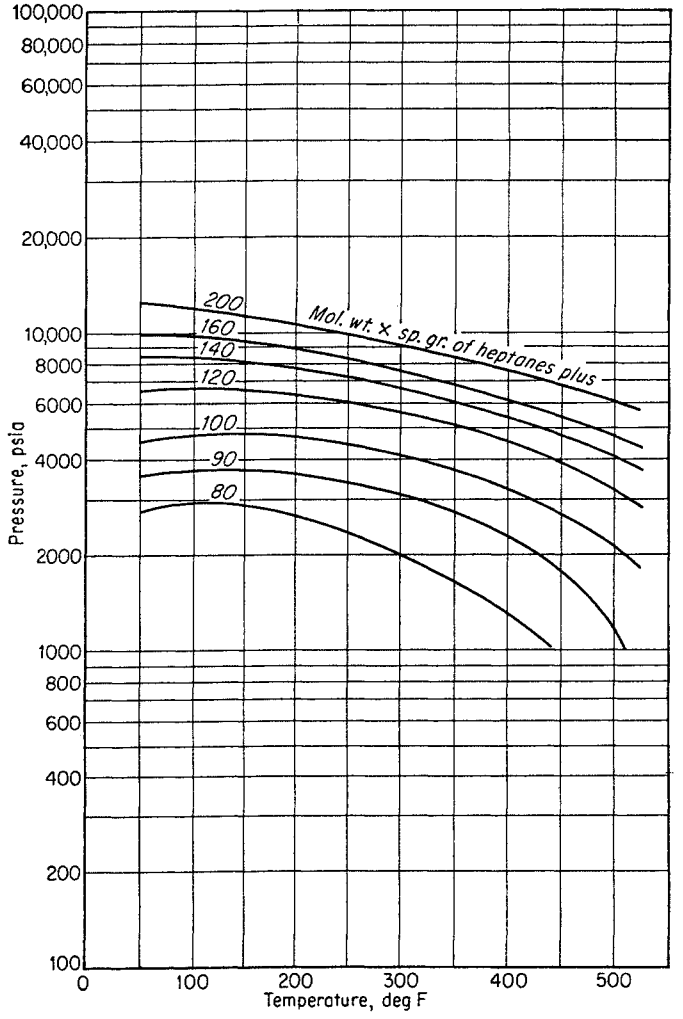

Fig. 6-42. Convergence pressure from temperature and properties of heptanes-and-heavier fraction. (*Rzasa, Glass, and Opfell,* 6-51. *Courtesy AIChE.*)

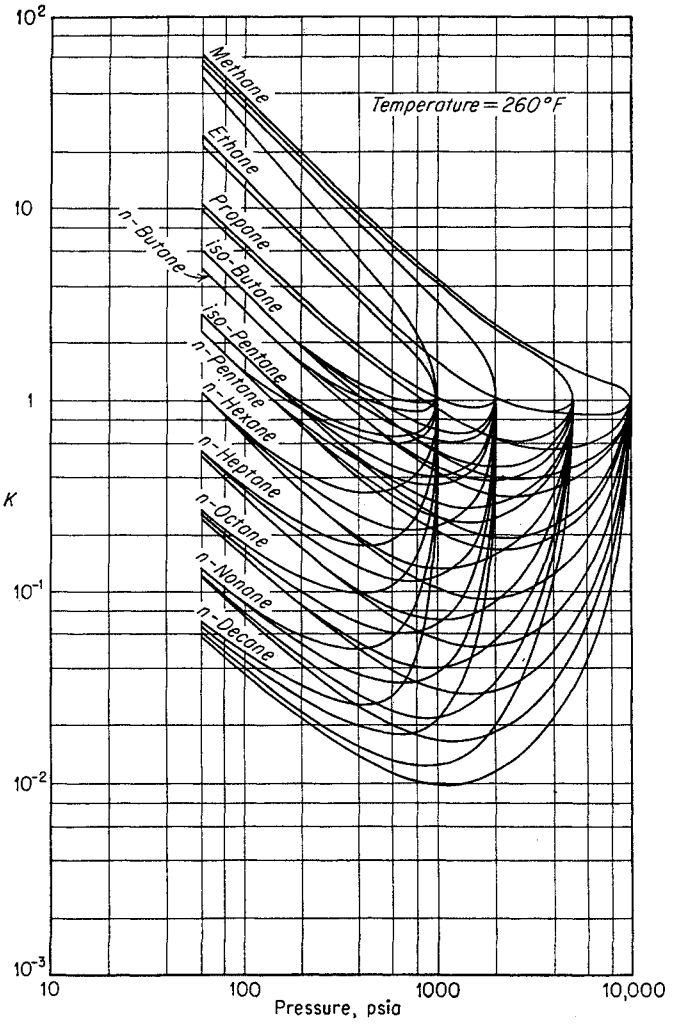

Fig. 6-43. Equilibrium constants for various convergence pressures at 260°F. (*Rzasa, Glass, and Opfell,* 6-51.)

Equilibrium or Flash-vaporization calculations may be made for a mixture that divides into two phases at a certain temperature and pressure (Fig. 6-72). At that temperature and pressure, all the vapor is in equilibrium with all the liquid. This may be a batch or a continuous-flow process. Equations will be derived for trial-and-error computation of the quantity of vapor and liquid formed and of the resultant compositions of the vapor and liquid.

Let F = moles of feed
V = moles of vapor
L = moles of equilibrium liquid
z = mole fraction of a constituent in the feed
x = mole fraction of a constituent in liquid
y = mole fraction of a constituent in vapor
i = any constituent

By equilibrium,

$$\frac{y_i}{x_i} = K_i \tag{6-5}$$

By material balance, over-all,

$$F = L + V \tag{6-6}$$

By material balance on a constituent,

$$zF = xL + yV \tag{6-7}$$

Substituting for x from Eq. (6-5),

$$zF = \frac{y}{K} L + yV \tag{6-8}$$

Multiplying numerator and denominator by K and dividing by V,

$$y = \frac{zF}{L/K + V} = \frac{F}{V} \frac{Kz}{K + L/V} \tag{6-9}$$

Table 6-9. Example of Computation of Bubble Point
Compute bubble-point pressure of the following mixture at 120°F (measured value 1,225 psia).

Constituent	Mole fraction x	At 120°F and 1400 psi		At 120°F and 1,200 psia	
		K	Kx	K	Kx
Methane	0.2208	3.4	0.7507	3.9	0.8611
Ethane	0.0739	0.97	0.0716	1.02	0.0755
Propane	0.0775	0.44	0.0341	0.44	0.0341
Isobutane	0.0203	0.255	0.0052	0.245	0.0050
n-Butane	0.0420	0.212	0.0089	0.208	0.0087
Isopentane	0.0170	0.126	0.0021	0.115	0.0020
n-Pentane	0.0270	0.108	0.0029	0.10	0.0027
Hexane	0.0477	0.056	0.0027	0.048	0.0023
Heptanes plus	0.4738	0.0051	0.0024	0.0042	0.0020
			0.8806		0.9934

By extrapolation, bubble point at 120°F $= 1{,}200 - \frac{0.0066}{0.1194} \times 200 = 1{,}188$ psia.

Table 6-10. Example of Computation of Dew Point
Compute dew-point temperature of fractionator overhead at 130 psia.

Constituent	Mole fraction y	At 130 psia and 130°F		At 130 psia and 150°F	
		K	y/K	K	y/K
Propane	0.025	1.85	0.0135	2.2	0.0114
Isobutane	0.904	0.88	1.2730	1.1	0.8218
n-Butane	0.071	0.65	0.109	0.83	0.0085
			1.3955		0.8417

By interpolation, dew point at 130 psia is 144°F.

or, letting $F = 1.0$,

$$y = \frac{Kz}{(K-1)V+1} \tag{6-10}$$

For all constituents

$$\sum y = 1 = \sum \frac{F}{V}\frac{Kz}{K + L/V} \tag{6-11}$$

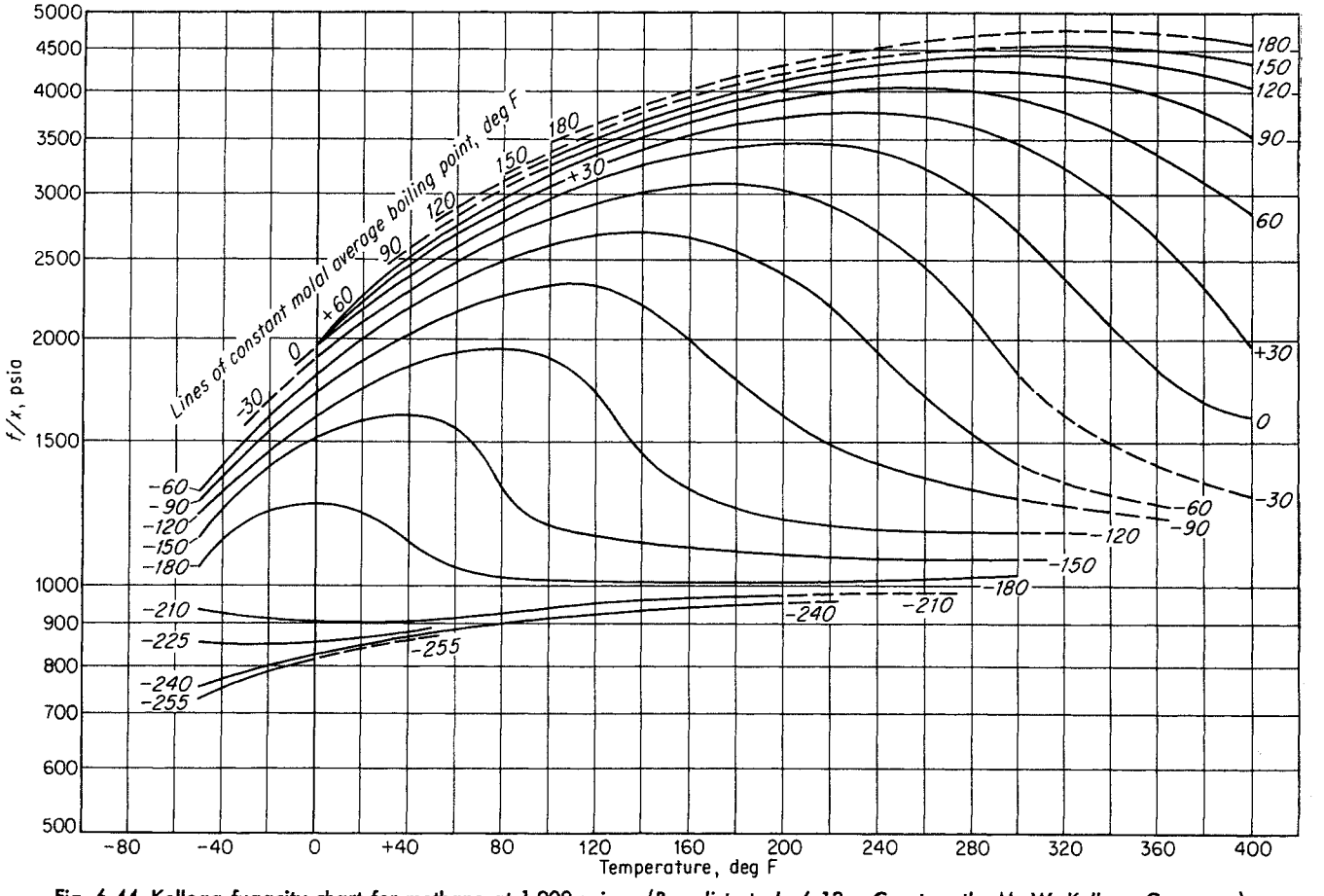

Fig. 6-44. Kellogg fugacity chart for methane at 1,000 psia. *(Benedict et al., 6-13. Courtesy the M. W. Kellogg Company.)*

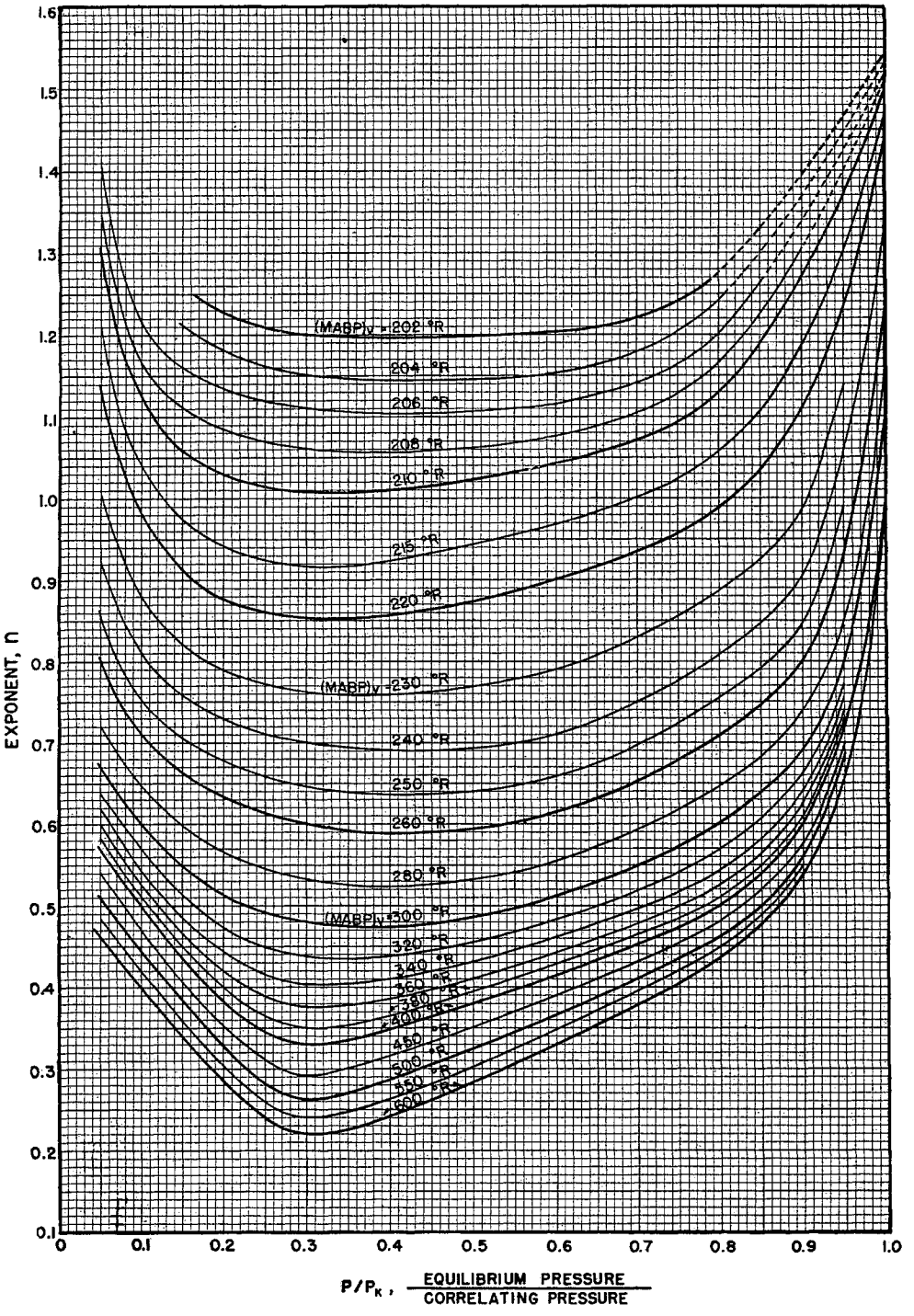

Fig. 6-45. Chart 1 for predicting convergence pressure. (*Organick and Brown, 6-37. Courtesy Chem. Eng. Progr.*)

Similarly, substituting for y in Eq. (6-7),

$$x = \frac{F}{V}\frac{z}{K + L/V} = \frac{z}{(K-1)V + 1} \qquad (6\text{-}12)$$

$$\sum x = 1 = \sum \frac{F}{V}\frac{z}{K + L/V} \qquad (6\text{-}13)$$

Letting $F = 1$ mole, by Eqs. (6-11) and (6-13),

$$V = \sum \frac{Kz}{K + L/V} = \sum \frac{z}{K + L/V} \quad (6\text{-}14)$$

Given a composition of feed and equilibrium constants for a selected temperature and pressure, a value of V is assumed and either the $\Sigma Kz/(K + L/V)$ or the $\Sigma z/(K + L/V)$ terms are calculated to find whether the correct value was assumed. A plot of V assumed versus V calculated is given in Fig. 6-73. It should be noted that the curves approach the origin even though the correct solution is somewhere along the 45° line. Table 6-11 gives an example calculation.

Alternative methods of combining Eqs. (6-5) to (6-7) give alternative methods of handling the trial-and-error solution. By subtracting Eq. (6-12) from Eq. (6-11) one obtains

$$\sum y - \sum x = 0 = \sum \frac{z(K - 1)}{V(K - 1) + 1} \quad (6\text{-}15)$$

For the correct value of V, the right-hand member of Eq. (6-15) equals 0; for other values of V, the summation takes on values of the type shown in Fig. 6-74.

A method of choosing successive values of V after the first trial, known as Newton's method, involves the slope of the curve at the V initially assumed (Fig. 6-74). The slope of the curve at V is obtained by differentiating the expression with respect to V.

$$\frac{\partial \left[\sum \frac{z(K - 1)}{V(K - 1) + 1}\right]}{\partial V} = \sum \frac{z(K - 1)^2}{[V(K - 1) + 1]^2} \quad (6\text{-}16)$$

The first trial value of $z(K - 1)/[V(K - 1) + 1]$ and the slope of the curve permit computation of the ΔV, which is applied to the first trial value to obtain the second trial value.

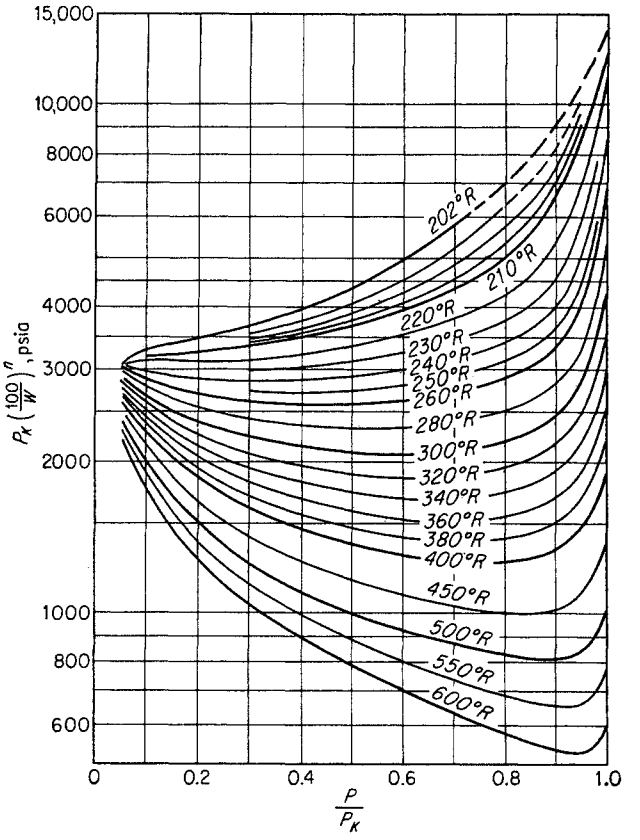

Fig. 6-46. Chart 2 for predicting convergence pressure. (*Organick and Brown, 6-37. Courtesy Chem. Eng. Progr.*)

Table 6-11. Example of Equilibrium Vaporization Problem

Compute the quantity and composition of liquid and vapor when the following mixture is flashed at 1,600 psia and 120°F.

Constituent	Mole fraction of mixture z	At 1,600 psia and 120°F K	Assume V = 0.9009		Assume V = 0.885		Mole fraction	
			$K + 0.11$	$z/(K + L/V)$	$K + 0.13$	$z/(K + L/V)$	Liquid	Vapor
Carbon dioxide	0.0046	1.65	1.76	0.0026	1.78	0.0026	0.0029	0.0048
Methane	0.8345	3.09	3.20	0.2603	3.22	0.2595	0.2943	0.9050
Ethane	0.0381	0.72	0.83	0.0459	0.85	0.0449	0.0510	0.0360
Propane	0.0163	0.39	0.50	0.0326	0.52	0.0314	0.0356	0.0137
Isobutane	0.0050	0.21	0.32	0.0156	0.34	0.0147	0.0167	0.0035
n-Butane	0.0074	0.175	0.285	0.0422	0.305	0.0242	0.0275	0.0048
Pentanes	0.0287	0.093	0.203	0.1413	0.223	0.1288	0.1463	0.0134
Hexanes	0.0220	0.065	0.175	0.1258	0.195	0.1130	0.1283	0.0083
Heptanes plus	0.0434	0.036	0.146	0.2970	0.166	0.2620	0.2974	0.0105
Total	1.0000	.....	.....	0.9633	.....	0.8811	1.0000	1.0000

By extrapolation, V = 0.887 mole vapor, L = 0.113 mole liquid.
Molecular weight C_7+ = 196; specific gravity C_7+ = 0.850.

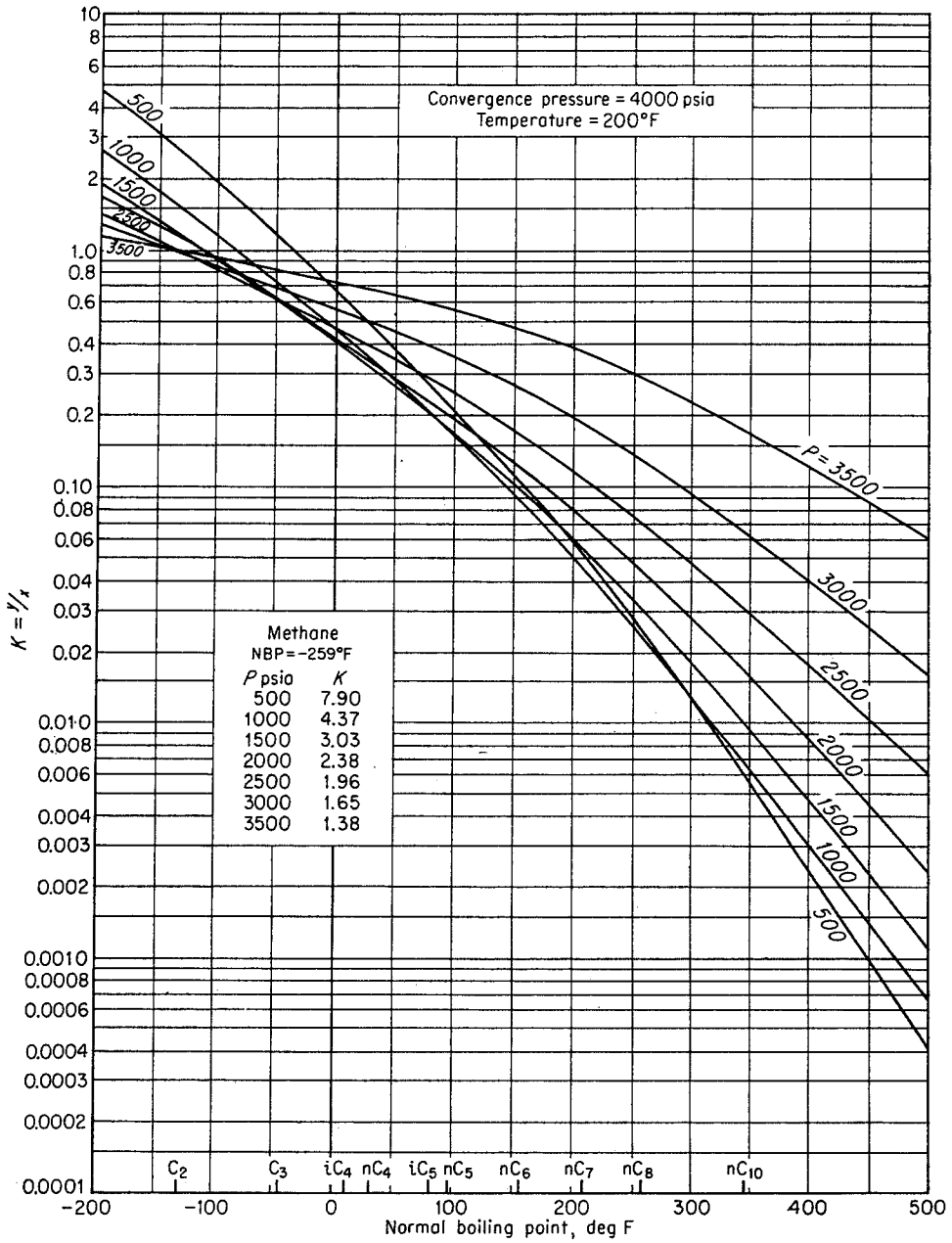

Fig. 6-47. Equilibrium constants as a function of normal boiling point of constituent at 4,000 psia convergence pressure.

$$V_2 = V_1 + \frac{\sum \frac{z(K-1)}{V(K-1)+1}}{\sum \frac{z(K-1)^2}{[V(K-1)+1]^2}} \qquad (6\text{-}17)$$

The shape of the curve may deviate from a straight line between the first and second points (Fig. 6-74) and, for the required accuracy, a third trial may be necessary. The value of V_3 is obtained from V_2 as V_2 was obtained from V_1. Table 6-12 is an example problem.

Two streams may be mixed before the combined stream is passed into a vapor-liquid separator. By retaining the compositions of individual streams throughout the calculations, it is possible to determine the amount of each constituent in the liquid and in the vapor that came from each of the original streams.

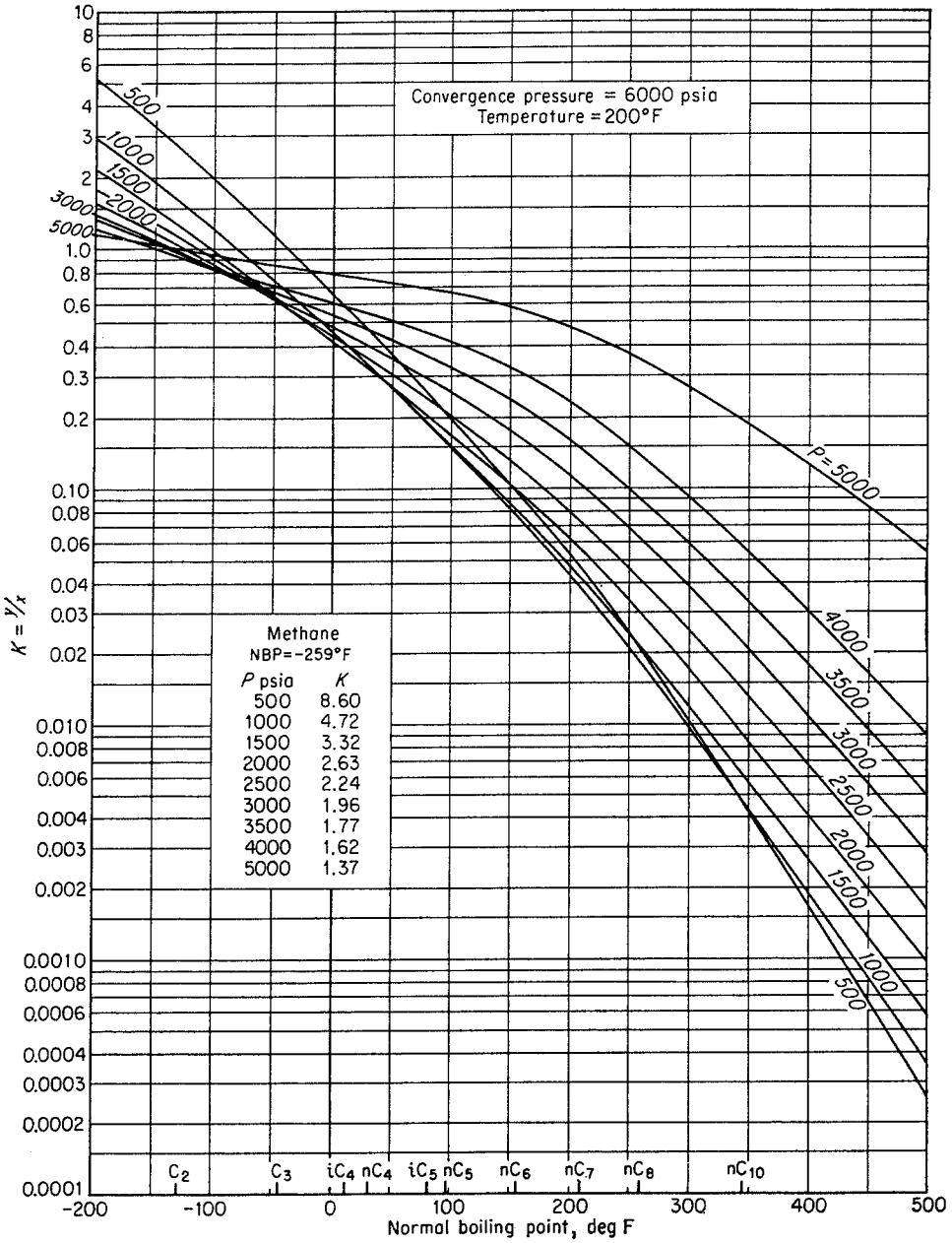

Fig. 6-48. Equilibrium constants as a function of normal boiling point of constituent at 6,000 psia convergence pressure.

DIFFERENTIAL VAPORIZATION

Differential vaporization differs from equilibrium flash vaporization in that the vapor is removed from contact with the liquid as fast as it is formed. The equilibrium vapor formed in this differential process is a result of a change in temperature and/or pressure. Each successive increment dW of vapor formed changes the composition of the liquid, which in turn requires a change in equilibrium pressure and/or temperature if the next increment is to form.

Differential-vaporization calculations are based on a statement of material balance, in which the quantity of a constituent in an increment of vapor is equated with the decrease in the quantity of that constituent in the liquid, according to Eq. (6-18).

Table 6-12. Example of Equilibrium-Vaporization Cal-

Component	Mole fraction z	K at 1,600 psia and 120°F	$K-1$	$z(K-1)$	$z(K-1)^2$	Assume $V = 0.80$				
						$V(K-1)$	$V(K-1)+1$	$\frac{z(K-1)}{V(K-1)+1}$	$[V(K-1)+1]^2$	$\frac{z(K-1)^2}{[V(K-1)+1]^2}$
Carbon dioxide..	0.0046	1.65	0.65	0.00299	0.00194	0.52000	1.52000	0.00197	2.3104	0.00084
Methane.....	0.8345	3.09	2.09	1.74411	3.64518	1.67200	2.67200	0.65273	7.13958	0.51055
Ethane.....	0.0381	0.72	−0.28	−0.01668	0.00467	−0.22400	0.77600	−0.02149	0.60218	0.00776
Propane.....	0.0163	0.39	−0.61	−0.00991	0.00605	−0.48800	0.51200	−0.01935	0.26214	0.02308
Isobutane.....	0.0050	0.21	−0.78	−0.00390	0.00304	−0.62400	0.37600	−0.01037	0.14138	0.02150
n-Butane.....	0.0074	0.175	−0.825	−0.00611	0.00504	−0.66000	0.34000	−0.01797	0.11560	0.04360
Pentanes.....	0.0287	0.093	−0.907	−0.02603	0.02361	−0.72560	0.27440	−0.09486	0.07530	0.31354
Hexanes.....	0.0220	0.065	−0.935	−0.02057	0.01923	−0.74800	0.25200	−0.08163	0.06350	0.30283
Heptanes+.....	0.0434	0.036	−0.964	−0.04184	0.04033	−0.77120	0.22880	−0.18287	0.05235	0.77039
								0.22616		1.99409

$$V_2 = 0.8 + \frac{0.22616}{1.99409} = 0.8 + 0.1134 = 0.913$$

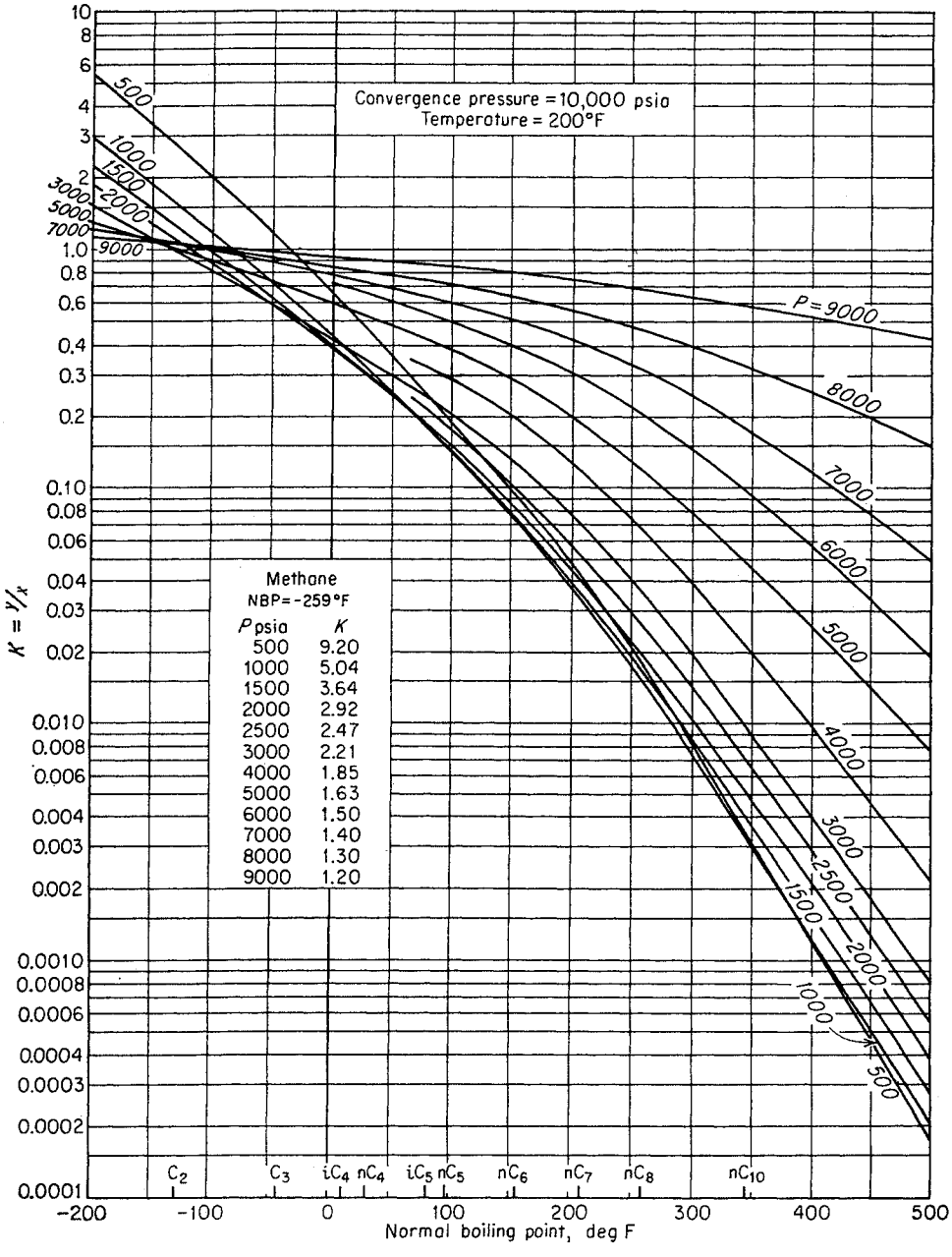

Fig. 6-49. Equilibrium constants as a function of normal boiling point of constituent at 10,000 psia convergence pressure.

culation with Successive Trials by Newton's Method

Assume $V = 0.913$					Assume $V = 0.8886$				
$V_2(K-1)$	$V_2(K-1)+1$	$\frac{z(K-1)}{V(K-1)+1}$	$[V(K-1)+1]^2$	$\frac{z(K-1)^2}{[V(K-1)+1]^2}$	$V_3(K-1)$	$V_3(K-1)+1$	$\frac{z(K-1)}{V(K-1)+1}$	$[V(K-1)+1]^2$	$\frac{z(K-1)^2}{[V(K-1)+1]^2}$
0.59345	1.59345	0.00188	2.53908	0.00076	0.57759	1.57759	0.00189	2.48879	0.00078
1.90817	2.90817	0.59972	8.45745	0.43100	1.85717	2.85717	0.61043	8.16342	0.44652
−0.25564	0.74436	−0.02241	0.55407	0.00843	−0.24881	0.75119	−0.02220	0.56428	0.00828
−0.55693	0.44307	−0.02237	0.19631	0.03082	−0.54205	0.45795	−0.02164	0.209718	0.02885
−0.71214	0.28786	−0.01355	0.08286	0.03669	−0.69311	0.30689	−0.01271	0.094181	0.03228
−0.75323	0.24677	−0.02476	0.06089	0.00828	−0.73310	0.26690	−0.02289	0.07123	0.07076
−0.82809	0.17191	−0.15142	0.02955	0.79898	−0.80596	0.19404	−0.13415	0.03765	0.62709
−0.85366	0.14634	−0.14056	0.02142	0.89775	−0.83084	0.16916	−0.12160	0.02862	0.67190
−0.88013	0.11987	−0.34904	0.01437	2.80654	−0.85661	0.14339	−0.29179	0.02056	1.96157
		−0.12251		5.01925			−0.01466		3.84803

$$V_3 = 0.913 - \frac{0.12251}{5.01925}$$
$$= 0.913 - 0.0244$$
$$= 0.8886$$

$$V_4 = 0.8886 - \frac{0.01466}{3.84803}$$
$$= 0.8886 - 0.00381$$
$$= 0.88479$$

Component	Assume $V = 0.8848$				
	$V_4(K-1)$	$V(K-1)+1$	$\frac{z(K-1)}{V(K-1)+1}$	Mole fraction	
				x	y
Carbon dioxide	0.57511	1.57511	0.00189	0.00292	0.00482
Methane	1.84921	2.84921	0.61213	0.29289	0.90503
Ethane	−0.24774	0.75226	−0.00217	0.05065	0.03647
Propane	−0.53972	0.46028	−0.02153	0.03541	0.01381
Isobutane	−0.69014	0.31986	−0.01219	0.01563	0.00328
n-Butane	−0.72995	0.27005	−0.02263	0.02740	0.00479
Pentanes	−0.80250	0.19750	−0.13179	0.14532	0.01351
Hexanes	−0.82728	0.17272	−0.11909	0.12737	0.00828
Heptanes+	−0.85294	0 14706	−0.28451	0.29512	0.01062
			0.00011		

$\therefore V = 0.8848$

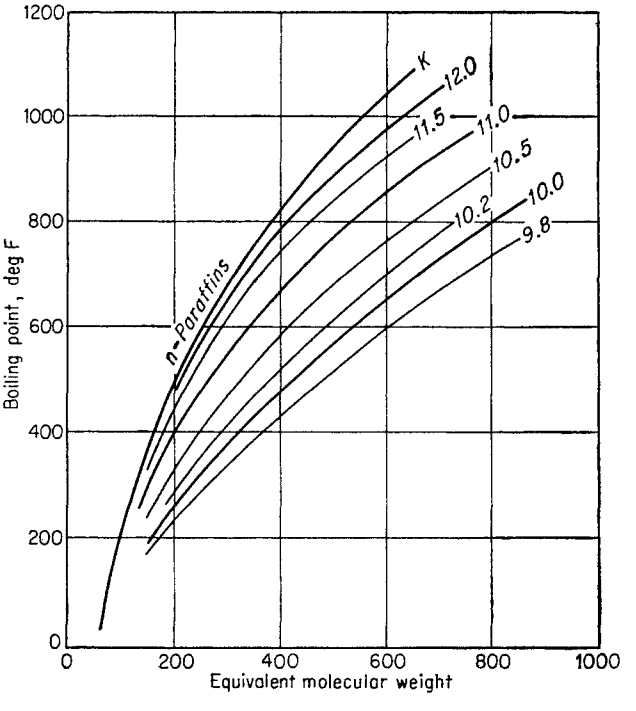

Fig. 6-50. Equivalent molecular weights of hydrocarbons. (*Organick and Brown, 6-37. Courtesy AIChE.*)

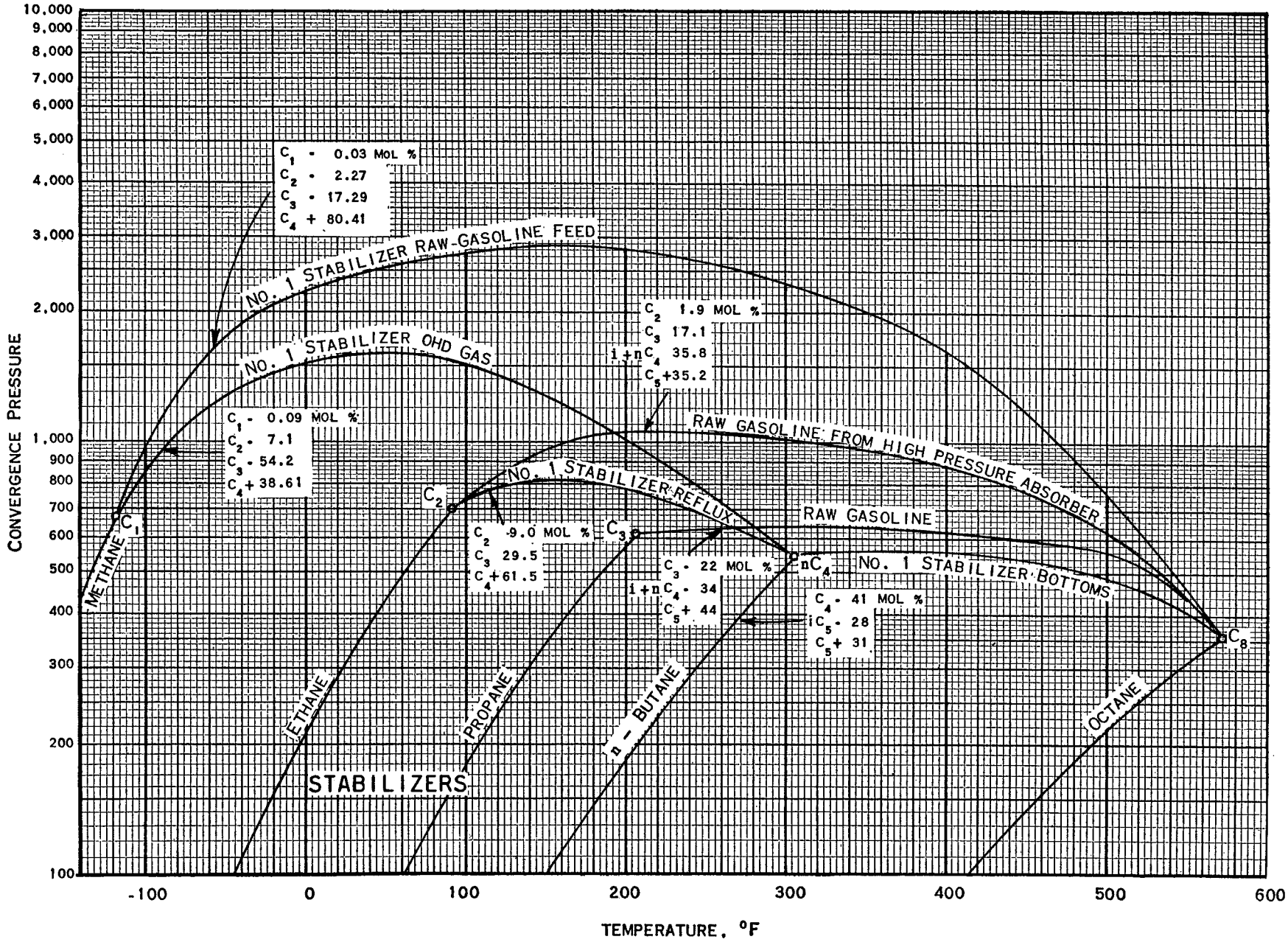

Fig. 6-51. Convergence pressures for typical stabilizer mixtures. (6-40. *Courtesy NGAA.*)

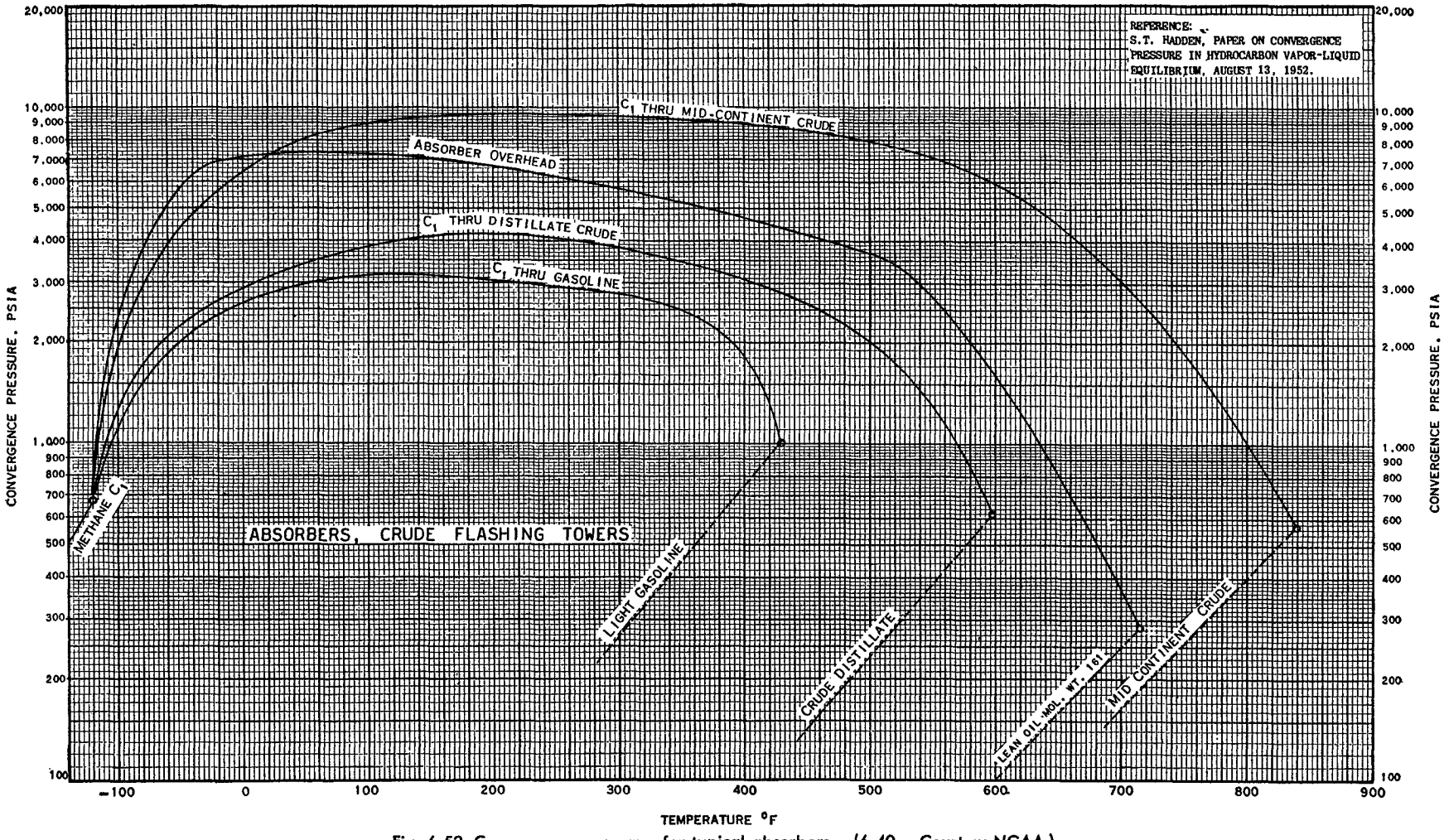

Fig. 6-52. Convergence pressures for typical absorbers. (6-40. *Courtesy NGAA.*)

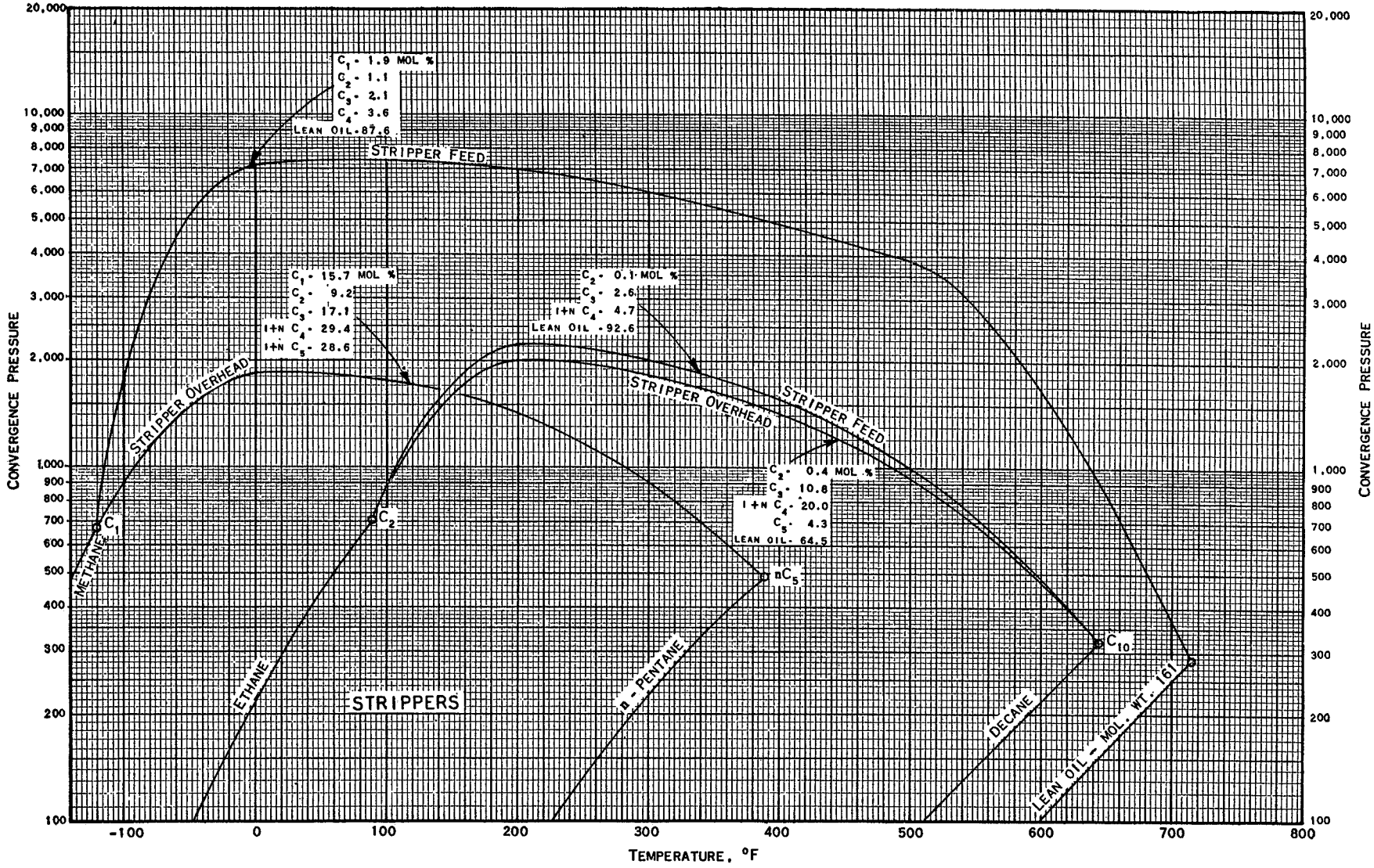

Fig. 6-53 Convergence pressures for typical strippers. (6-40. *Courtesy NGAA.*)

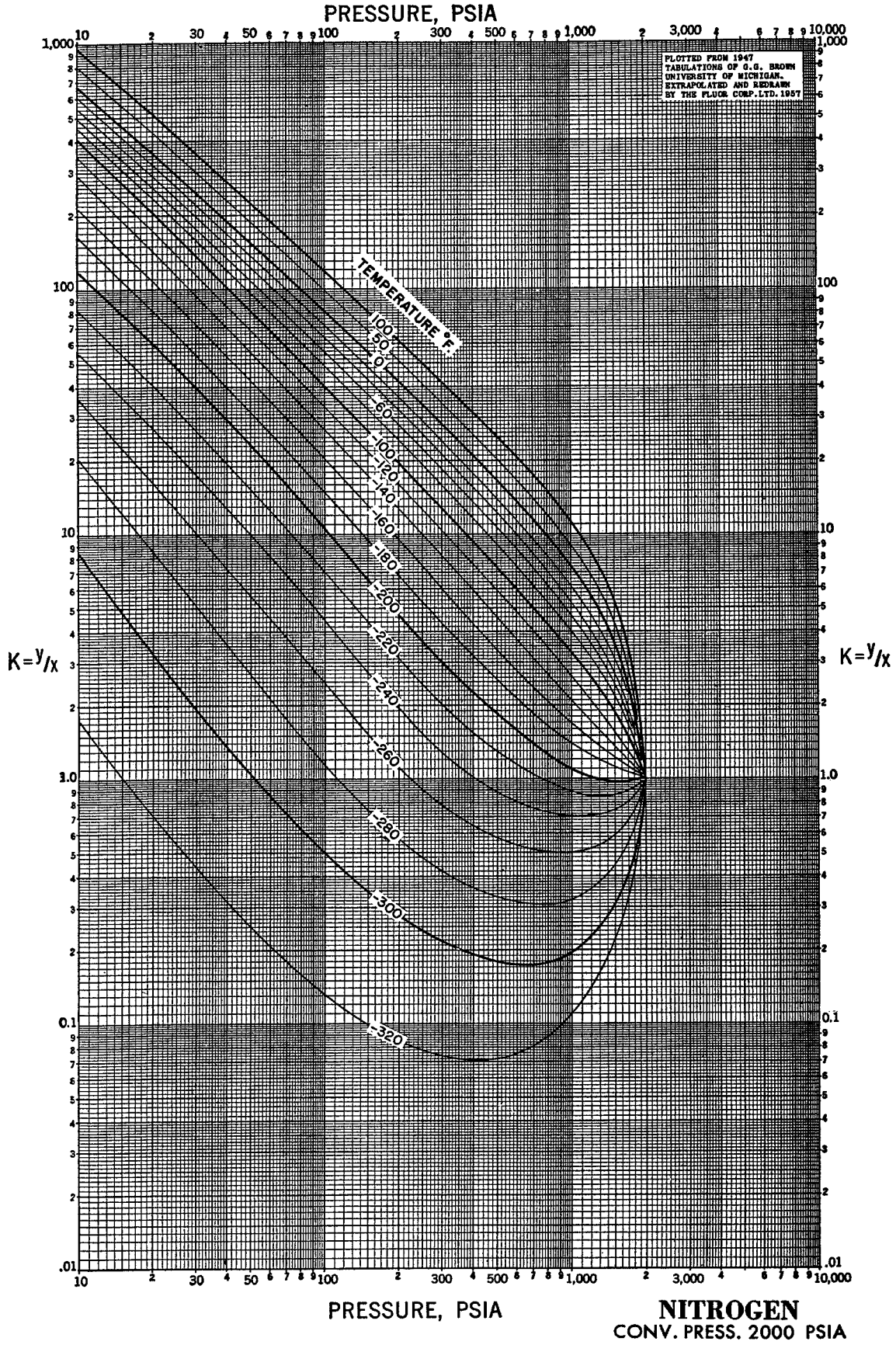

Fig. 6-54. Equilibrium constants for natural gas constituents at 2,000 psia convergence pressure. (6-40. *Courtesy NGAA.*)

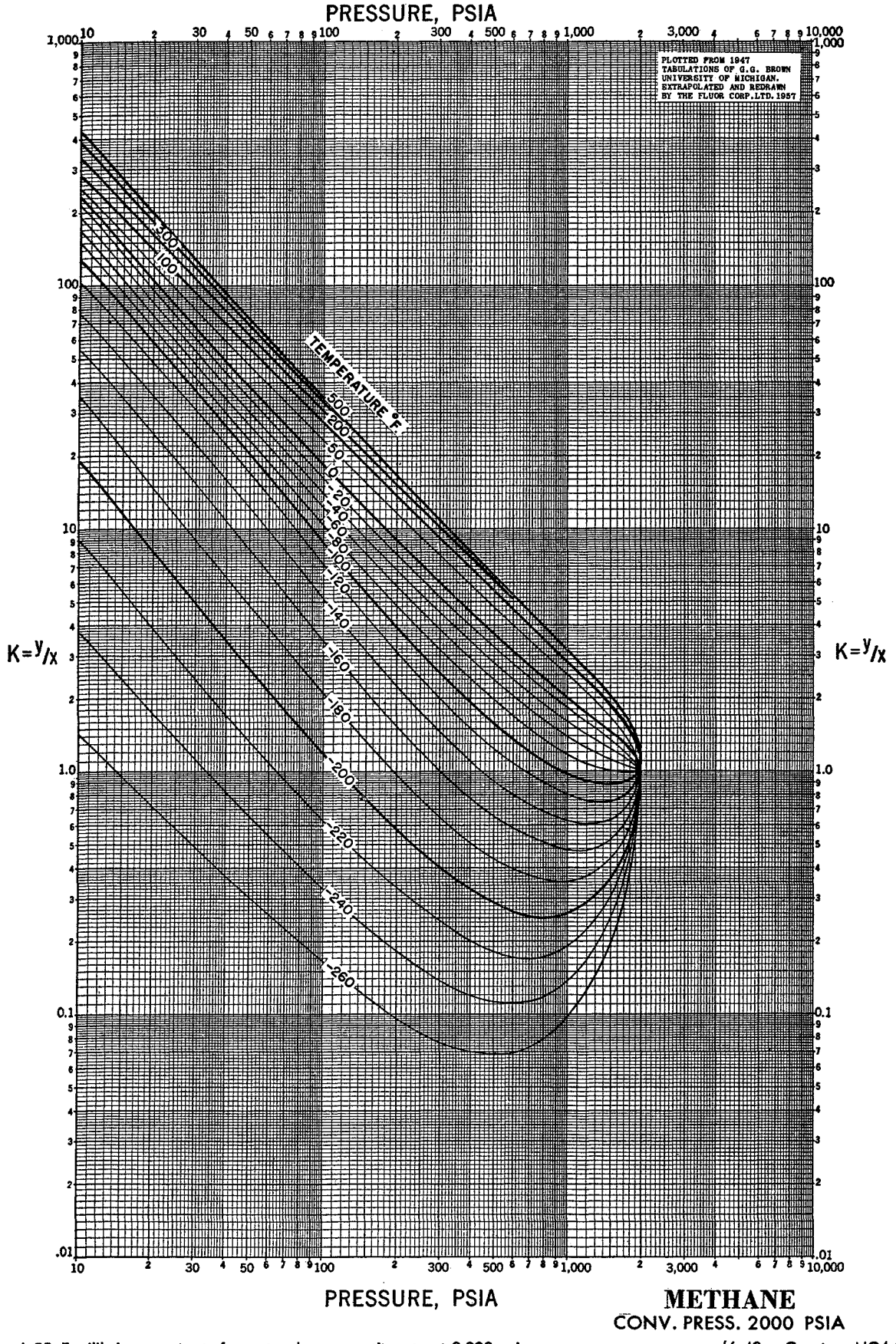

Fig. 6-55. Equilibrium constants for natural gas constituents at 2,000 psia convergence pressure. (6-40. *Courtesy NGAA.*)

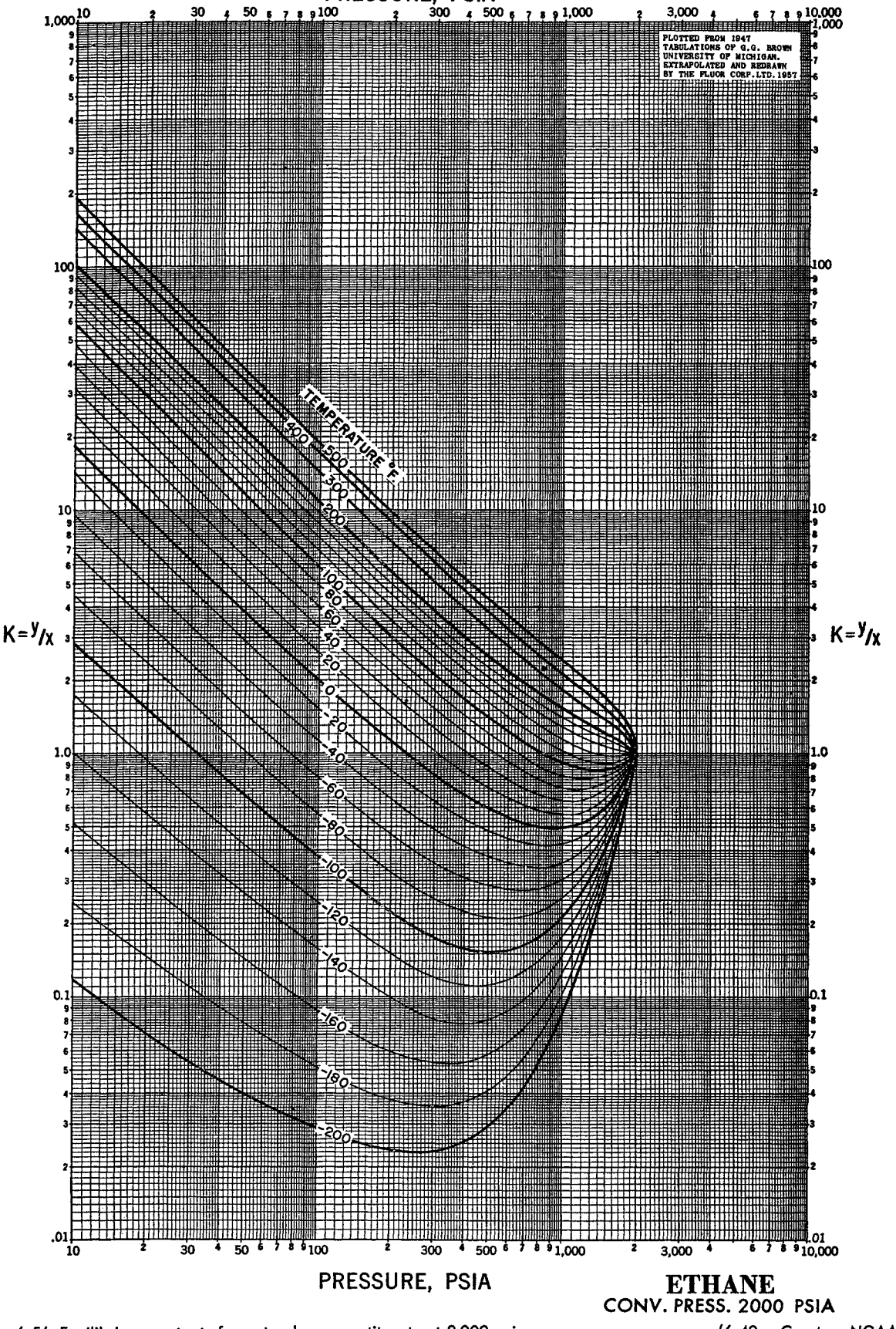

Fig. 6-56. Equilibrium constants for natural gas constituents at 2,000 psia convergence pressure. (6-40. *Courtesy NGAA.*)

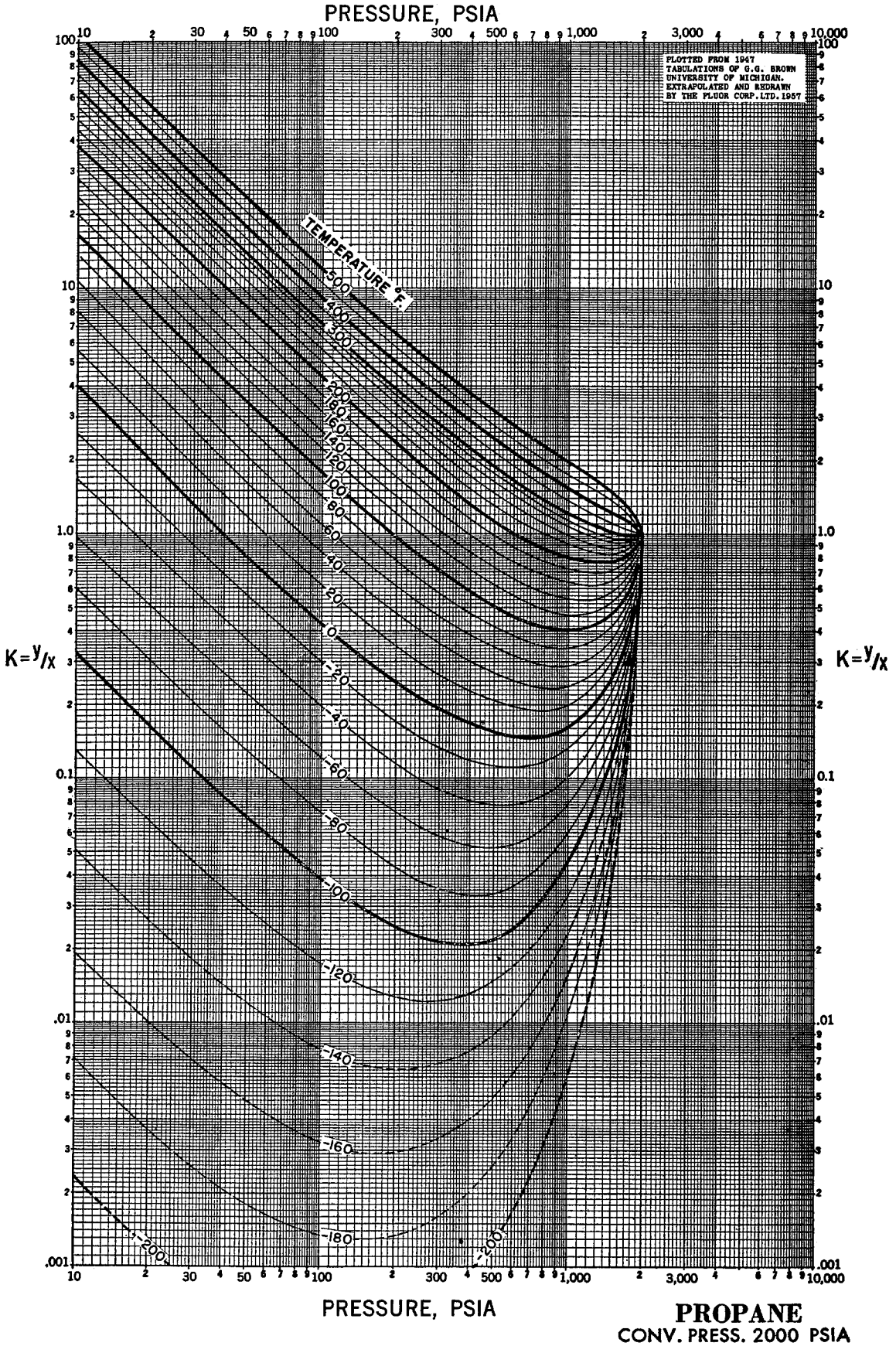

Fig. 6-57. Equilibrium constants for natural gas constituents at 2,000 psia convergence pressure. (6-40. *Courtesy NGAA.*)

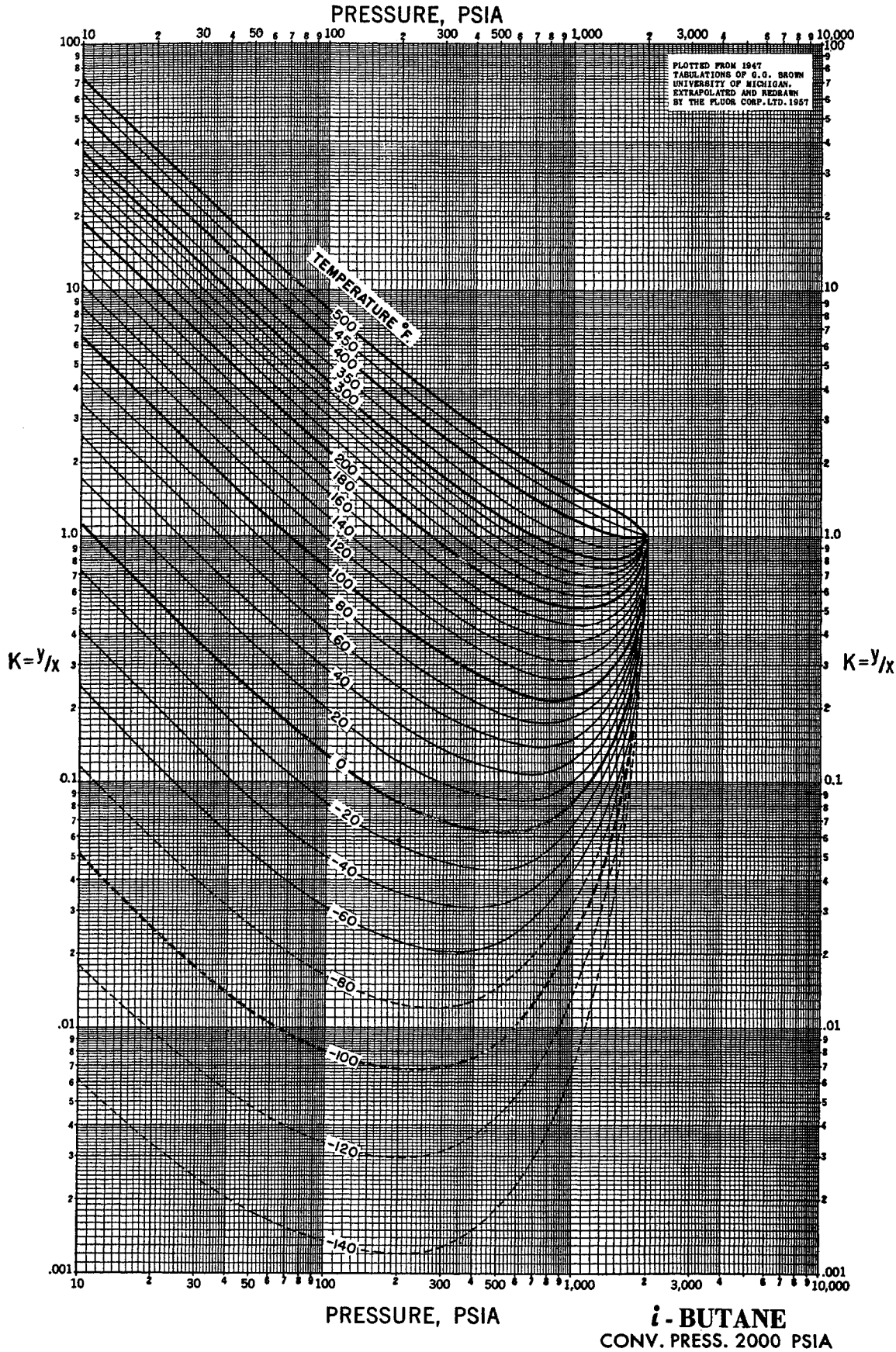

Fig. 6-58. Equilibrium constants for natural gas constituents at 2,000 psia convergence pressure. (6-40. *Courtesy NGAA.*)

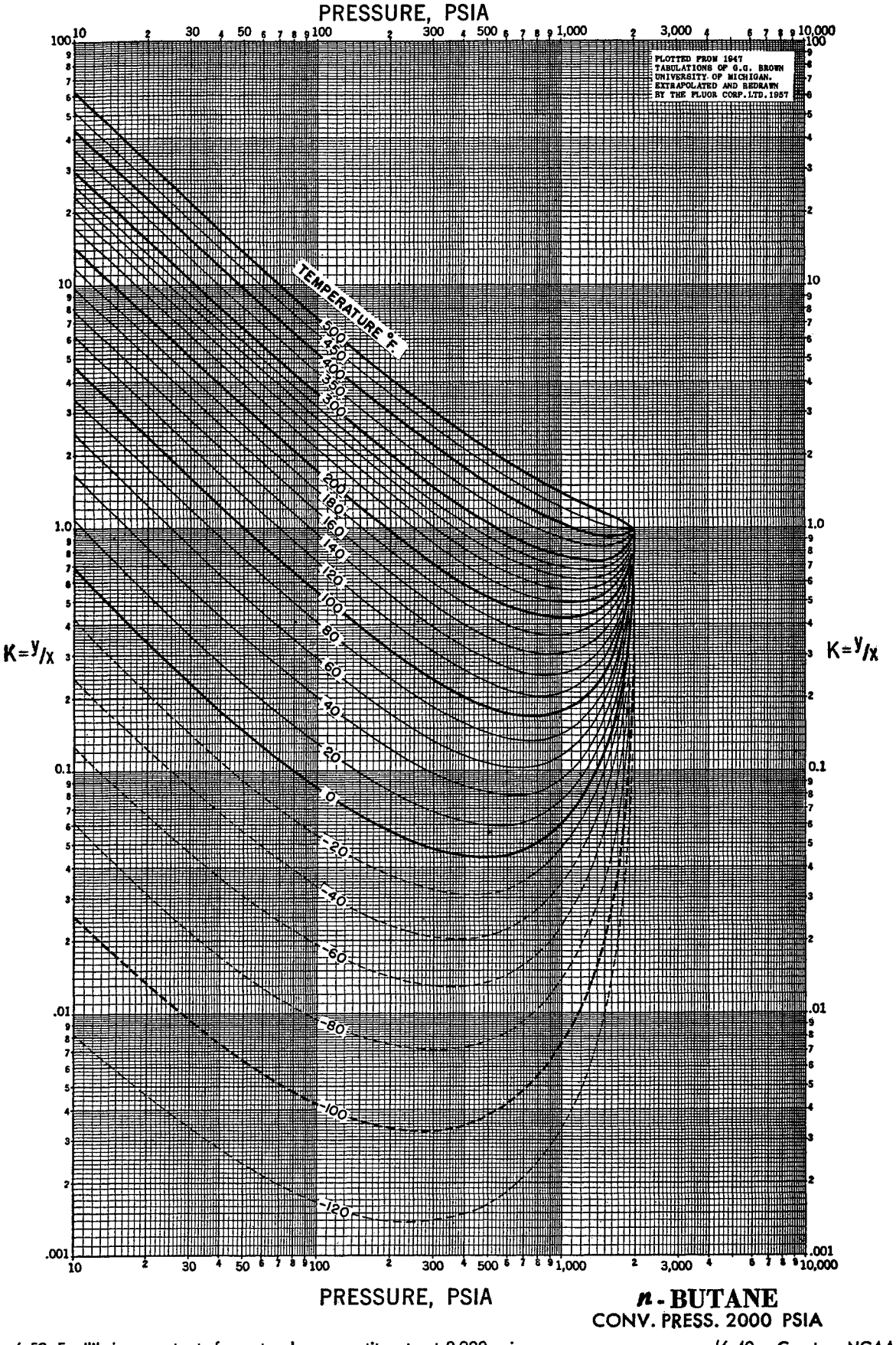

Fig. 6-59. Equilibrium constants for natural gas constituents at 2,000 psia convergence pressure. (6-40. *Courtesy NGAA.*)

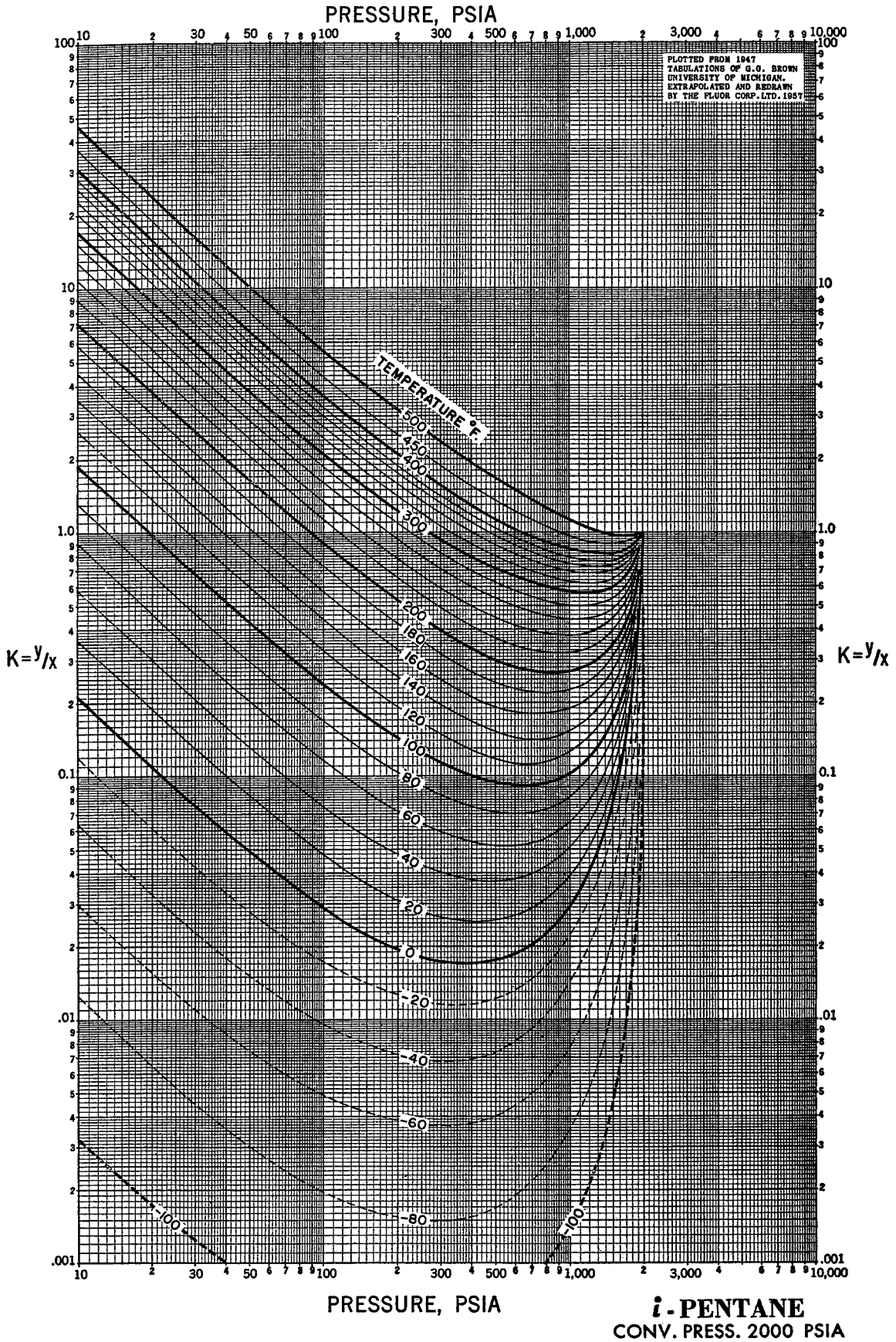

Fig. 6-60. Equilibrium constants for natural gas constituents at 2,000 psia convergence pressure. (6-40. *Courtesy NGAA.*)

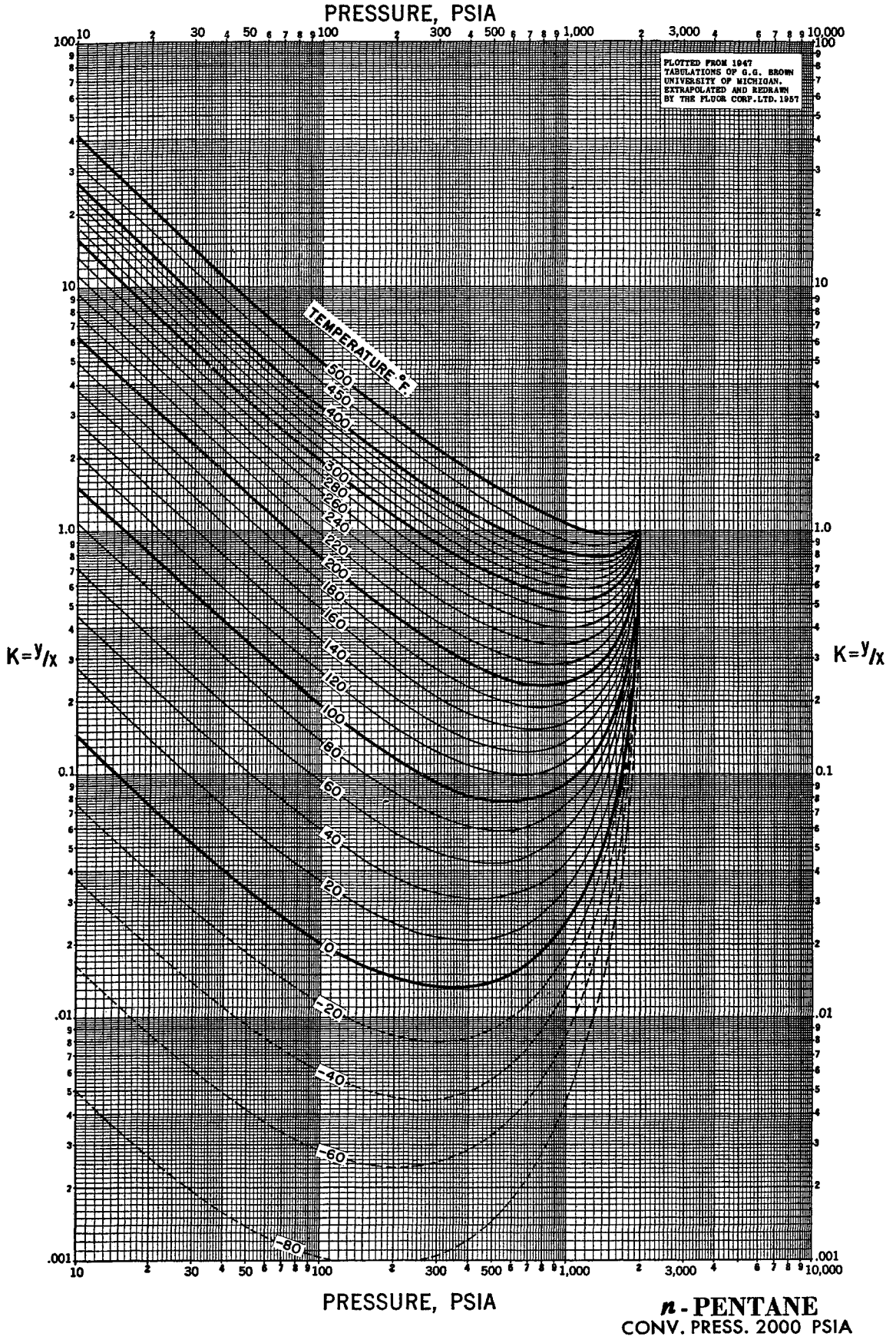

Fig. 6-61. Equilibrium constants for natural gas constituents at 2,000 psia convergence pressure. (6-40. *Courtesy NGAA.*)

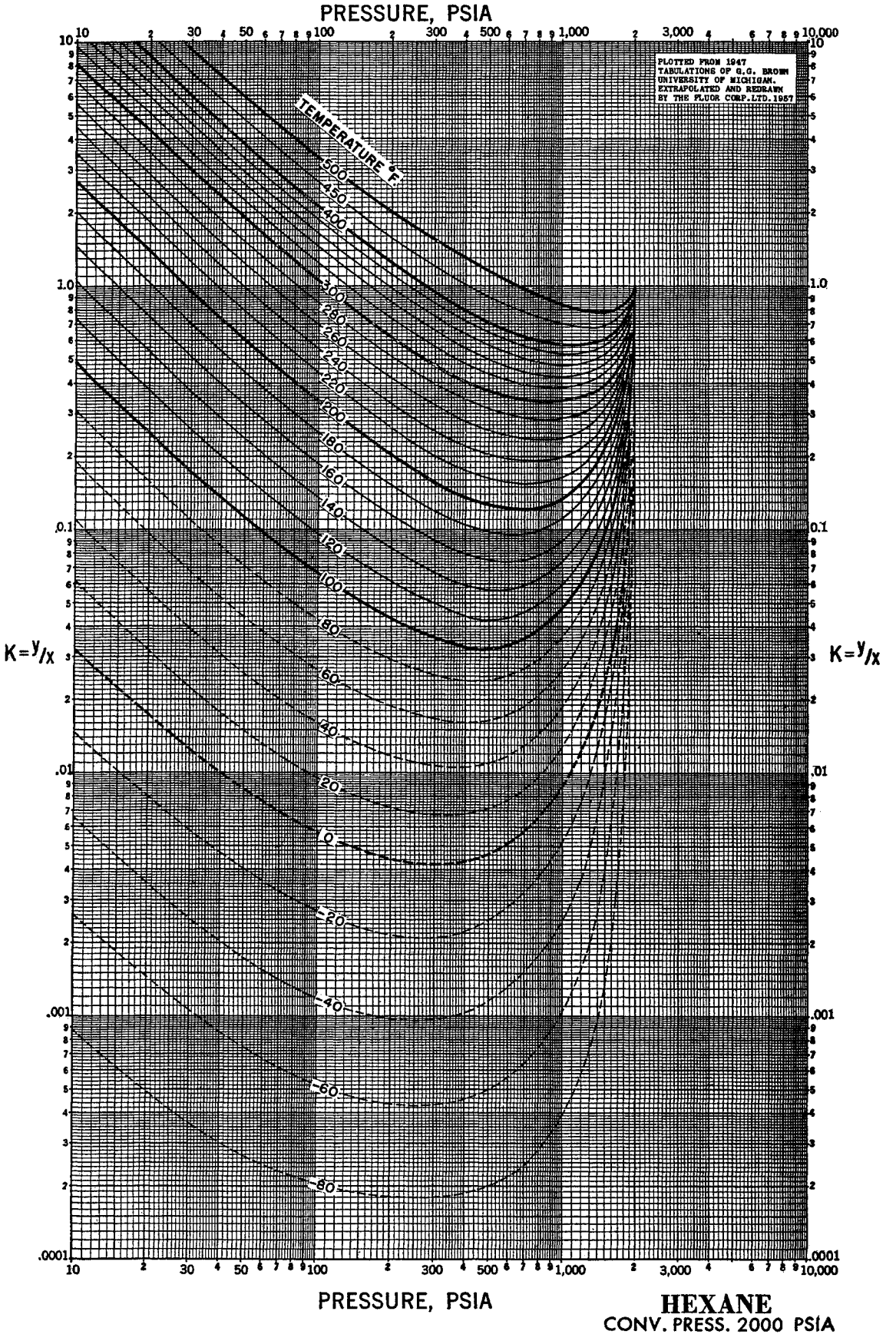

Fig. 6-62. Equilibrium constants for natural gas constituents at 2,000 psia convergence pressure. (6-40. *Courtesy NGAA.*)

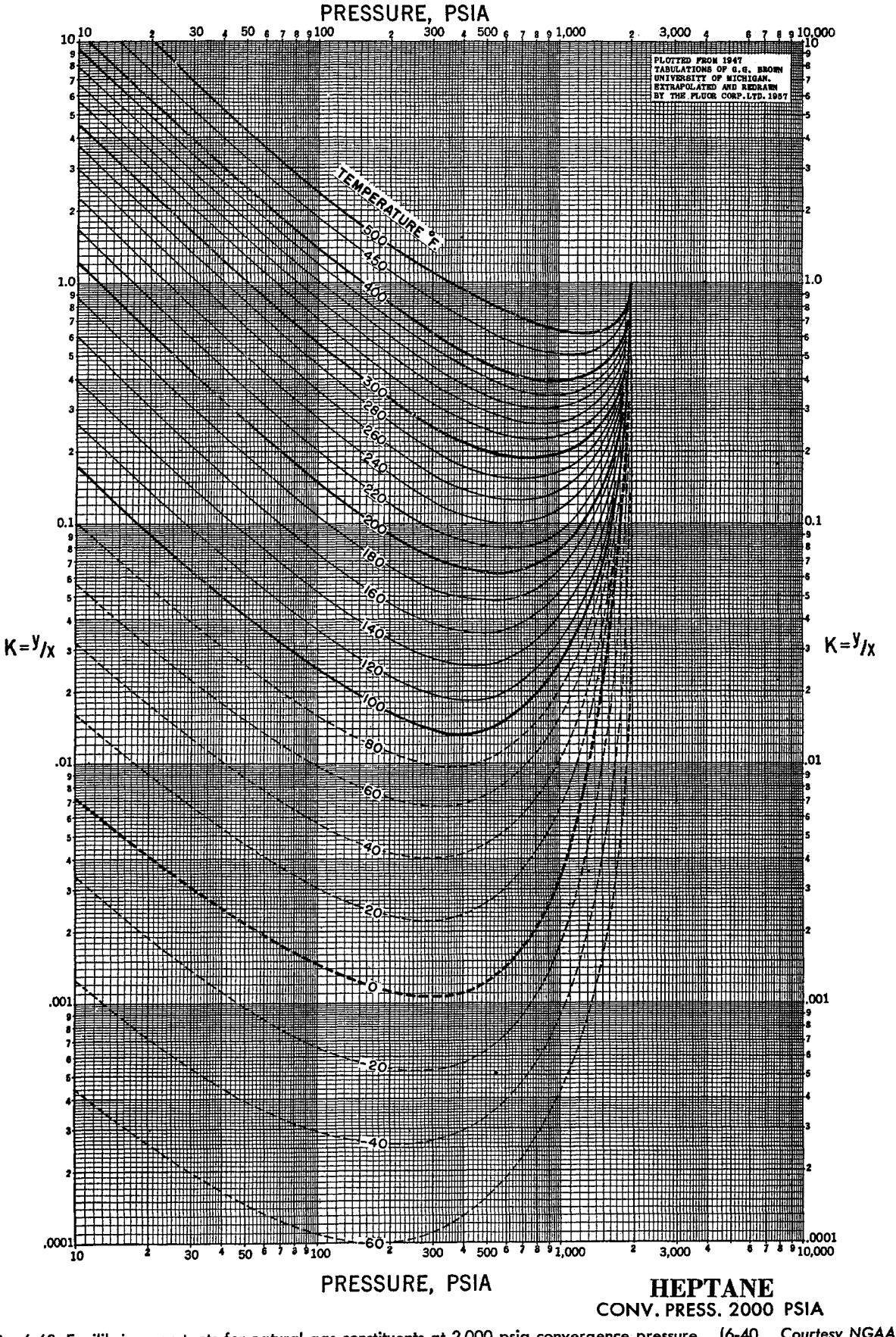

Fig. 6-63. Equilibrium constants for natural gas constituents at 2,000 psia convergence pressure. (6-40. *Courtesy NGAA.*)

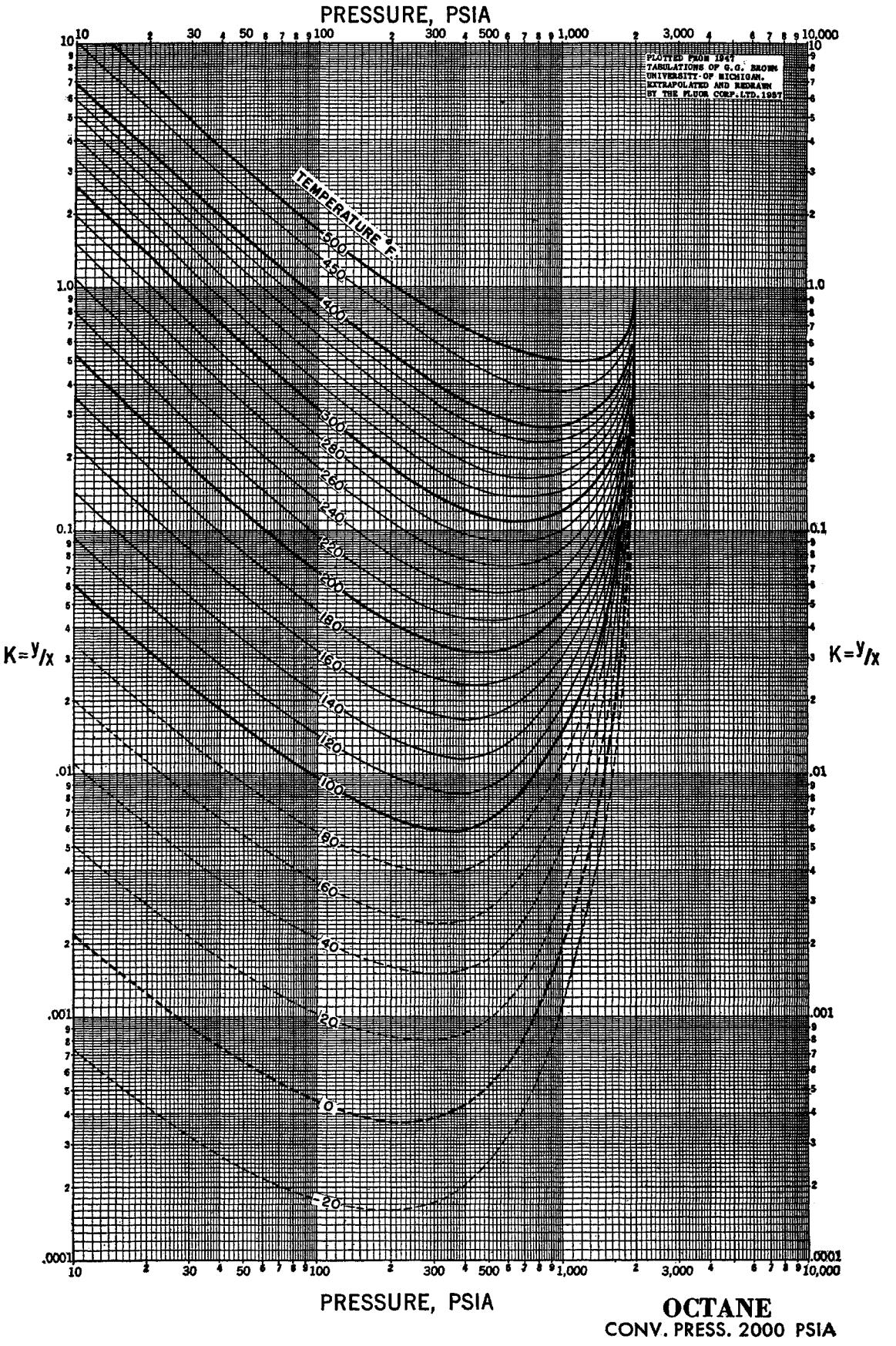

Fig. 6-64. Equilibrium constants for natural gas constituents at 2,000 psia convergence pressure. (6-40. *Courtesy NGAA.*)

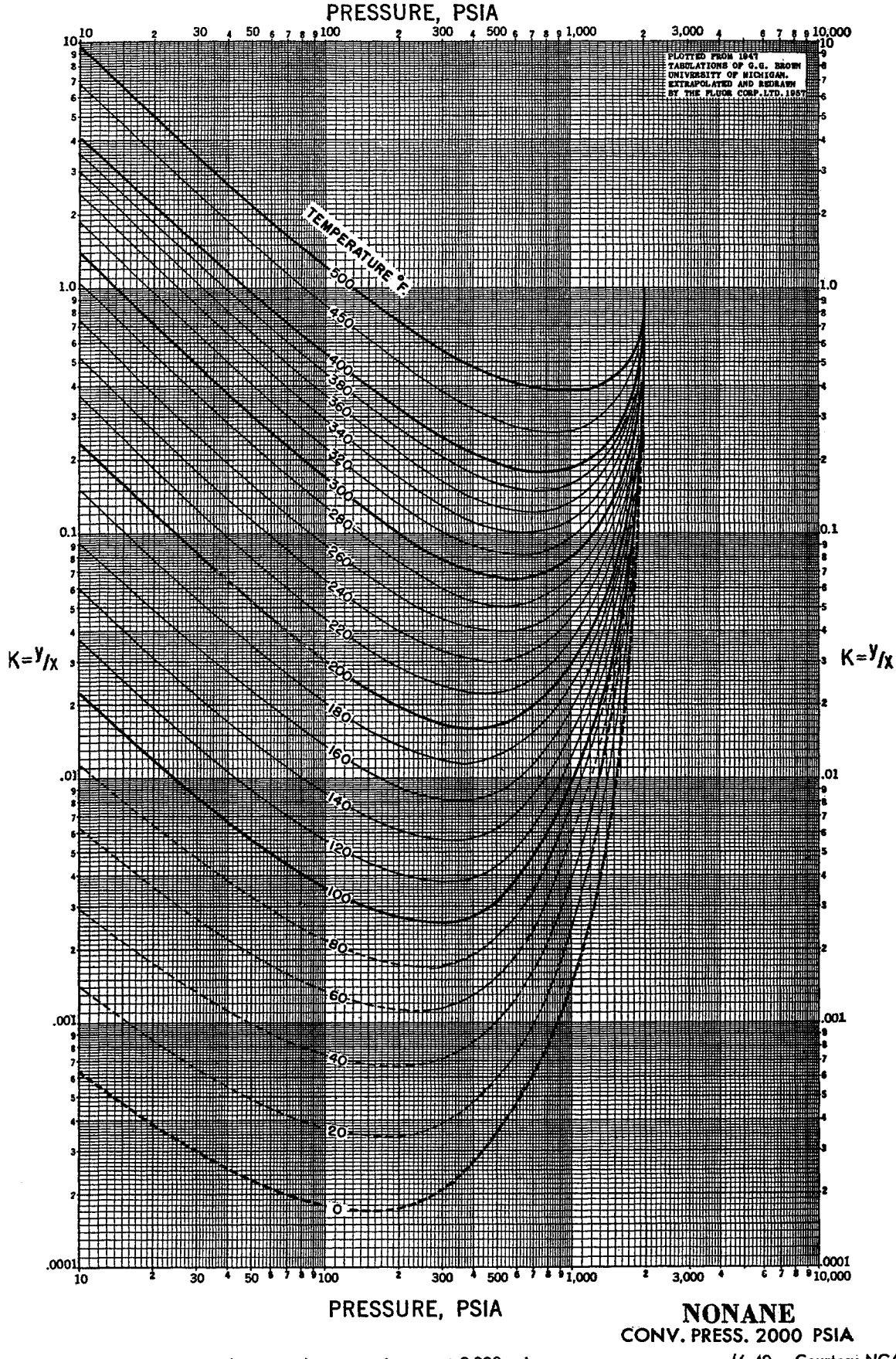

Fig. 6-65. Equilibrium constants for natural gas constituents at 2,000 psia convergence pressure. (6-40. Courtesy NGAA.)

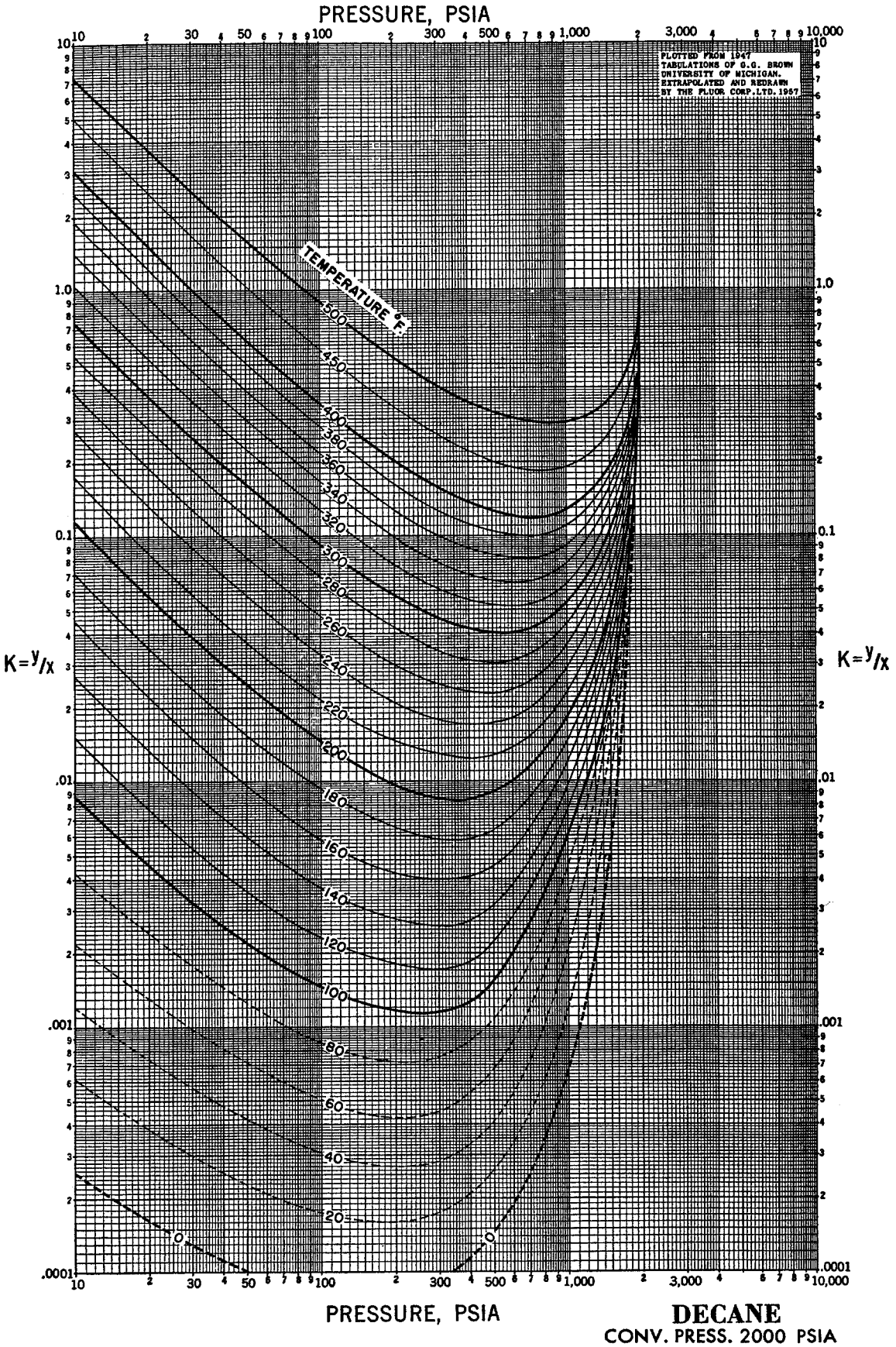

Fig. 6-66. Equilibrium constants for natural gas constituents at 2,000 psia convergence pressure. (6-40. *Courtesy NGAA.*)

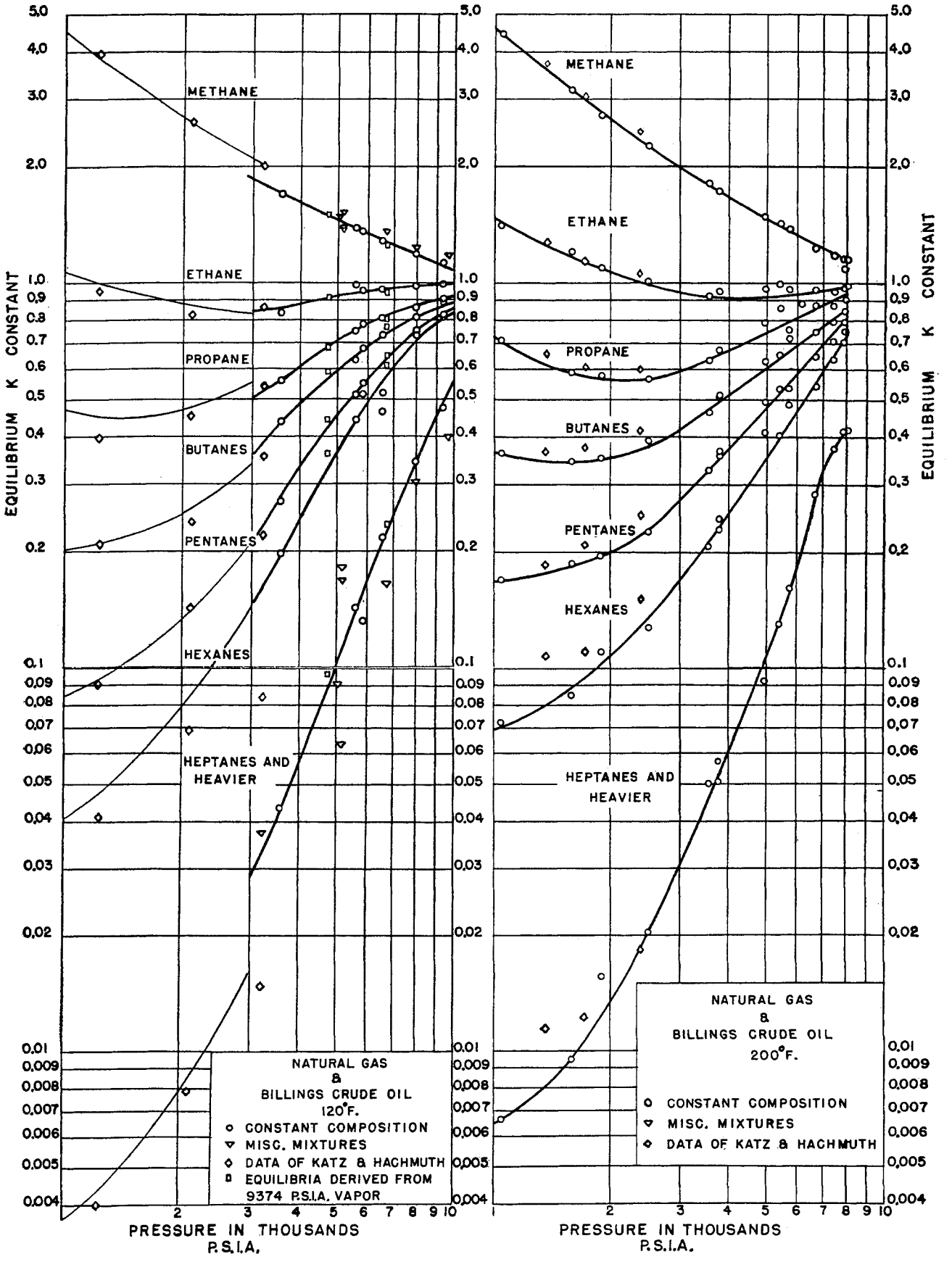

Fig. 6-67. Vapor-liquid equilibrium constants for natural gas and Billings crude oil at 120°F. (*Roland*, 6-50. *Courtesy Ind. Eng. Chem.*)

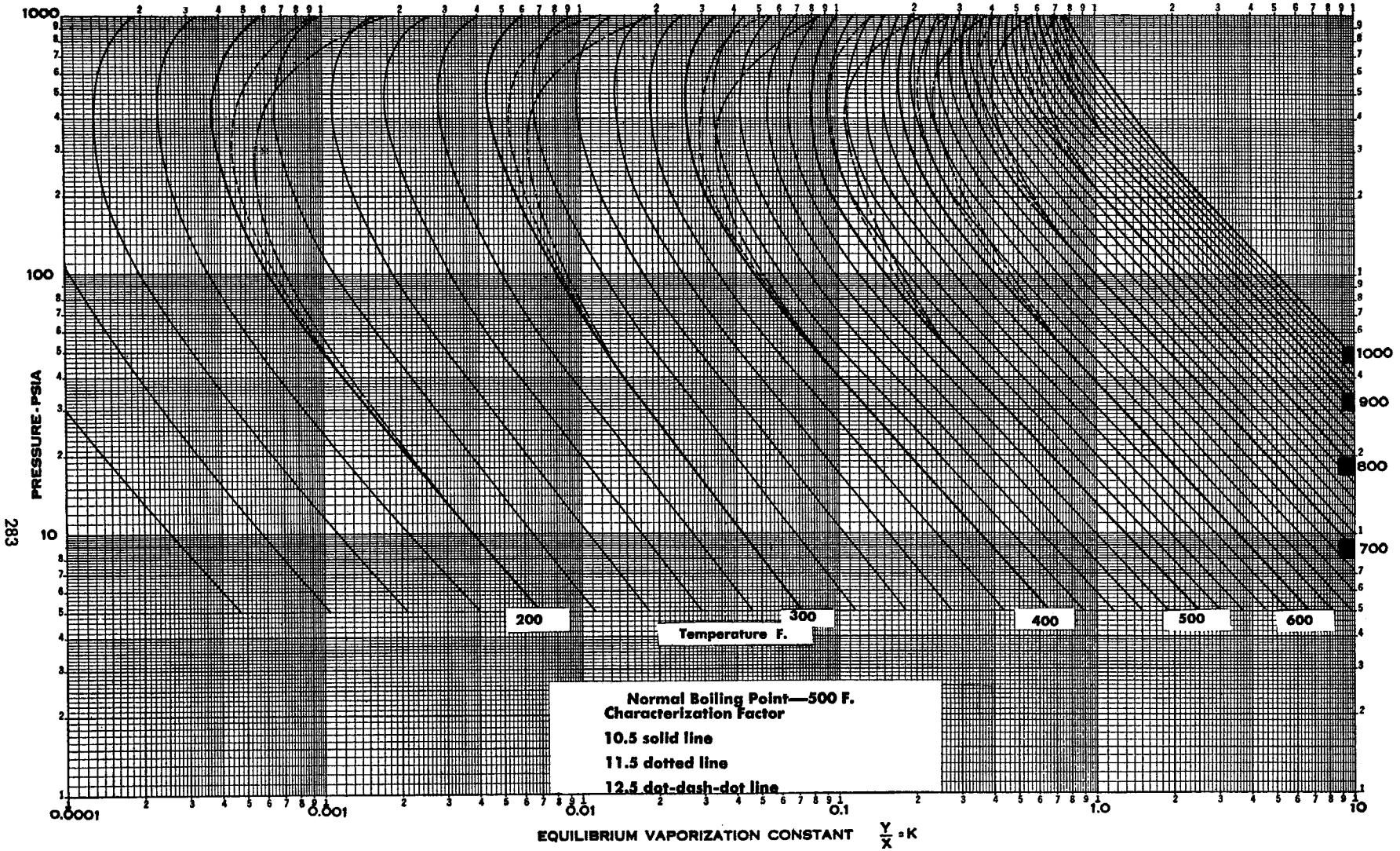

Fig. 6-68. Equilibrium-constant chart for constituents with a normal boiling point of 500°F. (*Poettmann and Mayland, 6-46. Courtesy Petrol. Refiner.*)

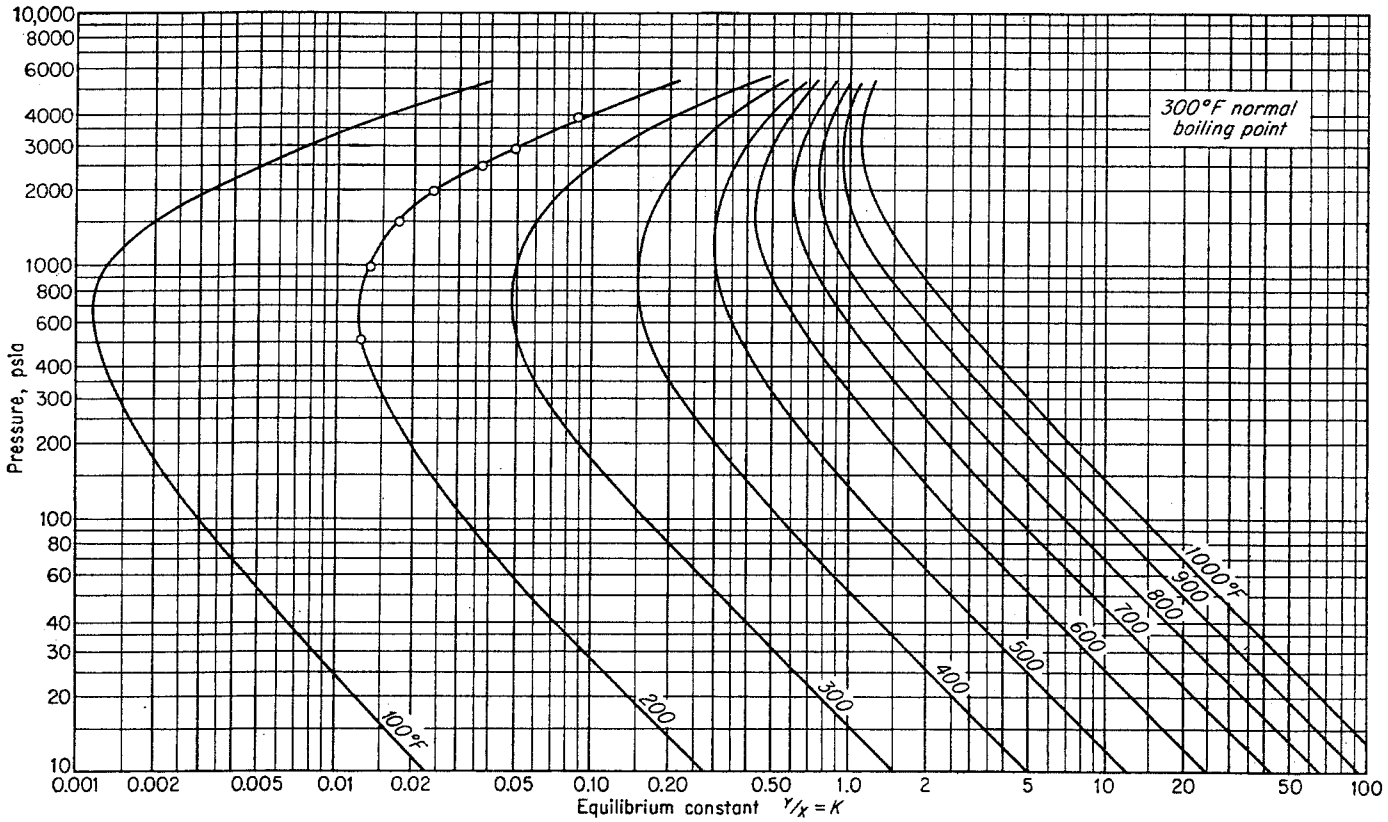

Fig. 6-69. Equilibrium constants for constituent boiling at 300°F.

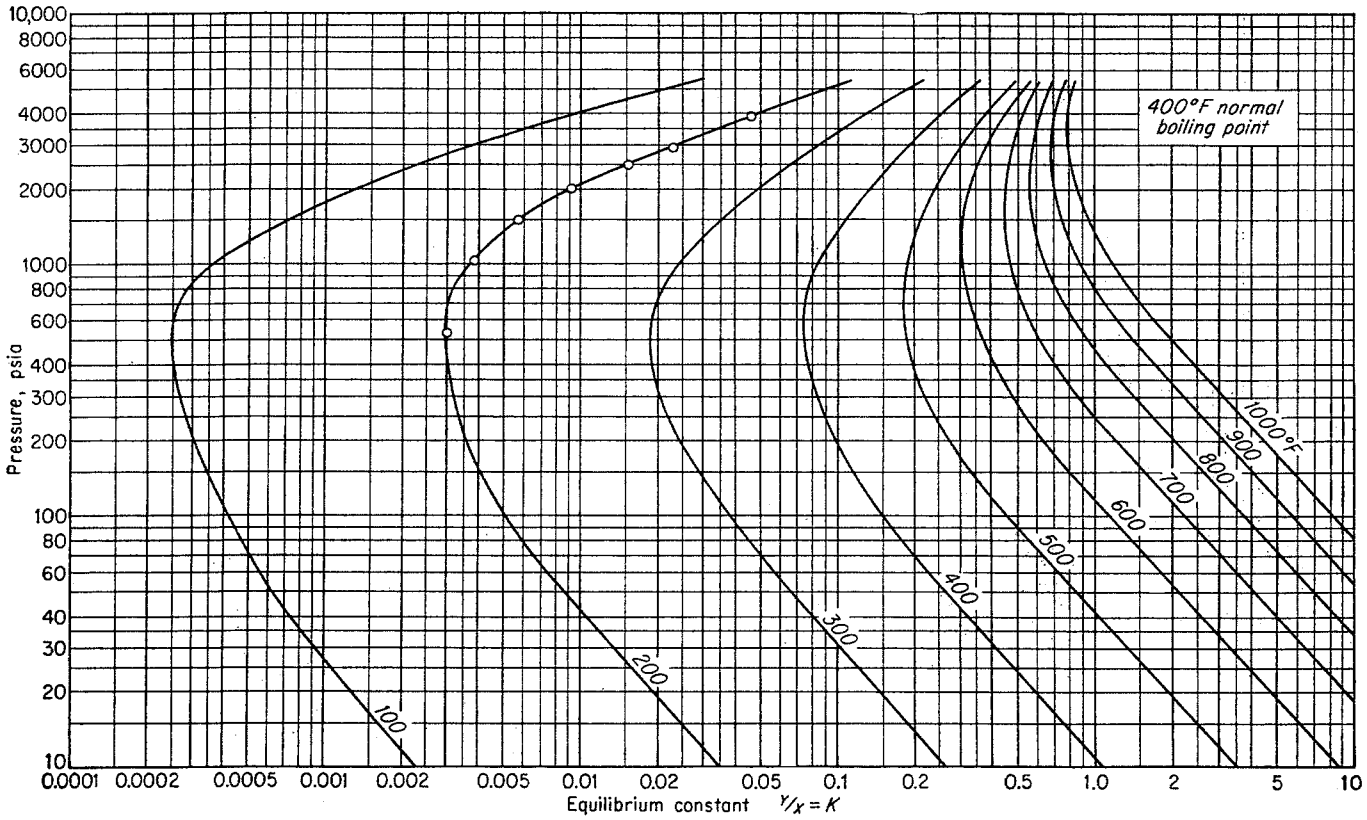

Fig. 6-70. Equilibrium constants for constituent boiling at 400°F.

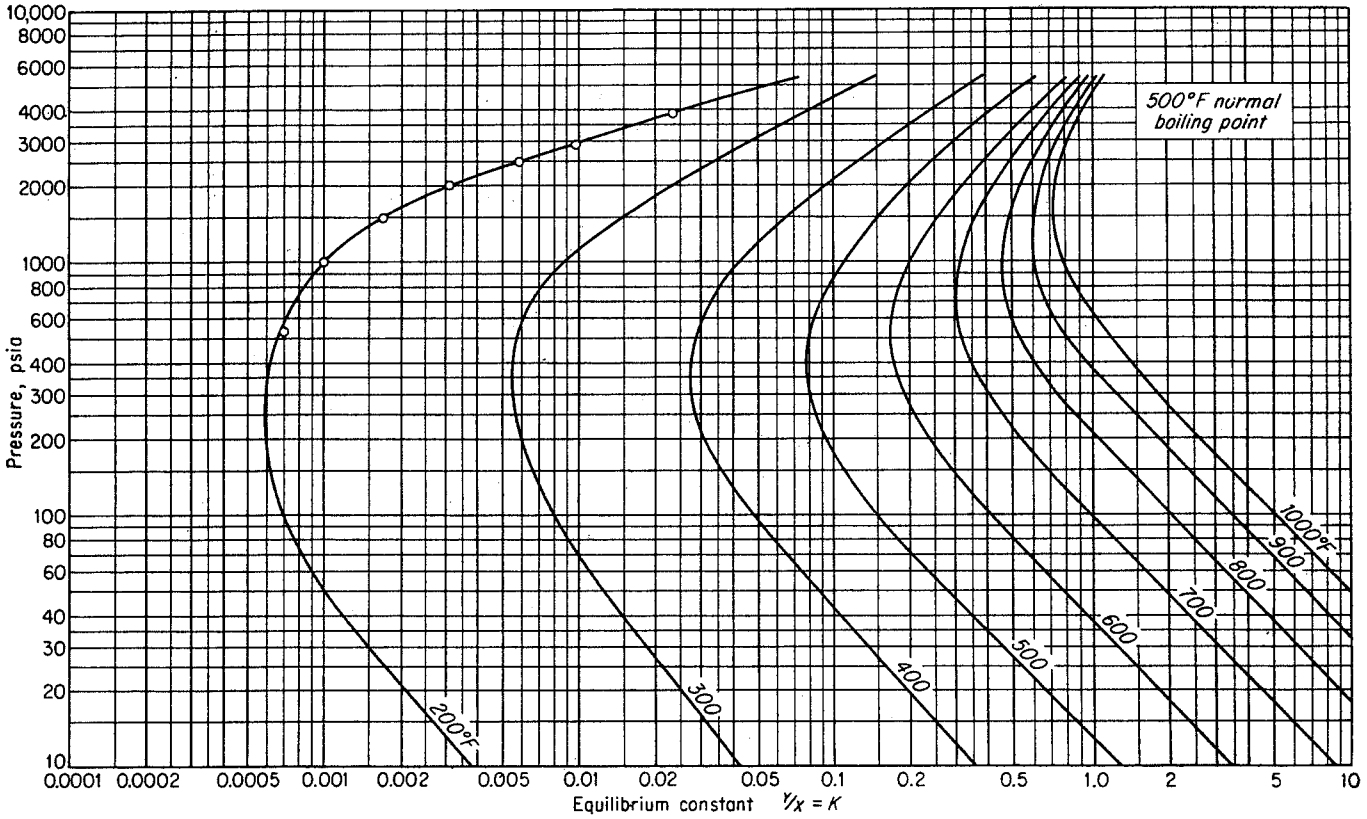

Fig. 6-71. Equilibrium constants for constituent boiling at 500°F.

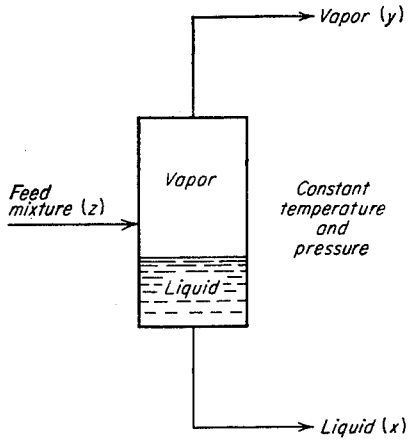

Fig. 6-72. Equilibrium vaporization.

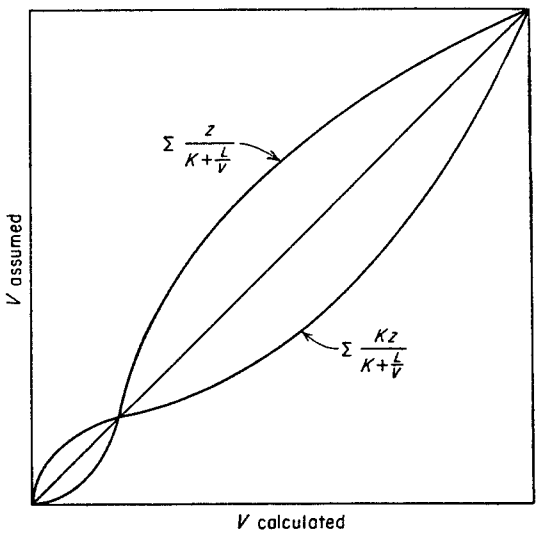

Fig. 6-73. Solution to equilibrium-vaporization equation (6-14).

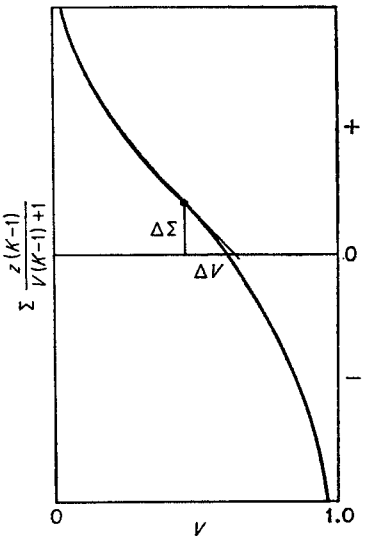

Fig. 6-74. Solution to equilibrium-vaporization equation by Newton's method, Eq. (6-15).

$$y\,dW = Wx - (W - dW)(x - dx) \quad (6\text{-}18)$$

where W = moles of liquid
x = mole fraction in liquid
y = mole fraction in vapor

Expanding, neglecting $dw\,dx$, and using $y = Kx$,

$$x\,dW + W\,dx = Kx\,dW \quad (6\text{-}19)$$

Rearranging and integrating, with K assumed constant,

$$\int_{W_o}^{W_f} \frac{dW}{W} = \frac{1}{K-1}\int_{x_o}^{x_f} \frac{dx}{x} \quad (6\text{-}20)$$

where subscript o = original condition and subscript f = final condition. Integrating,

$$\ln \frac{W_f}{W_o} = \frac{\ln (x_f/x_o)}{K-1} \quad (6\text{-}21)$$

$$\frac{W_f}{W_o} = \left(\frac{x_f}{x_o}\right)^{\frac{1}{K-1}} \quad (6\text{-}22)$$

$$\frac{x_f}{x_o} = \left(\frac{W_f}{W_o}\right)^{K-1} \quad (6\text{-}23)$$

At the end of the process,

$$\Sigma x_f = 1 \quad (6\text{-}24)$$

$$\Sigma K_f x_f = 1 \quad (6\text{-}25)$$

An example problem shows the calculation procedure.

Illustrative Problem

What quantity of vapor must be removed differentially at a constant temperature of 100°F in order to produce a liquid with a bubble-point pressure of 300 psia from a liquid containing 11.13 mole % methane and 88.87 mole % propane? The bubble point of the liquid is 470 psia at 100°F.

Solution

Using K values from Fig. 3-31:

Trial 1

Component	$(X_i)_o$	Assumed $\frac{W_f}{W_o}$	Assumed P_{me}, psia	K_n	$K_n - 1$	$\left(\frac{W_f}{W_o}\right)^{K_n-1}$	$(X_i)_f$	K (assume P_f = 300 psia)	$(y_i)_f$
C_1	0.1113	0.805	385	6.19	5.19	0.3245	0.0361	8.13	0.2935
C_3	0.8887	0.805	385	0.617	−0.383	1.0865	0.9640	0.720	0.695
							$\Sigma = 1.0001$		$\Sigma = 0.9885$
					Trial 2				
C_1	0.1113	0.8120	385	6.19	5.19	0.3395	0.0378	8.13	0.307
C_3	0.8887	0.8120	385	0.617	−0.3831	1.0828	0.962	0.720	0.693
							$\Sigma = 0.9998$		$\Sigma = 1.000$

Therefore, 18.8 per cent of the liquid must be differentially vaporized.

Similar equations may be developed, replacing K with the ratio K_n/K_1. Thus the K does not have to be constant for the above equation, but the ratio of the K's must be approximately constant. If the ratio of the K's varies considerably over the pressure or temperature range in which the vaporization occurs, the process must be broken down into a number of steps. The K's used in Eq. (6-23) are neither the average K's nor the K's at the average pressure and temperature, but the K's for the several constituents at the mean effective pressure, which must be determined to satisfy Eqs. (6-23) to (6-25). One can always check the accuracy of the procedure by using one step and then two or more steps for the same process. The final compositions and conditions found should be the same.

Illustrative Problem

Determine the final pressure to vaporize differentially 25 mole % of a mixture containing 32 mole % methane and 68 mole % propane at a temperature of 100°F. The bubble point is 1,000 psia.

Solution

Using K values from Fig. 3-31:

Trial 1
Assume P_{me} = 900 psia

Component	K_n	$K_n - 1$	$\left(\frac{W_e}{W_o}\right)^{K_n-1}$	$(X_i)_f$
C_1	2.295	1.295	0.6890	0.2205
C_3	0.511	−0.489	1.1510	0.783
				$\Sigma = 1.0035$

Trial 2

Assume P_{me} = 883 psia

Component	$(X_i)_o$	K_n	$K_n - 1$	$\left(\frac{W_f}{W_o}\right)^{K_n-1}$	$(X_i)_f$
C_1	0.320	2.350	1.350	0.678	0.217
C_3	0.680	0.510	−0.490	1.1515	0.783
					$\Sigma = 1.000$

$\therefore P_{me}$ = 883 psia

Determination of final pressure by computation of bubble point of final liquid:

Trial 1

Assume P_f = 800 psia

Component	K_n	$(y_i)_f$
C_1	2.66	0.576
C_3	0.50	0.3915
		$\Sigma = 0.9675$

Trial 2

Assume P_f = 765 psia

Component	K_n	$(y_i)_f$
C_1	2.805	0.6085
C_3	0.500	0.3915
		$\Sigma = 1.0000$

P_{me} = mean pressure
P_f = final pressure
$\therefore P_f$ = 765 psia

Use of Electronic Computers for Vaporization Calculations

A slide rule can be used to compute vaporizations with some accuracy and considerable expenditure of time. Desk calculators improve the accuracy, but they require considerable manpower for multiple-vaporization calculations. Electronic digital computers are rapidly taking over all such repetitive and time-consuming calculations as vaporization computations (6-39, 6-48, 6-36, 6-16).

The digital electronic computer (6-7, 6-28, 6-66, 6-15, 6-5, 6-4) is a device for conducting numerical operations at a very rapid rate, more than 100,000 operations/sec. The machine takes data and instructions from card or tape and stores them; then it is able to carry out the instructions. Basically the machine can add and tell whether a number is zero or not. All usual calculations can be reduced to numerical operations involving addition. The results of a computation, stored in the memory units, can be printed as tables or taken from the machine as cards or tape.

When considering the use of a digital computer for solving a problem, two factors need to be taken into account, machine time and cost of manpower. Computing time on this type of equipment is expensive. So the increase in knowledge about the problem and the increase in accuracy must warrant this expense. The cost of technical manpower to prepare or "program" the problem for the computer must also be considered. When the problem needs to be solved for only one set of conditions or has one unique solution, use of the computer may be uneconomical. However, when a problem needs to be solved for a number of sets of conditions, the programming expense is usually low, since, for each solution after the first one, it is necessary only to place the new conditions in the original program without additional preparation or programming.

It is apparent from these observations that many problems cannot be solved by means of a digital computer. In problems practical for a digital computer, all variables must be related by means of mathematical equations or by semimathematical means such as tables. In cases where such equations (or reasonable approximations thereof) are not available, the analogue computer has to be considered. In some cases, the mathematical relationships involve convergence and stability difficulties that make solution by means of a digital computer impractical, if not impossible. In spite of these limitations, the digital computer has wide application in the solution of engineering problems. The following discussion applies generally to digital computers, although certain comments may be pertinent only to the Datatron machines (6-4).

Programming

Once the decision to use the digital computer has been reached, the problem must be prepared for the computer. This preparation is usually referred to as *programming* or *coding;* its product is known as a *program* or *code.* The programming of most routine engineering calculations does not warrant use of the time of a programmer to obtain optimum use of the computing equipment; this is in contrast with many business problems that are periodically performed a relatively large number of times on a routine basis. Although most engineering codes do not result in the optimum use of the computer, they do result in the optimum use of the combination of technical manpower and computer time, since it is possible for technical people to code their own problems with little or no knowledge of the computing equipment itself. After a little experience, possibilities for shortening computer time become readily apparent.

Programming is not difficult to learn, for anyone who has solved a problem has in reality already pro-

grammed it. Programming is essentially writing a set of instructions for solving a problem for a clerk who has no knowledge of mathematics or engineering but who knows how to operate a desk calculator. Since the trend is toward the stored-program, single-address type of digital computer, the discussion here will be limited to this type. Modifications in method for a two-address system are rather easily made; two-address machines can be used essentially as single-address systems. The programmer may treat the computer as a so-called "black box" and for the most part ignore the detail of the mechanism by which the computer accomplishes the calculation. Only features of the equipment that are necessary for the programmer to understand are discussed here.

Storage

The computer has a series of storage locations in which instructions or data can be placed. These storage locations are numbered in sequence; one of the problems of the programmer is to keep a record of the content of each of these locations. Whenever a piece of information is stored in a location, any previous information in that location is erased or lost. However, removing data or instructions from a storage location for use in the computation leaves the information in the location unchanged. The number of each storage location is known as the "address" of that location. The computer performs the instructions stored in the memory or storage locations in sequence according to address, unless it is instructed to change the sequence by starting at an address other than the first.

Registers

The programmer must understand also that the arithmetical portion of the computer contains a number of registers in which the number being operated on appears during various stages of the process. These registers are similar to those found on a desk calculator. The numbers are handled by these registers in almost the same way as they are by a desk calculator, but with one important exception: the answer always appears in the same register. This register has twice as many digits as can be stored in any memory location plus a sign. When a number is added, the answer, or number plus sign, appears in the left half of the register. When a number in this register is multiplied by another number from memory, the product plus sign appears in the full length of the register. On the other hand, when a number in this register is divided by a number from memory, the quotient plus sign appears in the left half of the register and the remainder appears in the right half. This register, for convenience, is divided into two portions. The left, or answer, portion is known as the A register. The right half, where the remainder appears after a division, is called the R register. A number must be in the A register before it can be operated on by another number. After the operation, the answer automatically appears in some form in the A and R registers and it in turn is ready to be operated on by another number. When the sum of two numbers is too long to be contained in the A register, the register omits the remaining far left digits. This omission is again similar to the action of a desk calculator, except that the digital computer automatically stops when this happens and turns on a light to indicate that an "overflow" has occurred. Therefore, the data must be positioned in each memory location or in the A registers in such a way as to prevent overflow from occurring. Some computers have other registers that can be of great assistance to the programmer, but a discussion of these is beyond the scope of this elementary treatment. The A register and each memory location contain a number of digits plus a sign. These digits plus a sign are known as a "word." A "word" in most computers contains ten digits plus a sign; the word length is the factor that determines the size of numbers handled.

Word Construction

A digital computer of the type being discussed has a number of storage or memory locations in which one word of information may be placed. Words placed in the computer can contain either instructions or data points. The data have to be positioned within the digits of a word so that the position of the decimal point has a known relation to the decimal point of the other data used. Also, a memory location or address must be assigned to each data point.

Block Diagram

Once the addresses for all the data points have been assigned, a block diagram showing in some detail the steps in the calculation is prepared (Fig. 6-75). For purposes of illustration, the flash-vaporization computations will be programmed by a method that shows the flexibility of this type of computer; Eq. (6-15),

$$\sum y - \sum x = \sum \frac{z(K-1)}{V(K-1)+1} = F(V) = 0 \tag{6-15}$$

is in suitable form to be solved on a digital computer. A plot of the right-hand member of the equation for various values of V (as shown in Fig. 6-74) is used as a starting point. Since the computer itself cannot exercise any judgment when selecting a value for V

that might satisfy Eq. (6-15), a method for systematically selecting the V must be devised. Rachford and Rice (6-48) have proposed the use of the 20-questions method. The values of the function of V are determined for a series of V's (questions) chosen in such a way as to narrow the values of V that have not been proved impossible solutions for Eq. (6-15). First, a value for V equal to 0.5 is used to determine the function of V. From Fig. 6-74 it can be seen that, if the value for $\Sigma Z(K-1)/[V(K-1)+1]$ is positive, the value for V is too small to satisfy Eq. (6-15); so the value for V is greater than 0.5. If the value of the function is negative, the value for V is too large to satisfy Eq. (6-15); so the value for V is less than 0.5. The first value for V narrowed the range of values not proved impossible to half the previous range 0 to 1. Now, if another value of V, in the middle of the range of values not proved impossible, is used to determine the function of V, the sign of the function of V will determine which half of the remaining range is impossible. By repeating this process twenty times, an answer for V can be determined that will result in a value of the function of V that is 0 to eight places. After determining the value for V that satisfies Eq. (6-15), this value is used in Eqs. (6-10) and (6-12) to complete the solution. Although the method outlined would be too long to be practical with a desk calculator, a digital computer can use this method to obtain a solution within a minute after the data and program have been entered into it.

Another approach to the problem of determining V involves a process known as Newton's method. The slope of the function of V with respect to V is determined at the point for the value of V. The function of V divided by the slope becomes the correction to be added to the first V used. The new value for V will be much closer to the value that will satisfy Eq. (6-15). Derivation of the method is as follows:

$$F(V) = 0 \tag{6-26}$$

$$F(V) = F(V_j) + (V_{j+1} - V_j)F'(V_j) + \cdots \tag{6-27}$$

where j = trial number. Neglecting second-order terms,

$$V_{j+1} - V_j = -\frac{F(V_j)}{F'(V_j)} \tag{6-28}$$

$$V_{j+1} = V_j - \frac{F(V_j)}{F'(V_j)} \tag{6-29}$$

$$F'(V_j) = \sum_n \frac{(K_n - 1)^2 z}{[(K_n - 1)V_j + 1]^2} \tag{6-30}$$

Thus, successive approximations of V can be made by using Eq. (6-29) until the function of V approximates 0 to the desired number of places. For this problem, Newton's method converges to an answer in a very few steps and would prove more rapid than the 20-questions method. However, both methods are satisfactory for most cases and, only in the event that the equation would have to be solved a great number of times in conjunction with a larger problem, would reprogramming from the 20-questions method to Newton's method warrant use of the technical manpower required. A block diagram of the steps used in Newton's method is shown in Fig. 6-75. The purpose of this block diagram is to give the programmer a chance to view the calculation procedure as a whole and to discover which intermediate results should be retained for future use, such as those in block C that are needed in block J and in block N. A block diagram also allows the steps to be easily rearranged to give the least number of operations and thus to produce an optimum program.

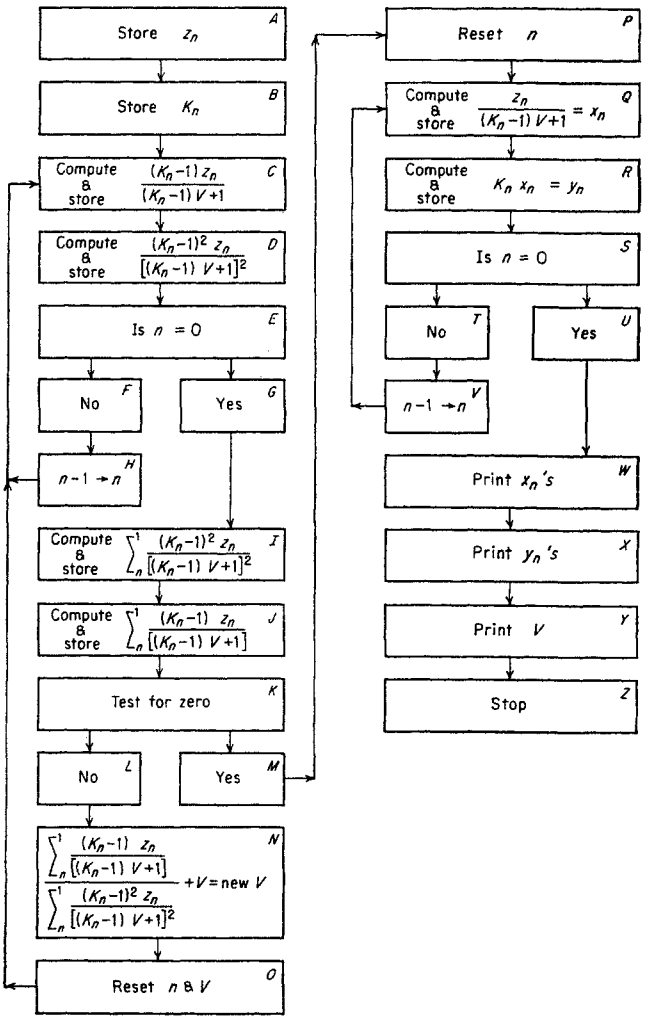

Fig. 6-75. Block diagram for computation by digital computer.

Instructions

After preparing the block diagram, steps indicated are translated into instructions for the computer. A computer instruction is made up of three parts: (1) the address or memory location where the instruction will be stored, (2) the operation or order to be carried out, and (3) the address of the number with which the operation is to be performed. A partial list of possible commands is given in Table 6-13.

Programming

Before coding the flash-vaporization problem, the code for the solution of the following equation is presented as a simplified example:

Table 6-13. Command List for Calculator

Command	*Explanation*
Arithmetical Commands	
Clear, add	Clear the *A* register, and add the contents of the cell whose address is in the instruction.
Add	Add the contents of the cell whose address is in the instruction to the contents of the *A* register.
Clear, subtract	Clear the *A* register, and subtract the contents of the cell whose address is in the instruction from the contents of the *A* register.
Subtract	Subtract the contents of the cell whose address is in the instruction from the contents of the *A* register.
Multiply	Multiply the contents of the cell whose address is in the instruction by the contents of the *A* register, and insert the 20-digit product in the *A* and *R* registers.
Multiply, round	Multiply the contents of the cell whose address is in the instruction by the contents of the *A* register. Round the product to ten digits and clear the *R* register.
Divide	Divide the 20-digit contents of the *A* register and *R* register by the contents of the cell whose address is in the instruction.
Manipulation and Transfer of Information	
Store	Store the contents of the *A* register in the cell whose address is in the instruction.
Store, clear	Store the contents of the *A* register in the cell whose address is in the instruction, and clear the *A* register.
Shift left	Shift the contents of the *A* and *R* registers to the left by the number of places indicated by the number in the address location of the instruction. The sign does not move.
Shift right	Shift the contents of the *A* and *R* register to the right by the number of places indicated by the number in the address portion of the instruction. The sign does not move.
Clear *R*	Clear the *R* register.
Round	Round the 20-digit contents of the *A* and *R* registers to ten digits, and clear the *R* register.
Decision Making and Branching	
Stop	Stop machine operation.
Overflow *on*, for sign difference	If the sign of the *A* register differs from the sign of the cell whose address is in the instruction, overflow indicates *on*.
Change on nonzero	Test the contents of the *A* register (not the sign) for 0. (*a*) If the *A* register setting is 0, set the sign of the *A* register at 0 and continue control in sequence. (*b*) If the *A* register is not 0, change the control to the cell whose address is in instruction.
Change on zero	Test the contents of the *A* register (not the sign) for 0. (*a*) If the *A* register setting is not 0, continue control in sequence. (*b*) If the content of the *A* register is 0, change control to the cell whose address is in instruction.
Change conditionally	If overflow indicates *on*, change control to the cell whose address is in the instruction, and reset overflow. If overflow indicates *off*, continue control in sequence.
Change unconditionally	Change control to the cell whose address is in the instruction.
Read ( )	Read the number of instructions and data points indicated by the number in parentheses, and transfer them to consecutive storage cells, beginning with the cell whose address is in instruction.
Write ( )	Write the contents of the number of storage locations indicated by the number in the parentheses, beginning with the cell whose address is in the instruction.
Read, start	Read the data or instructions continuously and store them in consecutive storage cells, beginning with the cell whose address is in the instruction, until a start command is reached; transfer control to the address of the cell whose address appears in that command.
Start	Start computing by transferring control to the cell whose address is in the instruction.

$$x = (D + B)C$$

where $D = 110.2345$, $B = 22.445566$, and $C = 33.557799$. The code is shown in Table 6-14 on one type of form used.

The first step in the program instructs the computer to store the following in sequence, starting with storage location 0001. When *input* reaches the last word on the tape or card, the *input* will stop, and control will be transferred to cell 0004. Here the calculation is started by the instruction to clear the A register and add the content of cell 0001, or D, to the A register. When the computer has completed this operation, the next instruction is executed and the content of cell 0002, B, is added to the A register, which then contains the sum $D + B$. Then the computer advances one more step, and the instruction to multiply by the content of cell 0003 is carried out. A and R registers now contain the product $(D + B)C$.

Decimal-point Alignment

In multiplication and division, the computer always interprets the numbers with a decimal point before the first digit. But, when the decimal point belongs in reality at another position in both numbers multiplied (or divided), its proper position will move when the multiplication (or division) is executed.

In order to realign the decimal point after a division or multiplication, shift-right and shift-left orders are provided. The instruction in cell 0007 repositions the product in the computer so that the decimal point is in the same position as in the data originally stored. The next instruction adds 1 to the last digit in the A register if the first digit in the R register is 5 or greater. The next two instructions result in a print-out of the answer to $(D + B)C$. The instruction in cell 0011 completes the process.

Flash Program

Table 6-15 shows a program for solution of a flash-vaporization problem using Newton's method. For simplicity, only ten components are used. The program is arranged so that a number of solutions may be obtained after the code has been entered into the computer, simply by reading in the z_n, K_n, and the first assumed value V for each solution. Storage locations 0001 to 0010 contain the feed composition data z_n and locations 0011 to 0020 contain the equilibrium-constant data K_n for each component arranged in the same sequence as the feed compositions for each component. Cells 0021 to 0090 are reserved for storing intermediate results. The values stored from 0091 to 0099 will be discussed as they are used in the program. Feed-composition data are positioned in the storage cell so that the decimal point is between the first and second digits from the left. The decimal point for equilibrium constants is placed between the third and fourth digits from the left, and the V decimal point is placed at the left of the first digit.

Before discussion of the program, it should be stated that the code was designed to show flexibility in available approaches rather than to give a refined and polished code. Also, no attempt was made to conserve storage space, for it was assumed that the computer had more available space than the 250 addresses used.

The commands in cells 0100 to 0113 show clearly the steps in the calculation. First, registers are cleared and the value in cell 0011 is added. Since the value in cell 0011 is K_1, K_1 appears in the A register as indicated in the explanation column. The result of each step in the computation to 0113 is shown in the explanation column. Steps from 0100 to 0113 can be repeated nine additional times, once for each component. The only changes necessary will be in address instructions of cells 0100, 0102, 0103, 0107, 0110, 0111, and 0113. The address in the instruction of each cell will require the addition of 1 each time the step is repeated. Thus, for K_2 the command in cell 0100 will be "clear, add 0012," and it will be stored in cell 0114.

Table 6-14. Example of a Program
Program for $X = (D + B)C$

Address where information is stored	Instructions or data		Explanation
	Order	Address	
....	Read, start	0001	Read program card data into computer beginning at storage address 0001 until an instruction word containing the start command is reached; store D at address 0001
0001	0110234500	....	Store D at address 0001
0002	0022445566	....	Store B at address 0002
0003	0033557799	....	Store C at address 0003
0004	Clear, add	0001	Clear and add D
0005	Add	0002	Add B ($D + B$ is then in A register)
0006	Multiply	0003	Multiply by C
0007	Shift left	0004	Realign decimal point
0008	Round	....	Round off the digits in the R register
0009	Store	0013	Store $(D + B)C$ in cell 0011
0010	Write (1)	0013	Write $(D + B)C$
0011	Stop	....	Stop calculation
0012	Start	0004	Stop input and start calculation at cell 0004

Table 6-15. Program for Flash-vaporization Calculation by Newton's Method

Storage address	Order	Address	Explanation
....	Read	0001	Read data into computer
0001	C_1	....	Store feed composition z, mole fraction
0002	C_2		
0003	C_3		
0004	C_4		
0005	C_5		
0006	C_6		
0007	C_7		
0008	C_8		
0009	C_9		
0010	C_{10}		
0011	K_1	....	Store equilibrium constants K
0012	K_2		
0013	K_3		
0014	K_4		
0015	K_5		
0016	K_6		
0017	K_7		
0018	K_8		
0019	K_9		
0020	K_{10}		
....	Read, start	0093	Read first assumed V into computer
0093	0000000001	....	Store constant 1 for address modification
0094	0000000009	....	Store constant 9 for address modification
0095	0000000009	....	9
0096	Stop	0096	Intermediate storage
0097	5000000000	....	Store constant .5
0098	5000000000	....	.5
0099	0010000000	....	1
0100	Clear, add	0011	Clear and add K
0101	Subtract	0099	$K - 1$
0102	Store	0021	
0103	Clear, add	0021	$K - 1$
0104	Multiply	0098	$(K - 1)V$
0105	Add	0099	$(K - 1) + 1$
0106	Store	0096	
0107	Clear, add	0021	$K - 1$
0108	Divide	0096	$\frac{K - 1}{(K - 1)V + 1}$
0109	Store	0096	
0110	Multiply	0001	$\frac{(K - 1)z}{(K - 1)V + 1}$
0111	Store	0041	
0112	Multiply	0096	$\frac{(K - 1)^2 z}{(K - 1)V + 1}$
0113	Store	0051	
0114	Clear, add	0100	
0115	Add	0095	
0116	Store	0120	

Table 6-15. Program for Flash-vaporization Calculation by Newton's Method (*Continued*)

Storage address	Order	Address	Explanation
0117	Clear, add	0102	
0118	Add	0095	
0119	Store	0122	
0120	Stop	0120	From 0116
0121	Subtract	0099	
0122	Stop	0122	From 0119
0123	Clear, add	0095	
0124	Change on zero	0128	
0125	Subtract	0093	Subtract 1 from the address modifier
0126	Store	0095	
0127	Change unconditionally	0114	
0128	Clear, add	0094	
0129	Store	0095	
0130	Clear, add	0103	
0131	Add	0095	
0132	Store	0145	
0133	Clear, add	0107	
0134	Add	0095	
0135	Store	0149	
0136	Clear, add	0110	
0137	Add	0095	
0138	Store	0152	
0139	Clear, add	0111	
0140	Add	0095	
0141	Store	0153	
0142	Clear, add	0113	
0143	Add	0095	
0144	Store	0155	
0145	.....	....	From 0132, $K - 1$
0146	Multiply	0098	$(K - 1)V$
0147	Add	0099	$(K - 1)V + 1$
0148	Store	0096	
0149	.....	....	From 135, $K - 1$
0150	Change unconditionally	0241	Correct for decimal-point position, and compute $\frac{K - 1}{(K - 1)V + 1}$
0151	Store	0096	
0152	.....	....	From 0138, $\frac{(K - 1)z}{(K - 1)V + 1}$
0153	.....	....	From 0141, store
0154	Change unconditionally	0244	Correct for decimal-point position and compute $\frac{(K - 1)^2 z}{(K - 1)V + 1}$
0155	.....	....	From 0144, store
0156	Clear, add	0095	
0157	Change on zero	0161	If zero, all components computed
0158	Subtract	0093	Reduce address modifier
0159	Store	0095	
0160	Change unconditionally	0145	Return to compute next component
0161	Clear, add	0094	Restore address modifier

Table 6-15. Program for Flash-vaporization Calculation by Newton's Method (*Continued*)

Storage address	Order	Address	Explanation
0162	Store	0095	
0163	Clear, add	0041	$\frac{(K-1)z}{(K-1)V+1}$
0164	Add	0042	
0165	Add	0043	
0166	Add	0044	
0167	Add	0045	
0168	Add	0046	
0169	Add	0047	
0170	Add	0048	
0171	Add	0049	
0172	Add	0050	$\frac{(K-1)z}{(K-1)V+1} = F(V)$
0173	Store	0092	
0174	Add	0051	
0175	Clear		
0176	Store	0091	Store 0 in 0091 $\frac{(K-1)^2z}{(K-1)V+1}$ 2 accumulation
0177	Clear, add	0174	
0178	. . . . .	0095	
0179	Store	0181	
0180	Clear, add	0091	
0181	Stop	0181	From 0179
0182	Store	0091	$\frac{(K-1)^2z}{(K-1)V+1}$ 2
0183	Clear, add	0095	
0184	Change on zero	0188	
0185	Subtract	0093	
0186	Store	0095	
0187	Change unconditionally	0177	
0188	Clear, add	0092	$F(V)$
0189	Shift right	0002	Test $F(V)$ for 0 to eight places
0190	Change on zero	0205	
0191	Clear, add	0092	$F(V)$
0192	Divide	0091	$\frac{F(V)}{F^1(V)}$
0193	Add	0098	New $V_{j+1} = V_j + \frac{F(V)}{F^1(V)}$
0194	Store	0098	
0195	Change unconditionally	0128	
0196	Clear, add	0121	$K - 1$
0197	Multiply	0098	$(K-1)V$
0198	Add	0099	$(K-1)V + 1$
0199	Clear, add	0001	z
0200	Shift right	0004	
0201	Divide	0096	$\frac{z}{(K-1)V+1} = y$
0202	Store	0061	

Table 6-15. Program for Flash-vaporization Calculation by Newton's Method (*Continued*)

Storage address	Order	Address	Explanation
0203	Multiply, round	0011	$Kx = y$
0204	Store	0071	
0205	Clear, add	0195	
0206	Add	0095	
0207	Store	0220	
0208	Clear, add	0199	
0209	Add	0095	
0210	Store	0224	
0211	Clear, add	0202	
0212	Add	0095	
0213	Store	0227	
0214	Clear, add	0203	
0215	Add	0095	
0216	Store	0228	
0217	Clear, add	0204	
0218	Add	0095	
0219	Store	0229	
0220	Stop	0220	From 0207, $K - 1$
0221	Multiply	0098	$(K-1)V$
0222	Add	0099	$(K-1)V + 1$
0223	Store	0096	
0224	Stop	0224	From 0210, z
0225	Shift right	0004	
0226	Divide	0096	$\frac{z}{(K-1)V+1} = x$
0227	Stop	0227	From 0213, store x
0228	Stop	0228	From 0216, $Kx = y$
0229	Stop	0229	From 0219, store y
0230	Clear, add	0095	
0231	Change on zero	0235	If zero, all components computed
0232	Subtract	0093	Reduce address modifier
0233	Store	0095	
0234	Change unconditionally	0205	Return to compute next component
0235	Write (20)	0001	Print out z and K
0236	Write (1)	0098	Print out V
0237	Write (20)	0061	Print out x and y
0238	Clear, add	0094	Address modifier
0239	Store	0095	Restore modifier
0240	Stop	0240	
0241	Shift right	0001	
0242	Divide	0096	
0243	Change unconditionally	0151	
0244	Multiply	0096	
0245	Shift left	0001	
0246	Round		
0247	Change unconditionally		
. . . .	Start	0114	

Address Modification

The computer must accomplish all this automatically; therefore, instructions 0114 to 0162 are designed to accomplish address modification. The instruction in cell 0114 treats the instruction in cell 0100 as data and adds it to the A register; then contents of cell 0095 are added to it. Since cell 0095 contains the number 0000000009, the A register contains a number that, if translated into an instruction, would read "clear, add 0020," which is the instruction to add the K for the last component. This instruction is then stored in cell 0120, where it will be performed in the normal sequence. Thus, an order has been computed by modifying its address. The cell 0120, where the computed command is placed, initially contains the order "stop 0120" as a dummy command so that other commands would be stored in their proper cells when read into the computer. A stop instruction is used in order to stop the computer on reaching this step if the computer instruction is not properly handled. This is of importance only during the checking of a code for errors. For this reason, the address of the cell is given in instruction to aid the operator in locating the error.

The next three orders 0017, 0118, and 0119 modify the address of instruction 0102 and store it in cell 0122. The code for the next three steps now reads:

0120: clear, add 0020
0121: subtract 0099
0122: store 0030

This sequence is the same as the first three instructions with one exception: instead of computing $K - 1$ for the first component, it computes $K - 1$ for the last (or tenth) component.

Next, the address modifier is added to register A and tested for 0. Since it is not 0, the next step is performed: 1 is subtracted from the modifier, making it 8. The new modifier is stored in the cell that contained the old one, which is destroyed. Then the step in cell 0127 changes the sequence in which the computer proceeds to cell 0114. Thus, the above address modification and computation are repeated. However, since cell 0095 now contains 8 instead of 9, $K - 1$ is computed for the ninth component. This process is repeated until $K - 1$ has been computed for all the components. At that time the contents of cell 0095 will have been reduced to 0; so when the address modifier is tested for 0 by order 0124, the sequence is changed so that steps 0125 to 0127 are skipped. Instructions of 0128 and 0129 restore the original value for the address modifier to cell 0095 for future use. This is the reason for storing the value for the address modifier twice.

The process of address modification and calculation just outlined in detail is repeated in cells 0130 to 0162 for the instructions in cells 0103 to 0113. It should be noted that instructions 0101, 0104, 0105, 0106, 0108, 0109, and 0112 are not necessary to the program since they do not need to be modified; they are included here only to simplify the explanation. It should also be noted that the computation is started at cell 0114. Instructions 0163 to 0173 show the computation of $\Sigma_n(K_n - 1)z_n/[(K_n - 1)V + 1]$ without address modification; cells 0174 to 0187 illustrate the calculation of a similar sum, $\Sigma(K - 1)^2z/[(K - 1)V + 1]^2$, with address modification. Eleven commands are necessary to sum and store the sum without address modification; 14 are required with address modification. In this case, the computing time and the number of storage cells required are at a minimum without address modification. However, if the digital computer is equipped with an address-modification register, the difference in time will not be appreciable and fewer storage spaces will be required. Also, if more components are involved, the address-modification system requires less storage space.

Branching

Commands 0188 to 0190 test

$$\sum \frac{(K_n - 1)z_n}{(K_n - 1)V + 1}$$

for 0 to eight places, which determine whether or not Eq. (6-15) has been satisfied. Order 0189 shifts the last two digits out of the register. They are replaced in the process by 0's entering the first two digits. After this shift, if the first eight digits in $F(V)$ are 0's, the A register will be all 0's. By changing the number of shifts, a number may be tested for 0 to any number of places. If $F(V)$ is not 0, a new V is computed by Newton's method in commands 0188 to 0193. The new V is then placed in 0098, erasing the old V. Cell 0195 changes the sequence of operation and returns to the start of the program to recompute the values for the new V. This is repeated until $F(V)$ becomes 0 to eight places.

After Eq. (6-15) has been satisfied, x_n and y_n are computed, using the address-modification system, by instructions 0196 to 0234. Then all the pertinent values associated with the solution are printed out by the instructions in cells 0235 to 0237. Instructions 0238 and 0239 restore the address modifier, so that, for the next problem, it is necessary only to enter the z_n, K_n, with new data and restart the computer. The cell 0240 instruction stops the computer, since the calculation is complete.

Corrections

The next group of instructions are examples of corrections to the program. When an attempt to run

the program was made, an overflow occurred after a division that was called for by cell 0150.

A check revealed that the decimal point was not aligned for this division. The correction was made by replacing the instruction with a change in sequence order to the end of the program cells 0241 to 0243. Here the decimal point is aligned, the division performed, and the computation returned to the former sequence at cell 0151. If the decimal-point-alignment instruction had been inserted directly into the program, all addresses of the subsequent instructions would have needed to be changed; some of the addresses in the instructions would also have had to be redetermined. It was also found necessary to readjust the decimal point after originally multiplying at cell 0154. This, as well as the rounding off of the product, was accomplished by replacing cell 0154 with a change in sequence order and instructions in cells 0243 to 0246.

Subroutines

The coding principles illustrated above have been further simplified by the use of subroutines. Common mathematical functions such as sine, cosine, tangent, cotangent, logarithm, exponential, etc., have been coded for most computers in the form of subroutines. These subroutines are stored in the computer so that the programmer can place a number in the A register, change the sequence to a subroutine address that will compute the function, and then return the control to the main program. Such a subroutine determines a mathematical function by expanding a series equal to the function. This method must be used, since the computer, like a desk computer, can perform only a limited number of operations. Any book on numerical analysis will be useful in finding a mathematical approach suitable for the digital computer.

Table Lookup

Some mathematical functions representing data are too complex and involved to determine and code in a reasonable time. Under these conditions a "table-lookup" procedure can be used. For purposes of illustration, a small section of such a table is included as Table 6-16.

Table 6-16. Function of X to Illustrate Table-lookup Procedure

X	$F(X)$
0	84270
1	84681
2	85084
3	85478
4	85865
5	86244
6	86614
7	86977
8	87333
9	87680
10	88021

In order to use the "table-lookup" method, the table must be stored in sequence at some predetermined address. In this case the values for the function are stored beginning at address 1200. The value for X, or the argument, is determined and stored at 1199 as a part of the main program. The computation of the function of X is programmed as follows.

In this program the first three digits of the argument X plus 1200 form the address at which the function is stored. Thus, the tabulated values of the function just above and just below the actual value may be determined by making the first three digits in the argument X a part of the address of an instruction. The program is entered at cell 1505, and X is positioned in the A register so that the first three digits appear in the last three digits on the right. When this value is added to the instructions in cells 1502 and 1504, the order to add the function of X for the nearest tabulated value below X is formed. When an identical value is added to the instruction in cell 1503, the order to subtract the function of X, for the nearest tabulated value above X, is formed. A straight-line interpolation between these two tabulated values is obtained by placing X in the A register and shifting to the left a sufficient number of times to move the first three digits out of the A register. The number remaining is the interpolation factor by which the difference between the nearest tabulated values is multiplied.

The resulting value is added to the nearest value of the function tabulated below X to give a close approximation of the function for the value of X.

Greater accuracy may be obtained by storing additional values in the table. Or the three nearest points may be read from the table to form the data with which the computer is to determine the equation of a parabola. This equation is then used to determine the value of the function for the value of X.

A few of the broad procedures used in a stored-program digital computer have been presented by use of the symbolic-instruction system. Although general procedures are the same for all equipment, specific details must be obtained from the supplier of the equipment to be used by the programmer. Also, suppliers of some equipment maintain exchange libraries from which codes for many common problems may be obtained.

Figures 6-76 and 6-77 show computers typical at the time of this writing.

Fig. 6-76. The IBM 650 Magnetic Drum Data Processing Machine, a data-processing machine for commercial use, consists of three units. The drum and electronic calculating components are housed in two separate cabinets, one of which is provided with a console. The third unit provides input and output facilities.

This machine is designed to meet the vast accounting and computing requirements in areas between those now served by the company's "giant brains" and those served by its widely used smaller machines. It has up to 20,000 memory positions which are used for storage of data and operating instructions. (*Courtesy International Business Machines Corp.*)

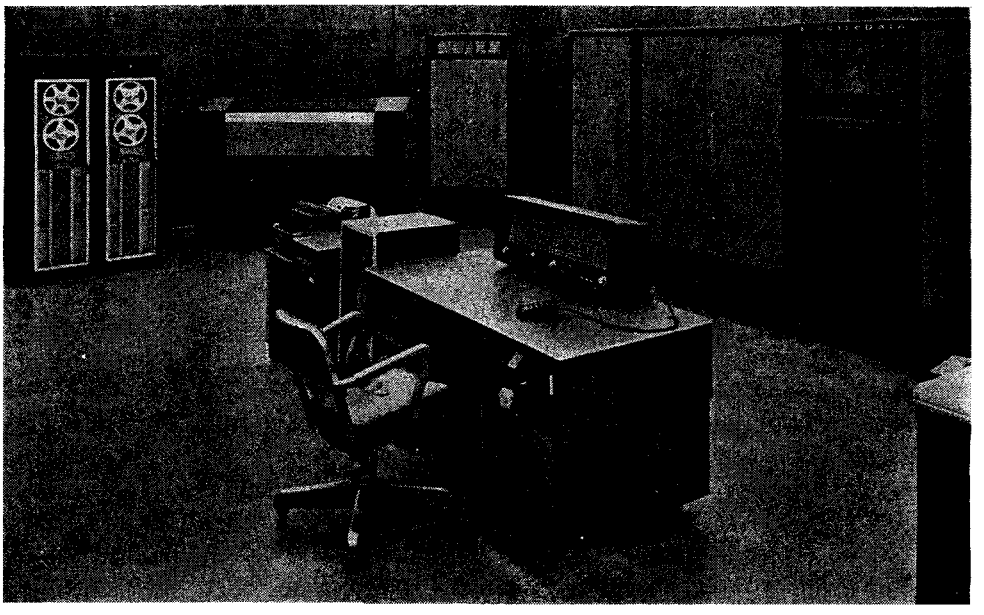

Fig. 6-77. Close-up of Burroughs ElectroData Division contract computing center. Included in the Datatron electronic data-processing system is ElectroData's latest product addition—the Datafile multiple magnetic-tape unit. The size of an ordinary deepfreeze, Datafile provides compact storage and rapid access to virtually unlimited volumes of information. Datafile's new design concept physically "segmentizes" information by eliminating conventional tape reels, using 50 short lengths of magnetic tape to store 20 million characters. Up to ten Datafiles may be used with one Datatron electronic data-processing system. (*Courtesy ElectroData, Div. Burroughs Corp.*)

Table 6-17. Program for Computing $F(X)$ by "Table Lookup"

Storage address	Order	Address	Explanation
1199	0010345000	....	X = 001.0345000
1200	0842700000		
1201	0846810000		
1202	0850840000		
1203	0854780000		
1204	0858650000		
1205	0862440000		
1206	0866140000		
1207	0869770000		
1208	0873330000		
1209	1876800000		
1210	0880210000		
1500	.....	....	00000001.03
1501	.....	....	4500000000
1502	Clear, add	1100	
1503	Subtract	1101	
1504	Add	1100	
1505	Clear, add	1199	X = 001.0345000
1506	Shift right	0005	A register contains 00000001.03
1507	Store	1500	
1508	Clear, add	1199	
1509	Shift left	0005	A register contains 4500000000
1510	Store	1500	
1511	Clear, add	1502	A register contains: Clear, add 1100

Table 6-17. Program for Computing $F(X)$ by "Table Lookup" (*Continued*)

Storage address	Order	Address	Explanation
1512	Add	1500	A register contains: Clear, add 1203
1513	Store	1520	Instruction to look up first X
1514	Clear, add	1503	A register contains: Subtract 1101
1515	Add	1500	A register contains: Subtract 1204
1516	Store	1521	Instruction to look up and subtract second X
1517	Clear, add	1504	A register contains: Add 1100
1518	Subtract	1500	A register contains: Add 1203
1519	Store	1523	Instruction to look up and subtract first X
1520	Stop	1520	Instruction from 1513: $F(X)$ = 0854780000
1521	Stop	1521	Instruction from 1516: $F(X) - F(X)_2 = -0003870000$
1522	Multiply	1501	Interpretation: $[F(X)_1 - F(X)]$ $[F(X)_1 - F(X)_2]$ $= -0001741500$
1523	Stop	1523	Instruction from 1519: $F(X)$ = 0856521500
1523	Store		

CHAPTER 7

Flow and Compression Calculations

If utility is to be derived from its use, natural gas must be transported efficiently from reservoir to ultimate consumer. Efficient transportation of natural gas involves application of the principles of fluid flow.

The earliest records of the transportation and use of natural gas are Chinese. As early as 900 A.D., the Chinese transmitted natural gas, issuing from coal beds, in bamboo pipe to their salt workings, where brine was evaporated by heat supplied by the burning gases. Parts of Peking were illuminated by gas transmitted in bamboo pipe. In use of natural gas for domestic and industrial purposes, the Chinese outstripped by centuries the peoples of the Western hemisphere. It was not until early in the nineteenth century that natural gas for industrial and domestic purposes was used in the West.

In 1827 lead pipe was used for the short-distance transportation of gas in the town of Fredonia, N.Y. The gas was used to supply about a hundred street lights.

One of the earliest means used in the United States for transporting gas for long distances was wooden pipe. In 1870, the Bloomfield and Rochester Natural Gas Light Company initiated the construction of a 25-mile wooden pipeline from wells in the West Bloomfield, N.Y., area to Rochester. The pipe was constructed of Canadian white pine 12½ in. in diameter and in sections 2 to 8 ft long. The inside diameter of the pipe was 8 in. Bell-and-spigot-type joints were used. The pipe was tarred both inside and out. As a result of overpressuring during a test, the line sprang so many leaks that it was beyond repair and could not deliver gas pressure much above 1 psi.

The use of wood soon proved unsatisfactory. Lead was too expensive. Cast iron was limited to small-size pipe because of the nature of the joints and the inability of the pipe to withstand high pressure. One of the first uses of steel pipe was in the Titusville, Pa., area in 1872. The first really large-diameter line was used by the Equitable Gas Company of Pittsburgh, Pa.; this was a 36-in. line 21½ miles long, south of Pittsburgh. The pipe was made of ¼-in. steel plate riveted together and then caulked to prevent leakage. The development of steel pipe introduced the era of long-distance high-pressure gas transmission.

Interesting discussions of the early history of the production and transportation of natural gas can be found in the introductory chapters of J. C. Diehl's "Natural Gas Handbook" (7-14), in "Natural Gas Engineering" by M. M. Stephens and O. F. Spencer (7-40), and in "A Practical Treatise on Petroleum" by Crew (1-5).

The production and transmission of natural gas in the United States have reached a high degree of technological development. Table 1-1 shows that 10.2 trillion cu ft of gas was transported to market in 1956. The great bulk of this gas was transported from the oil- and gas-producing provinces of the Southwest for domestic and industrial use in the urban centers of the North and Northeast. The natural gas pipelines are shown in Fig. 1-1.

Along with this development has come new knowledge of the factors that enter into the design of gas-transmission systems, such as the physical and thermodynamic properties of the natural gas and the manner in which these properties affect the flow characteristics of the gas. It is the purpose of this chapter to present and discuss the various equations used in describing the flow and compression behavior of natural gas.

THE FLOW EQUATION

The basis of any fluid-flow calculation is a statement of energy balance on the fluid flowing between any two points of the system under consideration. It is well known that a certain amount of energy is necessary to overcome the resistance that any flowing fluid encounters in its path. The basic energy relationship of any fluid-flow process stems from the law of conservation of energy, which states merely that the energy of the fluid entering the conduit minus the energy dissipated in the conduit through irreversible

effects plus any work energy added to the fluid is equal to the energy of the fluid leaving the conduit. This is expressed by the well-known thermodynamic-flow equation for a unit mass of fluid in transit between two points, such as 1 and 2 of Fig. 7-1 (7-9).

$$\Delta H + \Delta \frac{v^2}{2g_c} + \frac{g}{g_c} \Delta X = q - w \qquad (7\text{-}1)$$

where $\Delta H = H_2 - H_1$ = the increase in enthalpy between the initial and final states

$\Delta \frac{v^2}{2g_c}$ = difference in kinetic energy (v = velocity, ft/sec) of flowing fluid, $\frac{(\text{sq ft})(\text{ft-lb force})(\text{sec}^2)}{(\text{sec}^2)(\text{ft-lb mass})(\text{ft})}$

g = acceleration of gravity, ft/sec^2

g_c = 32.174, conversion factor, [ft-lb mass/(ft)(lb force)](ft/sec^2)

$\Delta X = X_2 - X_1$ = difference in elevation, ft

q = heat absorbed by system from surroundings, ft-lb force/lb mass

w = work done by the fluid while in flow, ft-lb force/lb mass

This equation is useful when heat is transferred or when the system is adiabatic ($q = 0$). However, it does not permit the identification of the energy lost because of irreversibilities through friction. An alternative equation (7-2) may be derived, which includes a term lw for the work energy dissipated through irreversibilities such as fluid friction.

$$\int_1^2 V\,dP + \Delta \frac{v^2}{2g_c} + \frac{g}{g_c} \Delta X + lw + w = 0 \qquad (7\text{-}2)$$

where V = the specific volume of flowing fluid, cu ft/lb mass

P = pressure, lb force/sq ft

lw = work energy lost in overcoming friction, ft-lb force/lb mass

This equation states that the sum of the changes in potential energy of compression or expansion, $\int V\,dP$; the kinetic energy $\Delta v^2/2g_c$; the potential energy $(g/g_c)\,\Delta X$ of position; the potential energy lw lost through irreversibilities; and the work w done by the flowing fluid must equal zero. Equation (7-2) contains no limiting assumptions about compression, kinetic, and position energies; it can be made the basis of any specific fluid-flow relationship when surface, electrical, and chemical energies are negligible. The units of all the terms are foot-pounds force per pound mass. Noting that a pound mass is the equivalent of a pound force due to gravity, one converts the quantities to read directly in feet, and finds head in feet of fluid flowing.

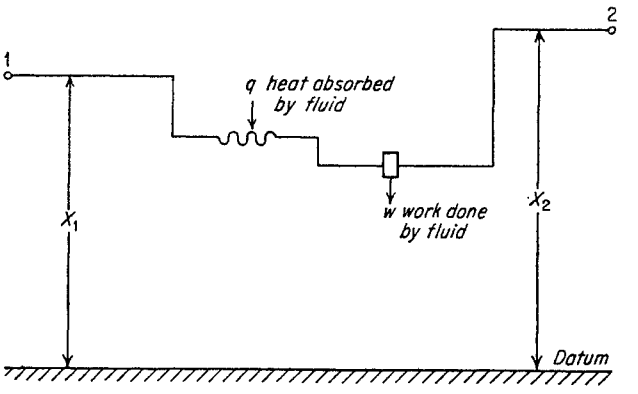

Fig. 7-1. Continuous-flow system.

CALCULATION OF STATIC BOTTOM-HOLE PRESSURE IN GAS WELLS

A knowledge of the static bottom-hole pressure of a gas reservoir is of prime importance in predicting the reserves and deliverability of the gas in the reservoir. Because of the importance of this factor, much attention has been paid to its measurement and to its calculation from known surface properties. Because of the time and expense involved in direct measurement of static bottom-hole pressures, methods of calculating these pressures from surface information are preferred. Calculation methods have been developed which, in general, are well within the range of accuracy of present physical measurement methods (7-17, 7-30, 7-32, 7-34).

All of the calculation methods developed are based on the general flow equation (7-2). A static column of gas with no fluid velocity, friction, or work is just a special case of Eq. (7-2), which reduces to

$$\int_1^2 V\,dP + \frac{g}{g_c} \Delta X = 0 \qquad (7\text{-}3)$$

Assuming

$$g = g_c$$

numerically, replacing V by $znRT/P$ from Eq. (4-2), and letting $n = 1/29G$, one obtains

$$\Delta X = \int_1^2 \frac{zRT}{29GP}\,dP \qquad (7\text{-}4)$$

Given certain assumptions, Eq. (7-4) becomes the starting point for the derivation of equations for calculating static bottom-hole pressures of gas wells. Needless to say, the equation involving the least assumptions should be the most accurate. In all cases, four factors must be known: well effluent composition, well depth, wellhead pressure, and well-bore temperature. The gas composition is used to calculate the

pseudocritical properties of the gas, from which is estimated the value of the compressibility-factor function used in the calculations. Quite often gas composition is not known, and gas gravity must be used to estimate the pseudocritical properties (Fig. 4-22).

The well depth–temperature traverse is quite often a straight-line relationship (Fig. 1-32). When this is the case, it can be shown that the log mean temperature is the rigorous average temperature to be used in calculating static bottom-hole pressure, as follows.

Writing the temperature T in terms of depth X,

$$T = aX + b \tag{7-5}$$

and

$$dT = a\,dX \tag{7-6}$$

By writing Eq. (7-4) in differential form and substituting Eq. (7-6) in (7-4), one obtains

$$\frac{dT}{aT} = \frac{zR}{29GP}\,dP \tag{7-7}$$

Integrating,

$$\frac{1}{a}\ln\frac{T_2}{T_1} = \int_1^2 \frac{zR}{29GP}\,dP \tag{7-8}$$

Since

$$a = \frac{T_2 - T_1}{\Delta X}$$

$$\frac{\Delta X}{(T_2 - T_1)/[\ln\,(T_2/T_1)]} = \frac{\Delta X}{T_{\text{lm}}} = \int_1^2 \frac{zR}{29GP}\,dP \tag{7-9}$$

Equation (7-4) can be solved when T and z are assumed to be constant average values as follows:

$$\frac{\Delta X\,29G}{T_a z_a R} = \int_1^2 \frac{dP}{P} = \ln\frac{P_2}{P_1} \tag{7-10}$$

or

$$\frac{P_2}{P_1} = \exp\frac{29G\,\Delta X}{T_a z_a R}\,* \tag{7-11}$$

or

$$P_2 = P_1 \exp\frac{29G\,\Delta X}{T_a z_a R} \tag{7-12}$$

or

$$P_2 - P_1 = P_1\left(\exp\frac{29G\,\Delta X}{T_a z_a R} - 1\right) \tag{7-13}$$

Rawlins and Schellhardt in monograph 7 (7-32) used this form of the equation for a gas temperature of 80°F and ideal gases. Converting to field units, as suggested by Rzasa and Katz (7-34), one obtains Eq. (7-14).

$$\Delta P = P_2 - P_1 = P_1\left(\exp\frac{0.01877GX}{T_a z_a} - 1\right) \tag{7-14}$$

where P_2 = bottom-hole pressure, psia
P_1 = wellhead pressure, psia
G = gas gravity
X = depth of well, ft
T_a = average well-bore temperature, °R
z_a = compressibility factor at mean well-bore temperature and pressure

In deriving this equation, the compressibility factor and temperature are assumed to be constant. This equation involves a trial-and-error solution for the compressibility factor, but in many cases is not very sensitive to the pressure. Values of P_2 are assumed in order to obtain a value of z_a; P_2 is then calculated. The procedure is repeated until the value of P_2 assumed in obtaining z and the calculated values of P_2 are in agreement.

Another method reported by Rzasa and Katz (7-34) assumes a constant average pressure, temperature, and compressibility factor, and field units the same as in Eq. (7-14).

$$\Delta P\left(1 - \frac{0.00938XG}{z_a T_a}\right) = 0.01877\,\frac{XG}{z_a T_a}\,P_1 \tag{7-15}$$

This equation, like Eq. (7-14), is solved by trial and error. The smaller one takes the increment of depth, the greater is the accuracy of the result. At the limit, Eq. (7-4) may be integrated, using the actual relationship between T and depth if this is known and assuming values of P versus X until the equation is solved.

The method presented by Fowler (7-17) and Sukkar and Cornell (7-41) involves integrated values of the compressibility factor with pressure; it is a direct method of calculating bottom-hole pressure, the only assumption being that average temperature is constant. By using the log mean temperature for conditions where temperature varies linearly with depth, the assumption of constant temperature can be confined to the value within the integral. Converting Eq. (7-9),

$$\frac{X29G}{T_{\text{lm}}R} = \frac{0.01877XG}{T_{\text{lm}}} = \int_1^2 \frac{z}{P}\,dP = \int_1^2 \frac{z}{P_r}\,dP_r \tag{7-16}$$

Also

$$\int_{0.2}^{P_{r,2}} \frac{z}{P_r}\,dP_r - \int_{0.2}^{P_{r,1}} \frac{z}{P_r}\,dP_r = \int_1^2 \frac{z}{P_r}\,dP_r \tag{7-17}$$

$$\int_{0.2}^{P_{r,2}} \frac{z}{P_r}\,dP_r = 0.01877\,\frac{XG}{T_{\text{lm}}} + \int_{0.2}^{P_{r,1}} \frac{z}{P_r}\,dP_r \tag{7-18}$$

The term corresponding to the tubing pressure,

$$\int_{0.2}^{P_{r,1}} \frac{z}{P_r}\,dP_r$$

is obtained directly from Table A-4, given the reduced temperature and pressure at the surface. The term

* Note that $\exp y = e^y$, where e is the base of the natural logarithms.

$0.01877XG/T_{lm}$ can be directly evaluated; the sum of the two then gives the term

$$\int_{0.2}^{P_{r,2}} \frac{z}{P_r}\, dP_r$$

corresponding to the bottom-hole pressure. The pseudoreduced bottom-hole pressure corresponding to this value can then be obtained from Table A-4. Multiplying this pseudoreduced pressure by the pseudocritical pressure gives the static bottom-hole pressure.

Illustrative Problem

Calculate the static bottom-hole pressure of a gas well having a depth of 5,790 ft. The gas gravity is 0.600 and the pressure at the wellhead is 2,300 psia. The average temperature of the flow string is 117°F.

From Fig. 4-22 $T_c = 358°R$

$P_c = 672$ psia

$$T_r = \frac{T}{T_c} = \frac{117 + 460}{358} = 1.612$$

$$P_{r,1} = \frac{P}{P_c} = \frac{2,300}{672} = 3.423$$

From Table A-4

$$\int_{0.2}^{P_{r,1}} \frac{z}{P_r}\, dP_r = 2.629$$

$$\frac{0.01877XG}{T_{lm}} = \frac{0.01877 \times 5,790 \times 0.600}{577} = 0.113$$

From Eq. (7-18)

$$\int_{0.2}^{P_{r,2}} \frac{z}{P_r}\, dP_r = 2.629 + 0.113 = 2.742$$

From Table A-4

2.742 at a T_r of 1.612 corresponds to a $P_{r,2}$ of 3.918

Therefore

$$P_2 = 3.918 \times 672 = 2,633 \text{ psia}$$

Fowler's method provides a direct, accurate solution for the static bottom-hole pressure of a gas well.

Solution by Eq. (7-14)

$$P_2 - 2,300 = 2,300\left(\exp \frac{0.01877 \times 0.6 \times 5,790}{577 \times z_a} - 1\right)$$

Assume $P_2 = 2,500$ psia. Then $P_{av} = 2,400$.

$$P_r = \frac{2,400}{672} = 3.57 \qquad T_r = \frac{577}{358} = 1.612 \qquad z = 0.822$$

$$P_2 - 2,300 = 2,300\left(\exp \frac{0.1127}{z_a} - 1\right) = 2,300(\exp 0.137 - 1)$$

$e^{0.137}$ found on log-log slide rule: 137 on D scale; 1.147 on $LL2$ scale.

$$P_2 - 2,300 = 2,300(1.147 - 1) = 338 \text{ psi}$$

$$P_2 = 2,638 \text{ psia}$$

Second trial:

$$P_{av} = 2,469 \qquad P_r = 3.67 \qquad z_a = 0.822$$

No change in z_a for this case; so first trial is sufficient.

Solution by Eq. (7-15)

$$\Delta P\left(1 - \frac{0.00938GX}{T_a z_a}\right) = 0.01877 \frac{XG}{T_a z_a} P_1$$

Evaluate $\dfrac{0.01877XG}{T_a z_a} = \dfrac{0.01877 \times 0.6 \times 5,790}{577 \times 0.822} = 0.137$

$$\Delta P\left(1 - \frac{0.137}{2}\right) = 0.137 \times 2,300$$

$$\Delta P = \frac{0.137 \times 2,300}{0.9315} = 0.147 \times 2,300 = 338 \text{ psi}$$

Figure 7-2 gives a plot of calculated pressure gradients in gas wells for a gas gravity of 0.7 and typical depth-pressure-temperature relationship (7-34).

For shallow fields where the compressibility factor is a relatively minor factor, the ΔP may be expressed according to Eq. (7-14) in the following form:

$$P_2 = P_1 \exp c = P_1 c' \qquad (7\text{-}19)$$

For example, for wells 1,200 ft deep, with average temperature 55°F, and containing 0.62 gravity gas, the equation becomes

$$P_2 = P_1 \exp \frac{0.01877 \times 0.62 \times 1,200}{515}$$

$$= P_1 \exp 0.0271 = 1.028P_1 \qquad (7\text{-}20)$$

FRICTION IN PIPE

The term lw of Eq. (7-2) represents all energy losses resulting from irreversibilities of the flowing stream. In the case of single-phase flow, such as flow of gas in pipe, these irreversibilities consist primarily of friction losses, both internal losses due to viscosity effects and losses due to the roughness of the wall of the confining flow string.

With the exception of completely laminar flow, the energy losses lw of actual systems cannot be predicted theoretically, but must be determined by actual experiment and then correlated as some function of the flow variables. Such a relationship is the well-known equation

$$lw = \int_1^2 \frac{fv^2}{2g_c D}\, dL = \frac{fv^2 L}{2g_c D} \qquad (7\text{-}21)$$

where the factor f is a dimensionless correlating function, the friction factor. By means of dimensional analysis it can be shown that the friction factor f is a function of the Reynolds number $Dv\rho/\mu$ and of the relative roughness e/D, which is the ratio of absolute roughness to pipe diameter. Roughness is defined as the distance from peaks to valleys in pipe-wall irregularities. Figure 7-3 shows a plot of f as a function of Reynolds number and relative roughness, as presented by Moody (7-25). Quite often the Fanning friction factor f' is used; $f' = f/4$. The Reynolds number Re

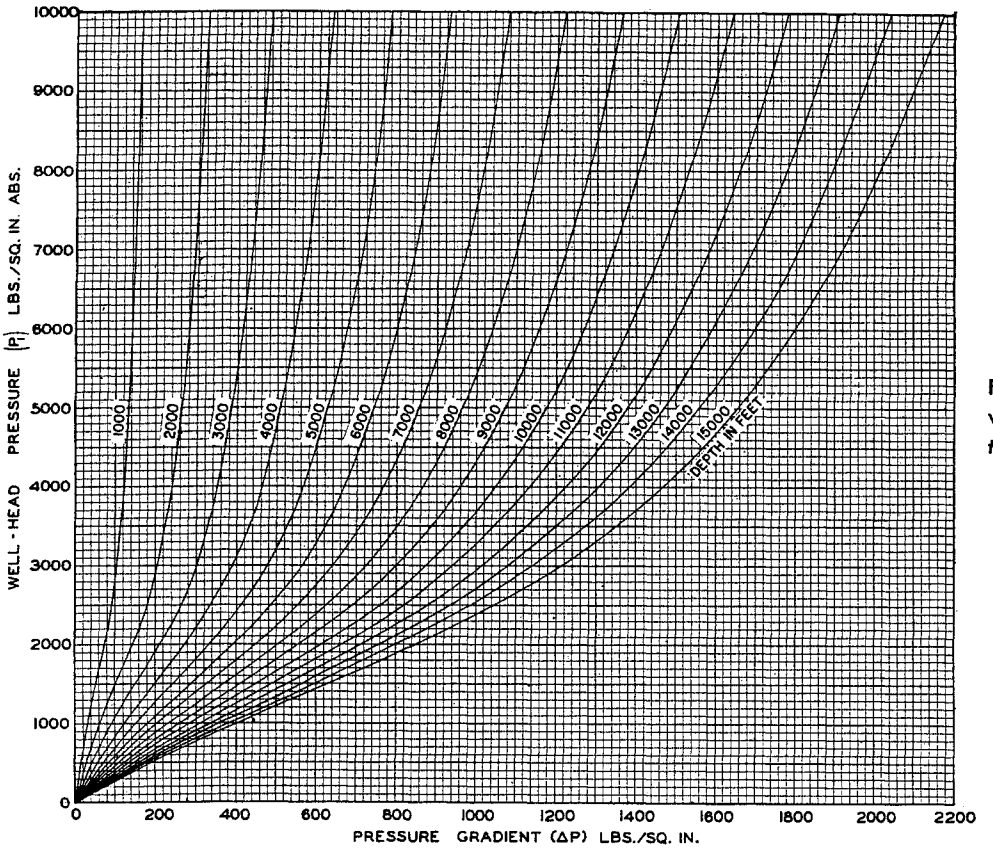

Fig. 7-2. Pressure gradients in gas wells. (*Katz and Rzasa, 7-34. Courtesy AIME.*)

is dimensionless,* but may be converted to field units.

$$\mathrm{Re} = \frac{Dv\rho}{\mu} = \frac{DW}{\mu A} = \frac{4dQ \times 12 \times 29G \times 1{,}000}{\mu 24\pi d^2 \times 379 \times 2.42} = 20.0\,\frac{QG}{\mu d} \qquad (7\text{-}22)$$

where Q = gas flow at 60°F and 14.7 psia, Mcf/day
G = gas gravity
W = mass flow, lb mass/hr
d = diameter of pipe, in.
μ = viscosity, centipoises
A = flow area, sq ft

Fluid flow ranges in nature between two extremes, laminar or streamline flow and turbulent flow (Fig. 7-3). For Reynolds numbers up to 2,100, flow is in the laminar region and f can be expressed by $f = 64/\mathrm{Re}$, which is the equation for the straight line in Fig. 7-3. It is to be noted that, in the laminar region of flow, the f factor is independent of pipe roughness. The stagnant film on the pipe surface minimizes the roughness of the pipe, and resistance to flow is due primarily to the internal resistance to shear, that is, the viscosity of the fluid.

* In dimensionless form

$$\mathrm{Re} = \frac{D\ (\mathrm{ft})\ v\ (\mathrm{ft/sec})\ \rho\ (\mathrm{lb/cu\ ft})}{\mu\ [\mathrm{lb/(ft)(sec)}]}$$

μ in pounds per foot per second = centipoises × 0.000672.

For Reynolds numbers between 2,100 and 4,000, flow is in an unstable region, as indicated by the shaded area of Fig. 7-3. At Reynolds numbers greater than 4,000, flow is partially turbulent, falling in the region of transition; it definitely becomes a function of relative roughness, with viscosity effects becoming less significant. In this region of transition (Fig. 7-3) the f factor is expressed by the empirical equation proposed by Colebrook (7-11).

$$\frac{1}{\sqrt{f}} = 2\log\frac{D}{e} + 1.14 - 2\log\left(1 + 9.34\,\frac{D/e}{\mathrm{Re}\sqrt{f}}\right) \qquad (7\text{-}23)$$

Smith and coworkers (7-36, 7-37, 7-38) have shown from carefully executed experimental studies that in actuality the f factors in the region of transition lie between those empirically predicted by the Colebrook relationship (7-11) and those predicted by Nikuradse (7-28) using pipes artificially roughened with coatings of uniform sand grains. According to these studies, use of the Colebrook expression in the transition region will lead to conservative design results.

For turbulent flow in smooth pipe—that is, pipe of zero roughness—the f factor (Fig. 7-3) over the entire range of Reynolds numbers can be expressed by the following relationship (7-28):

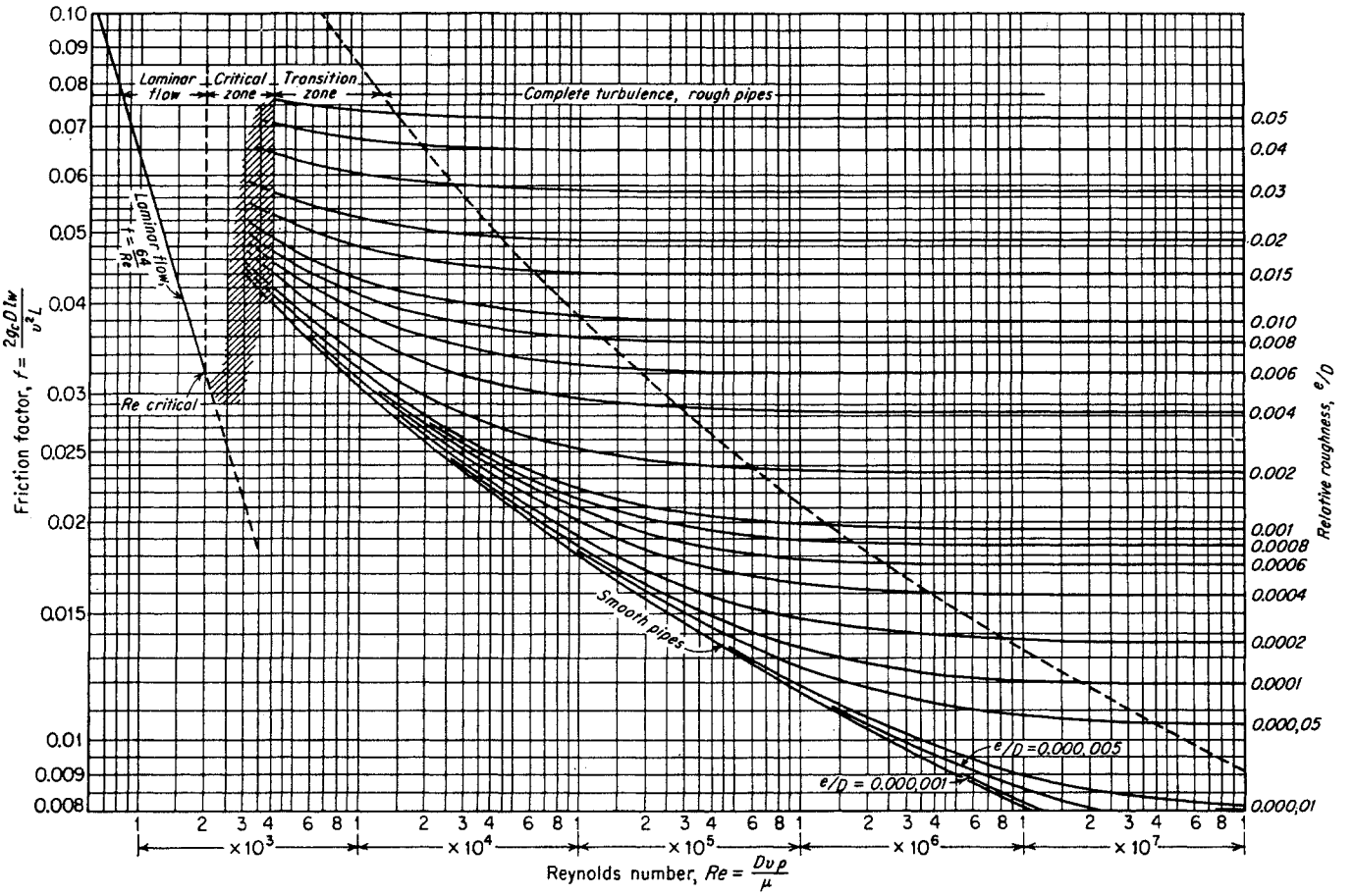

Fig. 7-3. Friction factor for flow of fluids in pipe. (Moody, 7-25. Courtesy ASME.)

$$\frac{1}{\sqrt{f}} = 2 \log (\mathrm{Re}\sqrt{f}) - 0.80 \qquad (7\text{-}24)$$

When flow becomes completely turbulent—that is, beyond the transition region—it is no longer a function of the Reynolds number, but becomes a function of relative roughness e/D only. This is shown in Fig. 7-3, where the f-factor lines are horizontal at high Reynolds numbers. Figure 7-4 shows the variation of f as a function of e/D only for completely turbulent flow. Gas flow at high pressure drops occurs at these high Reynolds numbers. The f factor in this region of flow is completely independent of the physical properties of the flowing fluid. For fully turbulent flow the f factor is expressed by an equation obtained experimentally by Nikuradse (7-28).

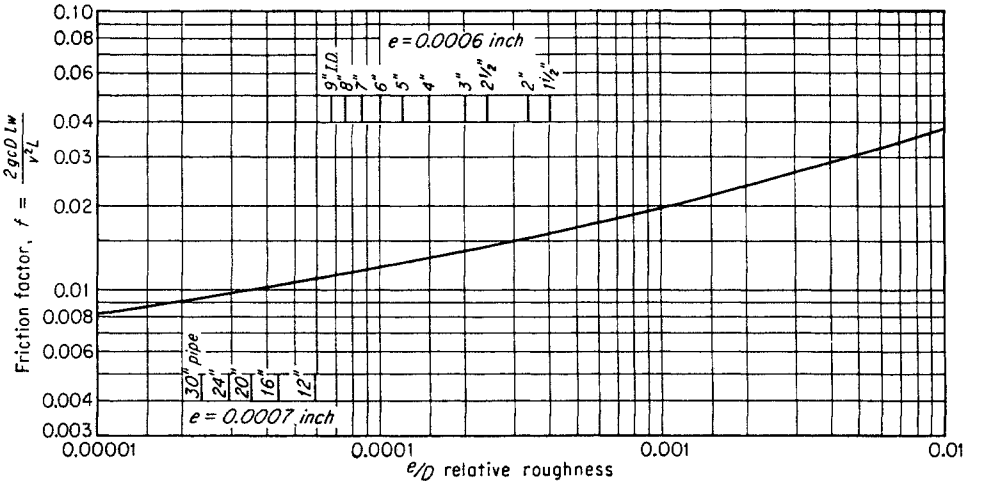

Fig. 7-4. Friction factor at completely turbulent flow as function of roughness.

$$\frac{1}{\sqrt{f}} = 2 \log \frac{D}{e} + 1.14 \qquad (7\text{-}25)$$

Figure 7-5 is a plot of relative roughness e/D as a function of diameter D and absolute roughness e for various types of pipe (7-25). Absolute roughness is best evaluated by an analysis of experimental flow data. Smith and coworkers (7-37, 7-38) have summarized, from their own experimental tests and from data available in the literature, absolute-roughness values for gas-transmission lines, flow strings in gas wells, and experimental pipelines (Table 7-1). These values are valid for clean steel pipe.

For turbulent flow in rough pipelines, the presence of liquid enough to wet the pipe wall will increase the flow capacity of the pipe. However, for laminar flow, the presence of a liquid film will decrease the flow capacity of the pipeline because the viscosity of the liquid in the surface layer is greater than the viscosity of the gas when the pipe is dry.

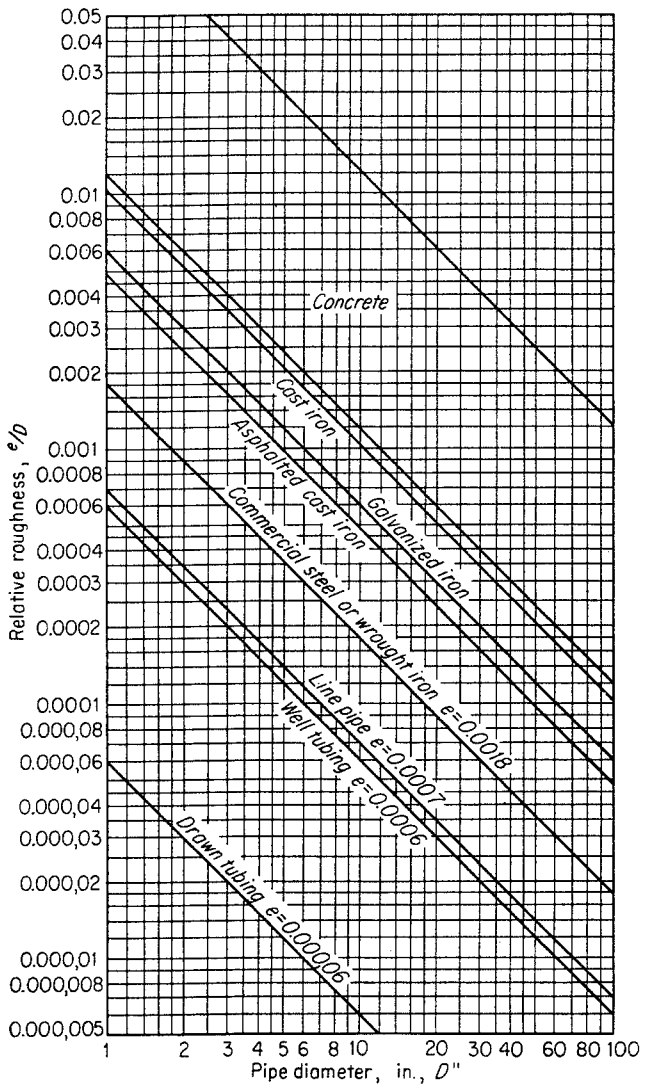

Fig. 7-5. Relative roughness of various pipes. (Moody, 7-25. Courtesy ASME.)

Table 7-1. Values of Roughness for Gas Lines

Reference	Description	Diameter, in.	Absolute roughness e, in.
Smith (7-38).....	Gas-transmission lines (avg)	10–26	0.0007
Smith (7-37).....	Gas wells	1¼–7	0.00065
Cullender (7-13)....	Gas wells	1¼–8⅝	0.0006
Smith (7-38).....	Experimental pipelines	2–8	0.00055–0.0019

PIPELINE-FLOW CALCULATIONS

Engineering of long-distance transportation of natural gas by pipeline requires a knowledge of flow formulas for calculating capacity and pressure requirements. In the early development of the natural gas–transmission industry, pressures were low and the equations used for design purposes were simple and adequate. However, as pressures increased in order to meet increased capacity demands, equations were developed to meet the new requirements.

As stated previously, Eq. (7-2) is the starting point of all fluid-flow relationships involving the evaluation of friction losses. In the case of natural gas transmission, the initial assumptions usually made in the derivation of any specific flow equation are as follows:

1. The kinetic-energy change is negligible and can be taken as zero. With this assumption, Eq. (7-2) becomes

$$\int_1^2 V\,dP + \frac{g}{g_c}\Delta X + lw + w = 0 \qquad (7\text{-}26)$$

2. The flow is steady-state and isothermal.
3. The flow is horizontal.
4. There is no work done by the gas in flow.

Given these assumptions, Eq. (7-2) reduces to

$$\int_1^2 V\,dp + lw = 0 \qquad (7\text{-}27)$$

Substituting for lw from Eq. (7-21) then leaves

$$\int_1^2 V\,dP + \int_1^2 \frac{fv^2}{2g_cD}\,dL = 0 \qquad (7\text{-}28)$$

By making various additional assumptions, Eq. (7-28) can be made the starting point for the derivation of specific flow equations for the transmission of natural gas.

One of the earliest of such equations was that of Weymouth (7-42), now modified to include the compressibility factor (7-9).

$$Q = 3.22 \frac{T_0}{P_0} \left[\frac{(P_1^2 - P_2^2)d^5}{GTLfz_a} \right]^{0.5} \quad (7\text{-}29)$$

where Q = gas flow measured at T_0 and P_0, std cu ft/hr
L = length of line, miles
d = internal diameter (ID), in.
P = pressure, psia
G = gas gravity (air = 1)
T = average line temperature, °R
z_a = average compressibility factor (in Weymouth's original equation $z = 1$)
f = friction factor from Fig. 7-3 or 7-4

Weymouth assumed that f varied as a function of the diameter in inches as follows:

$$f = \frac{0.032}{d^{1/3}} \quad (7\text{-}30)$$

Equation (7-29) then results in

$$Q = 18.062 \frac{T_0}{P_0} \left[\frac{(P_1^2 - P_2^2)d^{16/3}}{GTLz_a} \right]^{0.5} \quad (7\text{-}31)$$

Another equation, the "Panhandle" formula, assumes that f varies as follows:

$$\frac{1}{f} = 52 \left(\frac{GQ}{d} \right)^{0.1461} \quad (7\text{-}32)$$

resulting in

$$Q = 435.87E \left(\frac{T_0}{P_0} \right)^{1.07881} \left(\frac{P_1^2 - P_2^2}{L} \right)^{0.5394} \left(\frac{1}{T} \right)^{0.5394} \left(\frac{1}{G} \right)^{0.4606} d^{2.6182} \quad (7\text{-}33)$$

where Q = gas flow measured at T_0 and P_0, cu ft/day
d = pipe ID, in.
E = efficiency factor (0.92 average)
L = length of pipe, miles
T = mean flowing temperature, °R
P = pressure, psia
G = gravity of gas (air = 1)

The Ford, Bacon, and Davis flow formula for design of pipelines is given by Eq. (7-34).

$$Q = 840EMNd^{2.625} \left(\frac{P_1^2 - P_2^2}{L} \right)^{0.541} \quad (7\text{-}34)$$

where Q = gas flow measured at P_0 and T_0, cu ft/day
E = line flow efficiency (used as 94 per cent)
M = measurement-base adjustment factor

$$M = \frac{14.735}{P_0} \frac{T_0}{520}$$

P_0 = base pressure, psia
T_0 = base temperature, °R
N = gas-characteristic adjustment factor

$$N = B^{0.54} \left(\frac{0.6}{G} \right)^{0.46} \left(\frac{7.0}{\mu} \right)^{0.08} \left(\frac{520}{T} \right)^{0.54}$$

B = $1/z$, or 1+ deviation from Boyle's law at average pressure
G = specific gravity (air = 1.0)
μ = viscosity, English absolute units $\times 10^6$ (centipoises $\times$ 672)
T = flowing temperature, °R
d = pipe ID, in.
P_1 = line input pressure, psia
P_2 = line output pressure, psia
L = length of pipeline, miles

Equation (7-34) applies for 6- to 24-in. lines; the constant becomes 824 for 30-in. lines.

In addition to the Weymouth, Panhandle, and Ford, Bacon, and Davis equations, many others (7-23), such as the Cox and Pittsburgh, have been derived. Hanna and Schomaker (7-20) have presented a revised Panhandle formula, employing the AGA compressibility factors for natural gas.

The specific flow equation of Clinedinst (7-10) takes rigorously into consideration the deviation of natural gas from ideal behavior. This equation is a rigorous integration of Eq. (7-28). The only assumptions are those made in arriving at Eq. (7-28).

$$Q = 3{,}973.0 \frac{z_0 T_0 P_c}{P_0} \left[\frac{D^5}{GTLf} \left(\int_0^{P_{r,1}} \frac{P_r}{z} dPr - \int_0^{P_{r,2}} \frac{P_r}{z} dP_r \right) \right]^{0.5} \quad (7\text{-}35)$$

where Q = volumetric flow rate, Mcf/day
P_c = pseudocritical pressure, psia
D = pipe ID, ft
L = length of pipe, ft
T = flowing temperature, °R
G = gas gravity
z_0 = compressibility factor at T_0 and P_0, normally accepted as 1.0
P_r = pseudoreduced pressure

Values of the integral functions

$$\int_0^{P_r} \frac{P_r}{z} dP_r$$

are obtained from Table A-6.

The use of the Clinedinst equation is perhaps best explained by means of a numerical example.

Illustrative Problem

A pipeline 100 miles long has an internal diameter of 13.375 in. The inlet pressure is 1,300 psia and the pressure at the end of

the line is 300 psia. The temperature of the flowing gas is 40°F, and its composition is as follows:

	Mole %
Methane	75
Ethane	21
Propane	4
	100

Calculate the volumetric flow rate measured at 14.65 psia and 60°F.

Solution

Calculation of pseudocritical and reduced conditions:

Component	Mole fraction	Molecular weight	Lb/mole	P_c, psia	Psia	T_c, °R	°R
Methane..	0.75	16	12.0	673	505	343	257
Ethane....	0.21	30	6.2	708	148	550	115
Propane...	0.04	44	1.7	617	25	666	26
			19.9		678		398

$$G = 0.686$$

$$P_{r,1} = \frac{1{,}300}{678} = 1.91$$

$$P_{r,2} = \frac{300}{678} = 0.44$$

$$T_r = \frac{460 + 40}{398} = 1.25$$

The integral terms, as read from Table A-6, are

$$\int_0^{1.91} \frac{P_r}{z}\,dP_r = 2.43 \qquad \int_0^{0.44} \frac{P_r}{z}\,dP_r = 0.10$$

Using a roughness of 0.0006 in., $e/D = 0.000045$, the f factor as obtained from Fig. 7-4 is

$$f = 0.0104$$

for completely turbulent flow conditions. Then, from Eq. (7-35)

$$Q = \frac{3{,}973.0 \times 1.000 \times 520 \times 678}{14.65} \left[\frac{(1.1145)^5}{0.0104 \times 5.28 \times 10^5 \times 0.686 \times 500}(2.43 - 0.10)\right]^{0.5}$$

$$= 140{,}000 \text{ Mcf/day} \qquad \text{at 14.65 psia and 60°F}$$

In actual practice, transmission lines often deviate considerably from the horizontal. Given all the previous assumptions with the exception of horizontal flow, Eq. (7-2) reduces to

$$\int_1^2 V\,dP + \frac{g}{g_c}\Delta X + \int_1^2 \frac{fv^2}{2g_cD}\,dL = 0 \quad (7\text{-}36)$$

This equation is the starting point for any flow calculations that take into consideration differences in elevation.

One such equation was that developed by Ferguson (7-16), to which has been added a term correcting for the compressibility of the gas.

$$Q = 3.22\,\frac{T_0}{P_0}\left[\frac{(P_1^2 - e^S P_2^2)d^5}{GT_a f z_a L_e}\right]^{0.5} \quad (7\text{-}37)$$

where $e = 2.7183$
d = pipe ID, in.
Q = gas flow, std cu ft/hr, measured at T_0 and P_0
P = pressure, psia
G = gas gravity
T_a = average line temperature, °R
z_a = average compressibility factor
$S = 0.0375GX/T_a z_a$
X = change in elevation, ft (X is positive if outlet is higher than inlet)
L_e = effective length of pipeline, miles

The effective length L_e of the pipeline is based upon the profile of the line between pressure-measuring stations. If the slope is uniform

$$L_e = \frac{e^S - 1}{S} L = JL \quad (7\text{-}38)$$

where $J = (e^S - 1)/S$.

If the slope is not uniform, the profile should be divided into sections of nearly uniform slope; the effective length is then calculated as follows:

$$L_e = L_1J_1 + L_2e^{S_1}J_2 + L_3e^{S_2}J_3 + \cdots + L_ne^{S_{n-1}}J_n \quad (7\text{-}39)$$

where $J_1, J_2, J_3, \ldots J_n$ are calculated for the increase or decrease in elevation in L_1, L_2, L_3, and so forth, and $e^{S_1}, e^{S_2}, e^{S_3}, \ldots e^{S_{n-1}}$ are calculated for the rise or drop from the inlet of the line to the end of sections $L_1, L_2, L_3, \ldots L_{n-1}$, respectively.

As the demand for gas changes and as old transmission systems are extended and paralleled in order to increase line capacity, a knowledge of the relationships involved in the solution of complex pipeline problems becomes necessary. Johnson and Berwald, in Bureau of Mines monograph 6 (7-23), were the first to develop these relationships, using as a basis the Weymouth equation in which the f factor was expressed as a power function of the internal diameter of the pipe. Recently Smith and coworkers (7-38) derived these relationships, but without expressing the f factor in terms of any of its variables.

The philosophy involved in deriving the special relationships used in the solution of complex transmission systems is to express the various lengths and diameters of the pipe in the system as equivalent lengths of a common diameter or equivalent diameters of a common length.

Where the flow of gas, pressure differential, temperature, gas gravity, and compressibility are the same for two different pipes, the relationship of diameters and pipe lengths is expressed as follows:

$$L_1 = \frac{f_2}{f_1}\left(\frac{d_1}{d_2}\right)^5 L_2 \tag{7-40}$$

or

$$d_1 = \left(\frac{f_1}{f_2}\frac{L_1}{L_2}\right)^{1/5} d_2 \tag{7-41}$$

where L_1 is the length of a pipe of diameter d_1 and factor f_1 equivalent to the length L_2 of a pipe of diameter d_2 and factor f_2, or where d_1 is the diameter of a pipe of length L_1 and factor f_1 equivalent to the diameter d_2 of a pipe of length L_2 and factor f_2.

The flow of gas in parallel lines (Fig. 7-6) is obtained by adding the rate of flow through each individual line and combining like terms.

$$Q = 3.22\,\frac{T_0}{P_0}\left(\frac{P_1^2 - P_2^2}{GTLz}\right)^{0.5}\left(\frac{d_1^{2.5}}{f_1^{0.5}} + \frac{d_2^{2.5}}{f_2^{0.5}} + \frac{d_3^{2.5}}{f_3^{0.5}} + \cdots + \frac{d_n^{2.5}}{f_n^{0.5}}\right) \tag{7-42}$$

where d_1, d_2, . . . d_n are the internal diameters of the individual lines having f factors f_1, f_2, . . . f_n respectively.

The diameter d_0 of a single line having the same capacity as the set of parallel lines is given by Eq. (7-43) or (7-44).

$$\frac{d_0^{2.5}}{f_0^{0.5}} = \frac{d_1^{2.5}}{f_1^{0.5}} + \frac{d_2^{2.5}}{f_2^{0.5}} + \cdots + \frac{d_n^{2.5}}{f_n^{0.5}} \tag{7-43}$$

$$\text{or } d_0 = \left[\left(\frac{f_0}{f_1}\right)^{0.5} d_1^{2.5} + \left(\frac{f_0}{f_2}\right)^{0.5} d_2^{2.5} + \cdots + \left(\frac{f_0}{f_n}\right)^{0.5} d_n^{2.5}\right]^{0.4} \tag{7-44}$$

Most often in the design of complex transmission systems, only a part of the line is paralleled. Equations have been derived for determining the size of pipe to be used in completely or partially paralleling an original line in order to increase the system capacity by a fixed amount. The equations were derived on the basis that, after a line had been paralleled, the temperature, gas gravity, mean compressibility, and pressures at the inlet and outlet of the original lines were the same as they were before paralleling.

The following expression gives the fraction of the total length of original line that must be paralleled in order to increase the flow rate by a fixed amount.

$$Y = \frac{(Q_0/Q_L)^2 - 1}{1/(1 + W)^2 - 1} \tag{7-45}$$

where Y = fraction of original line paralleled, starting downstream
Q_0 = rate of flow through system before paralleling
Q_L = rate of flow through system after paralleling

$$W = \left(\frac{d_2}{d_1}\right)^{2.5}\left(\frac{f_1}{f_2}\right)^{0.5} \tag{7-46}$$

where d_1 = ID of original line
d_2 = ID of parallel line
f_1 = f factor of original line
f_2 = f factor of parallel line

The above equation can be rearranged in several different ways, for example, with the system rate of flow after paralleling as the dependent variable or with W as the dependent variable.

$$Q_L = \frac{Q_0}{\{Y[1/(1 + W)^2 - 1] + 1\}^{0.5}} \tag{7-47}$$

$$W = \left[\frac{Y}{(Q_0/Q_L)^2 - 1 + Y}\right]^{0.5} - 1 \tag{7-48}$$

When $Y = 1$ and the entire length of the original line has been paralleled,

$$W = \frac{Q_L}{Q_0} - 1 \tag{7-49}$$

If the diameter and f factor of the parallel line are the same as those of the original line, then $W = 1$.

$$Y = \tfrac{4}{3}\left[1 - \left(\frac{Q_0}{Q_L}\right)^2\right] \tag{7-50}$$

and

$$\frac{Q_L}{Q_0} = \frac{2}{(4 - 3Y)^{0.5}} \tag{7-51}$$

Figure 7-7 shows the relationship expressed by Eq. (7-45). Use of these curves will materially reduce the time required for calculating and designing complex transmission systems. In addition, the curves serve to illustrate quite clearly the interesting relationships among the variables. In the case where $W = \infty$, Y is the minimum portion of the line that must be paralleled in order to give the desired increase in flow rate. When $W = 1$, the parallel line has the same diameter and f factor as the original line. For small values of diameter of a parallel line, the length of the parallel line will be considerably greater for the same increase in flow than is necessary for a larger-

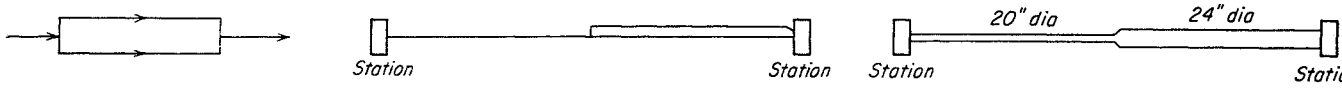

(a) Parallel flow in gas lines (b) Looped gas line (c) Change in size for series flow

Fig. 7-6. Flow diagrams for gas systems.

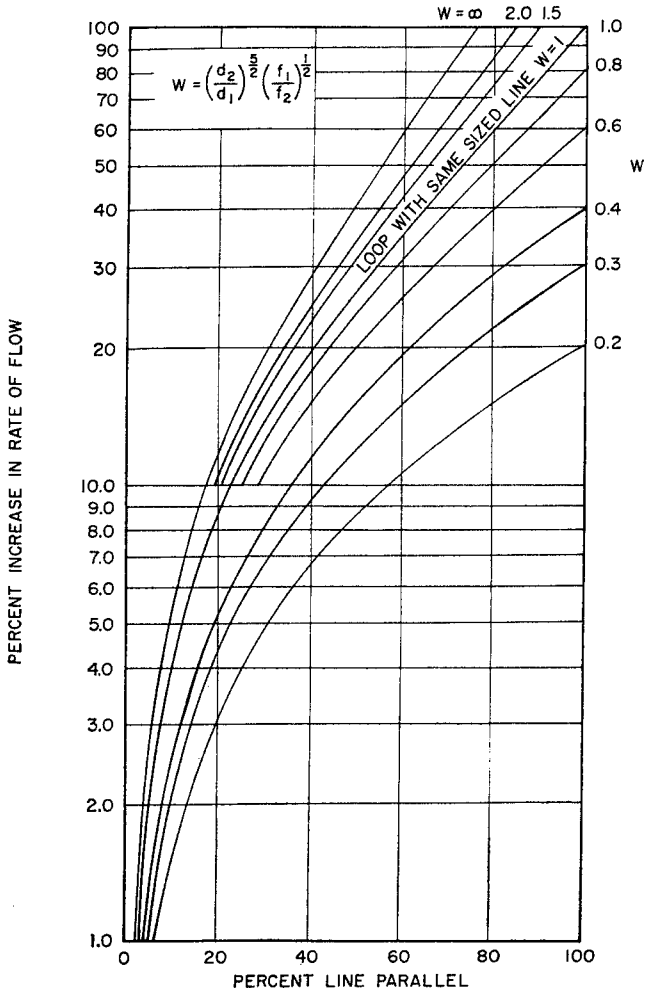

Fig. 7-7. Design of parallel line. *(Smith et al., 7-38.)*

diameter parallel line. However, as the parallel-line diameter increases further, the corresponding decrease in the length required becomes less.

STORAGE CAPACITY OF PIPELINES

During "off-peak" periods the pressure drop in natural gas–transmission lines will be less than during peak-load periods and, as a result, the average pressure along the line will be greater; the line thus serves an important secondary function, that of storage. Weymouth defined the storage capacity of a natural gas pipeline as the difference between the gas contents of the pipeline under packed and unpacked conditions. A pipeline is said to be "packed" when withdrawal from the line is at a minimum and when, therefore, for a constant supply of gas, the discharge pressure is a maximum. Similarly, a pipeline is "unpacked" when withdrawals are a maximum and pressure is a minimum for a constant supply of gas to the line. Using this definition of storage capacity and the Clinedinst equation, an expression can be derived that takes into consideration the variation in compressibility of the gas with pressure (7-29). The content of a natural gas pipeline under conditions of isothermal flow is then

$$V_0 = \frac{ALz_0T_0P_c}{P_0T} \frac{\int_0^{P_{r,1}} (P_r/z)^2\,dP_r - \int_0^{P_{r,2}} (P_r/z)^2\,dP_r}{\int_0^{P_{r,1}} (P_r/z)\,dP_r - \int_0^{P_{r,2}} (P_r/z)\,dP_r} \tag{7-52}$$

where V_0 = volume of gas in pipeline measured at T_0 and P_0, cu ft
A = cross-sectional area of pipe, sq ft
L = length of pipe, ft
T = temperature, °R
P_c = pseudocritical pressure of gas, psia
P_0 = standard measurement pressure, psia
T_0 = standard measurement temperature, °R

Values of the integrals

$$\int_0^{P_r} \left(\frac{P_r}{z}\right)^2 dP_r \text{ and } \int_0^{P_r} \frac{P_r}{z}\,dP_r$$

can be obtained from Tables A-7 and A-6 respectively.

The increments of temperature and pressure in the table have been taken small enough so that linear interpolation can be used.

The use of Eq. (7-52) in calculating storage capacity of a gas-transmission line is illustrated by the following example.

Illustrative Problem

Using the description of the pipeline given in the previous example, calculate the storage capacity of this line in cubic feet of gas measured at 60°F and 14.65 psia when for unpacked conditions the pressure at the outlet end of the line is 300 psia and for packed conditions it is 1,000 psia.

Solution

The conditions are the same as in the flow problem, except for the following:

Packed conditions:

P_1 = 1,300 psia $\quad P_{r,1}$ = 1.91
P_2 = 1,000 psia $\quad P_{r,2}$ = 1.47

Unpacked conditions:

P_1 = 1,300 psia $\quad P_{r,1}$ = 1.91
P_2 = 300 psia $\quad P_{r,2}$ = 0.44

Values of the integrals as obtained from Tables A-6 and A-7:

$$\left[\int_0^{1.91} \frac{P_r}{z}\,dP_r\right]_{T_r=1.25} = 2.43 \qquad \left[\int_0^{1.47} \frac{P_r}{z}\,dP_r\right]_{T_r=1.25} = 1.30$$

$$\left[\int_0^{0.44} \frac{P_r}{z}\,dP_r\right]_{T_r=1.25} = 0.10$$

$$\left[\int_0^{1.91} \left(\frac{P_r}{z}\right)^2 dP_r\right]_{T_r=1.25} = 4.52 \qquad \left[\int_0^{1.47} \left(\frac{P_r}{z}\right)^2 dP_r\right]_{T_r=1.25} = 1.71$$

$$\left[\int_0^{0.44}\left(\frac{P_r}{z}\right)^2 dP_r\right]_{T_r=1.25} = 0.032$$

$$V_{\text{packed}} = \frac{[\pi(1.1145)^2/4] \times 5.28 \times 10^6 \times 1 \times 520 \times 678}{14.65 \times 500} \times \frac{4.52 - 1.71}{2.43 - 1.30}$$

$$= 2.4826 \times 10^7 \left(\frac{2.81}{1.13}\right) = 6.1736 \times 10^7 \text{ cu ft}$$

$$V_{\text{unpacked}} = 2.4826 \times 10^7 \left(\frac{4.52 - 0.03}{2.43 - 0.10}\right)$$

$$= 2.4826 \times 10^7 \left(\frac{4.49}{2.33}\right) = 4.7841 \times 10^7$$

$$\text{Storage capacity} = (6.1736 - 4.7841) \times 10^7 = 1.3895 \times 10^7$$
$$= 13{,}895{,}000 \text{ cu ft}$$
$$= 13{,}895 \text{ Mcf}$$

For the same problem Joffe (7-22) gives a value for the storage capacity of 15,210 Mcf. If an integrated Weymouth equation had been used, the calculation would have given a capacity of from 18,720 to 19,980 Mcf, depending on the method of determining the average compressibility factor.

FLOW IN NATURAL GAS WELLS

Just as knowledge of the static bottom-hole pressure of a gas reservoir is of prime importance in predicting the reserves and deliverability of the gas in the reservoir, so also knowledge of the flowing bottom-hole pressure of a gas well is important in determining the deliverability of the well. For this purpose, flowing sand-face pressures are either measured directly by means of a bottom-hole pressure gauge, calculated from a static-gas column (such as occurs when gas is flowing through the tubing with an unobstructed static column of gas in the annulus or the reverse), or, finally, calculated from the flowing-gas column.

One of the first methods used to calculate flowing sand-face pressures employed the well-known Weymouth formula, Eq. (7-29). This equation was used to calculate the pressure drop due to frictional effects. The pressure due to the weight of a column of gas was then calculated. The sum of these two pressure drops was then taken to be the difference between the bottom-hole and wellhead pressures.

General equations for calculating the flow of gas in a vertical flow string can, like the equations for horizontal flow, be derived by starting with Eq. (7-2).

By assuming that

1. The kinetic-energy change is negligible and can be taken as zero
2. The flow is steady and isothermal
3. There is no work done by the gas in flow

one arrives at Eq. (7-36). Equation (7-36) then becomes the basis for the derivation of any specific equation for the flow of gas through a vertical flow string.

R. V. Smith (7-36) has derived an equation for the vertical flow of gas similar to the Weymouth equation for horizontal flow.

$$Q = 200{,}000\left[\frac{d^5}{GT_a z_a f X}(P_2^2 - e^S P_1^2)\frac{S}{e^S - 1}\right]^{0.5} \tag{7-53}$$

where Q = volume rate of flow measured at 4.65 psia and 60°F, cu ft/day
z_a = effective compressibility factor of the gas
T_a = effective average temperature, °R
d = ID of pipe, in.
P_2 = sand-face pressure at depth X, psia (sometimes written P_S)
P_1 = wellhead pressure, psia (sometimes written P_W)
e = 2.7183
$S = 0.0375GX/T_a z_a$
G = gas gravity
X = difference in elevation between pressures P_1 and P_2, ft
f = friction factor, from Fig. 7-3 or 7-4

In addition to the assumptions made in arriving at the basic equation, Eq. (7-53) assumes a constant effective compressibility factor and constant average temperature.

Poettmann (7-30) has derived an expression for calculating the sand-face pressure of flowing gas wells in which the variation of the compressibility factor of the gas with pressure is taken into consideration. The same integral factors (Table A-4) used in calculating static bottom-hole pressures by Eq. (7-18) are employed.

$$X = \frac{X_S}{1 + 0.9521 \times 10^{-6} \times fQ^2G^2X_S^2/D^5(\Delta P)^2} \tag{7-54}$$

where X = difference in elevation between pressures P_1 and P_2, ft
Q = gas flow at 14.65 psia and 60°F, MMcf/day
D = ID of tubing, ft
$\Delta P = P_2 - P_1$, psia
G = gas gravity
f = friction factor, from Fig. 7-3 or 7-4

$$\text{Then } X_S = \frac{53.241T_a}{G}\left(\int_{0.2}^{P_{r,2}}\frac{z}{P_r}dP_r - \int_{0.2}^{P_{r,1}}\frac{z}{P_r}dP_r\right) \tag{7-55}$$

Cullender and Binckley (7-13) and Smith (7-37) have shown by analysis of experimental data that absolute roughnesses of 0.0006 and 0.00065 in., respectively, are satisfactory values to use for the roughness of clean pipe ranging in size from 1¼ to 8⅝ in.

For a roughness of 0.0006 in., Cullender and Binckley (7-13) have expressed the f factor as a power function of the Reynolds number and the pipe diameter. In terms of Q, G, D, and viscosity

$$f = 30.9208 \times 10^{-3} \frac{Q^{-0.065} D^{-0.058} G^{-0.065}}{\mu^{-0.065}} \quad (7\text{-}56)$$

Substituting Eq. (7-56) in (7-54) gives

$$X = \frac{X_S}{1 + 2.944 \times 10^{-8} \times Q^{1.935} G^{1.935} X_S^2 \mu^{0.065} / D^{5.058} (\Delta P)^2} \quad (7\text{-}57)$$

where μ = viscosity, lb/(ft)(sec) [when μ is in micropoises (centipoises × 10,000), 2.944 becomes 1.0069; when d is in inches and μ in micropoises, 2.944×10^{-8} becomes 2.911×10^{-3}].

In case of flow through the annulus of a well, D^5 (or d^5) of Eqs. (7-54) and (7-53) must be replaced by

$$D^5 = (D_1 + D_2)^2 (D_1 - D_2)^3$$

and $D^{5.058}$ of Eq. (7-57) must be replaced by

$$D^{5.058} = (D_1 + D_2)^{1.935} (D_1 - D_2)^{3.123}$$

where D_1 = internal diameter of casing, ft
D_2 = external diameter of tubing, ft

For evaluating the Reynolds number when determining f from Fig. 7-3 or 7-4 for flow through the annulus, D is replaced by $D_1 - D_2$.

In arriving at Eq. (7-54), it should be noted that Eq. (7-36) consists of the sum of three energies: the compression energy, the potential energy of position, and the energy lost due to the irreversibilities of the system in flow. The compression energy must equal the sum of the other two.

In deriving Eq. (7-54), the compression energy and potential energy of position are handled rigorously. That is, the compressibility factor and pressure are integrated rigorously within the assumptions made in arriving at Eq. (7-36), in particular, the assumption of constant temperature. However, in handling the energy-loss function lw, the assumption is made that the gas velocity $\bar{v}$ is constant and equal to the integrated average value with pressure. That is to say,

$$\bar{v} = \frac{\int_1^2 v \, dP}{P_2 - P_1} = \frac{(W/A)(RT/29G) \int_1^2 (z/P_r) \, dP_r}{\Delta P} \quad (7\text{-}58)$$

In order to present an idea of the accuracy of the results calculated with field data, Table 7-2 was prepared. Comparisons are made on twenty flowing conditions in dry-gas wells from one field and eleven flowing conditions in gas-condensate wells from different fields. Equation (7-57) was used to calculate the pressure traverses, and only sand-face pressures were compared. The deviations shown reflect to a considerable degree the accuracy of the data used in making the calculations and the accuracy with which the flowing pressures are recorded, rather than the soundness of the mathematical development. In the case of dry-gas wells, for example, most of the deviations are negative, indicating that perhaps, for the tubing in this field, the absolute roughness and thus the factor f were slightly underestimated. However, the agreement between the calculated and observed results is good.

The application of Eqs. (7-54) and (7-56) to gas-condensate wells is limited by the amount of liquid phase in the flow string. However, it is of interest to note that, for a ratio as low as 40,000 cu ft/bbl, reasonable agreement is still obtained when one uses the composite well stream to obtain G and z. The higher the gas-oil ratio, the more accurate one can expect the calculated results to be. It is likely that the procedures can be applied to wells with ratios considerably lower than 40,000 cu ft/bbl without appreciable error in the computed results, as long as the fluid velocity is high enough to keep the liquid droplets completely dispersed in the flow stream, so that the flow-stream properties can be adequately described on an average basis.

The gas gravity G of Eqs. (7-54) and 7-56) can be calculated from the composition of the flow stream or measured experimentally. In the case of condensate wells, if composition is not available, the gas gravity of the composite flow stream may be obtained from Fig. 7-8 or calculated from the following equation:

$$G = \frac{G_g + 4{,}591\rho/R}{1 + 1{,}123/R} \quad (7\text{-}59)$$

where G = well-fluid gravity
G_g = separator-gas gravity
ρ = specific gravity of condensate, grams/cu cm
R = gas-liquid ratio, cu ft/bbl

Standing presented a similar plot, but with gas gravity as an added parameter (1-19).

The pseudocritical temperature and pressure of the gas are calculated from the gas composition. If composition is not available, Fig. 4-22 may be used to estimate these properties from gas gravity.

The viscosity of the natural gas may be obtained from Figs. 4-106 and 4-107.

Table 7-3 shows a comparison of flowing bottom-hole pressures calculated for flow through the annulus between various sizes of tubing and casing, with the flowing bottom-hole pressure calculated from the static gas column in the tubing by Eq. (7-18) and with the flowing bottom-hole pressure experimentally measured by means of a pressure gauge. In general

Table 7-2. Comparison of Observed Data and Calculated Results for Flow of Gas in Vertical Pipe

Part A. Dry-gas Wells

Test no.	Tubing size, in.		Q, MMcf/day	Depth X, ft	T_a, °F	Sp gr flowing fluid	P_w, psia	P_s, psia		Deviation	
	Nominal	ID						Obs	Calc	Psia	%
1	2½	2.441	5.109	5,190	92	0.600	1,253.0	1,495	1,490	−5	−0.334
2	2½	2.441	9.514	5,190	94	0.600	1,112.4	1,478	1,483	+5	+0.338
3	2½	2.441	14.068	5,190	96	0.600	832.0	1,475	1,500	+25	+1.695
4	2½	2.441	6.299	4,922	91	0.605	1,297.4	1,593	1,554	−39	−2.448
5	2½	2.441	5.695	5,195	92	0.595	1,210.0	1,462	1,455	−7	−0.479
6	2½	2.441	9.298	5,195	93	0.595	1,084.4	1,452	1,451	−1	−0.069
7	2½	2.441	13.176	5,195	94	0.595	802.4	1,438	1,412	−26	−1.808
8	2½	2.441	4.827	4,750	93	0.602	1,188.4	1,411	1,392	−19	−1.346
9	2½	2.441	8.025	4,750	93	0.602	1,099.4	1,411	1,389	−22	−1.559
10	2½	2.441	13.680	4,750	95	0.602	764.4	1,401	1,382	−19	−1.356
11	2½	2.441	2.432	4,764	90	0.599	1,102.4	1,260	1,261	+1	+0.079
12	2½	2.441	4.127	4,764	90	0.599	1,043.4	1,216	1,236	+20	+1.618
13	2½	2.441	6.167	4,764	90	0.599	923.4	1,156	1,148	−8	−0.692
14	2½	2.441	3.810	5,242	93	0.591	1,433.4	1,690	1,654	−36	−2.130
15	2½	2.441	5.379	5,242	93	0.591	1,302.4	1,579	1,550	−29	−1.837
16	2½	2.441	7.663	5,195	92	0.595	919.4	1,257	1,220	−37	−2.943
17	2½	2.441	10.598	5,195	92	0.595	680.4	1,247	1,173	−76	−6.308
18	2½	2.441	11.841	5,195	92	0.595	650.4	1,247	1,227	−20	−1.604
19	2½	2.441	4.384	5,195	92	0.595	1,028.4	1,240	1,223	−17	−1.371
20	2½	2.441	6.585	5,195	92	0.595	966.4	1,230	1,226	−4	−0.325

Part B. Distillate Wells

Test no.	Tubing size, in.		Q, MMcf/day	Depth X, ft	T_a, °F	Gas-oil ratio, Mcf/bbl	Gravity liquid	Sp gr flowing fluid	P_w, psia	P_s, psia		Deviation	
	Nominal	ID								Obs	Calc	Psia	%
21	2.0	1.995	4.461	5,529	122.5	341.2	47.7	0.7083	1,873	2,266	2,307	+41	+1.809
22	2.0	1.995	3.765	5,529	122.5	341.2	47.7	0.7083	1,951	2,276	2,370	+94	+4.130
23	2.0	1.995	3.055	5,529	121.0	341.2	47.7	0.7083	1,953	2,287	2,348	+61	+2.667
24	2.0	1.995	2.675	9,110	157.5	40.7	54.0	0.7163	1,979	2,688	2,593	−95	−3.534
25	2½	2.441	4.803	8,226	164.0	65.8	51.3	0.761	2,272	2,893	2,944	+51	+1.763
26	2½	2.441	3.207	8,226	161.0	65.8	51.3	0.761	2,320	2,902	2,970	+68	+2.343
27	2½	2.441	1.338	8,226	160.0	65.8	51.3	0.761	2,373	2,911	3,003	+92	+3.160
28	2.0	1.995	5.153	5,790	121.5	787.89	35.3	0.604	2,122	2,565	2,556	−9	−0.351
29	2.0	1.995	3.522	5,790	119.0	787.89	35.3	0.604	2,202	2,593	2,580	−13	−0.501
30	2.0	1.995	2.760	5,790	118.5	787.89	35.3	0.604	2,232	2,601	2,593	−8	−0.308
31	2.0	1.995	2.046	5,790	117.5	787.89	35.3	0.604	2,260	2,605	2,610	+5	+0.192

there is very good agreement between the calculated bottom-hole pressures. The agreement between measured and calculated pressure is also good; the measured values, however, are all less than the calculated values, indicating perhaps a systematic error in the measured values or in the data used in arriving at the calculated values.

Illustrative Problem

Calculate the sand-face pressure of a flowing gas-condensate well from the following surface measurements:

Q = 5.153 MMcf/day.
D = 0.1663 ft; d = 1.995 in.
Gravity of separator gas = 0.600.
Gravity of condensate = 35.3°API.
Separator gas–liquid ratio = 787.89 Mcf/bbl.
Depth of well = 5,790 ft.
Bottom-hole temperature = 160°F.
Wellhead flowing temperature = 83°F.
Tubing-head pressure = 2,122 psia.

Solution Using Eq. (7-57)

$$X = \frac{X_S}{1 + 2.911 \times 10^{-3} \times \mu^{0.065} Q^{1.935} G^{1.935} X_S^2 / d^{5.058} (\Delta P)^2}$$

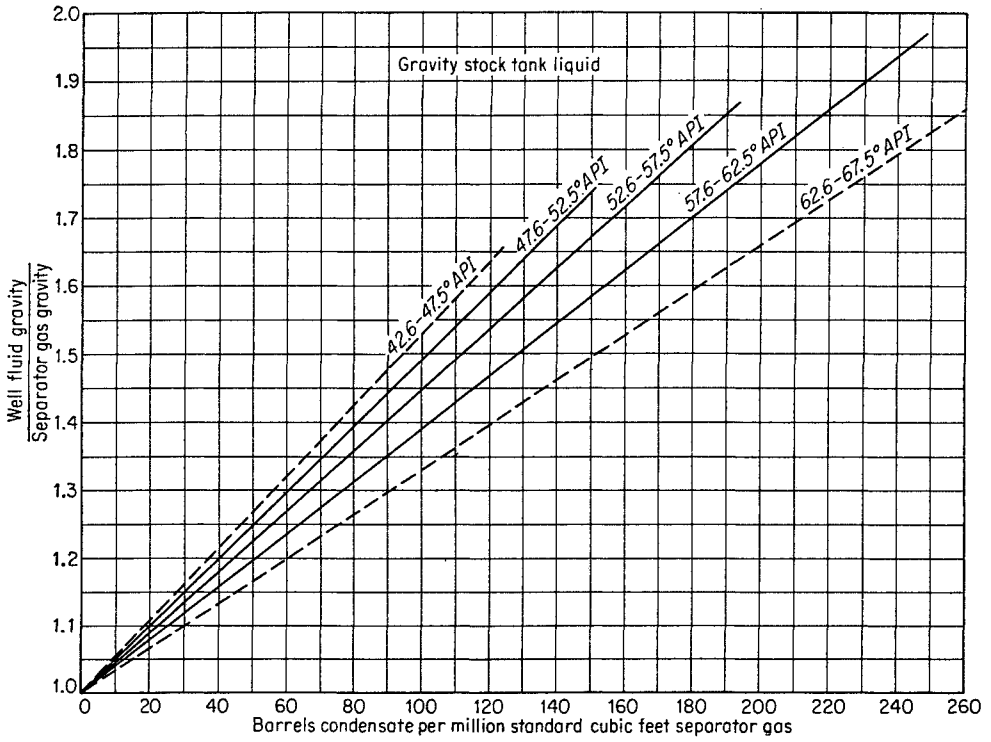

Fig. 7-8. Well-fluid gas gravity from separator-gas gravity and liquid content. *(Nisle and Poettmann, 7-29. Courtesy Petrol. Engr.)*

Flowing-gas gravity, from Eq. (7-59):

$$G = 0.600 + \frac{4{,}591 \times 0.8483/787{,}890}{1 + 1{,}123/787{,}890} = 0.604$$

Average flowing temperature:

$$\frac{160 + 83}{2} = 121.5°\text{F} \quad \text{or} \quad 581.5°\text{R}$$

Reduced conditions:

$$P_c = 671 \text{ psia} \qquad T_c = 360°\text{R}$$

(from Fig. 4-22)

$$T_R = \frac{581.5}{360} = 1.615 \qquad P_R = \frac{P}{671}$$

Viscosity at 121.5°F and 2,500 psia (Fig. 4-107):

$$\mu = 0.0175 \text{ centipoise} \quad \text{or } 175 \text{ micropoises}$$
$$\mu^{0.065} = 175^{0.065} = 1.398$$
$$Q^{1.935} = 5.153^{1.935} = 23.6$$
$$G^{1.935} = 0.604^{1.935} = 0.377$$
$$d^{5.058} = 1.995^{5.058} = 33$$

Then

$$X = \frac{X_S}{1 + 2.911 \times 10^{-3} \times 1.398 \times 23.6 \times 0.377 X_S^2/33 \times (\Delta P)^2}$$

$$= \frac{X_S}{1 + 0.00110 X_S^2/\Delta P^2}$$

$$X_S = \frac{53.24 \times 581.5}{0.604}\left(\int_{0.2}^{P_{r,2}} \frac{z}{P_r}\,dP_r - \int_{0.2}^{P_{r,1}} \frac{z}{P_r}\,dP_r\right)$$

We set up a table to compute values of X_S for various pressures down the well bore.

P, psia	P_r	$\int_{0.2}^{P_r} \frac{z}{P_r}\,dP_r$	$\int_{P_{r,1}}^{P_{r,2}} \frac{z}{P_r}\,dP_r$	X_S
2,122	3.162	2.564		
2,300	3.428	2.632	0.068	3,490
2,600	3.875	2.734	0.170	8,730

At 2,300 psia

$$X = \frac{3{,}490}{1 + 0.00110(3{,}490/178)^2} = 2{,}445 \text{ ft}$$

At 2,600 psia

$$X = \frac{8{,}730}{1 + 0.00110(8{,}730/478)^2} = 6{,}365 \text{ ft}$$

Figure 7-9 shows the pressure gradient in the flowing gas well. The pressure is read at 5,790 ft as 2,556 psia.

Sukkar and Cornell (7-41) have developed an expression for calculating the flowing bottom-hole pressures of gas wells by numerically integrating Eq. (7-36). The integration is rigorous within the assumptions made in arriving at Eq. (7-36), that is, negligible kinetic energy, steady-state isothermal flow, and no work done by the gas in flow.

$$\int_{P_{r,1}}^{P_{r,2}} \frac{z/P_r}{1 + B(z/P_r)^2}\,dP_r = \frac{0.01877GX}{T_a} \qquad (7\text{-}60)$$

where $B = 667fQ^2T_a^2/d^5P_c^2$
G = gas gravity
X = depth, ft

T_a = average temperature, °R
Q = flow rate at 60°F and 14.65 psia, MMcf/day
d = diameter of pipe, in.
P_c = pseudocritical pressure, psia
z = compressibility factor of gas
P_r = pseudoreduced pressure P/P_c
f = friction factor, from Fig. 7-3 or 7-4

In order to evaluate the integral on the left side of Eq. (7-60), tables of integral factors using an arbitrary reference point were prepared. Table A-8 was prepared for the low-pressure range: reduced pressures P_r from 1.0 to 5.0, or pressure from around 600 to 3,200 psia. The reference P_r was taken as 3.0 to simplify interpolation. In order to avoid negative values of the integral factors, 0.5 was added to all of the integrals. Table A-8 gives values of

$$\left[0.5 + \int_{P_r}^{3} \frac{z/P_r}{1 + B(z/P_r)^2}\, dP_r\right]_{T_r}$$

for values of constant B ranging from 0 to 20 and of T_r from 1.5 to 1.7.

In order to determine the bottom-hole pressure from Table A-8 using Eq. (7-60), where $P_{r,2}$ is the pseudoreduced bottom-hole pressure and $P_{r,1}$ is the pseudoreduced surface pressure, we use

$$\left[0.5 + \int_{P_{r,2}}^{3} \frac{z/P_r}{1 + B(z/P_r)^2}\, dP_r\right]_{T_r} = \left[0.5 + \int_{P_{r,1}}^{3} \frac{z/P_r}{1 + B(z/P_r)^2}\, dP_r\right]_{T_r} - \frac{0.01877GX}{T_a} \tag{7-61}$$

Since all the quantities on the right-hand side of Eq. (7-61) are known, the value of the integral factor corresponding to the bottom-hole pressure can be calculated and the pseudoreduced bottom-hole pressure obtained from Table A-8.

Similarly, Table A-9 was prepared for the high range: reduced pressures from 2.0 to 12.0, or pressures above 2,000 psia. Adequate overlap has been provided so that most problems can be worked out entirely from one table. Values of B range from 0 to 10, and pseudoreduced temperature from 1.5 to 1.7.

In order to determine the pseudoreduced bottom-hole pressure from Table A-9, a procedure similar to the foregoing is followed.

$$\int_{P_{r,2}}^{12} \frac{z/P_r}{1 + B(z/P_r)^2}\, dP_r = \int_{P_{r,1}}^{12} \frac{z/P_r}{1 + B(z/P_r)^2}\, dP_r - \frac{0.01877GX}{T_a} \tag{7-62}$$

The value of $P_{r,2}$ corresponding to the value of the left side of Eq. (7-62) is obtained from Table A-9.

Illustrative Problem

Repeat the previous example using the method of Sukkar and Cornell.

1. Calculate B.

$$B = \frac{667fQ^2T^2}{d^5P_c^2}$$

$f = 0.015$ from Fig. 7-3

$$B = \frac{667 \times 0.015 \times 5.153^2 \times 581.5^2}{1.955^5 \times 671^2}$$

$$= 7.01$$

2. Calculate

$$\frac{0.01877GX}{T_a} = \frac{0.01877 \times 0.604 \times 5{,}790}{581.5} = 0.112$$

3.
$$P_{r,1} = \frac{2{,}122}{671} = 3.162$$

$$T_r = \frac{581.5}{360.0} = 1.615$$

4. From Table A-9, read

$$\int_{P_{r,1}}^{12} \frac{z/P_r}{1 + B(z/P_r)^2}\, dP_r = 1.0840$$

5. From Eq. (7-62)

$$\int_{P_{r,2}}^{12} \frac{z/P_r}{1 + B(z/P_r)^2}\, dP_r = 1.0840 - 0.112 = 0.972$$

6. From Table A-9

$$P_{r,2} = 3.81$$
$$P = 3.81 \times 671 = 2{,}557 \text{ psia}$$

This agrees well with the calculated value of 2,556 psia obtained with the previous method.

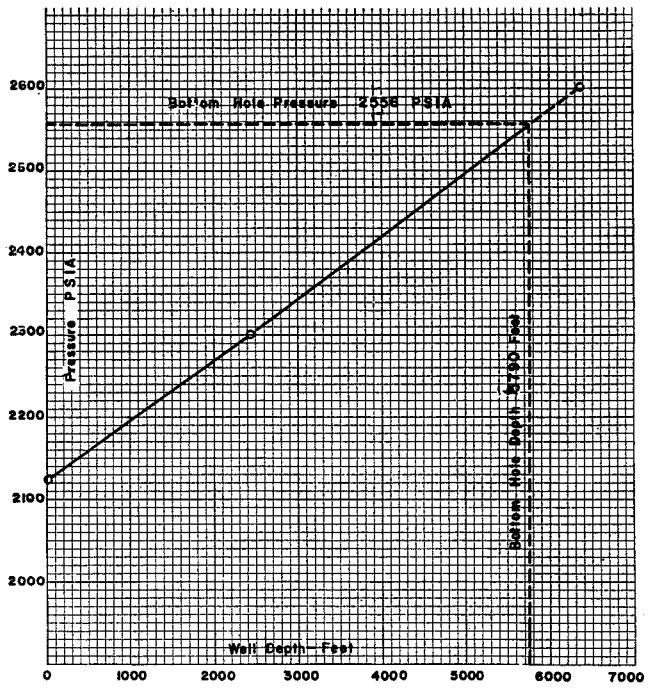

Fig. 7-9. Pressure gradient in flowing gas well.

Table 7-3. Flow of Gas through Annulus

Test no.	Annulus dimensions		Q at 14.65 psia and 60°F, MMcf/day	X, ft	T_a, °R	Specific gravity G	Wellhead pressure, psia		Sand-face pressure, psia		
	ID of casing, in.	OD of tubing, in.					Static, tubing	Flowing, annulus	Measured	Calculated	
										From static column	From flowing column
1	6.336	2.875	14.609	5,090	552	0.597	1,061.7	1,043.2	.....	1,198	1,202
2	6.336	2.875	23.389	5,090	553	0.595	1,230.7	1,192.2	.....	1,422	1,390
3	6.336	2.875	16.821	5,090	552	0.597	1,078.7	1,052.7	.....	1,208	1,205
4	4.892	2.875	20.590	4,647	548	0.602	1,227.7	1,040.2	.....	1,395	1,380
5	6.336	2.875	23.738	5,138	553	0.600	1,280.7	1,219.7	.....	1,538	1,468
6	4.892	2.375	8.743	4,470	546	0.599	1,055.2	1,036.2	.....	1,179	1,175
7	6.336	2.875	25.450	4,377	556	0.598	1,132.7	1,095.7	.....	1,265	1,257
8	6.336	2.875	4.316	4,372	552	0.598	1,126.7	1,120.7	1,227	1,259	1,252
9	6.336	2.875	8.051	4,372	553	0.598	1,122.7	1,114.7	1,223	1,264	1,258
10	6.336	2.875	16.165	4,372	555	0.598	1,113.7	1,091.7	1,212	1,243	1,248
11	6.336	2.875	24.833	4,372	556	0.598	1,098.7	1,054.7	1,197	1,218	1,210
12	6.336	2.875	4.637	4,372	552	0.598	1,128.7	1,119.7	1,229	1,259	1,257
13	6.336	2.875	11.707	4,377	554	0.598	1,159.7	1,152.7	.....	1,300	1,310
14	6.336	2.375	21.947	4,360	553	0.591	1,708.7	1,753.7	.....	1,907	1;918
15	6.336	2.375	9.874	4,360	552	0.591	1,790.7	1,786.7	.....	1,990	1,992
16	6.336	2.375	5.490	4,360	550	0.591	1,796.7	1,794.7	.....	1,997	1,998
17	6.336	2.875	5.489	4,724	550	0.600	962.2	958.7	.....	1,073	1,074
18	4.892	2.875	4.325	4,647	550	0.600	1,029.2	1,018.2	.....	1,150	1,158

Quite often, for instance in pressure maintenance, in gas cycling, and in designing of gas-lift installations, it is desirable to know the variation of pressure with depth for the injection of gas into the tubing of a well. Equations (7-53), (7-54), and (7-57), previously developed for the upward flow of gas in the tubing or annulus of a well, can be rearranged so that the pressure traverse for the vertical flow downward can be calculated. The nomenclature is the same as used in the corresponding equations.

$$Q = 200{,}000\left[\frac{d^5}{GT_a z_a f X}\,(e^S P_1^2 - P_2^2)\,\frac{S}{e^S - 1}\right]^{0.5} \tag{7-63}$$

$$X = \frac{X_S}{[0.9521 \times 10^{-6} f Q^2 G^2 X_S^2 / D^5 (\Delta P)^2] - 1} \tag{7-64}$$

$$X = \frac{X_S}{[2.94409 \times 10^{-8} Q^{1.935} G^{1.935} X_S^2 / D^{5.058} \mu^{-0.065} (\Delta P)^2] - 1} \tag{7-65}$$

The difference between these equations and (7-53) and (7-54) is due to the fact that the potential-energy change of Eq. (7-36) is negative for upward flow.

It is of interest to note the possibility of either a positive or a negative pressure gradient for the downward flow of gas. At low flow rates the gradient is positive; at high flow rates it is negative. This is because, as the flow rate increases, the energy loss increases and can be overcome only by a decrease in the change of compression energy or PV energy of the system. The decrease in potential energy due to elevation is constant, and the change in kinetic energy is usually negligible.

Illustrative Problem

A well is produced by gas-lifting the reservoir fluid through the annulus between 2-in. (4.7 lb/ft) tubing and 6⅝-in. (24.0 lb/ft) casing. Natural gas is injected downward through the tubing and enters the annulus at a depth of 4,000 ft. To produce the well at three different flow rates requires the following three injection pressures and corresponding gas rates:

Injection pressure at 4,000 ft, psia	*Injected-gas flow rate, MMcf/day*
920	0.282
740	0.783
560	1.677

Assuming that there is no pressure drop across the injection point, calculate the minimum injection-gas pressure at the wellhead for the above rates and pressure at 4,000 ft.

The average flowing temperature in the tubing is 140°F; gas gravity is 0.625.

Assume a pipe roughness of 0.0006 in.

Solution

The ID of 2-in. 4.7-lb/ft tubing is 1.995 in.

Since we know the pressure at the bottom, we use this as the reference point and calculate upward. By substituting the constant factors in Eq. (7-65), this can be reduced to an equation for the depth as a function of pressure. For example, for a rate of 0.783 MMcf/day and a pressure of 740 psia at 4,000 ft, Eq. (7-65) reduces to

$$X = \frac{X_S}{[3.003 \times 10^{-5} X_S/(\Delta P)^2] - 1}$$

This is then solved as follows:

Pressure at 4,000 ft, psia	P_r	A^*	$A_2 - A_1$	X_S	ΔP	X	Depth, 4,000 − X
740	1.10	1.656	0	.....	...	0	4,000
695	1.04	1.607	0.049	2,504	45	2,760	1,240
650	0.97	1.540	0.116	5,929	90	6,817	−2,817

$^* A = \int_{0.2}^{P_r} (z/P_r)\, dP_r.$

The depth is plotted versus pressure, and, at zero depth, the tubing pressure is 680 psia. Figure 7-10 shows the pressure traverses for the three injection pressures and gas rates. Table 7-4 shows a comparison of the wellhead pressures calculated by means of both Eqs. (7-63) and (7-65). The agreement is satisfactory.

CALCULATION OF WORK REQUIRED TO COMPRESS NATURAL GAS

There are two basic approaches that can be used to calculate the horsepower theoretically required to compress a natural gas. One is the use of analytical expressions. In the case of adiabatic compression, the relationships are complicated, and all are usually based on the ideal-gas equation. When used for real gases where deviation from the ideal-gas law is appreciable, they are empirically modified to take into consideration the compressibility factor of the gas. The second approach is the use of an enthalpy-entropy or Mollier diagram for real gases (Figs. 4-62 to 4-64). Such a diagram permits one to use a simple, direct, and rigorous procedure for determining the horsepower theoretically necessary to compress the gas.

Table 7-4. Calculated Wellhead Pressures When Injecting Gas to a Given Pressure at 4,000 Ft

Injected-gas flow rate, MMcf/day	Injection pressure at 4,000 ft, psia	Wellhead pressure, psia	
		Eq. (7-65)	Eq. (7-63)
0.282	920	846	845
0.783	740	680	688
1.677	560	562	558

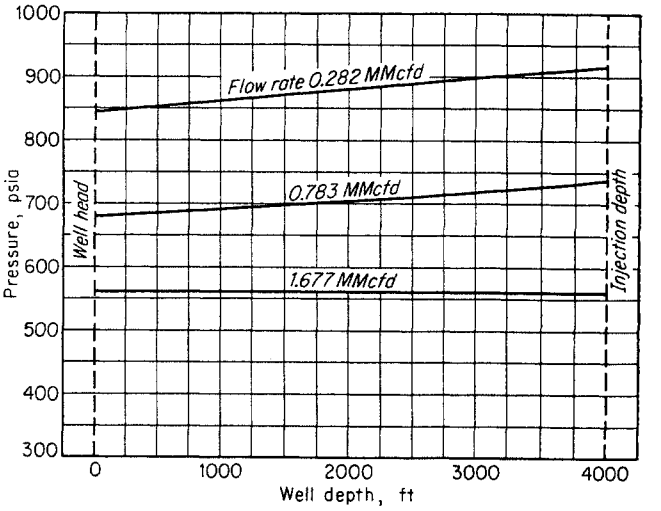

Fig. 7-10. Pressure traverse for gas injection.

When a real gas is compressed in a single-stage compression, the compression is polytropic, tending to approach adiabatic or constant-entropy conditions. Adiabatic-compression calculations give the maximum theoretical work or horsepower necessary to compress a gas between any two pressure limits, whereas isothermal-compression calculations give the minimum theoretical work or horsepower necessary to compress a gas. Adiabatic and isothermal work of compression thus give the upper and lower limits of work or horsepower requirements to compress a gas. One purpose of intercoolers between multistage compressors is to reduce the horsepower necessary to compress the gas. The more intercoolers and stages, the closer the horsepower requirement approaches the isothermal value.

The basis of the derivation of all analytical expressions for calculating the theoretical work required to compress a gas is Eq. (7-2). The changes in kinetic energy, potential energy of position, and energy losses are taken as zero. The equation then reduces to

$$-w = \int_{P_1}^{P_2} V\, dP \qquad (7\text{-}66)$$

For the isothermal work required to compress an ideal gas, Eq. (7-66) can be reduced to

$$-w = \frac{53.241T}{G} \ln \frac{P_2}{P_1} \quad \text{or} \quad w = \frac{53.241T}{G} \ln \frac{P_1}{P_2} \qquad (7\text{-}67)$$

where $-w$ = isothermal work required to compress an ideal gas, ft-lb/lb

T = temperature, °R

G = gas gravity
P_1 = initial pressure, psia
P_2 = final pressure, psia

The work of compression is defined as $-w$, and the work derived from the fluid as $+w$.

For real gases at constant temperature

$$V\,dP = RTd(\ln f) \tag{7-67a}$$

$$-w = \frac{53.241T}{G} \ln \frac{f_2}{f_1} \tag{7-67b}$$

where f = fugacity of gas. It can be shown that

$$\ln \frac{f_2}{f_1} = \int_0^{P_{r,1}} \frac{z\,dP_r}{P_r} - \int_0^{P_{r,2}} \frac{z\,dP_r}{P_r} \tag{7-67c}$$

For a real gas, Eq. (7-66) for isothermal work reduces to

$$-w = \frac{53.241T}{G} \left(\int_{0.2}^{P_{r,2}} \frac{z}{P_r} dP_r - \int_{0.2}^{P_{r,1}} \frac{z}{P_r} dP_r \right) \tag{7-68}$$

where values of the function

$$\int_{0.2}^{P_r} \frac{z}{P_r} dP_r$$

are obtained from Table A-4.

If we express the work in terms of isothermal theoretical horsepower required to compress 1 std MMcf/day at 60°F and 14.65 psia, we obtain

$$-w = 0.08531T \left(\int_{0.2}^{P_{r,2}} \frac{z}{P_r} dP_r - \int_{0.2}^{P_{r,1}} \frac{z}{P_r} dP_r \right) \tag{7-69}$$

For the adiabatic compression or expansion of an ideal gas, the change of state is represented by

$$PV^k = \text{constant} \tag{7-70}$$

where k is the ideal-gas specific-heat ratio C_p/C_v.

Substituting into Eq. (7-66) and integrating, we obtain the theoretical adiabatic work of compression in foot-pounds per pound of gas.

$$-w = \frac{k}{k-1} \frac{53.241T_1}{G} \left[\left(\frac{P_2}{P_1} \right)^{(k-1)/k} - 1 \right] \tag{7-71}$$

Where deviation from ideal-gas behavior is appreciable, the above equation is empirically modified (7-33, 7-15, 7-22a). One such modification presented by Joffe (7-22a) is as follows:

$$-w = \frac{k}{k-1} \frac{53.241T_1}{G} \left[\left(\frac{P_2}{P_1} \right)^{z(k-1)/k} - 1 \right] \tag{7-72}$$

where $-w$ is the work in foot-pounds per pound of gas and where z and k are evaluated at suction conditions.

To find the adiabatic theoretical horsepower required to compress 1 MMcf/day at 60°F and 14.65 psia the above equation is written as follows:

$$-w = 0.08531 \frac{k}{k-1} T_1 \left[\left(\frac{P_2}{P_1} \right)^{z(k-1)/k} - 1 \right] \tag{7-73}$$

where $k = C_p/C_v$ for gas at suction conditions
z = compressibility factor for gas at suction conditions
P_1 = suction pressure, psia
P_2 = discharge pressure for gas, psia
T_1 = suction-gas temperature, °R

The above equation gives results that are in reasonably good agreement with those calculated by means of an enthalpy-entropy diagram.

In developing the use of an enthalpy-entropy (H-S) diagram for calculating the horsepower required to compress a gas, Eq. (7-1) best describes the process. Kinetic energy and potential energy due to differences in elevation are usually neglected, leaving

$$\Delta H = q - w \tag{7-74}$$

For isothermal and frictionless conditions

$$\Delta H = T\,\Delta S - w \tag{7-75}$$

or

$$-w = \Delta H - T\,\Delta S \tag{7-76}$$

where T is the absolute temperature and ΔS is the difference in entropy.

To find the theoretical horsepower required to compress isothermally 1 MMcf/day at 60°F and 14.65 psia, Eq. (7-76) is written

$$-w = 0.0432(\Delta H - T\,\Delta S) \tag{7-77}$$

where ΔH is in Btu per pound mole and ΔS is in Btu per pound mole per degree Rankine.

By following a line of constant temperature on an enthalpy-entropy diagram between initial and final pressure conditions, ΔH and ΔS can be determined.

In the case of adiabatic compression, q of Eq. (7-74) is also zero; so

$$-w = \Delta H \tag{7-78}$$

That is, at adiabatic or constant-entropy conditions for a single stage of compression, the work necessary to compress the gas is equal to the difference in enthalpy between the initial and final stages of compression.

Expressing the adiabatic theoretical work necessary to compress 1 MMcf/day at 14.7 psia and 60°F in terms of horsepower results in

$$-w = 0.0432\,\Delta H \tag{7-79}$$

where ΔH is expressed in Btu per pound mole. For multistage compression the ΔH must be calculated separately for each stage and then totaled.

In addition to the horsepower, the final temperature of compression and the heat removed in the inter-

coolers can be rigorously obtained from the enthalpy-entropy diagrams.

In the case of multistage compression for a given number of stages, the compression ratios per stage for minimum work are the same; so the relationship of the compression ratio (CR) per stage to the over-all compression ratio is

$$\text{CR} = \left(\frac{P_f}{P_1}\right)^{1/n} \tag{7-80}$$

where n = number of stages
P_f = discharge pressure from compressor, psia
P_1 = suction pressure to compressor, psia

It is very seldom that the CR is greater than 6. The above relationship will give the minimum horsepower for multistage compression for the number of stages considered. If the CR for each stage were not the same, then the horsepower requirement for the compression would be greater.

The procedure for calculating horsepower from an enthalpy-entropy diagram can best be shown diagrammatically and then demonstrated by means of an example. Figure 7-11 is a qualitative sketch of an enthalpy-entropy diagram. Point 1 is the initial state of the gas as it enters the compressor. Path 1-2 shows the first stage of compression (constant entropy). The gas is then cooled in the intercooler at constant pressure (path 2-3); the difference in enthalpy along this path is equal to the heat removed in the intercooler. Path 3-4 shows the second stage of compression. The temperatures at points 2 and 4 are the temperatures of the gas at the end of the first and second stages of compression. The temperature at point 3 is the temperature to which the gas is cooled in the intercooler.

To demonstrate the use of the *H-S* charts in calculating both the adiabatic and the isothermal horsepower theoretically necessary to compress a gas, the solution of the following example is shown.

Illustrative Problem

Calculate the adiabatic and the isothermal theoretical horsepower required to compress 1 MMcf/day of a 0.6 gravity natural gas at 100 psia and 80°F to 1,600 psia. Intercoolers cool the gas to 80°F. In the case of the adiabatic compression, what is the heat load on the intercoolers and what is the final gas temperature? Use the *H-S* diagrams in the solution to this problem.

Solution

Adiabatic Compression Using Enthalpy-Entropy Charts

1. Since the over-all CR is 16, two-stage compression, each stage with a CR of 4, should be used.

$$\text{CR} = \sqrt{\frac{1,600}{100}} = 4$$

2. The first stage of compression will be from 100 to 400 psia. Determine the difference in enthalpy by following a vertical line (constant entropy) between 100 and 400 psia, using the 0.6 gravity *H-S* chart (Fig. 4-62).

$$\Delta H_{1-2} = H_2 - H_1 = 1990 - 380 = +1610 \text{ Btu/lb mole}$$

3. The gas is then cooled to 80°F. Follow the 400-psia line down to 80°F, and determine the difference in enthalpy. This is the amount of heat removed from the gas in the intercoolers.

$$\Delta H_{2-3} = H_3 - H_2 = 220 - 1990 = -1770 \text{ Btu/lb mole}$$

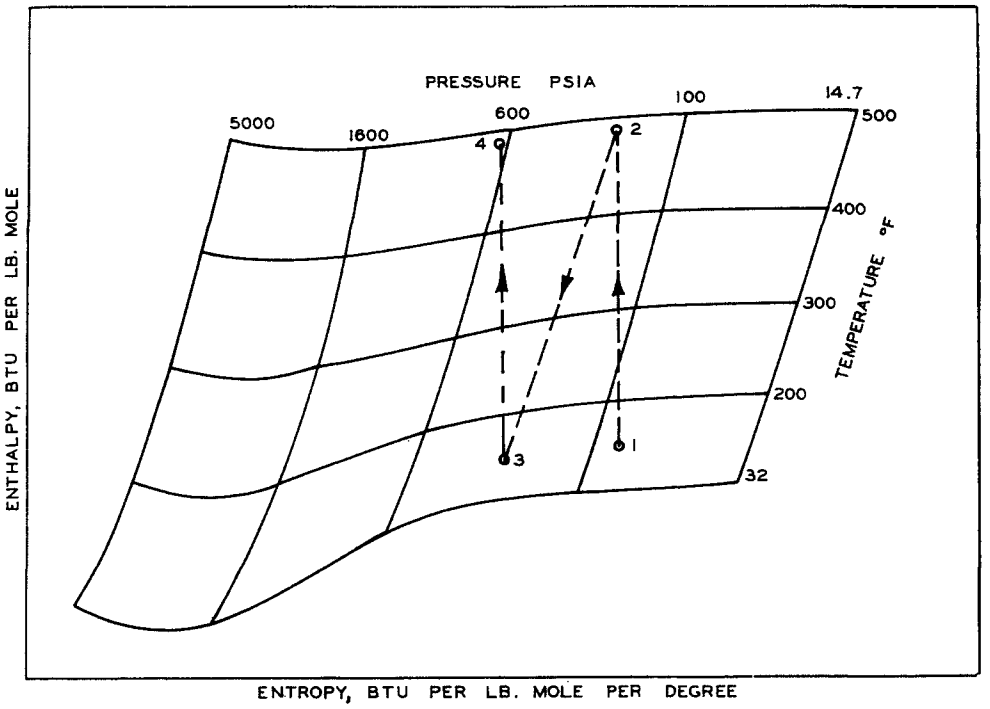

Fig. 7-11. Example of use of enthalpy-entropy diagram to find adiabatic work of compression.

4. The second stage of compression is from 400 to 1,600 psia. Repeat the procedure of step 1.

$$\Delta H_{3-4} = H_4 - H_3 = 1920 - 220 = +1700 \text{ Btu/lb mole}$$

5. The adiabatic theoretical horsepower necessary to compress the gas is thus

$$\begin{aligned} -w &= 0.0432(\Delta H_{1-2} + \Delta H_{3-4}) \\ &= 0.0432 \times (1{,}610 + 1{,}700) \\ &= 0.0432 \times 3{,}310 \\ &= 143 \text{ hp/(MMcf)(day)} \end{aligned}$$

6. The heat load on the intercoolers is

$$\Delta H_{2-3} = -1700 \text{ Btu/lb mole}$$

or, in terms of 1 MMcf/day,

$$\begin{aligned} \Delta H_{2-3} &= \frac{-1700 \times 1{,}000{,}000}{379} \\ &= -4.67 \times 10^6 \text{ Btu/(MMcf)(day)} \end{aligned}$$

7. The final gas temperature is read from the chart at point 4.

$$T = 278°F$$

Isothermal Compression Using Enthalpy-Entropy Chart

By following the 80°F constant-temperature line on the 0.6 gravity H-S diagram (Fig. 4-62), ΔH and ΔS can be determined.

The enthalpy and entropy at 80°F and 100 psia are

$$\begin{aligned} H_1 &= 380 \text{ Btu/lb mole} \\ S_1 &= -3.2 \text{ Btu/(lb mole)(°R)} \end{aligned}$$

At 80°F and 1,600 psia,

$$\begin{aligned} H_2 &= -480 \text{ Btu/lb mole} \\ S_2 &= -9.75 \text{ Btu/(lb mole)(°R)} \end{aligned}$$

Thus
$$\begin{aligned} \Delta H &= H_2 - H_1 = -480 - 380 = -860 \\ \Delta S &= S_2 - S_1 = -9.75 + 3.2 = -6.55 \end{aligned}$$

The isothermal theoretical horsepower then is

$$\begin{aligned} -w &= 0.0432(-860 + 540 \times 6.55) \\ &= 0.0432 \times 2{,}677 \\ &= 115.7 \text{ hp} \end{aligned}$$

This is the absolutely minimum horsepower necessary to compress the gas. An actual compressor with an infinite number of intercoolers and stages of compression would approach isothermal conditions if the gas were cooled to the initial temperature in the intercoolers. Qualitatively, Fig. 7-12 shows horsepower requirements versus number of compression stages. The horsepower approaches the isothermal value as the number of stages increases.

Illustrative Problem

Calculate the adiabatic and isothermal theoretical horsepower for the conditions of the previous problem using Eqs. (7-73) and (7-69), respectively.

Solution for Adiabatic Compression with Eq. (7-73)

$$-w = 0.08531 \frac{k}{k-1} T_1 \left[\left(\frac{P_2}{P_1} \right)^{z(k-1)/k} - 1 \right]$$

$$\begin{aligned} k &= 1.28 \\ T_1 &= 540°R \\ \frac{P_2}{P_1} &= 4 \\ T_C &= 358°R \\ P_C &= 671 \text{ psia} \\ T_r &= 1.51 \\ P_{r,1} &= 0.149 \\ P_{r,2} &= 0.595 \\ z_1 &= 0.985 \quad \text{at 80°F and 100 psia} \\ z_2 &= 0.940 \quad \text{at 80°F and 400 psia} \end{aligned}$$

First stage:

$$-w = 0.08531 \times \frac{1.28}{0.28} \times 540 \times (4^{0.985(0.28/1.28)} - 1)$$

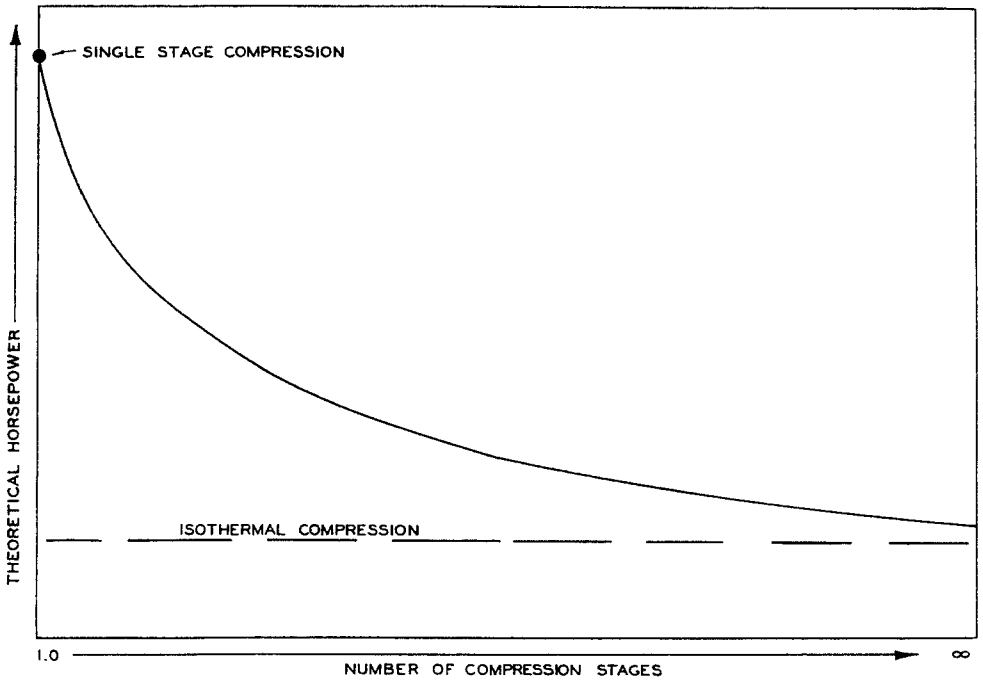

Fig. 7-12. Variation of compression horsepower with number of stages.

$$= 210.6 \times (4^{0.2165} - 1)$$
$$= 210.6 \times 0.348$$
$$= 73.3 \text{ hp} \quad \text{in first stage}$$

Second stage:

$$-w = 0.08531 \times \frac{1.28}{0.28} \times 540 \times (4^{0.940(0.28/1.28)} - 1)$$
$$= 210.6 \times 0.330$$
$$= 69.5 \text{ hp} \quad \text{in second stage}$$

Total work: $-w = 69.5 + 73.3$
$= 142.8$ hp/(MMcf)(day)

Solution for Isothermal Compression with Eq. (7-69)

$$-w = 0.08531T\left(\int_{0.2}^{P_{r,2}} \frac{z}{P_r}\,dP_r - \int_{0.2}^{P_{r,1}} \frac{z}{P_r}\,dP_r\right)$$
$$T = 540$$
$$T_r = 1.51$$
$$P_{r,1} = 0.149$$
$$P_{r,2} = 2.382$$
$$\int_{0.149}^{0.2} \frac{z}{P_r}\,dP_r = 0.291$$
$$\int_{0.2}^{2.382} \frac{z}{P_r}\,dP_r = 2.283$$
$$-w = 0.08531 \times 540 \times (2.283 + 0.291)$$
$$= 0.08531 \times 540 \times 2.574$$
$$= 118.6 \text{ hp}$$

For the above specific example the agreement between values for horsepower calculated by means of the equations and those calculated by means of the enthalpy-entropy diagram is good. However, use of the *H-S* charts is preferred.

Theoretical horsepower can be converted to brake horsepower (horsepower input into the compressor) by the application of the proper factors. The factors involved include the compression efficiency (compressor-valve losses) and the mechanical efficiency of the compressor. The losses vary with equipment design, speed, ratio of compression, and other factors. The combined efficiencies have been shown to vary with compression ratio, as shown in Fig. 7-13, and can be used (7-33) for determining brake horsepower from theoretical horsepower as obtained from the enthalpy-entropy diagrams or from the analytical equations.

$$\text{Efficiency} = \frac{\text{adiabatic theoretical horsepower}}{\text{brake horsepower}}$$

The 143 hp found for theoretical adiabatic compression at a CR of 4 converts to 143/0.827 = 172.9 brake horsepower.

SIMULTANEOUS FLOW OF LIQUID AND GAS

Two-phase flow occurs in horizontal pipelines on the surface of the ground and in vertical well bores.

Horizontal Flow. The mechanics and characteristics of two-phase horizontal-flow systems have been of interest for some time. In pipelines, chemical reactors, and heat exchangers, two-phase flow is an everyday occurrence. In the simultaneous production of gas and oil it is quite often desirable to transport both phases in a common pipeline. Centrally located stock-tank batteries in oil fields have resulted in long gathering lines which must be designed for multiphase-flow conditions. Increases in the efficiency of artificial lift equipment quite often require that surface gathering systems be redesigned to handle increased production. This is particularly true of gas-lift installations.

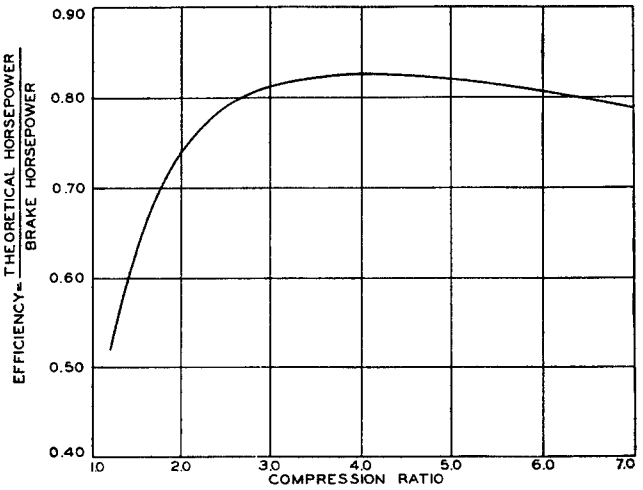

Fig. 7-13. Compressor efficiency. (*Ridgeway*, 7-33.)

The general problem of predicting the pressure drop for the simultaneous flow of gas and liquid is complicated. One of the main difficulties is that there may be flow patterns of widely different configurations. The types of flow that can occur are: bubble, plug, stratified, slug, wave, annular, spray, and froth flow (Fig. 7-13*a*). However, the same variables that determine the flow pattern also determine the energy losses, and it would seem reasonable to assume that a generalized solution, independent of flow pattern, is possible.

In designing two-phase flow systems, the problem is to predict the relationships among pipe diameter, pipe length, fluid properties, flow rates, and pressure drop. The literature contains many articles dealing with specific multiphase-flow problems.

Lockhart and Martinelli proposed a general solution for horizontal multiphase flow (7-24). The basis of their correlation is the assumption that the two-phase pressure drop is equal to the pressure drop of one phase as if it were flowing through the pipe alone, multiplied by a factor which was found to be a function of the ratio of the single-phase pressure drop of the liquid to the single-phase pressure drop of the gas, as well as of the flow mechanism. Flow mechanisms

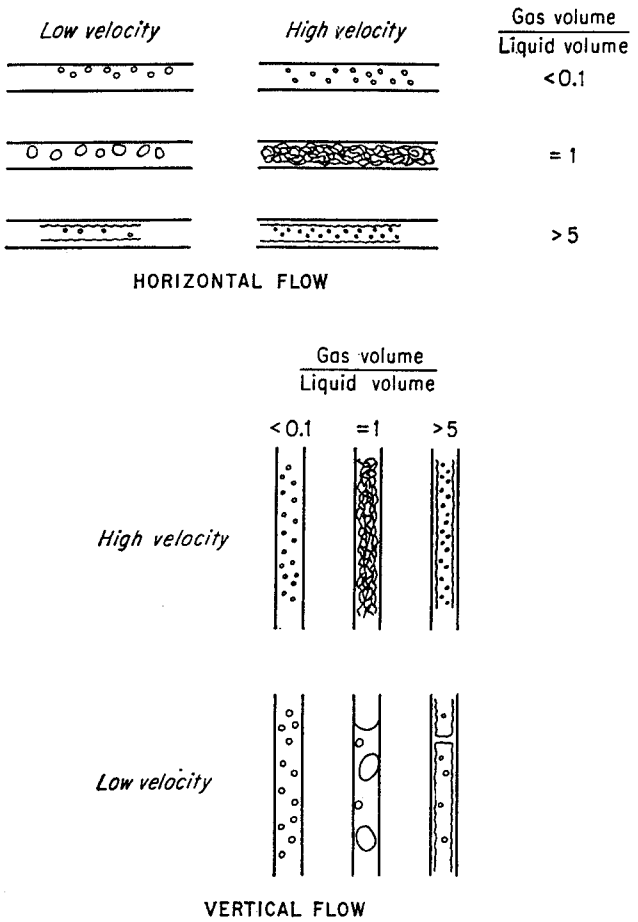

Fig. 7-13a. Mechanisms of two-phase flow.

are defined in terms of viscous or turbulent flow for each phase.

There have been some attempts to improve on this method. Alves (7-1) demonstrated that different flow patterns are possible for the various flow mechanisms used by Martinelli. Baker (7-4) attributes deviations from Martinelli's correlation to variations in flow pattern. Using Martinelli's procedure, Baker correlated data for each flow pattern for the turbulent-turbulent flow mechanism. A disadvantage of Baker's procedure is that one must determine flow pattern to find the correct chart for performing the pressure-drop calculations. Procedures for defining flow patterns are not well established.

The procedure for using Lockhart and Martinelli's correlation is as follows.

1. Calculate the pressure gradient or pressure drop for the liquid phase and for the gas phase, assuming during each calculation that it represents the only fluid flowing. The X parameter is then calculated.

$$X = \sqrt{\frac{(\Delta P/\Delta L)_L}{(\Delta P/\Delta L)_G}} = \sqrt{\frac{\Delta P_L}{\Delta P_G}} \qquad (7\text{-}81)$$

The pressure gradient or pressure drop for the gas phase can be calculated using Eq. (7-29) or (7-35). The pressure gradient or pressure drop for the liquid phase is calculated from the following relationship and from Fig. 7-3.

$$\Delta P_L = \frac{34 \times 10^{-10} f Q^2 L \rho_L}{g_c D^5} \qquad (7\text{-}82)$$

where f is obtained from Fig. 7-3

Q = liquid flow, bbl/day
L = length of pipeline, ft
ρ_L = liquid density, lb/cu ft
D = pipe diameter, ft
ΔP_L = pressure drop for liquid, psia
g_c = 32.174

2. Calculate the Reynolds numbers for both liquid and gas phases as though each phase were flowing in the pipe by itself. Then, from Table 7-5, determine the type of flow mechanism involved, that is, for example, liquid viscous–gas turbulent, etc.

Table 7-5. Flow Mechanisms

Flow mechanism	Reynolds number	
	Liquid	Gas
Liquid turbulent–gas turbulent	>2,000	>2,000
Liquid viscous–gas turbulent	<1,000	>2,000
Liquid turbulent–gas viscous	>2,000	<1,000
Liquid viscous–gas viscous	<1,000	<1,000

3. From Fig. 7-14, using the value of X calculated in step 1 and the type of flow mechanism found in step 2, obtain the value of ϕ. Use the ϕ_L curves when the pressure gradient or pressure drop for the liquid is used and the corresponding curves for ϕ_G when the pressure gradient or pressure drop for the gas is used. The two-phase pressure drop is then calculated.

$$\left(\frac{\Delta P}{\Delta L}\right)_{T,P} = \phi^2 \left(\frac{\Delta P}{\Delta L}\right)_{L \text{ or } G} \qquad (7\text{-}83)$$

or

$$\Delta P_{T,P} = \phi^2 (\Delta P)_{L \text{ or } G} \qquad (7\text{-}84)$$

Bertuzzi and coworkers have recently published a paper on horizontal multiphase flow in which the concept of a two-phase f factor was used (7-8). This concept has been successfully used in predicting pressure drop for multiphase vertical flow and for the flow of a flashing mixture of steam and water in pipes (7-6). The authors attempt to eliminate the need to establish a flow pattern for predicting pressure drop and they reduce their method to a simplified graphic procedure suitable for field use. The development is based on a total energy balance for the flowing two-phase mixture under steady-state conditions. Energy

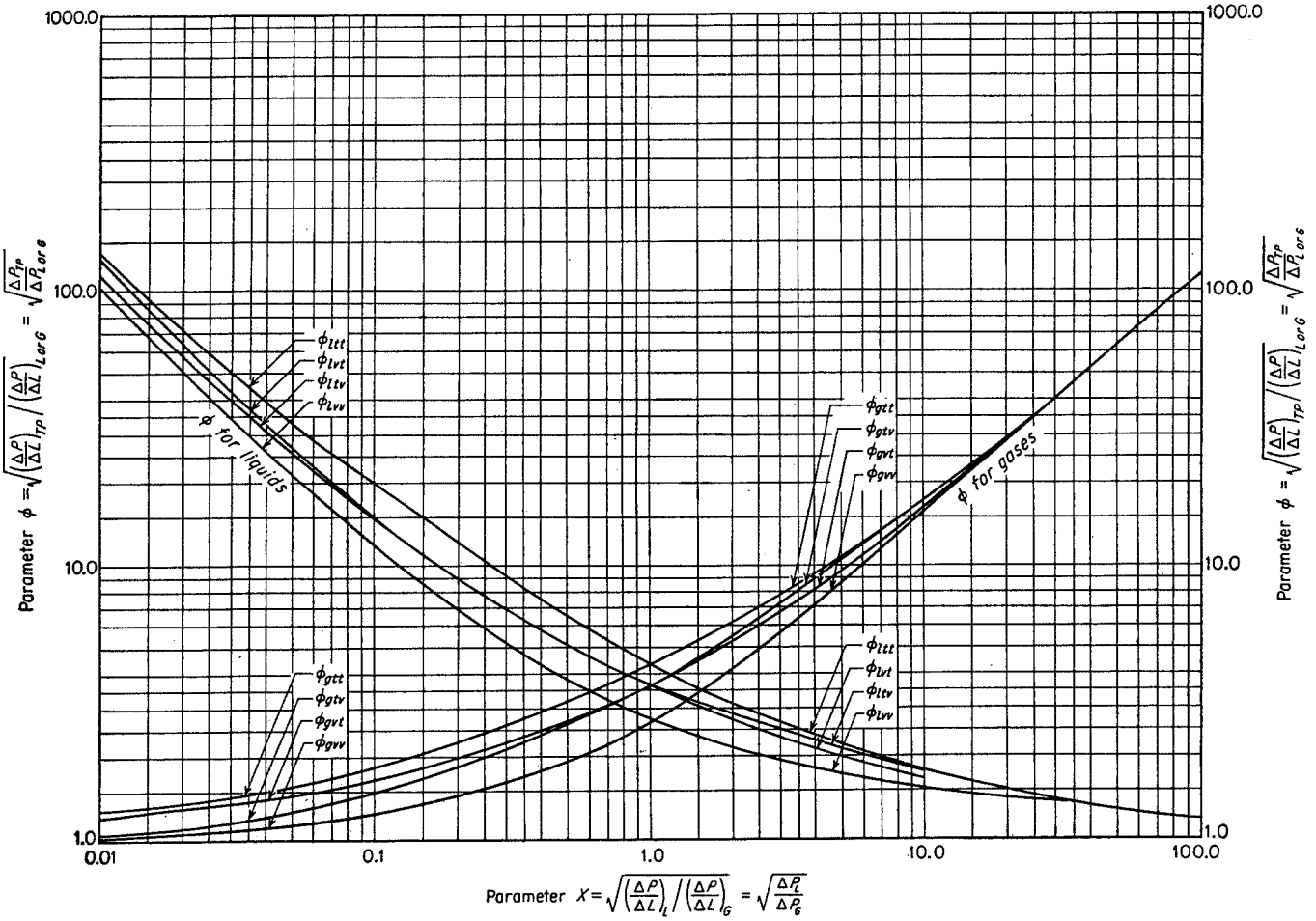

Fig. 7-14. Correlation for multiphase flow. (*Alves, 7-1. Courtesy Chem. Eng. Progr.*)

dissipated is expressed in terms of the two-phase f factor. This factor was found to correlate best in terms of a liquid- and a gas-phase Reynolds number, each based on pipe diameter and gas-liquid mass ratio (Fig. 7-15). [It should be noted that the f' used in this correlation is defined so that its value is one-fourth that for the Moody chart (Fig. 7-3).]

$$f' = \phi\left[\left(\frac{DW_g}{\mu_g}\right)^a \left(\frac{DW_L}{\mu_L}\right)^b\right] \qquad (7\text{-}85)$$

where D = diameter, ft
W_g = mass velocity of gas, lb/(sq ft)(sec)
W_L = mass velocity of liquid, lb/(sq ft)(sec)
$a = k/(1 + k)$
$b = 1/e^{0.1k}$
k = gas mass rate/liquid mass rate

The correlation was developed from laboratory data available in the literature.

On the basis of about 250 experimental measurements available from the literature, the pressure gradients calculated by means of this correlation and compared with experimental values showed a bias of +0.82 per cent and a standard deviation of 20.8 per cent from the algebraic average. Calculations on the same data using Martinelli's correlation (7-24) resulted in a bias of +14.4 per cent and a standard deviation from the algebraic average of 27.5 per cent.

In order to simplify the calculation of the pressure drop, the calculations were reduced to graphical form, as shown in Figs. 7-16 and 7-17, where

QM = total mass flow rate, lb/day
D = diameter, ft
R = gas-liquid ratio, cu ft/bbl (of stock-tank oil)
S = solubility of gas in oil, cu ft/bbl (of stock-tank oil)
G_g = gas gravity (air = 1)
ρ_L = specific gravity of liquid (water = 1)
μ_g = viscosity of gas at pressure P, lb/(ft)(sec)
μ_L = viscosity of liquid at pressure P, lb/(ft)(sec)
ρ = flowing density entering at pressure P, lb/cu ft
$r = 0.12a$

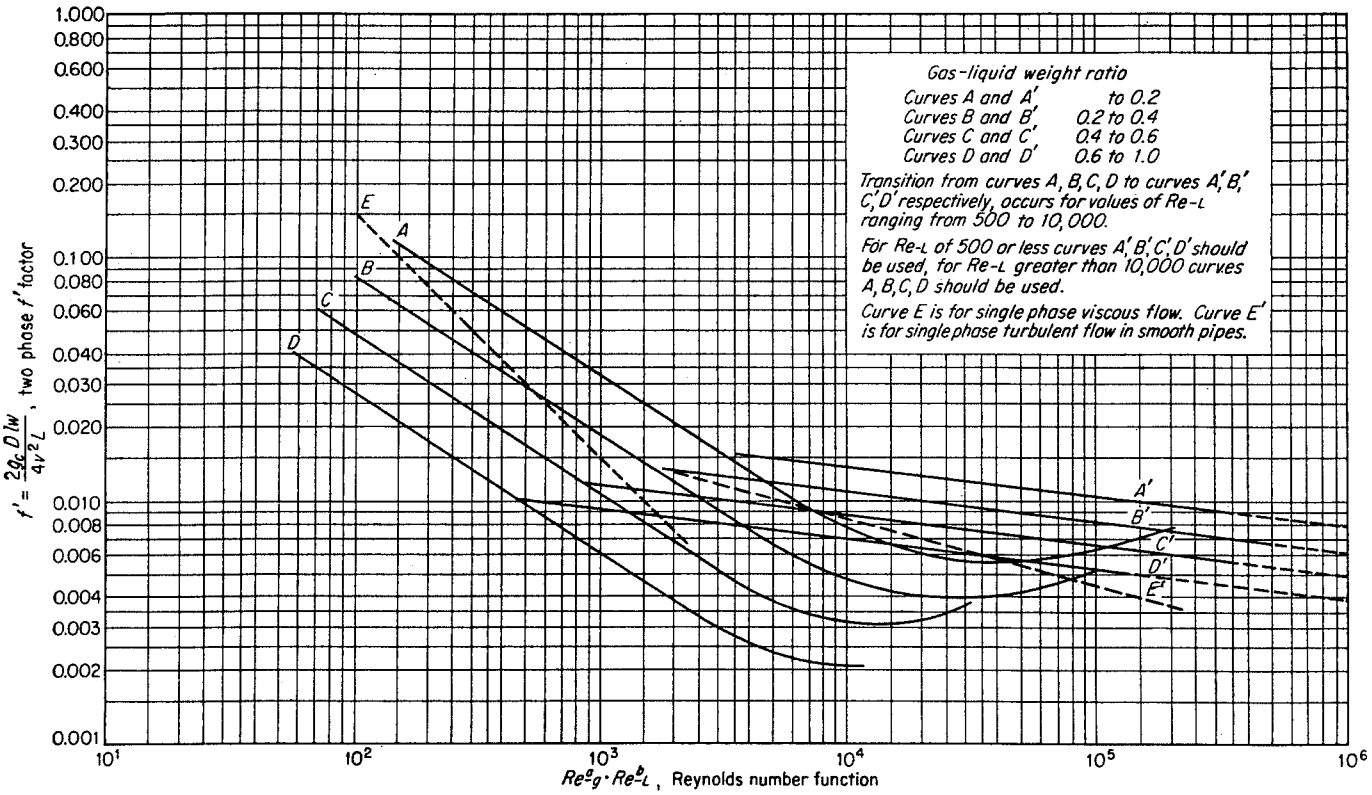

Fig. 7-15. Composite energy-dissipation chart for two-phase flow. (*Bertuzzi, Tek, and Poettmann, 7-8. Courtesy AIME.*)

$s = 0.12b$
$t = 0.12(a + b)$
$u = 2 - 0.12(a + b)$
$v = 5 - 0.12(a + b)$

Figures 7-16 and 7-17 should not be used for liquid Reynolds numbers Re_L less than 10,000. For most practical field cases Re_L will be greater than 10,000 for gas-liquid volume ratios less than 5,000.

The equations and procedure for calculating the variation of pressure with length for the multiphase flow of liquid and gas through a horizontal flow string is as follows.

1. Determine the mass flow rate QM in pounds of total fluid per day. Q is expressed in barrels of stock-tank fluid per day, and M is the total mass of gas and liquid associated with one barrel of fluid flowing into and out of the pipe. M can be calculated as follows:

$$M = 5.61 \times 62.4\rho_L + 0.0764G_gR \qquad (7\text{-}86)$$

2. Determine inside pipe diameter in inches.
3. Calculate the product $R(G_g/\rho_L)$.
4. Calculate the value of $\mu_g{}^r\mu_L{}^s/\rho$.

The value of this function depends on the physical properties of the fluid and, as such, is a function of pressure. Calculation of this function establishes the pressure gradient for a given pressure along the flow string. The function is calculated for various increments of pressure along the tubing, and the corresponding pressure gradients dP/dL are determined from Fig. 7-16.

$$\rho = \frac{M}{V_m} \qquad (7\text{-}87)$$

where
$$V_m = 5.61B + \frac{P_0T_az}{PT_0}(R - S) \qquad (7\text{-}88)$$

wherein B = formation volume factor of oil at pressure P in barrels of reservoir oil per barrel of stock-tank oil; the formation volume factor should be measured at the average flow-string temperature; however, this information is seldom available and the formation volume factor at reservoir temperature must be used
S = solubility of gas in oil at pressure P, cu ft/bbl
T_a = arithmetic average temperature in the flow string, °R
P = pressure, psia
P_0 = base pressure, psia
T_0 = base temperature, °R
z = compressibility factor of the gas in the tubing at temperature T_a and pressure P

If the gas solubility is nearly zero, such as in the case of air-and-water mixtures, or if the pressure level

is low, so that gas solubility can be neglected, then

$$V_m = 5.61 + \frac{P_0 T_a z R}{P T_0} \qquad (7\text{-}89)$$

The viscosity of the oil may be estimated by the method of Beal (4-99). Gas viscosity can be determined using Fig. 4-107.

5. Calculate the correction dP/dL for the pressure gradients from Fig. 7-17.

6. Determine the variation of pressure along the length of the flow string by incremental integration. Plot to give pressure at desired depth.

Illustrative Problem (7-8)

A well is being produced by gas lift at a rate of 400 bbl/day of stock-tank oil with a total gas-oil ratio of 1,000 cu ft/bbl. The separator, which is 1,000 ft from the wellhead, is operated at a pressure of 50 psia, and the fluid is transported to the separator through a 2-in., 1.995-ID horizontal line. In gas-lift operations, it is desirable to maintain a low wellhead pressure for efficient lifting. Calculate (*a*) the wellhead pressure for the 2-in. pipe, (*b*) the wellhead pressure if 3-in. (2.992-ID) or 4-in. (3.990-ID) pipe had been used. Plot diameter of pipe versus wellhead pressure.

Other pertinent data are:

$T_a = 75°\text{F}$
$G_g = 0.65$
$\rho_L = 0.80$
$\mu_g = 0.014$ centipoise
$= 9.4 \times 10^{-6}$ lb/(ft)(sec) at 75°F and 50 psia
$\mu_L = 0.60$ centipoise
$= 4.0 \times 10^{-4}$ lb/(ft)(sec) at 75°F and 50 psia

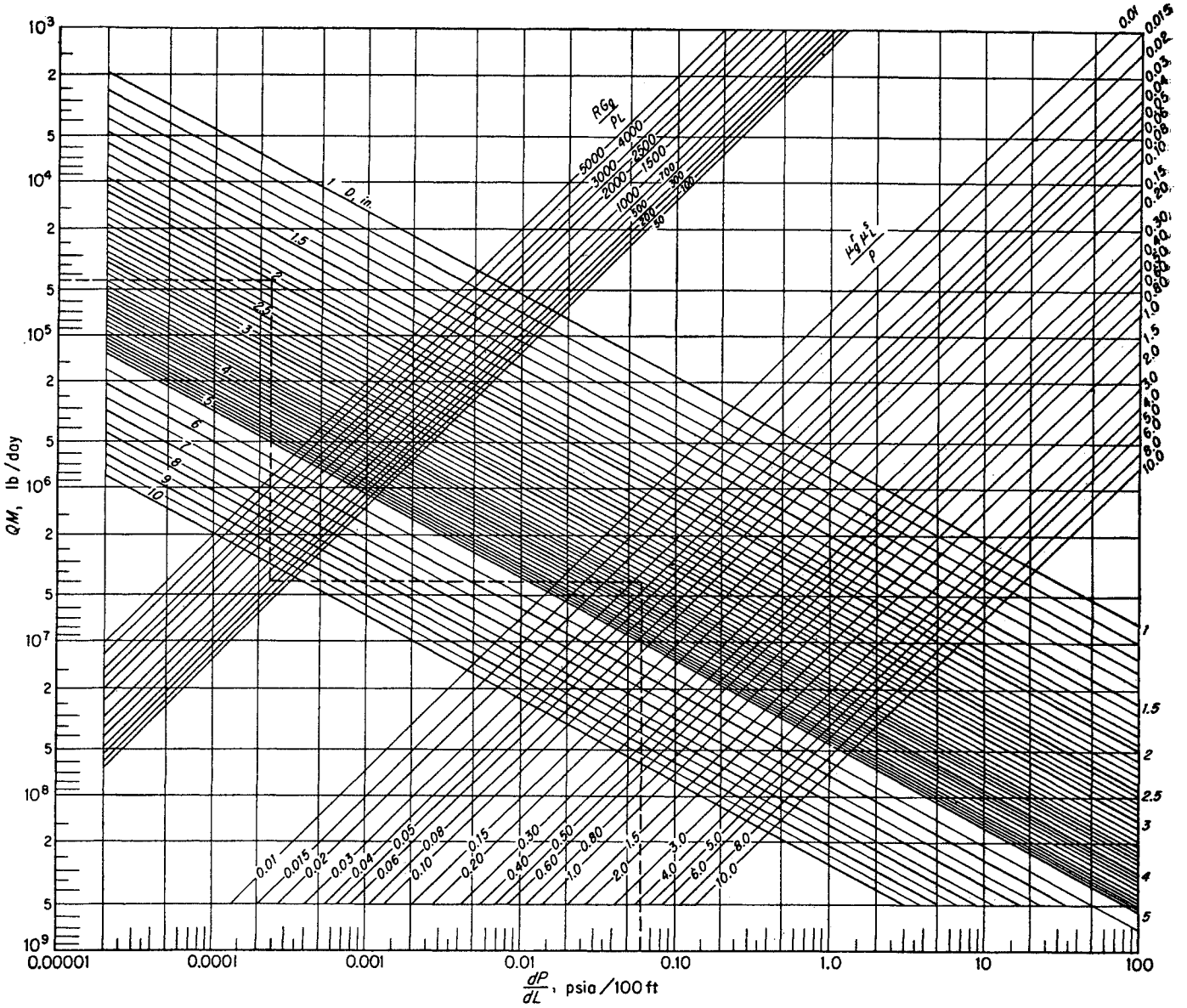

Fig. 7-16. Chart for estimating pressure drop for horizontal multiphase flow of fluid in pipes. (*Bertuzzi, Tek, and Poettmann, 7-8. Courtesy AIME.*)

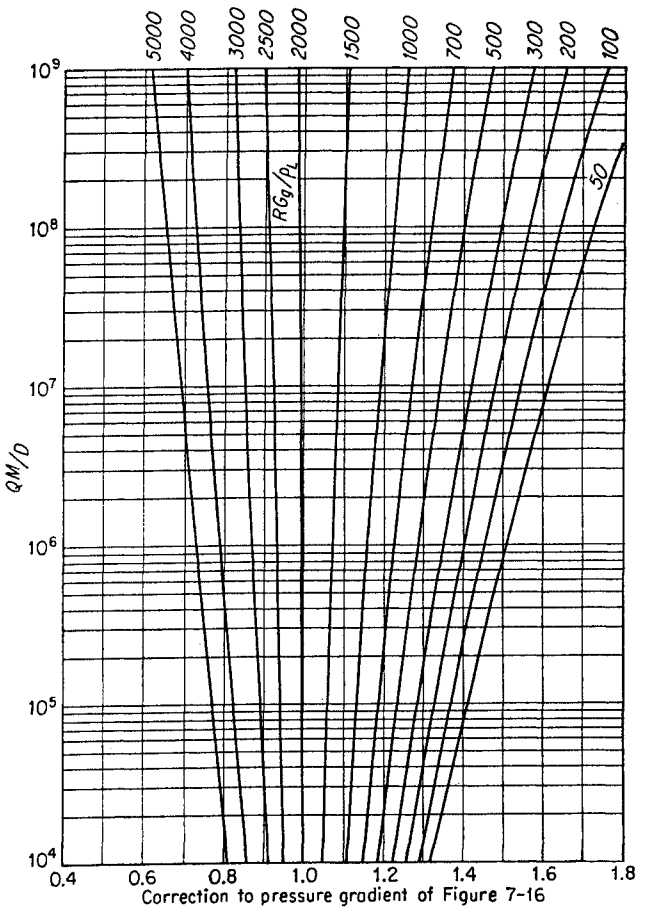

Fig. 7-17. Multiplication correction for Fig. 7-16. (*Bertuzzi, Tek, and Poettmann, 7-8. Courtesy AIME.*)

Solution

(*a*) Calculate QM.

$Q = 400$ bbl/day

$M = 350.1\rho_L + 0.0764G_gR$

$M = 329.7$ lb/bbl

$QM = 400 \times 329.7 = 131{,}880$ lb/day

(*b*) $D = 1.995$ in.

(*c*) Calculate $R(G_g/\rho_L)$.

$$R\left(\frac{G_g}{\rho_L}\right) = 1{,}000 \times \frac{0.65}{0.80} = 812.5$$

(*d*) Calculate $\mu_g{}^r\mu_L{}^s/\rho$.

Fluid viscosity at outlet conditions was used. If pressure drop is expected to be less than 100 psi, change in fluid viscosity with pressure can be neglected. Similarly, if the pressure level is low, gas solubility can also be neglected, and Eq. (7-88) can be used for calculating V_m.

$$a = \frac{k}{k+1} = \frac{812.5 \times 0.000219}{812.5 \times 0.000219 + 1} = 0.151$$

$$b = \frac{1}{e^{0.1k}} = \frac{1}{e^{0.0178}} = 0.980$$

$$r = 0.12a = 0.018$$

$$s = 0.12b = 0.118$$

$$\mu_g{}^r = (9.4 \times 10^{-6})^{0.018} = 0.812$$

$$\mu_L{}^s = (4.0 \times 10^{-4})^{0.118} = 0.397$$

$$\mu_g{}^r\mu_L{}^s = 0.322$$

$$\rho = \frac{M}{V_m} = \frac{329.7}{V_m}$$

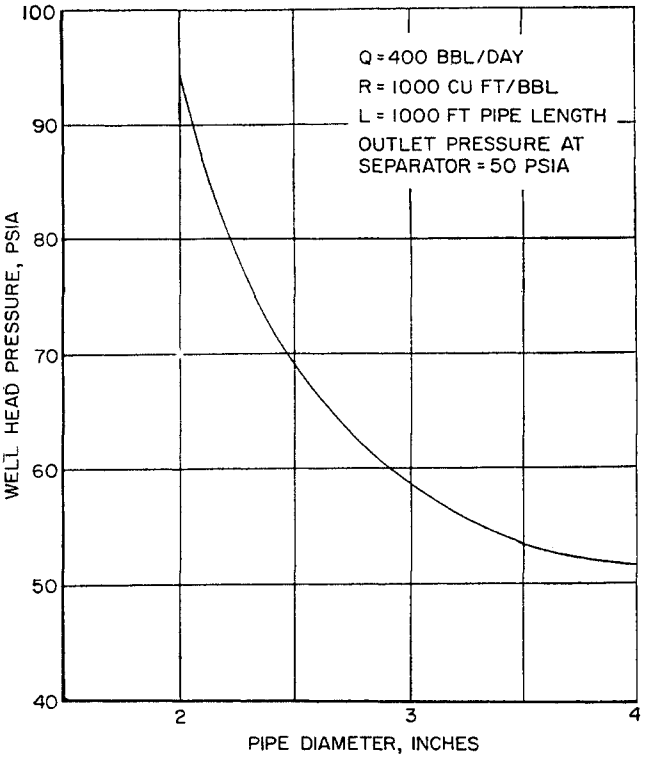

Fig. 7-18. Solution to illustrative problem. (*Bertuzzi, Tek, and Poettmann, 7-8. Courtesy AIME.*)

$$V_m = 5.61 + \frac{P_0T_a}{T_0}R\frac{z}{P}$$

$$V_m = 5.61 + \frac{14.65 \times 535 \times 1{,}000}{520}\frac{z}{P}$$

$$V_m = 5.61 + 15{,}073\,\frac{z}{P}$$

Assuming $z = 1.0$, calculate z/P for values of P of 50, 60, 70, 80, 90, and 100 psia. V_m corresponding to these values can then be calculated. Then values of the function $\mu_g{}^r\mu_L{}^s/\rho$ are calculated, and dP/dL is established from Fig. 7-16.

(1) P, psia	(2) V_m	(3) $\rho = \frac{M}{V_m}$	(4) $\frac{\mu_g{}^r\mu_L{}^s}{\rho}$	(5) $\frac{dP}{dL}$, psi/100 ft
50	304.05	1.084	0.297	5.7
60	254.31	1.296	0.248	4.6
70	218.79	1.507	0.214	4.0
80	191.19	1.724	0.187	3.6
90	170.57	1.933	0.167	3.25
100	153.32	2.150	0.150	3.0

(*e*) Correct gradients obtained in step *d* by use of Fig. 7-17. Calculate QM/D, where D is the pipe diameter expressed in feet.

$$\frac{QM}{D} = 131{,}880 \times \frac{12}{1.995} = 793{,}260$$

$$R\frac{G_g}{\rho_L} = 812.5$$

Correction factor = 1.21.

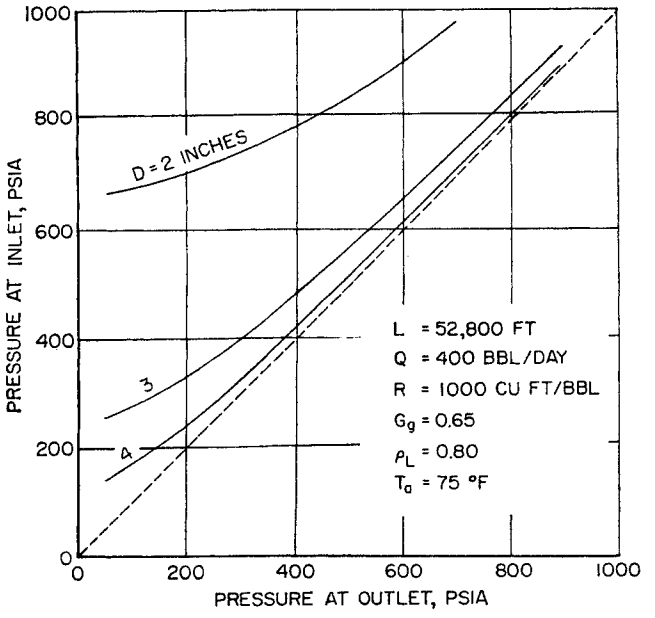

Fig. 7-19. Effect of pipe diameter on pressure drop at different pressure levels. (*Bertuzzi, Tek, and Poettmann, 7-8. Courtesy AIME.*)

(1) P, psia	(2) $\frac{dP}{dL}$	(3) Correct $\frac{dP}{dL}$
50	5.7	6.9
60	4.6	5.6
70	4.0	4.8
80	3.6	4.4
90	3.25	3.9
100	3.0	3.6

(*f*) Integrate $\frac{dP}{dL}$.

(1) P	(2) ΔP	(3) $\frac{\Delta P}{dL}$	(4) $\left(\frac{dP}{dL}\right)_{av}$	(5) $\Delta L = \frac{(2)}{(4)}$	(6) L
50	...	6.9	....	...	0
60	10	5.6	6.25	160	160
70	10	4.8	5.2	192	352
80	10	4.4	4.6	217	569
90	10	3.9	4.15	241	810
100	10	3.6	3.75	267	1,077

A plot of P versus L gives a value of 97 psia at 1,000 ft, a pressure drop of 47 psi.

The identical procedure gives a wellhead pressure of 59 psia for the 3-in.-diameter pipe and of 52 psia for the 4-in.-diameter pipe. A plot of the results is shown in Fig. 7-18. Going from a 2-in. to a 3-in. pipe would result in a considerable decrease in pressure at the wellhead, with resultant increase in the performance efficiency of the gas-lift operations.

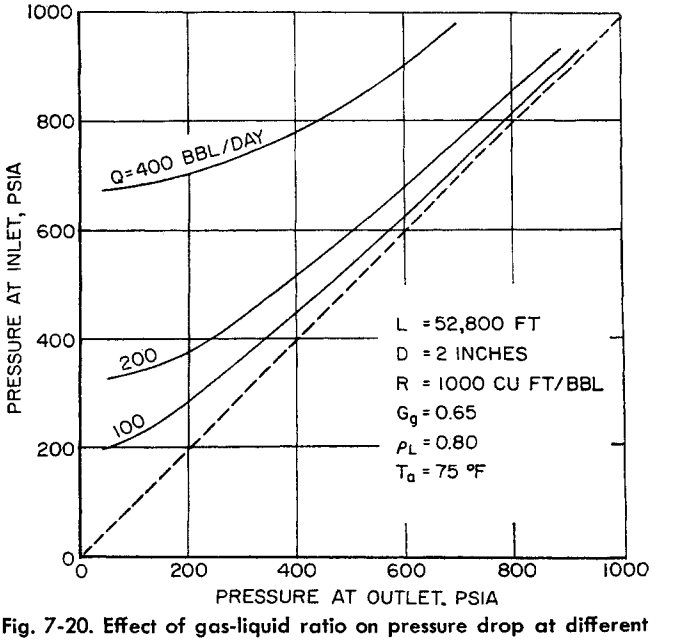

Fig. 7-20. Effect of gas-liquid ratio on pressure drop at different pressure levels. (*Bertuzzi, Tek, and Poettmann, 7-8. Courtesy AIME.*)

In order to show the effect of the different flow variables upon one another, Figs. 7-19 to 7-21 were plotted. Pipe length, gas and liquid gravity, and temperature were held constant. Figure 7-19 shows the effect of pipe diameter on pressure drop; Fig. 7-20 shows the effect of production rate on pressure drop; and Fig. 7-21 shows the effect of gas-liquid ratio on pressure drop.

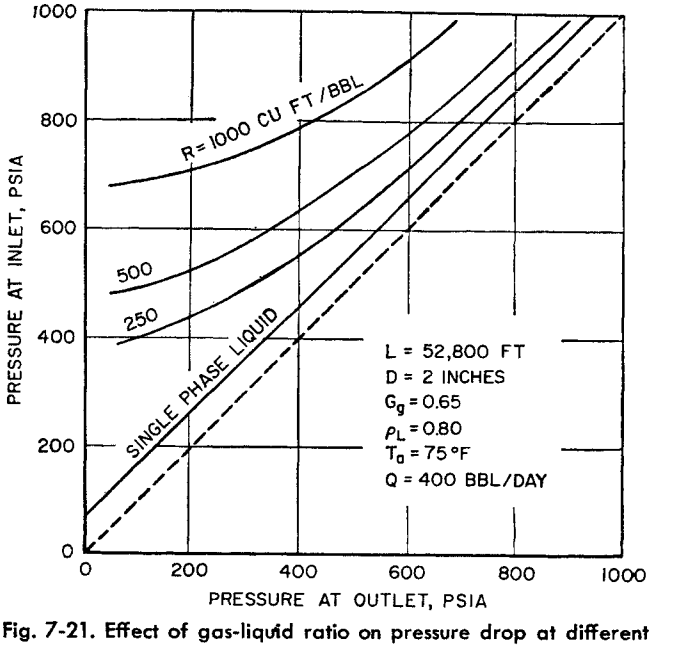

Fig. 7-21. Effect of gas-liquid ratio on pressure drop at different pressure levels. (*Bertuzzi, Tek, and Poettmann, 7-8. Courtesy AIME.*)

Vertical Flow. The general statements characterizing horizontal flow apply also to vertical flow. However, the "state of the art" for vertical multiphase flow is more advanced than that for horizontal multiphase flow, probably because the nature of the flow characteristics for vertical flow is better understood. The problem is to predict the variation of pressure with elevation along the length of the flow string for known conditions of flow. The ability to do this for flowing wells would provide a means of evaluating the effect on one another of tubing size, flow rate, bottom-hole pressure, and a number of other variables. It would be particularly useful in designing the installation of gas-lift wells. From such calculations one would obtain information about where to inject the gas, the pressure at which to inject the gas, the rate at which to inject the gas, the ideal horsepower requirements to lift the oil, and the effect of production rate and tubing size on these quantities (7-7). In other words, it would provide a means of studying systematically the effects of the different variables upon one another, a study which would be impractical in actual field testing.

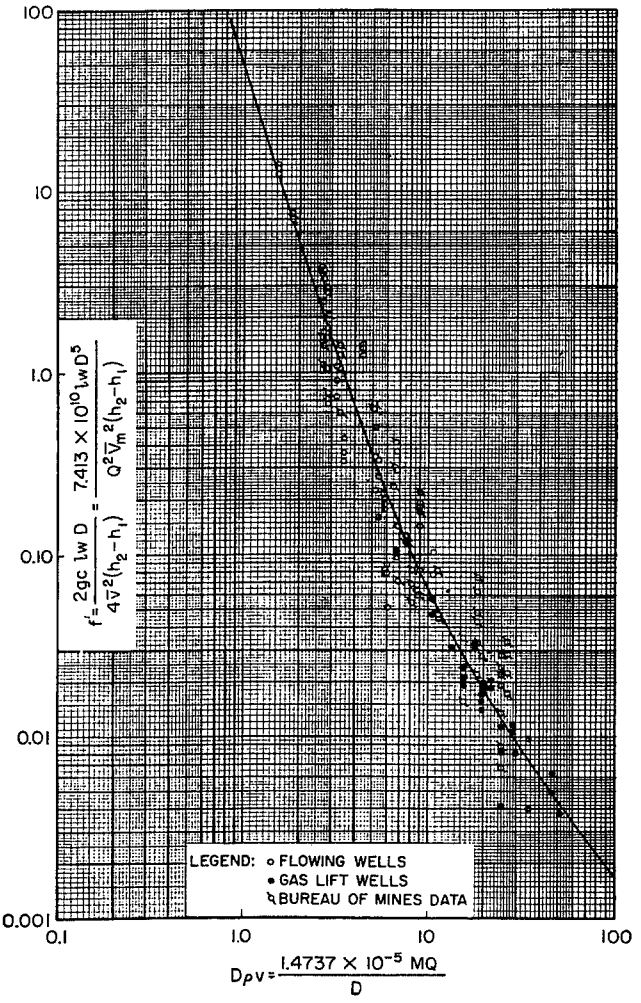

Fig. 7-22. Correlation of field data on flowing and gas-lift wells. (*Poettmann and Carpenter, 7-31. Courtesy API Drill. Prod. Practice.*)

Considerable work has been done on the laws governing the multiphase flow of fluid and gas mixtures in vertical tubing. However, only recently has anything approaching a general solution applicable to flowing oil wells and to gas-lift wells been found (Poettmann and Carpenter, 7-31). The basic differences between the treatment employed by Poettmann and Carpenter and methods previously used by other investigators are as follows:

[1] The correlation is based on field data covering a wide range of operating conditions. Use of field data eliminates the problem of extrapolating laboratory data to field conditions.

[2] The flowing fluid was treated as though it were a single homogeneous phase and the energy losses were correlated on this basis.

[3] The total flowing density or flowing specific volume was used rather than an "in situ" density or specific volume. Under steady-state conditions, a given amount of liquid and gas enters and leaves the tubing per unit of time. When liquid hangup or slippage occurs, gas flows at a greater linear velocity than the liquid. As a result the mass of liquid in the tubing at any instant, relative to that of the gas in the tubing at the same instant, is greater than the relative mass of liquid to gas as both components enter and leave the tubing. As a result the "in situ" specific volume is smaller than the flowing specific volume. It is from the flowing specific volume that the energy necessary to overcome the irreversibilities inherent in fluid flow is obtained. The energy entering and leaving the tubing by virtue of the flowing fluid is a function of the pressure-volume properties of the fluid entering and leaving the tubing and not of the pressure-volume properties of the fluid in place.

[4] In calculating the flowing density or flowing specific volume, mass transfer between the flowing phases is taken into consideration as well as the entire mass of the gas and liquid phases. No assumptions were made as to the type of flow existing in the flow string, other than that the fluid flowing in the vertical flow string is in a high degree of turbulence. Because of this, energy loss resulting from viscous shear is negligible, and flow can be considered independent of viscosity effects.

The treatment consists of developing an f' factor (Fig. 7-22) from field data on 49 flowing and gas-lift wells operating over a wide range of conditions. It should be noted that the f' used in this multiphase-flow correlation has been defined so that its value is one-fourth of that used in Fig. 7-3. From this f' factor,

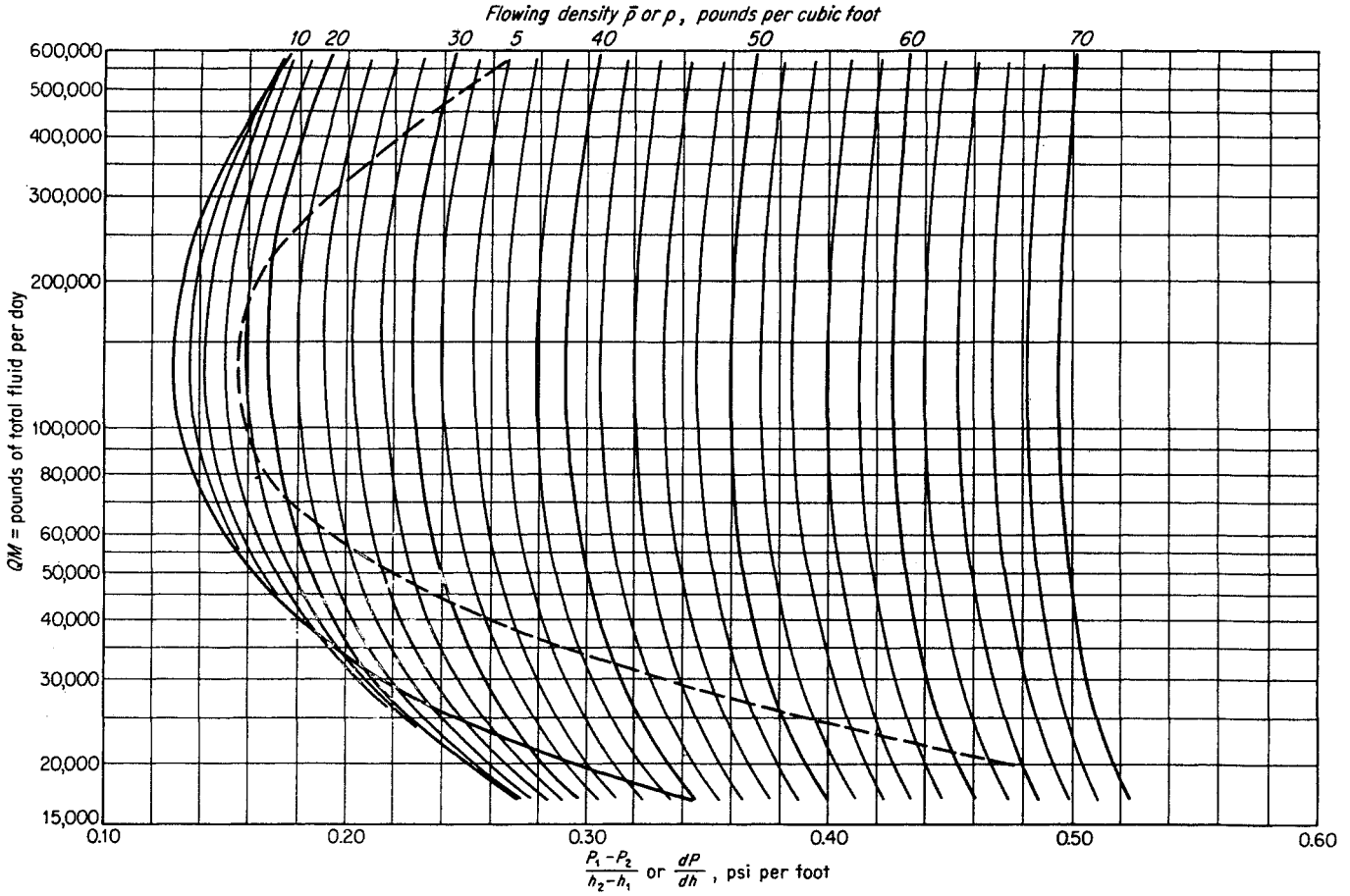

Fig. 7-23. Calculation of pressure traverse in 2-in. tubing (1.995 in. ID). (*Poettmann and Carpenter, 7-31. Courtesy API Drill. Prod. Practice.*

correlation charts were prepared for various tubing sizes, on which were plotted the total mass-producing rate QM versus the pressure gradient dP/dh or $(P_1 - P_2)/(h_2 - h_1)$ regarded as a function of the flowing density ρ or $\bar{\rho}$, respectively. The charts are shown in Figs. 7-23 to 7-25. Additional curves for tubing diameters other than those cited can be constructed, assuming that the f'-factor correlation will hold for the new diameters.

By determining the density at any pressure, dP/dh can be evaluated for that pressure. The pressure traverse can then be established by plotting the reciprocal of dP/dh versus the pressure and integrating. Another method of establishing the pressure traverse is to determine an average integrated density $\bar{\rho}$ between the pressure limits P_1 and P_2. This then determines the value of $(P_1 - P_2)/(h_2 - h_1)$. Dividing this value of $(P_1 - P_2)/(h_2 - h_1)$ into $P_1 - P_2$, the limits used in determining $\bar{\rho}$, we determine the difference in elevation between the pressure limits. The complete pressure traverse can then be constructed.

The curvature of the lines shown in Figs. 7-23 to 7-25 is significant. At high flow rates, there are high velocities and no slippage or liquid hangup. The pressure gradients in this region are primarily the result of frictional effects, and as the velocity (flow rate) decreases, the gradient decreases. At low rates of flow and low velocities, considerable slippage or liquid hangup exists in the flow strings. The pressure gradient under these conditions is primarily the result of the slippage effects, and as the velocity (flow rate) decreases, slippage increases, which in turn further increases the pressure gradient. The combination of these two effects for a gas-liquid mixture of constant density results in the curvature of the lines as shown in the figures.

The equations and procedure for calculating the pressure traverse for the multiphase flow of liquid and gas through vertical flow strings are as follows:

1. Determine the mass flow rate QM in pounds of total fluid per day, where Q is expressed in barrels of stock-tank oil per day and where M is the total mass, in pounds, of gas, oil, and water, associated with one barrel of stock-tank oil flowing into and out of the

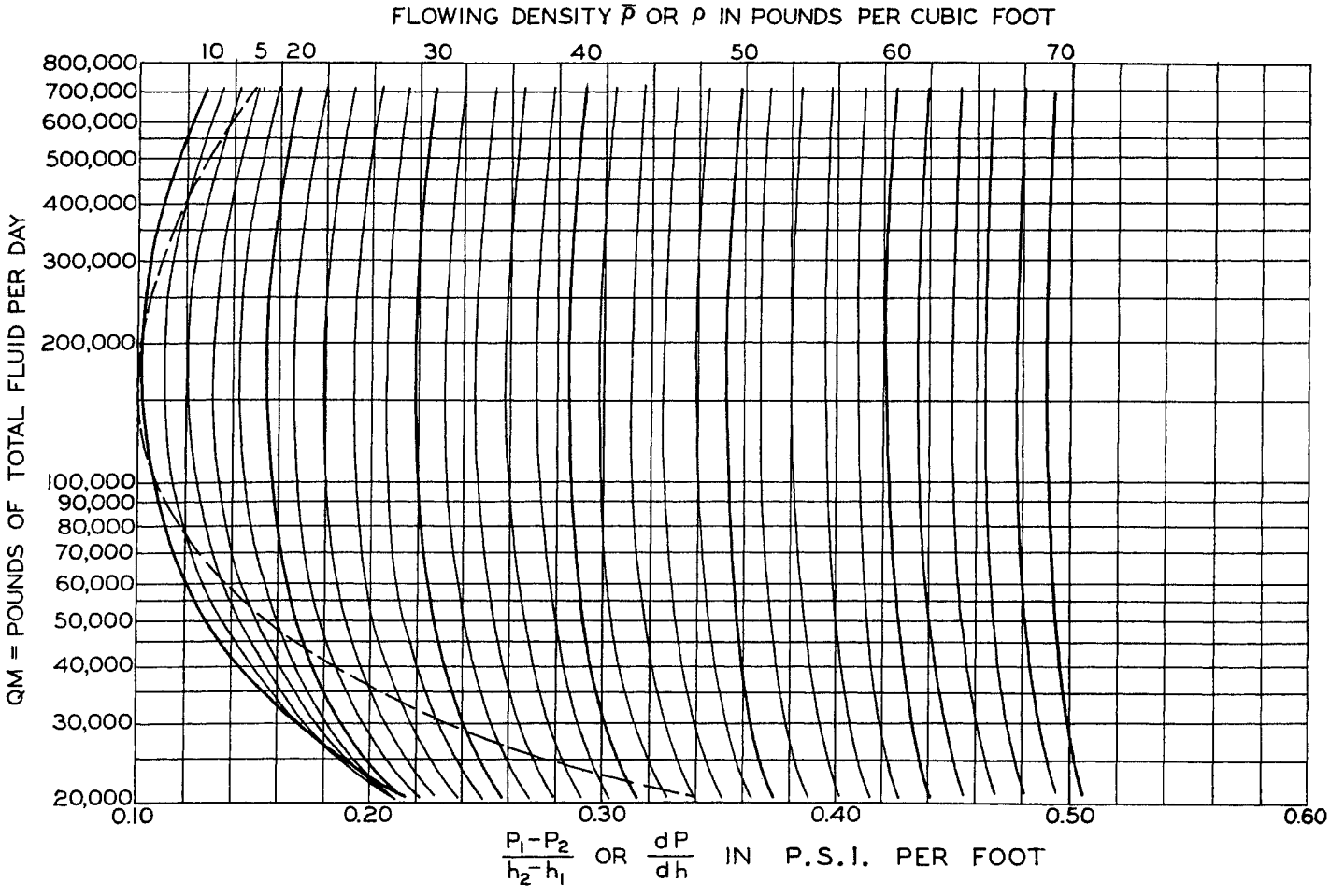

Fig. 7-24. Calculation of pressure traverse in 2.5-in. tubing (2.44 in. ID). (*Poettmann and Carpenter, 7-31. Courtesy API Drill. Prod. Practice.*)

flow string. M can be calculated from the following expression:

$$M = 5.61 \times 62.4\rho_o + 0.0764GR + 62.4\rho_w V_w \quad (7\text{-}90)$$

where M = total fluid production rate, lb/bbl (of stock-tank oil)
ρ_o = specific gravity of stock-tank oil
G = separator-gas gravity (air = 1)
ρ_w = specific gravity of produced water
R = producing gas-oil ratio, cu ft/bbl (of stock-tank oil)
V_w = water production rate, cu ft/bbl (of stock-tank oil)

2. Starting with the reference pressure (usually the tubing or bottom-hole pressure), assume various pressures along the flow string and calculate ρ or $\bar{\rho}$, where

$$\rho = \frac{M}{V_m} \quad (7\text{-}91)$$

and

$$\bar{\rho} = \frac{M}{\bar{V}_m} \quad (7\text{-}92)$$

V_m is the cubic feet of mixed gas, oil, and water at pressure P per barrel of stock-tank oil, based on the ratio of fluids flowing into and out of the flow string.

$$V_m = 5.61B + \frac{P_0 T_a z}{P T_0}(R - S) + V_w \quad (7\text{-}93)$$

where B = formation volume factor of the oil at pressure P in barrels of reservoir oil per barrel of stock-tank oil; the formation volume factor should be measured at the average flow-string temperature; however, this information is seldom available, and the formation factor at reservoir temperature must be used
S = solubility of gas in oil at pressure P, cu ft/bbl
T_a = arithmetic average temperature in the flow string, °R
P = pressure, psia
P_0 = base pressure at which gas is measured, psia

T_0 = base temperature at which gas is measured, °R

z = compressibility factor of the gas in the tubing at temperature T_a and pressure P

It is often possible to express the formation volume factor and the gas solubility as straight-line functions of pressure over the range of pressure under consideration. V_m can then be calculated as follows:

$$V_m = 5.61 n_f P + 5.61 B_i + \frac{P_0 T_a z}{T_0}\left(\frac{R}{P} - n_s - \frac{S_i}{P}\right) + V_w \quad (7\text{-}94)$$

where n_f = slope of formation-volume-factor curve

B_i = intercept of line on formation-volume-factor curve

n_s = slope of solubility curve

S_i = intercept of solubility curve

$\bar{V}_m$ is defined as follows:

$$\bar{V}_m = \frac{\int_{P_2}^{P_1} V_m \, dP}{P_1 - P_2} \quad (7\text{-}95)$$

If Eq. (7-94) is used to define V_m, then $\bar{V}_m$ can be evaluated from the following:

$$\bar{V}_m = 2.805 n_f (P_1 - P_2) + 5.61(B_i + V_w) + \frac{P_0 T_a}{T_0 (P_1 - P_2)}\left[(R - S_i)\int_{P_{r,2}}^{P_{r,1}} \frac{z}{P_r} dP_r - n_s P_c \int_{P_{r,2}}^{P_{r,1}} z \, dP_r\right] \quad (7\text{-}96)$$

The integrals can be evaluated from the tables in the Appendix.

3. Having evaluated ρ or $\bar{\rho}$ at various values of pressure or over pressure increments, determine from the appropriate chart (from among Figs. 7-20 to 7-25) the pressure gradient corresponding to the pressure or pressure increment. From this can then be calculated the pressure traverse.

Illustrative Problem

An oil well is flowing at a rate of 60 bbl/day. The static bottom-hole pressure is 4,478 psia. The producing formation is at a depth of 10,961 ft. Calculate the flowing bottom-hole pressure and productivity index of the well. Additional pertinent data are:

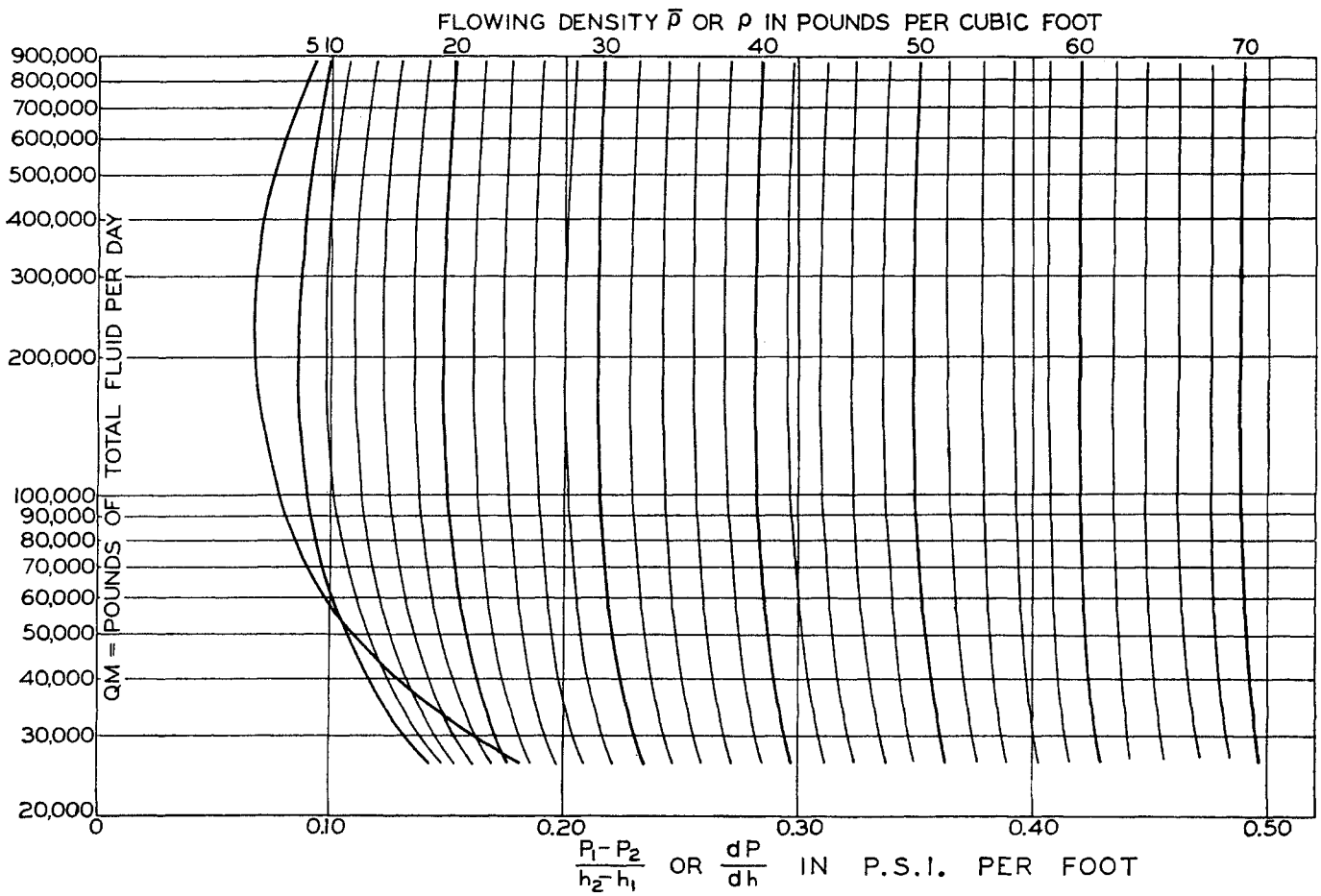

Fig. 7-25. Calculation of pressure traverse in 3.0-in. tubing (3.068 in. ID). (*Poettmann and Carpenter, 7-31. Courtesy API Drill. Prod. Practice.*)

Flowing tubing pressure	1,264 psia
Tubing ID	2.441 in.
Gas-oil ratio	2,250 cu ft/bbl
Formation volume factor	Fig. 7-26
Solubility	Fig. 7-27
Gravity of stock-tank oil at 60°F	44.4°API
Separator-gas gravity (air = 1)	0.796
Reservoir temperature	189°F
Tubing-head temperature (assumed)	75°F

Solution

(*a*) Calculate M using Eq. (7-90).

$\rho_o = 0.8044$ (44.4° API)
$G_g = 0.796$
$R = 2{,}250$
$V_w = 0$
$M = 5.61 \times 62.4 \times 0.8044 + 0.0764 \times 0.796 \times 2{,}250$
$= 418.3$ lb/bbl of oil

(*b*) Calculate QM.

$$QM = 60 \times 418.3 = 25{,}100 \text{ lb/day}$$

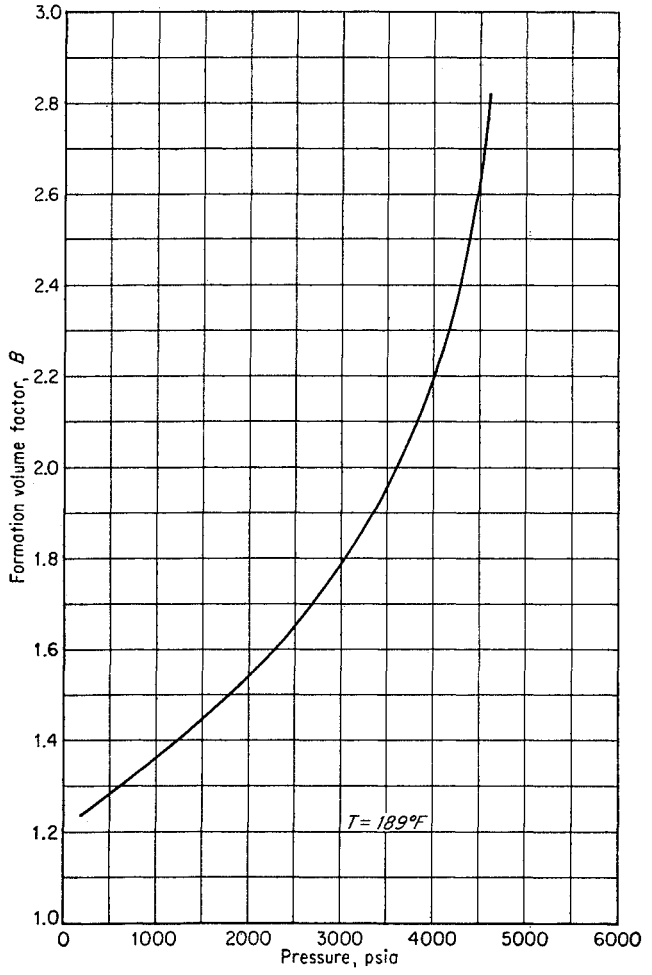

Fig. 7-26. Formation volume factor of oil in illustrative problem. (*Poettmann and Carpenter, 7-31. Courtesy API Drill. Prod. Practice.*)

(*c*) Calculate V_m using Eq. (7-93) and Figs. 7-26 and 7-27. Use 600-psi increments. Calculations are shown in Table 7-6.

(*d*) Calculate density at pressure, using Eq. (7-91). Using Fig. 7-24, determine the pressure gradient dP/dh corresponding to the pressure P. Using the average gradient over the pressure increment, calculate the depth increment corresponding to the pressure. The calculations for step *d* are shown in Table 7-7.

Figure 7-28 shows a plot of the calculated pressure traverse. The pressure at 10,961 ft is 3,870 psia.

(*e*) Calculate productivity index.

$$\frac{60}{4{,}478 - 3{,}870} = 0.0987 \text{ bbl/psi}$$

The field-measured bottom-hole pressure was 3,875 psia (7-31).

Table 7-6. Calculation of V_m in Illustrative Problem

(1) P	(2) P_r	(3) z	(4) B	(5) $5.61B$	(6) $\frac{16.39z}{P}$	(7) S	(8) $2{,}250 - S$	(9) (6) × (8)	(10) V_m = (5) + (9)
1,264	1.91	0.780	1.415	7.94	0.01011	590	1,660	16.78	24.72
1,800	2.71	0.725	1.512	8.48	0.00660	785	1,465	9.67	18.15
2,400	3.62	0.713	1.632	9.16	0.00487	1,050	1,200	5.84	15.00
3,000	4.52	0.740	1.778	9.97	0.00404	1,360	890	3.60	13.57
3,600	5.43	0.791	1.985	11.14	0.00360	1,780	470	1.69	12.83

Table 7-7. Calculation of Pressure Traverse

(1) P	(2) V_m	(3) $\rho = \frac{M}{V_m}$	(4) $\frac{dP}{dh}$	(5) $\left(\frac{dP}{dh}\right)_{av}$	(6) $P/(5)$	(7) Depth h, ft
1,264	24.72	16.95	0.191			
1,800	18.15	23.05	0.212	0.2015	2,660	2,660
2,400	15.00	27.90	0.237	0.2245	2,665	5,325
3,000	13.57	30.85	0.253	0.2450	2,450	7,775
3,600	12.83	32.60	0.263	0.2580	2,325	10,000

The agreement between calculated and measured pressure in this case is fortuitously close. The choice of the pressure increments over which the calculations are made, the calculation procedure employed, that is, use of ρ or $\bar{\rho}$, and the integration method used will result in some differences in the calculated pressure traverses. For example, using the $\bar{\rho}$ procedure and integrating V_m over the same pressure increments used in the above example resulted in a calculated bottom-hole pressure of 3,780 psia.

The calculation procedure used in the above example (Table 7-7) is recommended. The smaller the increments of pressure, the more accurate the results should be.

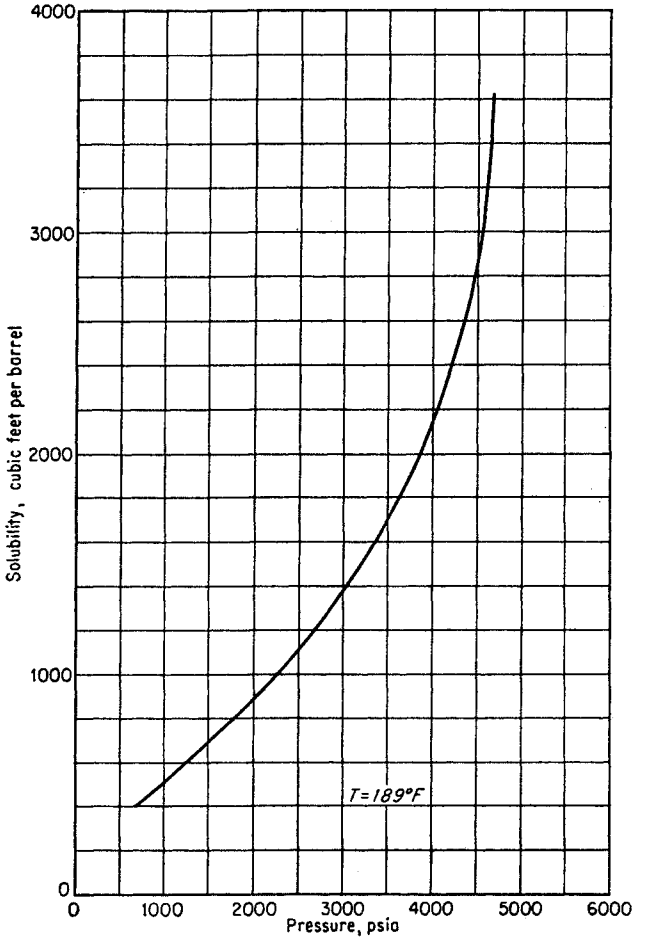

Fig. 7-27. Solubility curve for gas in oil for illustrative problem. (Poettmann and Carpenter, 7-31. Courtesy API Drill. Prod. Practice.)

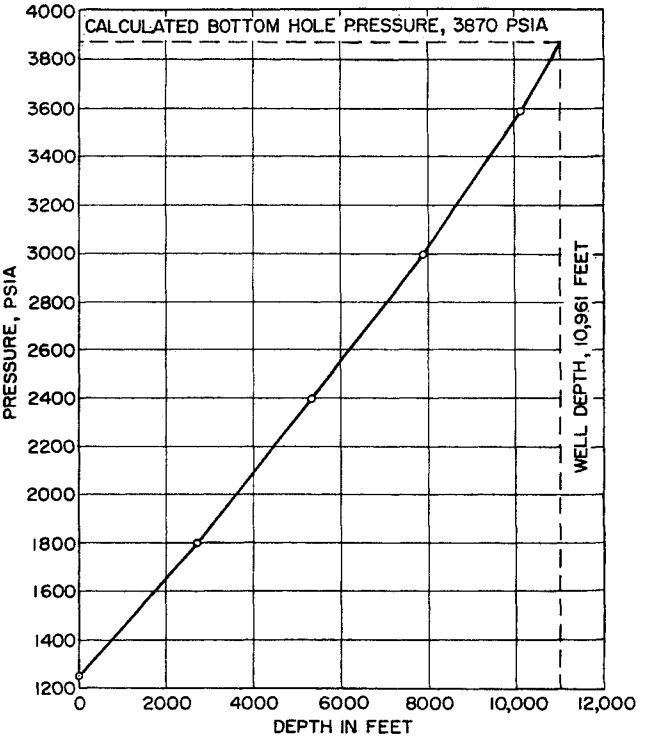

Fig. 7-28. Calculated pressure traverse in flowing oil well. (Poettmann and Carpenter, 7-31. Courtesy API Drill. Prod. Practice.)

For the application of the above-described calculation procedure to the design details of gas-lift installations, Refs. 7-7 and 7-31 should be consulted.

LIQUID PRODUCT LINES

Aude (7-3) has evaluated the friction factor versus Reynolds number for lines conveying gasoline and kerosene. His formula, an adaptation of the Hazen-Williams formula, is

$$B = 0.871k \frac{1}{\mu^{0.104}} \frac{P^{0.552} d^{2.656}}{\rho^{0.448}} \qquad (7\text{-}97)$$

where B = liquid flow, bbl/hr
μ = oil viscosity, centipoises
P = friction pressure drop, psi/mile
d = ID of pipe, in.
ρ = specific gravity of oil, grams/cu cm
k = factor for roughness (1.0 for new steel pipe)

Table 8-1. Principal Types of Meters

Dynamic measurement	*Volumetric measurement*
Orifice meter	Diaphragm meter
Venturi meter	Laboratory wet-test meter
Flow nozzle	
Critical-flow prover	
Pitot tube	
Rotameter	
Choke	

CHAPTER 8

Gas-flow Measurements

Natural gas is in continuous flow from the time it leaves the reservoir until it reaches its ultimate use, usually in a burner. Unlike other products, it is not packaged or put in warehouses where inventory can be taken. Measurement of gas purchases and deliveries is made on a flowing stream of gas; hence accurate measurement of the total quantity of gas that has passed through a given section of pipe over a period of time is of paramount importance to the gas industry. For example, an error of only 1.0 per cent in the measurement of natural gas in a pipeline delivering 300 MMcf per day of gas at 45 cents per Mcf will amount to a loss to either the seller or the purchaser of half a million dollars a year.

Because of the evident importance of accurate measurement of the quantity of gas delivered, various technical societies have combined their efforts to arrive at standards and procedures for quantitative measurement of gas that are mutually acceptable to both purchasers and sellers of gas products. Also, there is interest in the orifice meter throughout industry in general (8-17, 8-19, 7-9). The American Gas Association (AGA) (8-2), the American Society of Mechanical Engineers (ASME) (8-3), the California Natural Gasoline Association (CNGA) (4-3), and the Natural Gasoline Association of America (NGAA) (8-5, 8-9) have sponsored research and field-test programs supported by their member organizations and companies and have endeavored to set up standards of gas measurement for the industry as a whole. These efforts have culminated in Orifice Metering of Natural Gas, AGA Gas Measurement Committee Report 3, published in 1955 (8-2).

Two general classes of metering devices are available for measuring gas rates: dynamic and volumetric meters (Table 8-1). For measuring large volumes, the orifice flow meter is the primary type. In these meters, the pressure drop occurring at a restriction indicates the flow rate. With the exception of domestic or space-heating sales, essentially all transactions are based on orifice-meter measurements. The second class of meter, which is used for domestic sales, is the volumetric meter; this meter receives mechanically a definite volume of gas from an upstream source, counts the volume, and discharges it downstream. There are many varieties of meters and devices used in special applications or in research activities.

MEASUREMENT BY ORIFICE METERS

By far the greatest number of gas-metering installations depend upon the orifice meter for measuring the rate of flow of gas. The advantages of the orifice meter in terms of accuracy, ruggedness, simplicity, ease of installation and maintenance, range of capacity, and low cost readily account for its widespread use. Other factors of importance are the acceptance of the orifice meter for gas measurement by the joint AGA-ASME committee and the availability of standard tables of meter factors for orifice meters of standard design which are recognized by the industry as a common basis for gas measurement.

Orifices

The two types of orifice meters, flange taps and pipe taps, are illustrated in Fig. 8-1. The restriction in the flow path causes a velocity increase and a corresponding pressure drop. With a liquid flowing, the pressure profile can be observed by a manometer, as indicated. In general, the conversion of pressure energy into velocity head is virtually complete, but the regeneration of pressure when the gas is slowed down beyond the restriction is rather inefficient. The venturi meter and flow nozzle (Fig. 8-2) operate on similar principles; the former is more efficient than an orifice in converting kinetic energy to pressure energy.

The recording of pressure and of pressure differential with gas under pressure is accomplished by meters employing mercury U tubes (Fig. 8-3). A clock turns the chart under recording pens, so that there is provided a continuous record of the pressure and of the pressure differential.

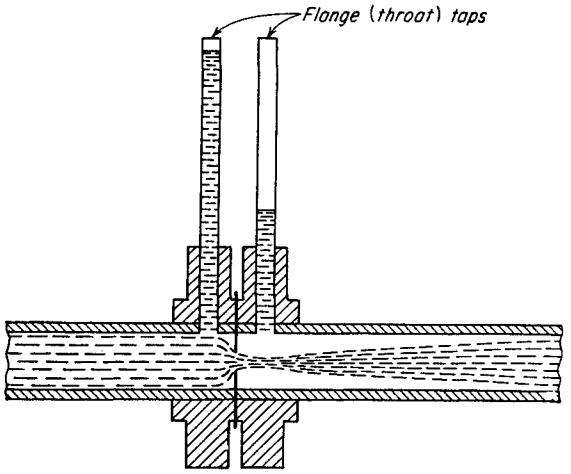

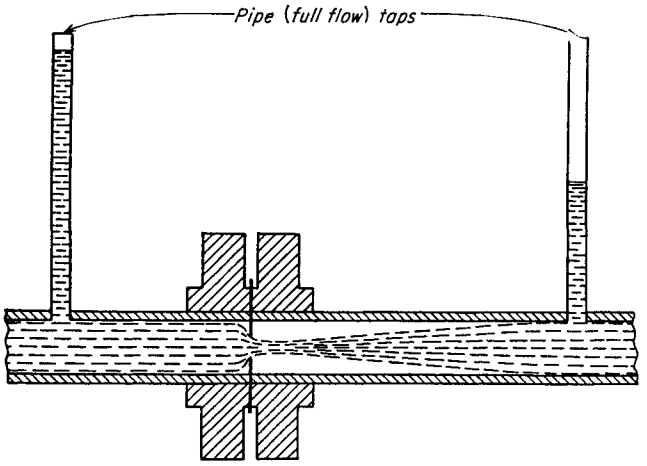

Fig. 8-1. Orifice meters: flange taps, pipe taps.

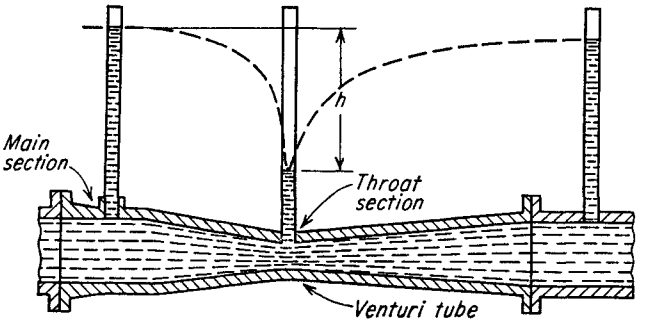

Venturi

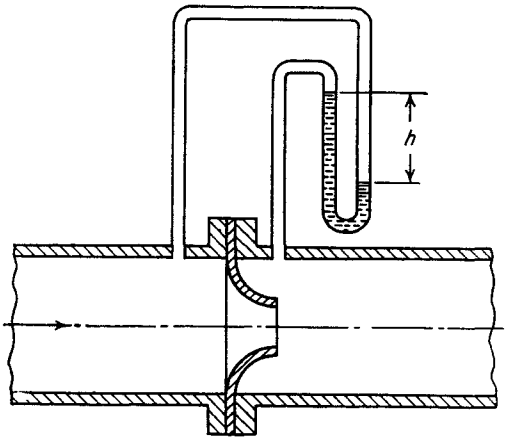

Flow nozzle

Fig. 8-2. Venturi and flow nozzle.

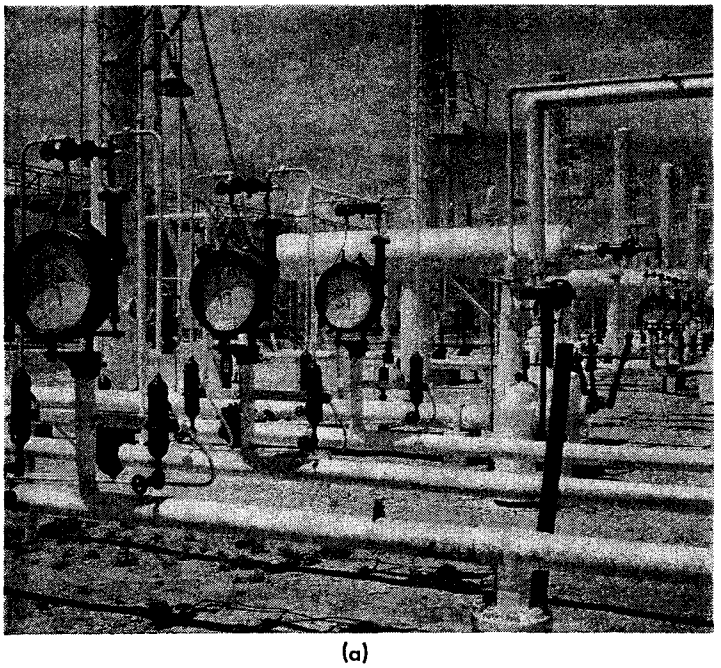

(a)

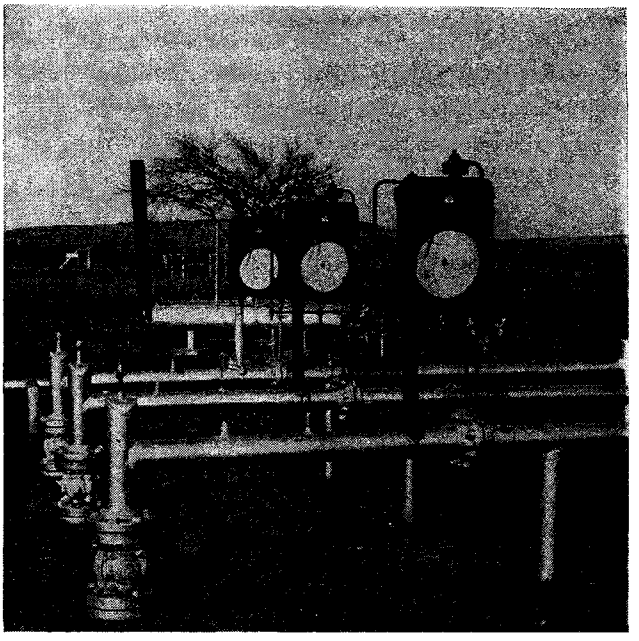

(b)

Fig. 8-3. Recording orifice meters. (a) (*Courtesy Foxboro Company.*) (b) (*Courtesy American Meter Company and Oil Gas J.*)

Derivation of Orifice-meter Formulas

The general energy equation, one form of which is given as Eq. (8-1), is the basis for all flow calculations for metering instruments that depend upon the dynamic or flowing characteristics of the fluid stream. Like Eq. (7-1) or (7-2), this equation may be written between any two points in the flowing stream, such as points 1 and 2 of Fig. 8-4.

$$\int_1^2 V\,dP + \int_1^2 v\frac{dv}{g_c} + \int_1^2 g\frac{dX}{g_c} = -w - lw \qquad (8\text{-}1)$$

where V = specific volume, cu ft/lb (the reciprocal of the density ρ)
P = pressure, lb/sq ft
v = average linear-flow velocity, ft/sec
g_c = conversion factor: 32.17 (lb mass/lb force) (ft/sec^2)
g = acceleration due to gravity, ft/sec^2
X = vertical distance above datum, ft
w = work done by flowing fluid, ft-lb/lb
lw = work energy lost due to frictional effects, ft-lb/lb

For most meters, changes dX in elevation between points 1 and 2 are zero and, since no work is done, $w = 0$. The lost-work term lw expresses the frictional losses due to viscosity and turbulence of the fluid. These losses can be handled in a manner convenient for meter calculations without reference to friction factor. The term $\int_1^2 V\,dP$ is a measure of the pressure head occurring across the orifice and the term $\int_1^2 v\,dv/g_c$ is the velocity head. The manometers a to f of Fig. 8-4 show, first, the conversion of pressure head into velocity head from b to c, and second, the conversion of velocity head back to pressure head from c to f.

The basic orifice equation is Eq. (8-2).

$$C^2\int_1^2 V\,dP + \int_1^2 v\frac{dv}{g_c} = 0 \qquad (8\text{-}2)$$

To compensate for any frictional effects between points 1 and 2, an empirical factor C^2 is inserted into the equation. The point of highest velocity and lowest pressure in the fluid flowing through an orifice is at point 3, called the *vena contracta*. The diameter of the stream at 3 is less than at 2, but the velocity is known only at 2 because the orifice diameter is known but the diameter of the *vena contracta* at 3 is not known. The discharge coefficient C compensates for the difference in the two diameters and for the fact that the velocity is computed in the orifice at 2 rather than at the lowest pressure (3). The coefficient C will always be less than 1.0 and appears as C^2 in Eq. (8-2) in order that the final flow equation may contain C raised to the first power only.

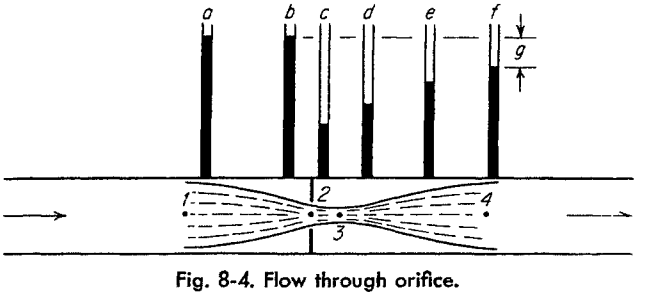

Fig. 8-4. Flow through orifice.

Use of Eq. (8-2) requires knowledge of the relationship between the specific volume V and the pressure P between points 1 and 2, but for real gases the integration becomes too complicated for routine use. Since the pressure differential is small as compared with the pressure, an average value $\bar{V}$ of V or an average value $\bar{\rho}$ of its reciprocal, the density ρ, is used and this variable is removed from under the integral as if it were constant. Integration of Eq. (8-2) then gives Eq. (8-3).

$$C^2(P_2 - P_1)\bar{V} = C^2\frac{P_2 - P_1}{\bar{\rho}} = -\frac{v_2^2 - v_1^2}{2g_c} \qquad (8\text{-}3)$$

or, as more commonly written,

$$\sqrt{v_2^2 - v_1^2} = C\sqrt{2g_c\frac{P_1 - P_2}{\bar{\rho}}} \qquad (8\text{-}4)$$

Velocity in linear feet per second may be converted to pounds per second, W, by Eq. (8-5).

$$W = \rho v A \qquad (8\text{-}5)$$

Substituting for v in Eq. (8-4); recognizing that v_1 is measured at area A_1, the pipe, and v_2 at A_2, the orifice; and defining $\beta = D_{\text{orifice}}/D_{\text{pipe}}$, one obtains Eq. (8-6).

$$W = CA_2\sqrt{\frac{2g_c\bar{\rho}(P_1 - P_2)}{1 - \beta^4}} \qquad (8\text{-}6)$$

The value of C in Eq. (8-4) or (8-6) varies with the area ratio β as well as with the flow rate. Figure 8-5 shows values of C, based on data with liquids, with the variation in flow rate given as a Reynolds number through the orifice. For liquids at appreciable velocities, the orifice coefficient becomes 0.610; for liquefied gases see Ref. 8-11.

Equation (8-4) may be reduced to a single velocity v_1 or v_2 by inserting a function of β as follows:

$$v_1 = v_{\text{pipe}} = C\sqrt{\frac{2g_c\beta^4(P_1 - P_2)}{(1 - \beta^4)\bar{\rho}}} \qquad (8\text{-}7)$$

$$v_2 = v_{\text{orifice}} = C\sqrt{\frac{2g_c(P_1 - P_2)}{(1 - \beta^4)\bar{\rho}}} \qquad (8\text{-}8)$$

These formulas apply for single-phase fluids, either liquids or gases. However, for natural gas, further simplifications are made to permit the use of simple factors.

In Eqs. (8-6) to (8-8)
P = pressure, lb/sq ft
$\bar{\rho}$ = density, lb/cu ft
v = velocity, ft/sec
A = area, sq ft
g_c = 32.2
$\beta = D_0/D_i$

Orifice-meter Formulas for Natural Gas

The orifice-meter formulas, Eqs. (8-4) and (8-6), have included the average density $\bar{\rho}$ of the gas. For gases, the average density may be expressed in terms of pressure, temperature, and compressibility factor.

$$\bar{\rho} = \frac{29G\bar{P}}{\bar{z}R\bar{T}} \tag{8-9}$$

The average values of pressure, temperature, and compressibility factor from points 1 to 2 in the meter should be used. It is customary to use either the upstream pressure or the downstream pressure, the flowing (stagnation) temperature, and the compressibility factor at the flowing temperature and pressure selected.

In using an orifice formula for thousands of measurements each day, it is necessary to devise calculation procedures that can be followed easily in a routine manner. This has been done for the orifice formula, with the development of a series of factors or corrections that can be taken from tables.

To convert Eq. (8-6) into units and form similar to those used for natural gas, the following conversions will be made.

$$Q = \frac{W \times 3{,}600 \times 379}{29G} \tag{8-10}$$

where Q = gas flow at 60°F and 14.7 psia, cu ft/hr
G = gas gravity (air = 1.0)
W = mass velocity, lb/sec

Combining Eqs. (8-9), (8-10), and (8-6),

$$Q = \frac{3{,}600 \times 379}{29G} \frac{CA_2}{\sqrt{1-\beta^4}} \sqrt{2g_c \frac{(P_1 - P_2)29GP}{zRT}} \tag{8-11}$$

$$Q = \frac{3{,}600 \times 379\sqrt{64.34}\,CA_2}{\sqrt{29}\sqrt{R}\sqrt{G}\sqrt{T}\sqrt{z}\sqrt{1-\beta^4}} \sqrt{(P_1 - P_2)P} \tag{8-12}$$

Since the differential pressure h is measured in inches of water and $P_1 - P_2$ is in pounds per square foot,

$$h = \frac{(P_1 - P_2)12}{62.43} \qquad P_1 - P_2 = \frac{62.43h}{12} \tag{8-13}$$

$$Q = \frac{3{,}600 \times 379}{\sqrt{29}\sqrt{10.73}} \sqrt{\frac{62.43}{12}} \frac{\sqrt{64.34}\,CA_2}{\sqrt{GTz}\sqrt{1-\beta^4}} \sqrt{hP} \tag{8-14}$$

This equation gives the flow volumes computed at base conditions of 60°F and 14.7 psia. Since other base conditions may be used on occasion, factors are used to convert base conditions.

$$F_{pb} = \frac{14.7}{P_b} \qquad F_{tb} = \frac{T_b}{520} \qquad \text{for } T_b \text{ in °R}$$

It is customary to establish the value to give Q for a flowing temperature of 60°F (520°R), a gas gravity of 1.0, and a compressibility factor of 1.0. To do this, the standard values are inserted.

$$\frac{1}{\sqrt{GTz}} = \sqrt{\frac{520}{T}}\sqrt{\frac{1}{G}}\sqrt{\frac{1}{z}}\sqrt{\frac{1}{520}} \tag{8-15}$$

$$\therefore Q = \frac{3{,}600 \times 379\sqrt{62.43}\sqrt{64.34}\,CA_2}{\sqrt{29}\sqrt{10.73}\sqrt{12}\sqrt{520}\sqrt{1-\beta^4}} \times \sqrt{\frac{520}{T}}\sqrt{\frac{1}{G}}\sqrt{\frac{1}{z}}(F_{pb}F_{tb})\sqrt{hP} \tag{8-16}$$

The numerical constants C, β, A_2 are grouped as a single constant F_b. The other factors are defined:

The flowing-temperature factor $F_{tf} = \sqrt{\frac{520}{T}}$.

The gas-gravity factor $F_g = \sqrt{\frac{1}{G}}$.

The supercompressibility factor $F_{pv} = \sqrt{\frac{1}{z}}$.

Equation (8-16) thus becomes Eq. (8-17).

$$Q = F_bF_{tb}F_{pb}F_{tf}F_gF_{pv}\sqrt{hP} \qquad \text{cu ft/hr} \tag{8-17}$$

where h = orifice differential, in. of water
P = pressure of gas at orifice, psia

The flowing pressure and temperature are taken normally as upstream values. The expansion of the gas through the orifice is essentially adiabatic. Under these conditions, the density of the stream changes because of the pressure drop and the adiabatic temperature change, according to Eq. (7-70); an expansion factor Y, computed for the adiabatic and reversible case, is included in the formula to correct for this variation in density. To find z or F_{pv}, the upstream values of pressure and temperature are used. In present practice no consideration is given to the expansion effect on the temperature and pressure in this connection.

The values of C, and hence of F_b, vary with the Reynolds number and the diameter ratio β, but the changes are small at the relatively high velocities used in gas meters. Correction factors for variations in

Reynolds numbers are given as F_r, with F_b considered to be a constant for a given meter installation. The values of F_b based on gas-flow data are given in Table A-10 for pipe taps and for flange taps.

Illustrative Problem

For a pipe of 5.761-in. ID with an orifice of 1.000 in. and a Reynolds number of 1,000,000 through the orifice, compute F_b, using the value of C for liquids. Compare the value with the one in Table A-10.

Solution

From Eq. 8-16,

$$F_b = \frac{3{,}600 \times 379 \sqrt{62.43}\sqrt{64.34}\,CA_2}{\sqrt{29}\sqrt{10.73}\sqrt{12}\sqrt{520}\sqrt{1-\beta^4}}$$

For Reynolds number of 1,000,000 through the orifice,

$C = 0.61$, from Fig. 8-5, by extrapolation.

Orifice diameter $A_2 = \frac{\pi \times 1^2}{4 \times 144} = 0.00546$ sq ft.

$\beta = \frac{1.00}{5.761} = 0.17358$; $\beta^4 = 0.09078$; $1 - \beta^4 = 0.90922$.

$$F_b = \frac{3{,}600 \times 379 \times 0.61 \times 0.00546\sqrt{62.43}\sqrt{64.34}}{\sqrt{29}\sqrt{10.73}\sqrt{12}\sqrt{520}\sqrt{0.90922}} = 216.6.$$

The values from Table A-10:

Pipe taps	204.84
Flange taps	200.96

The coefficient 0.61 taken from Fig. 8-5 for liquids is too high.

C for pipe taps = 0.577
C for flange taps = 0.566

The density of the gas opposite the mercury influences the differential indicated. Since the calibration is normally made at or near atmospheric pressure, corrections should be used for the gas density at high pressures. This correction factor F_m is

$$F_m = \sqrt{\frac{\rho_{Hg} - \rho_f}{\rho_{Hg}}}$$

where ρ_{Hg} is the density of mercury and ρ_f is the density of the fluid opposite the mercury column in the meter. The AGA table (Table A-19) for manometer factor F_m gives these corrections for gas opposite the mercury. The corrections are less than 0.4 per cent for all natural gases at 1,000 psia and below.

The complete orifice equation used in AGA Report 3 is

$$Q = F_b F_r Y F_{pb} F_{tb} F_{tf} F_g F_{pv} F_m \sqrt{hP} \qquad (8\text{-}18)$$

where Q = gas flow measured at base temperature and pressure, cu ft/hr
h = pressure differential across orifice, in. of water at 60°F
P = absolute static pressure on gas, psia
F_b = basic orifice factor provided in tables based on pipe diameter, orifice diameter, and type of meter
F_r = Reynolds-number factor
Y = expansion factor
F_{pb} = pressure-base factor = $14.73/P_b$
F_{tb} = temperature-base factor = $T_b/520$ (T_b in °R)
F_{tf} = flowing-temperature factor = $\sqrt{520/T}$ (T in °R)
F_g = gas-gravity factor = $\sqrt{1/G}$
F_{pv} = supercompressibility factor = $\sqrt{1/z}$
F_m = manometer factor = $\sqrt{(\rho_{Hg} - \rho_f)/\rho_{Hg}}$, where ρ_f = density of fluid opposite mercury in meter

Tables of the above factors are provided by the AGA (8-3), and abridged tables are given in Tables A-10 to A-19.

To obtain the quantity of gas flowing through an orifice meter from the above equation and the AGA tables, the following data are required:

Diameter of pipe
Diameter of orifice
Differential across meter
Pressure on meter
Flowing temperature
Gas gravity
Carbon dioxide and nitrogen content of gas
Type of meter, pipe or flange taps

Illustrative Problem

Compute the daily flow rate of natural gas through an orifice meter for the following conditions:

Barometer	14.5 psia
Diameter of pipe	11.938 in. (12-in. schedule 40)
Orifice diameter	4.000 in.
Differential across meter	27.0 in. of water
Static pressure on meter	678 psig
Flowing temperature	75°F
Gas gravity	0.63
Mole fraction CO_2	0.013
Mole fraction N_2	0.031
Type of meter	Flange taps
Temperature base	60°F
Pressure base	14.65 psia

Solution

Daily flow rate = $24F_bF_rYF_{tb}F_{pb}F_{tf}F_gF_{pv}F_m\sqrt{hP}$

$\sqrt{hP} = \sqrt{27(678 + 14.5)} = 136.7$. Extension tables are available for looking up this square root, given the differential and pressure.

$F_b = 3{,}260$ (from Table A-10 for flange taps).

$$F_r = 1 + \frac{b}{\sqrt{hP}} = 1 + \frac{0.0206}{136.7} = 1.00015 \text{ (b from Table A-11)}$$

Y is a function of

$$\frac{d}{D} = \frac{4.000}{11.938} = 0.335$$

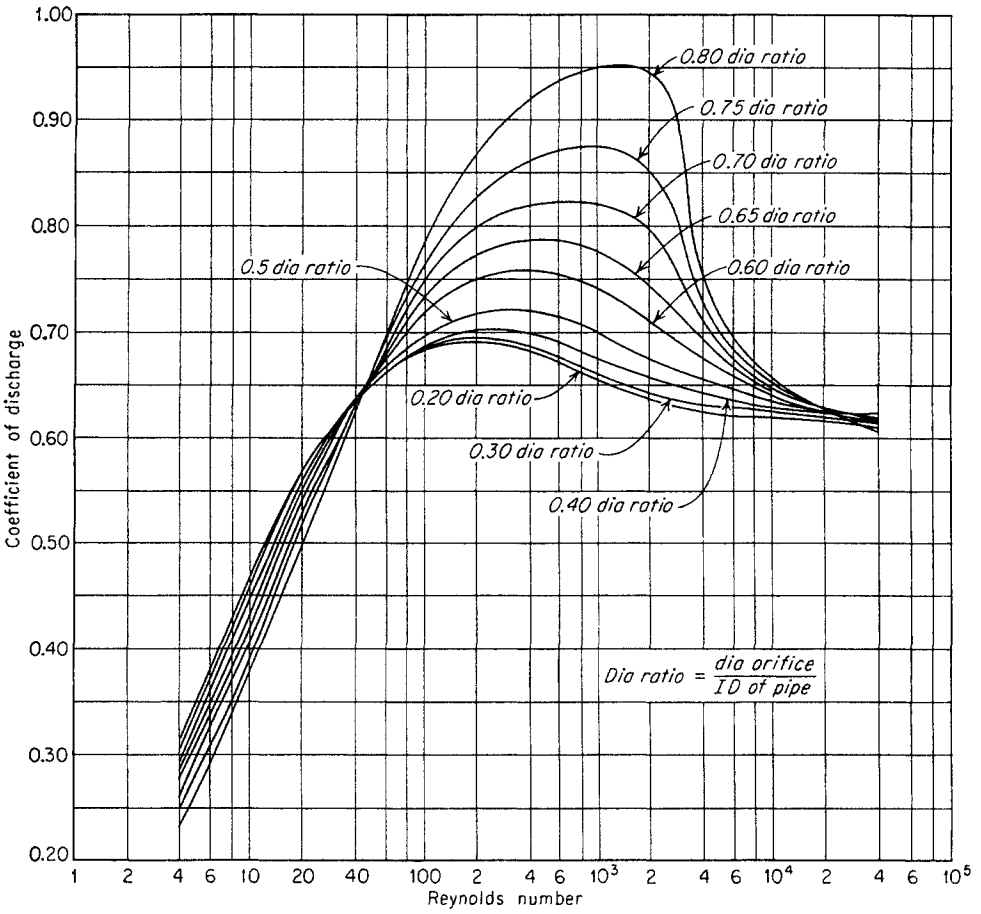

Fig. 8-5. Discharge coefficient for liquids with sharp-edged orifices. (*Tuve and Sprenkle*, 8-20.)

and of

$$\frac{h}{P} = \frac{27.0}{692.5} = 0.039 \qquad \text{from Table A-12}$$

$\therefore$ $Y = 0.9996$ by interpolation

$F_{tb} = 1.0$ (since 60°F is used).

$$F_{pb} = \frac{14.73}{14.65} = 1.0055.$$

$F_{tf} = 0.9859$ (from Table A-14).
$F_g = 1.2599$ (from Table A-13).

For F_{pv} the adjusted temperature and pressure must be found based on $G = 0.63$, $X_c = 0.013$, $X_n = 0.031$.

From Table A-17, obtain ΔT.

$$f_{tg} = G - 0.472X_c - 0.793X_n$$
$$= 0.630 - (0.472 \times 0.013) - (0.793 \times 0.031)$$
$$= 0.599$$

From Table A-17, by interpolation, $\Delta T = 0.50$.

From Table A-16, obtain ΔP.

$$f_{pg} = G - 13.84X_c + 5.420X_n$$
$$= 0.630 - (13.84 \times 0.013) + (5.420 \times 0.031)$$

From Table A-16, at $f_{pg} = 0.618$, $\Delta P = 0.57$.

Adjusted temperature = 75 + 0.5 = 75.5°F.
Adjusted pressure = 678 + 0.57 = 678.6 psig.
$F_{pv} = 1.0504$ by interpolation (Table A-15).
$F_m = 0.9985$ (from Table A-19).

$$Q_{24\text{ hr}} = 24 \times 3{,}260 \times 1.00015 \times 0.9996 \times 1.0055 \times 0.9859 \times 1.2599 \times 1.0504 \times 0.9985 \times 136.7$$
$$= 14{,}007{,}000 \text{ cu ft per 24 hr}$$
$$= 14{,}007 \text{ Mcf/day}$$

Correction for F_{pv}

The correction for the deviation from ideal-gas law is $F_{pv} = \sqrt{1/z}$. The compressibility of a particular gas can be measured as a function of temperature and pressure and the F_{pv} calculated. The values can be computed from the temperature, pressure, and gas gravity, using procedures given in AGA Report 3. Earlier methods are given in the Texas Railroad Commission booklet (7-5) on back-pressure tests for natural gas wells and in the CNGA tables (4-3).

When the composition of a gas is known, the compressibility factors may be computed, as shown in Table 4-8, from the reduced-temperature and reduced-pressure chart after the pseudocritical temperature and pressure have been found. Pseudocritical properties of gases may be found from gas gravities for various groups of gases, as shown in Fig. 4-22.

If there is occasion to prepare values of F_{pv} for a particular series of gases, a combined factor for gravity, temperature, and F_{pv} can easily be prepared, as described in Ref. 8-9. Inasmuch as F_{pv} depends

upon gas gravity, temperature, and pressure, a single value for the compressibility, gas gravity, and temperature correction factors has the same accuracy as individual factors and will reduce by 2 the number of readings on tables and also the number of multiplications.

$$F_{GTz} = F_{pv}F_gF_{tf} = \sqrt{\frac{520}{GTz}} \qquad (8\text{-}19)$$

A comparison of the factors $\sqrt{1/z}$ and $\sqrt{520/GTz}$ is given for a 0.6 gravity gas in Fig. 8-6.

Illustrative Problem

Compute F_{pv} for the following natural gas by various methods:

Flowing temperature..... 75°F
Meter pressure..... 692.5 psia

Constituent	*Mole fraction*
Nitrogen	0.031
Carbon dioxide	0.013
Methane	0.872
Ethane	0.065
Propane	0.013
Isobutane	0.006
	1.000

Solution

(*a*) Calculation by Compressibility-factor Chart (Fig. 4-16)

Constituent	Mole fraction	Mol. wt	Moles of mixture	P_c, psia	Pseudo-critical pressure, psia	T_c, °R	Pseudo-critical temp, °R
N_2	0.031	28	0.87	492	15.3	227	7.0
CO_2	0.013	44	0.57	1,072	14.0	548	7.1
CH_4	0.872	16	13.97	673	586	344	300
C_2H_6	0.065	30	1.95	712	46.3	550	35.8
C_3H_8	0.013	44	0.57	617	8.0	666	8.7
$i\text{-}C_4H_{10}$	0.006	58	0.35	528	3.2	734	4.4
			18.28		672.8		363.0

$$G = \frac{18.28}{29.0} = 0.630$$

$$T_r = \frac{460 + 75}{363.0} = 1.472$$

$$P_r = \frac{692.5}{672.8} = 1.029$$

$$z = 0.895 \quad \text{from Fig. 4-16}$$

$$F_{pv} = \sqrt{\frac{1}{0.895}} = \sqrt{1.118} = 1.057$$

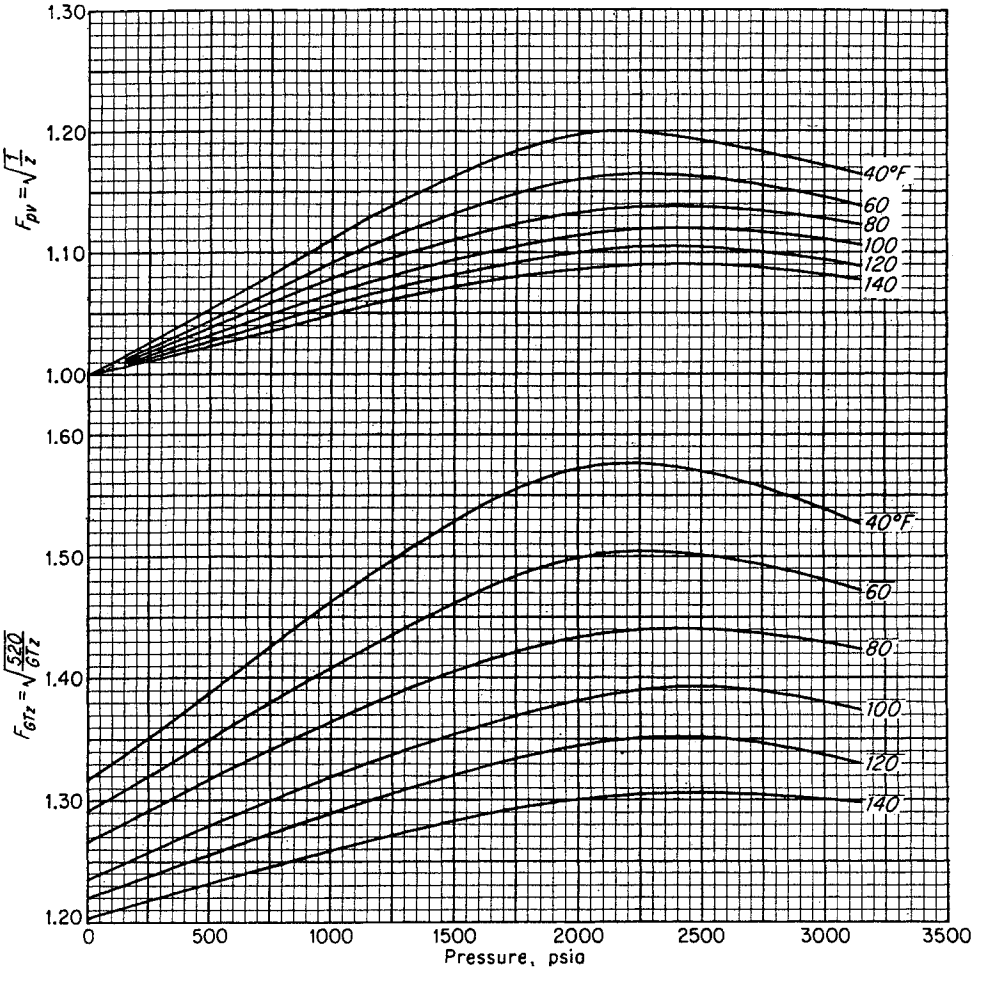

Fig. 8-6. Comparison of F_{pv} with F_{GTz} for 0.6 gravity natural gas.

(*b*) Calculation by AGA Report 3. Use of Tables A-15 to A-17 gives a value of 1.0504 as a solution to this problem.

(*c*) Calculation from Gas Gravity Using CNGA tables. The Texas Railroad Commission booklet gives the following values from CNGA TS-461, neglecting carbon dioxide and nitrogen content, for gas gravity of 0.63:

$$T_r = {}^{535}\!/_{368} = 1.452$$

$$P_r = \frac{692.5}{670} = 1.033$$

$$F_{pv} = 1.062$$

It appears that the compressibility chart, the AGA method, and the CNGA tables give values for this gas within 1 per cent of one another.

Effect of Condensate in Metered Gas Stream

Gas in transit to market seldom contains condensate, but gas flowing from high-pressure wells may contain substantial amounts of hydrocarbon condensate as well as some water. Tests were made (8-5) on a horizontal and on a vertical meter run 4 in. in diameter to determine the effect of the presence of condensate at 1,400 psi, with subsequent separation and measurement of the two phase streams. Figure 8-7 gives the correction factors found when the quantity of gas calculated from the meter data was compared with that calculated from a composite of the single-phase gas meter and the condensate converted to gas volumes.

Studies of *P-V-T* data on gases that enter the two-phase region (8-9) showed that the compressibility factor gave an adequate representation of the composite density of a two-phase stream even though liquid were present. For meters at 1,000 psi or more, one or two gallons of hydrocarbon condensate per Mcf can be appropriately accounted for as gas with an F_{pv} based on the gravity of the total stream. This behavior of hydrocarbon systems explains the small corrections at low liquid content in Fig. 8-7.

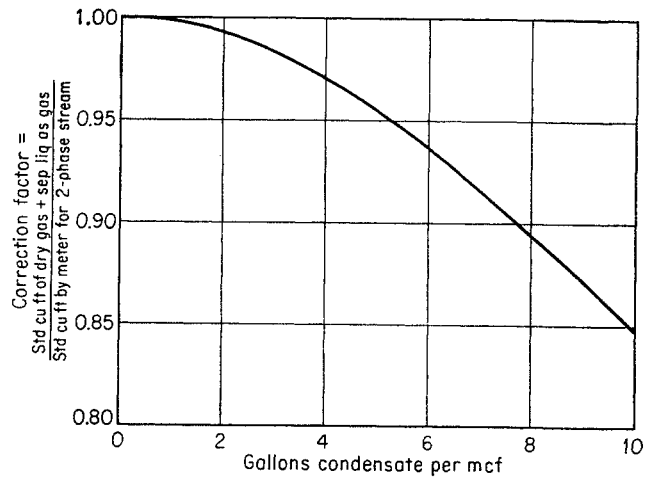

Fig. 8-7. Correction for condensate in metered gas stream. (*Brown and Katz*, 8-5.)

Meter Installations

The nature of the flow of gas through an orifice and the resultant pressure drop depends somewhat upon the type of flow pattern occurring in the stream approaching the orifice. An asymmetrical velocity profile will give different pressure differentials than a symmetrical velocity profile. Accordingly, meter formulas must be based on flow conditions that can be adequately described and duplicated. In general, it is necessary to eliminate disturbances in flow upstream of the orifice, so that the flow patterns are dependent only upon the pipe size and flow rate.

To give uniformity to the performance of orifice meters, installations for metering gas have become standardized with respect to certain dimensions. The installation is often called a "meter run." Irregular flow patterns caused by disturbances in a piping system may be brought to the pattern for straight pipe by the use of straightening vanes (Fig. 8-8). Bundles of smaller tubes are placed in the pipe some distance ahead of the orifice to eliminate swirls and cross currents. AGA specifications require (1) that the maximum transverse dimension a shall not exceed one-fourth of the inside pipe diameter, (2) that the cross-sectional area A of any passage shall not exceed one-sixteenth of the cross-sectional area of the pipe, and (3) that the length L shall be at least ten times the dimension a. Shapes other than circular may be used,

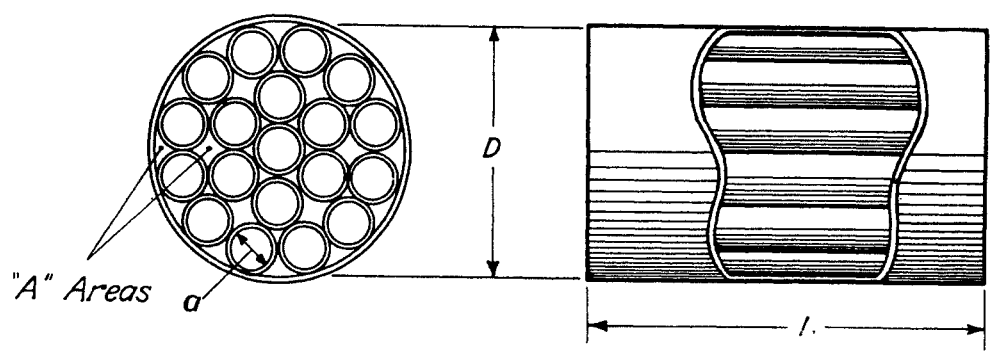

Fig. 8-8. Straightening vanes for orifice installation. (*AGA Gas Measurement Committee Rept.* 3.)

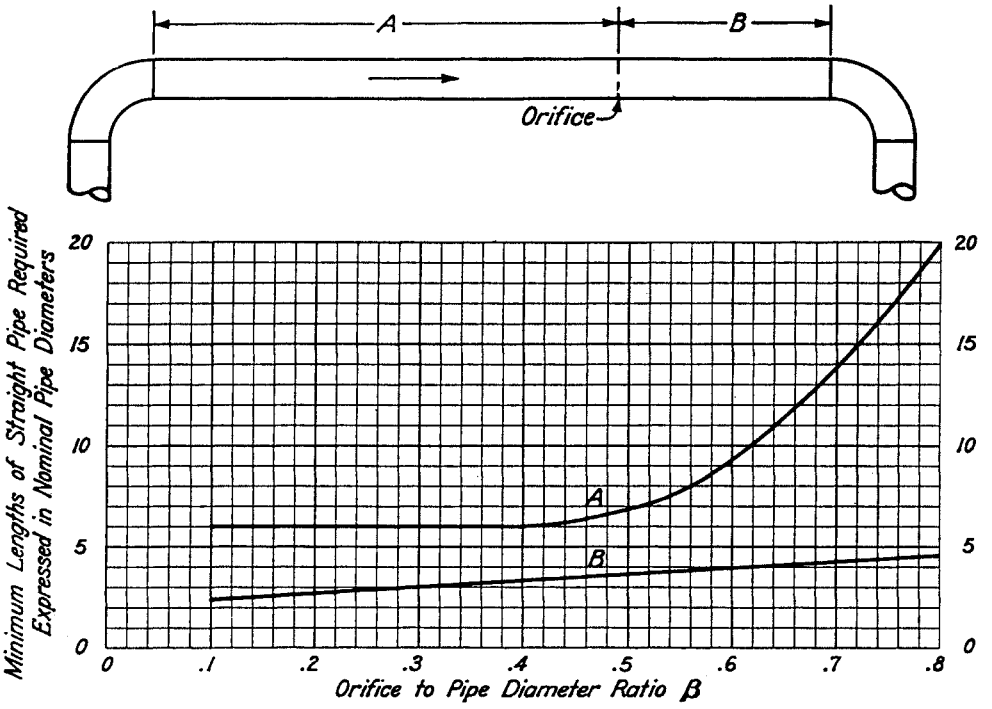

Fig. 8-9. Installation with one ell preceding meter tube. (*AGA Gas Measurement Committee Rept. 3.*)

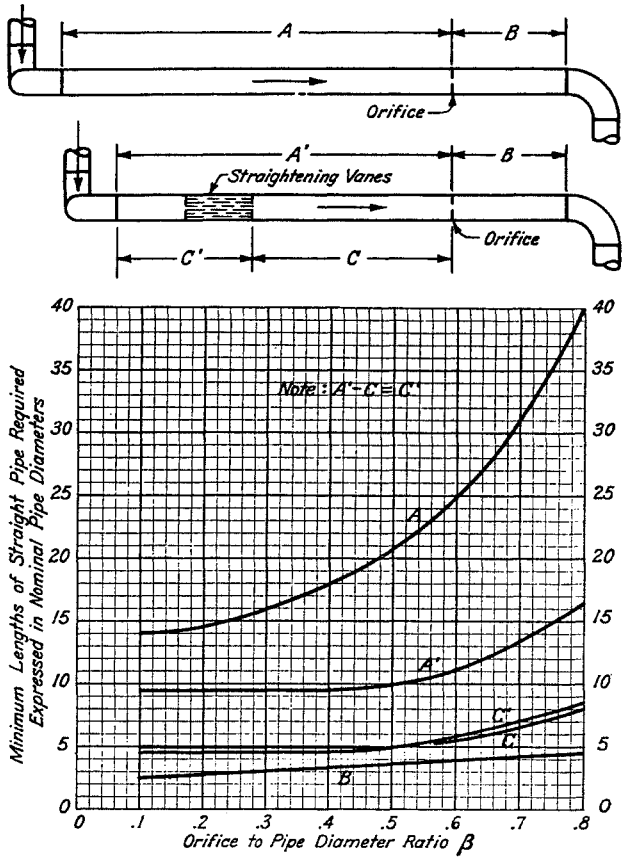

Fig. 8-10. Installation with two ells or bends preceding the meter tube, bends not in the same plane. (*AGA Gas Measurement Committee Rept. 3.*)

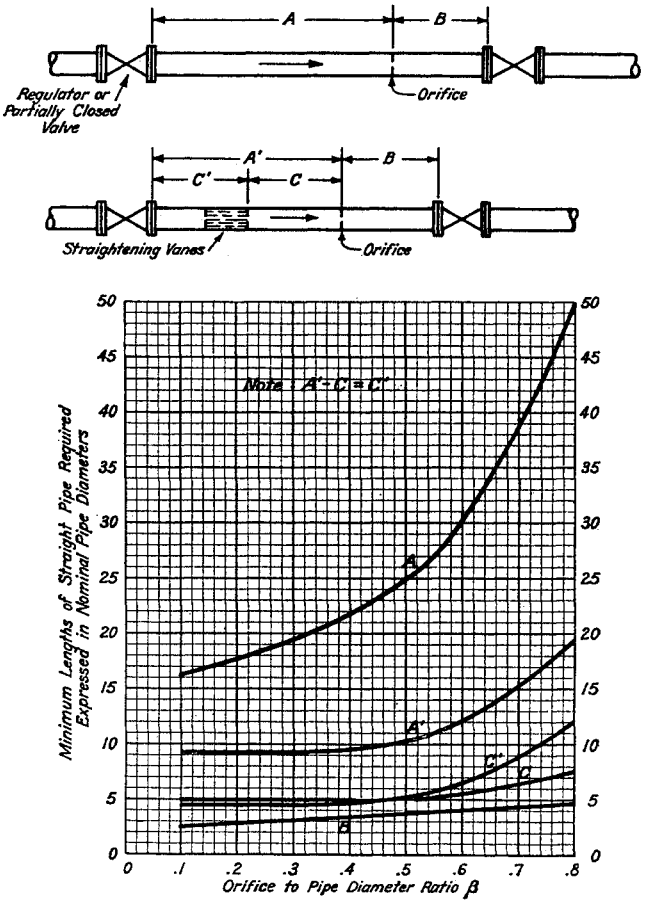

Fig. 8-11. Installation with valve or regulator preceding meter tube. (*AGA Gas Measurement Committee Rept. 3.*)

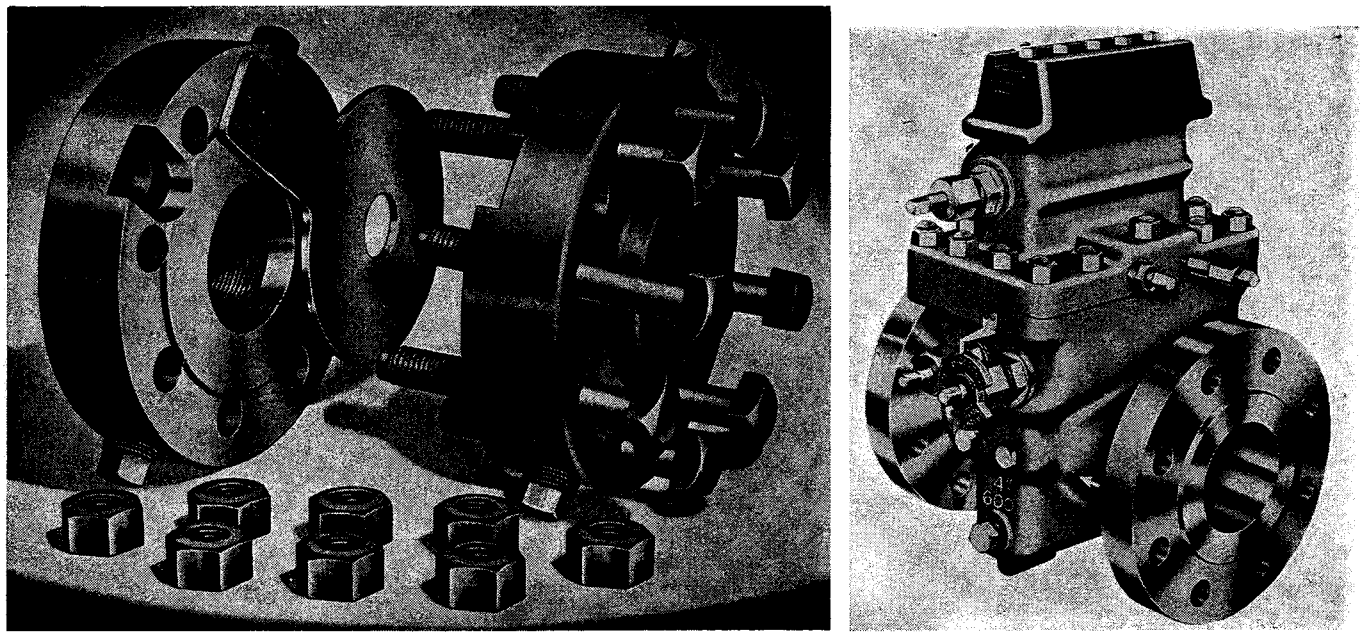

(a) (b)

Fig. 8-12. Orifice plates. (a) Standard plates. (*Courtesy Foxboro Company.*) (b) Orifice assembly permitting changing of orifices under pressure. (*Courtesy Daniel Orifice Fitting Company.*)

as well as a variety of sizes, provided the arrangement is symmetrical.

The AGA has specifications for the minimum lengths of straight pipe upstream and downstream of an orifice, depending on the disturbance ahead of the installation, on whether straightening vanes are used, and on the maximum size orifice to be used. Figure 8-9 shows the lengths A and B for various β values when only a single ell is upstream of the meter. Installations often have demands for handling increased flow rates and should provide for orifice sizes permitted by β of at least 0.6. The minimum lengths for A and B are given in Fig. 8-10 for two ells not in the same plane and in Fig. 8-11 for a valve or regulator upstream. Similar charts are available (8-2) for reducers and for two ells in the same plane upstream of the orifice.

Meter Plates

Meter plates are changed when flow rates do not permit reading the differential with the recorder. The range of flow rate for a single plate is about 2 to 1 from 20 to 100 in. of differential. Figure 8-12 shows typical orifice installations and plates. The size, measured to ± 0.0005 in., is normally stamped on the ear for identification. Special types of installation permit quick changing of orifice plates when the meter is under pressure (Fig. 8-12*b*). The influence of hydrate or foreign-material accumulation adjacent to orifice plates is discussed by Kehoe (8-10).

Temperature Measurement

The temperature is often measured by a mercury-in-glass thermometer inserted in a well either downstream from the orifice more than dimension B or upstream of straightening vanes by 1 pipe diameter. Recorders are used with the sensing element in the well when a continuous record is desired (Fig. 8-13).

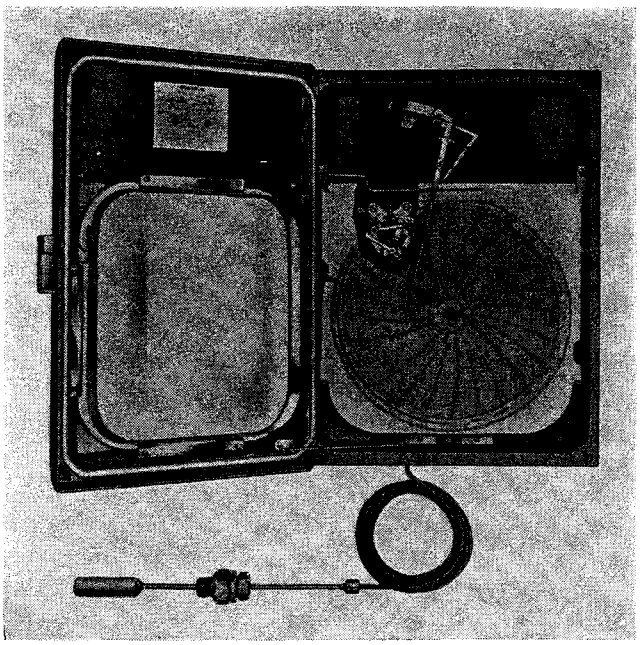

Fig. 8-13. Temperature recorder. (*Courtesy Bristol Company.*)

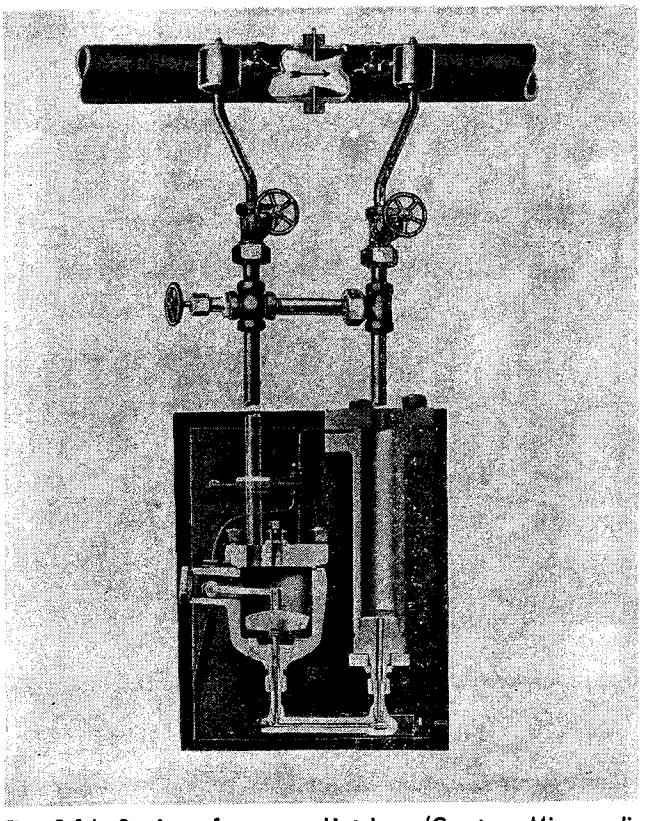

Fig. 8-14. Section of mercury U tube. (*Courtesy Minneapolis-Honeywell Regulator Company.*)

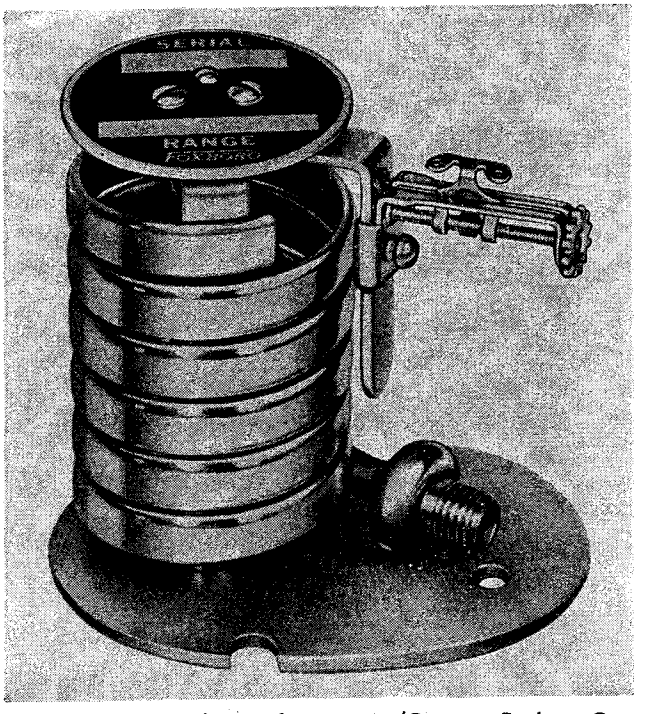

Fig. 8-15. Pressure element for meter. (*Courtesy Foxboro Company.*)

Recording Devices for Pressure and Differential

Recording devices may be installed individually for meters, as shown in Fig. 8-3, or they may be placed in a meter house for a group of meter runs. The mercury U tube on the meter is equipped with a float which actuates the differential pen (Fig. 8-14). The pressure element is a modified bourdon tube (Fig. 8-15).

Differential elements are normally for 50 in. or 100 in. of water differential. Pressure elements are available in various ranges such as 0 to 500 psi, 0 to 1,000 psi, 0 to 2,000 psi, etc.

There are two principal types of meter charts, shown in Fig. 8-16. The first is the direct-reading chart for the differential in inches of water and the pressure in pounds per square inch. The second is a chart that reads the square root.

Clocks turn the charts at desired speed, one turn each day or other time period.

Reading of Charts

Charts contain places for recording pertinent data such as pipe size, orifice size, gas gravity, and temperature. The F_b is usually available and may be recorded. The differential usually varies over the time period and must be averaged. Chart integrators (Fig. 8-17) are available for routine work.

Pulsation

Many meter runs are adjacent to compression stations. The action of a group of compressor pistons operating on natural gas causes pulsation of flow in varying degrees. The pulsation is a result of the short-time discharge period of the compressor. The pressure waves caused by the discharge of gas from a compressor travel with the velocity of sound. The greatest surges in pressure often may result from the combined effects of several piston discharges occurring together.

Pulsation causes errors in metering because the pressure differential indicated is not the true average. Many papers have been written on the subject (8-4, 8-6 to 8-8, 8-12, 8-14, 8-15, 8-18, 8-19). The meter indicates that more gas is passing through the orifice than is actually passing. The relationship between flow rate and orifice differential is given in Fig. 8-18. Consider the unpulsed differential at A and pulsation differentials reaching B. The recorder will indicate an average differential along the straight line between A and B although the flow rate actually varies as the square root of the differential along the curve between A and B. The calculation of the flow rate from differential C gives a value for the flow of E which is above the true value D. A meter that recorded the

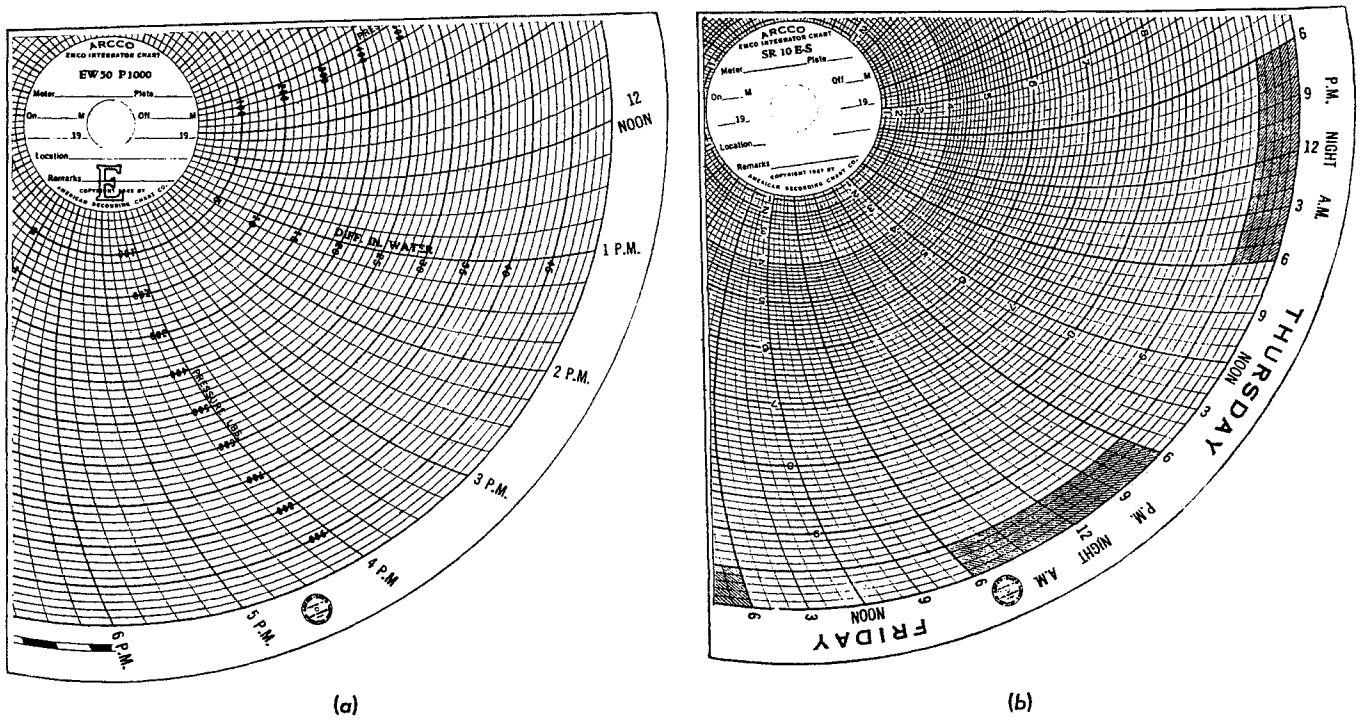

(a) (b)

Fig. 8-16. Orifice-meter charts. (a) Direct-reading chart. (b) Square-root chart. (Courtesy Rockwell Register Corp.)

root-mean-square differential $h_{rms} = \sqrt{(h^2)_{av}}$ would eliminate the error, since the square of the differential is a linear function of the flow rate.

A chart giving the error in metering due to pulsation has been devised by Hardway (8-7, Fig. 8-19). He computed the error mathematically by assuming regular pressure waveforms: sinusoidal, square, and sawtooth waves. He evaluated the h_{rms} as compared to h_{av} and computed the error corresponding to the ratio as

$$\text{Per cent error} = \frac{100}{8}\left(\frac{h_{rms}}{h_{av}}\right)^2 \qquad (8\text{-}20)$$

For small fluctuations, the error is the same for the three waveforms. At higher pulses, the several waveforms give different curves, but the point is soon reached where reversals in flow through the orifice take place. At this condition satisfactory corrections are no longer possible, for the orifice equation is not followed.

A suitable instrument for measuring the root-mean-square differential h_{rms} is available (8-7). The pressure fluctuations are converted to an alternating current by a pressure transducer of the strain-gauge type. This alternating current is amplified and measured in a thermomilliammeter. Such an instrument measures the heat generated in a resistor, which is proportional to the root-mean-square value of the current.

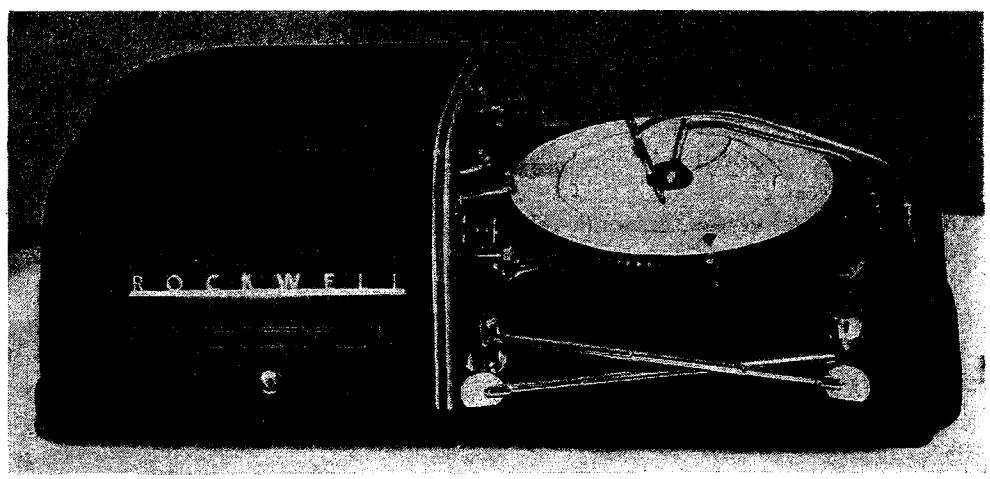

Fig. 8-17. Integrator for meter charts. (Courtesy Rockwell Register Corp.)

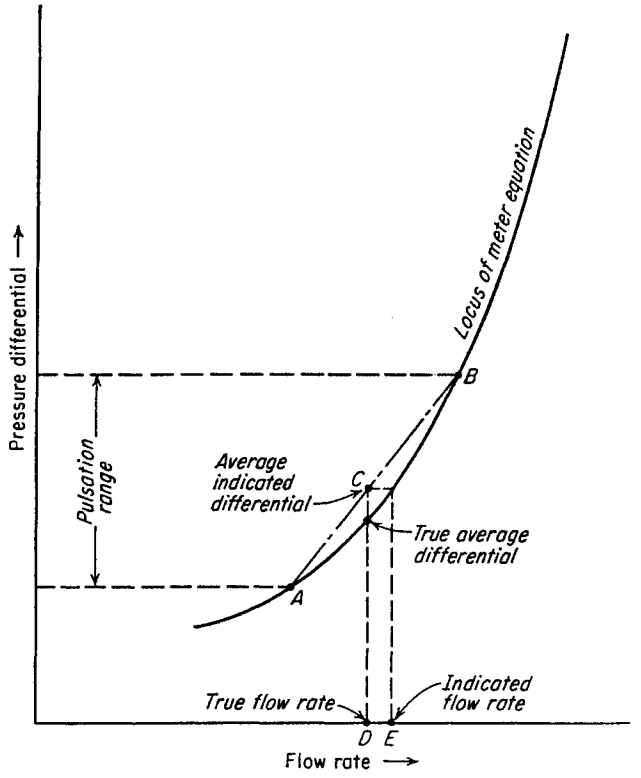

Fig. 8-18. Illustration of error in metering due to pulsation.

The Pulsometer

The mechanical pulsometer shown in Fig. 8-20 (8-12) consists of two cylindrical volumes, A and B, separated by a sylphon bellows C. The two volumes separated by the bellows are connected to the inlet (upstream) side and outlet (downstream) side of the meter connection. A coil spring A is mounted in the chamber connected to the high-pressure tap. The tension on the spring is adjusted by handwheel E with the degree of movement indicated by scale F. Electrical contacts in volume B permit adjustment of spring tension so that the bellows is at a fixed position. The tension on the spring is gradually increased until the contact is broken, indicating that the bellows has come to a standard position and that the spring tension offsets the maximum differential pressure occurring at any time. The scale F may be calibrated by a manometer placed across the connections with steady pressure.

Experimental data augmented by theoretical calculations have been used to present a curve of pulsometer reading versus meter reading, which shows a 1 per cent error in metering [Fig. 8-21 (8-12)]. Test points falling below the curve indicate less than 1 per cent error due to pulsations, and points falling above the curve indicate more than 1 per cent error.

Design to Minimize Pulsation

The volume of the piping system between the compressors and the meters is the important variable in designing meter installations adjacent to compressor stations. The ratio of the volume of gas entering or leaving the system when the valve of the compressor operates to the volume of the system determines in a general way the magnitude of the pulse. The usual procedure for dampening pulses is to insert a flow chamber in the line between the meter and compressor. The basis for the design of such a system to minimize pulsation is the Hodgson number (8-15):

$$\text{Hodgson number} = \frac{Vf(P_0 - P_1)}{WvP} \qquad (8\text{-}21)$$

where V = volume of entire flow system between meter and compressor, cu ft
f = frequency of pulsations, cycles/sec
$P_0 - P_1$ = differential across meter and piping to surge chamber, psi
W = flow rate, lb/sec
v = specific volume of gas, cu ft/lb
P = pressure in surge chamber, psia

Low Hodgson numbers are favorable to low errors in metering, but no direct relationship is given for gas-pipeline applications. In the absence of a quantitative relationship, a value of 1 to 3 for the Hodgson number is suggested for sizing the surge tank inserted in compressor-station lines. Although no distinction is made in the formula between volume of pipe and surge tank, it is known that, for the same volume, considerable advantage occurs from a surge tank with a 2:1 length-diameter ratio and a tank diameter at least twice the pipe diameter, as shown in Fig. 8-22.

It may be of interest to predict pressure pulsations in line pressure. Chilton and Handley (8-6) give a chart for relating per cent pulsation to volume of the system, volume of compressors, gas properties, and compressor characteristics (Fig. 8-23).

In the design of compression stations adjacent to metering facilities, the size and arrangement of piping may be selected and dampeners added to give a minimum of pulsation. Figure 8-24 shows a comparison of conventional design with an integral pulsation-dampener system design. Figure 8-25 shows dampeners in place on compressors, and Fig. 8-26 shows the internal construction of a dampener that has the added feature of an interconnecting pipe between two chambers. When systems already in operation exhibit undesirable pulsation characteristics, it is possible to design dampeners to minimize the effects after taking measurements of the instantaneous pressure fluctuations (8-4, 8-18). Design methods are relatively complicated and are subject to change as more is learned about this baffling problem.

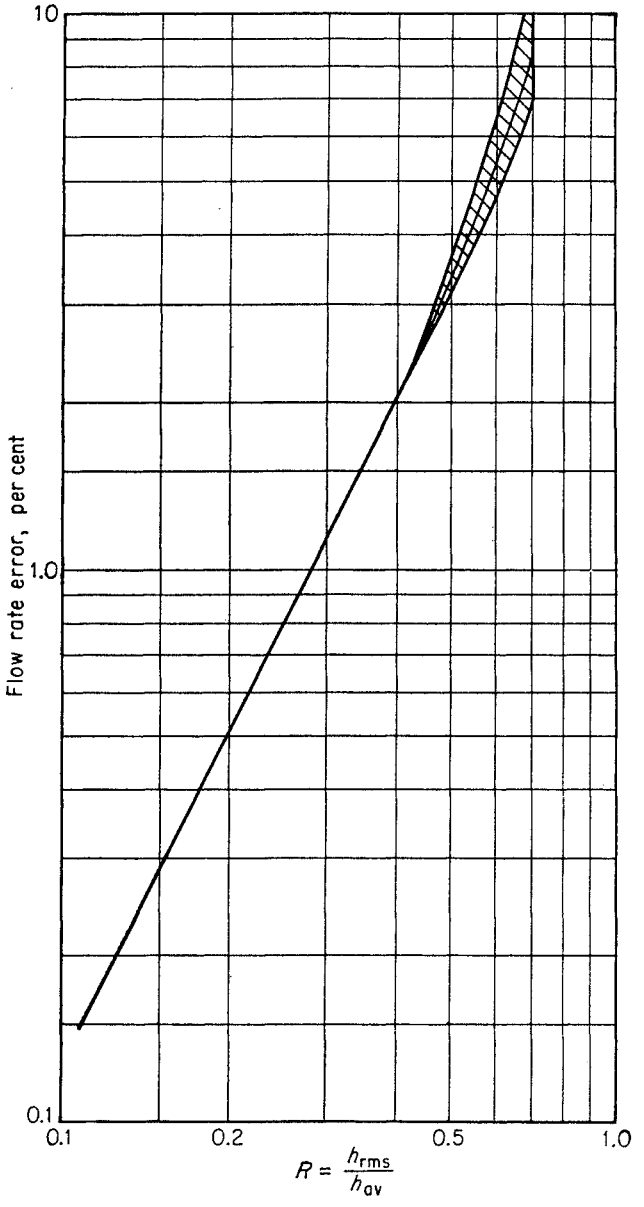

Fig. 8-19. Pulsation error for orifice meters. (*Hardway, 8-7. Courtesy Instruments.*)

The design of the lead lines from the orifice to the manometer may influence metering accuracy when pulsation is serious (8-21). The use of "snubbers" or dampeners in the lead lines can reduce the effect of pulsation on metering error but cannot eliminate the basic problem.

CRITICAL-FLOW PROVERS

Critical-flow provers are used for metering when gas can be blown to the air or when a large pressure drop is available. The device is very simple (Fig. 8-27); it involves only the upstream pressure, upstream temperature, gas gravity, and flow-nozzle size. Criti-

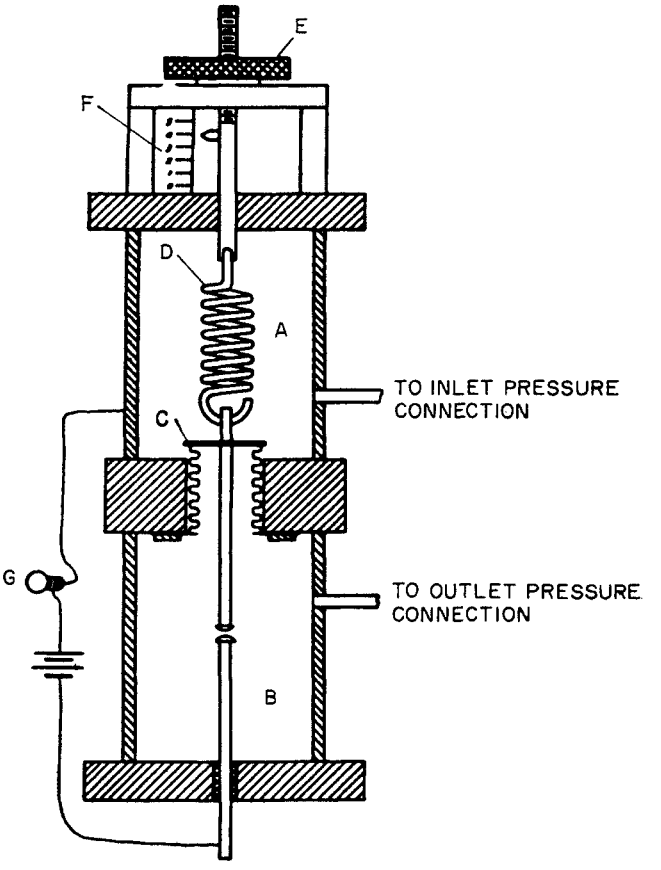

Fig. 8-20. Mechanical pulsometer. (*Lindahl, 8-12. Courtesy ASME.*)

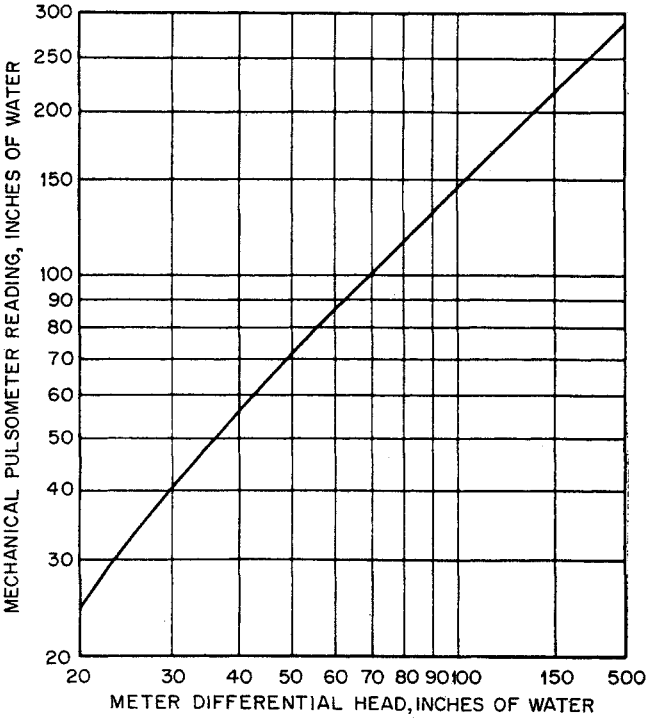

Fig. 8-21. Relationship between meter differential and pulsometer reading for 1 per cent error. (*Lindahl, 8-12; Stearns et al., 8-19. Courtesy ASME.*)

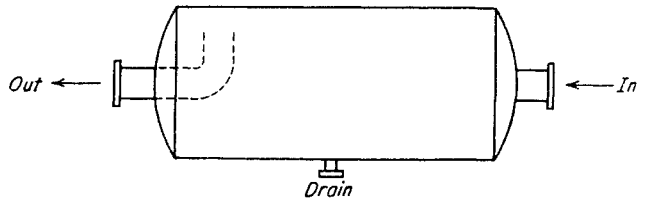

Fig. 8-22. Pulsation dampener tank.

cal flow occurs when the critical pressure ratio is exceeded and acoustical velocities are attained in the throat of the nozzle. For ideal gases, the critical pressure ratio is found from Eq. (8-22).

$$\frac{P_c}{P_1} = \left(\frac{2}{k+1}\right)^{k/(k-1)} \qquad (8\text{-}22)$$

where P_c = pressure in throat of prover nozzle
P_1 = pressure upstream
$k = C_p/C_v$

For air $P_c = 0.528\,P_1$.

For 0.6 gravity natural gas, $k = 1.299$ and

$$P_c = 0.546P_1$$

The equation for flow of an ideal gas in a converging adiabatic nozzle may be found from Eq. (7-1):

$$\Delta H + \Delta X \frac{g}{g_c} + \frac{\Delta v^2}{2g_c} = q - w \qquad (7\text{-}1)$$

For ideal gases in adiabatic and reversible flow,

$$P_1 V_1^k = PV^k = \text{constant} \qquad (8\text{-}23)$$

Real gases follow the relationship

$$PV = znRT \qquad (4\text{-}2)$$

For ideal gases,

$$\Delta H = 778 \int_1^2 \frac{C_p\,dT}{M} \qquad (8\text{-}24)$$

where ΔH = enthalpy increase, ft-lb/lb
C_p = specific heat, Btu/lb mole
M = molecular weight

Solving these equations simultaneously when $q = 0$ (adiabatic), $w = 0$ (no work done), and $\Delta X = 0$ (horizontal) gives

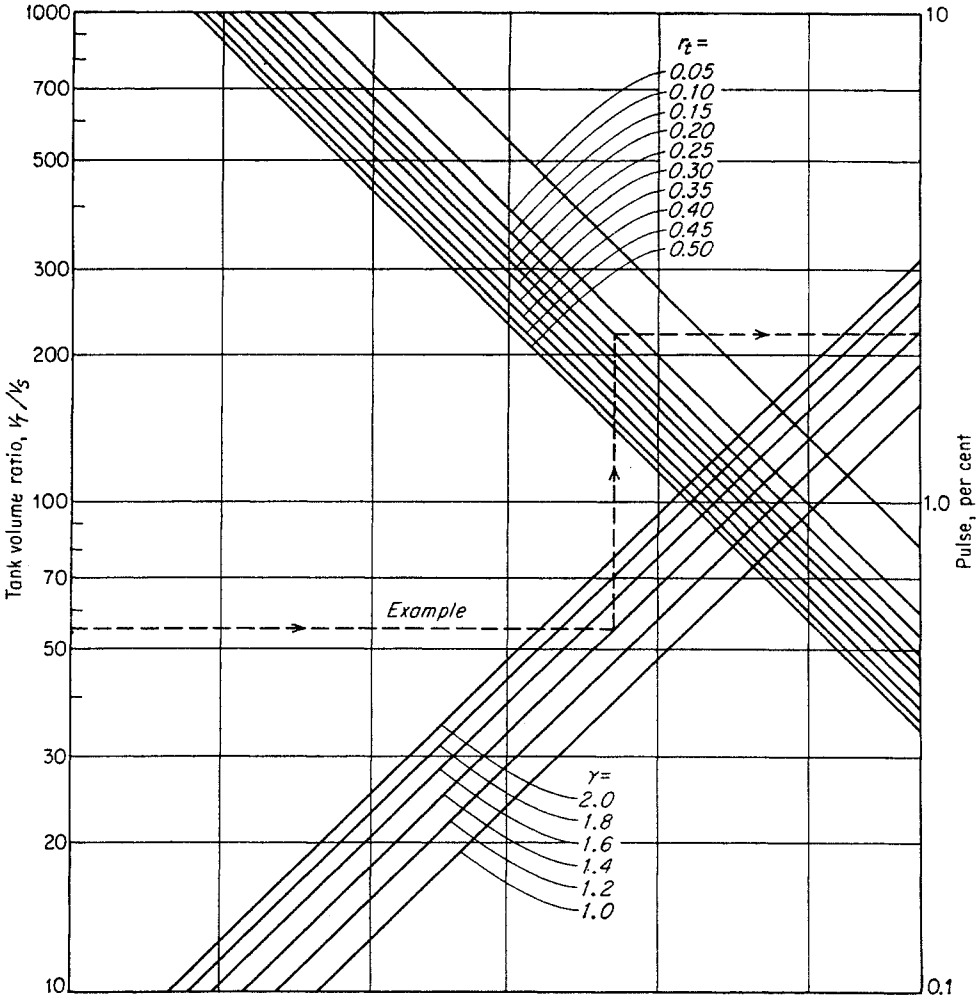

V_T = tank volume
V_s = gas volume flowing per stroke
r_t = ratio of valve-open time to piston period

$$\%\,\text{pulse} = \frac{\text{peak-to-peak pulse}}{\text{av abs pressure}} \times 100$$

γ = ratio of specific heats

Fig. 8-23. Tank volume vs. pulse amplitude for single-tank dampener. (*Chilton and Handley*, 8-6. *Courtesy ASME.*)

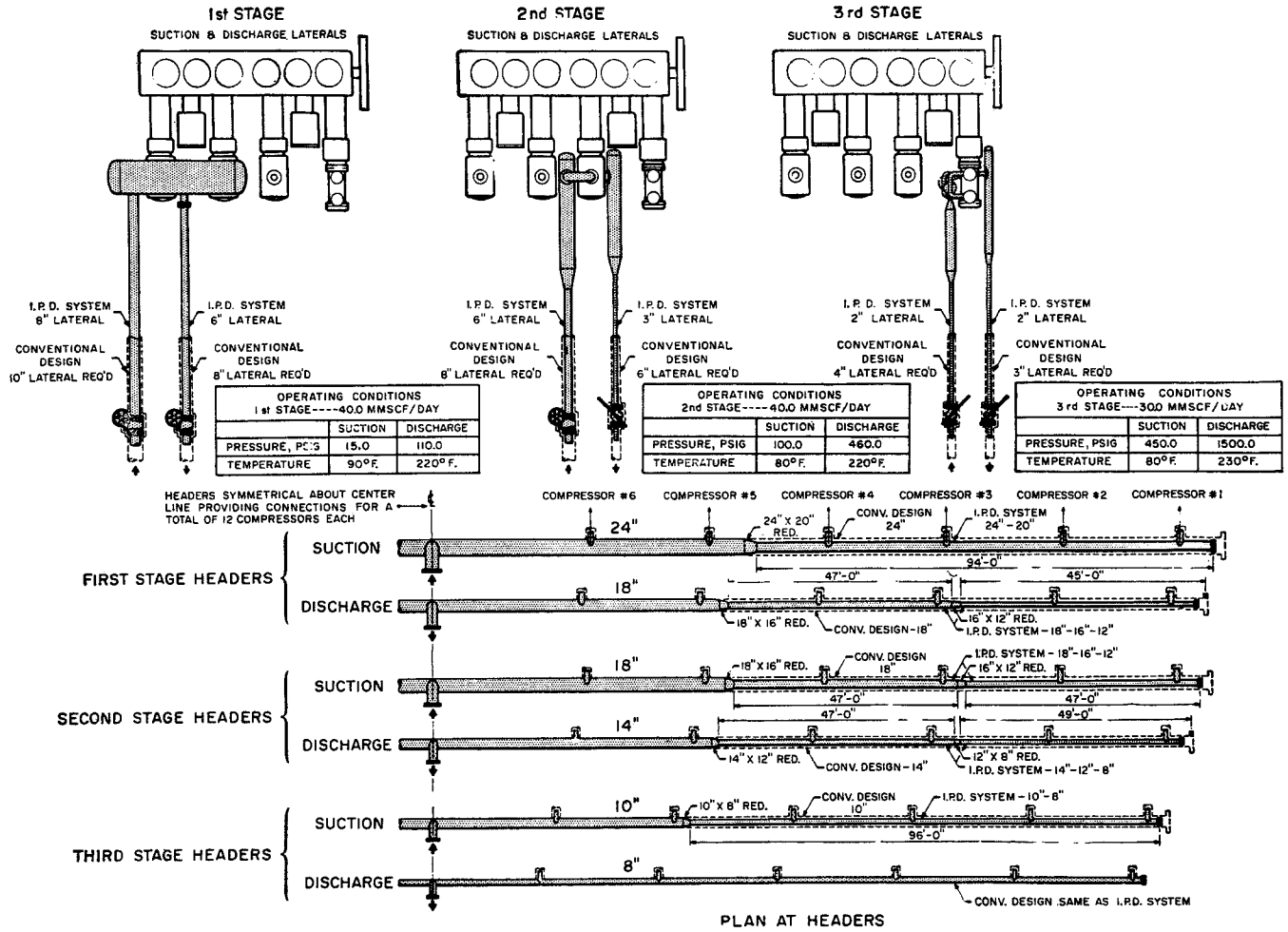

Fig. 8-24. Comparison of design to minimize meter pulsation with conventional design. (*Courtesy Fluor Products Company.*)

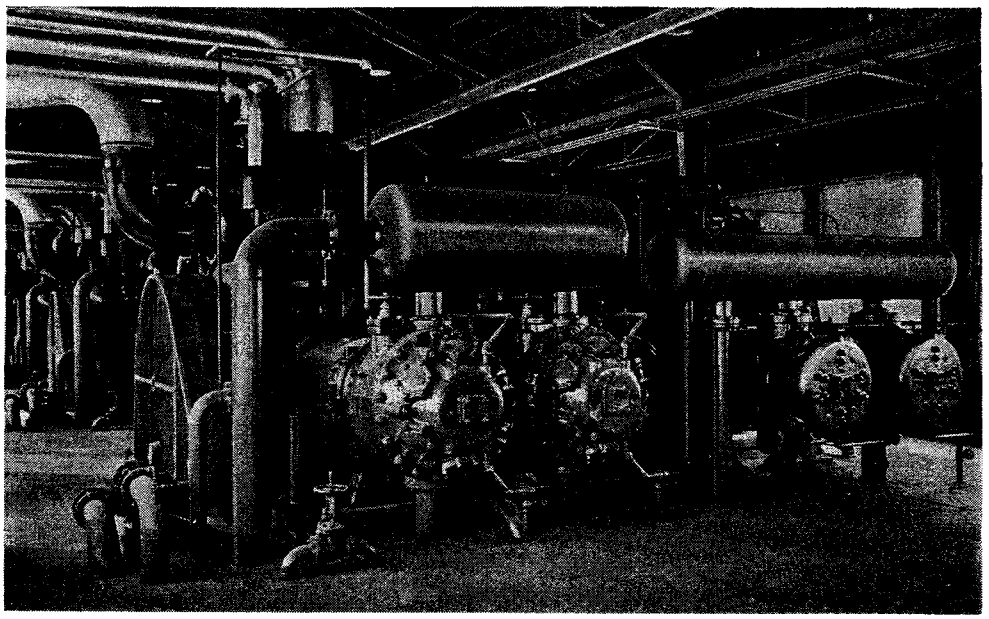

Fig. 8-25. Installation of pulsation dampeners on first-stage suction and on second-stage suction of compressor. (*Courtesy Fluor Products Company.*)

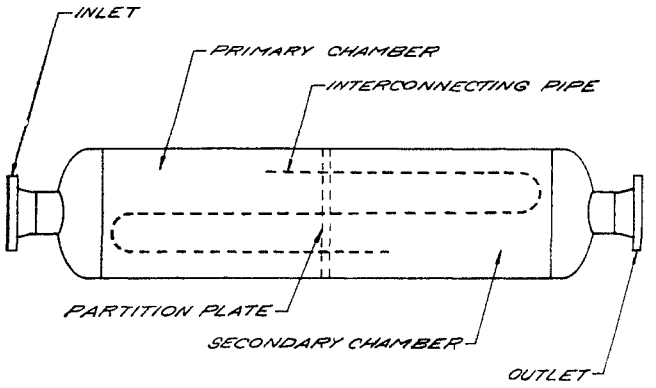

Fig. 8-26. Section of pulsation dampener. (Courtesy Fluor Products Company.)

$$v_2 = \sqrt{778 \times 2g_c \frac{C_p T_1}{29G}\left[1 - \frac{z_2}{z_1}\left(\frac{P_2}{P_1}\right)^{(k-1)/k}\right] + v_1^2} \tag{8-25}$$

For ideal gases $z_2/z_1 = 1$.

This equation gives the velocity in the orifice (v_2, ft/sec) as a function of the pressure at 2, but imposes no limitation on the degree of expansion. When the ratio P_2/P_1 reaches the value P_c/P_1 in a converging nozzle, the gas will expand no further, since the acoustical velocity is reached in the nozzle. For adiabatic and reversible flow of an ideal gas, the flowing temperature is given by Eq. (8-26).

$$T_2 = T_1\left(\frac{P_2}{P_1}\right)^{(k-1)/k} \tag{8-26}$$

The velocity may be converted to standard cubic feet by Eq. (8-27),

$$Q = v_2 A_2 \times 3{,}600 \frac{P_2}{P_b}\frac{T_b}{T_2}\frac{1}{z_2} \quad \text{cu ft/hr} \tag{8-27}$$

not assuming ideal gases at this point. Selecting 14.4 psia for the pressure-measurement base P_b and 520°F for T_b, and combining with Eq. (8-25),

$$Q = \frac{3{,}600 \times 520}{14.4 T_2}\frac{A_2 P_2}{z_2}$$
$$\sqrt{778 \times 2g_c \frac{C_p T_1}{29G}\left[1 - \frac{z_2}{z_1}\left(\frac{P_2}{P_1}\right)^{(k-1)/k}\right] + v_1^2} \tag{8-27a}$$

Combining Eqs. (8-27a), (8-26), and (8-22) and neglecting the v_1^2 term,

$$Q = \frac{3{,}600 \times 520 \times \sqrt{778}\,\sqrt{64.4}\,A_2\sqrt{C_p}}{14.4\sqrt{29}\,z_2\sqrt{GT_1}}$$
$$\left(\frac{2}{k+1}\right)^{1/(k-1)}\sqrt{\frac{k+1-2z_2/z_1}{k+1}}P_1 \tag{8-28}$$

This equation may be written simply:

$$Q = \frac{CP_1}{\sqrt{GT_1}} \tag{8-29}$$

where C = coefficient for given-sized orifice
Q = gas flow at 14.4 psia and 60°F, cu ft/hr
G = gas gravity
P_1 = upstream pressure, psia
T_1 = upstream temperature, °R

This is the critical-flow equation used with provers; it applies only when the value of P_1 is greater than the downstream pressure by an amount sufficient to give critical flow. Upstream pressure must be at least twice atmospheric pressure when exhausting to the atmosphere.

Rawlins and Schellhardt (7-32) presented calibrations (Table 8-2) for orifices in 2-in. pipe and 4-in. pipe and for plates ⅛ in. thick. Commercial devices give the constants for various plates.

The value of C can be computed from Eq. (8-28). Rawlins and Schellhardt did not make corrections

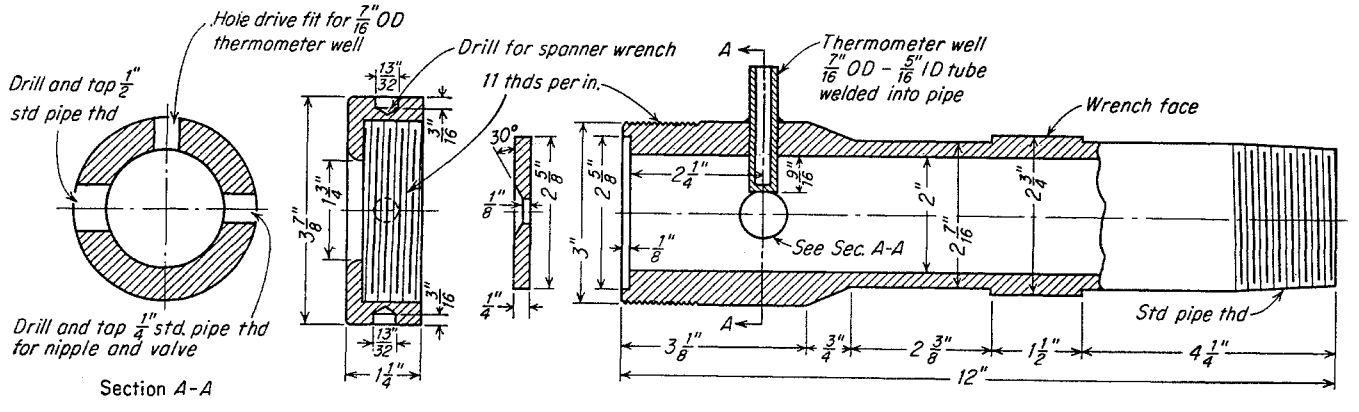

Fig. 8-27. Design of 2-in. critical slow prover. (Rawlins and Schellhardt, 7-32.)

Table 8-2. Coefficients for Critical-flow Prover and Choke Nipple

$$Q = \frac{CP}{\sqrt{GT}}$$

P = upstream pressure, psia
G = gas gravity
T = upstream temperature, °R
C = coefficient
Q = flow rate measured at 14.4 psia and 60°F, Mcf/day

Orifice size, in.		Value of C		
		Critical-flow prover		Choke nipple
		2-in. pipe	4-in. pipe	
1/16	0.063	1.524		
3/32	0.094	3.355		
1/8	0.125	6.301	.....	6.25
3/16	0.188	14.47	.....	14.44
7/32	0.218	19.97		
1/4	0.250	25.86	24.92	26.51
5/16	0.313	39.77	.....	43.64
3/8	0.375	56.58	56.01	61.21
7/16	0.438	81.09	.....	85.13
1/2	0.500	101.8	100.2	112.72
5/8	0.625	154.0	156.1	179.74
3/4	0.750	224.9	223.7	260.99
7/8	0.875	309.3	304.2	
1	1.000	406.7	396.3	
1 1/8	1.125	520.8	499.2	
1 1/4	1.250	657.5	616.4	
1 3/8	1.375	807.8	742.1	
1 1/2	1.500	1,002.0	884.3	
1 3/4	1.750	.....	1,208	
2	2.000	.....	1,596	
2 1/4	2.250	.....	2,046	
2 1/2	2.500	.....	2,566	
2 3/4	2.750	.....	3,177	
3	3.000	.....	3,904	

SOURCE: Rawlins and Schellhardt (7-32).

Table 8-3. Critical Expansion Ratios

Gas	C_p Btu/(lb mole) (°F)	$k = C_p/C_v$ at 1 atm, 60°F	$\frac{P_c}{P_1}$	Acoustical velocity at 60°F, ft/sec
Air.....	7.00	1.410	0.528	1,031
Helium.....	4.968	1.66	0.486	2,840
Methane....	8.44	1.308	0.545	1,350
Ethane.....	12.30	1.193	0.565	967
Propane....	17.10	1.133	0.577	793
Isobutane...	22.4	1.097	0.585	681
n-Butane...	23.0	1.094	0.585	680
0.6 gravity..	8.84	1.299	0.546	1,309
0.7 gravity..	9.77	1.279	0.550	1,035

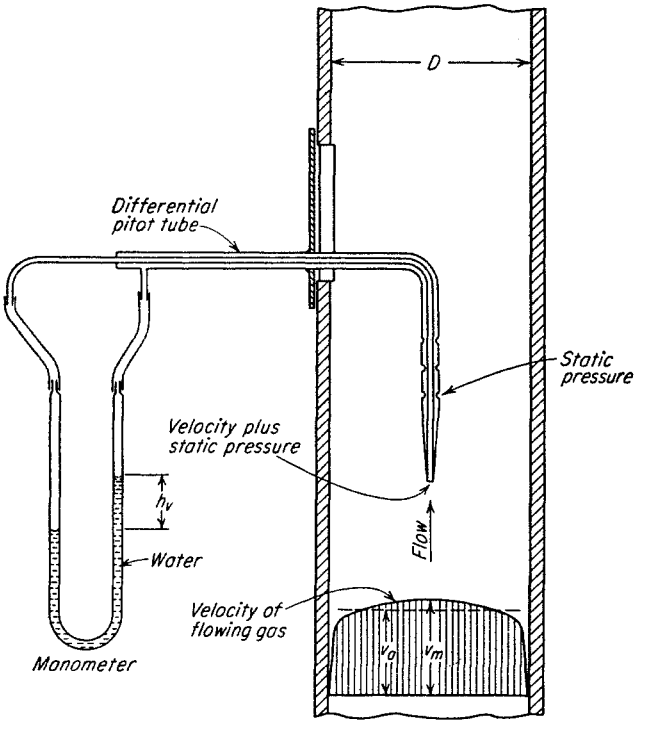

Fig. 8-28. Pitot tube.

in the meter volumes or in the critical-flow prover for deviation from ideal gases, or they assumed $z_1 = z_2 = 1.0$. Their measurements were made on a gas well with closed-in wellhead pressure of 480 psi.

Critical-expansion ratios and acoustical velocities are given for natural gas constituents in Table 8-3.

PITOT TUBE

The pitot tube measures flow rate from the impact pressure of a flowing stream. Figure 8-28 shows a differential pitot tube with manometer. The differential between the impact and static pressures is measured, since the static pressure is observed adjacent to the point where the impact pressure is taken. For high flow rates, mercury may be used in the manometer instead of water. For flow rates below those giving 0.5 in. of water on a vertical manometer, an inclined manometer or draft gauge will improve the accuracy of the reading.

The formula for computing flow in a pipe by pitot tube is

$$Q = CD^2 \sqrt{\frac{h_v P}{G} \frac{520}{T_f}} \qquad (8\text{-}30)$$

where Q = flow rate at 14.7 psia and 60°F, Mcf/day
C = constant = 7.00
D = diameter of pipe, in.

T_f = flowing temperature, °R
G = gas gravity
P = static pressure, psia
h_v = velocity or impact head, in. of water

For a 0.6 gravity gas, T_f of 60°F, and P at 14.7 psia,

$$Q = 34.7D^2\sqrt{h_v} \tag{8-31}$$

This formula is derived below on the basis of the known ratio of the velocity at the center to the average velocity for flow in pipes. It is the same formula as that published earlier (7-32, 8-16).

When a mercury manometer is used to indicate the impact velocity h_v in Eq. (8-30), C becomes $7.00\sqrt{13.55} = 25.8$; when h_v is in psi, C becomes $7.00\sqrt{27.75} = 36.9$.

When a pitot tube is held at the outlet of a vent pipe and the static pressure is taken at the side of the vent pipe 4 diameters from the end, the same formula applies (7-32), provided that the static pressure has not reached the point—about 15 psi—where critical flow is reached at the end of the pipe.

Derivation of Pitot-tube Formula

A pitot tube inserted in a flowing stream measures the velocity or impact head (Fig. 8-28). This head, measured in feet of fluid flowing, is equal to the kinetic energy $v^2/2g_c$ of the gas stream. The velocity v is at the tip of the pitot tube. When the pitot is placed in the center of the pipe, it registers the maximum velocity v_m for a stable velocity distribution. The ratio of the average velocity v_a of the full stream to the maximum velocity v_m is a function of the Reynolds number of the flowing stream.

The quantity Q of gas flowing through a pipe is obtained as a product of the velocity v_a and the pipe area $\pi D^2/4$. The problem is to obtain Q in Mcf per day at a standard pressure (14.7 psia) and temperature (60°F).

$$Q = Av_a \tag{8-32}$$

$$Q = \frac{\pi D^2}{4 \times 144} v_a \frac{3{,}600 \times 24}{1{,}000} \quad \text{Mcf/day at flowing pressure and temperature} \tag{8-33}$$

$$Q = \frac{3{,}600 \times 24}{1{,}000 \times 4 \times 144} \pi D^2 v_a \frac{P}{14.7}\frac{520}{T} \quad \text{Mcf/day measured at 14.7 psia and 60°F} \tag{8-34}$$

where A = area of pipe, sq ft
D = pipe ID, in.
P = pressure of flowing gas, psia
T = temperature of flowing gas, °R
v_a = average velocity, ft/sec

The average velocity is obtained from a reading of the impact-velocity head h_v, usually in inches of water.

$$\frac{v_a}{v_m} = f \tag{8-35}$$

$$\frac{v_m^2}{2g_c} = \text{head of gas, ft of gas} \tag{8-36}$$

where v_m = maximum velocity, ft/sec
f = ratio of velocities

$$v_a = f\sqrt{\frac{2g_c h_v(\text{density of water})}{12(\text{density of gas})}} \tag{8-37}$$

$$\frac{29GP}{RT} = \frac{29GP}{10.73T} = \text{density of gas, lb/cu ft} \tag{8-38}$$

$$v_a = f\sqrt{\frac{62.4h_v}{12}\frac{10.73 \times T \times 64.4}{29GP}} \tag{8-39}$$

where G = gas gravity
R = gas-law constant
h_v = velocity head of pitot at center of pipe, in. of water

Combining Eqs. (8-34) and (8-39),

$$Q = \frac{3{,}600 \times 24 \times 520 \times \pi D^2 P}{1{,}000 \times 4 \times 144 \times 14.7 \times T} f\sqrt{\frac{62.4 \times 10.73 \times T \times 64.4}{12 \times 29}\frac{h_v}{GP}} \tag{8-40}$$

$$Q = 185.7fD^2\sqrt{\frac{h_v P}{GT}} \tag{8-41}$$

For a flowing temperature of 60°F (520°R) and a ratio $f = v_a/v_m = 0.86$ (for Reynolds number range 30,000 to 1,000,000),

$$Q = 185.7 \times 0.86D^2\sqrt{\frac{h_v P}{G \times 520}} \tag{8-42}$$

$$Q = CD^2\sqrt{\frac{h_v P}{G}} \quad \text{where } C = 7.00 \tag{8-43}$$

For a flowing pressure of 14.7 psia and a gas gravity of 0.6,

$$Q = 7.00D^2\sqrt{\frac{14.7h_v}{0.6}} = 34.7D^2\sqrt{h_v} \tag{8-44}$$

SIDE STATIC PRESSURE

The static side pressure 4 diameters from the end of a pipe flowing to the atmosphere is an indication of the flow rate when critical flow is occurring at the end of the pipe. A formula developed by Reid (7-32) gives the flow rate.

$$Q = 20.13D^2(M + 30) = 41.05D^2(P + 14.7) \tag{8-45}$$

where Q = gas flow at 14.7 psia and flowing temperature for a 0.6 gravity gas, Mcf/day
D = pipe diameter, in.
M = static side pressure, in. Hg above atmosphere
P = static side pressure, psig

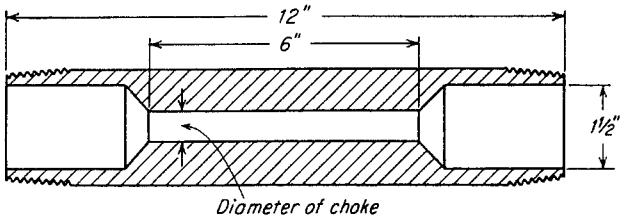

Fig. 8-29. Choke nipple.

CHOKE NIPPLES

Choke nipples (Fig. 8-29) are often used in controlling the flow of oil or gas from wells. For gas flowing through a choke nipple under critical flow, the values of C in Table 8-2 are given in the literature (7-32).

VOLUMETRIC METERS

Volumetric diaphragm meters are used in domestic installations. They depend for accurate metering upon periodic calibration. In the laboratory, wet-test meters are used frequently (Fig. 4-81). Gas not saturated with water must be presaturated or it will pick up an unknown quantity of water vapor in the meter. For accurate work a wet-test meter should be calibrated by water displacement. Gasometers (Fig. 8-30) are normally used for volumetric displacement of large gas volumes in experimental work. The center concentric cylinder is balanced by weights and pulleys, and the movement of the cylinder at a constant pressure on the gas indicates the volume of gas displaced.

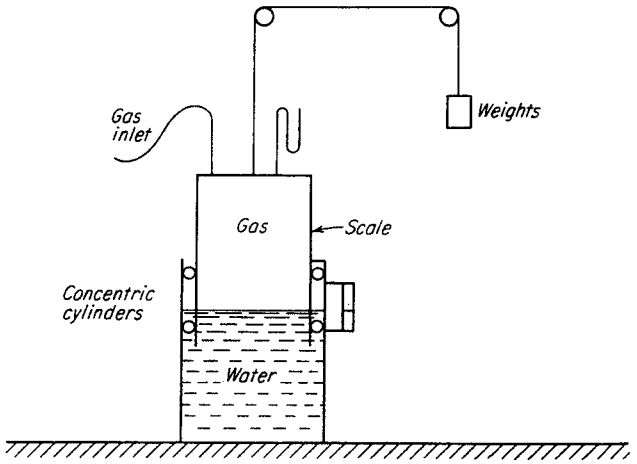

Fig. 8-30. Gasometer.

CHAPTER 9

Drilling and Testing of Natural Gas Wells

The drilling of some 58,000 wells in the United States in 1956 constituted a major activity. In round numbers, some 10 per cent of all wells drilled are gas wells, 40 per cent are dry holes, and 50 per cent produce crude oil. There is no difference between drilling an oil well and drilling a gas well down to the top of the producing horizon, but there may be differences in completion methods. In addition to drilling of wells, topics worthy of discussion include drill-stem testing, cementing of the casing, perforating of casing to the producing horizon, acidization, and fracturing processes. The logging of wells to determine the characteristics of the rock is a science in itself and will be covered. Once a gas well is completed, tests are made to aid in evaluating its gas content and flow capacity.

Fig. 9-1. Spring-pole drilling rig. *(Courtesy Baroid Division, National Lead Company.)*

DRILLING OF WELLS

The two methods of drilling a well are the rotary method and the cable-tool method. The cable-tool method is the older of the two methods; it employs a heavy bit and stem on the end of a cable. The bit is alternately raised and dropped, chipping its way into the formation. Water is flushed into the hole and the resulting suspension is removed by bailing. In the rotary method, a bit is attached to a length of steel pipe, which revolves by means of a turntable. As the bit bores a hole, lengths of pipe are added. Drilling fluid, "mud," is pumped down the drill pipe and up the annulus, its purpose being to flush cuttings from

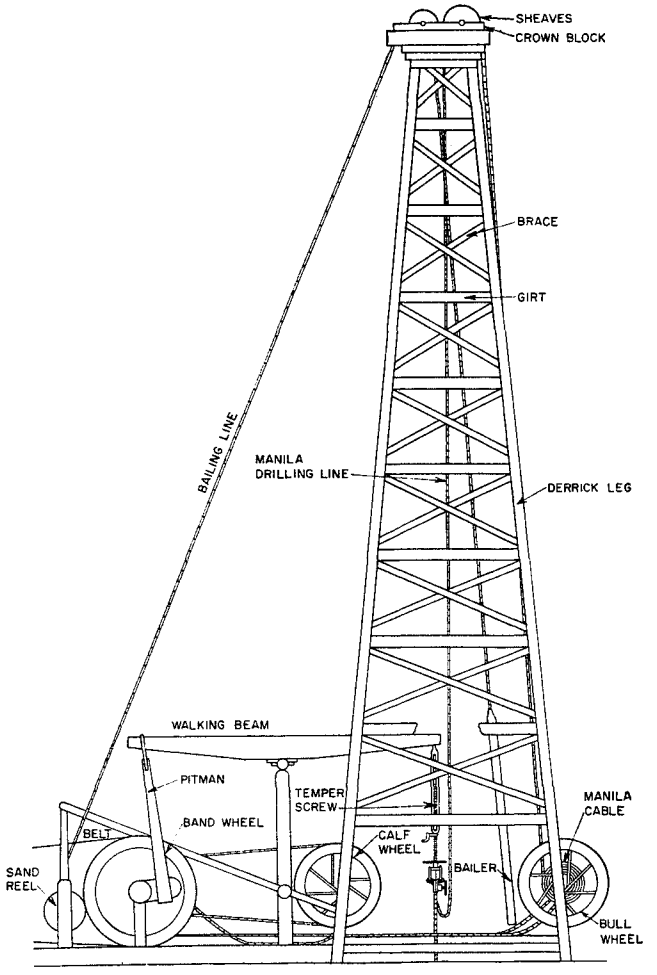

Fig. 9-2. Typical derrick cable-tool rig. *(Courtesy Standard Oil Company of New Jersey.)*

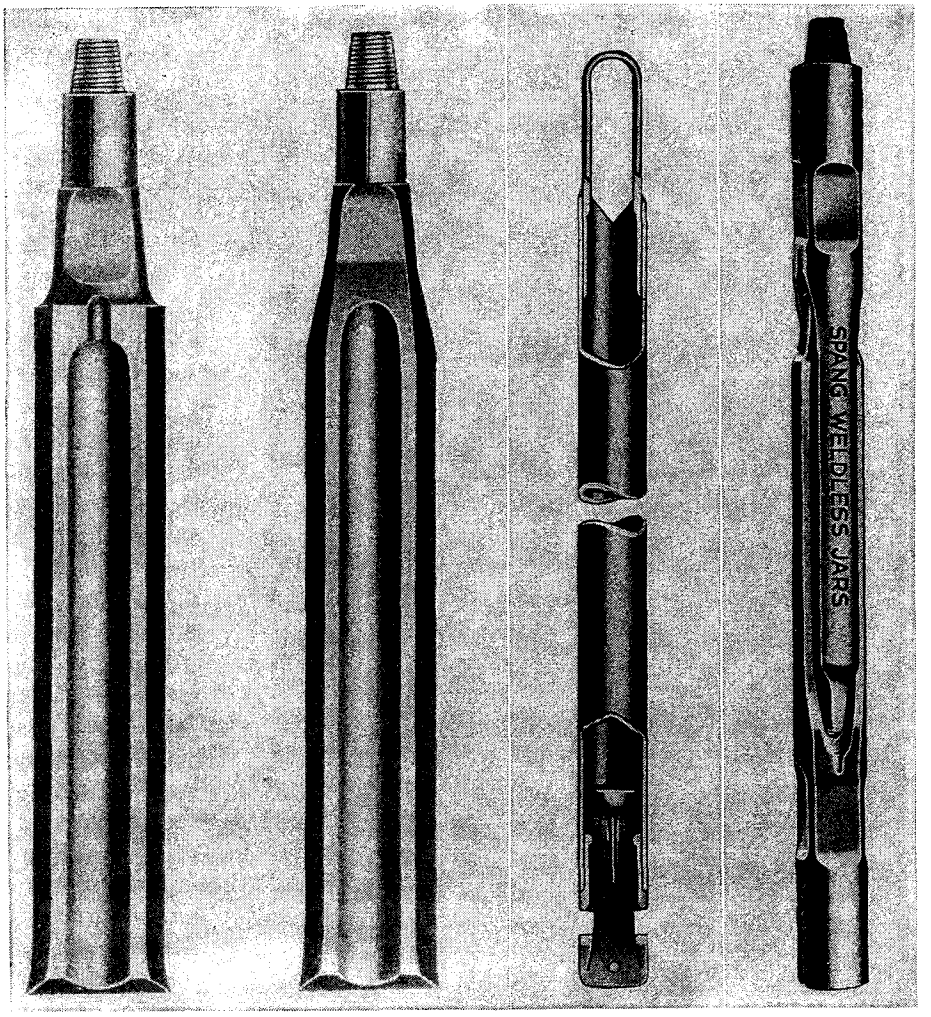

Fig. 9-3. Cable-tool bits, jars, and bailer. (*Courtesy Spang and Company.*)

the well, cool the bit, and form a mud cake on the walls of the hole.

Cable-tool Drilling

The Chinese were the first to practice the art of well drilling, using a cable-tool type of rig. As early as 256 B.C., they drilled deep brine wells. Early in the nineteenth century, "spring-pole" rigs were popular in the United States [Fig. 9-1 (9-30)]. The spring-pole rig usually consisted of a springy log anchored at an angle, at the tip of which the drilling tools were suspended by a rope. When the tip of the pole was pulled down, the tools fell into the hole and, when the pole was released, it lifted the tools out of the hole. The spring-pole rig was the forerunner of the cable-tool rig as we know it today. The development of the cable-tool rig came with the drilling of the Drake well in 1859, and continued as the sole method of drilling wells until about 1901. As late as 1952, cable-tool rigs drilled 17½ per cent of all oil and gas wells drilled. Figure 9-2 is a sketch of a typical cable-tool rig of the type that drilled the Drake well.

Photographs of bits, of jars coupled between the line and the bits, and of bailers used to remove cuttings and mud are given in Fig. 9-3. Most cable-tool drilling is either for completing wells into the producing zone after the well has been cased or for the complete drilling of relatively shallow wells. These operations can be conducted with portable rigs (Fig. 9-4). Cable-tool rigs require the services of only two men and are relatively simple to move and operate. Some formations are adaptable to the percussion action of the cable-tool bit; so this method of drilling is still economical. In general, the economic limit of cable-tool operation is about 5,000 ft. Recent developments in percussion drilling include a bit that removes the cuttings as they are formed [Fig. 9-5 (9-20)]. The energy of the bit is then expended entirely on cutting rock rather than on reducing the size of the cuttings. The drill consists of a percussion bit (1), bailer (2), central pipe (3), trap or bailer for cuttings (4), and pump (5). The pump circulates the fluid up through the bit into the trap when the cuttings fall out. The flow of fluid is controlled by the two valves (6 and 7),

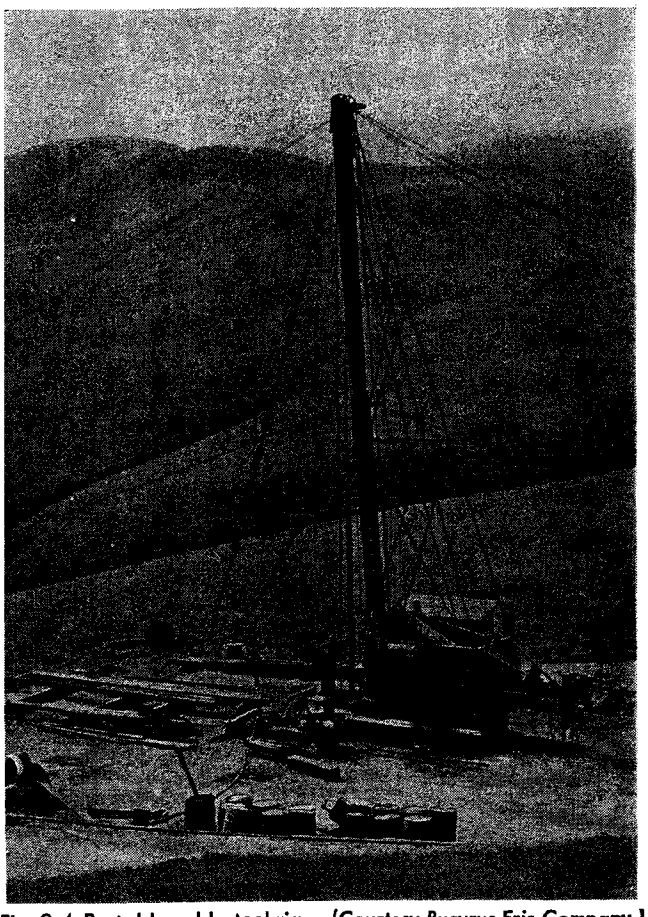

Fig. 9-4. Portable cable-tool rig. (*Courtesy Bucyrus Erie Company.*)

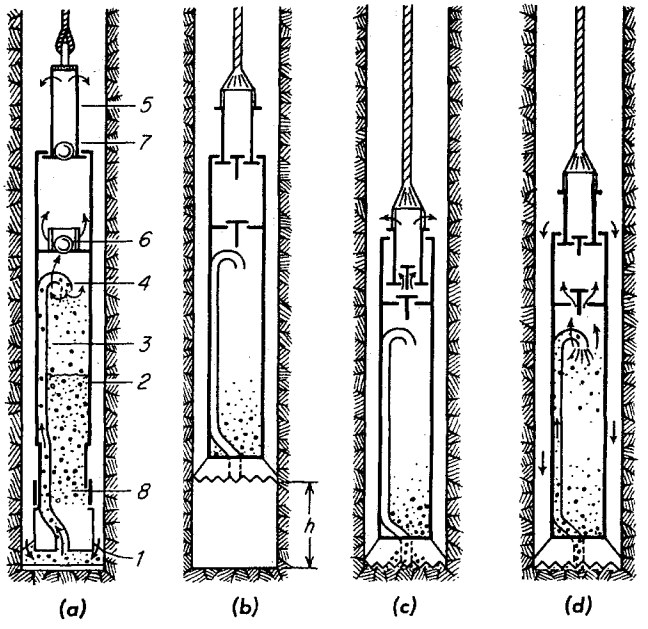

Fig. 9-5. Russian percussion bit. (Sterger, 9-20. *Courtesy Drilling.*)

which allow the fluid inside the drill to move from the bottom up and outside the unit downward. When the bailer is full, drilling is stopped, the drill is withdrawn from the hole, and the cuttings are removed through gate 8. Figure 9-5*b*, *c*, and *d* demonstrates the operation of this bit.

Rotary Drilling

Although the power-driven-rotary principle of drilling a well had been formulated at the time of the Drake well, no real application of the principle had been made. In 1860, a Frenchman drilled a well using a power-driven rotary drill with a diamond bit. New developments and improvements gradually followed, developed particularly by men in the mining industry. However, it was not until the drilling of the famous Spindletop well by Captain Lucas at Beaumont in 1901 that rotary drilling came into its own. Spindletop was to the rotary what the Drake well was to cable-tool drilling.

Figure 9-6 depicts the key components of a modern rotary rig; Fig. 9-7 is a photograph of such a rig. Modern rigs are so designed that they can drill to depths of 22,000 to 23,000 ft, and are flexible, so that they are readily portable to new locations. The com-

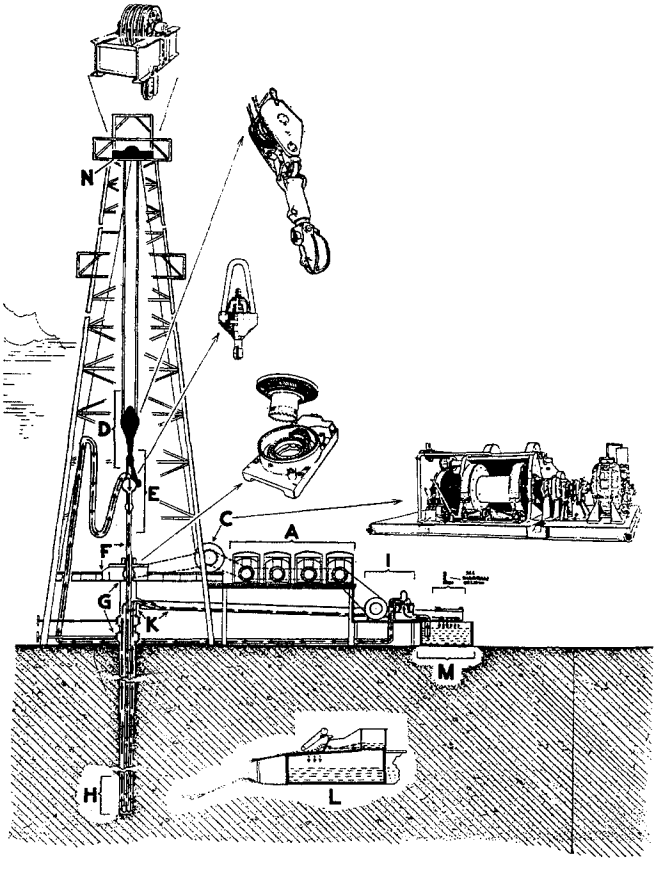

Fig. 9-6. Modern rotary rig: sketch. (*Courtesy Ohio Oil Company.*)

ponent parts of a modern rig, as indicated in Fig. 9-6, are as follows: The engines A drive the drawworks C. The drawworks consist of a hoisting drum around which is spooled steel cable. The steel cable is strung around the sheaves of the crown block N and the traveling block D, which raises and lowers the drill string. The drill string is made up of the swivel and kelly E, drill pipe, drill collars, and the bit H. The drill collars have a heavier wall than the drill pipe to give additional weight on the bit. The kelly is square-shaped so that, as it moves downward through the rotary table F, the entire drill string is rotated. The rotary table is driven by the drawworks C.

The engines A also power the slush pump I, which pumps mud out of the mud tank M. The path taken by the mud is shown by the arrows; it leaves the pump, flows up the standpipe, through the flexible rotary hose and into the swivel connection, down the kelly, drill pipe, drill collars, and out the holes in the bit. It then flows up the annular space and is vented out the casing G into a trough K and then to the shale shaker L. From the shale shaker the mud flows back to the mud pit, and the cycle is repeated. The purpose of the shale shaker is to remove the cuttings brought up by the mud. Tool joints and bits used in rotary drilling are shown in Fig. 9-8.

The cost of drilling a well may vary anywhere from a few thousand dollars for shallow wells to over a million dollars for very deep wells or offshore wells. In 1955–1956, the average cost for all wells drilled was about $90,000 per well. A slight increase or decrease in the time necessary to drill a well can change the cost of these wells by many thousands of dollars. The basic cost per day of operating a drilling rig once it is "rigged up" is no different whether 25 or 2,500 ft of hole is drilled in a day.

Thus, a continuing effort is made to speed the rate at which footage is being made. Drilling at minimum cost requires an optimum combination of several factors, among them: (1) average penetration rate, (2) footage that can be drilled with a given bit, (3) round-trip time required, (4) bit cost, and (5) operating cost of a rig.

The average drilling cost per foot can be simply calculated as follows:

$$\text{Cost per foot} = \frac{(\text{rig cost per hr})(\text{rotating hr} + \text{trip hr}) + (\text{bit cost})}{\text{bit footage}}$$

In the effort to reduce drilling costs, research in new and better methods of drilling as well as in modifying and improving present methods is being carried on continuously. There are at present three different devices under development or undergoing field tests. Two are percussion tools and the third is a turbodrill. In contrast with the percussion cable tools described in the previous section and with the standard rotary rig, all three of these devices place the power in the bottom of the hole at the bit. As a result of friction of the rotating pipe in the mud and walls of the hole, the conventional rotary drill rapidly loses much of its power as depth increases below 6,000 ft, with the result that the power and speed at the bit are not at their optimum for the best drilling conditions. Any drilling process, therefore, that keeps the power available at the bit, regardless of depth, would have a decided advantage over the conventional rotary.

The two percussion drills under development are a magnetostrictive drill by Drilling Research, Inc., and a sonic drill being developed by Borg-Warner. The magnetostrictive drill is operated by alternating electric current through a magnetostrictive motor which

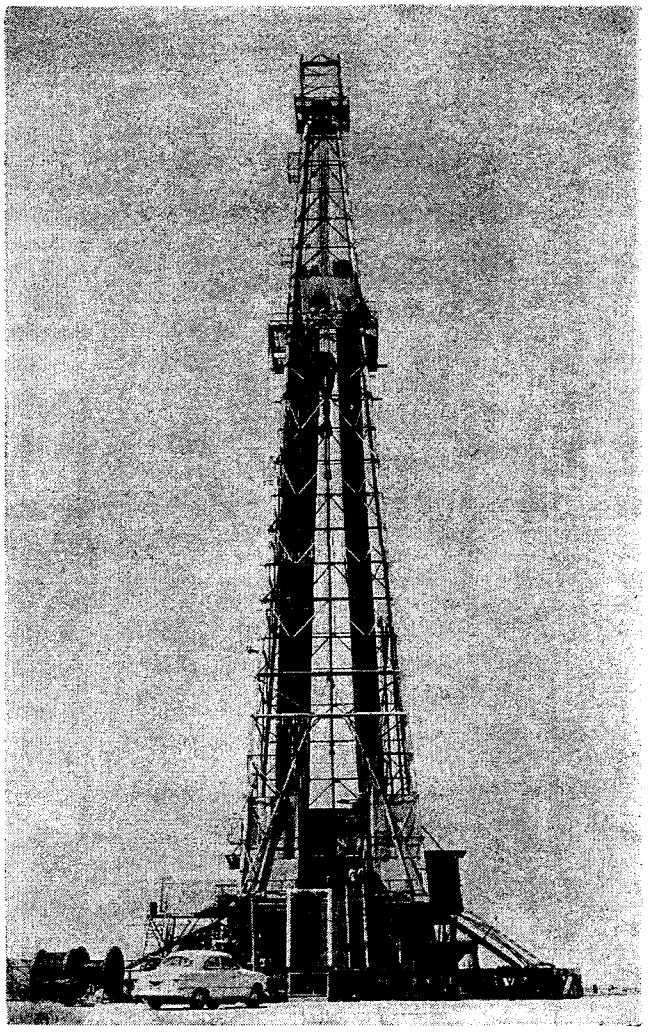

Fig. 9-7. Modern rotary rig. (*Courtesy Ohio Oil Company.*)

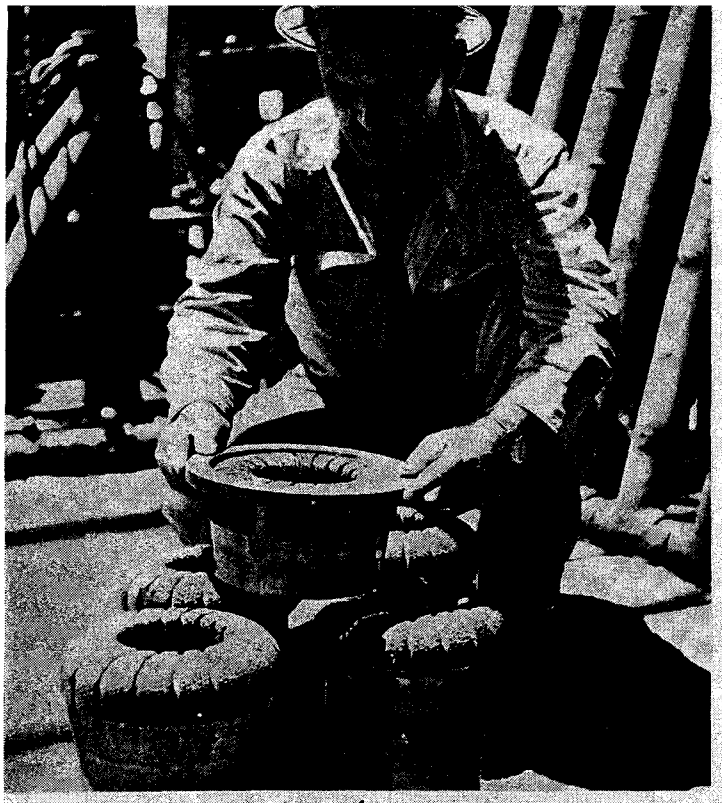

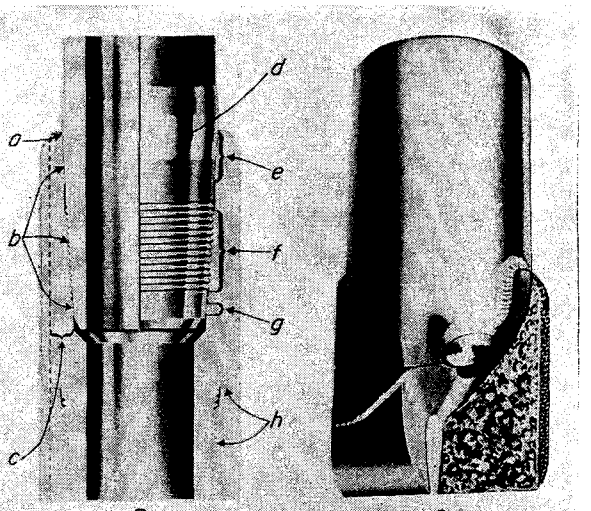

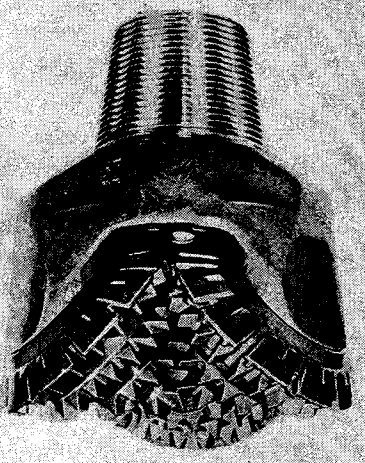

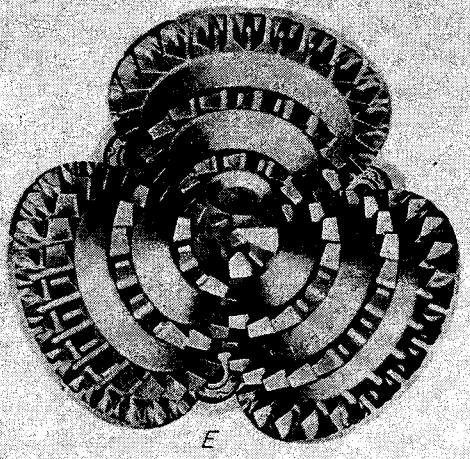

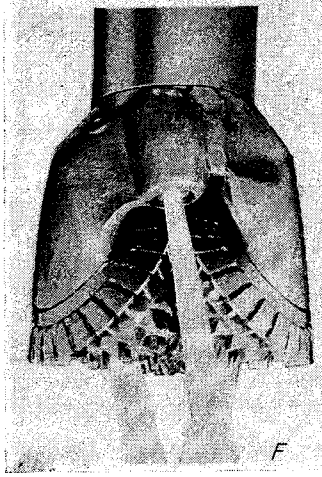

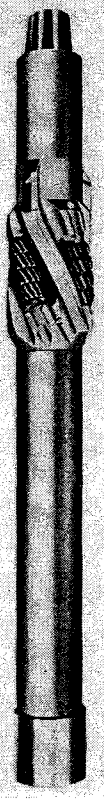

Fig. 9-8. (A) Gauging diamond core bits. (*Courtesy Ohio Oil Company.*) (B) Drill-pipe joint (tool joint). (*a*) Steep taper permits thick section at point of last contact between pipe and tool joint where bending loads in pipe are greatest. (*b*) All mating surfaces—the outer seal, pipe threads, and inner seal—are on the same taper. This provides uniformity of fit on initial and *replacement* installations. The three points of engagement of the Seal-Grip joint provide a *friction grip* stronger than the torsional strength of the pipe. (*c*) Even on badly worn tool joints, steep taper permits thick section where bending loads in tool joint are greatest. (*d*) This critical area of the pipe is *cold-rolled* at the mill for greater strength, using equipment and techniques developed by Hughes engineers. (*e*) Outer seal engagement. (*f*) Engaged thread strength in shear is greater than two times the strength of the drill pipe. (*g*) Inner seal is on taper to ensure uniformity of fit and positive seal against leakage on both original and replacement installations. This prevents corrosive fluids from attacking threads. (*h*) Copper-plating of threads and shoulders of Hughes tool joints protects against scoring and galling. (*Courtesy Hughes Tool Company.*) (C) "Fishtail" or unitized blade bit, jet type. (*Courtesy Reed Roller Bit Company.*) (D) Standard roller bit. (*Courtesy Hughes Tool Company.*) (E) Tooth view, hard-formation jet-type three-cone rock bit. (*Courtesy Reed Roller Bit Company.*) (F) Jet bit. (*Courtesy Security Engr. Div., Dresser Operations, Inc.*) (G) Reamer. (*Courtesy Security Engr. Div., Dresser Operations, Inc.*)

vibrates the bit at several hundred cycles per second. The Borg-Warner tool is also a vibratory drill; however, the power is transmitted to a downhole turbomotor by means of the flowing mud stream, and as a result, the frequency of vibration is considerably less.

The drill that is in the most advanced state of development is the turbodrill. It has already found widespread use in Russia and is being extensively field-tested in the United States (9-2, 9-23). The turbodrill consists of an external nonrotating body, a central shaft guided by rubber thrust and radial bearings, which holds the bit on the bottom, and 80 to 100 turbine stages. The stators are mounted on the external nonrotating body and the rotor elements on the central shaft. The mud flowing downward drives the turbine in addition to lubricating and cooling the bearings. The latest turbodrills have power outputs ranging from 300 to 450 hp, bit speeds from 500 to 900 rpm, with bit loadings from 20 to 35 tons.

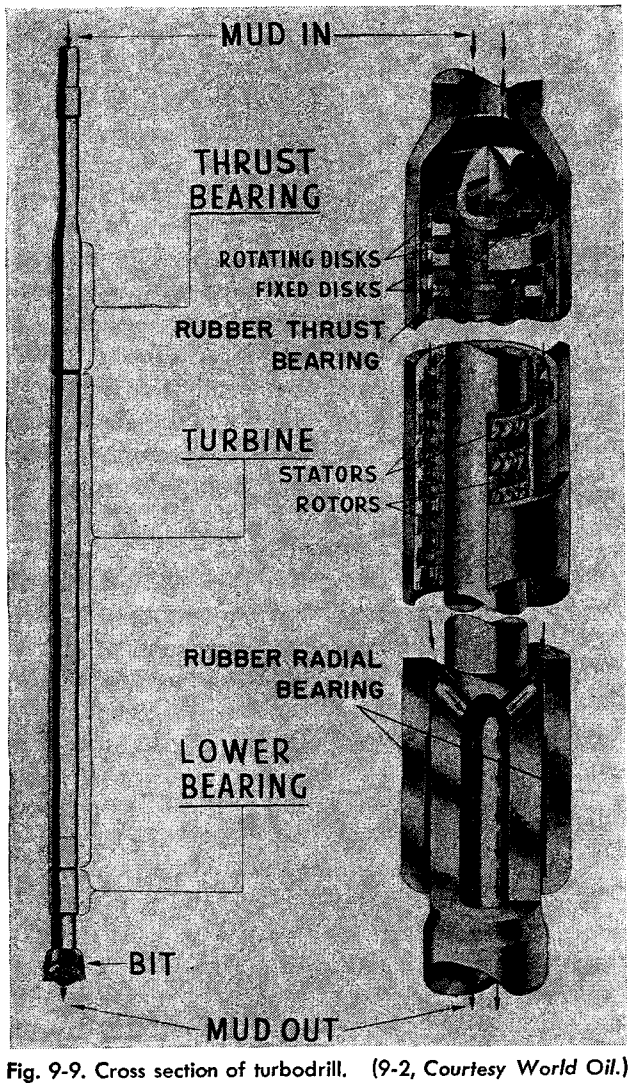

Fig. 9-9. Cross section of turbodrill. (9-2, *Courtesy World Oil.*)

Figure 9-9 is a cutaway drawing of a turbodrill, showing the important components (9-2). Table 9-1 shows a comparison of the power available at a 12-in. bit for cable tool, conventional rotary, and turbodrill.

A further comparison of the conventional rotary with the turbodrill is shown in Fig. 9-10, showing penetration rates in a hard formation (9-2). The use of the turbodrill appears to be the most significant development in the field of rotary drilling since Captain Lucas drilled his famous Spindletop well in 1901.

Drilling Fluids

As indicated above, drilling fluids are employed primarily in rotary drilling. The primary functions performed by a drilling fluid are as follows:

1. Removal of cuttings from the hole. This function depends upon the velocity, viscosity, and gel strength of the drilling fluid.
2. Cooling the drill bit.

Table 9-1. Comparison of Power Available at Bit for Conventional Rotary and Turbodrills

Tool	*Available power at 12-in. diameter bit, hp*
12-in. cable tool	26
12-in. rotary (maximum conditions)	70
10-in. turbodrill	190–285 (with 300 maximum)
8-in. turbodrills connected in tandem	210–285 (with 380 maximum)

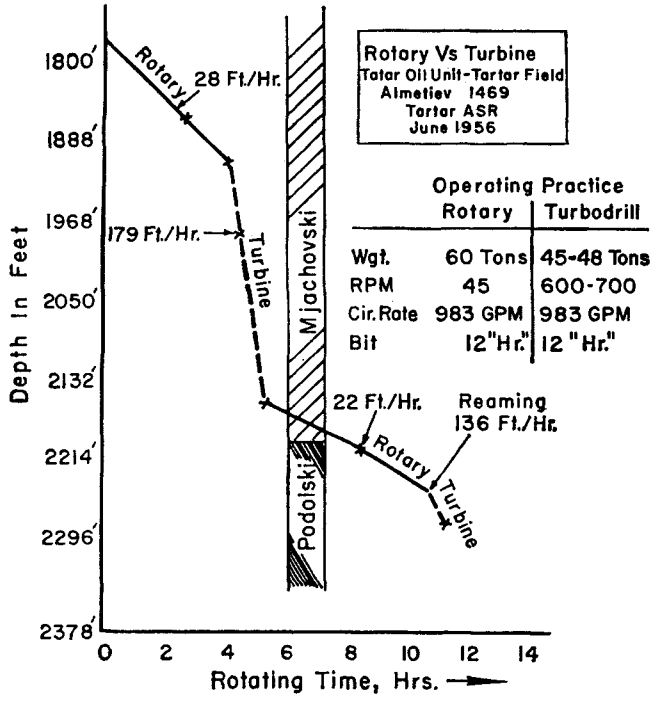

Fig. 9-10. Comparison of turbodrill and conventional drilling rates. (9-2, *Courtesy World Oil.*)

3. Preventing blowouts. By controlling the weight of the drilling fluid, the bottom-hole pressure opposite the formation being drilled can be maintained at a pressure higher than the fluid pressure in the formation, thus confining the fluid to the formation.

4. Preventing caving of the hole. This is accomplished by pressure, by consolidation of loose particles, by the thixotropic action of the drilling fluid, and by preventing water intrusion in such formations as shales, which would disintegrate on contact with water.

5. Lubricating the drill pipe and bit.

6. Preventing cuttings from settling in the hole and sticking the bit during periods of noncirculation during shutdown. This function is primarily a result of the thixotropic or gel-strength behavior of the fluid.

Drilling fluids vary widely in composition, depending on type of drilling involved. In general, drilling fluids can be classified as (1) water-base, (2) oil-base, or (3) emulsion. They consist of liquids, colloidal solids, noncolloidal solids, and dissolved solids. The liquid phase consists of water, oil, or both; the colloidal phase generally consists of clays such as bentonite or attapulgite. These clays to a large degree determine the thixotropic properties of the fluid. The magnitude of these thixotropic properties is controlled by the dissolved chemicals, such as polyphosphates, tannins, and lime. Organic colloids, such as starch or carboxymethylcellulose, are added to control filtration rates. The noncolloidal solids consist of sand, cuttings, and weight material such as barium sulfate.

A water-base mud, as the term implies, has water as the liquid medium. An oil-base mud has oil as the liquid medium. Various agents are used to control viscosity, increase gel strength, and control filter loss. The usefulness of oil-base muds is that the filtrate, being oil, does not react with the clays in productive formations. Emulsion muds are dispersions of oil and water. An emulsion of oil in water is the most common. It has the advantages of lighter weight,

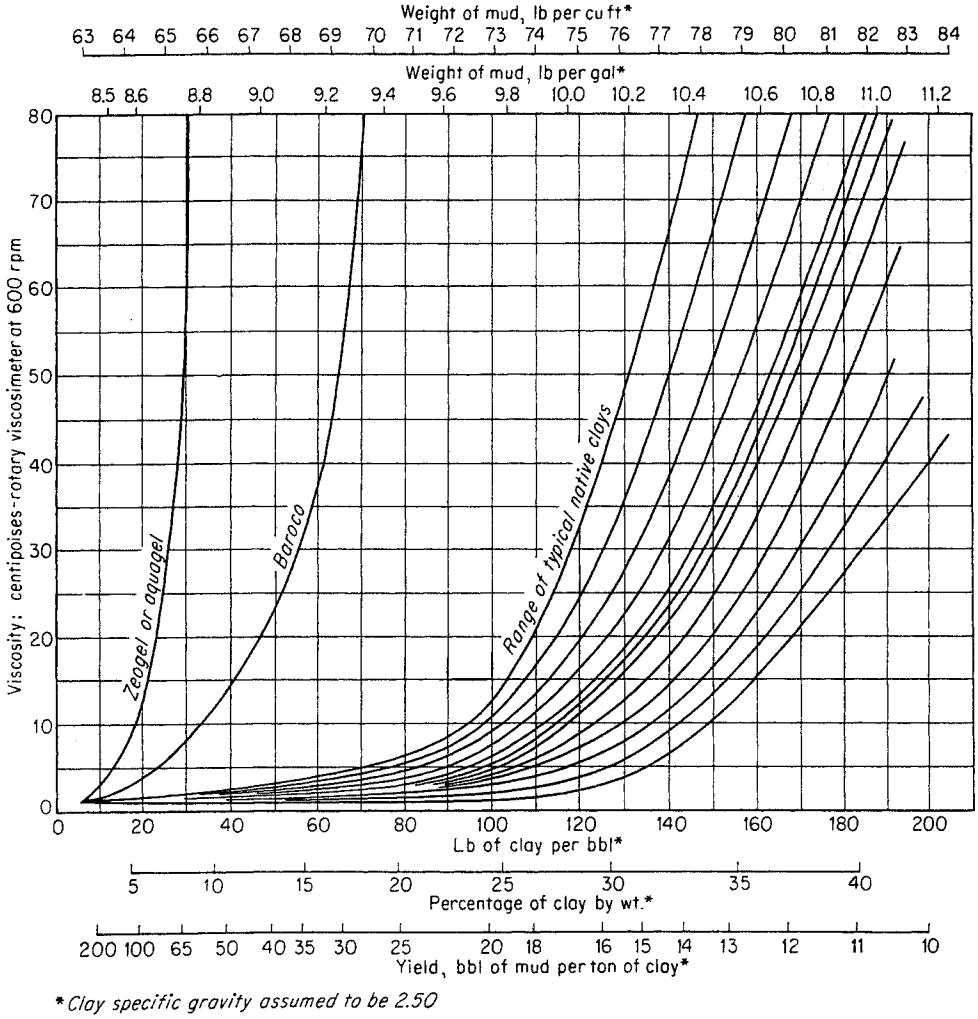

Clay specific gravity assumed to be 2.50

Fig. 9-11. Viscosity-proportion relationship of clays in fresh water. (9-30, *Courtesy National Lead Company.*)

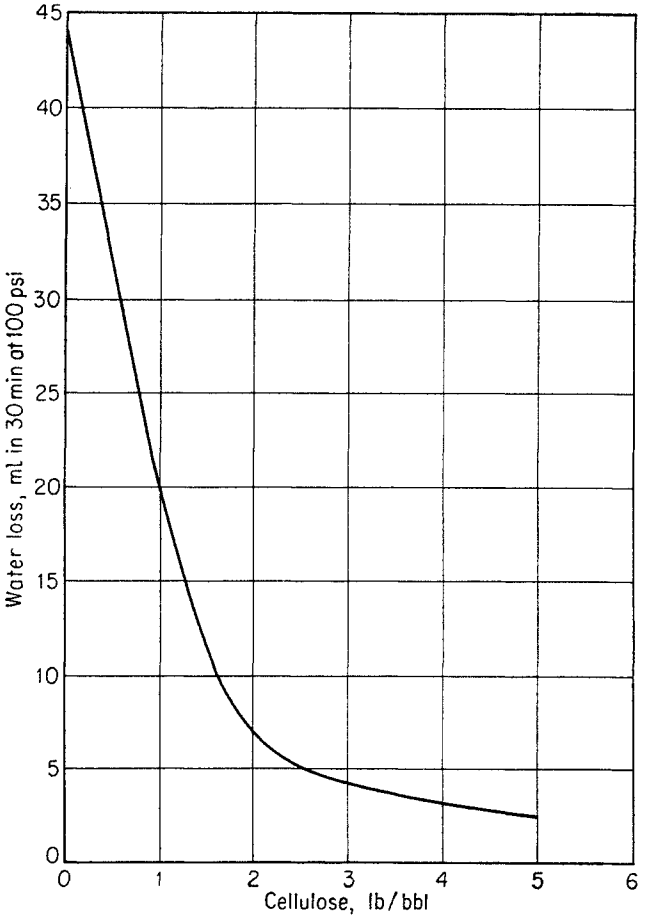

Fig. 9-12. Effect of carboxymethylcellulose on mud-fluid loss. (*Kaveler, 9-41. Courtesy Petrol. Engr.*)

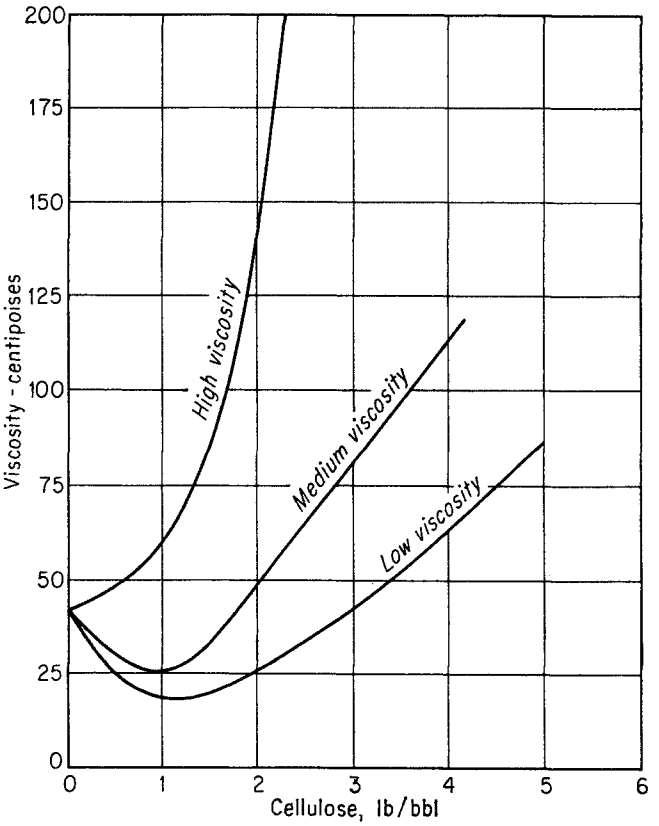

Fig. 9-13. Effect of various grades of carboxymethylcellulose on mud viscosity. (*Kaveler, 9-41. Courtesy Petrol. Engr.*)

lower filter loss, increased lubricity, and thinner filter cake. It is advantageous if the emulsifier used also acts as a thinner.

Figure 9-11 is a plot showing the "viscosity-proportion relationship" of various clays in fresh water (9-30). Aquagel, Zeogel, Baroco, etc., are trade names for special-purpose, commercially prepared clays. Some of these, for example, are especially resistant to flocculation as a result of salt contamination.

As an example of the effect of a chemical agent in controlling filter loss, Fig. 9-12 shows the result of using carboxymethylcellulose for this purpose. Similarly, Fig. 9-13 shows the effect of this same additive on viscosity (9-41).

Figure 9-14 shows the effect of quebracho, the most commonly used viscosity-reducing agent for muds, on a bentonite-kaolinite mud (9-43).

One of the most recent developments in the mechanical treatment of drilling muds has been the use of liquid cyclones to remove clay solids and sands that accumulate in the muds and to reclaim barite. The use of cyclones has materially reduced mud costs by cutting down on chemical and barite consumption. It is being used as a mechanical means of controlling viscosity by removal of the dispersed clay solids. Fig. 9-15 shows a layout of the equipment used in an actual field installation (9-45). A manifold of ten

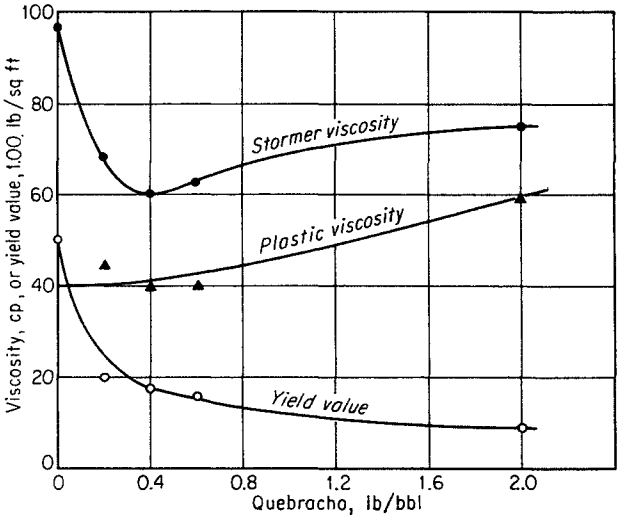

Fig. 9-14. Effect of quebracho on a bentonite-kaolinite mud. (*Melrose and Lilienthal, 9-43.*)

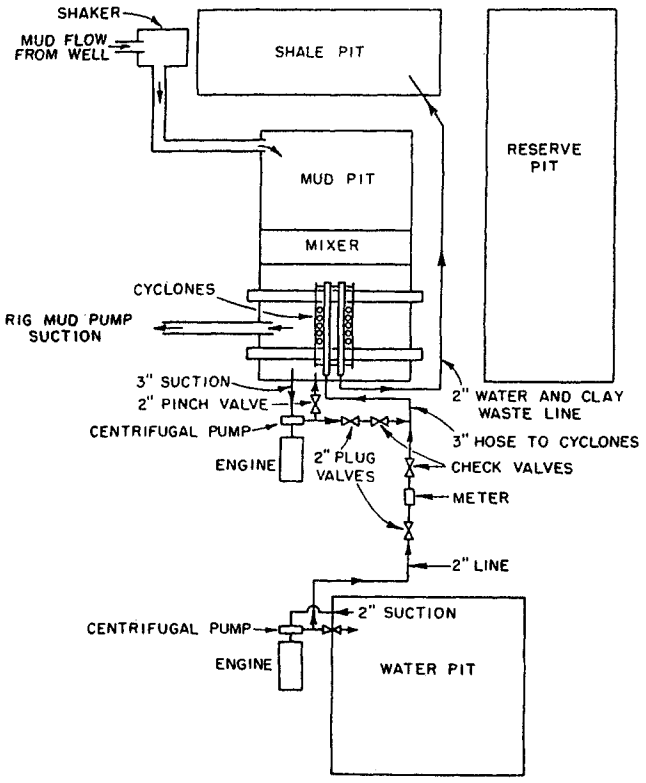

Fig. 9-15. Liquid-cyclone separator system. (*Scott and Lummers, 9-45. Courtesy Oil Gas J.*)

3-in. cyclones was used. Fluid is fed to the cyclones by means of two centrifugal pumps. In most applications, the mud is diluted with water in order to reduce the viscosity of the fluid passing through the cyclone.

Figure 9-16*a* shows diagrammatically a cross section of a cyclone (9-29). It consists of four elements: a central overflow for liquid and light-solids discharge, a sludge discharge, a conical gravitation section, and a cylindrical separation chamber, into which the feed enters tangentially. As the feed enters tangentially, the fluid acquires a vortex motion imparting a centrifugal force to the particles, which are thrown to the boundary where they then gravitate down along the stationary walls. Figure 9-16*b* shows the design of an actual test cyclone (9-33). Tables 9-2 and 9-3 illustrate the type of separation possible with unweighted and weighted muds (9-35). The weighted muds were diluted to 10.3 to 10.5 lb/gal prior to cyclone treatment. It is quite apparent that a 3-in. cyclone can remove from muds tonnage amounts of clay and barite per day.

Table 9-2. Separation of Clay or Drilled Solids from Unweighted Muds Using the 3-in. Cyclone

	Mud 1	Mud 2	Mud 3
Flow rate, gpm:			
Feed (at 120–125 psi)	27.3	26.3	26.7
Overflow	26.1	23.1	25.2
Sludge	1.2	3.2	1.5
Density, lb/gal:			
Feed	9.6	9.6	9.05
Overflow	9.45	9.2	8.75
Sludge	12.55	12.2	12.8
Solids content, wt %:			
Feed	21.5	21.5	12.0
Overflow	19.2	15.2	7.8
Sludge	55.5	51.6	57.0
Solids removed in sludge:			
Lb/lb in feed	0.15	0.37	0.38
Tons/day	6.03	14.4	7.8
Dilution savings, per cent	78	74	90

SOURCE: Bergman, Engle, Marvel, and Tek (9-35).

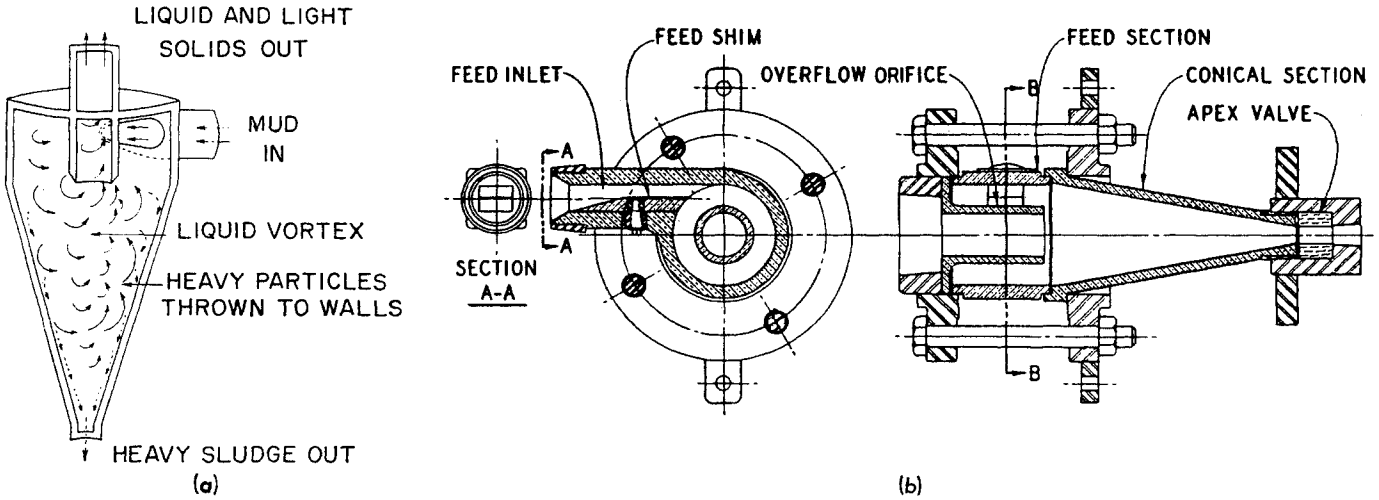

Fig. 9-16. Design of test cyclone. (*Bergman et al., 9-33; 9-29. Courtesy Oil Gas J.*)

Table 9-3. Recovery of Barite Using the 3-in. Cyclone

	Mud 1	Mud 2	Mud 3
Flow rates, gpm:			
Feed (at 125–150 psi)...	29.9	29.9	29.6
Overflow.....	27.3	25.0	22.6
Sludge.....	2.6	4.9	7.0
Density, lb/gal:			
Feed.....	10.3	10.3	10.5
Overflow.....	9.3	9.2	9.0
Sludge.....	21.5	16.3	17.9
Solids content, wt %:			
Feed.....	26.6	27.1	26.5
Overflow.....	15.3	14.0	10.8
Sludge.....	78.0	65.8	69.4
$BaSO_4$ content, wt %:			
Feed.....	58.1	58.5	91.5
Overflow.....	21.4	16.6	76.5
Sludge.....	90.4	85.0	97.8
$BaSO_4$ recovered:			
Lb/lb in feed.....	0.795	0.890	0.805
Tons/day.....	28	32	44

SOURCE: Bergman, Engle, Marvel, and Tek (9-35).

Air or Gas Drilling

The use of air or gas as the circulating fluid rather than mud, using the conventional rotary rig, has been successful under certain circumstances (9-8, 9-11, 9-17, 9-19). With air drilling, only a nominal fluid pressure is present on the formation being drilled. It is used advantageously when the formations being drilled do not slough or produce appreciable quantities of water. It is particularly applicable where the producing formations are susceptible to injury from drilling-fluid filtrate or particle penetration, where there is severe loss in circulation, and where drilling fluid is expensive or unavailable. Other advantages are longer bit life, higher penetration rates, and less tendency to contaminate cores and cuttings. The method has found particular application in San Juan gas field, N.M. (9-19).

Figure 9-17 shows a typical hookup used for air or gas drilling. As the air travels down the tubing and up the annulus, the fine particles travel up with the gas. The larger cuttings tumble in the rising air stream until they are ground to lifting size and are removed. This process is rapid enough so that there is little possibility of the cuttings sticking the pipe when circulation ceases. Figure 9-18 shows the relationship between gas velocity required to float a given-sized particle at a given gas density (9-19).

If a reduction of circulation occurs, the velocity in the annulus is reduced and the size of the cuttings carried out decreases as a result of the reduced velocity. The air velocities are such that particles

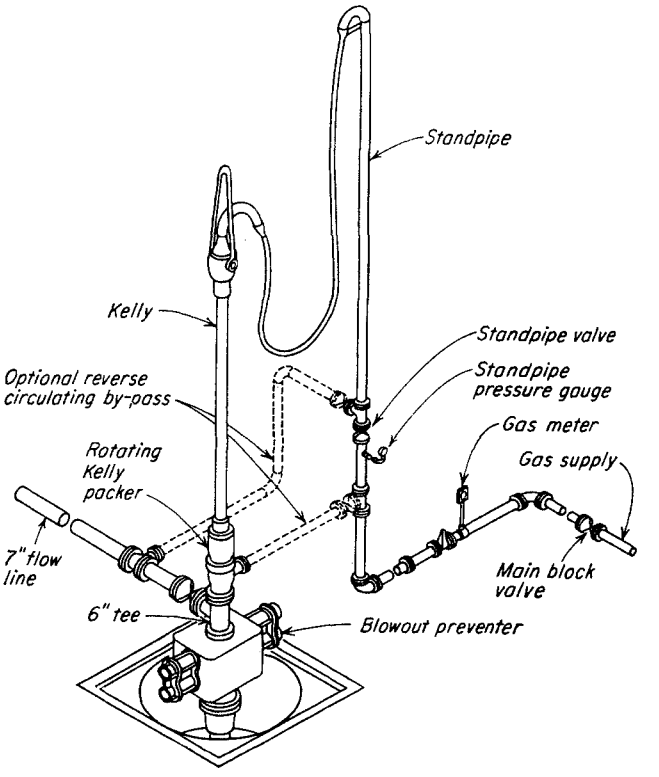

Fig. 9-17. Air drilling. (*Kirkpatrick*, 9-12. Courtesy Petrol. Engr.)

make their appearance at the surface within seconds after drilling starts. A sudden stoppage of dust during drilling indicates moisture in the hole. Reverse circulation of the air or gas is occasionally used because the higher velocities in the tubing will carry the cutting better than the annulus.

Drilling with Mud Aeration

In drilling with liquids, the most universally used remedial practice to prevent loss of circulation involves reduction of mud density and the addition of sealing agents to the drilling fluid. A recent development involves the injection of air or gas in a conventional mud to produce a low-density system. Like air or gas drilling, this system has the additional advantages of increased drilling rates and longer bit life. In addition, it has certain advantages over gas drilling, such as the elimination of fire and dust hazards and applicability to any type of formation —hard or soft, wet or dry—unlike gas drilling, which requires a dry condition. When necessary, the mud density can be rapidly increased to stop salt-water flow or to prevent blowout. In addition, the hole may be conditioned to withstand a higher-density mud, permitting full-depth logging and more successful cementing operations.

Figure 9-19 is a schematic diagram of an aerated-

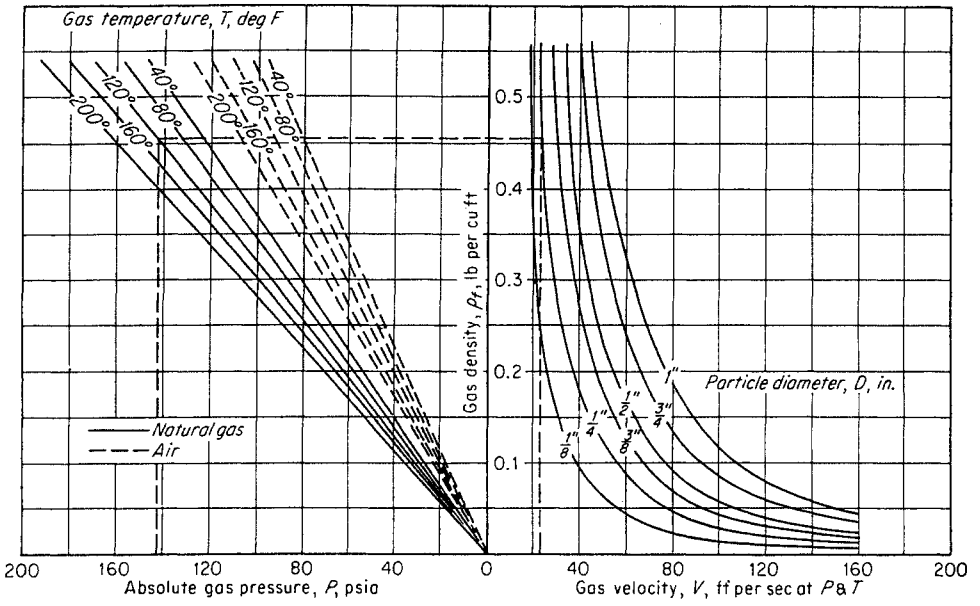

Fig. 9-18. Gas and air lifting capacity. (*Nicolson, 9-19. Courtesy Petrol. Engr.*)

mud system used in an actual test (9-32). The air is delivered from the compressor into the standpipe downstream from the mud pumps.

When oil or water is used as the drilling fluid, the minimum fluid density will be in the range of 7 to 8.3 lb/gal. This would correspond to pressure gradients of 0.37 to 0.43 psi per foot of depth. With air or gas drilling and with aerated-mud drilling, even much lower pressure gradients can be achieved. Figures 9-20 and 9-21 can be used to estimate the amount of air that may be injected into any mud to obtain the desired effective mud density at depths from 1,000 to 10,000 ft. For most wells the bottom-hole circulating temperature will not exceed 150°F at 10,000 ft, and the discharge temperature will be 10 to 25°F lower than the bottom-hole circulating temperature (9-44).

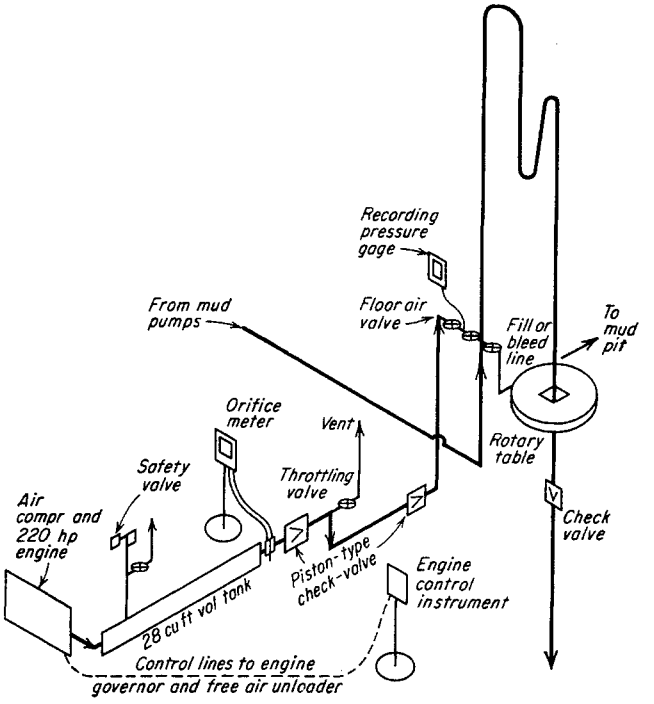

Fig. 9-19. Aerated-mud system. (*Bobo, Ormsby, and Hoch, 9-32. Courtesy Oil Gas J.*)

Drilling Rate

The rate at which a hole is drilled through a subsurface formation depends upon other factors: formation characteristics, bit design, weight on the bit, rotary speed, and drilling fluids employed. The physical properties of different formations make it necessary to design rock bits of different mechanical and metallurgical properties. Bits range from those designed for soft formations to those for extremely hard formations. Bits for soft formations usually have long, slender cutters faced far apart. The cones usually consist of a steel casting or forging with a carburized or tungsten carbide surface. Hard-formation bits are characterized by short, stubby cutters spaced close together. The bit is usually fabricated from a steel forging with the surface carburized with a small amount of tungsten carbide hard facing. Figure 9-8 shows some examples of bit types. The life of a bit is terminated when the cutters are so worn that the penetration rate is reduced below the economic limit or when the bit bearings become so worn that further drilling might result in the loss of a cone, which would lead to a subsequent fishing job. Formations are characterized as either hard or soft, with various degrees of abrasiveness. A rock with high compressive strength is classified as hard, one with

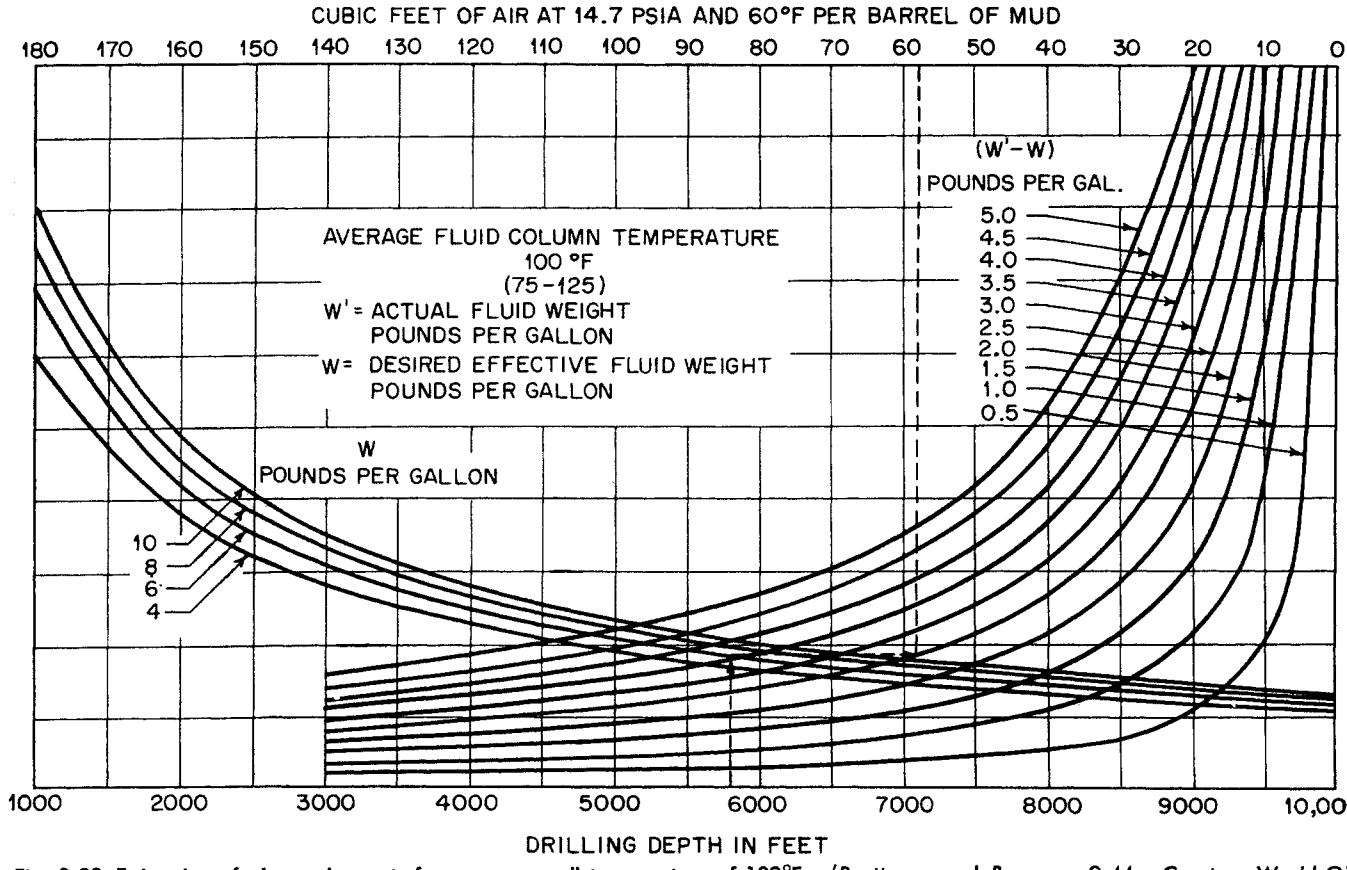

Fig. 9-20. Estimation of air requirements for average well temperature of 100°F. (*Poettmann and Bergman, 9-44. Courtesy World Oil.*)

relatively low compressive strength as soft. Rock abrasiveness is measured by the rapidity with which the bit cutters wear.

There are many factors that influence penetration rate, but two that are most easily varied are weight on the bit and rotary speed. Any generalization on the effect of these two variables assumes that all other variables remain constant. In general, increasing bit weight will always increase penetration rate, up to the weight at which the bit flounders. Crooked holes

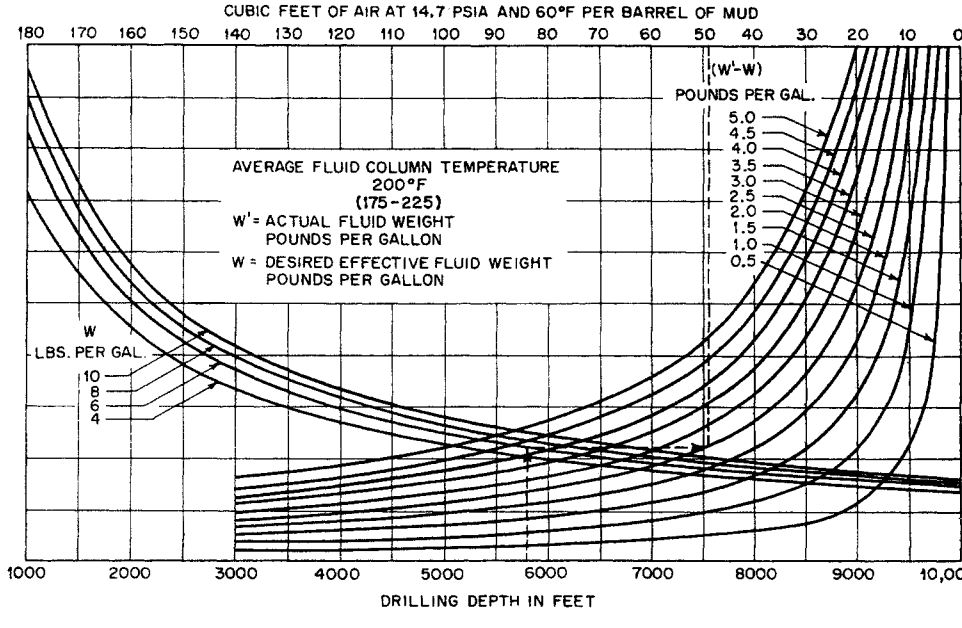

Fig. 9-21. Estimation of air requirements for average well temperature of 200°F. (*Poettmann and Bergman, 9-44. Courtesy World Oil.*)

often result from too much bit weight. One other limitation on bit weight is the size of the bit and the bearing area available to support the weight. Within the above limitations, on soft formations increased bit weight usually increases the rate of penetration in direct proportion to the weight on the bit. In hard formations, however, doubling bit weight quite often increases penetration rate from two to four times.

Increasing the rotary speed will increase the instantaneous penetration rate, everything else remaining constant. In soft formations, where high rotary speeds are usually employed, the rate of penetration varies with rotary rpm as 1 to 2; i.e., doubling speed increases the penetration rate by 50 per cent. In soft formations, rotary speeds as high as 300 rpm are used. As formations become harder, rotary speeds are usually reduced, resulting in increased bit and drill-collar life. In very hard formations, speeds greater than 100 rpm are generally avoided.

The drilling fluid employed greatly affects the penetration rate and the performance of the bit in both soft and hard formations. The primary function of the drilling fluid with respect to the performance of the bit is to remove cuttings from the hole as fast as they are formed and carry them to the surface. Therefore, the higher the circulation rate for a given fluid, the greater the penetration rate. This is why, under certain conditions, jet bits (Fig. 9-8) outperform conventional bits. Circulation rate, of course, is limited by the physical limitations of the equipment involved. The use of water and air as drilling fluids will always give better penetration rates and bit performance than mud. However, because of other drilling requirements, they cannot always be used. In general, better bit performance can be obtained by using fluids having the lowest possible densities. The greater the depth, the greater the effect of reduced pressure on bit performance. To summarize: improved bit performance and penetration rate can be obtained by holding the viscosity, yield value, density, and solids content of the drilling fluid as low as practically possible, within limitations dictated, of course, by other requirements. In addition, high circulation rates and/or the use of jet bits increase the rate at which the cuttings are removed from the bottom of the hole and thus improve bit performance.

Fig. 9-22. Three-blade, soft-formation core bit for wire-line core barrel. (*Courtesy Reed Roller Bit Company.*)

Coring

Coring is the operation of sampling the subsurface formation by cutting cylinders 1 to 4 in. in diameter (Fig. 2-2). Although the most complete coring programs sample an amount of formation that at best represents only one part in a million of the whole, the sample may be reasonably representative, since all the material making up the formation was exposed to a similar environment during its formation. The recovery and examination of a core is one of the most critical and important operations in the drilling of an exploratory well. The success or failure of a well may quite often be determined from core evidence. The data obtained from a core include (1) permeability, (2) porosity, (3) oil saturation (9-6), (4) water saturation, and (5) gas-oil, gas-water, and oil-water contacts. Choice of drilling fluids that will not diminish a formation's ability to produce oil may be made from core evidence.

The information listed above is used in establishing reserve estimates, in increasing the value of electric and radioactive logs by providing a basis for their quantitative or semiquantitative interpretation in uncored wells, and in determining feasibility of secondary recovery projects; it serves as a basis for more realistic unitization agreements, determining the completion practice to be followed; and it serves as

source material for research on new oil-recovery methods. The information obtained from cores is only part of the data necessary for the intelligent drilling, completion, production, and reserve estimation of a petroleum reservoir; however, it could mean the difference between efficient and inefficient production of a field.

There are two main types of core barrels and coring methods in use in drilling: the ordinary or conventional method, and the wire-line retrievable method (9-12, 9-21). Figures 9-22 and 9-23 show core bits for the two methods. In the ordinary method, the drill string has to be pulled in order to recover the core; in the wire-line retrievable method, the core can be recovered without pulling the drill string. The ordinary rotary core barrel consists of an outer rotating barrel and an inner stationary barrel. The core is held in place within the inner barrel by four clips of spring steel referred to as the "core catcher." It is important that the core catcher be in good condition for each run of the core barrel. When the core barrel is run to bottom, the driller will usually circulate mud for some time to flush out cuttings that may have fallen to bottom during the round trip in and out of the hole. Core recovery depends to a large extent upon the manner in which the driller proceeds. Weight on bit, rotary speed, pump pressure, and mud properties determine to a large degree the recoveries that can be expected. Loose sands, shale breaks, rapid changes in hardness, such as occur in limestones and dolomites, make core recovery difficult.

The wire-line retrievable method enjoys considerable popularity, since it allows selective intervals to be cored without removing the drill pipe. As the name indicates, the core barrel is recovered by means of a wire line.

When the core run is finished and the driller has brought the core barrel to the surface, the cores are usually washed and boxed and then sent to a laboratory for analysis. Core samples containing oil or gas saturation should be selected immediately, canned, and properly labeled. As a further precaution, the canned cores may be immediately frozen in dry ice. The importance of speed in properly sealing and freezing the sample cannot be overemphasized. The core not canned should be given a lithological description. Among the data recorded in describing a core are the nature of the rock, particle size, extent and type of porosity, degree of crystallization, estimated permeability, and oil and gas content.

In addition to the two methods of coring described, there are other methods. Side-wall cores are taken after a well has been drilled (9-12, 9-15) and chip coring is done with cable tools (9-13). Cores have been taken under pressure to determine the virgin content of the rock (9-18, 9-22).

Fig. 9-23. Hard-formation cutterhead. (*Courtesy Hughes Tool Company.*)

Cementing the Casing in Wells

When the drilling has been completed, the mud is circulated to clean the hole and the drill pipe is removed. Casing is lowered into the well, a joint at a time, and, when in place, is cemented to seal the annulus between the casing and the drill hole. The cement seals off horizons productive of petroleum or of water. The casing may be cemented immediately above the oil or gas-bearing formation (open-hole completion) or it may be set through the producing formation (cased completion). In the latter instance, holes are shot through the casing and column of hardened cement to permit the flow of oil or gas into the well bore.

In cementing the casing, it is important that the bond between the formation and the cement be such that no communications between the upper formations exist. When such flow or communication occurs, it is usually caused by channeling of the cement

when it is pumped into place. Channeling can occur because the mud cake on the walls of the formation has not been properly washed off. Quite often the casing is equipped with "scratchers," which are scrapers or wires protruding from the surface of the casing. When the casing is lowered into the well, it is rotated or reciprocated so that the scratchers remove the mud from the formation at those points where a good bond between the formation and the cement is necessary.

When a primary cement job is unsatisfactory, it is necessary to do what is called a "squeeze-cementing" job. In this operation, the cement slurry is forced through perforations in the casing at the point where the previous cement job failed, in order to effect the proper seal.

The procedure of cementing a casing into a well consists of several steps. Briefly, the casing is lowered into the mud-filled hole to within a short distance of the bottom. The mud is circulated down through the casing and up along the walls of the hole in order to remove scrapings. After a period of time, water or salt solution is usually pumped on top of the mud column. In subsequent operations, this water or salt solution washes the mud from the formation and also minimizes contamination of the cement slurry with mud and mud chemicals. A "plug" is then placed on top of the water or salt solution, and the amount of cement slurry calculated to fill the annulus between the formation and casing is pumped in on top of the plug. This bottom plug is so designed that, when it reaches bottom and the pressure increases, the center portion will shear out and allow the cement to pass through. Another plug is placed on top of the cement-slurry column, and mud is usually pumped on top of it until the cement slurry has been forced into the annulus. The cement is then allowed to harden sufficiently so that drilling can be resumed or so as to allow perforating.

An oil-well cement must meet two basic criteria.

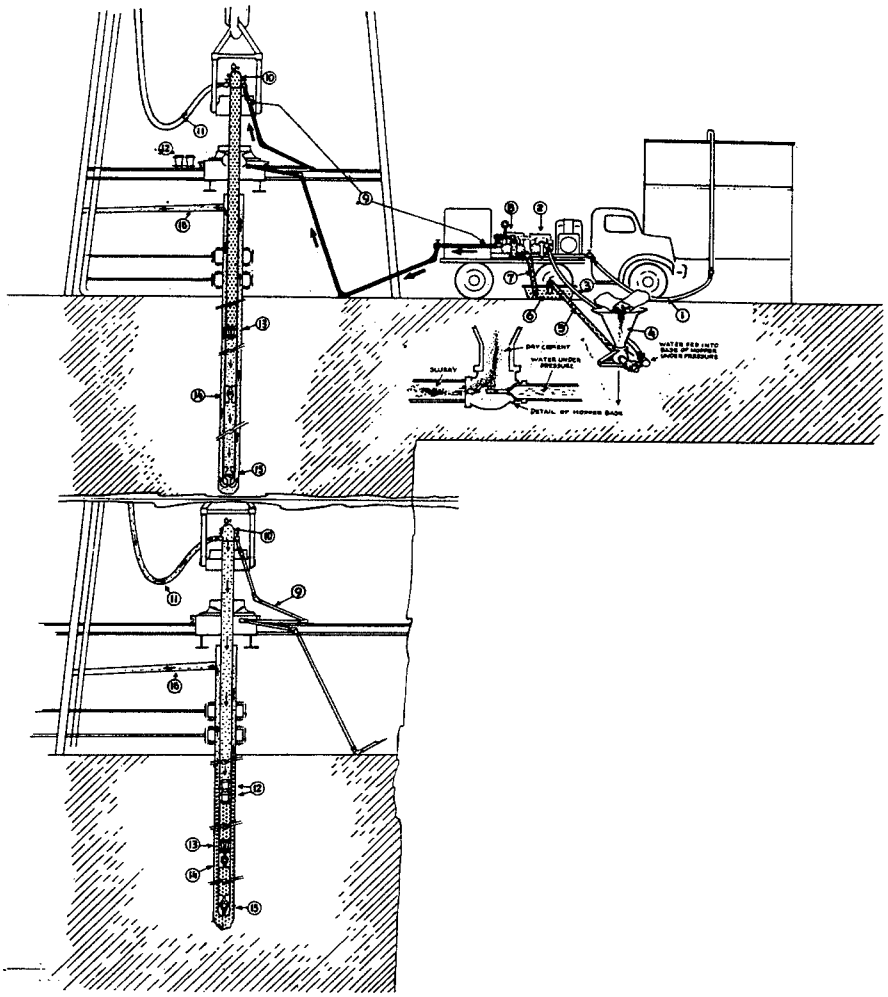

Fig. 9-24. Cementing operation. (*Courtesy Ohio Oil Company.*)

It must remain in a pumpable or fluid condition long enough to be pumped into place. It must remain in this condition when subject to pressures from atmospheric up to 20,000 psi and at temperatures ranging from atmospheric up to 300 or 400°F. Secondly, once in place it must harden or set rapidly after the desired period of fluidity is passed. The total cementing time, therefore, is the sum of the time required to mix the cement slurry and the time required to pump the slurry into final position.

Figure 9-24 depicts the key equipment and steps in a cementing operation. The cementing operation of a well, like many of the other operations of completing a well, is usually performed by a cementing service company. All equipment for the operation is provided by the company; this includes large trucks on which are mounted engines, pumps, tanks, and other equipment. The cementing service company also provides cementing lines, mixing hoppers, and calibrated devices for measuring the components going into the cement slurry. The operation, as indicated in Fig. 9-24, is as follows. The water feed line (1) takes water from the tank through the pump (2). The water is discharged from the pump (2) at high pressure through an orifice in the bottom of the cement hopper (4, see insert). Dry cement enters the hopper and is caught in the jet of water to form a slurry. The slurry then moves downline (5) into the tank (6). From the tank (6) the slurry moves through line (7) into the suction side of the pump (8). From the pump (8) the slurry moves through line (9) to the cementing head (10) on the derrick floor. The rotary hose is line (11). Top cementing plugs (12) and the bottom cementing plug (13), which is being pumped ahead of the slurry, are shown. As the slurry moves down the casing, the mud is displaced up the annulus between the casing and the formation; (14) and (15) are the float collar and guide shoe, respectively, and are used to control the placing (landing) of the casing (Fig. 9-25). The guide shoe acts to prevent the casing from hanging on the side of the well as it is being lowered. The float collar is a back-pressure valve which permits a floating action, thus taking off much of the load on the derrick while the casing is being run. It also prevents the backflow of cement and acts as a stop for the cement plugs. The mud-flow line is (16).

As stated previously, while the cement is being pumped into place the driller rotates and works the casing up and down in the well to prevent channeling of the cement.

After the correct amount of cement is placed in the well, the pumps are stopped, the valve on the cementing line is closed, the cementing head (10) is broken, and the top plug or plugs are placed in the casing on top of the column of cement. The head is made up, and mud is pumped on top of the plugs, forcing the plugs (12) down the casing as shown in the lower part of Fig. 9-24. The cement is forced through the bottom plug (13), through the float collar and shoe (14 and 15), and up the annulus. When the top plugs (12) "bump" the bottom plug, as indicated on the mud-line pressure gauge, pumping is stopped. The valve on the cementing head is closed. Operations are then shut down for 24 to 72 hr until the cement has set. Quite often the entire length of casing is cemented, so that cement returns follow the mud out of the flow line (16).

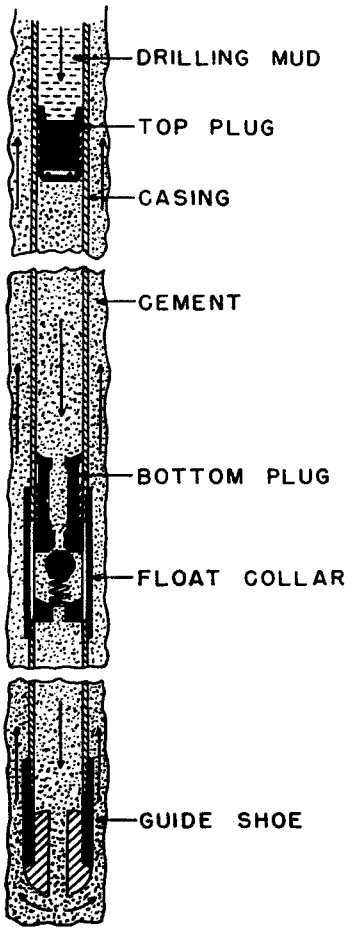

Fig. 9-25. Float collar and guide shoe in place for cementing wells. (*Anderson*, 9-28.)

After the cement has set, the plugs, float collar, float shoe, and the cement in the bottom joint of the casing and in the hole are drilled out. Drilling is then continued or the well completed.

In the case of deep wells, as many as two and three trucks (Fig. 9-26) are employed to pump the cement in place in the allowed time.

The cement used in cementing oil and gas wells is

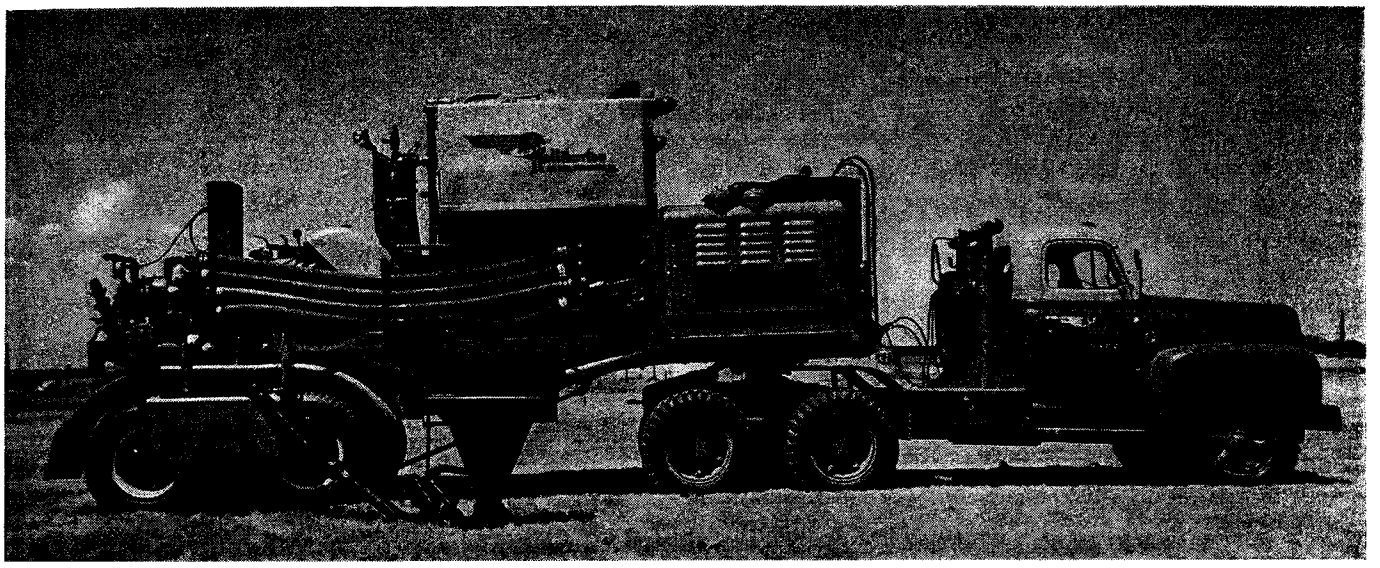

Fig. 9-26. Truck for cementing wells. (*Courtesy Halliburton Oil Well Cementing Company.*)

ordinary portland cement. However, because of the special conditions under which the cementing operation takes place and the requirements imposed by the pressure, temperature, and physical characteristics of the formation, many special additives with portland cement have been developed to meet these requirements. Additives to retard the set of cement so that they may be placed in deep wells have been developed. Low-water-loss additives to prevent flash setting are another recent development. In cementing deep wells, it is quite often impossible to impose the entire weight of a column of cement on the formation for fear of fracturing. In order to prevent fracturing, the cement is placed in stages. Another recent advance in cement technology has been the development of very-light-weight cements that do away with stage cementing operations in deep wells.

Table 9-4 shows the hydrostatic pressure for cement slurries of different densities at various depths.

Table 9-4. Hydrostatic Pressure of Fluids at Various Depths

Depth, ft	Pressure for fluid indicated, psi				
	Water, lb/gal	Drill mud or cement slurry, lb/gal			
	8.33	11.0	13.0	15.0	17.0
1,000	433	572	676	780	884
5,000	2,165	2,860	3,380	3,900	4,420
10,000	4,330	5,720	6,760	7,800	8,840
15,000	6,495	8,580	10,140	11,700	13,260
20,000	8,660	11,440	13,520	15,600	17,680

Table 9-5 shows both the circulating and the static temperatures of oil wells for various flow rates and depths. As discussed above, this information is necessary in designing a cementing operation.

Cements for oil and gas wells can be generally classified into three categories, as follows (9-28):

1. ASTM type I. Common portland cement used to 6,000 ft. By using an additive to retard the set, its use range may be extended to 14,000 ft.
2. ASTM type III. High-early-strength cement. Usually obtained by modifying the composition by increasing the $3CaO \cdot SiO_2$ content and by finer grinding.
3. Special oil-well cements.
   a. Retarded-set cements. The set of the cement may be retarded by modifying the clinker composition or by use of a chemical additive. These

Table 9-5. Temperature Data on Drilling Wells*

Well	Circulation rate, gpm	Depth of well, ft	Mud-circulating temperature, °F		Bottom-hole temperature, °F	
			Suction	Discharge	Circulating	Static
1	426	5,310	96	105	109.5	136
2	175	8,150	110	115	122.0	195
2	365	8,150	114	116	121.5	195
3	507	8,300	117	121	127.5	215
4	405	9,923	117	121	137.0	192
5	408	10,924	128	133	156.0	244

* R. Floyd Farris, "A Practical Evaluation of Cements for Oil Wells," American Petroleum Institute, Division of Production, November, 1941.

cements can be used to depths of 16,000 ft or more.

b. Sulfate-resisting cements. The composition of these cements has been altered to resist the disintegrating action of sulfate waters.

c. Low-water-loss cements. Cements contain additives to reduce water loss and, thus, to prevent possible flash setting of the cement.

d. Low-density cements. The ideal cement-slurry density is equal to the density of the drilling mud. By use of admixtures with such materials as bentonite, pozzolanic materials, and diatomaceous earth, low densities can be achieved.

e. Pozzolan cements. Pozzolans are reactive silicas which, when mixed with cement, impart special properties, such as resistance to high-sulfate waters.

Table 9-6 shows the effect of temperature and pressure on the time of initial set and compressive strength of a 50 per cent slurry (100 parts cement, 50 parts water) or portland cement type I. Elevated pressure decreases the setting time and increases strength. Increased temperature accelerates the set but also decreases the strength.

Slow-set or retarded cements, as stated previously, are obtained either by modifying the chemical composition of the cement or by the use of an additive. In modifying the chemical composition of the cement, the "ratio of Al_2O_3 to Fe_2O_3 is such that, theoretically, the $3CaO \cdot Al_2O_3$ content of the cement would be zero and the Fe_2O_3 content would be somewhat in excess of that required to convert all of the Al_2O_3 to $4CaO \cdot Al_2O_3 \cdot Fe_2O_3$" (9-39). The other method is to add materials that will retard the rate of reaction of the cement minerals with water. These retarders usually fall into one of three categories: (1) starches or celluloses, (2) sugars, and (3) acids or salts containing one or more hydroxyl groups. Carboxymethyl hydroxyethyl cellulose (CMHEC) is an example of a cellulose; glucose is an example of sugar; and the calcium salt lignin-sulfonic acid is an acid used as a retarder. CMHEC also has the property of being an excellent water-loss control agent when used in cements in concentrations from 1 to 2 per cent.

Contaminants, from drilling muds and other sources, have considerable effect on the thickening time of cements. In general, the inorganic salts, such as sodium chloride, decrease the pumpable time whereas the organic materials, such as quebracho, increase the pumpable time. Table 9-7 shows the effect of sodium chloride on the thickening time of a retarded cement. A few per cent of calcium chloride is often used to accelerate the set of a cement if this is desired.

One of the most recent developments has been a low-water-loss, low-density cement (9-28). Slurry densities as slow as 10.5 lb/gal have been achieved, matching that of the drilling muds used. To obtain this low water loss and low density, two special additives are used, CMHEC and a special grade of diatomaceous earth. The diatomaceous earth permits the use of a high percentage of water in the cement, thus resulting in the low densities.

Table 9-6. Effect of Temperature and Pressure on Time of Initial Set and Compressive Strength with a 50 Per Cent Slurry of Portland Cement*

Temperature, °F	Atmospheric results		Hydraulic results		
	Time for initial set, min	Compressive strength at 72 hr, psi	Autoclave pressure gauge, psi	Time for initial set, min	Compressive strength at 72 hr, psi
130	98	.....	500	87	
180	63	2,240	2,000	54	3,950
180	63	.....	4,000	53	3,900
205	56	405	2,000	43	3,780
250	...	.....	2,000	29	3,815
275	...	.....	2,000	...	2,680
300	...	.....	2,000	...	765
325	...	.....	2,000	...	760

* Data by Craft, Johnson, and Kirkpatrick, *Trans. AIME*, **114**: 68 (1935).

SOURCE: (9-39).

Acidization

The treatment of wells with acid to increase the productivity of the wells had its beginning in 1896 when a patent was issued to Frash (9-55) for a method of treating a well with hydrochloric acid. However, this

Table 9-7. Data Showing Effect of Sodium Chloride on Thickening Time of Retarded Oil-well Cement

Well depth, ft	Thickening time in Stanolind pressure thickening-time tester for concentration of NaCl indicated, ppm									
	None		5,000		20,000		100,000		300,000	
	hr	min	hr	min	hr	min	hr	min	hr	min
8,000	3	19	2	42	2	08	1	58	5	36
10,000	2	56	2	04	1	27	1	24	3	57
12,000	2	18	1	53	1	12	1	09	2	37
14,000	2	04	1	49	1	10	1	01	2	10

SOURCE: Hansen (9-39).

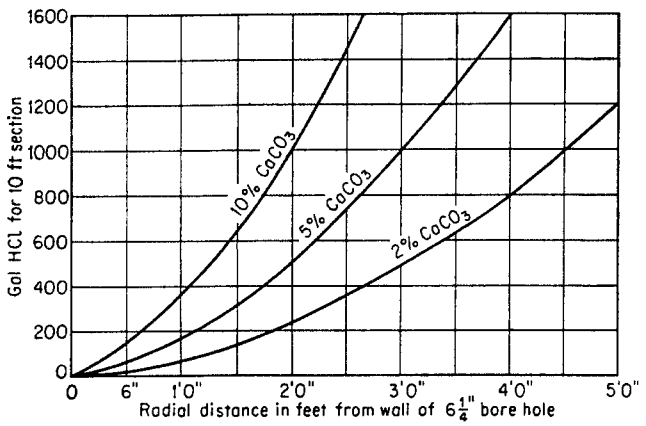

Fig. 9-26a. Curves showing amount of 15 per cent hydrochloric acid required to remove varying amounts of calcium carbonate for a formation 10 ft thick. (*Lehnhard, 9-62. Courtesy Petrol. Engr.*)

method did not become popular because there was no way to prevent excessive corrosion of the steel equipment by the acid. In 1932, thirty-six years after the Frash patent was issued, a patent was issued to Grebe and Sanford (9-56), outlining the use of corrosion inhibitors in acids for oil- and gas-well treating. Since that time, numerous inhibitors, as well as other special-purpose additives, have been developed and have markedly extended the value and usefulness of acid treating.

The object of acidizing an oil or gas well is to increase the permeability around the well bore and thus increase the rate of production or recovery of oil and gas, and to increase the ultimate recovery by increasing the economic life of the well. Of course, treating a well with acid does not mean that the above objectives will always be met.

In evaluating the possibilities of success in acid-treating a well, certain information on the rock characteristics is required, such as type of formation, porosity, permeability, stratigraphy, and structural characteristics. Other factors of importance are formation pressure, temperature, oil and water saturation, interfacial and wetting characteristics, and dissolved-gas content. If cores are available, it is desirable to run laboratory tests in order to determine optimum acid formulations. Any formation that is moderately soluble in acid should undergo an improvement in permeability leading to increased production capacity. However, it does not necessarily follow that production will improve if the formation is treated with acid. Solubility data are essential information, since such data permit one to predict when an acid treatment will be successful.

The velocity of the chemical reaction that occurs during the acid treatment is important, since this determines to a large degree the rate at which the acid should be pumped into the formation. In the case of fast-reacting limestones, for example, unless the solution is pumped rapidly, the acid will spend itself ineffectually by simply enlarging the well bore. Quite often, in the case of sandstone formations, the solubility is too low to make reaction rate of any significance. Most acid treatments are made using 15 per cent hydrochloric acid. This selection results from several factors. Commercial acid contains about 30 per cent hydrochloric acid, so a simple 1:1 dilution is all that is required. Higher concentrations lead to difficulty in cleaning up a well because the viscosity of the spent acid with its dissolved salts and suspended material is high. Higher concentrations require too high injection rates to prevent the acid from becoming spent before it has a chance to penetrate back into the formation. Concentrations lower than 15 per cent may dissolve too little of the formation. Figure 9-26*a* shows the amount of 15 per cent hydrochloric acid required to remove varying amounts of calcium carbonate from a formation 10 ft thick (9-62).

Another acid that is used quite often is called "mud acid." This is a mixture of 15 per cent hydrochloric, 3 to 6 per cent of a fluoride, plus some wetting and surface-tension-reducing agents; it is used primarily, as its name implies, to attack and dissolve clay particles around the well bore which have resulted from the drilling mud or which are originally present in the formation. Table 9-8 shows the solubility of a typical Gulf Coast producing formation in mud acids and in 15 per cent hydrochloric acid, and Table 9-9 shows the effect of mud acid on the permeability of mud cakes (9-62). One gallon of mud acid dissolves 0.33 lb of bentonite.

In addition to the regular hydrochloric acid and mud acid, a wide variety of less frequently used, special-purpose acids are occasionally recommended by the service companies: acids, such as the highly viscous hydrochloric acid solution "penetrating acid," which have surface-tension reducers in them, and acids containing tracers so that the acid movement can be followed.

Before a well is acidized, as much data as possible on the well should be collected. In addition to bottom-hole temperature and pressure, formation solubility, formation composition, mud type, and fluid loss, other information should be available, such as formation thickness, permeability, oil and gas saturation, oil, gas, and water level, and method used in completing the well. It is informative to have a decline curve on the well before and after treatment,

Table 9-8. Solubility of Producing Formation in 15 Per Cent HCl and Mud Acid

Pool	Area	Formation	Depth, ft	Average solubility, %	
				Mud acid	15% HCl
Alice	Texas Gulf Coast	.....	5,150	51	17
Bexar County	Southwest Texas	.....	963	66	17
Carrizo	Texas Gulf Coast	.....	.....	17	2
High Island	Texas Gulf Coast	Miocene	4,680–5,440	32–60	2–10
Luby	Texas Gulf Coast	Oakville	5,612–5,632	30–60	0–9
Agua Dulce	Texas Gulf Coast	Catahoula	4,735–4,765	43	30
			6,360–6,390	41–60	14–46
			5,485–5,500	53–61	8–12
Angleton	Texas Gulf Coast	Frio	9,900–10,490	.....	Less than 2
Ganado	Texas Gulf Coast	Frio	5,069–5,108	23–33	2–3
Esperson Dome	Texas Gulf Coast	Cockfield	7,025	20	2
			8,500	22–42	3–5
Joes Lake	Texas Gulf Coast	Wilcox	7,686	15	1
Loma Novia	Texas Gulf Coast	Government Wells	2,720–2,850	20–60	2–7
Manvel	Texas Gulf Coast	Marginulina	5,355–5,389	23–42	2–4
Louise	Texas Gulf Coast	Frio	5,150	22	4
Nueces County	Texas Gulf Coast	Frio	5,300–5,323	45–50	9–24
N. Sweden	Texas Gulf Coast	Jackson	4,750–4,790	50	16–30
Old Ocean	Texas Gulf Coast	Frio	10,065–10,092	45	34
				25	1
Placedo	Texas Gulf Coast	Frio	4,747–4,765	24	4
Rowan	Texas Gulf Coast	Frio	8,600–9,220	.....	2–7
Rincon	Texas Gulf Coast	.....	3,809–3,927	60	24
Segno	Texas Gulf Coast	Wilcox	8,030–8,090	35–40	4–13
Starr County	Texas Gulf Coast	.....	1,930	63	24
Turkey Creek	Texas Gulf Coast	Frio	5,860	50	
White Creek	Texas Gulf Coast	Government Wells	1,500	45	1
Black Bayou	La. Gulf Coast	Miocene	4,326–4,402	24–55	3–17
Charenton	La. Gulf Coast	Miocene	950	44	4
Eola	La. Gulf Coast	Sparta	5,887–6,010	20–65	5
		Wilcox	8,500–8,600	16–25	2–8
Golden Meadow	La. Gulf Coast	Miocene	5,300	24	1
Ville Platte	La. Gulf Coast	Haas	8,832–8,837	21	2
		Taite	9,088–9,097	23	1
		Wilcox	9,900–10,300	22–35	3–5
Long Lake	North Texas	Woodbine	5,294–5,304	30	3
East Texas	East Texas	Woodbine	3,600	8–45	1–28
Hawkins	East Texas	Woodbine	4,419–4,425	15–25	5
Tinsley	Mississippi	Eutaw	4,931–4,967	20–27	12–27

SOURCE: Lehnhard (9-62).

in order to assess the success or failure of the job.

The mechanics of treating wells varies widely. However, there are a few common methods that will be described. The Carr method (9-49) was used shortly after acidization became routine as the result of the use of inhibitors. It consisted in (1) filling the casing and tubing with oil and closing the casing valve, (2) filling the tubing with acid while bleeding off the oil through the casing valve, and (3) pumping oil into the tubing valve and displacing acid into the formation. The sequence of action is shown in Fig. 9-27. The Carr method has certain shortcomings, such as not being sufficiently selective, and the possibility, in uncased holes, of losing both oil and acid in upper barren formations.

Another method is to treat under a packer (1-20). In this method a packer is seated in the annulus between the casing and the tubing to confine the acid to the zone to be treated. Quite often the pressure on top of the packer is sufficient to keep it in position but, in cases where the acid is being injected under high pressure, a second pump is used to exert pressure on the oil above the packer to prevent it from becoming unseated.

Where the formation to be acidized consists of several zones of different permeability, in order to prevent

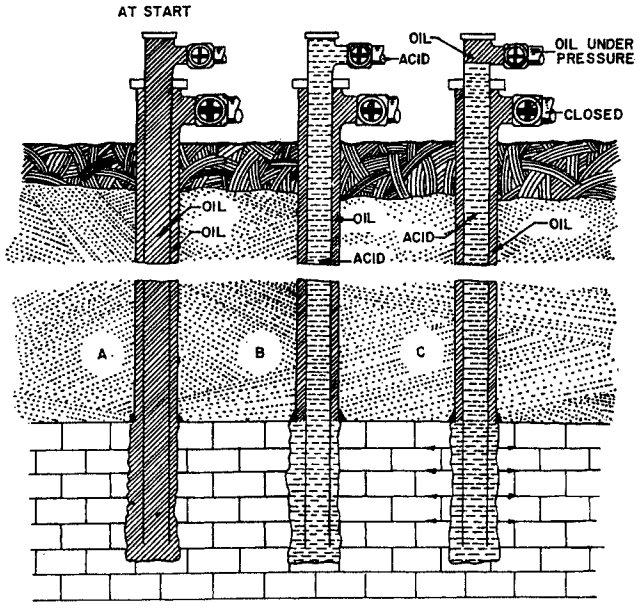

Fig. 9-27. The Carr method of acid treatment. (9-49.)

the acid from penetrating only the zone of greatest permeability to the detriment of the tighter zone, which should be treated, a viscous gel is used to block the most permeable zone. The acid is forced into the tighter zones, and then the gel is broken to allow the entire formation to produce.

One important point to consider in preparing for an acidization job is the volume of acid necessary to accomplish the purpose. The amount used depends upon formation thickness, solubility, permeability, and the distance to which the penetration is desired; it can vary from 100 to as high as 50,000 gal. Quite often the treatment is in stages. The volume is increased in each successive stage, the acid being forced farther and farther back into the formation. For a given volume of acid, stage treatment possesses certain advantages, for it allows any solids loosened by the treatment to be flushed out before very large quantities can settle out and cause plugging and, secondly, production tests are made after each stage to ascertain the need for further stages. In this way, optimum volume is determined.

As stated previously, pumping rate is important, and, in most cases, the treatment consists of injecting and removing the acid as rapidly as possible. In some cases, formation pressure is high enough to eject the spent acid, but in others swabbing is necessary.

In the case of new wells, routine acidization as a completion practice has been the general trend, for several reasons. The allowable production from a well is frequently based on production capacity on completion, wells clean up easily after acidization when pressure is high, and wells that have been invaded by mud produce to full capacity faster when acidized.

Fracturing

A new method of stimulating the production of wells has been developed since 1949, starting with the paper by Clark (9-51) on fracturing (9-48, 9-52 to 9-54, 9-57 to 9-58a, 9-60, 9-67). It has been known, since the days of water injection during water flood, that injection rates would rise sharply at some level of water pressure. Yuster and Calhoun (9-67a) report that the pressures for "formation parting" on a group of wells occur at about 1 psi per foot of depth, with two wells exhibiting the phenomenon at 0.5 psi per foot of depth. The stimulation by fracturing consists of forming partings in the formation by liquid injection along with the addition of sand or other foreign material to hold the partings open. Upon relief of fluid injection, the permeability of the formation may be increased several times.

The key to fracturing is the rate and quantity of fluid injection with the attendant pressure rise in the well bore to cause the fractures. As much as 250,000 gal of water with 200,000 lb of sand has been used on one well. Rates up to 50 bbl/min of liquid are used.

Theories and concepts on the nature of fracturing vary (9-67, 9-58a). Hubbert and Willis state that fractures produced should be approximately perpendicular to the axis of least stress. They believe that, when pressure reaches overburden, the fracture is likely to be horizontal (9-58a).

There are many trade names and procedures for stimulating the production of wells, including the use of acids (9-47).

Completion and Testing of Wells

The drilling and completion of wells can be covered here only briefly. Such operations as directional drilling (9-9, 1-26), whereby a well can be sidetracked and completed a considerable horizontal distance from the surface operations, will not be described. This type of operation is necessary in killing wild wells or in offshore operations from a drilling platform (9-3).

When wells are cased through the producing horizon, the casing is perforated with bullets to allow the fluid to enter the well bore; this is called "gun perforating" (9-4). This method of completing wells permits the opening to production of narrow zones. It also makes it possible to close off one zone with cement before opening a new zone.

Screens or slotted pipes are used to prevent sand flow when open-hole completions are used (9-5).

When sand is loose, gravel packs (9-26) or treatments with plastics are used to prevent sand from coming into wells. The pressure losses occurring with such processes have been studied (9-14, 9-16).

Wells are completed as "dual completions" with the deeper formation open to the tubing and a shallower formation open to the annulus (9-25, 9-27). Figure 9-27*a* shows a wellhead for a dually completed well. Permanent-type well completions permit wells to be perforated and reworked through tubing (9-10).

Once a well is opened to the producing horizon, it is often tubed and allowed to flow the mud and water to a pit and give a test flow of oil and gas. For some wells, it may be necessary to circulate water to clean the mud from the hole or to lower the pressure on the formation by swabbing water from the tubing or casing. Oil wells are often reported as making a given number of barrels of oil per day when flowing through a given-sized choke. Gas wells are usually tested and their flow rates reported.

Testing of Wells. One important test is made in drilling wells before the last casing is set: drill-stem testing (9-80, 1-20). A tool is placed on the bottom of the drill pipe and the pipe is lowered into the hole full of mud. A cushion of 1,000 to 2,000 ft of water may be placed in the bottom of the drill pipe. By manipulating the drill pipe, the tool seals off the mud column in the annulus and opens the formation at the bottom of the hole to the inside of the drill pipe. High-pressure oil and gas will issue from the porous rock and produce through the drill stem, establishing beyond all doubt that oil and gas are present. When salt water fills the zone, the drill pipe will fill with water, showing the absence of oil and gas in commercial quantities. Pressure gauges are installed in the drill-stem tool to show the pressure rise in the bottom of the hole when the tool closes off the flow at the conclusion of the test.

For a gas well, pressures and temperatures in the reservoir are needed to give the reserve of gas per unit of reservoir space. The temperature is measured with a recording gauge (9-77, 9-78) or with maximum thermometers placed in a pressure gauge. Precautions must be taken relative to effects of cement setting and mud circulation on deviations of the temperature gradient from that of the normal earth gradient (Fig. 1-31).

Pressures are taken at the wellhead with deadweight testers, and reservoir pressures are computed as discussed in Chap. 7. Subsurface pressure gauges are often employed to obtain both static and flowing bottom-hole pressures (9-69, 9-70, 9-73, 9-79, 9-82 to 9-84). Figure 9-28 shows the pressure chart for a typical run into a well bore, with *A* representing the base line; *B*, the tubing head; *C* and *D*, intermediate stops; and *E*, the bottom-hole pressure. The modulus, or psi per inch of pen movement on the chart, is found by calibration at known temperatures. Smith and Dewees show the results of repeated calibrations under carefully controlled conditions (Table 9-10).

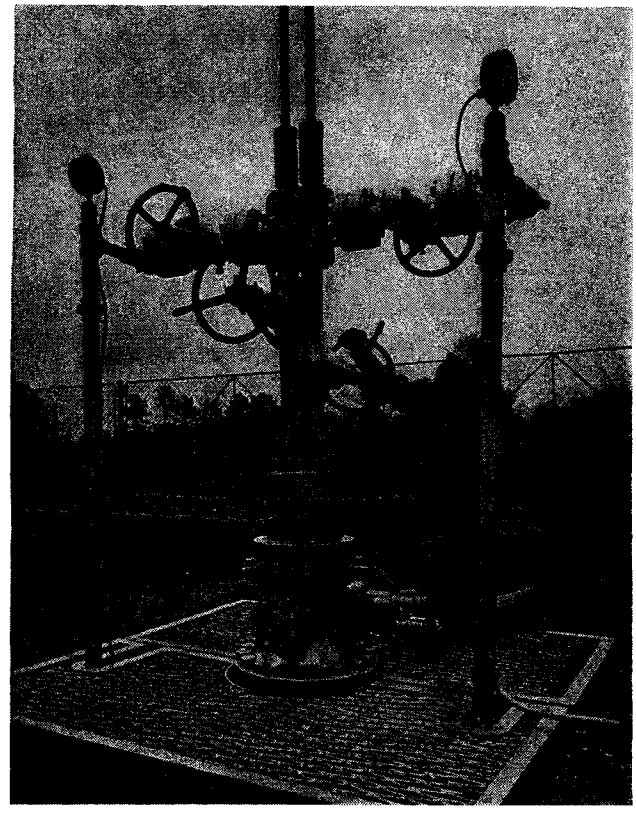

Fig. 9-27*a*. Wellhead for a dual completion. (*Courtesy National Supply Company.*)

Temperature surveys are made to detect casing leaks on gas wells (9-77) and flows between zones behind the casing. The flowing and expanding gas is likely to create an anomaly in the temperature gradient.

Gas-condensate wells are flowed into separators to obtain the gas-liquid ratio. Sometimes, small-scale

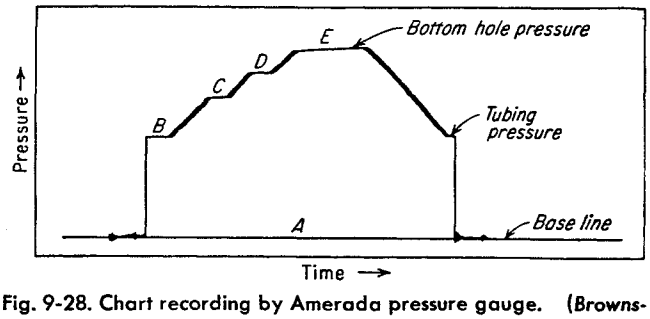

Fig. 9-28. Chart recording by Amerada pressure gauge. (*Brownscombe and Conlon, 9-70. Courtesy AIME.*)

Table 9-9. Effect of Mud Acid on the Permeability of Mud Cakes

Mud no.	Pool	County and state	Water flow through mud cake, cu cm/min		Per cent increase in flow rate or permeability by mud acid treatment
			Before mud acid	After mud acid	
1	English Bayou	Calcasieu, La.	0.466	3.67	690
2	University	Baton Rouge, La.	1.460	46.0	3,100
3	Port Barre	St. Landry, La.	1.130	44.0	3,800
4	Port Barre	St. Landry, La.	1.55	80.0	5,000
5	Jennings	Arcadia, La.	1.00	8.7	770
6	Eola	Avoyelles, La.	0.40	13.35	3,250
7	Tepatate	Acadia, La.	1.00	166.6	16,500
8	Ainse La Butte	Lafayette, La.	1.07	125.0	12,400
9	Paradise	St. Charles, La.	0.333	85.0	2,450
10	Wildcat	St. Marys, La.	0.67	150.0	22,500
11	Wildcat	La Fourche, La.	0.05	Infinity*	Infinity*
12	Stark	Calcasieu, La.	1.67	250.0	15,000

* Mud cake disintegrated after treatment.

sampling cells are used to process a small stream taken from the full-scale stream, as shown in Fig. 9-29 (9-68, 9-72, 9-74, 9-76).

The rate of withdrawing the small-scale sample influences the measurement of liquid content, as shown in Fig. 9-30. It appears that slowing down the sampling rate permits more droplets of liquid from the main stream to enter the sampling tip than would ordinarily accompany the gas, and high rates of sampling bring only more gas. At low flow rates from the well, the small-scale sampling may be unsuccessful because of unknown phase distribution in the flow system. When using the conditions shown in Table 9-11 and a velocity in the tip of 94 per cent of the velocity in the main flow stream, reliable small-scale samples can be obtained by using the following procedure (9-76):

The agreement among all of the tests run either in well tubings, or at Katy, or at Erath indicate that the methods used will give identical results in different equipment of different sizes provided the following procedure is used.

1. Straight-pipe sampling section
   a. Length 60 diameters or more.
   b. Inside diameter must be known and the tubing should be clean, smooth, and straight.
   c. The recommended minimum flow rate per inch of pipe diameter and the corresponding maximum pipe diameter per million cubic feet of flow rate are given below:

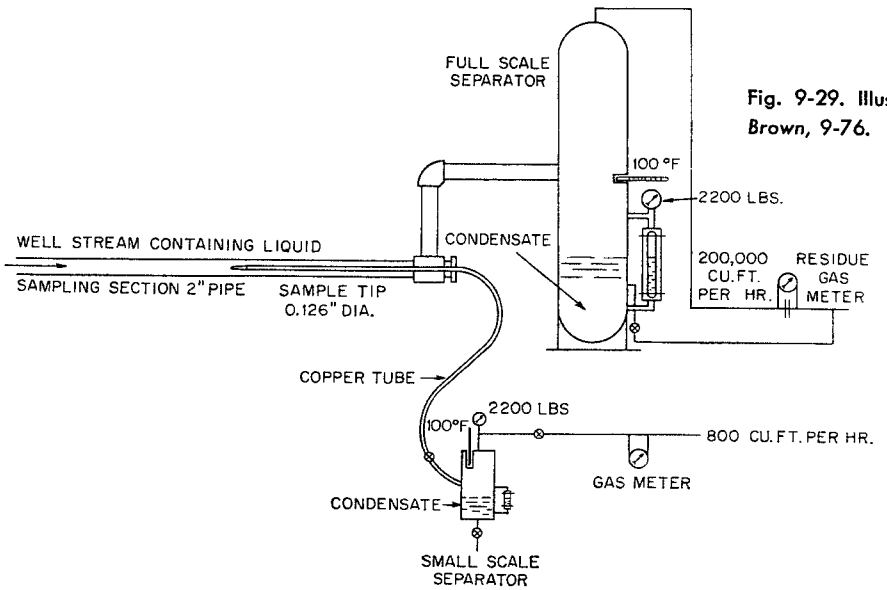

Fig. 9-29. Illustrative sketch of sampling system. (*Katz and Brown, 9-76. Courtesy NGAA.*)

d. In vertical sampling sections the tip position should be not less than 45 pipe diameters downstream from the last disturbance with 15 diameters of the straight section continued downstream from the tip. The flow rate should be not less than that indicated in Table 9-11 for a velocity ratio of 0.94.

e. In horizontal straight-tube sampling section, the tip should be placed at approximately 45 diameters downstream from the last disturbance in a straight sampling section of at least 60 pipe diameters in length, and flow rate should be not less than that indicated in Table 9-11 for a velocity ratio of 0.94.

2. Tips
   a. Sharp-edge tips.
   b. The sample tube supporting the tip and connecting the sample to the sample separator should be of the minimum consistent diameter.
   c. The tips should be well centered by a sturdy centering device or spider downstream from the tip.
   d. Tips can be permanently fixed in sample sections or inserted by any suitable means provided their position is known and controlled.
   e. Size of the tip should be, preferably, not less than ⅛ inch ID and generally as large as is practical and still bracket the velocity ratio of 0.94 without exceeding the capacity of the small-scale separator.
3. Sample separator
   a. Must be so designed as to give complete separation of gas from the liquid under the conditions of use.
   b. The gas-handling capacity must be at least adequate to handle the maximum flow rates with a tip not less than ⅛ inch ID.

Table 9-10. Gauge Modulus Determinations for a 1,200-lb-range Subsurface-pressure Gauge

Calibration date	Modulus, psi, corresponding to 1 in. deflection, at calibration temperatures, °F			
	60	80	100	120
Nov. 24, 1947.....	634.9	633.1	629.3	626.9
(Gauge was used extensively in this interval)				
Jan. 2, 1948.....	633.1	630.3	628.3	625.9
May 17, 1948.....	634.7	631.3	629.1	627.1
May 20, 1948.....	634.8	631.8	628.9	627.1
May 25, 1948.....	635.0	632.8	630.6	628.4
May 27, 1948.....	635.0	632.1	629.6	627.1
June 1, 1948.....	634.6	631.8	629.7	627.6
June 3, 1948.....	634.6	632.1	629.8	627.3
June 7, 1948.....	634.7	632.1	629.8	627.5
June 11, 1948.....	634.5	632.2	629.7	627.1
June 15, 1948.....	634.5	631.8	629.7	627.7
June 17, 1948.....	633.7	631.3	629.3	627.3
Average.....	634.5	631.9	629.5	627.3

SOURCE: Smith and Dewees (9-83).

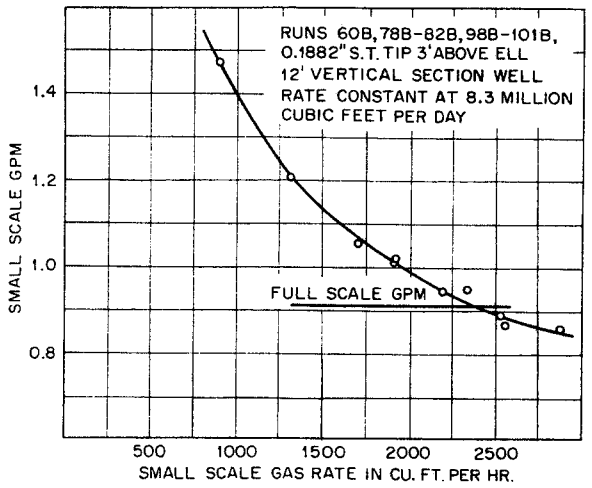

Fig. 9-30. Effect of sampling rate on liquid content of small-scale separator. (*Katz and Brown, 9-76. Courtesy NGAA.*)

In the sampling of gas from static wells, the possible concentration gradients, due to gravitational and temperature effects, in the well bore should be noted (9-81).

Back-pressure or performance tests on gas wells are used to demonstrate the flow capacity of the well (7-32, 9-71, 9-75, 9-84, 9-85). Recent work, discussed in Chap. 10, shows that for low-permeability formations, the isochronal flow tests are the best, for they give the correct slope of the performance curve. The test procedure consists of measuring the closed pressure and then, after opening the well to a fixed flow rate for a fixed period of time, measuring the flowing pressure. The well is closed in, preferably long enough to allow the pressure to return to its original value before the second test at a higher flow rate. The second and all succeeding tests should use the same length of time as the first flow test. In case the closed pressure after a flow test does not return to the original closed pressure in a reasonable period of time, the succeeding flow test should use the closed pressure just prior to opening the well for the test. Third and fourth flow points are usually taken. Table 9-11 and Fig. 9-31 show a sample back-pressure test on a well. It is necessary to calculate the flowing bottom-hole pressure to plot the difference in squares of the closed formation pressure P_f and the flowing sand-face pressure P_s against the flow rate Q. The value of Q at the P_f^2 is called the "absolute open flow," since it is the maximum flow rate for the well with zero back pressure on the sand.

Illustrative Problem

Back-pressure-test data for a well in the Pledger field are shown on page 376.

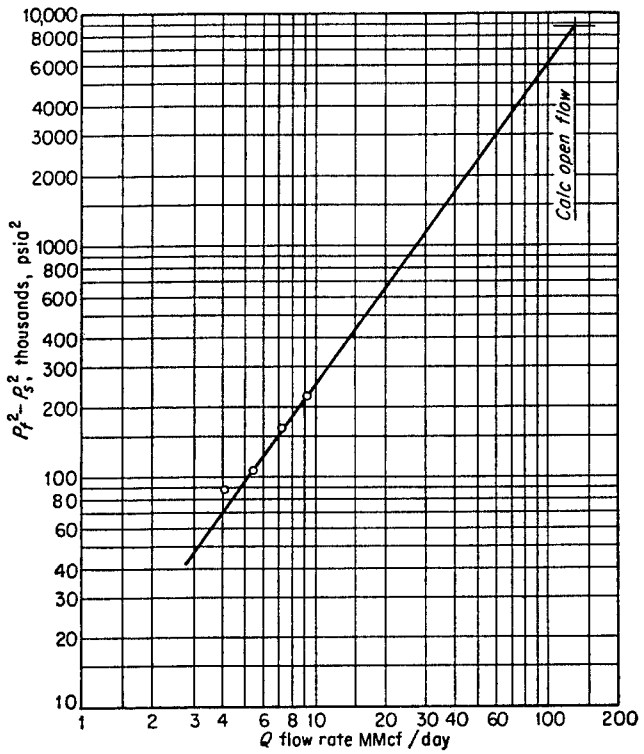

Fig. 9-31. Back-pressure curve on gas well.

Flow rate, Mcf/day	Wellhead pressure, psia	Wellhead temperature, °F
0	2,512	78.0
4,080	2,490	105.5
5,440	2,467	110.0
7,200	2,425	114.3
9,160	2,363	119.8

Separator-gas gravity = 0.6127
Separator-liquid gravity = 50°API
Gas/oil ratio = 426 Mcf/bbl
Tubing diameter = 2.441 in.
Depth of well = 6,830 ft
Reservoir temperature = 171°F

Table 9-11. Minimum Flow Rates and Maximum Pipe Diameters for Plain Tube Sampling with a Velocity Ratio of 0.94

Pressure not less than, psi	Minimum flow rate, MMcf per inch of pipe diameter		Maximum pipe diameter, in. per MMcf of flow rate	
	Vertical	Horizontal	Vertical	Horizontal
1,200	2.5	4.3	0.4	0.23
1,800	1.7	...	0.6	
2,200	1.5	3.0	0.66	0.33

SOURCE: Katz and Brown (9-76).

(a) *Solution Using the Moody-friction-factor Table*

$G = 0.619$ from Eq. (7-59) for well fluid gravity
$P_c = 670$ psia from Fig. 4-22
$T_c = 364$°R from Fig. 4-22
$d^5 = 2.441^5 = 86.6$

The solution will be carried out using the following equation' a form of Eq. (7-53), the nomenclature and the table for the Moody friction factor f.

$$P_s^2 - e^s P_w^2 = \frac{6.67 \times 10^{-4}(QT_a z_a)^2(e^s - 1)f}{d^5} = b$$

P_s = flowing sand-face pressure, psia
P_w = flowing wellhead pressure, psia
P_a = average well-bore pressure, psia
$e = 2.71828 \cdots$
G = gas gravity of well fluid (air = 1.0)
L = well depth, ft
T_a = average well temperature, °R
μ = viscosity of gas, centipoises
z_a = average compressibility factor
$s = \dfrac{0.0375GL}{T_a z_a}$
Q = flow rate, Mcf/day
f = Moody friction factor, function of GQ/μ according to Table A-22
d = inside diameter of pipe, in.

The calculations by this method are shown in Table 9-12.

(b) *Solution Using the Cullender and Binckley Friction Group*

An alternative method of solution is that of Cullender and Binckley (7-13). Their equation is

$$P_s^2 - e^s P_w^2 = \frac{0.1f'Q^2T_a^2z_a^2(e^s - 1)}{0.0375d^5}$$

Define R^2 such that

$$R^2 = (F_d Q)^{1.935}(e^s - 1) = P_s^2 - e^s P_w^2$$

and

$$P_s^2 = e^s P_w^2 + R^2 \qquad \text{(all pressures squared in thousands)}$$

where P_s = flowing sand-face pressure, psia
P_w = flowing wellhead pressure, psia
G = gas gravity
L = depth, ft
T_a = average well temperature, °R
z_a = average compressibility factor
$s = \dfrac{0.0375GL}{T_a z_a}$
f' = Fanning friction factor $f/4$
Q = flow rate, MMcf/day
F_d = friction group from Table A-23
d = inside pipe diameter, in.

The calculations according to the above equation are shown in Table 9-13.

This method has many advantages if repetitive calculations are to be made in a field where average conditions for flowing gas can be used. The F_d of Table A-23 uses $T_a = 540$°R; $z_a = 1.0$; $\mu = 0.0109$ centipoise; $G = 0.720$; and absolute roughness = 0.0006 in. To correct the F_d for other conditions,

$$F_d \text{ (new)} = F_d \text{ (Table A-23)} \left(\frac{Tz}{540}\right)^{1.0336} \left(\frac{0.720\mu}{0.0109G}\right)^{0.0336}$$

When it can be assumed that the F_d values are virtually the same for all flow points in a test, their use is very advantageous.

Table 9-12. Calculation of Back-pressure Test Using Moody Friction Factors

Item	Static	1	2	3	4
1. Flow rate, Mcf/day	.....	4,080	5,440	7,200	9,160
2. P_w, wellhead pressure, psia	2,512	2,490	2,467	2,425	2,363
3. T_a, avg well temp, °R	585	598	600	603	606
4. P_a assumed, psia	2,730	2,714	2,700	2,677	2,644
5. $P_r = P_a/P_c$	4.08	4.05	4.03	3.99	3.95
6. $T_r = T_a/T_c$	1.608	1.645	1.649	1.658	1.663
7. z_a	0.822	0.835	0.835	0.837	0.840
8. μ, centipoises	.....	0.018	0.018	0.018	0.018
9. GQ/μ	.....	140,000	187,000	247,000	315,000
10. f, from Table A-22	.....	0.0152	0.0151	0.0149	0.0148
11. $s = 0.03754GL/T_az_a$	0.330	0.317	0.316	0.314	0.312
12. e^s	1.391	1.373	1.372	1.369	1.366
13. $e^s - 1$	0.391	0.373	0.372	0.369	0.366
14. $(QT_az_a)^2$	.....	4.15×10^{12}	7.45×10^{12}	1.32×10^{13}	2.17×10^{13}
15. $b = 6.67 \times 10^{-4}(QT_az_a)^2(e^s - 1)f/d^5$	.....	181,000	322,000	559,000	905,000
16. P_w^2	6,310,000	6,200,000	6,086,000	5,881,000	5,584,000
17. $e^sP_w^2$	8,770,000	8,500,000	8,340,000	8,050,000	7,640,000
18. $P_s^2 = b + e^sP_w^2$	.....	8,681,000	8,662,000	8,609,000	8,545,000
19. P_f^2	8,770,000				
20. P_f, psia	2,961				
21. P_s, psia	.....	2,946	2,943	2,934	2,923
22. $P_f^2 - P_s^2$, psia², thousands	.....	89	108	161	225

This amounts to neglecting small differences in μ, T, and z as they influence the friction in the well. Examination of the set of calculations for this problem shows that this assumption is valid.

LOGGING OF WELLS

Before the casing is set and with the hole full of mud, an electric log is run to determine the characteristics of the rocks that the drill hole has penetrated. Certain logs may be run after the casing has been set.

In the early thirties the Schlumberger brothers introduced a geophysical technique, electrical logging, to the oil and gas industry. Records made by geologists and drillers to describe strata pierced during a drilling process are called logs. Records made by inserting electrodes into well bores and making a traverse of the strata penetrated are termed "electrical logs," for they constitute a description of the rock including its fluid content and they consist of electrical measurements. Radiation logs, caliper logs, and temperature logs, as well as many types of electrical log, have become so commonplace in the industry that one or more of these are run in each well drilled. Logging service is generally available throughout the world.

Electrical logs are run on uncased well bores containing drilling fluid (see Fig. 9-32). Elements of logging equipment are (1) the electrodes, which are lowered into the well and which are contained in a tube called the *sonde;* (2) the electric conductor and measuring line used to lower the sonde into the bore hole to known depths and to transmit signals between sonde and surface; and (3) surface equipment, which is housed in a truck and which consists of mechanical equipment used to lower and raise the sonde and electrical gear to generate, measure, and record potentials.

The logging operation is conducted between the drilling and casing of the well. A truck equipped with a sonde containing a maximum-indicating ther-

Table 9-13. Calculation of Back-pressure Test Using Cullender and Binckley Factors

Item	Static	1	2	3	4
1. Flow rate, MMcf/day	.....	4.080	5.440	7.200	9.160
2. P_w, wellhead pressure, psia	2,512	2,490	2,467	2,425	2,363
3. T_a, avg well temp, °R	585	598	600	603	606
4. P_a assumed, psia	2,730	2,714	2,700	2,677	2,644
5. $P_r = P_a/P_c$	4.08	4.05	4.03	3.99	3.95
6. $T_r = T_a/T_c$	1.608	1.645	1.649	1.658	1.663
7. z_a	0.822	0.835	0.835	0.837	0.840
8. μ, centipoises	.....	0.018	0.018	0.018	0.018
9. F_d, from Table A-23	.....	6.376	6.376	6.376	6.376
10. $(T_z/540)^{1.0336}$	.....	0.924	0.925	0.933	0.940
11. $(0.720\mu/0.0109G)^{0.0336}$	.....	1.022	1.022	1.022	1.022
12. F_d (new)	.....	6.02	6.03	6.09	6.14
13. $s = 0.03754GL/T_az_a$	0.330	0.317	0.316	0.314	0.312
14. e^s	1.391	1.373	1.372	1.369	1.366
15. $e^s - 1$	0.391	0.373	0.372	0.369	0.366
16. $R^2 = (F_dQ)^{1.935}(e^s - 1)$	.....	181	322	559	905
17. P_w^2, psia², thousands	6,310	6,200	6,086	5,881	5,584
18. $e^sP_w^2$, psia², thousands	8,770	8,500	8,340	8,050	7,640
19. $P_s^2 = R^2 + e^sP_w^2$	.....	8,681	8,662	8,609	8,545
20. P_f^2, psia², thousands	8,770				
21. P_f, psia	2,961				
22. P_s, psia	.....	2,946	2,943	2,934	2,923
23. $P_f^2 - P_s^2$, psia², thousands	.....	89	108	161	225

mometer comes to the well site. After the sonde is placed in the wellhead, a zero depth measurement relative to some base such as the derrick floor is obtained. After the sonde is lowered to the bottom of the hole, it is raised slowly and various electrical responses are recorded as a function of depth. Auxiliary measurements are made of the resistivity of the mud and of the mud filtrate both at a known temperature and at the temperature at the bottom of the well. The electrical log is a chart of self-potential and electrical-resistivity measurements versus depth, along with certain other well data.

Radiation logs are run with equipment similar to that used for electrical logs. Radiation logs can be run in cased wells, since steel casing reduces but does not completely absorb the neutrons emitted from the sonde and the gamma rays returning from the formation. The procedure used to make the log and obtain the charts is similar to the procedure used for electrical logs.

Electrical and radiation logs have two purposes. The first is to identify similar strata in adjacent wells for stratigraphic studies. The second is to determine porosity and water saturation of the formation. Any fluid other than water is considered to be oil or gas.

Caliper logs on uncased wells measure the diameter of the hole. This information is needed for cementing the casing and for interpreting electrical and radiation logs.

Temperature logs are effective in finding the level of cement behind the casing and in locating casing leaks by temperature abnormalities which are created by flowing gas, oil, or water.

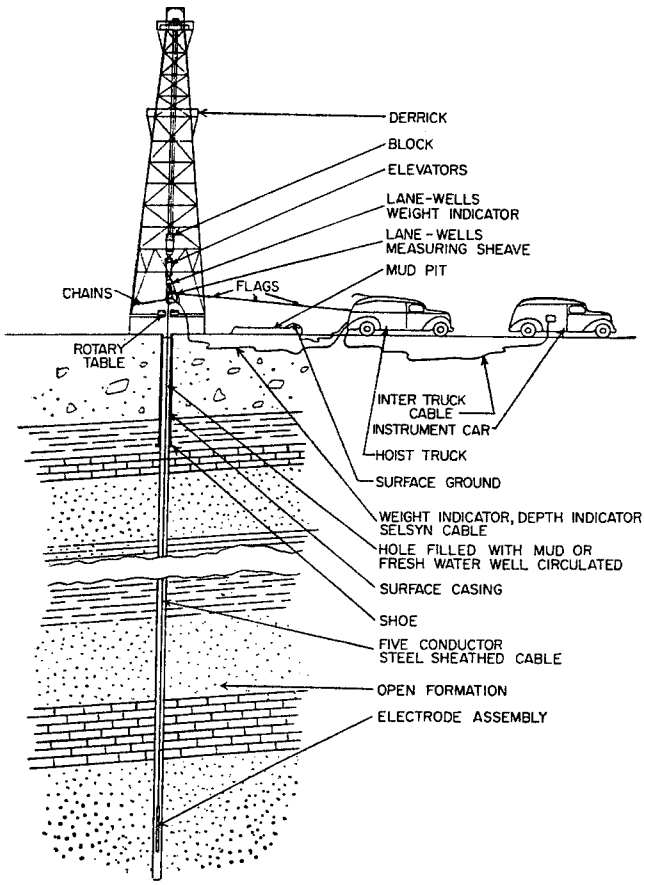

Fig. 9-32. Arrangement of equipment used in electric logging. *(Courtesy Lane Wells Company.)*

Electrical Logs

An electrical log measures two quantities. First, the penetration of the various formations with a bore hole filled with mud generates various electric currents. The electrical log measures the potential associated with these currents. These currents are caused by natural conditions; hence the curve formed by plotting variations in potential with depth is called the "spontaneous potential" or "self-potential." This term is often shortened to SP; an SP curve is illustrated in Fig. 9-33.

The other quantity measured is resistivity of formations penetrated. Resistivity is the resistance to flow of electric current afforded by a volume of material of unit cross-sectional area and of unit length. Units of resistivity are ohms times square meters per meter, or ohm-meters. The reciprocal of resistivity is the conductivity of the material, or the ability of the material to carry electric current.

Except for a few "metallic ores," most formations of rock will not conduct electricity when they are dried. In other words, dry rock is a fairly good insulator, or has infinite resistivity; the ability of most formations to conduct current is due to the fluid content and not to the rock. Also, both oil and gas are nonconductors of current. Therefore, variations in resistivity or conductivity of the formation must reflect the conductivity and the quantity of water present in the formation.

Resistivity of Water

Since water in the rock pores forms the conducting path for current, factors affecting resistivity of water must be known in order to interpret electrical logs. Pure water will not conduct electric current. Dissolved salts form charged ions which bear the electrons, or charges of current. The mobility as well as concentration of these ions determines the conductivity of a solution. Mobility of ions in a solution depends upon two factors: the ions themselves and the temperature. Each chemical ion has its own mobility. However, the determination of solution

conductivity from a chemical analysis and from ion-mobility data is impractical.

The over-all effects of various ions present in naturally occurring "salt" water can be determined with sufficient accuracy by one direct or indirect measurement of resistivity at a known temperature. The variation of resistivity with temperature for sodium chloride solutions is shown in Fig. 9-34. Since most dissolved salts in naturally occurring or connate waters are sodium chloride and since the change with temperature in the mobility or resistivity of other dissolved salts approximates the corresponding change for sodium chloride, Fig. 9-34 can be used in general to determine the effect of temperature on resistivity. First, resistivity measured at a known temperature is used to determine a pseudo salt concentration, and this concentration is used to find the resistivity at other temperatures.

Resistivity of Formations Saturated with Water

As stated above, minerals comprising the matrix of rocks are for the most part insulators. Current must flow through the pores, which contain conducting fluids and are interconnected. Thus, pore geometry forms an electrical network. The cross-sectional area available for flow in this network is proportional to porosity and to ratio of length of core to length of flow path. The flow path is longer than the porous medium containing this network, for the flow path is tortuous. Equation (9-1) may be written using an equivalent length L_e of flow path.

$$R_0 = R_w \frac{L_e^2}{\phi L^2} \tag{9-1}$$

where R_0 = resistivity of rock
R_w = resistivity of water
L_e = length of flow path
L = length of core
ϕ = porosity

Archie (9-86) introduces the concept of a formation factor F which is the ratio of resistivity of rock filled with water to resistivity of the water with which it is filled.

$$F = \frac{R_0}{R_w} \tag{9-2}$$

The relationship between porosity and formation factor may be obtained by substituting Eq. (9-1) for R_0 in Eq. (9-2).

$$F = \frac{L_e^2}{\phi L^2} \tag{9-3}$$

Since the detailed pore geometry necessary to obtain L_e is not available, Archie suggests that this factor might also vary with porosity in the following manner:

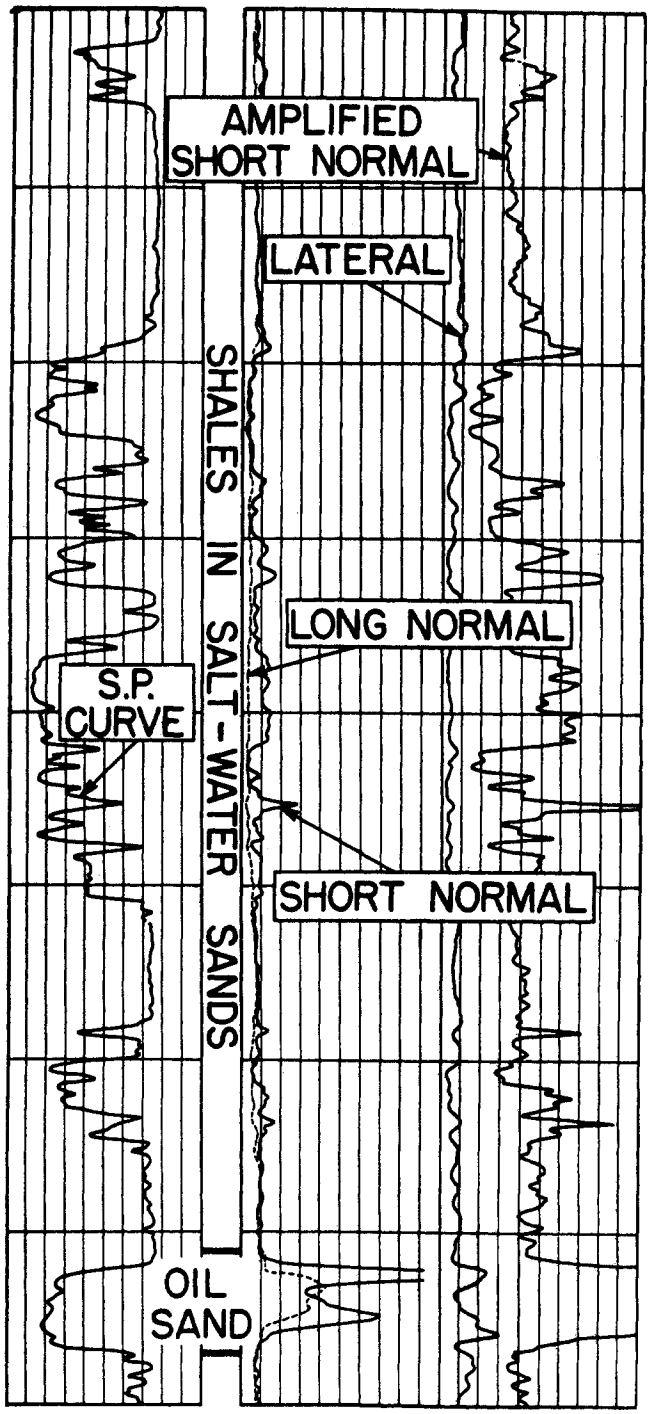

Fig. 9-33. Electrical log.

$$F = \frac{1}{\phi^m} \tag{9-4}$$

Archie shows that m ranged from 1.3 for unconsolidated sand to 2.0 for consolidated sand. For this reason, m is called the "cementation factor." Figure 9-35 is a plot of this equation.

Winsauer, Shearin, Masson, and Williams (9-150)

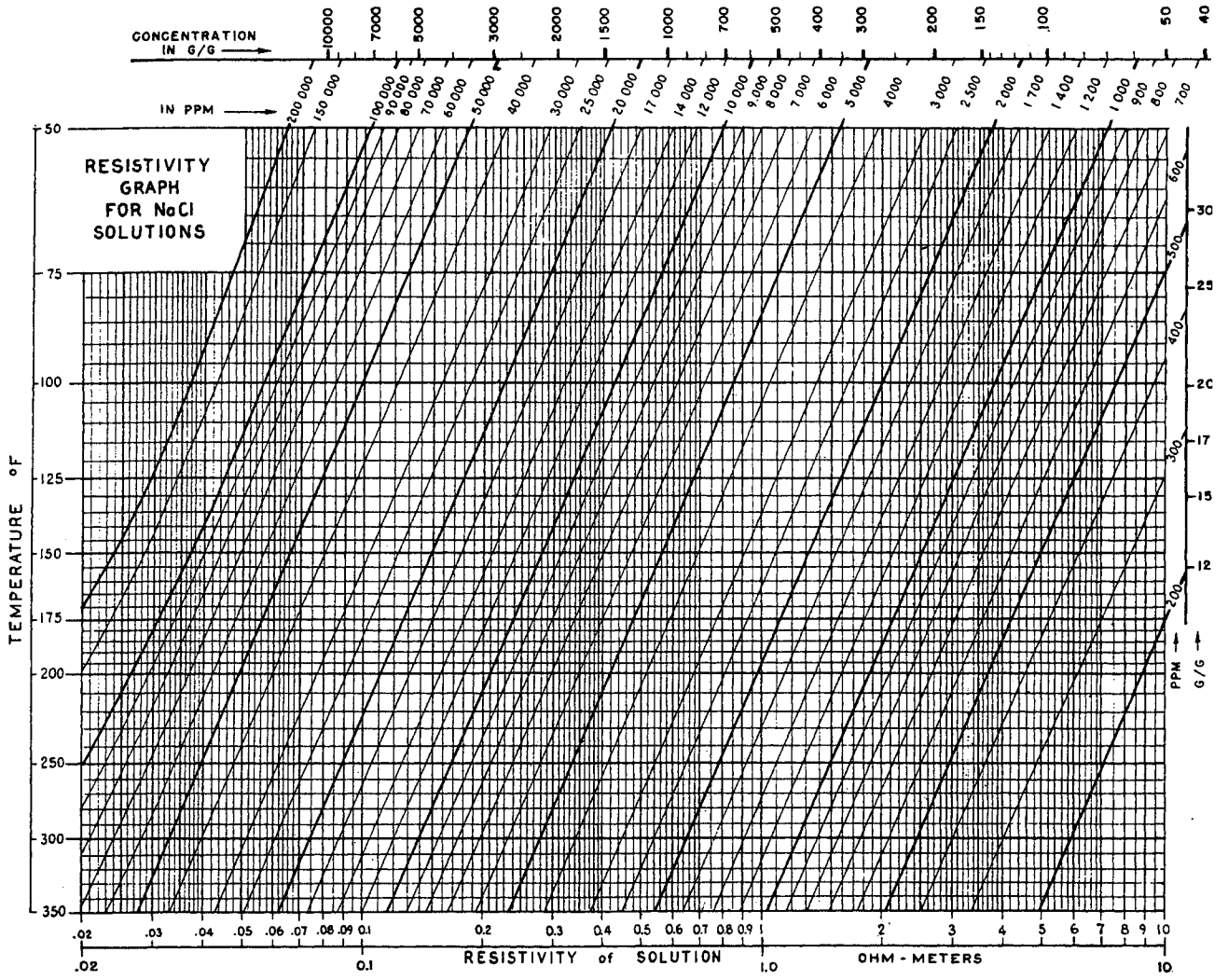

Fig. 9-34. Resistivity of sodium chloride solutions. (*Courtesy Schlumberger Well Surveying Corp.*)

propose the following modification, known as the Humble formula:

$$F = \frac{0.062}{\phi^{2.15}} \tag{9-5}$$

Both Eqs. (9-4) and (9-5) are in use. When Eq. (9-4) is used, m is usually determined from wells in the locality, for which complete information—resistivity, porosity, etc.—is available.

Shale and Clay

The above discussion assumes that rock matrix does not conduct. This is true for clean sand and for hard formations. But some formations contain shale or clay, and these have very fine matrix which, when penetrated with water, will conduct electric current. Numerous investigators have shown that resistivity of these clays or conductive solids is not truly dependent upon resistivity of formation water; therefore, the formation factor changes with resistivity of formation water. Patnode and Wyllie (9-126) have discussed these effects. Their data indicate that the effect of clay or shale decreases with increase in water resistivity and decreases also at water resistivities below 0.1 ohm-meter, as shown in Fig. 9-36, which was computed by Winn (9-148a). These effects will be further discussed with resistivity-departure curves.

Fluid Saturation and Resistivity

Resistivity of rock increases when part of a pore space is occupied by insulating material such as oil or gas. Resistivity is determined not only by degree of water saturation, but also by the relative position occupied by the hydrocarbon and the water. This is discussed in the section on properties of reservoir rock. For substantially clean formations all these factors can be related by the equation

$$S_w = \left(\frac{R_0}{R_t}\right)^{1/n} \tag{9-6}$$

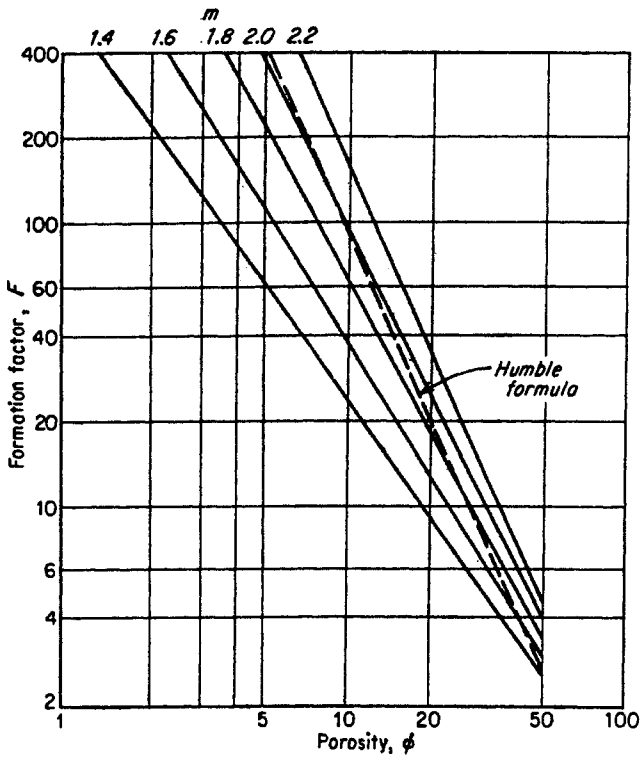

Fig. 9-35. *Porosity vs. formation factor.* (9-136, *Courtesy Schlumberger Well Surveying Corp.*)

where S_w = water saturation
R_t = resistivity of formation
R_0 = resistivity of formation when entirely saturated with water
n = exponent depending upon character of rock

A plot of this equation is shown in Fig. 9-37. Where complete data on porosity, resistivity, and water saturation are available, the value for n can be obtained from information for wells in the locality. Where this information is not available, $n = 2$ is used as a good approximation.

The above considerations are basic for the interpretation of electrical logs. However, the real problem in electrical-log interpretation lies in converting readings obtained from various devices into values required by the foregoing equations.

Self-potential Curve

Electrical logs also record the natural potentials that occur in a bore hole filled with mud. Curves are used for two purposes: location of pores in permeable formations, and estimation of formation-water resistivity.

Determination of Formation-water Resistivity

Mounce and Rust (9-125) propose use of the "shale cell" as the point of origin of the SP; this proposal has been generally accepted. The shale cell

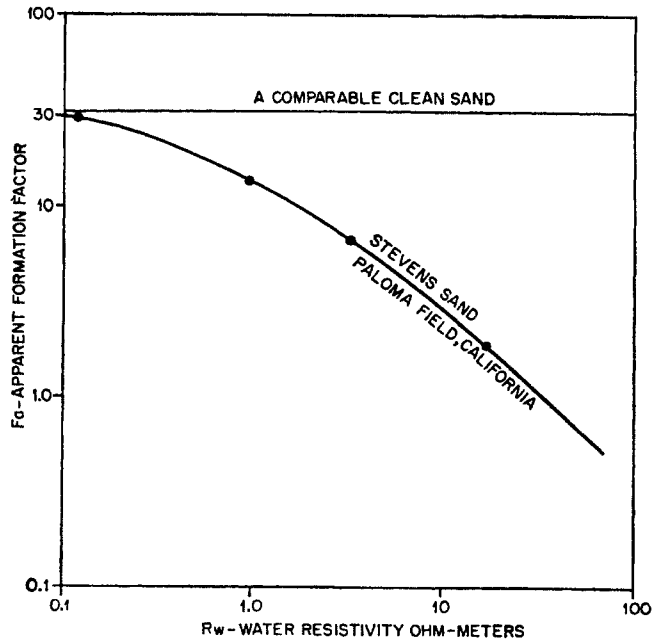

Fig. 9-36. Apparent formation factor vs. water resistivity for Stevens sand of Paloma field, Calif. (*Patnode and Wyllie*, 9-126. *Courtesy AIME.*)

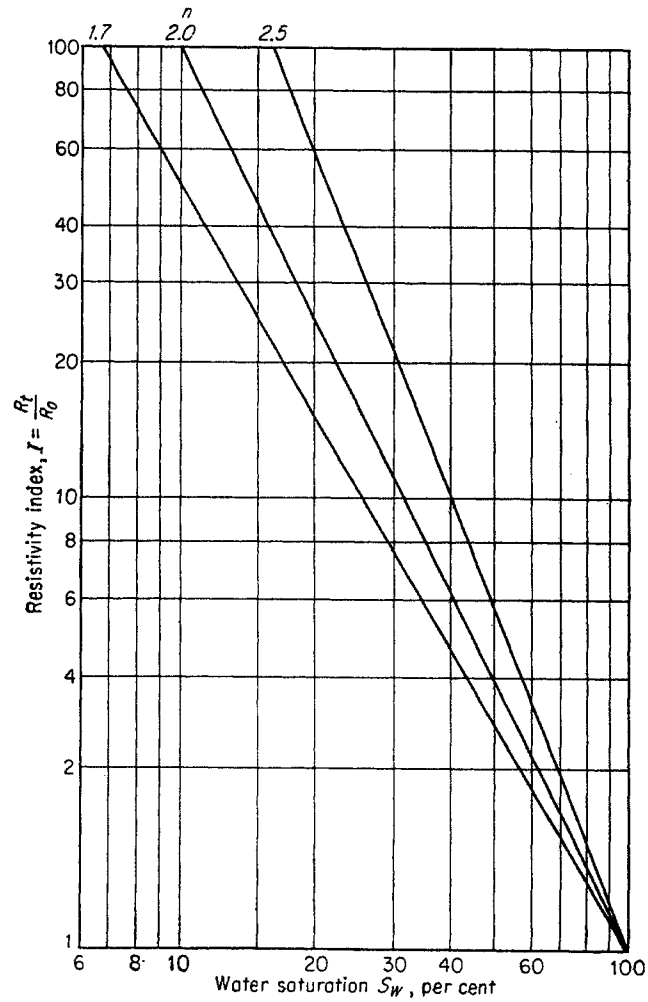

Fig. 9-37. Water saturation vs. resistivity index. (9-136, *Courtesy Schlumberger Well Surveying Corp.*)

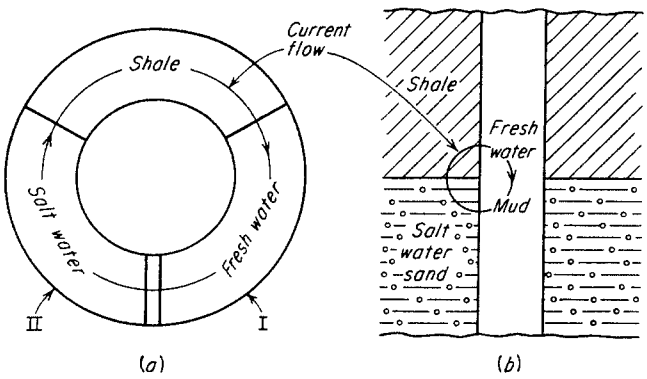

Fig. 9-38. Mounce and Rust shale cell. (9-125. Courtesy AIME.)

involves electrochemical forces resulting from contact of two solutions of different concentrations, as illustrated in Fig. 9-38. Wyllie (9-156) presents the following theoretical equation:

$$emf = K \log \frac{a_w}{a_{mf}} \tag{9-7}$$

where a_w = activity of interstitial water
a_{mf} = activity of the mud filtrate

If all the salts dissolved are sodium chloride, the equation for the coefficient is

$$K = 2.303 \frac{RT}{zF}\left(1 + \frac{u - v}{u + v}\right) \tag{9-8}$$

where R = gas-law constant = 8.32 joules
F = faraday = 96,450 coulombs
T = temperature, °K
z = ion valencies
u = mobility of the chloride ion
v = mobility of the sodium ion

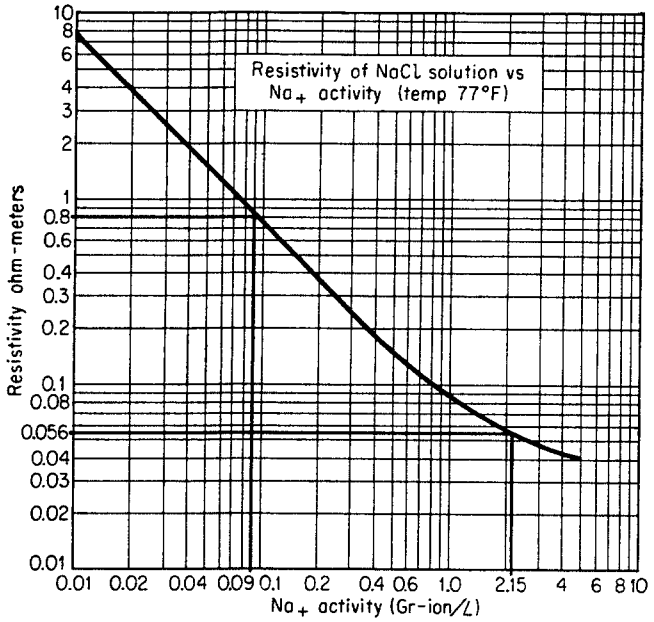

Fig. 9-39. Resistivity of sodium chloride vs. sodium-ion activity. (9-136, Courtesy Schlumberger Well Surveying Corp.)

Activity can be determined from a variety of measurements and can be related to resistivity (Fig. 9-39). Equation (9-8) is plotted for sodium chloride solution in Fig. 9-40. Assuming all dissolved salts to be sodium chloride, Figs. 9-39 and 9-40 may be used with the SP curve and with resistivity of mud filtrate to estimate resistivity of formation water. If formation-water resistivity is between 0.08 and 0.3 ohm-meter, resistivity of sodium chloride solutions is inversely proportional to activity, that is,

$$\frac{a_w}{a_{mf}} = \frac{R_{mf}}{R_w} \tag{9-9}$$

and Fig. 9-40 can be used directly to estimate R_w.

The above method of estimating formation-water resistivity is satisfactory if a large proportion of the dissolved salts is sodium chloride. However, when other ions such as calcium and magnesium form a substantial proportion of the dissolved salts, considerable error is introduced. For this reason, data on resistivities of formation waters are being compiled by various organizations such as the AIME and API. This information should be used whenever it is available for the formation in a specific locality.

Another problem in interpreting the SP curve is that an observed effect may be the result of an additional source of potential called "streaming potential." At one time this streaming potential was considered to be the source of the SP. Wyllie (9-157) investigated the effect of streaming potential and presented data allowing the estimation of this component of the SP curve. However, in the majority of cases this factor does not need to be considered.

Factors Influencing the Measured SP

Shale and Permeable Beds. The SP, as mentioned above, is the value that would result from an ideal shale cell. These conditions exist in the center of thick formations and where mud has high resistivity. Figure 9-41 is a schematic diagram of the ideal or static SP distribution and the actual SP curve. In the static case no current is flowing and the entire potential is available at the point of generation. In practice, current will flow along the paths indicated, producing a potential change in the mud before the point of origin is reached. This effect also dissipates part of the potential at points of origin, resulting in the indicated SP curve. Low mud resistivities, large bore-hole diameters, thin sections, and mud-filtrate invasion all increase spreading of current-flow lines and reduce the peak value of the SP curve. Doll (9-95) correlates these factors in Fig. 9-42, which is used to estimate the static SP for determining R_w.

Invasion of mud filtrate may be considered as increasing effective bore-hole diameter.

Doll (9-95) also reports the effect of interbedded sand and shale strata on the SP curve (Fig. 9-42*a*). Qualitative interpretation of the SP curve from these formations and from shaly sand will be discussed in conjunction with resistivity-departure curves and micrologs. Doll shows that the boundary between a thick-shale and a clean-sand formation produces an inflection in the SP curve which may be used to determine accurately the location and, thus, the thickness of these formations. The precision of this determination decreases as resistivity of the mud decreases. This method is not reliable for thin formations, as is indicated in Fig. 9-43.

Dense Formations—Limestones. The SP curve obtained from permeable strata adjacent to or interbedded in dense, highly resistant formations such as limestones differs in form from the SP curve observed when permeable strata are adjacent to low-resistivity formations such as shale.

In the case of the shale-sand-mud system, the low-resistivity shale and sand and the large, horizontal cross-sectional area form only a small part of the total resistance to current flow, as shown in the shale cell (Fig. 9-38). Resistance in mud controls the amount of current flow. Doll (9-95) shows that in the case of permeable sections surrounded by dense, highly resistant formations, resistance of the dense formation must also be considered. The geometry of the system is such that a vertical path is the path of least resistance across these dense resistive beds. Thus currents circulate within the formation (Fig. 9-41) until they come to a formation of low resistance such as a shale bed, where they return to the mud column. Figure 9-44 shows the analysis of SP curves in highly resistive formations made from characteristic shapes with the aid of the resistivity curve.

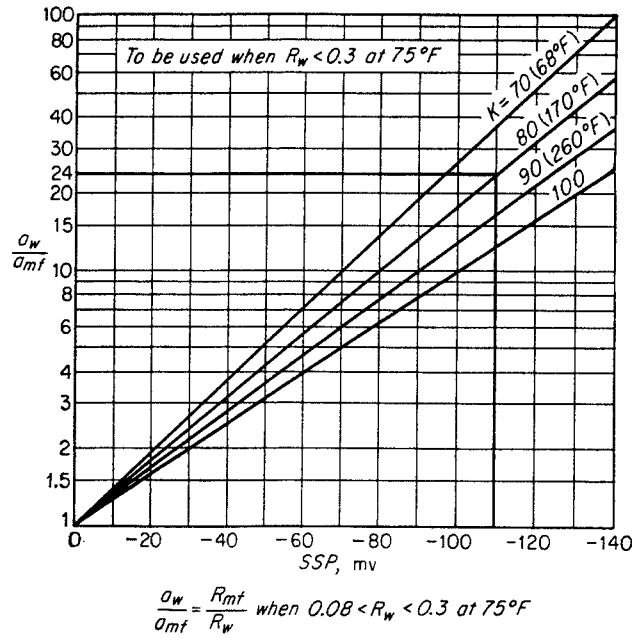

Fig. 9-40. Activity ratio vs. self-potential. (9-136, *Courtesy Schlumberger Well Surveying Corp.*)

Resistivity from Normal and Lateral Devices

Since the device to determine resistivity cannot be inserted into the formation but must remain in the bore hole, an instrument must be designed to correct for surroundings in the measurement of resistivity. All devices for measuring resistivities of formations give a response that is caused not only by resistance of the formation opposite the device but also by resistivities of the mud, mud filtrate, invaded zone, and surrounding formations; thickness of formation; diameter of bore hole and invaded zone; and the dimensions of the device. The effect of these factors may

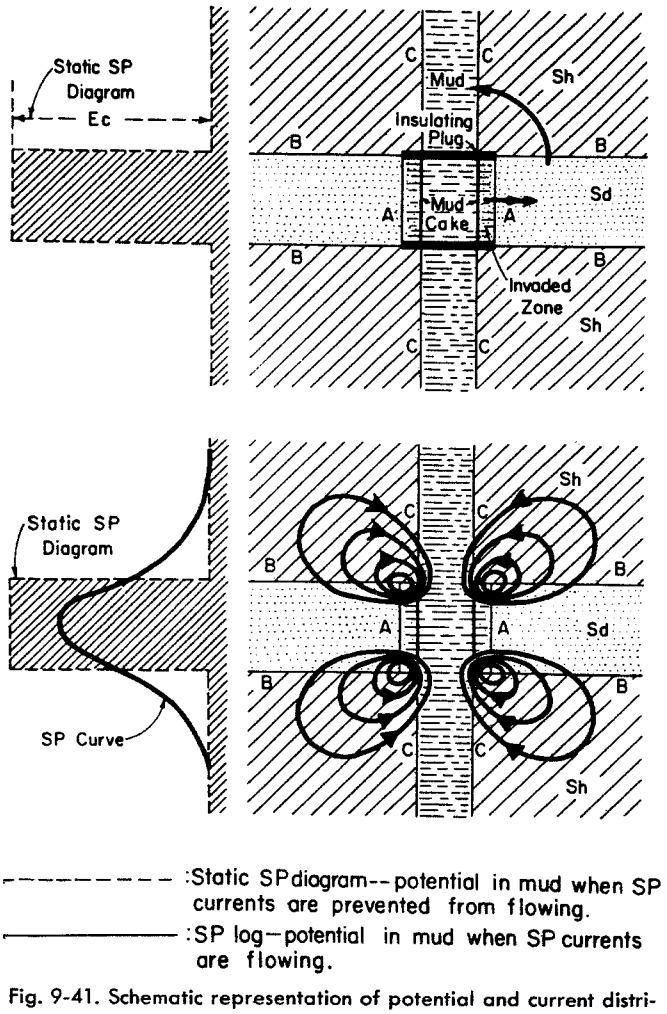

Fig. 9-41. Schematic representation of potential and current distribution in and around a permeable bed. (9-136, *Courtesy Schlumberger Well Surveying Corp.*)

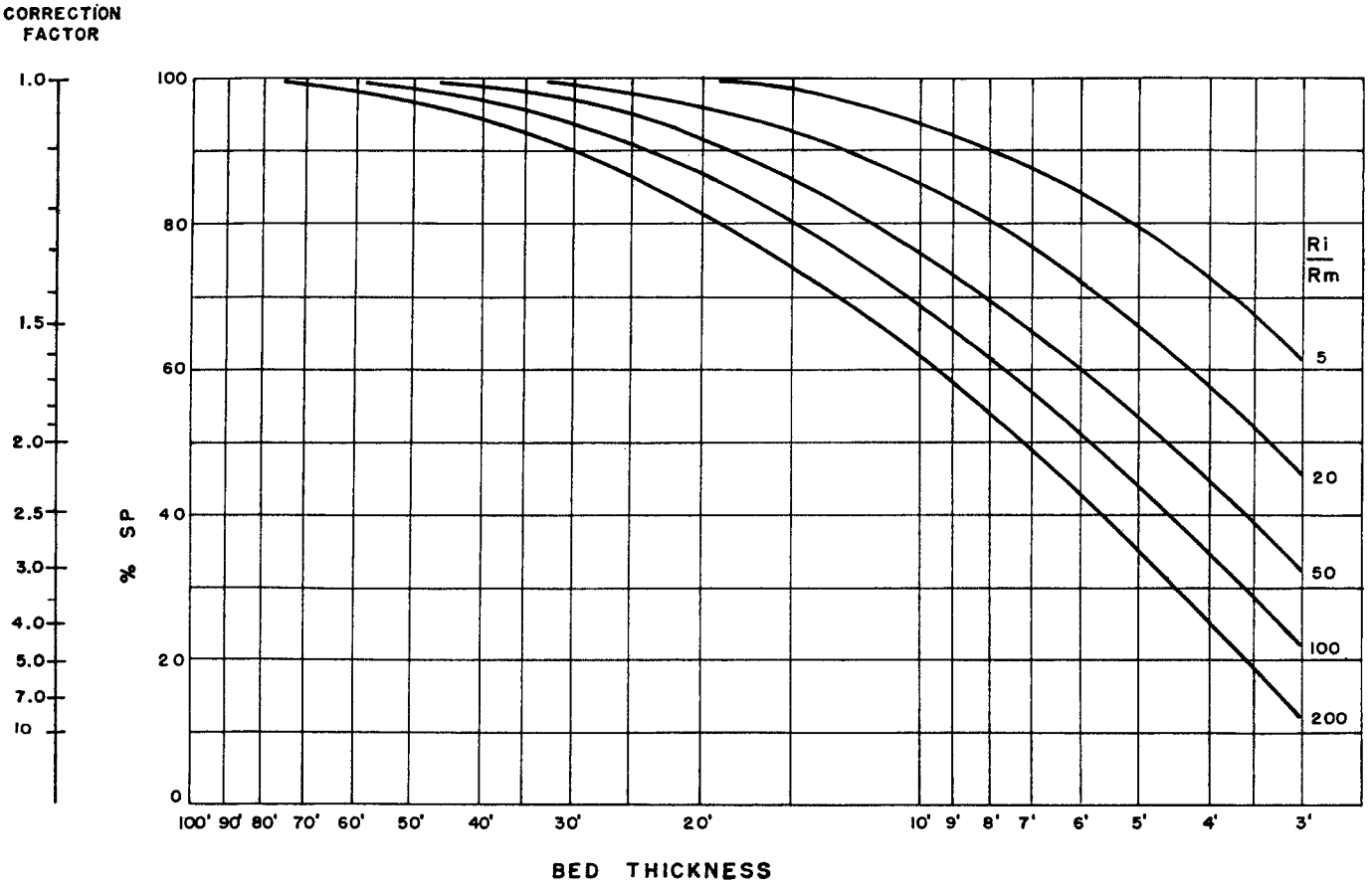

Fig. 9-42. SP correction chart. (9-136, Courtesy Schlumberger Well Surveying Corp.)

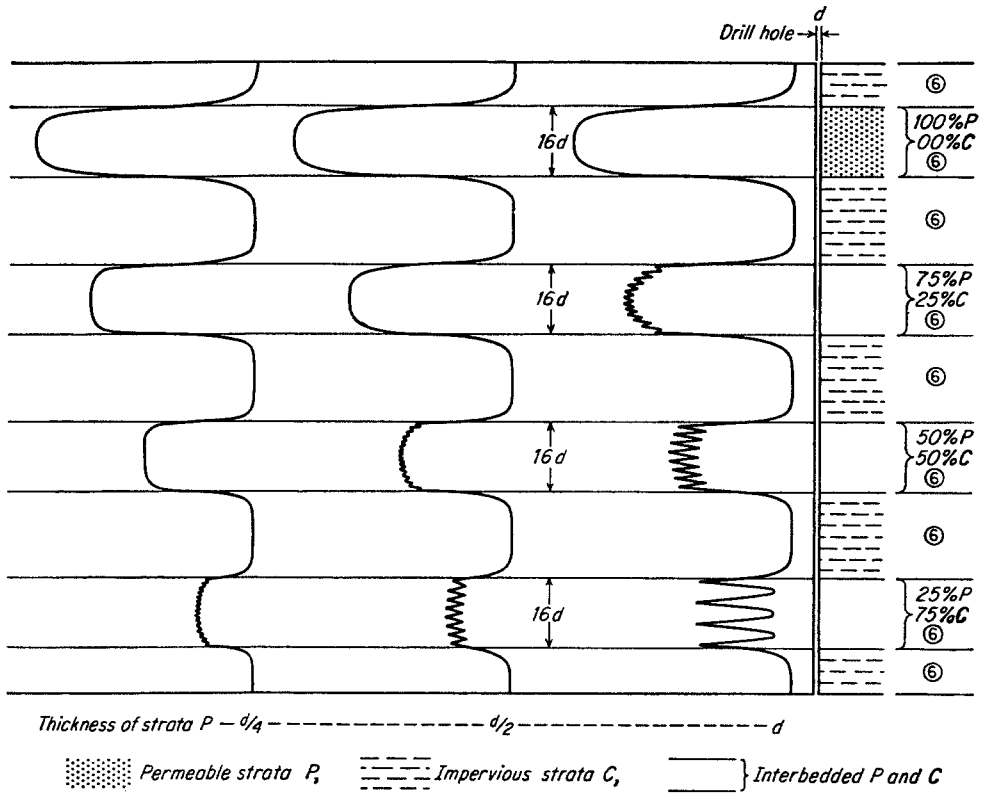

Fig. 9-42a. Effect of interbedded sand and shale strata on the self-potential curve. (Doll, 9-95. Courtesy AIME.)

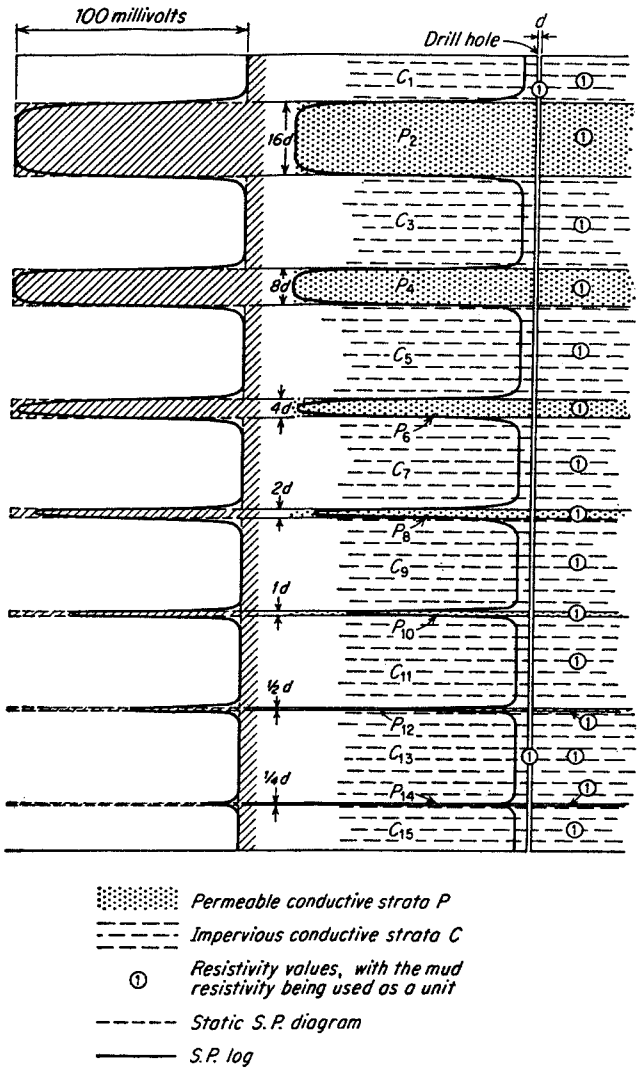

Fig. 9-43. Effect of bed thickness on the self-potential curve. (Doll, 9-95. Courtesy AIME.)

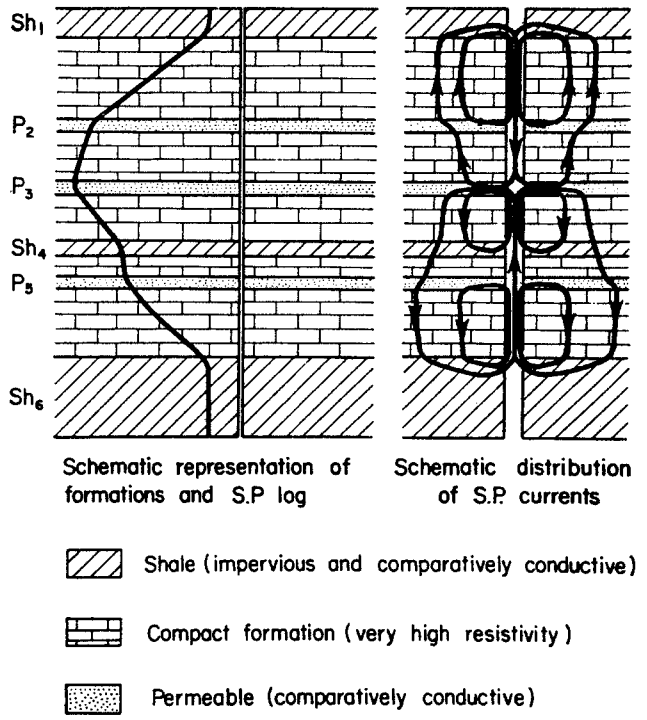

Fig. 9-44. Effect of adjacent dense formation on self-potential curve. (9-136, Courtesy Schlumberger Well Surveying Corp.)

be seen in the simple diagram, Fig. 9-45. Voltage is applied to or current emitted from electrode A, and a voltage drop is measured that is either part or all of the potential change between A and the point M. The potential drop is converted to resistivity by assuming that measurement is made in an infinite homogeneous medium with a bore hole of zero diameter. However, this last assumption is not strictly accurate, for measurement is really an "average" of all factors within the sphere. Since current lines will not radiate as straight lines from point A, but are bent or refracted as they pass through a material of one resistivity to a material of another resistivity, Fig. 9-45 more nearly illustrates the actual case. Radius of the sphere in Fig. 9-45 is called the "radius of investigation." This sphere should not be considered a fixed volume within which measurement is determined, but should be used only as an approximation of zone boundaries. When the device has a small radius of investigation, resistivity measured will be greatly influenced by bore-hole diameter, mud resistivity, and condition of the formation adjacent to

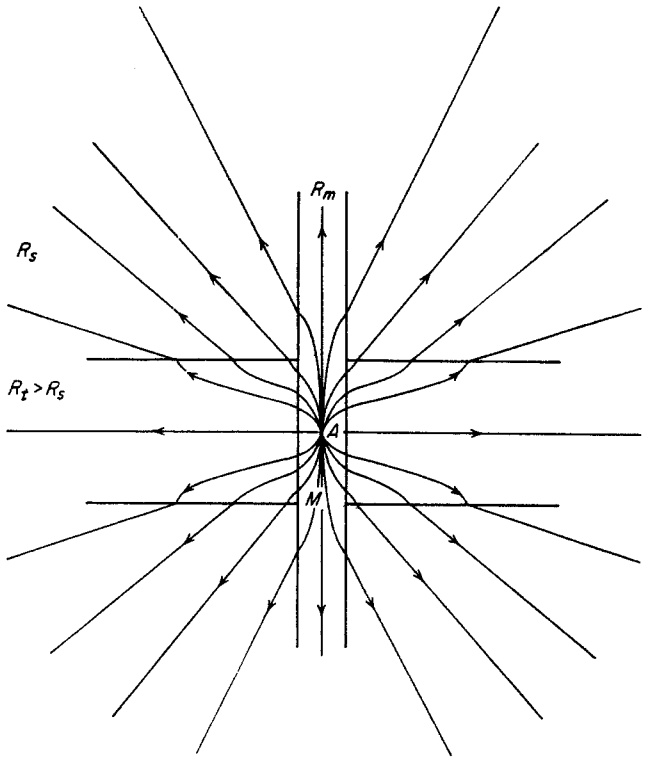

Fig. 9-45. Current distribution.

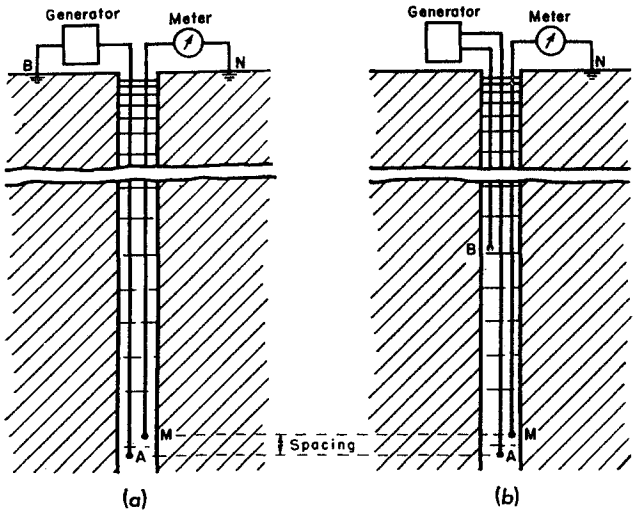

Fig. 9-46. (a) Two-electrode circuit; (b) actual circuit. (9-136, Courtesy Schlumberger Well Surveying Corp.)

the hole, and the effect of surrounding beds will be at a minimum. Large radii of investigation minimize effects of the bore-hole mud and of the invaded zone, but have the disadvantage of being greatly affected by surrounding formations, especially if the bed is thin. Present-day logs measure resistivity using devices with several radii of investigation in an attempt to separate the variables.

Normal or Two-electrode Devices. A schematic diagram, as presented by Russell (9-132), of the normal or two-electrode instrument for measuring resistivity is shown in Fig. 9-46. A direct or low-frequency alternating current is supplied by the generator and the potential difference between M and N is measured. Since B is remote from A, current would spread out radially in a homogeneous medium, as discussed above. The potential difference recorded is an indirect measurement of the potential difference from point A to point M. Thus, the device investigates a sphere whose center is A. The distance AM is referred to as the "spacing" of the device, and radius of investigation is considered to be twice the spacing. Laboratory curves presented by Russell (9-132, 9-133) and shown in Fig. 9-47 show the type of curve obtained by a normal device when formations have not been invaded with mud filtrate.

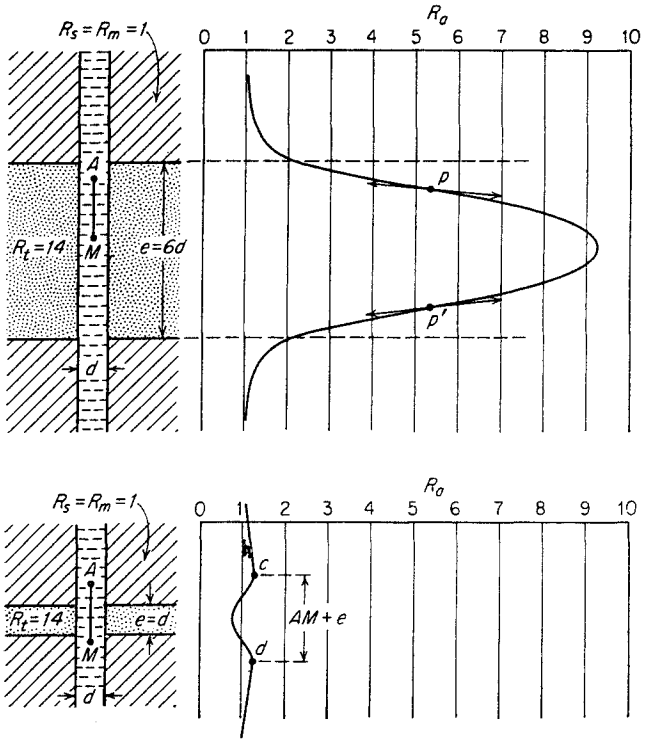

Fig. 9-47. Response of normal device. (9-136, Courtesy Schlumberger Well Surveying Corp.)

Lateral or Three-electrode Devices. The lateral or three-electrode device for measuring resistivity is shown in the schematic diagram, Fig. 9-48. In the same manner as in the normal device, a direct or low-frequency alternating current is applied by the generator; and the potential drop between points M and N, which are close together, is measured. Again, since B is remote from A, the current-flow line will spread out radially from A. However, in this homogeneous medium, a potential drop between the two closely spaced points M and N will equal the voltage drop between two concentric spheres of radius AM and AN. Thus, the spacing AO of this instrument is considered equal to the radius of investigation. Figure 9-49 shows the response to a lateral device for two thicknesses of uninvaded formations. The response is markedly asymmetrical, because current lines do not flow radially from the current electrode as they would if the device were in a homogeneous medium. Opposite a resistive formation, current concentrates more in the bore hole than it does opposite a conductive formation. This results in a "blind zone" and in a reflection when thin beds are logged. For this reason, thin beds in the blind zone could be overlooked. Also, in thin beds the maximum apparent resistivity is greater than true resistivity. The presence of highly resistive formations magnifies these effects and makes interpretation impossible.

Interpretation of Normal and Lateral Responses. The departure of apparent or measured resistivity from true resistivity has been computed by the Schlumberger Well Surveying Corporation (9-136) to assist in determining porosity and water saturation by Eqs. (9-4) to (9-6). These resistivity-departure curves show conditions at which the effects of the bore hole, surrounding formation, invasion, etc., are negligible so that apparent resistivity approaches true resistivity. When complicating factors are not negligible, departure curves are of little practical use since

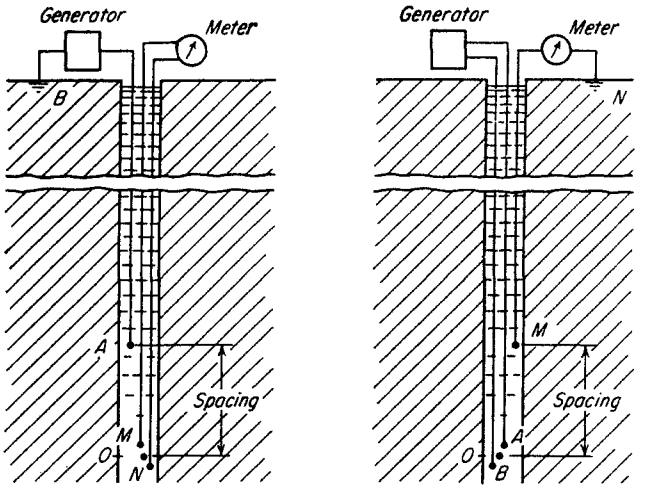

Fig. 9-48. Lateral sonde. (9-136, *Courtesy Schlumberger Well Surveying Corp.*)

it is impossible to estimate accurately such factors as effective diameter of the invaded zone. Departure curves show that lateral and normal devices can be used to determine true resistivities for thick beds in the sand-shale series if there are no highly resistive beds present such as lignite streaks. Also, depth of invasion must be less than twice the diameter of the bore hole and the formation must be logged shortly after drilling. Under these conditions the following rules can be used to determine true resistivity from normal and lateral measurements:

1. When the ratio between the resistivity values shown by the short normal (R_{sn}) and by the mud (R_m) is less than 10 and when bed thickness e is 4 times the spacing of the long-normal device or more, true resistivity R_t is equal to the value R_{ln} shown by the long-normal device.

   Conditions:
   Short normal $R_{sn}/R_m < 10$
   Long normal $e > 4AM$
   Response:
   Long normal $R_{ln} = R_t$

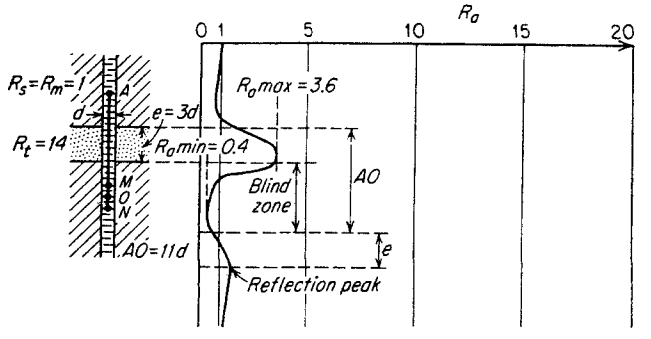

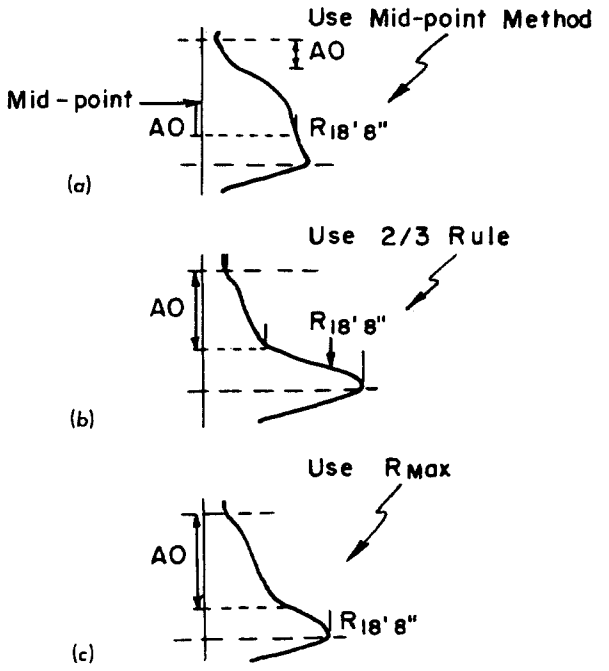

Fig. 9-49a to c. Lateral logs. (9-136, *Courtesy Schlumberger Well Surveying Corp.*)

2. When the ratio between the resistivity values shown by the short normal and by the mud is less than 50 and when bed thickness is twice the lateral spacing or more, the value at the mid-point of the lateral-device curve is equal to true resistivity.

   Conditions:
   Short normal $R_{sn}/R_m < 50$
   Lateral $e > 2AO$
   Response:
   Lateral $R_{\text{mid-point}} = R_t$ (see Fig. 9-49*a*)

3. When the ratio between the resistivity values shown by the short normal and by the mud is less

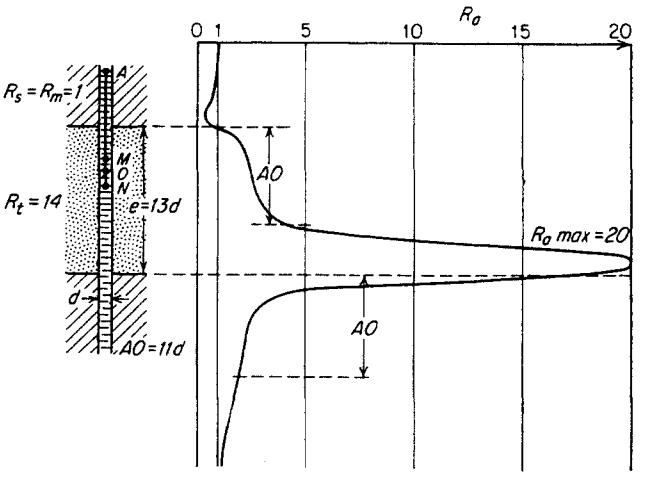

Fig. 9-49. Response of lateral device. (9-136, *Courtesy Schlumberger Well Surveying Corp.*)

than 50 and when bed thickness is 1½ times the lateral spacing, a value of the lateral value at the distance of the lateral spacing below the top of the bed plus two-thirds the maximum lateral value is equal to true resistivity.

Conditions:
Short normal $R_{sn}/R_m < 50$
Lateral $e = 1.5AO$
Response:
Lateral (see Fig. 9-49*b*)

4. When the ratio between the resistivity values shown by the short normal and by the mud is less than 50 and when bed thickness is 1.3 times the lateral spacing, the maximum resistivity of the lateral device is equal to true resistivity.

Conditions:
Short normal $R_{sn}/R_m < 50$
Lateral $e = 1.3AO$
Response:
Lateral $R_{max} = R_t$ (see Fig. 9-49*c*)

For conditions not included above, resistivity-departure curves can be used to determine true resistivity if information is not available from more suitable devices.

Summary. Normal and lateral devices give excellent results in determining porosities in low- to medium-resistive formations of great thickness, if the mud is not contaminated with salt.

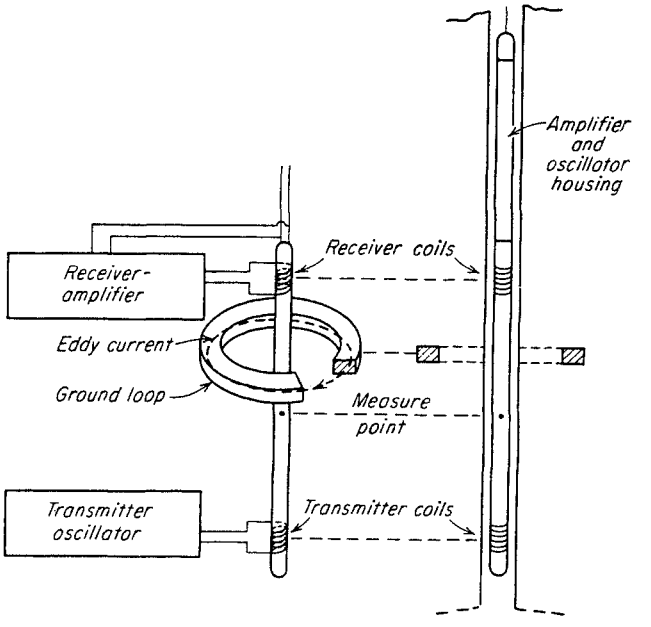

Fig. 9-50. Induction-log equipment. (9-136, *Courtesy Schlumberger Well Surveying Corp.*)

Induction Logging

The induction-logging device was developed in an attempt to overcome some of the difficulties found in determining true resistivity of formations. Figure 9-50 is a schematic diagram of an induction logging device. Alternating current is applied to the transmitter coils. This current sets up an alternating magnetic field around the coil, and the magnetic field induces electric "Foucault" currents in conductive formations. These electric currents, which are proportional to the conductivity of the formation, also develop their own alternating magnetic fields, which in turn induce a current in the receiver coils. This latter current is amplified, rectified, and sent to the surface to be recorded.

In addition to the two coils just described, additional or auxiliary coils are included and so operated as to minimize the effects of bore-hole mud and adjacent formations. These auxiliary coils focus the generated magnetic field on the bed opposite the device instead of permitting the field to fan out radially in all directions.

The distance between the two main coils is termed "spacing." Depth measurement is taken at a point midway between the main coils. Since there is no need for an electrical contact, induction logs may also be run in empty holes or with oil-base mud in the hole.

The signal of induction logs is proportional to the conductivity of the medium surrounding the device and is recorded as conductivity at the surface. As stated previously, conductivity is the reciprocal of resistivity, which is also recorded, for comparison with other logs.

Interpretation. The apparent conductivity recorded by the instrument is the result of the combined effects of the bore hole, invaded zone, uncontaminated zone, and adjacent formations. The geometrical locations of each of these regions, as well as their conductivities, determine the reading obtained. Since resistivity is the reciprocal of conductivity, these factors may be related by the following equation.

$$\frac{1}{R_a} = \frac{G_m}{R_m} + \frac{G_i}{R_i} + \frac{G_t}{R_t} + \frac{G_s}{R_s} \qquad (9\text{-}10)$$

where R_a = average resistivity
G_m = geometrical factor for mud column
G_i = geometrical factor for invaded zone
G_t = geometrical factor for uncontaminated zone
G_s = geometrical factor for adjacent formations

and where $G_m + G_i + G_t + G_s = 1 \qquad (9\text{-}11)$

Geometrical Factors. Geometrical factors are the result of two special considerations: a set of concen-

tric cylinders about the bore hole and sets of essentially horizontal beds of formations. The concentric cylinders are the mud column, the invaded zone, and the uncontaminated zone. Geometrical factors for various-diameter cylinders of infinite height are shown in Fig. 9-52 for two induction-log devices with spacings of 27 in. and 40 in. These were computed by Doll (9-96).

Curves show that the effect of the bore hole is negligible if it is less than 10 in. in diameter. In practice, however, this is true only if mud resistivity is greater than 0.5 ohm-meter, for muds of lower resistivities or higher conductivities become major factors in the equation even if G_m is small.

Figure 9-51 gives the geometrical factors of 27 in. and 40 in. spacing for horizontal conductive beds surrounding the bed, when the device is in the center of the formation. When bed thickness is twice the device spacing, surrounding beds do not affect the reading obtained. This figure may be used to determine the G_s to be used in Eq. (9-10). Other geometrical factors may be obtained from Fig. 9-52, since the geometry of the rest of the system may be considered as being a series of concentric cylinders. However, to accomplish this, diameter of the invaded zone must be known. Also, resistance of the invaded zone must be determined in order to determine R_t by Eqs. (9-10) and (9-11). For these reasons, the induction log is used in combination with other logs. The most useful of these combinations includes the laterolog and will be discussed following the discussion of the laterolog.

Formation Boundaries. When the device is located at a bed boundary, half of the reading results from the conductivity of one formation and the other half from the other formation, as shown by the equation presented by Doll (9-96).

$$\frac{1}{R_b} = \frac{0.5}{R_a} + \frac{0.5}{R_s} \qquad (9\text{-}11a)$$

Here R_b is the resistivity at the bed boundary, and R_a and R_s are the resistivities read at the centers of the two beds under consideration.

Effect of Mud Column. Fresh-water muds with resistivities greater than 0.5 ohm-meter in bore holes of normal diameter contribute very little to readings obtained from induction-logging devices. However, if the bore-hole diameter has been enlarged by caving, the contribution could be considerable. If mud resistivity is less than 0.5 ohm-meter, as it is for salt-contaminated muds, the mud column acts essentially as a shield, masking the effects of the formations themselves.

Since induction-logging devices have no electrodes and no electrical connections with or through mud,

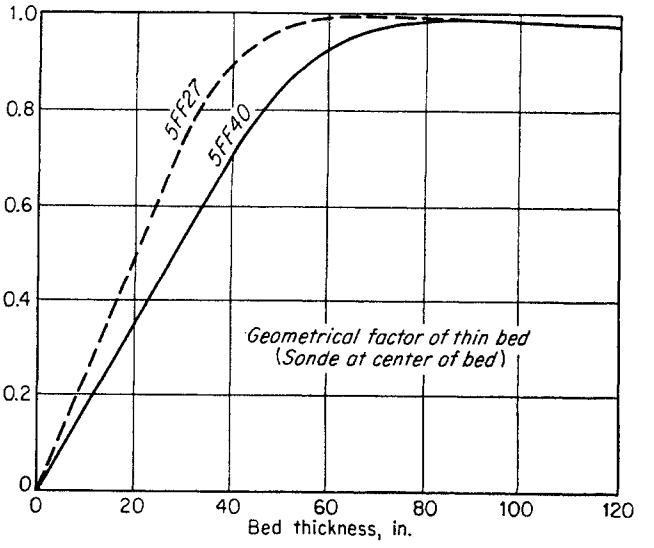

Fig. 9-51. Geometrical factor of thin bed. (9-136, *Courtesy Schlumberger Well Surveying Corp.*)

this type of log may run in an empty hole or in one containing oil-base mud. However, casing in the well would shield the device completely.

Effect of Invasion. As stated above, induction-log readings may be corrected for invasion effect if diameter and resistivity of the invaded zone are known. The problem of determining resistivity of the invaded zone is very difficult if penetration has been great. First, the entering mud filtrate not only displaces oil, but also displaces original connate water. In deeply invaded zones three distinct areas develop: (1) the area nearest the bore hole, which has a water saturation of residual mud filtrate and, if oil or gas is present, a hydrocarbon saturation; (2) the middle area, which has a residual hydrocarbon saturation and

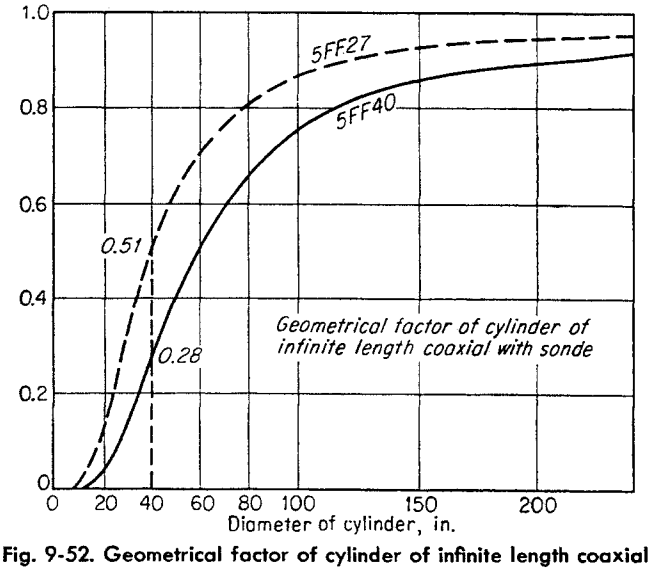

Fig. 9-52. Geometrical factor of cylinder of infinite length coaxial with sonde. (9-136, *Courtesy Schlumberger Well Surveying Corp.*)

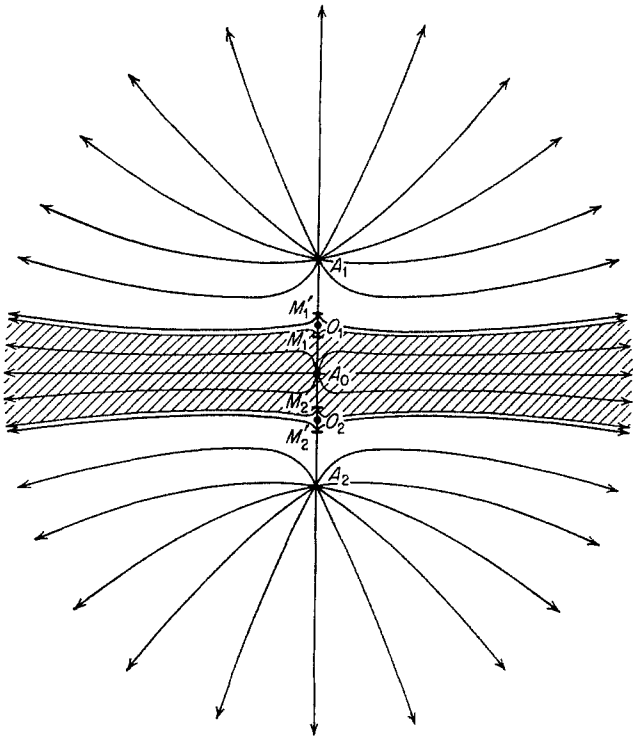

Fig. 9-53. Laterolog. (9-136, Courtesy Schlumberger Well Surveying Corp.)

a water saturation comparable to those of the first area but where the water is connate water; and (3) the last area, which contains a transition zone into the undisturbed zone.

The first area contributes little to the reading obtained in induction logging if the invaded zone is not too deep and if mud-filtrate resistivity is greater than 0.5 ohm-meter. However, with a mud filtrate of lower resistivity, conductivity of the zone may be high enough to act as a shield and mask effects of the undisturbed zone. The second area is of most importance since it contains only residual oil, the remaining fluid being connate water, which normally contains a large quantity of dissolved salts and has very low resistivity. If the formation is deeply invaded, all induced current will circulate in this second area of high conductivity. Thus, the undisturbed region will be shielded from effects of the device. For this reason, if muds of high water loss are used, the induction log should be run as soon as possible after the drilling of the formation.

Laterolog

The advantage of a measuring instrument that will focus on and penetrate deeply into the formation is apparent from the foregoing discussion. The laterolog is such an instrument. Figure 9-53 shows modification of the laterolog and distribution of current lines around it in a homogeneous medium, as described by

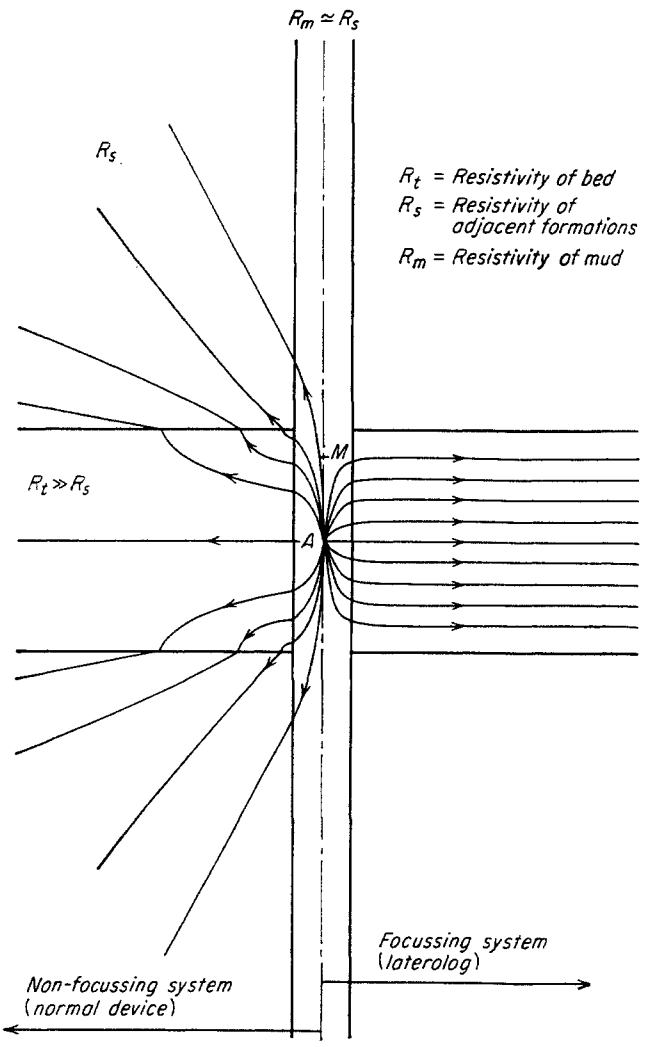

Fig. 9-54. Laterolog and nonfocusing current distributions. (9-136, Courtesy Schlumberger Well Surveying Corp.)

Doll (9-99). A_0 is the central-current electrode, which operates similarly to those in more conventional devices. A_1 and A_2 are a pair of auxiliary-current electrodes which are connected together. M_1, M_2 and M_1', M_2' are two pairs of measuring electrodes.

A controlled secondary current of the same polarity that supplied the central electrode is furnished to the auxiliary-current electrodes A_1 and A_2 so that the potential difference between electrodes M_1, M_2 and M_1', M_2' is maintained near zero. Doll (9-99) shows that the effect of the current supplied to the auxiliary electrodes A_1 and A_2 is to force current emitted from the central electrode to be focused on or flow into the formation opposite the device, as illustrated in Fig. 9-54. Figure 9-54 also shows the pattern formed by current-flow lines established by the laterolog. The instrument measures a potential at one of the M electrodes, interprets this measurement as resistivity, and records the result.

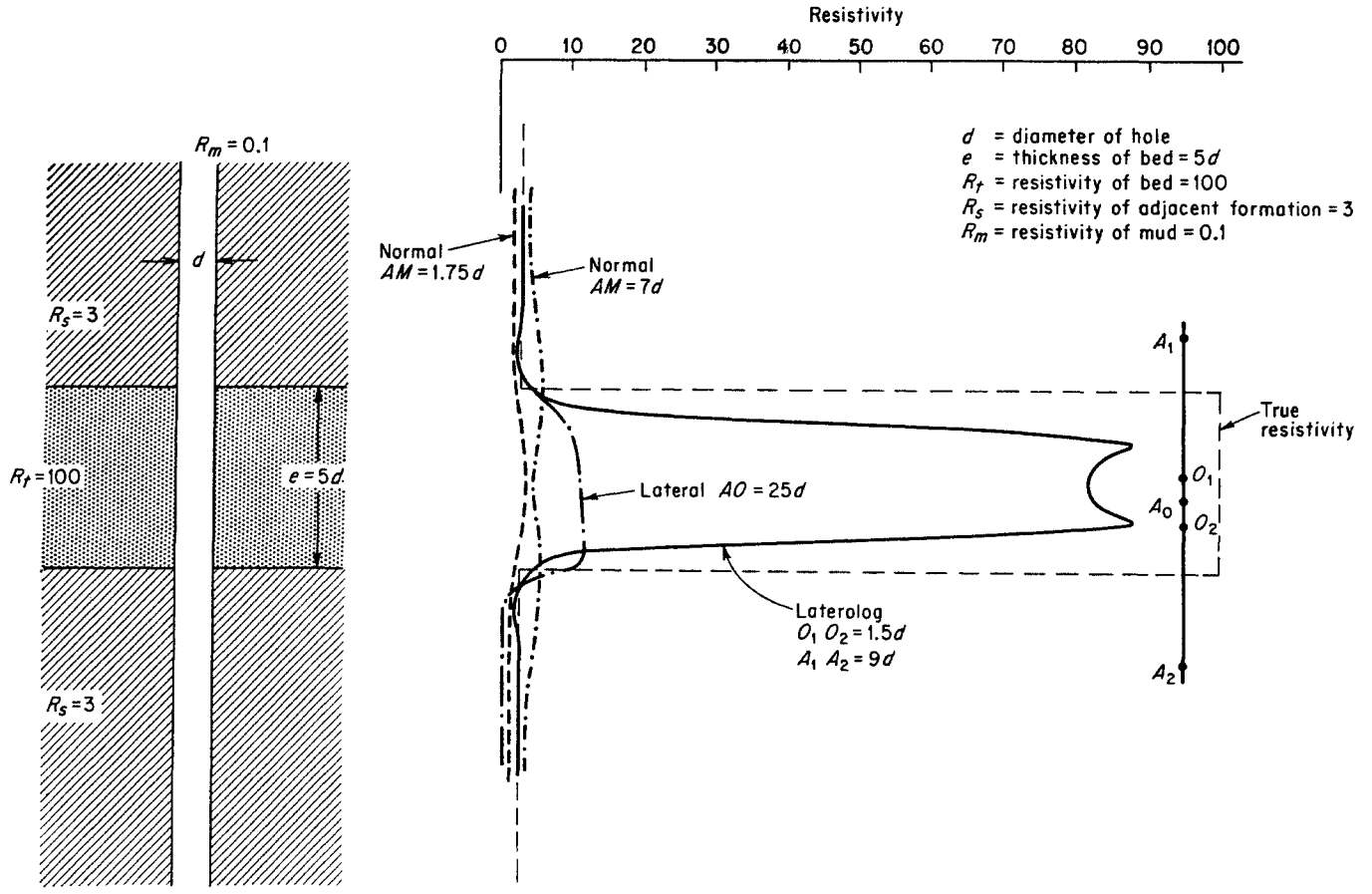

Fig. 9-54a. Response of laterolog and conventional devices. (*Courtesy Schlumberger Well Surveying Corp.*)

Effect of Bed Thickness. Since the laterolog focuses current on the formation and prevents it from spreading out, thin beds are delineated much better than by normal or lateral devices. Doll illustrates this in Fig. 9-54. The response of the instrument, as indicated by Doll (9-99), is shown in Fig. 9-54*a* for a thin noninvaded zone. This illustration also shows curves obtained with conventional short-normal, long-normal, and lateral devices, which respond hardly at all to these conditions. Boundaries are sharply indicated by the laterolog; however, bed thickness indicated is smaller than actual bed thickness by about the spacing of the device. The apparent bed resistivity is about 80 per cent of the true resistivity. If resistivity of adjacent beds is greater than resistivity of the bed opposite the device and if the bed is thicker than 4 ft, resistivity measured is equal to true bed resistivity. Therefore, when bed thickness is greater than 4 ft, laterolog value is usually considered equal to true resistivity, provided the bed is not deeply invaded.

Effect of Invaded Zone. The focusing feature of the instrument causes current used in measurement to flow horizontally and radially through the invaded zone, thus minimizing its effect on measurement. In a deeply invaded zone this effect can be computed, provided the resistivity and diameter of this zone can

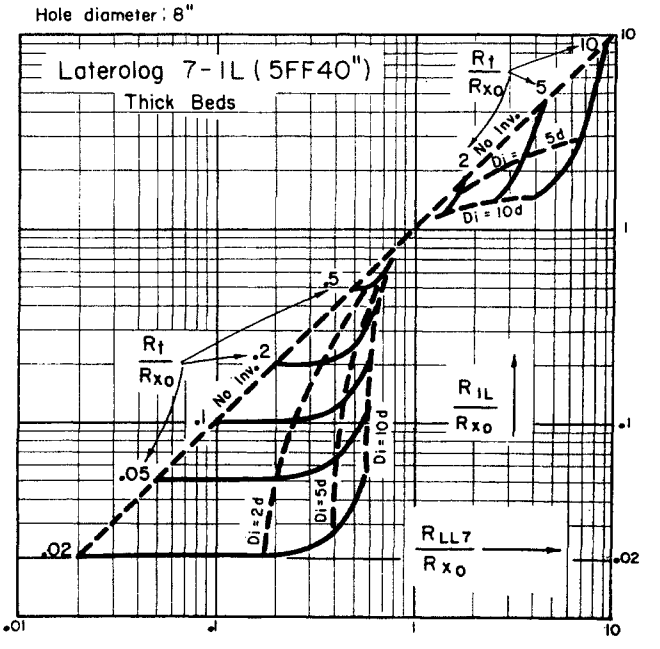

Fig. 9-55. Combination of induction and laterologs. (9-136, *Courtesy Schlumberger Well Surveying Corp.*)

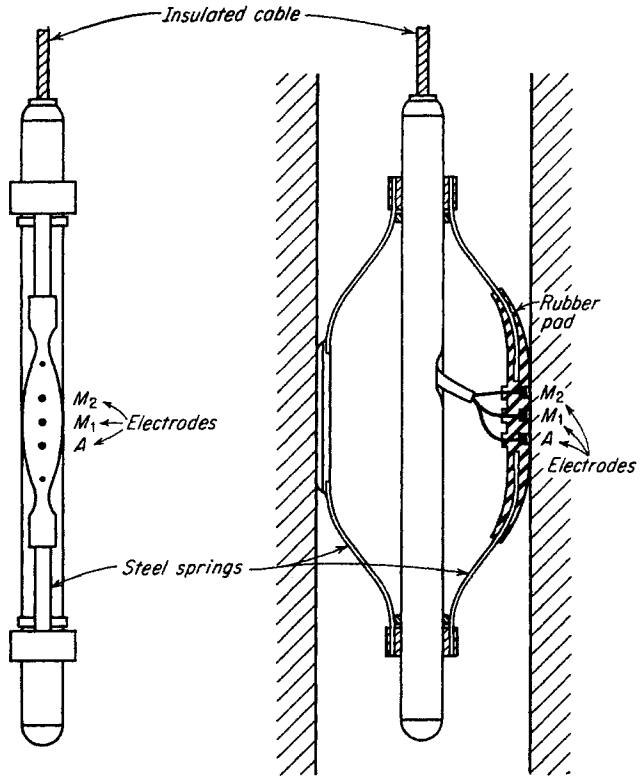

Fig. 9-56. Microlog sonde. (9-136, Courtesy Schlumberger Well Surveying Corp.)

be eliminated from the calculations by using the laterolog in combination with the induction log.

Effect of Mud. Since current is forced to flow directly from the instrument into the formation, it cannot be short-circuited through low-resistive or highly conductive mud to the measuring electrode. For this reason the laterolog is the only device that can be used where mud has been contaminated with salt.

Combination of Induction and Laterologs

Since both induction and laterolog devices contain focusing features, the same environmental conditions affect the two instruments if their spacings are equal. Current-flow lines produced in the formation by the induction device circulate in loops which cross at the current-flow paths produced by the laterolog. Therefore, the two measurements are not equally affected by mud, diameter of bore hole, invaded zone, etc., and values obtained complement each other. Where one device is ineffective, the other is useful. When measurements from these two devices are available, Fig. 9-55 is used to determine true resistivity of formation. The value for $R_{x,0}$, resistivity of flushed zone near bore holes, may be determined from a microlog or a microlaterolog, which are discussed immediately below.

Micrologs

The desire to delineate permeable and porous formations in greater detail, especially in hard rocks, led to development of the microlog, shown schematically in Fig. 9-56. It consists of three electrodes in a rubber pad mounted on a spring arm which presses the pad against the bore-hole wall. Current is supplied to one electrode A; the potential difference between the other two electrodes M_1 and M_2 is measured, converted to resistivity, and recorded as a function of depth to form the microinverse curve. Potential between electrode M_2 and the surface is treated similarly to form the micronormal curve. Separation of the two spring arms is used to determine bore-hole diameter and is recorded as the microcaliper curve. In operation the microlog sonde is lowered into the hole with the spring arms collapsed. Mud resistivity is then measured and recorded as a function of depth (since these measurements are very sensitive to mud resistivity). After the desired depth is reached, the spring arms are released, and microinverse, micronormal, and microcaliper curves are recorded as the sonde is withdrawn from the hole.

The formations and the rubber pad shield the electrodes from the short-circuiting effect of the mud column, since the electrodes are pressed against the hole. The electrode arrangement is approximately the same as that of closely spaced normal and lateral devices, and the general principles previously discussed therefore apply. The radii of investigation of both microinverse and micronormal curves are very small; that of the microinverse is the smaller. The position and spacing of these electrodes make it possible to measure the effects of a small volume which includes mud cake on the side of the hole, and approximately a 3-in. penetration into the formation. Resistivity of the mud cake is usually measured at surface conditions by forming a cake in mud-filter-loss equipment with a sample of the mud; the resistivity of the mud is also measured, along with the mud cake and the filtrate. With these values corrected for temperature and with the microlog reading, thickness of the mud cake can be determined, since the microinverse curve with the smaller radius of investigation includes more of the mud cake in its value than does the micronormal curve. The correlation of these values, presented by Doll (9-97), is shown in Fig. 9-57. The presence of the mud cake smooths out the readings, since it covers drill-hole irregularities. The type of formation where no mud cake has formed produces microlog readings that change sharply and frequently and give a ragged curve, for bore-hole irregularities frequently allow mud to remain between the pad and the formations. Mud-cake thickness can also be estimated from the microcaliper curve and drill-hole diameter.

Invaded Zone. A microlog is effective in determining resistivity of the flushed-out region of a deeply

invaded formation. In this case, the formation investigated by the microlog contains only the region, immediately surrounding the bore hole, that has been completely flushed by the invading mud filtrate. The fluids contained in this region are mud filtrate and/or residual oil. Usually mud-filtrate resistivity at formation temperatures can be determined more accurately than formation-water resistivity estimated from the SP curve. Thus, the formation factor (the ratio of water resistivity to resistivity of rock saturated with water) can be determined using microlog curves.

Where oil or gas is present, residual-hydrocarbon content must be taken into account; usually a value of 20 per cent can be used without introducing appreciable error. The formulas (9-4) and (9-6) are used in computing formation factor and porosity. The true resistivity of the flushed region used in these computations may be estimated from the microlog curves and nomographs presented in Figs. 9-58 and 9-59. Interpretations are shown for two companies that employ

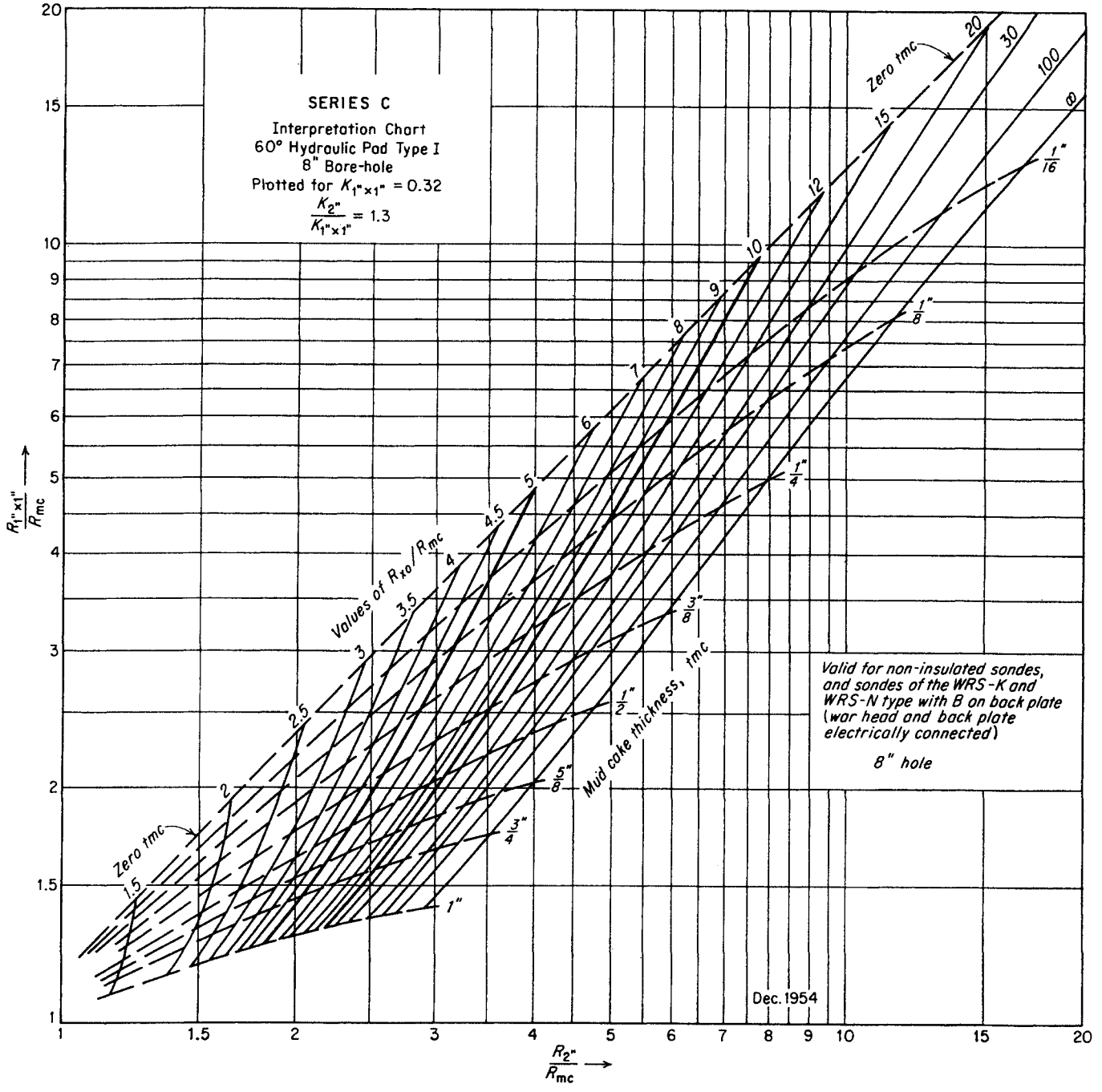

Fig. 9-57. Microlog interpretation. (9-136, Courtesy Schlumberger Well Surveying Corp.)

NOMOGRAPHIC "MICROLOG" CHART — HYDRAULIC PAD

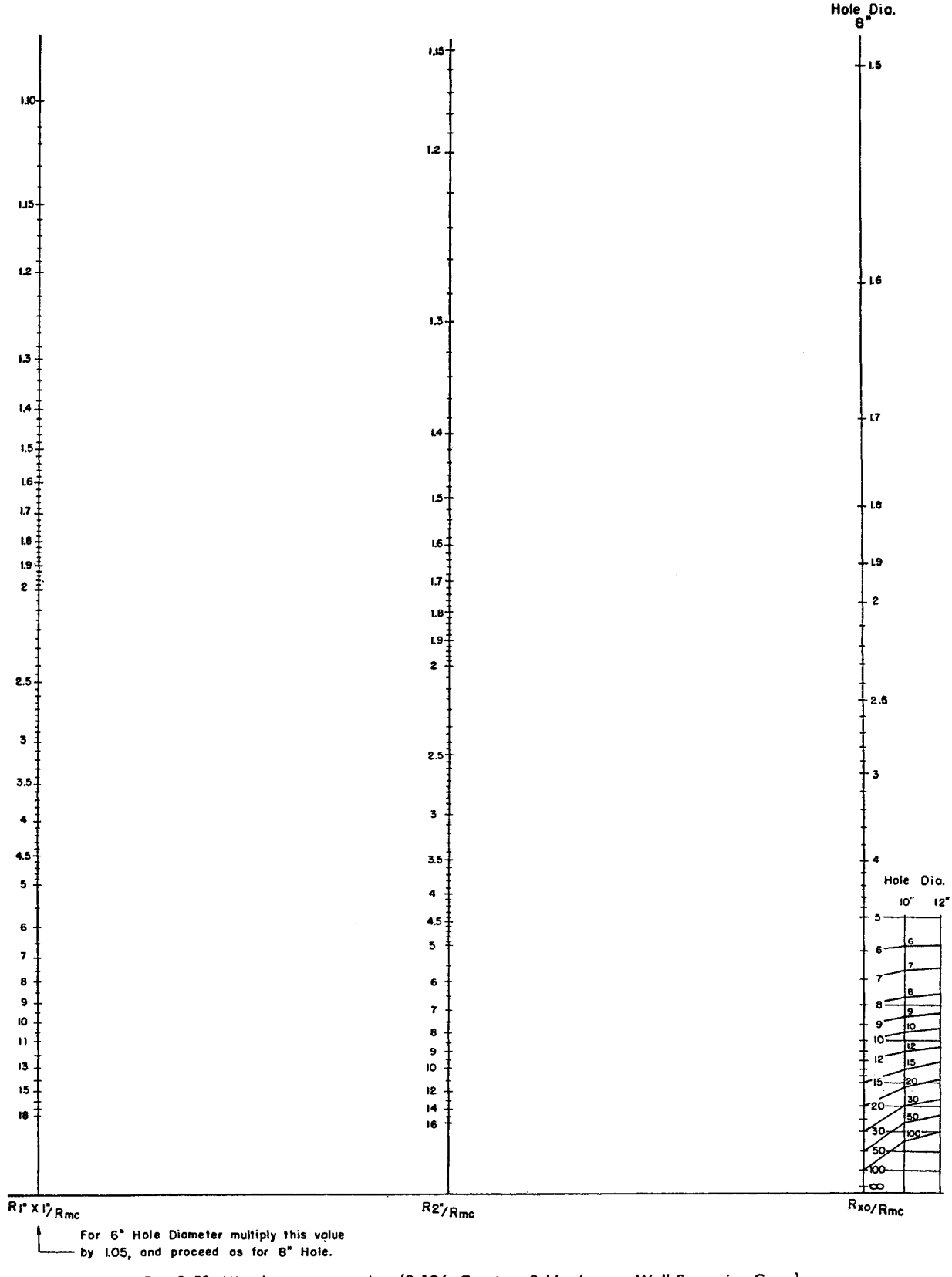

Fig. 9-58. Microlog nomograph. (9-136, *Courtesy Schlumberger Well Surveying Corp.*)

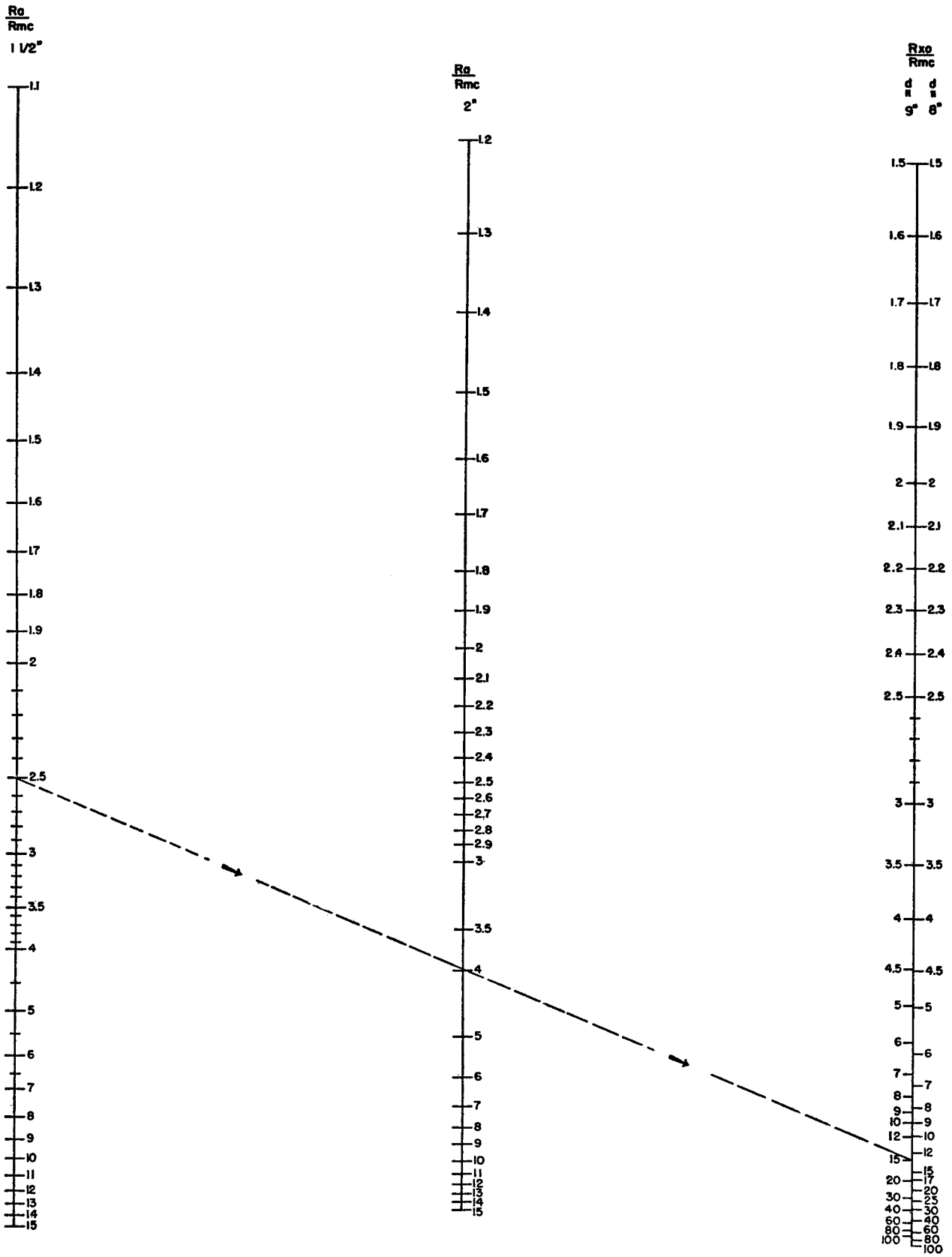

Fig. 9-59. Microlog nomograph. (*Courtesy Halliburton Electrical Well Services.*)

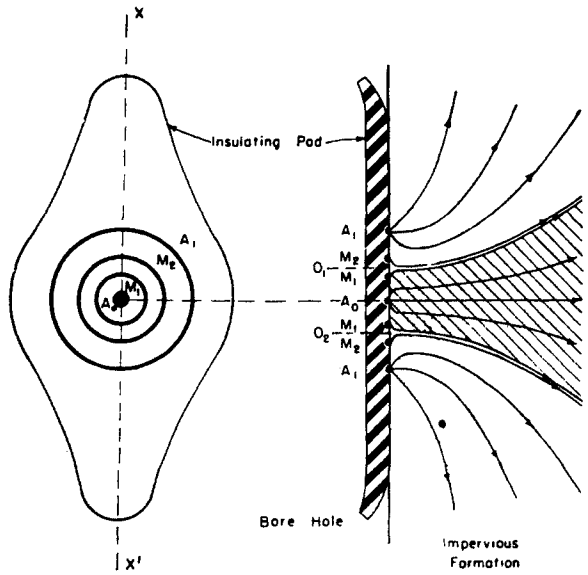

Fig. 9-60. Microlaterolog sonde. (9-136, *Courtesy Schlumberger Well Surveying Corp.*)

essentially the same devices. Differences indicated in Figs. 9-58 and 9-59 are the result of construction and interpretation details.

In case of deep invasion, the mud cake usually has a lower resistivity than does the flushed region, which results in a lower reading from the microinverse than from the micronormal curve (which has a greater radius of investigation). Under these conditions,

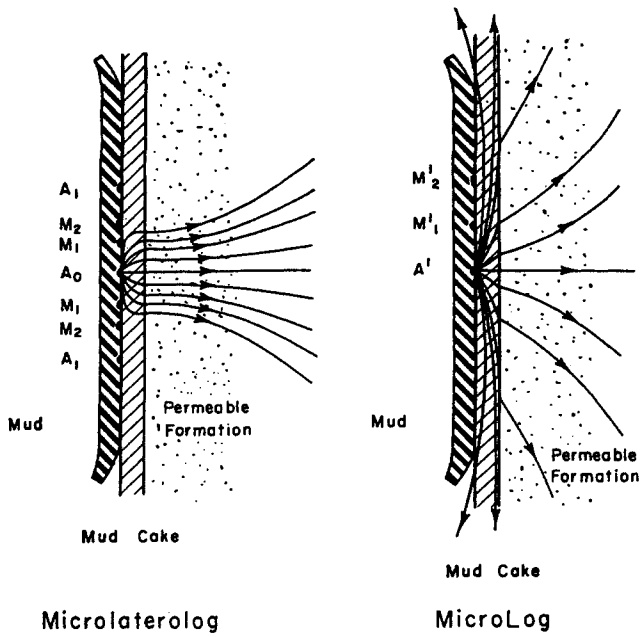

Fig. 9-61. Current distribution for microlaterolog and microlog. (9-136, *Courtesy Schlumberger Well Surveying Corp.*)

separation of the two curves is called positive and is taken as a qualitative indication of porous and permeable beds (Doll, 9-97).

In case of a shallow invasion, mud cakes are thin, and resistivity of the formation volume investigated is not greatly affected by mud-filtrate invasion. This is the case where capillary forces are low. When the bed is saturated with salt or low-resistivity water, separation of the microlog is negative, for the mud cake will usually be more resistive than the formation. However, when formations contain hydrocarbons and invasion is shallow, the formation investigated is usually more resistive than the mud cake and a positive separation is obtained, again qualitatively indicating porosity and permeability. Where invasion is shallow the microlog is not very effective in quantitative estimations.

Cavings. The presence of cavings complicates microlog interpretation. Where caving is extensive, the electrodes are not pressed against the formation. It is possible that only the mud is within the volume investigated, in which case both curves would yield an estimate of mud resistivity. However, if caving is of such magnitude that the electrodes are not pressed against the formation and some of the formation is included in the measurement, the separation will be positive, for mud is usually less resistive than formation. This could cause a dense zone to be interpreted as a permeable zone. The microcaliper curve is very useful in eliminating this error.

Formation Boundaries. Since spacing is very small, microlog curves change sharply at bed boundaries. The microlog is therefore extremely useful in determining bed thickness.

Microlaterolog

When porosity is less than 15 per cent, formation resistivity is so high that most of the current emitted by a microlog circulates in the mud cake, which has a relatively low resistance. Under these conditions, microlog sensitivity is decreased to a point where it is ineffective in determining resistivity of the flushed region. In order to overcome this condition, a focusing log with small spacing was developed. Since it employs the same principles as the laterolog, it is called a microlaterolog. A schematic diagram of the tool, as presented by Doll (9-100), is shown in Fig. 9-60. The instrument consists of the insulated pad shown in Fig. 9-60 mounted on a spring arm, as used in the microlog. Mounted in the insulated pad is a central-point electrode A_0 surrounded by three concentric-ring electrodes M_1, M_2, and A_1. A secondary current of the same polarity is supplied to the outside concentric-ring electrode A_1 in such a way as to maintain the potential difference between the two inner

concentric-ring electrodes near *O*, as in the laterolog. The resulting current distribution, presented by Doll, is shown in Fig. 9-61. Doll also compares the distribution of measuring currents for the microlaterolog and the microlog (Fig. 9-61). The measuring current is forced to flow directly across the mud cake into the formation and is not permitted to spread out, thus decreasing its effect on the reading. The spacing of the electrodes is such that about three inches of the material directly in front of the pad is investigated.

Tight Formations and Shales. When the tool is opposite a tight formation or shale, the presence of a thin film of mud or a thin mud cake does not affect the reading obtained, so the instrument records resistivity of the bed. However, if there has been extensive caving (as occurs in shales) the spring arms will not be able to maintain contact between formation and pad. Under these conditions, the volume affecting the reading may be only mud, or partly mud and partly formation. Thus, the reading will be an "average" of the resistivities of the volume affecting the reading. The presence of these conditions can be determined with the aid of the microcaliper and SP curves.

Porous and Permeable Sections. In tightly permeable sections capillary forces are large, resulting in deep invasion of these sections. In these conditions the microlaterolog is especially effective in determining flushed-region resistivity and, thus, formation factor and porosity. If mud-cake thickness is less than $\frac{3}{8}$ in., Doll (9-97) shows that the microlog value is equal to resistivity of the flushed region. When the mud cake is thicker, another measurement is needed to correct the reading for the effect of the mud cake. Doll correlates the microlaterolog information with the microinverse data (shown in Fig. 9-62) in order to determine flushed-region resistivity in the presence of

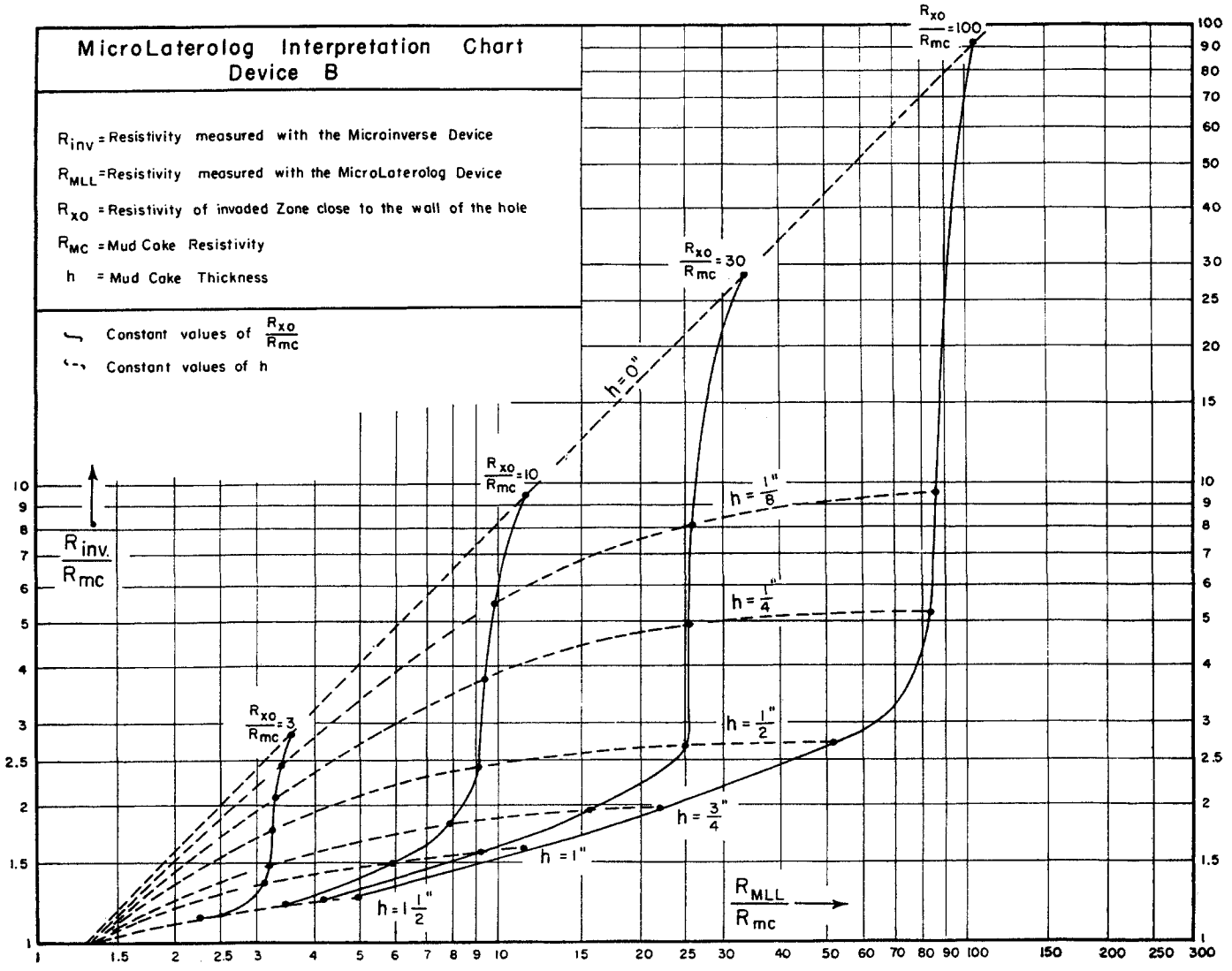

Fig. 9-62. Microlaterolog interpretation chart. (*Doll, 9-97. Courtesy AIME.*)

thick mud cakes. The microlaterolog is effective in determining resistivity of the flushed region when mud is contaminated with salt, for this type of mud usually produces thin cakes and deeply invaded regions.

Interpretations in Shaly Sands

The presence of shale, either interbedded or disbursed in sand, affects formation resistivity. Since it is a conductive solvent, any shale present must be taken into account in computing porosity and water saturation from electrical-log data.

Poupon, Loy, and Tixier (9-129) study the effects of shale in sand formations on both formation resistivity and generated SP. They employ laboratory and field data as well as theoretical considerations. Their data, as well as those of Doll (9-98), indicate that the SP value is reduced by shale. Poupon et al. use the term "pseudostatic self-potential" (PSP) to represent the value of self-potential in an infinitely thick section of shaly sand. In practice, the measured value of a shaly sand may be corrected for the effect of adjacent beds by using Fig. 9-43, which is used also for clean sands; the static self-potential is the value that would have been obtained if the shale had been a bed of clean sand.

Poupon et al. also present data showing that PSP is lowered even further by the presence of oil in shaly sand. Using these data and theoretical equations for SP, the correlation shown in Fig. 9-63 for determining water saturation in shaly sands was developed. Data needed to obtain water saturation are flushed-region resistivity, undisturbed-region or true resistivity, and static self-potential for determinations of the ratio of mud-rate resistivity to formation resistivity. The ratio of mud-filtrate resistivity to formation-water resistivity is preferred to the static self-potential. However, when resistivity of formation water is not available, static self-potential of clean sands in the locality may be used in the interpretation.

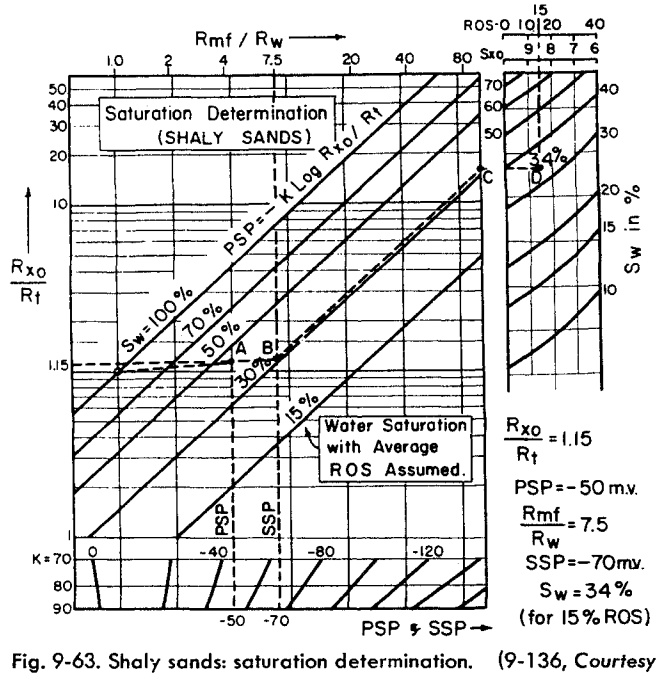

Fig. 9-63. Shaly sands: saturation determination. (9-136, *Courtesy Schlumberger Well Surveying Corp.*)

Poupon et al. further correlate their data (Fig. 9-64) so that porosity can be determined for shaly sands. Data used here are ratio of flushed-region resistivity to true resistivity, ratio of flushed-region resistivity to mud-filtrate resistivity, and ratio of pseudostatic to static self-potential. While these correlations leave much to be desired from the standpoint of rigorous development, they serve as excellent guides in interpretation of data for shaly sands.

RADIATION LOGGING

The first radiation log was run in 1935 (9-114) to determine natural radiation of formation traversed. This type of log was run as a commercial service in 1940 (9-110), and in 1941 commercial measurements of neutron-induced radiation were made available.

The procedure followed in obtaining these gamma-and-neutron-ray logs is similar to that used for electrical logs. The sonde containing the sensing device —a geiger or scintillation counter—is lowered into the bore hole on a measuring line containing conductors which transmit signals to the surface. At the surface these signals are received, modified, and recorded as a function of depth, using equipment mounted in a truck which contains also hoisting and depth-measuring equipment.

Rate Factor

In order to interpret radiation logs it is necessary to know effects of time, or "rate factors." These factors are important since radiation received and measured by the sensing device varies with time and is not constant, as are electrical-log signals. This variation in radiation occurs because the reactions that produce radiation are governed by the laws of probability. In other words, the amount of radiation produced in one instant may be very high and in the next instant very low, but the average over a period of time is constant for the times under consideration here. Rate meters that record radiation reaching the sensing device integrate, or average, the receiving rate over a period of time. The longer the time period the more nearly will the value read approximate the true average rate. However, in the meantime, the sensing device is being raised continuously; so the reading is affected

not only by radiation at the depth recorded, but also by some radiation received at depths below the depth being recorded. This carry-over or lag displaces the curve upward. The amount of displacement depends on two things: the time constant used in the counting-rate instrument, and the logging speed. Lengthy time constants and fast logging speeds yield high displacements. Also, radiation comes from all directions, not simply from the direction perpendicular to the bore hole, and thus radiation received at any given instant does not originate from just one depth but from a range of several feet. The amount received from any one depth decreases as distance from the instrument increases.

Gamma-ray Log

The gamma-ray log measures natural radioactivity of formations penetrated by the bore hole. Commercial equipment in current use does not distinguish among the natural sources of radiation: potassium, thorium, and uranium-radium series. However, equipment is now being developed and tested to determine not only the amount of radiation, but the source. This will allow even greater ability to determine lithology of beds penetrated.

At present, the gamma-ray log is used principally as a qualitative manifestation of lithology. Highly radioactive formations are most often sandstones. However, these qualitative considerations do not always hold. A shale saturated with water that contained a large amount of dissolved radioactive potassium would be a highly radioactive formation and, given insufficient knowledge of the geology of the area, might be misinterpreted as a sandstone. In special cases (9-132) where the oil-field formation is highly radioactive, the gamma-ray log is used to determine water-oil content, since the presence of oil decreases the radioactivity of a formation.

Neutron and Neutron–gamma-ray Logs

Neutron or neutron–gamma-ray logs use the same type of instrumentation as gamma-ray logs, except that the sonde contains a source of high-energy neutrons, which is shielded and placed some distance from the radiation-sensing element. The sensing element is adjusted to measure either low-energy neutrons resulting from bombardment of the formation with high-energy neutrons, or gamma rays produced by the capture of low-energy neutrons resulting from bombardment. In the first case, a neutron log is recorded and, in the second, a neutron–gamma-ray log is recorded. Actually both methods measure the resulting concentration of low-energy or thermal neutrons. Thus, any factors that decrease neutron

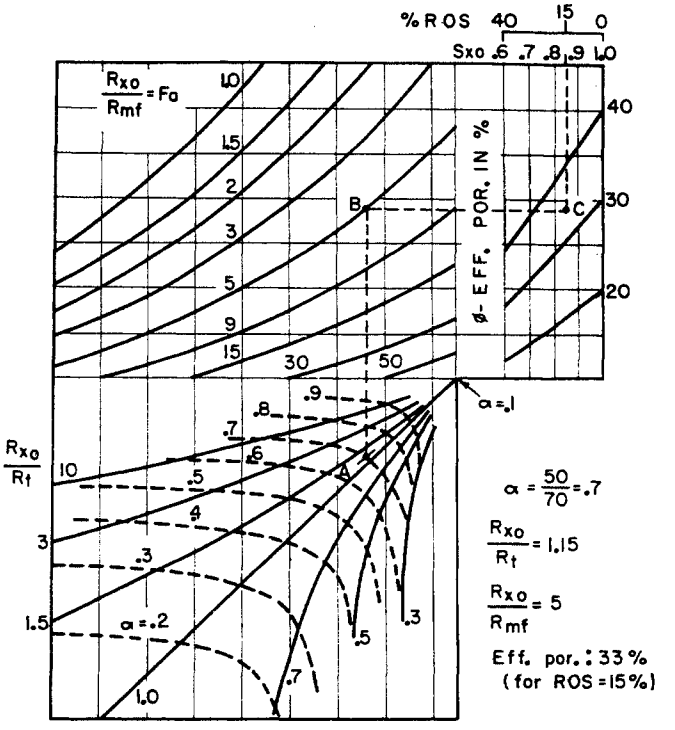

Fig. 9-64. Shaly sands: porosity determination. (9-136, *Courtesy Schlumberger Well Surveying Corp.*)

energy control values obtained in this type of logging.

Energy Loss of Neutrons. A high-energy neutron loses energy by colliding with nuclei of elements composing the formation. When this happens, chemical combination of elements into molecules is not a factor. There are two factors that must be considered, however, in determining loss of energy: the effect of collision with the nucleus of any element, and the probability of such collision, or the average number of collisions taking place over an interval with the nuclei of each element. Although the laws of classical mechanics are not strictly applicable to these phenomena, they do yield satisfactory results for our purposes. Thus, collision of two masses such as a neutron and a nucleus will result in redistribution of the kinetic energy of the two masses, depending on the angle at which they approach each other and upon the relative size of the masses.

In determining differences in energy-loss rate of high-velocity or high-energy neutrons, angle of approach is unimportant, but relative weight of the mass is important. Of the two masses, the neutron is traveling at a high velocity and the formation-element nucleus is relatively slow. In this situation, when a small mass "bounces off" the large mass, it maintains about the same speed or energy it had before the collision. However, when two equal masses collide while traveling at differing speeds, the collision may result in a complete energy exchange (head-on colli-

sion), a very limited energy exchange, or any degree of exchange ranging between these extremes. The probability is that equal masses will have the same velocity—and equal energy—after the collision.

The mass of most elements contained in a formation is greater than the neutron mass by a factor of at least 10. Collisions with these elements reduce energy of the high-velocity neutron very little. However, the presence of hydrogen changes this situation, for example, in a porous formation containing water and/or oil and gas. Hydrogen nuclei are very effective in reducing velocity of high-energy neutrons.

The other factor that affects the rate at which neutrons lose energy is the probability that collision will occur with any one element. Increasing the number of atoms of an element in a unit volume will increase probability of collision with that element. Also, the larger the nucleus in relation to a neutron, or the greater the "cross section," the greater the chance that collision will occur. A nucleus cross section for an element varies with the amount of neutron energy. Both concentration of various elements and constitution of their varying "cross section" are used by Tittman (9-144) to compute probability of collision with various elements in a water-saturated sand formation (Fig. 9-65).

Hydrogen is the most important factor causing a neutron to lose or dissipate energy. As neutrons scatter in all directions from the source, the average neutron energy at any given distance from the source will depend more on the amount of hydrogen present than on any other factor. Large concentration of hydrogen results in high loss of neutron energy close to the source. Eventually, average velocity of the neutron is decreased to the speed that a gas of equal mass would have at the same temperature, that is, the neutron reaches thermal energy. In this phase of its history, the neutron diffuses through the medium much as a gas would, until it is "captured."

Thermal-neutron Capture. A collision of a thermal neutron and a nucleus may yield two results. They may "bounce off" each other, or the neutron may be captured by the nucleus, thus producing one or more gamma rays. The latter result reduces the concentration of thermal neutrons. Therefore, the average life of a thermal neutron depends upon concentration and "capture power" of various elements present. In porous sand or in limestone saturated with water most neutrons are captured by hydrogen nuclei, thus producing a gamma ray. As the porosity decreases, "capture" by rock-matrix elements becomes important; however, this phenomenon usually occurs where porosity is too low to be commercially important.

The one other element besides hydrogen that must be considered is chlorine. Chlorine is usually present as the ion of a dissolved salt, and has a capture power approximately 100 times as strong as hydrogen. If mud filtrate contains dissolved chlorides above 30,000 ppm, the counting rate for the neutron log will be low and the counting rate for the neutron–gamma-ray log will be high. Chlorine reduces thermal-neutron concentration and neutron counting rate, and, since it emits two gamma rays for each thermal neutron it captures, it increases the gamma counting rate. The presence of chlorine ions in connate water does not affect either log when a flushed region exists, for mud filtrate displaces chloride in connate water to a point beyond the penetration obtained with these logs.

Interpretation. The total effect of these factors is to establish a thermal-neutron-concentration gradient around the high-energy-neutron source. In the absence of hydrogen, neutrons lose energy rather slowly and are not very efficiently captured; thus, high neutron and gamma-ray counts are obtained at relatively long distances from the source. In the area of interest here, a plot of logarithm of hydrogen concentration in a formation versus counting rate has been found to form a straight line (9-93, 9-105, 9-133, 9-138, 9-143). This fact has been used to calibrate various devices available. Since hydrogen concentration is

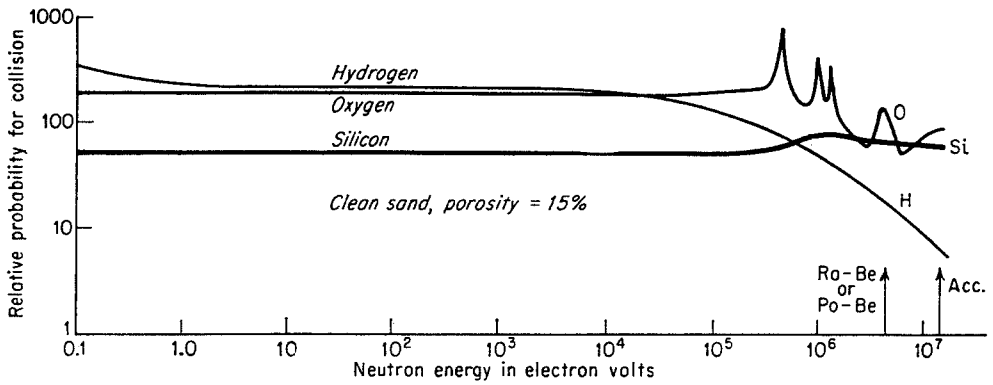

Fig. 9-65. Collision probability. (9-136, *Courtesy Schlumberger Well Surveying Corp.*)

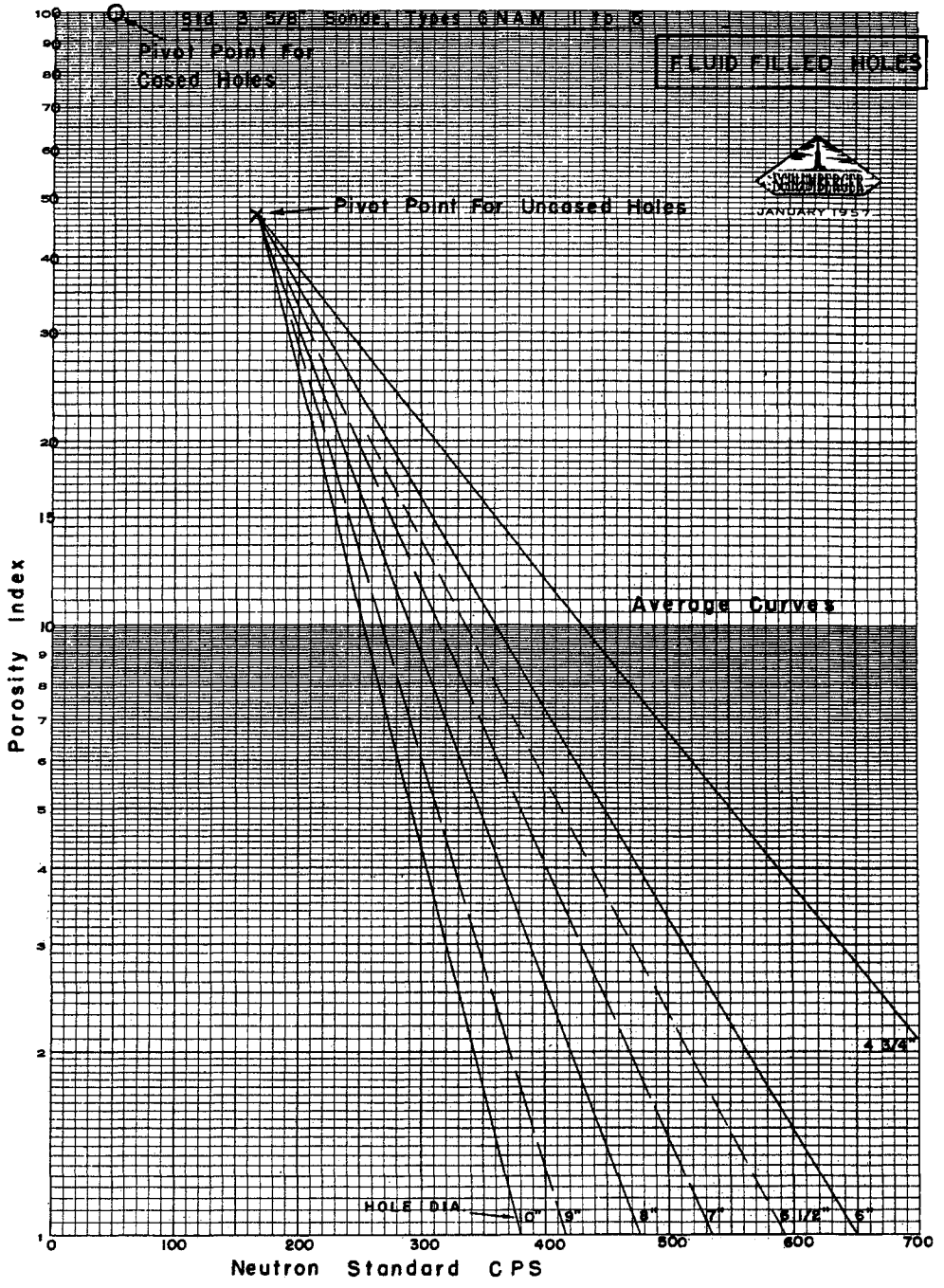

Fig. 9-66. Effect of bore-hole diameter. (9-136, *Courtesy Schlumberger Well Surveying Corp.*)

approximately the same for both water and oil, it is proportional to porosity except where large quantities of chemically bound water are present, such as in clay or shale. Thus, neutron or neutron–gamma-ray logs are effective instruments for determining porosity and formation factors.

The presence of mud that contains large amounts of hydrogen decreases not only the counting rate obtained but also the porosity sensitivity of the device by masking partially the effects of the formation (Fig. 9-66). The differences among the three lines obtained are due to the increased amount of mud surrounding the device in the larger-diameter holes. If the sonde is absolutely centered in the hole, the effect will be more pronounced. However, although nothing is done to guarantee that the sonde is against the hole

wall, it is usually assumed to be there. Also, the presence of dissolved chlorides in mud has the same effect as increasing the bore-hole diameter.

Casing reduces the counting rate but does not appreciably affect the sensitivity of the device. However, cement reduces both the counting rate and the sensitivity.

As illustrated in Fig. 9-66, a plot of the logarithm of hydrogen concentration, or porosity, versus counting rates results in approximately a straight line in the region of interest. For this reason, a calibration curve can be established from known field data in the locality. The calibration curve can then be modified to fit conditions of a given bore hole, by observing the reading obtained from a formation whose porosity is known to be 1 per cent or less. The counting rate observed is plotted against the logarithm of porosity (1, if porosity is less than 1 per cent), and the calibration curve is drawn by connecting this point with the region where the curves on Fig. 9-66 appear to converge at a porosity or hydrogen index of 40 per cent.

SUMMARY

Electrical and radiation logs can be used in stratigraphic studies, quantitative estimation of fluid content, and determination of porous and permeable zones.

The relation between self-potential and true-formation resistivities of zones affected and unaffected by drilling mud and the relation between porosity and water saturation are fairly well established. The difficulty in quantitative interpretation of logs lies in conversion of various readings, which are affected by a number of factors, to electrical properties of the formation alone. Combined readings from several devices surmount this problem in most cases and allow reliable quantitative estimates of porosity and fluid saturation to be made.

CHAPTER 10

Steady- and Unsteady-state Flow in Reservoirs

Flow through porous media in reservoirs may be treated as steady-state when conditions do not change with time or as unsteady-state when conditions do change with time. Pressure depletion of a gas field upon gas withdrawal is an unsteady-state phenomenon; however, under certain conditions, steady-state flow formulas find considerable use. Such conditions might include flow in areas adjacent to a producing well or flow from a well that is said to have become "stabilized."

Much of the material on steady- and unsteady-state flow is given in the two books by Muskat (1-11, 1-12). The works of Van Everdingen and Hurst (10-27), Aronofsky, Jenkins, et al. (10-1 to 10-5, 10-19, 10-20), Peaceman, Rachford, et al. (10-6, 10-14), and MacRoberts (10-21) serve, with Muskat, as a basis for the presentation here. Further contributions have been made by Chatas (10-7), Matthews, Brons, and Hazebroek (10-22), Cornell and Katz (2-42, 10-11), Janicek and Katz (10-18), and Warren (10-28).

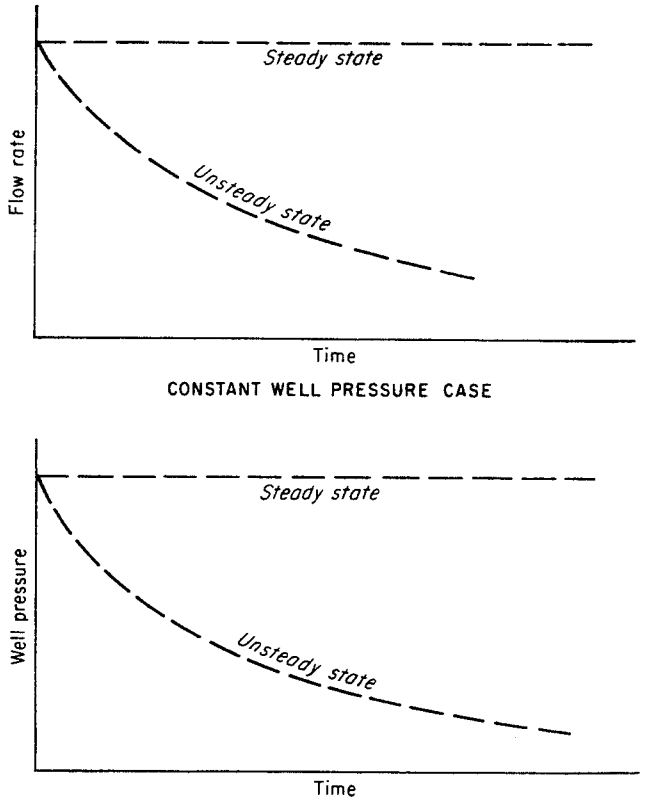

Fig. 10-2. Illustrations of steady and unsteady state.

Figure 10-1 illustrates a well producing liquid or gas either from a reservoir of limited extent or from one large enough to be considered infinite in extent. In either case, a change in pressure at the well will cause flow to occur radially in the producing formation to or from the well in the direction of lowest pressure.

Figure 10-2 shows the pressure and flow characteristics at the sand face in the well bore for steady- and unsteady-state production of fluid from wells that are controlled either to a constant flow rate or to a constant flowing pressure. High-permeability reservoirs approach the steady-state curve as a limiting case; low-permeability reservoirs show a greater de-

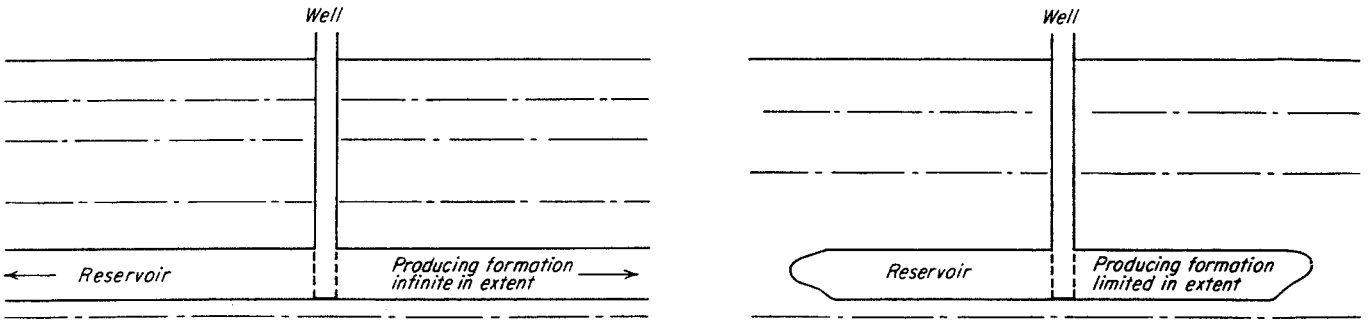

Fig. 10-1. Well producing from finite and infinite reservoirs.

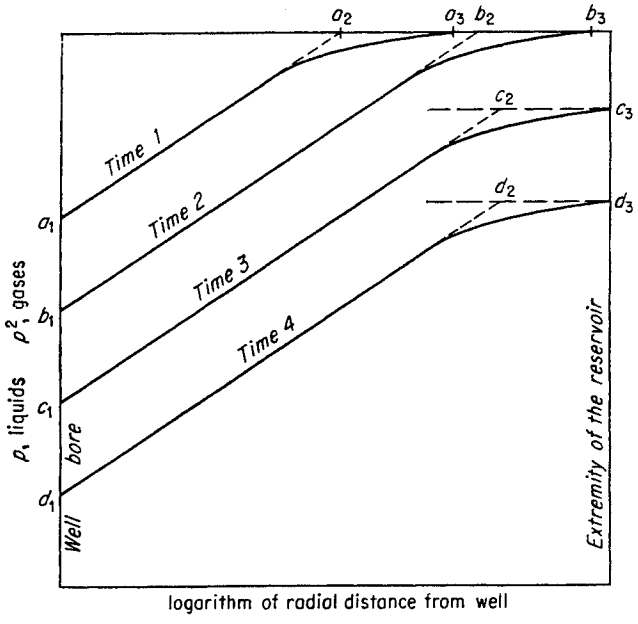

Fig. 10-3. Typical variation of pressure in a reservoir with time.

gree of unsteady-state behavior. Other reservoir characteristics, to be taken up later, are also important in determining the magnitude of unsteady-state effects.

The general behavior of unsteady-state pressure distributions in a reservoir producing from a single well at a constant production rate is given in Fig. 10-3. For steady-state flow the pressure gradient is a straight line when plotted as p* for liquids or p^2 for gases against a logarithmic distance scale. The unsteady-state pressure-distribution curve is essentially straight near the well, but leaves the straight line as shown to become tangent to the horizontal at the maximum reservoir pressure. The pressure gradient moves outward with time through the reservoir until the extremity of the reservoir is reached. At this point the reservoir pressures begin to decline uniformly, and the outward movement ceases.

First the steady-state flow formulas will be developed and then the unsteady-state flow formulas.

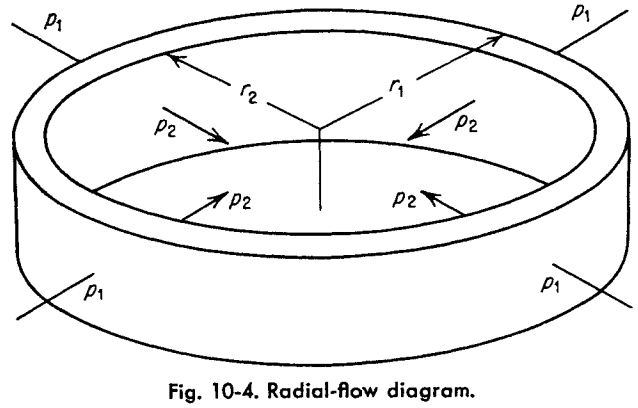

Fig. 10-4. Radial-flow diagram.

* Lower-case p is used for pressure in this chapter rather than capital P, since P is useful as a dimensionless value.

STEADY-STATE FLOW EQUATIONS

Steady-state flow equations are based on Darcy's law expressed in Eq. (2-1) for viscous flow. The equation is integrated for changing area to obtain radial flow. At high flow rates, turbulence becomes a factor and the radial-turbulent-flow formula needs to be used for reservoirs.

Radial Viscous Flow of Gas

Radial flow such as would be encountered in flow toward a producing well or away from an injection well is shown in Fig. 10-4. The area A of the flow path is a variable in radial flow that must be considered in the integration of Eq. (2-1). Let $A = 2\pi rh$, where r is radius in feet and h is formation thickness in feet. For radial flow of gas Eq. (2-1) becomes Eq. (10-1).

$$Q = \frac{0.0004476\pi hKp(\pm dp)\dagger}{zT\mu\, dr/r} \qquad (10\text{-}1)$$

The integrated radial-flow equation for constant values of K, T, h, μ, and z is

$$Q = \pm \frac{0.0007030hK(p_1^2 - p_2^2)\dagger}{zT\mu \ln (r_1/r_2)} \qquad (10\text{-}2)$$

The units for Eqs. (10-1) and (10-2) are:

h = sand thickness, ft
K = permeability, millidarcys
p = pressure, psia
z = compressibility factor
T = absolute flowing temperature, °R
μ = viscosity, centipoises
Q = gas flow rate measured at 14.7 psia and 60°F, Mcf/day

This set of units will be referred to hereafter as the "field units" for gas flow. The term ln (r_1/r_2) is the natural logarithm of the ratio of the radii measured from the center of the well bore. For gas flowing from a reservoir to a well, point 1 is out in the reservoir and point 2 is the sand face at the well bore. For gas injected into a well, point 1 is at the well bore and point 2 is out in the reservoir.

Illustrative Problem

Five thousand Mcf/day of 0.6 gravity natural gas, measured at 14.7 psia and 60°F, is being injected into one well of a con-

† The sign on dp is $-$ for injection of gas and $+$ for production from the reservoir. Note that during production $-dr$ is the increment of distance; also ln $(r_2/r_1) = -$ ln (r_1/r_2).

densate reservoir during a cycling operation. Reservoir data are:

h = 20 ft
K = 60 millidarcys
T = 186°F + 460 = 646°R
Well-bore radius r_w = 0.33 ft

The injection pressure in the well at the sand face is 2,300 psia. Calculate the pressure at a point in the formation 50 ft away from the center of the well, assuming steady-state, viscous, radial flow.

Solution

It is necessary to assume a mean pressure for finding the viscosity and compressibility factor. Assume p = 2,250 psia.

Pseudo p_c = 671 psia Pseudo p_r = 3.35
Pseudo T_c = 358°R Pseudo T_r = 1.803

z = 0.893 from Fig. 4-16
μ = 0.017 centipoise from Fig. 4-107

$$p^2 = 2{,}300^2 - \frac{5{,}000 \times 0.893 \times 646 \times 0.017 \times 5.01}{0.0007030 \times 20 \times 60}$$

p = 2,236 psia at 50 ft

Radial Viscous Flow of Liquid

The formula for radial viscous flow of liquid is found, like the formula for gases, to be Eq. (10-3).

$$Q = \frac{0.03976hK(p_1 - p_2)}{\mu \ln (r_1/r_2)} \qquad (10\text{-}3)$$

where Q = flow rate of liquid, cu ft/day (0.03976 becomes 0.007087 for flow rate, bbl/day)
h = formation thickness, ft
K = permeability, millidarcys
p = pressure, psia
μ = liquid viscosity, centipoises
r = radius, ft
subscript 1 refers to reservoir; 2, to well bore

Equations (10-2) and (10-3) are for the cases in which the well completely penetrates the producing strata. Muskat (1-12) has provided a chart (Fig. 10-5) for correcting the flow rate when the well partially penetrates the producing formation. In this chart Q/Q_0 is the production capacity of a partially penetrating well over the production capacity of a completely penetrating well. Solid curves are for well radius of ¼ ft, and dashed curves are for ½ ft. The external-boundary radius is 660 ft in all cases.

Turbulent Flow

The linear turbulent-flow formula [Eq. (2-14)] may be converted to field units and rearranged as follows (2-42):

$$\frac{p_1^2 - p_2^2}{L} = \frac{zT\mu Q}{0.0001119AK} + \frac{1.254 \times 10^{-10} zTGQ^2\beta}{A^2} \qquad (10\text{-}4)$$

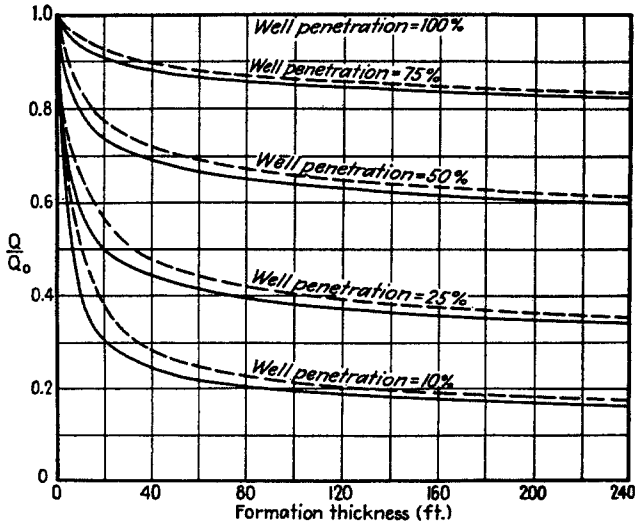

Fig. 10-5. Correction to flow for partially penetrating wells (*Muskat, 1-12. Courtesy McGraw-Hill Book Company, Inc.*)

Likewise, Eq. (2-11) may be converted to an expression involving cross-sectional area and quantity flowing followed by the integration for changing area to give the radial turbulent-flow formula for gases.

$$p_1^2 - p_2^2 = \frac{1{,}424\mu zTQ \ln (r_1/r_2)}{hK} + \frac{3.161 \times 10^{-12}\beta GQ^2zT(1/r_2 - 1/r_1)}{h^2} \qquad (10\text{-}5)$$

The field units for Eqs. (10-4) and (10-5) are the same as for Eq. (10-2) and

G = gas gravity
β = turbulence factor from laboratory measurements on cores or from Fig. 2-23, 1/ft

Equation (10-5) can be used to calculate the radial-flow pressure gradient near an injection or producing gas well. Elenbaas and Katz (10-15) derived a turbulent-flow formula for unconsolidated porous media using friction factors for sand particles.

Illustrative Problem

Given the following information on a gas well, compute the effective permeability of the reservoir sand.

Well radius	0.5 ft
Radius to neighboring closed-in well	450 ft
Thickness of gas zone	29 ft
Well penetration	11 ft

On a flow test the well produced 38,861 Mcf/day with a sand-face pressure p_2 = 705.2 and a reservoir pressure p_1 = 722.9 in the neighboring well. The flowing temperature in the reservoir is 63°F and the gas gravity is 0.6. To solve Eq. (10-5), the gas compressibility factor is obtained by usual procedures; it is 0.892. The gas viscosity, obtained from Fig. 4-107, is 0.0117 centipoise. The fact that the well is partially penetrating means that it will produce 62 per cent as much as a completely penetrating well, according to Fig. 10-5. Sixty-two per cent of 29 ft = 18 ft; so the equivalent formation thickness h = 18 ft.

Solution

Solving Eq. (10-5) for K and leaving β as a variable, since it is dependent upon K,

$$722.9^2 - 705.2^2 = \frac{1{,}424 \times 0.0117 \times 0.892 \times 523 \times 38{,}861 \ln (450/0.5)}{18K} + \frac{\beta \times 3.161 \times 10^{-12} \times 0.6 \times (38{,}861)^2 \times 0.892 \times 523}{18^2} \times \left(\frac{1}{0.5} - \frac{1}{450}\right)$$

$$25{,}244 = \frac{114{,}000{,}000}{K} + 0.00825\beta$$

or

$$K = \frac{114{,}000{,}000}{25{,}244 - 0.00825\beta}$$

Neglecting β, which is equivalent to assuming viscous flow, $K = 114{,}000{,}000/25{,}244 = 4{,}520$ millidarcys. From Fig. 2-23, $\beta = 5.8 \times 10^5$ at 4,520 millidarcys. Inserting this value of β in the equation for K above,

$$K = \frac{114{,}000{,}000}{25{,}244 - 4{,}780} = 5{,}570 \text{ millidarcys}$$

UNSTEADY STATE

In steady-state flow the same quantity of fluid enters the flow system as leaves it. In unsteady-state flow the flow rate into an element of volume of a porous medium may not be the same as the flow rate out of that element. Accordingly, the fluid content of the porous medium changes with time. Such changes in the amount of fluid in the porous medium are possible with a compressible fluid. The variables in unsteady-state flow additional to those already used for steady-state flow, therefore, become: time, the porosity of the formation, and the compressibility of the fluid. The porosity of the formation is a measure of the ability of the porous medium to contain fluids; and the compressibility or expansibility determines the change in fluid content with pressure changes.

Several steps are always followed in the original solution of an unsteady-state flow problem:

1. A material-balance equation that accounts for every pound mass of fluid produced, injected, or remaining in the reservoir is established for the flow-system geometry to be considered. This is called the "continuity equation."

2. The continuity equation is combined with the equation for fluid motion and with the equation for fluid density as a function of temperature and pressure, to obtain the partial-differential flow equation. The equation for fluid motion is taken as Darcy's law.

3. Boundary conditions stating that fluids cannot move past impermeable boundaries of the system, that fluids are produced or injected at a specified rate, that pressures start out or follow a specified pattern, or other similar limitations on the problem are set up mathematically.

4. The partial-differential equation is solved, using the desired boundary conditions to obtain engineering solutions in terms of pressures, flow rates, distances, and times for the system geometry and boundary conditions selected.

For most engineering work it is not necessary to go through all of these steps every time a problem is repeated. Integrated solutions for a given type of problem may be used to find unsteady-state flow rates or pressure drops with no more difficulty than that encountered in steady-state problems. Most engineering problems can be solved by the use of prepared solutions presented in the form of working charts or tables. Only when a completely new type of problem must be solved is it necessary to return to the steps outlined above, using the system geometry and boundary conditions that describe the new problem. However, there is value in following the derivations, for the engineer must be prepared to handle new problems on occasion; and the derivations increase his comprehension of the usefulness and limitations of the working charts.

The Continuity Equation

The continuity equation may be derived by considering the flow into and out of a small element of volume. Such flow is best expressed as mass per unit time. The net flow into the element equals the accumulation of fluid with time, as in Eq. (10-6).

$$\text{Input} - \text{output} = \text{accumulation} \qquad (10\text{-}6)$$

The continuity equation will be derived first for the general three-dimensional case and then for the radial-flow case, following the procedure of Streeter (10-26a).

For the three-dimensional case, Fig. 10-6 shows an element of volume having sides of length Δx, Δy, and Δz in the x, y, z coordinate system. The superficial-fluid velocities u, v, and w in the x, y, and z directions, respectively, at the center of the element will be considered. Superficial velocities are velocities based on the entire cross-sectional flow area without regard to the fractional porosity of the porous medium. The fluid density at the center of the element is ρ.

The velocity in the x direction entering the left face of the volume element is $[u - (\partial u/\partial x)(\Delta x/2)]$ and the velocity leaving the right face is $[u + (\partial u/\partial x)(\Delta x/2)]$. Similarly, the fluid density at the left face is $[\rho - (\partial \rho/\partial x)(\Delta x/2)]$ and the density at the right face is $[\rho + (\partial \rho/\partial x)(\Delta x/2)]$. The area of each of the two faces is $\Delta y\, \Delta z$.

The mass rate of flow through any face is (velocity)

(density)(area). Accordingly, the mass rate of flow in the x direction into the left face is

$$\left[u - \left(\frac{\partial u}{\partial x}\right)\left(\frac{\Delta x}{2}\right)\right]\left[\rho - \left(\frac{\partial \rho}{\partial x}\right)\left(\frac{\Delta x}{2}\right)\right](\Delta y\ \Delta z)$$

and the mass rate of flow in the x direction out of the right face is

$$\left[u + \left(\frac{\partial u}{\partial x}\right)\left(\frac{\Delta x}{2}\right)\right]\left[\rho + \left(\frac{\partial \rho}{\partial x}\right)\left(\frac{\Delta x}{2}\right)\right](\Delta y\ \Delta z)$$

The net rate of flow into the volume element in the x direction is found by multiplying out the above expressions term by term, neglecting squares of Δx, subtracting the output from the input, and remembering that

$$d(\rho u) = \rho\, du + u\, d\rho \tag{10-7}$$

Equation (10-8) is obtained.

$$\text{Input} - \text{output} = -\Delta x\ \Delta y\ \Delta z\left[\frac{\partial(\rho u)}{\partial x}\right] \tag{10-8}$$

Similarly, the net mass flow rates into the volume element in the y and z directions, respectively, are $-\Delta x\ \Delta y\ \Delta z[\partial(\rho v)/\partial y]$ and $-\Delta x\ \Delta y\ \Delta z[\partial(\rho w)/\partial z]$.

The accumulation of fluid within the volume element also has the units of mass rate of flow. Such an accumulation is due to a change in the density of the fluid within the volume element with time, or $\phi\ \Delta x\ \Delta y\ \Delta z(\partial \rho/\partial t)$, where ϕ is the fractional porosity of the porous medium and t is the time.

Setting the net input equal to the accumulation and canceling the $\Delta x\ \Delta y\ \Delta z$ terms gives the equation of continuity:

$$\frac{\partial(\rho u)}{\partial x} + \frac{\partial(\rho v)}{\partial y} + \frac{\partial(\rho w)}{\partial z} = -\phi\left(\frac{\partial \rho}{\partial t}\right) \tag{10-9}$$

No assumptions have been made in deriving the continuity equation.

For the radial-flow case, a similar type of derivation will establish the equation of continuity. The volume element is shown in Fig. 10-6. Flow occurs only in the radial direction at a velocity denoted by u. The volume element is bounded by circles of radii r and $(r + \Delta r)$ and by the angle Δa, and may be considered to be of thickness h and porosity ϕ.

The mass rate of flow into the element is

$$\left[u - \left(\frac{\partial u}{\partial r}\right)\left(\frac{\Delta r}{2}\right)\right](rh\ \Delta a)\left[\rho - \left(\frac{\partial \rho}{\partial r}\right)\left(\frac{\Delta r}{2}\right)\right]$$

and out of the element is

$$\left[u + \left(\frac{\partial u}{\partial r}\right)\left(\frac{\Delta r}{2}\right)\right][(r + \Delta r)h\ \Delta a]\left[\rho + \left(\frac{\partial \rho}{\partial r}\right)\left(\frac{\Delta r}{2}\right)\right]$$

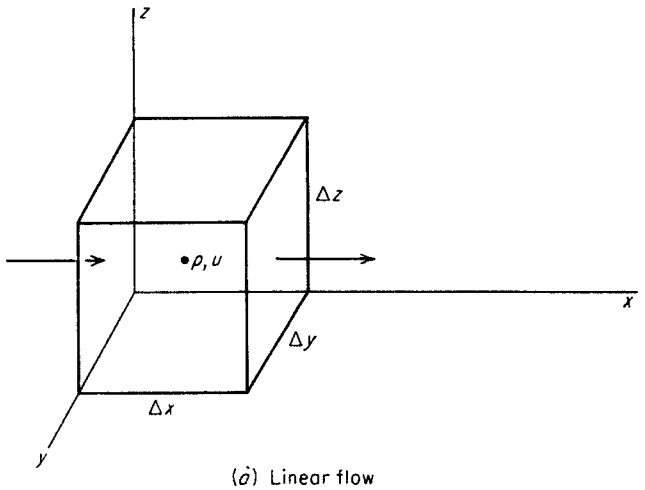

(*a*) Linear flow

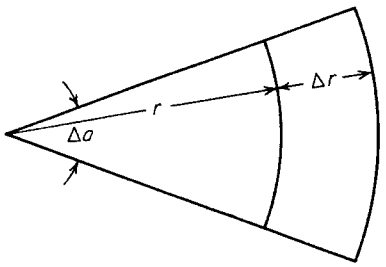

(*b*) Radial flow

Fig. 10-6. Element of volume for derivation of continuity equation.

The accumulation of fluid in the element is $\phi rh\ \Delta a\ \Delta r\ \partial \rho/\partial t$. Proceeding as before, the equation of continuity is found to be Eq. (10-10).

$$\frac{\partial(\rho u)}{\partial r} + \frac{\rho u}{r} = -\phi\left(\frac{\partial \rho}{\partial t}\right) \tag{10-10}$$

Unsteady-state-flow Differential Equations

The particular case of unsteady-state radial flow of gases will be considered as an illustration of the procedures by which such equations are obtained. Equation (2-1) with r replacing L gives Darcy's law for radial flow:

$$u = \frac{-K}{\mu}\frac{\partial p}{\partial r} \tag{10-11}$$

Darcy's law may be combined with the radial-flow continuity equation (10-10) by direct substitution to give Eq. (10-12).

$$\rho\frac{\partial^2 p}{\partial r^2} + \frac{\partial p}{\partial r}\frac{\partial \rho}{\partial r} + \frac{\rho}{r}\frac{\partial p}{\partial r} = \frac{\mu\phi}{K}\frac{\partial \rho}{\partial t} \tag{10-12}$$

Equation (10-12) is written in terms of four variables p, r, t, and ρ, one of which must be eliminated before

the equation can be solved. The density ρ can be eliminated by means of Eq. (10-13) for the gas density.

$$\rho = \frac{Mp}{zRT} \tag{10-13}$$

In Eq. (10-13) M is the molecular weight, or gas gravity $\times$ 29; R is the gas constant; T is the absolute temperature; and z is now the compressibility factor. The gas constant R has the value 10.73 (Table 4-1) for density in pounds mass per cubic foot, pressure in psia, and temperature in degrees Rankine.

Combining Eqs. (10-12) and (10-13) to eliminate the gas density, the radial-flow unsteady-state equation for gases is obtained.

$$\frac{\partial^2 p^2}{\partial r^2} + \frac{1}{r}\frac{\partial p^2}{\partial r} = \frac{\mu\phi}{Kp}\frac{\partial p^2}{\partial t} \tag{10-14}$$

In deriving Eq. (10-14), the general mathematical relationship given in Eq. (10-15) is used to arrive at the form of the equation presented.

$$\frac{1}{2}\frac{\partial^2 p^2}{\partial r^2} = p\frac{\partial^2 p}{\partial r^2} + \left(\frac{\partial p}{\partial r}\right)^2 \tag{10-15}$$

The assumptions that μ, K, z, and T are constants and that Darcy's law applies are embodied in Eq. (10-14).

A variety of special unsteady-state-flow partial-differential equations can be derived in the foregoing manner for gas or liquid flow in linear or radial systems. Table 10-1 gives a summary of several such equations. Those for liquid flow are based on the density relationship given in Eq. (10-16).

$$\rho = \rho_0 e^{c(p-p_0)} \tag{10-16}$$

where ρ_0 is the density at some reference pressure p_0, c is a constant having the units of 1/pressure, and p is the pressure at which the density is to be calculated.

Most unsteady-state liquid-flow calculations have, however, been based on equations with one further assumption. For simplicity, such terms as $c(\partial p/\partial x)^2$ or $c(\partial p/\partial r)^2$ have been neglected. For slightly compressible liquids, this assumption is probably satisfactory. Such may not be the case in all applications, however.

Dimensionless Numbers in Unsteady-state Flow

A great simplification in handling unsteady-state-flow problems is brought about by the use of dimensionless numbers or groups of variables. It would be next to impossible to show separately the effect of all the variables such as permeability, porosity, viscosity, flow rates, pressures, well-bore size, time, etc., on the unsteady-state behavior of a reservoir. Instead, these variables may be grouped together to form a few dimensionless combinations which are easily used and which bear a simple relationship to one another.

Table 10-2 lists several of the common dimensionless groups. The most important relationship is dimensionless time t_D. The distance that transients move in a reservoir is, for example, dependent upon dimensionless time. The dimensionless flow rate is the slope of the steady-state pressure gradient, as given by Eq. (10-3) or (10-5) or as shown in Fig. 10-3.

Table 10-1. Unsteady-state Flow Equations

Fluid	Fluid-density equation	System geometry	Continuity equation	Unsteady-state flow equation for Darcy flow
Gas	$\rho = Mp/zRT$	Linear flow	$\frac{\partial(\rho u)}{\partial x} = -\phi\frac{\partial \rho}{\partial t}$	$\frac{\partial^2 p^2}{\partial x^2} = \frac{\mu\phi}{Kp}\frac{\partial p^2}{\partial t}$ (10-17)
Liquid	$\rho = \rho_0 e^{c(p-p_0)}$	Linear flow	$\frac{\partial(\rho u)}{\partial x} = -\phi\frac{\partial \rho}{\partial t}$	$\frac{\partial^2 p}{\partial x^2} + c\left(\frac{\partial p}{\partial x}\right)^2 = \frac{\phi\mu c}{K}\frac{\partial p}{\partial t}$ (10-18)
Slightly compressible liquid	$\rho = \rho_0 e^{c(p-p_0)}$*	Linear flow	$\frac{\partial(\rho u)}{\partial x} = -\phi\frac{\partial \rho}{\partial t}$	$\frac{\partial^2 p}{\partial x^2} = \frac{\phi\mu c}{K}\frac{\partial p}{\partial t}$ (10-19)
Gas	$\rho = Mp/zRT$	Radial flow	$\frac{\partial(\rho u)}{\partial r} + \frac{\rho u}{r} = -\phi\frac{\partial \rho}{\partial t}$	$\frac{\partial^2 p^2}{\partial r^2} + \frac{1}{r}\frac{\partial p^2}{\partial r} = \frac{\phi\mu}{Kp}\frac{\partial p^2}{\partial t}$ (10-14)
Liquid	$\rho = \rho_0 e^{c(p-p_0)}$	Radial flow	$\frac{\partial(\rho u)}{\partial r} + \frac{\rho u}{r} = -\phi\frac{\partial \rho}{\partial t}$	$\frac{\partial^2 p}{\partial r^2} + c\left(\frac{\partial p}{\partial r}\right)^2 + \frac{1}{r}\frac{\partial p}{\partial r} = \frac{\phi c\mu}{K}\frac{\partial p}{\partial t}$ (10-20)
Slightly compressible liquid	$\rho = \rho_0 e^{c(p-p_0)}$†	Radial flow	$\frac{\partial(\rho u)}{\partial r} + \frac{\rho u}{r} = -\phi\frac{\partial \rho}{\partial t}$	$\frac{\partial^2 p}{\partial r^2} + \frac{1}{r}\frac{\partial p}{\partial r} = \frac{\phi c\mu}{K}\frac{\partial p}{\partial t}$ (10-21)

* $c(\partial p/\partial x)^2$ is small and is negligible.

† $c(\partial p/\partial r)^2$ is small and is negligible.

Since dimensionless flow rate is a slope, the symbol m has been given to it. Several dimensionless pressure ratios are shown in Table 10-2. These include simple ratios of the pressure p to the initial shut-in pressure p_i of the reservoir; of the pressure difference $p - p_i$ from the shut-in pressure, to the shut-in pressure p_i; and of the pressure difference $p - p_i$ to the maximum possible pressure difference $p_e - p_i$, where p_e is a constant external pressure. For gas flow, the pressures are squared, as in the steady-state formulas.

Unsteady-state flow solutions are frequently given in terms of a dimensionless pressure-change number P_t for constant-production-rate problems or in terms of a dimensionless production number Q_t for constant-flowing-pressure problems. Values of P_t have been found for a number of types of problems, and, for any value of dimensionless time, this number will permit the pressure drawdown or build-up due to fluid production or injection to be calculated. Similarly, values of the dimensionless production number Q_t are available and can be used to compute fluid-production quantities for a number of types of reservoir problems.

A variety of other forms of the important dimensionless groups has been used by different workers for similar problems. Although each variation has its advantage in certain types of calculation procedures, the necessity for a common set of dimensionless groups is evident. Accordingly, the dimensionless groups used by various workers will be expressed in terms of the dimensionless groups given in Table 10-2 whenever possible.

An effort should be made to think in terms of dimensionless groups rather than in terms of the individual variables. In gas flow, for example, the reservoir pressure or fluid viscosity will be just as important as the time in determining the value of dimensionless time and, hence, the extent to which a transient has moved through the reservoir.

Table 10-2. Dimensionless Groups for Unsteady-state Flow

Name of group	Symbol	Dimensionless group in field units	
		Liquid flow	Gas flow
Dimensionless time (linear flow)	t_D	$\frac{2.634 \times 10^{-4} Kt}{\mu c \phi x^2}$	$\frac{2.634 \times 10^{-4} Kt\bar{p}}{\mu \phi x^2}$
Dimensionless time (radial flow)	t_D	$\frac{2.634 \times 10^{-4} Kt}{\mu c \phi r^2}$	$\frac{2.634 \times 10^{-4} Kt\bar{p}}{\mu \phi r^2}$
Dimensionless radial distance	R	$\frac{r}{r_w}$ or $\frac{r}{r_b}$	$\frac{r}{r_w}$ or $\frac{r}{r_b}$
Dimensionless pressure ratios	....	p/p_i $(p - p_i)/p_i$ $(p - p_i)(p_e - p_i)$	$(p/p_i)^2$ $(p^2 - p_i^2)/p_i^2$ $(p^2 - p_i^2)/(p_e^2 - p_i^2)$
Dimensionless pressure change	P_t	Varies with problem	Varies with problem
Dimensionless total production	Q_t	Varies with problem	Varies with problem
Dimensionless flow rate (linear flow)	m	$\frac{158.5\mu Q}{hKp_i}$	$\frac{8{,}930\bar{\mu}\bar{z}TQ}{hKp_i^2}$
Dimensionless flow rate (radial flow)	m	$\frac{25.1\mu Q}{hKp_i}$	$\frac{1{,}424\bar{\mu}\bar{z}TQ}{hKp_i^2}$

The Radius-of-drainage Concept

Use is made of the idea of a "radius of drainage" around a producing well, not only in visualizing reservoir behavior, but also in formulating mathematical solutions for unsteady-state flow problems. Several definitions of this radius exist for different purposes. In general, the term "radius of drainage" indicates the distance within which the fluid is moving toward a producing well.

Theory states that any change in pressure at the well rapidly creates at least an infinitesimal disturbance throughout the entire reservoir. In a strict sense, therefore, the radius of drainage is that of the entire producing formation supplying gas to a well. However, because such pressure changes may be only infinitesimal, such a definition is not always useful and is seldom employed.

One important definition is that of the "steady-state radius of drainage" or the "apparent radius of drainage." For given flowing pressure, formation pressure, flow rate, reservoir characteristics, and gas properties, the steady-state radial-flow formula may be used to calculate the radius of the reservoir through which the fluid is apparently flowing. All of the fluid appears to originate at this apparent radius of drainage. This amounts to extrapolating the straight-line portion of the pressure gradient near the well in Fig. 10-3 out to the maximum reservoir pressure. Points a_2, b_2, c_2, and d_2 are the steady-state or apparent radii of drainage for the four times shown in Fig. 10-3.

Another definition is that of the "effective" radius of drainage r_e. Points a_3, b_3, c_3, and d_3 in Fig. 10-3 are such effective values. The effective radius of drainage is greater than the steady-state radius of drainage; however, only negligible changes in pressure have occurred beyond the effective radius of drainage. After the limit of the producing area has been reached, the effective radius of drainage is the same as the radius of the producing area. More exact definitions of the effective radius of drainage will be given later.

The movement of the radius of drainage is important in reservoir behavior. The steady-state and effective radii of drainage move outward while a well

is being produced at a constant rate and the effective radius of drainage has not yet reached the reservoir limit. However, this outward movement ceases when the limit of the producing area is reached. While the radius of drainage is moving, the well is said to be "unstabilized" and, when such movement ceases, the well is said to be "stabilized," even though both cases are unsteady-state. These terms will be considered further in the development of well-performance characteristics.

Methods of Solving Unsteady-state Flow Equations

Several methods are available for solving the various unsteady-state flow equations of Table 10-1. These include:

1. Rigorous analytical solutions
2. Analytical solutions with one or more simplifying assumptions
3. Difference equations
   - *a.* Numerical solutions
   - *b.* Graphical solutions
   - *c.* Digital-computer solutions
4. Analogue-computer solutions
   - *a.* Pneumatic analogues
   - *b.* Electrical analogues
   - *c.* Electronic analogues

Rigorous analytical solutions are available for the slightly-compressible-liquid case, including solutions adapted from heat-transfer problems and summarized by Churchill (10-8) and solutions presented by Van Everdingen and Hurst (10-27). In a sense, however, there are no rigorous analytical solutions for these unsteady-state problems; for, in deriving the equations, it was necessary to assume that viscosity, compressibility factors, temperature, and permeability were constants, that Darcy's law applied, and that certain terms in the equations could be neglected. However, if these assumptions are accepted, straightforward mathematical integrations can be carried out to give analytical solutions for Eqs. (10-19) and (10-21) of Table 10-1.

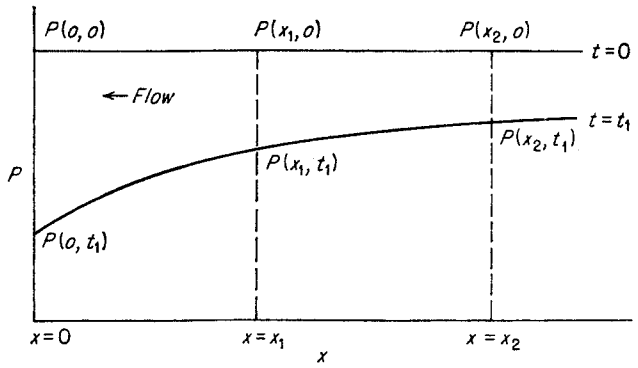

Fig. 10-7. Linear-flow diagram.

The mathematical derivation for linear flow of slightly compressible liquids has been given in detail for heat-flow problems by Churchill (10-8). Figure 10-7 illustrates the linear-flow problem. The first symbol following each pressure indicates the point at which the pressure is measured, and the second symbol indicates the time at which the measurement is made. Accordingly, $p(x_1,t_1)$ indicates the pressure at point x_1 measured at time t_1. For simplicity, the constant initial pressure is called p_f and the constant applied external pressure is called p_e. The fluid flow in Fig. 10-7 is to the left, the fluid leaving the porous medium at the $x = 0$ face.

Several solutions can be obtained, depending on the boundary conditions chosen. Three cases are solved by Churchill. In each case, the initial pressure p_f is constant at zero time, and the pressure gradient is zero at $x = \infty$ for any value of time.

Case I. Pressure at the $x = 0$ Face Maintained Constant. Linear Flow. In case I the pressure at the face $x = 0$ is suddenly changed from p_f to p_e. The pressure $p(x,t)$ at any point and time can be calculated from Eq. (10-22) as derived by Churchill.

$$\frac{p(x,t) - p_f}{p_e - p_f} = -\operatorname{erfc}\frac{1}{2t_D^{1/2}} \qquad (10\text{-}22)$$

The dimensionless time t_D is given in Table 10-2, and the term "erfc" signifies "complementary error function." Values of the error function may be found readily in standard tables (10-25). The sign of Eq. (10-22) is minus for production of fluid and plus for injection of fluid.

$$\text{erfc} = 1 - \text{probability integral} \qquad (10\text{-}22a)$$

The calculation procedure for obtaining the unsteady-state pressure distribution is:

1. Calculate the dimensionless time t_D for the point and time at which the pressure is desired. In linear flow, the distance from the $x = 0$ face is used in place of r in the dimensionless time as given in Table 10-2.
2. Calculate $1/2t_D^{1/2}$.
3. Find the value of erfc $(1/2t_D^{1/2})$ in suitable tables.
4. Calculate $p(x,t)$, knowing p_f and p_e.

Illustrative Problem

In the laboratory, a long pipe is completely filled with large core samples having a permeability of 15.6 millidarcys and a porosity of 12 per cent. The system is saturated with a liquid having a viscosity of 0.20 centipoise and a compressibility of 0.00061 at the existing temperature. The pressure is 500 psia initially and is suddenly lowered at one end to 300 psia. What will be the pressure at a point 20 ft from the producing

end of the pipe after 0.1 hr of flow, assuming that the pipe is of great length?

Solution

$$t_D = \frac{2.634 \times 10^{-4} \times 15.6 \times 0.1}{0.20 \times 0.00061 \times 0.12 \times 20^2} = 0.0704$$

$$\frac{1}{2 \times 0.0704^{1/2}} = 1.89$$

$$\text{erfc } (1.89) = 1 - 0.99248 = 0.00752$$

$$p(20,0.1) = 500 - 200 \times 0.00752 = 498.5 \text{ psia}$$

Case II. Constant Production Rate at the $x = 0$ Face. Linear Flow. If liquid is allowed to flow out through the $x = 0$ face at a constant rate, the pressure at any point and time for unsteady-state liquid flow is given by Eq. (10-23).

$$\frac{p(x,t) - p_f}{p_f} = -mP_t \qquad (10\text{-}23)$$

The dimensionless group m is defined in Table 10-2 for linear liquid flow, and the dimensionless pressure-change number P_t is calculated from Eq. (10-24), derived by Churchill.

$$P_t = \frac{2t_D^{1/2}}{\pi^{1/2} e^{1/4 t_D}} - \text{erfc } \frac{1}{2t_D^{1/2}} \qquad (10\text{-}24)$$

The sign of the right-hand side of Eq. (10-23) is minus for production of liquid and plus for injection.

Since the value of $x = 0$ cannot be substituted directly into Eq. (10-23) or (10-24), a special form of the equation for the case $x = 0$ is needed. Equation (10-25) gives this relationship in the centimeter-second-atmosphere-centipoise-darcy system of units.

$$p(0,t) - p_f = \frac{2Q}{A}\left(\frac{\mu t}{K\phi c\pi}\right)^{1/2} \qquad (10\text{-}25)$$

Ordinarily, Eq. (10-25) would not be used because the assumption of linear flow is not justified near individual wells.

Case III. Arbitrary Pressure Behavior at the $x = 0$ Plane. If the pressure at the $x = 0$ plane varies with time in an arbitrary manner,

$$p(0,t) = f(t) \qquad (10\text{-}26)$$

the solution (10-8) for the pressure at any point and time becomes

$$p(x,t) - p_f = \frac{2}{\pi^{1/2}} \int_{1/2t_D^{1/2}}^{\infty} f\left(t - \frac{t}{4t_D\lambda^2}\right) e^{-\lambda^2}\, d\lambda \qquad (10\text{-}27)$$

where λ is a new variable of integration. Equation (10-27) reduces to Eq. (10-22) for $f(t) =$ constant.

Case IV. Constant Well Pressure. Infinite Radial Reservoir. By following procedures very similar to those for linear flow, radial-flow solutions for slightly compressible liquids were developed by Van Everdingen and Hurst (10-27). The dimensionless equations will be given together with values for the dimensionless groups tabulated by Van Everdingen and Hurst and by Chatas (10-7) for the various cases treated. A uniform pressure distribution at $t = 0$ and a zero pressure gradient at the outer extremity of the reservoir are assumed in the infinite reservoir and in the finite, closed-reservoir cases.

For the constant-well-pressure, infinite-radial-reservoir case, the total cumulative liquid flowing radially into a well over a period of time is designated by the symbol Q_T.

$$Q_T = \int_0^t uA\, dt = \int_0^{t_D} \frac{K}{\mu}\left(\frac{\partial p}{\partial r}\right)_{r=r_w} 2\pi r_w h \frac{\mu\phi c r_w^2}{K}\, dt_D = 2\pi\phi c r_w^2 h(p_e - p_f)Q_t \qquad (10\text{-}28)$$

where Q_t is a dimensionless total-production number defined by Eq. (10-29).

$$Q_t = \frac{\int_0^{t_D}\left[\frac{\partial p}{\partial(r/r_w)}\right]_{r=r_w} dt_D}{p_e - p_f} \qquad (10\text{-}29)$$

If r_w and h are expressed in feet in Eq. (10-28), Q_T is given in cubic feet of liquid measured at the reservoir conditions. Pressure p and compressibility c should be in the same units, either psia or atmospheres. The value of Q_t for any value of dimensionless time t_D is given in Table 10-4. Figure 10-8 by Chatas (10-7) gives values of Q_t for case IV.*

Illustrative Problem

A shut-in well initially at 2,000 psia has been opened to flow at a constant pressure of 1,500 psia for several hours. The value of dimensionless time has been calculated to be 1,500 for this production period. $r_w = 0.5$ ft, $h = 15$ ft, $\phi = 0.20$, and $c = 0.00012$ psia^{-1}. Compute the cubic feet of liquid produced during this flow period for radial flow from an infinite reservoir.

Solution

For $t_D = 1{,}500$, Q_t is found to be 416.220, from Table 10-4.

$$\therefore Q_T = 2\pi \times 15 \times 0.20 \times 0.00012 \times 0.5^2 \times 500 \times 416.220 = 117.8 \text{ cu ft}$$

Case V. Constant Production Rate. Infinite Radial Reservoir. In the case of a constant production rate, the pressure at any point and time is calculated from Eq. (10-30) for radial liquid flow.

$$\frac{p(r,t) - p_f}{p_f} = -mP_t \qquad (10\text{-}30)$$

The sign of the right-hand term of Eq. (10-30) is minus for production problems and plus for injection problems. The value of m may be calculated from

* r_e/r_w of Figs. 10-8 and 10-9 is same as r_b/r_w of text.

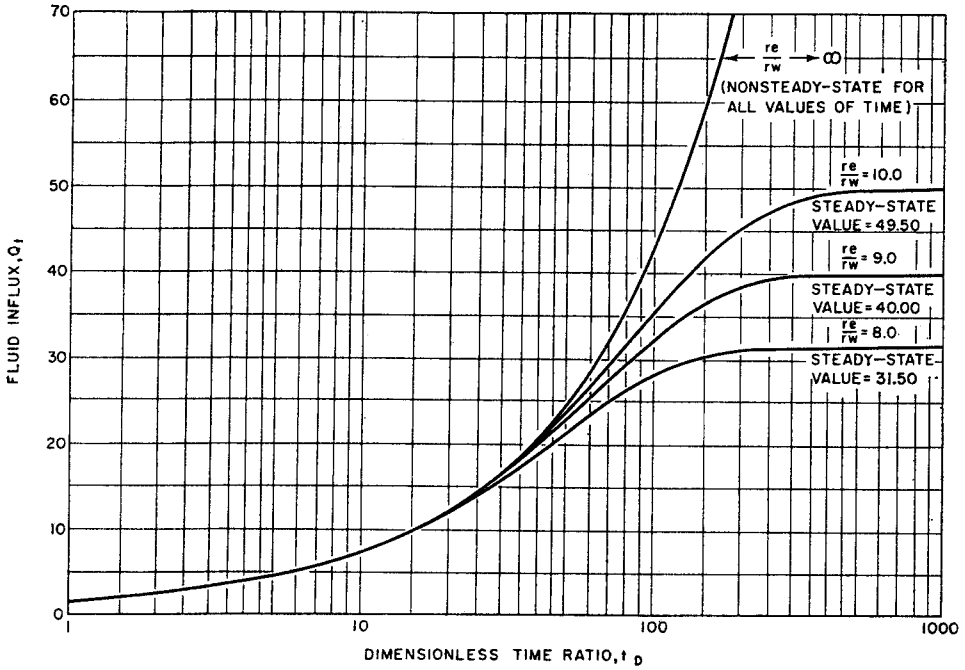

Fig. 10-8. Finite radial system with closed exterior boundary, constant pressure. (*Chatas*, 10-7. *Courtesy Petrol. Engr.*)

the expression given in Table 10-2. The dimensionless pressure-change function P_t depends only on the dimensionless time. For values of t_D less than 1,000, P_t is given in Table 10-5 and in Fig. 10-9. For t_D values greater than 1,000, Eq. (10-31) is used to calculate P_t.

$$P_t = \tfrac{1}{2}(\ln t_D + 0.80907) \qquad (10\text{-}31)$$

In calculating the pressure at any radius, the value of dimensionless time must be calculated using that particular radius.

Illustrative Problem

The well of the preceding illustrative problem is opened to flow at a constant liquid-production rate of 100 bbl/day. Compute the pressure at the well after 24 hr of flow if in this case K = 100 millidarcys and μ = 1.8 centipoises.

Solution

$$t_D = \frac{2.634 \times 10^{-4} \times 100 \times 24}{1.8 \times 0.00012 \times 0.20 \times 0.5^2} = 58{,}400$$

$$P_t = \tfrac{1}{2}(\ln 58{,}400 + 0.80907) = 5.88$$

$$m = \frac{25.1 \times 1.8 \times 100 \times 5.61}{15 \times 100 \times 2{,}000} = 0.00845$$

$$\frac{p(0.5,24) - 2{,}000}{2{,}000} = -0.00845 \times 5.88 = -0.0497$$

$$p(0.5,24) = 1{,}901 \text{ psia}$$

Case VI. Constant Well Pressure. Finite Reservoir with Closed Exterior Boundary. Radial Flow. For a constant flowing pressure at the well bore, Eq. (10-28) may be used together with the values of Q_t given in Table 10-6 or Fig. 10-8 for finite reservoirs. For any value of t_D, Q_t is read for the desired $R = r_b/r_w$ ratio and used in Eq. (10-28) together with the value of m, as in case IV. The additional factor to consider is the radius r_b of the outer boundary of the producing area, which must be used in looking up values of Q_t.

For large values of dimensionless time not covered by Table 10-6 or by Fig. 10-8, Eq. (10-31a) (Chatas, 10-7) may be used to evaluate Q_t.

$$Q_t = \frac{(r_b/r_w)^2 - 1}{2} \qquad (10\text{-}31a)$$

Case VII. Constant Production Rate. Finite Reservoir with Closed Exterior Boundary. Radial Flow. Case VII for a constant flow rate from a single well in a finite reservoir resembles case V except that values of P_t to be used in Eq. (10-30) are obtained from Table 10-7 or Fig. 10-9 for the proper value of R.

For large values of dimensionless time not covered by Table 10-7 or by Fig. 10-9, Eq. (10-31b) (Chatas, 10-7) may be used to evaluate P_t.

$$P_t = \frac{0.5 + 2t_D}{R^2 - 1} - \frac{3R^4 - 4R^4(\ln R) - 2R^2 - 1}{4(R^2 - 1)^2} \qquad (10\text{-}31b)$$

where $R = r_b/r_w$.

Case VIII. Constant Production Rate. Finite Reservoir with Fixed Pressure at Exterior Boundary. Radial Flow. Equation (10-30) and values of P_t given in Table 10-8 will permit the calculation of pressure gradients for the constant-production-rate case with a fixed pressure at the outer boundary of a finite reservoir.

Case IX. Multiple Transients. Constant Production Rates. If the flow rate is changed one or more times, the pressure distribution at any time can still

be calculated readily. The pressure change for the first flow rate is calculated for the entire time under consideration. The pressure change for the next *change* in flow rate is then calculated for the total length of time elapsed after that change took place. Pressure changes due to subsequent changes in flow rate are calculated for the total time elapsed after each change took place. All of these pressure changes are then added together to give the total pressure change from the initial pressure.

The pressure change after two or more successive constant-production-rate periods is calculated from Eq. (10-32).

$$\frac{p(r,t) - p_i}{p_i} = m_1 P_{t_1} + (m_2 - m_1)P_{t_2} + (m_3 - m_2)P_{t_3} + \cdots + (m_n - m_{n-1})P_{t_n} \quad (10\text{-}32)$$

where t_1 = total elapsed time since the first flow rate began
t_2 = total elapsed time since the second flow rate began
t_n = total elapsed time since the nth flow rate began
m_1 = first dimensionless flow rate
m_2 = second dimensionless flow rate
m_n = nth dimensionless flow rate
P_{t_1} = dimensionless pressure-change number evaluated at dimensionless time t_{D_1} for time t_1
P_{t_n} = dimensionless pressure-change number evaluated at dimensionless time t_{D_n} for time t_n

Such a direct calculation of the total pressure drop for several successive flow periods by direct addition is called superposition of the transients. By dividing variable-flow-rate problems into several constant-flow-rate periods, problems that do not involve a constant production rate can be solved. Variable-pressure problems can be solved in this way also.

Analytical Solutions with Simplifying Assumptions for Gases

Several simplifying assumptions have been used to obtain analytical solutions for gas flow. Roberts (10-26) presented a solution in which the function $ax + b$ was used to replace p in the $Kp/\mu\phi$ term of the linear-flow equation. MacRoberts (10-21) developed an analytical solution that was used to estimate the behavior of radial-flow transients. Janicek and Katz (10-18) derived an analytical solution using the assumption that dp/dt is independent of radius. If an average pressure $\bar{p}$ is used in place of $1/c$ in the dimensionless time group, then the preceding solutions found for slightly compressible liquids apply to gas flow (10-12, 10-13). Such an assumption will not introduce errors greater than the uncertainty of the reservoir-property values unless very large pressure changes take place. In such cases the problem can be broken down into several parts to reduce the error.

The form of the solutions will be modified in that pressure squared will appear in the equations where pressures appeared for liquid flow. Values of dimensionless time and for flow-rate groups must be calculated using the gas formulas given in Table 10-2.

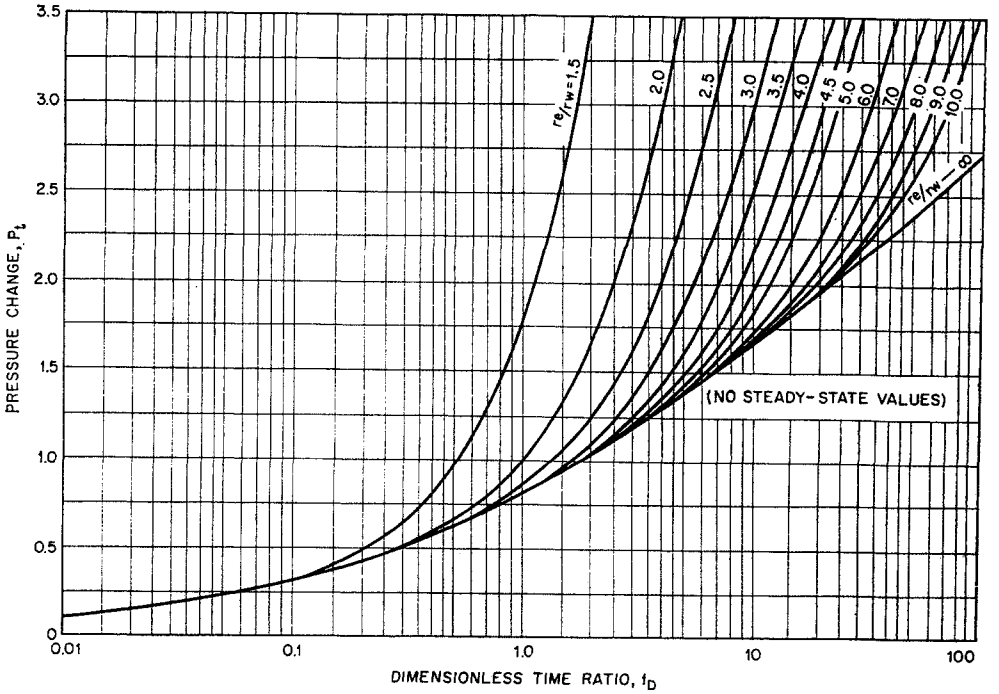

Fig. 10-9. Finite radial system with closed exterior boundary, constant rate. (*Chatas*, 10-7. *Courtesy Petrol. Engr.*)

Case X. Pressure at the $x = 0$ Face Maintained Constant. Linear Gas Flow. This case corresponds to case I for liquid flow. Equation (10-33) applies for case X.

$$\frac{p^2(x,t) - p_f^2}{p_e^2 - p_f^2} = \text{erfc}\,\frac{1}{2t_D^{1/2}} \qquad (10\text{-}33)$$

Case XI. Constant Production Rate at the $x = 0$ Face. Linear Gas Flow. Case XI for gas flow, as given by Eq. (10-34), is similar to case II for liquid flow.

$$\frac{p^2(x,t) - p_f^2}{p_f^2} = -mP_t \qquad (10\text{-}34)$$

The dimensionless pressure-change group P_t is evaluated using Eq. (10-24).

Case XII. Constant Well Pressure. Infinite Radial Reservoir. Gas Flow. The chief difference between case XII and case IV for liquids is that the total cumulative gas production is usually expressed in Mcf per day measured at standard conditions rather than in cubic feet of gas at the reservoir conditions. Accordingly, the gas-production equation becomes

$$Q_T = \frac{2\pi\phi r_w^2 h}{1{,}000\bar{p}}\,\frac{520}{T}\,\frac{p_s}{14.7}\,(p_s - p_f)Q_t \qquad (10\text{-}35)$$

Values of Q_t are found in Table 10-4 or in Fig. 10-8.

Case XIII. Constant Production Rate. Infinite Radial Reservoir. Gas Flow. Equation (10-30) in case V is modified for application to gas-flow problems by using the squares of the pressure terms.

$$\frac{p^2(r,t) - p_f^2}{p_f^2} = -mP_t \qquad (10\text{-}36)$$

Values of P_t are taken from Table 10-5, Fig. 10-9, or Eq. (10-31).

Case XIV. Constant Well Pressure. Finite Reservoir with Closed Exterior Boundary. Radial Gas Flow. The procedure to be followed is the same as that given in case VI except that Eq. (10-35) is to be used.

Case XV. Constant Production Rate. Finite Reservoir with Closed Exterior Boundary. Radial Gas Flow. This type of problem is solved like problems of case VII, using Eq. (10-36) and values of P_t from Table 10-7, Fig. 10-9, or Eq. (10-31*b*).

Case XVI. Constant Production Rate. Finite Reservoir with Fixed Pressure at Exterior Boundary. Radial Gas Flow. Problems of this type are solved like problems of case VIII, using Eq. (10-36) and values of P_t from Table 10-8.

Case XVII. Multiple Transients. Constant Gas-production Rates. For gas flow, Eq. (10-32) of case IX becomes

$$\frac{p^2(r,t) - p_f^2}{p_f^2} = m_1P_{t_1} + (m_2 - m_1)P_{t_2} + (m_3 - m_2)P_{t_3} + \cdots + (m_n - m_{n-1})P_{t_n} \qquad (10\text{-}37)$$

where the symbols have the same meanings as in Eq. (10-32).

Succession-of-steady-states Assumption for Gases

Janicek and Katz (10-18) obtained an analytical solution for unsteady-state radial-gas-flow equations assuming that $\partial p/\partial t$ is independent of radius at any given instant of time. This assumption has been called by Muskat (1-11) the "assumption of a succession of steady states" and has been applied to reservoir problems by Matthews, Brons, and Hazebroek (10-22). Such an assumption is most nearly correct for finite reservoirs once a constant-production-rate transient has reached the extremity of the reservoir. The derivation of Janicek and Katz was made for this condition and then applied to infinite reservoirs by analogy with more rigorous solutions. The importance of the Janicek and Katz derivation lies in its mathematical simplicity, which, with many problems, leads to a ready understanding impossible with the involved mathematics of more rigorous treatments.

Equation (10-14) for unsteady radial gas flow may be restated:

$$\frac{\partial p^2}{\partial t} = \frac{Kp}{\mu\phi r^2}\,\frac{\partial^2 p^2}{\partial(\ln r)^2} \qquad (10\text{-}38)$$

If the dimensionless quantities $P = p/p_f$, $R = r/r_w$, and $t_D = k\bar{p}t/\mu\phi r_w^2$ are used, Eq. (10-38) becomes Eq. (10-39).

$$\frac{\partial P^2}{\partial t_D} = \frac{1}{R^2}\,\frac{\partial^2 P^2}{\partial(\ln R)^2} \qquad (10\text{-}39)$$

Assuming $\partial P^2/\partial t_D$ to be independent of R, this equation can be rewritten:

$$\frac{dP^2}{dt_D} = \frac{1}{R^2}\,\frac{d^2P^2}{d(\ln R)^2} \qquad (10\text{-}40)$$

The boundary condition for a constant production rate is given in Eq. (10-41).

$$\frac{dP^2}{d(\ln R)} = m \qquad \text{at } R = 1 \qquad (10\text{-}41)$$

The boundary condition at the extremity of the reservoir is

$$\frac{dP^2}{d(\ln R)} = 0 \qquad \text{at } R = R_e \qquad (10\text{-}42)$$

where R_e is the ratio r_e/r_w previously discussed. Equation (10-40) may be integrated between $R = 1$ and $R = R_e$.

$$\frac{dP^2}{dt_D}\int_1^{R_e} R^2 d(\ln R) = \left[\frac{dP^2}{d(\ln R)}\right]_{R=1}^{R=R_e} \quad (10\text{-}43)$$

The result is

$$-\frac{dP^2}{dt_D} = \frac{2m}{R_e^2 - 1} \quad (10\text{-}44)$$

Equation (10-44) gives the rate of pressure decline at any radius for any dimensionless production rate m and effective radius of drainage R_e.

The value of dP^2/dt_D from Eq. (10-44) can now be used in Eq. (10-40) to find the pressure gradient at any time.

$$\frac{dP^2}{d(\ln R)} = \frac{2m}{R_e^2 - 1}\int_R^{R_e} R^2 d(\ln R) = m \times \left(1 - \frac{R^2 - 1}{R_e^2 - 1}\right) \quad (10\text{-}45)$$

$$P_f^2 - P_s^2 = \frac{m}{2}\left[\left(1 + \frac{R_w^2}{R_e^2 - R_w^2}\right)\left(\ln \frac{R_e^2}{R_w^2}\right) - \delta\right] \quad (10\text{-}46)$$

where $P_f^2 = p_f^2/p_f^2 = 1$ and where $R_w^2 = r_w/r_w = 1$. In this derivation the term δ has a value of 1.0 for finite reservoirs when the pressure gradient has reached the limit of the reservoir. By analogy with other derivations, δ = Euler's constant = 0.5772 for infinite reservoirs or for those cases in which the effective radius of drainage is still moving in a finite reservoir.

A number of other useful equations are derived by Janicek and Katz by extension of the methods just given for the unsteady-state pressure gradient. For gas flow in an infinite reservoir, the equation for the pressure change at the well bore with time is found to be

$$P_f^2 - P_s^2 = \frac{m}{2}\ln(4t_D e^{-\delta} + 1) \quad (10\text{-}47)$$

The effective radius of drainage is found from Eq. (10-48).

$$R_e^2 = 4t_D \quad (10\text{-}48)$$

This equation is similar to but not identical with the expression reported by MacRoberts (10-21).

To find the ratio of the apparent or steady-state radius of drainage to the effective radius of drainage, Janicek and Katz suggest using the ratio 0.749 while the effective radius of drainage is moving and 0.606 when the effective radius of drainage becomes stationary at the reservoir boundary.

When the effective radius of drainage reaches the extremity of the reservoir, as calculated from Eq. (10-48), and no longer moves, the relationship for pressure decline with time is given by the equation

$$p_{f_1} - p_{f_2} = \frac{0.375zT(t - t_b)Q}{h\phi r_b^2} \quad (10\text{-}49)$$

where p_{f_1} = formation pressure at r_b and t_b, psia
p_{f_2} = formation pressure at r_b and t, psia
t = total flow time, hr
t_b = time of flow for effective radius to reach r_b, hr
r_b = radius of outer boundary of area serving a well, ft

and where z, T, h, ϕ, and Q are field units.

The principle of superposition applied to these equations gives an equation for extrapolating the pressure-build-up curves on closed wells.

$$\frac{p_{s_2}^2 - p_{s_1}^2}{1{,}000Q_1} = \frac{1.635\mu zT}{hK}\log\frac{5.93 \times 10^{-4}K\bar{p}(t_2 - t_1)}{\mu\phi r_w^2} \quad (10\text{-}50)$$

where p_{s_1} = sand-face pressure at time t_1 when the well is closed in, psia
p_{s_2} = sand-face pressure at time t_2, psia
Q_1 = constant production rate prior to the shut-in for t_1 hr, Mcf/day

and where μ, z, T, h, K, $\bar{p}$, ϕ, and r_w are field units.

Difference Equations

The unsteady-flow equations may be solved by using finite increments of pressure, distance, and time rather than by using the differentials ∂p, ∂x, and ∂t. The partial differential equation written in terms of such finite increments is called a difference equation. The partial differential equation is first arranged so that all the partial derivatives with respect to distance are on one side and the partial derivatives with respect to time are on the other side. Then, starting with a known initial-pressure distribution with distance, the changes of pressure with distance are evaluated over small increments of distance and used in the equation to evaluate the change in pressure for the proper increment of time. Thus, a pressure-distribution curve at later periods of time can be calculated in a step-by-step manner and the unsteady-state equation can be solved.

Partial derivatives of pressure with respect to time at a fixed distance are expressed as in Eq. (10-51).

$$\frac{\partial p^2}{\partial t} = \frac{\Delta p^2}{\Delta t} = \frac{p^2(x, t + \Delta t) - p^2(x,t)}{\Delta t} \quad (10\text{-}51)$$

Since the above derivative is a derivative in which x is not a variable, both of the two p^2 terms are evaluated at the same point x. The value of p^2 is, however, evaluated at times t and $t + \Delta t$; so the right-hand expression in Eq. (10-51) is the partial derivative with respect to time at point x.

Second derivatives are expressed in a similar manner. As an example, a partial derivative with respect to x at a constant value of t will be used.

$$\frac{\partial^2 p^2}{\partial x^2} = \frac{\Delta(\Delta p^2)}{(\Delta x)^2}$$
$$= \frac{[p^2(x + \Delta x, t) - p^2(x,t)] - [p^2(x,t) - p^2(x - \Delta x, t)]}{(\Delta x)^2}$$
$$= \frac{p^2(x + \Delta x, t) - 2p^2(x,t) + p^2(x - \Delta x, t)}{(\Delta x)^2} \quad (10\text{-}52)$$

Equation (10-14) for unsteady-state radial flow of a gas, written in terms of the above finite-difference relationships, becomes

$$p^2(r, t + \Delta t) = \frac{\Delta t\, Kp}{(\Delta r)^2 \mu\phi}\left[\left(1 - \frac{\Delta r}{2r}\right) p^2(r - \Delta r, t) + \left(1 + \frac{\Delta r}{2r}\right) p^2(r + \Delta r, t)\right] \quad (10\text{-}53)$$

Graphical Solution of Difference Equations

The Schmidt graphical method, which is widely used for solving unsteady-state heat-transfer problems, has been adapted (10-11) to the solution of unsteady-state gas-flow problems. This method is versatile and can be used to solve many problems involving various boundary conditions. It is generally applicable to reservoir problems, can be used effectively with a minimum of mathematical background, and requires no expensive computing equipment.

A constant average pressure $\bar{p}$ is assumed in the coefficient of the right-hand side of Eq. (10-14). The value of the time increment Δt is chosen to be about

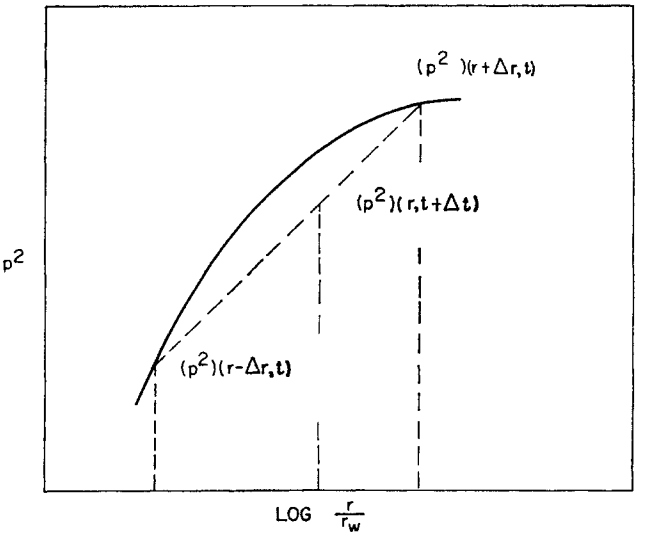

Fig. 10-10. Graphical solution of unsteady-state radial flow. (Cornell and Katz, 10-11. Courtesy AIME.)

$\frac{1}{10}$ to $\frac{1}{20}$ of the total time of the transient to be calculated, and Δr is then calculated from Eq. (10-54).

$$\Delta t = \frac{(\Delta r)^2 \mu\phi}{2K\bar{p}} \quad (10\text{-}54)$$

Using the value of Δr given by Eq. (10-54), Eq. (10-53) becomes Eq. (10-55).

$$p^2(r, t + \Delta t) = \tfrac{1}{2}\left[\left(1 - \frac{\Delta r}{2r}\right) p^2(r - \Delta r, t) + \left(1 + \frac{\Delta r}{2r}\right) p^2(r + \Delta r, t)\right] \quad (10\text{-}55)$$

Equation (10-55) can be used to make unsteady-state radial-flow calculations as shown in Fig. 10-10. This figure shows a pressure gradient drawn on a plot of p^2 versus log (r/r_w) at a given instant of time. Three vertical lines each a distance Δr apart are drawn on the plot. The intersection of the line drawn from $p^2(r - \Delta r, t)$ to $p^2(r + \Delta r, t)$ with the vertical line at radius r gives the value of p^2 at r an interval of time Δt later than that of the original pressure gradient. In this way the entire pressure gradient at later periods of time can be determined and the unsteady-state equation can be solved. This graphical calculation procedure based on Eq. (10-55) amounts to taking a weighted average of p^2 at two points $2\,\Delta r$ apart to find the pressure at a later time. The weighting factor is seen from Eq. (10-55) to be inversely proportional to r. The use of a logarithmic scale in r is indicated for the graphical calculation, since $d(\ln r) = dr/r$ and $\Delta(\ln r) = \Delta r/r$.

The graphical calculations for a single viscous-flow transient in an infinite reservoir initially at a constant pressure are carried out as follows in order to compute the pressure gradient in the reservoir at the end of the transient. It is necessary to know the values of K, h, p_f, $\bar{\mu}$, ϕ, $\bar{z}$, T, Q, $\bar{p}$, and r_w. An estimate of the average pressure in the disturbed portion of the reservoir must be made beforehand to obtain values of $\bar{\mu}$, $\bar{z}$, and $\bar{p}$. A sheet of semilogarithmic graph paper is then laid out with the proper range of values of p^2 on the linear scale as the ordinate and r on the logarithmic scale as the abscissa. Values of Δt and Δr are selected using Eq. (10-54), and vertical lines are drawn at $r = \Delta r$, $2\,\Delta r$, $3\,\Delta r$, and so on, up to $10\,\Delta r$ or $20\,\Delta r$, as may be necessary. Figure 10-11 shows such a diagram.

The slope of the steady-state pressure gradient is next determined from Eq. (10-2), setting $p_1 = p_f$, $r_1 = 2\,\Delta r$, and $r_2 = r_w$. The value of p_1^2, which is p_s^2 in this case, is then calculated from Eq. (10-2) and plotted at $r = r_w$, yielding a line similar to line 1-1 in Fig. 10-11. This line establishes the slope of the

steady-state pressure gradient. All other steady-state pressure gradients at the same flow rate will be parallel to this line.

As is shown in Fig. 10-10, the pressures at r_w, Δr, and $3\,\Delta r$ an interval of time Δt later are given as points 2-2-2 in Fig. 10-11. At time $2\,\Delta t$ later the pressure gradient is given as points 3-3-3 on Fig. 10-11. Note that the slope of the pressure gradient near the well bore is always that of the steady-state flow and that the effect of the unsteady-state flow is to alter the slope at points farther out in the reservoir. The solution is continued in the same manner until the desired transient time has elapsed.

If necessary, the steady-state viscous-flow pressure gradient near the well bore may be corrected for turbulence, using Eq. (10-56), which is derived from Eq. (10-5) for radial, turbulent flow.

$$-(p^2_{\text{turbulent}} - p^2_{\text{laminar}}) = \frac{3.161 \times 10^{-12}\bar{z}TGQ^2\beta}{h^2r} \tag{10-56}$$

This equation was derived by subtracting the equation for the pressure under viscous-flow conditions from the equation for the pressure when turbulence is present, neglecting the reciprocal of r_1 as compared with the reciprocal of r_2. Corrections for turbulence calculated from Eq. (10-56) are shown in Fig. 10-11.

Figure 10-12 shows the procedure for calculating two successive transients. At the end of the first flow rate, the slope of the steady-state pressure gradient near the well bore is changed to that of the new flow rate and the calculation procedure is carried on as before the change. Figure 10-13 shows the procedure to be used for a finite reservoir closed at the extremity. In this case the pressure gradient is zero at the extremity; otherwise, the calculations are carried out as before.

Successive flow rates are handled by changing the slope of the steady-state gradient near the well bore to correspond to the changed flow rate. Cornell (10-10) has given a sample problem involving a series of four increasing flow rates with turbulence corrections. Figure 10-14 shows the graphical part of this problem.

The pressure gradients in a gas reservoir produced at a constant rate of flow after the reservoir has been shut in long enough so that initially the pressure is uniform have been calculated (10-9, 2-42) and are given in Fig. 10-15 in terms of the dimensionless flow-rate group m, distance ratio R, pressure ratio P, and dimensionless-time group t_D. Figure 10-15 is prepared for viscous flow and, for high flow rates, must be corrected for turbulence near the well bore.

A variety of problems may be solved using Fig.

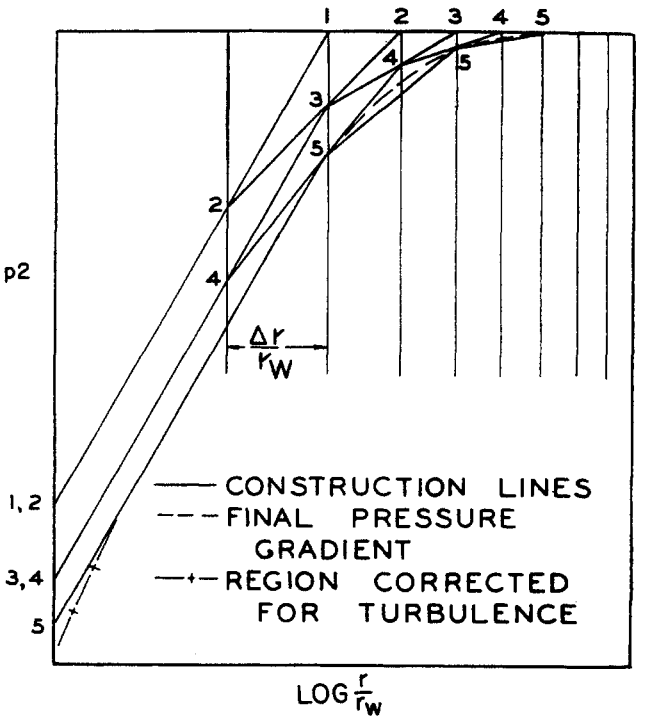

Fig. 10-11. Graphical solution of reservoir pressure gradients for a single constant-rate transient. (*Cornell and Katz*, 10-11. *Courtesy AIME.*)

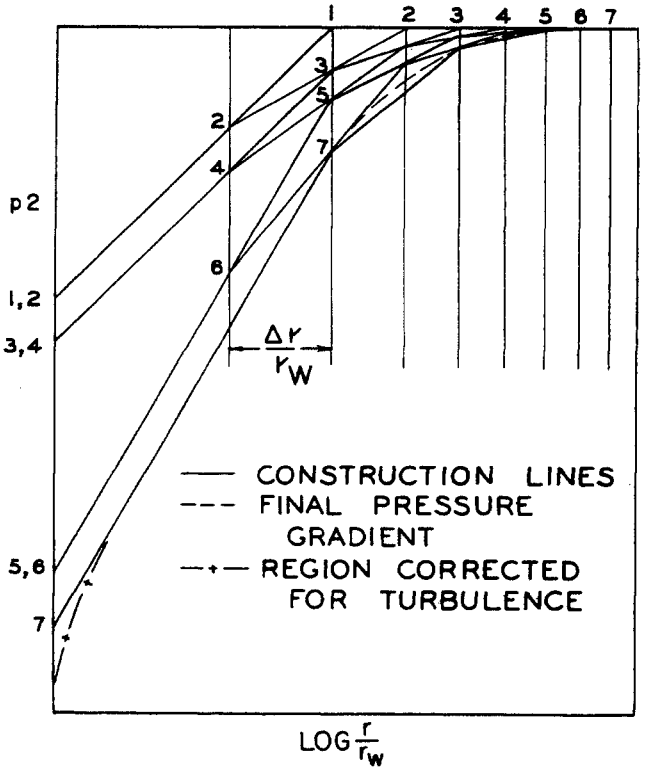

Fig. 10-12. Graphical solution of reservoir pressure gradients for two constant-rate transients, rate 2 > rate 1. (*Cornell and Katz*, 10-11. *Courtesy AIME.*)

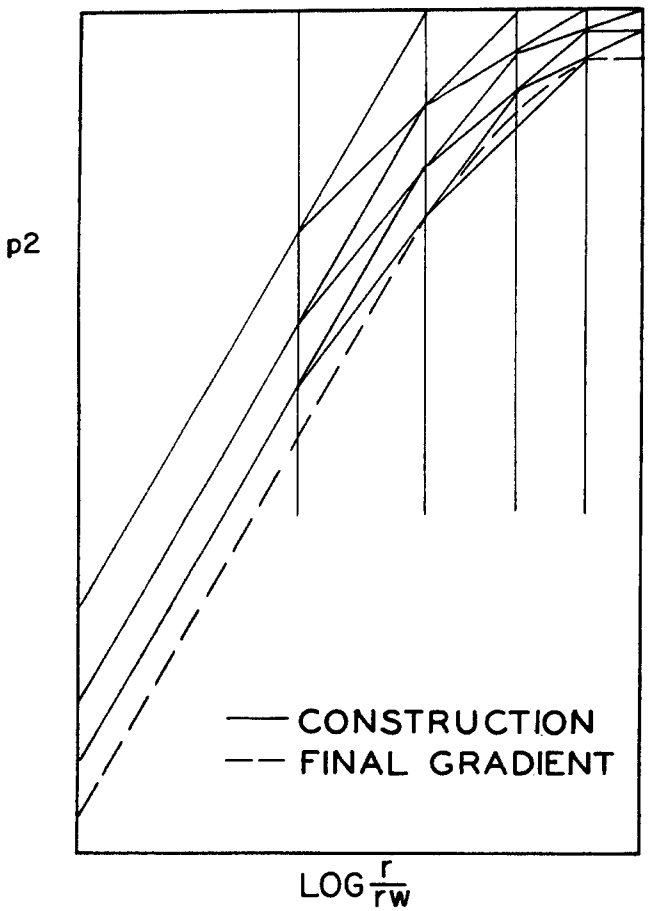

Fig. 10-13. Graphical solution of reservoir pressure gradients for a single constant-rate transient in an infinite reservoir. (*Cornell and Katz, 10-11. Courtesy AIME.*)

10-15. For example, drawdown pressures at the well bore may be calculated from the fluid properties, reservoir properties, reservoir conditions, and flow rate. The entire pressure gradient in the reservoir is given by Fig. 10-15. Or a knowledge of the pressure-decline curve together with the fluid properties and reservoir conditions permits an estimate of the formation permeability. The following illustrative problem shows how a drawdown pressure can be computed using Fig. 10-15.

Illustrative Problem

A natural gas well that has been shut in for some time is to be produced at a rate of 5,000 Mcf/day. The characteristics of the formation and of the gas are given below. Compute the bottom-hole pressure expected after flowing the well for 20 hr, assuming viscous flow.

$\mu = 0.022$ centipoise $\quad z = 0.865$
$T = 652°R \quad K = 60$ millidarcys

Fractional porosity $\phi = 0.17$
Thickness $h = 12$ ft
Closed pressure $p_i = 3{,}500$ psia
Well-bore radius $r_w = 0.33$ ft

Solution

$$m = \frac{1{,}424 \times 0.022 \times 0.0865 \times 652 \times 5{,}000}{12 \times 60 \times 3{,}500^2} = 0.010$$

$$t_D = \frac{60 \times 3{,}400 \times 20 \times 2{,}634 \times 10^{-4}}{0.022 \times 0.17 \times 0.33^2} = 2{,}640{,}000$$

The average pressure value of 3,400 psia was assumed in calculating t_D. From Fig. 10-15,

$$\left(\frac{p}{p_i}\right)^2 = 0.922 \qquad \text{at } \frac{r_w}{r} = 1.0$$

$$p_s = 3{,}500 \times 0.922^{1/2} = 3{,}360 \text{ psia}$$

No further trial is needed.

Since Fig. 10-15 is made up only for the value of $m = 0.010$, the pressure gradients in Fig. 10-15 must be corrected for other rates of flow. The pressures may be corrected by means of Eq. (10-57).

$$\left(\frac{p}{p_i}\right)^2_{\text{corrected}} = 1.0000 - \left[1.000 - \left(\frac{p}{p_i}\right)^2_{\text{Fig. 10-15}}\right] 100m \tag{10-57}$$

Illustrative Problem

Re-solve the previous illustrative problem using a flow rate of 2,500 Mcf/day.

Solution

$$m = 0.005 \qquad t_D = 2{,}640{,}000$$

$$\left(\frac{p}{p_i}\right)^2 = 1.0000 - (1.0000 - 0.922)(100 \times 0.005) = 0.961$$

$$p_s = 3{,}500 \times 0.961^{1/2} = 3{,}430 \text{ psia}$$

Digital-computer Solutions of Differential Equations

A wide variety of solutions is now available as a result of work done using punched-card digital computers. Solutions must be obtained by such computers, rather than by the analytical or graphical methods previously discussed, whenever such simplifying assumptions as the use of average compressibility factors, average viscosity, or average pressure do not apply or whenever the geometry of the reservoir considered leads to problems of undue complexity. Table 10-9 summarizes this work and describes briefly the conditions chosen in each computer study.

Because of the special nature of each problem solution obtained by computer means, it is not possible to present general solutions based on single concise tables as we did for each of the analytical solutions. Instead, numerous tables or charts must be used to cover the range of conditions employed in each computer study. Since it is not feasible to include all such tables or charts here, a few typical results will be presented and described. Problems involving ranges of variables not covered here can be solved by consulting the complete solutions in the original references.

Linear Gas Flow. Several linear gas-flow problems not involving the assumption of an average pressure in the solution were solved by Aronofsky and Jenkins

(10-1). As an example of this work, Fig. 10-16 shows their constant-terminal-pressure solutions for the infinite-reservoir case. The proper units are indicated on the chart, and the parameter N is the ratio of the initial pressure p_0 to the constant pressure p_1.

Radial Gas Flow. Radial gas-flow solutions obtained without assuming an average gas pressure have been computed by Jenkins and Aronofsky (10-19) and by Bruce, Peaceman, Rachford, and Rice (10-6). A typical result from the work of Jenkins and Aronofsky is given as Fig. 10-17. This chart gives the variation of bottom-hole pressure with time for a number of injection and depletion flow rates. This family of curves replaces the single curve for the previous analytical solution of Van Everdingen and Hurst.

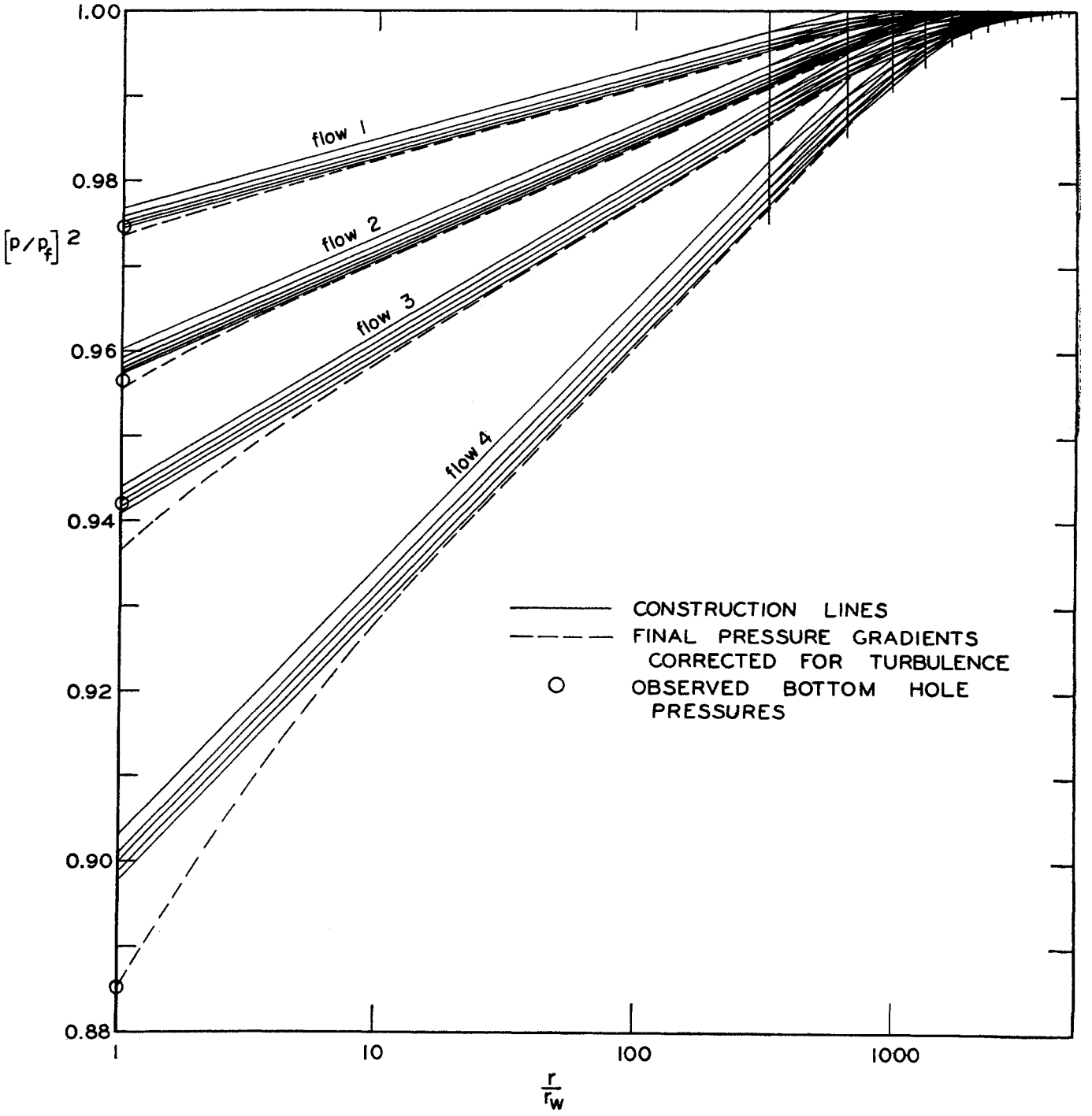

Fig. 10-14. Calculated pressure gradients for a back-pressure test. (*Cornell*, 10-10.)

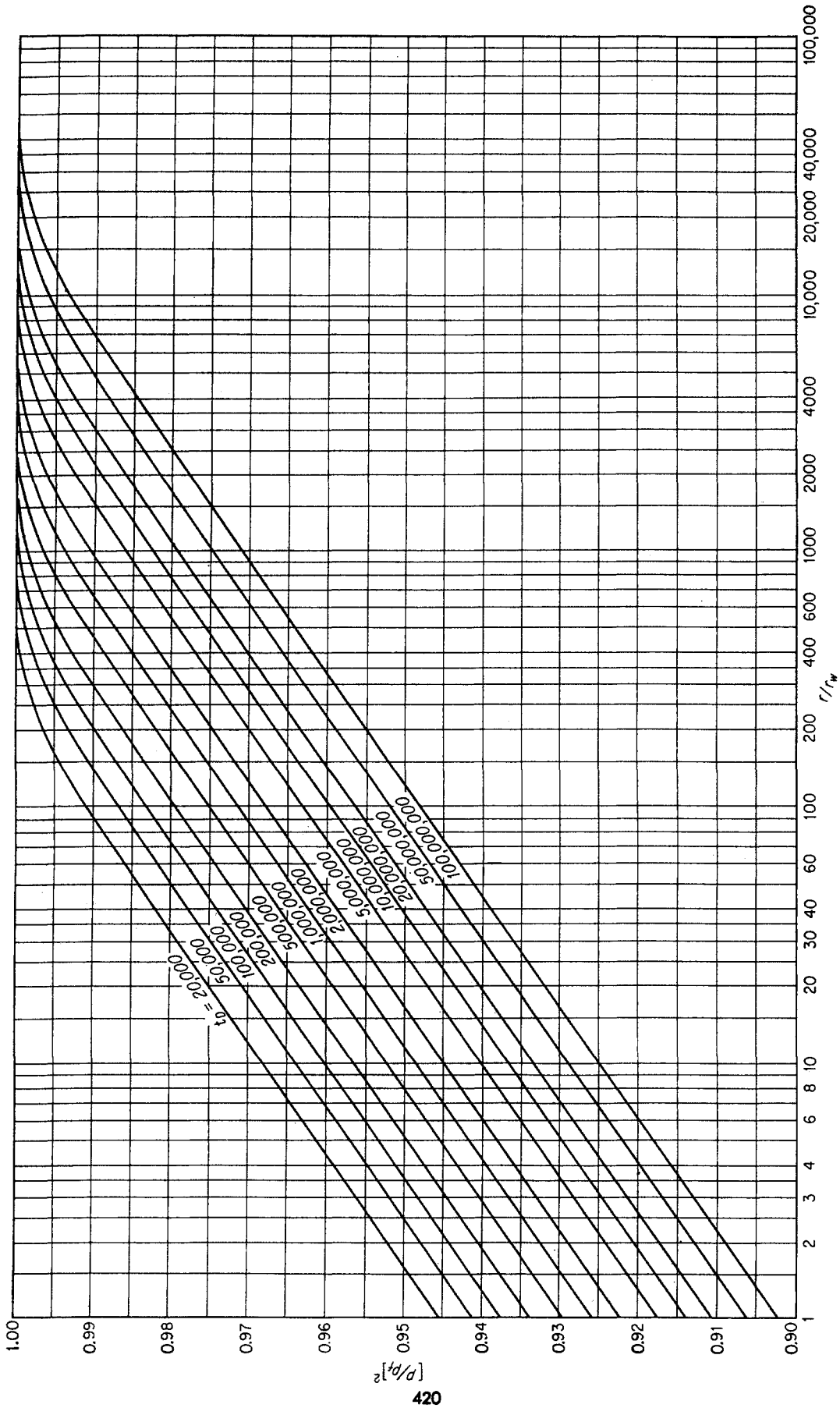

Fig. 10-15. Generalized chart for reservoir pressure gradients in terms of dimensionless groups, $m = 0.010$. (*Cornell and Katz, 2-42.*)

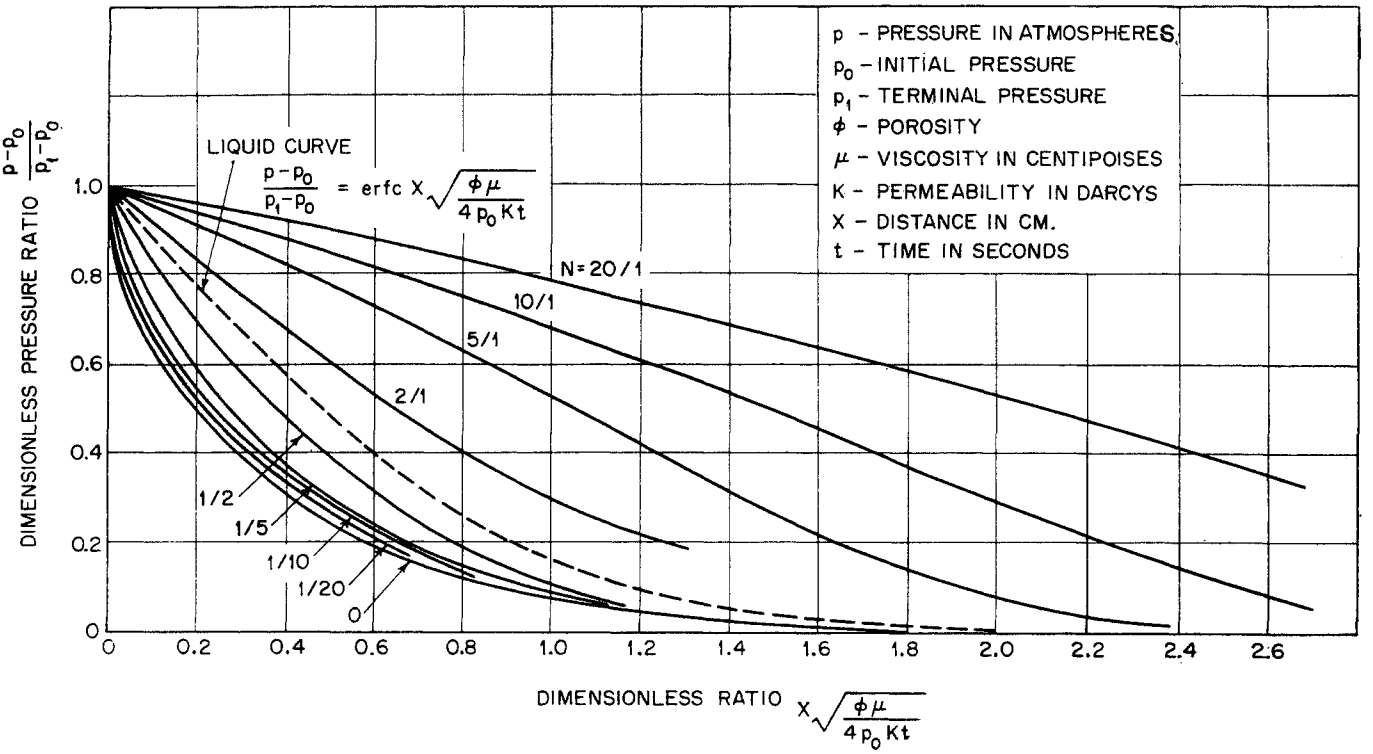

Fig. 10-16. Pressure distribution in a linear gas-flow system of infinite length. (*Aronofsky and Jenkins*, 10-1. *Courtesy ASME.*)

The separation of the curves is due to the fact that pressure is now taken as a variable in all parts of the differential equation.

Representative charts by Bruce, Peaceman, Rachford, and Rice (10-6) for unsteady-state, constant-rate production from a finite radial reservoir are given in Fig. 10-18*a* to *c*. These charts may be used to calculate the pressure at any point in the reservoir for the given dimensionless parameter mt_D, the product of dimensionless time and the dimensionless flow rate.

Analogue-computer Solutions

Unsteady-state differential equations can be solved by setting up electrical, electronic, or mechanical systems that obey laws similar to Darcy's law, *P-V-T* relationships, and the continuity equation. For example, an electrical network can be set up with electrical capacitance instead of formation volume, porosity, and compressibility; electrical resistance instead of reciprocal of permeability, viscosity, and

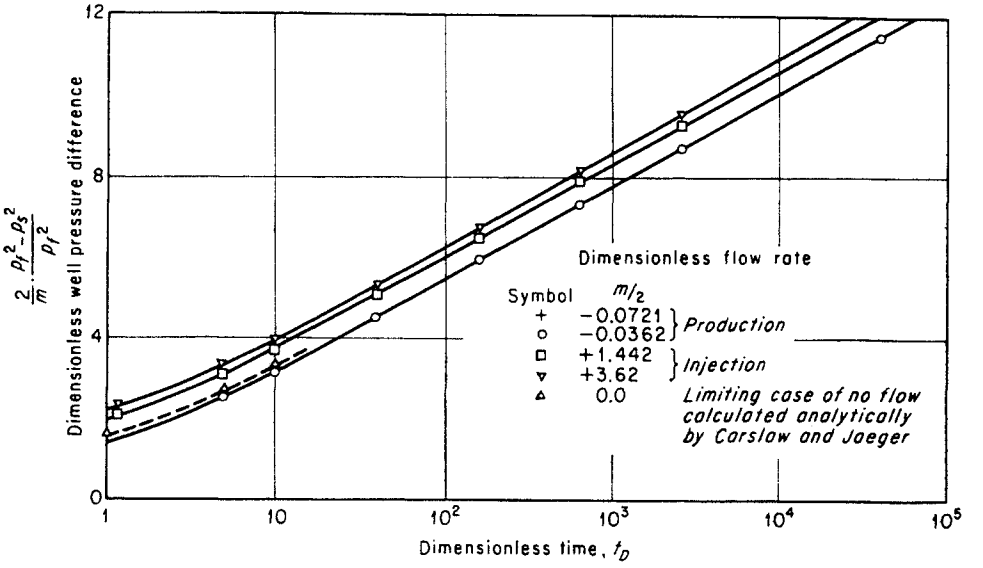

Fig. 10-17. Well-pressure change with time for various production rates, infinite radial gas reservoir. (*Jenkins and Aronofsky*, 10-19.)

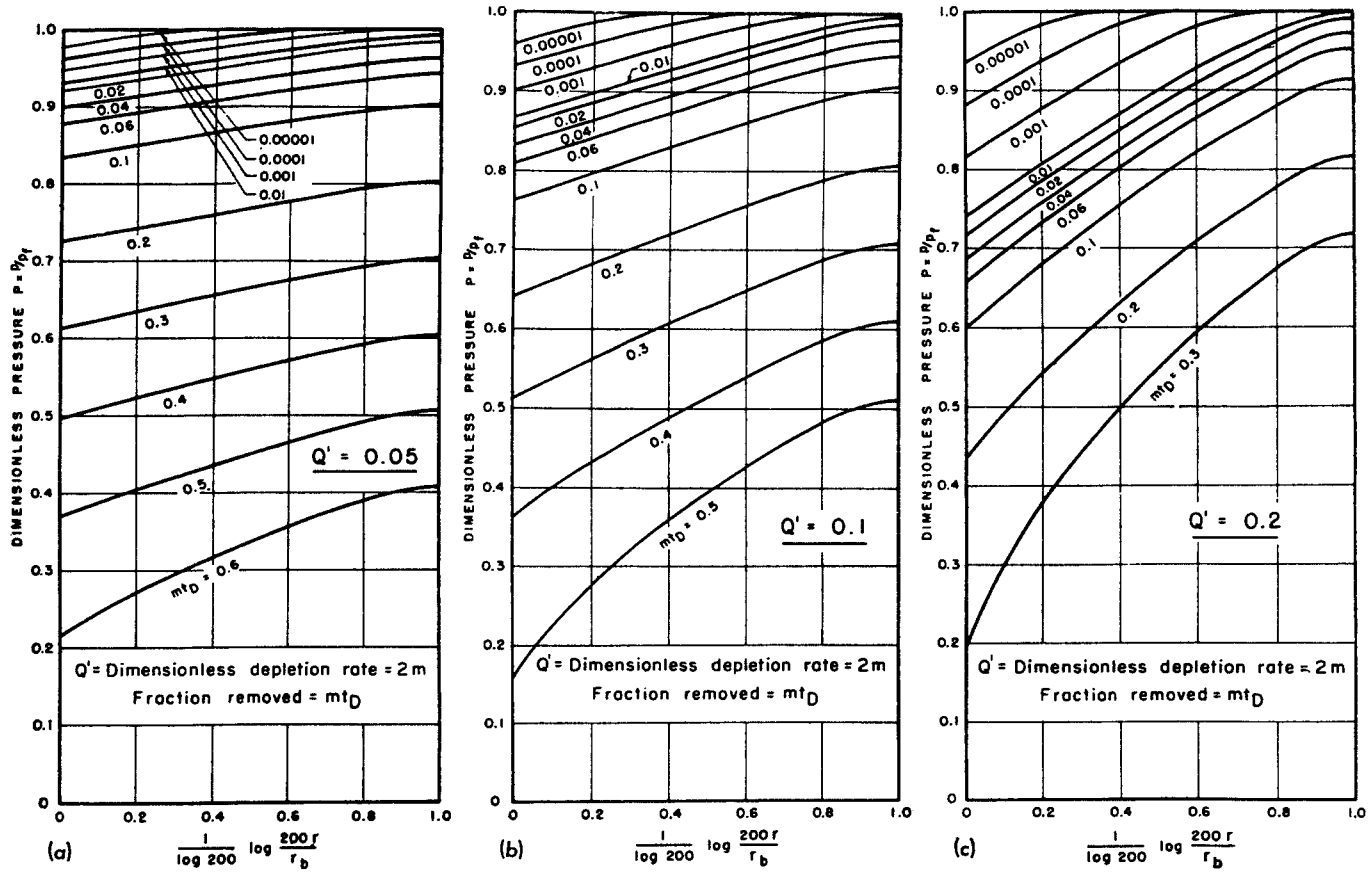

Fig. 10-18. Calculation of pressure distribution for depletion of radial gas reservoir. Note that t_D is based on radius of outer boundary of reservoir r_b. (*Bruce, Peaceman, Rachford, and Rice, 10-6. Courtesy AIME.*)

reciprocal of sand thickness; electrical current instead of flow; and voltage instead of pressure. Withdrawal of current at a constant rate from such a system would then simulate the constant-production-rate, unsteady-state behavior of the reservoir being studied.

A pneumatic analogue is possible using combinations of capillary restrictions and gas-storage volumes to represent unsteady-state gas-flow systems. Or tubes filled with sand can be used to simulate unsteady-state gas-flow systems.

Electronic circuits that can differentiate, integrate, or compute other necessary functions can be combined to obtain electronic-analogue solutions for differential equations.

Analogue-computer solutions that are available include the pneumatic-analogue results of Houpeurt (10-17) and the resistor-capacitor network of Green and Wilts (10-16). Miller, Dyes, and Hutchinson (10-23) also used a resistor-capacitor network to solve pressure-build-up-rate problems for shut-in wells.

Determination of Equalized Reservoir Pressures

Periodic measurements of the shut-in or formation reservoir pressure must be made in order to calculate gas reserves and to correct the back-pressure curve as the field is depleted. In low-permeability formations appreciable pressure differences may exist between various points even after long shut-in times. These differences are due to the low rates at which gas can flow through the low-permeability formation to reach the depleted zones. Such pressure differences should be recognized and taken into account by the calculation and use of an "equalized reservoir pressure." The equalized reservoir pressure is the uniform pressure that would exist in the reservoir after such a long time had passed that flow of gas to the depleted areas had ceased and that, for practical purposes, no pressure gradients existed in the reservoir.

The method of Matthews, Brons, and Hazebroek (10-22) involves the use of a build-up curve with time. After producing a well for a time t_f, the well is shut in. Sand-face pressures are recorded at time intervals Δt following the shut-in, and a plot of sand-face pressure versus log $\Delta t/(t_f + \Delta t)$ is made (Fig. 10-19). The straight-line portion of such a plot, which develops after a short time following the shut-in, is extrapolated to $\Delta t/(t_f + \Delta t) = 1$, or infinite shut-in time. This extrapolated pressure, denoted by p^*, is greater

than the equalized shut-in pressure, because of the over-all decline in the reservoir pressure as a whole, which will have taken place when the equalization is complete. The equalized reservoir pressure is then found from Fig. 10-20. It may be used for either liquid or gas reservoirs with appropriate coordinates.

Illustrative Problem

The use of Fig. 10-20, prepared by Matthews, Brons, and Hazebroek (10-22), for calculating the equalized reservoir pressure of a finite reservoir from the straight-line portion of a build-up curve will be shown. In this example, however, sufficient information will be given to permit calculation of the equalized reservoir pressure in three ways:

1. A simple material-balance calculation will be made.
2. The unsteady-state calculation procedures will be used to calculate the pressure after a period sufficiently long to reach the equalized condition.
3. The equalized reservoir pressure will be obtained from the initial part of the build-up curve, using Fig. 10-20.

Deviations from simple theory due to skin effect, etc., will be omitted in order to show clearly the basic calculation procedure.

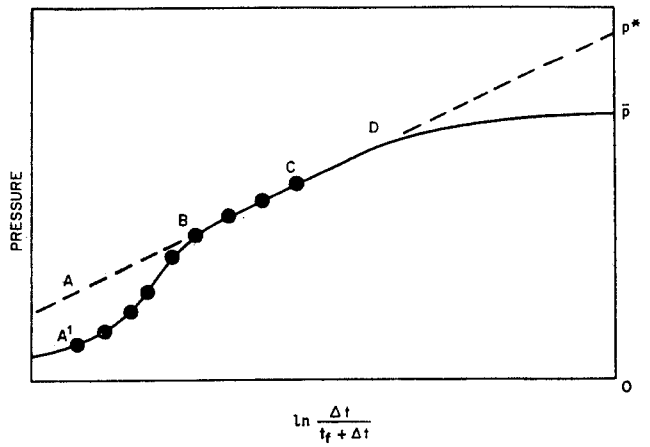

Fig. 10-19. Pressure build-up curve. (*Matthews, Brons, and Hazebroek, 10-22. Courtesy AIME.*)

Conditions:

Radius of outer reservoir boundary	r_b	= 400 ft
Radius of well bore	r_w	= 0.5 ft
Gas gravity	G	= 0.6
Reservoir temperature	T	= 640°R
Initial shut-in formation pressure	p_i	= 2,000 psia
Viscosity of reservoir gas	μ	= 0.016 centipoise
Compressibility factor of reservoir gas	z	= 0.89
Formation thickness	h	= 50 ft
Formation permeability	K	= 20 millidarcys
Fractional porosity	ϕ	= 0.15
Constant production rate prior to shut-in	Q	= 3,000 Mcf/day
Length of production time prior to shut-in	t_f	= 24 hr

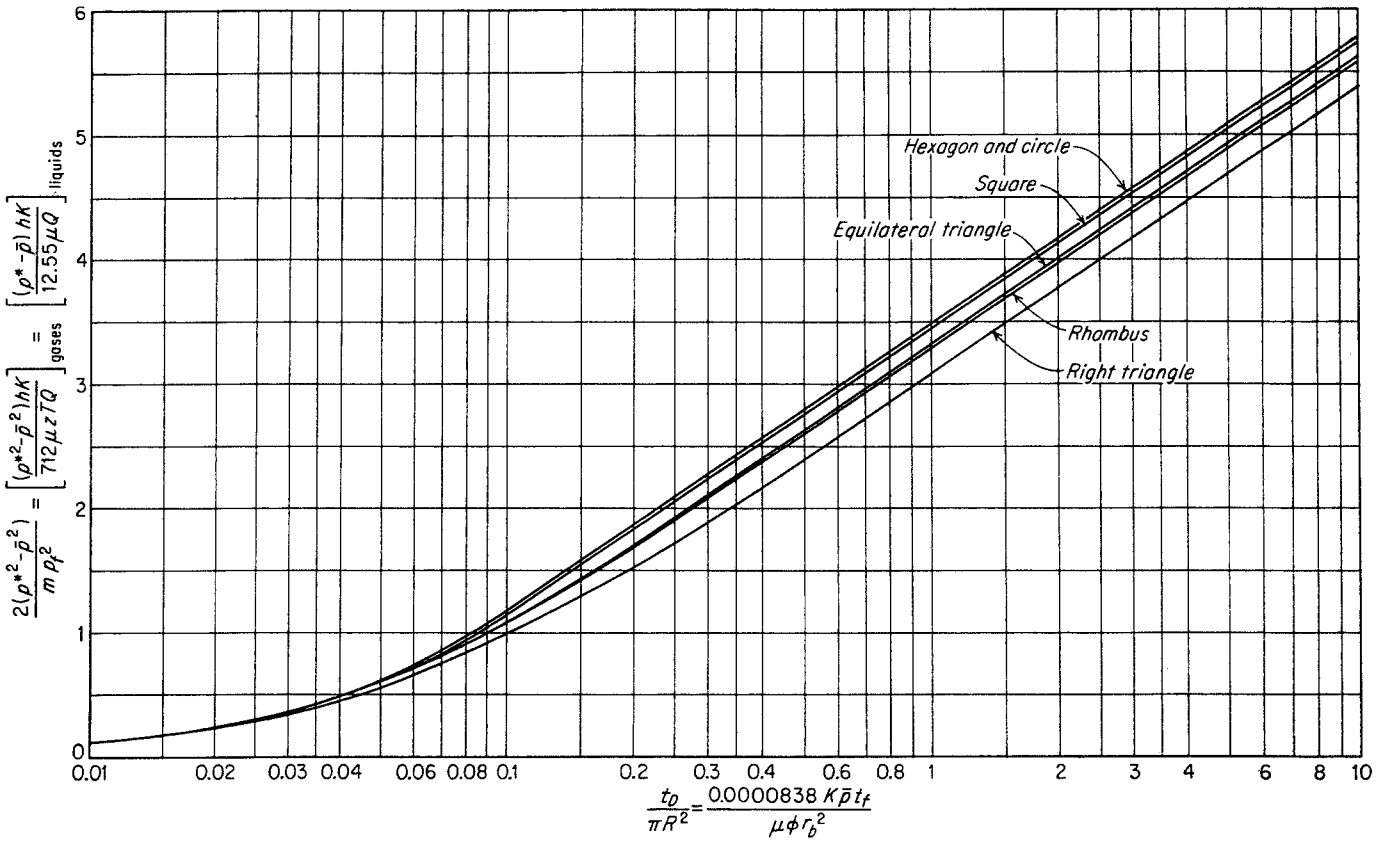

Fig. 10-20. Pressure function of one well in center of equilateral figures. (*Matthews, Brons, and Hazebroek, 10-22. Courtesy AIME.*)

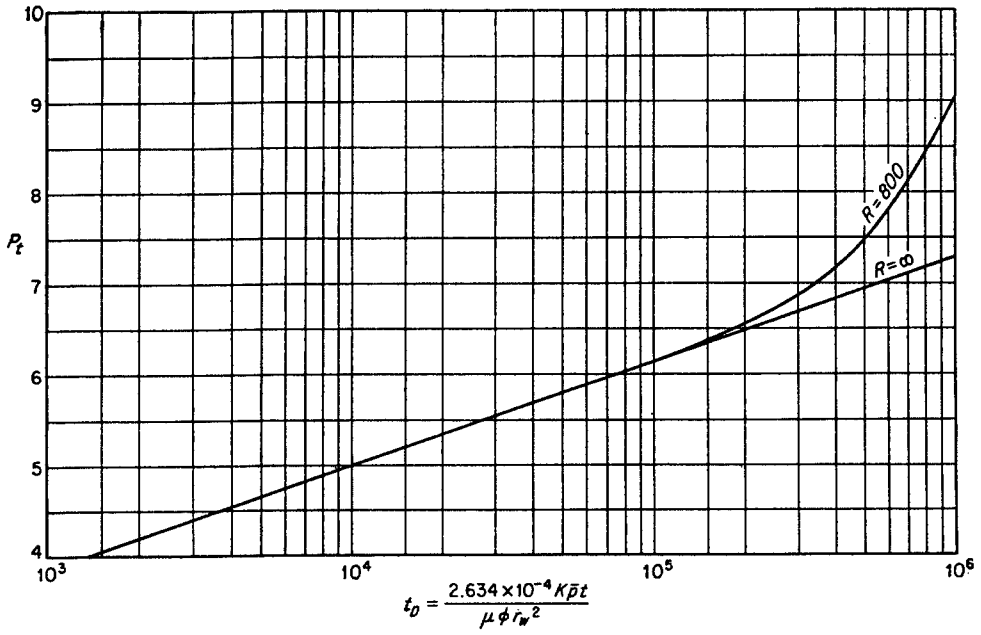

Fig. 10-21. Dimensionless pressure change for a constant-production-rate, finite reservoir with a closed exterior boundary, $R = r_b/r_w = 800$.

1. Volumetric Material Balance. Before we proceed with the build-up calculations, the true equalized reservoir pressure will be calculated from a material balance. A constant compressibility factor will be assumed.

$$\text{Pressure decline} = \frac{3{,}000{,}000 \times 0.89 \times 10.731 \times 640}{379\pi \times 400^2 \times 50 \times 0.15}$$

$$= 13 \text{ psia}$$

$$\bar{p} = 2{,}000 - 13 = 1{,}987 \text{ psia}$$

2. Unsteady-state Drawdown and Build-up Curves. Assume an average pressure of 1,900 psia for calculating the dimensionless time.

$$t_D = \frac{2.634 \times 10^{-4} \times 20 \times 1{,}900t}{0.016 \times 0.15 \times 0.5^2}$$

$$= 16{,}682t$$

The dimensionless flow rate is

$$m = \frac{1{,}424 \times 0.016 \times 0.89 \times 640 \times 3{,}000}{50 \times 20 \times 2{,}000^2}$$

$$= 0.009732$$

Values of P_t for $R = 800$ and a constant production rate from a finite radial reservoir with a closed outer boundary must be calculated. For large values of t_D, Chatas (10-7) gives Eq. (10-31*b*). For $R = 800$ this equation becomes

Table 10-3. Drawdown and Build-up Calculations

Total time, hr	Δt shut-in time, hr	t_D		P_t			$p_f^2 - p_s^2$, psia^2	p_s^2, psia$^2 \times 10^3$	$\frac{\Delta t}{t_f + \Delta t}$	p_s, psia
		Flow	Shut in	Flow	Shut in	Difference				
0	...	0	.....	0	....	0	0	4,000	.....	2,000
1	...	16,682	.....	5.26	....	5.26	204,800	3,795	.....	1,948
4	...	66,728	.....	5.96	....	5.96	232,000	3,768	.....	1,942
8	...	133,456	.....	6.30	....	6.30	245,200	3,755	.....	1,938
12	...	200,184	.....	6.55	....	6.55	255,000	3,745	.....	1,936
16	...	266,912	.....	6.76	....	6.76	263,200	3,737	.....	1,934
20	...	333,640	.....	6.97	....	6.97	271,300	3,729	.....	1,931
24	0	400,368	0	7.16	0	7.16	278,700	3,721	0	1,929
26	2	433,732	33,364	7.31	5.61	1.70	66,180	3,933.8	0.077	1,983
27	3	450,410	50,046	7.33	5.81	1.52	59,170	3,940.8	0.111	1,985
28	4	467,096	66,728	7.37	5.96	1.41	54,890	3,945.1	0.143	1,986
32	8	533,824	133,456	7.62	6.30	1.32	51,385	3,948.6	0.250	1,987
36	12	600,552	200,184	7.83	6.55	1.28	49,830	3,950.2	0.333	1,987
40	16	667,280	266,912	8.02	6.76	1.26	49,050	3,951.0	0.400	1,987
44	20	734,008	333,640	8.23	6.97	1.26	49,050	3,951.0	0.454	1,987
48	24	800,736	400,368	8.42	7.16	1.26	49,050	3,951.0	0.500	1,987

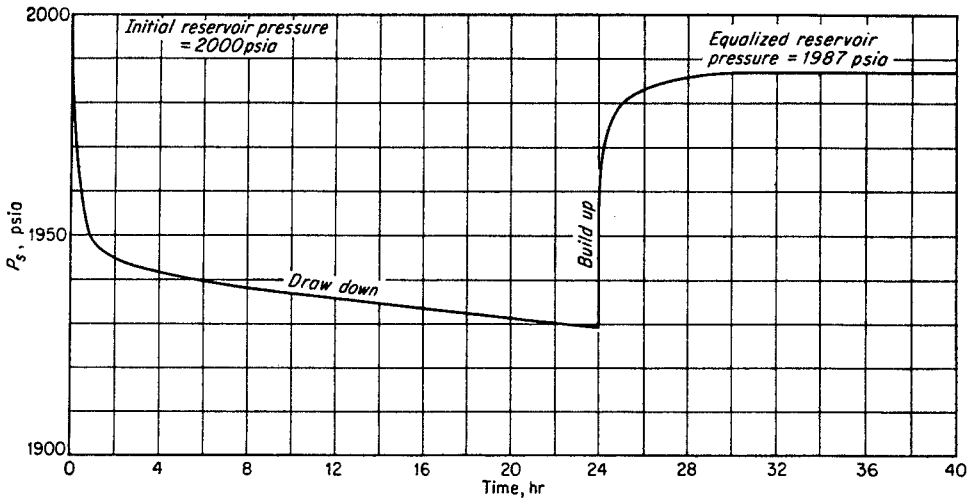

Fig. 10-22. Calculated drawdown and build-up curves for a finite reservoir.

$$P_t = \frac{t_D}{3.2 \times 10^5} + 5.934$$

For somewhat smaller values of t_D and for $R = \infty$, Eq. (10-31) applies. Figure 10-21 shows the P_t function for $R = 800$ and $R = \infty$.

Complete calculations of the hypothetical drawdown and build-up curves by means of Eq. (10-37) and the P_t values of Fig. 10-21 are tabulated in Table 10-3.

Figure 10-22 shows the calculated drawdown and build-up curves. In this case the equalized pressure reaches the value of 1,987 psia that was calculated by means of a material balance in a relatively short time.

$$\bar{p} = 1{,}987 \text{ psia}$$

3. Method of Matthews, Brons, and Hazebroek. Figure 10-23 shows a plot of the build-up pressures. The initial points form a straight line that extrapolates to a value of $(p^*)^2 = 3{,}983{,}200$ psia^2. The actual pressure variation is also shown; however, this portion of the curve would not usually be available. Note that $(p^*)^2$ has a different value than $p_f^2 = 4{,}000{,}000$ because a finite reservoir is being considered.

The value of dimensionless time for the production period is

$$t_D = 16{,}682 \times 24 = 400{,}000$$

The value of the abscissa of Fig. 10-20 is

$$\frac{t_D}{\pi R^2} = \frac{400{,}000}{\pi \times 800^2} = 0.199$$

From Fig. 10-20 for circular reservoirs,

$$\frac{[(p^*)^2 - \bar{p}^2] \times 2}{mp_f^2} = 1.85$$

Solving for $\bar{p}^2$,

$$\bar{p}^2 = 3{,}947{,}600 \text{ psia}^2$$

and

$$\bar{p} = 1{,}987 \text{ psia}$$

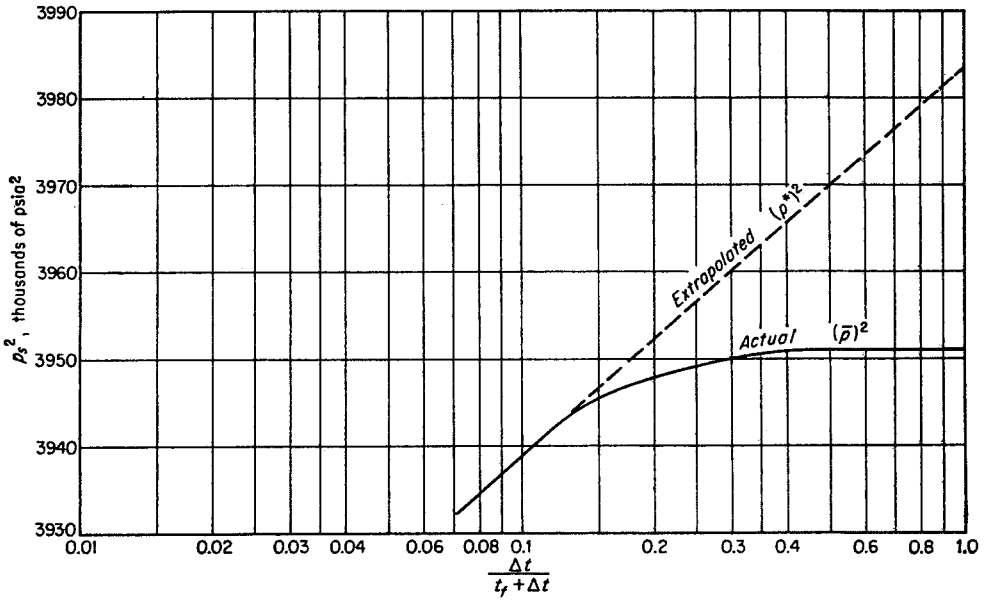

Fig. 10-23. Calculated build-up pressure plot to determine p^*.

Table 10-4. Solutions to Unsteady-state Flow Equations, Infinite Radial System, Constant Well Pressure

Dimensionless time t_D	*Fluid influx* Q_t	*Dimensionless time* t_D	*Fluid influx* Q_t
0.00	0.000	41	21.298
0.01	0.112	42	21.701
0.05	0.278	43	22.101
0.10	0.404	44	22.500
0.15	0.520	45	22.897
0.20	0.606	46	23.291
0.25	0.689	47	23.684
0.30	0.758	48	24.076
0.40	0.898	49	24.466
0.50	1.020	50	24.855
		51	25.244
0.60	1.140	52	25.633
0.70	1.251	53	26.020
0.80	1.359	54	26.406
0.90	1.469	55	26.791
1	1.569	56	27.174
2	2.447	57	27.555
3	3.202	58	27.935
4	3.893	59	28.314
5	4.539	60	28.691
6	5.153	61	29.068
7	5.743	62	29.443
8	6.314	63	29.818
9	6.869	64	30.192
10	7.411	65	30.565
11	7.940	66	30.937
12	8.457	67	31.308
13	8.964	68	31.679
14	9.461	69	32.048
15	9.949	70	32.417
16	10.434	71	32.785
17	10.913	72	33.151
18	11.386	73	33.517
19	11.855	74	33.883
20	12.319	75	34.247
21	12.778	76	34.611
22	13.233	77	34.974
23	13.684	78	35.336
24	14.131	79	35.697
25	14.573	80	36.058
26	15.013	81	36.418
27	15.450	82	36.777
28	15.883	83	37.136
29	16.313	84	37.494
30	16.742	85	37.851
31	17.167	86	38.207
32	17.590	87	38.563
33	18.011	88	38.919
34	18.429	89	39.272
35	18.845	90	39.626
36	19.259	91	39.979
37	19.671	92	40.331
38	20.080	93	40.684
39	20.488	94	41.034
40	20.894	95	41.385

Table 10-4. Solutions to Unsteady-state Flow Equations, Infinite Radial System, Constant Well Pressure (Continued)

Dimensionless time t_D	*Fluid influx* Q_t	*Dimensionless time* t_D	*Fluid influx* Q_t
96	41.735	355	121.966
97	42.084	360	123.403
98	42.433	365	124.838
99	42.781	370	126.270
100	43.129	375	127.699
105	44.858	380	129.126
110	46.574	385	130.550
115	48.277	390	131.972
120	49.968	395	133.391
125	51.648	400	134.808
130	53.317	405	136.223
135	54.976	410	137.635
140	56.625	415	139.045
145	58.265	420	140.453
150	59.895	425	141.859
155	61.517	430	143.262
160	63.131	435	144.664
165	64.737	440	146.064
170	66.336	445	147.461
175	67.928	450	148.856
180	69.512	455	150.249
185	71.090	460	151.640
190	72.661	465	153.029
195	74.226	470	154.416
200	75.785	475	155.801
205	77.338	480	157.184
210	78.886	485	158.565
215	80.428	490	159.945
220	81.965	495	161.322
225	83.497	500	162.698
230	85.023	510	165.444
235	86.545	520	168.183
240	88.062	525	169.549
245	89.575	530	170.914
250	91.084	540	173.639
255	92.589	550	176.357
260	94.090	560	179.069
265	95.588	570	181.774
270	97.081	575	183.124
275	98.571	580	184.473
280	100.057	590	187.166
285	101.540	600	189.852
290	103.019	610	192.533
295	104.495	620	195.208
300	105.968	625	196.544
305	107.437	630	197.878
310	108.904	640	200.542
315	110.367	650	203.201
320	111.827	660	205.854
325	113.284	670	208.502
330	114.738	675	209.825
335	116.189	680	211.145
340	117.638	690	213.784
345	119.083	700	216.417
350	120.526	710	219.046

Table 10-4. Solutions to Unsteady-state Flow Equations, Infinite Radial System, Constant Well Pressure (*Continued*)

Dimensionless time t_D	*Fluid influx* Q_t	*Dimensionless time* t_D	*Fluid influx* Q_t
720	221.670	1,175	337.142
725	222.980	1,180	338.376
730	224.289	1,190	340.843
740	226.904	1,200	343.308
750	229.514	1,210	345.770
760	232.120	1,220	348.230
770	234.721	1,225	349.460
775	236.020	1,230	350.688
780	237.318	1,240	353.144
790	239.912	1,250	355.597
800	242.501	1,260	358.048
810	245.086	1,270	360.496
820	247.668	1,275	361.720
825	248.957	1,280	362.942
830	250.245	1,290	365.386
840	252.819	1,300	367.828
850	255.388	1,310	370.267
860	257.953	1,320	372.704
870	260.515	1,325	373.922
875	261.795	1,330	375.139
880	263.073	1,340	377.572
890	265.629	1,350	380.003
900	268.181	1,360	382.432
910	270.729	1,370	384.859
920	273.274	1,375	386.070
925	274.545	1,380	387.283
930	275.815	1,390	389.705
940	278.353	1,400	392.125
950	280.888	1,410	394.543
960	283.420	1,420	396.959
970	285.948	1,425	398.167
975	287.211	1,430	399.373
980	288.473	1,440	401.786
990	290.995	1,450	404.197
1,000	293.514	1,460	406.606
1,010	296.030	1,470	409.013
1,020	298.543	1,475	410.214
1,025	299.799	1,480	411.418
1,030	301.053	1,490	413.820
1,040	303.560	1,500	416.220
1,050	306.065	1,525	422.214
1,060	308.567	1,550	428.196
1,070	311.066	1,575	434.168
1,075	312.314	1,600	440.128
1,080	313.562	1,625	446.077
1,090	316.055	1,650	452.016
1,100	318.545	1,675	457.945
1,110	321.032	1,700	463.863
1,120	323.517	1,725	469.771
1,125	324.760	1,750	475.669
1,130	326.000	1,775	481.558
1,140	328.480	1,800	487.437
1,150	330.958	1,825	493.307
1,160	333.433	1,850	499.167
1,170	335.906	1,875	505.019

Table 10-4. Solutions to Unsteady-state Flow Equations, Infinite Radial System, Constant Well Pressure (*Continued*)

Dimensionless time t_D	*Fluid influx* Q_t	*Dimensionless time* t_D	*Fluid influx* Q_t
1,900	510.861	4,050	990.108
1,925	516.695	4,100	1,000.858
1,950	522.520	4,150	1,011.595
1,975	528.337	4,200	1,022.318
2,000	534.145	4,250	1,033.028
2,025	539.945	4,300	1,043.724
2,050	545.737	4,350	1,054.409
2,075	551.522	4,400	1,065.082
2,100	557.299	4,450	1,075.743
2,125	563.068	4,500	1,086.390
2,150	568.830	4,550	1,097.024
2,175	574.585	4,600	1,107.646
2,200	580.332	4,650	1,118.257
2,225	586.072	4,700	1,128.854
2,250	591.806	4,750	1,139.439
2,275	597.532	4,800	1,150.012
2,300	603.252	4,850	1,160.574
2,325	608.965	4,900	1,171.125
2,350	614.672	4,950	1,181.666
2,375	620.372	5,000	1,192.198
2,400	626.066	5,100	1,213.222
2,425	631.755	5,200	1,234.203
2,450	637.437	5,300	1,255.141
2,475	643.113	5,400	1,276.037
2,500	648.781	5,500	1,296.893
2,550	660.093	5,600	1,317.709
2,600	671.379	5,700	1,338.486
2,650	682.640	5,800	1,359.225
2,700	693.877	5,900	1,379.927
2,750	705.090	6,000	1,400.593
2,800	716.280	6,100	1,421.224
2,850	727.449	6,200	1,441.820
2,900	738.598	6,300	1,462.383
2,950	749.725	6,400	1,482.912
3,000	760.833	6,500	1,503.408
3,050	771.922	6,600	1,523.872
3,100	782.992	6,700	1,544.305
3,150	794.042	6,800	1,564.706
3,200	805.075	6,900	1,585.077
3,250	816.090	7,000	1,605.418
3,300	827.088	7,100	1,625.729
3,350	838.067	7,200	1,646.011
3,400	849.028	7,300	1,666.265
3,450	859.974	7,400	1,686.490
3,500	870.903	7,500	1,706.688
3,550	881.816	7,600	1,726.859
3,600	892.712	7,700	1,747.002
3,650	903.594	7,800	1,767.120
3,700	914.459	7,900	1,787.212
3,750	925.309	8,000	1,807.278
3,800	936.144	8,100	1,827.319
3,850	946.966	8,200	1,847.336
3,900	957.773	8,300	1,867.329
3,950	968.566	8,400	1,887.298
4,000	979.344	8,500	1,907.243

Table 10-4. Solutions to Unsteady-state Flow Equations, Infinite Radial System, Constant Well Pressure (*Continued*)

Dimensionless time t_D	*Fluid influx* Q_t	*Dimensionless time* t_D	*Fluid influx* Q_t
8,600	1,927.166	2.5×10^7	2.961×10^6
8,700	1,947.065	3.0×10^7	3.517×10^6
8,800	1,966.942	4.0×10^7	4.610×10^6
8,900	1,986.796	5.0×10^7	5.689×10^6
9,000	2,006.628	6.0×10^7	6.758×10^6
9,100	2,026.438	7.0×10^7	7.816×10^6
9,200	2,046.227	8.0×10^7	8.866×10^6
9,300	2,065.996	9.0×10^7	9.911×10^6
9,400	2,085.744	1.0×10^8	1.095×10^7
9,500	2,105.473	1.5×10^8	1.604×10^7
9,600	2,125.184	2.0×10^8	2.108×10^7
9,700	2,144.878	2.5×10^8	2.607×10^7
9,800	2,164.555	3.0×10^8	3.100×10^7
9,900	2,184.216	4.0×10^8	4.071×10^7
10,000	2,203.861	5.0×10^8	5.032×10^7
12,500	2,688.967	6.0×10^8	5.984×10^7
15,000	3,164.780	7.0×10^8	6.928×10^7
17,500	3,633.368	8.0×10^8	7.865×10^7
20,000	4,095.800	9.0×10^8	8.797×10^7
25,000	5,005.726	1.0×10^9	9.725×10^7
30,000	5,899.508	1.5×10^9	1.429×10^8
35,000	6,780.247	2.0×10^9	1.880×10^8
40,000	7,650.096	2.5×10^9	2.328×10^8
50,000	9,363.099	3.0×10^9	2.771×10^8
60,000	11,047.299	4.0×10^9	3.645×10^8
70,000	12,708.358	5.0×10^9	4.510×10^8
75,000	13,531.457	6.0×10^9	5.368×10^8
80,000	14,350.121	7.0×10^9	6.220×10^8
90,000	15,975.389	8.0×10^9	7.066×10^8
100,000	17,586.284	9.0×10^9	7.909×10^8
125,000	21,560.732	1.0×10^{10}	8.747×10^8
1.5×10^5	2.538×10^4	1.5×10^{10}	1.288×10^9
2.0×10^5	3.308×10^4	2.0×10^{10}	1.697×10^9
2.5×10^5	4.066×10^4	2.5×10^{10}	2.103×10^9
3.0×10^5	4.817×10^4	3.0×10^{10}	2.505×10^9
4.0×10^5	6.267×10^4	4.0×10^{10}	3.299×10^9
5.0×10^5	7.699×10^4	5.0×10^{10}	4.087×10^9
6.0×10^5	9.113×10^4	6.0×10^{10}	4.868×10^9
7.0×10^5	1.051×10^5	7.0×10^{10}	5.643×10^9
8.0×10^5	1.189×10^5	8.0×10^{10}	6.414×10^9
9.0×10^5	1.326×10^5	9.0×10^{10}	7.183×10^9
1.0×10^6	1.462×10^5	1.0×10^{11}	7.948×10^9
1.5×10^6	2.126×10^5	1.5×10^{11}	1.17×10^{10}
2.0×10^6	2.781×10^5	2.0×10^{11}	1.55×10^{10}
2.5×10^6	3.427×10^5	2.5×10^{11}	1.92×10^{10}
3.0×10^6	4.064×10^5	3.0×10^{11}	2.29×10^{10}
4.0×10^6	5.313×10^5	4.0×10^{11}	3.02×10^{10}
5.0×10^6	6.544×10^5	5.0×10^{11}	3.75×10^{10}
6.0×10^6	7.761×10^5	6.0×10^{11}	4.47×10^{10}
7.0×10^6	8.965×10^5	7.0×10^{11}	5.19×10^{10}
8.0×10^6	1.016×10^6	8.0×10^{11}	5.89×10^{10}
9.0×10^6	1.134×10^6	9.0×10^{11}	6.58×10^{10}
1.0×10^7	1.252×10^6	1.0×10^{12}	7.28×10^{10}
1.5×10^7	1.828×10^6	1.5×10^{12}	1.08×10^{11}
2.0×10^7	2.398×10^6	2.0×10^{12}	1.42×10^{11}

SOURCE: Chatas (10-7).

Table 10-5. Solutions to Unsteady-state Flow Equations, Infinite Radial System, Constant Production Rate

Dimensionless time t_D	*Pressure change* P_t	*Dimensionless time* t_D	*Pressure change* P_t
0	0	2.0	1.0195
0.005	0.0250	3.0	1.1665
0.001	0.0352	4.0	1.2750
0.002	0.0495	5.0	1.3625
0.003	0.0603	6.0	1.4362
0.004	0.0694	7.0	1.4997
0.005	0.0774	8.0	1.5557
0.006	0.0845	9.0	1.6057
0.007	0.0911	10.0	1.6509
0.008	0.0971	15.0	1.8294
0.009	0.1028	20.0	1.9601
0.01	0.1081	30.0	2.1470
0.015	0.1312	40.0	2.2824
0.02	0.1503	50.0	2.3884
0.025	0.1669	60.0	2.4758
0.03	0.1818	70.0	2.5501
0.04	0.2077	80.0	2.6147
0.05	0.2301	90.0	2.6718
0.06	0.2500	100.0	2.7233
0.07	0.2680	150.0	2.9212
0.08	0.2845	200.0	3.0636
0.09	0.2999	250.0	3.1726
0.1	0.3144	300.0	3.2630
0.15	0.3750	350.0	3.3394
0.2	0.4241	400.0	3.4057
0.3	0.5024	450.0	3.4641
0.4	0.5645	500.0	3.5164
0.5	0.6167	550.0	3.5643
0.6	0.6622	600.0	3.6076
0.7	0.7024	650.0	3.6476
0.8	0.7387	700.0	3.6842
0.9	0.7716	750.0	3.7184
1.0	0.8019	800.0	3.7505
1.2	0.8672	850.0	3.7805
1.4	0.9160	900.0	3.8088
		950.0	3.8355
		1,000.0	3.8584

SOURCE: Chatas (10-7).

Table 10-6. Solutions to Unsteady-state Flow Equations, Finite Reservoir, Closed Exterior Boundary, Constant Well Pressure

$R = 1.5$		$R = 2.0$		$R = 2.5$		$R = 3.0$		$R = 3.5$		$R = 4.0$		$R = 4.5$		$R = 5.0$		$R = 6.0$		$R = 7.0$		$R = 8.0$		$R = 9.0$		$R = 10.0$	
t_D	Q_t	t_D	Q_t	t_D	Q_t	t_D	Q_t	t_D	Q_t	t_D	Q_t	t_D	Q_t	t_D	Q_t	t_D	Q_t	t_D	Q_t	t_D	Q_t	t_D	Q_t	t_D	Q_t
5.0×10^{-2}	0.276	5.00×10^{-2}	0.278	1.0×10^{-1}	0.408	3.0×10^{-1}	0.755	1.00	1.571	2.00	2.442	2.5	2.835	3.0	3.195	6.0	5.148	9.00	6.861	9	6.861	10	7.417	15	9.965
6.0×10^{-2}	0.304	7.50×10^{-2}	0.345	1.5×10^{-1}	0.509	4.0×10^{-1}	0.895	1.20	1.761	2.20	2.598	3.0	3.196	3.5	3.542	6.5	5.440	9.50	7.127	10	7.398	15	9.945	20	12.32
7.0×10^{-2}	0.330	1.00×10^{-1}	0.404	2.0×10^{-1}	0.599	5.0×10^{-1}	1.023	1.40	1.940	2.40	2.748	3.5	3.537	4.0	3.875	7.0	5.724	10	7.389	11	7.920	20	12.26	22	13.22
8.0×10^{-2}	0.354	1.25×10^{-1}	0.458	2.5×10^{-1}	0.681	6.0×10^{-1}	1.143	1.60	2.111	2.60	2.893	4.0	3.859	4.5	4.193	7.5	6.002	11	7.902	12	8.431	22	13.13	24	14.09
9.0×10^{-2}	0.375	1.50×10^{-1}	0.507	3.0×10^{-1}	0.758	7.0×10^{-1}	1.256	1.80	2.273	2.80	3.034	4.5	4.165	5.0	4.499	8.0	6.273	12	8.397	13	8.930	24	13.98	26	14.95
1.0×10^{-1}	0.395	1.75×10^{-1}	0.553	3.5×10^{-1}	0.829	8.0×10^{-1}	1.363	2.00	2.427	3.00	3.170	5.0	4.454	5.5	4.792	8.5	6.537	13	8.876	14	9.418	26	14.79	28	15.78
1.1×10^{-1}	0.414	2.00×10^{-1}	0.597	4.0×10^{-1}	0.897	9.0×10^{-1}	1.465	2.20	2.574	3.25	3.334	5.5	4.727	6.0	5.074	9.0	6.795	14	9.341	15	9.895	28	15.59	30	16.59
1.2×10^{-1}	0.431	2.25×10^{-1}	0.638	4.5×10^{-1}	0.962	1.00	1.563	2.40	2.715	3.50	3.493	6.0	4.986	6.5	5.345	9.5	7.047	15	9.791	16	10.361	30	16.35	32	17.38
1.3×10^{-1}	0.446	2.50×10^{-1}	0.678	5.0×10^{-1}	1.024	1.25	1.791	2.60	2.849	3.75	3.645	6.5	5.231	7.0	5.605	10.0	7.293	16	10.23	17	10.82	32	17.10	34	18.16
1.4×10^{-1}	0.461	2.75×10^{-1}	0.715	5.5×10^{-1}	1.083	1.50	1.997	2.80	2.976	4.00	3.792	7.0	5.464	7.5	5.854	10.5	7.533	17	10.65	18	11.26	34	17.82	36	18.91
1.5×10^{-1}	0.474	3.00×10^{-1}	0.751	6.0×10^{-1}	1.140	1.75	2.184	3.00	3.098	4.25	3.932	7.5	5.684	8.0	6.094	11	7.767	18	11.06	19	11.70	36	18.52	38	19.65
1.6×10^{-1}	0.486	3.25×10^{-1}	0.785	6.5×10^{-1}	1.195	2.00	2.353	3.25	3.242	4.50	4.068	8.0	5.892	8.5	6.325	12	8.220	19	11.46	20	12.13	38	19.19	40	20.37
1.7×10^{-1}	0.497	3.50×10^{-1}	0.817	7.0×10^{-1}	1.248	2.25	2.507	3.50	3.379	4.75	4.198	8.5	6.089	9.0	6.547	13	8.651	20	11.85	22	12.95	40	19.85	42	21.07
1.8×10^{-1}	0.507	3.75×10^{-1}	0.848	7.5×10^{-1}	1.299	2.50	2.646	3.75	3.507	5.00	4.323	9.0	6.276	9.5	6.760	14	9.063	22	12.58	24	13.74	42	20.48	44	21.76
1.9×10^{-1}	0.517	4.00×10^{-1}	0.877	8.0×10^{-1}	1.348	2.75	2.772	4.00	3.628	5.50	4.560	9.5	6.453	10	6.965	15	9.456	24	13.27	26	14.50	44	21.09	46	22.42
2.0×10^{-1}	0.525	4.25×10^{-1}	0.905	8.5×10^{-1}	1.395	3.00	2.886	4.25	3.742	6.00	4.779	10	6.621	11	7.350	16	9.829	26	13.92	28	15.23	46	21.69	48	23.07
2.1×10^{-1}	0.533	4.50×10^{-1}	0.932	9.0×10^{-1}	1.440	3.25	2.990	4.50	3.850	6.50	4.982	11	6.930	12	7.706	17	10.19	28	14.53	30	15.92	48	22.26	50	23.71
2.2×10^{-1}	0.541	4.75×10^{-1}	0.958	9.5×10^{-1}	1.484	3.50	3.084	4.75	3.951	7.00	5.169	12	7.208	13	8.035	18	10.53	30	15.11	34	17.22	50	22.82	52	24.33
2.3×10^{-1}	0.548	5.00×10^{-1}	0.983	1.0	1.526	3.75	3.170	5.00	4.047	7.50	5.343	13	7.457	14	8.339	19	10.85	35	16.39	38	18.41	52	23.36	54	24.94
2.4×10^{-1}	0.554	5.50×10^{-1}	1.028	1.1	1.605	4.00	3.247	5.50	4.222	8.00	5.504	14	7.680	15	8.620	20	11.16	40	17.49	40	18.97	54	23.89	56	25.53
2.5×10^{-1}	0.559	6.00×10^{-1}	1.070	1.2	1.679	4.25	3.317	6.00	4.378	8.50	5.653	15	7.880	16	8.879	22	11.74	45	18.43	45	20.26	56	24.39	58	26.11
2.6×10^{-1}	0.565	6.50×10^{-1}	1.108	1.3	1.747	4.50	3.381	6.50	4.516	9.00	5.790	16	8.060	18	9.338	24	12.26	50	19.24	50	21.42	58	24.88	60	26.67
2.8×10^{-1}	0.574	7.00×10^{-1}	1.143	1.4	1.811	4.75	3.439	7.00	4.639	9.50	5.917	18	8.365	20	9.731	25	12.50	60	20.51	55	22.46	60	25.36	65	28.02
3.0×10^{-1}	0.582	7.50×10^{-1}	1.174	1.5	1.870	5.00	3.491	7.50	4.749	10	6.035	20	8.611	22	10.07	31	13.74	70	21.45	60	23.40	65	26.48	70	29.29
3.2×10^{-1}	0.588	8.00×10^{-1}	1.203	1.6	1.924	5.50	3.581	8.00	4.846	11	6.246	22	8.809	24	10.35	35	14.40	80	22.13	70	24.98	70	27.52	75	30.49
3.4×10^{-1}	0.594	9.00×10^{-1}	1.253	1.7	1.975	6.00	3.656	8.50	4.932	12	6.425	24	8.968	26	10.59	39	14.93	90	22.63	80	26.26	75	28.48	80	31.61
3.6×10^{-1}	0.599	1.0	1.295	1.8	2.022	6.50	3.717	9.00	5.009	13	6.580	26	9.097	28	10.80	51	16.05	100	23.00	90	27.28	80	29.36	85	32.67
3.8×10^{-1}	0.603	1.1	1.330	2.0	2.106	7.00	3.767	9.50	5.078	14	6.712	28	9.200	30	10.98	60	16.56	120	23.47	100	28.11	85	30.18	90	33.66
4.0×10^{-1}	0.606	1.2	1.358	2.2	2.178	7.50	3.809	10.00	5.138	15	6.825	30	9.283	34	11.26	70	16.91	140	23.71	120	29.31	90	30.93	95	34.60
4.5×10^{-1}	0.613	1.3	1.382	2.4	2.241	8.00	3.843	11	5.241	16	6.922	34	9.404	38	11.46	80	17.14	160	23.85	140	30.08	95	31.63	100	35.48
5.0×10^{-1}	0.617	1.4	1.402	2.6	2.294	9.00	3.894	12	5.321	17	7.004	38	9.481	42	11.61	90	17.27	180	23.92	160	30.58	100	32.27	120	38.51
6.0×10^{-1}	0.621	1.6	1.432	2.8	2.340	10.00	3.928	13	5.385	18	7.076	42	9.532	46	11.71	100	17.36	200	23.96	180	30.91	120	34.39	140	40.89
7.0×10^{-1}	0.623	1.7	1.444	3.0	2.380	11.00	3.951	14	5.435	20	7.189	46	9.565	50	11.79	110	17.41	500	24.00	200	31.12	140	35.92	160	42.75
8.0×10^{-1}	0.624	1.8	1.453	3.4	2.444	12.00	3.967	15	5.476	22	7.272	50	9.586	60	11.91	120	17.45			240	31.34	160	37.04	180	44.21
		2.0	1.468	3.8	2.491	14.00	3.985	16	5.506	24	7.332	60	9.612	70	11.96	130	17.46			280	31.43	180	37.85	200	45.36
		2.5	1.487	4.2	2.525	16.00	3.993	17	5.531	26	7.377	70	9.621	80	11.98	140	17.48			320	31.47	200	38.44	240	46.95
		3.0	1.495	4.6	2.551	18.00	3.997	18	5.551	30	7.434	80	9.623	90	11.99	150	17.49			360	31.49	240	39.17	280	47.94
		4.0	1.499	5.0	2.570	20.00	3.999	20	5.579	34	7.464	90	9.624	100	12.00	160	17.49			400	31.50	280	39.56	320	48.54
		5.0	1.500	6.0	2.599	22.00	3.999	25	5.611	38	7.481	100	9.625	120	12.0	180	17.50			500	31.50	320	39.77	360	48.91
				7.0	2.613	24.00	4.000	30	5.621	42	7.490					200	17.50					360	39.88	400	49.14
				8.0	2.619			35	5.624	46	7.494					220	17.50					400	39.94	440	49.28
				9.0	2.622			40	5.625	50	7.497											440	39.97	480	49.36
				10.0	2.624																	480	39.98		

SOURCE: Van Everdingen and Hurst (10-27).

Table 10-7. Solutions to Unsteady-state Flow Equations, Finite Radial System with Closed Exterior Boundary, Constant Production Rate

$R = 1.5$*		$R = 2.0$		$R = 2.5$		$R = 3.0$		$R = 3.5$		$R = 4$		$R = 4.5$		$R = 5$		$R = 6.0$		$R = 7.0$		$R = 8.0$		$R = 9.0$		$R = 10$	
t_D	P_t	t_D	P_t	t_D	P_t	t_D	P_t	t_D	P_t	t_D	P_t	t_D	P_t	t_D	P_t	t_D	P_t	t_D	P_t	t_D	P_t	t_D	P_t	t_D	P_t
6.0×10^{-2}	0.251	2.2×10^{-1}	0.443	4.0×10^{-1}	0.565	5.2×10^{-1}	0.627	1.0	0.802	1.5	0.927	2.0	1.023	3.0	1.167	4.0	1.275	6.0	1.436	8.0	1.556	10.0	1.651	12.0	1.732
8.0×10^{-2}	0.288	2.4×10^{-1}	0.459	4.2×10^{-1}	0.576	5.4×10^{-1}	0.636	1.1	0.830	1.6	0.948	2.1	1.040	3.1	1.180	4.5	1.322	6.5	1.470	8.5	1.582	10.5	1.673	12.5	1.750
1.0×10^{-1}	0.322	2.6×10^{-1}	0.476	4.4×10^{-1}	0.587	5.6×10^{-1}	0.645	1.2	0.857	1.7	0.968	2.2	1.056	3.2	1.192	5.0	1.364	7.0	1.501	9.0	1.607	11.0	1.693	13.0	1.768
1.2×10^{-1}	0.355	2.8×10^{-1}	0.492	4.6×10^{-1}	0.598	6.0×10^{-1}	0.662	1.3	0.882	1.8	0.988	2.3	1.072	3.3	1.204	5.5	1.404	7.5	1.531	9.5	1.631	11.5	1.713	13.5	1.784
1.4×10^{-1}	0.387	3.0×10^{-1}	0.507	4.8×10^{-1}	0.608	6.5×10^{-1}	0.683	1.4	0.906	1.9	1.007	2.4	1.087	3.4	1.215	6.0	1.441	8.0	1.559	10.0	1.653	12.0	1.732	14.0	1.801
1.6×10^{-1}	0.420	3.2×10^{-1}	0.522	5.0×10^{-1}	0.618	7.0×10^{-1}	0.703	1.5	0.929	2.0	1.025	2.5	1.102	3.5	1.227	6.5	1.477	8.5	1.586	10.5	1.675	12.5	1.750	14.5	1.817
1.8×10^{-1}	0.452	3.4×10^{-1}	0.536	5.2×10^{-1}	0.628	7.5×10^{-1}	0.721	1.6	0.951	2.2	1.059	2.6	1.116	3.6	1.238	7.0	1.511	9.0	1.613	11.0	1.697	13.0	1.768	15.0	1.832
2.0×10^{-1}	0.484	3.6×10^{-1}	0.551	5.4×10^{-1}	0.638	8.0×10^{-1}	0.740	1.7	0.973	2.4	1.092	2.7	1.130	3.7	1.249	7.5	1.544	9.5	1.638	11.5	1.717	13.5	1.786	15.5	1.847
2.2×10^{-1}	0.516	3.8×10^{-1}	0.565	5.6×10^{-1}	0.647	8.5×10^{-1}	0.758	1.8	0.994	2.6	1.123	2.8	1.144	3.8	1.259	8.0	1.576	10.0	1.663	12.0	1.737	14.0	1.803	16.0	1.862
2.4×10^{-1}	0.548	4.0×10^{-1}	0.579	5.8×10^{-1}	0.657	9.0×10^{-1}	0.776	1.9	1.014	2.8	1.154	2.9	1.158	3.9	1.270	8.5	1.607	11.0	1.711	12.5	1.757	14.5	1.819	17.0	1.890
2.6×10^{-1}	0.580	4.2×10^{-1}	0.593	6.0×10^{-1}	0.666	9.5×10^{-1}	0.791	2.0	1.034	3.0	1.184	3.0	1.171	4.0	1.281	9.0	1.638	12.0	1.757	13.0	1.776	15.0	1.835	18.0	1.917
2.8×10^{-1}	0.612	4.4×10^{-1}	0.607	6.5×10^{-1}	0.688	1.0	0.806	2.25	1.083	3.5	1.255	3.2	1.197	4.2	1.301	9.5	1.668	13.0	1.801	13.5	1.795	15.5	1.851	19.0	1.943
3.0×10^{-1}	0.644	4.6×10^{-1}	0.621	7.0×10^{-1}	0.710	1.2	0.865	2.50	1.130	4.0	1.324	3.4	1.222	4.4	1.321	10.0	1.698	14.0	1.845	14.0	1.813	16.0	1 867	20.0	1.968
3.5×10^{-1}	0.724	4.8×10^{-1}	0.634	7.5×10^{-1}	0.731	1.4	0.920	2.75	1.176	4.5	1.392	3.6	1.246	4.6	1.340	11.0	1.757	15.0	1.888	14.5	1.831	17.0	1.897	22.0	2.017
4.0×10^{-1}	0.804	5.0×10^{-1}	0.648	8.0×10^{-1}	0.752	1.6	0.973	3.0	1.221	5.0	1.460	3.8	1.269	4.8	1.360	12.0	1.815	16.0	1.931	15.0	1.849	18.0	1.926	24.0	2.063
4.5×10^{-1}	0.884	6.0×10^{-1}	0.715	8.5×10^{-1}	0.772	2.0	1.076	4.0	1.401	5.5	1.527	4.0	1.292	5.0	1.378	13.0	1.873	17.0	1.974	17.0	1.919	19.0	1.955	26.0	2.108
5.0×10^{-1}	0.964	7.0×10^{-1}	0.782	9.0×10^{-1}	0.792	3.0	1.328	5.0	1.579	6.0	1.594	4.5	1.349	5.5	1.424	14.0	1.931	18.0	2.016	19.0	1.986	20.0	1.983	28.0	2.151
5.5×10^{-1}	1.044	8.0×10^{-1}	0.849	9.5×10^{-1}	0.812	4.0	1.578	6.0	1.757	6.5	1.660	5.0	1.403	6.0	1.469	15.0	1.988	19.0	2.058	21.0	2.051	22.0	2.037	30.0	2.194
6.0×10^{-1}	1.124	9.0×10^{-1}	0.915	1.0	0.832	5.0	1.828			7.0	1.727	5.5	1.457	6.5	1.513	16.0	2.045	20.0	2.100	23.0	2.116	24.0	2.090	32.0	2.236
		1.0	0.982	2.0	1.215					8.0	1.861	6.0	1.510	7.0	1.556	17.0	2.103	22.0	2.184	25.0	2.180	26.0	2.142	34.0	2.278
		2 0	1.649	3.0	1.596					9.0	1.994	7.0	1.615	7.5	1.598	18.0	2.160	24.0	2.267	30.0	2.340	28.0	2.193	36.0	2.319
		3.0	2.316	4.0	1.977					10.0	2.127	8.0	1.719	8.0	1.641	19.0	2.217	26.0	2.351	35.0	2.499	30.0	2.244	38.0	2.360
		5.0	3.649	5.0	2.358							9.0	1.823	9.0	1.725	20.0	2.274	28.0	2.434	40.0	2.658	34.0	2.345	40.0	2.401
												10.0	1.927	10.0	1.808	25.0	2.560	30.0	2.517	45.0	2.817	38.0	2.446	50.0	2.604
												11.0	2.031	11.0	1.892	30.0	2.846					40.0	2.496	60.0	2.806
												12.0	2.135	12.0	1.975							45.0	2.621	70.0	3.008
												13.0	2.239	13.0	2.059							50.0	2.746		
												14.0	2.343	14.0	2.142										
												15.0	2.447	15.0	2.225										

* $R = r_b/r_w$.

SOURCE: Van Everdingen and Hurst (10-27).

Table 10-8. Solutions to Unsteady-state Flow Equations, Finite Radial System with Constant Pressure at Exterior Boundary, Constant Production Rate

$R = 1.5$		$R = 2.0$		$R = 2.5$		$R = 3.0$		$R = 3.5$		$R = 4.0$		$R = 6.0$		$R = 8.0$		$R = 10$		$R = 15$		$R = 20$		$R = 25$		$R = 30$	
t_D	P_t	t_D	P_t	t_D	P_t	t_D	P_t	t_D	P_t	t_D	P_t	t_D	P_t	t_D	P_t	t_D	P_t	t_D	P_t	t_D	P_t	t_D	P_t	t_D	P_t
5.0×10^{-2}	0.230	2.0×10^{-1}	0.424	3.0×10^{-1}	0.502	5.0×10^{-1}	0.617	5.0×10^{-1}	0.620	1.0	0.802	4.0	1.275	7.0	1.499	10.0	1.651	20.0	1.960	30.0	2.148	50.0	2.389	70.0	2.551
5.5×10^{-2}	0.240	2.2×10^{-1}	0.441	3.5×10^{-1}	0.535	5.5×10^{-1}	0.640	6.0×10^{-1}	0.665	1.2	0.857	4.5	1.320	7.5	1.527	12.0	1.730	22.0	2.003	35.0	2.219	55.0	2.434	80.0	2.615
6.0×10^{-2}	0.249	2.4×10^{-1}	0.457	4.0×10^{-1}	0.564	6.0×10^{-1}	0.662	7.0×10^{-1}	0.705	1.4	0.905	5.0	1.361	8.0	1.554	14.0	1.798	24.0	2.043	40.0	2.282	60.0	2.476	90.0	2.672
7.0×10^{-2}	0.266	2.6×10^{-1}	0.472	4.5×10^{-1}	0.591	7.0×10^{-1}	0.702	8.0×10^{-1}	0.741	1.6	0.947	5.5	1.398	8.5	1.580	16.0	1.856	26.0	2.080	45.0	2.338	65.0	2.514	100	2.723
8.0×10^{-2}	0.282	2.8×10^{-1}	0.485	5.0×10^{-1}	0.616	8.0×10^{-1}	0.738	9.0×10^{-1}	0.774	1.8	0.986	6.0	1.432	9.0	1.604	18.0	1.907	28.0	2.114	50.0	2.388	70.0	2.550	120	2.812
9.0×10^{-2}	0.292	3.0×10^{-1}	0.498	5.5×10^{-1}	0.638	9.0×10^{-1}	0.770	1.0	0.804	2.0	1.020	6.5	1.462	9.5	1.627	20.0	1.952	30.0	2.146	60.0	2.475	75.0	2.583	140	2.886
1.0×10^{-1}	0.307	3.5×10^{-1}	0.527	6.0×10^{-1}	0.659	1.0	0.799	1.2	0.858	2.2	1.052	7.0	1.490	10.0	1.648	25.0	2.043	35.0	2.218	70.0	2.547	80.0	2.614	160	2.950
1.2×10^{-1}	0.328	4.0×10^{-1}	0.552	7.0×10^{-1}	0.696	1.2	0.850	1.4	0.904	2.4	1.080	7.5	1.516	12.0	1.724	30.0	2.111	40.0	2.279	80.0	2.609	85.0	2.643	165	2.965
1.4×10^{-1}	0.344	4.5×10^{-1}	0.573	8.0×10^{-1}	0.728	1.4	0.892	1.6	0.945	2.6	1.106	8.0	1.539	14.0	1.786	35.0	2.160	45.0	2.332	90.0	2.658	90.0	2.671	170	2.979
1.6×10^{-1}	0.356	5.0×10^{-1}	0.591	9.0×10^{-1}	0.755	1.6	0.927	1.8	0.981	2.8	1.130	8.5	1.561	16.0	1.837	40.0	2.197	50.0	2.379	100	2.707	95.0	2.697	175	2.992
1.8×10^{-1}	0.367	5.5×10^{-1}	0.606	1.0	0.778	1.8	0.955	2.0	1.013	3.0	1.152	9.0	1.580	18.0	1.879	45.0	2.224	60.0	2.455	105	2.728	100	2.721	180	3.006
2.0×10^{-1}	0.375	6.0×10^{-1}	0.619	1.2	0.815	2.0	0.980	2.2	1.041	3.4	1.190	10.0	1.615	20.0	1.914	50.0	2.245	70.0	2.513	110	2.747	120	2.807	200	3.054
2.2×10^{-1}	0.381	6.5×10^{-1}	0.630	1.4	0.842	2.2	1.000	2.4	1.065	3.8	1.222	12.0	1.667	22.0	1.943	55.0	2.260	80.0	2.558	115	2.764	140	2.878	250	3.150
2.4×10^{-1}	0.386	7.0×10^{-1}	0.639	1.6	0.861	2.4	1.016	2.6	1.087	4.5	1.266	14.0	1.704	24.0	1.967	60.0	2.271	90.0	2.592	120	2.781	160	2.936	300	3.219
2.6×10^{-1}	0.390	7.5×10^{-1}	0.647	1.8	0.876	2.6	1.030	2.8	1.106	5.0	1.290	16.0	1.730	26.0	1.986	65.0	2.279	100	2.619	125	2.796	180	2.984	350	3.269
2.8×10^{-1}	0.393	8.0×10^{-1}	0.654	2.0	0.887	2.8	1.042	3.0	1.123	5.5	1.309	18.0	1.749	28.0	2.002	70.0	2.285	120	2.655	130	2.810	200	3.024	400	3.306
3.0×10^{-1}	0.396	8.5×10^{-1}	0.660	2.2	0.895	3.0	1.051	3.5	1.158	6.0	1.325	20.0	1.762	30.0	2.016	75.0	2.290	140	2.677	135	2.823	220	3.057	450	3.332
3.5×10^{-1}	0.400	9.0×10^{-1}	0.665	2.4	0.900	3.5	1.069	4.0	1.183	7.0	1.347	22.0	1.771	35.0	2.040	80.0	2.293	160	2.689	140	2.835	240	3.085	500	3.351
4.0×10^{-1}	0.402	9.5×10^{-1}	0.669	2.6	0.905	4.0	1.080	5.0	1.215	8.0	1.361	24.0	1.777	40.0	2.055	90.0	2.297	180	2.697	145	2.846	260	3.107	600	3.375
4.5×10^{-1}	0.404	1.0	0.673	2.8	0.908	4.5	1.087	6.0	1.232	9.0	1.370	26.0	1.781	45.0	2.064	100	2.300	200	2.701	150	2.857	280	3.126	700	3.387
5.0×10^{-1}	0.405	1.2	0.682	3.0	0.910	5.0	1.091	7.0	1.242	10.0	1.376	28.0	1.784	50.0	2.070	110	2.301	220	2.704	160	2.876	300	3.142	800	3.394
6.0×10^{-1}	0.405	1.4	0.688	3.5	0.913	5.5	1.094	8.0	1.247	12.0	1.382	30.0	1.787	60.0	2.076	120	2.302	240	2.706	180	2.906	350	3.171	900	3.397
7.0×10^{-1}	0.405	1.6	0.690	4.0	0.915	6.0	1.096	9.0	1.250	14.0	1.385	35.0	1.789	70.0	2.078	130	2.302	260	2.707	200	2.929	400	3.189	1,000	3.399
8.0×10^{-1}	0.405	1.8	0.692	4.5	0.916	6.5	1.097	10.0	1.251	16.0	1.386	40.0	1.791	80.0	2.079	140	2.302	280	2.707	240	2.958	450	3.200	1,200	3.401
		2.0	0.692	5.0	0.916	7.0	1.097	12.0	1.252	18.0	1.386	50.0	1.792			160	2.303	300	2.708	280	2.975	500	3.207	1,400	3.401
		2.5	0.693	5.5	0.916	8.0	1.098	14.0	1.253											300	2.980	600	3.214		
		3.0	0.693	6.0	0.916	10.0	1.099	16.0	1.253											400	2.992	700	3.217		
																				500	2.995	800	3.218		
																						900	3.219		

Table 10-8. Solutions to Unsteady-state Flow Equations, Finite Radial System with Constant Pressure at Exterior Boundary, Constant Production Rate (*Continued*)

$R = 40$		$R = 50$		$R = 60$		$R = 70$		$R = 80$		$R = 90$		$R = 100$		$R = 200$		$R = 300$		$R = 400$		$R = 500$		$R = 600$		$R = 700$	
t_D	P_t	t_D	P_t	t_D	P_t	t_D	P_t	t_D	P_t	t_D	P_t	t_D	P_t	t_D	P_t	t_D	P_t	t_D	P_t	t_D	P_t	t_D	P_t	t_D	P_t
120	2.813	200	3.064	3.0×10^2	3.257	5.0×10^2	3.512	6.0×10^2	3.603	8.0×10^2	3.747	1.0×10^3	3.859	1.5×10^3	4.061	6.0×10^3	4.754	1.5×10^4	5.212	2.0×10^4	5.356	4.0×10^4	5.703	5.0×10^4	5.814
140	2.888	220	3.111	4.0×10^2	3.401	6.0×10^2	3.603	7.0×10^2	3.680	9.0×10^2	3.806	1.2×10^3	3.949	2.0×10^3	4.205	8.0×10^3	4.898	2.0×10^4	5.356	2.5×10^4	5.468	4.5×10^4	5.762	6.0×10^4	5.905
160	2.953	240	3.154	5.0×10^2	3.512	7.0×10^2	3.680	8.0×10^2	3.747	1.0×10^3	3.858	1.4×10^3	4.026	2.5×10^3	4.317	10.0×10^3	5.010	3.0×10^4	5.556	3.0×10^4	5.559	5.0×10^4	5.814	7.0×10^4	5.982
180	3.011	260	3.193	6.0×10^2	3.602	8.0×10^2	3.746	9.0×10^2	3.805	1.2×10^3	3.949	1.6×10^3	4.092	3.0×10^3	4.408	12.0×10^3	5.101	4.0×10^4	5.689	3.5×10^4	5.636	6.0×10^4	5.904	8.0×10^4	6.048
200	3.063	280	3.229	7.0×10^2	3.676	9.0×10^2	3.803	10.0×10^2	3.857	1.3×10^3	3.988	1.8×10^3	4.150	3.5×10^3	4.485	14.0×10^3	5.177	5.0×10^4	5.781	4.0×10^4	5.702	7.0×10^4	5.979	9.0×10^4	6.105
220	3.109	300	3.263	8.0×10^2	3.739	10.0×10^2	3.854	12.0×10^2	3.946	1.4×10^3	4.025	2.0×10^3	4.200	4.0×10^3	4.552	16.0×10^3	5.242	6.0×10^4	5.845	4.5×10^4	5.759	8.0×10^4	6.041	10.0×10^4	6.156
240	3.152	350	3.339	9.0×10^2	3.792	12.0×10^2	3.937	14.0×10^2	4.019	1.5×10^3	4.058	2.5×10^3	4.303	5.0×10^3	4.663	18.0×10^3	5.299	7.0×10^4	5.889	5.0×10^4	5.810	9.0×10^4	6.094	12.0×10^4	6.239
260	3.191	400	3.405	10.0×10^2	3.832	14.0×10^2	4.003	15.0×10^2	4.051	1.8×10^3	4.144	3.0×10^3	4.379	6.0×10^3	4.754	20.0×10^3	5.348	8.0×10^4	5.920	6.0×10^4	5.894	10.0×10^4	6.139	14.0×10^4	6.305
280	3.226	450	3.461	12.0×10^2	3.908	16.0×10^2	4.054	16.0×10^2	4.080	2.0×10^3	4.192	3.5×10^3	4.434	7.0×10^3	4.829	24.0×10^3	5.429	9.0×10^4	5.942	7.0×10^4	5.960	12.0×10^4	6.210	16.0×10^4	6.357
300	3.259	500	3.512	14.0×10^2	3.959	18.0×10^2	4.095	18.0×10^2	4.130	2.5×10^3	4.285	4.0×10^3	4.478	8.0×10^3	4.894	28.0×10^3	5.491	10.0×10^4	5.957	8.0×10^4	6.013	14.0×10^4	6.262	18.0×10^4	6.398
350	3.331	550	3.556	16.0×10^2	3.996	20.0×10^2	4.127	20.0×10^2	4.171	3.0×10^3	4.349	4.5×10^3	4.510	9.0×10^3	4.949	30.0×10^3	5.517	11.0×10^4	5.967	9.0×10^4	6.055	16.0×10^4	6.299	20.0×10^4	6.430
400	3.391	600	3.595	18.0×10^2	4.023	25.0×10^2	4.181	25.0×10^2	4.248	3.5×10^3	4.394	5.0×10^3	4.534	10.0×10^3	4.996	40.0×10^3	5.606	12.0×10^4	5.975	10.0×10^4	6.088	18.0×10^4	6.326	25.0×10^4	6.484
450	3.440	650	3.630	20.0×10^2	4.043	30.0×10^2	4.211	30.0×10^2	4.297	4.0×10^3	4.426	5.5×10^3	4.552	12.0×10^3	5.072	50.0×10^3	5.652	12.5×10^4	5.977	12.0×10^4	6.135	20.0×10^4	6.345	30.0×10^4	6.514
500	3.482	700	3.661	25.0×10^2	4.071	35.0×10^2	4.228	35.0×10^2	4.328	4.5×10^3	4.448	6.0×10^3	4.565	14.0×10^3	5.129	60.0×10^3	5.676	13.0×10^4	5.980	14.0×10^4	6.164	25.0×10^4	6.374	35.0×10^4	6.530
550	3.516	750	3.688	30.0×10^2	4.084	40.0×10^2	4.237	40.0×10^2	4.347	5.0×10^3	4.464	6.5×10^3	4.579	16.0×10^3	5.171	70.0×10^3	5.690	14.0×10^4	5.983	16.0×10^4	6.183	30.0×10^4	6.387	40.0×10^4	6.540
600	3.545	800	3.713	35.0×10^2	4.090	45.0×10^2	4.242	45.0×10^2	4.360	6.0×10^3	4.482	7.0×10^3	4.583	18.0×10^3	5.203	80.0×10^3	5.696	16.0×10^4	5.988	18.0×10^4	6.195	35.0×10^4	6.392	45.0×10^4	6.545
650	3.568	850	3.735	40.0×10^2	4.092	50.0×10^2	4.245	50.0×10^2	4.368	7.0×10^3	4.491	7.5×10^3	4.588	20.0×10^3	5.227	90.0×10^3	5.700	18.0×10^4	5.990	20.0×10^4	6.202	40.0×10^4	6.395	50.0×10^4	6.548
700	3.588	900	3.754	45.0×10^2	4.093	55.0×10^2	4.247	60.0×10^2	4.376	8.0×10^3	4.496	8.0×10^3	4.593	25.0×10^3	5.264	10.0×10^4	5.702	20.0×10^4	5.991	25.0×10^4	6.211	50.0×10^4	6.397	60.0×10^4	6.550
800	3.619	950	3.771	50.0×10^2	4.094	60.0×10^2	4.247	70.0×10^2	4.380	9.0×10^3	4.498	9.0×10^3	4.598	30.0×10^3	5.282	12.0×10^4	5.703	24.0×10^4	5.991	30.0×10^4	6.213	60.0×10^4	6.397	70.0×10^4	6.551
900	3.640	1,000	3.787	55.0×10^2	4.094	65.0×10^2	4.248	80.0×10^2	4.381	10.0×10^3	4.499	10.0×10^3	4.601	35.0×10^3	5.290	14.0×10^4	5.704	26.0×10^4	5.991	35.0×10^4	6.214			80.0×10^4	6.551
1,000	3.655	1,200	3.833			70.0×10^2	4.248	90.0×10^2	4.382	11.0×10^3	4.499	12.5×10^3	4.604	40.0×10^3	5.294	15.0×10^4	5.704			40.0×10^4	6.214				
1,200	3.672	1,400	3.862			75.0×10^2	4.248	10.0×10^3	4.382	12.0×10^3	4.500	15.0×10^3	4.605												
1,400	3.681	1,600	3.881			80.0×10^2	4.248	11.0×10^3	4.382	14.0×10^3	4.500														
1,600	3.685	1,800	3.892																						
1,800	3.687	2,000	3.900																						
2,000	3.688	2,200	3.904																						
2,500	3.689	2,400	3.907																						
		2,600	3.909																						
		2,800	3.910																						

Table 10-8. Solutions to Unsteady-state Flow Equations, Finite Radial System with Constant Pressure at Exterior Boundary, Constant Production Rate (*Continued*)

$R = 800$		$R = 900$		$R = 1{,}000$		$R = 1{,}200$		$R = 1{,}400$		$R = 1{,}600$		$R = 1{,}800$		$R = 2{,}000$		$R = 2{,}200$		$R = 2{,}400$		$R = 2{,}600$		$R = 2{,}800$		$R = 3{,}000$	
t_D	P_t	t_D	P_t	t_D	P_t	t_D	P_t	t_D	P_t	t_D	P_t	t_D	P_t	t_D	P_t	t_D	P_t	t_D	P_t	t_D	P_t	t_D	P_t	t_D	P_t
7.0×10^4	5.983	8.0×10^4	6.049	1.0×10^5	6.161	2.0×10^5	6.507	2.0×10^5	6.507	2.5×10^5	6.619	3.0×10^5	6.710	4.0×10^5	6.854	5.0×10^5	6.966	6.0×10^5	7.057	7.0×10^5	7.134	8.0×10^5	7.201	1.0×10^6	7.312
8.0×10^4	6.049	9.0×10^4	6.108	1.2×10^5	6.252	3.0×10^5	6.704	2.5×10^5	6.619	3.0×10^5	6.710	4.0×10^5	6.854	5.0×10^5	6.966	5.5×10^5	7.013	7.0×10^5	7.134	8.0×10^5	7.201	9.0×10^5	7.260	1.2×10^6	7.403
9.0×10^4	6.108	10.0×10^4	6.161	1.4×10^5	6.329	4.0×10^5	6.833	3.0×10^5	6.709	3.5×10^5	6.787	5.0×10^5	6.965	6.0×10^5	7.056	6.0×10^5	7.057	8.0×10^5	7.200	9.0×10^5	7.259	10.0×10^5	7.312	1.4×10^6	7.480
10.0×10^4	6.160	12.0×10^4	6.251	1.6×10^5	6.395	5.0×10^5	6.918	3.5×10^5	6.785	4.0×10^5	6.853	6.0×10^5	7.054	7.0×10^5	7.132	6.5×10^5	7.097	9.0×10^5	7.259	10.0×10^5	7.312	12.0×10^5	7.403	1.6×10^6	7.545
12.0×10^4	6.249	14.0×10^4	6.327	1.8×10^5	6.452	6.0×10^5	6.975	4.0×10^5	6.849	5.0×10^5	6.962	7.0×10^5	7.120	8.0×10^5	7.196	7.0×10^5	7.133	10.0×10^5	7.310	12.0×10^5	7.401	16.0×10^5	7.542	1.8×10^6	7.602
14.0×10^4	6.322	16.0×10^4	6.392	2.0×10^5	6.503	7.0×10^5	7.013	5.0×10^5	6.950	6.0×10^5	7.046	8.0×10^5	7.188	9.0×10^5	7.251	7.5×10^5	7.167	12.0×10^5	7.398	14.0×10^5	7.475	20.0×10^5	7.644	2.0×10^6	7.651
16.0×10^4	6.382	18.0×10^4	6.447	2.5×10^5	6.605	8.0×10^5	7.038	6.0×10^5	7.026	7.0×10^5	7.114	9.0×10^5	7.238	10.0×10^5	7.298	8.0×10^5	7.199	16.0×10^5	7.526	16.0×10^5	7.536	24.0×10^5	7.719	2.4×10^6	7.732
18.0×10^4	6.432	20.0×10^4	6.494	3.0×10^5	6.681	9.0×10^5	7.056	7.0×10^5	7.082	8.0×10^5	7.167	10.0×10^5	7.280	12.0×10^5	7.374	8.5×10^5	7.229	20.0×10^5	7.611	18.0×10^5	7.588	28.0×10^5	7.775	2.8×10^6	7.794
20.0×10^4	6.474	25.0×10^4	6.587	3.5×10^5	6.738	10.0×10^5	7.067	8.0×10^5	7.123	9.0×10^5	7.210	15.0×10^5	7.407	14.0×10^5	7.431	9.0×10^5	7.256	24.0×10^5	7.668	20.0×10^5	7.631	30.0×10^5	7.797	3.0×10^6	7.820
25.0×10^4	6.551	30.0×10^4	6.652	4.0×10^5	6.781	12.0×10^5	7.080	9.0×10^5	7.154	10.0×10^5	7.244	20.0×10^5	7.459	16.0×10^5	7.474	10.0×10^5	7.307	28.0×10^5	7.706	24.0×10^5	7.699	35.0×10^5	7.840	3.5×10^6	7.871
30.0×10^4	6.599	40.0×10^4	6.729	4.5×10^5	6.813	14.0×10^5	7.085	10.0×10^5	7.177	15.0×10^5	7.334	30.0×10^5	7.489	18.0×10^5	7.506	12.0×10^5	7.390	30.0×10^5	7.720	28.0×10^5	7.746	40.0×10^5	7.870	4.0×10^6	7.908
35.0×10^4	6.630	45.0×10^4	6.751	5.0×10^5	6.837	16.0×10^5	7.088	15.0×10^5	7.229	20.0×10^5	7.364	40.0×10^5	7.495	20.0×10^5	7.530	16.0×10^5	7.507	35.0×10^5	7.745	30.0×10^5	7.765	50.0×10^5	7.905	4.5×10^6	7.935
40.0×10^4	6.650	50.0×10^4	6.766	5.5×10^5	6.854	18.0×10^5	7.089	20.0×10^5	7.241	25.0×10^5	7.373	50.0×10^5	7.495	25.0×10^5	7.566	20.0×10^5	7.579	40.0×10^5	7.760	35.0×10^5	7.799	60.0×10^5	7.922	5.0×10^6	7.955
45.0×10^4	6.663	55.0×10^4	6.777	6.0×10^5	6.868	19.0×10^5	7.089	25.0×10^5	7.243	30.0×10^5	7.376	51.0×10^5	7.495	30.0×10^5	7.584	25.0×10^5	7.631	50.0×10^5	7.775	40.0×10^5	7.821	70.0×10^5	7.930	6.0×10^6	7.979
50.0×10^4	6.671	60.0×10^4	6.785	7.0×10^5	6.885	20.0×10^5	7.090	30.0×10^5	7.244	35.0×10^5	7.377	52.0×10^5	7.495	35.0×10^5	7.593	30.0×10^5	7.661	60.0×10^5	7.780	50.0×10^5	7.845	80.0×10^5	7.934	7.0×10^6	7.992
55.0×10^4	6.676	70.0×10^4	6.794	8.0×10^5	6.895	21.0×10^5	7.090	31.0×10^5	7.244	40.0×10^5	7.378	53.0×10^5	7.495	40.0×10^5	7.597	35.0×10^5	7.677	70.0×10^5	7.782	60.0×10^5	7.856	90.0×10^5	7.936	8.0×10^6	7.999
60.0×10^4	6.679	80.0×10^4	6.798	9.0×10^5	6.901	22.0×10^5	7.090	32.0×10^5	7.244	42.0×10^5	7.378	54.0×10^5	7.495	50.0×10^5	7.600	40.0×10^5	7.686	80.0×10^5	7.783	70.0×10^5	7.860	10.0×10^6	7.937	9.0×10^6	8.002
70.0×10^4	6.682	90.0×10^4	6.800	10.0×10^5	6.904	23.0×10^5	7.090	33.0×10^5	7.244	44.0×10^5	7.378	56.0×10^5	7.495	60.0×10^5	7.601	50.0×10^5	7.693	90.0×10^5	7.783	80.0×10^5	7.862	12.0×10^6	7.937	10.0×10^6	8.004
80.0×10^4	6.684	10.0×10^5	6.801	12.0×10^5	6.907	24.0×10^5	7.090							64.0×10^5	7.601	60.0×10^5	7.695	95.0×10^5	7.783	90.0×10^5	7.863	13.0×10^6	7.937	12.0×10^6	8.006
100.0×10^4	6.684			14.0×10^5	6.907											70.0×10^5	7.696			10.0×10^6	7.863			15.0×10^6	8.006
				16.0×10^5	6.908											80.0×10^5	7.696								

SOURCE: Van Everdingen and Hurst (10-27).

Table 10-9. Digital-computer Solutions of Difference Equations

Year	Author(s)	Fluid	System geometry	Terminal condition	Exterior boundary conditions		Other conditions	Reference
					Extent	Condition		
1936	Muskat and Meres	Liquid + gas	Linear	.....	.....	.....	.....	10-24
1952	Aronofsky and Jenkins	Gas	Linear	Constant pressure	Infinite	.....	.....	10-1
1952	Aronofsky and Jenkins	Gas	Linear	Constant production rate	Infinite	.....	.....	10-1
1952	Aronofsky and Jenkins	Gas	Linear	Constant pressure	Finite	Constant pressure	.....	10-1
1952	Aronofsky and Jenkins	Gas	Linear	Constant pressure	Finite	Closed	.....	10-1
1952	Jenkins and Aronofsky	Gas	Radial	Constant production rate	Infinite	.....	.....	10-19
1952	Jenkins and Aronofsky	Gas	Radial	Constant production rate	Finite	Closed	.....	10-19
1952	Jenkins and Aronofsky	Gas	Radial	Constant pressure	Finite	Closed	.....	10-19
1953	Bruce, Peaceman, Rachford, and Rice	Gas	Linear	Constant production rate	Finite	Closed	.....	10-6
1953	Bruce, Peaceman, Rachford, and Rice	Gas	Radial	Constant production rate	Finite	Closed	.....	10-6
1953	Jenkins and Aronofsky	.....	.....	.....	.....	.....	See Jenkins and Aronofsky, 1952 (10-19).	10-20
1954	Aronofsky	Gas	Linear	Constant pressure	Finite	Closed	Permeability varies with pressure.	10-3
1954	Aronofsky	Gas	Linear	Constant pressure	Finite	Closed with dead volume	Permeability varies with pressure.	10-3
1954	West, Garvin, and Sheldon	Liquid + gas	Linear	Constant-production-rate period followed by a constant-pressure period	Finite	Closed	Viscosities, formation volume factor, and gas solubility vary with pressure. Relative permeability varies with saturation.	10-29
1954	West, Garvin, and Sheldon	Liquid + gas	Radial	Constant-production-rate period followed by a constant-pressure period	Finite	Closed	Viscosities, formation volume factor, and gas solubility vary with pressure. Relative permeability varies with saturation.	10-29
1954	Aronofsky and Jenkins	.....	.....	.....	.....	.....	See Jenkins and Aronofsky, 1952 (10-19).	10-2
1954	Aronofsky and Ferris	Gas	Linear	Constant pressure	Finite	Closed	Viscosity and compressibility factor are functions of pressure.	10-4
1955	Douglas, Peaceman, and Rachford	Gas	Square	Constant production rate	Finite	Closed	Well in center of square.	10-14
1956	Aronofsky and Porter	Gas	Radial	Constant pressure	Finite	Closed	Viscosity and compressibility factor are functions of pressure.	10-5
1956	Warren	Gas	Linear	Constant pressure	Finite	Closed	Viscosity and compressibility factor are functions of pressure.	10-28

CHAPTER II

Development and Operation of Gas Fields

Once a gas field has been discovered by drilling one or more wells, a plan is needed for developing the field and placing the gas on the market. Estimates of gas reserves are needed as a basis for marketing the gas. Sufficient wells must be planned to produce the gas at the rates projected for delivery of the gas. The operation of the field to depletion completes the enterprise.

GAS-WELL CAPACITY

Gas-well capacities are determined by performance flow tests on the wells. Conventional back-pressure tests (7-32) may be sufficient for high-permeability reservoirs but, for low-permeability reservoirs, either long-time flow tests with pressure-build-up tests upon shutting in the well or isochronal tests may be required (9-71, 11-27). Core data may be used to predict flow capacity and production; or drill-stem tests may be used to estimate performance.

Before taking up the various test and calculation procedures in detail, an explanation must be given of three distinct types of behavior of gas wells, as predicted by theory and confirmed by field data. The general characteristics of these three phenomena will be described in connection with their effect on the testing methods. Reference should be made to Chap. 10 for the theory underlying the description.

Flow of gas from wells may first be considered as *steady-state* only. Gas-well performance can be calculated readily from Darcy's law, provided that a radius of drainage is somehow specified. Such calculations form the basis of the back-pressure-test equation and of many of the gas-reservoir calculations today. A second case arises, however, when it is recognized that over a certain period of time the radius of drainage is receding from the well. This period is best referred to as the *unsteady-state* flow period. The isochronal test and unsteady-state flow calculations have been devised to handle well behavior during the unsteady-state flow period. A third case—called stabilized flow—arises when the effective radius of drainage reaches the limit of the reservoir or, more commonly, when the pressure gradients from two adjacent wells meet and the radius of drainage becomes fixed. These two events have the same effect. It is surprising to note that, once the radius of drainage stops moving, although the flow is still of an unsteady-state nature, the steady-state equations once again apply, provided only that the appropriate values for pressure and radius of drainage are used in these equations. The new reservoir pressure at any time must be used, with a steady-state radius of drainage approximately equal to 0.606 times one-half the distance between wells (10-18). For a group of adjacent wells with different flow rates, the total area may be divided among the wells, with radii proportional to the average production rate (10-22).

Table 11-1 has been prepared to summarize the importance of the three flow mechanisms: steady-

Table 11-1. Types of Behavior of Gas Wells

Item	Steady-state flow	Unsteady-state flow	Stabilized flow
Features establishing which type of flow exists	Fixed radius of drainage and constant reservoir pressure	Moving radius of drainage and constant reservoir pressure at a distance	Fixed radius of drainage and changing reservoir pressure
Type of flow tests that are valid	Back-pressure and isochronal	Isochronal only	Back-pressure and isochronal
Reciprocal slope n of a back-pressure curve	Constant. Determined by viscous- or turbulent-flow condition only	Variable. Depends on unsteady state. Increases with increasing rate series or decreases with decreasing rate series of flow rates. Varies also with turbulent-flow condition	Constant. Determined by viscous- or turbulent-flow condition only
Reciprocal slope n of an isochronal performance curve	Constant. Determined by viscous- or turbulent-flow condition only	Constant. Determined by viscous- or turbulent-flow condition only	Constant. Determined by viscous- or turbulent-flow condition only
Coefficient C of back-pressure equation or isochronal curve	Constant	Decreases with increased length of flow time	Constant

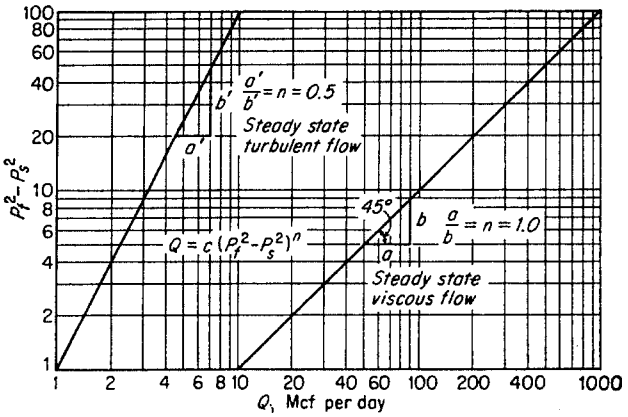

Fig. 11-1. Variation of slope of back-pressure curves for steady-state viscous and turbulent flow.

state, unsteady-state, and stabilized, in relation to the testing of gas wells and the prediction of performance characteristics.

In flow calculations, units can become a large part of the problem. Field units as follows are used herein unless otherwise specified.

Q = flow rate at 14.7 psia and 60°F, Mcf/day
T = temperature, °R (°F + 460)

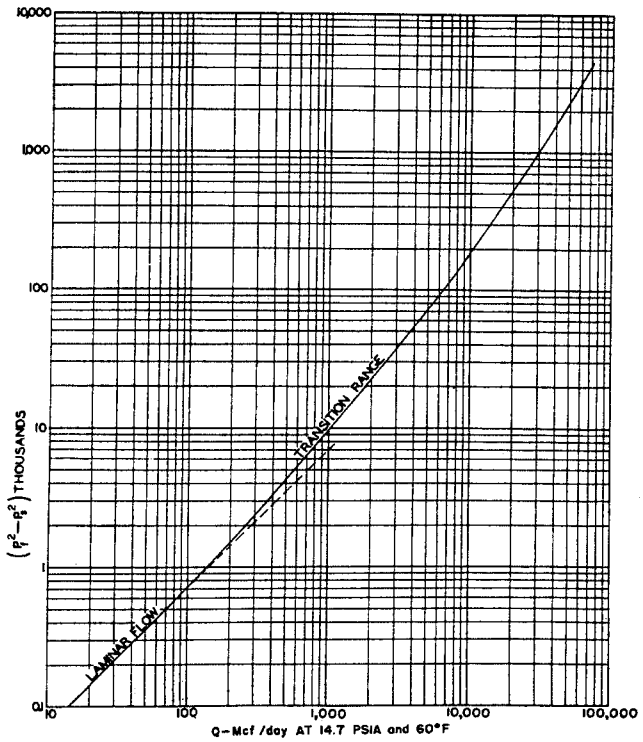

Fig. 11-2. Calculated back-pressure curve showing transition from laminar to turbulent flow. (*Elenbaas and Katz*, 10-15. *Courtesy AIME.*)

μ = viscosity, centipoises
K = permeability, millidarcys
h = formation thickness, ft
ϕ = porosity, fractional
P^* = pressure, psia
r = radius, ft
t = time, hr
β = turbulence factor, ft^{-1}
G = gas gravity, mol. wt ÷ 29.0

Back-pressure Tests

Back-pressure tests on gas wells have been used for many years to determine flow capacity. Monograph 7 by Rawlins and Schellhardt (7-32) outlines early knowledge of the subject. The back-pressure curve of Fig. 9-31 is an example of a record of the performance of a well.

The slope of the back-pressure curve [Eq. (11-1)] is not completely predictable as yet.

$$Q = C(P_f^2 - P_s^2)^n \qquad (11\text{-}1)$$

where P_f = closed-formation pressure
P_s = flowing sand-face pressure

It is customary to represent the reciprocal slope by the value of n in Eq. (11-1). This is the reciprocal of the slope of the line plotted on log-log paper. For completely laminar steady-state flow the line should be a 45° line with $n = 1.0$. For steady-state flow with turbulence, the value of n decreases and can reach 0.5 for complete turbulence, as shown in Fig. 11-1. Elenbaas and Katz (10-15) show that the back-pressure curve could have curvature resulting from the onset of turbulence as in Fig. 11-2. With unsteady-state effects entering the picture, it has been found that the flow time for the test points and the sequence of flow rates can influence the value of n for the curve.

For high-permeability reservoirs the performance of a well over the life of the field can be predicted from a single back-pressure curve. By using the difference in squares between the closed-in reservoir pressure and the flowing pressure, one can predict the flow rate for a given drawdown. For the flow test of Fig. 11-3 on a Carthage gas well, the flow capacities at various reservoir pressures are given in Fig. 11-4. The well has a computed open flow of 92 MMcf/day at the reservoir pressure of 3,127 psia. At a reservoir pressure of 1,000 psia, the open flow is 13.2 MMcf/day. Since some wells are rated at 25 per cent of open flow and some at flowing pressures equal to 0.8 shut-in pressure, both of these curves are shown in Fig. 11-4.

* Since P is no longer needed for dimensionless groups, we will return to the use of P for pressure, instead of p (Chap. 10 only).

It may be necessary to test the well at intervals to assure that the sand face is clean. The presence of water or shale cavings in open holes can reduce the flow capacities of wells.

It is of interest to analyze the back-pressure-equation coefficient C to bring out the variables that make up the coefficient. For the case of $n = 1$, Eq. (11-1) may be compared to Eq. (10-2). Solving for C, Eq. (11-2) is obtained:

$$C = \frac{0.0007030hK}{zT\mu \ln (r_d/r_w)} \qquad (11\text{-}2)$$

The back-pressure equation can also be put in dimensionless form, as in Eq. (11-3).

$$m = \frac{1}{\ln (r_d/r_w)} \frac{P_f^2 - P_s^2}{P_f^2} \qquad (11\text{-}3)$$

where m is the dimensionless flow rate (Table 10-2).

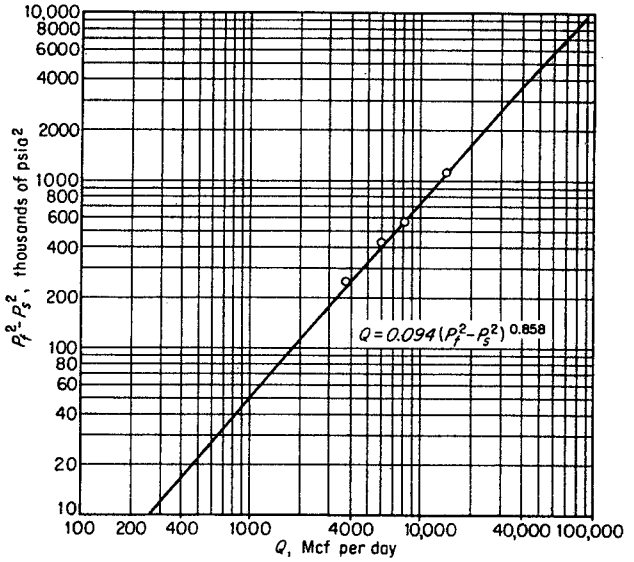

Fig. 11-3. Back-pressure curve of Carthage gas well. (*Baumel and Breitung, 7-5.*)

Computation of Steady-state Performance Curves from Core Data

The core data on a well give the porosity and permeability of the producing formation. Knowledge of the gas properties, reservoir temperature, formation thickness, and the well-spacing plan may be used to predict performance curves in the absence of actual test information.

For high-permeability reservoirs that stabilize rapidly, one can compute the flow from the steady-state radial-flow formula, Eq. (10-5). The only difficult problem is that of selecting the proper steady-state radius of drainage to use in such calculations. A stabilized well is one for which the effective radius of drainage has stopped at the reservoir limit or halfway between producing wells. For this condition, Janicek and Katz (10-18) have shown (see Chap. 10) that the steady-state radius of drainage is 0.606 times one-half the well spacing. A correction can be made

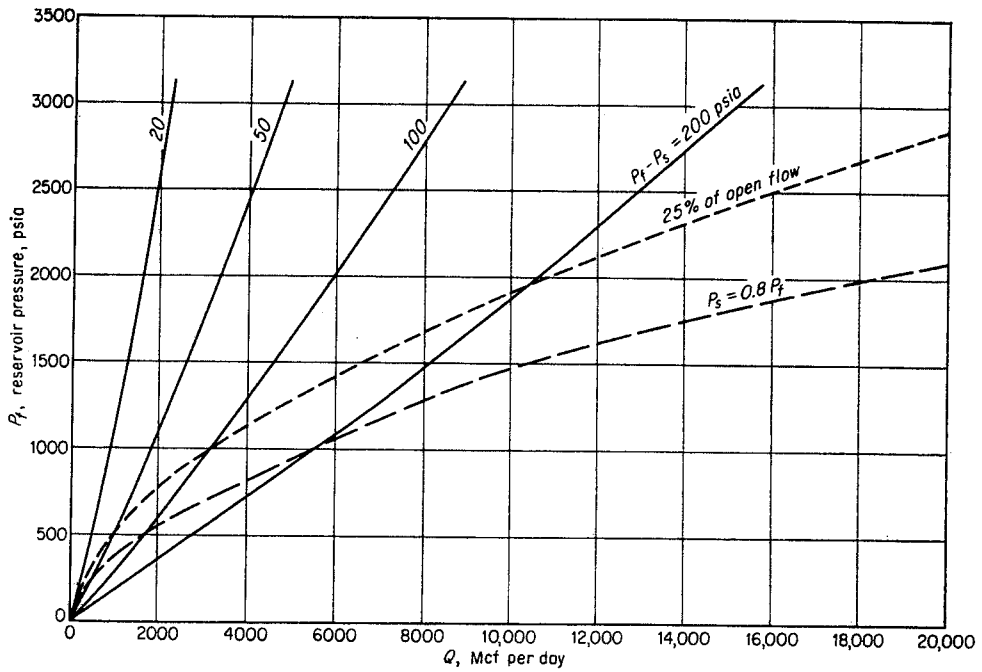

Fig. 11-4. Flow capacity of Carthage well over life of the reservoir.

to compensate for the difference between a square and a circular limit (10-14). Accordingly, r_1 in Eq. (10-5) becomes 0.606 times one-half the well spacing.

In order to simplify routine calculation of performance curves from core data, calculations have been made for the constants in the performance-curve equation for a set of commonly occurring conditions (Table 11-2). Equation (10-5) can be simplified to the form given as Eq. (11-4) for a given gas gravity, well spacing, and well-bore diameter:

$$P_f^2 - P_s^2 = A\frac{Q}{hK} + B\left(\frac{Q}{hK}\right)^2 \qquad (11\text{-}4)$$

A further generalization can be made with regard to formation temperature. High formation temperatures are usually associated with high initial reservoir shut-in pressures. A straight-line relationship from 75 to 350°F for pressures of 0 to 10,000 psia is a typical relationship and will be used. Accordingly, for the conditions shown at the bottom of Table 11-2 and the typical temperature–discovery pressure relationship, calculations for the values of A and B in Eq. (11-4) are made. Values of Q/hK in Eq. (11-4) are in Mcf per day per millidarcy-foot, and pressures are in psia. An average reservoir pressure has been used in estimating z and μ. In Fig. 11-5, the performance curves corresponding to the values of A and B of Table 11-2 are plotted. The procedure for converting the values of A and B in Table 11-2 to the performance curves of Fig. 11-5 is as follows:

1. Select values of A and B corresponding to the discovery pressure and the permeability, from Table 11-2.
2. Select four flow rates Q of interest, and calculate Q/hK and $(Q/hK)^2$ for each rate.
3. Knowing A and B, calculate $P_f^2 - P_s^2$ for each flow rate, from Eq. (11-4).
4. Plot $P_f^2 - P_s^2$ versus Q on log-log paper, as shown in Fig. 11-5.

The performance curve thus obtained will be the steady-state curve with the correct slope for that reservoir. In the calculations for Fig. 11-5, a constant viscosity and compressibility factor are used for a given discovery pressure. Further refinement could consist of obtaining new A's and B's for each mean pressure level with new values for z and μ.

Figure 11-5 gives directly the flow per millidarcy-foot when hK is taken as unity. This calculated performance does not take into account any damage or effects of stimulation at the well bore.

The Unsteady State

Some wells have such high permeability that the flowing well pressure for a given flow rate remains constant with time. Other wells have a gradual reduction in flowing well pressure at constant rate.

Table 11-2. Computation of Gas-well Performance Curve from Core Data for 0.6 Gravity Gas*

$$P_f^2 - P_s^2 = A\frac{Q}{hK} + B\left(\frac{Q}{hK}\right)^2\dagger$$

Initial shut-in reservoir pressure P_f, psia	$\bar{P} = \frac{P_f}{2}$, psia	T, °R	$\bar{P}_R$ for $\frac{P_f}{2}$	T_R	$\bar{z}$ for $\bar{P}_R$ and T_R	$\bar{\mu}$ for $\bar{P}_R$ and T_R, cp	A for 1.0 md-ft	B for 1.0 md-ft with K as indicated, md		
								10	100	1,000
500	250	546	0.372	1.523	0.964	0.0113	65,875	554	2,606	12,280
1,000	500	560	0.745	1.562	0.935	0.0117	67,812	551	2,592	12,214
2,000	1,000	589	1.490	1.643	0.902	0.0131	77,066	560	2,630	12,392
3,000	1,500	616	2.235	1.719	0.892	0.0145	88,243	578	2,720	12,819
4,000	2,000	644	2.980	1.797	0.896	0.0159	101,600	607	2,856	13,460
5,000	2,500	672	3.725	1.875	0.910	0.0172	116,516	644	3,027	14,267
6,000	3,000	700	4.470	1.953	0.935	0.0184	133,391	689	3,240	15,267
7,000	3,500	727	5.215	2.028	0.963	0.0195	151,182	737	3,466	16,336
8,000	4,000	755	5.960	2.106	1.000	0.0205	171,475	795	3,737	17,614
9,000	4,500	782	6.705	2.182	1.032	0.0213	190,430	850	3,994	18,830
10,000	5,000	810	7.450	2.260	1.065	0.0219	209,273	908	4,270	20,128

* Data: $G = 0.6$
$T_c = 358$°R
$P_c = 671$ psia
$hK = 1.0$ millidarcy-foot
160-acre spacing; $r_1 = 1{,}320 \times 0.606 = 800$ ft
8-in.-diameter well bore; $\ln(r_1/r_2) = 7.78$

† $A = 1{,}424\bar{\mu}\bar{z}T \ln(r_1/r_2)$
$B = 3.161 \times 10^{-12}\beta K^2\bar{z}T(1/r_2)G$

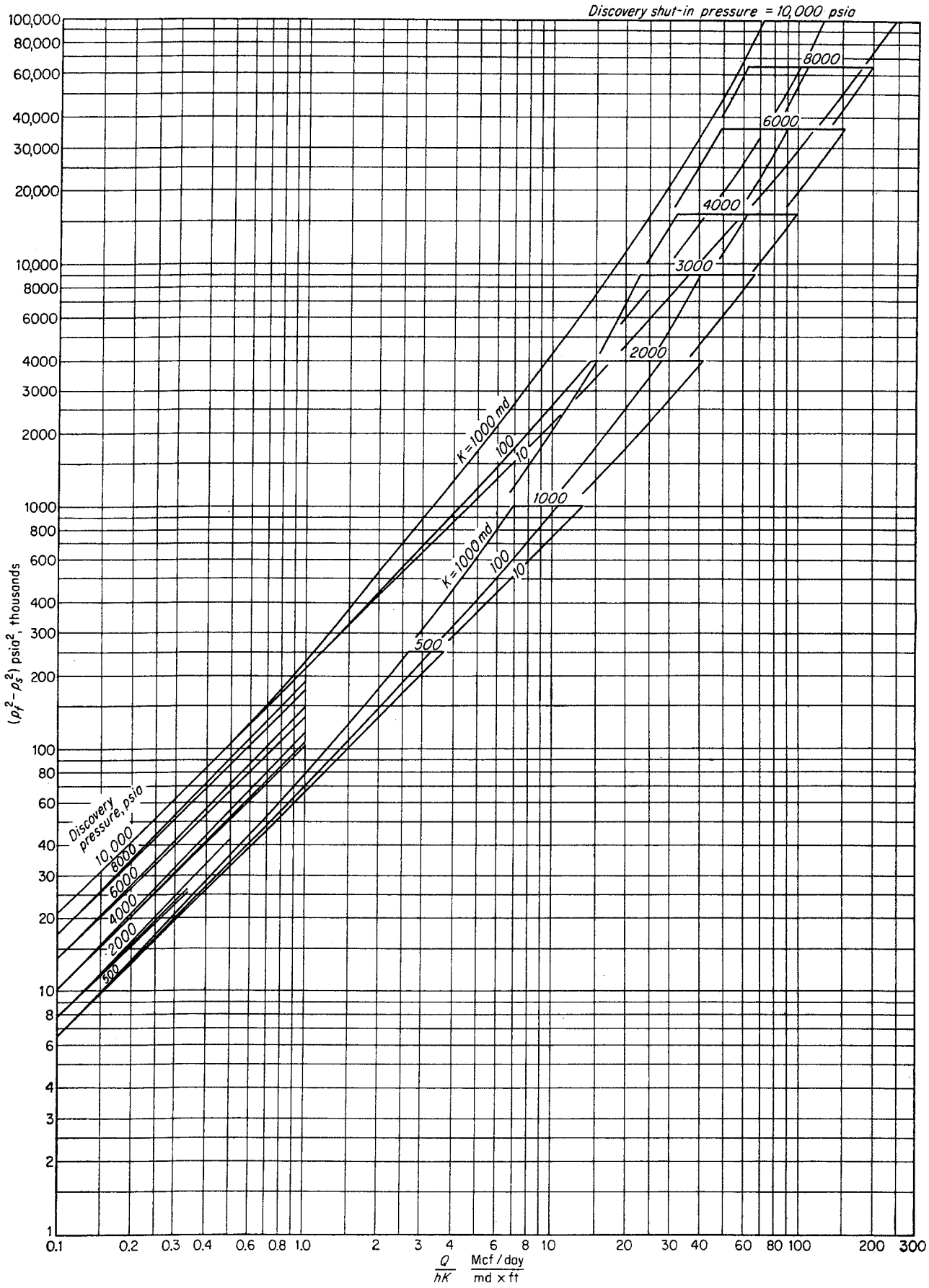

Fig. 11-5. Performance curves from core data for 0.6 gravity gas.

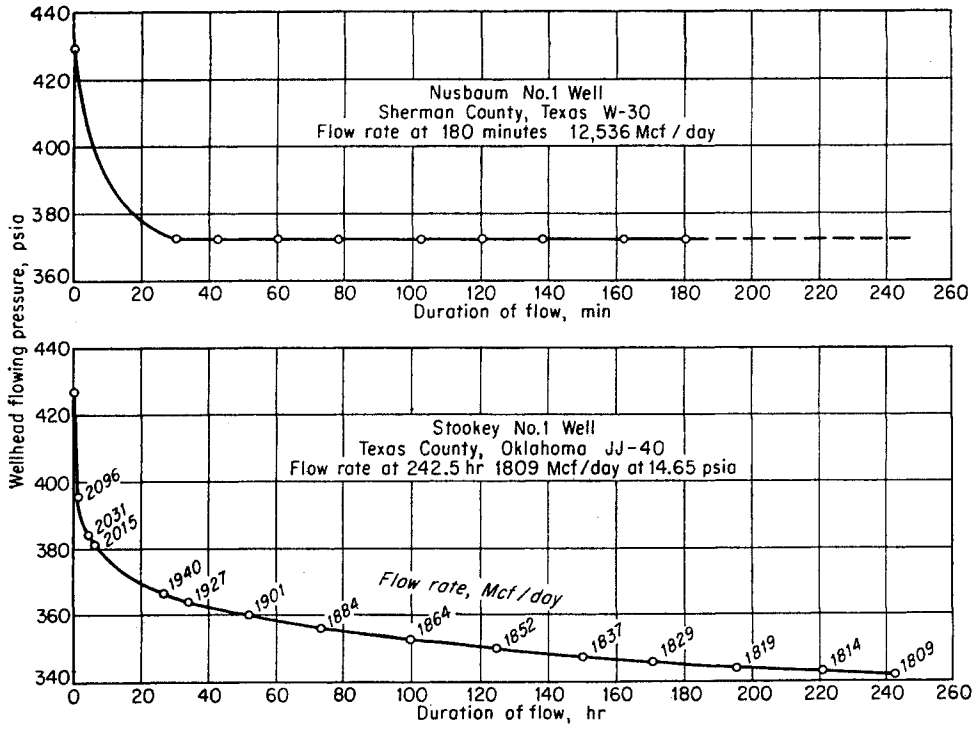

Fig. 11-6. Drawdown of flowing wellhead pressure on high- and low-permeability Hugoton wells. (*Katz*, 11-20.)

Figure 11-6 shows the performance of two such wells in the Hugoton field. The problems involved in predicting the flow capacity for the low-permeability wells will be considered.

Figure 11-7 illustrates the changes in reservoir pressure that take place for wells like the Stookey. This behavior is equivalent to that shown in Fig. 10-3: the pressure gradients become straight lines when pressure squared and logarithm of ratio of drainage radius to well-bore radius are used. At time 3 in Fig. 11-7, the pressure gradient has reached the point of interference of another well or the extremity of the reservoir. Between time 3 and time 4, the pressure on the entire reservoir is falling rather uniformly and the flow may be considered to be "stabilized." The value of C in Eq. (11-1) may be computed using wellhead pressures when pipe friction is negligible. This has been done with values of C plotted in Fig. 11-8.

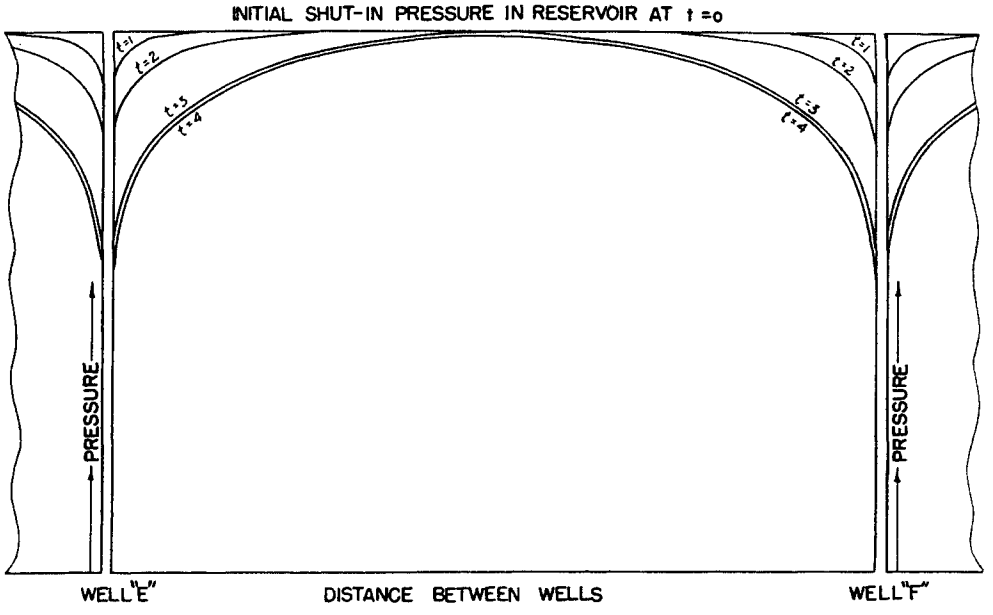

Fig. 11-7. Illustration of radius of drainage. (*Katz*, 11-20.)

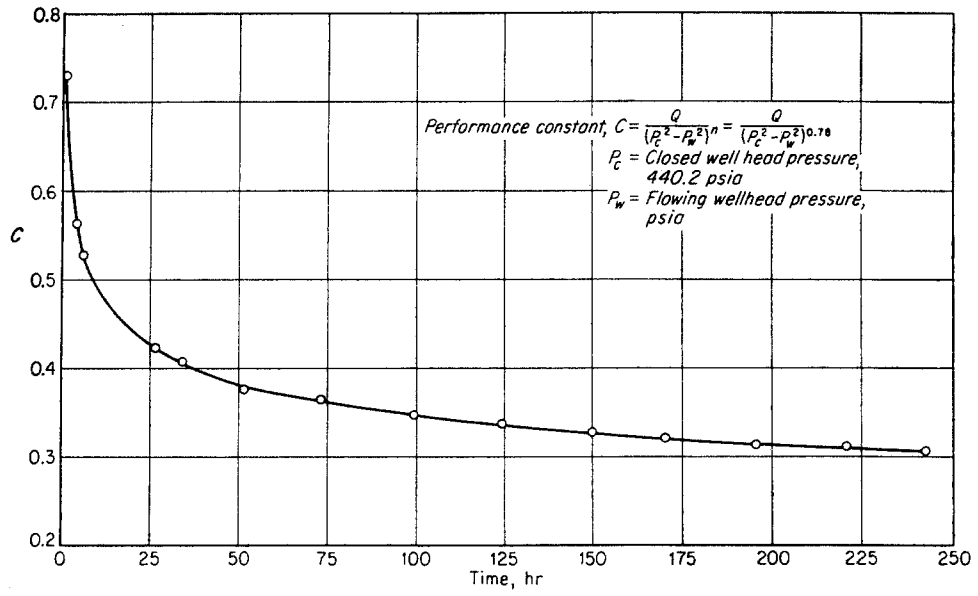

Fig. 11-8. Stabilization of performance constant for Stookey No. 1 well in November, 1944. (Katz, 11-20.)

The corresponding performance curves with an n of 0.78 are drawn in Fig. 11-9.

At the point in the drawdown procedure when the entire reservoir pressure declines and the well is stabilized, new closed-reservoir or wellhead pressures should be used. It was found that the use of these declining reservoir pressures along with the performance curves of Fig. 11-9 gave correctly the performance point measured in a 3-day test some five years after the flow test of Fig. 11-6. The problem is to find the position of the stabilized-performance curve for a well exhibiting unsteady-state characteristics. At Hugoton, the 10-day curve appears to give a reliable prediction of performance with time if the closed-reservoir pressure P_f is adjusted at intervals of time.

Problems similar to that illustrated by the drawdown curve of Fig. 11-6 occur when wells in low-permeability reservoirs are closed in to find the

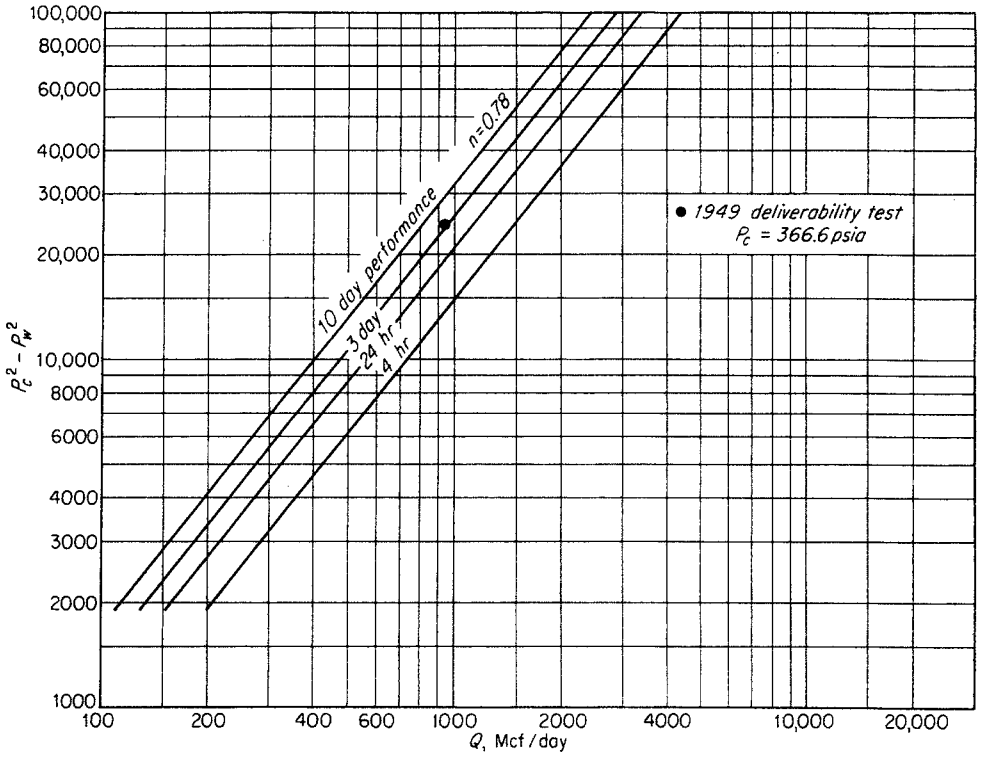

Fig. 11-9. Performance curves for Stookey No. 1 corresponding to the drawdown curve of Fig. 11-6. (Katz, 11-20.)

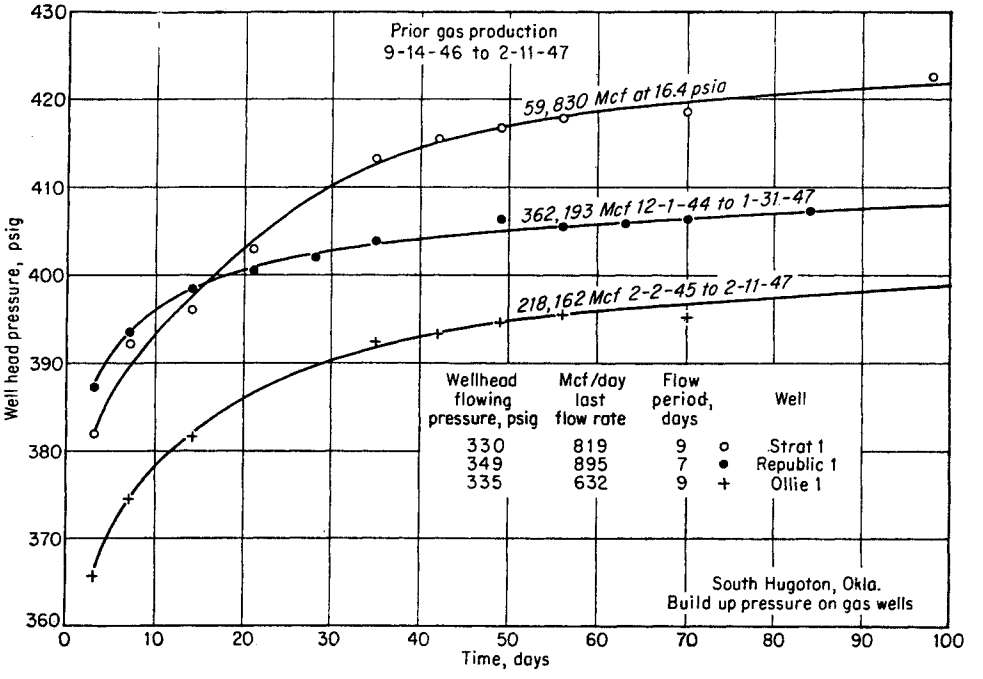

Fig. 11-10. Build-up pressures on closed-in Hugoton gas wells. (*Katz*, 11-20.)

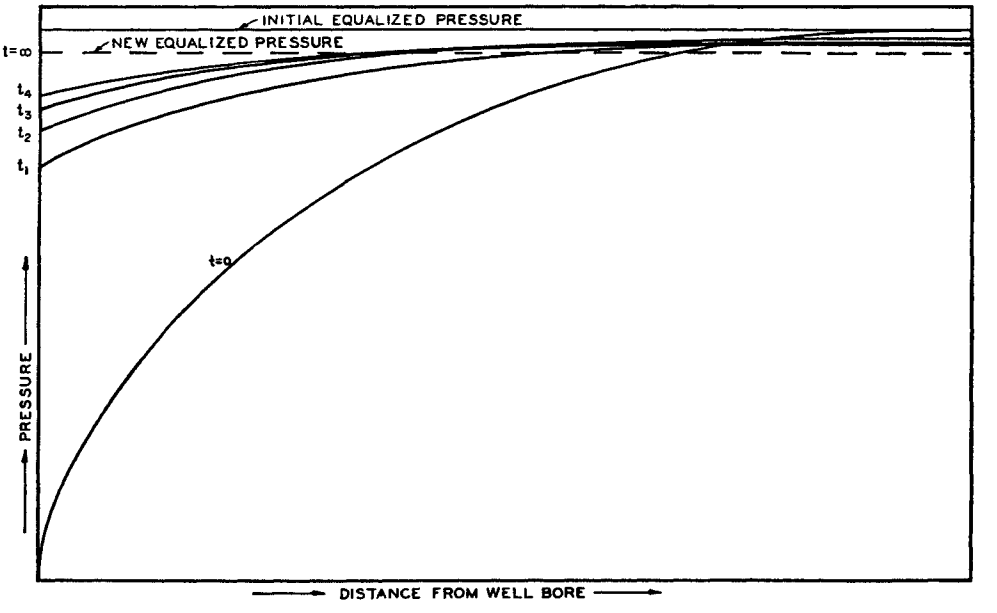

Fig. 11-11. Pressure gradients around a closed-in gas well. (*Katz*, 11-20.)

reservoir pressure. Figure 11-10 shows build-up curves on other Hugoton wells. Figure 11-11 illustrates the nature of the pressure-equalization process by which a new equalized pressure is obtained. For low-permeability wells on stream to serve a pipeline, it may be almost impossible to measure the true equalized reservoir pressure at a given time.

Not only must the position of the performance curve with time be considered, but also its slope. The slope of all curves will be the same when constant flow times are used in the isochronal procedure (9-71).

Equation for the Radius of Drainage

The steady-state or apparent radius of drainage is required for use in the back-pressure equation. Combining the dimensionless back-pressure equation (11-3) with the unsteady-state flow equation (10-36), a relationship is obtained between the radius of drainage and the dimensionless pressure change P_t defined in Table 10-2.

$$\ln \frac{r_d}{r_w} = P_t \qquad (11\text{-}5)$$

Using Eq. (10-31), the variation of the radius of drainage with dimensionless time is obtained for large values of t_D and for the condition of viscous flow.

$$\frac{r_d}{r_w} = 1.498 t_D^{0.5} \tag{11-6}$$

This value of r_d/r_w may be used to find an expression for the coefficient of the back-pressure equation for viscous-flow conditions.

$$C = \frac{0.001406hK}{\mu z T(\ln t_D + 0.80907)} \tag{11-7}$$

where C = coefficient of back-pressure equation for P in psia and Q in Mcf/day
hK = millidarcy-feet
z = compressibility factor
T = absolute temperature, °R
μ = viscosity, centipoises
t_D = dimensionless time (Table 10-2)

Effect of Unsteady State on n of Conventional Back-pressure Curve

The contribution of unsteady-state effects to the slope of a conventional back-pressure curve can be derived from Eq. (10-37). Equation (11-8) is first obtained from Eq. (11-1) at two different flow rates.

$$\frac{Q_1}{Q_2} = \left[\frac{(P_f^2 - P_s^2)_1}{(P_f^2 - P_s^2)_2}\right]^n \tag{11-8}$$

Solving for n, Eq. (11-9) is obtained.

$$n = \frac{\ln (Q_1/Q_2)}{\ln [(P_f^2 - P_s^2)_1/(P_f^2 - P_s^2)_2]} = \frac{\ln (Q_1/Q_2)}{\ln \{(Q_1 P_{t_1})_1/[Q_1 P_{t_1} + (Q_2 - Q_1)P_{t_2}]_2\}} \tag{11-9}$$

For any combination of flow rates and flow times the value of n can be calculated from the Van Everdingen and Hurst P_t values. The effect of turbulence on n should be considered separately using Eq. (10-5).

Illustrative Problem

The first two flow rates of a conventional back-pressure test are 2,000 and 4,000 Mcf/day, and each is continued for 1.0 hr. The dimensionless-time group is equal to $10{,}000t$, where t is in hours. Compute the value of n for the conventional back-pressure curve, considering unsteady-state effects only.

$$n = \frac{\ln \frac{2{,}000}{4{,}000}}{\ln \frac{\frac{1}{2}(\ln 10{,}000 + 0.80907)2{,}000}{\frac{1}{2}(\ln 20{,}000 + 0.80907)2{,}000 + \frac{1}{2}(\ln 10{,}000 + 0.80907)(4{,}000 - 2{,}000)}}$$

$$= 0.952$$

Calculation of the Effective Reservoir Permeability from a Drawdown Curve

The effective permeability of a formation can be determined (11-6, 10-18) from an unsteady-state drawdown curve, using Eqs. (10-31) and (10-36) as combined in Eq. (11-10).

$$P_s^2 = -\frac{mP_f^2 \ln t}{2} + \text{constant} \tag{11-10}$$

This equation applies for infinite reservoirs with laminar flow at large values of dimensionless time. If we plot P_s^2 versus the logarithm of time for a drawdown at a constant flow rate, the slope of this curve is $-mP_f^2/2$. This slope can be used to evaluate the permeability, using Eq. (11-11).

$$K = \frac{1{,}424\mu z T Q}{2h \times \text{slope of } P_s^2 \text{ plot}} \tag{11-11}$$

A convenient way of finding the slope is to determine the change in P_s^2 for one cycle on a semilogarithmic graph. The slope then reads in psia² per cycle, divided by 2.303.

Illustrative Problem

Given the drawdown data in a shallow gas well in Illinois (Table 11-3 and Fig. 11-12), compute the effective permeability of the sand.

Solution

The data are plotted in Fig. 11-13 as P_s^2 versus log t. From the data the slope of the line is found to be 7,800 psia² per time cycle. Using Eq. (11-11),

$$K = \frac{1{,}424\mu z T Q}{2h \times \text{slope}} = \frac{1{,}424 \times 0.0113 \times 0.92 \times 544 \times 1{,}465 \times 2.303}{2 \times 17 \times 7{,}800}$$

$$= 103 \text{ millidarcys}$$

It is sometimes more convenient to plot P_s versus log t than P_s^2 versus log t. In this case Eq. (11-10) can be rewritten using an average pressure

$$\bar{P} = \frac{P_f + P_s}{2}$$

as in Eq. (11-12).

$$P_s = \frac{-mP_f^2 \ln t}{4\bar{P}} + \text{constant} \tag{11-12}$$

The permeability may be found from the slope of such a plot evaluated in (psia per cycle) ÷ 2.303, using Eq. (11-13).

$$K = \frac{1{,}424\mu z T Q}{4h\bar{P} \times \text{slope of } P_s \text{ plot}} \tag{11-13}$$

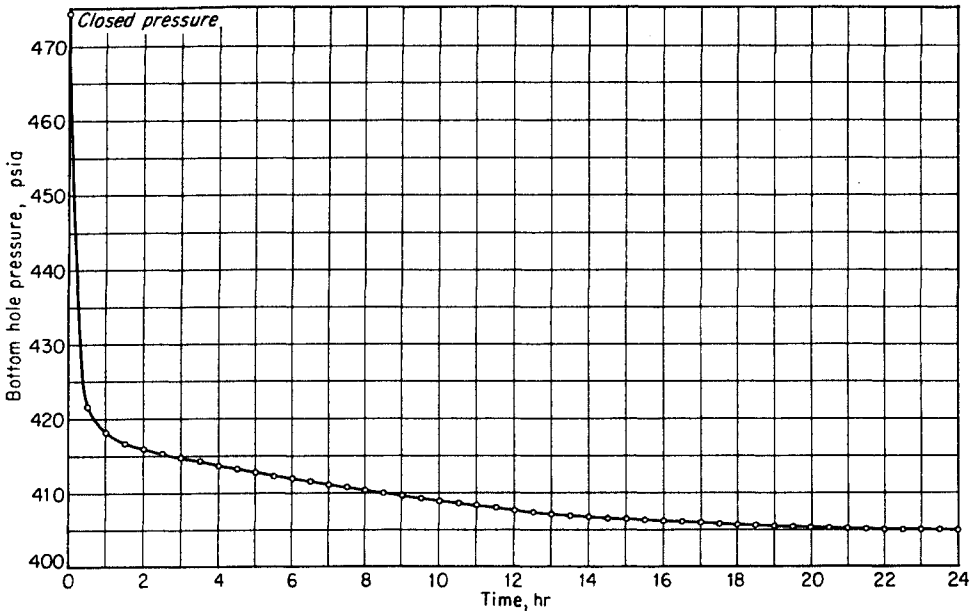

Fig. 11-12. Drawdown data on shallow gas well. (*Courtesy Illinois Power Company.*)

Table 11-3. Data on a Shallow Gas Well*

Depth, ft	1,190
Reservoir temperature, °F	84
Gas gravity	0.62
Sand porosity, per cent	20.5
Sand permeability, millidarcys	74
Sand thickness, ft	17
Gas compressibility factor in reservoir	0.92
Gas viscosity at 460 psia, centipoises	0.0113
Closed reservoir pressure, psia	474.7
Flow rate on drawdown test, Mcf/day:	
Range	1,500–1,430
Average	1,465

* Courtesy K. W. Robertson, Illinois Power Company.

Calculation of Effective Reservoir Permeability from a Build-up Curve

A build-up curve may be used for the evaluation of the effective permeability of the formation. Specific applications of pressure build-up to the calculation of permeability of natural gas reservoirs have been made by Hurst (11-18), Tek, Grove, and Poettmann (11-27), and Janicek and Katz (10-18). In practice, a gas well is shut in after it has been flowing for a long period of time at a fixed production rate. Equation (10-37) with m_2, m_3, . . . , m_n all equal to zero

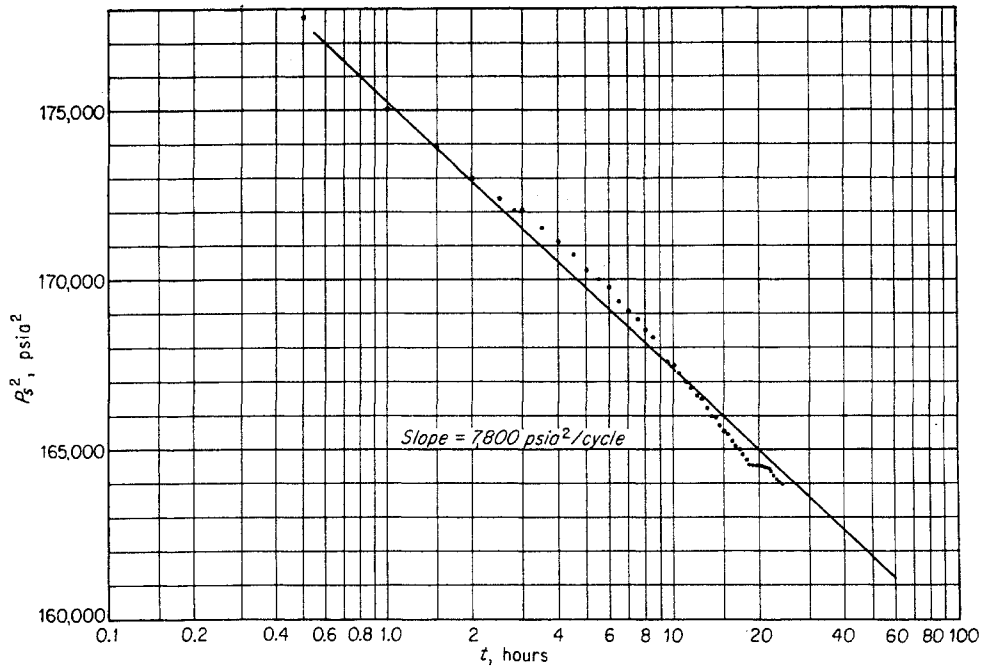

Fig. 11-13. Drawdown curve for permeability evaluation.

applies. P_t may be evaluated using Eq. (10-31) if large values of dimensionless time are involved.

$$\frac{P_s^2 - P_f^2}{P_f^2} = -\frac{m_1}{2}(\ln t_{D_1} - \ln t_{D_2}) \quad (11\text{-}14)$$

or

$$P_s^2 = -\frac{m_1 P_f^2}{2}[\ln (t_f + \Delta t) - \ln \Delta t] + P_f^2 \quad (11\text{-}15)$$

where t_f = length of time that the well was flowing at the constant dimensionless rate m_1 prior to shut-in, Δt = length of time since the shut-in, and P_s, P_f are in psia.

Two types of operation must be considered, depending on the length of time that the well was producing before the shut-in took place. If only a short period of flow was used, Eq. (11-16) shows that P_s^2 versus the logarithm of $(t_f + \Delta t)/\Delta t$ should be plotted.

$$P_s^2 = -\frac{m_1 P_f^2 \ln [(t_f + \Delta t)/\Delta t]}{2} + P_f^2 \quad (11\text{-}16)$$

The permeability is determined from such a plot using Eq. (11-11).

For long periods of flow, however, a simpler type of data plot may be used. Differentiating Eq. (11-15) with respect to Δt, Eq. (11-17) is obtained.

$$\frac{dP_s^2}{d(\Delta t)} = -\frac{m_1 P_f^2}{2}\left(\frac{1}{t_f + \Delta t} - \frac{1}{\Delta t}\right) \quad (11\text{-}17)$$

If t_f is very long compared to Δt, the term $1/(t_f + \Delta t)$ will be negligible and Eq. (11-17) will become

$$\frac{dP_s^2}{d(\ln \Delta t)} = -\frac{m_1 P_f^2}{2} = \text{slope of a curve of } P_s^2 \text{ versus } \ln \Delta t \quad (11\text{-}18)$$

Accordingly, the slope of the build-up curve of P_s^2 versus the logarithm of the build-up time will establish the formation permeability in this special case, using Eq. (11-11) and taking the flow rate Q_1 as the production rate prior to the shut-in. Alternatively, a plot of P_s versus the logarithm of Δt may be used together with Eq. (11-13) to find the permeability.

It is of interest to note that the slopes of the drawdown and build-up curves for long production times are the same but opposite in sign. This constitutes a test of field data for reliability. For shorter production times the slopes of the P_s^2 versus log t for the drawdown and P_s^2 versus log $(t_f + \Delta t)/\Delta t$ for the build-up may be compared.

Illustrative Problem

Given the data on the shallow gas well in Illinois of Table 11-3 and the pressure-build-up curve of Fig. 11-14, compute the effective permeability of the formation.

Solution

Because of the relatively short drawdown period t_f = 24 hr, a plot of P_s^2 versus log $(t_f + \Delta t)/\Delta t$ is required as in Fig. 11-14. The slope of this curve is 6,800 psia² per cycle. From Eq. (11-11), the permeability is

$$K = \frac{1{,}424\mu z T Q_1}{2h \times \text{slope}}$$

$$= \frac{1{,}424 \times 0.0113 \times 0.92 \times 544 \times 1{,}465 \times 2.303}{2 \times 17 \times 6{,}800}$$

$$= 118 \text{ millidarcys}$$

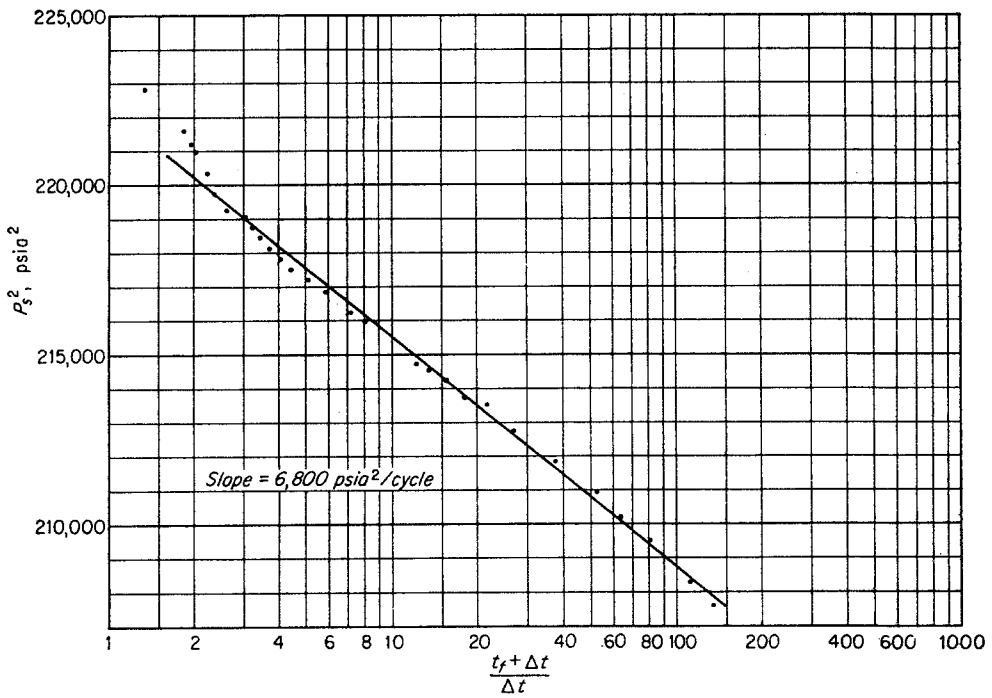

Fig. 11-14. Build-up curve for permeability evaluation. (*Data Courtesy Illinois Power Company.*)

A difference exists between the permeability calculated from the drawdown curve and the permeability calculated from the build-up curve. This is probably due to the fact that the flow rate was not quite constant during the drawdown. The use of the build-up curve to compute permeability is preferable since any effect of well-bore damage is canceled in Eq. (11-15).

Permeability at the Well Bore

The permeabilities just computed are representative of the formation at distances from the well bore. In some cases, the rock adjacent to the well bore may be contaminated with drilling mud and the well-bore permeability reduced. This effect has been called the "skin effect" by Van Everdingen (11-29) and Hurst (11-18). The behavior has been studied by others (11-1, 11-15, 11-16, 11-24a, 11-28, 10-23, 11-31). It is possible that the permeability adjacent to the well bore is increased by acid or other means. Changes in permeability at the well bore may be represented by effective well-bore radii for laminar flow as well as by altered permeability.

Drawdown or build-up curves like Figs. 11-13 and 11-14 usually do not follow a straight line during early flow or shut-in times. Although, after an initial period, the slopes of these drawdown or build-up curves do accurately represent the formation permeability and flow conditions, as given by Eqs. (11-10) and (11-16) (Hurst, 11-18), the observed data during the initial period do not agree with those equations or with the extrapolated curves. The deviations are due to such factors as turbulence, permeability alterations near the well bore, increases in the well-bore radius, and the fact that Eq. (10-31) does not apply for small values of dimensionless time. The volume of gas in the tubing and casing must also be considered.

A zone of decreased permeability adjacent to the well bore will increase the actual pressure drop over that calculated from the permeability of the main portion of the formation. Unsteady-state flow calculations will not be altered because only a small volume of the reservoir is involved. The increase in pressure drop will depend upon the dimensionless flow rate and the permeability change as in Eq. (11-19).

$$\frac{(P_f^2 - P_s^2)_{\text{skin effect}}}{P_f^2} = mS \qquad (11\text{-}19)$$

The term $(P_f^2 - P_s^2)_{\text{skin effect}}$ represents an additional pressure drop that is to be added to the pressure drop calculated by means of such equations as Eq. (11-10) or (11-16). The quantity S is a dimensionless factor depending upon the ratio of the formation permeability K to the altered permeability K' out to a radius r'. Hawkins (11-15) has expressed this relationship in Eq. (11-20).

$$S = \left(\frac{K}{K'} - 1\right) \ln \frac{r'}{r_w} \qquad (11\text{-}20)$$

The additional pressure drop given by Eq. (11-19) may be added to the pressure drop given by Eq. (10-36) to yield Eq. (11-21).

$$P_f^2 - P_s^2 = mP_f^2(P_t + S) = \frac{mP_f^2}{2}(\ln t_D + 0.80907 + 2S) \qquad (11\text{-}21)$$

Knowledge of the formation and gas properties permits the calculation of m and t_D in Eq. (11-21). For a given flow test the factor S may then be calculated from Eq. (11-21).

Advantage may be taken of the fact that the skin effect cancels out in build-up equation (11-15). Van Everdingen (11-29) and Hurst (11-18) both recommend that build-up-test data be extrapolated back to very small values of Δt using Eq. (11-16). At this point the difference between the observed $P_f^2 - P_s^2$ and the extrapolated $P_f^2 - P_s^2$ is considered to be due to the skin effect. Horner (11-16) shows that this extrapolation to very short times is valid. The error is less than ¼ per cent for $t_D = 25$, a condition that will ordinarily be met within a few seconds after closing in the well. Further work may be expected to evaluate such effects as turbulent flow near the well bore.

The value of the skin-effect factor S is found from Eq. (11-21a) in field units.

$$P_f^2{}_{\text{extrapolated to } \Delta t = 1.0 \text{ sec}} - P_f^2{}_{\text{final flowing pressure}} = \frac{1{,}424\mu z T Q}{2hK}\left(\ln \frac{2.634 \times 10^{-4} K \bar{P}\,\Delta t}{\mu \phi r_w^2} + 0.80907 + 2S\right) \qquad (11\text{-}21a)$$

Illustrative Problem (11-18)

Hurst (11-18) gives the straight-line portion of a build-up curve for a natural gas well, plotted as P_s in psig versus Δt in minutes, as $P_s = 5{,}068.58894 + 47.88033 \log \Delta t$.

h = 81 ft
Q_1 = 5,304 Mcf/day
μ = 0.02 centipoise
ϕ = 0.187
r_w = 0.25 ft
T = 717°R
z = 1.026
$\bar{P}$ = 5,155 psia (assumed)

The sand-face pressure just prior to the shut-in is 4,166 psig. Calculate (*a*) the pressure drop due to skin effect, and (*b*) the factor S, assuming that the calculated pressure after a build-up time of 1.0 sec may be compared with the final flowing bottom-hole pressure.

Solution

(*a*) Pressure Difference Due to Skin Effect. The straight-line portion of the build-up curve extrapolated to $\Delta t = 1.0$ sec gives $P_s = 4{,}983.4$ psig.

(*b*) The Skin-effect Factor S. The effective reservoir permeability is calculated from the slope of the build-up curve 47.88/2.303 = 20.8 and from Eq. (11-13).

$$K = \frac{1{,}424 \times 0.02 \times 1.026 \times 717 \times 5{,}304}{20.8 \times 81 \times 4 \times 5{,}155}$$
$$= 3.2 \text{ millidarcys}$$

The skin-effect factor S is calculated from Eq. (11-21*a*).

$$\ln \frac{2.634 \times 10^{-4} \times 3.2 \times 5{,}155}{0.02 \times 0.187 \times 0.25^2 \times 3{,}600} = \ln 5.2$$
$$= 1.65$$
$$\frac{1{,}424 \times 0.02 \times 1.026 \times 717 \times 5{,}304}{2 \times 81 \times 3.2} = 214{,}000$$
$$4{,}983.4^2 - 4{,}166^2 = 214{,}000(1.65 + 0.80907 + 2S)$$
$$2S = \frac{7{,}480{,}000}{214{,}000} - 1.65 - 0.80907$$
$$S = 16.3$$

If the damaged formation extends to a radius of 5 ft, from Eq. (11-20), the permeability of this zone is 0.5 millidarcy. This value of S differs slightly from that calculated by Hurst because Hurst evaluated the gas volume at the maximum reservoir pressure.

Computation of Reservoir Pressure Gradients in Unsteady-state Flow

The procedure for calculating reservoir pressure gradients and the isochronal performance curves from the unsteady-state flow theory of Chap. 10 will now be given. The experimental permeability (Table 11-3) of the previous illustrative problem will be used to calculate pressure gradients in the reservoir after 8 and 16 hr time.

The pressure in the reservoir may be computed by Eq. (10-36), which requires the use of dimensionless time and the functions of Van Everdingen and Hurst (Table 11-4).*

$$\frac{P^2(r,t) - P_f^2}{P_f^2} = -mP_t \qquad (10\text{-}36)$$

or
$$P^2(r,t) = P_f^2(1 - mP_t)$$

where P_t = function of dimensionless time,

$$t_D = \frac{2.634K\bar{P}t}{\mu\phi r^2} \times 10^{-4}$$

Then

$$t_D = \frac{2.634 \times 74 \times 442t}{0.0113 \times 0.205r^2} \times 10^{-4} = 3{,}810\,\frac{t}{r^2} \qquad (11\text{-}22)$$

The results calculated are plotted in Fig. 11-15.

Table 11-4. Computation of Pressure Gradient in Reservoir

t, hr	r, ft	r^2, sq ft	t_D	P_t	$mP_t = 0.0422P_t$	$1 - mP_t$	$P_{r,t}^2 = P_f^2(1 - mP_t)$, psia^2 × 10^{-4}
8	20	400	76.2	2.590	0.1092	0.8908	20.0
	100	10,000	3.05	1.1719	0.0495	0.9505	21.4
	300	90,000	0.339	0.5048	0.0213	0.9787	22.0
	600	360,000	0.0847	0.2917	0.0123	0.9877	22.3
16	20	400	152.4	2.928	0.1237	0.8763	19.7
	100	10,000	6.10	1.4426	0.0609	0.9391	21.1
	300	90,000	0.678	0.6653	0.0281	0.9719	21.9
	600	360,000	0.1694	0.3940	0.0166	0.9834	22.1

* Use of Van Everdingen and Hurst P_t functions for calculation of pressure at points other than the well bore is not rigorous. For such calculations, $P_{t,r}$ functions are required. However, P_t functions represent a close approximation except at small values of t_D.

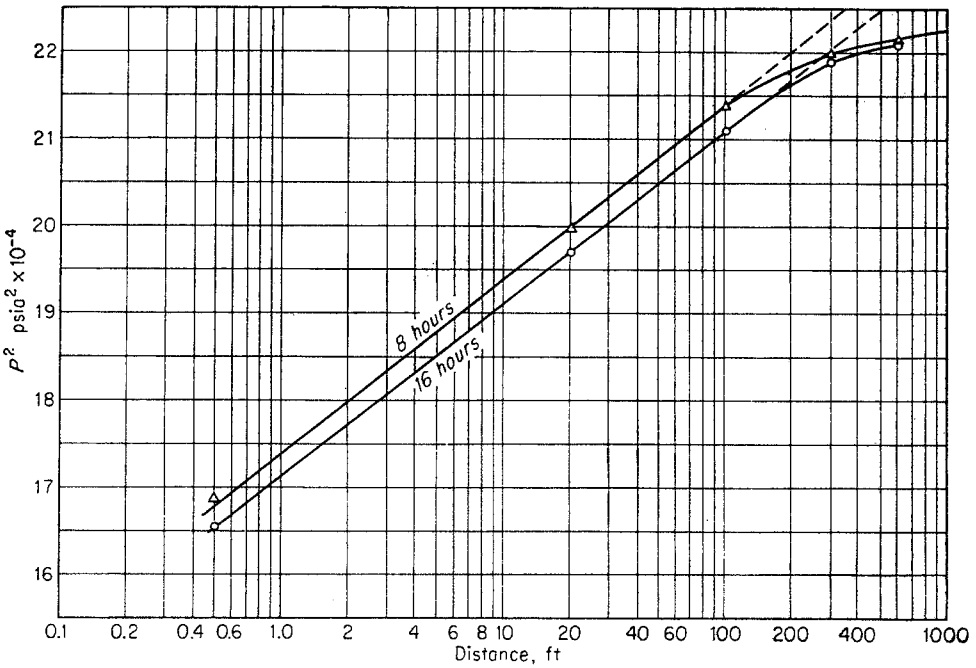

Fig. 11-15. Calculated pressure gradients in shallow gas reservoir at various times.

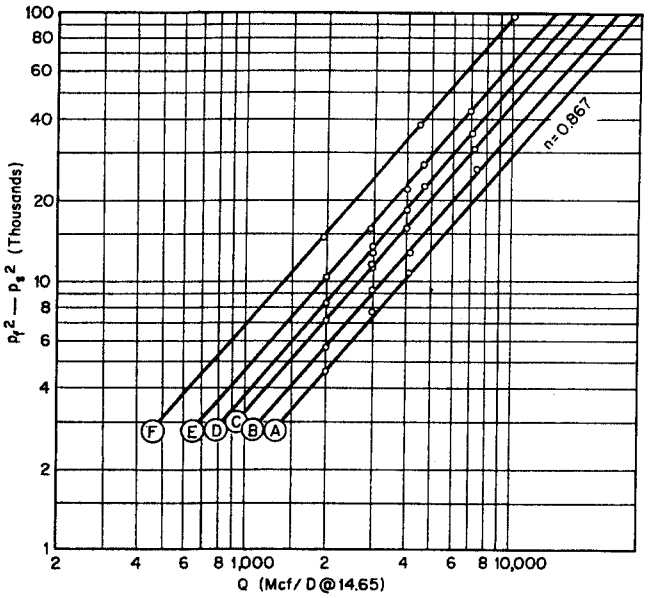

Fig. 11-16. Isochronal performance curves of gas well No. 1. Duration of flow: (A) 0.1 hr, (B) 0.2 hr, (C) 0.5 hr, (D) 1.0 hr, (E) 3.0 hr, and (F) 24.0 hr. (*Cullender, 9-71. Courtesy AIME.*)

By using a series of flow rates and extrapolating to the well bore, a well-performance test is obtained.

An alternative method of making these calculations is by use of Fig. 10-15 (Cornell and Katz, 2-42) with the pressure and radius ratios. The chart is for $m = 0.010$, and for $m = 0.0422$, the value $1 - (P/P_f)^2$ must be multiplied by 4.22.

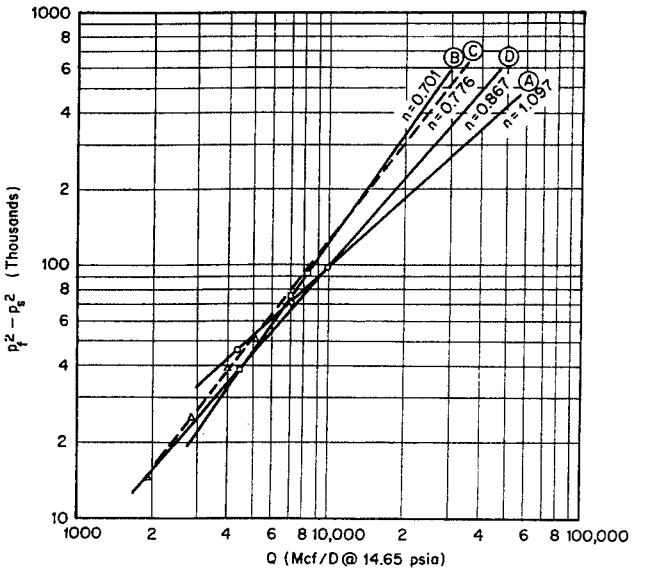

Fig. 11-17. Back-pressure test data on gas well No. 1. Curve A: 24-hr reverse-sequence back-pressure test. Curve B: 24-hr normal-sequence back-pressure test. Curve C: 24-hr normal-sequence back-pressure test. Curve D: 24-hr isochronal performance curve. (*Cullender, 9-71. Courtesy AIME.*)

Isochronal Flow Tests

Cullender proposed (9-71)—and unsteady-state theory predicts—that a series of flow tests at different rates for the same length of time will give a performance curve for a well that has the proper slope throughout the life of the field, regardless of unsteady-state effects. The well should be closed in between tests to permit the well pressure to return to the equalized reservoir pressure. In actual practice, a closed-in period equal to the flow period may give satisfactory results if the new closed-in pressure is used for P_f in calculating the difference in squares for the next flow. The pressure build-up between flow periods will be as shown in Fig. 11-11. The pressure gradient in the reservoir must have returned to a plateau out to the radius of drainage of the next flow.

The basic principle behind the isochronal test is that the radius of drainage depends only on dimensionless time, as established in Chap. 10. Flow rate is not a factor. Accordingly, separate flow-rate tests conducted for the same length of time will reach the same radius of drainage. A performance curve based on isochronal flow data will, therefore, be for a fixed radius of drainage. As shown in Table 11-1, a fixed radius of drainage is required for a steady-state or stabilized performance curve. Likewise, as shown in Table 11-1, the slope of such an isochronal curve is fixed and is the same as that of a steady-state or stabilized performance curve.

The discovery of the isochronal performance curve by Cullender was the result of careful tests made on gas wells in the Hugoton field. Figure 11-16 shows a series of six isochronal tests on one gas well. Figure 11-17 shows a series of four conventional back-pressure tests on the same well. The variable nature of n and C for the back-pressure tests, as contrasted with the definite character of the isochronal test, is shown conclusively by Cullender's paper (9-71).

Figure 11-18 shows in more detail the pressure gradients existing throughout a reservoir during an isochronal test. The initial pressure gradient before each new flow rate is shown by a dashed line. The final pressure gradient after each flow rate is shown by a solid line. The extrapolation of the straight-line portion of each final pressure gradient to the apparent radius of drainage R_a is shown by a broken line. Because the separate flow periods are of equal duration, the apparent radius of drainage is the same in each case. The need for using the new closed-in pressure before the start of each flow rate rather than the reservoir shut-in pressure in calculating the individual points on the isochronal performance curve is shown by this figure.

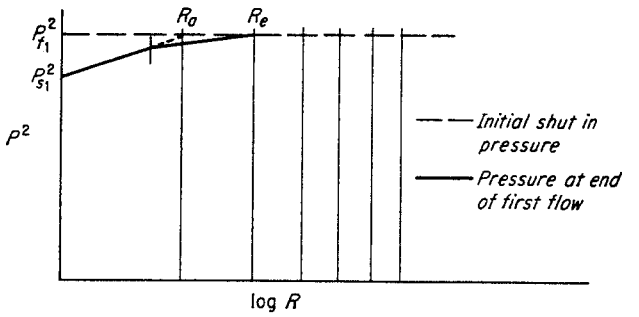

Fig. 11-18. Reservoir pressure gradients during isochronal test.

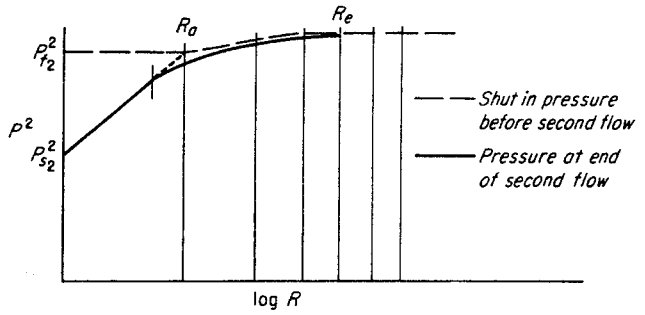

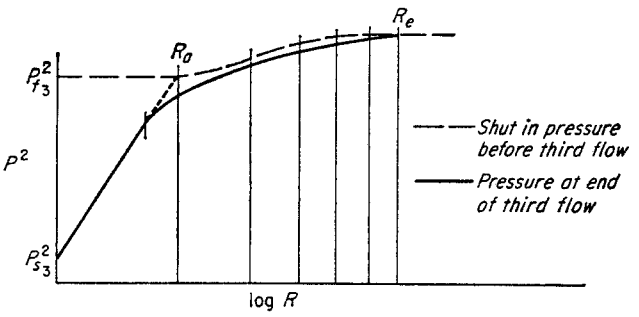

Conversion of Back-pressure Test Data to Isochronal Performance Curves

At the same time that the isochronal test was reported, a method for converting conventional back-pressure test data to an isochronal basis was presented (11-7). The first point on a back-pressure test is the same as the corresponding point on the isochronal performance curve. Successive points have too large values of $P_f^2 - P_s^2$, however, because of the increase in radius of drainage. Figure 11-19 gives correction factors by which the successive points of a conventional back-pressure test may be multiplied to obtain isochronal points. Only flow rates increasing in the ratios indicated and flow periods of equal duration are considered.

A more general procedure would be to use Eq. (10-37) for any combination of flow rates and times (11-4). The correction factors are given for the general case in Table 11-5.

Table 11-5. Factors to Convert Conventional Back-pressure Test Data to Isochronal Data

Flow period	*Correction factor*
1	No correction
2	$\dfrac{Q_2 P_{t,1}}{Q_1 P_{t,1} + (Q_2 - Q_1) P_{t,2}}$
3	$\dfrac{Q_3 P_{t,1}}{Q_1 P_{t,1} + (Q_2 - Q_1) P_{t,2} + (Q_3 - Q_2) P_{t,3}}$
4	$\dfrac{Q_4 P_{t,1}}{Q_1 P_{t,1} + (Q_2 - Q_1) P_{t,2} + (Q_3 - Q_2) P_{t,3} + (Q_4 - Q_3) P_{t,4}}$

SOURCE: (11-4).

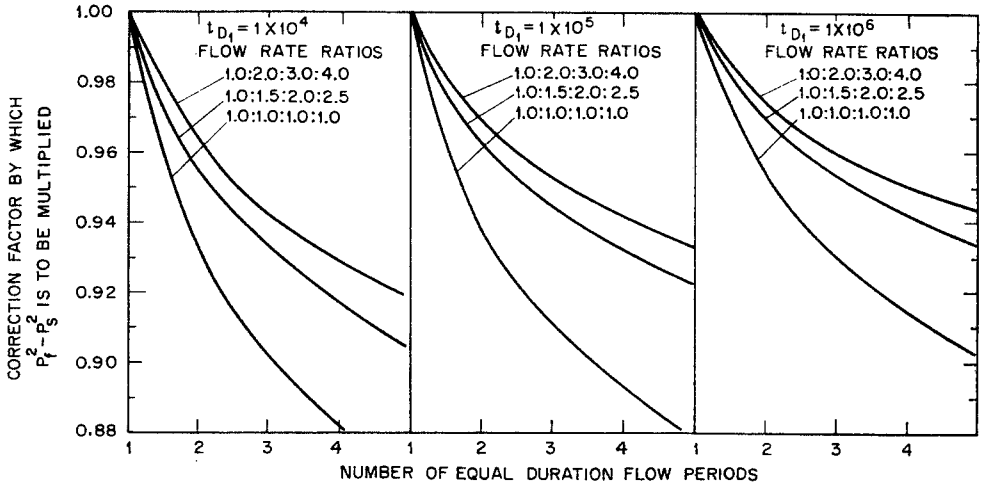

Fig. 11-19. Charts for converting conventional back-pressure test data to isochronal basis. (*Cornell, 11-7. Courtesy AIME.*)

Illustrative Problem (2-42)

The following information has been obtained from a back-pressure test of a natural gas well.

Flow period	Bottom-hole pressure, psia	Flow rate, Mcf/day	Duration of flow, min
Shut-in	2,800		
I	2,700	1,800	60
II	2,653	2,700	60
III	2,596	3,600	60
IV	2,532	4,500	60

The properties of the producing formation and reservoir gas are estimated to be as follows:

K = 110 millidarcys
μ = 0.021 centipoise
ϕ = 0.15
r_w = 0.50 ft

Calculate and plot

(*a*) The back-pressure curve
(*b*) The 1.0-hr performance curve
(*c*) The 24-hr performance curve
(*d*) The 7.0-day performance curve

Solution

Back-pressure Curve

Flow period	Observed $P_f^2 - P_s^2$, psia^2	Flow-rate ratio Q/Q_1	Correction factor (Fig. 11-19)	Corrected $P_f^2 - P_s^2$ (1.0 hr), psia^2
I	496,000	1.000	1.000	496,000
II	802,000	1.5	0.962	770,000
III	1,101,000	2.0	0.944	1,040,000
IV	1,429,000	2.5	0.933	1,330,000

24-hr Performance Curve

$$t_D = \frac{4.39 \times 10^{-6} \times 110 \times 2{,}755 \times 24 \times 60}{0.021 \times 0.15 \times 0.25} = 2.43 \times 10^6$$

m_1 can be obtained from the back-pressure test data as follows:

$$\left(\frac{P}{P_f}\right)_1^2 = \frac{7{,}344{,}000}{7{,}840{,}000} = 0.937$$
$$t_D = 1.012 \times 10^5$$

For $m_1 = 0.010$ and $t_{D_1} = 1.012 \times 10^5$ (Fig. 10-15), $\left(\frac{P}{P_f}\right)_1^2 = 0.938$. The value of m_1 is, therefore, 0.010. At $m_1 = 0.010$ and $t_D = 2.43 \times 10^6$, $\left(\frac{P}{P_f}\right)_1^2 = 0.921$.

$$\frac{P}{P_f} = 0.960$$
$$P_s = 0.960 \times 2{,}800 = 2{,}688 \text{ psia}$$
$$P_s^2 = 7{,}225{,}000$$
$$P_f^2 - P_s^2 = 615{,}000 \text{ psia}^2$$
$$Q = 1{,}800 \text{ Mcf/day}$$

Points 2, 3, and 4 can be found readily by drawing the 24-hr performance curve parallel to the 1.0-hr performance curve.

7-Day Performance Curve

$$t_D = 1.70 \times 10^7$$
$$\left(\frac{P_s}{P_f}\right)_1^2 = 0.912$$
$$\frac{P_s}{P_f} = 0.955$$
$$P_s = 2{,}670$$
$$P_s^2 = 7{,}129{,}000$$
$$P_f^2 - P_s^2 = 711{,}000 \text{ psia}^2$$
$$Q = 1{,}800 \text{ Mcf/day}$$

Figure 11-20 shows the 1-hr, 24-hr, and 7-day performance curves.

Adjustment of Stabilized Performance Curves for Changes in the Reservoir Pressure (2-42)

When gas is withdrawn from a reservoir over a period of time and the reservoir pressure P_f falls, the stabilized performance curve must be corrected for the decline in reservoir pressure. This correction is important in evaluating the producing capacity of a field over a long period of time.

Two effects occur as the pressure declines. The maximum possible flow rate decreases and the family of stabilized performance curves shifts slightly to higher flow rates and spreads apart. Examination of dimensionless time t_D shows that the average pressure is just as important as the elapsed time or the permeability in determining unsteady-state effects. As the reservoir pressure declines, all the stabilized performance curves for a given duration of flow will shift to the right because of the decreased value of t_D. The new maximum flow rate can then be found at $P_f^2 - P_s^2 = P_f^2$ using the new value of P_f. An illustrative problem shows the calculation procedure to use in such cases.

Illustrative Problem

At some later date the shut-in reservoir pressure for the gas well of the previous illustrative problem will have dropped to 2,000 psia. Compute and plot the 7-day stabilized performance curve to be expected at the new reservoir pressure.

Solution

$$\bar{\mu} = 0.018 \text{ centipoise}$$

The value of m_1 is corrected for the change in P_f and viscosity by use of ratios.

$$m_1 = \frac{0.010 \times 0.018 \times 2{,}800^2}{0.021 \times 2{,}000^2} = 0.0168$$

The value of t_{D_1} is corrected for the change in $\bar{z}$, $\bar{P}$, and $\bar{\mu}$ by use of ratios. Because of the limited data available in this problem the change in $\bar{z}$ will be neglected and the change in $\bar{P}$ will be taken the same as the change in P_f.

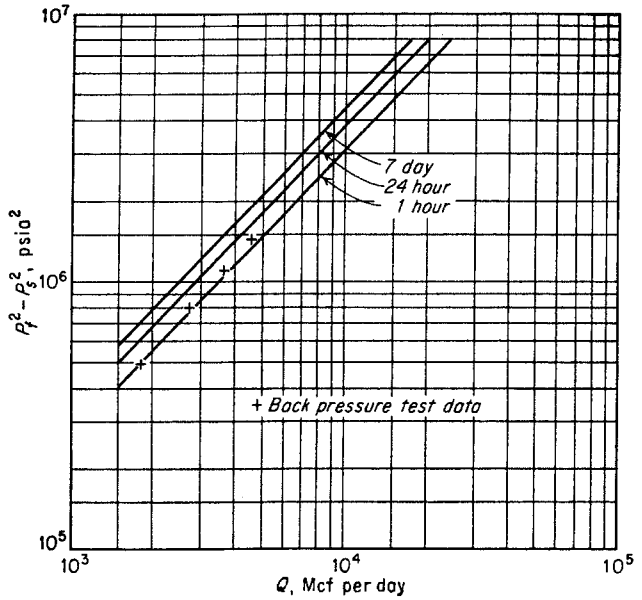

Fig. 11-20. Performance curves for illustrative problem. (*Katz and Cornell*, 2-42.)

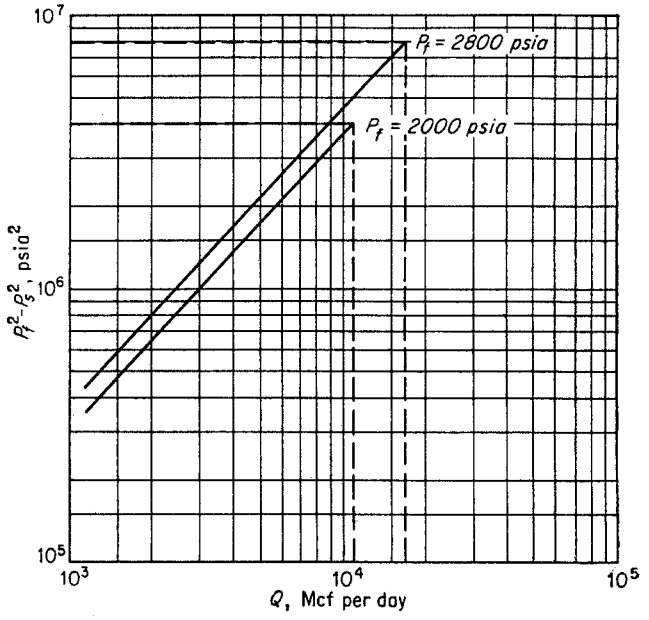

Fig. 11-21. Adjustment of the 7.0-day performance curve for changes in reservoir pressure. (*Katz and Cornell*, 2-42.)

$$t_D = \frac{1.70 \times 10^7 \times 2{,}000 \times 0.021}{2{,}800 \times 0.018}$$

$$= 1.415 \times 10^7$$

$$\left(\frac{P_s}{P_f}\right)^2 = 0.913 \qquad \text{(Fig. 10-15, } m = 0.010\text{)}$$

$$\left(\frac{P_s}{P_f}\right)^2 = 0.854 \qquad (m = 0.0168$$

$$P_s^2 = 0.854 \times 4{,}000{,}000 = 3{,}416{,}000$$

$$(P_f^2 - P_s^2) = 584{,}000 \text{ psia}^2$$

$$Q = 1{,}800 \text{ Mcf/day}$$

Figure 11-21 shows the 7-day performance curves at $P_f = 2{,}800$ and $P_f = 2{,}000$ psia.

Calculation of Performance Curves from Field Data

Tek, Grove, and Poettmann (11-27), using concepts from work by Houpeurt (10-17), have developed a method for predicting the stabilized performance curve of a gas well from a flow test and a pressure-build-up curve. They have found this method of considerable application at Hugoton and San Juan. The advantages of the method lie in its correlation of reciprocal slope n of the back-pressure curve with a coefficient of the back-pressure equation and in the development of work charts to speed the calculation of performance curves.

The back-pressure equation

$$Q = C(P_f^2 - P_s^2)^n \qquad (11\text{-}1)$$

is written as Eq. (11-23).

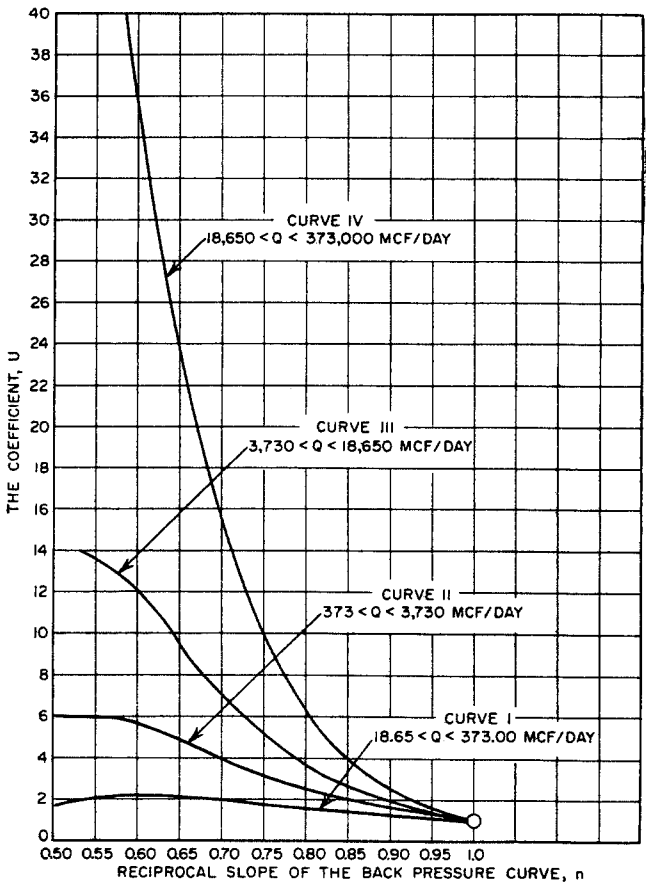

Fig. 11-22. Variation of U with the reciprocal slope of the back-pressure curve. (*Tek, Grove, and Poettmann*, 11-27. *Courtesy AIME.*)

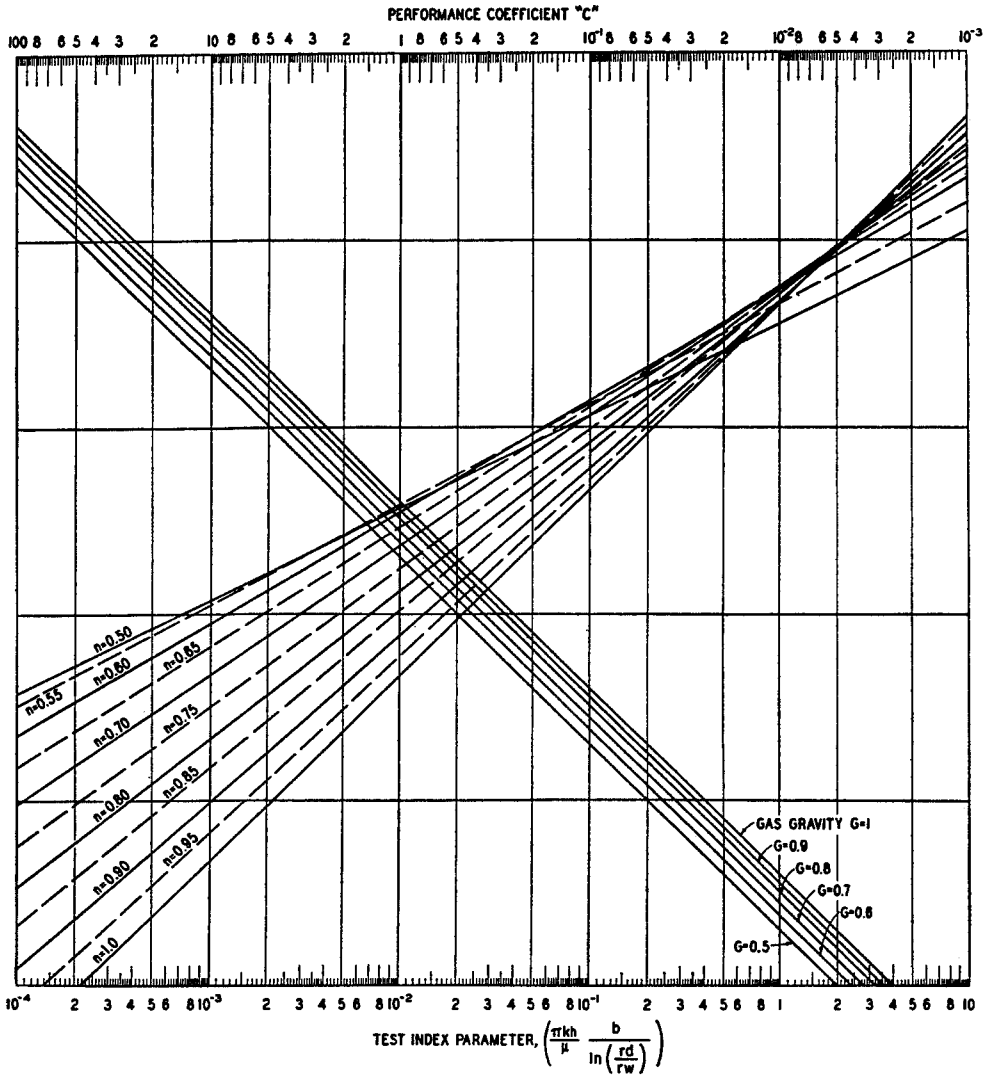

Fig. 11-23. Chart for predicting stabilized performance coefficient from pressure-build-up curve for wells with flow capacities of 18.65 to 373 Mcf/day. (*Tek, Grove, and Poettmann*, 11-27. *Courtesy AIME.*)

$$Q = \frac{2.49}{G}\,(4.659)^n\,U\left[\frac{\pi Kh}{\mu}\,\frac{b}{\ln\,(r_d/r_w)}\right]^n\,(P_f^2 - P_s^2)^n \qquad (11\text{-}23)$$

where Q = flow rate at 60°F and 14.65 psia, Mcf/day
G = gas gravity
n = slope of isochronal performance curve
U = a factor determined by range of production rates and n
K = permeability, darcys
h = formation thickness, cm
μ = viscosity, centipoises
r_d = radius of drainage, ft
r_w = radius of well bore, ft
b = ratio of gas density to pressure, grams/(cu cm)(atm)
P_f^2 = closed-reservoir pressure², psia² (thousands)
P_s^2 = flowing sand-face pressure², psia² (thousands)
C = performance coefficient (Figs. 11-23 to 11-26)

The factor U was related to the reciprocal slope n of the performance curve as shown in Fig. 11-22. Curves of U for ranges of flow are given, with the advice to use the closest curve rather than to interpolate. Working charts for solving Eq. (11-23) with the units as shown are given in Figs. 11-23 to 11-26 for the four ranges of flow rate. For $n = 1$, Eq.

(11-23) becomes Eq. (11-1) considering the different sets of units employed.

The procedure for determining the stabilized performance curve of a gas well using these charts consists of four parts. (1) The short-time performance curve (1 to 3 hr) for the well is determined by an isochronal flow test. This gives the value of n. (2) The well is produced over a period of time (such as one or more days) and then given a pressure-build-up test. This test gives the test index to use with Figs. 11-23 to 11-26, depending upon the flow rate. The test-index parameter is $\pi Kh/\mu$. (3) The radius of drainage is estimated by some means. (4) Finally, values of the performance coefficient C are read from the work charts. Figure 11-24 shows an example for a test index of 1.49, $n = 0.969$ and $G = 0.716$.

The test index is found by Eq. (11-24), using the slope S of a build-up curve.

$$\frac{\pi Kh}{\mu} = 78.1 \frac{QT}{P_f S} \tag{11-24}$$

where $\pi Kh/\mu$ = test index, darcys × cm/centipoise
Q = flow rate at 60°F and 14.65 psia, Mcf/day
T = absolute temperature, °R
P_f = final flowing bottom-hole pressure, psia
S = slope of straight-line section of build-up curve, psia/cycle

Equation (11-24) will be recognized as similar to Eq. (11-13).

Tek, Grove, and Poettmann recommend Eq. (11-25) for calculating the radius of drainage.

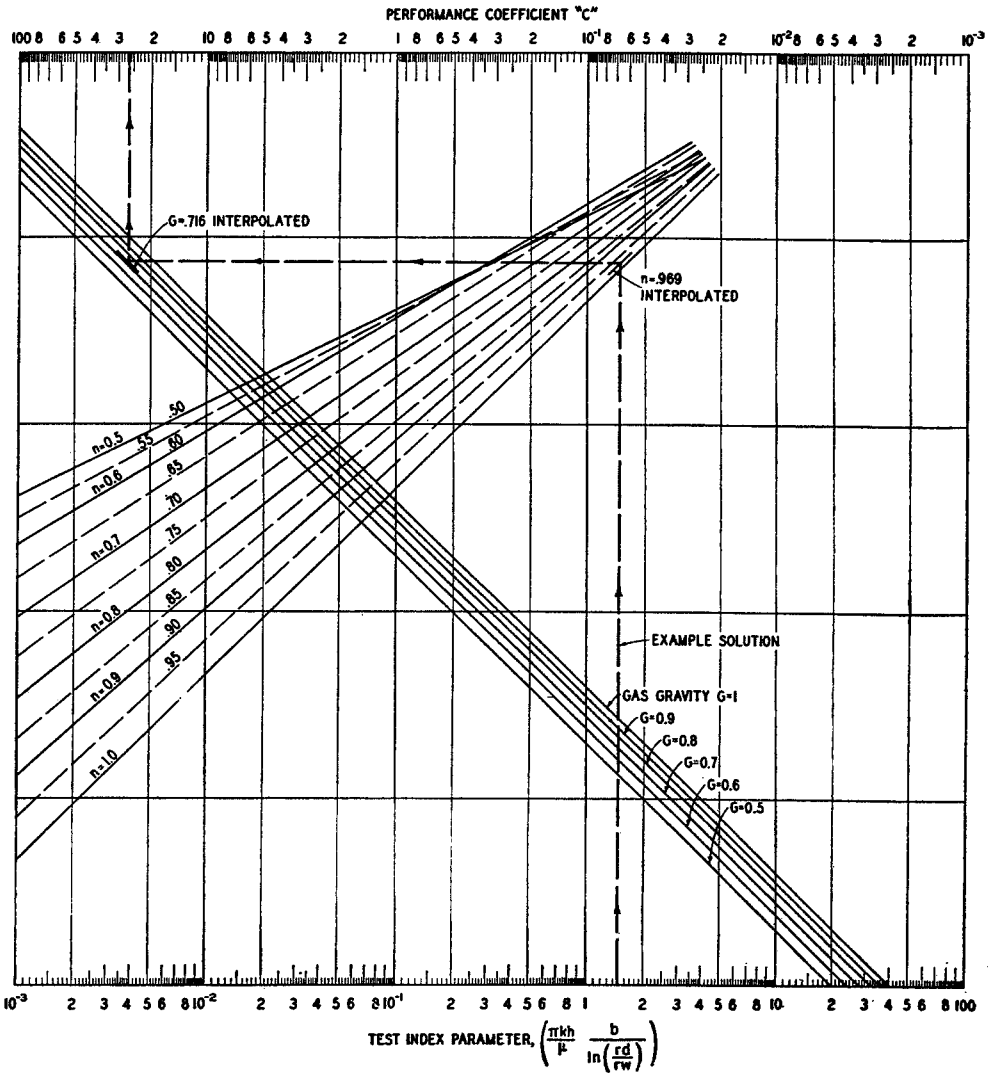

Fig. 11-24. Chart for predicting stabilized performance coefficient from pressure-build-up curve for wells with flow capacities of 373 to 3,730 Mcf/day. (*Tek, Grove, and Poettmann*, 11-27. *Courtesy AIME.*)

$$\frac{r_d}{r_w} = 4.29(t_D)^{1/2} \qquad (11\text{-}25)$$

The use of Eq. (11-6), derived from the work of Van Everdingen and Hurst, is probably a better choice. In any case, if the effective radius of drainage has reached the limit of the producing area, a value of 0.303 times the well spacing should be used. For calculation purposes, a test-index parameter is defined as

$$\frac{\pi Kh}{\mu} \frac{b}{\ln (r/r_w)} = \frac{49.9QG}{P_s Sz \ln (r/r_w)}$$

Illustrative Problem

Given the 3-hr performance curve on the Mesa 1-14 well at San Juan, Rio Arriba County, N. Mex., of Fig. 11-27, the drawdown curve of Fig. 11-28, and the pressure-build-up curve of Fig. 11-29, compute the stabilized performance of the well. The gas has a gravity of 0.650; the reservoir temperature is 156°F; the thickness of the producing formation is 648 ft; the porosity of the formation is 10 per cent. The flow test lasted 718 hr, and the average rate was 682.5 Mcf/day. The flowing pressure was 382 psia just before shut-in.

Solution

Curve *A* of Fig. 11-27 is the 3-hr isochronal performance curve, and will be used to obtain the reciprocal of the slope, or $n = 0.772$. The 6-hr and 30-day curves were determined for this well, but are not essential to the calculation. The solution required is the stabilized performance curve that will give the physical performance of the well for long flow times when using new values of P_f corresponding to the average pressure depletion at intervals.

The test-index parameter is computed from the straight-line portion of Fig. 11-29, using:

1. Average flow rate prior to closing well = 682.5 Mcf/day
2. Flowing pressure P_s prior to closing = 382 psia
3. Pressure rise for time cycle of 10 to 100 hr = 348 psia/cycle

The test-index parameter is computed:

$$\text{Parameter} = \frac{49.9QG}{P_s Sz \ln (r_1/r_2)} = \frac{49.9 \times 682.5 \times 0.65}{382 \times 348 \times z \ln (r_1/r_2)}$$

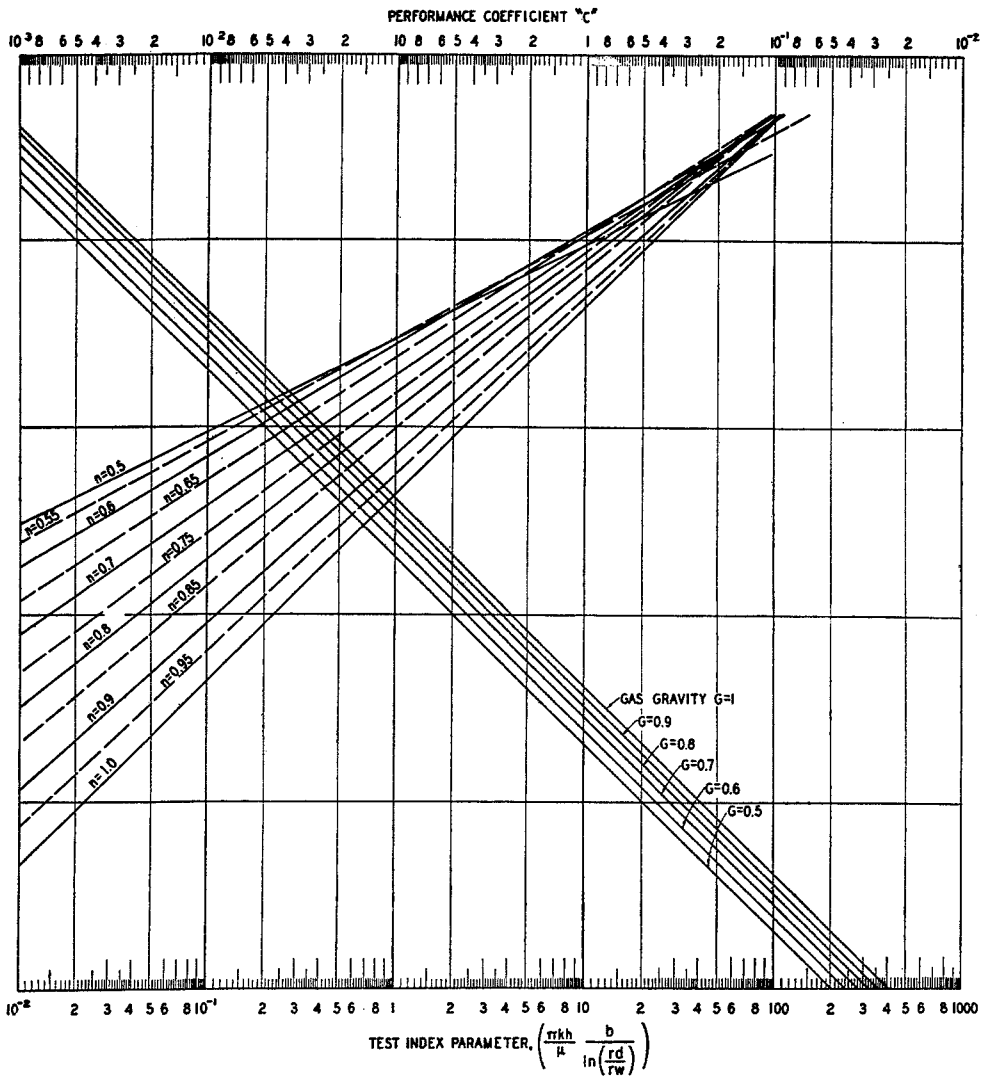

Fig. 11-25. Chart for predicting stabilized performance coefficient from pressure-build-up curve for wells with flow capacities of 3,730 to 18,650 Mcf/day. (*Tek, Grove, and Poettmann,* 11-27. *Courtesy AIME.*)

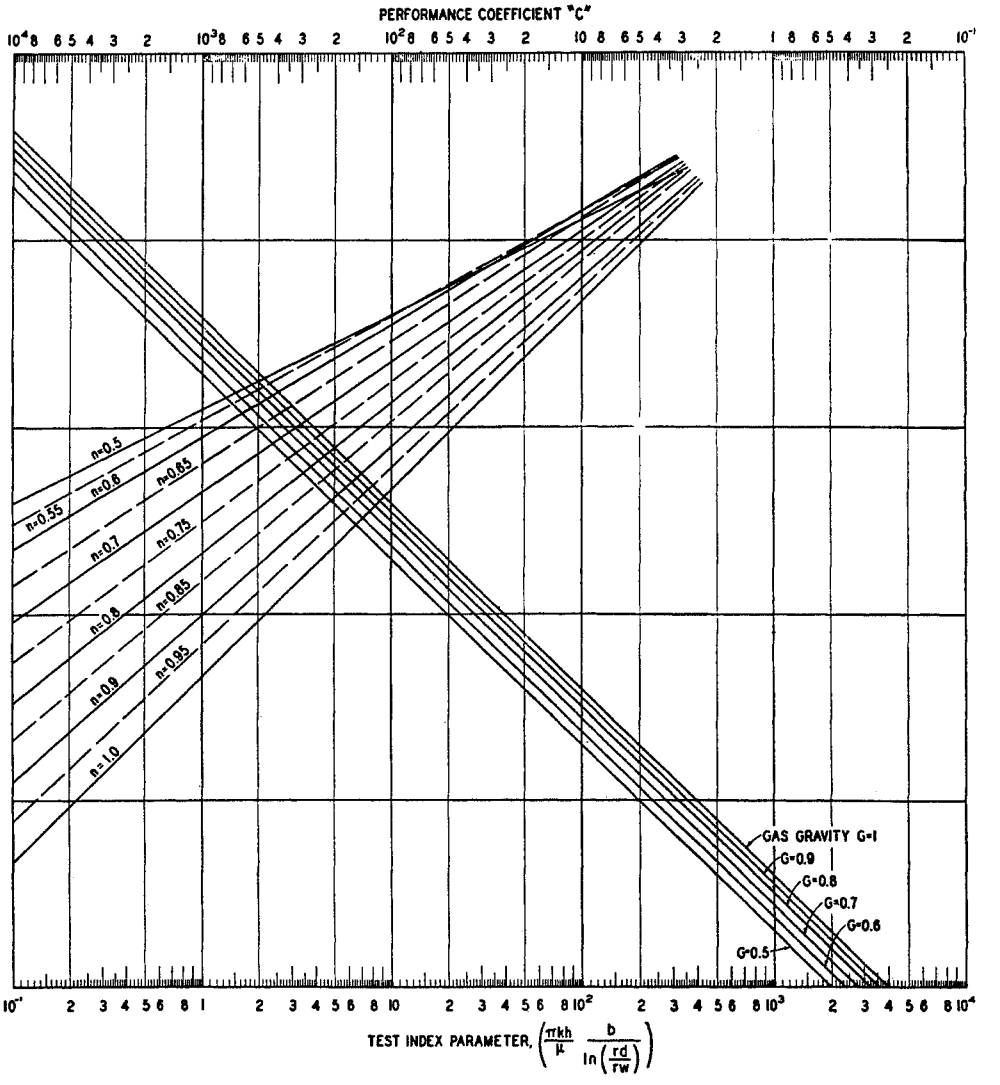

Fig. 11-26. Chart for predicting stabilized performance coefficient from pressure-build-up curve for wells with flow capacities of 18,650 to 373,000 Mcf/day. (*Tek, Grove, and Poettmann,* 11-27. *Courtesy AIME.*)

For 0.65 gravity gas

$$T_r = {}^{616}/_{374} = 1.65$$
$$P_r = {}^{483}/_{669} = 0.72$$
$$z = 0.95$$
$$\ln \frac{r_1}{r_2} = 3 + \frac{1}{2} \ln \frac{718}{10} + \frac{548 - 382}{2 \times 348}$$
$$= 3 + 2.13 + 0.238 = 5.37$$
$$\text{Test-index parameter} = \frac{49.9 \times 682.5 \times 0.65}{382 \times 348 \times 0.95 \times 5.37}$$
$$= 0.0325$$

From Fig. 11-27, this test-index parameter at $n = 0.772$ and $G = 0.650$ gives $C = 2.9$ Mcf/(day)(1,000 psia^2)^n for 1,000,000 difference of squares, and

$$Q = 2.9 \times 1{,}000^{0.772} = 610 \text{ Mcf/day}$$

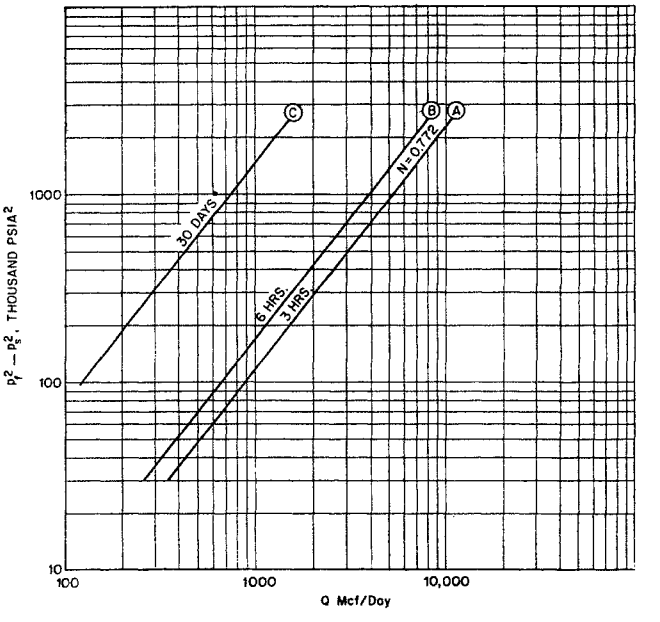

Fig. 11-27. Performance curves on 28-6 Mesa 1-14 San Juan well. (*Tek, Grove, and Poettmann,* 11-27. *Courtesy AIME.*)

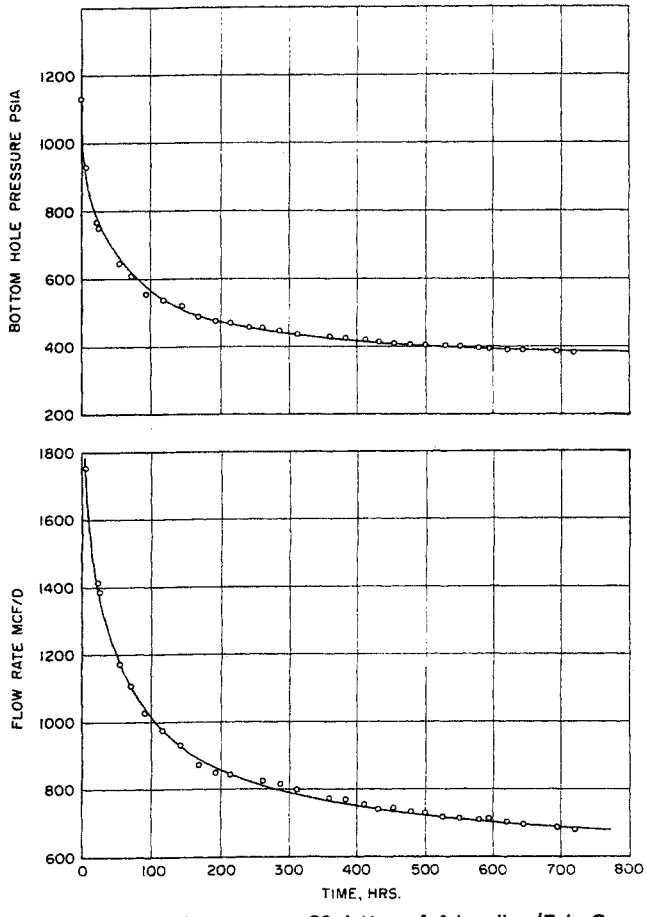

Fig. 11-28. Drawdown test on 28-6 Mesa 1-14 well. (Tek, Grove, and Poettmann, 11-27.)

This point is somewhat below the 30-day test curve in Fig. 11-27, but agrees perfectly with the computed performance from drawdown data by Tek, Grove, and Poettmann. They reported a computed performance some 20 per cent higher than actual.

Tek, Grove, and Poettmann used pressure build-up data to predict the effective well-bore radius r_2 as follows:

$$r_2 = 1.74\left(\frac{QTt_n}{\phi C_g P_s Sh}\right)^{1/2}\left\{\frac{1}{\log^{-1}[(P_n - P_s)/S - 0.3515]}\right\}^{1/2} \tag{11-26}$$

where r_2 = effective radius of well, ft
Q = flow rate prior to shut in, Mcf/day
T = flowing temperature, °R
t_n = build-up time, hr
ϕ = porosity, fractional
C_g = compressibility of gas, (vol)/(vol)(atm)
S = slope of build-up curve on semilog paper, psia/cycle
h = formation thickness, ft
P_n = well-bore pressure at time t_n, psia
P_s = final flowing sand-face pressure, psia

The radius of drainage r_1 is given by Eq. (11-27).

$$r_1 = 42\left(\frac{QT}{P_s Sh\phi C_g}\right)^{1/2} t_f^{1/2} \tag{11-27}$$

where r_1 = radius of drainage at time t, ft
Q = flow rate prior to shut-in, Mcf/day
T = gas temperature in reservoir, °R
P_s = flowing sand-face pressure prior to shut-in, psia
S = slope of build-up curve, psia/cycle
h = formation thickness, ft
ϕ = fractional porosity
C_g = compressibility of gas, vol/(vol)(atm)
t_f = flowing time, hr

Combining r_1/r_2 and taking ln (r_1/r_2), one obtains

$$\ln\frac{r_1}{r_2} = 3 + \frac{1}{2}\ln\frac{t_f}{t_n} + \frac{P_n - P_s}{2S} \tag{11-28}$$

where t_f = time of flow period, hr
t_n = closed-in time, hr
P_n = closed pressure at time t_n, psia
P_s = final flowing sand-face pressure, psia
S = slope of build-up curve, psia/cycle

GAS RESERVES

Gas reserves in gas fields may be estimated by two general methods, the volumetric or pore-volume method and the production–pressure-decline or material-balance method (11-13, 11-10). The first method may be used for new fields before production begins, but the second requires some production history. Gas reserves for gas associated with oil are treated in Chap. 12.

In discussing gas reserves, a distinction should be made between gas in place and gas recoverable in commercial operations. Most of the effort is required to determine the gas in place.

Volumetric Method

The volumetric method of estimating gas reserves is used for new fields before any significant production takes place. The items comprising a volumetric estimate are as follows:

1. Reservoir extent A and thickness h
2. Average porosity ϕ of producing formation
3. Fractional saturation S of pore space with connate water
4. Reservoir pressure P and temperature T
5. Compressibility factor z of gas, based on gas analysis or gas gravity

The volume of gas contained in a reservoir is computed by finding the volume of pore space containing gas and the gas content of a unit space from temperature, pressure, and the compressibility factor. For those desiring an equation, Eq. (11-29) is presented:

$$Q = 43{,}560Ah\phi(1 - S)\frac{PT_b}{P_b Tz} \tag{11-29}$$

where Q = gas in place measured at P_b and T_b, cu ft
A = areal extent, acres
h = thickness of formation, ft

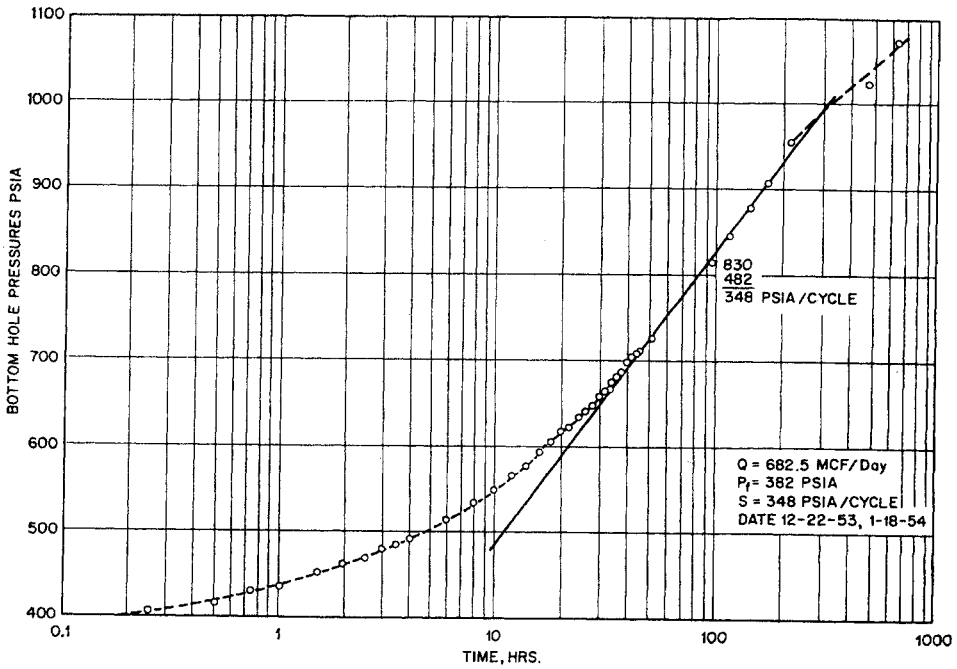

Fig. 11-29. Pressure build-up on 28-6 Mesa 1-14 well. (*Tek, Grove, and Poettmann,* 11-27. *Courtesy AIME.*)

ϕ = fractional porosity
S = fractional saturation of pore space with water
P = reservoir pressure, psia
P_b = measurement pressure base, psia
T = reservoir temperature, °R
T_b = measurement temperature base, °R
z = compressibility factor for gas

The areal extent and formation thickness are based on geological information and maps drawn to portray the structure. Figures 1-29 and 1-30 show a structural map and an isopachous map, which are used to determine the pore volume. A planimetering of the isopachous map gives the area of the zones with the indicated thicknesses. The average thickness times the areas gives the product Ah in acre-feet. The data used in preparing the structural and isopachous maps include all data on the wells such as electric logs, core data, drill-stem tests, logs from cuttings, drilling rate, etc. To obtain the water level, it is necessary to have one well reach the level. When the porosity occurs intermittently, it is customary to give a total formation thickness and a net pay thickness h to be used in computing the gas reserve.

The definition of the water table (11-21) and the possibility of tilted water tables for dynamic reservoirs should not be overlooked (11-17, 11-32, 1-34).

The porosity and connate-water content are determined by methods described in Chap. 2. Measurements on cores are desirable when working with unfamiliar formations. These values may be estimated from electrical logs, especially after experience has been gained in an area.

The compressibility-factor determination requires either the gas analysis or the gas gravity to identify the gas and the reservoir temperature and pressure, as discussed in Chap. 4. The ratio PT_b/P_bTz depends on the choice of base conditions, the reservoir pressure, the reservoir temperature, and the gas composition. It represents the standard cubic feet of gas per cubic foot of space. Figures 11-30 and 11-31 have been prepared for 0.6 and 0.7 gravity gases to give this quantity directly for measurement conditions of 14.73 psia and 60°F. Since the compressibility factors of the gases may be useful as well, Figs. 11-32 and 11-33 are provided to give the values for 0.6 and 0.7 gravity gases.

Illustrative Problem

Compute the gas reserve for the sand No. 44 at Deep Lake, La. The isopachous map is given in Fig. 1-30. Reservoir conditions are given in Table 1-9.

Solution

Find the acre-feet of sand by planimetering area between contours and multiplying by average sand thickness between contours.

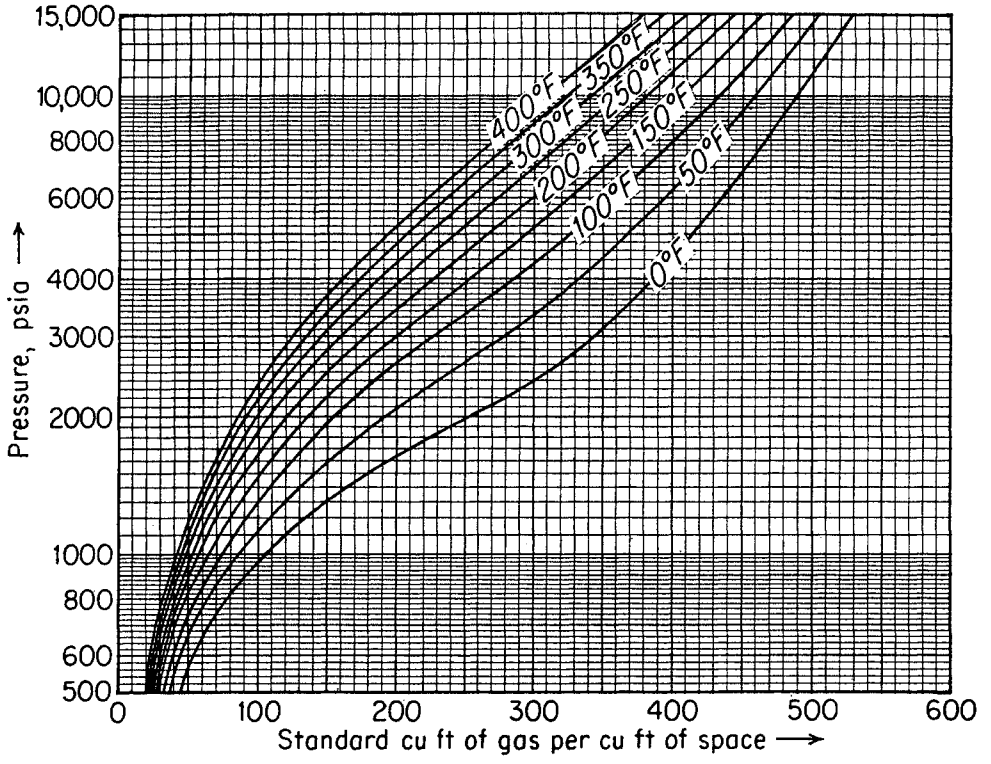

Fig. 11-30. Standard cubic feet of gas (14.73 psia, 60°F) per cubic foot of space, 0.6 gravity natural gas.

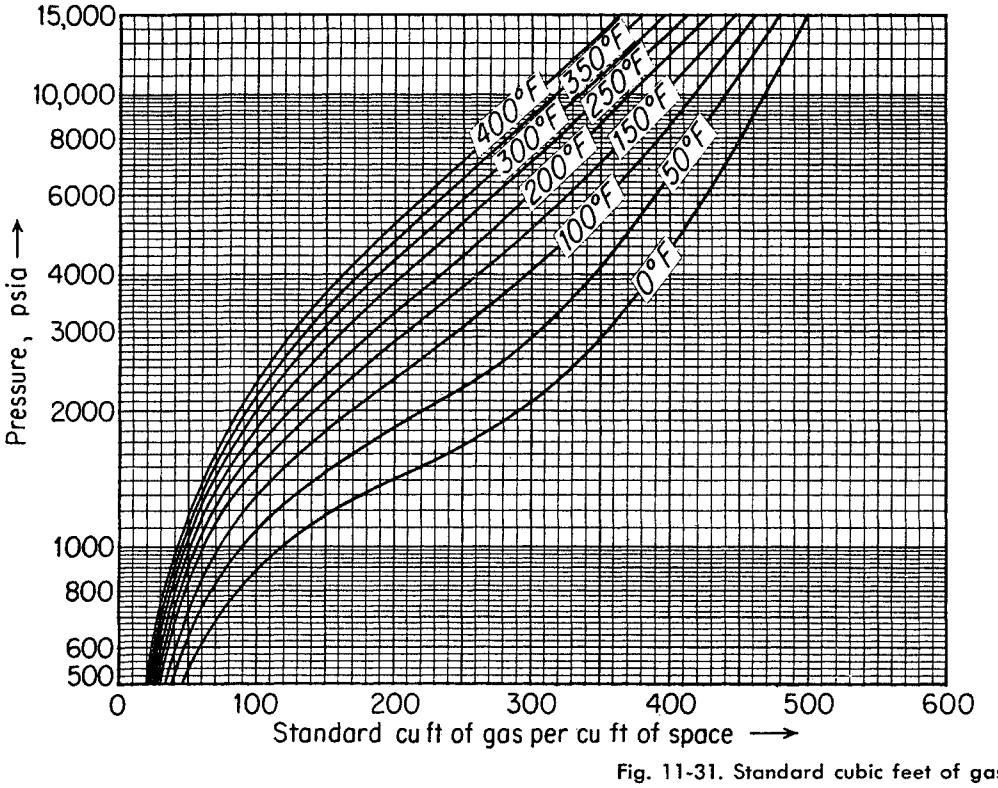

Fig. 11-31. Standard cubic feet of gas (14.73 psia, 60°F) per cubic foot of space, 0.7 gravity natural gas.

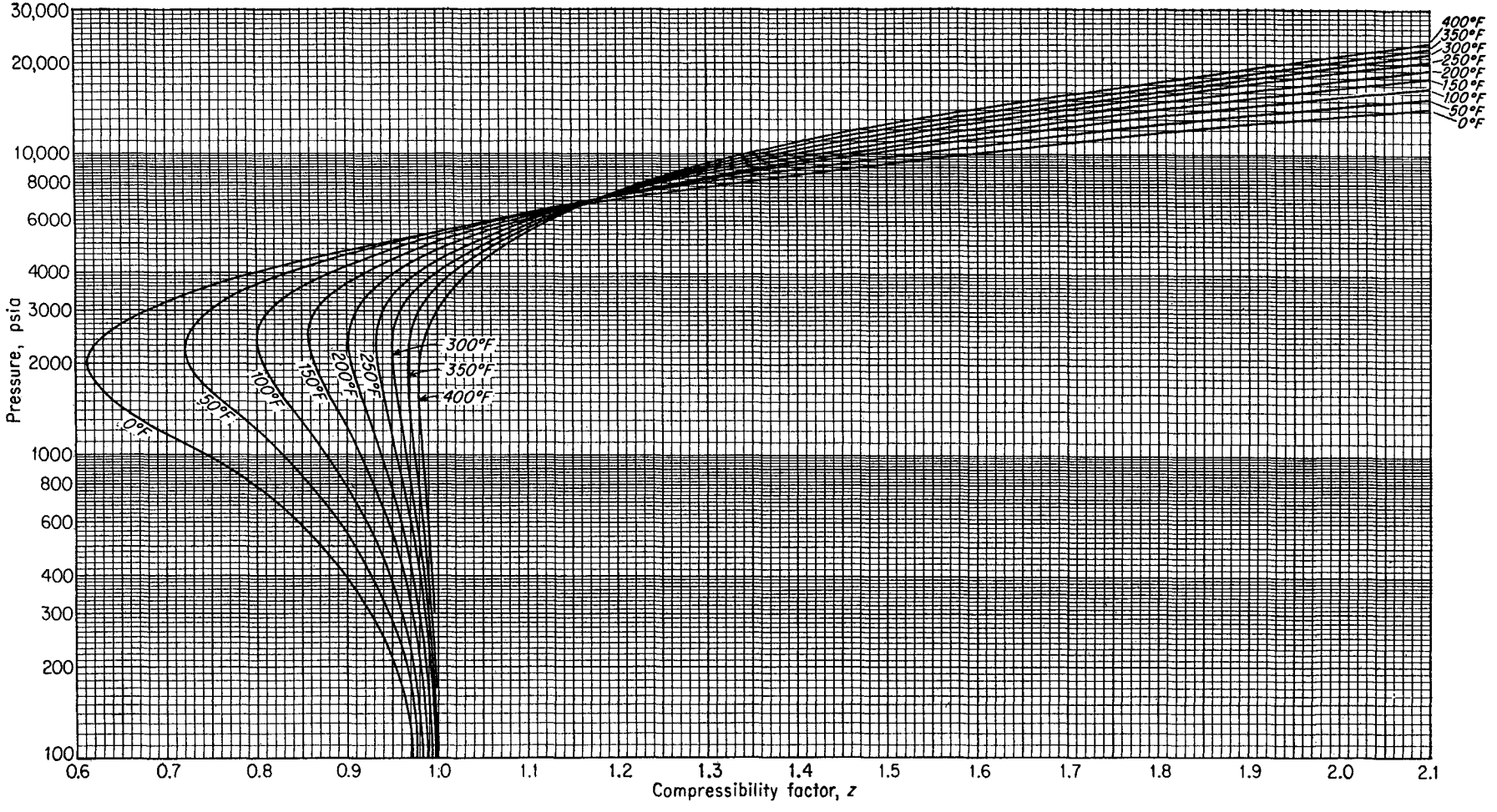

Fig. 11-32. Compressibility factors for 0.6 gravity natural gas.

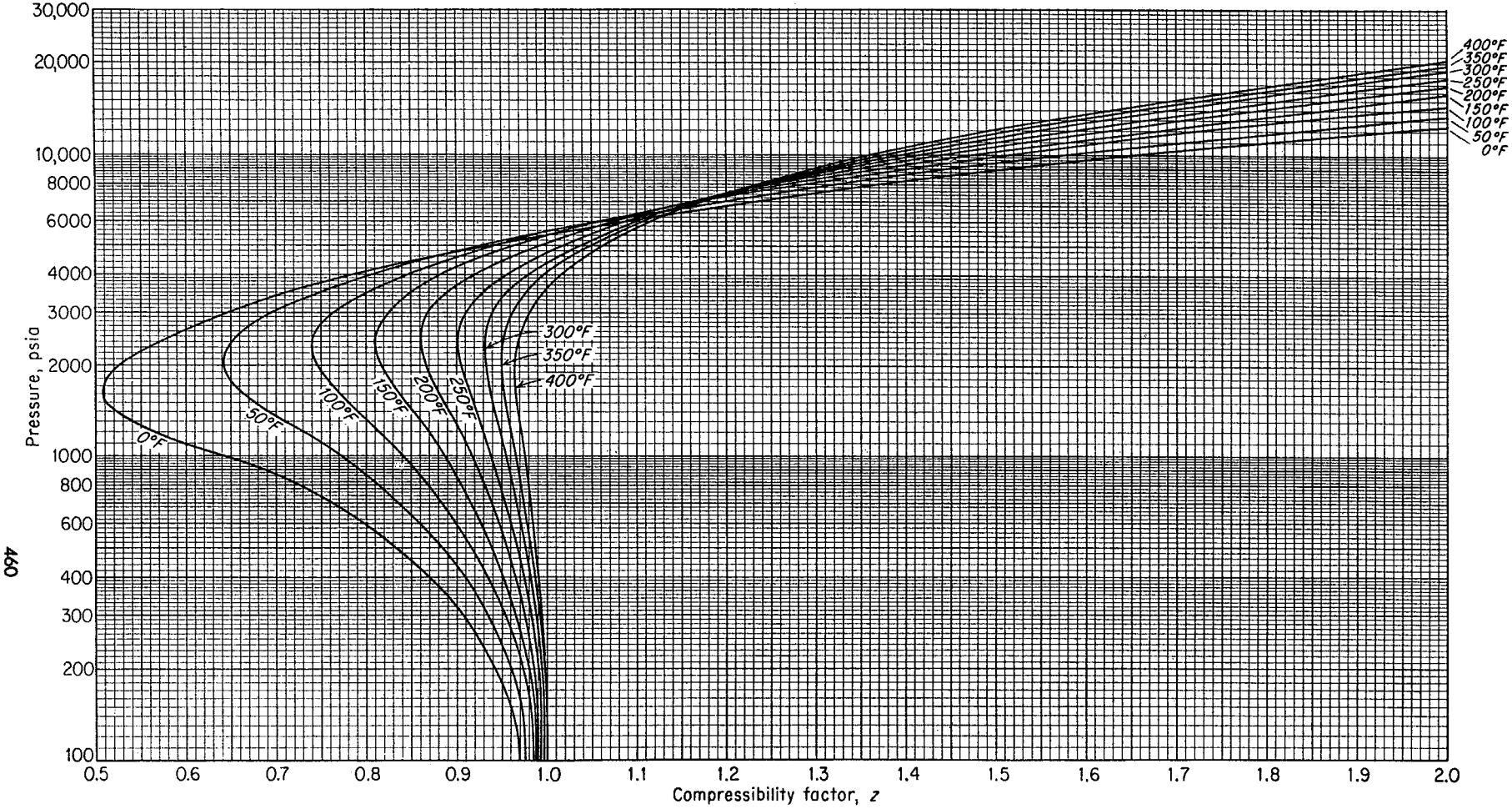

Fig. 11-33. Compressibility factors for 0.7 gravity natural gas.

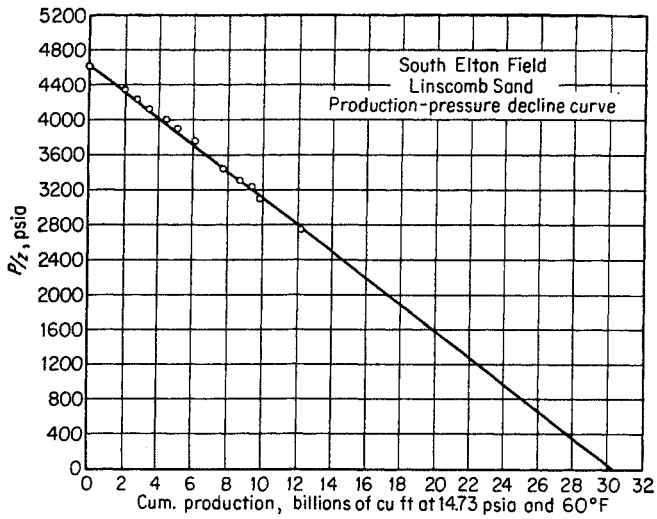

Fig. 11-34. Production–pressure-decline curve, South Elton field, Linscomb sand, Jefferson Davis Parish, La.

Contour interval	Area, acres (from planimeter)	Average thickness, ft	Volume, acre-ft
0–5	153.37	2.5	383.4
5–10	142.75	7.5	1,070.6
10–15	136.78	12.5	1,709.8
15–20	128.38	17.5	2,246.7
20–25	183.55	22.5	4,129.9
25–30	506.10	27.5	13,917.8
30–30	23.77	30.0	713.1
30–35	569.79	32.5	18,518.2
35–40	281.41	37.5	10,552.9
40–44	132.69	42.0	5,573.0
44–44	27.77	44.0	1,045.9
Total.....	2,286.36	....	59,861

Gas reserve per acre-foot (from Table 1-9):

$$43{,}560 \text{ sq ft/acre} \times 0.28 \times 0.75 \times \frac{5{,}164}{14.73} \times \frac{520}{657} \times \frac{1}{0.987}$$

$$= 2{,}572{,}000 \text{ cu ft/acre-ft}$$

$$\text{Gas reserve} = 59{,}861 \times 2{,}572{,}000 = 153{,}900{,}000{,}000 \text{ cu ft}$$

$$= 153.9 \text{ MMMcf}$$

In some low-permeability reservoirs, it may be necessary to select a permeability limit below which the gas, though present, is not counted in the reserve, since it cannot be produced in the usual time limits of depleting the field. The increase of connate-water content of low-permeability rock reduces the gas content of such low-permeability formations considerably.

Production–Pressure-decline Method

The use of pressure declines accompanying gas withdrawal to compute gas in place assumes that the space occupied by gas in the reservoir is constant. This method is not applicable to water-drive reservoirs.

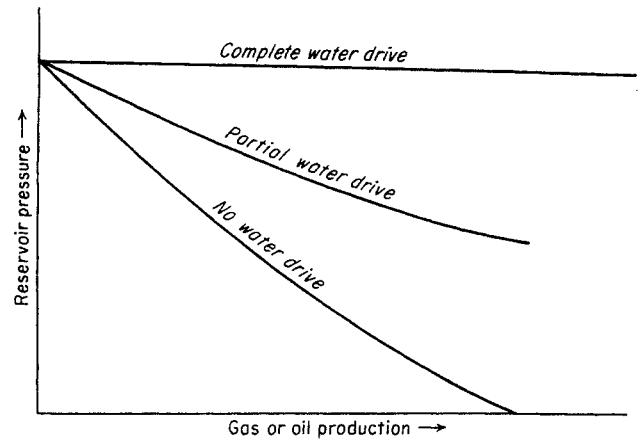

Fig. 11-34a. Effect of water drive on pressure decline.

Figure 11-35 shows the pressure-decline curve for a constant-volume space when gas is being withdrawn. It is because of the compressibility factor for the gas that the curve is not a straight line. A plot of P/z versus gas withdrawn is a straight line at constant temperature, as shown.

When, with pressure reduction, water enters the space occupied by gas, the pressures are maintained either almost completely or only in part, as shown in Fig. 11-34*a*. The water influx, unless it is in known

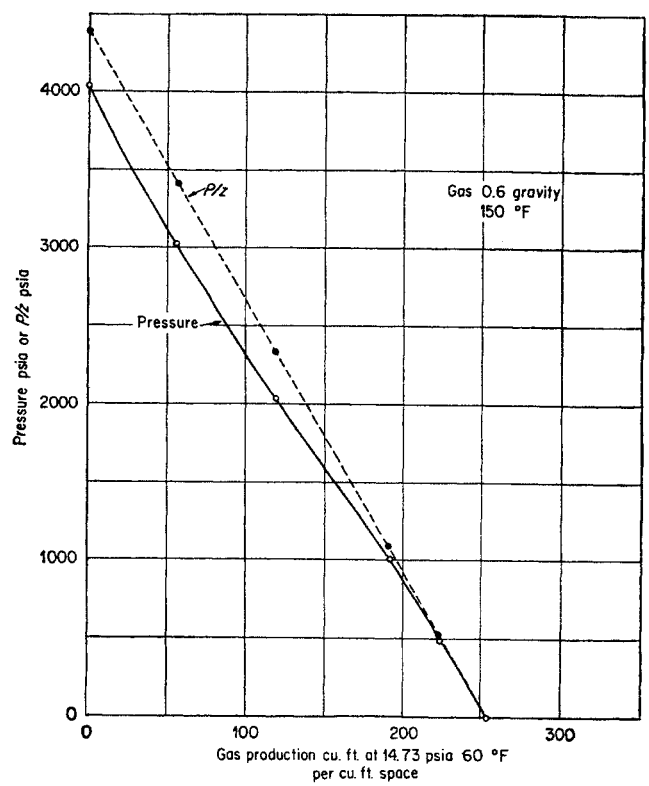

Fig. 11-35. Theoretical pressure-decline curves.

amounts, prevents the use of production–pressure-decline curves for estimating the gas content of reservoirs. The computation of gas in place for constant-volume reservoirs is made from initial pressure, a gas-production quantity, and the reservoir pressure at the end of the gas production.

Illustrative Problem

Given a reservoir initially at 4,030 psia and 150°F and containing gas of 0.6 gravity. When it had produced 1,600 MMcf of gas at 14.73 psia and 60°F, the reservoir pressure was 3,022 psia. Neglecting any water influx in the reservoir, compute its initial gas content.

Solution

At the initial condition, 1 cu ft of space contains

$$\frac{PT_b}{P_bTz} = \frac{4{,}030 \times 520}{14.73 \times 610 \times 0.919} = 253.8 \text{ cu ft of gas}$$

The values of z may be read directly from Fig. 11-32. At 3,022 psia, 1 cu ft of space contains

$$\frac{3{,}022 \times 520}{14.73 \times 610 \times 0.884} = 198.1 \text{ cu ft}$$

During the production process, each cubic foot of space gave up $253.8 - 198.1 = 55.7$ cu ft of gas. It follows that there is $1{,}600{,}000{,}000/55.7 = 28{,}720{,}000$ cu ft of space, which initially contained $28{,}720{,}000 \times 253.8 = 7{,}290{,}000{,}000$ cu ft of gas.

This problem can be solved by reading the cubic feet of gas per cubic foot of space directly from Fig. 11-30.

Illustrative Problem

Given the production–pressure-decline curve on the Linscomb sand of the South Elton field, La. (Fig. 11-34), what is the reserve?

Solution

Extending the pressure-decline line to zero gives total gas in place = 30.4 MMMcf for a constant-volume reservoir.

A formula can be derived to give the initial gas in place from production–pressure-decline data and compressibility factors:

$$Q_R = \frac{Q_P(P_1/z_1)}{P_1/z_1 - P_2/z_2} \tag{11-30}$$

where Q_R = gas in place at initial condition P_1
Q_P = gas produced from time 1 to time 2, std cu ft
P_1 = reservoir pressure at time 1, psia
P_2 = reservoir pressure at time 2, psia
z = compressibility factor

In computing gas reserves from reservoir pressure, it must be assumed that well pressures reflect the equalized reservoir pressures. For low-permeability reservoirs, pressure-build-up data on wells may be used to estimate equalized pressures, as discussed in Chap. 10.

Specifically, the procedure is to plot P_s^2 versus $\log [\Delta t/(t_f + \Delta t)]$ on semilog paper, as shown in Fig. 11-14. P_s is the closed bottom-hole pressure, Δt is the time the well has been closed, and t_f is the flow time prior to closing the well. The build-up curve is extrapolated to $\Delta t/(t_f + \Delta t) = 1$ (Fig. 11-14 or Fig. 10-19). The value of $P_s{}^{*2}$ read at this point is greater than the equalized reservoir pressure squared, excepting for reservoirs of great extent. Figure 10-20 gives the correction for P_s for finite reservoirs so that it represents the closed-in equalized pressure (10-22). Using dimensionless time over πR^2,

$$\frac{t_D}{\pi R^2} = \frac{0.0000838K\bar{P}t_f}{\mu\phi r_b{}^2}$$

from Fig. 10-20, the value of $(P^{*2} - \bar{P}^2)hK/712\mu zTQ$ is read. The closed pressure $\bar{P}$ is found as

$$\bar{P}^2 = P^{*2} - (\text{ordinate Fig. 10-20})\left(\frac{712\mu zTQ}{hK}\right)$$

where P^* = closed pressure for infinite reservoir from plot, psia
$\bar{P}$ = true equalized reservoir pressure, psia
K = permeability, millidarcys
t_f = flow time of well prior to shut in, hr
μ = viscosity of gas, centipoises
ϕ = fractional porosity of formation
r_b = radius of outer boundary, one-half distance between wells
t_D = dimensionless time, from Table 10-2
T = reservoir temperature, °R
h = formation thickness, ft
Q = flow rate of well prior to shut-in, Mcf/day
z = compressibility factor for gas
$R = r_b/r_w$

Recoverable Gas

For reservoirs producing by gas expansion and without water drive, there is no reason that essentially all the gas may not be produced, down to atmospheric pressure. However, the production rates decrease so rapidly when the pressure approaches atmospheric that some abandonment pressure is normally established for commercial production. These abandonment pressures are set as low as 50 psia for shallow reservoirs and may be as high as 500 psia or more for deep gas reservoirs. The initial gas content minus the content at a selected abandonment pressure gives the recoverable gas.

For water-drive reservoirs, the pressure decline is not the occasion for final depletion of the reservoir. Water production from the wells will drown out gas production when most of the gas has been produced. The exact effectiveness of water in displacing gas is not known for reservoir conditions. In long periods

of time the displacement is essentially complete, for one does not expect to find partial gas saturation below an initial water level. Data in the literature are conflicting (11-12, 11-25) and may be somewhat removed from actual behavior in the reservoir. In addition to direct displacement of gas by water, one should consider the position of wells on the structure and the ability to recomplete wells on the top portion of the producing formation. Many engineers and geologists use a recovery factor of 85 per cent for water-drive gas reservoirs. Field recoveries from reservoirs with good geological control should be studied to give the range of recoveries and any significant variations between reservoirs.

PRODUCTION PROBLEMS

The operator of gas wells expects to have a certain number of problems and is equipped to handle them. Corrosion in high-pressure condensate wells is an example. Water often comes into the well bore or accumulates from condensate flowing down the casing of low-capacity gas wells. The presence of water may reduce the flow capacity of the gas well.

Corrosion

Corrosion is a persistent problem in the petroleum industry. Special problems of corrosion occur in the tubing of high-pressure condensate wells (11-2). Figure 11-36 shows some tubing taken from a 1,300- to 4,500-ft depth in a gas well. It appears that corrosion is related to the presence of carbon dioxide and that enough organic acids of the acetic acid series are present to cause corrosion. In the tubing, water condenses from the cooling gas stream to provide the aqueous phase. Research and field tests are in progress to solve the problems of corrosion (11-3, 11-11, 11-14, 11-23, 11-26), but they become complicated by special conditions in each installation. Eilerts and associates (11-11) presented the results of injecting sodium chromates and alkalies into the annulus of flowing gas-condensate wells. Menaul and Spafford (11-23) show that the injection of ammonium hydroxide into the annuli of condensate wells will eliminate tubing corrosion when calcium and magnesium salts are not present in the water accompanying the well stream.

Water in Gas Wells

Water "coning" at the well bore is a term often used to describe entrance of water due to flow-pressure gradients (11-24, 11-22, 11-9, 1-12). Muskat and Wyckoff have presented theoretical calculations for static and dynamic conditions based on potential

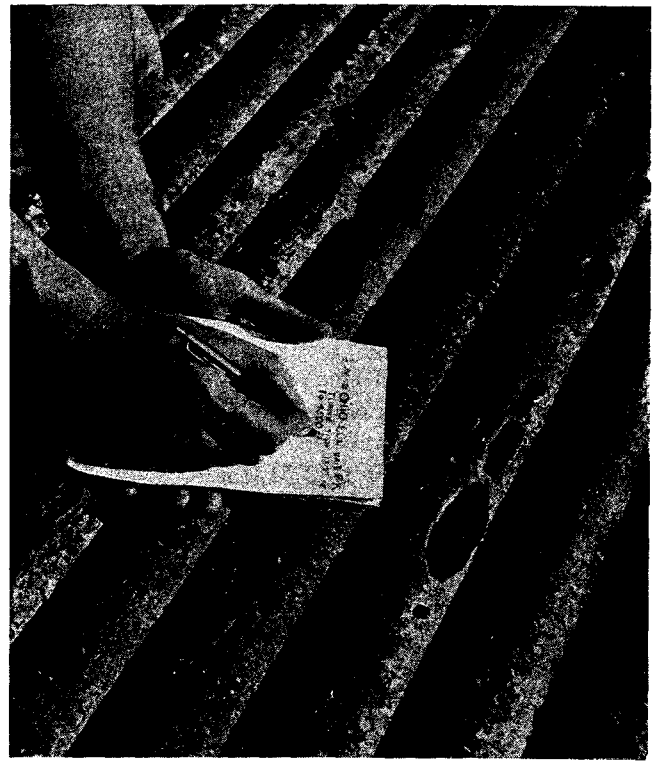

Fig. 11-36. Corrosion in tubing from gas well in North Markham field, Tex. (*Courtesy Ohio Oil Company.*)

theory. In essence, the theory states that a decrease in flowing bottom-hole pressure in the gas phase of 1 psi will be accompanied by a rise in the water cone below the well of 0.43 ft (Fig. 11-37). The theoretical treatment requires uniform horizontal and vertical permeability.

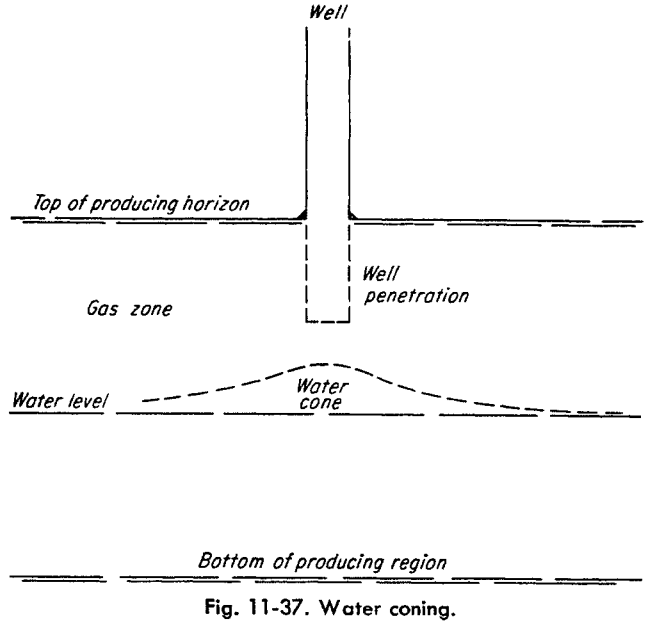

Fig. 11-37. Water coning.

Experience with this theoretical treatment indicates that it seldom applies to the practical case. For example, one well produced 41 MMcf/day for a period of 3 days, at the end of which the drawdown in bottom-hole pressure was from 696 to 650, or 46 psia. The known vertical distance between the bottom of the well and the water level was 28 ft. There were no signs of water coning or encroachment into the well. The sand had a permeability of around 1,000 millidarcys, and vertical permeabilities were about the same as the horizontal. There is a slight possibility that thin low-vertical-permeability layers occurred to prevent the water from coning.

In another case, a well produced from a sand conglomerate at the rate of 10.2 MMcf/day for 10 days without water coning to interfere with gas production. The well penetrated the gas zone a distance of 7 ft and was known, from data on a twin well to a deeper zone, to have a water level 14 ft below this point. The drawdown in bottom-hole pressure during the flow was from 1,338 to 1,080, or 258 psia. The permeability of the conglomerate was as much as 1,000 millidarcys in both horizontal and vertical directions. There was a layer having a permeability <1 millidarcy below the well completion depth and above the water level. Again, this low permeability barrier may have prevented coning.

Both bottom water and edge water enter gas wells on occasion. In general it appears that greater pressure drawdown in flowing-well pressures will be more liable to bring water into wells. If there is shale intermingled in the producing section or below the casing point for open-hole completions, water may cause sloughing of the shale and an accumulation of shale mud in the hole. Blowing of wells or bailing of the mud may renew the flow capacity. Yuster (11-33) indicates that well treatment with low-surface-tension liquids such as acetone–diethyl ether would remove the water around the well bore and restore the well capacity.

Delivery of Gas to Market

Once a gas reserve has been dedicated to market, its production rate on the average and maximum day is usually specified. Contracts often require that the average take-or-pay-for quantity shall be 1 MMcf/day per 8 MMMcf of reserve. This rate depletes 91.3 per cent of the reserve in 20 years.

The operator drills sufficient wells to ensure that he can maintain the maximum daily requirement, which may be 1.25 times the average daily rate. For water-drive fields, the flow rates are normally set to allow uniform advance of water into the producing zone. Once water reaches a well, water may be produced for a while along with gas. The well may be squeeze-cemented and recompleted at a higher level in the same zone or at another reservoir in a multiple-sand field.

Engineering work during operations includes studies of reservoir pressure changes, water-level movements, and other items that bear on the reserves. Charts may be developed for predicting bottom-hole pressures from wellhead values for the specific field (11-8). Well productivity is checked at intervals (11-30), and the deliverability of the field is computed to ensure that it can continue to meet the market requirement. Well remediation or new wells may be required at certain stages in the life. If the reservoir is producing by pressure depletion and the gas-sales contract calls for a minimum pressure for delivering gas, field compressors may be installed as the field approaches abandonment pressure.

CHAPTER 12

Gas from Condensate and Oil Fields

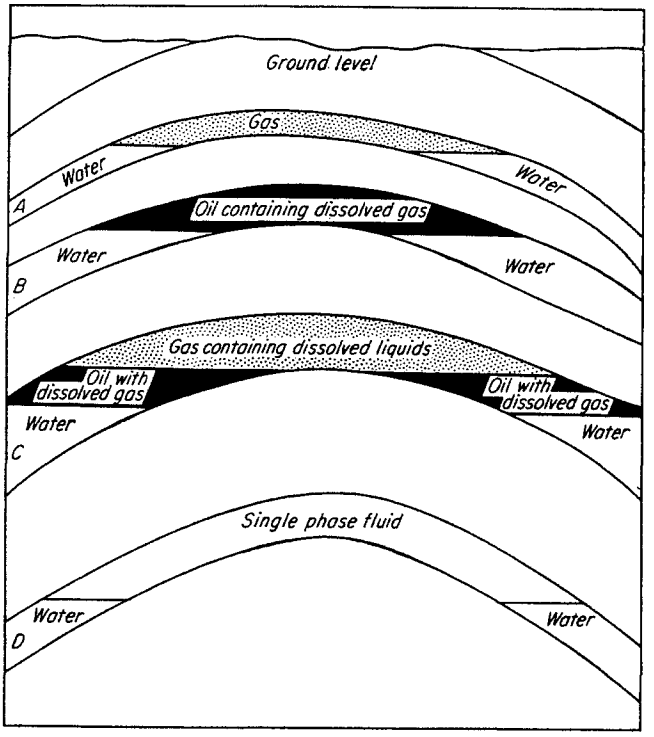

Fig. 12-1. Occurrence of oil and gas.

At low pressures in shallow fields, natural gas and crude oil appear as distinct substances in the reservoir (Fig. 12-1). As the pressure at which petroleum is found rises with increased depth, gas dissolves in crude oil, and high-boiling constituents dissolve in the gas phase. Some fields have oil and gas layers in contact (Fig. 12-1, reservoir C), and the gas phase is often called a gas cap. Deeper fields at pressures above some 4,000 psi and at temperatures of 200°F and more contain single-phase fluids that are not immediately distinctive as oil or gas fields. In general, wells produce from a single phase in the reservoir and the following discussion will assume that the well effluent from a virgin reservoir comes from a single phase.

There are two approaches to understanding the relationship of gas and oil in the reservoir. One is to consider the nature of the phase diagram for a reservoir fluid. The other is to use the gas-oil ratio as a criterion for the nature of the reservoir fluid. Figure 12-2 gives illustrative phase diagrams for reservoir fluids. The diagram for the liquid layer indicates that a gas phase forms as the pressure is reduced along path AB in the reservoir and along AA' for fluid flowing up the well bore. The diagram for a high-pressure gas layer containing dissolved liquid constituents shows that condensate will form upon pressure reduction either at constant temperature AB or at decreasing temperatures AA'. The liquid or crude oil layer occurs in the reservoir at a temperature below the critical point for the mixture and the gas phase at a temperature above its critical. As the mixture composition becomes such that its critical

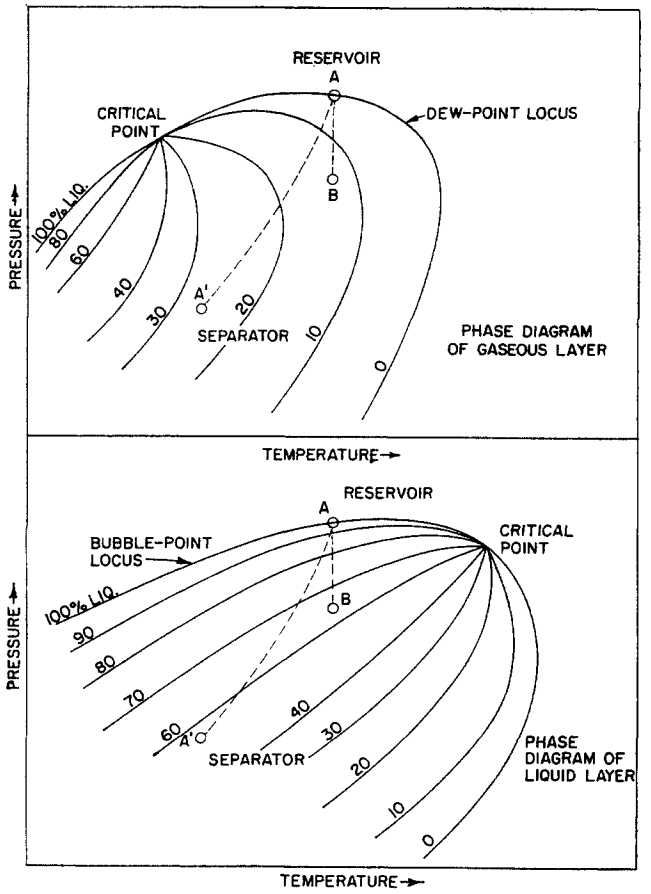

Fig. 12-2. Relative phase diagrams of liquid and vapor layers. (*Katz and Williams*, 1-38. *Courtesy AAPG.*)

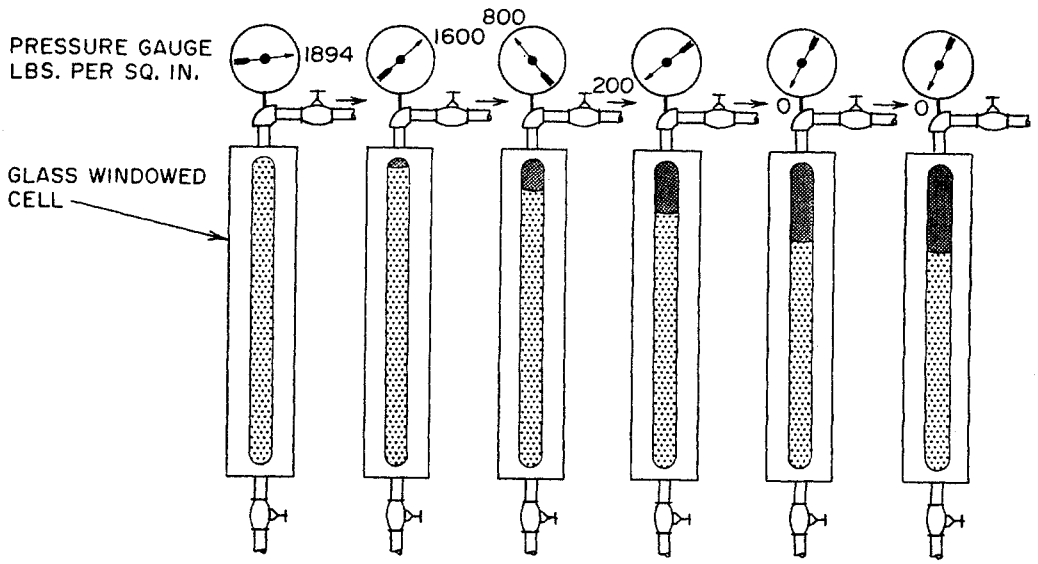

Fig. 12-3. Gas evolution causing shrinkage of crude oils. (*Katz and Williams*, 1-38. *Courtesy AAPG.*)

PRESSURE - LBS. PER SQ. IN. GAUGE	1894	1600	800	200	0	0
TEMPERATURE - DEGREES FAHRENHEIT	152	152	152	152	152	60
VOLUME LIQUID PHASE - BBLS.	1.40	1.36	1.26	1.16	1.04	1.00
VOLUME GAS PHASE - BBLS.	0.00	0.04	0.14	0.24	0.36	0.40
GAS EVOLVED - CU. FT. FROM PREVIOUS PRESSURE	0	88	238	212	208	0
GAS EVOLVED - CU. FT. ACCUMULATIVE	0	88	326	538	746	746

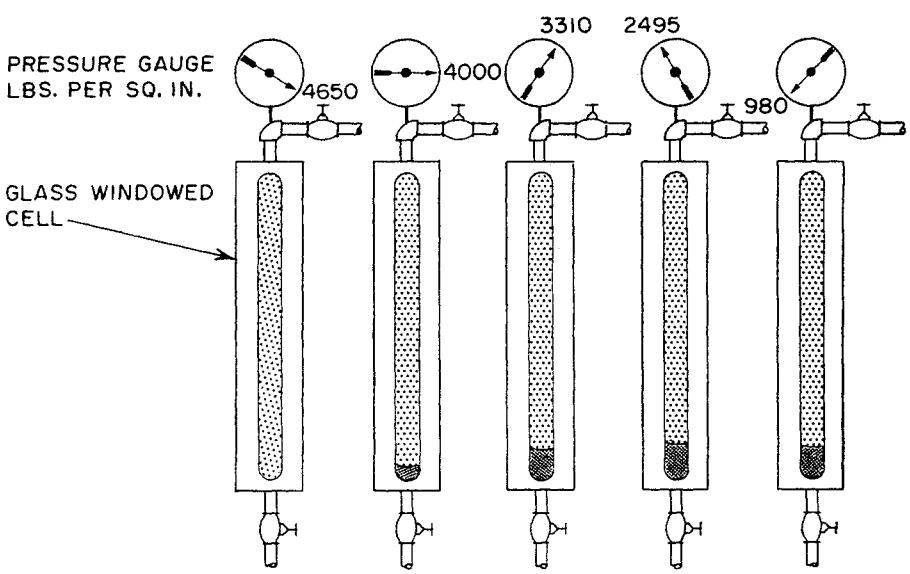

Fig. 12-4. Retrograde condensation from gas phase by pressure reduction. (*Katz and Williams*, 1-38. *Courtesy AAPG.*)

PRESSURE - LBS. PER SQ. IN. GAUGE	4650	4000	3310	2495	980
TEMPERATURE - DEGREES FAHRENHEIT	256	256	256	256	256
VOLUME LIQUID PHASE - C.C.	0	5.1	9.4	10.7	9.4
VOLUME GAS PHASE - C.C.	100	94.9	90.6	89.3	90.6
GAS WITHDRAWN - BETWEEN PRESSURES *	0	1770	2330	3600	6900
GAS WITHDRAWN - ACCUMULATIVE *	0	1770	4100	7700	14,600

* — — — C.C. MEASURED AT 60° F., 14.7 LB. PER SQ. IN.

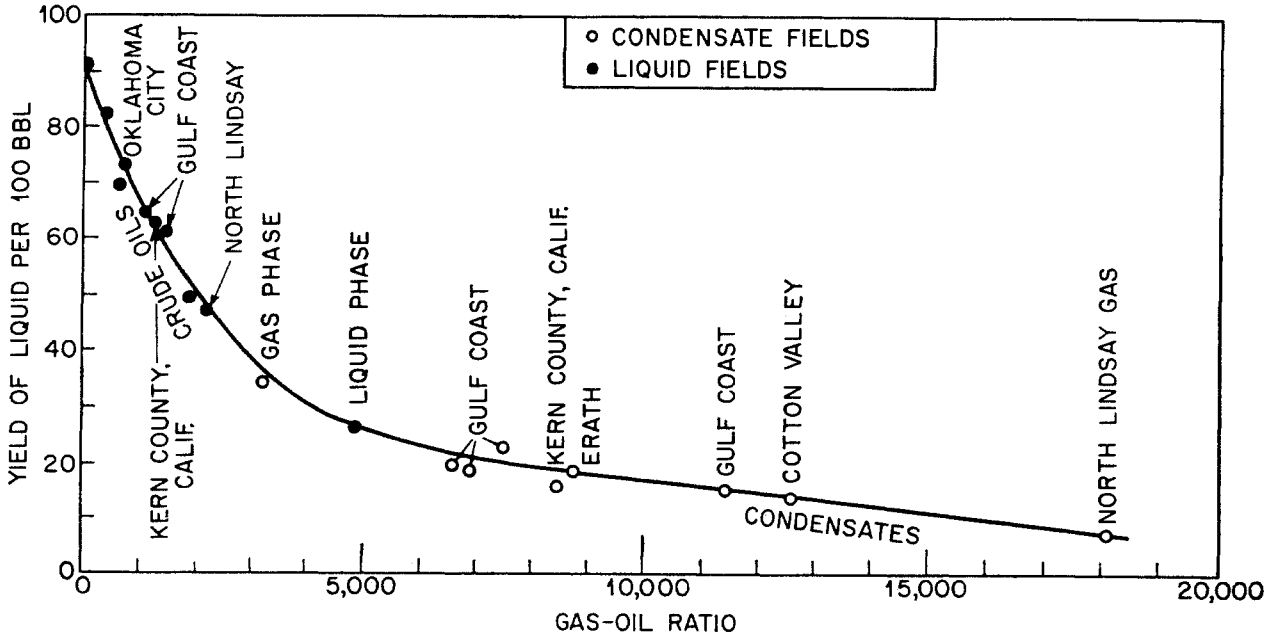

Fig. 12-5. Gas-oil ratio for condensate and oil fields. (*Katz and Williams*, 1-38, 12-44.)

temperature approaches or coincides with the reservoir temperature, the terms "gas" and "liquid" become meaningless. Near the critical temperature both liquids and gases change phase rapidly as the pressure is decreased and the two-phase region is entered. Production methods discussed later will indicate clearly the need for displacing this type of reservoir fluid as a single phase without permitting it to enter the two-phase region.

Procuring a reservoir sample and measuring its phase behavior provide a good way to learn about a reservoir fluid. A second criterion, however, for judging the nature of a reservoir fluid is the gas-oil ratio of the surface separator. Figures 1-19 and 1-20 show the separation conditions and gas-oil ratio for an oil reservoir and a gas-condensate reservoir. Figures 12-3 and 12-4 present the phase behavior that occurs for these two reservoir fluids. Similar data have been used to plot Fig. 12-5, which gives the gas-oil ratio versus barrels of liquid in the separator per 100 bbl of reservoir fluid. At gas-oil ratios below about 3,000 cu ft/bbl, the reservoirs are oil or liquid and the gas evolves from the liquid. At gas-oil ratios greater than about 6,000 cu ft/bbl, the fluids are gas phase in the sense that liquid is formed upon reduction of pressure. In the range of 3,000 to 6,000 cu ft/bbl, one cannot tell reservoir phase from the gas-oil ratio but one can be sure that the fluid is in the neighborhood of its critical temperature at the reservoir temperature for this gas-oil ratio range (12-41).

Since much gas production accompanies oil production, the nature of crude oils containing dissolved gas will be discussed along with the mechanism of oil production from reservoirs (1-3, 1-12, 1-14, 12-93). Discussion of the behavior of condensate fluids will precede that of cycling in condensate reservoirs.

SUBSURFACE SAMPLES OF CRUDE OIL

Methods for measuring the quantity of natural gas dissolved in crude oil were developed by Lindsly (12-47, 12-48) of the Bureau of Mines at Bartlesville, Okla. A bottom-hole sampler procured the oil at the reservoir pressure before the dissolved gas was released from solution. The quantity of gas evolved per barrel of residual oil is reported as solubility of the gas even though it is a measure of the composition of the naturally occurring system. Such solubility measurements are normally made at the reservoir temperature and either as approximate differential or constant-volume differential vaporizations (12-42). It soon became customary to obtain a hydrocarbon analysis of the subsurface sample of crude oil (examples are given in Table 1-8). When no extraneous gas accompanies the crude oil flowing into the well bore, samples of liquid and vapor from surface separators may be recombined in the proportions at which they were produced. The recombined mixture may be compressed with mercury and converted to a single-phase liquid, which may then be used in laboratory experiments similar to those for subsurface samples.

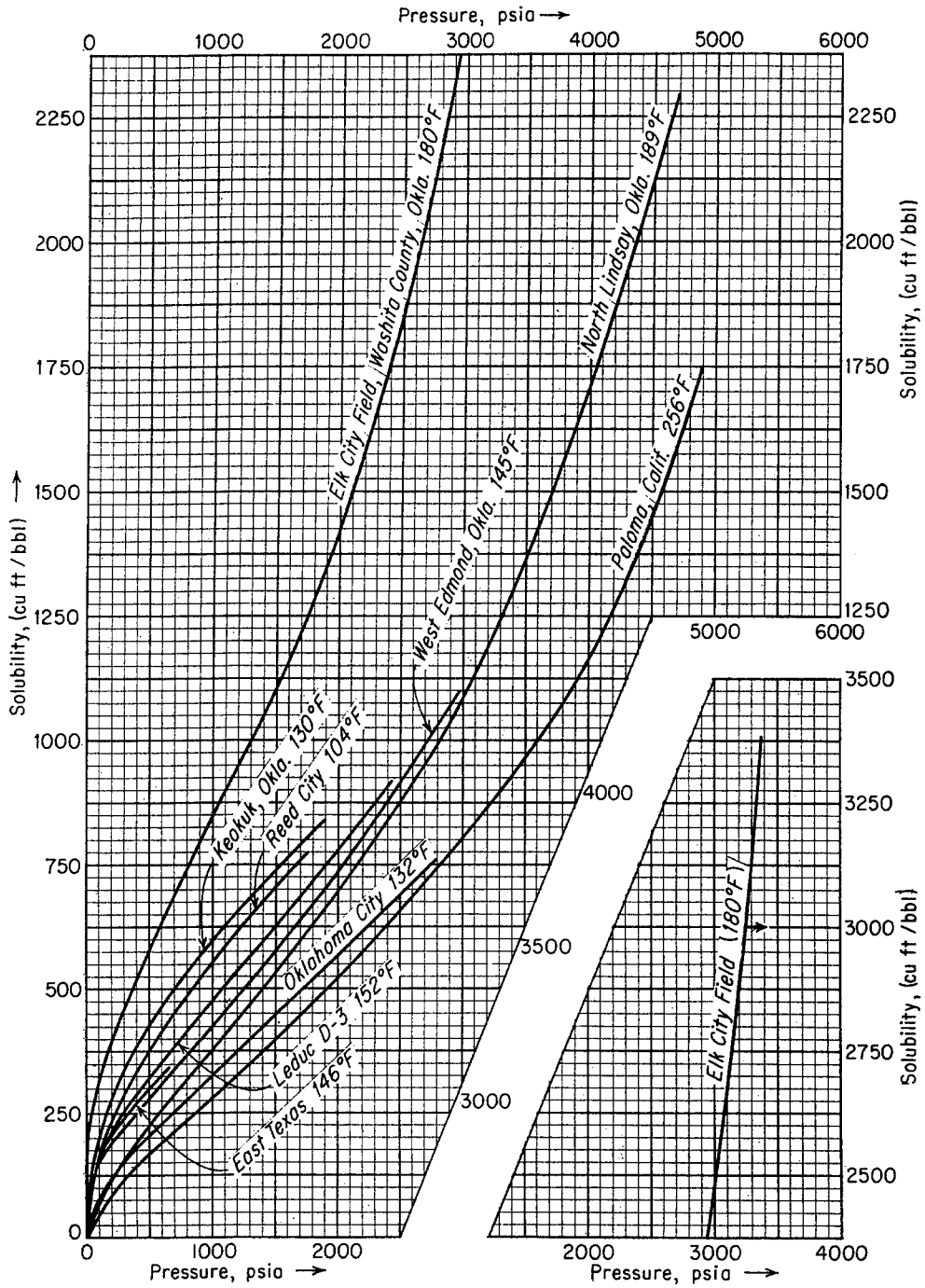

Fig. 12-6. Solubility curves for natural gas in crude oils.

Figure 12-6 gives the solubility curves for various crude oils at their reservoir temperature (12-16, 12-47, 12-42).

Shrinkage of the liquid phase takes place as the natural gas evolves from solution. Figure 12-7 gives the shrinkage that takes place corresponding to the gas evolution indicated in Fig. 12-6. The *formation volume factor* is the ratio of the reservoir volume to the volume of residual oil remaining after the pressure has been depleted to atmospheric and the oil cooled to 60°F. The formation volume factor multiplied by the quantity of stock-tank crude oil gives the volume that it occupied in the reservoir. As the pressure rises on the reservoirs and more gas is contained in solution, the crude oil liquids become more diluted with dissolved gas. Figure 12-8 illustrates this phe-

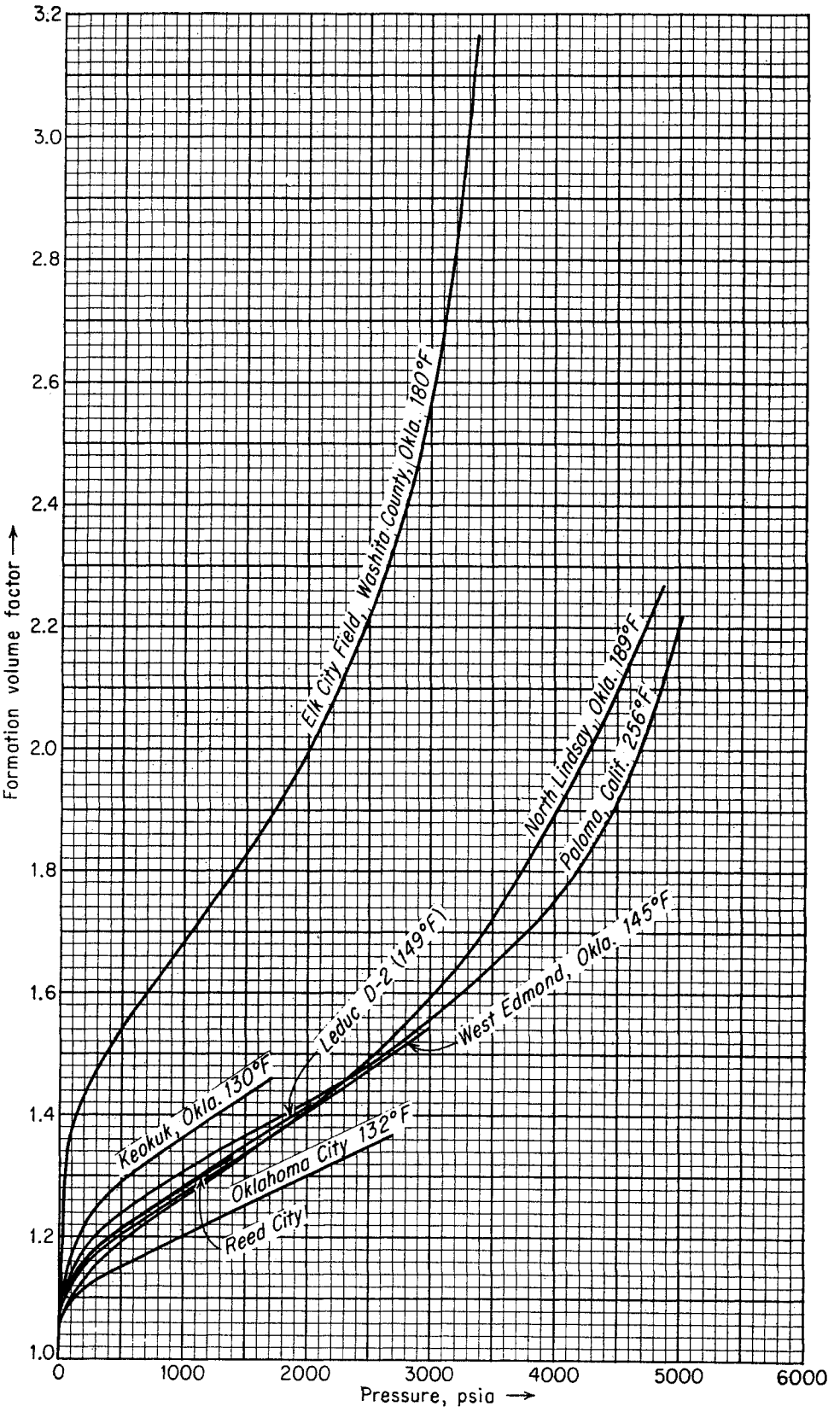

Fig. 12-7. Shrinkage of crude oils with gas evolution.

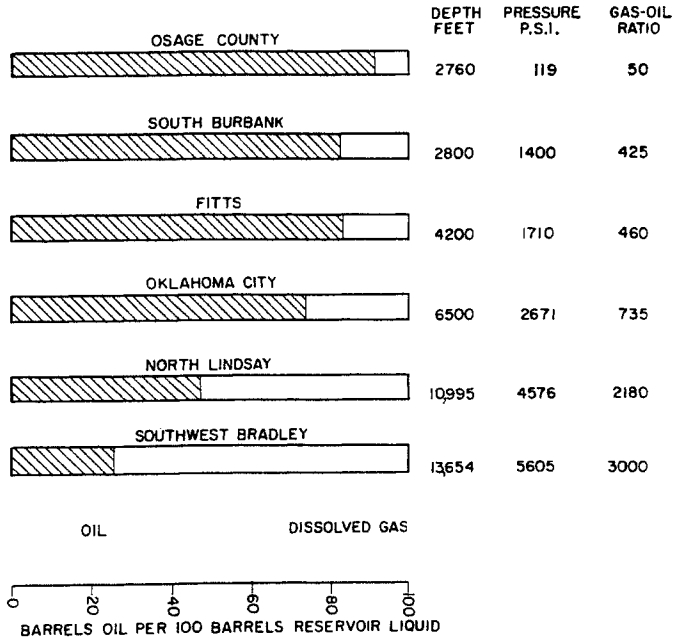

Fig. 12-8. The shrinkage of reservoir fluids.

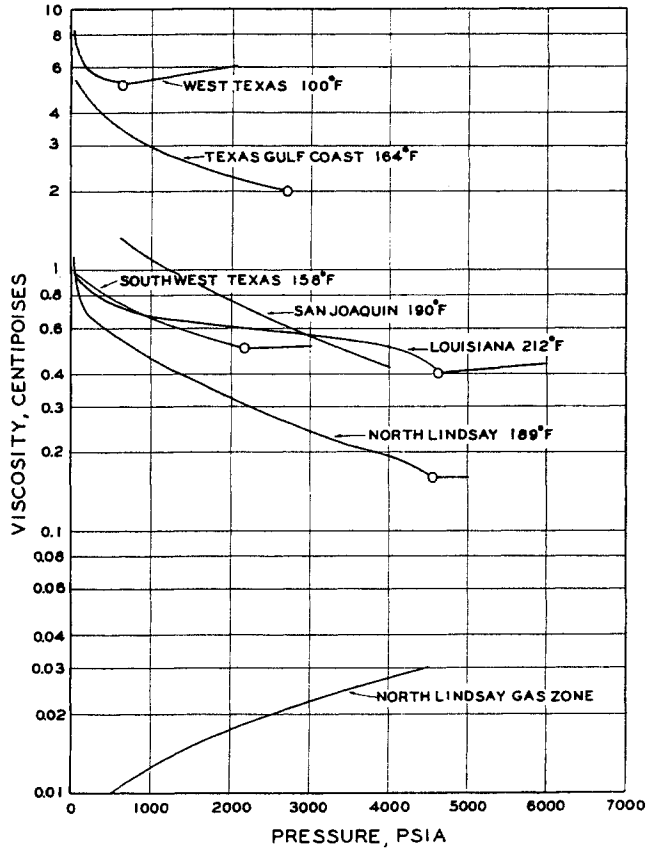

Fig. 12-9. Viscosity of crude oils with dissolved gas. (*Katz and Williams*, 1-38. *Courtesy AAPG.*)

nomenon and shows that the volatile liquid in the Southwest Bradley reservoir is 26 per cent by volume stock-tank oil and 74 per cent by volume dissolved gas. It follows that any action that causes gas to dissolve in crude oil will cause it to swell correspondingly.

The viscosity and surface tension of crude oils rise as gas is evolved and decrease with increased dissolved gas (Figs. 12-9 and 12-10). Viscosity measurement on the equilibrium liquid at various stages during gas evolution has become a routine measurement on reservoir crude oils (12-28, 12-65, 12-67, 4-112).

Prediction of Solubility and Shrinkage of Crude Oils

Since it is possible to compute the density of liquids containing dissolved gases (Chap. 6) it is possible to compute shrinkage from the composition and quantity of dissolved gas. Often the composition of the gas is not available but its gravity is known. The apparent densities of natural gases at 60°F and 1 atm are given in Fig. 12-11, based on solubility data (12-43). The effects of pressure and temperature on the liquid are given in Figs. 12-12 and 12-13. Rough approximations of shrinkage, gas solubility, and apparent density of dissolved gas are given by Figs. 12-14 to 12-16.

Illustrative Problem

A crude oil is saturated in the reservoir with natural gas at 108°F and 1,853 psia. It evolves 666 cu ft of natural gas, 1.031 gravity, per barrel of residual oil at 60°F, 32.8°API. Compute the formation volume factor for the crude oil in the reservoir.

Solution

From Fig. 12-11,

$$\text{Apparent density of dissolved gas} = 30.3 \text{ lb/cu ft}$$

$$\text{Molecular weight of air} = 29.0$$

$$= 379 \text{ cu ft/mole}$$

$$\frac{666 \text{ cu ft} \times 29.0 \times 1.031}{379 \text{ cu ft/mole}} = 52.5 \text{ lb of dissolved gas}$$

$$\frac{52.5}{30.3} = 1.73 \text{ cu ft of dissolved gas}$$

$$\begin{array}{l} 1.73 \text{ cu ft of dissolved gas} \\ \underline{5.61 \text{ cu ft of residual crude oil}} \\ 7.34 \text{ cu ft at 60° F and 1 atm} \end{array}$$

$$32.8°\text{API} = 301.5 \text{ lb/bbl}$$

$$\begin{array}{l} 301.5 \text{ lb of crude oil} \\ \underline{52.5 \text{ lb of dissolved gas}} \\ 354.0 \text{ lb total} \end{array}$$

Density at 60°F and 1 atm = 354.0/7.34 = 48.3 lb/cu ft.
By Fig. 12-12, 48.3 + 0.6 = 48.9 lb/cu ft at 60°F, 1,853 psia.

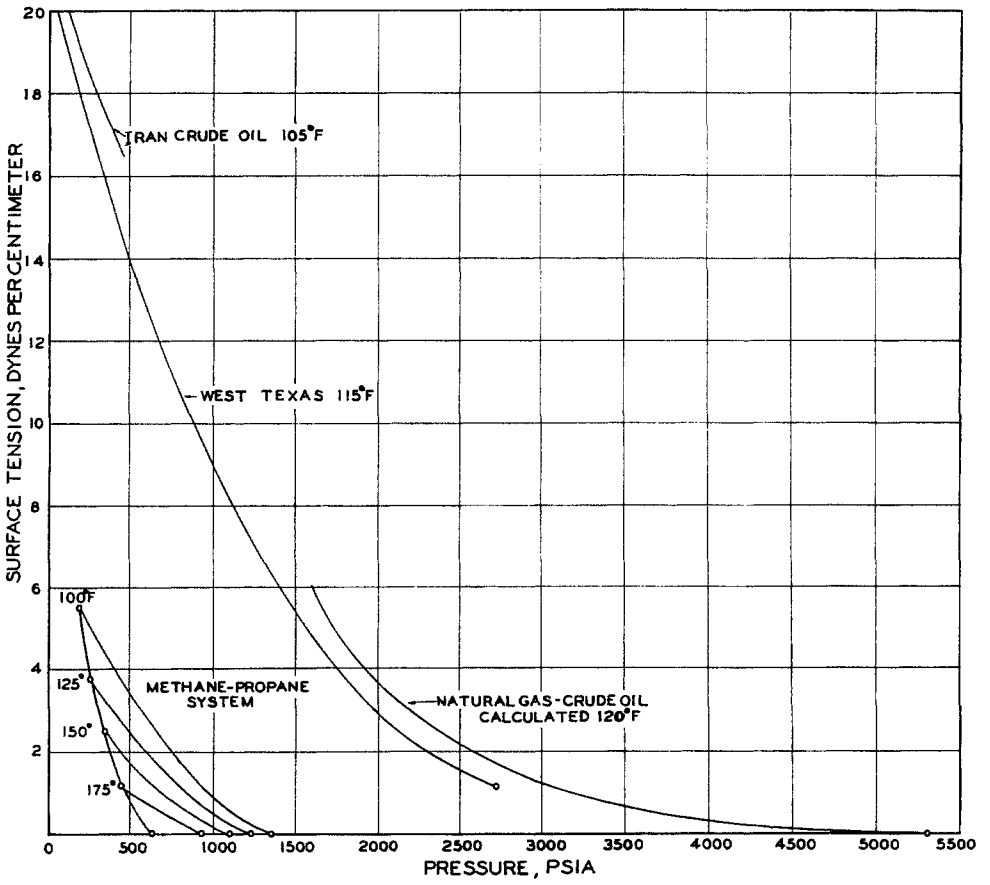

Fig. 12-10. Surface tension of crude oils with dissolved gas. (*Katz and Williams*, 1-38. *Courtesy AAPG.*)

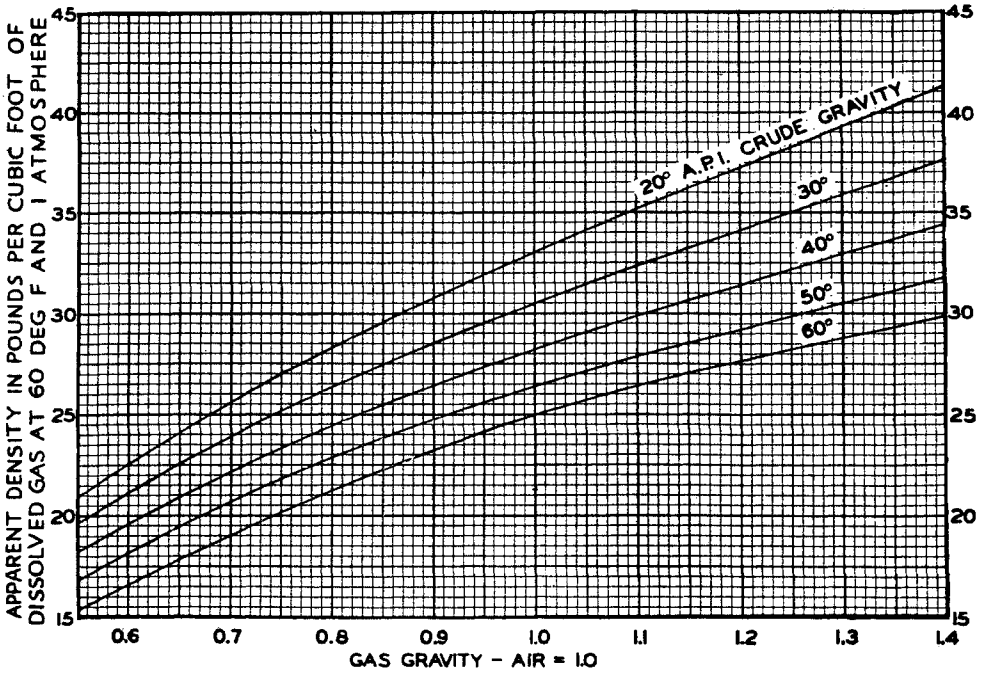

Fig. 12-11. Apparent density of natural gas dissolved in crude oil. (*Katz*, 12-43. *Courtesy API Drill. Prod. Practice.*)

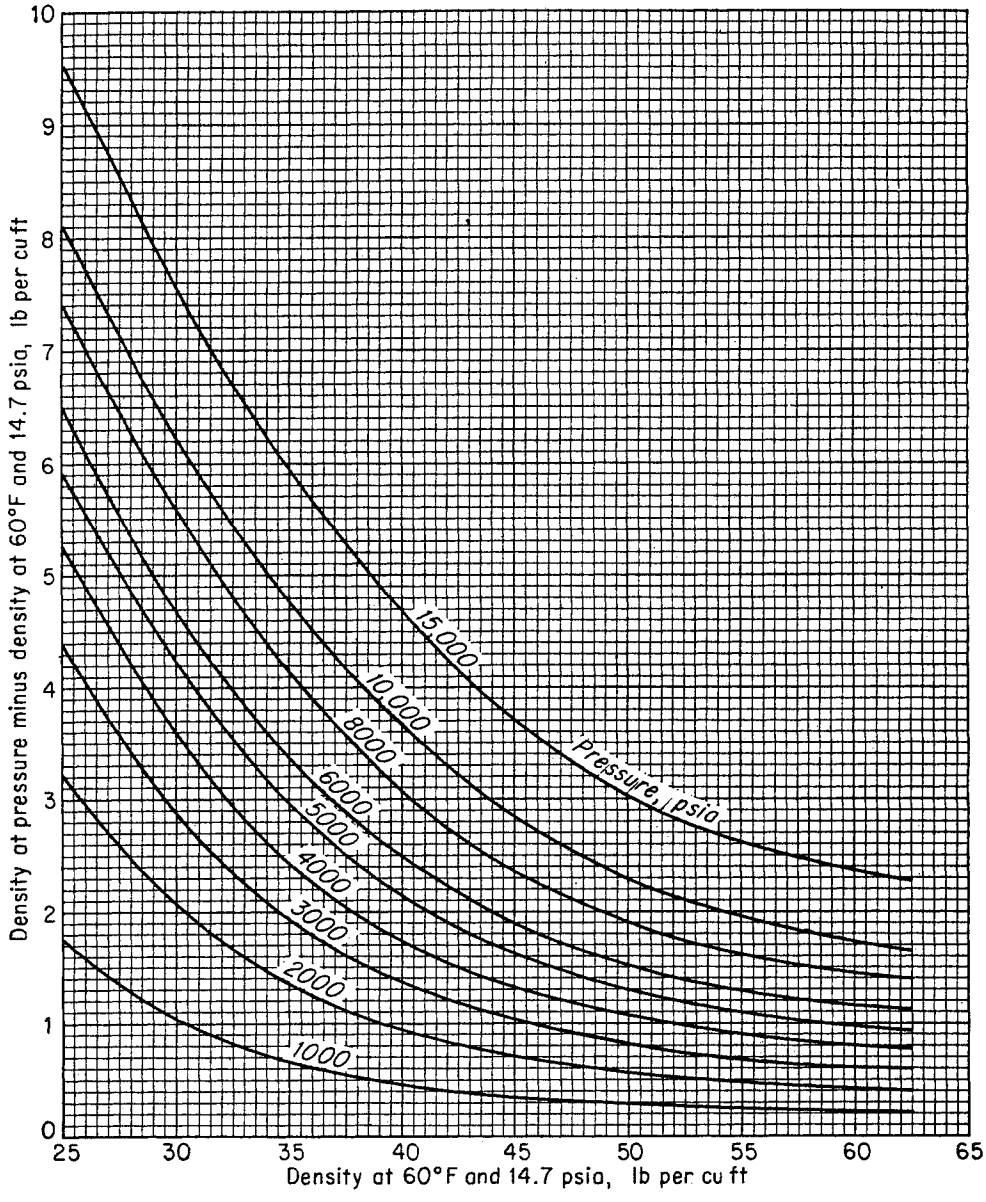

Fig. 12-12. Change of density of crude oils with pressure. (*Standing*, 1-19 *Courtesy Reinhold Publishing Corporation.*)

By Fig. 12-13, 48.9 goes to 47.7 lb/cu ft at 108°F, 1,853 psia.

$$\frac{354 \text{ lb}}{47.7} = 7.42 \text{ cu ft at } 108°\text{F, } 1{,}853 \text{ psia/bbl of residual oil}$$

5.61 cu ft crude oil in stock tank
1.81 cu ft dissolved gas

$$\text{Calculated shrinkage} = \frac{1.81}{5.61} = 32.3 \text{ per cent based on residual oil}$$

Experimental shrinkage = 34.9 per cent based on residual oil
Error = −7.4 per cent

Calculated formation volume factor = 1.323
Experimental formation volume factor = 1.349
Error = −1.9 per cent

Standing has prepared charts for relating bubble-point pressure and formation volume factor to gas-oil ratio (GOR), gas gravity, oil gravity, and temperature [Figs. 12-17 and 12-18 (12-84, 1-19)]. These charts assume that the gas-oil ratio in cubic feet per barrel of stock-tank oil represents the gas in solution at the bubble point.

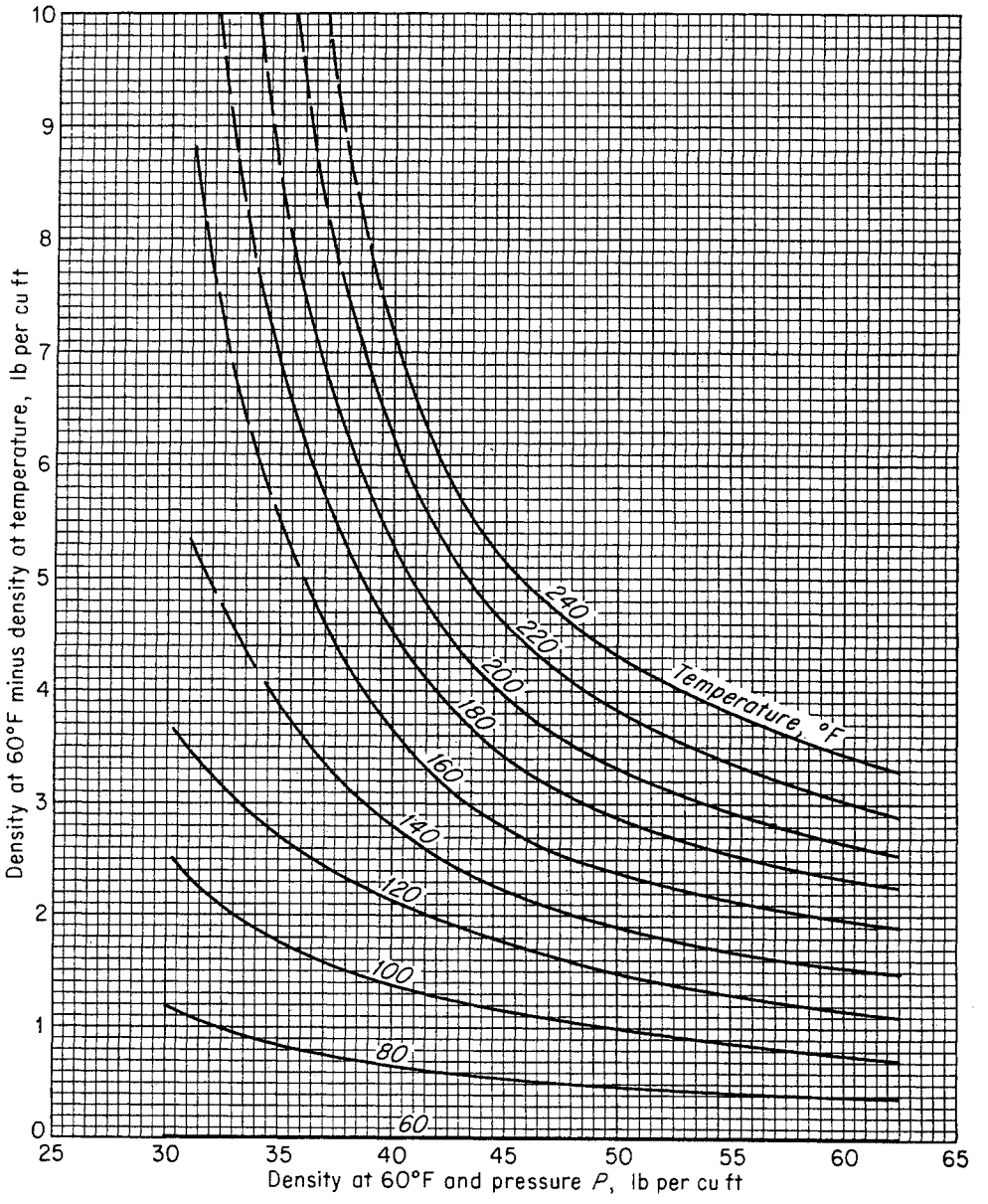

Fig. 12-13. Change of density of crude oils with temperature. (*Standing*, 1-19. *Courtesy Reinhold Publishing Corporation.*)

Borden and Rzasa (12-8) have presented correlations of bubble-point pressures, solubility, and formation volumes (Figs. 12-19 and 12-20).

Illustrative Problem (1-19)

A well produces 529 cu ft of gas per barrel of stock-tank oil. The gas is 0.726 gravity and the oil 27.4°API, 0.891 gram/cu cm. The reservoir is at 218°F. Compute the bubble point of the oil and the formation volume factor, by charts of Standing (Figs. 12-17 and 12-18).

Solution

To use Fig. 12-18, find

$$\frac{(\text{GOR})^{0.83}}{G}\,\frac{10^{0.00091T}}{10^{0.0125\text{API}}}$$

$$\left(\frac{529}{0.726}\right)^{0.83}\frac{10^{0.00091\times 218}}{10^{0.0125\times 27.4}} = 236 \times \frac{10^{0.198}}{10^{0.242}} = 213$$

From Fig. 12-18, the bubble point is 3,800 psia.
To use Fig. 12-17, find

$$\text{GOR}\left(\frac{G}{\rho_o}\right)^{0.5} + 1.25T$$

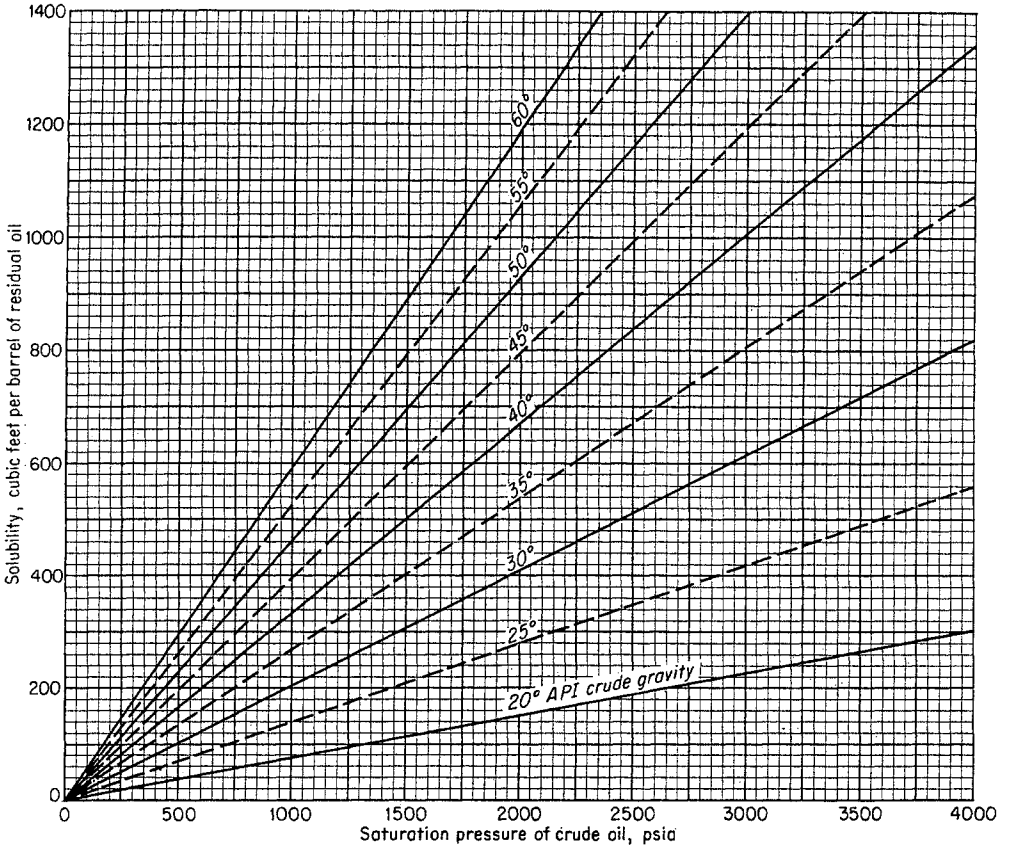

Fig. 12-14. Prediction of gas solubility from saturation pressure and residual crude oil gravity. (*Katz, 12-43. Courtesy API Drill. Prod. Practice.*)

$$529 \times \left(\frac{0.726}{0.891}\right)^{0.5} + 1.25 \times 218 = 529 \times 0.897 + 272.5 = 747$$

From Fig. 12-17, formation volume factor = 1.32.

MECHANISM OF OIL RECOVERY FROM RESERVOIRS

The following mechanisms recover oil from underground porous rock: (1) water drive, (2) dissolved gas drive, (3) gas-cap drive, and (4) gravity drainage (12-14, 12-15). Various combinations of these mechanisms occur in specific reservoirs. The energy for oil movement may be water pressure forcing oil to the well bore, the expansion of gas either from the dissolved state or as free gas, or the force of gravity causing oil to run downhill. Figure 12-21 illustrates these mechanisms, and Fig. 11-35 shows the pressure changes with production. Secondary recovery processes include water flooding (12-58, 12-101), gas injection (12-7), and combinations thereof. The initial fluid distribution in a reservoir is a basic consideration (12-61).

Water-drive Reservoirs occur in blanket sands containing water. The water in contact with the oil expands under pressure reduction and moves into the oil zone in an unsteady-state process. Since the source of the water is the expansion of the fluid in the aquifer, less fluid will be flowing toward the reservoir at greater distances. The water may enter the oil zone so readily that oil production reduces the reservoir pressure very little, as in the Kansas Arbuckle Lime reservoirs. The East Texas oil field maintains an intermediate reservoir pressure of 1,000 psi, as compared to 1,600 psi initially, by control of oil and water production and of water return (12-56). Figure 11-34*a* shows the nature of pressure change with and without water drive.

Gas production accompanying crude oil for a water-drive field will be directly proportional to the oil-production rate. Without any pressure reduction in the reservoir, no gas is evolved there and so only dissolved gas accompanies the produced crude oil. The pattern of oil production is that downstructure wells gradually go to water; eventually the oil recovery is

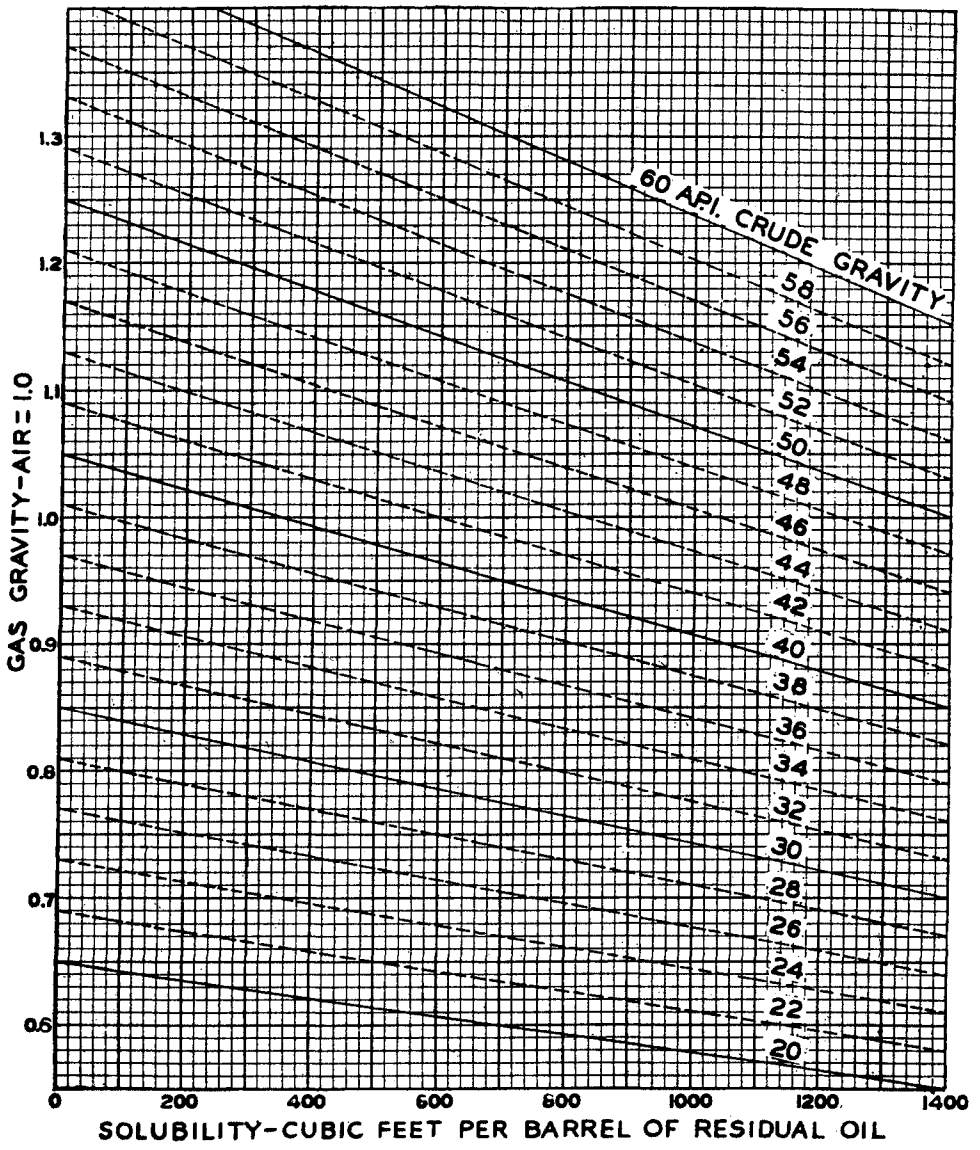

Fig. 12-15. Prediction of gas gravity from solubility and crude oil gravity. (*Katz*, 12-43. *Courtesy API Drill. Prod. Practice.*)

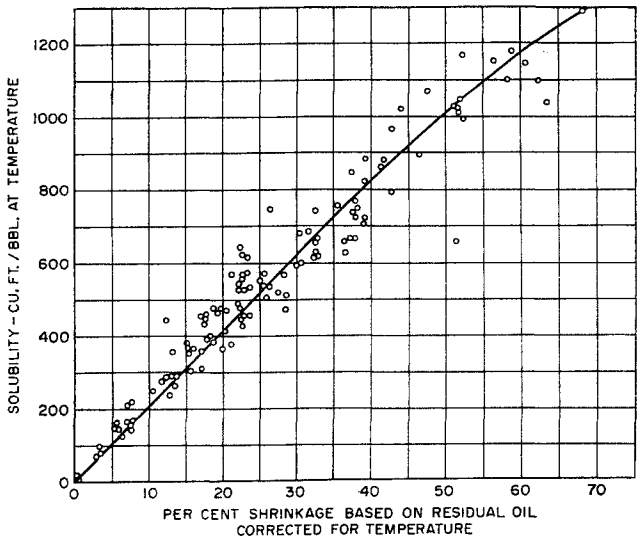

Fig. 12-16. Shrinkage vs. solubility of gas in crude oils. (*Katz*, 12-43. *Courtesy API Drill. Prod. Practice.*)

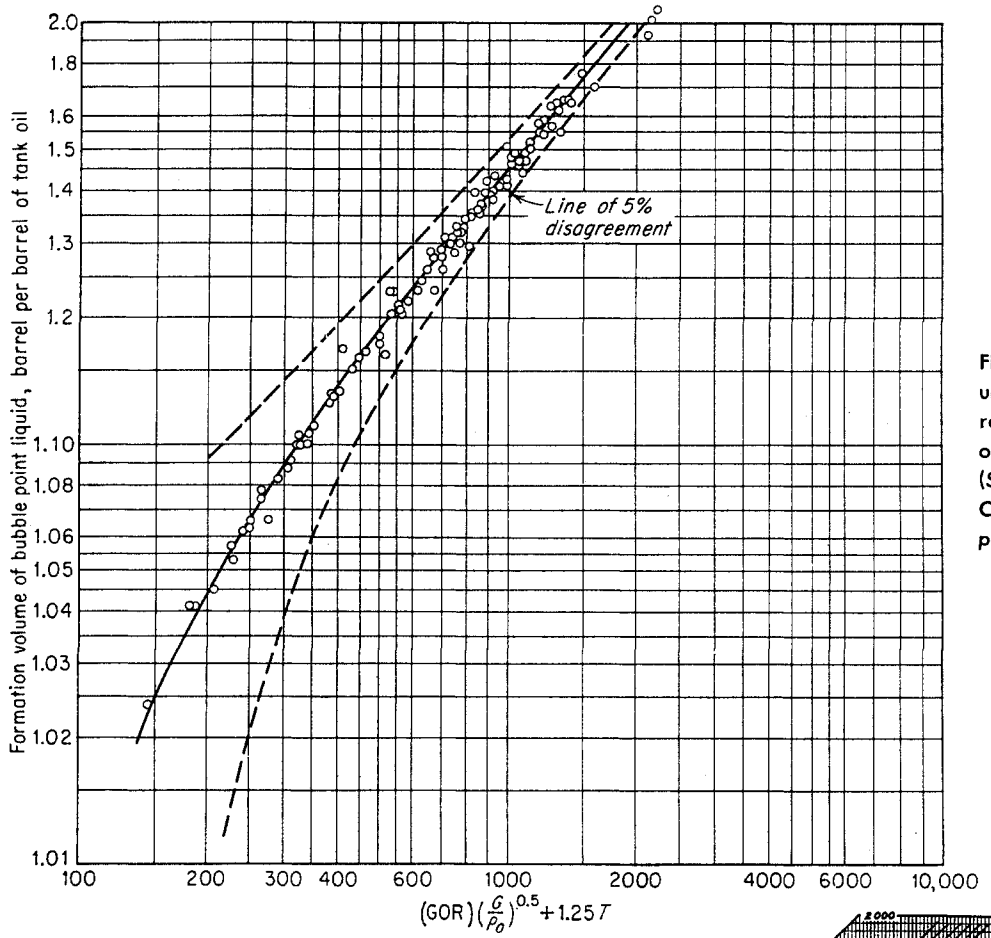

Fig. 12-17. Prediction of formation volume of bubble-point liquid from gas-oil ratio GOR, solution gas gravity G, tank oil gravity ρ_0, and temperature T. (*Standing*, 12-84. Copyright 1947, California Research Corp. Reprinted by permission.)

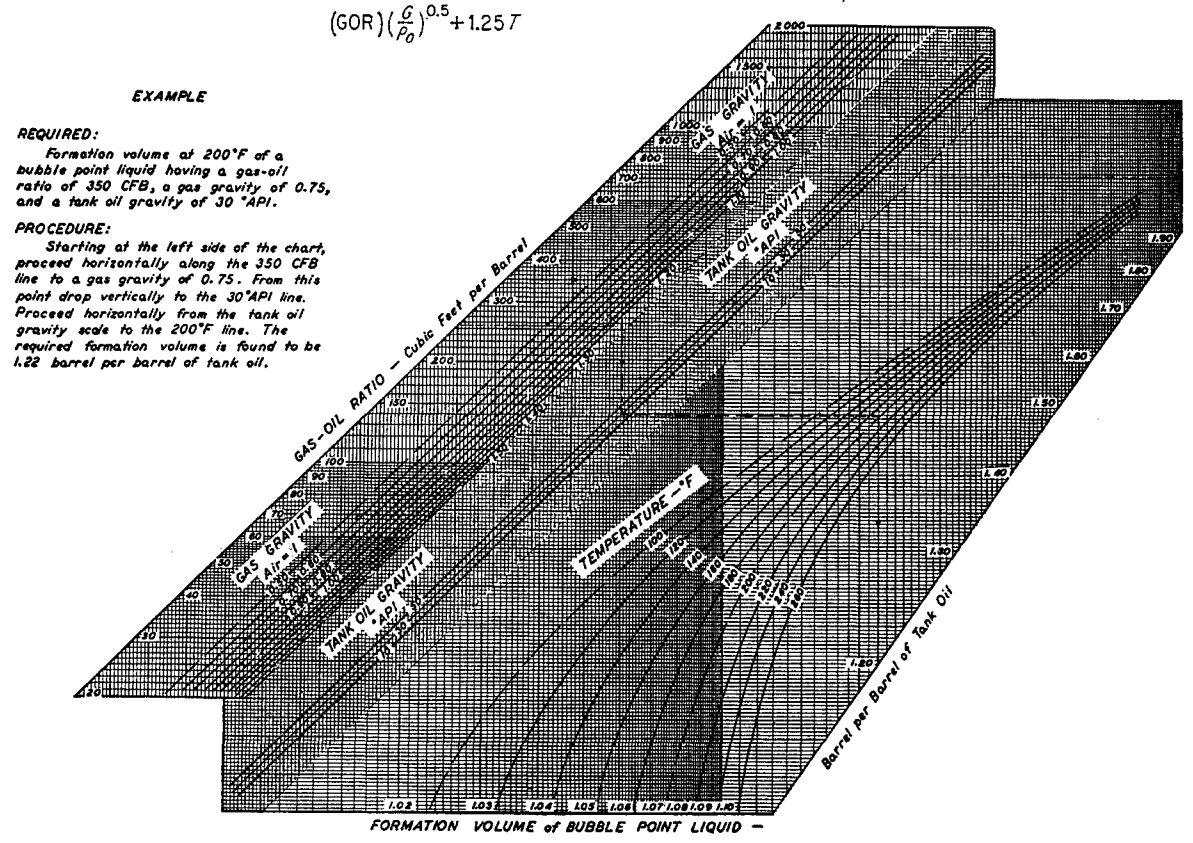

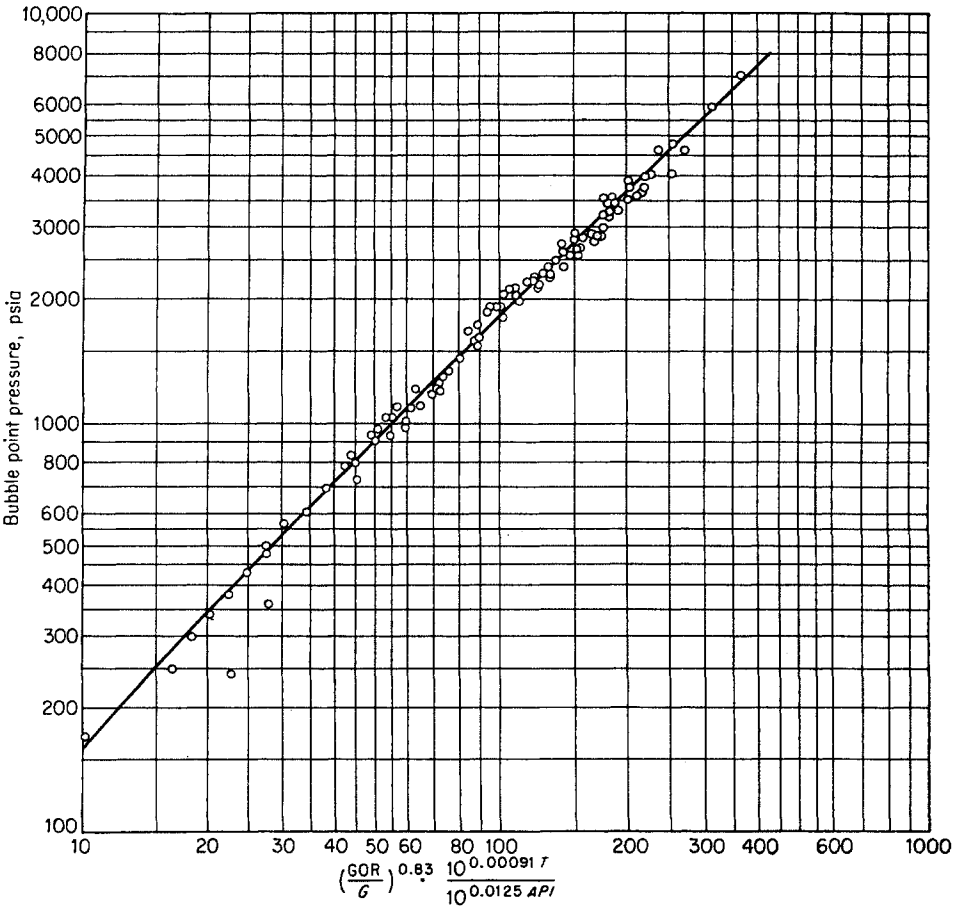

Fig. 12-18. Prediction of bubble-point pressure from gas-oil ratio GOR, solution gas gravity G, tank oil gravity API, and temperature T. (*Standing*, 12-84. *Copyright 1947, California Research Corp. Reprinted by permission.*)

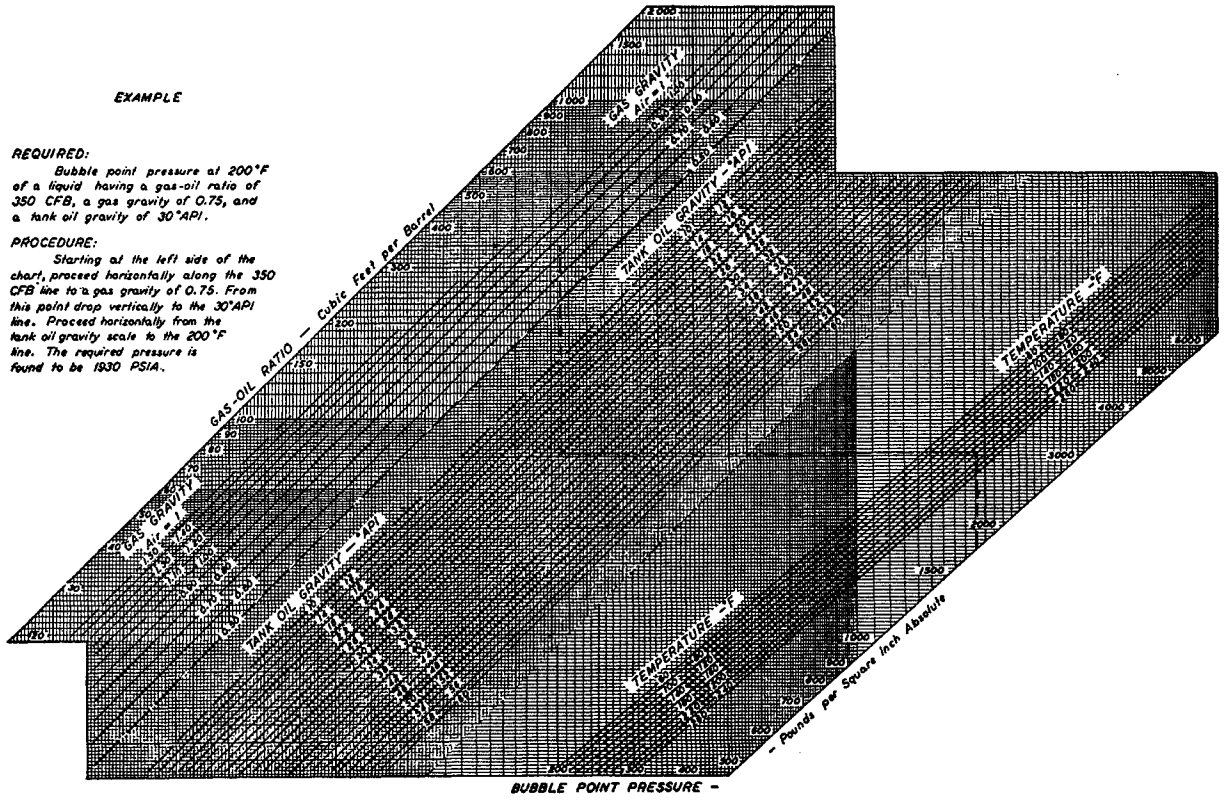

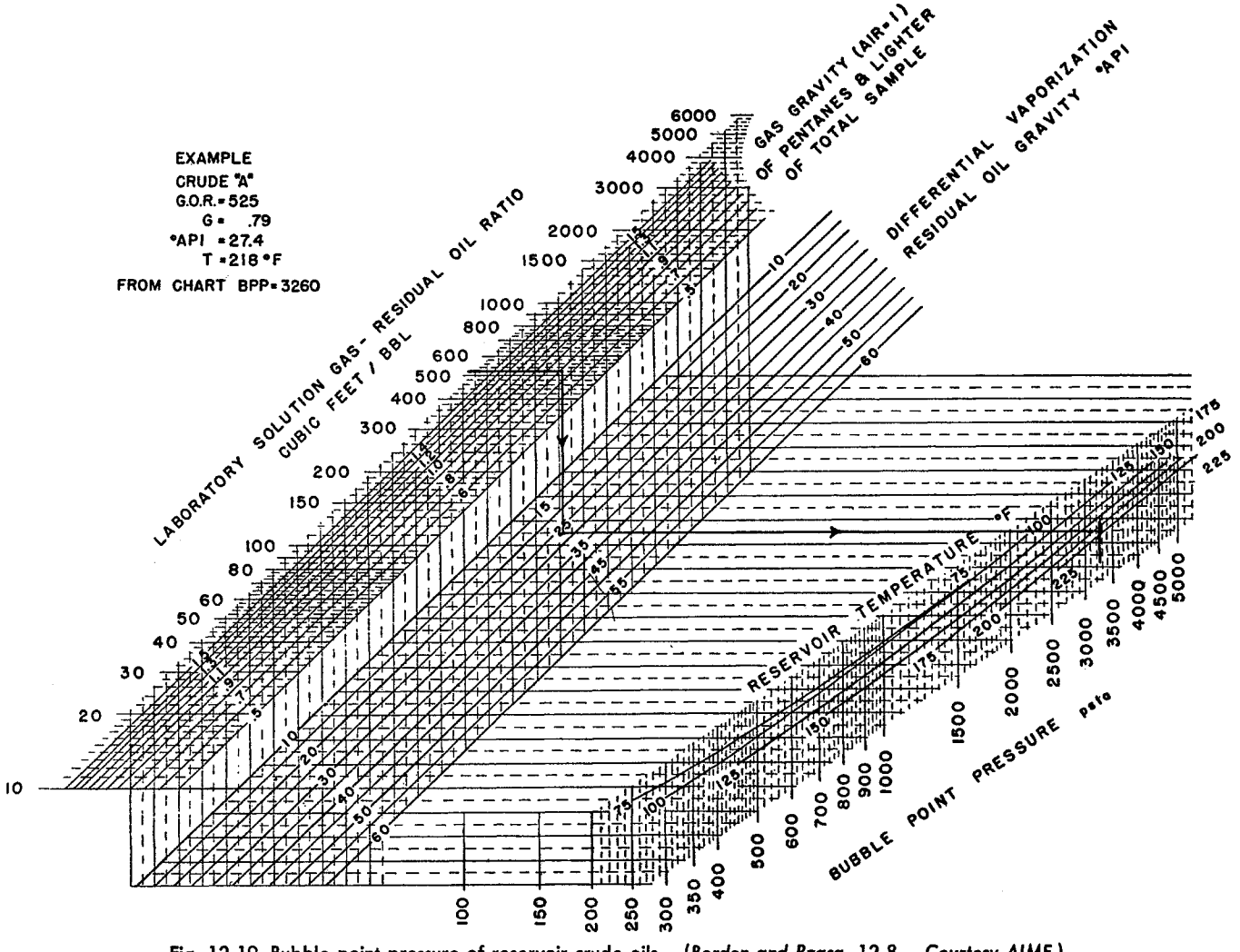

Fig. 12-19. Bubble-point pressure of reservoir crude oils. (*Borden and Rzasa*, 12-8. *Courtesy AIME.*)

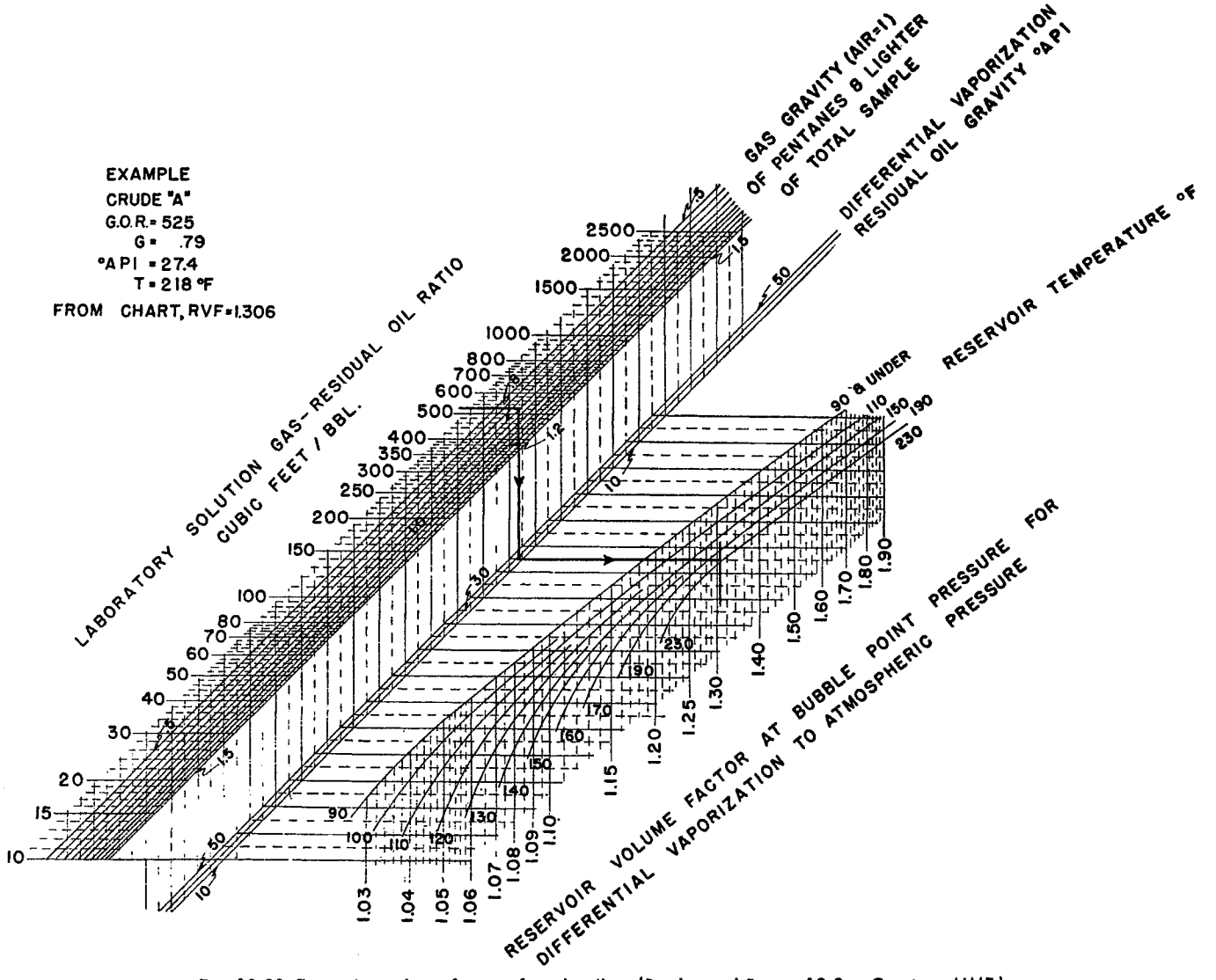

Fig. 12-20. Formation volume factor of crude oils. (*Borden and Rzasa*, 12-8. *Courtesy AIME.*)

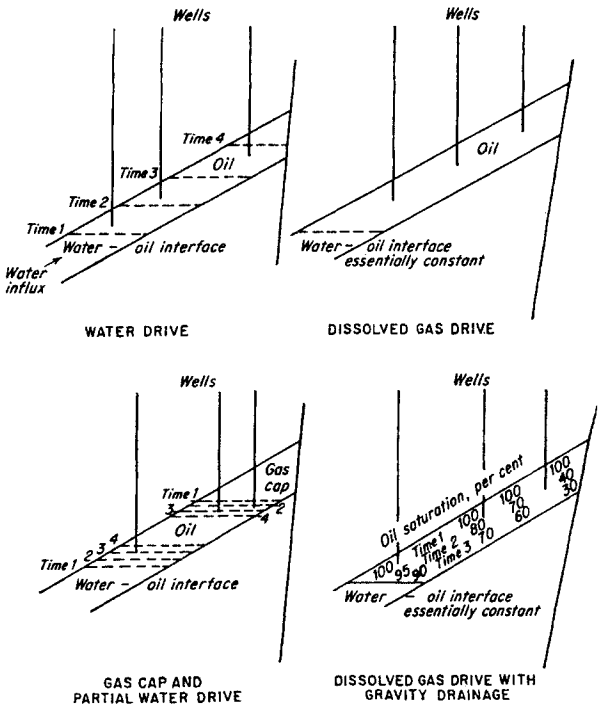

Fig. 12-21. Mechanisms of oil recovery.

so low that expenses are not met by oil production and the well is produced no longer. Criss and McCormick (12-22) have presented a case history for the Coldwater oil field, a water-drive reservoir. Figures 12-22 to 12-24 give the contour structure map and the degree to which water had entered the producing wells as of two successive dates. Production data are given in Fig. 12-25. By the end of 1952 the field had produced 12.7 million bbl of oil, and 69 out of an original 81 wells were producing at the rate of 3,600 bbl of oil and 21,000 bbl of water per day. The reservoir pressure decreased only 75 psi from its original pressure of 1,453 psi. Since the oil was saturated with gas only to 1,190 psi, no gas was evolved in the reservoir and the oil produced was always accompanied by the same amount of gas. Water was returned to wells open in horizons other than the Rogers City–Dundee zone. Often water is used to maintain the reservoir pressure by injecting it downstructure in the oil-production zone.

The Coldwater field is typical of complete water-drive fields. Gas production per barrel of oil is indi-

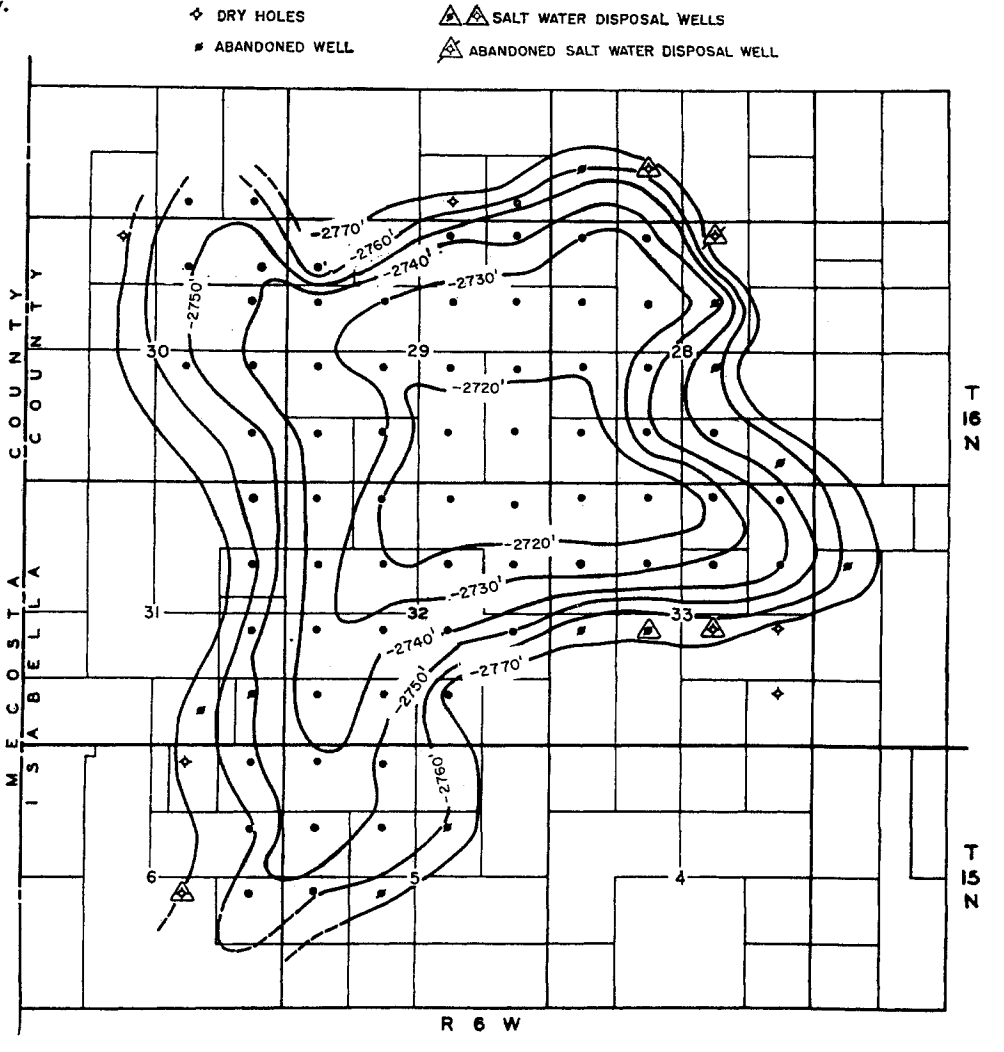

Fig. 12-22. Structural contour map of top of Rogers City dolomite, Coldwater field. (Criss and McCormick, 12-22. Courtesy AIME.)

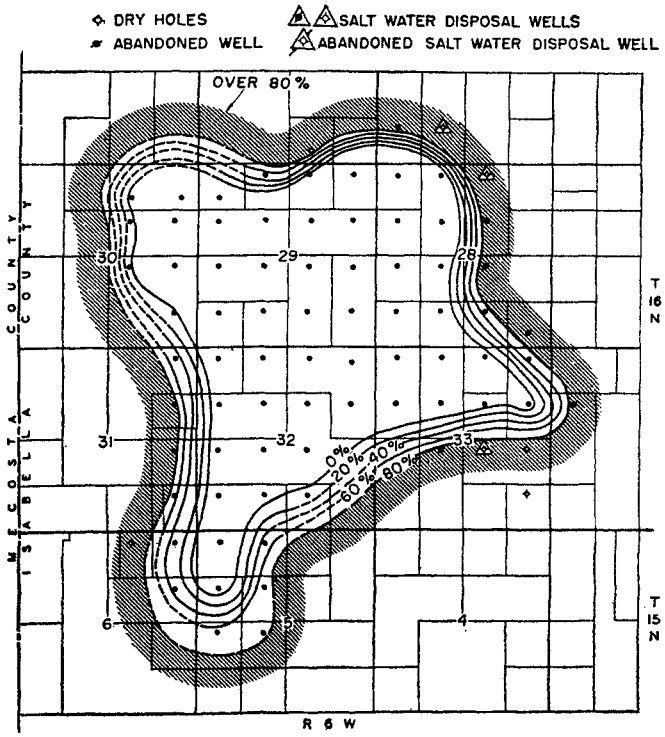

Fig. 12-23. Produced-water-percentage contours, Coldwater field, January, 1947. Contour interval: 20 per cent water. (*Criss and McCormick*, 12-22. *Courtesy AIME.*)

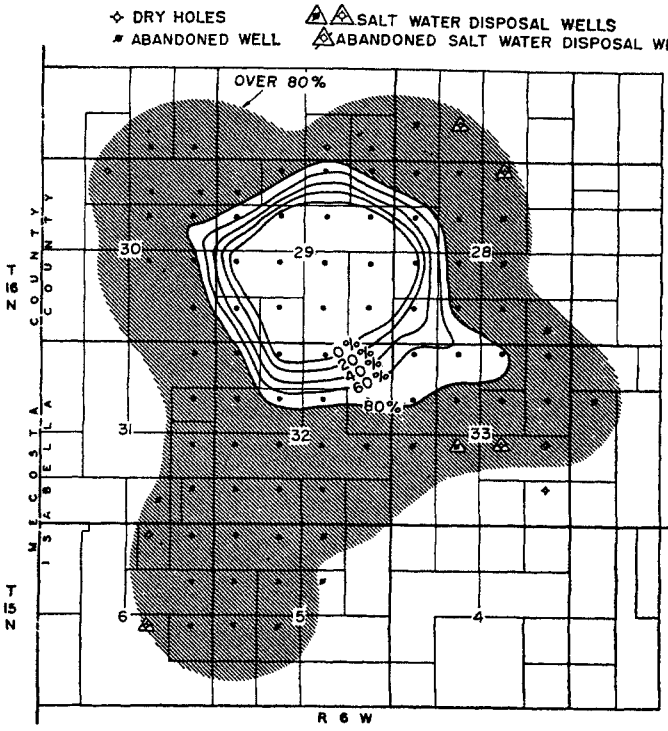

Fig. 12-24. Produced-water-percentage contours, Coldwater field, January, 1953. Contour interval: 20 per cent water. (*Criss and McCormick*, 12-22. *Courtesy AIME.*)

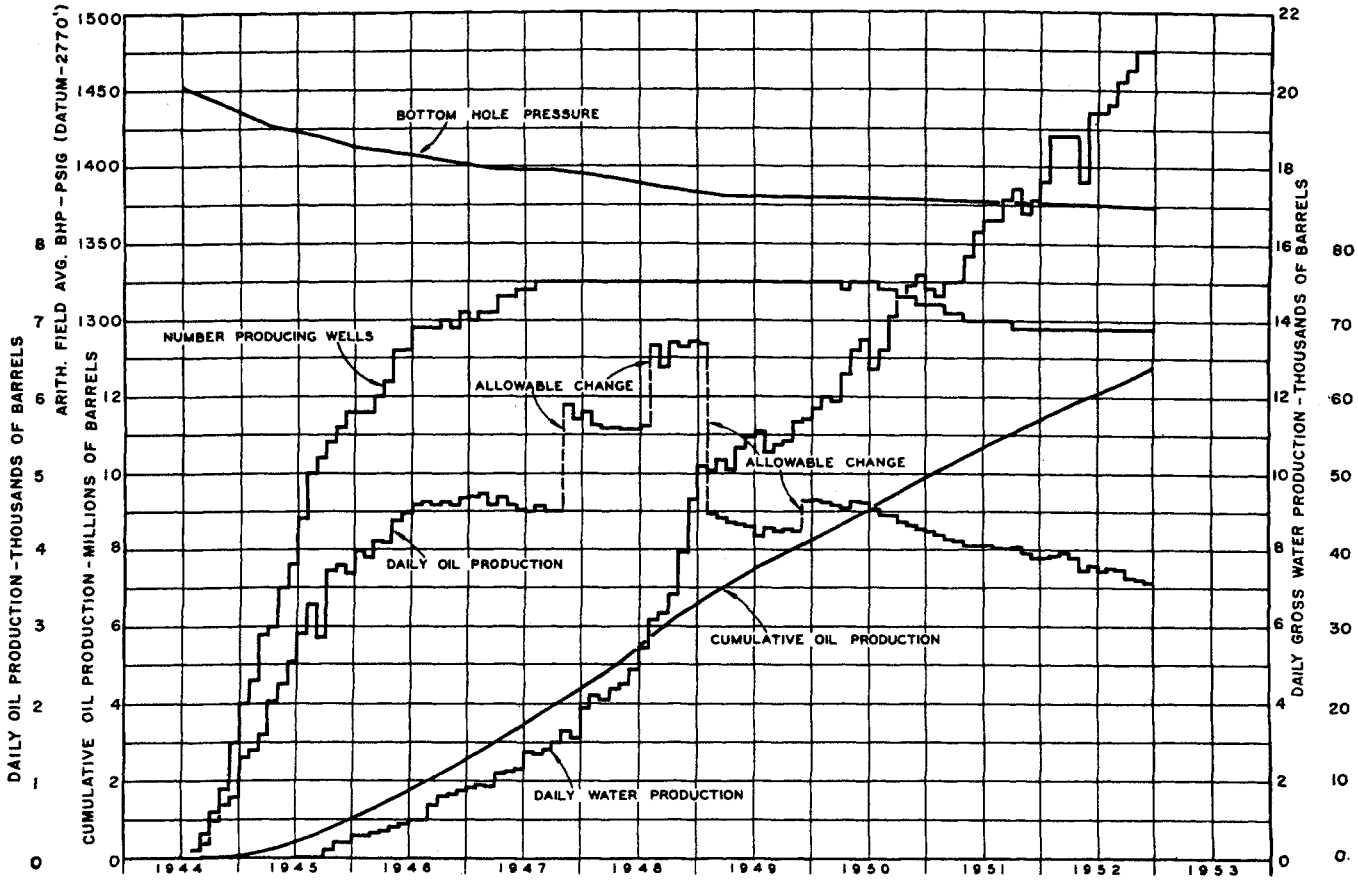

Fig. 12-25. Performance of the Rogers City–Dundee reservoir of Coldwater field. (*Criss and McCormick*, 12-22. *Courtesy AIME.*)

cated from the solubility data, 512 cu ft/bbl. To find the gas reserve, it is necessary to predict oil production. The oil in place is found from the pore volumes determined by contour maps, pay section, porosity, and connate water. Oil recoveries may be in the range of 20 to 80 per cent of the initial oil in place, and vary with type of pore space, viscosity ratio of oil to water, and nature of structure (12-20, 12-25, 12-49, 12-96, 12-98).

For reservoirs that have partial water drive, the influence of production rate on pressure decline can be predicted from calculations involving unsteady-state phenomena in the aquifer (12-6, 12-55).

The Dissolved-gas-drive Reservoir is considered to have a constant pore volume. Oil is forced to the well bore by gas evolving from solution in the crude oil as the pressure is lowered. The reservoir may or may not have an initial gas cap. The main deterrent to high oil recovery is the fact that because of the high relative permeability of rock to gas, once the liquid saturation is down to 70 or 80 per cent, gas bypasses oil on the way to the wells. Reservoirs containing oil with 700 cu ft per bbl of dissolved gas may produce oil with gas-oil ratios of 3,500 cu ft/bbl. In essence this means that four out of five barrels of oil remain in the reservoir because the gas from these four barrels helps to produce the single barrel of oil. It should be noted that all the gas dissolved in the oil is produced and that the initial oil content is of interest when finding gas reserves, not the oil production.

Gravity segregation of oil takes place in varying degrees in gas-drive reservoirs and must be considered. Likewise, some water may encroach on the reservoir and reduce its volume.

Methods of estimating the original oil and gas content of a constant-volume reservoir have been devised, using solubility and shrinkage data. Coleman, Wilde, and Moore (12-13) published a paper in 1930 on the "quantitative effect of gas-oil ratio on decline in average rock pressure." In 1936, papers by Schilthuis (12-79) and Katz (12-40) gave alternative procedures for estimating the oil content of a gas-drive reservoir. Schilthuis presented the calculations in equation form, now described as the *material-balance equation*. Katz gave a tabulative procedure intended to give an understanding of the reservoir production mechanism. The material-balance equation has proved advantageous for the utilization of mathematical calculations on reservoirs.

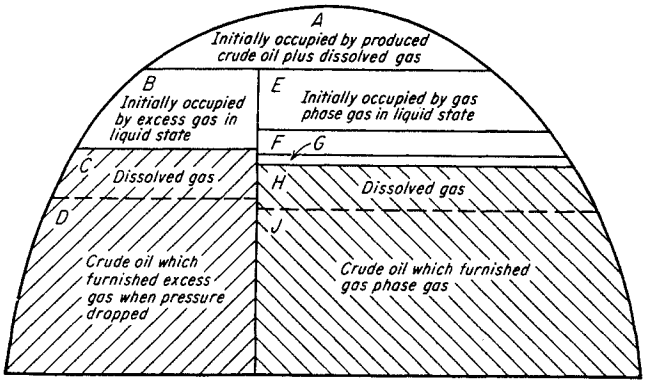

Fig. 12-26. Graphical allocation of initial reservoir fluid. (Katz, 12-40. Courtesy AIME.)

The Material-balance Procedure presented by Katz (12-40, 2-40) states that the initial crude oil is equal to the oil produced as of a given date, plus the oil which supplied the gas produced in excess of that initially dissolved in the produced crude oil, plus the oil which supplied the gas-phase gas to maintain the reservoir pressure. The data required are (1) initial or saturation pressure for reservoir crude oil; (2) reservoir temperature; (3) oil production; (4) gas production; (5) reservoir pressure at end of oil and gas production; (6) solubility and shrinkage data; (7) gas-oil ratio of saturated crude oil at separator conditions; (8) information on any gas cap; and (9) water production from or water influx into the reservoir.

Figure 12-26 illustrates the allocation of initial space in a reservoir containing saturated crude oil, without water production or influx.

The production process removes oil and gas from the reservoir. The space occupied by the crude oil plus its dissolved gas (space A) can be computed from the oil production and the formation volume factor or shrinkage. Gas that was produced in excess of that dissolved in the crude oil came from oil still in the reservoir. With the reservoir pressure known as of a given date in the producing life, the solubility curve gives the cubic feet of gas per barrel that have been evolved by each barrel in the reservoir. The excess gas and the rate of shrinkage per unit of evolved gas permit computation of the space voided (space B) when this gas vaporized from the crude oil. The quantity of crude oil (D and C) that is required to supply this gas is known from the quantity of excess gas and the gas evolved per barrel of oil during the pressure drop in the reservoir.

These spaces A and B are filled with gas phase by vaporization of crude oil still in the reservoir. Space E is voided when crude oil is vaporized to fill gas phase A and B; space F is voided when space E is filled with gas from solution in the crude oil. Space G is voided when F is filled, etc. To find the gas-cap space without using a trial-and-error procedure, a solution to a converging series is employed. Spaces H and J con-

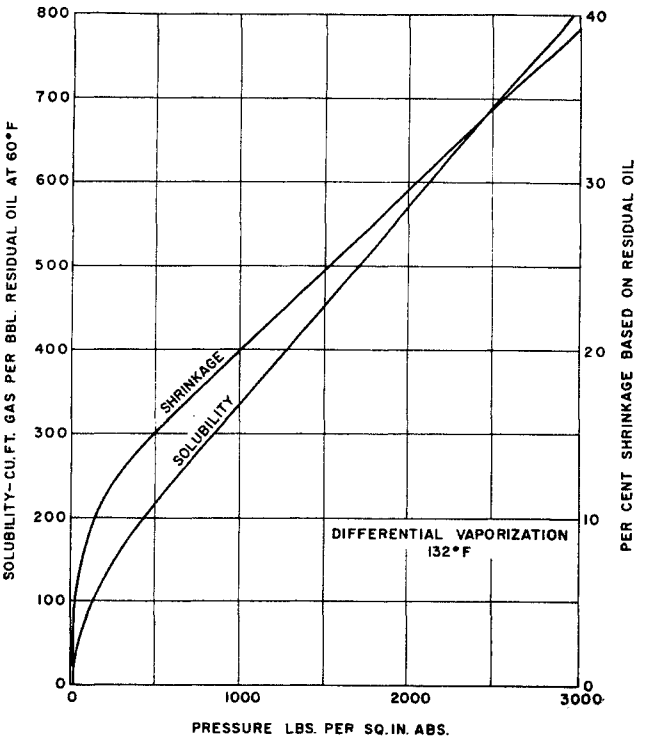

Fig. 12-27. Solubility and shrinkage curves for Oklahoma City crude oil. (*Katz, 2-40. Courtesy AIME.*)

tain the crude oil and dissolved gas that furnished the gas to fill the gas phase. The total initial crude oil as stock-tank barrels equals the produced crude oil, the oil D that provided the excess gas, and the oil that provided the gas-phase gas J.

An example of a material-balance tabulation is given by Table 12-1 (2-40). The reservoir was calculated to have an initial gas cap with 10.3 MMMcf (60°F, 14.65 psia) of gas in it. The gas produced from the cap during a given pressure reduction is removed from the total production of gas to find the gas produced from the oil reservoir. The solubility and shrinkage data were taken from curves of Fig. 12-27. Table 12-1 gives the computations at seven annual intervals of the initial oil and gas content, assuming the reservoir volume a constant. Items 1 to 7 are given or are obvious. Item 8 is the product of crude oil production and 735 cu ft/bbl as solution

Table 12-1. Computation of Initial Oil Content of Wilcox Pool, Oklahoma City
Calculations made from reservoir conditions at dates indicated

Item	Unit	1/1/33	1/1/34	1/1/35	1/1/36	1/1/37	1/1/38	1/1/39
1. Crude oil produced	MMbbl	69.8	119	166	212	255	301	333
2. Gas produced	MMMcf	177	378	550	630	701	751	780
3. Bottom-hole pressure	Psia	1,640	895	430	203	111	58	34.8
4. Gas dissolved in crude at bottom-hole pressure	Cu ft/bbl	487	308	198	132	94	57.5	32
5. Gas evolved initial condition to bottom-hole pressure	Cu ft/bbl	248	427	537	603	641	677.5	703
6. Shrinkage crude from bottom-hole pressure to atmospheric	Per cent	26.0	18.9	14.2	11.3	9.4	7.7	6.2
7. Shrinkage crude from initial pressure to bottom-hole pressure	Per cent	10.1	17.2	21.9	24.8	26.7	28.4	29.9
8. Solution gas for produced crude	MMMcf	51.3	87.5	122	156	188	222	245
9. Compressibility factor reservoir gas	Ratio	0.82	0.885	0.926	0.955	0.97	0.985	0.99
10. Gas from initial gas cap	MMMcf	4.0	7.1	8.8	9.6	9.9	10.1	10.2
11. Excess gas produced	MMMcf	121.7	283.4	419.2	464.4	503.1	518.9	524.8
12. Volume 1 std cu ft gas at reservoir conditions	Cu ft	0.0083	0.0165	0.0359	0.0785	0.146	0.283	0.475
13. Volume produced oil and dissolved gas	MMcf	533	910	1,270	1,620	1,950	2,300	2,540
14. Initial volume excess gas in liquid state	Cu ft/std cu ft	0.00228	0.00226	0.00229	0.00231	0.00234	0.00235	0.00238
15. Initial volume excess gas	MMcf	277	640	961	1,072	1,178	1,219	1,249
16. Reservoir volume total production oil and gas	MMcf	810	1,550	2,231	2,692	3,128	3,519	3,789
17. $a = 16/12$	MMMcf	97.6	94.0	62.1	34.3	21.4	12.4	8.0
18. $1/b = 14/12$	Ratio	0.275	0.137	0.064	0.029	0.016	0.008	0.005
19. $a/(1 - 1/b)$ = gas-cap gas	MMMcf	135	109	66	35.4	21.7	12.5	8.0
20. Crude for gas-cap gas	MMbbl	544	255	123	59	34	18	11
21. Crude for excess gas	MMbbl	490	664	781	770	785	766	747
22. Total initial crude	MMbbl	1,104	1,038	1,070	1,041	1,074	1,085	1,091
23. Total initial fluid	MMbbl	1,503	1,411	1,457	1,419	1,462	1,478	1,487

Solubility at 2,686 psia. 735 cu ft/bbl residual oil. Shrinkage: 36.1 per cent. Reservoir temperature: 132°F. Average initial residual oil: 1,072 MMbbl. Reservoir fluid: 1,460 MMbbl.

SOURCE: (2-40).

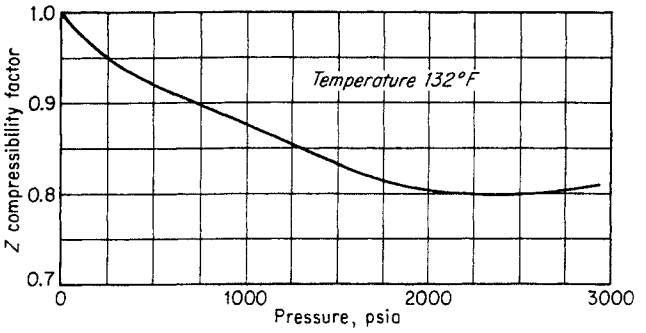

Fig. 12-28. Compressibility factors for Oklahoma City reservoir gas. (Katz, 2-40. Courtesy AIME.)

gas either by differential vaporization at 132°F or by flash vaporization in separators. Item 9 is taken from Fig. 12-28, which gives compressibility factors calculated from gas compositions occurring at the reservoir pressures. Item 10 is the initial gas-cap gas that left the reservoir as the pressure dropped to the pressure of item 3. Item 11 equals item 2 minus the sum of items 8 and 10. Item 13 equals item 1 times 5.61 and times 1.361. Item 14 equals item 7 divided by item 5 and multiplied by 5.61. Item 15 is item 11 times item 14. Item 16 equals items 13 plus 15. The computation of the quantity of gas in the gas phase or in the developed gas cap where the evolution of gas creates more space is found by using the expression for a converging series, item 19. Items *a* and *b* in the expression for the gas-cap gas (*A*, *B*, *E*, *F*, *G*, etc., Fig. 12-26) are given by items 17 and 18. Item 20 is item 19 divided by item 5. Item 21 is item 11 divided by item 5. The calculated average quantity of initial residual crude oil is 1,072 million bbl.

The initial gas reserve is 1,072 million bbl × 735 cu ft/bbl or 789 MMMcf + 10 MMMcf in the initial gas-cap, or 799 std MMMcf. By 1939, the Oklahoma City Wilcox reservoir had produced 780 MMMcf of gas and the pressure was approaching atmospheric. By January 1, 1957, it had produced 563 million bbl of crude oil, or 52.4 per cent of its initial content, and was still producing at the rate of 6,500 bbl/day.

The production of water or the intrusion of water into the reservoir can be used to account for changes in the gas-phase volume in the above procedure.

The Material-balance Equation may be derived on the basis of a gas balance as follows (12-73, 12-79, 12-92, 1-3, 1-14) using the nomenclature of Table 12-2.

Original gas = produced gas + gas in solution + gas-phase gas

$$NS_0 = R\,\Delta N + (N - \Delta N)S + \frac{[NB_0 - (N - \Delta N)B]5.61}{v} \quad (12\text{-}1)$$

Table 12-2. Nomenclature for Material-balance Equation

N	Initial oil content of reservoir, stock-tank barrels
ΔN	Accumulative oil production at given time, stock-tank barrels
g	Original gas content of reservoir in gas phase, std cu ft
R	Gas-oil ratio, std cu ft/bbl
R_s	Gas-oil ratio for saturated crude oil, std cu ft/bbl
S_0	Solubility of gas at initial pressure and reservoir temperature, std cu ft/bbl
S	Solubility of gas at any pressure, std cu ft/bbl
v	The formation volume of 1 std cu ft of gas, cu ft/std cu ft; subscript 0 for initial conditions
B	Formation volume factor for crude oil, bbl liquid in reservoir per bbl stock-tank oil; subscript 0 for initial conditions
m	Ratio of initial gas-cap pore volume to initial oil-phase pore volume
w	Accumulative water production, cu ft
W	Accumulative water influx into reservoir, cu ft

Multiplying through by v and regrouping terms,

$$N[B + v(S_0 - S) - B_0] = \Delta N[B + v(R - S)] \quad (12\text{-}2)$$

$$N = \Delta N \frac{5.61B + v(R - S)}{5.61B + v(S_0 - S) - 5.61B_0} \quad (12\text{-}3)$$

This equation applies for constant-volume reservoirs without water intrusion or water production, and without an initial gas cap. When these two items are included in a consideration of the material balance for natural gas, Eq. (12-4) results.

$$NS_0 + g = R\,\Delta N + (N - \Delta N)S + \frac{5.61NB_0 - 5.61(N - \Delta N)B + gv_0 + w - W}{v} \quad (12\text{-}4)$$

Rearranging as before,

$$N = \frac{\Delta N[5.61B + v(R - S)] - g(v - v_0) + w - W}{5.61B + v(S_0 - S) - 5.61B_0} \quad (12\text{-}5)$$

An alternative equation may be used, appropriate when the initial gas-cap volume is known relative to the oil volume.

$$m = \frac{\text{gas cap volume}}{\text{oil volume}}$$

$$N = \frac{\Delta N[B + v(R - S)] + w - W}{B + v(S_0 - S) - B_0 + mB_0(v - v_0)/v_0} \quad (12\text{-}6)$$

Table 12-3 gives the solution to Eq. (12-3) for the data of Table 12-1 and the dates 1/1/33 and 1/1/37. The answers found are equal to those of Table 12-1. The numerical manipulations appear to be equivalent. Pirson (12-73) has shown that the material-balance procedure of Table 12-1 is equivalent to solving Eq. (12-3) as in Table 12-3. The procedure of Table 12-1 gives some sense of the physical phenomena occurring in the reservoir and may be preferred in teaching for

Table 12-3. Solution to Material-balance Equation

Item	Symbol	Unit	Data as of Jan. 1, 1933	Data as of Jan. 1, 1937	Initial condition
1. Crude oil produced	ΔN	MMbbl	69.8	255	
2. Gas produced	$R\Delta N$	Std MMMcf	177	701	
3. Gas-oil ratio	R	Std cu ft/bbl	2,540	2,750	735
4. Reservoir pressure	P	Psia	1,640	111	2,686
5. Formation volume factor	B	.....	1.26	1.094	1.361
6. Solubility of gas	S	Std cu ft/bbl	487	94	735
7. Compressibility factor of reservoir gas	Z	.....	0.82	0.97	0.802
8. Reservoir volume of 1 std cu ft of gas in gas phase	v	Cu ft/std cu ft	0.0083	0.146	0.00498
9. Gas in initial gas cap	g	Std MMMcf	.....	.....	10.3
10. $R - S$	....	Std cu ft/bbl	2,053	2,656	
11. $v(R - S)$	....	Cu ft/bbl	17.02	387.5	
12. $5.61B + v(R - S)$	....	Cu ft/bbl	24.10	393.6	
13. $\Delta N[5.61B + v(R - S)]$	....	MMcf	1,682	100,300	
14. $v - v_0$	....	Cu ft/std cu ft	0.00332	0.141	
15. $g(v - v_0)$	....	MMcf	34.2	1,450	
16. Item 13 − item 15	....	MMcf	1,648	98,850	
17. $S_0 - S$	....	Std cu ft/bbl	248	641	
18. $v(S_0 - S)$	....	Cu ft/bbl	2.06	93.6	
19. $5.61B + v(S_0 - S) - 5.61B_0$	....	Cu ft/bbl	1.49	92.1	
20. Item 16 ÷ item 19	N	MMbbl	1,105	1,071	
21. Initial gas content	....	Std MMMcf	864	789	

acquainting students with the concepts of reservoir behavior. The equation has the advantage that it can be combined with other equations for reservoir calculations. The material balance on the gas gives a simpler equation than would result if the material balance on crude oil used in Table 12-1 were reformulated in equation form.

Both of these procedures assume that crude oil and gas are distinct substances although the method of separation may cause greater or lesser quantities of gas to be evolved. The proportion of gas evolved from saturated crude oil by differential vaporization at the reservoir temperature may not be equal to the gas-oil ratio in a flash separation at the wellhead. Therefore, the solubility S_0 may not equal the gas-oil ratio R_0, and different values may be used in the procedures given.

The initial reservoir pressure may be well above the saturation pressure of the crude oil. In this case, the time zero is the condition at which the saturation pressure is reached. Estimates of oil in place may be made from fluid compressibilities in the period of production before the saturation pressure is reached (12-31, 12-33).

Normally reservoir crude oils are rather uniform, but examples of variation in reservoir oils have been noted when the reservoir was extensive or had high relief.

Woods and Muskat (12-99) present an analysis of material-balance calculations when water is entering the reservoir in a partial-maintenance process in unsteady state. The water influx may be evaluated from unsteady-state formulas in conjunction with the material-balance equation to give the most reliable estimate of the initial oil in place.

A Typical Production History for a gas-drive field produced by pressure depletion is a gradual rise in the gas-oil ratio for a period, followed by a rapid rise when the gas phase in the reservoir has reached sufficient saturation to give the gas a high relative permeability. By using a relative-permeability curve and material-balance calculations, the future production history can be projected. Simple calculations in small increments of production will show how the gas-oil ratio rises as the percentage of gas phase in the reservoir increases. Such calculations neglect any effects of gravity on the segregation of oil and gas.

Smith and Henderson report the behavior of a solution gas-drive field (12-82). Figures 12-29 and 12-30 give the pressure, gas-oil ratio, and production history. About 20 per cent of the 26 million bbl of stock-tank oil had been produced when most of the wells in the field became marginal producers, 47 bbl/day from 18 wells, and the field was unitized to water flood. An oil recovery of 26.5 per cent was predicted using the assumed K_g/K_o curve of Fig. 12-31, which was based on the performance of Cromwell sand. The field-performance curve of Fig. 12-31 is in accord with the findings of Owens, Parrish, and Lamoreaux (12-70).

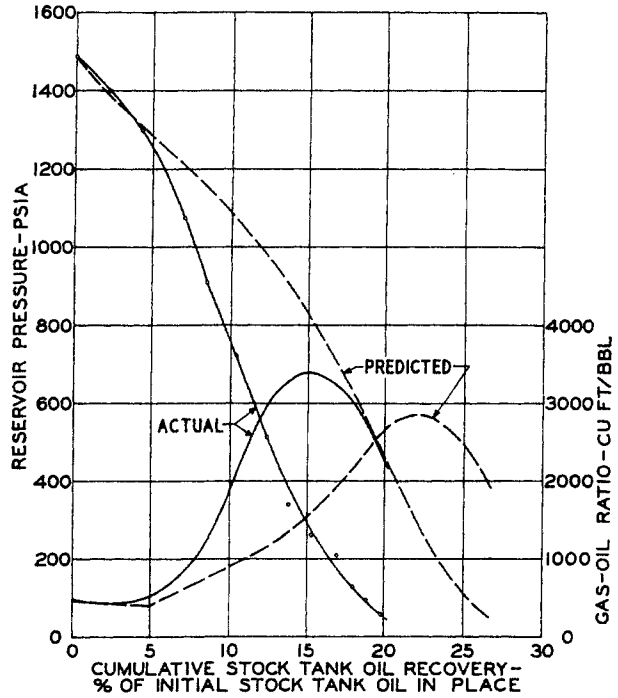

Fig. 12-29. Pressure and gas-oil-ratio history of Rosenwald pool. (*Smith and Henderson*, 12-82. *Courtesy AIME.*)

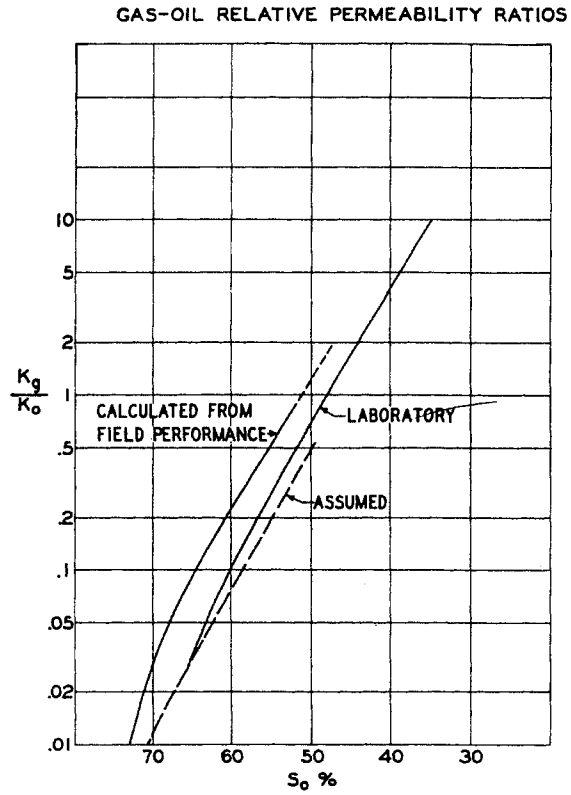

Fig. 12-31. Relative permeability ratio for gas and oil, Rosenwald pool. (*Smith and Henderson*, 12-82. *Courtesy AIME.*)

Muskat and Taylor (12-59) presented generalized solutions for the depletion of gas-drive reservoirs, giving gas-oil ratio and pressure histories for selected conditions. Figures 12-32 and 12-33 give the predicted histories of solution gas-drive fields with 30 per cent connate water, showing the influence of oil viscosity and gas solubility. The reversal in the gas-oil ratio curve is due to the lack of gas in the reservoir as atmospheric pressure is approached. Figure 12-34 gives the decrease in productivity of wells for oil production corresponding to the cases in Fig. 12-33, and shows that low oil recoveries are obtained by this process. Figure 12-35 gives pressure histories for reservoirs having initial gas caps.

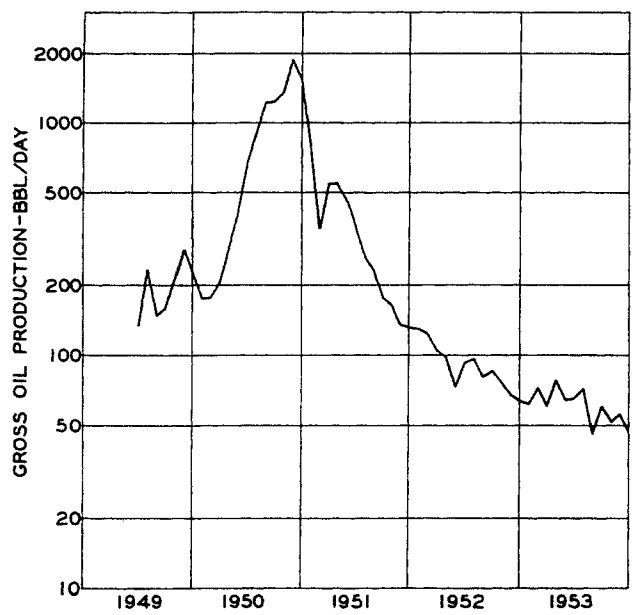

Fig. 12-30. Oil production, Rosenwald pool. (*Smith and Henderson*, 12-82. *Courtesy AIME.*)

Brinkman and Weinaug have presented a method of calculating the performance of a dissolved-gas-drive reservoir using the differential-vaporization procedures of Chap. 6, relative permeabilities, and fluid properties (12-9).

Other studies have been made on the use of the material-balance equation and flow from gas-drive reservoirs (12-10, 12-17, 12-57, 12-64, 12-92). Although the presence of increasing amounts of dissolved gas would appear to be very beneficial in bringing oil to the well bore, the shrinkage that occurs as the gas evolves is very detrimental since the gas phase created permits the gas to bypass oil as gas and oil flow together toward the well. For high-formation volume factors such as 2 or more, a single well on the crest of a structure could relieve almost all the gas

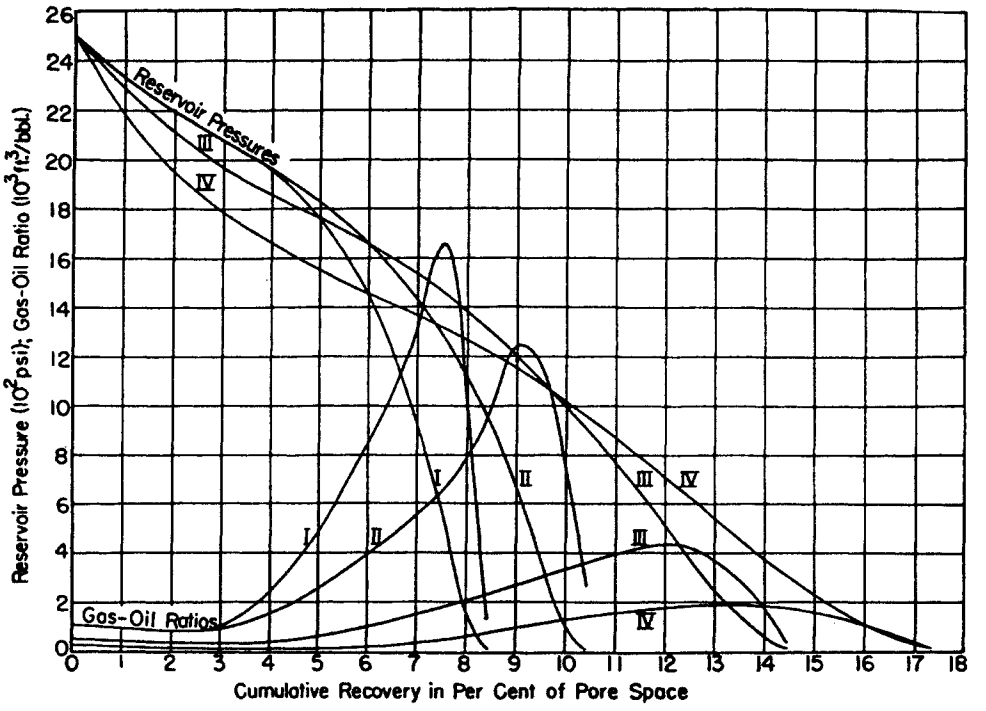

Fig. 12-32. Pressure and gas-oil-ratio histories of solution gas-drive reservoirs producing oil of different gas solubilities and viscosities. Curve I: gas solubility at 2,500 psia = 1,068 cu ft/bbl; viscosity at 1 atm = 2.76 centipoises; shrinkage from 2,500 psia = 61.6 per cent. Curve II: same as curve I except that viscosity at 1 atm = 1.38 centipoises. Curve III: gas solubility at 2,500 psia = 534 cu ft/bbl; viscosity at 1 atm = 1.38 centipoises; shrinkage from 2,500 psia = 30.8 per cent. Curve IV: gas solubility at 2,500 psia = 267 cu ft/bbl; viscosity at 1 atm = 1.38 centipoises; shrinkage from 2,500 psia = 15.4 per cent. (*Muskat and Taylor*, 12-59. *Courtesy AIME.*)

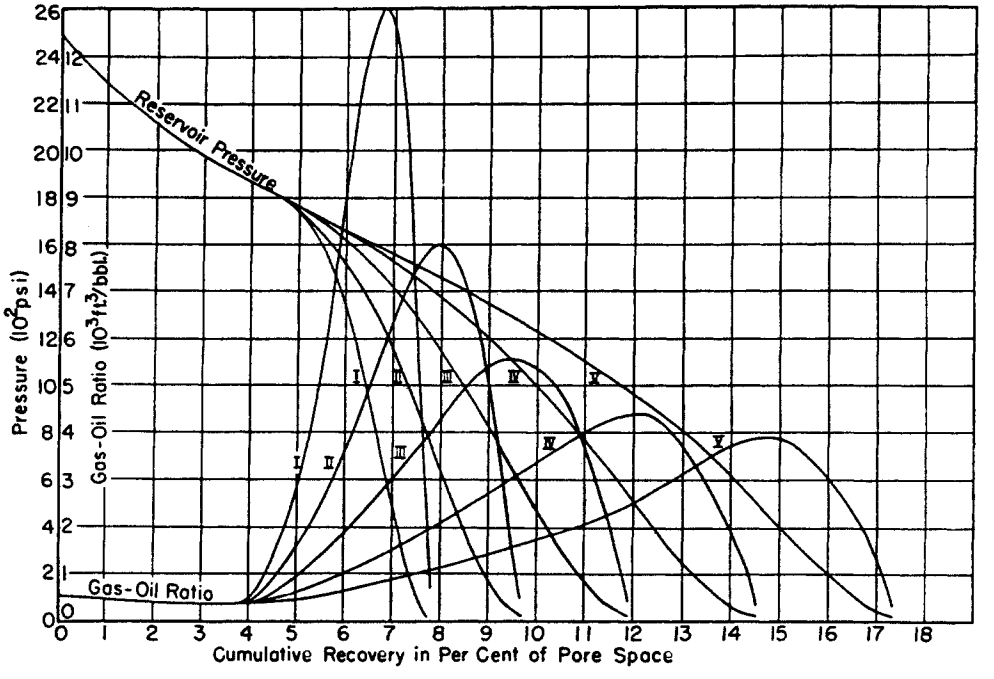

Fig. 12-33. Pressure and gas-oil-ratio histories of solution gas-drive reservoirs producing oil of different viscosities. Curve I: viscosity at 1 atm = 11.04 centipoises. Curve II: viscosity at 1 atm = 5.52 centipoises. Curve III: viscosity at 1 atm = 2.76 centipoises. Curve IV: viscosity at 1 atm = 1.38 centipoises. Curve V: viscosity at 1 atm = 0.69 centipoise. Gas solubility at 2,500 psia = 534 cu ft/bbl in all cases. (*Muskat and Taylor*, 12-59. *Courtesy AIME.*)

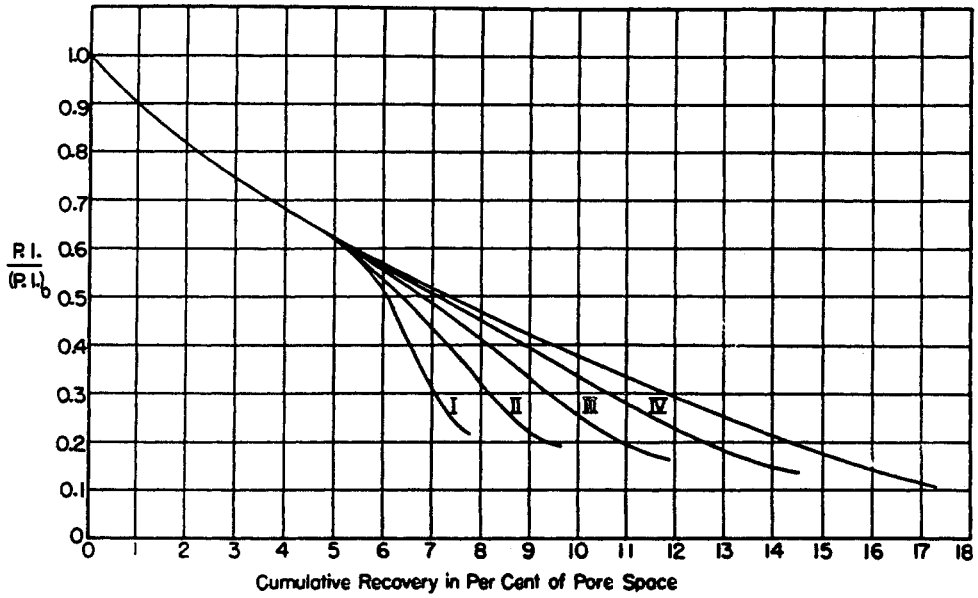

Fig. 12-34. Histories of productivity-index variations in gas-drive fields producing oil with different gas solubilities. $PI/(PI)_0$ = ratio of current-productivity index to initial-productivity index. Curve I: solubility at 2,500 psia = 1,068 cu ft/bbl; shrinkage = 61.6 per cent; viscosity at 1 atm = 2.76 centipoises. Curve II: same as curve I except that viscosity at 1 atm = 1.38 centipoises. Curve III: solubility at 2,500 psia = 534 cu ft/bbl; shrinkage = 30.8 per cent; viscosity at 1 atm = 1.38 centipoises. Curve IV: solubility at 2,500 psia = 267 cu ft/bbl; shrinkage = 15.4 per cent; viscosity at 1 atm = 1.38 centipoises. (*Muskat and Taylor*, 12-59. *Courtesy AIME.*)

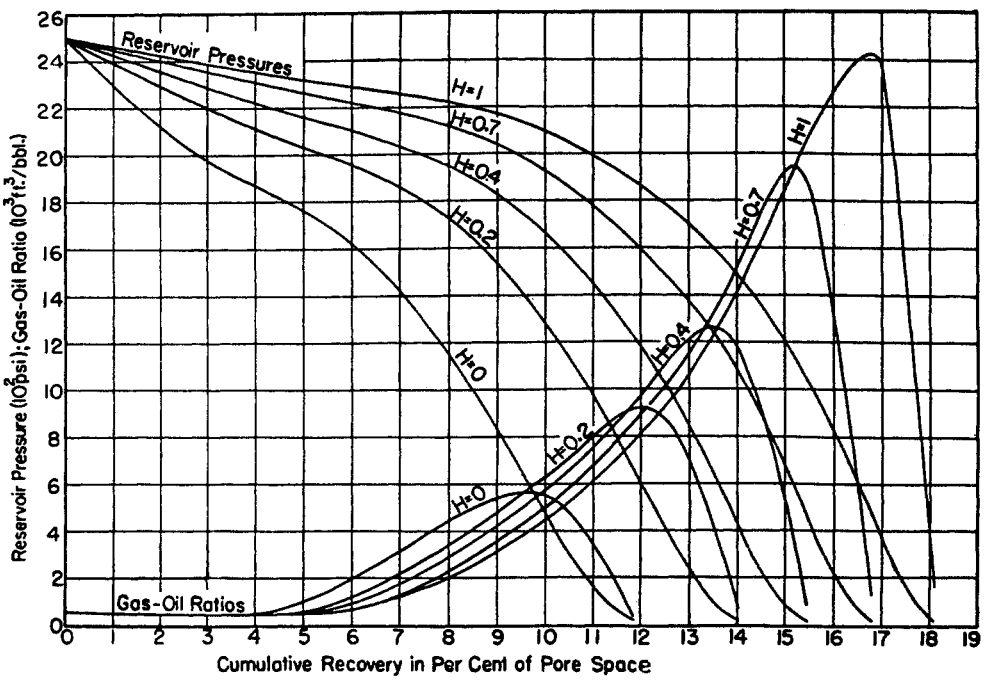

Fig. 12-35. Reservoir pressure and gas-oil-ratio histories of gas-drive reservoirs with various thicknesses of gas cap. H = ratio of thickness of gas cap to thickness of oil zone; gas solubility at 2,500 psia = 534 cu ft/bbl; shrinkage from 2,500 psia = 30.8 per cent; viscosity at 1 atm = 2.76 centipoises. (*Muskat and Taylor*, 12-59. *Courtesy AIME.*)

with little oil recovery, since little oil moves in a porous solid when its saturation has reached 50 per cent.

Conservation practices and the demands of economics have led to better procedures for producing gas-drive reservoirs without allowing them to "blow down" in the fashion described. Gas repressuring, selective production of oil from wells of low gas-oil rates, and water injection are some of the methods used for increasing recovery.

Gravity Drainage

The segregation of oil and gas systems into an oil layer and a gas cap is evidence that gravity had an important role in the accumulation process. That wells on the top of a structure in oil fields have high gas-oil ratios and that downstructure wells have lower ratios is an indication of the effects of gravity in producing operations. High permeability, high relief, low oil viscosity, and low surface tension of crude oils are factors that contribute to the movement of oil by gravity. In thin, flat formations with horizontal layers of impervious material, no gravity effects may occur. In such reservoirs as the Oklahoma City Wilcox sand (2-40), gravity reduced the saturation of oil in the upper hundred feet of sand to 7 to 12 per cent of the pore space, with sand of 400- to 600-millidarcy permeability. One well drilled downstructure after the reservoir was at atmospheric pressure pumped 900 bbl of oil per day for a period of months. An oil recovery of about 33 per cent had occurred by the time the reservoir reached atmospheric and 20 per cent has been recovered since that time, with a daily production rate of 6,520 bbl/day still occurring.

The saturation distribution of a liquid in a gravity-drainage process is shown by Figs. 2-40 and 2-43. Stahl, Martin, and Huntington (12-83) measured the saturation of Wilcox crude oil at 130°F (38.2°API, viscosity 4.3 centistokes at 130°F, surface tension 25.5 dynes/cm) in an unconsolidated sand column that had a porosity of 31.9 per cent and permeability of 7.5 darcys (Fig. 12-36). In the short column and with the extremely permeable sand, a time of 56 hr caused a reduction in oil saturation to 16 per cent.

Lewis (12-46) reviewed the practical aspects of gravity drainage in oil fields, pointing out examples of reservoirs where it was an important mechanism of oil recovery. The type of segregation that might be expected in multiple sands separated by impermeable barriers is shown in Fig. 12-37. Terwilliger et al. (12-91) conducted experimental studies on drainage of liquids from a column of sand and provided a calculation procedure for predicting recovery of liquid

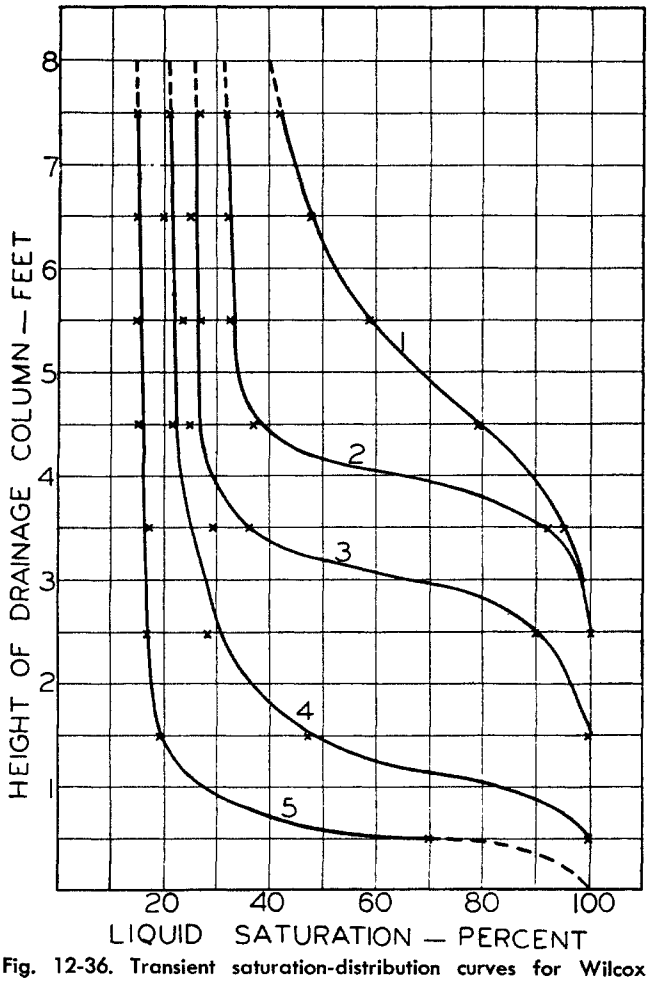

Fig. 12-36. Transient saturation-distribution curves for Wilcox crude oil at 130°F. The drainage production, in percentage of original oil in place, is as follows: at 35 min, 8.2 per cent (curve 1); at 1 hr 36 min, 16.4 per cent (curve 2); at 3 hr 51 min, 32.8 per cent (curve 3); at 8 hr, 49.2 per cent (curve 4); at 56 hr, 72.5 per cent (curve 5). (*Stahl, Martin, and Huntington, 12-83. Courtesy AIME.*)

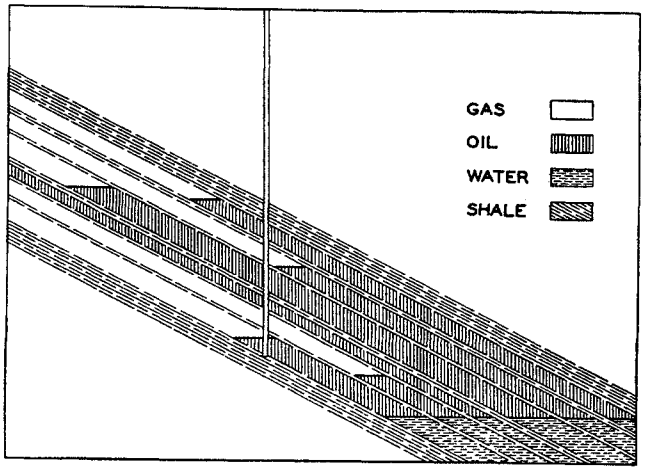

Fig. 12-37. Segregation of gas from oil in a multiple-sand section. (*Lewis, 12-46. Courtesy AIME.*)

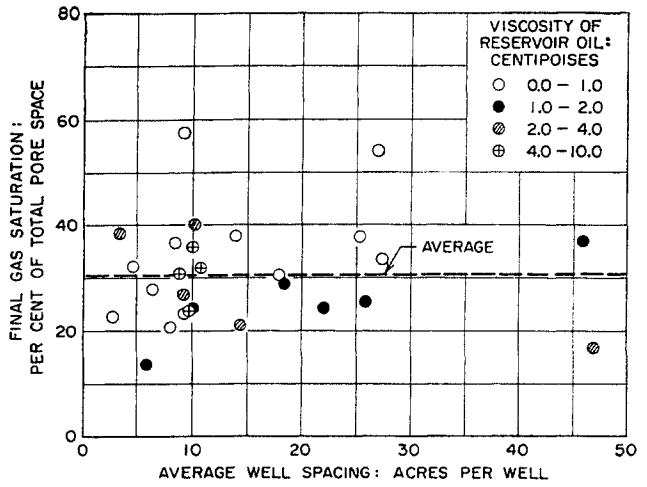

Fig. 12-38. Relation between final gas saturation and well spacing in gas-drive sand fields. (*Craze and Buckley*, 12-19. *Courtesy API Drill. Prod. Practice.*)

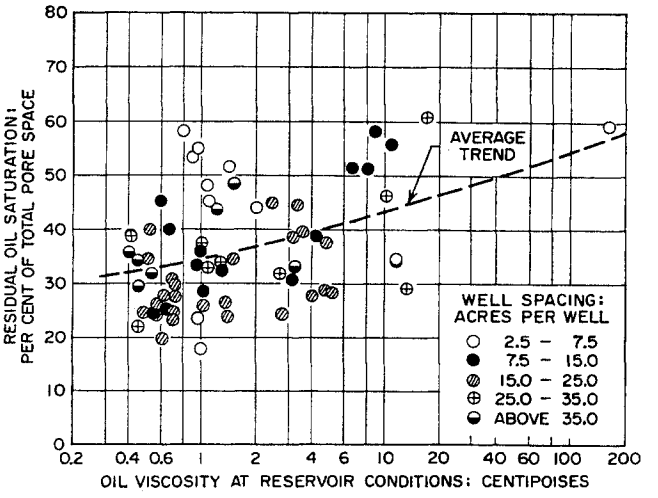

Fig. 12-40. Effect of oil viscosity on residual-oil saturation in water-drive sand fields. (*Craze and Buckley*, 12-19. *Courtesy API Drill. Prod. Practice.*)

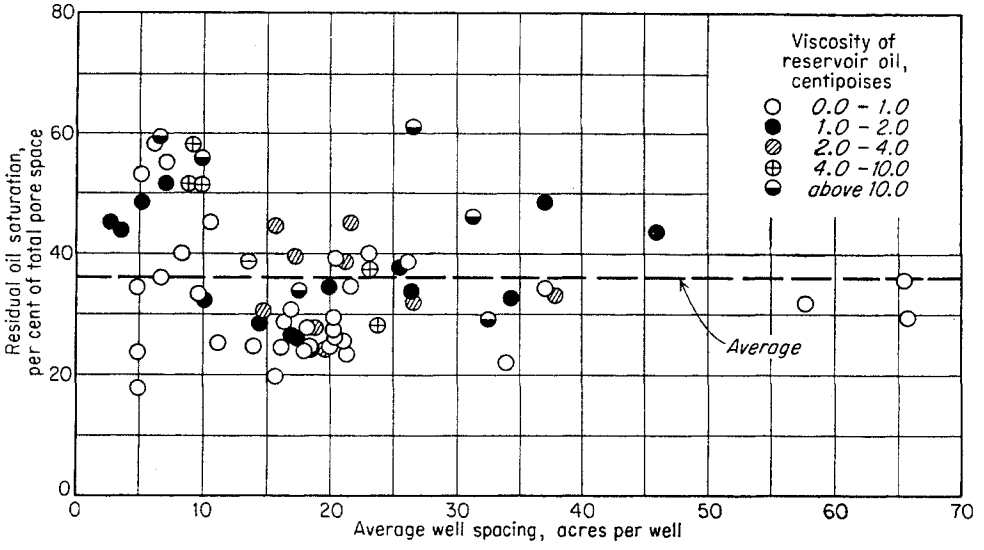

Fig. 12-39. Relation between residual-oil saturation and well spacing in water-drive sand fields. (*Craze and Buckley*, 12-19. *Courtesy API Drill. Prod. Practice.*)

by gravity drainage. Cardwell and Parsons (12-11) present a theory for predicting gravity drainage. The differential equation describing the process was used to predict the successive saturation curves for a column of porous medium after making simplifying assumptions. Matthews and Lefkovits (12-51) compare theoretical predictions with model studies for wells producing by gravity drainage.

The Prediction of Oil Recovery is of great importance to the oil industry. At one time, primary production was considered separate from secondary recovery by such projects as gas injection or water drive. Many reservoirs now experience modifications of the natural recovery process.

Craze and Buckley (12-19), in their study of the influence of well spacing, report the recoveries for many oil fields. Figures 12-38 to 12-40 give recoveries for gas-drive and water-drive sand fields. The connate water (28 per cent average for gas-drive sand fields) and shrinkage of crude oil must be taken into account in evaluating recovery from these figures.

Studies of procedures for estimating oil recoveries are given in the literature (12-4, 12-10, 12-18, 12-25, 12-34, 12-64, 12-96 to 12-98). An important factor in such studies is the mobility ratio K_g/K_o of oil and gas (12-5, 12-12, 12-57, 12-70).

Water and Gas Injection

Water and gas are often injected to aid the primary oil-producing processes or in an attempt to obtain secondary oil after natural production processes no longer will yield significant amounts of oil. In 1938,

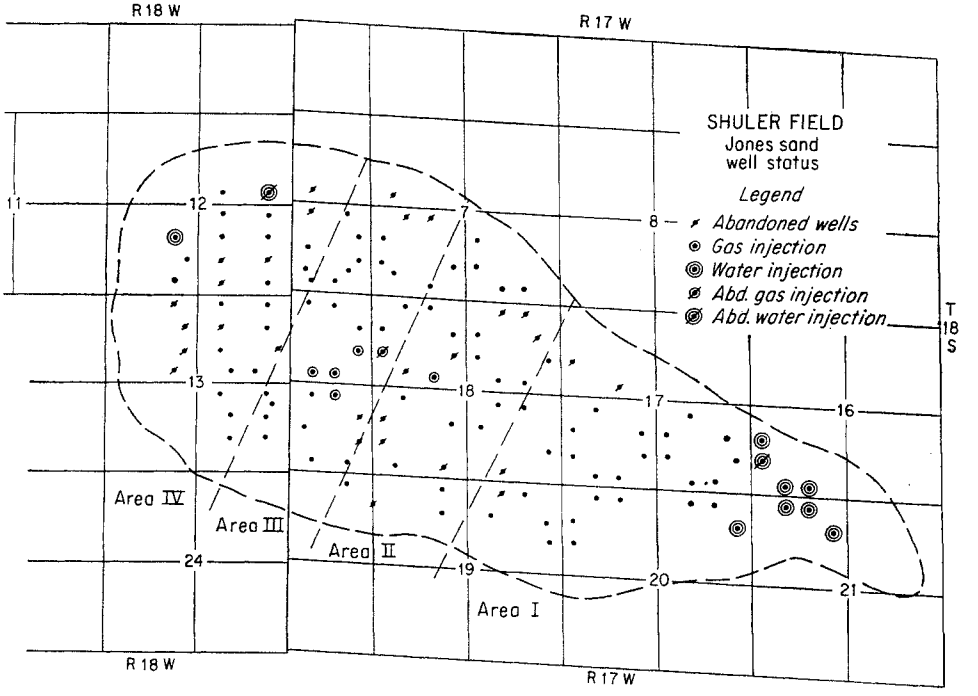

Fig. 12-41. Well status, Shuler field, Jones sand. (*Tarner, Evans, and Kaveler, 12-90. Courtesy AIME.*)

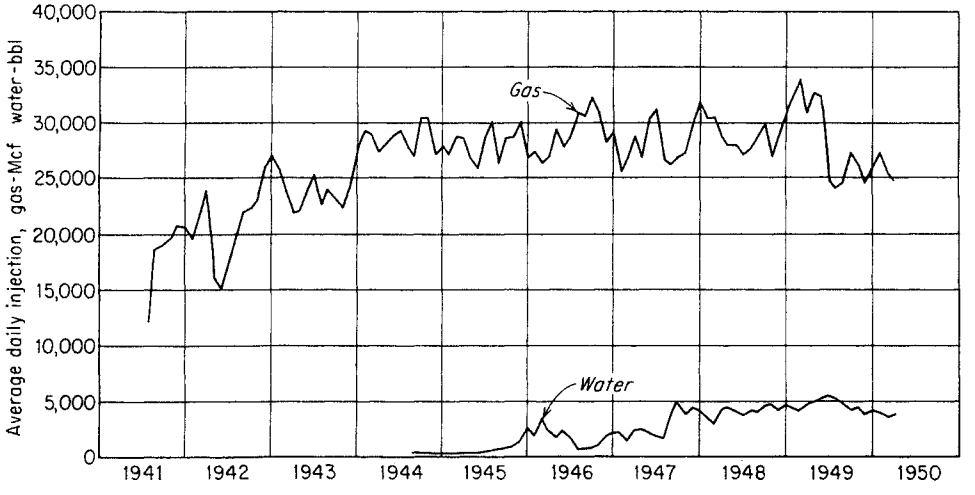

Fig. 12-42. Daily volumes of gas and water injected into Shuler unit. (*Tarner, Evans, and Kaveler, 12-90. Courtesy AIME.*)

Bennett described activities toward pressure maintenance by gas injection (12-7).

Water may be injected to maintain the natural water drive and decrease the pressure reduction (12-1). Water disposal is needed for water-drive fields, and return to the producing horizon downdip to help maintain pressure is a mutually advantageous procedure. The return of large volumes of water at East Texas is an excellent example of this process (12-6, 12-49, 12-56).

The operation of the Shuler field, Jones sand, is an example of gas injection to maintain pressure and later an example of water injection also. Figures 12-41 to 12-44 give information from the paper by Tarner, Evans, and Kaveler (12-90). A significant point in the operation is that over one-half the wells were closed in as soon as the field was placed under unit operation. By selecting wells with low gas-oil ratio, gas production was reduced. This action, plus the injection of produced gas, has maintained the reservoir pressure and increased oil recovery. A combined salt-water- and fresh-water-injection program was started some four years after unitization. This water also helps maintain reservoir pressure and aids in oil recovery. The Jones sand has a porosity of 20.2 per cent, a permeability of 400 millidarcys, and connate-water content of 25 to 35 per cent. The crude oil is saturated, for the reservoir had a small gas cap. The reservoir oil had a formation volume factor of 1.45; 750 cu ft of gas was evolved from the reservoir oil at 198°F when the reservoir fluid was expanding from 3,520 psia to atmospheric.

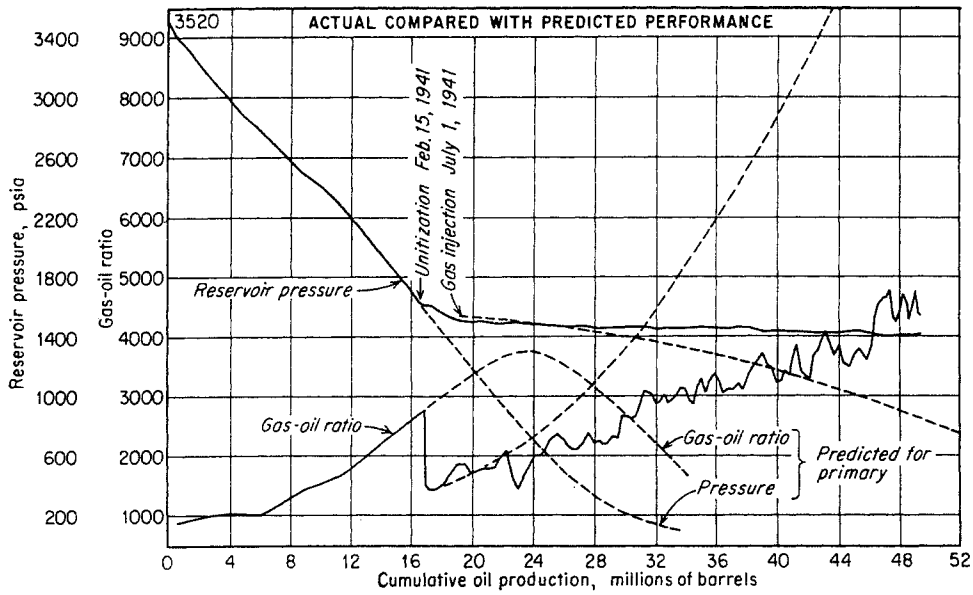

Fig. 12-43. Performance of Shuler Jones sand pool. (*Tarner, Evans, and Kaveler, 12-90. Courtesy AIME.*)

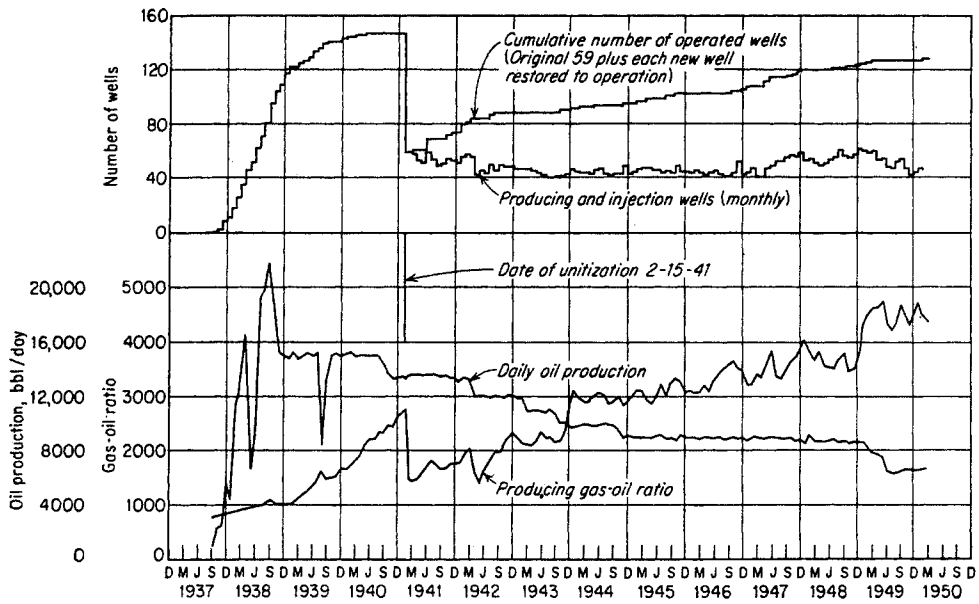

Fig. 12-44. Well and production data: Shuler field, Jones sand. (*Tarner, Evans, and Kaveler, 12-90. Courtesy AIME.*)

The injection of gas at high pressure into reservoirs containing undersaturated oils will cause the oils to swell. Liquid propane is used to blend a continuous phase between oil and the gas used to displace the fluid. The processes involve the use of gas and will produce gas to market at the end of their life (12-32, 12-81, 12-97).

Case histories of field operations and discussion of fluid injection are given in Refs. 12-1, 12-20, 12-27, 12-21, 12-24, 12-30, 12-39, 12-49, 12-52, 12-71, 12-86, 12-87, 12-95, 12-100.

CYCLING OF GAS-CONDENSATE RESERVOIRS

High-pressure natural gases containing substantial quantities of dissolved high-boiling hydrocarbons will

precipitate liquids with pressure reduction (paths AA' or AB, Fig. 12-2).

To compensate for this loss of hydrocarbon liquids in the reservoir from retrograde condensation, the contents of gas-condensate reservoirs often are displaced in a cycling operation. Rich gas is produced and stripped of liquefiable hydrocarbons at a high pressure; then the residue gas is compressed for injection into the reservoir (Fig. 12-45). When this process was started in the late 1930s it was called recycling and the liquid product was described as distillate (12-74). The economics of early cycling operations was based in part on the lack of an immediate market for the natural gas and on the relatively high rates of liquid production permitted per well. Sue and Miller (12-88) listed, as of 1944, 224 condensate fields in the United States and 37 gas-cycling plants. These plants returned 3 MMMcf of gas per day to the ground and recovered 86,000 bbl/day of condensate. The LaGloria (12-38), Cotton Valley (12-53), Katy (12-62), and Erath cycling plants are examples of large-scale operations.

The marketing of the contents of a gas-condensate reservoir in the most profitable manner requires knowledge of the phase behavior of the high-pressure fluid, the nature of the structure containing the deposit, the cost of a suitable condensate-recovery plant, and the value of the gas and liquefied products. Many gas-condensate fields have several reservoirs with variable liquid contents. Often the leaner gases are produced, stripped of propane, butane, and heavier products, and sent to market. The richer fluids are processed and the residue gases returned to the reservoir. The cycling process on a single reservoir may involve a time schedule of 5 to 10 years. At the end of cycling, a dry-gas supply of known quantity is available for the market.

Phase Behavior

The phase behavior of a condensate-gas mixture is normally determined in the laboratory or with portable equipment at the wellhead on a representative sample of the composite well fluid (3-11, 12-26, 12-80, 3-19). The phase diagram for the well fluid composed of 72.47 mass % separator gas and 27.43 mass % separator liquid was determined by Eilerts (3-19) using a laboratory cell and a mobile laboratory at the wellhead. Figure 12-46 presents the phase diagram and Table 12-4 gives the composition for this reservoir fluid.

Miller and Lents (12-53) report the liquid content of the Cotton Valley gas as a function of pressure

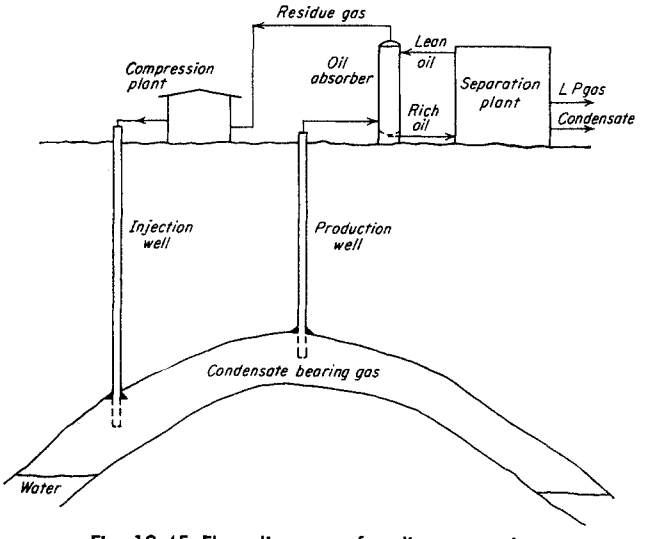

Fig. 12-45. Flow diagram of cycling operation.

(Fig. 12-47). The decline in reservoir pressure had reduced the butanes-plus content of the produced gas from 114 to 83 bbl/MMcf of gas before cycling started. Further drop in reservoir pressure during cycling caused more decline in the liquid content of the gas stream. Allen and Roe (12-3) present a case history of the decrease in condensate recovery accompanying production from a volumetric condensate reservoir without gas return (Fig. 12-48). Patten and Ivey (12-72) give the decline in condensate content accompanying the drop in reservoir pressure at LaBlanca.

Sage, Lacey, and coworkers have studied many naturally occurring systems (12-66, 12-75 to 12-78). Figure 12-49 gives the liquid content of system C from a Louisiana field studied by Reamer and Sage. Table 12-5 gives the composition of the mixture studied. Allen (12-2) has studied the phase relations of gas-oil mixtures. Figure 12-50 shows a phase diagram by Allen for a well effluent taken from a reservoir at 195°F and 2,350 psi. Had the reservoir temperature been as high as 263°F, no retrograde condensation would have occurred. Organick and Golding (12-68) presented a method of predicting saturation pressures for gas-condensate mixtures.

Reamer and Sage found a nearly linear variation in the formation volume factor for a given mixture with the gas-condensate ratio under isobaric-isothermal conditions. The following expression describes with reasonable accuracy the volumetric behavior of a system in the two-phase region as related to the yield of stock-tank oil.

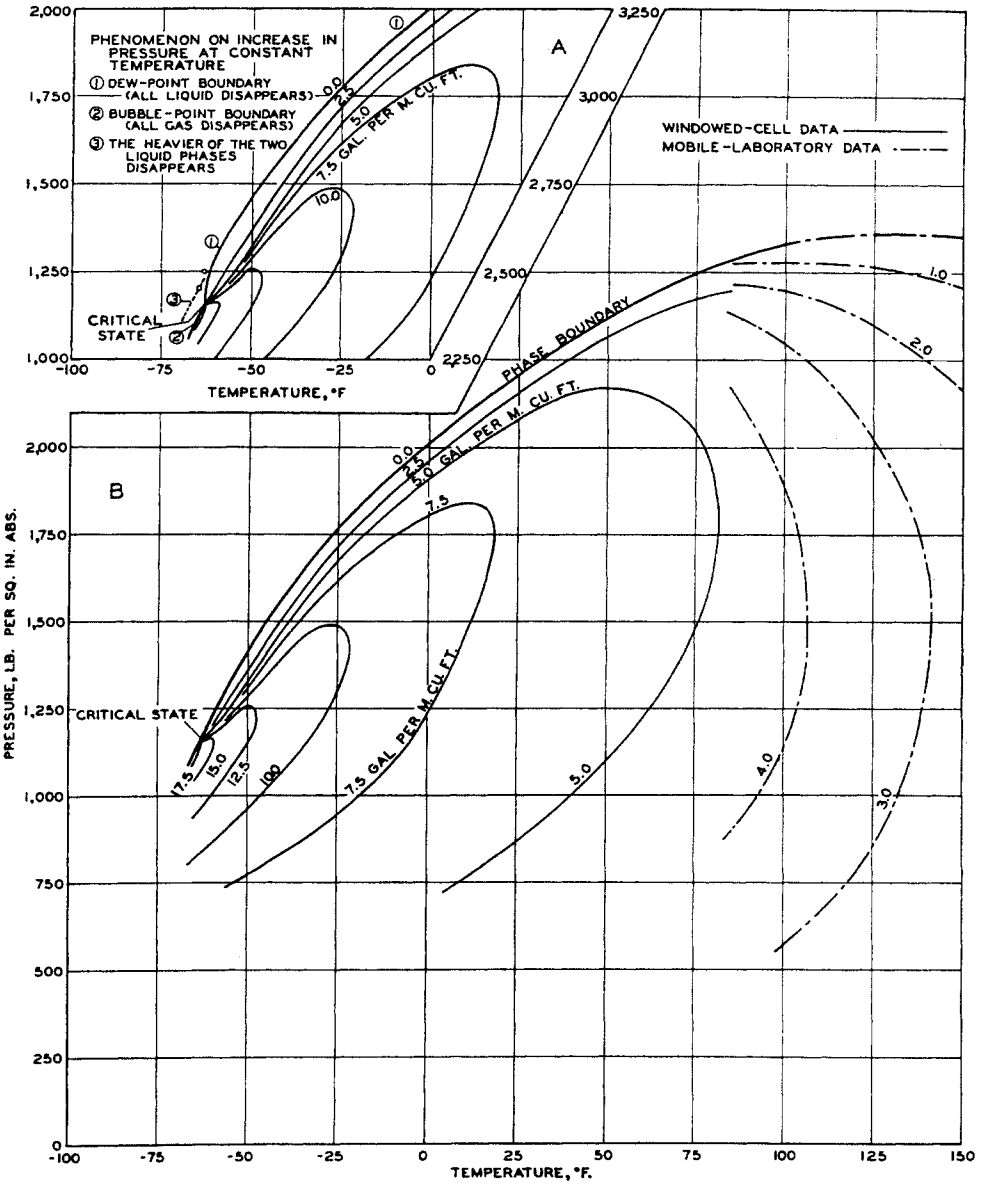

Fig. 12-46. Phase relations for a condensate well fluid. (*Eilerts et al.*, 3-19. *Courtesy Petrol. Engr.*)

Table 12-4. Composition of Composite Well Stream

72.47 mass % separator gas

Component	*Mole fraction*	*Component*	*Mole fraction*
Carbon dioxide	0.00794	Hexanes, 56–35	0.00661
Nitrogen	0.01375	Heptanes, 35–17	0.00290
		Heptanes 17	0.00295
Methane	0.76432	Octanes	0.01040
Ethane	0.07923	Nonanes	0.00613
Propane	0.04301	Decanes	0.00338
Isobutane	0.01198	Undecanes	0.00176
n-Butane	0.01862	Dodecanes	0.00153
Isopentane	0.00937	Tridecanes	0.00087
n-Pentane	0.00781		1.00000
Hexanes, 135–56	0.00744		

SOURCE: Eilerts et al. (3-19).

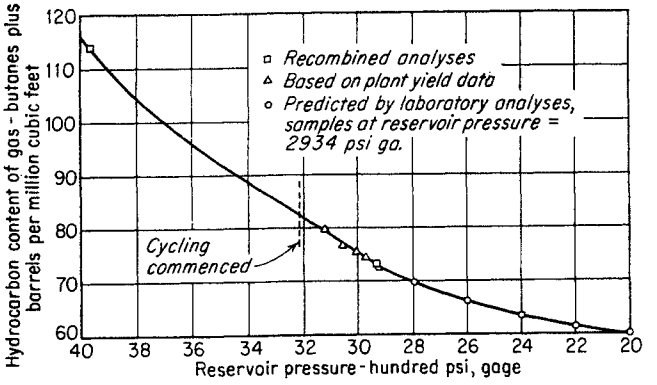

Fig. 12-47. Variation of butane+ content of produced gas with reservoir pressure, Bodcaw sand, Cotton Valley field, La. (*Miller and Lents, 12-53. Courtesy API Drill. Prod. Practice.*)

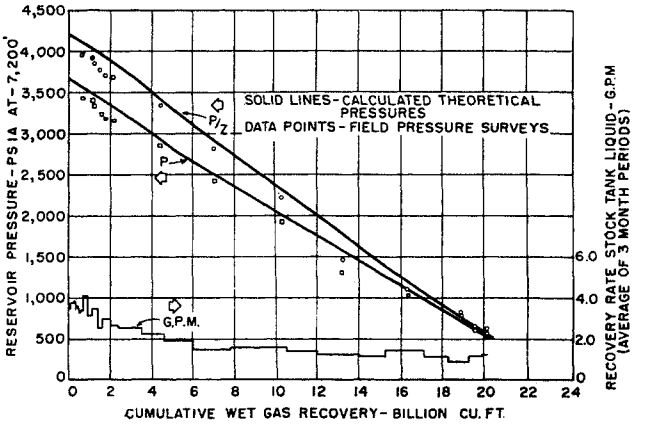

Fig. 12-48. Reservoir performance of Bacon Lime condensate reservoir, East Texas. (*Allen and Roe, 12-3. Courtesy AIME.*)

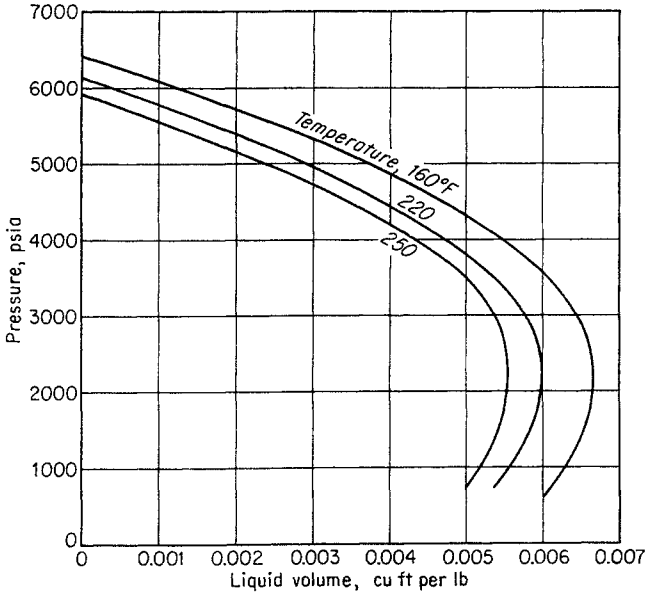

Fig. 12-49. Phase behavior of condensate-gas system from a Louisiana field. (*Reamer and Sage, 12-75. Courtesy AIME.*)

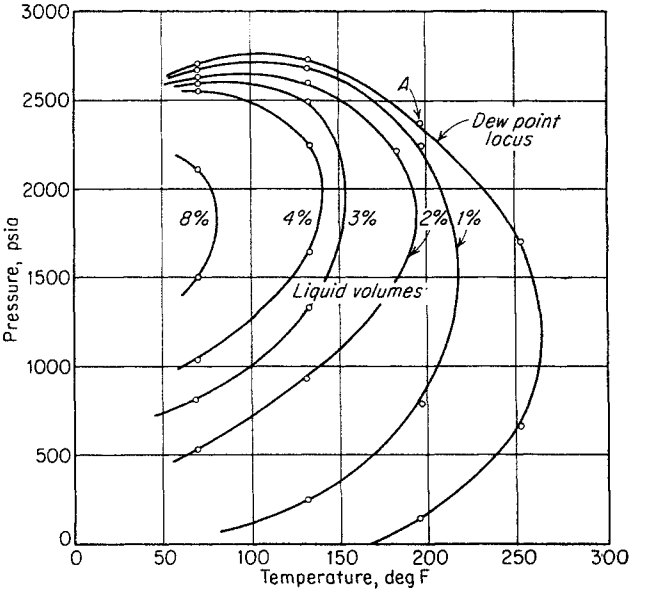

Fig. 12-50. Phase diagram of the well production mixture from field C. (*Allen, 12-2. Courtesy API Drill. Prod. Practice.*)

Table 12-5. Composition C Prepared from Separator Gas and Liquid from Louisiana Field

Component	*Mole fraction*	*Component*	*Mole fraction*
Air	0.0047	*n*-Butane	0.0082
Carbon dioxide	0.0065	Isopentane	0.0044
		n-Pentane	0.0022
Methane	0.8659	Hexanes	0.0062
Ethane	0.0376	Heptanes	0.0100
Propane	0.0161	Octanes and heavier*	0.0334
Isobutane	0.0048		1.0000

* Molecular weight, 167.6. 43.8°API.

SOURCE: Reamer and Sage (12-75).

$$v = \frac{ART}{P} \qquad (12\text{-}7)$$

where v = formation volume factor
$= \dfrac{\text{volume of mixture at conditions}}{\text{volume of stock-tank oil}}$
P = pressure, psia
R = gas-condensate ratio, cu ft/bbl
A = coefficient

Figure 12-51 is a plot of the values of A for gas-condensate mixtures from a Louisiana field (12-76).

Condensate fields may be discovered at pressures considerably above the retrograde dew point, and therefore may produce fluid of constant composition until the dew-point pressure is reached in the reservoir. Thereafter the liquid content of the well stream will normally decrease.

The revaporization of liquid condensed during the pressure reduction on a reservoir is a factor to be considered. Weinaug and Cordell (12-94) showed that sweep gas would attain equilibrium with any liquid in the porous medium through which it passes.

Computation of Pressure Depletion of a Retrograde Condensate Field with No Water Drive

Pressure decline at constant reservoir temperature results in the formation of retrograde condensate from naturally occurring condensate fluids. In many of these fluids the amount of condensate or liquid formed is insufficient to institute flow; however, as the amount of liquid changes, the composition of the gas phase, or production, changes. It is important to be acquainted with these changes in order to plan future operation of gasoline plants, etc., and to determine the economic advantages or disadvantages of cycling the reservoir.

If the reservoir has no water drive, the production mechanism is essentially a continuous removal of vapor from a constant-volume cell while the remaining

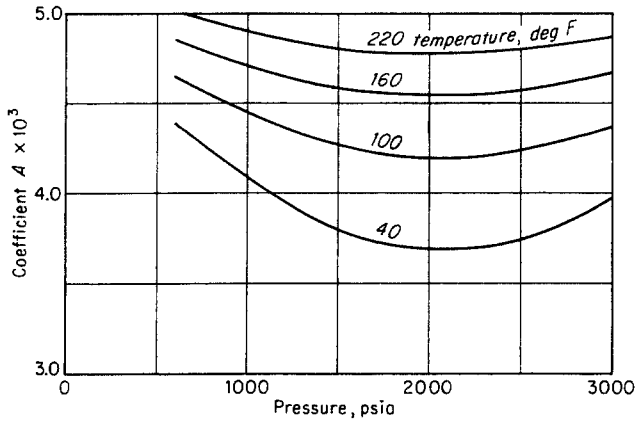

Fig. 12-51. Coefficient A in Eq. (12-7) for Louisiana gas-condensate mixtures. (*Sage and Reamer, 12-76. Courtesy AIME.*)

mixture is maintained at equilibrium. Determination of changes occurring under these conditions can be made by assuming that a plot of composition versus production forms a straight line over the increment of pressure decline under consideration. If the pressure increments are not too large, this assumption does not introduce any appreciable error.

The computation method involves a trial-and-error solution which is illustrated for two pressure steps in Table 12-6. Columns 2 and 3 list moles and original composition of reservoir fluid, which was at its dew point at 3,820 psia and 216°F. These are used to determine the volume of the reservoir, which is 166 cu ft. Next, the composition of the vapor at the end of pressure step 1, 3,500 psia, is assumed and listed in column 4. Average composition of material produced in lowering the pressure to 3,500 psia is calculated by adding the initial and assumed compositions, columns 3 and 4, and dividing by 2. Average composition is listed in column 5.

Next, the number of moles of production necessary to lower the pressure to 3,500 psia is assumed to be 6.8. The product of the number of moles produced and the average composition yields the amount of each constituent produced, column 6. This quantity subtracted from the total moles initially present (column 2) yields the moles of each constituent present at the end of the pressure step, column 7.

The amounts of liquid and vapor formed from the remaining material are determined by means of the flash-vaporization equation [Eq. (6-14)]. The equilibrium constants used were determined by methods described by NGAA (6-40) and are listed in column 8. The results of this computation are shown in columns 9 to 12. The computed composition of the vapor at 3,500 psia (column 10) is then compared with assumed composition (column 3). Although these compositions do not quite check, they are close enough.

After verifying the composition assumption, the production assumption is checked by determining the volume of the material remaining at 3,500 psia. The volume of the gas at 3,500 psia is 161.8 cu ft; the liquid occupied 4.19 cu ft; so the total volume was 166.0 cu ft. Since this volume is equal to the volume occupied by the original fluid, the assumed production must be correct, and a solution has been obtained for the first pressure step.

This procedure is repeated until abandonment pressure is reached.

Sweep Patterns

Wells for injection of lean gas and withdrawal of rich gas should be located to permit the lean gas to

Table 12-6. Calculation of Pressure Depletion for a Gas-condensate Reservoir

(1) Component	(2) Total moles present	(3) Vapor composition y	(4) Assumed vapor composition at 3,500 psia, y	(5) (3) + (4) / 2 Av vapor composition y_{av}	(6) (5) × 6.8 Moles produced	(7) (2) − (6) Total moles present	(8) K at 3,500 psia	(9) Moles of liquid*	(10) Moles of vapor*	(11) Vapor composition y	(12) Liquid composition X
CO_2	0.90	0.0090	0.00904	0.00902	0.0614	0.839	1.28	0.01607	0.823	0.00904	0.00707
CH_4	78.05	0.7805	0.7880	0.7842	5.3329	72.717	1.72	1.0418	71.675	0.78827	0.05830
C_2H_6	7.42	0.0742	0.0741	0.0742	0.5043	6.916	0.960	0.1755	6.740	0.07413	0.07720
C_3H_8	4.88	0.0488	0.0485	0.0487	0.3308	4.55	0.785	0.1404	4.409	0.04849	0.06176
i-C_4H_{10}	1.18	0.0118	0.0116	0.0117	0.0797	1.100	0.610	0.0433	1.051	0.01162	0.01905
n-C_4H_{10}	1.65	0.0165	0.0162	0.0164	0.1112	1.539	0.560	0.0658	1.473	0.01620	0.02896
i-C_5H_{12}	0.75	0.0075	0.00728	0.00739	0.503	0.700	0.430	0.0384	0.661	0.00723	0.01689
n-C_5H_{12}	0.60	0.0060	0.00580	0.00590	0.0401	0.560	0.395	0.0333	0.527	0.00579	0.01465
C_6H_{14}	1.04	0.0104	0.00988	0.01014	0.0690	0.971	0.300	0.0749	0.896	0.00986	0.03286
I C_{7+}	0.923	0.0923	0.00853	0.00888	0.0604	0.863	0.215	0.0899	0.773	0.00850	0.03955
II C_{7+}	0.843	0.0843	0.00750	0.00797	0.0542	0.789	0.154	0.1102	0.679	0.00746	0.04848
III C_{7+}	0.712	0.0712	0.00602	0.00657	0.0447	0.667	0.110	0.1236	0.544	0.00599	0.05437
IV C_{7+}	0.570	0.0570	0.00428	0.00499	0.0340	0.536	0.064	0.1506	0.386	0.00424	0.00625
V C_{7+}	0.482	0.0482	0.00318	0.00400	0.0272	0.455	0.042	0.1697	0.285	0.00314	0.07465
	100.00	.....	.....	.....	.....	93.2	.....		90.922		

* Computed by means of flash-vaporization equation.

Volume at 3,820 psia

Gas

$T_c = 427.3°\text{R}$

$P_c = 657.5$ psia

$$T_r = \frac{676}{427.3} = 1.58$$

$$P_r = \frac{3{,}820}{657.5} = 5.81$$

$Z = 0.875$

$$\text{Volume of gas} = \frac{0.875 \times 100 \times 10.71 \times 676}{3{,}820}$$

$= 166.0$ cu ft

Volume of liquid = 0

Total volume = 166.0 cu ft

Volume at 3,500 psia

Gas

$T_c = 421.2°\text{R}$

$P_c = 659.7$ psia

$$T_r = \frac{676}{421.2}$$

$$P_r = \frac{3{,}500}{659.7} = 5.305$$

$$\text{Volume of gas} = \frac{0.860 \times 90.922 \times 10.71 \times 676}{3{,}500}$$

$= 161.8$ cu ft

Liquid

Molecular weight = 63.91

Density = 0.555 gram/cu cm

$$\text{Volume} = \frac{63.91 \times 2.2731}{0.555 \times 62.4}$$

$= 4.19$ cu ft

Total volume = 161.8 + 4.2 = 166.0

166.0 = 166.0, the initial volume

All assumptions are correct

Volume at 3,000 psia

Gas

$T_c = 415.6°\text{R}$

$P_c = 662.0$ psia

$$T_r = \frac{676}{415.6}$$

$$P_r = \frac{3{,}000}{662.0}$$

$= 4.532$

$$\text{Volume of gas} = \frac{0.839 \times 78.228 \times 10.71 \times 676}{3{,}000}$$

$= 158.4$ cu ft

Liquid

Molecular weight = 66.92

Density = 0.570 gram/cu cm

$$\text{Volume} = \frac{66.92 \times 3.872}{0.570 \times 62.4}$$

$= 7.29$ cu ft

Total volume = 158.4 + 7.3 = 165.7 cu ft

$165.7 \neq 166.0$, the initial volume, but close enough

All assumptions are correct

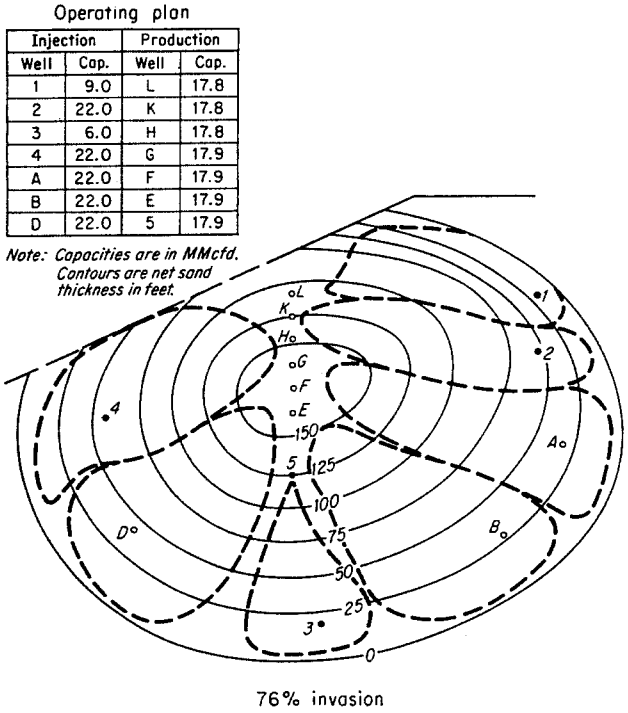

Fig. 12-52. Sweep pattern by electric model. (*Marshall and Oliver*, 12-50. *Courtesy AIME.*)

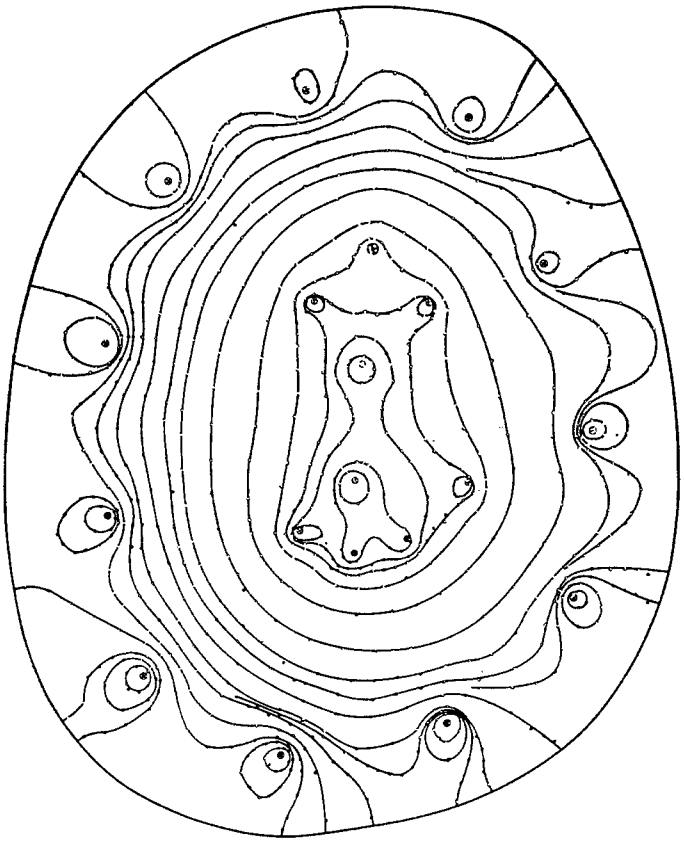

Fig. 12-53. Potential distribution in an electrical model. (*Hurst and McCarty*, 12-35. *Courtesy API Drill. Prod. Practice.*)

sweep the maximum amount of the rich gas from the reservoir. Flow patterns for specific well locations may be predicted for homogeneous porous media from potential theory or may be determined from models (12-50).

Early work by Wyckoff, Botset, and Muskat on sweep patterns was concerned with displacing oil by water in the water-flooding process (12-58, 12-101). Swearingen (12-89) and Hurst (12-35, 12-37) extended the potential theory and electrical-flow-model studies to problems of condensate reservoirs. The electrical models depend upon the transfer of ions in an electrolyte from one pole to another, leaving a colored background to represent the flooded area. The reservoir model may be made of blotting paper or agar gel scaled for relative thickness of the producing zone. Swearingen used a solution of zinc ammonium chloride in the model, with glass electrodes containing copper ammonium chloride as input wells and electrodes of zinc ammonium chloride as output wells. Under the influence of a potential between input and output wells, a blue coloration develops from the copper ion showing the sweep pattern at successive stages. Figure 12-52 shows a sweep pattern from an electrical model developed by Lee (12-45a). It is possible to control the relative input and output from each well by varying the potential imposed on the electrodes. Diffusion in the solution imposes limitations on such model studies especially when they are conducted over a period of time.

A potentiometric model was employed by Hurst and McCarty (12-35) to determine the lines of equipotential (or equipressure) for flow between wells. They immersed copper rods for wells into a copper sulfate solution, passed current from input to output wells, and found the lines of equipotential with an electrical probe. Figure 12-53 is an illustration of the potential distribution of the model with nine center-input wells and eleven outer-production wells. Flow takes place along streamlines normal to equipotential lines. These flow lines may be sketched in graphically. The position of the wavefront of the flowing gas at different times is determined from the rate of movement along the streamlines in proportion to the potential gradient. Figure 12-54 by Hurst and McCarty is a plot of the successive waveforms for the model of Fig. 12-53. Figure 12-55 gives the composition of the produced gas for this model. The "fluid-mapper" technique developed by Moore may be used as a means of obtaining streamlines, with the equipotential lines taken normal to the flow (12-54). Crystals of potassium permanganate are sprinkled on a plaster of paris base and a glass plate is laid on top with spacers. Water is allowed to run into the source

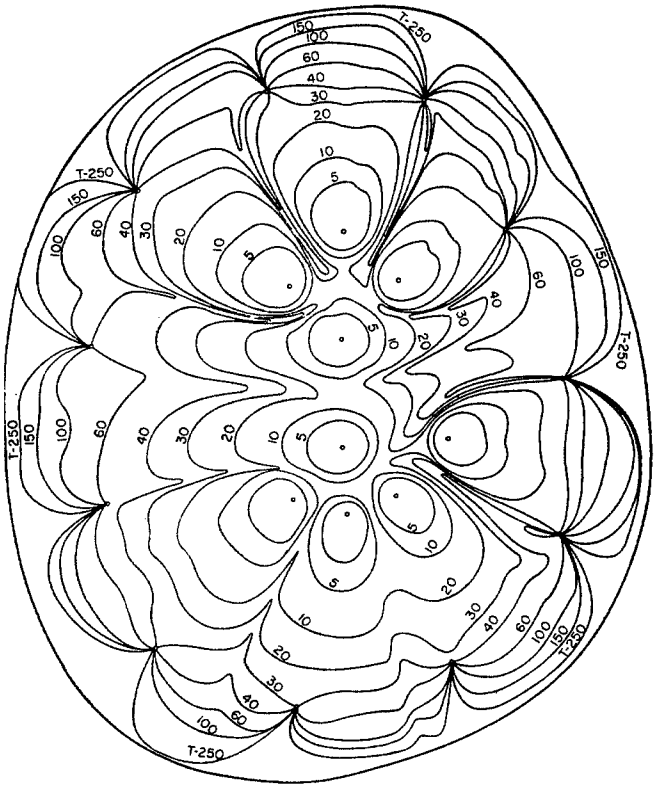

Fig. 12-54. Areas swept out at progressive times by dry gas. (*Hurst and McCarty*, 12-35. *Courtesy API Drill. Prod. Practice.*)

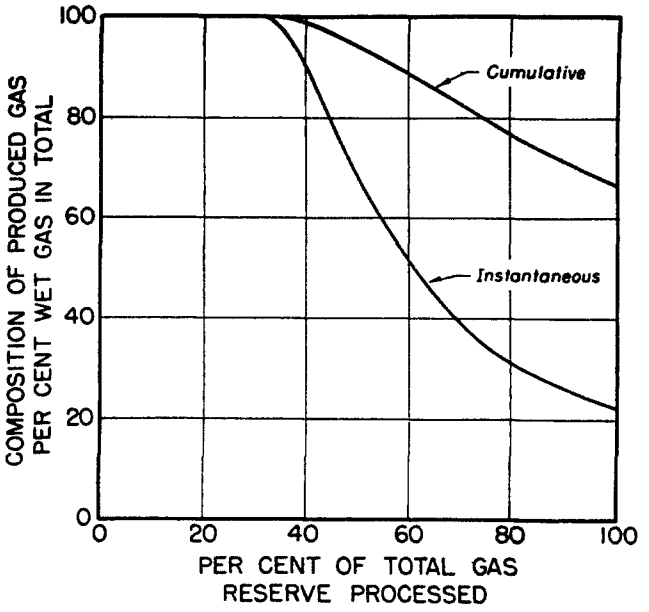

Fig. 12-55. Variation of composition of produced gas. (*Hurst and McCarty*, 12-35. *Courtesy API Drill. Prod. Practice.*)

A and out the sink B causing the color lines past the crystals (Fig. 12-55*a*).

The sweep patterns just mentioned all depend upon uniform porous media. In practice, a considerable variation occurs in the permeability of the various layers or strata. Should the producing formation contain several layers of different permeability, the

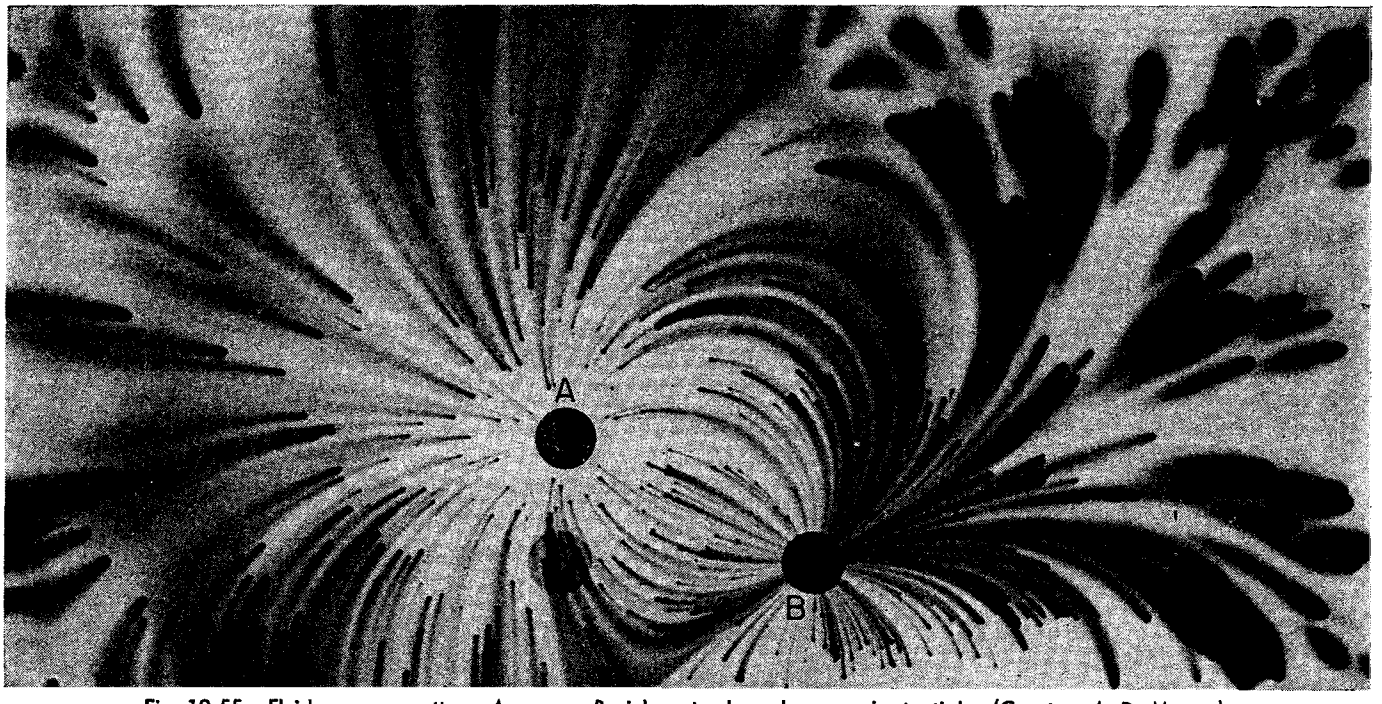

Fig. 12-55a. Fluid-mapper pattern: A, source; B, sink; outer boundary, equipotential. (Courtesy A. D. Moore.)

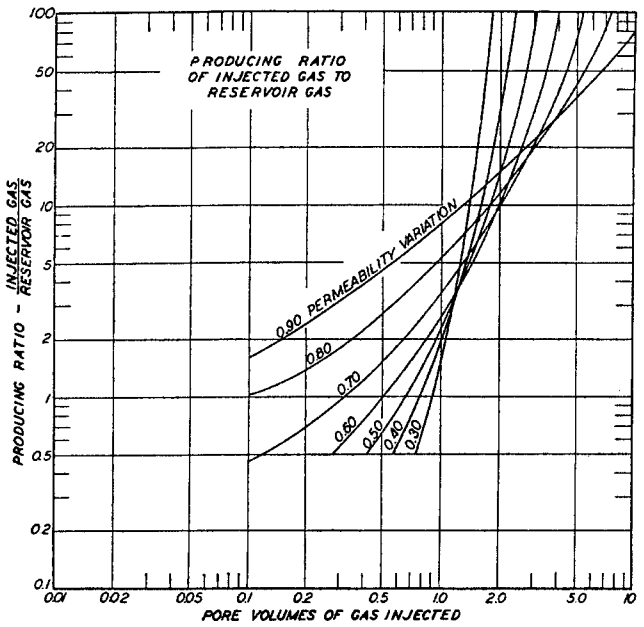

Fig. 12-56. Effect of permeability variation on producing ratio of injected to reservoir gas. (*Standing, Lindblad, and Parsons*, 12-85. *Courtesy AIME.*)

more permeable zone would sweep first and thus dilute the produced gas at a well with dry gas. It is desirable to isolate into separate zones as far as possible all strata of different permeability. Methods have been presented of predicting the over-all sweep results for reservoirs with variable permeability (12-37, 12-50, 12-60, 12-85). Standing, Lindblad, and Parsons (12-85) have presented a chart for showing the effect of permeability variation on the ratio of dry gas to wet gas in the production from wells (Fig. 12-56). Permeability variation is defined as the ratio of the difference between the median permeability and the permeability above which 84.1 per cent of the values lie, to the median permeability. The permeabilities are plotted on logarithmic-probability paper as permeability over maximum permeability versus "per cent larger than" (Fig. 12-57). The median permeability is read at the 50 per cent line. Muskat has developed charts for predicting sweep for various permeability distributions (12-60).

Organick studied a condensate field and came to the conclusion that some liquid phase flowed to the wells (12-69).

Processing Condensate Well Fluids

Cycling plants normally operate on fields with reservoirs having pressures enough in excess of 2,000 psi so that the gas-liquid mixtures may be delivered to the plant at around this pressure. The primary separation normally takes place at pressures around 2,000 psi, to allow recompression of the residue gas without undue horsepower requirements. Oil absorp-

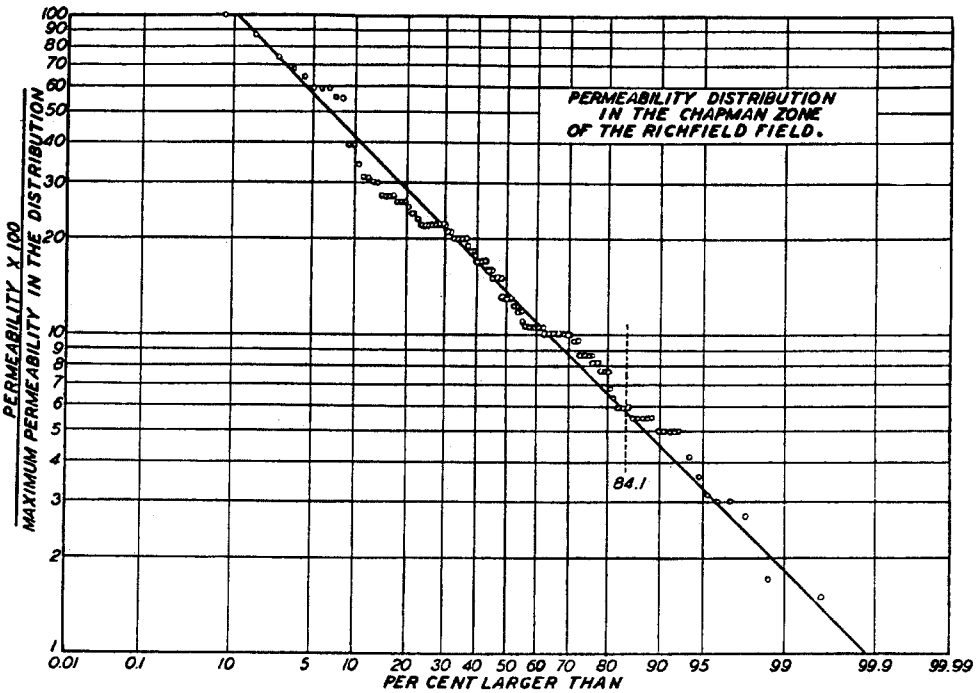

Fig. 12-57. Permeability variation in the Richfield field. (*Standing, Lindblad, and Parsons*, 12-85. *Courtesy AIME.*)

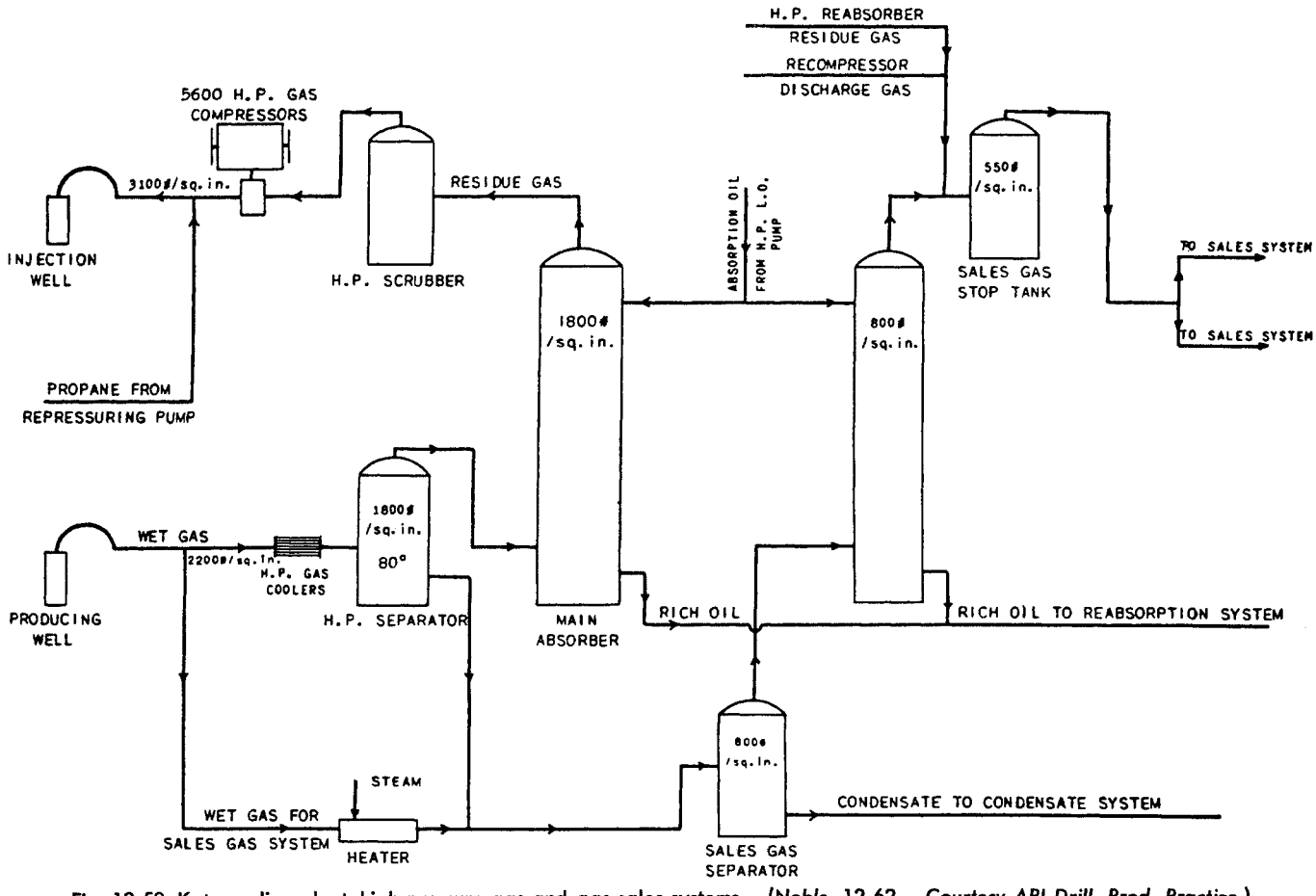

Fig. 12-58. Katy cycling plant: high-pressure-gas and gas-sales systems. (*Noble*, 12-62. *Courtesy API Drill. Prod. Practice.*)

tion is the common recovery process. Since high-boiling hydrocarbons are involved, cycling plants often make their absorption oil from the condensate produced. Cycling plants make condensate—either stabilized or blended with butane–butane, propane, and sometimes a natural gasoline.

Cycling plants have complexities akin to those in oil refineries even though no chemical conversion is involved in the usual processing operation. They operate throughout the year with shutdowns usually limited to an annual inspection.

A flow diagram for the Katy cycling plant, shown in Figs. 12-58 to 12-60, was presented by Noble (12-62). The plant processes gas for direct sale at 800 psi and cycles gas processed at 1,800 psi and compressed to 3,100 psi. The liquid products are condensate from the 45-lb still (Fig. 12-59), gasoline from the debutanizer (Fig. 12-60), butane from the debutanizer overhead, and propane.

In 1943 the plant processed 275 MMcf of gas per day with 80 per cent recovery of butanes, but has been doubled in size since then. The plant requires 14,000 gpm of cooling water in a cycle of 85 to 115°F. The electrical requirement is 1,740 kw and the steam requirement is 95,000 lb/hr. The absorber oil rate is 1,340 gpm.

Fifteen wells, three of which are dual completions, provide the gas-condensate mixture for the plant. The field lines are designed for a working pressure of 2,750 psi at 130°F and take 20 to 25 MMcf/day per well completion. The injection system is designed for a working pressure of 3,500 psi at 175°F, since the compressed gas is not cooled after compression. Even this hot gas caused a cooling of as much as 30°F in a reservoir temperature after several years of gas injection.

Processing operations are discussed in detail in later chapters.

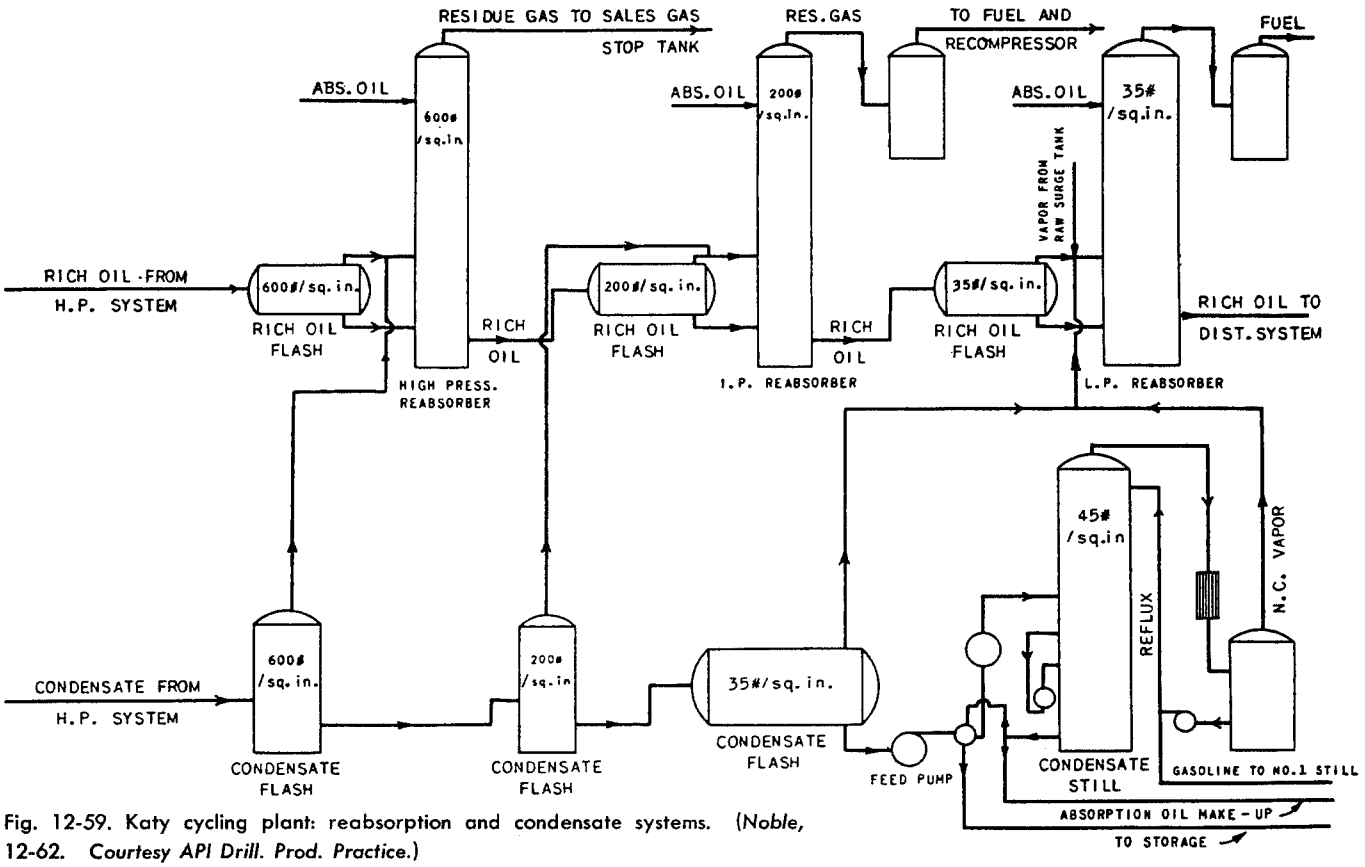

Fig. 12-59. Katy cycling plant: reabsorption and condensate systems. (*Noble*, 12-62. *Courtesy API Drill. Prod. Practice.*)

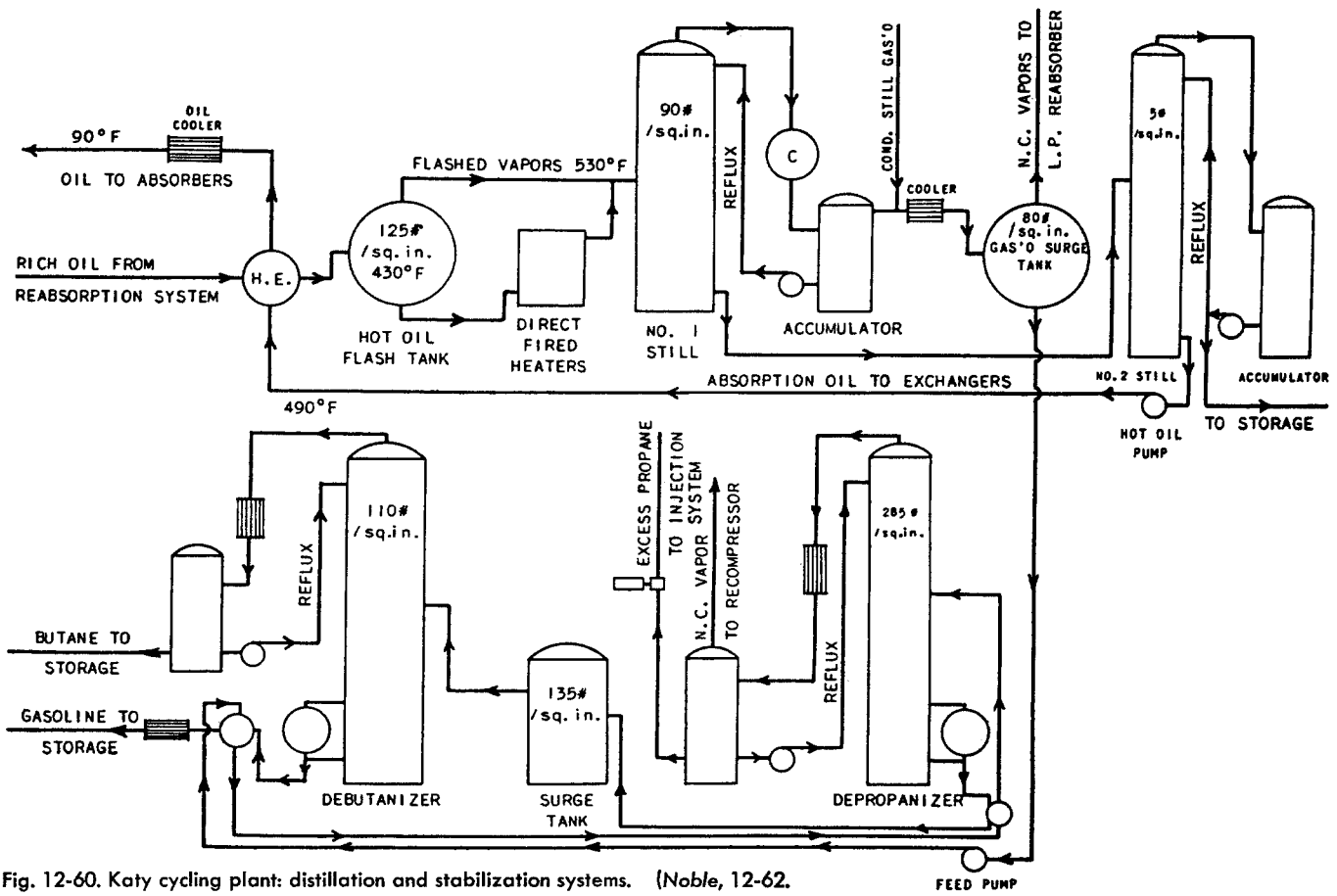

Fig. 12-60. Katy cycling plant: distillation and stabilization systems. (*Noble*, 12-62. *Courtesy API Drill. Prod. Practice.*)

CHAPTER 13

Field-separation and Oil-absorption Processes

Natural gas from high-pressure wells passes through separators at the well to remove hydrocarbon condensate and water. Most gases contain enough natural gasoline, butane, and propane to warrant processing plants for recovery of these liquefiable constituents (Fig. 13-1). The most common method of recovering them is by absorption in bubble-plate columns with a gas oil as absorbent. This oil, which is rich in light hydrocarbons, is stripped of propane, butane, and natural gasoline constituents, cooled, and returned to the absorber.

The natural gas, denuded of valuable liquefiable constituents, is ready for the gas market unless it contains hydrogen sulfide. When hydrogen sulfide is present, the gas is sweetened by absorption of the hydrogen sulfide in an amine solution. To prevent hydrate formation in transit to market, the gas is normally dehydrated either by a glycol absorption process or by passage over solid desiccants.

The liquids recovered by the oil-absorption process are fractionated into stable products, LP gas—propane or butane, natural gasoline, or stabilized condensate. These liquid products may be dehydrated by distillation. Alternative processes of liquid recovery include low-temperature separation, either by expansion or by refrigeration. The industry is considering the complete liquefaction of natural gas constituents for transportation to market by barges where pipelines are not feasible.

The rate processes of mass transfer, fluid flow, and heat transfer are treated in the chemical engineering literature, often under the heading of "unit operations." Phase-equilibria data with hydrocarbon systems or with hydrocarbons are necessary for finding the approach to equilibrium. These subjects have a voluminous literature which is abstracted for applications in natural gas processing, but such abstracting may appear to be incomplete and arbitrary in its choice of topics. Readers are referred to Refs. 13-1,

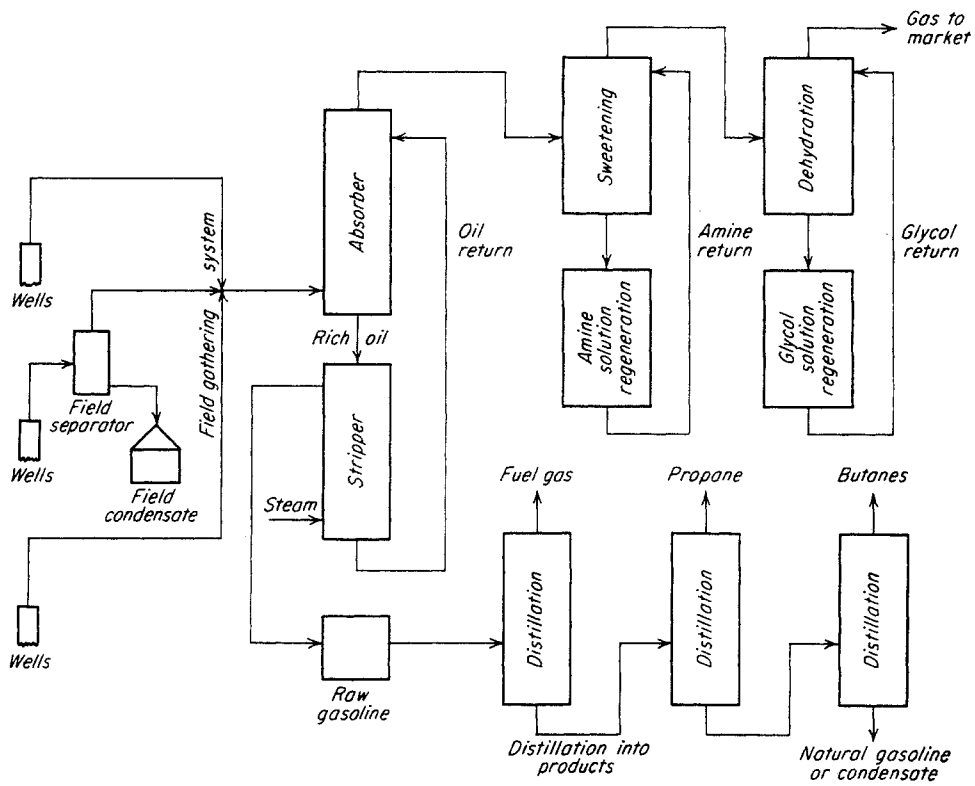

Fig. 13-1. Simplified flow diagram for gas processing.

13-2, 13-9, 13-19, 13-21, 13-22, 13-24, 13-25, 13-31, 13-35, 13-37, 13-39, and 7-9 for comprehensive treatises on the unit operations involved. The treatment here is designed primarily to provide the reader with introductory background on some of the unit operations involved and on their application to the processing of natural gas. A few processes are discussed that are not widely used but that may nevertheless find special applications. This chapter will treat field processing and the absorption-stripping process of natural gasoline or cycling plants.

FIELD SEPARATION

Fluids flowing from oil and gas wells generally include gas, one or more liquid phases, and frequently small quantities of solid phases. The hydrocarbon liquid phase is usually accompanied by brine or condensed water. The separation of these phases at the wellhead is ordinarily desirable. The variables to be considered in determining the optimum recovery of liquid hydrocarbon by means of wellhead separators are discussed below. Modifications of conventional separators have been made to increase the condensate recovery and to dehydrate the gas (13-3, 5-66, 13-5 to 13-7, 13-14, 13-15, 13-27, 13-34, 13-40). Figures 1-19 and 1-20 indicate the nature of the gas-liquid separation for crude oils containing dissolved gas and for gas-condensate systems. Table 6-4 gives hydrocarbon phase compositions for separator gases and liquids.

Figure 13-2 gives the flow sheet for a simple three-stage wellhead separation unit. The first stage includes provisions for the separation of water from the oil. Under certain conditions, where hydrate formation is likely to occur, the fluid stream may be heated at the wellhead. The factors influencing efficiency of recovery of hydrocarbons by such an arrangement include the phase behavior of the flowing mixture, the pressure and temperature of each stage, and the number of stages used. The choice of conditions and arrangement made for a given operation involves a study of these factors. Secondary variables such as foaming, emulsification, and entrainment may become serious considerations at times. Figures 13-3 and 13-4 show field-separator installations.

Usually the pressure and temperature of the stream at the wellhead are fixed by the characteristics of the reservoir and the history of travel of the fluid up the producing tubing. For instance, the wellhead temperatures are dependent on flow rate over a wide range, as shown in Fig. 13-5 (5-66). Further changes in stream conditions on the way to the separator take place through the transfer of heat to or from the surroundings and as a result of the pressure drop through the lines. The flowing wellhead conditions, nevertheless, provide the usual starting point for further computations. Measured values of wellhead temperature as a function of flow rate provide the most reliable values. It should be noted that flow temperature at a given flow rate increases with time after the well is opened.

When the composition of the well stream is known, the yield of liquid and the compositions of the gas-liquid stream can be computed from equilibrium constants as described in Chap. 6. In many cases, the well effluent composition is obtained by a recombination of gas and liquid compositions at measured flow rates. However, it may be desirable to find the yield and compositions at other separator temperatures and pressures. Also, the subsequent separations on the liquid in low-pressure separators or in the stock

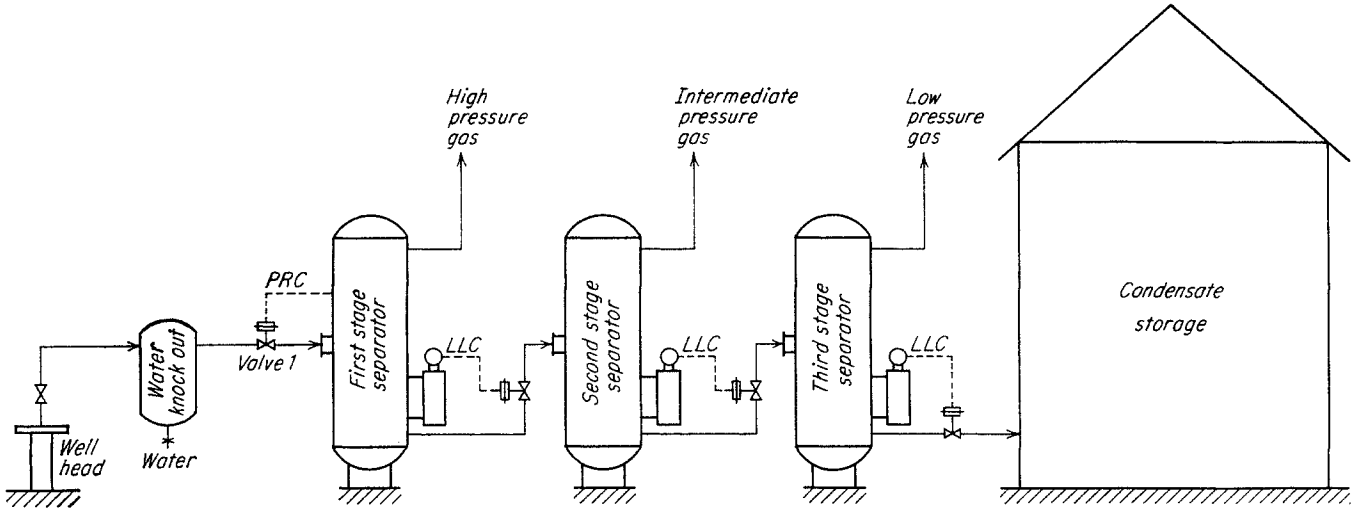

Fig. 13-2. Flow diagram for three-stage wellhead separation unit.

(a)

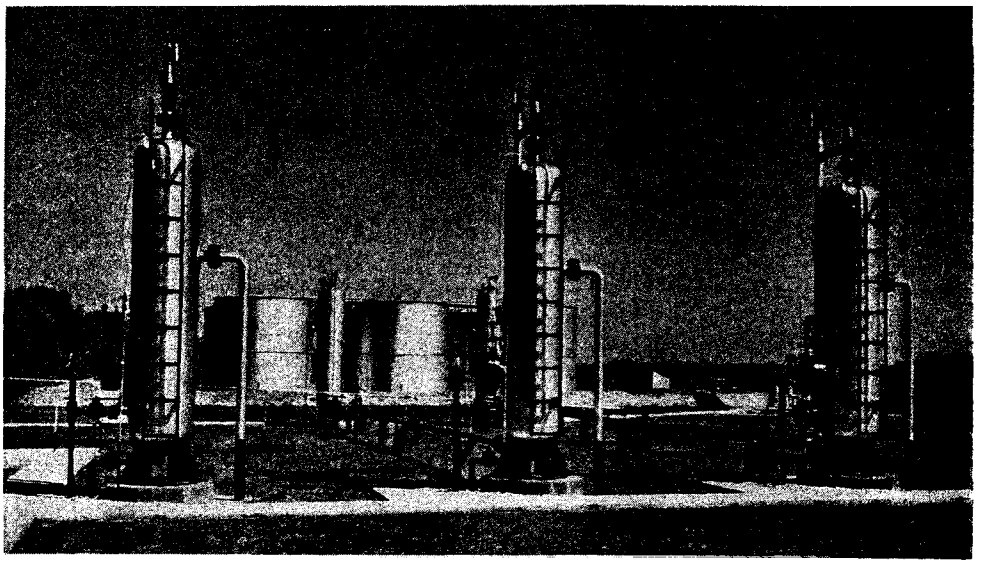

(b)

Fig. 13-3. (a) Field-separator installation. (*Courtesy National Tank Company.*)
(b) Field-separator installation. (*Courtesy Ohio Oil Company.*)

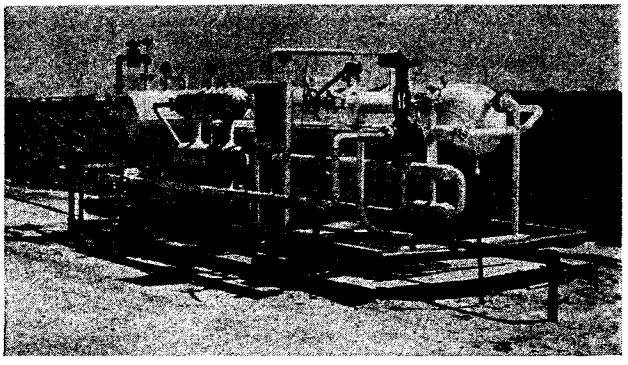

Fig. 13-4. Low-temperature field-separation installation. (*Courtesy National Tank Company and Oil Gas J.*)

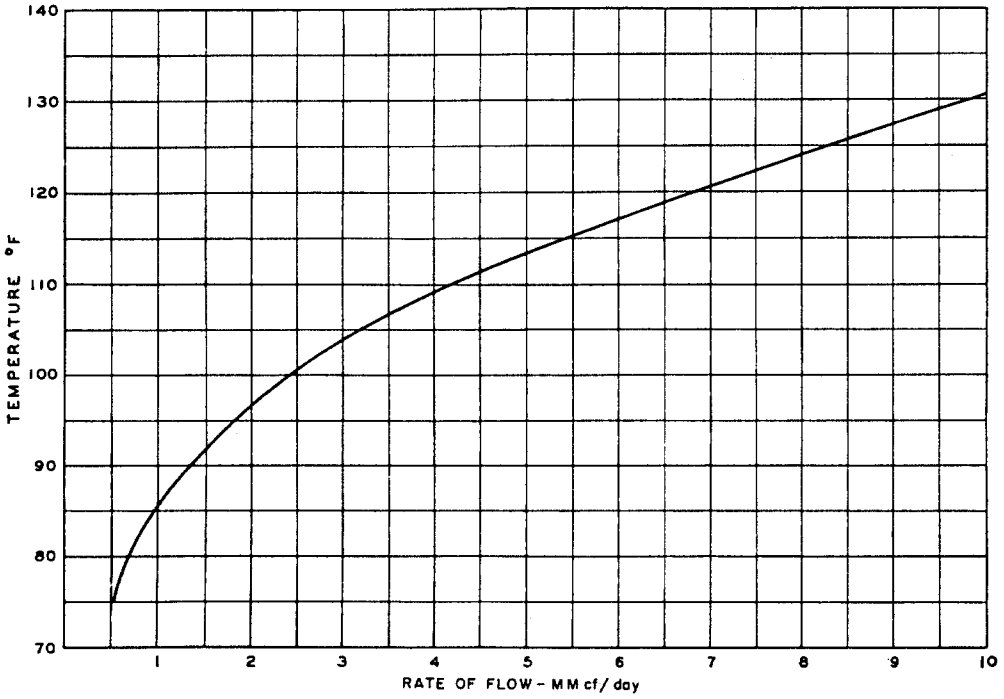

Fig. 13-5. Wellhead temperature as a function of flow rate for wells in southern Louisiana. (*Records and Seely, 5-66. Courtesy AIME.*)

tank can be computed (3-27, 13-34). Table 13-1 and Fig. 13-6 give an example calculation. The use of electronic computers for such calculations has been noted in Chap. 6.

The change in state of the fluid stream caused by the sudden reduction in pressure at valve 1 (Fig. 13-2) can be predicted. The effect produced by a sudden adiabatic pressure drop in which no work is done is termed a "free expansion" or Joule-Thomson expansion. It is clear that no useful work is done by the fluid, although the reduction in pressure is accompanied by a drop in temperature for pressures below some 5,000 psia (see Chap. 4). The amount of liquid present after the expansion can be computed by methods shown in Chap. 4. The use of enthalpy-entropy charts to find the temperature drop resulting

Table 13-1. Computation of Stage

Component	Well effluent mole fraction z	K at 115 psia and 60°F	Assume $V = 0.40$		Assume $V = 0.500$		Assume $V = 0.461$		1st separator mole fraction		K at 25 psia and 60°F	Assume $V = 0.119$		Assume $V = 0.145$	
			$K + 1.5$	$\frac{z}{K+1.5}$	$K + 1$	$\frac{z}{K+1}$	$K + 1.17$	$\frac{z}{K+1.17}$	Vapor	Liquid (new z)		$K + 7.4$	$\frac{z}{K+7.4}$	$K + 5.9$	$\frac{z}{K+5.9}$
Methane	0.303	30.0	31.5	0.0096	31.0	0.00976	31.17	0.00972	0.6158	0.0208	140	147.4	0.00014	145.9	0.00014
Ethane	0.131	3.7	5.2	0.0252	4.7	0.0279	4.87	0.0269	0.2150	0.0575	17.5	24.9	0.00231	23.4	0.00246
Propane	0.094	0.98	2.48	0.0379	1.98	0.0475	2.15	0.0437	0.0916	0.0936	4.2	11.6	0.00807	10.1	0.00927
Isobutane	0.018	0.400	1.90	0.0095	1.40	0.0129	1.57	0.0115	0.0098	0.0246	1.80	9.2	0.00267	7.7	0.00320
n-Butane	0.049	0.285	1.785	0.0272	1.285	0.0381	1.455	0.0336	0.0205	0.0720	1.30	8.7	0.00827	7.2	0.01000
Isopentane	0.020	0.120	1.62	0.0123	1.12	0.0179	1.29	0.0155	0.0398	0.0332	0.55	7.95	0.00418	6.45	0.00515
n-Pentane	0.025	0.094	1.594	0.0157	1.094	0.0228	1.264	0.0198	0.0040	0.0425	0.50	7.90	0.00538	6.40	0.00665
Hexanes	0.038	0.032	1.532	0.0248	1.032	0.0368	1.202	0.0316	0.0022	0.0677	0.131	7.531	0.00899	6.031	0.01122
Heptanes+	0.322	0.0022	1.5022	0.2140	1.0022	0.3210	1.1722	0.2745	0.0013	0.5881	0.0096	7.4096	0.07937	5.9096	0.09951
Total	1.000	.....	.....	0.3762	.....	0.5346	.....	0.4668	1.0000	1.0000	.....	.....	0.11938	.....	0.14760

Solution: $V = 0.45$

Solution:

$$\text{Density} = \frac{164.39}{202.2} = 0.813 \text{ gram/cu cm} \quad \text{at } 60°\text{F, 1 atm}$$

$$\equiv 42.6°\text{API}$$

$$\equiv 0.813 \times 350 = 284 \text{ lb/bbl}$$

Referring to Fig. 13-6 and the mole fractions vaporized in the three vaporizations, one can compute the moles of stock tank liquid per mole of inlet mixture to the first separator:

$$0.55 \times 0.881 \times 0.969 = 0.47 \text{ mole of liquid}$$

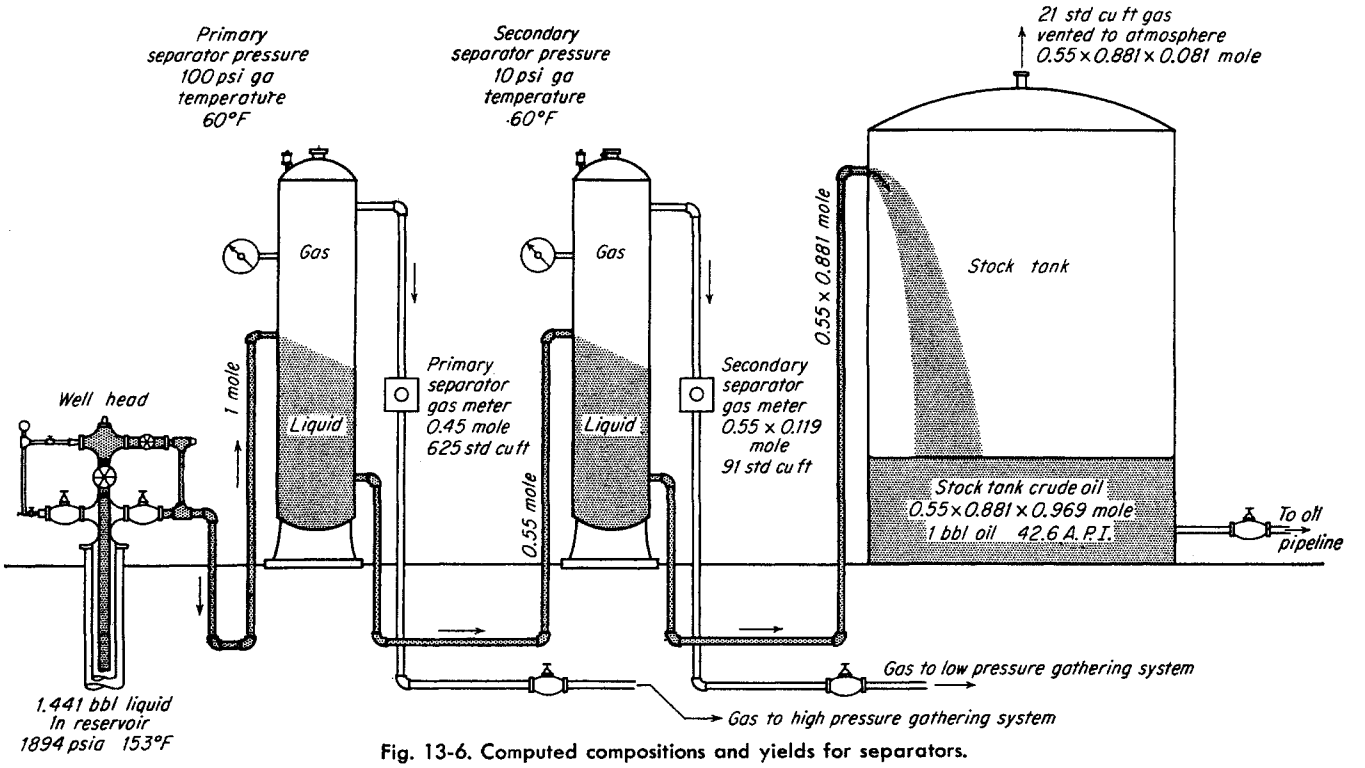

Fig. 13-6. Computed compositions and yields for separators.

from an expansion will give a value greater than the actual value when latent heat is evolved by liquid formation.

Separation of Condensate Fluids

The nature of gas-condensate systems and the nature of condensate reservoirs have been discussed; it was indicated that condensation in the well bore is attributed to simultaneous reduction of pressure and temperature on the fluid. One computation indicates that there is simultaneous two-phase flow of hydrocarbon liquid and gas through the porous medium to the well bore, which increases the liquid yield by 15 per cent (12-69). The variables to be considered

Separation from Analysis of Well Effluent

Assume $V = 0.10$		2d separator, mole fraction		K at 14.7 psia and 60°F	Assume $V = 0.0400$		Assume $V = 0.03571$		Assume $V = 0.0303$		Stock-tank fluid, mole fraction		Mol. wt	Liquid		
$K + 9.0$	$\frac{z}{K + 9.0}$	Vapor	Liquid (new z)		$K + 24$	$\frac{z}{K + 24}$	$K + 27$	$\frac{z}{K + 27}$	$K + 32$	$\frac{z}{K + 32}$	Vapor	Liquid		Grams/mole	Grams/cu cm	Cu cm/mole
149	0.00014	0.1692	0.00118	230	254	0.000004	257	0.00000	262	0.00000	0.0340	0.0001	16	0.0016	0.35	0.005
26.5	0.00217	0.3474	0.0193	29	53	0.000364	53	0.00036	61	0.000316	0.3000	0.0104	30	0.312	0.50	0.62
13.2	0.00708	0.2910	0.0676	6.2	30.2	0.002238	33.2	0.00203	38.2	0.001769	0.3600	0.0584	44	2.57	0.508	5.06
10.8	0.00227	0.0411	0.0223	3.2	27.2	0.000819	30.2	0.00074	35.2	0.000633	0.0665	0.0208	58	1.21	0.563	2.15
10.3	0.00699	0.0921	0.0692	2.2	26.2	0.002641	29.2	0.00236	34.2	0.002023	0.1462	0.0667	58	3.87	0.584	6.64
9.55	0.00348	0.0197	0.0350	0.94	24.94	0.001403	27.94	0.00125	32.94	0.001062	0.0330	0.0351	72	2.53	0.625	4.05
9.50	0.00448	0.0230	0.0450	0.72	24.72	0.001826	27.72	0.00162	32.72	0.001375	0.0327	0.0454	72	3.26	0.631	4.16
9.131	0.00742	0.0100	0.0753	0.22	24.22	0.003109	27.22	0.00276	32.22	0.002337	0.0170	0.0771	86	6.64	0.664	10.0
9.0096	0.06448	0.0065	0.6652	0.0138	24.0138	0.027704	27.0138	0.02462	32.0138	0.02078	0.0096	0.6860	210	144.00	0.850	169.5
	0.09851	1.0000	1.0000			0.040108		0.03574		0.030295	0.999	1.000		164.3936		202.185

$V = 0.119$ Solution: $V = 0.031$

Moles of fluid mixture to first separator per barrel of stock-tank liquid

$$\frac{284}{0.47 \times 164.4} = 3.67 \text{ moles}$$

Gas from separator I: $0.45 \times 3.67 \times 379 = 625$ cu ft

Gas from separator II: $0.55 \times 0.119 \times 3.67 \times 379 = 91$ cu ft

Gas from stock tank: $0.55 \times 0.881 \times 0.031 \times 3.67 \times 379 = 21$ cu ft

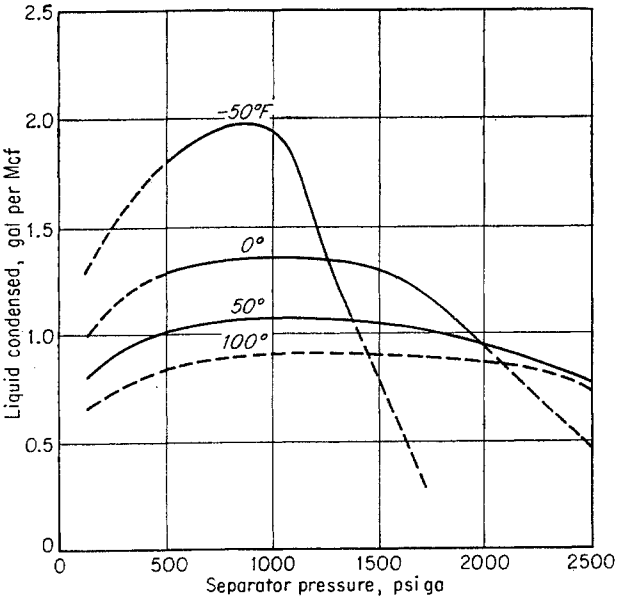

Fig. 13-7. Effect of separation temperature on gross liquid yield at various pressures. (*Buckley and Lightfoot*, 3-11. *Courtesy AIME.*)

in achieving the optimum recovery of liquid hydrocarbons from natural gas–condensate systems are substantially the same as the variables for natural gas–crude oil systems, but the optimum conditions of separation are much more peculiar to the particular mixture. The optimum conditions for separation may be determined by trial-and-error testing in the field or by computations based on equilibrium constants.

Huntington et al. (13-18, 13-30), Buckley and Lightfoot (3-11), and Eilerts et al. (3-19) made field studies of the factors influencing the yield of condensate from gas-condensate wells. The primary separator pressure was varied at constant temperature to demonstrate the existence of an optimum condensation in the primary separator temperatures. The composition of the gas phase as reflected by its specific gravity undergoes a minimum at the pressure of maximum liquid condensation.

Buckley and Lightfoot (3-11) made a study of the effect of pressure and temperature on the condensation of distillate from natural gas using an experimental field-separation unit. Table 13-2 gives the phase compositions for various separator conditions. Figure 3-26 gives the phase diagram for the well stream and Table 3-1 the well-stream composition based on the vapor and liquid compositions at 1,000 psia and 77°F. Figure 13-7 shows the separator yields for the well. The behavior shown is characteristic of fluid systems that show both isobaric and isothermal retrograde condensation. A phase diagram of this type by Eilerts et al. is presented in Fig. 12-46. Large amounts of methane, ethane, and propane are still dissolved in the high-pressure condensate from separators at high pressure. If this condensate is stabilized by stagewise reduction of pressure on the liquid phase, considerable shrinkage of the primary stage separator liquid takes place. The higher the primary separator pressure, the greater will be the shrinkage. Barry and Parks (13-3) show (Fig. 13-8) that the pressure of

Table 13-2. Hydrocarbon Analyses of Equilibrium Gas and Liquid Samples

Operating pressure, psig	500				1,000						1,500					
Temperature, °F	−47		−17	80	−42		12		77		−15		38		81	
Sample	Gas	Liquid	Gas	Gas	Gas	Liquid	Gas	Liquid	Gas	Liquid	Gas	Liquid	Gas	Liquid	Gas	Liquid
Mole percentage:																
Methane	96.8	22.86	96.3	.....	96.7	47.02	96.4	31.41	95.5	24.90	96.6	48.65	96.7	39.21	95.3	33.38
Ethane	2.54	7.62	2.59	98.8	2.49	8.90	2.41	5.12	2.63	3.95	1.90	3.80	2.04	5.35	2.71	4.65
Propane	0.49	8.85	0.70	.....	0.37	7.51	0.76	6.75	0.85	3.60	0.80	6.32	0.73	4.44	0.93	3.57
Isobutane	0.067	2.82	0.192	0.385	0.157	3.42	0.044	2.47	0.251	1.57	0.086	1.68	0.028	1.69	0.226	1.38
n-Butane	0.064	6.40	0.143	0.298	0.143	3.83	0.121	5.13	0.303	2.70	0.235	2.57	0.080	2.55	0.352	2.00
Isopentane	0.021	3.49	0.052	0.184	0.051	2.46	0.096	3.67	0.148	2.55	0.115	2.38	0.118	2.12	0.161	2.00
n-Pentane	0.003	3.46	0.011	0.078	0.020	1.86	0.036	1.74	0.059	1.61	0.064	0.96	0.071	1.60	0.063	1.17
Hexanes	.....	7.31	0.019	0.179	0.030	3.91	0.067	6.60	0.148	6.57	0.133	4.25	0.134	5.28	0.185	4.95
Heptanes	.....	8.06	.....	.....	.....	4.90	.....	8.59	.....	7.43	.....	5.70	.....	6.08	.....	6.18
Octanes	.....	4.99	.....	.....	.....	3.24	.....	4.15	.....	7.01	.....	3.67	.....	4.13	.....	5.71
Nonanes	.....	4.24	.....	.....	.....	1.96	.....	4.85	.....	6.22	.....	3.55	.....	5.14	.....	5.46
Heavier	0.008	19.90	0.007	0.037	0.013	10.99	0.022	19.52	0.071	31.89	0.060	16.47	0.083	22.41	0.091	29.55
Molecular weight	.....	182	.....	.....	.....	178	.....	175	.....	184	.....	176	.....	176	.....	181
Density at 60°F, grams/cu cm	.....	0.8124	.....	.....	.....	0.8094	.....	0.8106	.....	0.8119	.....	0.8102	.....	0.8099	.....	0.8120

SOURCE: Buckley and Lightfoot (3-11).

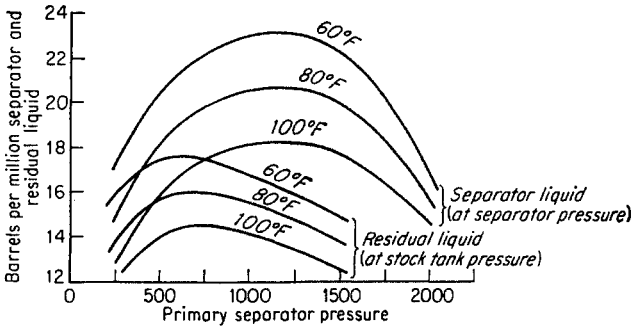

Fig. 13-8. Optimum pressure for maximum ultimate recovery of residual liquid is lower than the pressure for maximum separator liquid. (*Barry and Parks*, 13-3. *Courtesy World Oil.*)

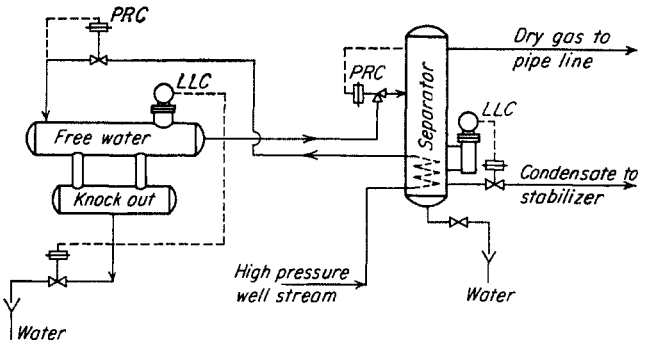

Fig. 13-9. Flow diagram for expansion-refrigeration system. (*Campbell and Laurence*, 13-5. *Courtesy Petrol. Refiner.*)

maximum condensation in the primary separator at separator pressure *does not* give the maximum ultimate recovery of hydrocarbons. The optimum separator pressure occurs considerably lower than the pressure of maximum condensation in the primary separator. However, the primary separator pressure chosen may be dictated by other factors, such as recompression cost and hydrate formation. The lower limits of pressure to which gases may be expanded without hydrate formation are presented in Figs. 5-48 to 5-50.

Barry and Parks recommend removal of the free water just prior to the first-stage pressure reduction (Fig. 13-2) in order to take advantage of the low water content of the high-pressure gas. Automatic controls are incorporated in stage separation units to control the stage pressures and the liquid levels.

Expansion-refrigeration Systems

The expansion-refrigeration system uses the Joule-Thomson effect to increase the recovery of condensate and at the same time lower the water content of the gas. When high wellhead pressures permit, hydrocarbon hydrates are intentionally formed to dehydrate the gas in accordance with the low-temperature gas-solid hydrate equilibrium relations (5-66, 13-40, 13-6). The temperatures that may be achieved through refrigeration by expansion also permit a considerable increase in the recovery of natural gasoline.

Figure 13-9 presents the flow diagram of one variation of the scheme used for an expansion-refrigeration system (13-5). The high-pressure well stream enters the heat-exchanger coil in the bottom of the low-temperature separator, where it exchanges heat with the solid hydrates and cold liquids. The cooled gas stream passes through the regenerative heat exchanger where it is further cooled (when permissible from hydrate formation standpoint) by countercurrent heat exchange with the cold-separator off-gas. Any water that has been condensed in the cooling process is removed in the free-water separator. From the water separator the stream passes through a pressure-reducing separator where the Joule-Thomson expansion occurs. The gas that is separated from the liquid and solids by gravity difference leaves the top of the separator. A temperature controller is set up so as to permit part of the cold dehydrated gas to bypass the regenerative heat exchanger when all the available refrigeration is not needed. The liquid condensate and water are removed through separate outlets from the bottom of the hydrate separator. The liquid hydrocarbons may be sent to storage or recombined with the dehydrated gas. Optimum location for the introduction of condensate in the stock tank should be such that the flash gas from the separator is not allowed to strip hydrocarbons from the stock tank.

Records and Seely reported the operation of a separator in which hydrates form when the gas is expanded (Fig. 13-10). The temperature drop with

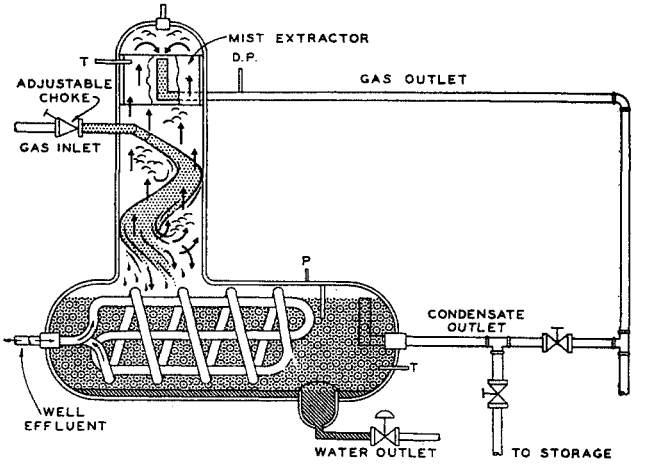

Fig. 13-10. Hydrate separators. (*Records and Seely, 5-66. Courtesy AIME.*)

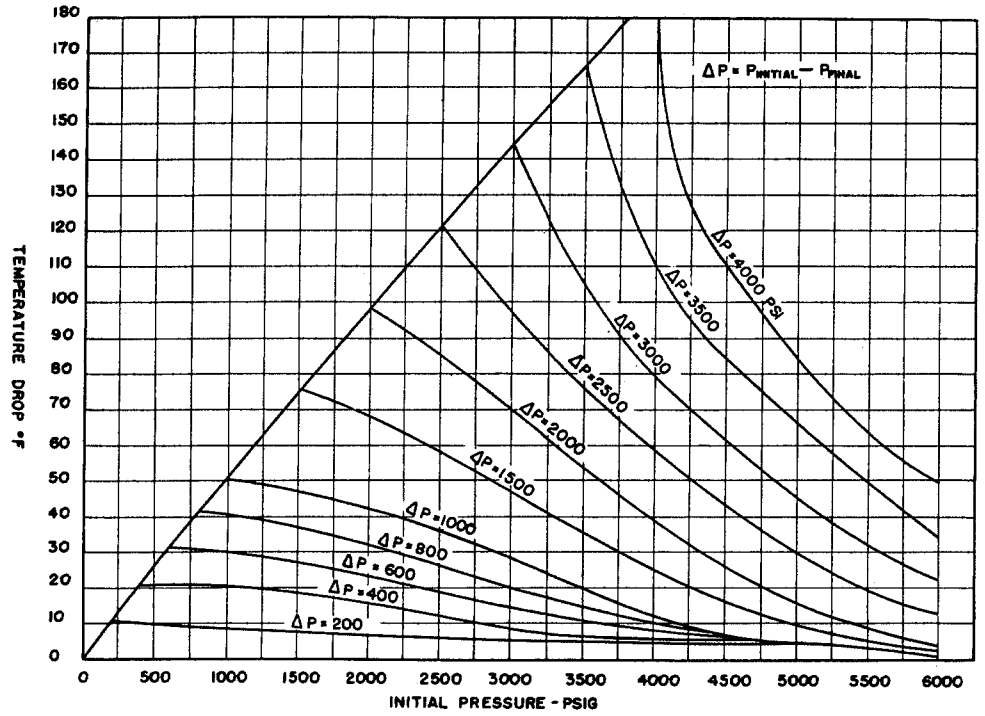

Fig. 13-11. Temperature drop accompanying pressure drop on expansion of a 0.64 gravity natural gas. (*Records and Seely, 5-66. Courtesy AIME.*)

Table 13-2a. Analysis of Well Effluent*

Component	*Mole %*
Carbon dioxide	0.20
Methane	92.80
Ethane	3.47
Propane	1.16
Isobutane	0.39
n-Butane	0.35
Isopentane	0.14
n-Pentane	0.11
Hexanes+	1.38
	100.00

* Gas gravity = 0.64.
SOURCE: Records and Seely (5-66).

expansion is given by Fig. 13-11. The gas composition used in these tests is given in Table 13-2*a* and the moisture-content curves in Fig. 13-12. To find the moisture content of the exit gas in Fig. 13-12, start with the separator inlet pressure and follow up the lines until the inlet temperature is reached. From this point read vertically to the hydrate-separator-pressure lines and the water-content scale. For example, a wellhead gas at 3,000 psig and 100°F will have 9.5 lb of water per MMcf of gas for a 1,000-psig separator pressure.

The difference between the water-dew-point temperatures and the hydrate-separator temperatures is given in Fig. 5-10. The dew-point temperatures are lower than the separator temperatures because the water dew point is a metastable water-gas equilibrium rather than a gas-hydrate equilibrium (see Chap. 5).

Usually, the desired water-content specification for pipeline gas is 6 to 8 lb of water per MMcf of gas at 60°F and 14.7 psia. With sufficient wellhead pressure the operating conditions can be adjusted to fulfill this requirement. The low-temperature dehydration process is continuous and limited only by the pressure drop available for the process. However, unusual cases of wax formation may hinder its operation. Campbell (13-6) gives the following summary of operating characteristics for the expansion-refrigeration system:

Recommended Operating Range

Where available pressure drop is sufficient to give a dew-point depression comparable to the other systems. The necessary drop is usually about 1,500 pounds per square inch gauge. A wide range of temperatures may be handled by suitable modification of the equipment with the necessary heat-exchange requirements.

Advantages

1. Usually the least expensive system where a pressure drop is necessary in a process anyway.
2. Increased revenue from most natural gas systems with the increased condensate recovery.
3. Low dew points when sufficient pressure drop is available.
4. Simple automatic operation requiring minimum attendance.

Disadvantages

1. Restricted to those applications where a large pressure drop is available.

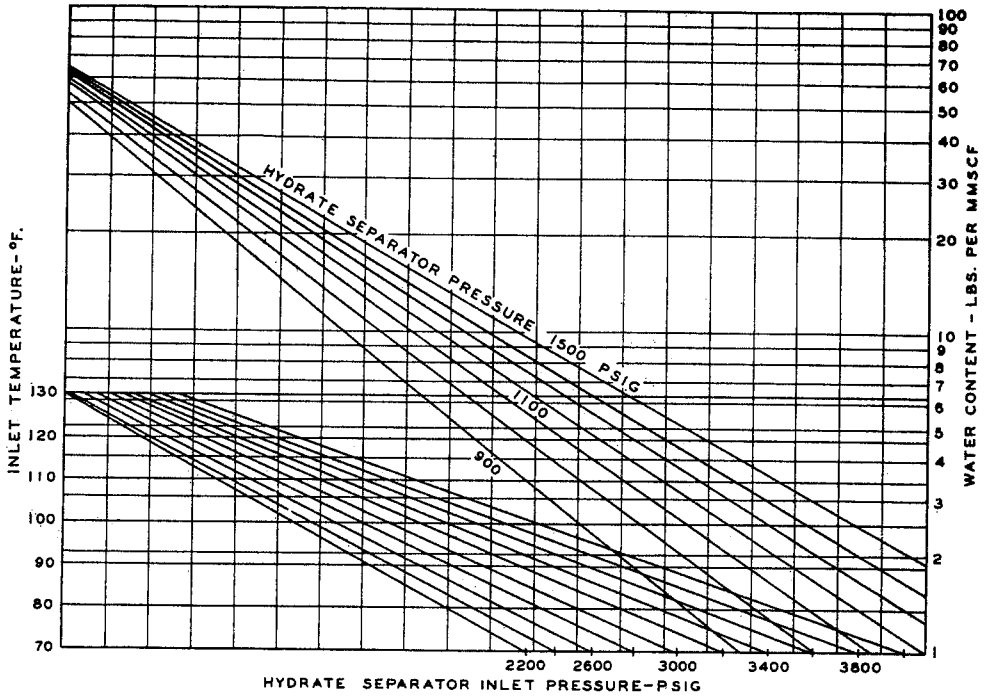

Fig. 13-12. Low-temperature dehydrator performance curves, based on 0.64 specific gravity gas. (*Records and Seely, 5-66. Courtesy AIME.*)

2. Effectiveness lost if pressures decline. In this case it must be supplemented by other equipment.

3. Danger of low-carbon-steel embrittlement and equipment failure if operated below −20°F.

4. Close control often necessary to prevent formation of hydrates prior to the low-temperature separator.

Low-temperature separation cannot usually be justified when used solely for gas dehydration.

Expansion-refrigeration Systems with Liquid Desiccant

The expansion-refrigeration process discussed in the previous section may be modified by the injection of 70 to 80 wt % solution of diethylene glycol into the fluid stream just ahead of the regenerative heat exchanger. This modification is applicable where well pressures are expected to vary appreciably or where not enough pressure is available to produce the necessary dehydration by expansion alone. A flow sheet for the expansion-refrigeration system as modified for glycol injection is presented in Fig. 13-13 (13-6).

The process shown is similar to the expansion-refrigeration process with regenerative heat exchange. The modifications consist of injection of glycol into the main gas stream just following the water knock-

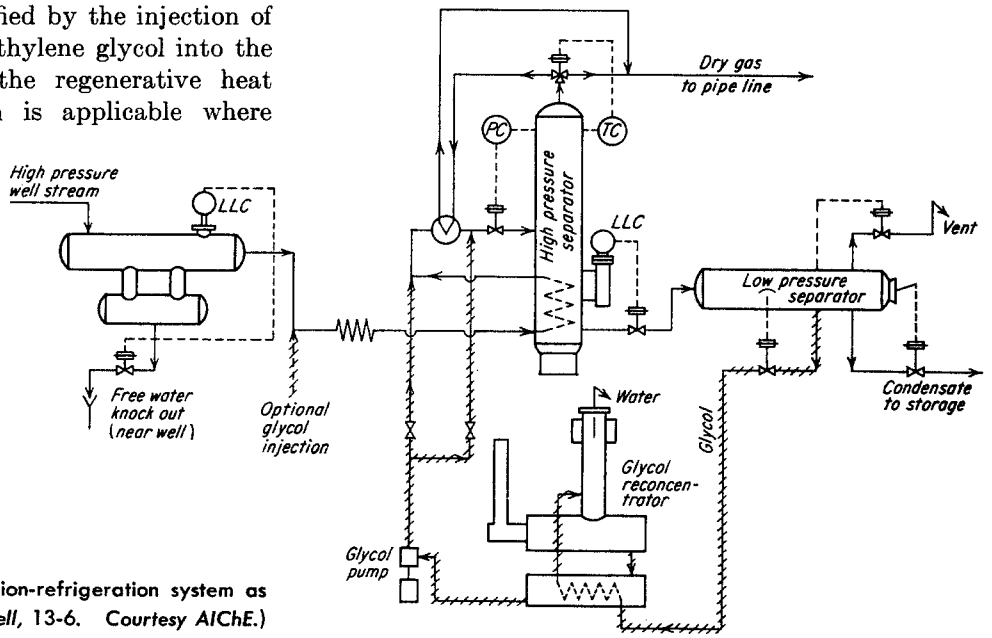

Fig. 13-13. Flow diagram for expansion-refrigeration system as modified for glycol injection. (*Campbell, 13-6. Courtesy AIChE.*)

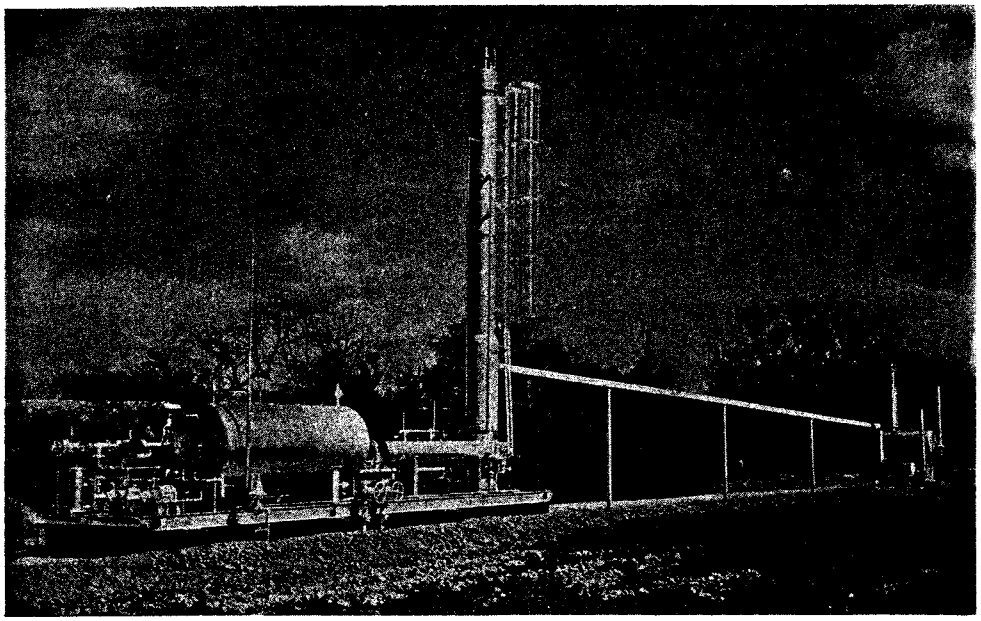

Fig. 13-13a. Well separator using hydrate inhibitor. (*Courtesy Black, Sivalls, and Bryson, Inc.*)

out separator and addition of a gas-glycol-condensate separator and of a glycol concentrator. A heater is customarily placed just before the gas-glycol-condensate separator so that the separation may be conducted at about 70°F to produce a relatively stable condensate.

The amount of glycol necessary depends on the pressure drop available and the water content specified. Additional factors to be considered in the choice of desiccant are the losses due to vaporization and to solubility in the hydrocarbon liquid.

The extent of glycol losses through vaporization (13-29, 13-32) and through solubility have been evaluated. Diethylene glycol is being used most widely as the desiccant in the presence of liquid hydrocarbons because of its relatively low vapor pressure and low solubility in the condensate. Large-scale dehydration and the economics of dehydration by several methods will be discussed in the section on gas dehydration. A summary of operating characteristics for the glycol-injection system is given by Campbell (13-6):

RATE OF INJECTION

Normal rate 0.2 to 0.4 gal glycol per 1,000,000 std cu ft/hr of gas passed.

TYPE OF GLYCOL RECOMMENDED

A 70 to 85 per cent solution of diethylene glycol. For such a solution the concentration of glycol in the hydrocarbon liquid recovered theoretically should not exceed 0.04 per cent by weight.

ADVANTAGES

1. Effective at lower pressure differentials since it gives dew-point depressions over and above those obtained by refrigeration alone.
2. High recoveries of natural gas condensate possible.
3. A compact unit with high salvage value.
4. Stabilization of the recovered liquid less expensive since this liquid is colder than that from a comparatively low-temperature separation system.
5. For flow rates above 17,000,000 cu ft/day, initial cost less than that for a low-temperature-separation unit.

DISADVANTAGES

1. Higher initial investment than the glycol absorption unit at rates less than 17,000,000 cu ft/day.
2. Slightly greater operating and maintenance cost than a low-temperature-separation system.
3. Return of glycol solution to injection point. The total quantity involved, however, is small.

Many gases are produced at insufficient pressure to permit processing for hydrocarbon recovery or dehydration by individual-well separation units. The propane-and-butane content may be high enough to warrant its recovery. Gases collected in connection with the production of crude oil are processed. The usual natural gasoline plant takes these gases and processes them to recover liquefiable hydrocarbons. The basic unit in the gasoline plant is the oil absorber, which removes the desired constituents from the field gas stream.

ABSORPTION AND STRIPPING

The absorption-stripping cycle for the recovery of liquefied petroleum (LP) gases and natural gasoline (Fig. 13-14) is widely used in the industry. The

desired constituents are removed from the gas in the absorber and separated from the absorbing medium in the stripper. A primary problem is the presence of methane and ethane in the rich oil, which makes it difficult to achieve complete separation between those hydrocarbons intended to be recovered as liquids and those expected to remain as part of the dry fuel gas.

Absorption is the countercurrent contacting of gas and liquid-solvent streams in multistage equipment, usually bubble-plate columns. Conventional absorption applies the physical principle that different gases have different solubilities in solvents. Absorption is used in place of distillation in order to accomplish the separation without lowering the temperature until the dry gas is at its hydrocarbon dew point at the column conditions. The usual natural gasoline absorber employs a relatively narrow-boiling gas-oil fraction boiling in the range of 400 to 600°F. The primary process taking place in an absorber is intimate contact of the phases, which results from bubbling the gas through the liquid to approach equilibrium.

For a given gas, the mole fraction of each component originally in the rich gas that is absorbed by the oil is a function of the equilibrium phase relation between the gas constituents and the absorber oil, of the ratio of liquid flow to gas flow, and of the number of equilibrium-contact stages. The equilibrium phase relation is, in turn, primarily a function of temperature and pressure, but is also influenced by phase compositions and the aromaticity of the solvent (6-31).

Since the oil that has been added to facilitate the recovery of light hydrocarbons is not desired in the final product, the light hydrocarbons are separated from the oil by the process called "stripping," which is the reverse of absorption. Figure 13-14 shows the absorption-stripping cycle and the nomenclature to be used in subsequent discussions. The stages enumerated refer to equilibrium or *ideal stages* and not to the actual stages in the column. The equilibrium or ideal stage is a hypothetical stage for which the vapor leaving the stage is in equilibrium with the liquid leaving the same stage.

The stripping of the hydrocarbons is facilitated by using low pressures and high temperatures and by injecting open steam into the bottom of the stripper. Equilibrium phase relationships show that low pressure and high temperature decrease the solubility of the light hydrocarbons in the absorber oil. The steam serves to lower the partial pressure of the light hydrocarbons in the gas phase, which is equivalent to lowering the effective pressure of the stripping operation. The steam also serves to hasten the approach of the system to equilibrium.

The objective of the following section is to treat

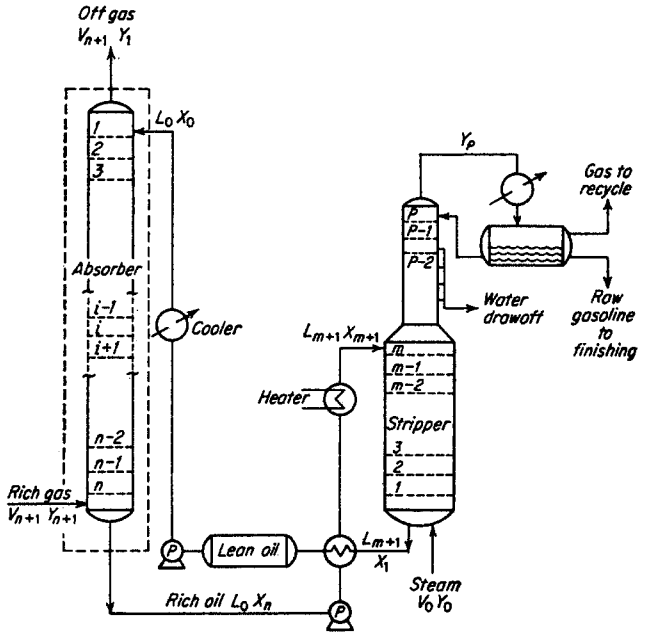

Fig. 13-14. Flow diagram for absorption and stripping.

several types of absorption-stripping calculations, in increasing order of rigor, and to point to the reason why simpler procedures fail to predict accurately the absorption or stripping carried out under actual operating conditions. All the calculations are based on the hypothetical equilibrium stage, which is to be distinguished from an actual contact stage. This concept permits the use of vaporization-equilibrium constants discussed in Chap. 6.

The stripping operation is essentially the reverse of absorption. Reflux is provided in the stripping column (Fig. 13-14) to reduce the loss of the absorber oil in the overhead product. Otherwise, the operation of the absorber and the operation of the stripper are sufficiently similar to permit parallel analytical treatment.

Kremser-Brown Absorption-factor Procedure

The Kremser-Brown absorption-factor procedure is the name given to the Souders-Brown (13-38, 13-4) modification of Kremser's theoretical analysis of the absorption process (13-26). It is an analytical method which relates the fraction of a component absorbed (or stripped) to the number of equilibrium plates or stages, to the liquid-gas ratio, and to the equilibrium-vaporization ratio of that component. The effects of pressure, temperature, and composition of the gas and liquid phases on the equilibrium-vaporization ratio have been covered in a previous section.

The derivation of the Souders-Brown modification of Kremser's analysis is as follows (7-9, 13-12).

The material balance around any plate i of an n-plate absorber is given by Eq. (13-1) and Fig. 13-14.

$$L_0(X_i - X_{i-1}) = V_{n+1}(Y_{i+1} - Y_i) \quad (13\text{-}1)$$

where L_0 = moles of lean oil entering absorber
V_{n+1} = moles of rich gas entering absorber
X_i = moles of component in liquid leaving plate i per mole of lean oil entering absorber
Y_i = moles of component in vapor from plate i per mole of rich gas entering absorber
X_{i-1} = moles of component in liquid to plate i per mole of lean oil entering absorber
Y_{i+1} = moles of component in vapor from plate $i + 1$ (or to plate i) per mole of rich gas entering absorber

The actual mole fractions of the vapor and liquid leaving plate i are, respectively,

$$y_i = \frac{Y_i V_{n+1}}{V_i} \quad (13\text{-}2)$$

$$x_i = \frac{X_i L_0}{L_i} \quad (13\text{-}3)$$

where y_i = mole fraction of component in vapor leaving plate i
x_i = mole fraction of component in liquid leaving plate i
V_i = moles of vapor leaving plate i
L_i = moles of liquid leaving plate i

Introducing the vaporization-equilibrium constant K_i by combining the definition

$$y_i = K_i x_i \quad (13\text{-}4)$$

with Eqs. (13-2) and (13-3) gives

$$Y_i = K_i \frac{L_0}{L_i} \frac{V_i}{V_{n+1}} X_i \quad (13\text{-}5)$$

Substituting in Eq. (13-1) for X_i and X_{i-1} from Eq. (13-5),

$$Y_i = \frac{Y_{i+1} + (L_{i-1}/K_{i-1}V_{i-1})Y_{i-1}}{1 + L_i/K_i V_i} \quad (13\text{-}6)$$

The absorption factor A is defined as

$$A_i = \frac{L_i}{K_i V_i} \qquad A_{i-1} = \frac{L_{i-1}}{K_{i-1}V_{i-1}} \quad (13\text{-}7)$$

Substituting (13-7) in (13-6),

$$Y_i = \frac{Y_{i+1} + A_{i-1}Y_{i-1}}{1 + A_i} \quad (13\text{-}8)$$

For a one-plate absorber, $i = 1$ and Eq. (13-8) becomes

$$Y_1 = \frac{Y_2 + A_0 Y_0}{1 + A_1} \quad (13\text{-}9)$$

where Y_2 = moles of a component in entering rich gas per mole of entering rich gas
Y_0 = moles of a component in gas in equilibrium with entering lean oil per mole of entering rich gas = 0 for all constituents absent from lean oil
A_0, A_1 = absorption factors for hypothetical plates 0 and 1, respectively

Using Eq. (13-5) by setting $i = 0$,

$$Y_0 = K_0 \frac{L_0}{L_0} \frac{V_0}{V_{n+1}} X_0 \quad (13\text{-}10)$$

or

$$A_0 Y_0 = \frac{L_0 X_0}{V_{n+1}} \quad (13\text{-}11)$$

Using Eq. (13-11) to eliminate A_0Y_0 from Eq. (13-9),

$$Y_1 = \frac{Y_2 + L_0X_0/V_{n+1}}{1 + A_1} \quad (13\text{-}12)$$

is obtained. The vapors from the second plate may be determined by applying Eq. (13-8) to give

$$Y_2 = \frac{Y_3 + A_1 Y_1}{1 + A_2} \quad (13\text{-}13)$$

Eliminating Y_1 and solving for Y_2 from Eqs. (13-12) and (13-13) extends the relationship (13-9) to a two-plate absorber:

$$Y_2 = \frac{(A_1 + 1)Y_3 + A_1L_0X_0/V_{n+1}}{A_1A_2 + A_2 + 1} \quad (13\text{-}14)$$

Similarly, for a three-plate absorber,

$$Y_3 = \frac{(A_1A_2 + A_2 + 1)Y_4 + A_1A_2L_0X_0/V_{n+1}}{A_1A_2A_3 + A_2A_3 + A_3 + 1} \quad (13\text{-}15)$$

In general, the composition of a given component in the gas phase from the nth plate may be related to the absorption factor for that component on each plate, the lean-oil rate, lean-oil composition for that component, and the rich-gas rate by

$$Y_n = \frac{\begin{array}{r}(A_1A_2A_3 \cdots A_{n-1} + A_2A_3 \cdots A_{n-1} \\ + \cdots + A_{n-1} + 1)Y_{n+1} \\ + A_1A_2 \cdots A_{n-1}L_0X_0/V_{n+1}\end{array}}{\begin{array}{r}A_1A_2A_3 \cdots A_n + A_2A_3 \cdots A_n \\ + \cdots + A_n + 1\end{array}} \quad (13\text{-}16)$$

Since it is more convenient to relate the external vapor compositions, the equation

$$L_0(X_n - X_0) = V_{n+1}(Y_{n+1} - Y_1) \quad (13\text{-}16a)$$

is combined with the equation

$$X_n = \frac{L_n V_{n+1}}{K_n L_0 V_n} Y_n \qquad (13\text{-}16b)$$

to yield

$$Y_n = \frac{Y_{n+1} - Y_1 + L_0 X_0 / V_{n+1}}{A_n} \qquad (13\text{-}17)$$

Equation (13-17) is used to eliminate Y_n in Eq. (13-16) and introduce a terminal composition Y_{n+1}, giving

$$\frac{Y_{n+1} - Y_1}{Y_{n+1}} = \frac{A_1A_2A_3 \cdots A_n + A_2A_3 \cdots A_n + \cdots + A_n}{A_1A_2A_3 \cdots A_n + A_2A_3 \cdots A_n + \cdots + A_n + 1} - \left(\frac{L_0X_0}{V_{n+1}Y_{n+1}}\right)\left(\frac{A_2A_3 \cdots A_n + A_3A_4 \cdots A_n + \cdots + A_n + 1}{A_1A_2A_3 \cdots A_n + A_2A_3 \cdots A_n + \cdots + A_n + 1}\right) \qquad (13\text{-}18)$$

It should be noted that the left-hand member of Eq. (13-18) represents the fraction of a component in the rich gas that is absorbed if the lean oil has been completely regenerated with respect to that component. Equation (13-18), though completely rigorous, does not lend itself simply to application without further simplification. The corresponding equation for stripping may be written as

$$\frac{X_{m+1} - X_1}{X_{m+1}} = \frac{S_1S_2S_3 \cdots S_m + S_2S_3 \cdots S_m + \cdots + S_m}{S_1S_2S_3 \cdots S_m + S_2S_3 \cdots S_m + \cdots + S_m + 1} - \left(\frac{V_0Y_0}{L_{m+1}X_{m+1}}\right)\left(\frac{S_2S_3 \cdots S_m + S_3 \cdots S_m + \cdots + S_m + 1}{S_1S_2S_3 \cdots S_m + S_2S_3 \cdots S_m + \cdots + S_m + 1}\right) \qquad (13\text{-}19)$$

where the "stripping factor" is given by

$$S_j = \frac{K_j V_j}{L_j} \qquad (13\text{-}20)$$

and where X_1 = moles of component in stripped lean oil leaving bottom of stripper per mole of rich oil entering absorber
X_{m+1} = moles of component in rich oil entering stripping section per mole of rich oil entering stripper
L_{m+1} = moles of rich oil entering stripper
V_0 = moles of stripping medium, usually steam, entering stripper
Y_0 = moles of component in stripping medium per mole of stripping medium entering stripper

To simplify Eq. (13-18), it is assumed that the absorption factor for each plate is constant and that it is possible to estimate this average value of A. Under these conditions,

$$\frac{Y_{n+1} - Y_1}{Y_{n+1}} = \frac{A^{n+1} - A}{A^{n+1} - 1} - \frac{Y_0}{Y_{n+1}} \frac{A^{n+1} - A}{A^{n+1} - 1} \qquad (13\text{-}21)$$

since $$\frac{A^{n+1} - A}{A - 1} = A^n + A^{n-1} + \cdots + A^2 + A \qquad (13\text{-}22)$$

and $$\frac{A^{n+1} - 1}{A - 1} = A^n + A^{n-1} + \cdots + A^2 + A + 1 \qquad (13\text{-}23)$$

Rearranging,

$$\frac{Y_{n+1} - Y_1}{Y_{n+1} - Y_0} = \frac{A^{n+1} - A}{A^{n+1} - 1} \qquad (13\text{-}24)$$

where A = average absorption factor
Y_1 and Y_{n+1} have been previously defined
Y_0 = moles of a component in vapor in equilibrium with lean oil per mole of entering wet gas
n = number of theoretical equilibrium stages in absorber

Since $Y_{n+1} - Y_1$ = moles of component absorbed per mole of entering gas, and $Y_{n+1} - Y_0$ = number of moles that would be absorbed if it were possible to bring the gas leaving into equilibrium with the entering liquid, the left-hand quotient of Eq. (13-24) represents the fraction of a component absorbed when passed through an n-plate absorber.

The corresponding equation for the stripping section of the stripping column is

$$\frac{X_{m+1} - X_1}{X_{m+1} - X_0} = \frac{S^{m+1} - S}{S^{m+1} - 1} \qquad (13\text{-}25)$$

where S = average stripping factor = KV/L
X_1, X_{m+1} have been previously defined
X_0 = moles of component in liquid in equilibrium with stripping medium per mole of entering rich oil
m = number of theoretical equilibrium stages in stripping portion of stripping column

Graphic solutions of Eqs. (13-24) and (13-25) may be shown by a family of curves as indicated in Figs. 13-15 and 13-16. The advantage of the Kremser-Brown procedure is its simplicity.

Illustrative Problem

A natural gas of the following composition is to be extracted with a 210 molecular weight 44°API gas oil at 200 psia and 90°F. Find the amount of each constituent extracted for an oil rate of 20 gal per Mcf of gas at 60°F and 14.7 psia when eight equilibrium stages are used.

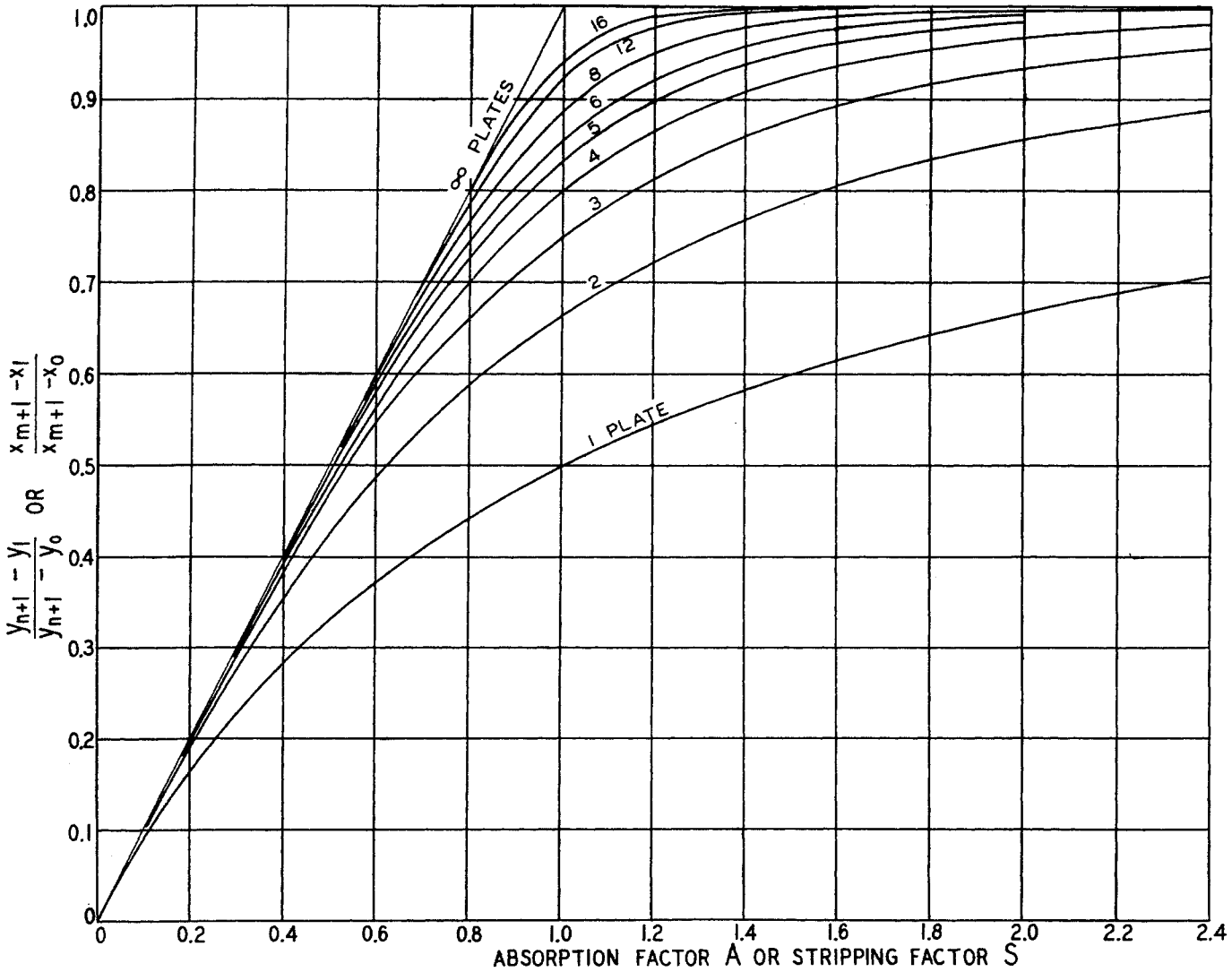

Fig. 13-15. Solution to absorption-factor and stripping-factor equation. (*Souders and Brown, 13-38. Courtesy Ind. Eng. Chem.*)

Solution

Component	Mole fraction	K at 90°F, 200 psia	$A = \frac{0.243^*}{K}$	% absorbed†	Gallons per Mcf‡	
					Absorbed	Remain in gas
Methane.....	0.8319	18.2	0.0133	1.33		
Ethane.....	0.0848	2.85	0.085	8.5		
Propane.....	0.0437	0.85	0.286	28.6	0.35	0.87
Isobutane....	0.0076	0.375	0.648	64	0.164	0.092
n-Butane.....	0.0168	0.282	0.861	81	0.441	0.104
Isopentane....	0.0057	0.131	1.85	99.6	0.207	0.001
n-Pentane....	0.0032	0.105	2.31	99.9	0.115	0.000
Hexanes.....	0.0063	0.038	6.40	99.9+	0.260	0.000

* $A = \frac{L}{KV}$ $\quad L = \frac{20 \times 8.33 \times 0.8063}{210} = 0.64$ mole

$V = \frac{1{,}000}{379} = 2.64$ moles

$\frac{L}{V} = 0.243$

† From Fig. 13-15.

‡ Cubic feet of vapor per gallon of liquid from Table A-1.

The shortcomings of this procedure are that the temperature is not constant and that the L/V varies as a result of the absorbed constituents entering the liquid phase.

The first difference of Eq. (13-24) [or (13-25)] with respect to the number n (or m) of trays gives the increase in fraction absorbed (or stripped) for a given increase in the theoretical trays. Figures 13-17 and 13-18 show curves of increase in the fraction absorbed (or stripped) as a function of absorption (or stripping) factor, and indicate the presence of a relative maximum for every value of the initial number of theoretical trays. Where the initial number of theoretical trays is greater than 2, the location of the relative maximum is in the neighborhood of A (or S) = 1.0. The marginal effects of adding theoretical trays to an absorber already possessing a large number of theoretical trays is evident from Fig. 13-18.

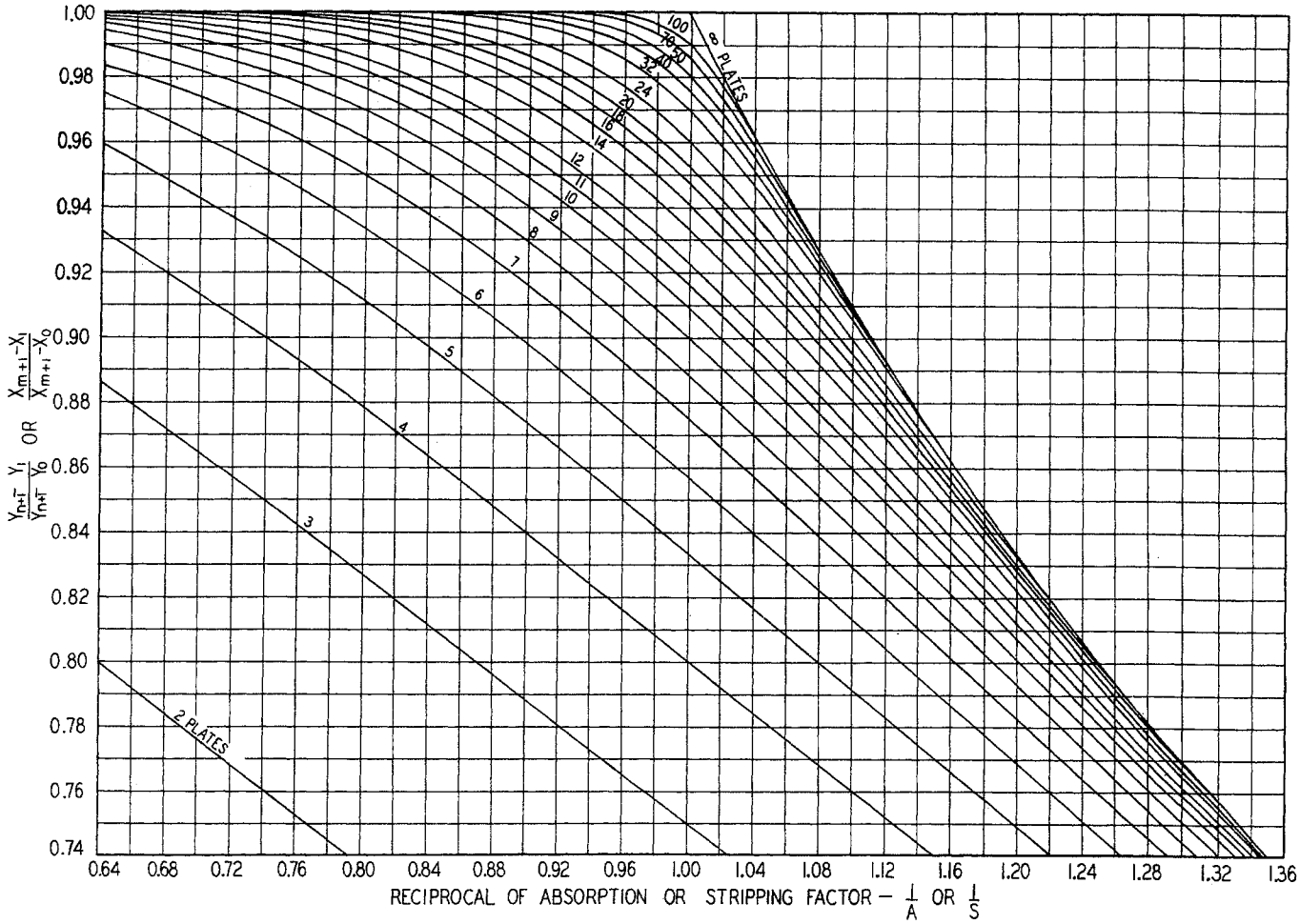

Fig. 13-16. Solution to absorption-factor and stripping-factor equation. (*Brown and Souders, 13-4. Courtesy Oxford University Press.*)

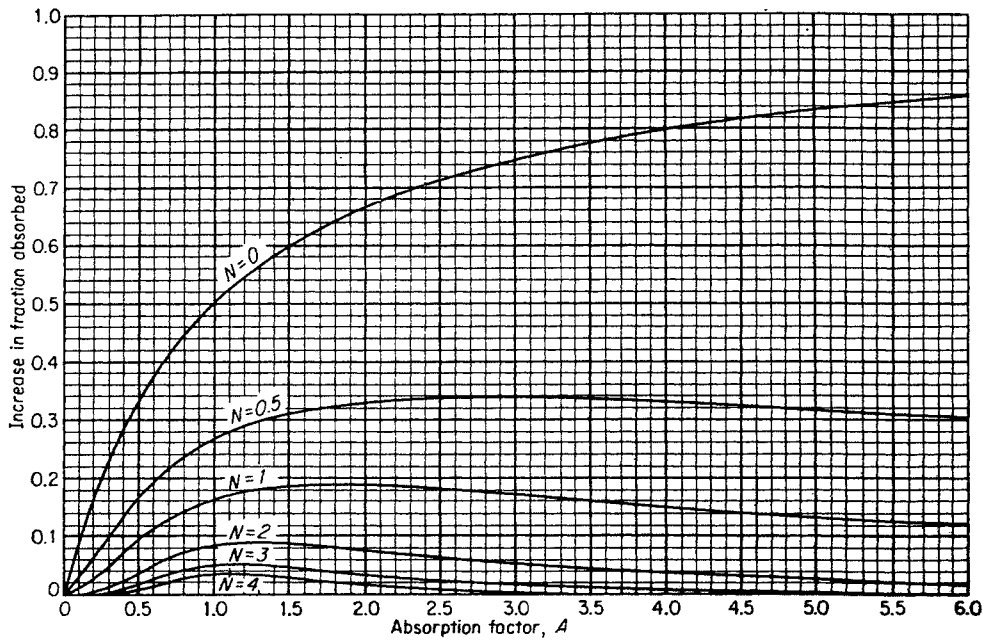

Fig. 13-17. Effect of adding one theoretical plate to an absorber with *n* theoretical plates.

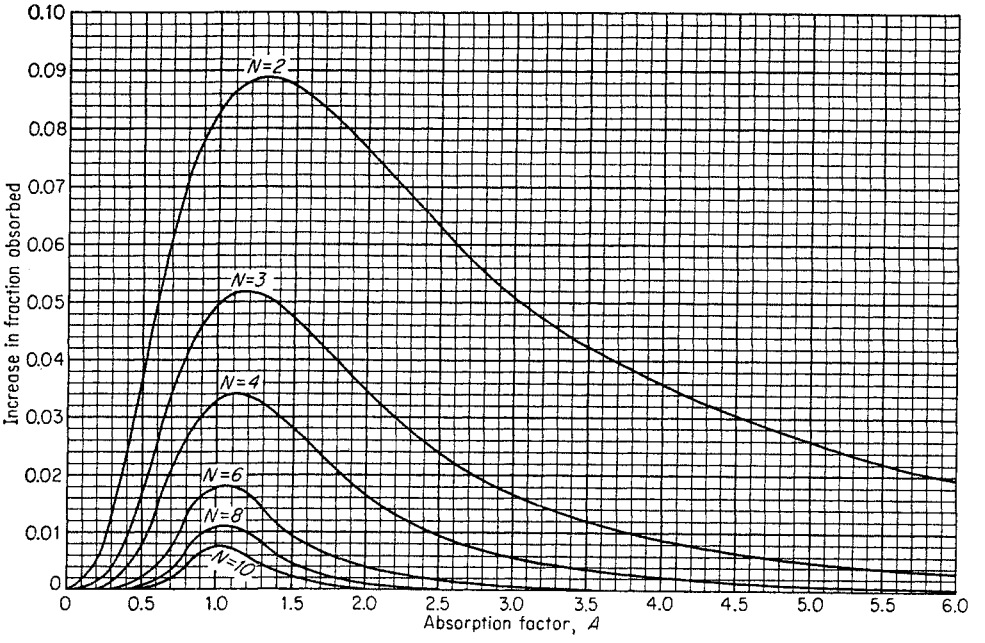

Fig. 13-18. Effect of adding one theoretical plate to an absorber with n theoretical plates.

The assumption that there is an average value of the absorption (or stripping) factor giving an exact solution to Eq. (13-24) is more serious than it may appear at first hand. The Kremser-Brown procedure *does not* provide a method by which the average absorption factors can be estimated. Also, the value of the number n of theoretical trays may be expected to vary from component to component since the tray efficiencies can be expected to vary from component to component (13-33).

The Kremser-Brown procedure approaches exactness for situations in which the liquid-gas rate L/V remains substantially constant throughout the length of the column. This would indicate that it works best for computing the absorption of slightly soluble gases for pressure and temperature conditions in which there is relatively little shrinkage of the gas phase *and also* relatively little increase in the liquid phase; for then the average absorption factor is easily estimated from the external-stream quantities and conditions. Estimation of an average absorption factor $(L/KV)_a$ can be resolved into separate estimations of the equilibrium-vaporization ratio K and the liquid-gas rate L/V. Most hydrocarbon absorption columns show a temperature profile qualitatively resembling the one shown in Fig. 13-19. The extent of the bulge appears to be primarily a function of the gas absorbed per pound of solvent and the extent of sensible heat gained or lost by the gas stream. As indicated by the correlation, Fig. 13-20 (13-37) applies to low-pressure light-hydrocarbon absorbers operating at pressures below 150 psi. The nomenclature for Fig. 13-20 is

t_1 = temperature of vapor leaving
T_1 = temperature of liquid leaving
T_2 = temperature of liquid entering
$\Delta G/G$ = pounds of vapor absorbed per pound of inlet vapor

A high-pressure absorber in which considerably greater absorption takes place may, nevertheless, show lower temperature rises because of the large decrease in heat of absorption with pressure (13-37). The nonisothermal condition resulting from heats of absorption may cause reversal in mass transfer and cause stripping rather than absorption somewhere in the column. Figure 13-21 shows a plot of the theoretical-plate number as a function of the reciprocal equilibrium constant $1/K$, L/V, and the absorption

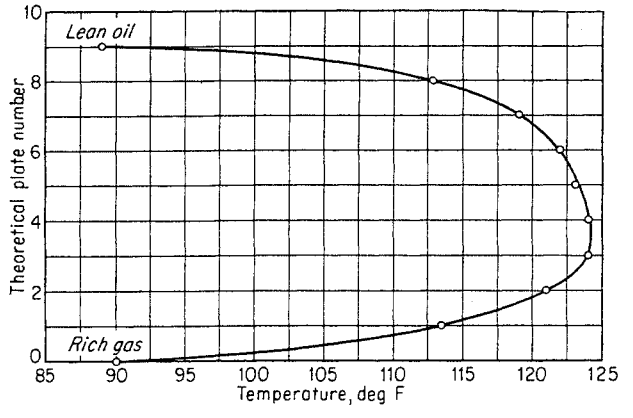

Fig. 13-19. Temperature profile in absorber. (*Ferro, Legatski, and Hachmuth,* 13-13.)

factor A for the same column as Fig. 13-19. The absorption-factor curve is seen to possess at least as great a bulge as either the $1/K$ profile or the L/V profile, since it is a product of the two.

The Kremser-Brown equations may be solved by successive approximations when allowances are made for temperature variation and L/V changes. The steps involved in the calculation of the total moles of light hydrocarbons absorbed with a given number of theoretical trays, absorption tray efficiency assumed equal for each of the trays, a given fraction absorbed of a key component, a given gas rate at a given temperature and pressure, and a completely stripped absorber oil, are as follows:

1. Enter fraction of key component absorbed on ordinate of Fig. 13-15 or 13-16, and intersect line of given number of theoretical trays.
2. Read required absorption factor A for the key component.
3. From an estimated temperature, determine the equilibrium-vaporization constant K of the key component.
4. Calculate L/V from this equilibrium ratio K and A of the key component.
5. Using this L/V and the equilibrium constant of the non-key components, determine the fraction absorbed from Fig. 13-15 or 13-16.
6. The product of the fraction absorbed and the moles of each constituent in the feed gas gives the moles of each component absorbed.

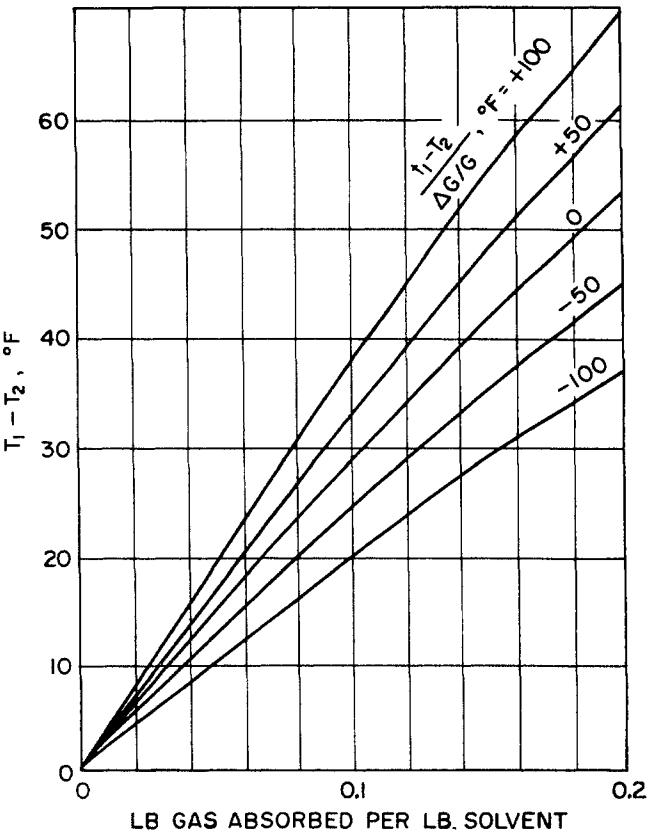

Fig. 13-20. Temperature rise due to absorption of light hydrocarbons at pressures up to 150 psi. (*Sherwood and Pigford*, 13-37. *Courtesy McGraw-Hill Book Company, Inc.*)

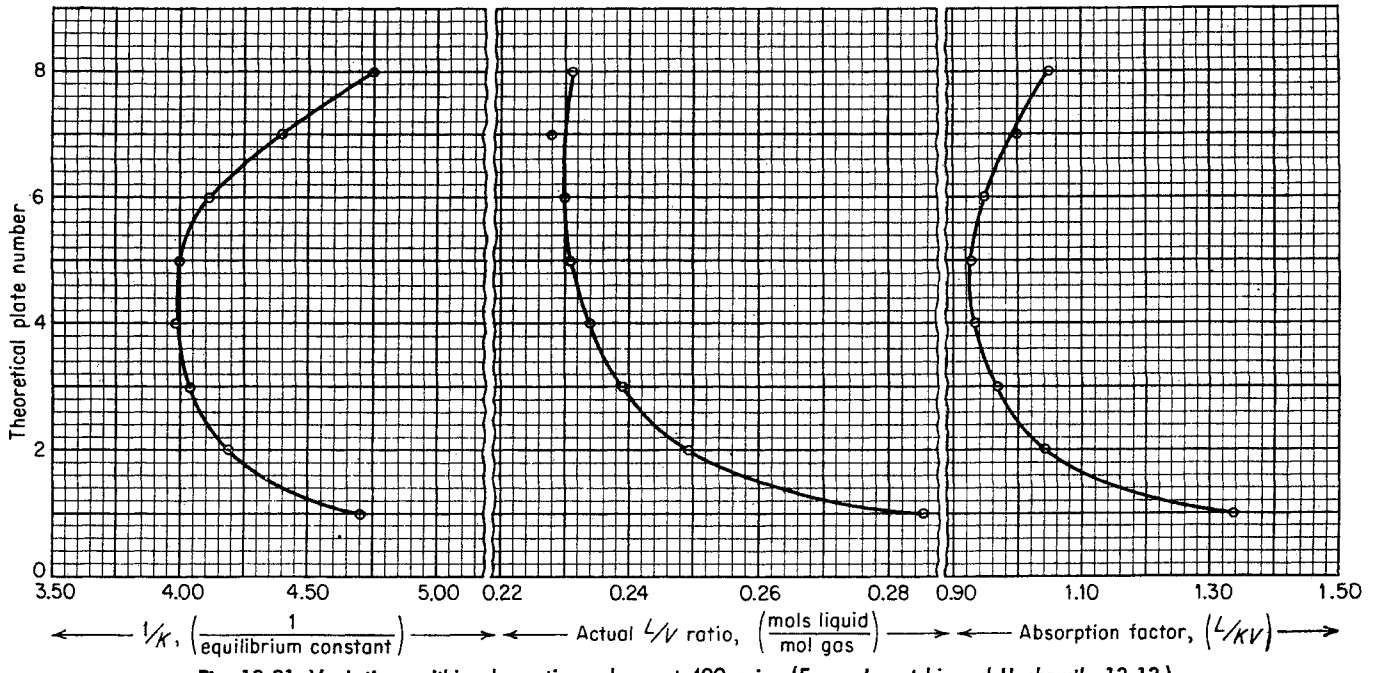

Fig. 13-21. Variations within absorption column at 400 psi. (*Ferro, Legatski, and Hachmuth*, 13-13.)

7. Determine the total moles of gas absorbed. Find the new temperature from Fig. 13-20.

8. Using the absorption factor of the key component and its K value adjusted to the new temperature, calculate the L/V for the key and obtain new K values and absorption factors for the non-keys.

9. Recompute the amount of the non-key components absorbed on the basis of the readjusted absorption factors for the non-key components.

10. Repeat the calculations until the temperature rise and the values of the components absorbed agree for two successive trial calculations.

Lewis-Sherwood Graphical Design Method for Absorption and Stripping

The Sherwood modification of W. K. Lewis's procedure for graphical calculation of absorbers (13-37) will be presented in order to illustrate pictorially the relationship that each component bears to other components. This method provides also an understanding of the mass transfer that is expected to take place as one proceeds from one end of the absorption column to the other.

The analytical equations which dictate the nature of the graphical constructions are discussed below. Equation (13-1) may be rewritten as

$$Y_{i+1} - Y_i = \frac{L_0}{V_{n+1}} (X_i - X_{i-1}) \qquad (13\text{-}26)$$

which is identified as the equation of a straight line in which the concentration units are defined on the basis of the external streams. Thus, all operating lines on the locus of concentrations of the equilibrium streams passing each other are straight lines, for they have a common slope L_0/V_{n+1}, which is invariant as long as the lean oil–rich gas ratio is set.

The simplicity in the operating line is gained at the expense of the equilibrium line, which now has to be redefined for the new coordinate system. For a given component a, the true mole fraction on plate i is given by

$$(y_a)_i = \left(\frac{v_a}{v_a + v_b + v_c + \cdots}\right)_i \qquad (13\text{-}27)$$

where v_a = moles of component a in vapor leaving plate (plate i in this case)

$v_a + v_b + \cdots$ = total moles of vapor leaving plate (plate i in this case)

Dividing the numerator and denominator of Eq. (13-27) by V_{n+1},

$$(y_a)_i = \left(\frac{\frac{v_a}{V_{n+1}}}{\frac{v_a}{V_{n+1}} + \frac{v_b}{V_{n+1}} + \frac{v_c}{V_{n+1}} + \cdots}\right)_i \qquad (13\text{-}28)$$

$$= \frac{Y_a}{\Sigma Y_i} \qquad (13\text{-}29)$$

A similar expression for the liquid x_i leaving plate i may be obtained by writing

$$(x_a)_i = \left(\frac{l_a}{L_0 + l_a + l_b + l_c + \cdots}\right)_i \qquad (13\text{-}30)$$

with the identity

$$(x_a)_i = \left(\frac{l_a/L_0}{L_0/L_0 + l_a/L_0 + l_b/L_0 + l_c/L_0 + \cdots}\right) \qquad (13\text{-}31)$$

where l_a = moles of liquid a leaving plate (plate i in this case)

$l_a + l_b + \cdots$ = total moles of absorbed hydrocarbons leaving plate (plate i in this case)

L_0 = moles of lean oil entering absorber, presumed to be constant throughout column

In abbreviated form

$$(x_a)_i = \frac{(X_a)_i}{1 + \Sigma X_i} \qquad (13\text{-}32)$$

Combining Eqs. (13-29) and (13-32) with the definition of the equilibrium-vaporization ratio,

$$\frac{(y_a)_i}{(x_a)_i} = (K_a)_i \qquad (13\text{-}33)$$

The final form of the equation for the equilibrium line is given by

$$\frac{Y}{X} = \frac{K\Sigma Y}{1 + \Sigma X} \qquad (13\text{-}34)$$

where ΣY = sum of all Y_i values for components in vapor phase

ΣX = sum of all X_i values for absorbed constituents in liquid phase

By similar reasoning, the equation for the equilibrium line during a stripping operation is given as

$$Y = KX \frac{1 + \Sigma Y}{1 + \Sigma X} \qquad (13\text{-}35)$$

It can readily be seen that the equation for the equilibrium line is substantially more complex than it is when expressed in mole-fraction units. Equation (13-34), however, is simplified to a straight-line form on the modified coordinate system when

$$\Sigma Y \to 1.0 \qquad (13\text{-}36a)$$

$$\Sigma X \to 0 \qquad (13\text{-}36b)$$

Condition (13-36a) is fulfilled when very little shrinkage of the gas phase takes place and condition (13-36b) is fulfilled when the concentration of the solute is low in the liquid phase. It is observed that these conditions are fulfilled in the absorption of slightly soluble gases and in the lean end of an absorption column or a stripping column where substantially complete stripping is accomplished.

Figure 13-22 schematically illustrated the application of the Lewis-Sherwood method to absorption of methane, propane, and butanes with an absorber oil. The key component, or the component whose absorption it is desired to control, is propane. *n*-Butane is almost completely absorbed, and the absorption of methane is relatively small. It is assumed that the equilibrium lines are straight, although this may not actually be so. It should be noted that the methane is absorbed near the top of the absorption column, propane throughout the length of the column, and the butanes most heavily near the bottom or rich end of the column. The horizontal lines of the step function may be pictured as representing the over-all liquid-phase diffusional driving force (including eddy diffusion) and the vertical lines the over-all gas-phase diffusional driving force. For high-pressure absorbers where the vaporization-equilibrium constants for methane approach a value less than 10.0, the absorption of methane in the neighborhood of the top plate causes large temperature rises. The temperature gradient near the bottom of the tower is likewise relatively large because of the absorption of the heavier hydrocarbons. This observation, i.e., that the absorption of hydrocarbons from hydrocarbon mixtures does not take place uniformly, has led to the development of the Horton and Franklin modification of the absorption-factor calculations (13-17).

The equilibrium lines are easily located where slightly soluble gases are involved; however, rich gases may cause considerable curvature in the equilibrium lines. The equilibrium line may be anchored at the lean end by noting that, at the lean end, $\Sigma X = 0$; Eq. (13-34) then reduces to

$$Y = K_L X(\Sigma Y_L) \qquad (13\text{-}37)$$

where K_L and the ΣY_L are taken at the lean end of the column. It will be necessary to determine ΣY_L by a trial solution using this or some other method, e.g., Kremser-Brown. K_L should represent the temperature of the top plate; hence it is taken at a temperature somewhat higher than the temperature of the lean oil. One method by which a fair estimate of the shape of the equilibrium line can be obtained is by calculating a hypothetical value of X, called X_R, corresponding to the rich-gas composition Y_R. This is accomplished by dividing each mole-fraction value y_R of the feed by its equilibrium-vaporization ratio at the rich gas-stream temperature and pressure, to get the mole-fraction composition x_R of the hypothetical equilibrium liquid. The difference between the Σx_R and 1.0 must be made up of absorber oil. From the given (or assumed) mole rate of flow of absorber oil, the total quantity in stream R is calculated; from this in turn the moles of each constituent are calculated.

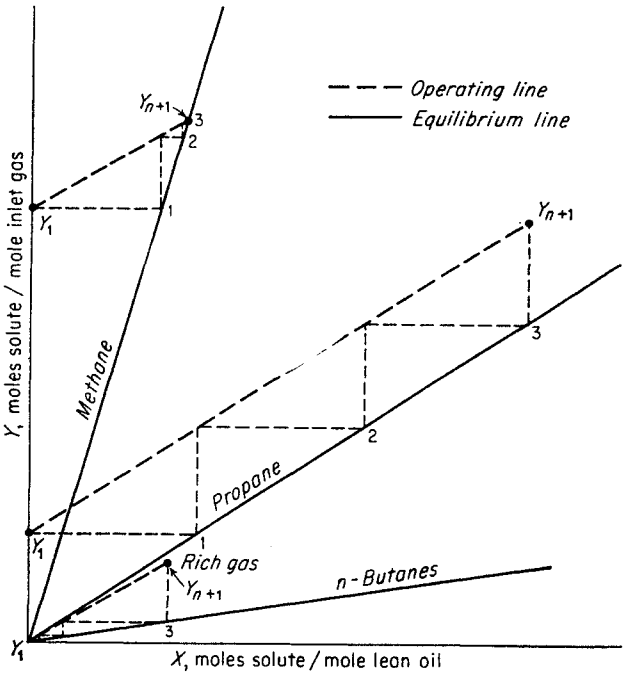

Fig. 13-22. Lewis-Sherwood method.

The values of X_R and Y_R are then calculated to give a point on each equilibrium line as well as the slope at the lean end. Thus, a "point-slope" approximation to the equilibrium line can be obtained.

Sufficient variables may be set to obtain the number of theoretical trays for one component. The position of the operating line is adjusted, keeping all operating lines parallel, until the number of theoretical trays for various components checks the one that was originally set.

The "minimum oil rate" is the lowest oil rate with which a given separation can be achieved, given an infinite number of theoretical trays. The minimum oil rate occurs, as in distillation, when zones of infinite plates develop. Figure 13-23 gives two ways in which infinite-tray zones may be generated in an absorber. In a column in which the equilibrium line is a straight line, the zones of infinite plates may be expected to occur either at the rich or at the lean end of the column, as shown in Fig. 13-23*a*. For columns whose equilibrium lines are curved, as in Fig. 13-23*b*, the infinite-plate zone may develop somewhere in the middle of the column.

The Lewis-Sherwood method does not permit rigorous solution, for it is not possible to predict the equilibrium curve exactly. Graphical procedures for multicomponent systems are cumbersome; so this method is used infrequently. However, its value in illustrating mass transfer in an absorption column is surpassed only by the tray-to-tray calculations.

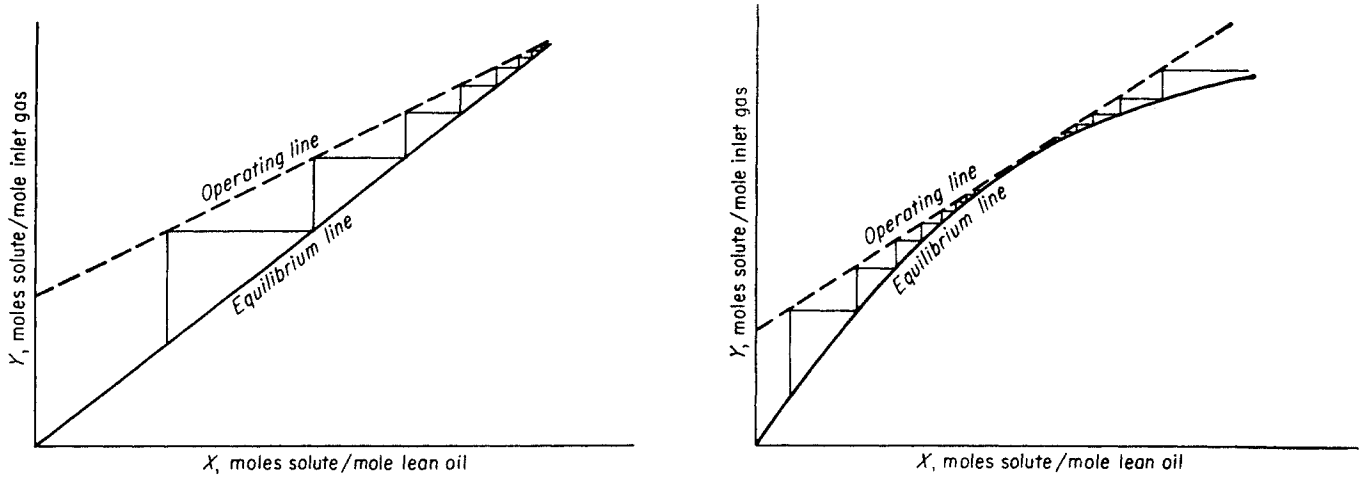

Fig. 13-23. Development of infinite-plate zones in absorbers.

Horton-Franklin Effective-absorption-factor Method

The Horton and Franklin (13-17) method of calculating absorbers recognizes that the absorption of hydrocarbons from a mixture does not take place uniformly throughout the column. Figure 13-22 indicates that this is a natural consequence of the differences in the equilibrium relationships of the various components. In Fig. 13-22, most of the trays used in the absorption of methane fall near the inlet methane concentration and most of the trays used in the absorption of butane fall near the outlet butane concentration. The key component, propane, on the other hand, is absorbed relatively uniformly throughout the tower. Horton and Franklin reason that the absorption factor should be taken in the region where it is representative of the greatest number of plates or where the absorption of a component is controlled, e.g., in the "pinch" zone for the absorption of methane and butanes in Fig. 13-22. The same conclusions could be obtained by studying the limits of the right-hand member of Eq. (13-24) for small values of the absorption factor and for values of the absorption factor appreciably greater than 1.0. Table 13-3 gives the relative locations of the effective absorption (or stripping) factor for various values of A (or S) which in the ultimate analysis have been located empirically (13-17).

Table 13-3. Location of Effective Absorption Factor

Value of A (or S)	*Ratio i:n or i:m*
0–0.1	1.0
0.1–0.4	0.9
0.4–1.0	0.8
1.0–4.0	0.7
4.0	0.6

* i = location of effective plate, numbering from lean end of column.

n or m = total number of theoretical trays in the absorber or the stripping section of the stripping column.

SOURCE: (13-17).

The evaluation of the effective absorption and stripping factors requires that the vapor load, liquid load, and temperature be estimated at the effective plates. It is assumed that the change in vapor quantity from plate i to plate $i + 1$ follows the exponential form:

$$\frac{V_i}{V_{i+1}} = \left(\frac{V_1}{V_{n+1}}\right)^{1/n} \tag{13-38}$$

where V_i = total moles of vapor on effective plate i
V_{i+1} = total moles of vapor entering effective plate i
V_1 = total moles of vapor leaving top plate
V_{n+1} = total moles of rich gas entering absorber
n = number of theoretical plates in absorber

Using as a basis 1 mole of wet gas, Eq. (13-38) may be written from plate 1 to plate i as

$$V_i = V_1^{(n+1-i)/n} \tag{13-39}$$

For the initial trial, V_1 may be calculated by the simpler Kremser-Brown method. A material balance around the top of the tower and the effective plate i yields

$$L_i = L_0 + V_{i+1} - V_1 \tag{13-40}$$

where L_i = total moles of liquid leaving effective plate i
L_0 = moles of lean oil

Equation (13-40) may be used to determine the liquid

flow from the effective plate, once V_{i+1} has been obtained from Eq. (13-38).

By assuming that the temperature change is approximately proportional to the total volume of gas absorbed, that is,

$$\frac{T_n - T_i}{T_n - T_0} = \frac{V_{n+1} - V_{i+1}}{V_{n+1} - V_1} \qquad (13\text{-}41)$$

it is possible to estimate the temperature of the effective plate i. For this particular trial calculation, the effective absorption factor for each component may be calculated from the equilibrium constant K_i on the effective plate, the total vapor volume V_i leaving the effective plate, and the total liquid rate L_i leaving the effective plate. The moles of each constituent can then be calculated from the Kremser-Brown relations, using the effective absorption factors.

Terminal-absorption-factor Methods

Two methods of calculating absorption from estimated values of the terminal (top and bottom plate) absorption and stripping factors are worthy of note (13-12, 13-13). In both procedures it is presumed that an effective absorption (or stripping) factor can be calculated from terminal values.

In the Edmister method, Eq. (13-24) is solved for a two-plate absorber to obtain the effective absorption factor as a function of the terminal absorption factor. This effective absorption factor is used in the Kremser-Brown relationship as the average or "effective" absorption factor for the particular component in question. Solutions for the effective-absorption-factor equations are presented in graphical form to facilitate their application to absorption, stripping, and fractionating problems (13-12). Illustrative problems are provided in the original reference.

The procedure of Ferro et al. (13-13) is also a terminal-absorption-factor method, but algebraic relations (geometric or arithmetic progression) are assumed to define the paths described by the absorption and stripping factors through the column. This procedure recognizes that both absorption and stripping may occur on the same trays for different components. The solutions to the progressions are presented graphically, and numerous sample problems are included and compared with rigorous plate-to-plate calculations.

Rigorous Plate-to-plate Calculation of Absorbers

Criteria for judging the accuracy of short-cut calculation procedures are rigorous calculations involving stagewise heat and material balances and precise operating data on absorbers. Short-cut procedures have rarely been compared with rigorous procedures in the literature (13-13, 13-23). One drawback to the use of rigorous calculation methods for high-pressure absorbers has been the lack of accurate heats-of-solution data for light hydrocarbons at high pressures.

Rigorous procedures can be adapted to computation by means of high-speed computers which hasten and improve the accuracy of the calculations (13-11). Rigorous calculations of absorbers from known inlet-stream compositions, amounts, and conditions and from the number of theoretical trays usually assume the composition of an outgoing stream (rich oil or lean gas) and calculate from one end of the column to the other on a tray-to-tray basis. From the assumed and calculated absorptions, a new trial outgoing stream is obtained, and the calculations are repeated. The agreement of the computed and the assumed streams is used as a check for the finality of the calculations.

Another method, which is believed to converge more rapidly to the exact answer, is attributed to Harbert (13-16). The procedure is based on direct computation of the composition of liquid and vapor leaving each tray from assumed liquid-gas ratios (L/V's) and temperatures on each plate through the column. The computed L/V leads to a check on the assumed values, and a heat-and-material balance on each plate permits the evaluation of a temperature check. The convergence of the L/V's and temperatures on each plate to unique values indicates that the solution has been completed. The procedure requires equilibrium constants and thermal data for the conditions and system encountered in the absorber.

Derivation of Algebraic Relationships for Harbert's Procedure

The derivation of the necessary algebraic relationships proceeds below. A material balance for each component around a general plate i in the absorber gives

$$(Vy)_{i+1} + (Lx)_{i-1} = (Vy)_i + (Lx)_i \qquad (13\text{-}42)$$

A heat balance for each component gives

$$(Vy\bar{H})_{i+1} + (Lx\bar{h})_{i-1} = (Vy\bar{H})_i + (Lx\bar{h})_i \qquad (13\text{-}43)$$

The following nomenclature is used:

- n = number of theoretical plates in absorber
- i = any theoretical plate
- V = total moles of vapor
- L = total moles of liquid
- x = mole fraction in liquid for a given component
- y = mole fraction in vapor for a given component
- $\bar{H}$ = partial enthalpy of a component (above some datum) in vapor state at absorber conditions, Btu per pound mole of component

$\bar{h}$ = partial enthalpy of a constituent in liquid state at absorber conditions, Btu per pound mole of constituent

$K = y/x$ = equilibrium constant

Thus,

$(Lx)_1$ = moles of a constituent in liquid leaving plate 1 or top plate

$(Vy)_{n+1}$ = moles of a component in vapor entering absorber

The equilibrium relationship for each component on plate i is

$$y_i = K_i x_i \tag{13-44}$$

Multiplying each side of Eq. (13-44) by $V_i L_i$,

$$(Vy)_i = \left(\frac{KV}{L}\right)_i (Lx)_i \tag{13-45}$$

Letting $A_i = L_i/V_i K_i$,

$$A_i(Vy)_i = (Lx)_i \tag{13-46}$$

Eliminating $(Lx)_{i-1}$ from Eq. (13-42) using Eq. (13-46) written for plate $i - 1$ leads to

$$(Lx)_i = (Vy)_{i+1} + A_{i-1}(Vy)_{i-1} - (Vy)_i \tag{13-47}$$

It should be recalled that Eq. (13-46) may be written for each component on each plate. Thus, for a three-plate absorber, the following series of equations for a given component may be written, the first three for balances around each plate of the absorber and the last one for a balance around the entire three-plate absorber.

$$(Lx)_3 = (Vy)_{n+1} + (Lx)_2 - (Vy)_3 \tag{13-48}$$
$$(Lx)_2 = (Vy)_3 + (Lx)_1 - (Vy)_2 \tag{13-49}$$
$$(Lx)_1 = (Vy)_2 + (Lx)_0 - (Vy)_1 \tag{13-50}$$
$$(Lx)_3 + (Vy)_1 = (Vy)_{n+1} + (Lx)_0 \tag{13-51}$$

Writing Eq. (13-46) for each plate gives

$$(Lx)_3 = A_3(Vy)_3 \tag{13-52}$$
$$(Lx)_2 = A_2(Vy)_2 \tag{13-53}$$
$$(Lx)_1 = A_1(Vy)_1 \tag{13-54}$$

For lean oil which has been stripped of the components for which the equations were written,

$$(Lx)_0 \equiv 0 \tag{13-55}$$

The simultaneous solution of Eqs. (13-48) to (13-55) yields an expression relating the moles of a component on a particular plate to the moles of the same component in the rich gas and its absorption factor on each plate. The resulting expression for plate 3 is

$$(Lx)_3 = \frac{(Vy)_{n+1}(A_3 + A_3A_2 + A_3A_2A_1)}{1 + A_3 + A_3A_2 + A_3A_2A_1} \tag{13-56}$$

For an absorber of n theoretical plates, the moles of a component on plate i may be written as

$$(Lx)_i = \frac{(Vy)_{n+1}(A_i + A_iA_{i-1} + A_iA_{i-1}A_{i-2} + \cdots + A_i \cdots A_2A_1)}{1 + A_n + A_nA_{n-1} + \cdots + A_nA_{n-1} \cdots A_2A_1} \tag{13-57}$$

The vapor composition follows from Eq. (13-57) by application of Eq. (13-46). On the basis of the assumed liquid-gas ratios L/V, the assumed temperature on each plate in the column, and the feed rate for a given component, the moles of each stream in the column are calculated. This leads to revised values of the L/V's.

There are three temperatures corresponding to the four streams leaving any given plate of an absorber, for two of the streams represented are in equilibrium. It is, therefore, convenient in making the heat balances to work from the top of the column down or from the bottom of the column up; one of the four streams is definitely known on plate 1 or plate n. Let it be imagined that a heat balance is made around the top tray. The temperature of the lean-oil stream is known, and the temperature of the top plate has been tentatively assumed. With regard to the top plate, there is one stream whose temperature is unknown, namely the vapor stream from the plate below. The heat balance around plate 1 is used to compute the temperature of this stream. It should be noted that the heat balance is used to check the temperature of the stream (gas in this case) coming onto the plate from an adjacent plate and *is not* used to check the assumed value of the temperature on that plate.

One proceeds in this way, making a heat balance on each plate, finally making a heat balance over the entire column using the computed and known streams, to check for an over-all heat balance. For a second-trial calculation the liquid-gas ratios and tray temperatures that were computed in the first trial serve as a guide for the new assumed liquid-gas ratios and the tray temperatures. Experience shows that the convergence is fairly rapid and that, in a few trials, the profile can be established within the accuracy of the thermal and equilibrium data.

A sample calculation for a three-plate absorber is included.

Illustrative Problem

Given the following gas composition and K's, compute the per cent absorbed for each constituent in an absorber with three equilibrium stages operating at 1,515 psia, (*a*) using Horton and Franklin's method and (*b*) using Harbert's method. The

gas enters the absorber at 82°F; the lean oil enters at 90°F; 903 gpm of 200 molecular weight, 36.7°API oil is circulated; and 288 MMcf/day of gas at 14.7 psia and 60°F is treated.

Gas composition		Equilibrium constants selected at 1,515 psia	
Constituent	Mole fraction	At 85°F	At 90°F
Methane	0.9302	3.30	3.36
Ethane	0.0373	0.78	0.835
Propane	0.0163	0.36	0.385
Isobutane	0.00444	0.19	0.020
n-Butane	0.00448	0.15	0.165
Isopentane	0.00279	0.083	0.0905
n-Pentane	0.001375	0.068	0.076
Hexanes	0.001563	0.035	0.0385
Heptanes+	0.00147	0.005	0.0056
	0.999918		

Solution

(*a*) Horton and Franklin's Method

$$\text{Oil rate} = \frac{903 \times 60 \times 8.33 \times 0.8413}{200} = 1{,}900 \text{ moles/hr}$$

$$\text{Gas rate} = \frac{288{,}000{,}000}{24 \times 379} = 31{,}600 \text{ moles/hr}$$

$$\text{Ratio of lean oil to rich gas} = \frac{1{,}900}{31{,}600} = 0.060 \text{ mole/mole}$$

The equilibrium constants are plotted log K versus temperature as straight lines over the temperature range of the absorber, with the values at two temperatures given above.

Table 13-4 presents a calculation of the composition of the lean gas when there are three theoretical or equilibrium plates for the absorber. The information required to make the calculations may be listed as follows:

1. The rich-gas composition, column 1, Table 13-4
2. The molal ratio of lean oil to rich gas, from data, in this case 0.06 mole of lean oil to 1 mole of rich gas
3. Table of ratio m/n of effective-plate number to total number of plates versus effective absorption factor (given by Table 13-3)
4. The number of theoretical plates (here arbitrarily assumed to be 3)
5. Empirical equations from Horton-Franklin, Eqs. (13-39) and (13-41):

$$V_i = V_1^{(n+1-i)/n} \tag{13-39}$$

where V_i = total moles of vapor on effective plate m
V_1 = total moles of lean vapor leaving absorber
n = number of theoretical plates in absorber
i = index number of effective plate for a constituent counting from top plate = 1 and bottom plate = n

$$V_{i+1} = \frac{V_i}{(V_1/V_{n+1})^{1/n}} \tag{13-58}$$

where V_{n+1} = moles of rich gas and is taken as unity.

By material balance,

$$L_i = L_0 + V_{i+1} - V_1 \tag{13-59}$$

where L_i = total moles of liquid on effective plate
L_0 = moles of lean oil

$$\frac{T_n - T_i}{T_n - T_0} = \frac{V_{n+1} - V_{i+1}}{V_{n+1} - V_1} \tag{13-60}$$

where T_n = temperature of bottom plate, °F
T_i = temperature of effective plate, °F
T_0 = temperature of lean oil, °F

It is necessary to assume the number of moles of gas absorbed per mole of rich gas entering. In this case, 0.0545 mole of gas leaves with the rich oil per mole of rich gas in Table 13-4. Table 13-4 is constructed as follows:

Table 13-4. Calculation of Absorber by Horton and Franklin Method

Horton and Franklin method for three theoretical plates
Assumed knockout or absorption, 0.0545 mole per mole of rich gas

Component	(1) Y_{n+1}, mole fraction of rich gas	(2) i/n assumed	(3) i for $n = 3$	(4) V_i, moles of vapor on effective plate	(5) V_{i+1} mole fraction	(6) L_i, moles of liquid on effective plate	(7) T_i, effective-plate temp, °F	(8) K_i, equilibrium constant at T_i	(9) A_{eff}	(10) $\frac{Y_{n+1} - Y_1}{Y_{n+1}}$ absorbed	(11) $Y_{n+1} - Y_1$	(12) Y_1, moles of lean gas
Methane	0.9302	1.0	3.0	0.9815	1.0000	0.1145	85.0	3.30	0.0354	0.0354	0.0329	0.8973
Ethane	0.0373	0.9	2.7	0.9760	0.9944	0.1089	85.5	0.783	0.1415	0.1414	0.00528	0.03202
Propane	0.0163	0.9	2.7	0.9760	0.9944	0.1089	85.5	0.362	0.308	0.298	0.00486	0.01144
Isobutane	0.00444	0.8	2.4	0.9706	0.9889	0.1034	86.0	0.191	0.559	0.514	0.02228	0.00216
n-Butane	0.00448	0.8	2.4	0.9706	0.9889	0.1034	86.0	0.152	0.701	0.606	0.00272	0.00176
Isopentane	0.00279	0.7	2.1	0.9652	0.9834	0.0979	86.5	0.084	1.208	0.815	0.00227	0.00052
n-Pentane	0.001375	0.7	2.1	0.9652	0.9834	0.0979	86.5	0.069	1.47	0.872	0.0012	0.000175
Hexanes	0.001563	0.7	2.1	0.9652	0.9834	0.0979	86.5	0.036	2.82	0.969	0.00152	0.000043
Heptanes+	0.00147	0.6	1.8	0.9598	0.9779	0.0924	87.0	0.00506	19.00	1.000	0.00147	
Total	0.999918	...	...	.....	.....	.....	....	.....	.....	.....	0.05450	0.945418

Column 1. Given
Column 2. Assumed, based on experience in calculations
Column 3. Calculated from column 2 and $n = 3$
Column 4. Calculated from Eq. (13-39) and column 3
Column 5. Calculated from Eq. (13-58) and column 4
Column 6. Calculated from Eq. (13-59) and molal ratio of lean oil to rich gas = 0.06 (item 2, above)
Column 7. Calculated from Eq. (13-60) and an assumed temperature of 85°F for bottom plate and 90°F for the lean oil
Column 8. Equilibrium constants for temperatures of column 7
Column 9. Calculated from columns 4, 6, and 8 ($A = L/KV$)
Column 10. Fraction absorbed, from absorption-factor plot (Fig. 13-15 or 13-16) for values of A (column 9) and three theoretical plates
Column 11. Column 10 times column 1, moles absorbed
Column 12. Column 1 minus column 11

(*b*) Harbert's Method

Table 13-5 shows an example calculation for a three-plate column using Harbert's method.

Table 13-5*a* lists the data given, the assumed temperatures, and assumed L/V ratios. For each constituent on each plate, an A value is found from the L/V and the K corresponding to the assumed temperature.

To solve Eq. (13-57) for a three-plate column, the three liquid compositions are found by the following equations, which are written for each constituent:

$$(Lx)_3 = \frac{(Vy)_{n+1}(A_3 + A_3A_2 + A_3A_2A_1)}{1 + A_3 + A_3A_2 + A_3A_2A_1} \quad (13\text{-}61)$$

$$(Lx)_2 = \frac{(Vy)_{n+1}(A_2 + A_2A_1)}{1 + A_3 + A_3A_2 + A_3A_2A_1} \quad (13\text{-}62)$$

$$(Lx)_1 = \frac{(Vy)_{n+1}A_1}{1 + A_3 + A_3A_2 + A_3A_2A_1} \quad (13\text{-}63)$$

It should be observed that the denominators for all three equations are the same and are calculated in Table 13-5*a* for each constituent.

Table 13-5*b* gives the calculations for the numerator for each constituent on plate 1 in such a form that terms added for the case of a larger number of plates may be conveniently handled. The solution of Eq. (13-63) is simply the ratio of numerator to denominator, giving $(Lx)_1$ or the moles of each constituent in the liquid leaving the top plate. The vapor off the top plate or the lean gas comes from the liquid composition and Eq. (13-64).

$$A_i(Vy)_i = Lx_i \quad (13\text{-}64)$$

Table 13-5a. Example of Calculation Using Harbert's Method

Given: composition of rich gas; temperature of rich gas = 82°F; ratio of lean oil to rich gas = 0.060 mole/mole; temperature of lean oil = 90°F

Assumptions:

Plate no	1	2	3
Assumed L/V	0.1025	0.104	0.114
Assumed temperature, °F	96	94	89

Absorption factors for each constituent on each plate:

Component	Plate 1		Plate 2		Plate 3	
	K_{96}	A	K_{94}	A	K_{89}	A
C_1	3.36	0.0305	3.35	0.0311	3.33	0.0342
C_2	0.835	0.123	0.825	0.126	0.800	0.1425
C_3	0.385	0.266	0.380	0.274	0.369	0.309
i-C_4	0.200	0.513	0.199	0.523	0.192	0.595
n-C_4	0.165	0.621	0.161	0.646	0.155	0.736
i-C_5	0.0905	1.13	0.089	1.17	0.086	1.318
n-C_5	0.076	1.35	0.074	1.41	0.0705	1.62
C_6	0.0385	2.66	0.038	2.74	0.036	3.17
C_7+	0.0056	18.30	0.0055	18.90	0.0052	21.95

Denominator of Eq. (13-57) for each constituent:

	C_1	C_2	C_3	i-C_4	n-C_4	i-C_5	n-C_5	C_6's	C_7+
$1 + A_3$	1.0342	1.1425	1.309	1.595	1.736	2.318	2.62	4.17	22.95
A_3A_2	0.00106	0.0180	0.0846	0.311	0.476	1.54	2.28	8.69	415
$A_3A_2A_1$	0.0000325	0.00221	0.0225	0.160	0.296	1.74	3.08	23.10	7,460
Sum	1.03529	1.1627	1.4161	2.066	2.508	5.598	7.98	35.96	7,898

Table 13-5b. Harbert's Method—Plate 1

Numerator of Eq. (13-63) for each constituent, plate 1:

	C_1	C_2	C_3	i-C_4	n-C_4	i-C_5	n-C_5	C_6	C_7+
$(Vy)_4$	0.9302	0.0373	0.0163	0.00444	0.00448	0.00279	0.001375	0.001563	0.00147
A_1	0.0305	0.123	0.266	0.513	0.621	1.13	1.35	2.66	18.30
$(Vy)_4A_1$	0.0284	0.00459	0.00434	0.00227	0.00278	0.00315	0.00186	0.00416	

	Solution to Eq. (13-63) $(Lx)_1$	Eq. (13-63) and Eq. (13-64) $(Vy)_1$	Mole fraction on plate 1		Mol. wt	Liquid						Vapor
			x	y		$x \times$ mol. wt	Wt fraction	Density, grams/ cu cm	Vol, cu cm	h_{96}	xh_{96}	$y \times$ mol. wt
C_1	0.0274	0.899	0.281	0.949	16.04	4.51	0.0340	.....	.....	990	278	15.24
C_2	0.00395	0.0321	0.0405	0.0339	30.07	1.22	0.0092	.....	.....	1,450	59	1.02
C_3	0.00306	0.0115	0.0314	0.01215	44.09	1.39	0.0105	0.510	0.0206	1,790	56	0.536
i-C_4	0.0011	0.00214	0.0113	0.00226	58.12	0.66	0.005	0.565	0.0089	2,040	23	0.131
n-C_4	0.00111	0.00179	0.0114	0.00189	58.12	0.66	0.005	0.585	0.0085	2,130	24	0.110
i-C_5	0.000564	0.000499	0.0058	0.00053	72.15	0.42	0.0032	0.625	0.0051	2,400	14	0.038
n-C_5	0.000233	0.000173	0.0024	0.000183	72.15	0.17	0.0013	0.631	0.0021	2,500	6	0.013
C_6	0.000116	0.00043	0.0012	0.000454	86.17	0.11	0.0008	0.664	0.0012	2,800	3	0.004
Absorber oil	0.0600	.....	0.615	.....	200	123.2	0.931	0.841	1.107	5,850*	3,610	
C_7+	.....	.....	.....	.....	127	.....	.....	0.782				
	0.09753	0.94763	1.0000	1.00037	.....	132.34	1.0000	.....	1.1534	.....	4,073	17.092

Calculated $\frac{L}{V} = \frac{0.0975}{0.9477} = 0.1029$ Specific gravity $= \frac{17.092}{28.9} = 0.591$ $H_{96} = 1{,}940$

* Enthalpy of absorber oil at 96°F and 0 psia $= 200 \times (96 - 32) \times 0.457$
$= 5850$ Btu/lb mole

Specific gravity of $C_3+ = \frac{1.0000 - 0.0340 - 0.0092}{1.1534} = \frac{0.9568}{1.1534} = 0.829$ gram/cu cm

Specific gravity of $C_2+ = 0.825$ gram/cu cm
Specific gravity of $C_1+ = 0.790$ gram/cu cm at 60°F and 1 atm
Enthalpy correction for pressure at 96°F and 1,515 psia = 4.14 Btu/lb or $132.3 \times 4.14 = 549$ Btu/lb mole
$\therefore$ Enthalpy of liquid on plate 1 $= 4073 + 549 = 4622$ Btu/lb mole

Heat balance around plate 1 to get temperature of V_2:

Heat Out

$h_{L_1} = 0.0975 \times 4{,}622 = 451$ Btu
$H_{V_1} = 0.9476 \times 1{,}940 = 1838$
2289 Btu

Heat In

$h_{\text{lean oil}} = 0.06 \times 6120 = 367$ Btu
$H_{V_2} \times 0.9844 = 1922$ Btu/mole of rich gas
$H_{V_2} = 1952$ Btu/mole of V_2

From 0.600 gravity, Table 13-5c, and Fig. 13-24,

Temperature of $V_2 = 93°F+$
Assumed temperature = 94°F

Table 13-5c. Harbert's Method—Plate 2

	C_1	C_2	C_3	i-C_4	n-C_4	i-C_5	n-C_5	C_6	C_7+
$(Vy)_4$	0.9302	0.0373	0.0163	0.00444	0.00448	0.00279	0.001375	0.001563	0.00147
A_2	0.0311	0.126	0.274	0.523	0.646	1.17	1.41	2.74	18.90
A_2A_1	0.00095	0.0155	0.073	0.268	0.402	1.32	1.90	7.30	346
Sum	0.03205	0.1415	0.347	0.791	1.048	2.49	3.31	10.04	364.9
$(Vy)_4 \times$ sum	0.0298	0.00529	0.00565	0.00351	0.0047	0.00695	0.00455	0.0157	0.536

	$(Lx)_2$	$(Vy)_2$	x	y	Liquid						Vapor
					$x \times$ mol. wt	Wt fraction	Sp gr	Vol, cu cm	h_{94}	xh_{94}	$y \times$ mol. wt
C_1	0.0288	0.926	0.279	0.941	4.49	0.0352	.....	.....	950	265	15.10
C_2	0.00454	0.0360	0.044	0.0365	1.32	0.0103	.....	.....	1,400	62	1.098
C_3	0.00399	0.0146	0.0386	0.0148	1.71	0.0134	0.510	0.0263	1,710	66	0.653
i-C_4	0.0017	0.00324	0.0165	0.00329	0.96	0.0075	0.565	0.0133	1,990	33	0.191
n-C_4	0.00187	0.0029	0.0181	0.00294	1.05	0.0082	0.585	0.0140	2,060	37	0.171
i-C_5	0.00124	0.00106	0.0120	0.00108	0.87	0.0068	0.625	0.0109	2,310	28	0.078
n-C_5	0.00057	0.000404	0.0055	0.00041	0.40	0.0031	0.631	0.0049	2,410	13	0.030
C_6	0.00044	0.000159	0.0043	0.00016	0.37	0.0029	0.664	0.0044	2,700	12	0.014
C_7+	0.00007	.....	0.0007	.....	0.09	0.0007	0.782	0.0009	4,200	3	
Absorber oil	0.0600	.....	0.5813	.....	116.3	0.912	0.841	1.083	5,660*	3,295	
Sum	0.1032	0.98436	1.0000	1.00018	127.56	1.000	.....	1.1577	.....	3,814	17.335

Calculated $\frac{L}{V} = \frac{0.1032}{0.9844} = 0.1049$ Specific gravity $= \frac{17.335}{28.9} = 0.600$ $H_{94} = 1965$ Btu/lb mole

* Enthalpy of absorber oil at 94°F and 0 psia $= 200 \times (94 - 32) \times 0.457 = 5660$ Btu/lb mole

Specific gravity of C_3+ $= \frac{1.000 - 0.0352 - 0.0103}{1.1577} = \frac{0.9545}{1.1577} = 0.825$ gram/cu cm

Specific gravity of C_2+ $= 0.819$ gram/cu cm

Specific gravity of C_1+ $= 0.784$ gram/cu cm

Correction for pressure at 94°F and 1,515 psia $= 4.17$ Btu/lb or $127.6 \times 4.17 = 532$ Btu/lb mole

$\therefore$ Enthalpy of liquid on plate 2 $= 3814 + 532 = 4346$ Btu/lb mole

Heat balance around plate 2:

Heat Out

$h_{L_2} = 0.1032 \times 4{,}346 = 449$ Btu

$H_{V_2} = 0.9844 \times 1{,}965 = 1932$

2381 Btu

Heat In

h_{L_1} from Table 13-5*b* $= 451$

$H_{V_3} \times 0.9884 = 1930$ Btu

$H_{V_3} = \frac{1930}{0.9884} = 1952$ Btu/mole of V_3

From Fig. 13-24, using gravity of 0.605 from Table 13-5*d*,

Temperature of $V_3 = 91$°F −
Assumed temperature $= 89$°F

However, differences are of the order of 20 Btu out of 1950, and can be accepted as within the error of the charts and calculations.

Table 13-5*d*. Harbert's Method—Plate 3

	C_1	C_2	C_3	i-C_4	n-C_4	i-C_5	n-C_5	C_6	C_7+
$(Vy)_4$	0.9302	0.0373	0.0163	0.00444	0.00448	0.00279	0.001375	0.001563	0.00147
A_3	0.0342	0.1425	0.309	0.595	0.736	1.318	1.62	3.17	21.95
A_3A_2	0.00106	0.0180	0.0846	0.311	0.476	1.54	2.28	8.69	415
$A_3A_2A_1$	0.0000325	0.00221	0.0225	0.160	0.296	1.74	3.08	23.10	7,460
Sum	0.0353	0.1627	0.4161	1.066	1.508	4.598	6.98	34.96	7,897
$(Vy)_4 \times$ sum	0.0328	0.00607	0.00672	0.00473	0.00675	0.00128	0.0096	0.0546	

	$(Lx)_3$	$(Vy)_3$	x	y	Liquid						Vapor
					$x \times$ mol. wt	Wt fraction	Sp gr	Vol, cu cm	h_{89}	xh_{89}	$y \times$ mol. wt
C_1	0.0317	0.926	0.280	0.9369	4.49	0.0370	.....	.....	870	246	15.02
C_2	0.00521	0.0366	0.0461	0.0370	1.39	0.0114	.....	.....	1,270	59	1.115
C_3	0.00475	0.01536	0.0420	0.0155	1.85	0.0152	0.510	0.0298	1,580	66	0.685
i-C_4	0.00229	0.00385	0.02025	0.0039	1.18	0.0097	0.565	0.0172	1,800	36	0.227
n-C_4	0.00269	0.00366	0.0238	0.0037	1.38	0.0113	0.585	0.0193	1,890	45	0.215
i-C_5	0.00229	0.00174	0.02025	0.00176	1.46	0.0120	0.625	0.0192	2,120	43	0.127
n-C_5	0.0012	0.00074	0.0106	0.00075	0.76	0.0062	0.631	0.0098	2,200	23	0.054
C_6	0.00152	0.00048	0.0134	0.00049	1.15	0.0091	0.664	0.0137	2,490	33	0.042
C_7+	0.00147	.....	0.0130	.....	1.65	0.0136	0.782	0.0174	3,800	49	0
Absorber oil	0.0600	.....	0.531	.....	106.2	0.8745	0.841	1.04	5,210*	2,770	
	0.11312	0.98843	1.0004	1.0000	121.51	1.0000	.....	1.1664	.....	3,370	17.485

Calculated $\frac{L}{V} = \frac{0.1131}{0.9884} = 0.1143$ Specific gravity $= \frac{17.485}{28.9} = 0.605$ $H_{89} = 1952$ Btu/lb mole

* Enthalpy of absorber oil at 89°F and 0 psia = 200 × (89 − 32) × 0.456 = 5210 Btu/lb mole

Specific gravity of C_3+ $= \frac{1.0000 - 0.0370 - 0.0114}{1.1664} = \frac{0.9516}{1.1664} = 0.816$ gram/cu cm

Specific gravity of C_2+ = 0.809 gram/cu cm
Specific gravity of C_1+ = 0.773 gram/cu cm
Correction for pressure at 89°F and 1,515 psia = 4.20 Btu/lb or 121.5 × 4.2 = 510 Btu/lb mole
∴ Enthalpy of liquid on plate 3 = 3370 + 510 = 3880 Btu/lb mole

Heat balance around plate 3:

Heat Out

$h_{L_3} = 0.1131 \times 3880 = 439$ Btu
$H_{V_3} = 0.9884 \times 1952 = 1930$
2369 Btu

Heat In

$h_{L_2} = 449$
$H_{\text{rich gas}} \times 1 = 1920$ Btu

From Fig. 13-24, using gravity 0.62, temperature of rich gas = 82°F.
The temperature given was 82°F.

Table 13-5e. Harbert's Method

Enthalpy of lean oil entering at 90°F:

$$200 \times (90 - 32) \times 0.457 = 5310 \text{ Btu/lb mole at 0 psia}$$

Correction for pressure at 90°F and 1,515 psia:

$$4.05 \text{ Btu/lb}$$

or $$200 \times 4.05 = 810 \text{ Btu/lb mole}$$

$\therefore$ Enthalpy of lean oil = 5310 + 810 = 6120 Btu/lb mole

Heat balance around absorber:

Heat In	
Lean oil at 90°F: 6120 × 0.06 =	367 Btu
Rich gas at 82°F (0.62 sp gr):	1915
	2282 Btu
Heat Out	
Rich oil at 89°F: 0.1131 × 3880 =	439 Btu
Lean gas at 96°F:	1838
	2277 Btu

The mole fractions are the $(Lx)_1$ or $(Vy)_1$ terms divided by the total moles.

Tables 13-5*c* and 13-5*d* give similar calculations for the vapor and liquid compositions on plates 2 and 3, respectively, completing the compositions of all streams in the three-plate absorber.

Tables 13-5*b* to *d* also give the heat-balance calculations. The summation of the mole fractions y in the vapor times molecular weight gives the molecular weight of the vapor. The molecular weight divided by 28.9 gives the gas gravity, which may be used with Fig. 13-24 to obtain the vapor enthalpy. The liquid enthalpy requires the liquid density, which is computed by the method of Standing and Katz (4-88). Additive volumes are assumed when the apparent densities for methane and ethane from Fig. 4-31 are used. The liquid enthalpies per pound mole at zero pressure at the plate temperature are read from Fig. 4-72. The mole fraction x in the liquid times the molal enthalpy h gives the partial enthalpy for each constituent. The total enthalpy must be corrected for pressure, using Fig. 4-73 and the liquid density.

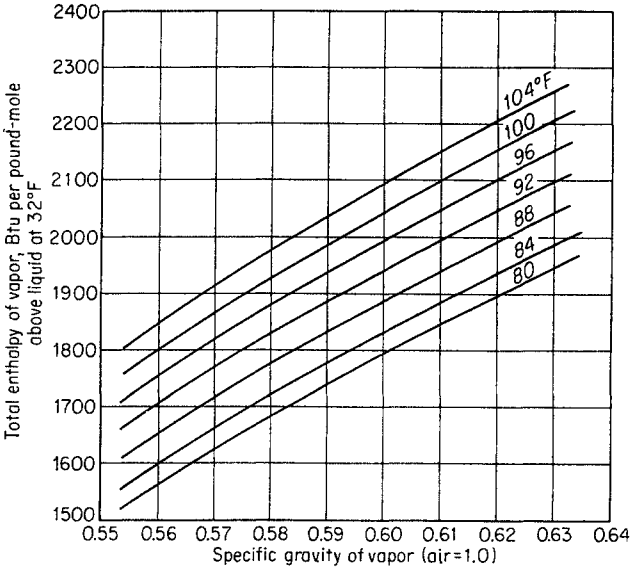

Fig. 13-24. Enthalpy of hydrocarbon vapors at 1,515 psia above liquid at 32°F and zero pressure. (*Katz and Rzasa*, 13-23.)

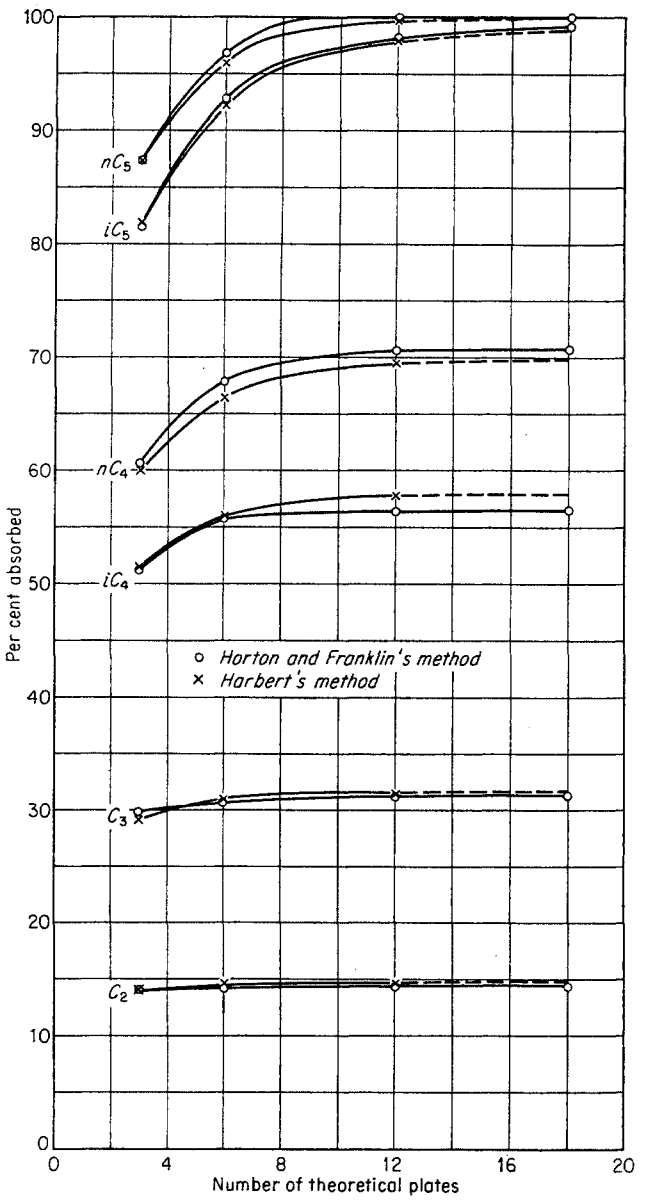

Fig. 13-25. Per cent absorbed for various constituents by Harbert's and Horton and Franklin's methods. (*Katz and Rzasa*, 13-23.)

Before making the enthalpy calculation of plate 2, a heat or enthalpy balance around plate 1 is made which gives the enthalpy of the vapor from plate 2. If the temperature corresponding to this enthalpy differs from that originally assumed for plate 2, the temperature just computed is used for finding the liquid enthalpy on plate 2, rather than that originally assumed. This enthalpy in turn gives the temperature for the vapors from plate 3. For a perfect solution, the balances made plate to plate should match the heat balance around the column.

In case the L/V ratios computed do not match the assumed

values, a second calculation is performed by solving Eqs. (13-61) to (13-63). New temperatures are required and they are assumed, based on the discrepancies found between the plate-to-plate heat balances and the over-all balance.

It can be seen that the selection of the top-plate temperature is critical in this procedure. If heat balances plate to plate through the tower give a different bottom-plate temperature from that computed by a heat balance around the tower, a new top-plate temperature is selected, with the assumption that the temperature-gradient curve throughout the tower remains about constant.

In case the L/V ratios are close to those assumed but the temperatures are not, heat-balance calculations plate to plate and around the absorber may be made for the temperatures of the second assumption without going through the composition calculations. Finally, however, a complete composition and enthalpy balance should be made like that given for the three-plate tower.

Calculations for six- and twelve-plate absorbers have been made using Harbert's method, with results shown in Table 13-6. The L/V ratios and temperatures resulting from the twelve-plate and the three-plate calculations are given in Fig. 13-25. The percentages absorbed are plotted in Fig. 13-26 along with the results by Horton and Franklin's method.

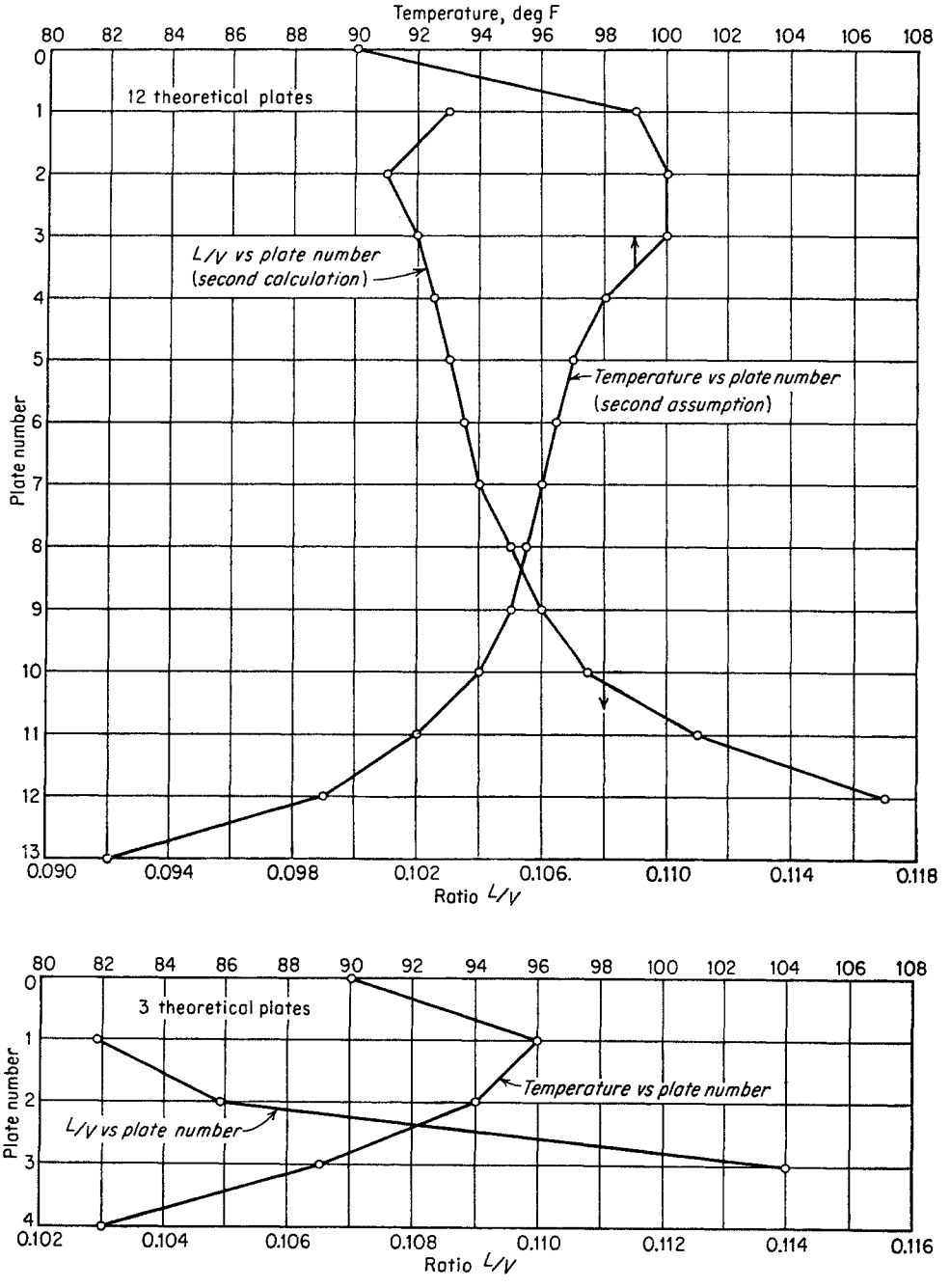

Fig. 13-26. Temperature and L/V profiles for the absorber. (*Katz and Rzasa*, 13-23.)

Table 13-6. Absorption Computed by Harbert's Method

No. of equilibrium plates	3	6	12
Absorption, per cent:			
Methane	3.41	3.56	3.56
Ethane	13.96	14.7	14.8
Propane	29.10	31.0	31.4
Isobutane	51.60	56.0	57.8
n-Butane	60.0	66.4	69.7
Isopentane	82.1	92.2	97.9
n-Pentane	87.4	96.0	99.4
Hexanes	97.1	99.8	100.0
Heptanes+	100.0	100.0	100.0
Temperature, °F:			
Lean oil	90	80	90
Rich gas	82	80	82
Top plate (calculated)	96	94	99
Bottom plate (calculated)	89	85	89

SOURCE: (13-23).

Stripping of Light Hydrocarbons from Absorber Oil

The absorption of light hydrocarbons from natural gas in absorber oils constitutes one step in their recovery. The absorbed hydrocarbons must be separated from the absorbing medium or lean oil by the unit operation known as "stripping." "Stripping" is the term applied to an operation in which the significant or desired transfer of material is from the liquid to the vapor phase. High temperatures and low partial pressures of the components to be stripped favor the mass transfer from the liquid to the gas phase. High temperatures are obtained by preheating the feed, and low partial pressures of the stripped gases over the liquid phase are obtained by operating the stripping columns at low pressures and by injecting an inert gas (generally steam) into the bottom of the column.

Stripping of light hydrocarbons from absorber oils, although essentially the reverse operation of absorption, is sufficiently different to warrant some discussion. For instance, commercial strippers are provided with a reflux section (Fig. 13-14) to carry out the relatively easy separation between the stripped light hydrocarbons and the absorber oil. Problems such as absorption of steam in the hot absorber oil and partial condensation of light hydrocarbon vapors in the overhead condenser should be recognized.

As in absorption, in stripping also the efficiency of one component may be assigned, and the stripping efficiencies of all the others will follow. The low-molecular-weight hydrocarbons such as butanes are completely stripped; so stripping performance is usually stated in terms of per cent of hexanes-and-heavier or heptanes-and-heavier components stripped. Two-stage stripping using a high- and a low-pressure stripping column in series yields high-pressure recycle vapors at the expense of low stripping efficiencies in the high-pressure column.

The absorption calculations that have been discussed or mentioned may be adapted to stripping calculations. The pressure may be set at a maximum of about 200 psi for the high-pressure step of a two-stage stripping; or a pressure in the neighborhood of 100 psi may be set if a single stripping column is used. The rich-oil feed to the stripping column is preheated, e.g., with a fired heater, to a temperature of from 350 to 500°F, depending on the thoroughness of the stripping desired and the stripping pressure. The first computation, then, is to establish the composition and the amounts of liquid and vapors entering the rectifying section of the stripper. Vaporization-equilibrium constants for high temperatures may be obtained from Chap. 6.

Neglecting the reflux of the hydrocarbons to the stripping section of the column, calculations using stripping-factor methods may be used to establish the degree of stripping obtained for an established number of equilibrium trays and an established value of liquid-gas ratio L/V. Actually, several cycles of calculations are required to establish a steady-state stripping value. Temperature drops of the order of 5 to 15°F in the stripping section of the stripping column may be expected as a result of overhead reflux and differences in the steam and hot-oil temperatures.

Once the steam rate has been established, including that of the dissolved steam (13-13) which leaves with the stripped oil as bottoms product, an approximate value for the vapors entering the rectifying section of the stripper is established. It is safe to assume that no free liquid water is formed in the stripping section. Hutchinson (13-20) has outlined a procedure to establish the reflux requirements in the rectifying section. The various streams may be resolved, as in Fig. 13-27, to simplify analysis of the rectifying section. The vapor rising to the rectifier from the feed plate consists of:

1. The vaporized portion of the feed
2. Stripped oil and the stripped hydrocarbons
3. Stripping steam not dissolved in lean oil

The liquid leaving the bottom plate of the rectifier section is primarily the refluxed absorber oil and some light hydrocarbons. The vapors leaving the top plate of the rectifying section may be divided into:

1. Water vapor associated with the hydrocarbon vapors at the top-plate temperature (around 200°F)
2. Hydrocarbon reflux plus overhead product

Condensed water is removed from the top plates of the

rectifying section. Only hydrocarbon is shown to be refluxed to the top plate, since oil is easily excluded from the overhead product.

The heat balance around boundary 1 can be used to determine the hydrocarbon reflux, provided all the other streams can be calculated or estimated. The heat balance around boundary 2 can be used to determine the condenser load. For the heat balance around boundary 1 to determine the reflux ratio, it is necessary to ascertain the quantities of each indicated stream from calculations of:

1. Vaporized feed, from a flash calculation
2. Stripped oil, from a stripping calculation
3. Stripped hydrocarbons, from a stripping calculation
4. Stripping steam, from a stripping calculation
5. Refluxed-absorber-oil quantity, from total absorber oil onto bottom rectifier plate
6. Water vapor leaving top plate of rectifier, written in terms of an unknown quantity: reflux plus overhead product
7. Water drawn off from the plates, from item 4 minus item 6

The heat balance can then be written in terms of one unknown, the quantity of reflux; and the reflux is thus determined. Item 6 may be written as

$$W = (R + O)\frac{p_w}{P - p_w}$$

where W = pound moles of water leaving top plate of rectifier
R = moles of hydrocarbon refluxed
O = moles of hydrocarbon taken overhead
p_w = partial pressure of water vapor at top-plate temperature
P = total pressure at top plate

The condenser heat load may be determined from an evaluation of the enthlapy balances for boundary 2. The quantity of each stream for boundary 2 follows from the solution of the previous heat-balance and material-balance equations.

In a design, the steady-state values of the feeds to the absorber and the stripper must be determined by successive approximations when the vapor from the partial condenser is recycled to the absorber. Since large variations of the feed to the stripping column may be expected because of seasonal and operational fluctuations in gas composition, actual design should be based on a substantial factor of safety (13-20). Ample liquid-handling capacity, both on the trays and in the downcomers, should be provided in the stripping column below the feed plate, since stripping columns characteristically have high ratios of liquid flow to gas flow.

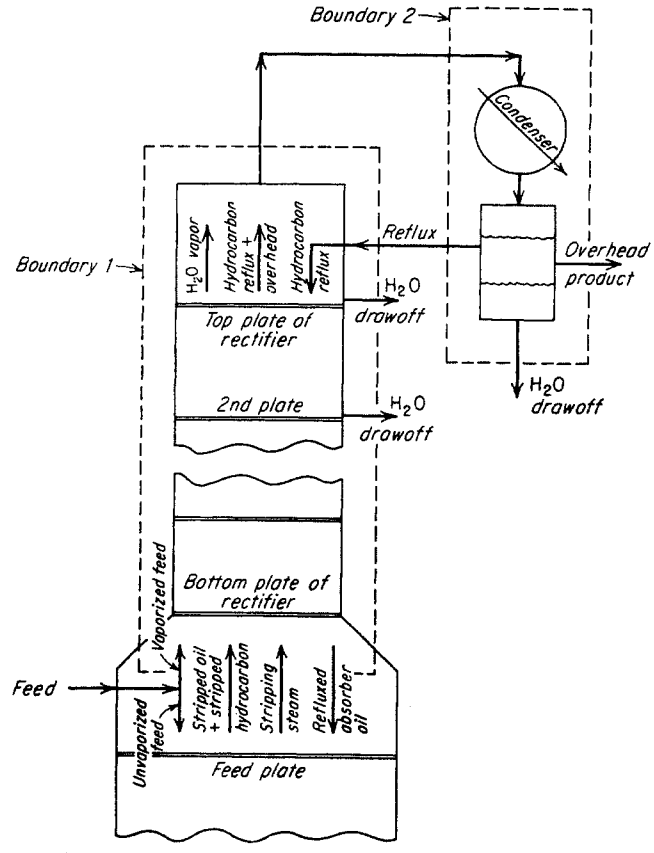

Fig. 13-27. Rectifying section of stripping column, showing breakdown of streams.

CHAPTER 14

Fractional Distillation

Fractional distillation, together with the absorption-stripping operation, is the most widespread means of purifying hydrocarbons. This chapter consists of an introductory treatment of fractional-distillation calculations by equilibrium stages for binary, ternary, and multicomponent systems, followed by a section on mass transfer of bubble-cap columns and tray hydraulics. More exhaustive treatment of these topics can be found in the many books and treatises which already exist in the field (14-2, 14-4, 14-7, 14-11, 14-16, 14-28, 14-39, 14-41). The purpose of this chapter is to present some of the fundamentals of distillation rather than to provide a catalogue of working relationships.

A fractionating column, represented schematically by Fig. 14-1, may be viewed as a combination of absorption and stripping columns. A fractionating column employs a reboiler at the bottom of the column to generate its own stripping vapors, which strip those constituents to be excluded from the bottom product, and employs a condenser at the top of the column to provide reflux or selective absorption of those constituents which must be excluded from the overhead products. Ferro, Legatski, and Hachmuth (14-18) have recognized that absorption and stripping take place simultaneously in a distillation column and have applied this basic principle to develop their absorption-and-stripping-factor method of fractionating-column design.

Since it is theoretically conceivable that a distillation could be conducted without any irreversibilities, that is, since the net work can theoretically be reduced to the work thermodynamically required for the separation, Benedict (14-3) has classified distillation as a potentially reversible process. Actual distillation columns are built with a finite number of plates, condenser areas, and reboiler areas, with consequent introduction of irreversibilities.

When the overheads cannot be condensed at ambient-cooling-water temperatures, absorption and stripping operations are combined. An example of such a hybrid process is the rich-oil deethanizer described in Fig. 14-2. The knockback of hydrocarbons that are to be retained in the bottoms product is achieved by using a lean-oil reflux; a reboiler at the bottom generates the stripping vapors required to exclude the volatile components from the bottoms (13-10). A reduction in the diameter of the column above the feed plate is permissible since the volume of liquid flow in the upper section of the column is considerably smaller than the volume of flow in the stripping section. Stripping vapors provided by the

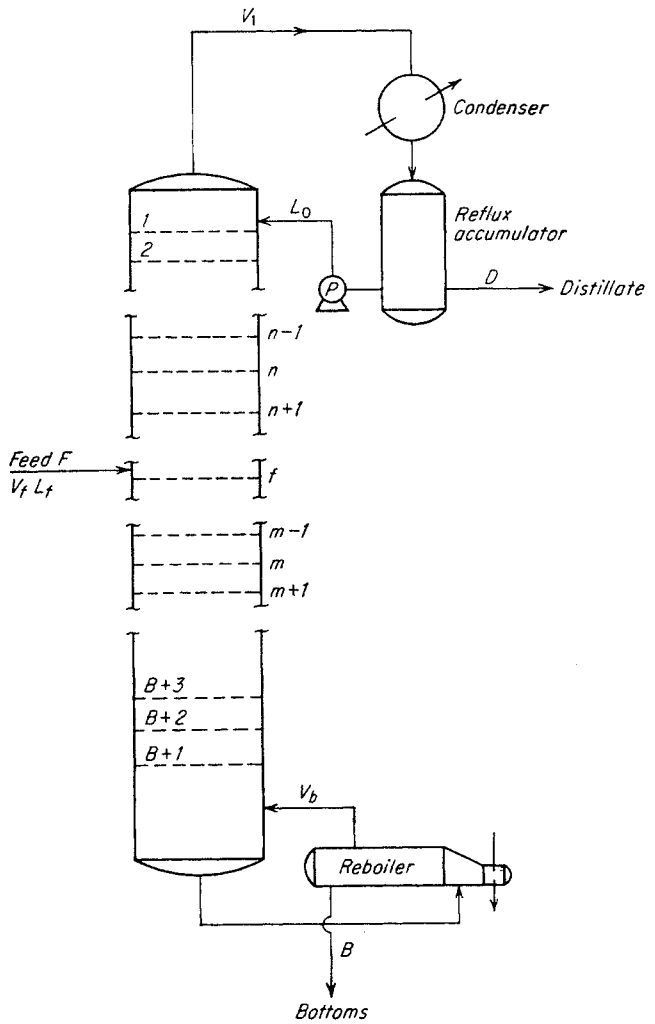

Fig. 14-1. Fractionating column with accessory equipment and nomenclature used.

reboiler have, on some occasions, been supplemented by introducing hydrocarbon vapors under a tray somewhere between the reboiler and the feed tray.

Figure 14-3 shows diagrammatically the combination of unit operations in a typical natural gasoline and liquefied-petroleum-gas recovery plant (14-37a). The main units of equipment are labeled, and the operating temperatures and pressures are given. Figure 14-4 is a photograph of the same plant.

A primary prerequisite to separation by vapor-liquid transfer is favorable phase-equilibrium relationships. The relative volatility of the components to be separated must be sufficiently high so that the separation can be achieved without excessive expenditure of thermal energy and without a prohibitive number of stages. Phase equilibria and other thermodynamic properties of hydrocarbons have already been treated in Chaps. 3 to 6.

BINARY DISTILLATION

Three primary methods of computing the number of equilibrium stages for a fractionator are presented: (1) the McCabe-Thiele graphical procedure, which does not use energy relationships directly, (2) the Ponchon-Savarit method, which combines phase and thermal behavior in a single graphical procedure, and (3) the analytical approach.

McCabe-Thiele Graphical Procedure

The McCabe-Thiele method (14-33), though not rigorous, provides a rapid method by which the significant variables in an equilibrium-stage binary calculation can be related. Despite the simplicity of this method, the only assumption required is that the liquid-vapor ratio in an adiabatic section of the column is constant.

Referring to Fig. 14-1, an over-all material balance around the top of the column intersects the material streams V_{n+1}, L_n, and D, yielding the material-balance equation

$$V_{n+1} = L_n + D \tag{14-1}$$

A component material balance over the same section of the column gives

$$V_{n+1}y_{n+1} = L_n x_n + Dx_D \tag{14-2a}$$

$$y_{n+1} = \frac{L_n}{V_{n+1}} x_n + \frac{Dx_D}{V_{n+1}} \tag{14-2b}$$

where V_{n+1} = moles of vapor leaving plate $n + 1$
y_{n+1} = concentration of more volatile component in V_{n+1}, mole fraction
L_n = moles of liquid leaving plate n

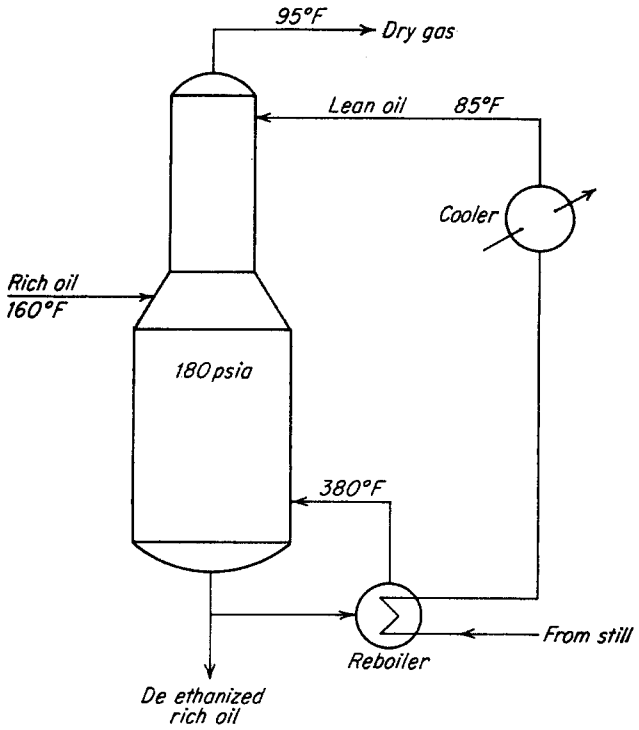

Fig. 14-2. Flow diagram for rich-oil deethanizer.

x_n = concentration of most volatile component in L_n, mole fraction
D = moles of distillate product removed from column
x_D = concentration of most volatile component in overhead distillate product, mole fraction

Since steady-state conditions in the column are assumed, the quantities V, L, and D may be taken to represent mass rate of flow as well as mass flow. Note that Eqs. (14-1) and (14-2) are both rigorous. Equations 14-2*a* and 14-2*b* relate the compositions of the adjacent countercurrent vapor and liquid streams (streams passing each other) in terms of the local liquid and vapor rate and of the rate of distillate production.

Equation (14-2*b*) is frequently referred to as the "equation of the operating line." In order to facilitate the construction of the operating line, the ratio L/D of the liquid flow is assumed to be constant. Then

$$y_{n+1} = \frac{L}{V} x_n + \frac{D}{V} x_D \tag{14-3}$$

which is, for a steady-state column, a straight line on a plot of the vapor composition versus the liquid composition in mole fractions (Fig. 14-5).

Setting $x_n = x_D$ in Eq. (14-3), $y_{n+1} = x_D$. Thus,

point (x_D, y_1) falls on the 45° line through the origin $(x = 0, y = 0)$ and the point $(x = 1.0, y = 1.0)$. The construction of the operating line with slope L/V, that is, of the line that relates the compositions of the streams passing each other, is illustrated in Fig. 14-5.

A discontinuity of the operating line is produced by the introduction of the feed into the column. A component balance around the bottom of the column gives

$$V'_{m+1}y_{m+1} = L'_m x_m - Bx_B \qquad (14\text{-}4)$$

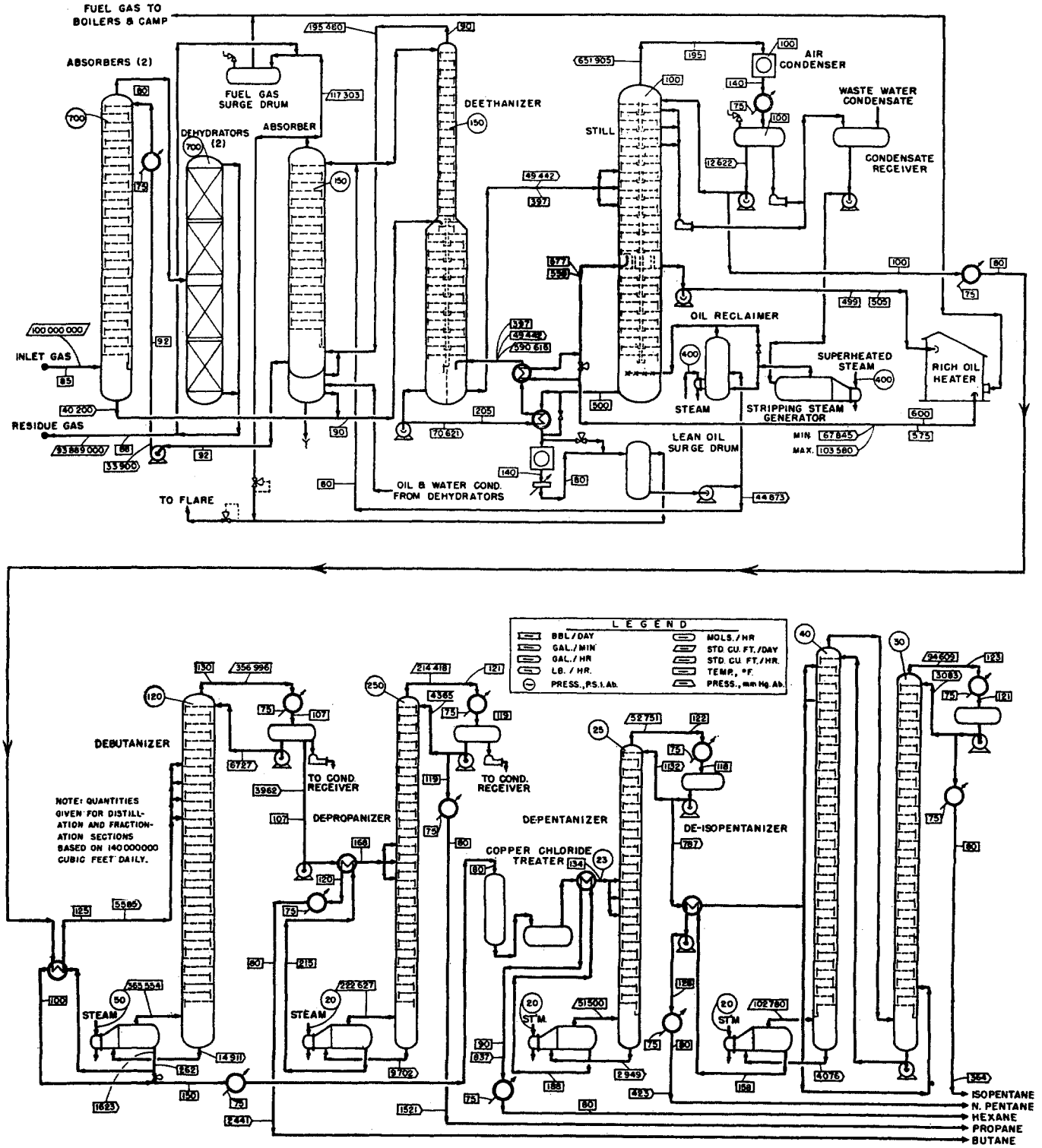

Fig. 14-3. Flow diagram for a complete natural gasoline plant. (*Panoma plant, after Nutter and Van Vliet, 14-37a. Courtesy Petrol. Refiner.*)

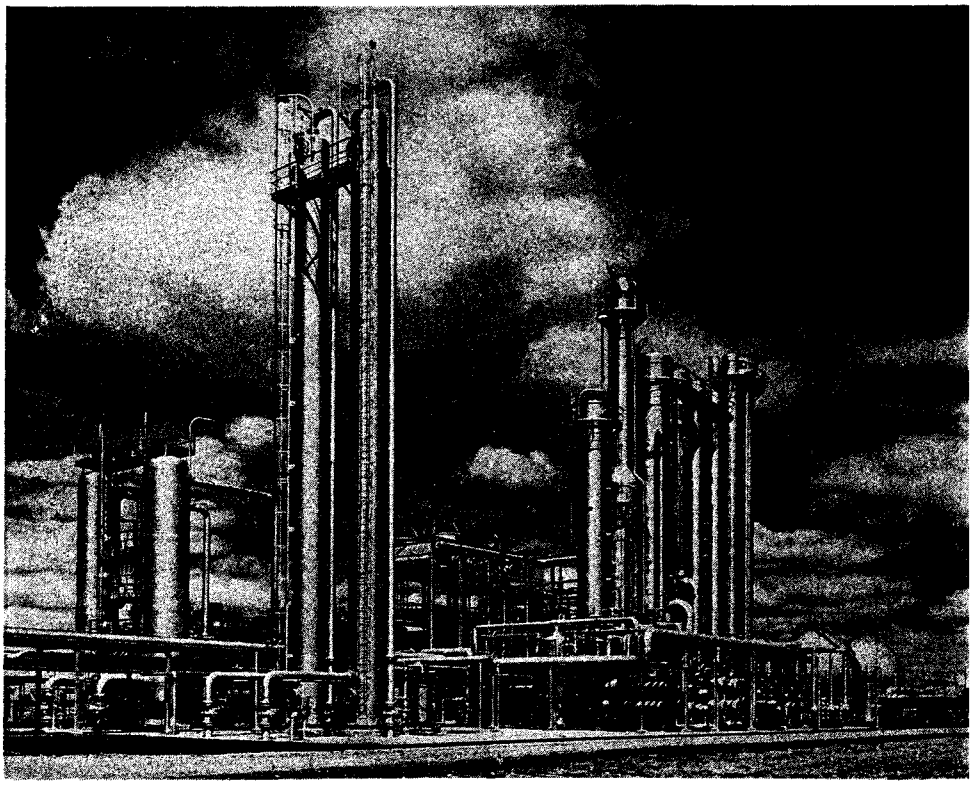

Fig. 14-4. View of Panoma's process area. (*Courtesy Dorchester Corp.*)

where V'_{m+1} = moles of vapor leaving plate $m + 1$, where stage $m + 1$ lies below feed plate

y_{m+1} = concentration of most volatile component in V_{n+1}, mole fraction

L'_m = moles of liquid leaving plate m, where m lies below feed plate

B = moles of bottom product

x_B = concentration of most volatile component in bottoms product, mole fraction

If the mole ratio of liquid to vapor is constant in the stripping section of the column,

$$y_{m+1} = \frac{L'}{V'} x_m - \frac{Bx_B}{V'} \qquad (14\text{-}5)$$

The requirement for constant liquid-vapor ratio in each section of the column is met for a column that satisfies the two conditions that:

1. No heat is transferred to or from the surroundings except at the reboiler and overhead condenser.
2. Molal heat of vaporization is constant for the concentration range over which the distillation takes place.

Neglecting such effects as entrainment, it will be seen that these are sufficient conditions for constant L/V or "constant molal overflow" in each section of the column. This will be demonstrated later, in the presentation of the Ponchon-Savarit rigorous method for binary-distillation calculations.

To interrelate Eqs. (14-3) and (14-5), the parameter q' defining the "state of the feed" is introduced.

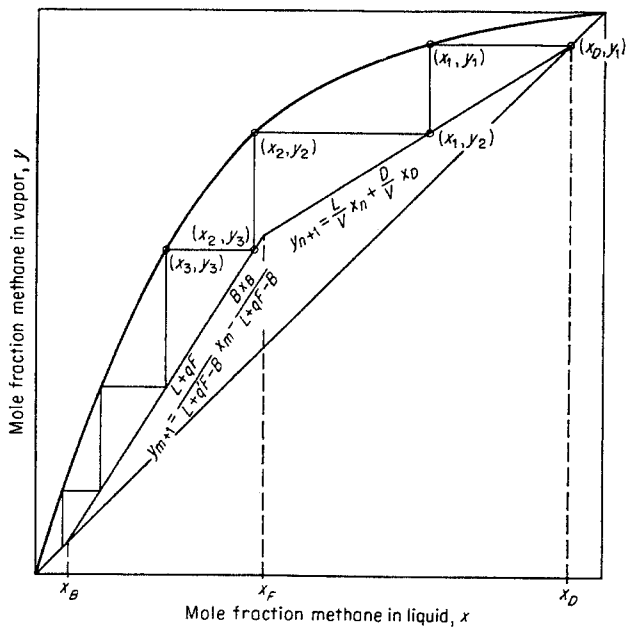

Fig. 14-5. McCabe-Thiele construction for a complete column.

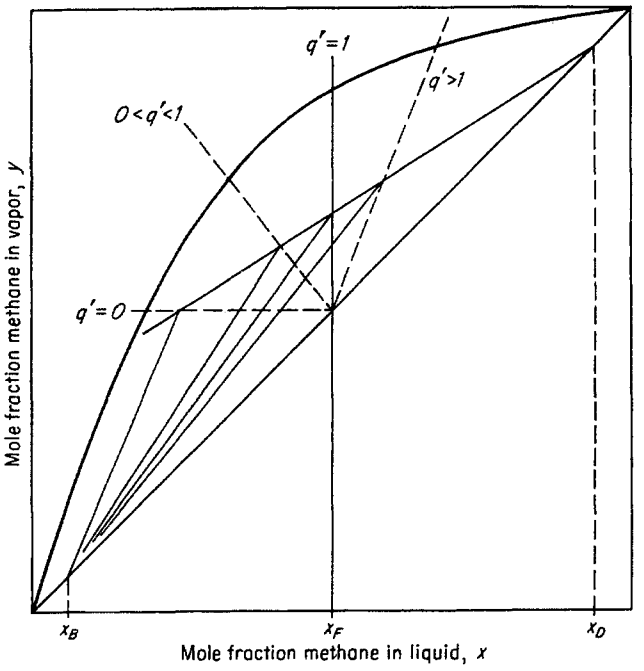

Fig. 14-6. Effect of state of feed q' on operating lines below feed for methane-ethane binary system at 500 psia.

$$L' = q'F + L \tag{14-6}$$

where q' = moles of saturated liquid formed on feed plate by introduction of 1 mole of feed
F = moles of feed

From an enthalpy-concentration diagram it is seen that

$$q' \sim \frac{H_{SV} - h_F}{H_{SV} - h_{SL}} \tag{14-7a}$$

and, if condition 2 above is met in the vicinity of the feed composition,

$$q' = \frac{H_{SV} - h_F}{H_{SV} - h_{SL}} \tag{14-7b}$$

where H_{SV} = enthalpy of saturated vapor, Btu/lb mole
h_F = enthalpy of feed, Btu/lb mole
h_{SL} = enthalpy of saturated liquid, Btu/lb mole

From Eq. (14-7b)

If $h_F = H_{SV}$ $\quad q' = 0$
If $h_F = h_{SL}$ $\quad q' = 1.0$
If $h_F > H_{SV}$ $\quad q' < 0$
If $h_F < h_{SL}$ $\quad q' > 1.0$

Since $V' = L' - B$, Eq. (14-5) may be rewritten in a more useful form:

$$y_{m+1} = \frac{L + q'F}{L + q'F - B} x_m - \frac{Bx_B}{L - q'F - B} \tag{14-8}$$

which is the equation for the operating line below the feed plate.

An alternative relation for V' may be obtained by writing a material balance around the feed plate.

$$\begin{aligned} L + V' + F &= L' + V \\ V' &= L + q'F + V - L - F \\ &= F(q' - 1) + V \end{aligned} \tag{14-9}$$

Another procedure for defining the operating line in one section of the column, from the operating line in the other section and the feed concentration together with its state, is to solve Eqs. (14-3) and (14-8) simultaneously, noting that the points of intersection fulfill the condition

$$(x_n, y_{n+1}) = (x_m, y_{m+1})$$

The resulting solution (14-2, 14-11) gives the equation for the "q line," which is the locus of intersections of the upper and lower operating lines.

$$y = \frac{q'}{q' - 1} x - \frac{x_F}{q' - 1} \tag{14-10}$$

The slope $q'/(q' - 1)$ of the curve for this equation is defined solely by the state q' of the feed. Equation (14-10) passes through the point ($y = y_F$, $x = x_F$), which lies on the 45° line.

Figure 14-6 shows the effect of the feed condition q' on the intersection of the upper and lower operating lines when all other conditions are held constant. The effect of the feed quality on the number of equilibrium stages required can be determined by stepping off the stages.

The operating lines in the rigorous representation of plate-to-plate calculations on a y-x diagram may be

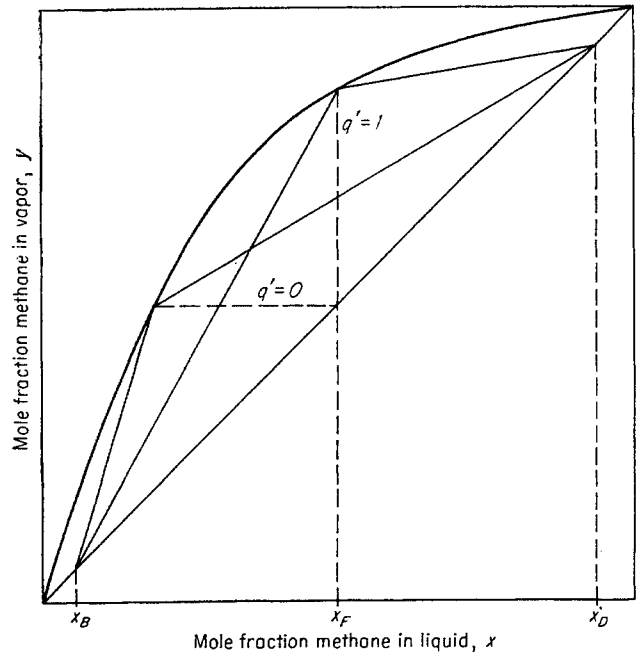

Fig. 14-7. Effect of feed conditions on the minimum reflux ratio for methane-ethane binary system at 500 psia.

curved lines. The application of the McCabe-Thiele method of rigorous calculation, however, gives way to the completely rigorous enthalpy-concentration calculation of binary distillation (14-40, 14-44). The application of McCabe-Thiele techniques to approximate multicomponent calculations has been successfully carried out (14-22, 14-23, 14-25).

Significant theoretical limits for a given separation are the minimum external-reflux ratio $(L_0/D)_{min}$ and the minimum number of equilibrium stages. The minimum reflux ratio corresponds to the reflux ratio required for a given separation when an infinite number of theoretical stages are permitted. The minimum reflux ratio also corresponds to the minimum theoretical energy with which a given distillation can be conducted. The operating lines corresponding to the minimum reflux ratio with a fixed feed composition but with various feed conditions are shown in Fig. 14-7. From the slopes of the operating lines, it is possible to obtain $(L/V)_{min}$ directly. The minimum external-reflux ratio $(L_0/D)_{min}$ is related to the minimum internal ratio $(L/V)_{min}$, according to the equation

$$\left(\frac{L}{V}\right)_{min} = \frac{(L_0/D)_{min}}{(L_0/D)_{min} + 1} \qquad (14\text{-}11)$$

Referring to Fig. 14-5, it is noted that the driving force for mass transfer diminishes to zero when the operating lines intersect the equilibrium line. The zone of zero driving force is known as the "pinch zone" within which no separation is achieved in going from one stage to another. For binary light-hydrocarbon separations, because of the regular shape of the equilibrium line, the pinch zone or the zone of infinite stages may be expected to coincide with the intersection of the q line and the equilibrium line. This may not be true of systems that exhibit serious deviations from ideal solutions in the liquid phase (14-7).

The minimum number of theoretical stages corresponds to a condition of total reflux, $L/V = 1.0$ or $L_0/D \rightarrow \infty$. Under these conditions the operating line coincides with the 45° line. The calculation of the minimum number of equilibrium stages for a given separation is illustrated in Fig. 14-8. At a given pressure, the minimum number of equilibrium stages is a function of the product compositions and the equilibrium relationship only.

Ponchon and Savarit Method Employing Enthalpy-Concentration Diagrams

This section presents the rigorous graphical procedure attributed to Ponchon (14-40) and Savarit (14-44) for stagewise binary-distillation calculations. Numerous extensions of their approach have been reported in the literature (14-43, 14-56, 14-57, 14-59).

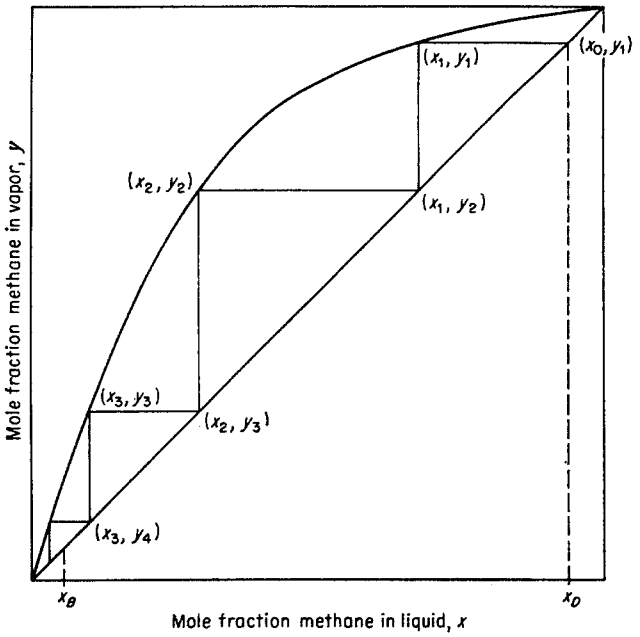

Fig. 14-8. Calculation of minimum number of equilibrium stages for methane-ethane binary system at 500 psia.

In its rigorous application, the procedure makes use of an enthalpy-concentration diagram together with vapor-liquid equilibrium data. Proper choice of state functions such as enthalpy and mass permits the heat and material streams to be added or subtracted linearly by graphical means.

In Fig. 14-9 a typical enthalpy-concentration dia-

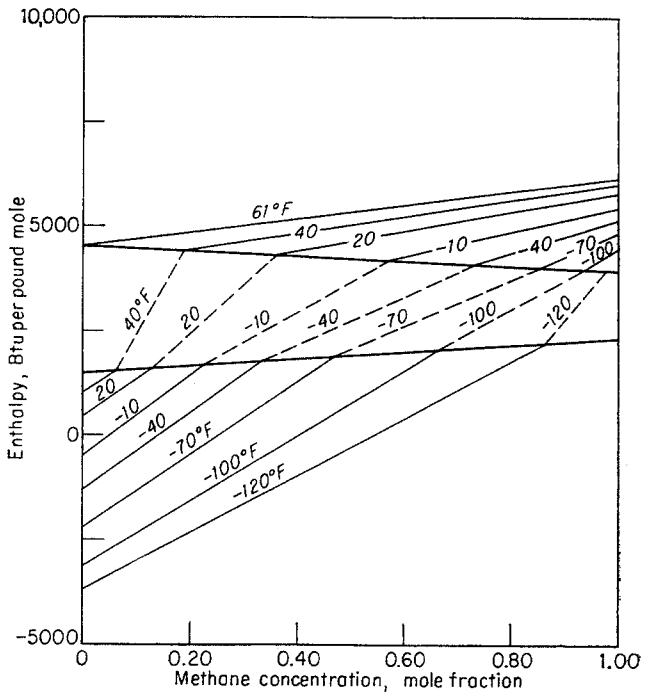

Fig. 14-9. Enthalpy-concentration diagram for methane-ethane system at 500 psia.

gram is shown for the methane-ethane system at 500 psia. The locus of enthalpies of the saturated liquid and vapor is shown with several equilibrium tie lines and their equilibrium temperatures. Experimental values of the enthalpy of mixtures of methane and ethane are not available, but have been estimated by assuming ideal solutions in both the vapor and liquid phases. A few isotherms in the superheated-vapor and subcooled-liquid regions are shown. Either enthalpy values in Btu per pound mole versus mole fractions or enthalpy values in Btu per pound versus mass fractions may be used.

The rigorous graphical determination of material and heat relationships for binary systems can be shown on an enthalpy-concentration diagram. The procedure is applied to the flow schemes presented in Figs. 14-10 and 14-11. Figure 14-10 represents an adiabatic case, and Fig. 14-11 a nonadiabatic case in which a quantity of heat q is added to the system. The stream compositions of F, V, and L are x_F, y, and x, respectively.

The material-balance and energy-balance equations for the scheme of Fig. 14-10 are

Over-all: $$F = V + L \tag{14-12}$$

Component: $$Fx_F = Vy + Lx \tag{14-13}$$

Total heat: $$Fh_F = VH_V + Lh_L \tag{14-14}$$

where H_V = enthalpy of vapor per unit mass
h_L = enthalpy of liquid per unit mass
h_F = enthalpy of feed per unit mass

Eliminating F from Eqs. (14-12) and (14-13) and from (14-12) and (14-14), respectively, gives

$$\frac{V}{L} = \frac{h_F - h_L}{H_V - h_F} = \frac{x_F - x}{y - x_F} \tag{14-15}$$

The elimination of L yields

$$\frac{V}{F} = \frac{h_F - h_L}{H_V - h_L} = \frac{x_F - x}{y - x} \tag{14-16}$$

or of V yields

$$\frac{L}{F} = \frac{H_V - h_F}{H_V - h_L} = \frac{y - x_F}{y - x} \tag{14-17}$$

Equations (14-15) to (14-17) state that the ratios of the magnitudes of the streams can be obtained by applying the lever-arm rule to the coordinate values of either the enthalpy or the concentration. The two right terms of Eq. (14-15) may be rearranged to give

$$\frac{H_V - h_F}{y - x_F} = \frac{h_F - h_L}{x_F - x} \tag{14-18}$$

Similarly, for Eq. (14-17),

$$\frac{H_V - h_F}{y - x_F} = \frac{H_V - h_L}{y - x} \tag{14-19}$$

Combining Eqs. (14-18) and (14-19) gives

$$\frac{H_V - h_F}{y - x_F} = \frac{h_F - h_L}{x_F - x} = \frac{H_V - h_L}{y - x} \tag{14-20}$$

These equations show that three points having the coordinates (x_F,h_F), (x,h_L), and (y,H_V) must lie on a straight line (Fig. 14-10*b*).

In this case, since L and V, which are in equilibrium, fall at the ends of the tie line, F is located at the value (x_F,h_F) in between.

The direction of either V or L may be reversed to show that the point representing the difference between two streams also lies along the straight lines through the two given streams. In this case, the point representing the difference between the two streams lies outside the two points whose differences are taken. The location of the "difference point" is achieved by applying the lever-arm rule to the ratios of the magnitudes of the streams. It should be emphasized that, although an equilibrium separation is treated in the example, the analysis is not restricted to phases in equilibrium.

The nonadiabatic case represented by Fig. 14-11*a* yields the following balances:

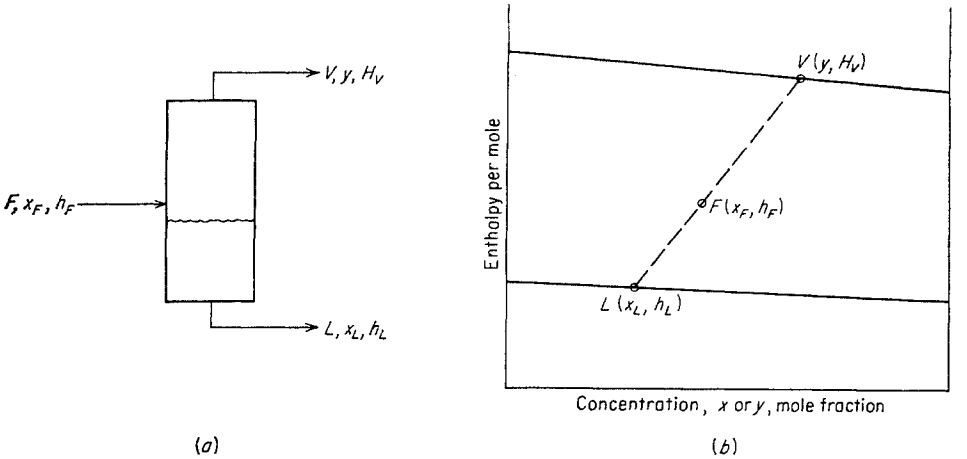

Fig. 14-10. (*a*) One-stage flash separation; (*b*) material-and-energy-balance solution to scheme of (*a*).

Fig. 14-11. (a) One-stage separation with heat added to the system; (b) material-and-energy-balance solution to scheme of (a).

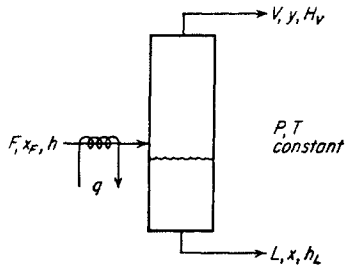

(a)

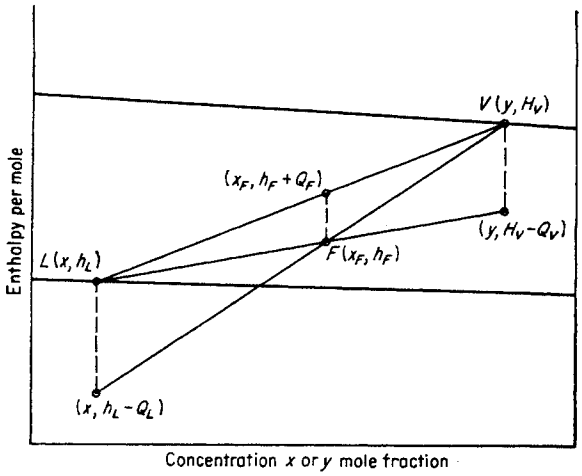

(b)

Over-all: $F = V + L$ (14-21)

Component: $Fx_F = Vy + Lx$ (14-22)

Total heat: $Fh_F + q = VH_V + Lh_L$ (14-23)

The total heat q may be represented on an enthalpy-concentration diagram by introducing the definitions that

$$q = FQ_F = VQ_V = LQ_L \tag{14-24}$$

where Q_F, Q_V, and Q_L represent the heat absorbed by the system from the surroundings per unit mass of F, V, and L, respectively. These definitions permit the combination of the heat stream q with any one of the mass streams. Manipulations similar to those carried out for the system of Fig. 14-10*a* and *b* yield the following relationships:

$$\frac{(h_F + Q_F) - h_L}{x_F - x} = \frac{H_V - (h_F + Q_F)}{y - x_F} = \frac{H_V - h_L}{y - x} \tag{14-25}$$

$$\frac{H_F - (h_L - Q_L)}{x_F - x} = \frac{H_V - h_F}{y - x_F} = \frac{H_V - (h_L - Q_L)}{y - x} \tag{14-26}$$

$$\frac{h_F - h_L}{x_F - x} = \frac{(H_V - Q_V) - h_F}{y - x_F} = \frac{(H_V - Q_V) - h_L}{y - x} \tag{14-27}$$

represented in Fig. 14-11*b*. The lever-arm rule is again used to obtain the mass ratios of the streams. Equations (14-25) to (14-27) are obtained by combining the heat stream q with F, V, and L, respectively.

The effect of combining the heat with a particular stream is to produce a vertical displacement from the point that actually represents the properties of that stream. The displacement is determined by the direction of the stream as well as by the direction of q (q is taken as positive when heat is absorbed from the surroundings). The direction of the displacement may be summarized as follows:

1. Mass stream in, q in: displacement upward or +
2. Mass stream out, q out: displacement upward or +
3. Mass stream in, q out: displacement downward or −
4. Mass stream out, q in: displacement downward or −

Figure 14-11*b* gives examples of case 4 when q is combined with either L or V and of case 1 when q is combined with F. The magnitude of the displacement equals q divided by the mass of the stream with which q is combined.

The three basic operations carried out in performing the Ponchon-Savarit calculations are:

1. Taking the sum of two streams to give the properties and amount of a third stream or an "addition point"
2. Taking the difference of two streams to give a third stream or a combination of streams, frequently called the "difference point"
3. Combining a pure heat stream with a mass stream

The operations are summarized in Fig. 14-12.

The application of the Ponchon-Savarit procedure to column calculations can be rigorously justified mathematically, provided that the analytical expressions for the enthalpy and equilibrium relations are not excessively cumbersome (14-35). Such an approach, however, will be abandoned in favor of the application of the three simple rules summarized in Fig. 14-12.

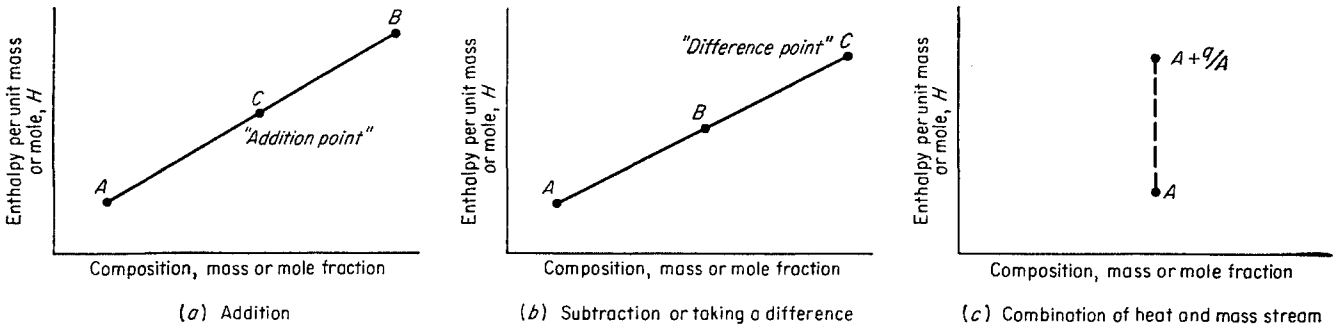

Fig. 14-12. Summary of three basic operations carried out on an enthalpy-concentration diagram.

Equilibrium-stage Calculation for Finite Reflux Ratio

The five external streams associated with the complete distillation column shown in Fig. 14-1 are F, B, D, q_c, and q_s, where

q_c = heat transferred in condenser
q_s = heat transferred in still

Three over-all heat and material-balance lines result from

1. Combining q_s with B, q_c with D
2. Combining q_s with F, q_c with D
3. Combining q_c with F, q_s with B

The three lines are shown in Fig. 14-13 and illustrate how the heat streams are combined with various mass streams. The line through the two difference points and the feed is the one of greatest significance, for its terminal points represent the difference points used in making the stagewise calculations.

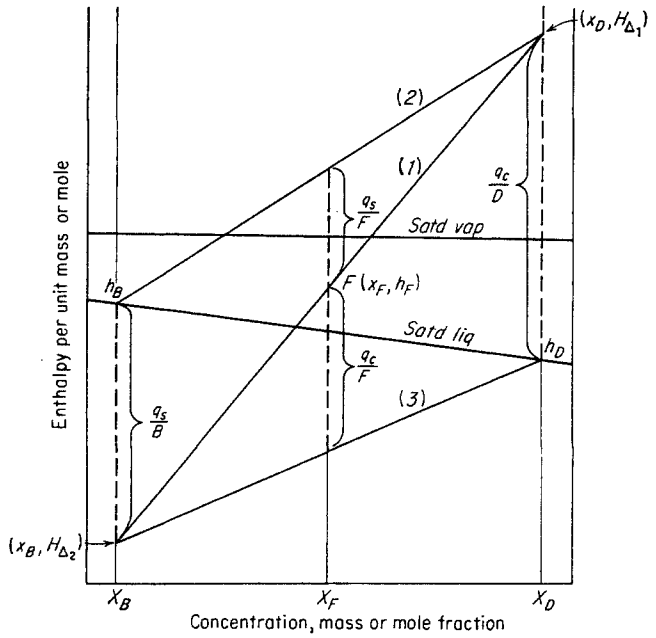

Fig. 14-13. Combination of heat streams with various mass streams for a complete column.

Although Fig. 14-13 indicates the way in which the over-all material-and-energy-balance lines may be drawn, the internal streams have yet to be interrelated. If a total condenser is used, the distillate-product composition is the same as the composition y_1 of the vapor leaving the top stage. The material and energy differences between D and q_c/D are precisely equal to the material and energy differences between any two streams passing each other within the column, until the feed is introduced. Let this fact be represented by the symbols

$$\left| h_D - \frac{q_c}{D} \right| = |H_{V_1} - h_{L_0}| = |H_{V_2} - h_{L_1}| = |H_{V_3} - h_{L_2}| = \cdots \quad (14\text{-}28)$$

But $|h_D - q_c/D|$ must represent a specific point which lies a distance q_c/D above the point (x_D,h_D), namely the point representing the combination of q_c/D with D. This is the point (x_D,H_{Δ_1}) in Fig. 14-14. Thus, all the difference lines down to the feed plate converge on the upper difference point (x_D,H_{Δ_1}). The vapor V_1 of composition y_1 is in equilibrium with (x_1,h_{L_1}) on the saturated-liquid line. (y_2,H_{V_2}) falls at the intersection of the difference line $\overline{(x_1,h_{L_1})(x_D,H_{D_1})}$ with the saturated-vapor line. By the alternative construction of equilibrium and difference lines, the streams are related up to the point where the feed is introduced. The optimum feed location, from a consideration of the number of trays required and the feed conditioning necessary, is usually found where a tie line and the over-all heat-and-material-balance line intersect.

Switching difference points is equivalent to introducing the feed. The calculations are continued as shown in Fig. 14-14, using the bottom difference point (x_B,H_{Δ_2}) in the stripping section, until the bottom composition x_B is reached. The total number of

equilibrium trays in the column may be obtained by counting the number of equilibrium stages or tie lines drawn during the construction. Fractional equilibrium stages may be estimated by interpolation along the saturated-vapor or saturated-liquid lines. The external-reflux ratio L_0/D for Fig. 14-14 is given by the ratio of the line $\overline{(y_1,H_{V_1})(x_D,H_{\Delta_1})}$ to $\overline{(y_1,H_{V_1})(x_D,h_D)}$.

Minimum Reflux Ratio

The minimum reflux ratio for a given separation will occur at the highest reflux ratio for which a tie line and a difference line coincide. To start the search for the minimum reflux ratio, it may be imagined that all tie lines are difference lines; the tie lines above the feed are extended until they intersect the line $x = x_D$, and those below the feed until they intersect the line $x = x_B$. The highest intersection point above the feed and the lowest one below the feed are of interest, since they represent the highest reflux ratios that fulfill the criterion of minimum reflux ratio.

Finally, lines through these two points and through the feed are drawn, to pick the higher reflux ratio of the two. The graphical determination of the minimum reflux ratio is illustrated in Fig. 14-15. Usually, for binary hydrocarbon mixtures and for systems showing regular equilibrium behavior, the tie line through the feed when extended corresponds to the minimum reflux ratio, producing the zone of constant composition at the feed plate. For systems such as ethanol-water, which show serious deviations from ideality in the liquid phase, the zone of infinite stages may occur elsewhere.

Minimum Number of Equilibrium Stages

The minimum number of equilibrium stages required to conduct a given separation corresponds to a condition of total reflux:

$$\frac{L_0}{D} \to \infty \qquad \text{or} \qquad \frac{L}{V} = 1.0$$

This requirement is met on an enthalpy-composition diagram when the upper and lower difference points are located "at" $+\infty$ and $-\infty$, respectively. The construction that results from these locations of the difference points is shown in Fig. 14-16. The difference lines now become vertical, since the streams passing each other have identical composition.

Other Calculations

The adaptation of the Ponchon-Savarit procedure to many other cases appears in the literature. For a two-feed column, there are three difference points.

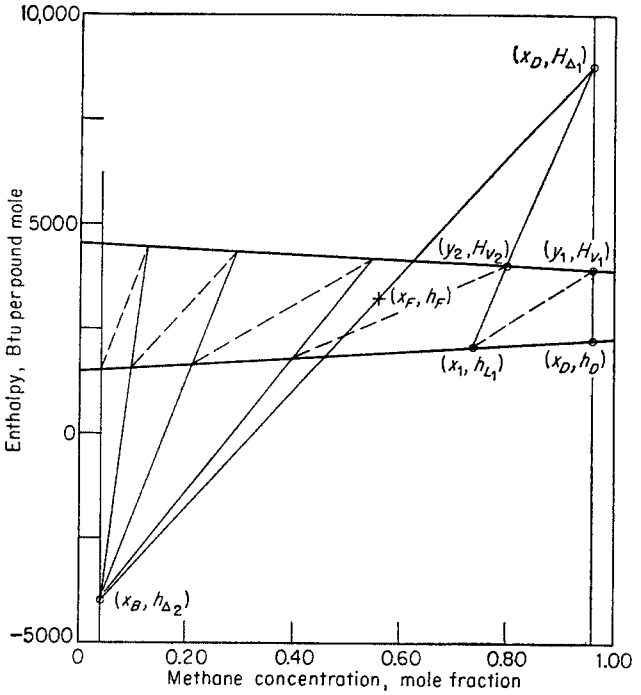

Fig. 14-14. Calculation of complete distillation column at finite reflux ratio.

The 0 point, representing the sum of the feeds F_1 and F_2, is located by applying the lever-arm principle

$$\frac{\text{Mass of } F_1}{\text{Mass of } F_2} = \frac{\overline{\text{OF}_2}}{\overline{\text{OF}_1}}$$

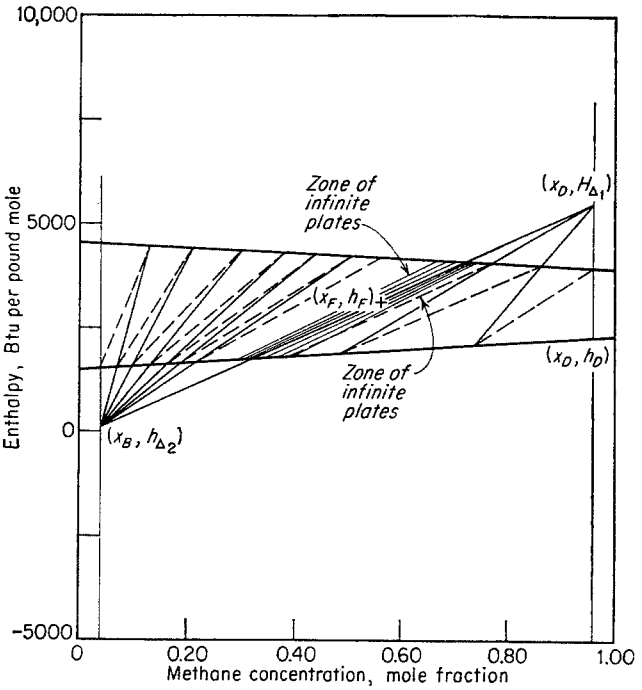

Fig. 14-15. Determination of minimum reflux ratio for methane-ethane system at 500 psia.

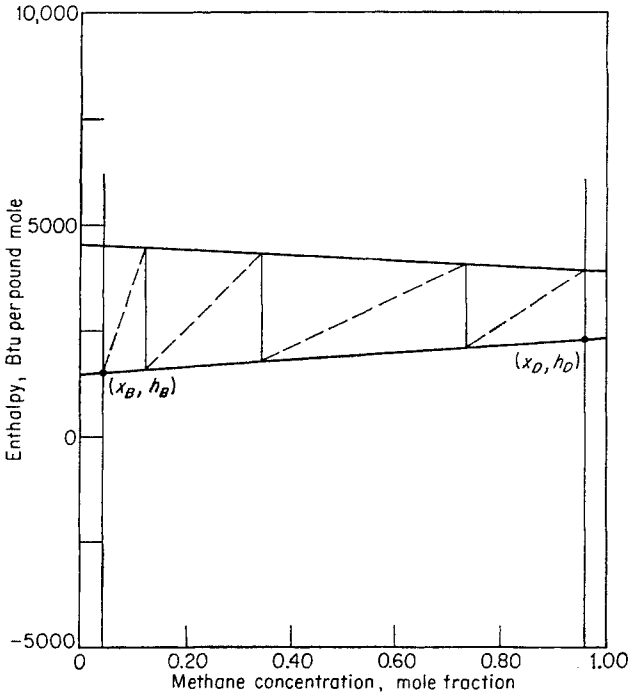

Fig. 14-16. Determination of minimum number of equilibrium stages for methane-ethane system at 500 psia.

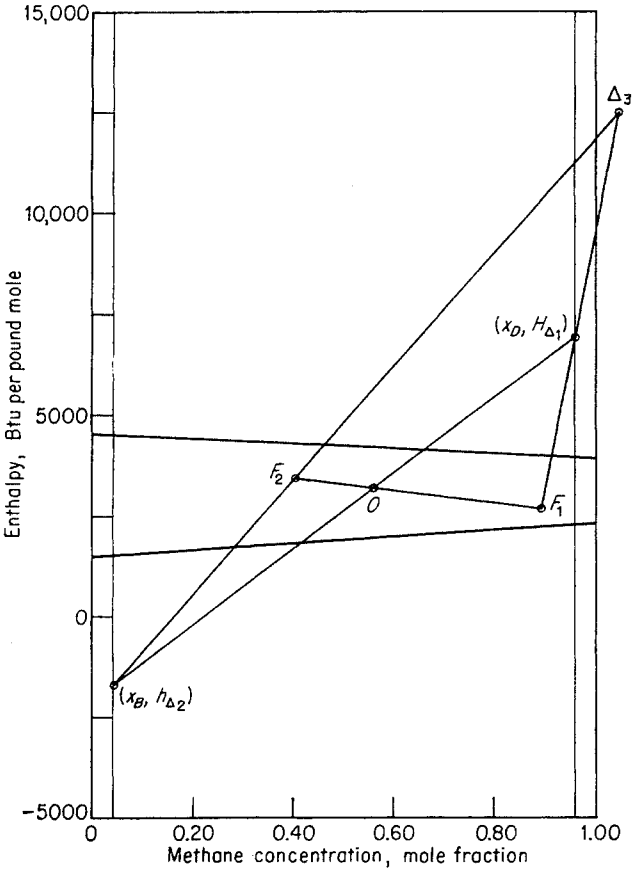

Fig. 14-17. Difference-point location for a two-feed column for methane-ethane system at 500 psia.

Figure 14-17 shows the construction of the difference points for the two-feed column.

The Murphree vapor efficiency for a single plate is defined as

$$E_0 = \frac{y_n - y_{n+1}}{y_n^* - y_{n+1}} \tag{14-29}$$

where y_n, y_{n+1} are actual vapor concentrations and where y_n^* is the composition of the vapor that would be in equilibrium with the average liquid composition x_n.

This equation gives the efficiency of contact of a single plate, based on vapor-phase concentrations. Since the efficiency for a single plate may not be equal to the over-all efficiency for the entire column (14-36), it may be necessary to include the plate efficiency in the stagewise calculations. Figure 14-18 indicates, for a few stages, how this is carried out.

When the enthalpy-concentration curves for the vapor and liquid phases on a molal basis are parallel, the Ponchon-Savarit and the McCabe-Thiele calculations give identical results. In the absence of thermal data for mixtures, the latent heat of vaporization of the pure component and the assumption of ideal solutions provide a reasonable estimate of the enthalpy-composition relationship for hydrocarbon systems.

Other stagewise distillation columns which have been successfully calculated by means of the Ponchon-Savarit procedure include columns with:

1. Multiple feed (14-59)
2. Sidestream removal (14-59)
3. Partial condenser (14-59)
4. Interstage heating or cooling (14-30)
5. Combined reboiler and open steam (14-30)
6. Open steam with complete liquid-phase miscibility (14-7)
7. Distillation of mixture with two liquid phases (14-30)
8. Double column of the Linde type (14-43, 14-59)

The large number of variations that have been handled by this method attests to the versatility of the procedure.

Analytical Method for Calculating Binary Distillation

Analytical methods for distillation calculation by the equilibrium-stage concept have been developed for the general multicomponent case with any number of distributed components, assuming constant relative volatility and constant molal overflow (14-37, 14-55). The general equations have evolved from previous treatments of binary (14-52) and ternary

(14-53, 14-54) distillation calculations employing the same fundamental assumptions.

Analytical calculations for binary distillation find application in many cases where distillation of two close-boiling components of a homologous series is undertaken. The following procedure (14-7), like other procedures (14-48, 14-52), assumes constant relative volatility and constant molal overflow in each section of the column. Because of the inherent errors in graphical methods, the analytical procedure may be comparatively accurate and convenient for separations requiring a large number of stages. Although it is understood that the basic equations for stagewise calculations are finite-difference equations (14-51), the foregoing attack employs algebraic equations exclusively (14-7).

The assumption of constant relative volatility specifies that

$$\alpha = \frac{K_a}{K_b} = \text{constant} \tag{14-30}$$

where $K_a = y/x$ of more volatile component a
$K_b = y/x$ of less volatile component b

Equation (14-30) may be restated in terms of the mole fraction y of a in the vapor phase and the mole fraction x of a in the liquid phase.

$$y = \frac{\alpha x}{1 + (\alpha - 1)x} \tag{14-31}$$

By means of the linear transformation of coordinates illustrated in Fig. 14-19, the operating lines became 45° lines. The shaded section, representing the area between the operating line in the rectifying section and the equilibrium line, can be made to fit between the 45° line and the transformed equilibrium line in the new $x' - y'$ plane. The operating line is thereby simplified, but some added complexities are introduced in the new equilibrium line. The necessary transformations are

$$x' = \frac{x - x_{\text{I}}}{x_{\text{II}} - x_{\text{I}}} \tag{14-32}$$

$$y' = \frac{y - y_{\text{I}}}{y_{\text{II}} - y_{\text{I}}} \tag{14-33}$$

where $(x_{\text{I}},y_{\text{I}})$ and $(x_{\text{II}},y_{\text{II}})$ are the coordinates of the lower and upper roots, respectively, of the equilibrium line expressed by Eq. (14-31) and of the original operating line in the rectifying section. Notice that, when $x = x_{\text{II}}$, $x' = 1.0$; and that, when $y = y_{\text{II}}$, $y' = 1.0$. Eliminating y in Eq. (14-33) through the use of Eq. (14-31),

$$\frac{\alpha x}{1 + (\alpha - 1)x} - \frac{\alpha x_{\text{I}}}{1 + (\alpha - 1)x_{\text{I}}} = y'\left[\frac{\alpha x_{\text{II}}}{1 + (\alpha - 1)x_{\text{II}}} - \frac{\alpha x_{\text{I}}}{1 + (\alpha - 1)x_{\text{I}}}\right] \tag{14-34}$$

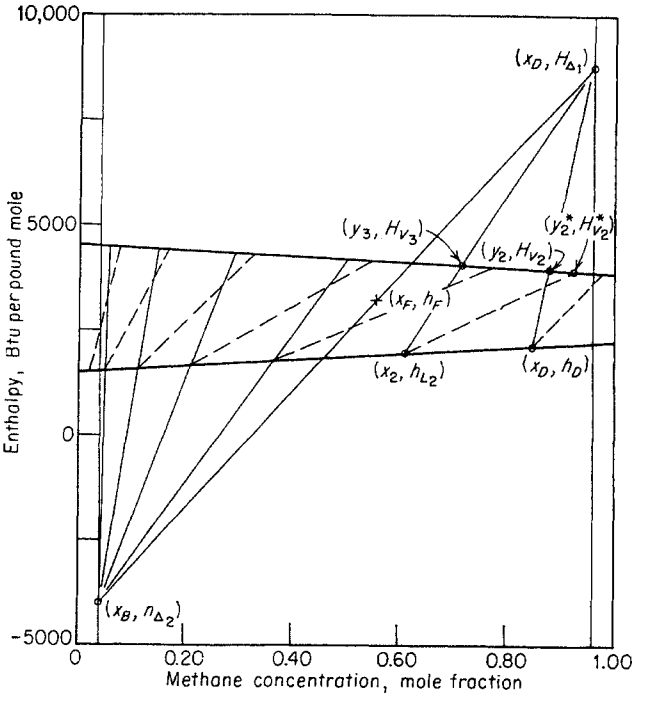

Fig. 14-18. Inclusion of Murphree plate efficiency based on vapor phase in Ponchon-Savarit calculation.

Solving for y',

$$y' = \frac{\dfrac{x}{1 + (\alpha - 1)x} - \dfrac{x_{\text{I}}}{1 + (\alpha - 1)x_{\text{I}}}}{\dfrac{x_{\text{II}}}{1 + (\alpha - 1)x_{\text{II}}} - \dfrac{x_{\text{I}}}{1 + (\alpha - 1)x_{\text{I}}}} \tag{14-35}$$

$$= \frac{x - x_{\text{I}}}{x_{\text{II}} - x_{\text{I}}} \frac{1 + (\alpha - 1)x_{\text{II}}}{1 + (\alpha - 1)x} \tag{14-36}$$

$$= x' \frac{1 + (\alpha - 1)x_{\text{II}}}{1 + (\alpha - 1)x} \tag{14-37}$$

Eliminating x from Eq. (14-37) by using (14-32),

$$y' = \frac{[1 + (\alpha - 1)x_{\text{II}}]x'}{1 + (\alpha - 1)x_{\text{I}} + (\alpha - 1)(x_{\text{II}} - x_{\text{I}})x'} \tag{14-38}$$

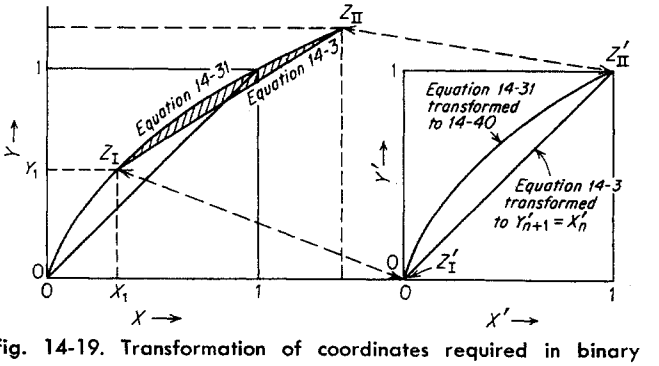

Fig. 14-19. Transformation of coordinates required in binary analytical calculations.

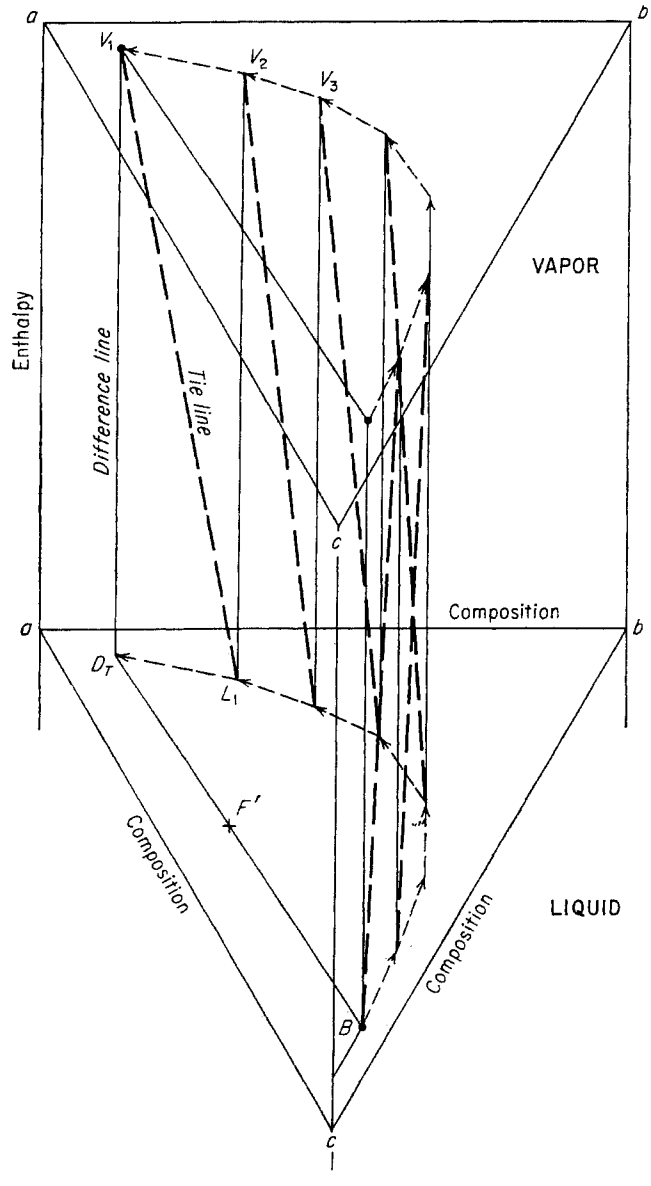

Fig. 14-20. Calculation of minimum number of stages by enthalpy-composition diagram for a ternary mixture.

Dividing the numerator and denominator of Eq. (14-38) by $1 + (\alpha - 1)x_I$ and introducing the definition

$$c = \frac{1 + (\alpha - 1)x_{II}}{1 + (\alpha - 1)x_I} \tag{14-39}$$

the following expression for the equilibrium line in the $x' - y'$ plane is obtained:

$$y' = \frac{cx'}{1 + (c - 1)x'} \tag{14-40}$$

The operating line is reduced to a 45° line on the $x' - y'$ plane, that is,

$$y' = x' \tag{14-41}$$

Dividing Eq. (14-40) by $1 - y'$ leads to a restatement of the equilibrium line on the $x' - y'$ plane:

$$\begin{aligned} \frac{y'}{1 - y'} &= \frac{cx'}{1 + (c - 1)x'} \frac{1}{1 - \dfrac{cx'}{1 + (c - 1)x'}} \\ &= \frac{cx'}{1 + (c - 1)x'} \frac{1 + (c - 1)x'}{1 - x'} \\ &= \frac{cx'}{1 - x'} \end{aligned} \tag{14-42}$$

For the general plate i,

$$\frac{y'_{i+1}}{1 - y'_{i+1}} = \frac{cx'_{i+1}}{1 - x'_{i+1}} \tag{14-43}$$

Since the stagewise relation of streams passing each other on the $x' - y'$ plane is that

$$x'_i = y'_{i+1} \tag{14-44}$$

y'_{i+1} can be eliminated; so

$$\frac{x'_i}{1 - x'_i} = \frac{cx'_{i+1}}{1 - x'_{i+1}} \tag{14-45}$$

For stages $i + 1$ and $i + 2$,

$$\frac{x'_{i+1}}{1 - x'_{i+1}} = \frac{cx'_{i+2}}{1 - x'_{i+2}} \tag{14-46}$$

Combining Eqs. (14-45) and (14-46),

$$\frac{x'_i}{1 - x'_i} = \frac{c^2x'_{i+2}}{1 - x'_{i+2}}$$

In general, the liquid composition from plate 0 may be related to that leaving plate n by

$$\frac{x'_0}{1 - x'_0} = \frac{c^n x'_n}{1 - x'_n} \tag{14-47}$$

or

$$n = \frac{\log [x'_0(1 - x'_n)/x'_n(1 - x'_0)]}{\log c} \tag{14-48}$$

where n = number of equilibrium stages required to distill from $x' = x'_0$ to $x' = x'_n$.

The form of Eq. (14-48) is precisely that of the Fenske-Underwood (14-17, 14-52) equation for the computation of the minimum number of stages under total-reflux conditions. In the Fenske-Underwood equation $\log c$ is replaced by $\log \alpha$.

The range of concentration over which the distillation is to be conducted in each section of the column can be obtained from Eq. (14-32), provided the values of x_I and x_{II} are known. x_I and x_{II} are the intersections of the equilibrium line, Eq. (14-31), and the operating line, Eq. (14-3).

$$y = \frac{L}{V} x + \frac{D}{V} x_D \tag{14-3}$$

The x coordinates may be obtained by eliminating y

from Eqs. (14-31) and (14-3) and solving the quadratic equation, obtaining

$$x_{I,II} = \frac{\left(-\left[\frac{L}{V} - \alpha + (\alpha - 1)\frac{D}{V}x_D\right] \pm \left\{\left[\frac{L}{V} - \alpha + (\alpha - 1)\frac{D}{V}x_D\right]^2 - \frac{4}{V^2}LDx_D(\alpha - 1)\right\}^{1/2}\right)}{2(\alpha - 1)\frac{L}{V}} \tag{14-49}$$

where $x_I > x_{II}$.

The values of x_I and x_{II} below the stripping section, which arise from the simultaneous solution of Eqs. (14-5) and (14-31), can be obtained by replacing L by L', V by V', D by $-B$, and x_D by x_B in Eq. (14-49). The streams above and below the feed were related by the equations

$$L' = L + qF \tag{14-6}$$
$$V' = F(q - 1) + V \tag{14-9}$$

At total reflux, since $D = 0$, $L/V = 1.0$.

$$x_I,\ x_{II} = 0,\ 1$$

which, when substituted into Eq. (14-49), states that $c = \alpha$ and reduces Eq. (14-48) to the Fenske-Underwood equation. Equation (14-48), applied to both the rectifying and the stripping sections of the column, yields the number of equilibrium stages required for the separation.

Graphical Representation of Ternary-distillation Calculations

The application of the enthalpy-concentration diagram to ternary-distillation calculations is thwarted by the need for three dimensions to represent the enthalpy and the two independent composition variables at constant pressure. The general use of the Ponchon-Savarit construction in three-dimensional space is impractical for routine calculations; it may, however, be used successfully as an instructive tool in developing an understanding of multicomponent calculations (14-58).

An enthalpy-concentration diagram, with the calculation of the minimum number of stages required for a separation, is presented in Fig. 14-20. The upper surface represents the saturated-vapor locus and the lower surface the saturated-liquid locus. Vapor-liquid equilibrium relationships can best be represented for multicomponent hydrocarbon systems by means of equilibrium-vaporization constants or K values. A given point in the upper surface is related to its equilibrium liquid phase by means of a dew-point calculation, and a given point in the lower surface is related to its equilibrium vapor phase by means of the bubble-point calculation. In three dimensions, the difference line becomes a set of lines in space and the difference point a point in space. From a knowledge of the difference point and of a point on the saturated-liquid (or vapor) locus, the third point is located as a piercing point on the saturated-vapor (or liquid) locus.

The difference points in Fig. 14-20 are located "at" $\pm\infty$, since the separation is conducted at total reflux. Note that, under these conditions, all the difference lines are drawn vertically. At total reflux, since $D = 0$, the compositions and amounts of the streams passing each other fall on the vertical difference lines at their respective saturated enthalpies.

In a multicomponent distillation, it is not always clear what variables can be fixed to establish a unique solution. For the projected total reflux calculation (Fig. 14-21) the system pressure or column pressure, the feed composition, and the concentrations of the most volatile component in the bottoms and of the least volatile component in the overheads are fixed. The restrictions on the overhead and bottoms products are set by the lines x_{cd} and x_{ab} of Fig. 14-21. A trial-and-error calculation is necessary to determine the remaining dependent concentration variables in the overhead and bottoms products. An assumed value of B_T leads to a consequent value of D_T since B_T, F, and D_T must all lie along a straight line. But the assumed B_T also yields a D_T value by stagewise computation up the column. The correct B_T has been

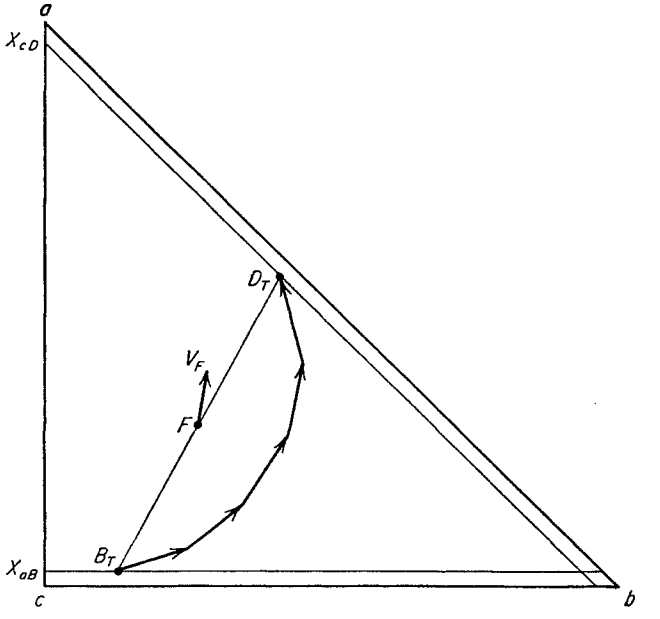

Fig. 14-21. Minimum reflux calculation projected on composition plane. (*White*, 14-58. *Courtesy Petrol. Processing.*)

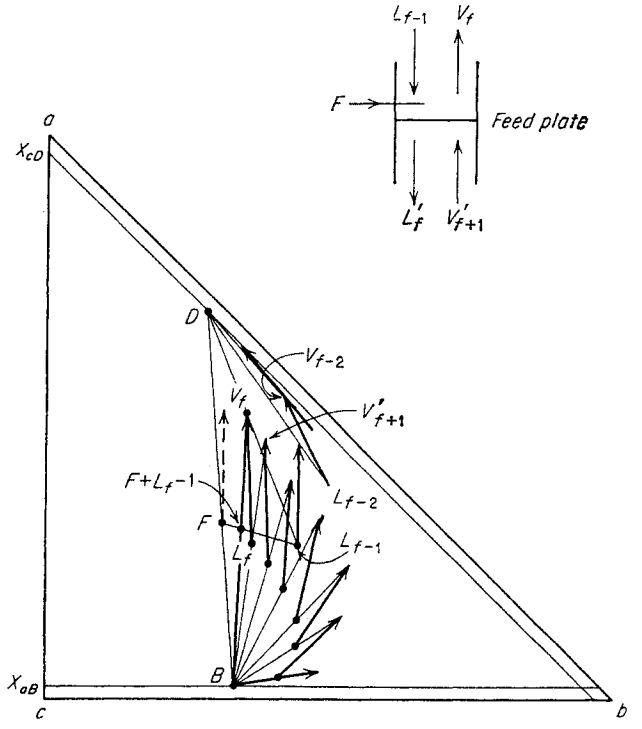

Fig. 14-22. Stagewise calculation of complete column at finite reflux. (*White*, 14-58. *Courtesy Petrol. Processing.*)

assumed when the D_T calculated by material balance and the D_T found by stagewise calculations concur. The minimum number of stages, not necessarily an integer, is obtained by counting the tie lines.

For three-component calculations, the tie lines and difference lines can be projected onto the composition

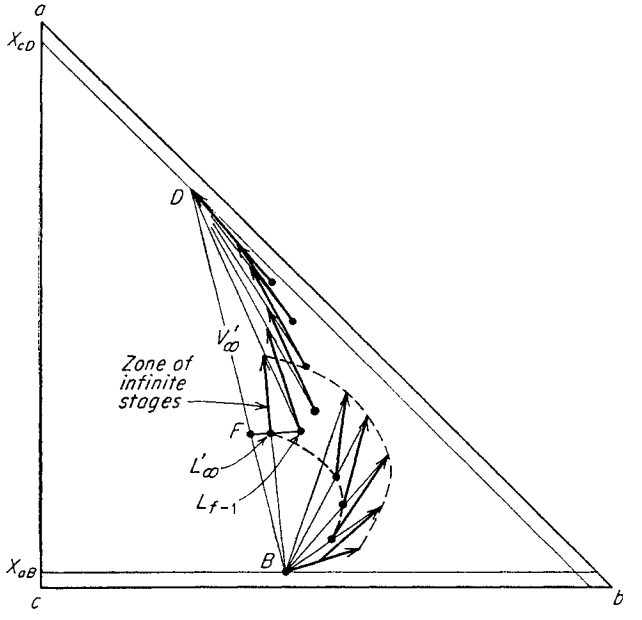

Fig. 14-23. Calculation of zone of infinite stages for a ternary mixture. (*White*, 14-58. *Courtesy Petrol. Processing.*)

plane with little loss of understanding, especially if the system under consideration possesses constant molal latent heat of vaporization over the concentration range of the separation. White's solution (14-58) for a complete column, assuming constant molal reflux, is shown in Fig. 14-22. For a complete column operating at an intermediate reflux ratio, for a three-component distillation, the following total number of variables may be listed:

1. Column pressure (1 variable)
2. Feed composition and its state (3 variables)
3. Composition of bottoms (2 variables)
4. Composition of overheads (2 variables)
5. Number of theoretical stages (1 variable)
6. Feed-plate location (1 variable)
7. Reflux ratio at one point in the column (1 variable)
8. State of distillate and reflux (1 variable)

Of these variables, let the column pressure, the feed composition and its state, the composition of the most volatile component in the bottoms, the composition of the least volatile component in the overhead, the reflux ratio defined by V_s/B or L_0/D, and the feed-plate location be fixed. The reboil ratio V_s/B is the ratio of the moles of stripping vapors to the moles of bottoms product. Again, a double trial-and-error solution is necessary to obtain the value of the other dependent variables. An additional composition in the bottoms is assumed, tentatively fixing the location of B. By material balance, the tentative D is established, since $B + D = F$. The feed plate may be specified by requiring the feed to be introduced at an optimum point in the column. To check the assumed bottoms composition, it is now necessary to make a stagewise calculation up through the column. The vapor V_s in equilibrium with B is located by a bubble-point calculation on the tentative bottoms composition. Since $V_s + B = L_{B+1}$, from the known ratio V_s/B the location of L_{B+1} may be established. Now, L_{B+1} is in equilibrium with V_{B+1}, and $V_{B+1} + B = L_{B+2}$. Assuming constant molal overflow,

$$\frac{V_s}{B} = \frac{B_{B+1}}{B} = \frac{V_{B+2}}{B} = \cdots \qquad (14\text{-}49a)$$

so the location of the liquid composition can be established after each bubble-point calculation. The calculation proceeds up the column until the ratio of the key components in the liquid portion of the feed is approximately equal to the ratio of the same components in the liquid leaving the feed tray.

The introduction of the feed is achieved by changing

difference points from B to D. The value of L/V above the feed plate corresponding to the value of V_s/B below the feed plate is obtained by means of a heat balance around the entire column. The heat balance around the column is given by

$$Fh_F + q_s = (V_1H_1 - V_1h_D) + Bh_B + Dh_D \qquad (14\text{-}50)$$

where F = mass of feed
h_F = enthalpy per unit mass of feed
q_s = total heat to still
V_1 = mass of vapor leaving top stage $L_0 + D$
H_1 = enthalpy of V_1 per unit mass
h_D = enthalpy of distillate product or reflux per unit mass
B = mass of bottoms product
h_B = enthalpy of bottoms product per unit mass

By using Eq. (14-50), it is possible to solve for V_1 and, hence, for the reflux ratio L/V above the feed plate. Referring to Fig. 14-22, the difference of the streams just above the feed stage is $V_f - L_{f-1} = D$, or

$$\frac{L_{f-1}}{V_f} = \frac{\overline{V_fD}}{\overline{L_{f-1}V_f}} \qquad (14\text{-}50a)$$

which permits the location of L_{f-1}. A bubble-point calculation gives V_{f-1}, from which L_{f-2} may be located. The calculation is continued up the column until the specification line x_{c_D} is crossed. A check on the assumed B is obtained only if a tie line intersects the specification line $x = x_{cd}$ to give a value of D which falls on a straight line $\overline{BFD}$. If a check is not obtained, a new value of B is assumed and the calculations are repeated. It is apparent that the final solution is obtained only as a result of a tedious iterative process.

The minimum reflux ratio is, again, that reflux ratio for which the tie lines and difference lines coincide in some section of the column as the reflux ratio is lowered from some higher workable value. This coincidence is equivalent to the development of a zone of infinite stages. Figure 14-23 gives White's illustration of the minimum-reflux-ratio calculation for a case in which the introduction of the feed is delayed (calculating up the column) until a zone of infinite stages develops below the feed stage. Note that, by switching difference points or by introducing the feed, it is possible to "work out" of the zone of infinite stages.

STAGEWISE MULTICOMPONENT CALCULATION METHODS

Stagewise multicomponent calculations have been developed and illustrated by Lewis and Matheson (14-32), Thiele and Geddes (14-50), and McIntire (14-34). In the first method, the number of ideal stages is determined from known terminal-product composition by effecting a feed-stage mesh. The second procedure also makes use of the feed-stage mesh, but the product compositions are found for a *given* number of ideal stages. The final method is based on an iterative procedure for correcting the assumed L/V and temperature profile through the column. Calculations are continued until there are no further changes in (1) the temperature gradient; (2) the vapor-volume gradient; (3) the stages in the absorbing section; and (4) the stages in the stripping section from one iteration to the next.

Lewis-Matheson Procedure

Of the methods listed, only the Lewis-Matheson procedure, which uses the notion of the feed-plate mesh, will be discussed here. Furthermore, the assumption will be made that only the adjacent key components are distributed. The treatment of separations in which more than two components are distributed may be attacked systematically by assuming constant relative volatility and constant molal reflux (14-55), or through the use of digital computers in the manner of Bonner (14-5). In the last-mentioned procedure, no distinction is made between "sharpness" and "sloppiness" of cut, since every component in the feed is assumed to be distributed in both the bottoms and overhead products.

With the simplifying assumption that only the adjacent key components are distributed in both the bottoms and the overhead products, the designation of the amount of a key component in each product stream permits a complete component material balance for the separation. Starting, then, with a knowledge of the tower pressure, the feed, overheads, bottoms, feed conditions, reflux ratio, and reflux state, the Lewis-Matheson method permits the calculation of the number of equilibrium stages by a plate-to-plate procedure.

A dew-point calculation on the overheads gives the top-stage temperature T_1 and the composition of the equilibrium liquid phase. A bubble-point calculation on the bottoms product gives the bottoms temperature T_B and the composition of the vapors V_B in equilibrium with it. Since the moles of V_1, L_0, and D and their states are known, the value of $|H_{V_1} - h_{L_0}|$, or the enthalpy difference in the streams passing each other in the rectifying section of the column, may be computed.

For the calculation down the column, the composition of L_1 is known, but its amount is not. Therefore, the amount of L_1 is assumed, giving a tentative value

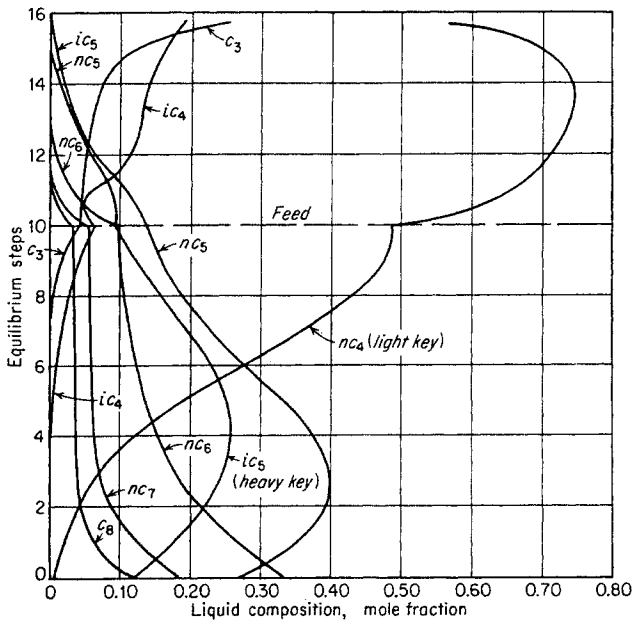

Fig. 14-24. Component-concentration curves for debutanizer at 120 psia. (*Shelton, McIntire, and Hachmuth, 14-46. Courtesy NGAA.*)

for the amount and composition of V_2 by material balance. A dew-point calculation on V_2 gives the temperature of stream V_2; so the heat-balance check for the required equality,

$$|H_{V_1} - h_{L_0}| = |H_{V_2} - h_{L_1}|$$

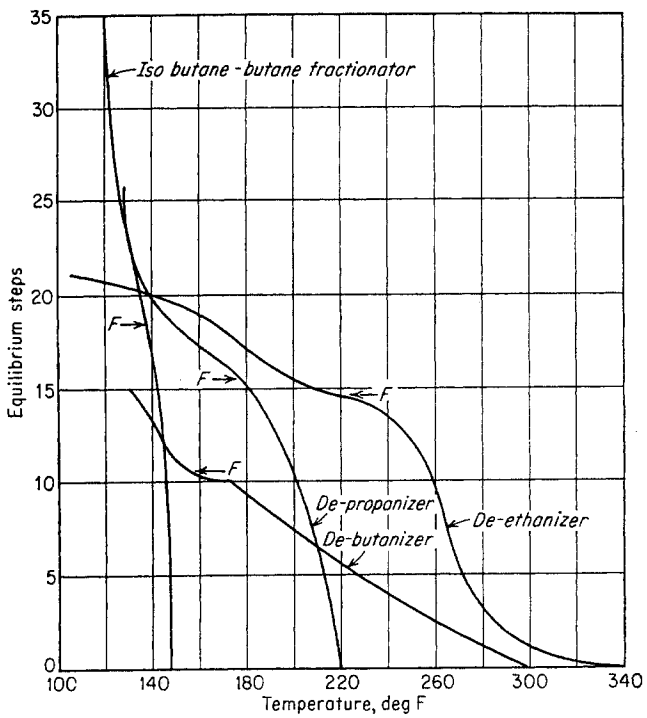

Fig. 14-25. Temperature gradients for four fractionators. (*Shelton, McIntire, and Hachmuth, 14-46. Courtesy NGAA.*)

can be made. If the difference equality does not hold, a new value of L_1 is assumed and the calculation is repeated. Usually, a heat balance can be obtained with two or three assumed values of L_1. The calculation for the next stage, 2, makes use of the liquid concentration L_2 obtained by the previous dew-point calculation on V_2. The correct amount of L_2 is calculated by trial and error, using the enthalpy difference $|H_{V_1} - h_{L_0}|$ as a check. These calculations down the column are continued until it is evident that the ratios of the key components in the liquid and in the liquid portion of the feed are identical or nearly so.

For the bottom section of the column, the difference between the enthalpies of the streams passing each other may be obtained by a heat-and-material balance around the rectifying section of the column, including the feed stage. The difference between the enthalpies of the streams passing each other in the stripping section may also be obtained by a heat balance around the bottom of the column, if the reboil ratio V_s/B is given rather than the reflux ratio L_0/V_1.

A bubble-point calculation on the bottoms product gives the composition of V_B, but not its amount. It is necessary to determine the amount of V_B such that

$$|q_s - h_B| = |H_{V_B} - h_{L_{B+1}}|$$

that is, such that the difference between the still heat and the heat in the bottoms is equal to the difference between the enthalpies of the adjacent vapor and liquid streams passing each other. With the correct value of V_B and the correct temperature of stream L_{B+1}, the calculation proceeds to the next stage by assuming an amount of V_{B+1}, etc. Stagewise calculations are made until the ratio of keys calculating upward is approximately equal to the ratio of keys in the liquid portion of the feed.

Up to this point, the calculations have completely neglected the appearance of the components lighter than the light key in the stripping section and of the components heavier than the heavier key in the rectifying section. But these components do have some bearing on the liquid, vapor, and concentration profiles in their respective sections, and must therefore be taken into account in any rigorous stagewise calculation. Therefore, in order to obtain the final feed-tray mesh, it is necessary to drop back a few trays, begin the addition of small amounts of the nondistributed components, and calculate back toward the feed tray from either side. If the amounts of nondistributed components are improperly added, the composition of the components will not mesh simultaneously at a common stage, the feed stage. The concentration profile of the key components will be

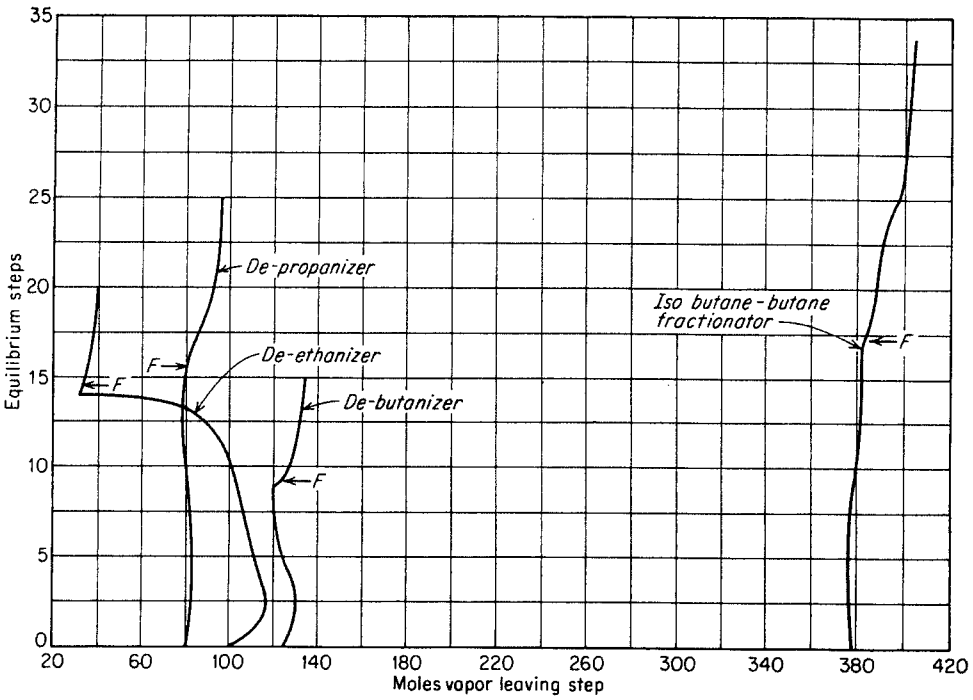

Fig. 14-26. Vapor quantities for four fractionators. (*Shelton, McIntire, and Hachmuth*, 14-46. Courtesy NGAA.)

altered somewhat by consideration of these nondistributed components.

A systematic procedure for effecting the feed-plate mesh is discussed by Brown (14-7). The final concentration, temperature, and vapor profiles for a commercial debutanizer operating at 120 psia is given in Figs. 14-24 to 14-26 (14-46). Note that a discontinuous but exact mesh occurs at the feed tray. Typical relative maxima with respect to concentration occur on some intermediate stage for the key component.

Examples of rigorous stagewise calculation of distillation columns by digital computers are now available in the literature (14-5, 14-34, 14-47).

RAPID CALCULATION PROCEDURES FOR DISTILLATION COLUMNS

Multicomponent-distillation calculations can be conducted rapidly by recourse to:

1. Digital computers employing intermediate or higher-speed computers
2. Short-cut procedures

The short-cut procedures are not without utility in preparing rigorous digital computations. The short-cut procedures may be programmed on digital computers to provide the basis for preliminary judgment before employing more rigorous procedures.

One short-cut procedure involves the following sequence of calculations:

1. Calculation of minimum reflux ratio
2. Calculation of minimum number of equilibrium stages
3. Calculation of actual number of equilibrium stages from the minimum reflux ratio and the minimum number of stages
4. Location of the feed stage or tray
5. Translation of the number of equilibrium stages to the actual number of stages

Underwood Minimum-reflux Calculations

For the case of constant relative volatility and constant molal reflux, Underwood has obtained the following equations for the computation of the minimum reflux ratio (14-55):

$$\frac{\alpha_1 x_{1,F}}{\alpha_1 - \phi} + \frac{\alpha_2 x_{2,F}}{\alpha_2 - \phi} + \frac{\alpha_3 x_{3,F}}{\alpha_3 - \phi} + \cdots + \frac{\alpha_n x_{n,F}}{\alpha_n - \phi} = 1 - q' \tag{14-51}$$

$$\frac{\alpha_1 x_{1,D}}{\alpha_1 - \phi} + \frac{\alpha_2 x_{2,D}}{\alpha_2 - \phi} + \frac{\alpha_3 x_{3,D}}{\alpha_3 - \phi} + \cdots + \frac{\alpha_n x_{n,D}}{\alpha_n - \phi} = R_{\min} + 1 \tag{14-52}$$

where the α's are the relative volatilities
the x's are the concentrations taken in mole fractions
subscript F denotes components in feed
subscript D denotes components in distillate
q' = moles of saturated liquid formed on feed plate by introduction of 1 mole of feed = $(H_{SV} - h_F)/(H_{SV} - h_{SL})$

ϕ = enrichment parameter defined by Eq. (14-51)

$R_{\min}$ = minimum reflux ratio L_0/D

Equation (14-51) arises from the elimination of the reflux ratios from Eq. (14-52) and its companion equation for the stripping column:

$$\frac{\alpha_1 x_{1,B}}{\alpha_1 - \phi} + \frac{\alpha_2 x_{2,B}}{\alpha_2 - \phi} + \frac{\alpha_3 x_{3,B}}{\alpha_3 - \phi} + \cdots + \frac{\alpha_n x_{n,B}}{\alpha_n - \phi} = -S \tag{14-53}$$

where ϕ = parameter for stripping column used to simplify algebraic manipulations

$S = (RD + q'F - B)/B$

Equations (14-51) and (14-52) may be solved for the general case for any number of components, including the special cases:

1. Where the separation between adjacent key components (components whose concentration it is desired to control) is not sharp
2. Where there are one or more distributed components between the key components

To solve for the minimum reflux ratio when the key components lie adjacent to each other and only the key components are distributed, one finds first the value of ϕ between the relative volatilities of the adjacent key components that satisfies Eq. (14-51). This value of ϕ is then used to calculate the minimum reflux ratio $R_{\min}$ in Eq. (14-52). For this solution, all the distillate concentrations were known because only the key components were distributed. For the case in which there are distributed components other than the key components, all the distillate-product compositions are not known and additional relations are required to solve for $R_{\min}$. If one component between the two keys is distributed, the two values of ϕ that fall between the relative volatilities of the key components provide two equations (14-52) which may be solved simultaneously to obtain the unknown concentration in the distillate and the minimum reflux ratio $R_{\min}$.

The application of the minimum-reflux equations to actual multicomponent separations must be carried out with caution because the original assumption of constant molal reflux and constant relative volatilities may not hold.

Nevertheless, the equations may be applied if judgment is used in selecting the values of the relative volatilities and in the final interpretation of the results. For instance, the selection of the relative volatilities at the average tower temperature or at the average of the pinch-zone temperatures has been recommended. The calculation of the latter is covered in the next section.

Colburn Minimum-reflux Relationship

The minimum reflux ratio implies the existence of at least one zone of infinite plates in a column. The number and location of the zones of infinite plates for the distillation of systems exhibiting regular equilibrium behavior (e.g., a mixture of hydrocarbons) may be summarized as follows:

1. For complete distribution of every component in the overheads and the bottoms product, the zone of infinite stages lies at the feed plate.
2. For one or more components absent from the overheads, the zone of infinite stages lies in the rectifying section.
3. For one or more components absent from the bottoms product, the zone of infinite stages lies in the stripping section.
4. For one or more components absent from each of the overhead and bottoms products, two zones of infinite stages occur, one in the rectifying section and the other in the stripping section.

In cases 2 to 4 the development of the zone of infinite stages is associated with the complete elimination of one or more components from a product stream.

Returning to the nomenclature of Fig. 14-1, the following sets of relations apply to the zone of infinite stages:

$$\left.\begin{aligned} V_{n+1}y_{n+1} &= L_n x_n + Dx_D \\ y_{n+1} &= Kx_{n+1} \\ x_{n+1} &= x_n \end{aligned}\right\} \quad \text{above the feed}$$

$$\left.\begin{aligned} V'_{m+1}y_{m+1} &= L'_m x_m - Bx_B \\ y_{m+1} &= Kx_{m+1} \\ x_{m+1} &= x_m \end{aligned}\right\} \quad \text{below the feed}$$

which lead to

$$x_n = \frac{Dx_D}{KD + L(K-1)} \quad \text{above the feed} \tag{14-54}$$

$$x_m = \frac{Bx_B}{KB + L'(1-K)} \quad \text{below the feed} \tag{14-55}$$

Note that Eqs. (14-54) and (14-55) must also satisfy the bubble-point condition $\Sigma x = 1.0$. Equation (14-54) or (14-55) combined with the bubble-point condition $\Sigma x = 1.0$ *cannot* be solved, even if the composition of the product stream is known. Equations (14-54) and (14-55) may also be expressed in terms of relative volatilities of K-value ratios.

$$x_n = \frac{x_D}{[(K/K_d)_n - 1](L/D)_{\min} + (K/K_d)_n(x_{d,D}/x_{d,n})} \tag{14-56}$$

$$x_m = \frac{x_B(K_c/K_d)_m}{[(K_c/K_d)_m - (K/K_d)_m](L'/B)_{\min} + (K/K_d)_m(x_{c,B}/x_{c,m})} \quad (14\text{-}57)$$

where c indicates more volatile key component
d indicates less volatile key component
n indicates upper infinite zone
m indicates lower infinite zone
concentrations x are in mole fractions

Colburn (14-10) has developed an empirical relation between the compositions of the two pinch zones of case 4 which permits the assumed minimum reflux of Eqs. (14-54) and (14-55) to be checked. The assumed temperature is checked for a given reflux ratio by means of the bubble-point requirement $\Sigma x = 1.0$. The empirical relation of Colburn is expressed by the following equation:

$$\frac{(x_c/x_d)_n}{(x_c/x_d)_m} = \left(1 - \sum c_m \frac{K_m x_m}{K_d}\right)\left(1 - \sum c_n x_n\right) \quad (14\text{-}58)$$

where $\Sigma c_m(K_m x_m/K_d)$ is the summation of $c_m(K_m x_m/x_d)$ for all components less volatile than the less volatile key component d, and where $\Sigma c_n x_n$ is the summation of $c_n x_n$ for all components more volatile than the more volatile key component c. The values of c_n and c_m are obtained from Fig. 14-27. The general behavior of the summations is such that, if the left-hand member of Eq. (14-58) is less than the right-hand member, the assumed minimum reflux ratio $(L/D)_{\min}$ is too high and it is necessary to make another trial assumption.

A detailed stage-to-stage minimum-reflux calculation carried out by Brown and Holcomb (14-6) is of interest.

Minimum Number of Stages

The minimum number of equilibrium stages may be calculated by properly applying the Fenske-Underwood equation:

$$n = \frac{\log [(x_c)_0(x_d)_n/(x_c)_n(x_d)_0]}{\log (K_c/K_d)} \quad (14\text{-}58a)$$

where n = number of theoretical stages required to distill from stage 0 to stage n in which liquid composition of keys changes from $(x_c,x_d)_0$ to $(x_c,x_d)_n$
x_c = mole fraction of light key component
x_d = mole fraction of heavy key component
K_c, K_d are K values of key components

It should be recalled that Eq. (14-58a) was derived assuming (1) a binary system and (2) constant relative volatility $\alpha = K_c/K_d$ throughout the column. Therefore, in a multicomponent distillation, in which neither of these assumptions is valid, Eq. (14-58a) should be applied with caution. A sound way in which to apply the Fenske-Underwood equation is to proceed as follows:

1. Make the product split.
2. Starting with the vapors leaving the top stage, calculate down a few stages by means of successive dew-point calculations until the temperature change from stage to stage becomes small or constant.
3. Starting with the still liquid, calculate a few stages upward by successive bubble-point calculations until the temperature change from stage to stage becomes small or constant.
4. Apply the Fenske-Underwood relation over the region of near-constant or low-temperature gradient, using an average relative volatility.

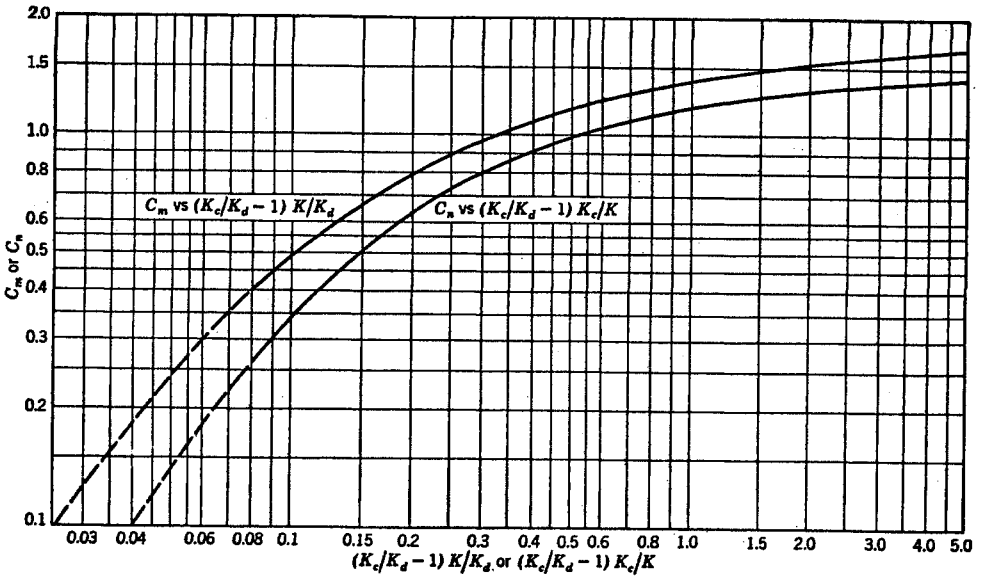

Fig. 14-27. Colburn's empirical functions for the minimum-reflux ratio. (14-10. *Courtesy AIChE.*)

5. Count the total number of stages; this represents the minimum number of stages.

For the stagewise calculations at total reflux, since $D = 0$, $B = 0$, the material-balance equations reduce to

$$V_{n+1} = L_n$$
$$y_{n+1} = x_n$$
$$y_{m+1} = x_m$$

Therefore, the liquid and gas streams passing each other have identical compositions as well as masses. The stagewise calculations are made employing the above assumptions.

Relations among Minimum Number of Stages, Minimum-reflux Ratio, Actual-reflux Ratio, and Actual Number of Stages

Martin and Brown (14-8) and Gilliland (14-21) have developed empirical correlations which may be used to obtain the actual number of stages required for a given separation at a given reflux ratio from a knowledge of the minimum number of stages and the minimum-reflux ratios. Figure 14-28 presents the empirical relation of Martin and Brown. The ordinate P is defined by

$$P = \left[\left(\frac{L'V}{V'L}\right)_{\text{actual}} - 1\right] \div \left[\left(\frac{L'V}{V'L}\right)_{\text{min reflux}} - 1\right]$$

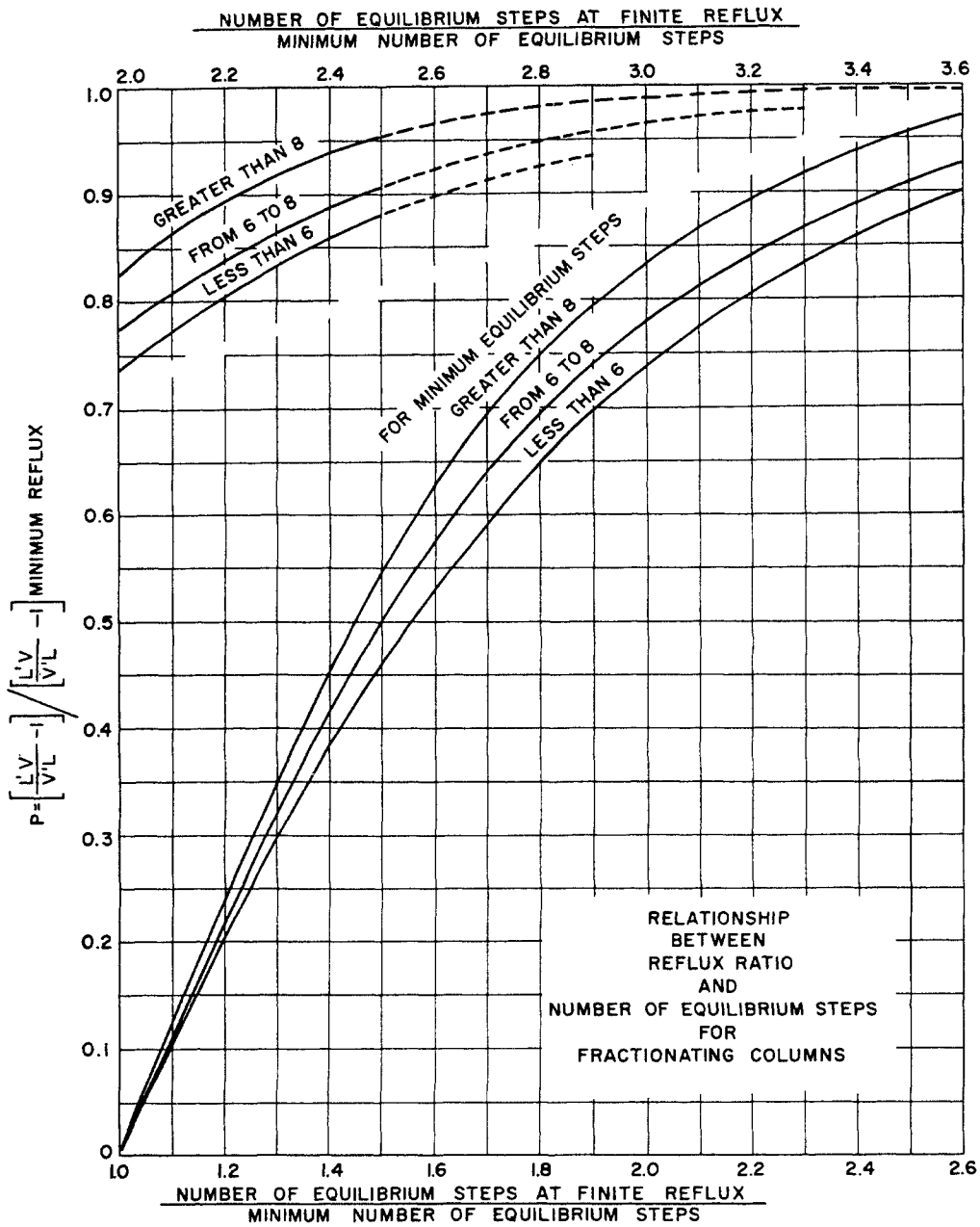

Fig. 14-28. Relationship between minimum number of stages and minimum-reflux ratio and actual number of stages and actual-reflux ratio. (*Brown and Martin*, 14-8. *Courtesy AIChE.*)

where L = average liquid flow above feed plate, moles
V = average vapor flow above feed plate, moles
L' = average liquid flow below feed plate, moles
V' = average vapor flow below feed plate, moles

The empirical relationships were developed originally from binary-distillation calculations and checked for multicomponent systems. They should be applied with caution when the feed composition approaches one of the terminal-product compositions and when the system exhibits nonideal equilibrium and enthalpy relations. The original correlation was developed for a saturated-liquid feed, and must be adjusted for the case in which the feed is not at saturation conditions (14-8).

Feed-plate Location

For a bubble-point feed, the optimum location of the feed entry may be approximated by the empirical relation (14-27)

$$\log \frac{n}{m} = 0.206 \log \left[\frac{B}{D} \frac{x_d}{x_c} \left(\frac{x_{c,B}}{x_{d,D}} \right)^2 \right] \qquad (14\text{-}59)$$

where n = number of ideal stages above feed plate
m = number of ideal stages below feed plate
x_c = light-key concentration in feed, mole fractions
x_d = heavy-key concentration in feed, mole fractions
$x_{d,D}$ = heavy-key concentration in overhead, mole fractions
$x_{c,B}$ = light-key concentration in bottom, mole fractions
B/D = mole ratio of bottoms to distillate product

Because of unpredictable variations in the composition of the feed, the distillation column should be equipped with more than one feed nozzle or entry. The optimum feed-plate location can be determined from the Underwood relations for the case of constant molal reflux and constant relative volatility (14-55).

RELATION BETWEEN THEORETICAL AND ACTUAL NUMBER OF STAGES

Mass-transfer considerations must be introduced to obtain the fundamental relations between the number of equilibrium or ideal stages required for a separation and the number of actual stages. However, approximate empirical correlations have been developed for absorption and fractionation which employ only the physical properties of the system (14-15, 14-38).

Method Based on Physical Properties

The first extensive empirical correlation of over-all plate efficiencies was developed by Drickamer and Bradford (14-15) using plant-test data as a basis. The over-all plate efficiency, defined as

$$E = \frac{n^*}{n}$$

where E = over-all tower-plate efficiency
n^* = number of equilibrium stages
n = number of actual stages

was correlated as an empirical function of the molal average viscosity of the feed at the average tower temperature.

Recognizing that plate-efficiency data on absorbers could not be correlated using these variables, O'Connell (14-38) developed a similar relation for the over-all efficiency of absorption as a function of the solubility of the absorbed gas expressed in terms of the Henry's law constant, the total pressure, and the viscosity (Fig. 14-29). It should be noted that some of the very-low-plate-efficiency points used were Murphree plate efficiencies. For fractionators, a second relation was developed, in which the over-all efficiency was plotted as a function of the relative volatility of the key component times the molal-average viscosity of the feed at the average tower temperature (Fig. 14-30).

Although these correlations provide rapid procedures for calculating the over-all tray efficiency, it has been demonstrated that efficiency depends also on mass-transfer variables governed by tray design, entrainment, and liquid mixing on the trays (14-19, 14-28).

Method Based on Physical Properties and Tray Dynamics

One general attack on the problem of theoretical correlation of tray efficiency begins with the correlation of the Murphree point efficiency, obtains next the integrated tray efficiency over an entire plate, and then relates the over-all efficiency of a single tray to the over-all efficiency of the column.

Gerster et al. (14-20) have related the individual-film resistance to the Murphree point efficiency E_p by the following relationship:

$$\frac{1}{-\ln (1 - E_p)} = \frac{V}{Zk_Ga} + \frac{mV}{Zk_La} \qquad (14\text{-}60)$$

where $E_p = (y_n - y_{n+1})/(y_n^* - y_{n+1})$ taken at a given point
V = gas flow rate per unit of active tray area, lb moles/hr per square foot of tower cross section
Z = vertical distance on plate in which gas contacts liquid, ft
k_Ga = gas film coefficient of mass transfer, lb

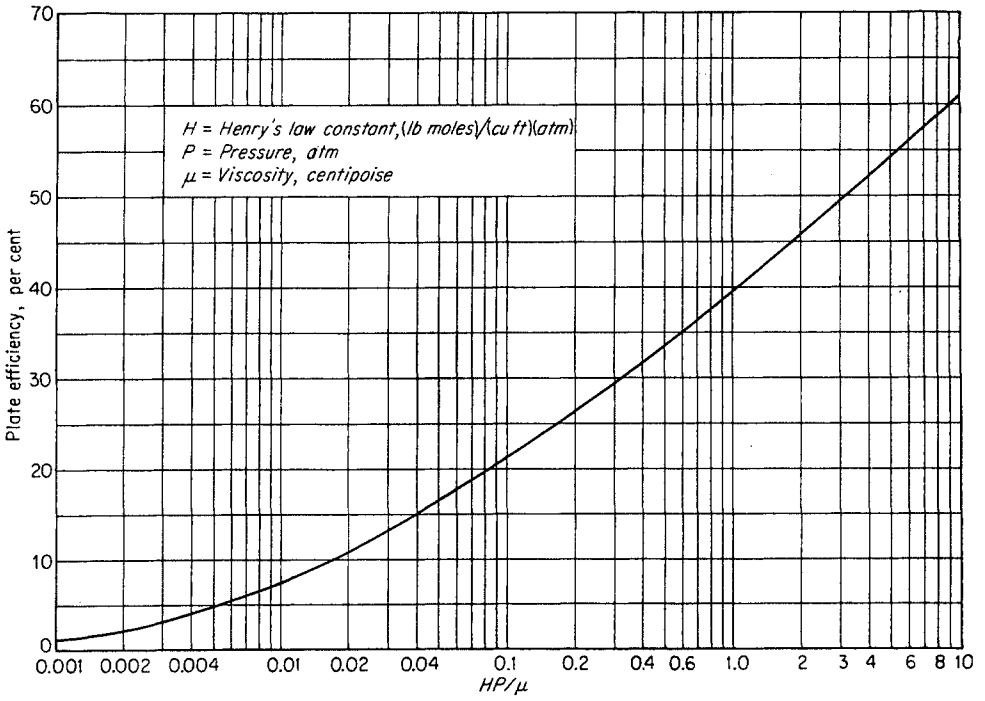

Fig. 14-29. Over-all plate efficiency (O'Connell, 14-38. Courtesy AIChE

moles/(hr)(cu ft) per unit of difference in gas mole-fraction concentration

$k_L a$ = liquid film coefficient of mass transfer, lb moles/(hr)(cu ft) per unit mole-fraction concentration difference in liquid

The application of Eq. (14-60) is hampered by the scarcity of data on film transfer coefficients.

Another method for obtaining the point efficiency would be to utilize plate-efficiency data for small columns. The local efficiencies should also be correlated more successfully than the over-all efficiencies using the original technique of O'Connell. Figure 14-31 gives the tentative correlation of local efficiencies as a function of relative volatility of the light key component to the heavier key component, times the viscosity.

Lewis (14-31) related the over-all efficiency of a single plate to the Murphree point efficiency for the limiting case where there is no liquid mixing on a plate. The three cases treated were:

1. Vapor of uniform composition entering a tray, liquid unmixed
2. Vapor entering a tray unmixed, unmixed liquid flowing in the same direction on successive trays
3. Vapor entering a tray unmixed, unmixed liquid flowing in opposite directions on successive trays

All three models show a substantial excess of the

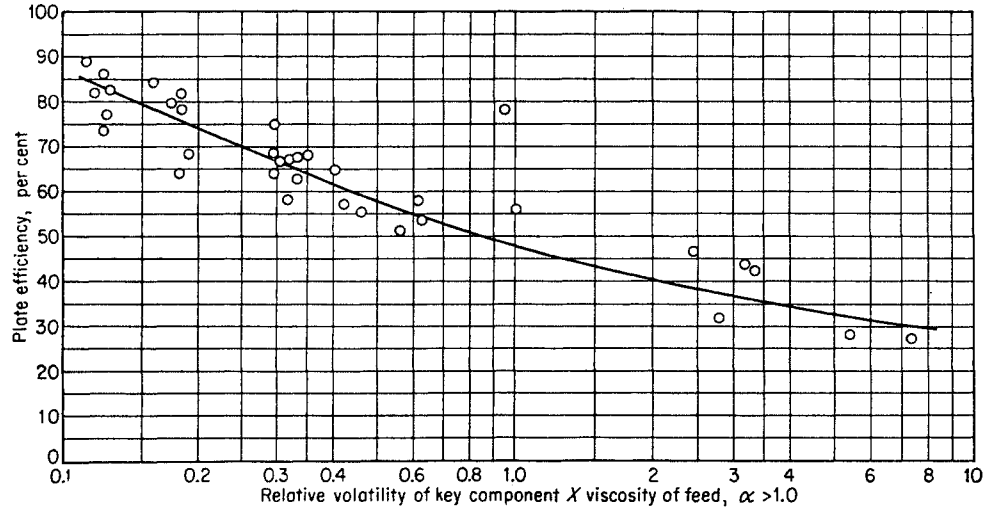

Fig. 14-30. Over-all tray efficiency vs. relative volatility of key component times viscosity of feed. (O'Connell, 14-38. Courtesy AIChE.)

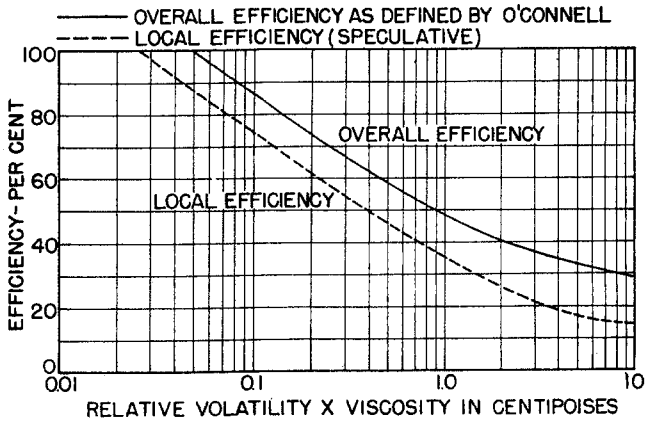

Fig. 14-31. Plate efficiency as a function of relative volatility times viscosity. (*Gautreaux and O'Connell*, 14-19. *Courtesy AIChE.*)

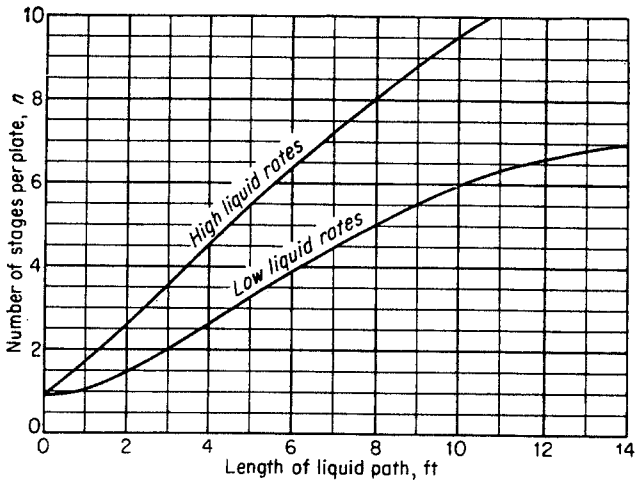

Fig. 14-32. Number of stages per plate vs. length of liquid path. (*Gautreaux and O'Connell*, 14-19. *Courtesy AIChE.*)

efficiency of the entire plate over the local or Murphree efficiency. The difference is shown to be greatest for case 2, the next greatest for case 1. The largest differences occur when the point efficiencies are already high and, for rectification, when the value of mV/L is greater than 1.0,

where m = slope dy^*/dx of the equilibrium line
V = gas rate, moles/hr
L = liquid rate, moles/hr

The actual excess in tray efficiency, which may be attributed to liquid cross flow, becomes appreciable only for large columns. Since the magnitude of the excess is so much smaller for actual columns, Lewis concludes that an appreciable amount of mixing occurs on the trays.

The point efficiency has been related to the over-all efficiency of a single plate by Gautreaux and O'Connell (14-19) in a paper which analyzes the effect of liquid cross flow and which takes into account the liquid mixing on each tray. Following the original analysis of Kirschbaum (14-28), Gautreaux and O'Connell imagine that the liquid on the tray is divided into stages, each stage consisting of pools of liquid each of which is completely mixed. They make the following additional simplifying assumptions:

1. Constant liquid and vapor loads enter each stage.
2. Vapors entering each stage are uniformly mixed.
3. The equilibrium relation is of the form

$$y^* = mx + b$$

4. Local efficiency is constant across the plate.
5. Entrainment and other effects are negligible.

They derive (14-19) the following equation for the over-all efficiency over a single plate:

$$E_0 = \frac{L}{VK}\left[\left(1 + \frac{E_p}{nL/VK}\right)^n - 1\right] \qquad (14\text{-}61)$$

where E_0 = over-all efficiency of a single plate and is defined by

$$E_0 = \frac{(y_n)_{av} - y_{n+1}}{y_n^* - y_{n+1}} \qquad (14\text{-}62)$$

n = number of hypothetical stages in series

Accordingly, the number of stages may be expected to:

1. Increase with increased liquid path
2. Increase with increased liquid rate
3. Increase with decreased vapor rate
4. Increase with tray-design factors that minimize liquid mixing

From test data on large columns and estimated point efficiencies, Eq. (14-48) was used to calculate the number n of hypothetical stages. The resulting values of n are plotted in Fig. 14-32, which may be used on a tentative basis.

Solutions of Eq. (14-61), for a constant local-efficiency value of 60 per cent, are presented in Fig. 14-33. The results indicate that, as n becomes very

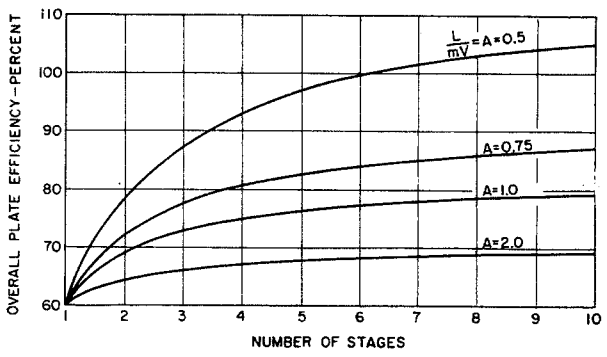

Fig. 14-33. Effect of number of stages on over-all plate efficiency for local efficiency = 60 per cent. (*Gautreaux and O'Connell*, 14-19. *Courtesy AIChE.*)

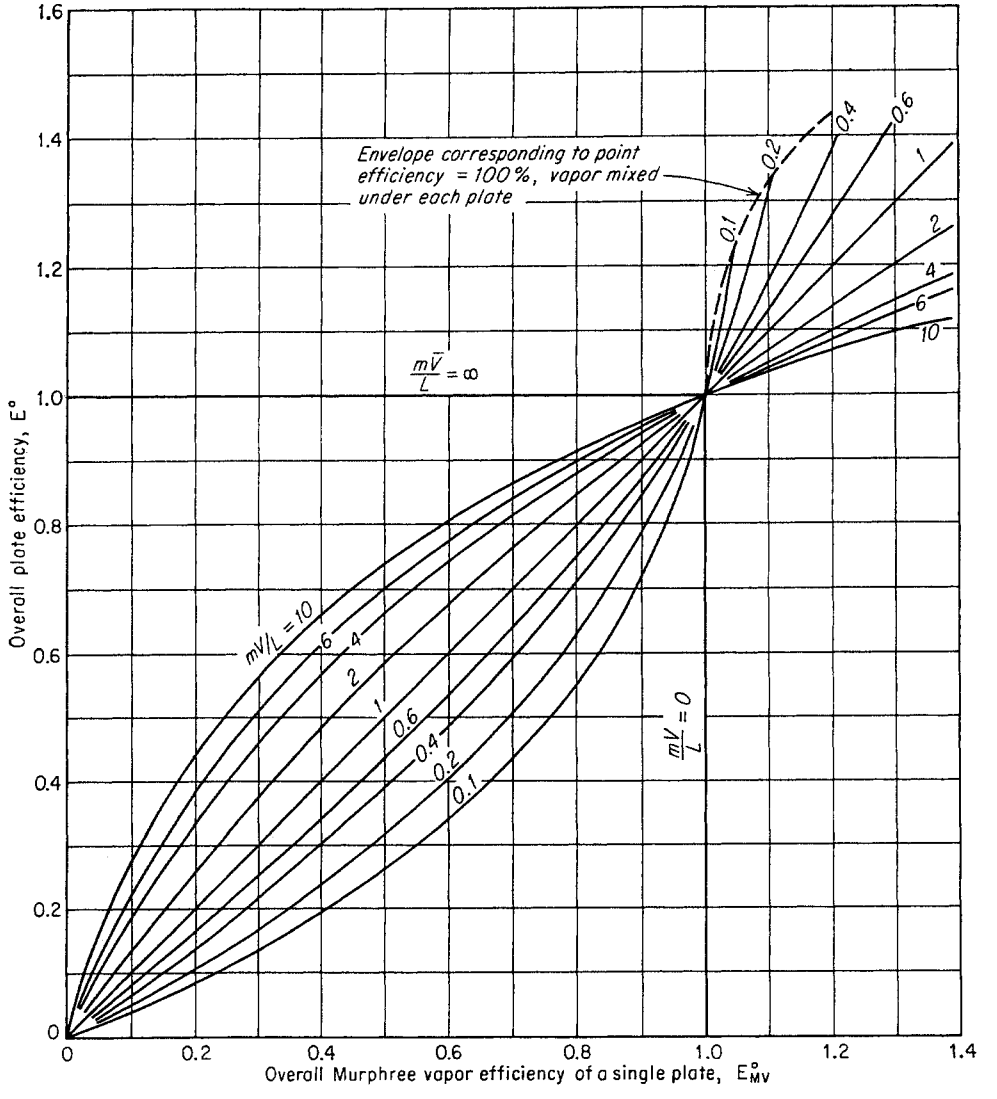

Fig. 14-34. Over-all Murphree vapor efficiency of a single plate. (*Marshall and Pigford, 14-36. Courtesy University of Delaware.*)

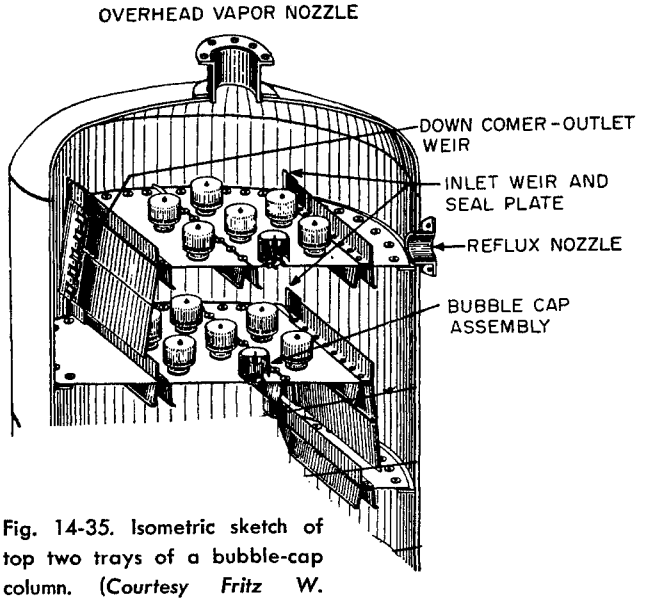

Fig. 14-35. Isometric sketch of top two trays of a bubble-cap column. (*Courtesy Fritz W. Glitsch and Sons, Inc.*)

large, the over-all efficiency of a single plate approaches a constant value, the value predicted by the Lewis relation for case 1 listed above.

It is frequently assumed that the over-all tray efficiency for a tower is equal to that of a single plate. This, however, does not always hold. Marshall and Pigford (14-36) have shown that, when the parameter mV/L is appreciably different from 1.0, as it frequently is for an absorber, the two efficiencies are not the same. Figure 14-34 shows Marshall and Pigford's results relating the over-all Murphree vapor efficiency for a single plate to the over-all efficiency for the entire absorber.

No satisfactory treatment on the effect of entrainment on tray efficiencies has been published to date. It has been observed that entrainment is a major variable in the correlation of tray efficiencies as the maximum tower capacity is approached.

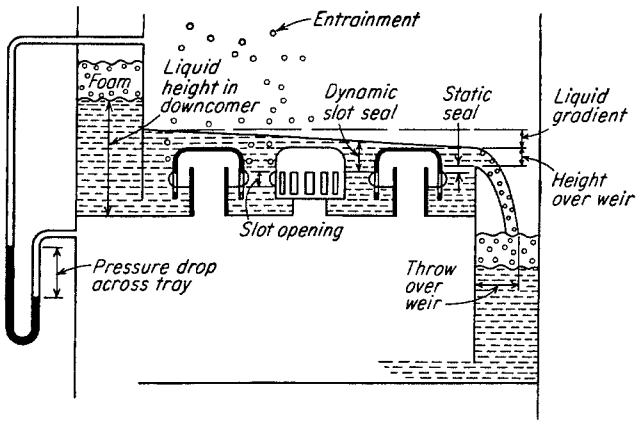

Fig. 14-36. Nomenclature of tray components in bubble-cap column. (*Bolles, 14-4. Courtesy Petrol. Processing.*)

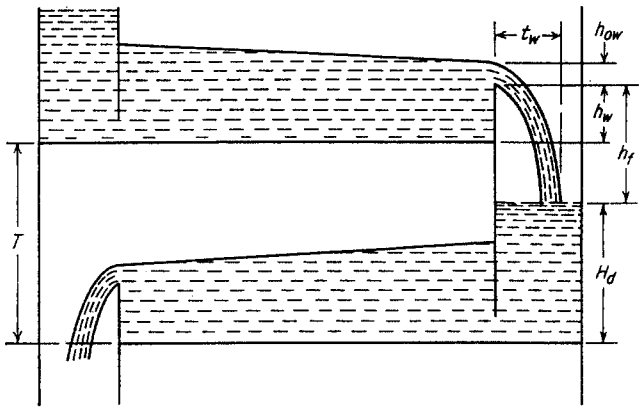

T = tray spacing, in.
t_w = horizontal projection of liquid over weir, in.
h_w = weir height, in.
h_{ow} = height of clear liquid flow over weir
H_d = clear liquid backup, in. of liquid
h_f = clearance, in. of liquid

Fig. 14-37. Nomenclature used in tray-dynamics discussion. (*Bolles, 14-4. Courtesy Petrol. Processing.*)

DESCRIPTION OF COLUMN SECTION AND TRAY ACTION

The bubble-cap tray is one of the many types of equipment designed to bring about intimate contact of a gas and a liquid. In this case the contact is carried out with the main purpose of transferring mass from one phase to the other, the transfer of heat occurring incidentally.

Figure 14-35 presents an isometric sketch of the two top trays of a fractionating column showing the caps, downcomers, and weirs. Chord-type weirs are shown, although occasionally circular weirs are used. An idealized diagram of the elevation of a bubble-cap tray in operation is presented in Fig. 14-36, giving the nomenclature generally used. The same elevation, giving the nomenclature symbolically, is presented in Fig. 14-37. It should be emphasized that Figs. 14-36 and 14-37 represent the actual dynamics only under limiting conditions of low gas flow.

For a tray-dynamics analysis, the tray components may be broken up into three functional groups:

1. Bubble-cap and associated components, which provide intimate contact of the gas and the liquid
2. Weirs, which provide distribution of the liquid on the trays
3. Downcomers, which provide segregation of gas from the liquid, directing the flow of the liquid to the tray below, and which provide a seal between trays

The dynamics on a tray of given physical design will vary appreciably with the liquid and vapor loading. Figure 14-38 gives qualitatively the limiting gas and liquid rates imposed by a given tray configuration and a given set of liquid and gas properties. For low vapor rates, unsatisfactory tray dynamics may be characterized by vapor pulsation, by dumping of liquid down the risers, or by uneven vapor distribution. At high vapor rates, excessive slot loading will eventually lead to flooding because the tray pressure drop becomes too high to permit liquid downflow from the tray above, because of increased liquid loading induced by entrainment, or because of a combination of these factors. On the other hand, at low liquid rates, the given weir height may not provide sufficient seal to give satisfactory liquid-gas contact. High liquid

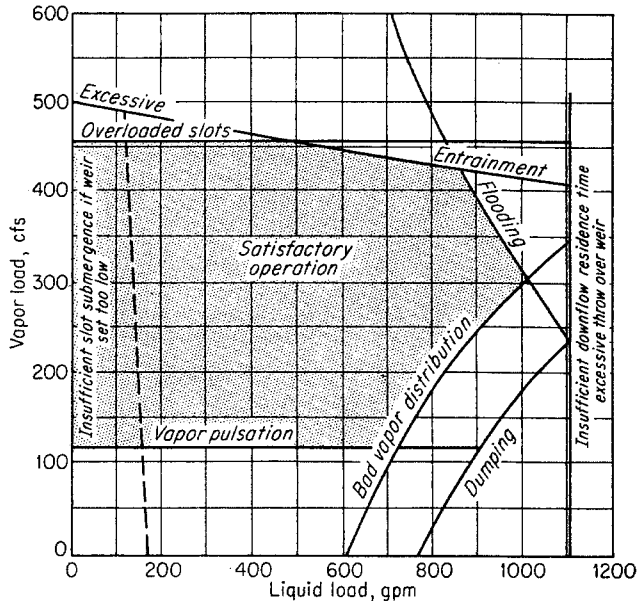

Fig. 14-38. Limits of satisfactory tray operation for a specific set of tray and fluid properties. (*Bolles, 14-4. Courtesy Petrol. Processing.*)

rates contribute to flooding when the vapor rate is moderate or high, but may lead to inadequate distribution of vapors at low vapor rates. Over a range defined by such boundaries, tray operation will usually be satisfactory.

Let it be imagined that, for a given liquid flow, the pressure differential of the gas across a tray is gradually increased. At some value of the pressure differential, equal to the hydrostatic head above the slot, bubbling action through the slot will just begin. For a level tray, since a gradient is produced by the resistance to flow across the tray, the bubbling action will begin on the outlet side of the tray. As the pressure differential is increased, bubbling through slots on caps further upstream will begin, and the rate of bubbling will increase in the slots that were originally activated. Since the slots cover a finite elevation, the lower portion of the slots will be sealed by the liquid until the pressure drop through the slot becomes equal to the height of the slot. At the pressure differential, when all the slots on a tray become active, the tray is said to be "stable."

Under satisfactory operating conditions, violent bubbling action on the tray produces a massive spray which lies above a denser gas-liquid mixture near the tray floor. Under these conditions, the bubbling action produces not isolated bubbles but a continuous chain of bubbles through a heterogeneous mixture of gas and liquid. Furthermore, the pressure drop from the outside of the slot to the free gas space above is *not* equal to the pressure drop determined by a hydrostatic head of clear liquid. The liquid that flows over the weir is associated with an appreciable amount of gas, which has to be substantially segregated from it in the downcomer. The limit to the permissible increase in pressure drop is reached when the pressure drop across the tray is so high that liquid can no longer flow to it from the tray above. This condition is termed "flooding." The height of the massive spray or froth may be expected to increase as the tray pressure drop or gas rate is increased. Many of the smaller liquid droplets will be carried up the riser into the next plate above, but the entrainment produced by small droplets is negligible. The sudden and serious rise in entrainment occurs when the massive spray reaches the bottom of the tray above. The entrainment produced is due primarily not to the suspension of particles by the gas phase, but rather to the projection of relatively large drops with high kinetic energy up to the tray above (14-24). The entrained liquid produces an internal recycle which increases the liquid loading in the column, eventually causing or seriously contributing to flooding. For a properly designed tray, the flooding caused by liquid backup in the downcomer should result appreciably from both sources: pressure drop and entrainment.

CRITERIA FOR BUBBLE-TRAY DESIGN

The choice of design criteria for bubble-cap columns must be based on a physical description of phenomena that take place in them. The appearance of basic data for fractionation equipment in recent years has led to the development of theories of mechanisms in bubble-cap columns and to improved criteria for their design. The purpose of this section is to provide an understanding of bubble-cap-tray dynamics and to present criteria for their design.

Rapid column-sizing methods have been used which do not take into account the tray layout (Souders and Brown, 14-49; Atkins and Wilson, 14-1). These procedures may be used in making preliminary calculations and cost estimates. Detailed methods (14-4, 14-14), on the other hand, provide a basis for the design and construction of bubble-cap columns.

Rapid Methods of Column Sizing

Rapid methods of tower sizing are based on an empirical application of the entrainment formula for droplets. For a given droplet of diameter d, which is just suspended in a rising vapor stream, the gravitational force acting on the droplet is equal to the resistance of the droplet, giving

$$\tfrac{1}{6}\pi d^3(\rho_L - \rho_V)g = \frac{R'}{\rho_V u^2}\frac{\pi d^2}{4}\rho_V u^2 \qquad (14\text{-}63)$$

where $R'/\rho_V u^2$ = drag coefficient
ρ_L = liquid density
ρ_V = gas density
u = gas velocity
d = particle diameter
g = gravitational constant

Under these conditions, the gas velocity is

$$u = c\sqrt{\frac{\rho_L - \rho_V}{\rho_V}} \qquad (14\text{-}64)$$

where $$c = \sqrt{\frac{2gd}{3R'/\rho_V u^2}}$$

Expressed in terms of mass velocity (mass flow per unit time per unit cross-sectional area) (14-49), Eq. (14-64) becomes

$$G = c\sqrt{\rho_V(\rho_L - \rho_V)} \qquad (14\text{-}65)$$

where G = mass velocity of vapor, lb/hr per square foot column cross section
c = a parameter empirically determined, ft/hr

ρ_L = liquid density at column conditions, lb/cu ft
ρ_V = vapor density at column conditions, lb/cu ft

Equation (14-65) has been used to determine the values of c for experimental and full-scale bubble-cap columns under various conditions of gas flow, liquid flow, gas density, plate spacing, tray design, etc. For a first approximation, the value of c has been found by Souders and Brown (14-49) to be a function of the plate spacing, the gas and liquid densities, and the surface tension (Fig. 14-39). Obviously, the correlation is an oversimplification of the real picture, but it provides a rapid means of calculating column cross-sectional areas, giving a value that falls 20 to 40 per cent below the ultimate or maximum vapor-handling capacity. The surface tension is given as a parameter, because the dispersion of liquid into fine droplets is expected to increase with decreased surface tension. However, Kirschbaum (14-28) could find but a small effect of surface tension on the allowable gas velocities.

Kirschbaum has systematically verified the significance of tray spacing in column design, especially its importance for spacings less than 12 to 16 in. At higher tray spacings (Fig. 14-40*a* and *b*) little increase in the ultimate vapor velocity is gained by an additional increase in the tray spacing, except at the higher gas densities. In Kirschbaum's correlation, the maximum allowable vapor velocity assumes the form

$$u = c'(\rho_V)^b \qquad (14\text{-}66)$$

where u = maximum allowable gas velocity
c' = an empirical function of plate spacing
ρ_V = vapor density
b = a function of plate spacing, varying from -0.425 to -0.545

Equation (14-66) follows from Eq. (14-64) if ρ_L is assumed to be large relative to ρ_V and if $\sqrt{\rho_L - \rho_V}$, therefore, is assumed to be a constant which is absorbed in c'.

A convenient method for sizing hydrocarbon fractionators has been developed by Atkins and Wilson (14-1). A Souders-Brown type of relationship is applied to the active area of the tray, which is the actual area given over to caps. Criteria for vapor-loading and liquid-loading capacities are given.

Some Criteria for Bubble-cap-tray Design

It has been seen from Fig. 14-40 that low tray spacing yields low ultimate vapor capacities. This can be attributed to entrainment, to liquid backup in the downcomers resulting from tray pressure drop, or to limited liquid-handling capacity in the downcomers.

Here, entrainment is referred to as the buildup on the tray of massive spray which reaches the tray above. A tray spacing of from 18 to 24 in. usually gives a good balance between tower capacity and tower height.

The effect of entrainment in increasing the ideal-stage requirements has been discussed in a previous section. The effect of entrainment on the efficiency of an actual tray can likewise be serious, for it brings about remixing of liquids already unmixed through the application of thermal energy. The sharp decrease in the tray efficiency in the vicinity of the ultimate vapor capacity may be due to entrainment. In Fig. 14-41, the coincidence of the vapor rates at which high entrainment and low tray efficiencies were obtained on a sieve plate illustrates this point.

Since entrainment is such a pronounced function of tray spacing, Hunt, Hanson, and Wilke (14-24) conclude that drag is an unimportant factor in entrainment. Observations indicate that most of the par-

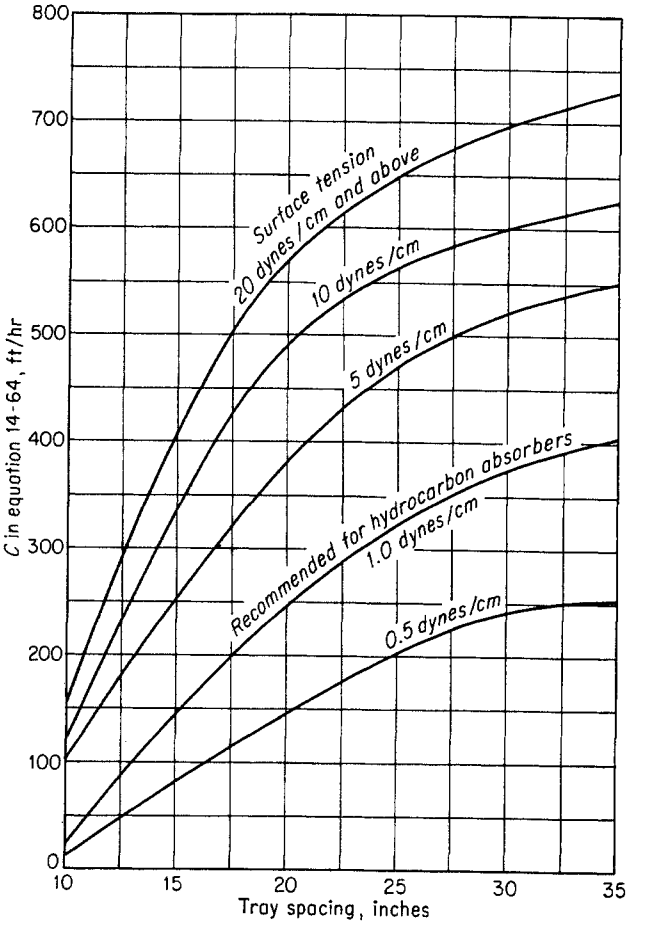

Fig. 14-39. Souders-Brown correlation for approximate tower sizing.

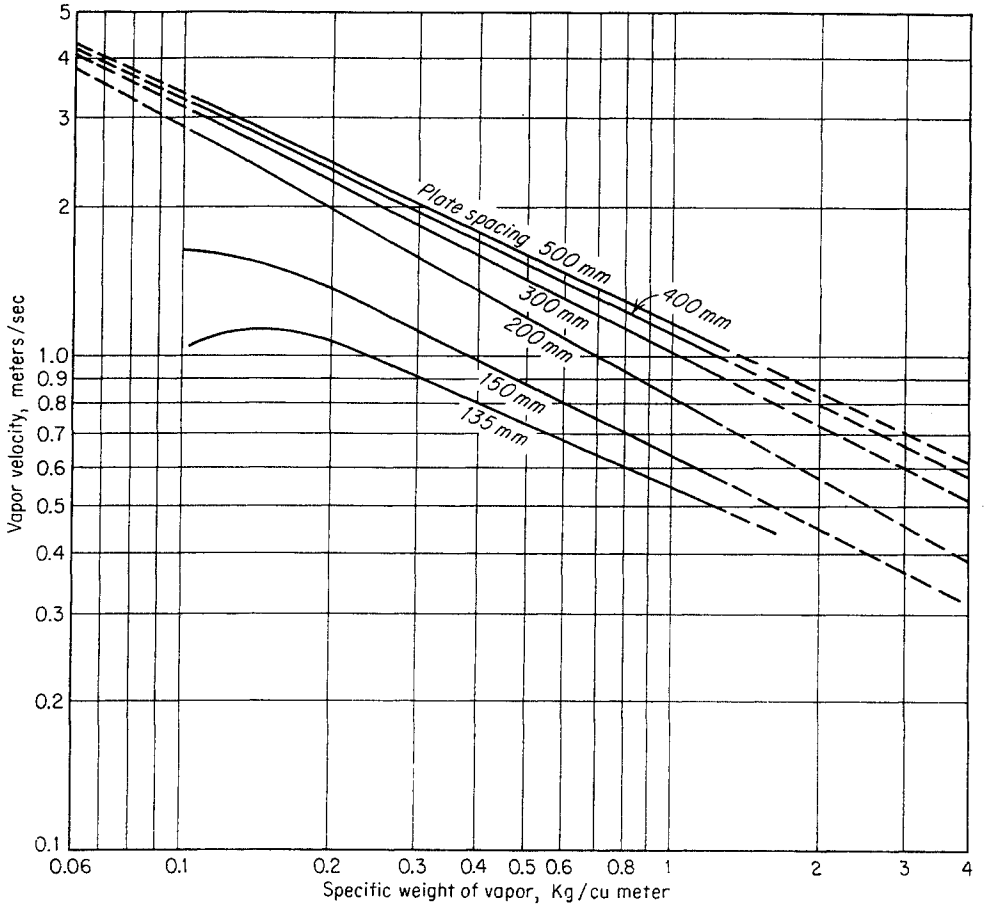

Fig. 14-40. (a) Permissible vapor velocities for different vapor densities and plate spacings. (b) Enrichment ratio plotted against plate spacing for various vapor velocities. Ethanol-water; reflux ratio $v = \infty$; final plate concentration $X_F = 50$ mole %. (*After Kirschbaum*, 14-28.)

ticipating droplets are large, of the order of ¼ in. in diameter, whereas calculations show that drag alone would require drop sizes of the order of 0.03 in. Simkin, Strand, and Olney (14-45) have developed an empirical correlation for entrainment in bubble-cap columns. Their correlation, presented in Fig. 14-42, though not completely general, indicates some major variables governing entrainment. The exponential relationship between entrainment and vapor flow rate is clearly demonstrated.

The depth to which the slots of a bubble cap are submerged should be sufficient to provide adequate contact between the gas and liquid phases. The tray efficiency as a function of slot submergence is given in Fig. 14-43 for the ethanol-water system (14-9, 14-28). It is evident that the plate efficiency is al-

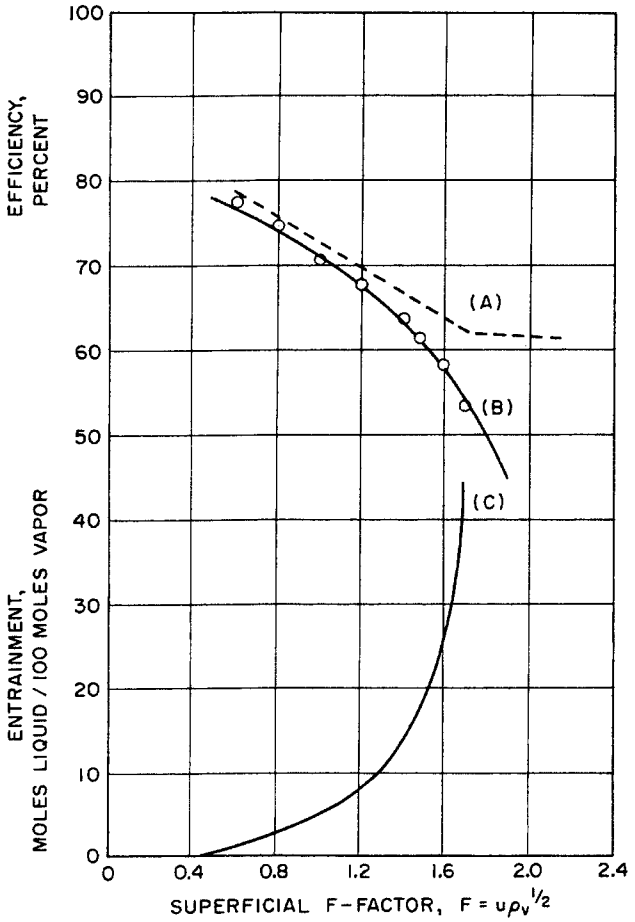

Fig. 14-41. Effect of entrainment on efficiency. Basis: sieve plate with 1/8-in.-diameter holes on 3/8-in. triangular centers; free area, 6.7 per cent; S_{av} = 1.5 in. (A) Experimental curve for entrainment-free plate (single plate). (B) Experimental efficiency curve for three plates on 12-in. plate spacing. (C) Experimental entrainment curve for three plates. Circles indicate calculated efficiency points for three plates on 12-in. spacing, based on curves A and C. (*Jones and Pyle*, 14-25a. *Courtesy AIChE.*)

	Kirschbaum	Carey et al.
Column diameter, in	4 1/3	6
Per cent slot area	4.55	3.53
Liquid-vapor ratio	0.5	1.0
Slot width, in	Triangular	0.25
Slot height, in	0.197	0.50

Fig. 14-43. Murphree tray efficiency as a function of liquid seal. (*Data from Carey et al.*, 14-9; *Kirschbaum*, 14-28.)

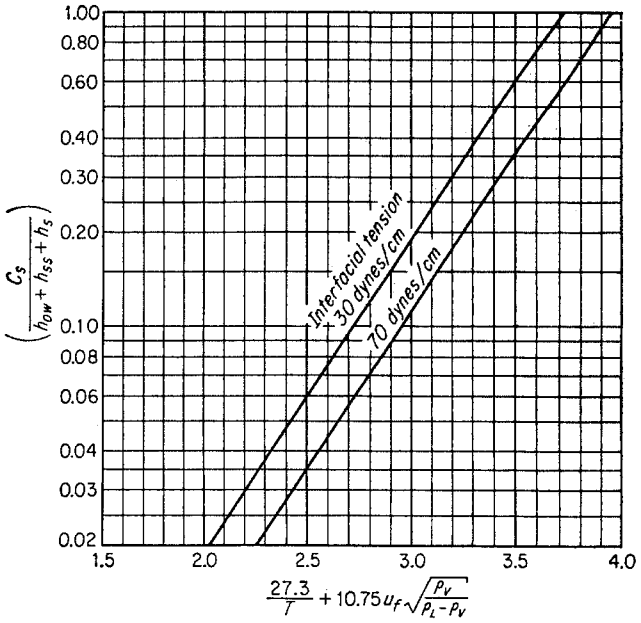

C_s = liquid-entrainment mass velocity based on active area, lb/(min)(sq ft)
h_{ow} = height of liquid crest over weir, in.
h_{ss} = static slot seal, in.
h_s = slot pressure drop, in.
u_f = vapor velocity based on active area, ft/sec
T = tray spacing, in.
ρ_L, ρ_V = liquid and vapor density, lb/cu ft

Fig. 14-42. Entrainment correlation of Simkin, Strand, and Olney. (14-45. *Courtesy AIChE.*)

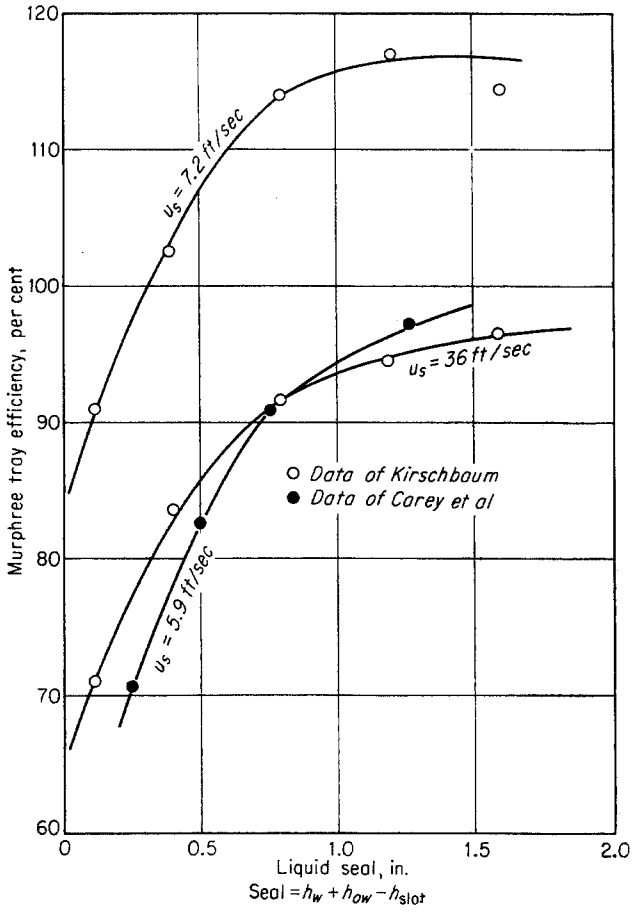

ready appreciable when the slot submergence, or the distance from the top of the slot to the top of the liquid level with no vapor flow, is zero. As the slot submergence increases above 1 in., little change in the efficiency of this system is experienced. Static slot submergence of 1 in. or more is satisfactory for light-hydrocarbon distillation. Adjusting the weir height provides a means of regulating the slot submergence. A weir height of 2 to 3 in. will usually provide sufficient slot submergence for an active tray.

Figure 14-44 gives the horizontal streaming distance l for the vapors issuing from a specific cap (14-28, 14-42). The horizontal streaming distance reaches an asymptotic value of about 1 in. at high vapor velocities. To avoid mutual interference of the vapor streams from adjacent caps, the minimum distance between caps is taken to be twice the maximum streaming distance or about 2 in. For the same velocity, high-density vapors may be expected to have greater horizontal streaming distance than low-density vapors. Rectangular caps with liquid flow parallel to the row of caps should have a minimum distance less than 4 in. Excessive distances between caps lead to channeling of the liquid and should be avoided by using a sufficiently high and uniform density of caps on the tray or through the use of distribution weirs which direct the flow of liquid across the tray.

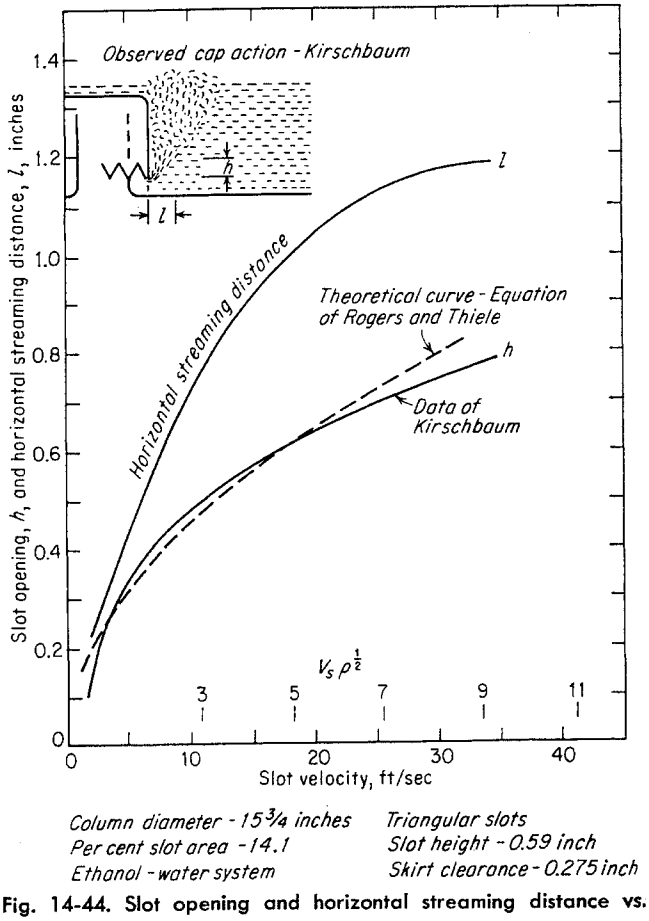

Fig. 14-44. Slot opening and horizontal streaming distance vs. vapor velocity. *(Data from Kirschbaum, 14-28; Rogers and Thiele, 14-42.)*

For a given cap diameter and vapor flow, the area distribution of the riser, reversal, and annular areas should be chosen to give the lowest pressure drop through the entire assembly. The effect of varying the annular area–riser area ratio on the pressure drop through these components is illustrated in Fig. 14-45 for the Dauphine equation (14-4, 14-12).

A stable tray is one on which all the bubble caps are active. The limit of stability is that vapor rate for which all the caps on a tray just become active. No simple criterion exists to determine tray stability, since it is influenced by cap size and shape, cap spacing, weir height, liquid properties, liquid and vapor loading, and length of liquid path. Davies (14-13) has developed a general procedure for predicting the liquid gradient. The method has been later elucidated by Bolles (14-4). Hydraulic gradient across towers under normal operation is primarily caused by the resistance of gas flow to the flow of the aerated mass and by the frictional drop of the aerated mass in its flow across the tray. With respect to design, the hydraulic gradient is important only in so far as it gives rise to tray instability at low gas rate. Once tray stability is attained, although the hydraulic gradient increases with increase in gas rate, it is not detrimental to tray operation.

The hydrostatic head at the outlet side is probably the most important factor determining the hydraulic gradient, and high outlet weirs are an effective way of combating tray instability at high liquid rates (14-29). Tray pressure drops of from 2 to 3 in. of liquid will usually be sufficient to avert tray instability for medium-size columns. The reader is referred to the more detailed analyses of Davies (14-14), Bolles (14-4), and Kemp and Pyle (14-26).

The downcomers provide residence time for the final segregation of the liquid and the vapor phases, transmit the liquid phase to the tray below, and provide a liquid seal for the vapors from the tray below. Davies (14-14) recommends a minimum downflow residence time of 5 sec. Atkins and Wilson (14-1) recommend downflow residence velocities of 0.21 to 0.35 ft/sec with a value of 0.28 for a 24-in. tray spacing; this converts to about 7 sec of residence time. To permit effective segregation of the gas and liquid in the downcomers, the liquid thrown over the weirs should be less than the width of the weir. For a single cross-flow tray, this requirement is met when

$$O_s > \sqrt{h_{ow}t} \qquad (14\text{-}67)$$

where O_s = average downcomer width, in.
t = tray spacing, in.
h_{ow} = height of clear liquid over weir, in.

For the central downcomer of a double-cross-flow weir,

$$O_s > 2\sqrt{h_{ow}t} \qquad (14\text{-}68)$$

since two streams meet at the center downcomer. Equations (14-67) and (14-68) are developed by considering the horizontal component of velocity of the liquid flowing across the weir and the maximum possible height over which the liquid falls. Under these conditions a sufficient fraction of the downcomer area will remain for vapor disengaging, unless the liquid has unusual frothing tendencies.

One of the most important criteria to be set is the clear liquid backup in the downcomers, which results from the hydrostatic head on the tray, the tray pressure drop, and resistance to flow in the downcomers. Present design practice is to allow approximately 50 per cent free height in the downcomers of fractionators and even up to 60 per cent free height in the more viscous absorber-oil systems. Data are being rapidly accumulated to permit calculation of the froth level in the downcomer from the calculated *clear-liquid* backup. The aeration factor in the downcomer,

$$A_f = \frac{\text{clear-liquid backup}}{\text{froth backup}}$$

varies both with the nature of the gas-liquid system and with the dynamics of the tray. For a given downcomer, the value of A_f decreases with increasing liquid rate, increasing gas rate, and increasing viscosity of the liquid.

DETAILED CALCULATION OF TRAY DYNAMICS

A sequence of calculation procedures, terminating with an estimate of the clear-liquid backup in the downcomers, will be followed. This represents one of several procedures outlined in the literature (14-4, 14-14, 14-27).

Pressure Drop through Caps

The pressure drop through the caps is obtained by summing the pressure drop through each component of the cap. The pressure drop through the riser, as given by Dauphine (14-12), is

$$h_r = 0.111\frac{d_r}{\rho_L}\left(\sqrt{\rho_V}\frac{V}{A_r}\right)^{2.09} \qquad (14\text{-}69)$$

where h_r = head loss in riser, in. of liquid
d_r = ID of riser, in.
ρ_L = liquid density, lb/cu ft

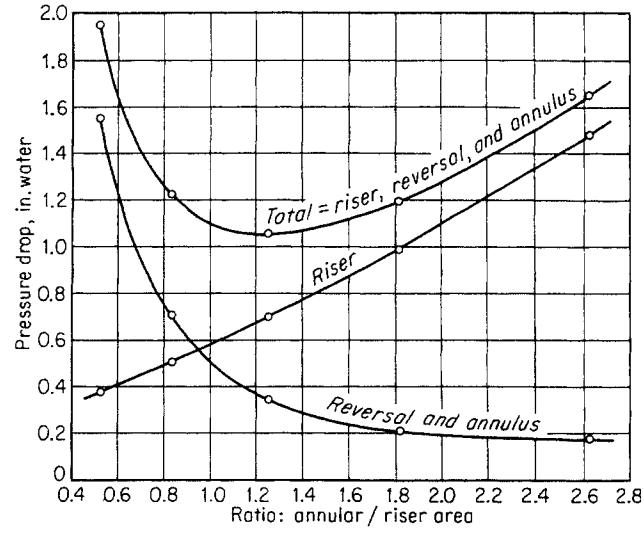

Fig. 14-45. Determination of optimum annular-riser relationship. (*Bolles, 14-4. Courtesy Petrol. Processing.*)

ρ_V = vapor density, lb/cu ft
V = total vapor load for tray under flowing conditions, cu ft/sec
A_r = total riser area per tray, sq ft

The pressure drop through the reversal and the annular area is given by the semiempirical relation

$$h_{ra} = 0.0109\frac{\rho_w}{\rho_L}\left(\sqrt{\rho_V}\frac{V}{A_u}\frac{2A_u^2}{A_mA_c}\right)^{1.71} \qquad (14\text{-}70)$$

where h_{ra} = head loss in reversal and annular area, in. of liquid
ρ_w = density of water, lb/cu ft
A_u = riser area per tray, sq ft/tray
A_m = smaller of two areas A_a and A_r
A_a = annulus area, sq ft/tray
A_c = total inside cross-sectional area of caps, sq ft/tray

Pressure Drop through Slots

The next pressure drop to be considered is the pressure drop of the gas as it passes through the slots. Bolles (14-4) has applied Rogers and Thiele's (14-42) approach to determine the slot opening and hence the slot pressure drop in trapezoidal slots, which include triangular and rectangular slots as limiting configurations. The following development has been taken from Bolles's article (14-4).

The orifice equation

$$u = K_s\sqrt{2g\frac{\rho_L - \rho_V}{\rho_V}\frac{h}{12}} \qquad (14\text{-}71)$$

may be applied to a differential area dA to give the rate of vapor flow.

$$dV_s = u\,dA = K_s\sqrt{2g\frac{\rho_L - \rho_V}{\rho_V}\frac{h}{12}}\frac{w_s\,dh}{144} \quad (14\text{-}72)$$

where V_s = vapor load per slot, cu ft/sec
u = slot velocity, ft/sec
K_s = slot-orifice coefficient
g = gravitational constant, ft/sec^2
ρ_L = liquid density, lb/cu ft
ρ_V = gas density, lb/cu ft
w_s = slot width, in.
h = slot height or head, in.

The width w of the actual flow element for a trapezoid is related to the elemental dimensions of the trapezoid by

$$w = w_{st} + (w_{sb} - w_{st})\frac{h_s - h}{H_s} \quad (14\text{-}73)$$

where w_{st} = width of slot at top, in.
w_{sb} = width of slot at bottom, in.
h_s = slot opening or slot drop, in.
H_s = slot height, in.

Combining Eqs. (14-72) and (14-73) yields the following:

$$dV_s = \frac{K_s}{144}\sqrt{\frac{2g}{12}\frac{\rho_L - \rho_V}{\rho_V}}\left[w_{st} + (w_{sb} - w_{st})\frac{h_s - h}{H_s}\right]h^{1/2}\,dh \quad (14\text{-}74)$$

The total vapor flow for a slot opening h_s is given by the integral

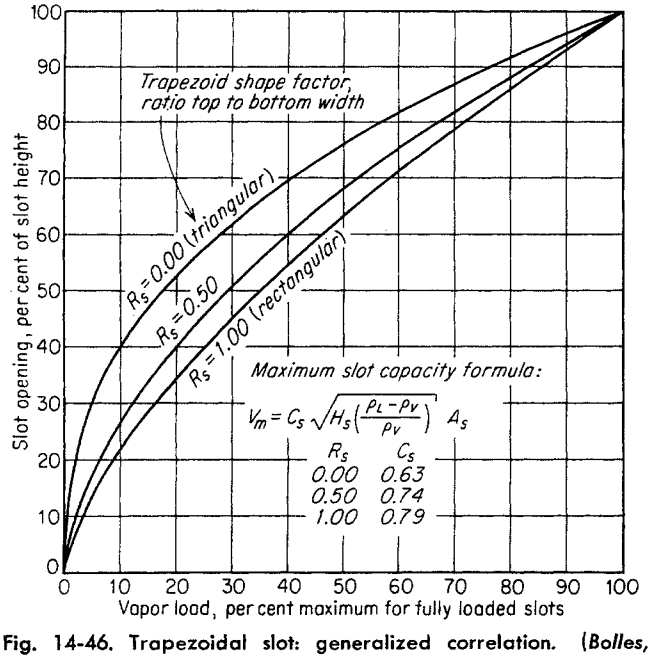

Fig. 14-46. Trapezoidal slot: generalized correlation. (Bolles, 14-4. Courtesy Petrol. Processing.)

$$V_s = \frac{K_s}{144}\sqrt{\frac{2g}{12}\frac{\rho_L - \rho_V}{\rho_V}}\left[\int_0^{h_s} w_{st}h^{1/2}\,dh + \int_0^{h_s}(w_{sb} - w_{st})\frac{h_s}{H_s}h^{1/2}\,dh - \int_0^{h_s}\frac{w_{sb} - w_{st}}{H_s}h^{3/2}\,dh\right] \quad (14\text{-}75)$$

Integrating,

$$V_s = \frac{K_s}{144}\sqrt{\frac{2g}{12}\frac{\rho_L - \rho_V}{\rho_V}}\left(\frac{2}{3}w_{st}h_s^{3/2} + \frac{2}{3}\frac{w_{sb} - w_{st}}{H_s}h_s^{5/2} - \frac{2}{5}\frac{w_{sb} - w_{st}}{H_s}h_s^{5/2}\right) \quad (14\text{-}76)$$

Using a value of $K_s = 0.51$ and collecting terms, the vapor volume for the whole tray gives

$$V = 0.00820N_sN_c\sqrt{\frac{\rho_L - \rho_V}{\rho_V}}\left[\frac{2}{3}w_{st}h_s^{3/2} + \frac{4}{15}\left(\frac{w_{sb} - w_{st}}{H_s}\right)h_s^{5/2}\right] \quad (14\text{-}77)$$

where N_s = number of slots per cap
N_c = number of caps per tray

In terms of the total slot area A_s, where

$$A_s = N_sN_cH_s\frac{w_{sb} + w_{st}}{2 \times 144} \quad (14\text{-}78)$$

$$V = 2.36\frac{A_s}{H_s}\sqrt{\frac{\rho_L - \rho_V}{\rho_V}}\left(\frac{2}{3}\frac{w_{st}}{w_{sb} + w_{st}}h_s^{3/2} + \frac{4}{15}\frac{w_{sb} - w_{st}}{w_{sb} + w_{st}}\frac{h_s^{5/2}}{H_s}\right) \quad (14\text{-}79)$$

This is simplified by introducing the parameter

$$R_s = \frac{w_{st}}{w_{sb}} \quad (14\text{-}80)$$

noting that $$\frac{w_{st}}{w_{sb} + w_{st}} = \frac{R_s}{1 + R_s} \quad (14\text{-}81)$$

and that $$\frac{w_{sb} - w_{st}}{w_{sb} + w_{st}} = \frac{1 - R_s}{1 + R_s} \quad (14\text{-}82)$$

The final equation is

$$V = 2.36\frac{A_s}{H_s}\sqrt{\frac{\rho_L - \rho_V}{\rho_V}}\left(\frac{2}{3}\frac{R_s}{1 + R_s}h_s^{3/2} + \frac{4}{15}\frac{1 - R_s}{1 + R_s}\frac{h_s^{5/2}}{H_s}\right) \quad (14\text{-}83)$$

It is not possible to solve Eq. (14-83) explicitly for the slot opening, but the solutions relating slot opening as a per cent of slot height to vapor loading as a per cent of fully loaded vapors may be presented graphically, as in Fig. 14-46. Note that the maximum vapor flow, or the flow corresponding to a fully opened slot, is

$$V_m = 2.36\left(\frac{2}{3}\frac{R_s}{1 + R_s} + \frac{4}{15}\frac{1 - R_s}{1 + R_s}\right)\sqrt{H_s\frac{\rho_L - \rho_V}{\rho_V}}A_s \quad (14\text{-}84)$$

since $h_s = H_s$ under this condition.

Three curves corresponding to triangular slots ($R_s = 0.00$), trapezoidal slots (with $R_s = 0.50$), and rectangular slots ($R_s = 1.00$) are shown in Fig. 14-46. The slot opening is equated to the slot pressure drop, since the pressure drop and, to some extent, the hydraulic gradient are directly responsible for the slot opening.

Estimation of Hydraulic Gradient

Davies (14-13) has developed a semitheoretical approach to the problem of estimating the hydraulic gradient in a bubble-cap column. Figure 14-47 presents an idealized sketch of a plate operating near the point of instability. The bubbling at D is presumed normal, and the bubbling at U is so slight that the resistance to flow may be equated to the gradient plus the slot submergence. The pressure drop at D, on the other hand, is the pressure drop through the slots plus the head due to the aerated liquid. Equating the two pressure drops,

$$h_r + h_{ra} + h_s + \psi_T S_m = \Delta + S_m \qquad (14\text{-}85)$$

where h_r = pressure drop through riser, in. of liquid
h_{ra} = pressure drop through reversal plus annular layer, in. of liquid
h_s = pressure drop through slots, in. of liquid
ψ_T = fraction of slot submergence that becomes pressure loss at outlet row of caps, U
S_m = slot submergence, in. of liquid
Δ = hydraulic gradient, in. of liquid

If $\psi_T = 1.0$, then $h_r + h_{ra} + h_s \geqq \Delta$ for the row of caps designated by U in Fig. 14-47 to bubble; and bubbling just begins when $h_r + h_{ra} + h_s = \Delta$. Actually, as the data of Kemp and Pyle (14-26) indicate, the values of ψ_T for the active caps are less than 1 when other portions of the cap are unstable; so we may write

$$h_r + h_{ra} + h_s + (\psi_T - 1)S_m = \Delta \qquad (14\text{-}86)$$

which states that the gradient may be slightly less than the pressure drop through the cap when tray instability begins.

But the liquid gradient Δ on a bubble-cap column is a complicated function of many variables (14-13), including:

1. Liquid rate
2. Liquid density
3. Vapor rate
4. Vapor density
5. Minimum seal
6. Cap-assembly details, including cap-pressure-drop characteristics

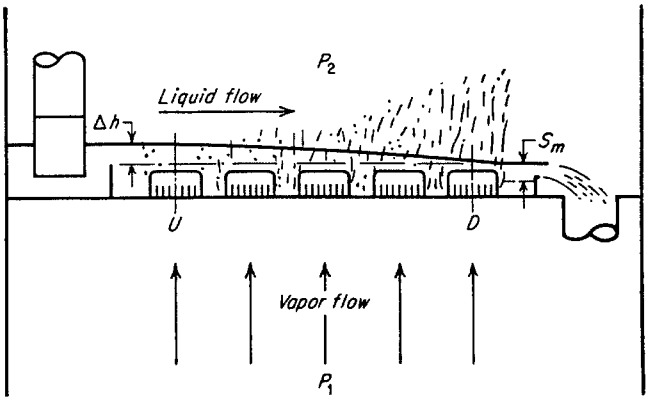

Fig. 14-47. Idealized sketch of a plate operating near point of instability. (Kemp and Pyle, 14-26. Courtesy AIChE.)

7. Cap spacing
8. Number of rows of caps
9. Clearance between the bottom of the cap and the plate, the "skirt clearance"

A summarizing curve of the hydraulic gradient, as a function of the slot factor F_s for a specific tray, is plotted in Fig. 14-48. Superimposed on the same diagram are the pressure drops at zero seal and the locus of tray stability.

Although the Davies method (14-13) of predicting tray hydraulics agrees only qualitatively with experimental fact (14-26), it is the only systematic approach that has been published. The derivation of the equation was based on the following assumptions and conditions:

1. Only clear liquid flowing across the tray, with clear-liquid level above the bottom of the cap but not over the top of the cap
2. Round caps and risers
3. Caps on isosceles-triangle spacing
4. All caps bubbling

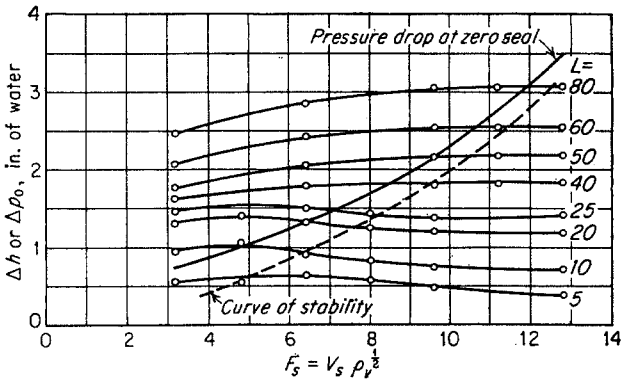

Fig. 14-48. Sample plot of effect of F on hydraulic gradient as used in preparation of liquid-handling-capacity charts. Sixteen rows of 3-in. caps, flush, on 4¼-in. equilateral triangular centers; minimum seal constant at 1.0 in. (Kemp and Pyle, 14-26. Courtesy AIChE.)

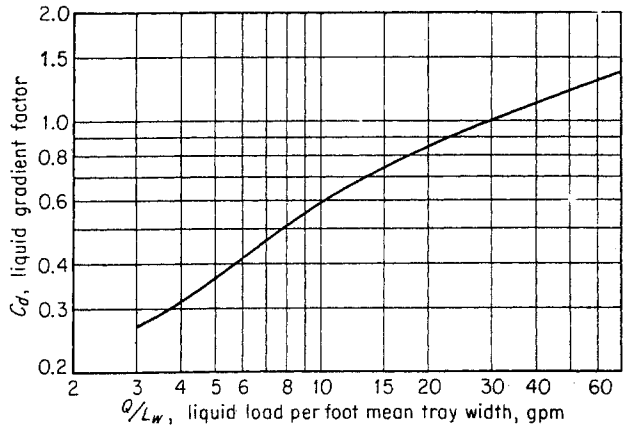

Fig. 14-49. Liquid-gradient-factor chart. (*Davies, 14-13. Courtesy Ind. Eng. Chem.*)

5. Uniform cap assembly and spacing
6. Level tray
7. Row of caps normal to direction of liquid flow
8. Cross-flow-type trays with essentially parallel flow of liquid streams
9. Main frictional resistance attributed to assembled cap
10. Steady-state flow conditions

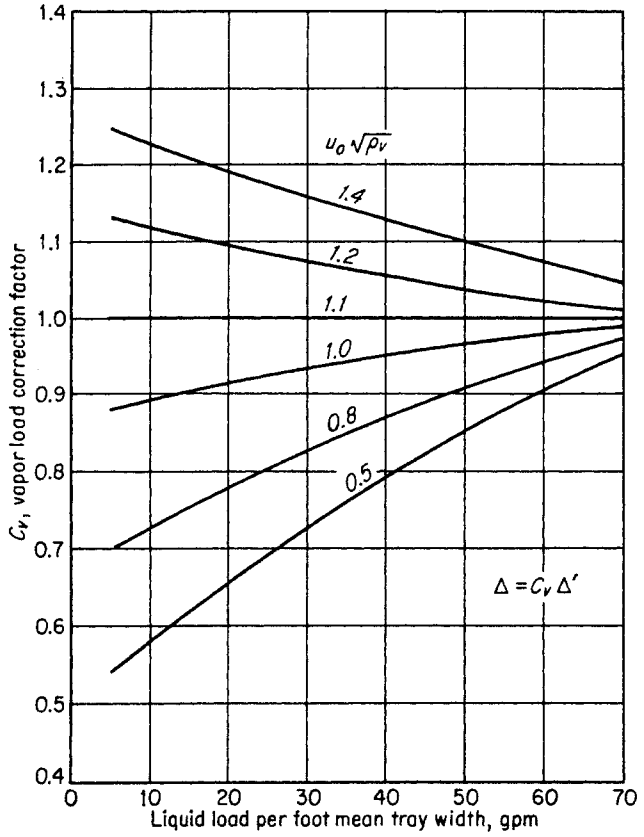

Fig. 14-50. Correction of liquid gradient for vapor load. (*Davies, 14-13. Courtesy Ind. Eng. Chem.*)

Using the submerged-orifice formula to calculate the frictional loss resulting from flow through the caps, together with experimental hydraulic-gradient data, Davies (14-14) developed the final equation relating the liquid gradient Δ' uncorrected for vapor flow to the other tray variables.

$$\sqrt{\Delta'}\left\{\Delta'\left[3\left(\frac{N_r}{2}-1\right)+\frac{2}{1+\frac{1}{4}\beta^2}\right]+3N_r\left[h_{l_0}+s(\alpha-1)\right]\right\}=\frac{N_r^{3/2}\sqrt{1+\frac{1}{4}\beta^2}\,Q}{2.4c_d l_c} \tag{14-87}$$

Bolles (14-4) makes the further assumptions that the caps are on equilateral triangular centers and that the riser diameter is approximately 0.7 times the cap diameter; so

$$\frac{Q/L_w}{c_d}=25.8\frac{\gamma}{1+\gamma}\sqrt{\Delta'_r}\left[1.6\Delta'_r+3\left(h_l+\frac{0.3s}{\gamma}\right)\right] \tag{14-88}$$

where N_r = number of rows of caps normal to flow
h = depth of clear liquid on tray, in.
h_{l_0} = depth of clear liquid at overflow weir, in.
l_c = total free width between caps normal to flow, in.
s = cap skirt clearance, in.
c_d = liquid-gradient factor
L_w = total flow width across tray normal to flow, ft
Q = liquid load for tray or tray section, gpm
α = ratio of distance between risers to distance between caps
Δ' = liquid gradient between caps, uncorrected for vapor load, in.
Δ'_r = liquid gradient per row of caps, uncorrected, in.
γ = ratio of distance between caps to cap diameter
β = ratio of distance between caps on parallel liquid pass to distance between caps on oblique liquid pass

Figure 14-49 gives a liquid-gradient-factor chart which may be employed with Eq. (14-88) to yield working charts for estimating hydraulic gradients on bubble-cap trays. Finally, the true hydraulic gradient is obtained by multiplying the uncorrected gradient by the vapor correction factor obtained from Fig. 14-50. A typical working chart drawn up by Bolles (14-4) is shown in Fig. 14-51.

Pressure Drop through Massive Spray

The vapor, just outside the slots, decreases in pressure as it flows through the massive spray above the

caps. The *actual* pressure drop through the massive spray is

$$h_A \leqq h_w + h_{ow} + \Delta - h_{ts} \qquad (14\text{-}89)$$

where h_A = actual pressure drop through massive spray, in. of liquid
h_w = height of weir, in. of liquid
h_{ow} = height of clear liquid flow over weir, in. of liquid
Δ = liquid head due to gradient at particular point on tray, in. of liquid
h_{ts} = height from tray floor to top of slot, in.

The ratio

$$\psi_T = \frac{h_A}{h_w + h_{ow} + \Delta - h_{ts}}$$

which is called the "aeration factor" on the tray, may be determined from experimental data, since

$$\psi_T = \frac{h_t - (h_r + h_{ra} + h_s)}{h_w + h_{ow} + \Delta - h_{ts}} \qquad (14\text{-}90)$$

where h_t = measured total tray pressure drop, in. of liquid. Adequate sources of ψ_T are not available. Kemp and Pyle (14-26) have found that the aeration factor for the air-water system varied from 0.50 to 0.80. High liquid levels and high vapor rates increased the value of ψ_T. Air–absorber oil systems yield ψ_T values of from 0.4 to 0.6, with a conservative value of 0.6. The aeration factors encountered in natural gasoline fractionation are not known, but use of a conservative value of 0.6 is recommended. The aeration factor is influenced by many variables, but vapor rate, slot submergence, and the system properties appear to be the outstanding variables. Tentatively, these values of ψ_T may be used to convert the static submergence S_m to actual pressure drop.

Head Loss Resulting from Downflow Baffle

The liquid head loss resulting from the flow of liquids under the downflow baffle is approximated by

$$h_d = 0.03\left(\frac{Q}{100A_d}\right)^2 \qquad (14\text{-}91)$$

where h_d = head loss, in. of liquid
Q = liquid load for tray or tray section, gpm
A_d = minimum area under downcomer, sq ft

Liquid Backup in Downcomer

The height of liquid at the tray inlet serves as a starting point for calculating the liquid backup in the downcomers. The height of liquid at the tray inlet is given by

$$h_{ti} = h_w + h_{ow} + \Delta \qquad (14\text{-}92)$$

where h_{ti} = height of clear liquid at tray inlet, in., and the other variables are defined as in Eq. (14-89). The total clear-liquid backup in the downcomer is

$$H_d = h_{ti} + h_d + h_r + h_{ra} + h_s + \psi_T S_m \qquad (14\text{-}93)$$

The actual backup in the downcomer will be considerably greater than this, because the liquid in the downcomer is also aerated. A few measurements are available for the downcomer aeration factor A_f, defined by

$$A_f = \frac{H_d}{H_f} \qquad (14\text{-}94)$$

where H_f = actual froth height in the downcomer, in. The aeration factor for the air-water system falls in the neighborhood of 0.8, with a conservative value of 0.75. On the other hand, the air–absorber oil system yielded a value of 0.5 to 0.7, with a conservative value of 0.5. A value of 0.45 for natural gasoline distillation is suggested. When the downcomer buildup reaches the top of the weir, the column may be expected to flood.

Downcomer buildup should be of the order of 60 per cent for a safe initial design.

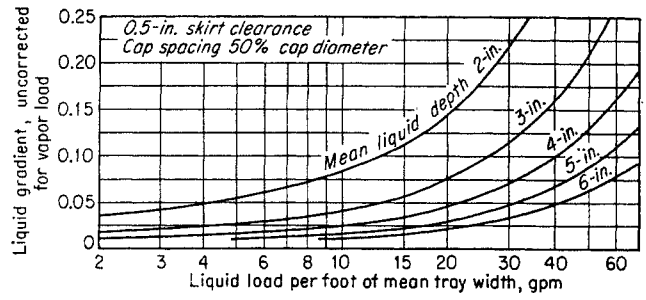

Fig. 14-51. Typical working chart for estimation of liquid gradient. (*Bolles, 14-4. Courtesy Petrol. Processing.*)

SUMMARY

An introductory treatment to the subject of distillation has been presented. The equilibrium-stage concept is used exclusively to relate stream flows and stream compositions. Tray efficiencies are used to relate the equilibrium number of stages to the actual number of trays. Both rapid and detailed methods of column sizing are discussed, with special attention paid to procedures that are descriptive rather than convenient.

CHAPTER 15

Low-temperature Processing

In the 1820s Sir Humphry Davy, Michael Faraday, M. Natterer, Cagnard de la Tour, and other scientists in Europe were discovering that all common gases could be liquefied and that critical phenomena occurred as the temperature was raised in gas-liquid systems (1-9). By 1900, hydrogen and helium had been liquefied and the present concept that all substances can occur in the gaseous, liquid, and solid states had been reached. Methane has a critical temperature of −116.5°F and a normal boiling temperature of −258.7°F. Processing operations at temperatures such as these have been limited, but the engineer is required to consider such processes on occasion. Liquid-oxygen manufacture has reached the tonnage stage, and experiences gained with liquid-oxygen plants is of value in other low-temperature operations (15-4, 15-22). Materials of construction must be selected specially for low temperatures. The phase-behavior information is limited to substances which are normally considered gases since their normal boiling points are below room temperature. Extraction of ethane from natural gas, liquefaction of natural gas, separation of nitrogen from natural gas, and helium extraction are actual or potential processes at low temperatures.

PHASE BEHAVIOR

General phase behavior discussed in Chap. 3 included methane, the methane-ethane system (3-8), and the methane-nitrogen system (3-7, 3-15). It should be noted that the maximum two-phase pressure for the methane-ethane system (Fig. 3-10) is 1,000 psia. This level is characteristic of the maximum pressure for two phases in hydrocarbon systems at low temperature; therefore, operations at low temperature are likely to be at moderate pressures. The proximity of the boiling points of the constituents in a mixture is responsible, in part, for the maximum two-phase pressures, and, when hydrogen is added to the light-

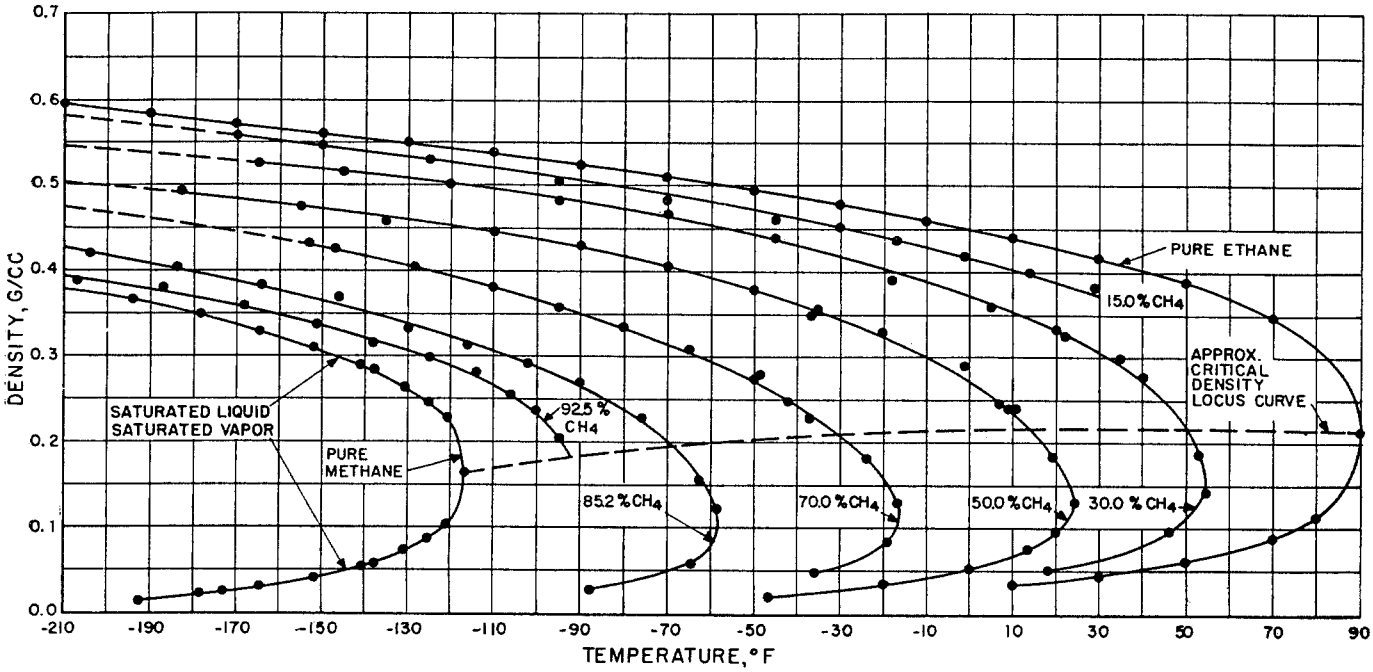

Fig. 15-1. Densities of saturated vapors and liquids in the methane-ethane system. *(By permission from "Physical Chemical Properties of Methane-Ethane Mixtures," by O. T. Bloomer, D. C. Gami, and J. D. Parent. Copyright 1953, Institute of Gas Technology.* 3-8.)

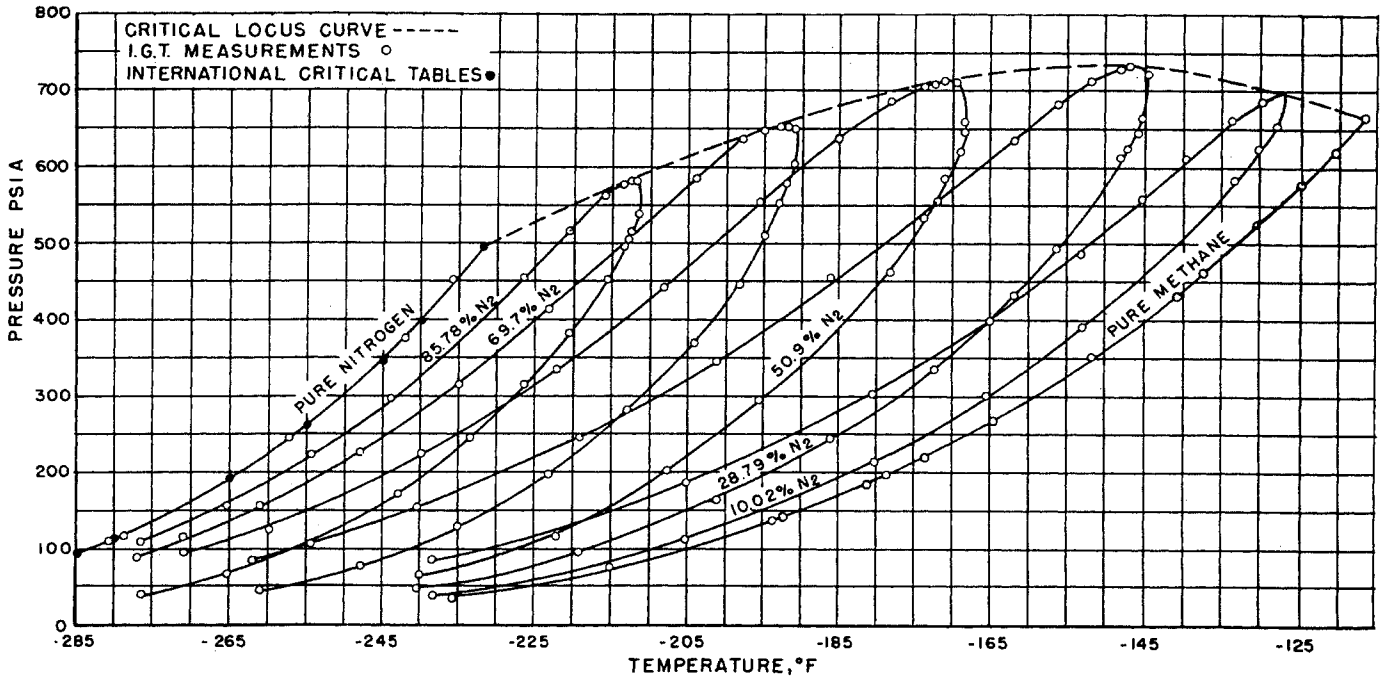

Fig. 15-2. Dew-point and bubble-point diagrams for the methane-nitrogen system. *(By permission from "Physical-Chemical Properties of Methane-Nitrogen Mixtures," by O. T. Bloomer and J. D. Parent. Copyright 1952, Institute of Gas Technology. 3-7.)*

hydrocarbon systems, two-phase regions occur up to 8,000 or 10,000 psia or more (15-3, 15-5, 15-6, 15-36). Ruhemann has summarized data on vapor-liquid equilibria for gaseous systems at low temperature (15-27).

It should be noted that the volatile hydrocarbons all have freezing points near −300°F (Table A-1) with pure methane freezing at −296.5°F. Propane has the lowest freezing point: −305.8°F; ethylene freezes at −272°F, and *n*-butane at −217°F. Although the pressure of dissolved hydrogen or nitrogen may lower the freezing points of the hydrocarbons, the effects at pressures up to 2,000 or 3,000 psia are not expected to be appreciable.

The methane-ethane system, already shown in Fig. 3-10 along with the nitrogen-methane system, exhibits important phase relations for low-temperature processing of natural gas. The orthobaric densities are given in Fig. 15-1. The equilibrium constants for the methane-ethane system are given in Table 15-1.

The nitrogen-methane system was investigated by Bloomer and Parent (3-7) and by Cines, Roach, Hogan, and Roland (3-15). Figures 15-2 to 15-6 give the behavior of this system. There is good agreement between the Phillips data (3-15) and the Institute of

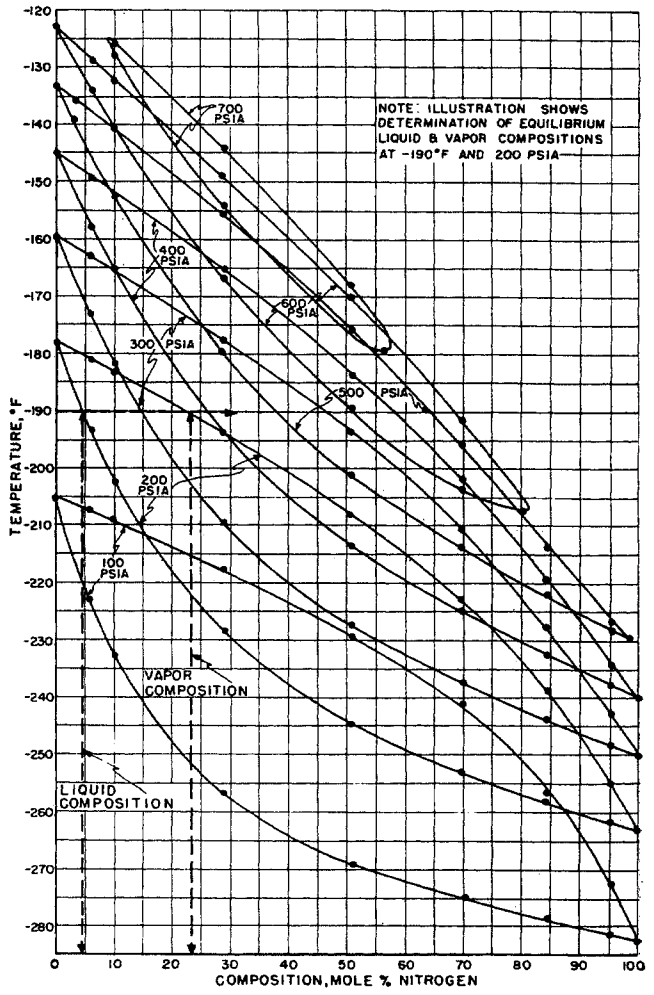

Fig. 15-3. Isobaric temperature-composition diagram for the methane nitrogen system. *(By permission from "Physical-Chemical Properties of Methane-Nitrogen Mixtures," by O. T. Bloomer and J. D. Parent. Copyright 1952, Institute of Gas Technology. 3-7.)*

Table 15-1. K Values in the Methane-Ethane System

K Values for Methane

Temp, °F	Pressure, psia								
	100	200	300	400	500	600	700	800	900
*	−205.5	−178.2	−159.5	−145.2	−132.9	−122.5	−110.5†	−88.4‡	−62.4‡
−200	1.16								
−180	2.02								
−160	2.99	1.44							
−140	4.06	2.01	1.36	1.06					
−120	5.45	2.68	1.82	1.38	1.13	1.02			
−100	6.95	3.33	2.28	1.76	1.42	1.20	1.06		
− 80	8.61	4.02	2.73	2.10	1.71	1.43	1.24	1.09	
− 60	9.78	4.85	3.17	2.43	1.97	1.67	1.44	1.28	1.08
− 40	.....	5.64	3.66	2.73	2.20	1.86	1.62	1.42	1.23
− 20	.....	6.23	4.16	3.05	2.40	2.00	1.74	1.52	1.33
0	.....	.....	4.46	3.37	2.63	2.18	1.87	1.59	1.39
20	.....	.....	.....	3.54	2.83	2.30	1.91	1.63	1.39
40	.....	.....	.....	3.62	2.85	2.36	1.91	1.63	1.23
60	.....	.....	.....	.....	.....	2.30	1.82		
80	.....	.....	.....	.....	.....	.....	1.61		
†	− 46.0	− 6.2	21.6	43.0	61.0	75.8	88.3	72.6‡	48.3‡

K Values for Ethane

Temp, °F	Pressure, psia								
	100	200	300	400	500	600	700	800	900
*	−205.5	−178.2	−159.5	−145.2	−132.9	−122.5	−110.5‡	−88.4‡	−62.4‡
−200	0.00735								
−180	0.0350								
−160	0.0710	0.0540							
−140	0.1291	0.0925	0.0890	0.1148					
−120	0.2225	0.1446	0.1257	0.1349	0.1712	0.2438			
−100	0.3550	0.2213	0.1822	0.1735	0.193	0.2515	0.398		
− 80	0.546	0.3265	0.264	0.2372	0.240	0.275	0.339	0.5645	
− 60	0.798	0.4571	0.363	0.3255	0.3115	0.322	0.358	0.441	0.718
− 40	.....	0.631	0.4798	0.421	0.405	0.405	0.421	0.462	0.583
− 20	.....	0.839	0.6237	0.540	0.510	0.497	0.506	0.533	0.619
0	.....	.....	0.7975	0.674	0.6175	0.596	0.5975	0.612	0.680
20	.....	.....	.....	0.815	0.739	0.703	0.6875	0.708	0.760
40	.....	.....	.....	0.980	0.873	0.814	0.790	0.807	0.894
60	.....	.....	.....	.....	0.995	0.926	0.881	0.929	
80	.....	.....	.....	.....	.....	.....	0.985		
†	−46.0	−6.2	21.6	43.0	61.0	75.8	88.3	72.6‡	48.3‡

* Saturation temperature for methane. † Saturation temperature for ethane. ‡ Critical temperature for the system.

SOURCE: Bloomer, Gami, and Parent (3-8).

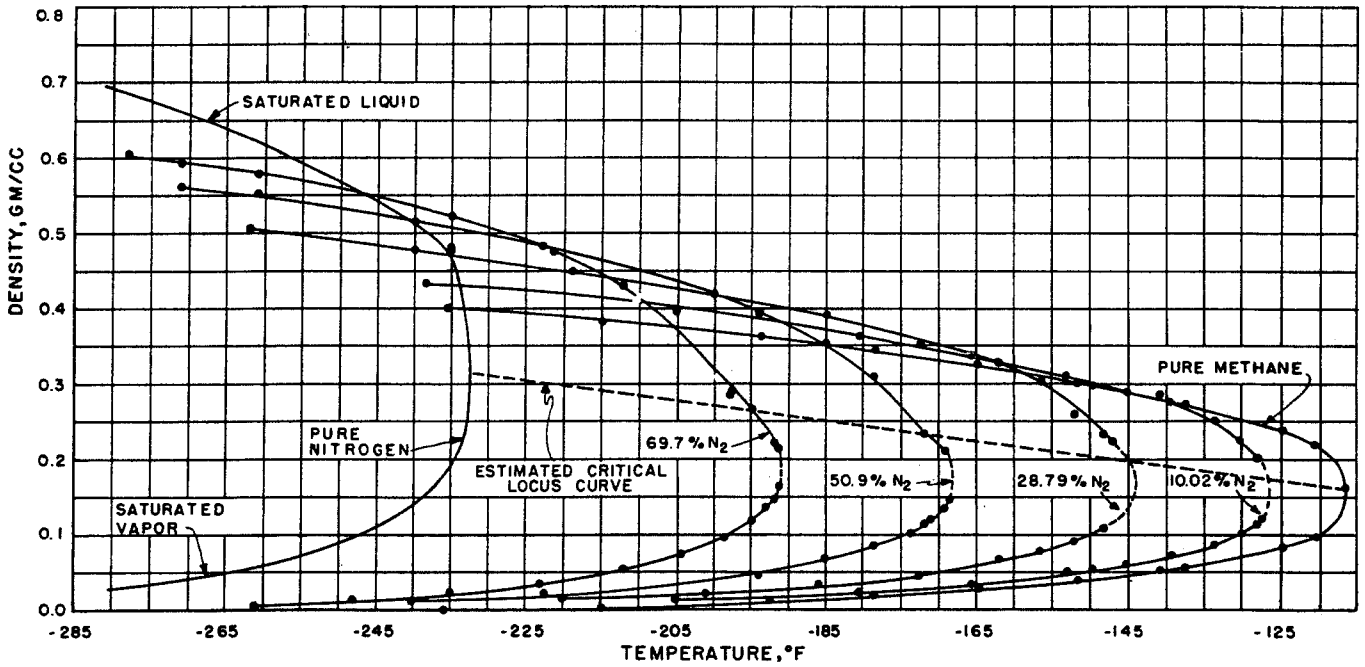

Fig. 15-4. Saturated vapor and liquid densities for methane-nitrogen system. (*By permission from "Physical-Chemical Properties of Methane-Nitrogen Mixtures," by O. T. Bloomer and J. D. Parent. Copyright 1952, Institute of Gas Technology.* 3-7.)

Gas Technology (IGT) data, as shown by Fig. 15-7 (3-8). The properties of nitrogen at low temperature are presented by Bloomer and Rao (15-7). Mollier diagrams for nitrogen and methane are given in Figs. 15-8 and 15-9. An enthalpy-composition chart for methane-nitrogen mixtures is given in Fig. 15-10 (15-8).

The behavior of the carbon dioxide–methane system is of interest since it represents the beginning of vapor-liquid-solid equilibria. Donnelly and Katz (15-15) presented the phase behavior (Figs. 15-11 and 15-12), showing the intrusion of the vapor-solid region into the normally vapor-liquid area. Methane lowers the freezing point of carbon dioxide as shown.

At low concentrations of carbon dioxide, the solid phase does not appear. Natural gases containing under about 1.5 per cent carbon dioxide should have no difficulties with solid formation down to liquefaction temperatures for methane.*

Price (15-26a) has studied the phase behavior of the methane-ethane-propane system and its associated binaries at low temperatures and at pressures up to the criticals for the mixtures. Such data may be applied to the recovery of ethane and propane at low temperatures. The data have been presented in the form of charts employing pressure, temperature,

* Since this statement was written, Kurata reports that liquid methane at atmospheric pressure in contact with solid carbon dioxide contains 0.2 mole % carbon dioxide.

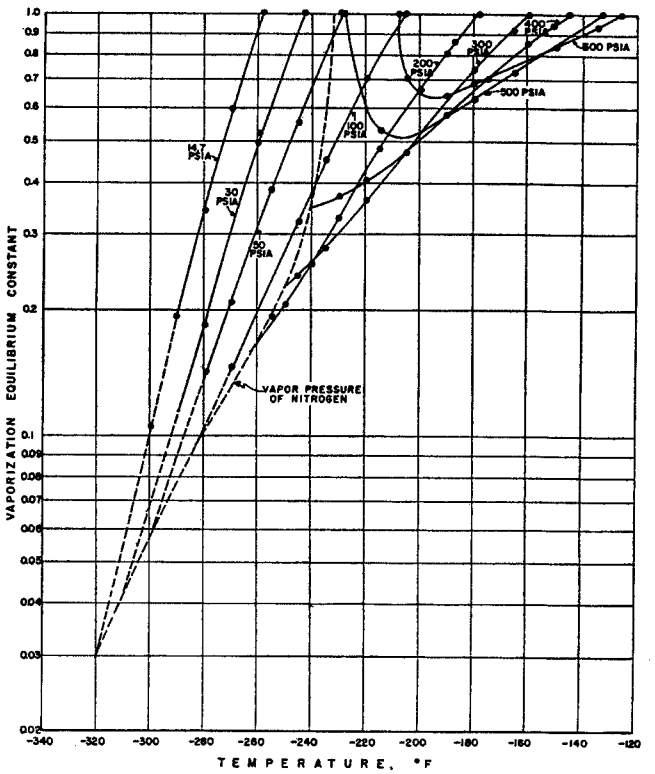

Fig. 15-5. Vaporization-equilibrium constants for methane in methane-nitrogen system. (*By permission from "Physical-Chemical Properties of Methane-Nitrogen Mixtures," by O. T. Bloomer and J. D. Parent. Copyright 1952, Institute of Gas Technology.* 3-7.)

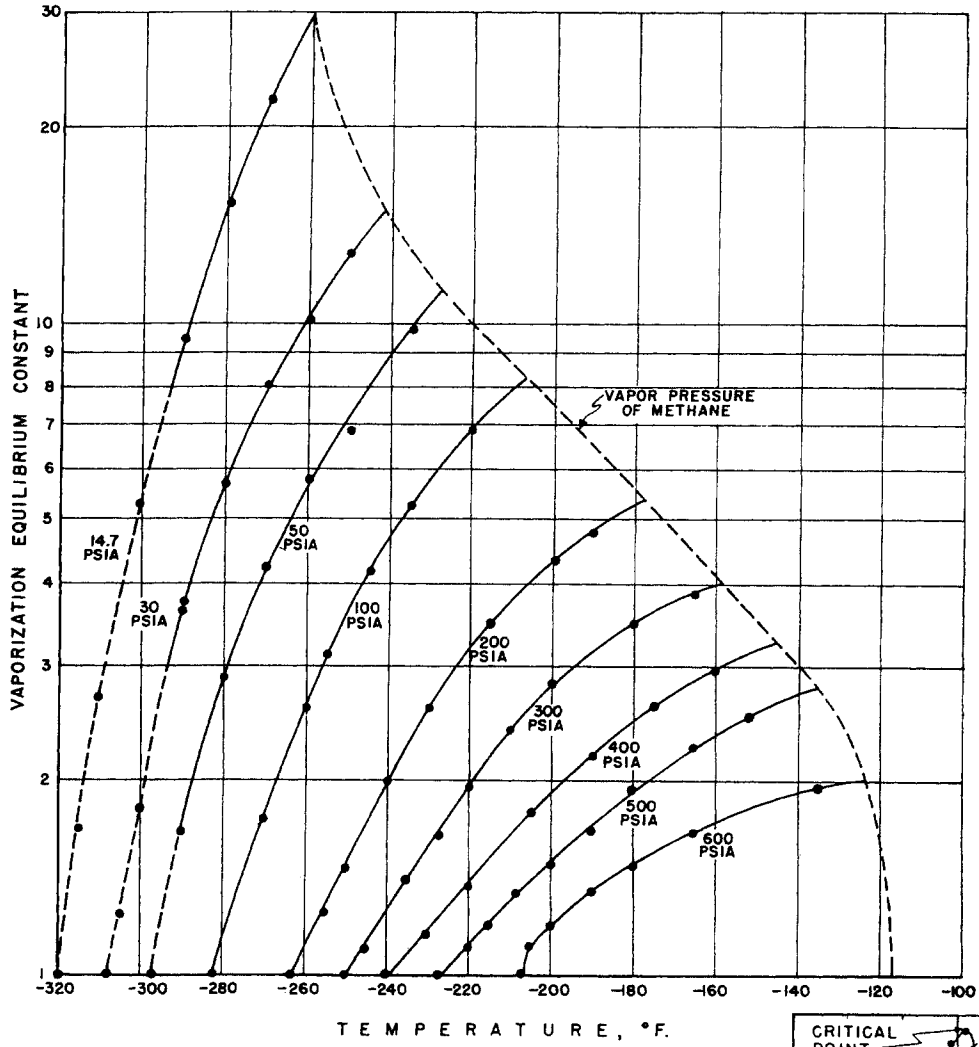

Fig. 15-6. Vaporization-equilibrium constants for nitrogen in the methane-nitrogen system. (*By permission from "Physical-Chemical Properties of Methane-Nitrogen Mixtures," by O. T. Bloomer and J. D. Parent. Copyright 1952, Institute of Gas Technology.* 3-7.)

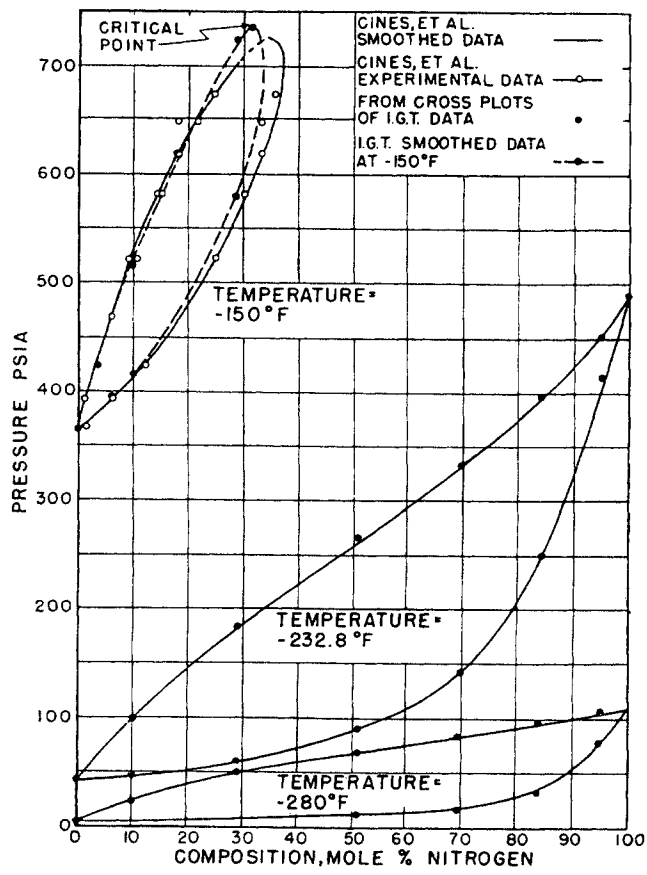

Fig. 15-7. Comparison of experimental data of Cines, Roach, Hogan, and Roland with IGT data. (*By permission from "Physical-Chemical Properties of Methane-Ethane Mixtures," by O. T. Bloomer, D. C. Gami, and J. D. Parent. Copyright 1953, Institute of Gas Technology.* 3-8.)

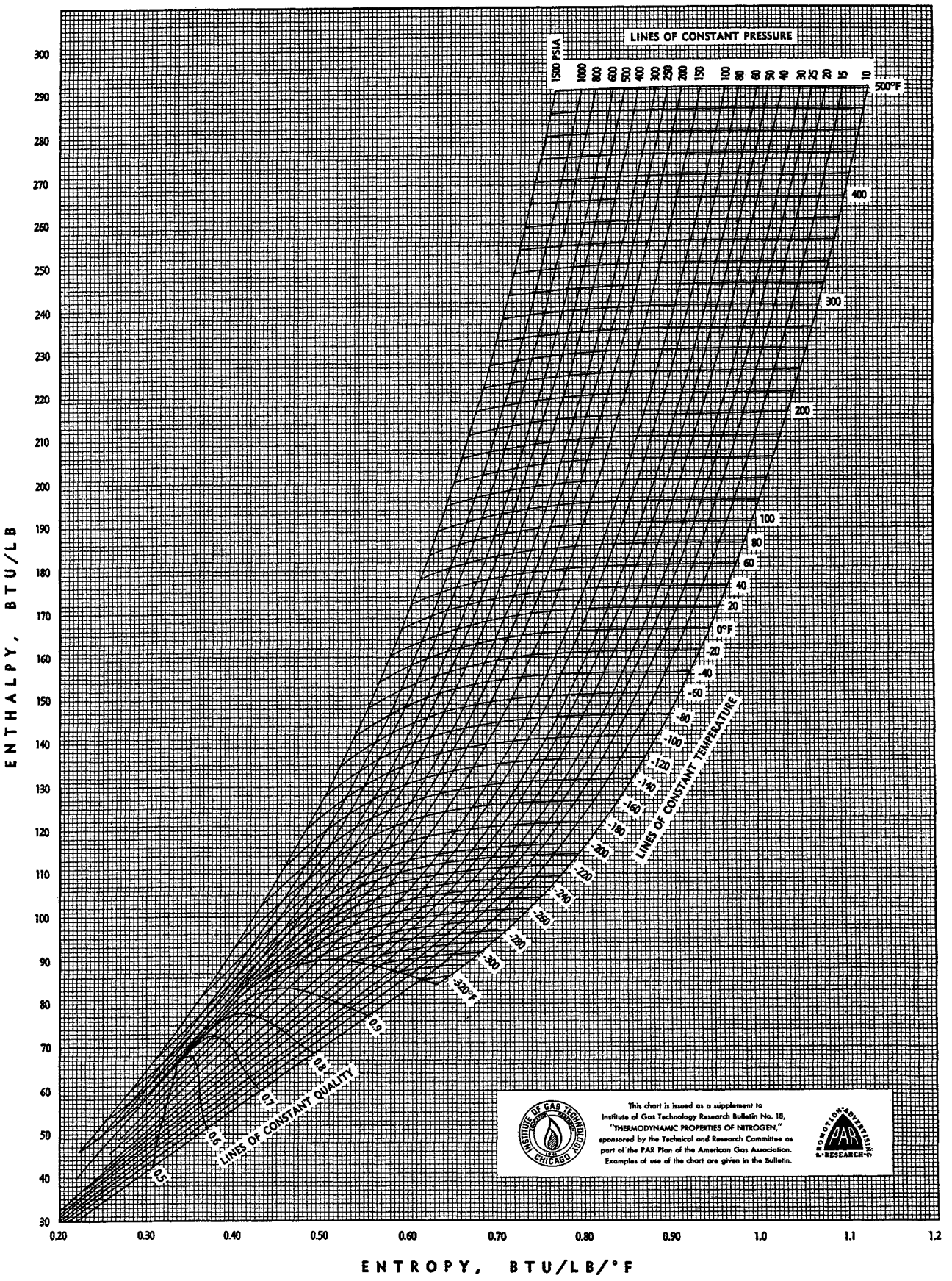

Fig. 15-8. Mollier chart for nitrogen. (*By permission from "Thermodynamic Properties of Nitrogen," by O. T. Bloomer and K. N. Rao. Copyright 1952, Institute of Gas Technology.* 15-7.)

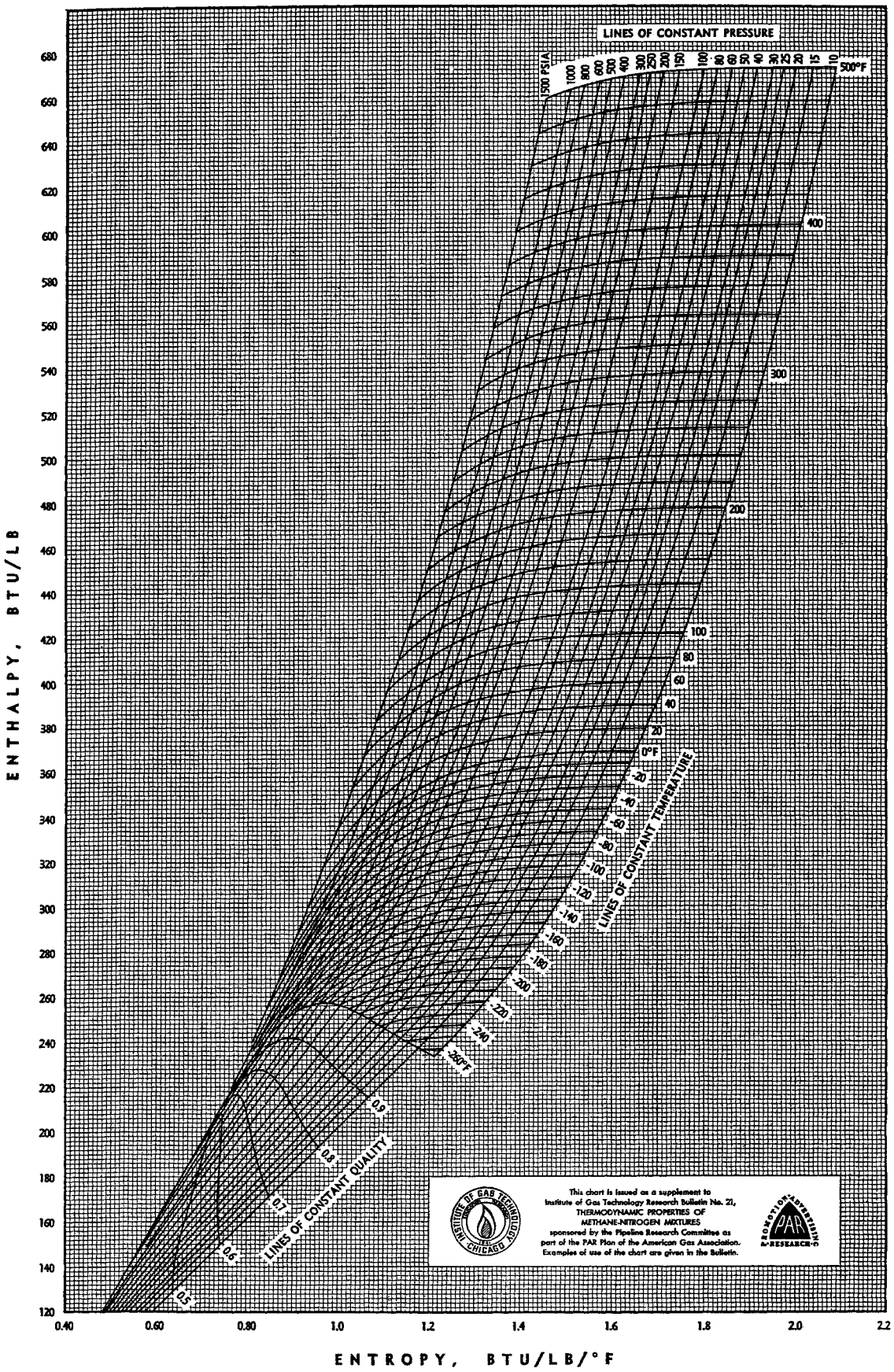

Fig. 15-9. Mollier chart for methane. (*By permission from "Thermodynamic Properties of Methane-Nitrogen Mixtures," by O. T. Bloomer, B. E. Eakin, R. T. Ellington, and D. C. Gami. Copyright 1953, Institute of Gas Technology.* 15-8.)

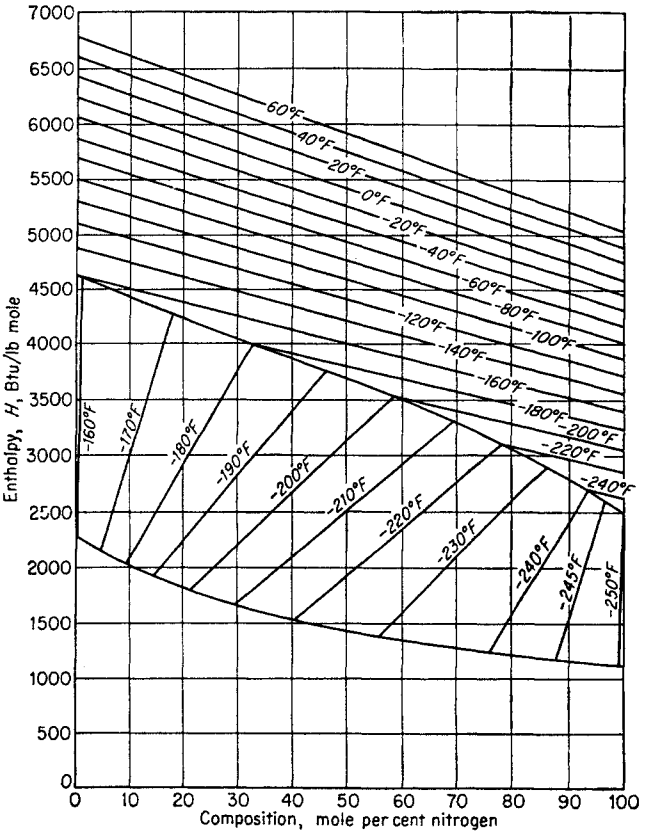

Fig. 15-10. Enthalpy-composition chart for methane-nitrogen mixtures at 300 psia. (*By permission from "Thermodynamic Properties of Methane-Nitrogen Mixtures," by O. T. Bloomer, B. E. Eakin, R. T. Ellington, and D. C. Gami. Copyright 1953, Institute of Gas Technology.* 15-8.)

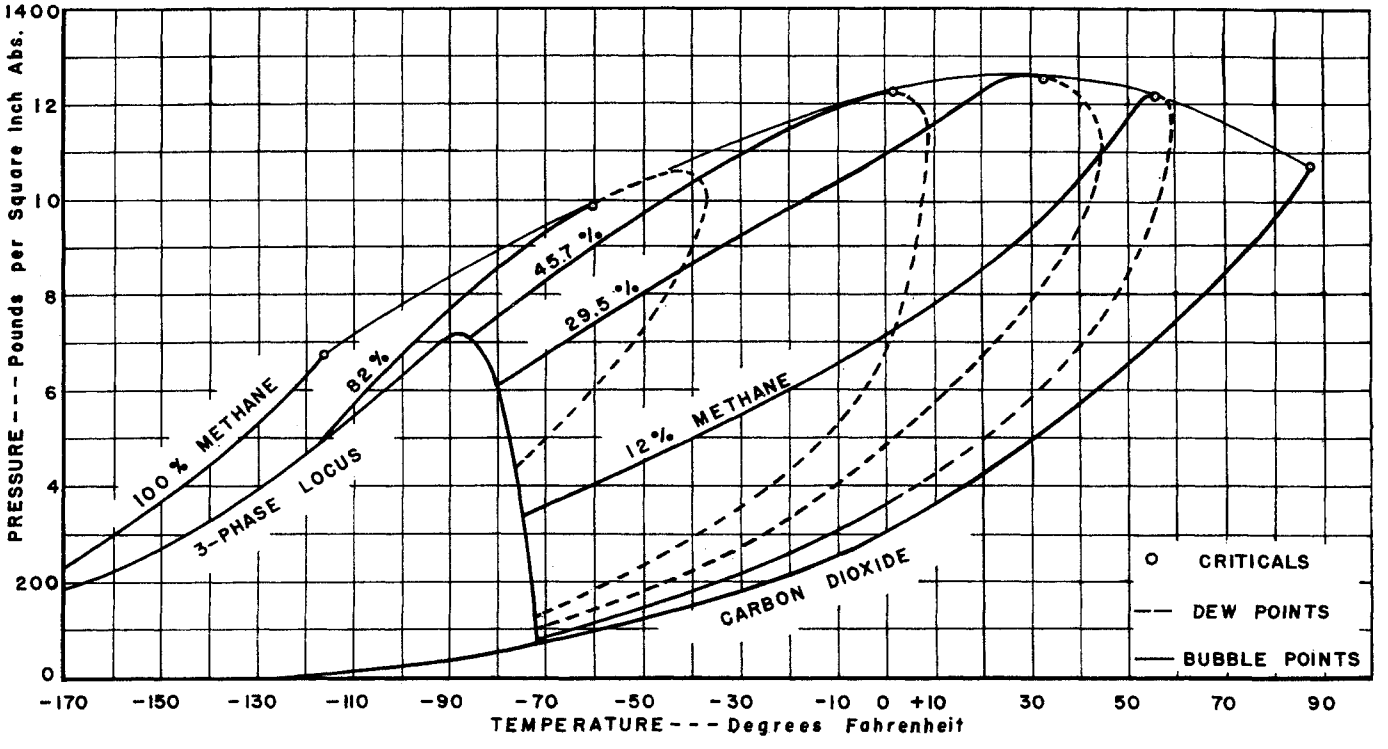

Fig. 15-11. Pressure-temperature diagram for carbon dioxide–methane system. (*Donnelly and Katz,* 15-15. *Courtesy Ind. Eng. Chem.*)

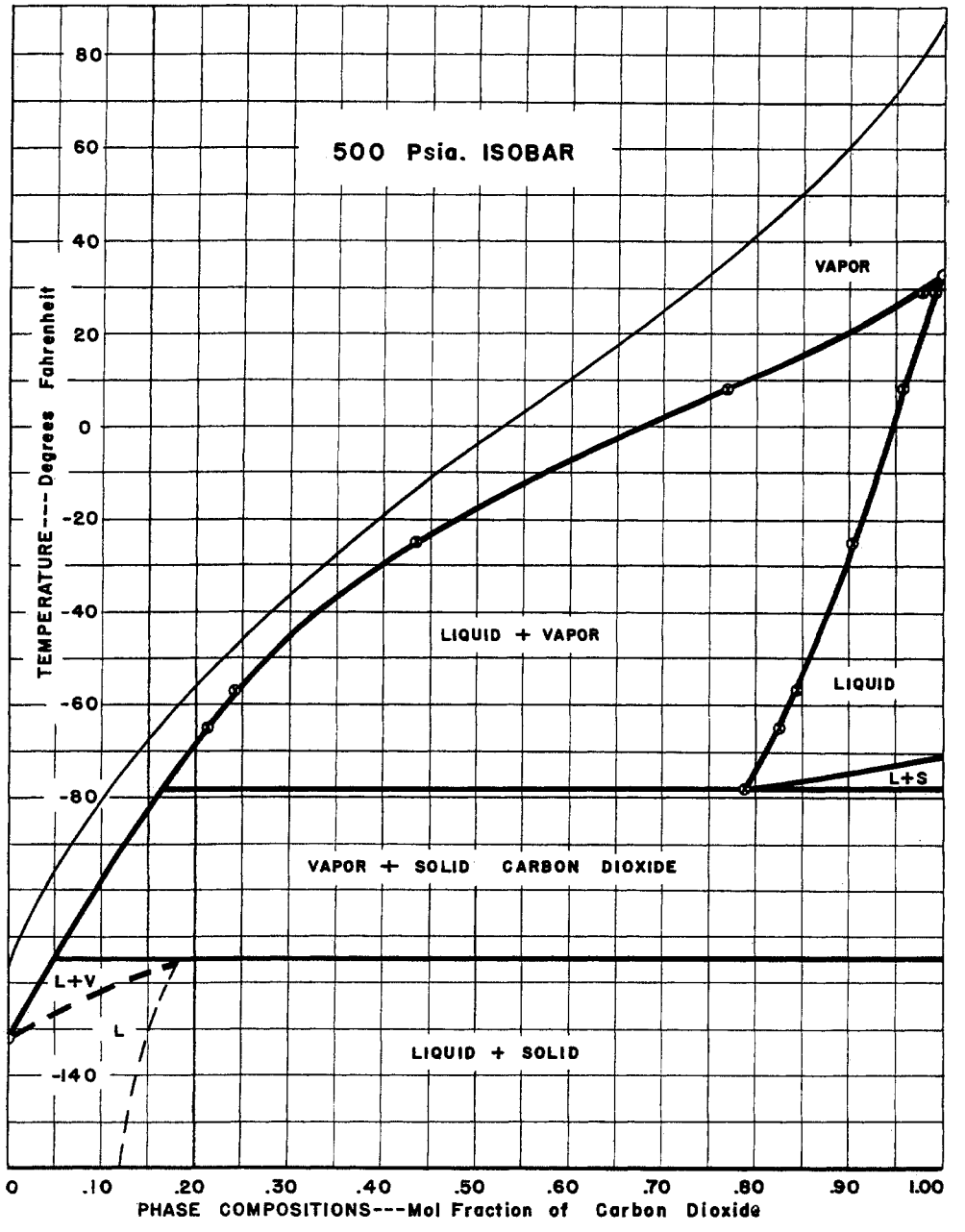

Fig. 15-12. Temperature-composition section of the carbon dioxide–methane system at 500 psia. (*Donnelly and Katz*, 15-15. *Courtesy Ind. Eng. Chem.*)

and phase molal-average boiling points as parameters (15-26b). Selected experimental data for the system are given in Table 15-2, and equilibrium constants for the methane-propane system are given in Figure 15-13.

Kurata and associates have studied the phase behavior of natural gases, determining phase diagrams and critical points at low temperatures (15-14, 15-18). Table 15-2 gives the compositions of the gases and the critical properties. Figures 15-14 and 15-15 give the phase behavior of mixture A-4, for which the composition is shown in Table 15-3. The compressibility-factor chart was extended down to the low-temperature region from experimental P-V-T data on the gases (Fig. 15-16). In some cases, two phases were present.

Table 15-2. Experimental Data for Methane-Ethane-Propane System

Code no.	Temp, °F	Pressure, psia	Liquid composition			Vapor composition			*K* Values		
			CH_4	C_2H_6	C_3H_8	CH_4	C_2H_6	C_3H_8	CH_4	C_2H_6	C_3H_8
1	50	100	0.0028*	.....	0.998	0.057	.....	0.943	20.5*	.....	0.945
2	50	100	0.0022*	0.0080	0.9897	0.0452	0.0280	0.9268	20.4*	3.50	0.936
4	50	100	.....	0.0236	0.9764	.....	0.0720	0.9280	.....	3.05	0.951
5	50	200	0.044*	.....	0.960	0.471	.....	0.529	10.7*	.....	0.551
6	50	200	0.044*	.....	0.962	0.471	.....	0.529	10.7*	.....	0.550
7	50	200	0.0396*	0.0655	0.8966	0.412	0.112	0.476	10.4*	1.86	0.531
8	50	200	0.0270*	0.160	0.811	0.275	0.284	0.441	10.1*	1.78	0.545
9	50	200	0.0128*	0.264	0.7193	0.127	0.476	0.397	9.95	1.80	0.552
10	50	200	.....	0.357	0.643	.....	0.612	0.388	.....	1.72	0.603
11	50	400	0.128	.....	0.872	0.685	.....	0.315	5.35	.....	0.361
12	50	400	0.110	0.175	0.715	0.557	0.193	0.250	5.06	1.10	0.350
13	50	400	0.0697	0.500	0.4303	0.306	0.535	0.159	4.39	1.07	0.369
14	50	400	0.0620	0.553	0.385	0.282	0.570	0.148	4.54	1.03	0.348
15	50	400	0.0302	0.7578	0.212	0.115	0.7989	0.0861	3.81	1.05	0.406
16	50	400	.....	0.9066	0.0934	.....	0.9616	0.0384	1.06	1.06	0.411
17	50	400	.....	0.9108	0.0892	.....	0.9606	0.0394	.....	1.05	0.442
18	50	600	0.216	.....	0.784	0.762	.....	0.238	3.53	.....	0.304
19	50	600	0.214	0.151	0.635	0.663	0.133	0.204	3.10	0.880	0.321
20	50	600	0.204	0.178	0.618	0.654	0.150	0.196	3.20	0.843	0.317
21	50	600	0.178	0.376	0.446	0.521	0.332	0.147	2.93	0.883	0.330
22	50	600	0.174	0.457	0.369	0.487	0.382	0.131	2.80	0.836	0.355
23	50	600	0.137	0.647	0.216	0.371	0.5501	0.0789	2.71	0.849	0.365
24	50	600	0.113	0.768	0.119	0.286	0.6668	0.0472	2.53	0.868	0.397
25	50	600†	0.083	0.917	.....	0.210	0.790	.....	2.53	0.861	
26	50	800	0.300	.....	0.700	0.788	.....	0.212	2.63	.....	0.303
27	50	800	0.286	0.121	0.593	0.7224	0.0906	0.187	2.53	0.749	0.315
28	50	800	0.268	0.359	0.373	0.588	0.282	0.130	2.19	0.786	0.348
29	50	800	0.255	0.454	0.291	0.534	0.357	0.109	2.10	0.787	0.374
30	50	800	0.237	0.566	0.197	0.4632	0.455	0.0818	1.95	0.803	0.415
31	50	800†	0.207	0.793	.....	0.325	0.675	.....	1.58	0.852	
32	50	1,000	0.413	.....	0.587	0.805	.....	0.195	1.95	.....	0.332
33	50	1,000	0.389	0.169	0.442	0.707	0.126	0.167	1.82	0.745	0.378
34	50	1,000	0.385	0.225	0.390	0.680	0.164	0.156	1.76	0.729	0.400
35	50	1,000	0.373	0.357	0.270	0.600	0.268	0.132	1.61	0.751	0.442
36	50	1,000	0.349	0.505	0.146	0.4826	0.431	0.0864	1.38	0.853	0.591
37	50	1,000	0.3755	0.5241	0.1004	0.4345	0.490	0.0755	1.16	0.933	0.751
38	50	1,100	0.451	.....	0.549	0.803	.....	0.197	1.78	.....	0.359
39	50	1,100	0.4365	0.0409	0.5226	0.7746	0.0306	0.1948	1.77	0.748	0.373
40	50	1,100	0.430	0.110	0.460	0.7341	0.0849	0.181	1.71	0.771	0.394
41	50	1,100	0.438	0.192	0.370	0.692	0.143	0.165	1.58	0.744	0.446
42	50	1,100	0.438	0.223	0.339	0.665	0.173	0.162	1.52	0.776	0.478
43	50	1,100	0.435	0.259	0.306	0.630	0.209	0.161	1.45	0.807	0.526
44	50	1,100	0.440	0.376	0.184	0.504	0.351	0.145	1.15	0.934	0.788
45	50	1,200	0.498	.....	0.502	0.784	.....	0.216	1.57	.....	0.430
46	50	1,200	0.4997	0.0375	0.4628	0.7558	0.0302	0.214	1.51	0.806	0.462
47	50	1,200	0.504	0.176	0.320	0.673	0.143	0.184	1.34	0.813	0.575
48	50	1,200	0.508	0.243	0.249	0.584	0.219	0.197	1.15	0.901	0.791

Table 15-2. Experimental Data for Methane-Ethane-Propane System (*Continued*)

Code no.	Temp, °F	Pressure, psia	Liquid composition			Vapor composition			*K* Values		
			CH_4	C_2H_6	C_3H_8	CH_4	C_2H_6	C_3H_8	CH_4	C_2H_6	C_3H_8
49	0	100	0.0358	.....	0.9642	0.573	.....	0.427	15.9	.....	0.445
50	0	100	0.0335	0.0174	0.9491	0.5589	0.0336	0.4075	16.7	1.93	0.430
51	0	100	0.0279	0.1284	0.8437	0.400	0.246	0.354	14.3	1.92	0.420
52	0	100	0.0210	0.166	0.813	0.325	0.349	0.326	15.5	2.10	0.401
53	0	100	0.0107	0.272	0.7173	0.159	0.534	0.307	14.9	1.96	0.428
54	0	100	.....	0.373	0.627	.....	0.692	0.308	.....	1.85	0.491
55	0	200	0.0904	.....	0.9096	0.768	.....	0.232‡	8.47	.....	0.256
56	0	200	0.0917	0.0127	0.8956	0.7717	0.0133	0.215	8.43	1.05	0.240
57	0	200	0.0702	0.250	0.6798	0.560	0.270	0.170	7.98	1.08	0.250
58	0	200	0.0457	0.4843	0.470	0.359	0.519	0.122	7.85	1.07	0.260
59	0	200	0.0127	0.8133	0.174	0.0778	0.8746	0.0476	6.12	1.08	0.274
60	0	200	.....	0.9013	0.0987	.....	0.9717	0.0283	.....	1.08	0.287
61	0	400	0.199	.....	0.801	0.862	.....	0.138	4.33	.....	0.172
62	0	400	0.159	0.347	0.494	0.6985	0.217	0.0845	4.39	0.626	0.171
63	0	400	0.1557	0.5293	0.315	0.6003	0.343	0.0567	3.86	0.648	0.180
64	0	400	0.1364	0.7243	0.1393	0.4869	0.4852	0.0279	3.57	0.670	0.200
65	0	400†	0.123	0.877	.....	0.410	0.590	.....	3.33	0.673	
66	0	600	0.311	.....	0.689	0.891	.....	0.109	2.86	.....	0.158
67	0	600	0.293	0.266	0.441	0.781	0.1377	0.0813	2.67	0.518	0.185
68	0	600	0.288	0.343	0.369	0.7514	0.184	0.0646	2.61	0.537	0.175
69	0	600	0.272	0.481	0.247	0.6896	0.260	0.0504	2.54	0.540	0.204
70	0	600	0.271	0.6204	0.1086	0.6138	0.361	0.0252	2.28	0.582	0.232
71	0	600†	0.256	0.744	.....	0.561	0.439	.....	2.18	0.591	
72	0	800	0.415	.....	0.585	0.899	.....	0.101	2.16	.....	0.173
73	0	800	0.391	0.188	0.421	0.8239	0.0939	0.0822	2.11	0.499	0.195
74	0	800	0.378	0.354	0.268	0.7727	0.1702	0.0517	2.05	0.481	0.213
75	0	800	0.380	0.418	0.202	0.7318	0.224	0.0442	1.93	0.536	0.219
76	0	800	0.380	0.5142	0.1058	0.6795	0.296	0.0245	1.80	0.576	0.232
77	0	800†	0.390	0.610	.....	0.619	0.381	.....	1.59	0.621	
78	0	1,000	0.522	.....	0.478	0.895	.....	0.105	1.71	.....	0.220
79	0	1,000	0.515	0.0780	0.407	0.8623	0.0443	0.0934	1.68	0.568	0.230
80	0	1,000	0.512	0.187	0.301	0.8174	0.1027	0.0799	1.60	0.549	0.266
81	0	1,000	0.514	0.239	0.247	0.791	0.140	0.0690	1.54	0.586	0.280
82	0	1,000	0.5161	0.3378	0.1461	0.7234	0.226	0.0506	1.40	0.669	0.346
83	0	1,000	0.5258	0.4467	0.0275	0.6357	0.349	0.0153	1.21	0.781	0.554
84	0	1,000‡	0.522	0.478	.....	0.569	0.431	.....	1.09	0.901	
85	0	1,100	0.582	.....	0.418	0.888	.....	0.112	1.53	.....	0.268
86	0	1,100	0.5759	0.0581	0.366	0.8619	0.0341	0.104	1.50	0.587	0.284
87	0	1,100	0.585	0.107	0.308	0.8377	0.0635	0.0988	1.43	0.593	0.321
88	0	1,100	0.584	0.157	0.259	0.8237	0.0928	0.0835	1.41	0.591	0.322
89	0	1,100	0.587	0.192	0.221	0.7947	0.1231	0.0822	1.35	0.641	0.372
90	0	1,100	0.582	0.228	0.190	0.7707	0.154	0.0753	1.32	0.675	0.396
91	0	1,100	0.5917	0.2483	0.1600	0.7545	0.1758	0.0697	1.275	0.708	0.436
92	0	1,100	0.6043	0.259	0.1367	0.7484	0.1855	0.0661	1.24	0.716	0.484
93	0	1,100	0.604	0.273	0.123	0.7142	0.2177	0.0681	1.18	0.797	0.554
94	0	1,200	0.637	.....	0.363	0.873	.....	0.127	1.37	.....	0.350
95	0	1,200	0.6456	0.0874	0.267	0.8218	0.0625	0.1157	1.27	0.716	0.433
96	0	1,200	0.653	0.106	0.241	0.8158	0.0751	0.1091	1.25	0.708	0.453
97	0	1,200	0.650	0.118	0.232	0.795	0.089	0.116	1.22	0.754	0.500
98	0	1,200	0.693	0.161	0.146	0.721	0.144	0.135	1.04	0.894	0.925

Table 15-2. Experimental Data for Methane-Ethane-Propane System (*Continued*)

Code no.	Temp, °F	Pressure, psia	Liquid composition			Vapor composition			*K* Values		
			CH_4	C_2H_6	C_3H_8	CH_4	C_2H_6	C_3H_8	CH_4	C_2H_6	C_3H_8
99	0	1,300	0.708	.....	0.292	0.845	.....	0.155	1.19	.....	0.531
100	0	1,300	0.7103	0.0297	0.260	0.8294	0.0246	0.146	1.17	0.828	0.561
101	0	1,300	0.7315	0.0345	0.234	0.8086	0.0322	0.1592	1.11	0.933	0.681
102	0	1,300	0.7364	0.0396	0.224	0.7978	0.0384	0.1638	1.08	0.970	0.731
103	−50	100	0.0769	.....	0.9231	0.840	.....	0.160	10.9	.....	0.173
104	−50	100	0.0614	0.1718	0.7668	0.7195	0.1628	0.1177	11.7	0.947	0.153
105	−50	100	0.0486	0.302	0.6494	0.605	0.292	0.103	12.4	0.967	0.159
106	−50	100	0.0479	0.399	0.5531	0.5287	0.380	0.0913	11.0	0.952	0.165
107	−50	100	0.0467	0.448	0.5053	0.4952	0.425	0.0798	10.6	0.949	0.158
108	−50	100	0.0261	0.7259	0.248	0.280	0.682	0.0380	10.7	0.939	0.153
109	−50	100†	0.006	0.994	.....	0.066	0.934	.....	11.0	0.940	
110	−50	200	0.146	.....	0.854	0.9216	.....	0.0784	6.31	.....	0.0918
111	−50	200	0.125	0.268	0.607	0.804	0.140	0.0560	6.43	0.522	0.0922
112	−50	200	0.125	0.368	0.507	0.7478	0.206	0.0462	5.98	0.560	0.0911
113	−50	200	0.119	0.627	0.254	0.6383	0.333	0.0287	5.35	0.531	0.115
114	−50	200	0.0968	0.9032	.....	0.505	0.495	.....	5.22	0.548	
115	−50	400	0.296	.....	0.704	0.9493	.....	0.0507	3.20	.....	0.0735
116	−50	400	0.292	0.126	0.582	0.920	0.0383	0.0417	3.15	0.304	0.0717
117	−50	400	0.271	0.289	0.440	0.8791	0.0907	0.0302	3.24	0.314	0.0687
118	−50	400	0.274	0.448	0.278	0.8245	0.154	0.0215	3.02	0.344	0.0773
119	−50	400	0.270	0.512	0.218	0.8084	0.1742	0.0174	2.99	0.340	0.0798
120	−50	400	0.277	0.523	0.200	0.7986	0.1880	0.0134	2.88	0.359	0.0805
121	−50	400	0.278	0.571	0.151	0.7901	0.194	0.0159	2.74	0.340	0.105
122	−50	400	0.282	0.718	.....	0.724	0.276	.....	2.57	0.384	
123	−50	600	0.438	.....	0.562	0.9585	.....	0.0415	2.19	.....	0.0739
124	−50	600	0.440	0.145	0.415	0.9179	0.0485	0.0336	2.06	0.334	0.0809
125	−50	600	0.424	0.150	0.426	0.919	0.0446	0.0364	2.17	0.298	0.0855
126	−50	600	0.443	0.243	0.314	0.8952	0.0790	0.0258	2.02	0.325	0.0822
127	−50	600	0.441	0.366	0.193	0.8637	0.119	0.0173	1.96	0.327	0.0896
128	−50	600	0.438	0.562	.....	0.800	0.200	.....	1.83	0.356	
129	−50	800	0.581	.....	0.419	0.959	.....	0.0410	1.65	.....	0.0978
130	−50	800	0.598	0.109	0.293	0.9275	0.362	0.0363	1.55	0.332	0.124
131	−50	800	0.611	0.249	0.140	0.8901	0.0886	0.0213	1.46	0.356	0.152
132	−50	800	0.622	0.378	.....	0.832	0.168	.....	1.34	0.445	
133	−50	1,000	0.736	.....	0.264	0.9458	.....	0.0542	1.29	.....	0.205
134	−50	1,000	0.7609	0.0651	0.174	0.9216	0.0331	0.0453	1.21	0.509	0.260
135	−50	1,000	0.7662	0.0892	0.1446	0.9026	0.0504	0.0470	1.18	0.565	0.325
136	−50	1,000	0.7749	0.1261	0.0990	0.8838	0.0758	0.0404	1.14	0.609	0.408
137	−50	1,000	0.7837	0.1491	0.0672	0.8631	0.1001	0.0368	1.10	0.671	0.547
138	−50	1,000	0.8332	0.1318	0.0350	0.8363	0.1288	0.0349	1.00	0.977	0.997
139	−100	100	0.125	.....	0.875	0.9591	.....	0.0409	7.67	.....	0.0468
140	−100	100	0.118	0.144	0.738	0.9186	0.0472	0.0342	7.78	0.328	0.0463
141	−100	100	0.110	0.320	0.570	0.8651	0.110	0.0249	7.77	0.344	0.0437
142	−100	100	0.110	0.580	0.310	0.7916	0.194	0.0144	7.20	0.334	0.0464
143	−100	100	0.101	0.899	.....	0.680	0.320	.....	6.73	0.356	
144	−100	200	0.222	.....	0.778	0.9792	.....	0.0208	4.41	.....	0.0268
145	−100	200	0.235	0.121	0.644	0.9615	0.0228	0.0157	4.09	0.188	0.0254
146	−100	200	0.232	0.435	0.333	0.9070	0.0840	0.00897	3.91	0.193	0.0269
147	−100	200	0.236	0.483	0.281	0.8926	0.0983	0.00909	3.78	0.204	0.0324
148	−100	200	0.250	0.750	.....	0.814	0.186	.....	3.26	0.248	

Table 15-2. Experimental Data for Methane-Ethane-Propane System (*Continued*)

Code no.	Temp, °F	Pressure, psia	Liquid composition			Vapor composition			*K* Values		
			CH_4	C_2H_6	C_3H_8	CH_4	C_2H_6	C_3H_8	CH_4	C_2H_6	C_3H_8
149	−100	400	0.477	.....	0.523	0.9855	.....	0.0145‡	2.06	.....	0.0277
150	−100	400	0.492	0.175	0.333	0.963	0.0266	0.0104	1.96	0.152	0.0312
151	−100	400	0.496	0.242	0.262	0.9562	0.0364	0.00741	1.93	0.150	0.0283
152	−100	400	0.504	0.308	0.188	0.9446	0.0486	0.00685	1.88	0.158	0.0364
153	−100	400	0.5191	0.386	0.0949	0.9321	0.0630	0.00486	1.80	0.163	0.0512
154	−100	400	0.528	0.472	.....	0.9165	0.0835	.....	1.72	0.177	
155	−100	600	0.744	.....	0.256	0.9852	.....	0.0148	1.32	.....	0.0556
156	−100	600	0.745	0.0520	0.203	0.9775	0.0119	0.0106	1.31	0.229	0.0522
157	−100	600	0.7647	0.1612	0.0741	0.9583	0.0366	0.00512	1.25	0.227	0.0691
158	−100	600	0.784	0.216	.....	0.9498	0.0502	.....	1.21	0.232	
159	−150	100	0.238	.....	0.762	0.9932	.....	0.0068	4.17	.....	0.0089
160	−150	100	0.242	0.258	0.500	0.9686	0.0282	0.0032	4.00	0.109	0.0064
161	−150	100	0.240	0.275	0.485	0.9653	0.0308	0.0039	4.02	0.112	0.0080
162	−150	100	0.249	0.446	0.305	0.9538	0.0433	0.0030	3.68	0.0970	0.0098
163	−150	100	0.252	0.6762	0.0718	0.9299	0.0682	0.0019	3.67	0.102	0.0265
164	−150	100	0.251	0.749	.....	0.9312	0.0688	.....	3.71	0.0918	
165	−150	200	0.502	.....	0.498	0.9955	.....	0.0045	1.98	.....	0.0090
167	−150	200	0.514	0.208	0.278	0.9806	0.0167	0.0027	1.91	0.0805	0.0097
168	−150	200	0.528	0.319	0.153	0.9742	0.0234	0.0024	1.84	0.0734	0.0157
169	−150	200	0.5532	0.400	0.0468	0.969	0.0294	0.0016	1.75	0.0735	0.0342
170	−150	200	0.561	0.439	.....	0.970	0.030	.....	1.73	0.0683	
171	−200	100	0.802	.....	0.198	0.9993	.....	0.0007	1.24	.....	0.0035
172	−200	100	0.8075	0.0735	0.119	0.9962	0.0021	0.0007§	1.23	0.0286	0.0059
173	−200	100	0.8187	0.124	0.0573	0.9961	0.0029	0.0007§	1.22	0.0234	0.012
175	−200	100	0.833	0.167	.....	0.9965	0.0035	.....	1.20	0.0210	

* Calculated by Henry's Law. † Bloomer (3-8). ‡ Interpolated. § Estimated.
SOURCE: Price (15-26a).

Katz and coworkers have studied phase behavior of systems of hydrogen and light hydrocarbons (15-3, 15-5, 15-6, 15-36). The hydrogen exhibits reversed solubility in these systems down to −300°F, the solidification point for the hydrocarbons. Figure 15-17 shows the critical locus for the hydrogen-methane system and Fig. 15-18, the equilibrium constants.

Ethylene is used as a refrigerant and is involved in low-temperature processing. A pressure-enthalpy diagram for ethylene by York and White (15-37) is given in Fig. 15-19.

The critical properties of natural gases at low temperature are of interest because processing operations may approach either the critical pressure or the critical temperature. Davis et al. (15-14) revised the critical-correlation chart of Kurata and Katz (4-52a) on the basis of their own measurements of critical conditions for natural gases. Figure 15-20 gives the revised chart. The method used for predicting critical temperature and pressure involves the computation of a weight-average critical temperature T'_c and correction of this value by Eq. (15-1).

$$T_c = T'_c + A_{1,2}m_1m_2 + A_{1,3}m_1m_3 + A_{1,4}m_1m_4 + \cdots \quad (15\text{-}1)$$

where T_c = true critical temperature, °R
T'_c = weight-average critical temperature, °R
$A_{1,2}$ = constant for system 1, 2 in Table 15-4
m = weight fraction
subscript 1 refers to constituent 1

All possible combinations of binaries should be included in Eq. (15-1). The pseudocritical (molal-average) pressure pP_c and temperature pT_c along with the true critical temperature and molal-average molecular weight M permit computation of the true critical pressure P_c for the mixture from Fig. 15-20. When nitrogen is present, M^* is used in Fig. 15-20,

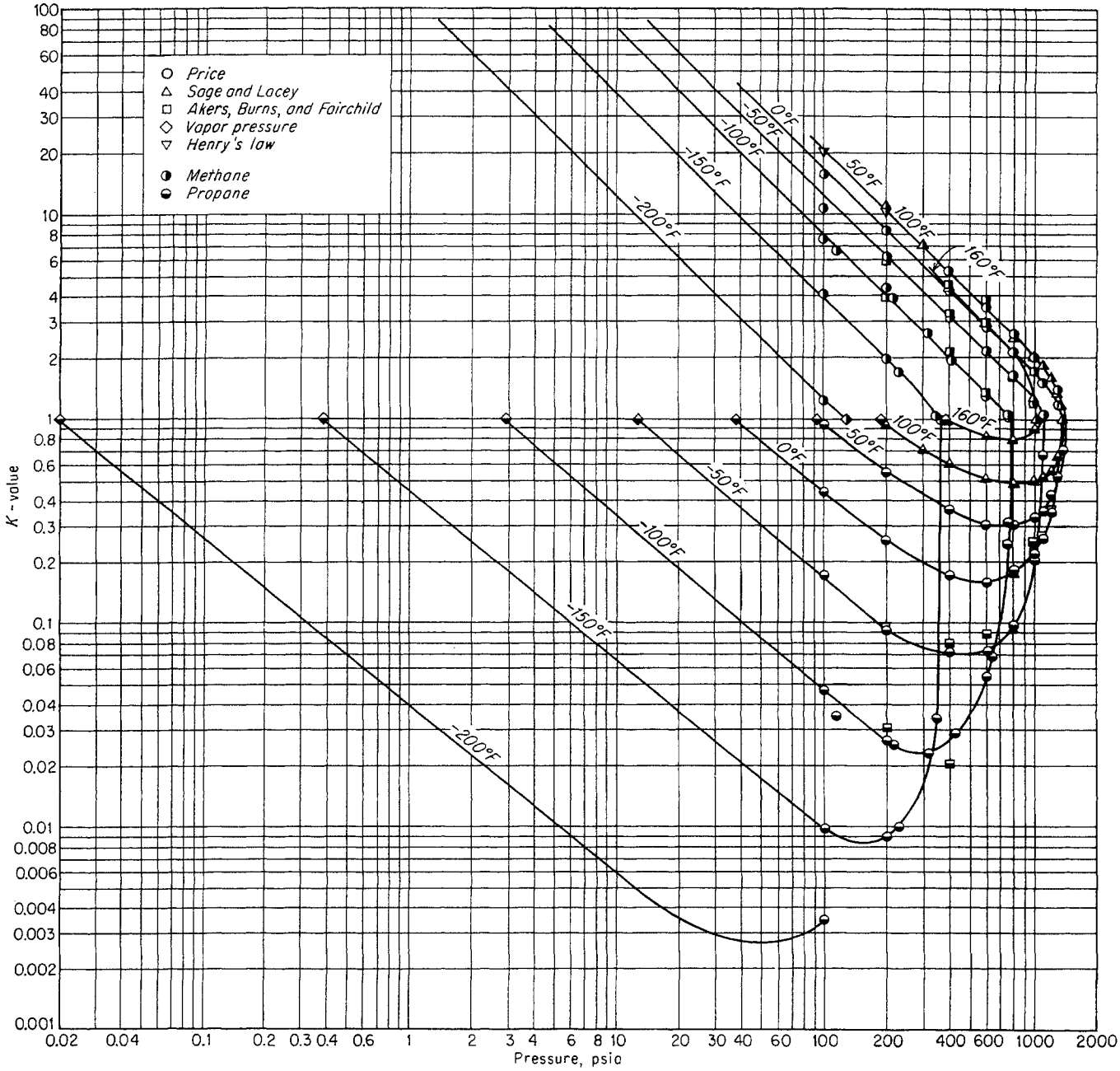

Fig. 15-13. Equilibrium constants for methane-propane system. (*Price*, 15-26a.)

based on the molecular weight and mole % of nitrogen. Helium increases the critical pressure by about 100 psi for each 1 mole % content.

LOW-TEMPERATURE PROCESSING OF NATURAL GAS

Pratt and Foskett give a general description of low-temperature processing (15-26). Katz, Schatz, and Williams (15-20) describe the equilibrium conditions for a low-temperature ethane-extraction plant like that operated by the Tennessee Gas Transmission Company near Greensburg, Ky. (15-21). They show that the pressure region for extraction of ethane and heavier hydrocarbons by low-temperature flash is near the convergence pressure for the system (Fig. 15-21). Experimental data on the liquefaction of natural gases containing small concentrations of ethane and heavier hydrocarbons are illustrated by

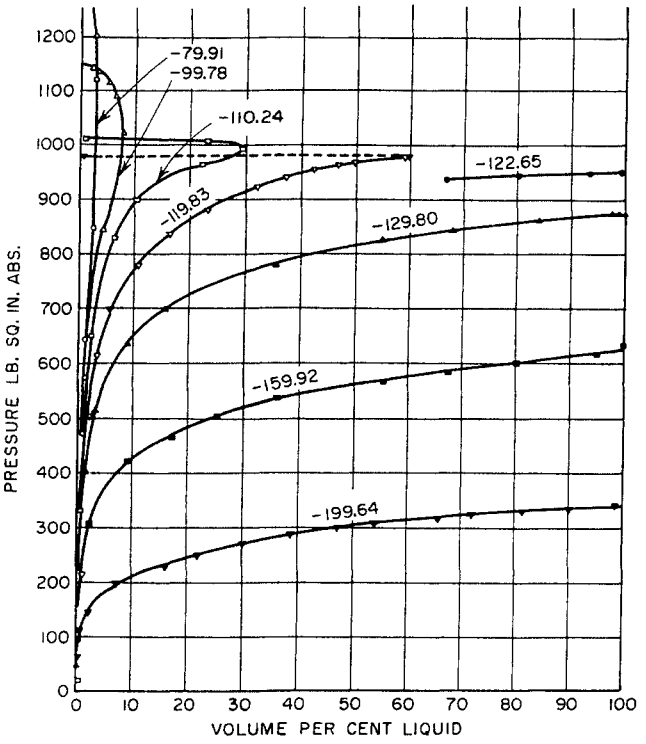

Fig. 15-14. Isotherms of mixture A-4. (*Davis, Bertuzzi, Gore, and Kurata*, 15-14. *Courtesy AIME.*)

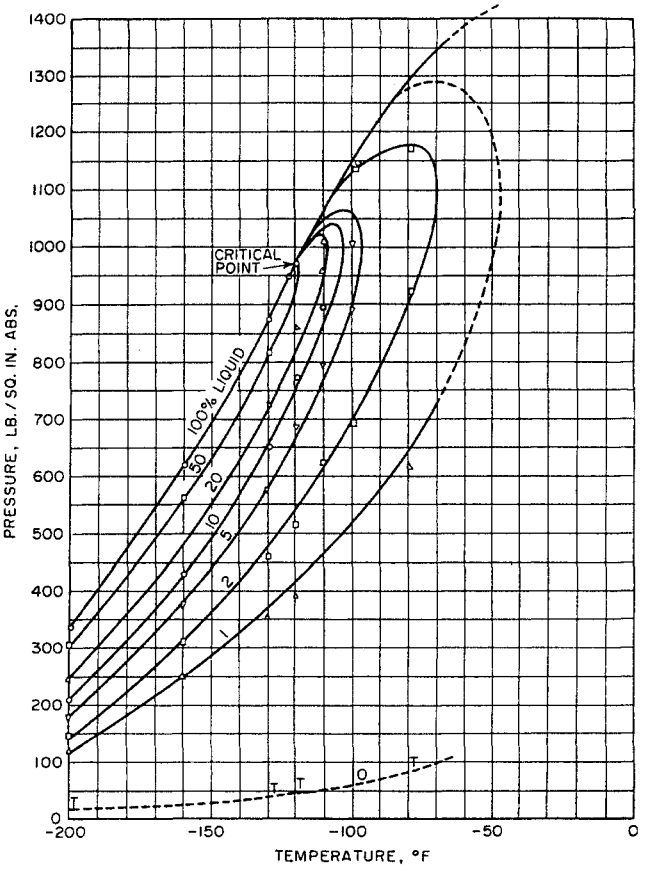

Fig. 15-15. Phase diagram for mixture A-4. (*Davis, Bertuzzi, Gore, and Kurata*, 15-14. *Courtesy AIME.*)

Table 15-3. Properties of Gases Studied

Gas	A-1	A-2	A-3	A-4	AB-1	AB-2	AB-3	B	C	D
Mole percentage:										
Carbon dioxide	1.20	1.09	1.00	0.91	0.44	0.30	0.20	0.13	0.20	0.25
Helium	.....	.....	.....	.....	.....	.....	.....	1.00	0.60	0.31
Nitrogen	.....	8.84	16.11	24.41	.....	11.30	24.00	11.46	13.50	7.05
Methane	90.89	82.86	76.25	68.70	96.68	85.80	73.64	76.65	75.15	85.32
Ethane	4.40	4.01	3.69	3.33	1.60	1.50	1.20	5.51	6.10	4.11
Propane	1.91	1.74	1.60	1.44	0.70	0.60	0.53	3.35	3.27	1.98
Isobutane	0.33	0.30	0.28	0.30	0.14	0.12	0.10	0.35	0.38	0.37
n-Butane	0.60	0.55	0.51	0.40	0.20	0.18	0.15	0.90	0.60	0.39
Isopentane	0.21	0.19	0.18	0.16	0.07	0.06	0.05	0.17		
n-Pentane	0.13	0.12	0.11	0.10	0.05	0.04	0.04	0.15	0.20	0.22
Hexanes	0.15	0.14	0.12	0.11	0.05	0.04	0.04	0.33		
Heptanes+	0.18	0.16	0.15	0.14	0.07	0.06	0.05			
Critical pressure, psia	925	955	968	973	765	790	815	1,143	1,107	918
Critical temperature, °R	381	368	356	340	359	343	329	376	370	364
Critical density, grams/mole	0.230	0.242	0.279	0.311	0.183	0.220	0.225	0.266	0.270	0.270
Mole av crit pressure, psia	676	659	646	631	674	653	630	644	644	658
Mole av crit temp, °R	369	356	346	334	353	339	322	358	354	354
Wt av crit temp, °R	409	386	368	349	370	344	320	397	380	379
Mole av mol. wt	18.40	19.25	19.94	20.75	16.90	18.11	19.56	20.02	19.98	18.60
Wt av equiv mol. wt (*W*)	22.26	21.47	20.80	20.22	18.54	18.00	17.62	22.85	21.25	20.19
MABP, °R	218	211	205	199	207	199	191	213	210	209

SOURCE: Davis, Bertuzzi, Gore, and Kurata (15-14), AIME.

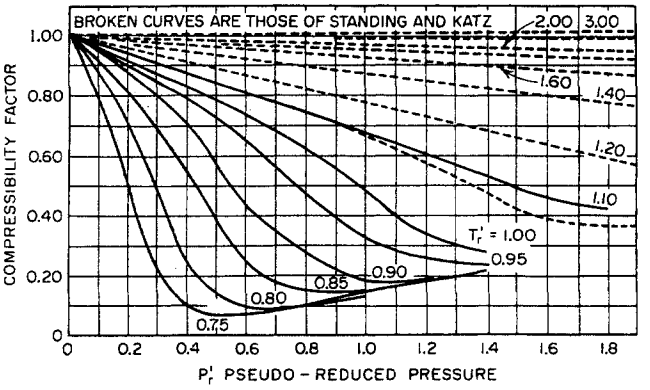

Fig. 15-16. Compressibility factors for natural gases at low temperature. (*Davis, Bertuzzi, Gore, and Kurata, 15-14. Courtesy AIME.*)

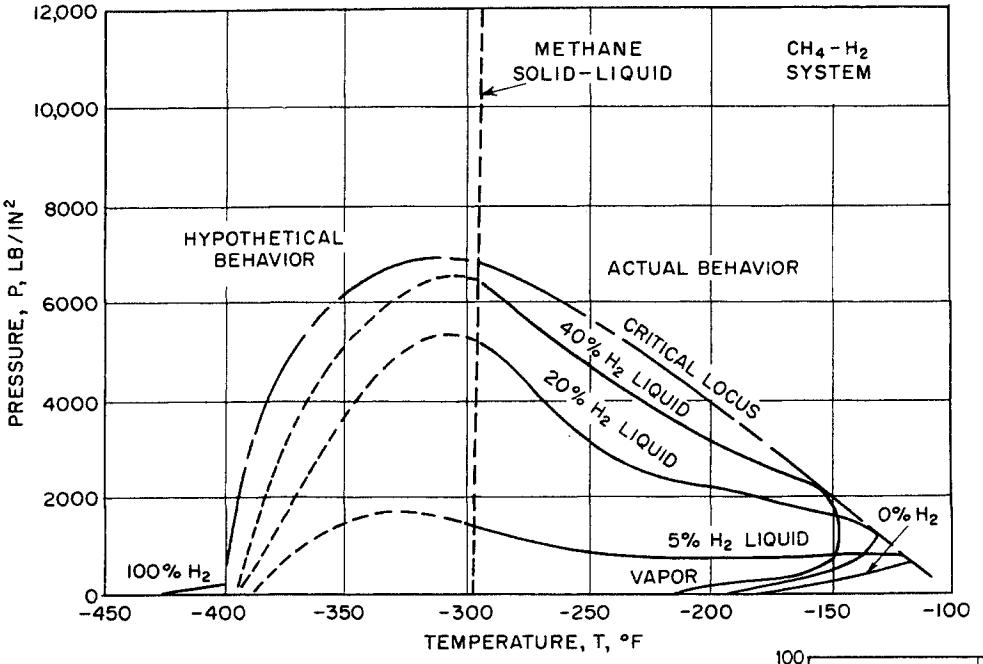

Fig. 15-17. Pressure-temperature diagram for hydrogen-methane system. (*Benham, Katz, and Williams, 15-5. Courtesy AIChE.*)

Table 15-4. Constants *A* for Eq. (15-1)

	N_2	C_1	C_2	C_3	C_4	C_5	C_6	C_7
N_2	0							
C_1	37 + 95(N_2)	0						
		−150						
C_2	+25	−400(C_1)	0					
C_3	0	−30	0	0				
C_4	−100	−180	−27	+10	0			
C_5	−300	−150	−50	−30	0	0		
C_6	−500	−400	−50	−50	0	−25	0	
C_7	−600	−400	−100	−50	−10	−100	0	0
C_8	−600	−400	−150	−50	−10	−100	0	0

SOURCE: (15-14).

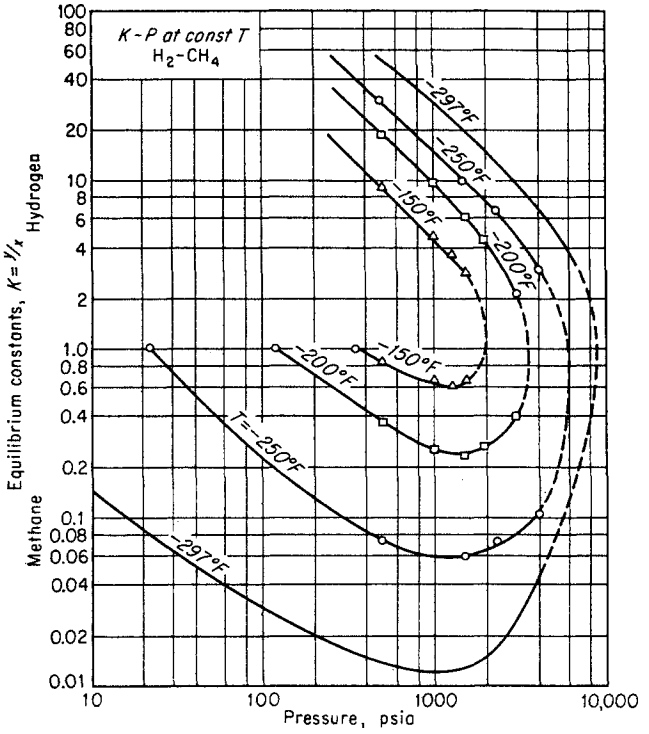

Fig. 15-18. Equilibrium constants for hydrogen-methane system. (*Benham and Katz, 15-6. Courtesy AIChE.*)

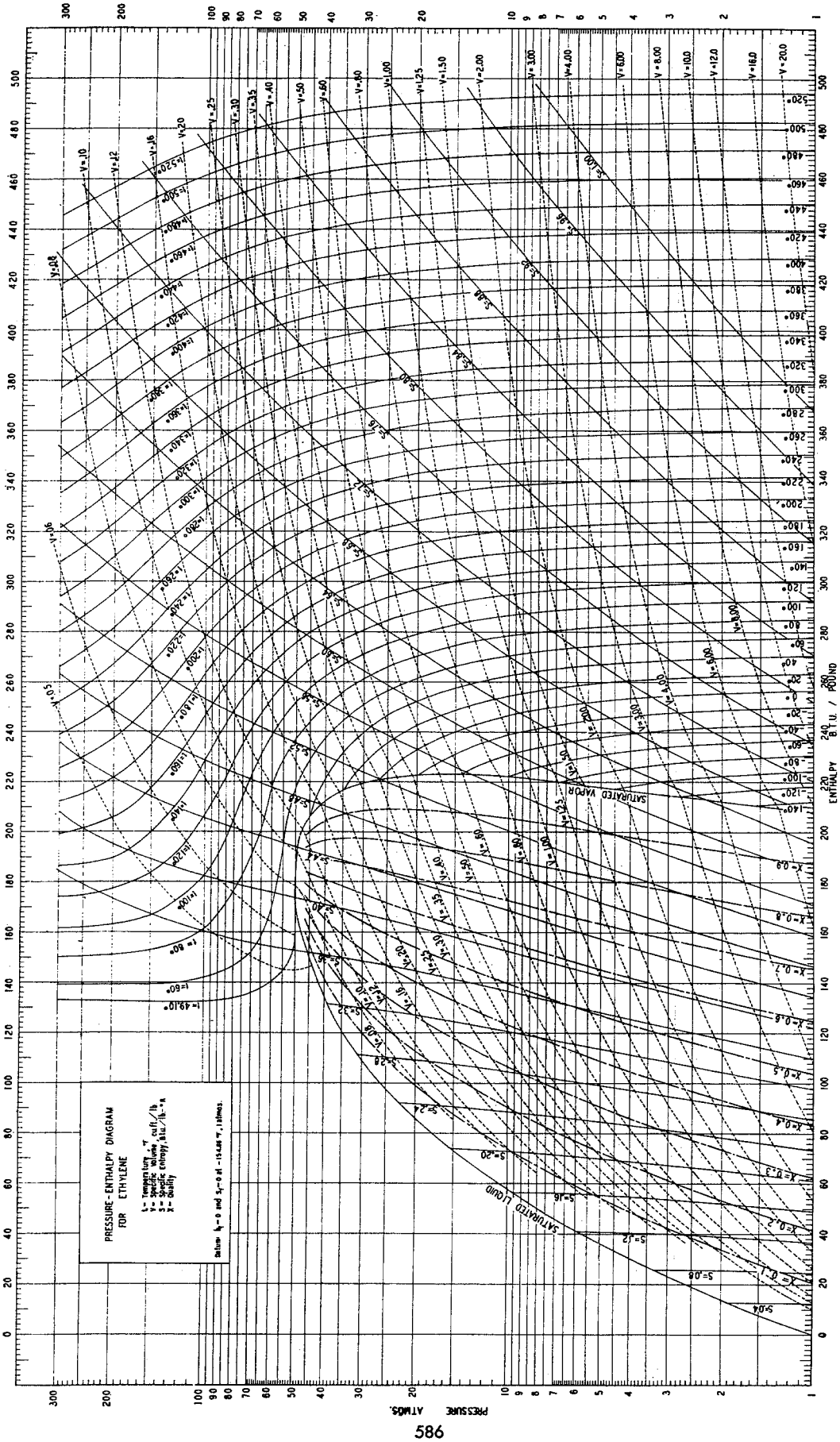

Fig. 15-19. Pressure-enthalpy diagram for ethylene. (*York and White*, 15-37. *Courtesy AIChE.*)

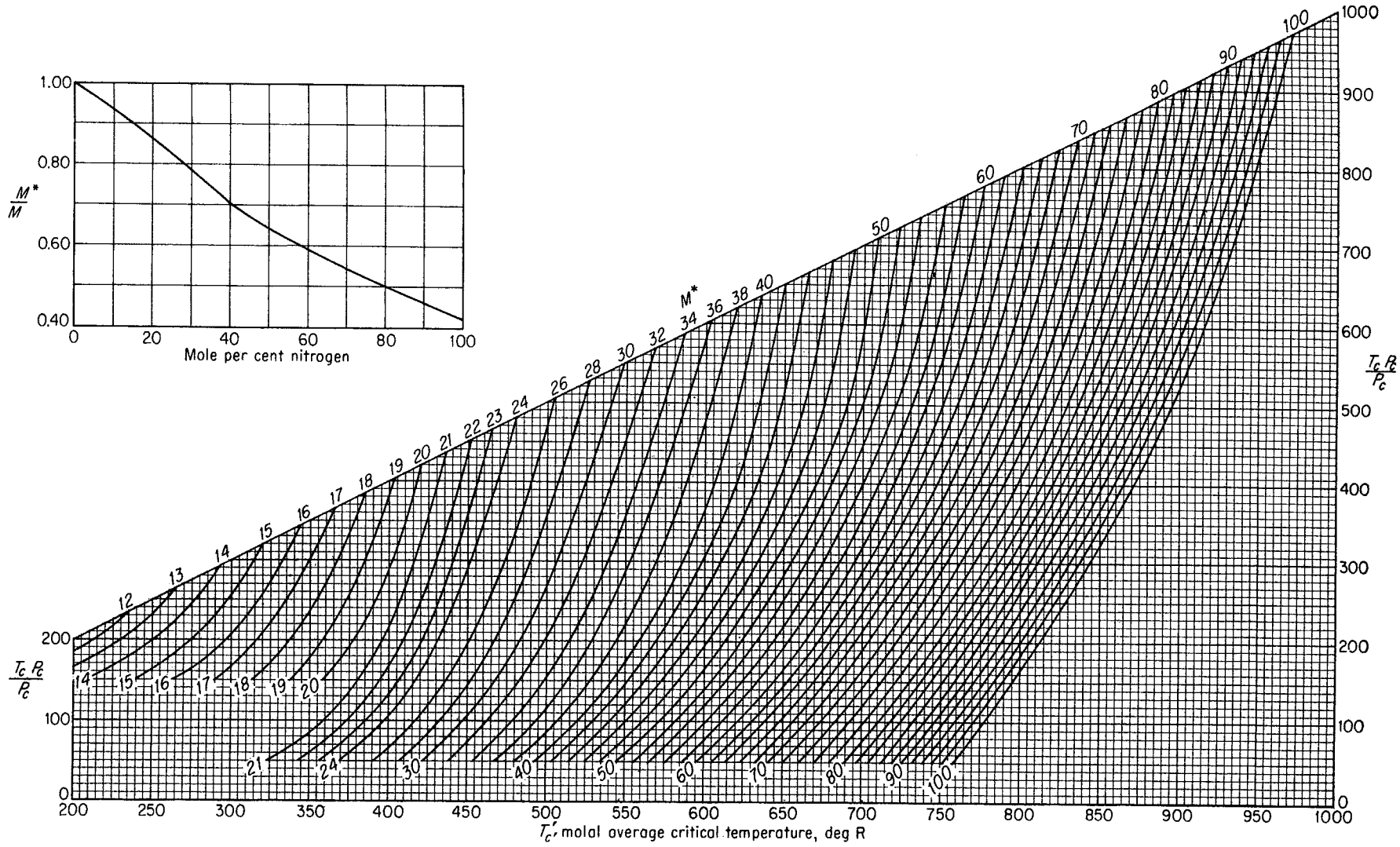

Fig. 15-20. Revised correlation chart for critical pressure of natural gases at low temperatures. ***(Davis, Bertuzzi, Gore, and Kurata, 15-14. Courtesy AIME.)***

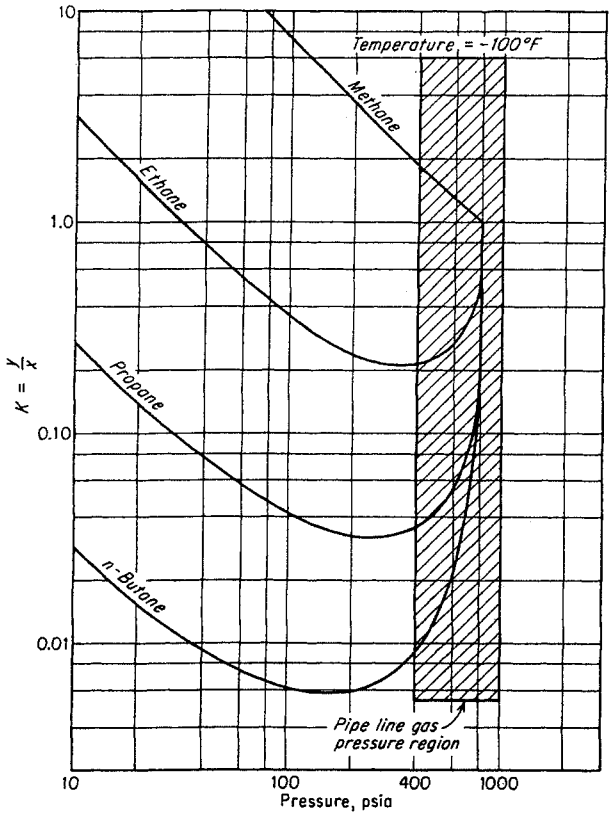

Fig. 15-21. Equilibrium constants for natural gases at −100°F. (Katz, Schatz, and Williams, 15-20. Courtesy NGAA.)

Fig. 15-14. The two-phase pressure range for the Tennessee gas from dew point to complete liquefaction at −100°F is no more than 150 psi.

The Tennessee Gas Transmission Company constructed an extraction plant for ethane and heavier hydrocarbons at Greensburg, Ky., which is described by King and Mertz (15-17, 15-21, 15-23). The plant processed initially 750 and later 950 MMcf/day of pipeline gas with a hydrocarbon-liquid production of 440,000 gal/day from the 950 MMcf. Figure 15-22 is a simplified flow sheet for the plant.

The gas is dehydrated to a dew point of −104°F by alumina desiccant. When problems of moisture occur, methanol additions have been made to prevent freeze-ups. The dried gas is heat-exchanged first with the residue gas, second with ethane refrigerant at −96°F, where the latent heat is extracted, and third with the flashed extraction liquid. The primary separation takes place at −104°F and 535 psi for a liquid yield of 5.5 mole per cent of the stream. The residue gas after heat exchange is compressed and returned to the pipeline. The ethane refrigeration system condenses at −5°F with propane as the condensing agent. The feed-gas and residue-gas compositions are given in Table 15-5. The liquid prod-

Table 15-5. Feed and Residue Gas Analyses, Tennessee Plant

Constituent	Mole fraction	
	Feed	Residue
Carbon dioxide	0.0035	0.0032
Nitrogen	0.0042	0.0044
Methane	0.9392	0.9577
Ethane	0.0364	0.0292
Propane	0.0101	0.0046
Isobutane	0.0018	0.0005
n-Butane	0.0024	0.0004
Pentanes	0.0011	0.0000
Hexanes	0.0009	0.0000
Heptanes+	0.0004	0.0000
Total	1.0000	1.0000

SOURCE: (15-21, 15-23).

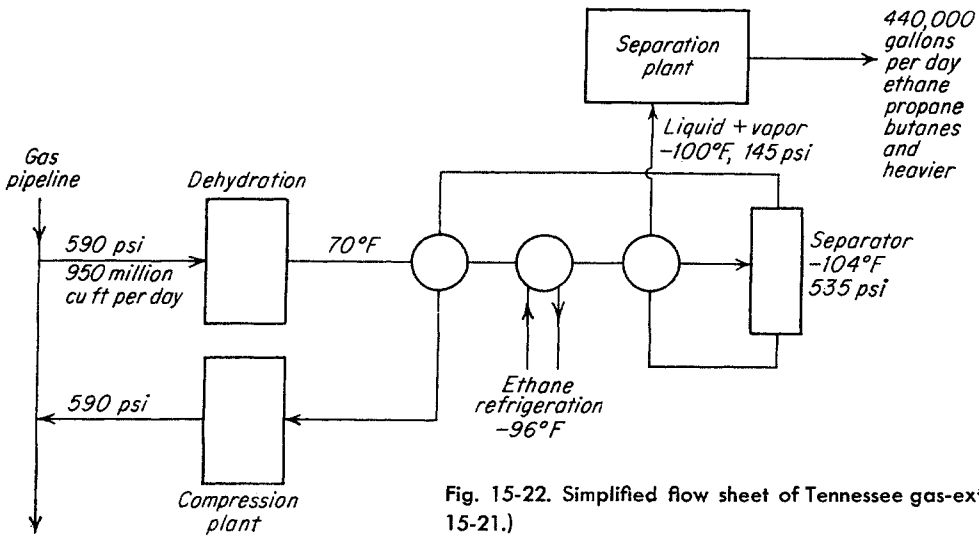

Fig. 15-22. Simplified flow sheet of Tennessee gas-extraction plant. (King and Mertz, 15-23, 15-21.)

ucts are piped to a nearby petrochemical plant. All materials of construction submitted to temperatures below −20°F are of nickel-alloy steel.

Stark (15-30) describes the Tuscola, Ill., plant of the National Petro-Chemicals Corporation. This plant in central Illinois operates on gas from the Panhandle Eastern Pipeline Company. The plant uses a dual-absorbent system of hexane at −10°F and a mineral oil of 180 molecular weight.

NATURAL GAS LIQUEFACTION

A natural gas liquefaction plant was constructed at Cleveland, Ohio, as a means of storing gas to supply peak loads (15-9, 15-10, 15-12). The general problems of liquefaction and regasification are discussed by Laverty and Edmister (15-21b). The Cleveland plant operated satisfactorily but was destroyed in a severe industrial fire which occurred when a storage tank ruptured (15-16). Liquid methane, though volatile, has considerable latent heat. When allowed to run onto the ground, it will act like any other liquid even though vaporizing as it flows. Lack of effective dikes around the tanks permitted more extensive damage than would otherwise have occurred.

The liquefaction process used an ethylene-ammonia cascade process (Fig. 15-23). At 600 psig, the gas was cooled to −139°F and then flashed to 55 psig and −218°F. The liquid formed was flashed to 10 psig and −258°F, the storage condition. Storage in spherical tanks was successful; one full storage tank survived the fire. Concentric steel spheres with 3 ft of cork between them were used. The inner tank was 57 ft in diameter and made of a 3.5 per cent nickel, 0.09 carbon steel (Fig. 15-23*a*).

The combination of the serious accident, war-time conditions, and the advent of cheaper underground storage caused interest to wane in liquefaction as a storage method.

The proposal to barge liquefied natural gas from the producing areas to points of consumption has revived interest in natural gas liquefaction (15-13, 15-2, 15-8a). For example, natural gas on the Gulf Coast could be liquefied and barged to Miami, or Venezuelan gas could be liquefied and brought to the eastern seaboard of the United States (15-13). The process appears to be about competitive with pipelines for long distances and has the advantage of alternate routes.

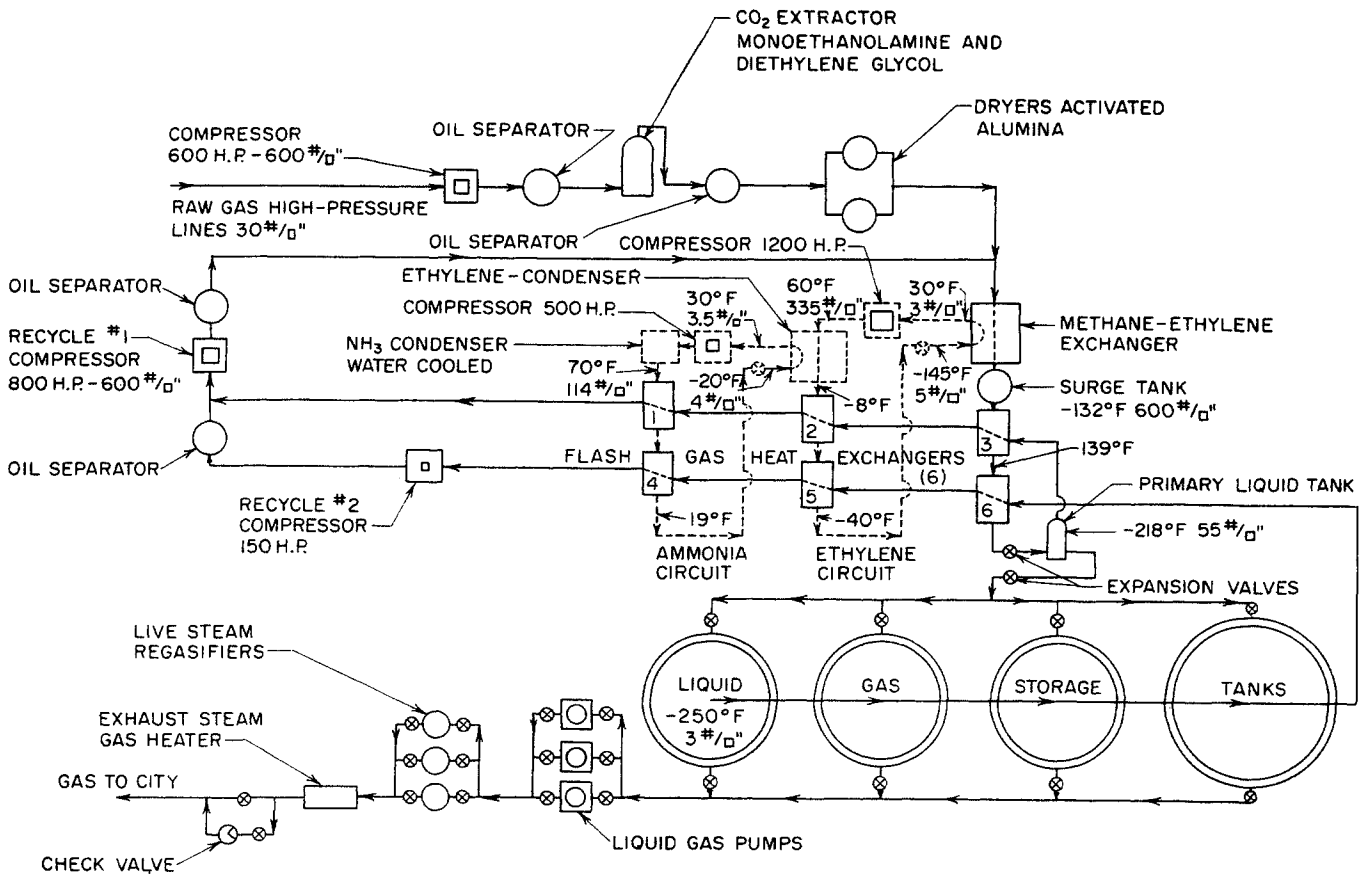

Fig. 15-23. Flow diagram for Cleveland liquefaction process. (*Elliott et al.*, 15-16.)

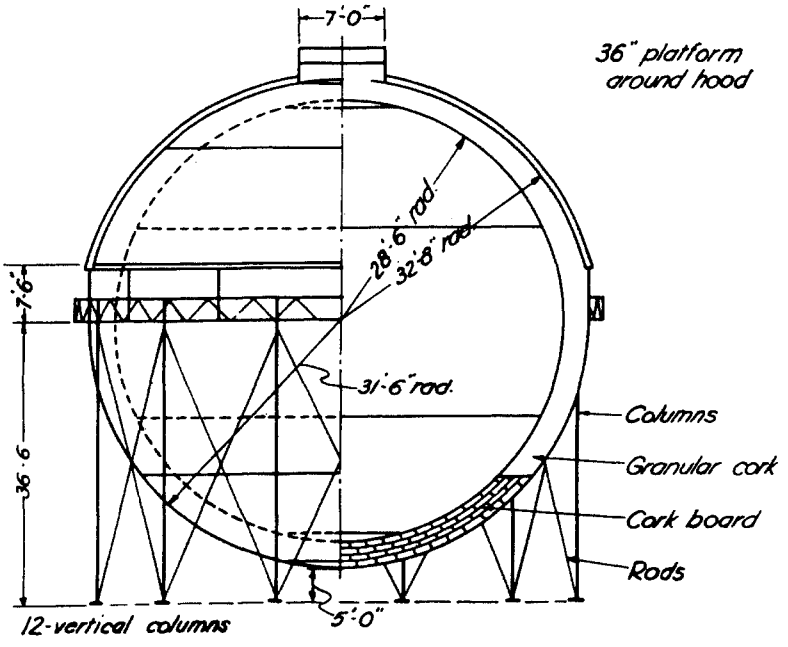

All seams inside and outside tanks to be butt welded
Plates for inside sphere to be 3½% nickel normalized
Remainder of steel to be std. carbon

Diameter of inside sphere 57'-0"

Basis of design
Maximum vapor pressure 10 #/□"
Weight of liquid methane 26 #/cu. ft.
Test hydrostatic to 125% of working stress in plates
Maximum working unit stress in plates · 13,750 #/□"
Net capacity 55,840,000 cu. ft gas, 89,300 cu ft. liquid
Vapor space 8.58% of net liquid volume.

55,840,000 cu. ft. container for liquid methane

Fig. 15-23a. Spherical storage tank for liquefied gas. (Elliott et al., 15-16.)

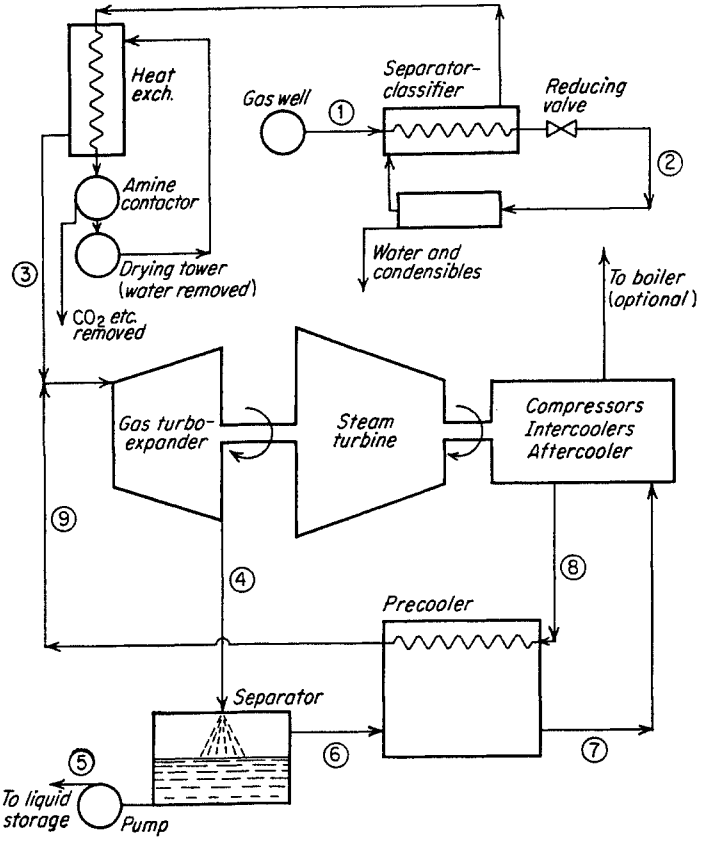

Fig. 15-24. Morrison cycle for gas liquefaction. (15-2.)

Station	1	2	3	4	5	6	7	8	9
P (psia)	2500	1050	1000	14.7	14.7	14.7	14.7	1000	1000
t (deg F)	80	0	10	-259	-259	-259	73	85	-95
h (Btu/lb)	333	323	333	186	19	237	407	385	201

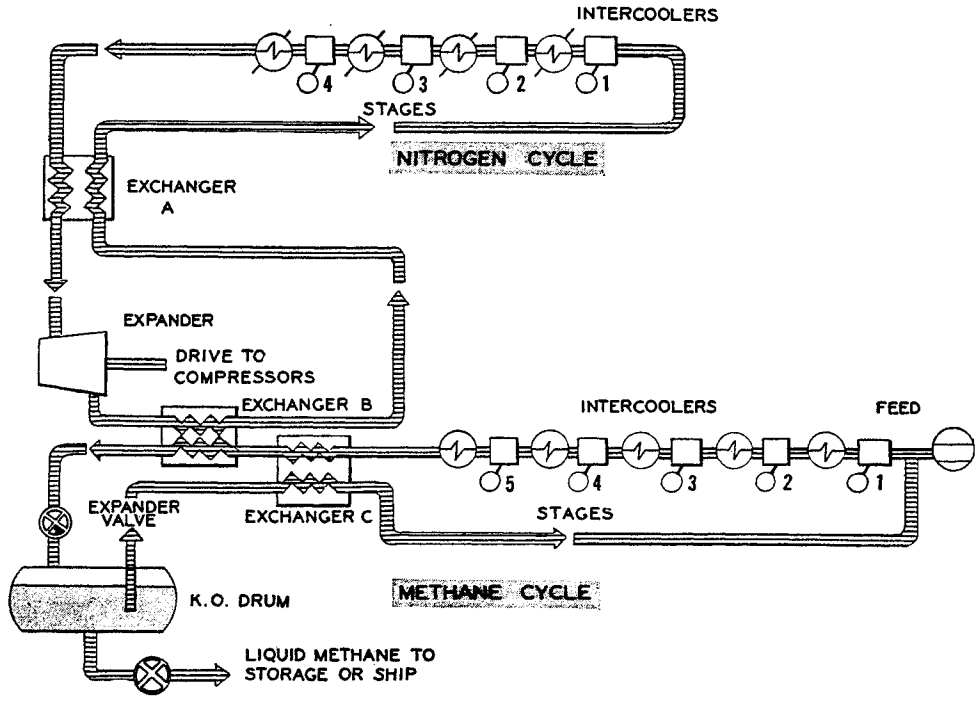

Fig. 15-25. Nitrogen refrigerated liquefaction cycle proposed for tanker. (Crecca, 15-13. *Courtesy Oil Gas J.*)

Processes proposed for liquefaction of natural gas are shown in Figs. 15-24 to 15-26. The expander used in Fig. 15-24 is advantageous thermodynamically; its use depends upon the availability of an efficient machine which can handle large percentages of liquid (15-31). In designing a liquefaction process, the prime concern is to find the conditions that will give both minimum investment cost for equipment and low operating expense. The most important item is compressors, both for recycling the nonliquefied gas and for external refrigerants. Various cycles require 400 to 700 hp per MMcf/day of liquefaction capacity. In general, the process requiring the least installed horsepower will meet the above requirement of lowest investment and operating cost.

Auxiliary Considerations

In addition to the selection of a liquefaction process, important considerations are heat exchangers, purification of gases, materials of construction, storage, and safety.

Heat-exchanger design (15-11, 15-22) is important because of the need for exchanging heat with low temperature differences. The accumulation of solids in heat exchangers can be avoided by the reversing of flow (Fig. 15-27) and by the use of scavenger streams to remove solids deposited. Construction materials for exchangers and fabrication methods have been

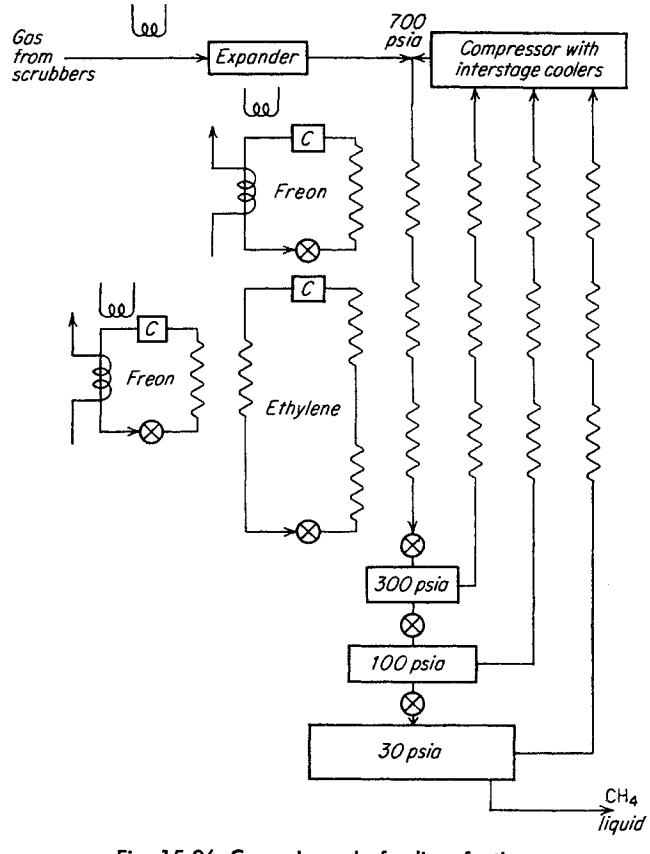

Fig. 15-26. Cascade cycle for liquefaction.

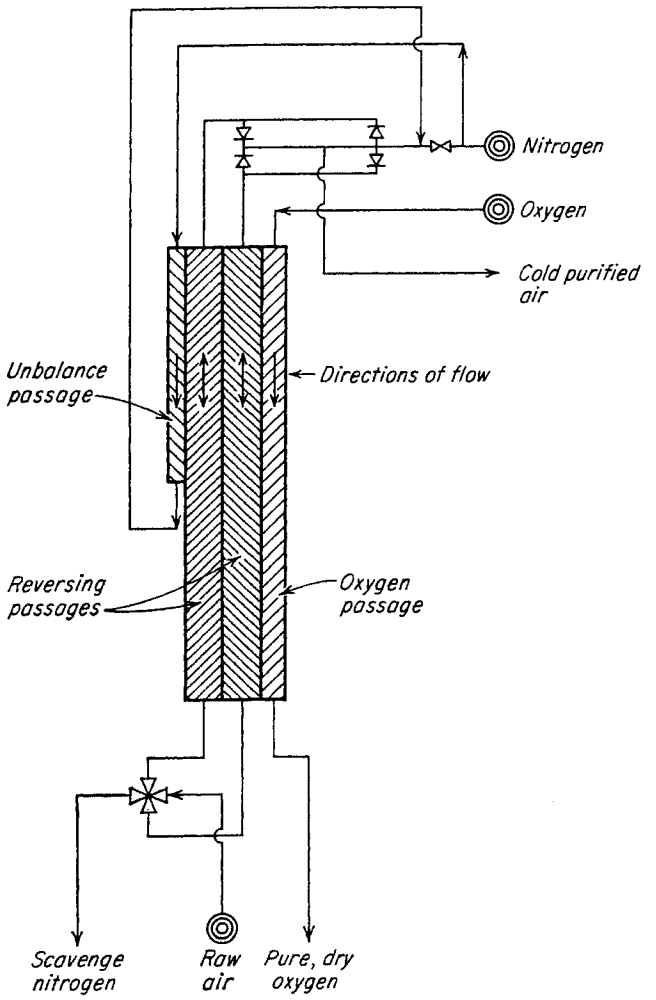

Fig. 15-27. Flow for reversing exchanger. (Lobo and Skaperdas, 15-22. Courtesy AIChE.)

developed in connection with tonnage oxygen plants (15-21, 15-22, 15-11, 15-4). Aluminum and copper have the desired conductivity and low-temperature properties; aluminum normally has a price advantage.

Dehydration and purification of gases may be important in a liquefaction process. The need for water removal is evident. An extension of normal dehydration procedures using solid desiccants can reduce the water content to almost any desired level. The use of reversing exchangers may be required to handle the last traces of water. Carbon dioxide concentrations in the gas of less than 1.5 per cent are believed to be low enough to prevent solid formation at processing pressures according to calculations based on extrapolation from the data of Donnelly and Katz (15-15). At atmospheric pressure the solubility of carbon dioxide in liquid methane is 0.2 mole % according to Kohn and Kurata (15-21a).

At low temperatures, ordinary steel becomes brittle and cannot be used safely. Austenitic steels, produced by addition of nickel and other alloying elements, can withstand low temperatures satisfactorily. Low carbon contents often increase the usefulness of steel as measured by Charpy impact tests at low temperature. Copper and aluminum and other solid solution–type metals do not become brittle enough to impair their usefulness, but their strength may increase at decreasing temperatures. A bibliography of 468 references on low-temperature characteristics of steels was prepared by Janis (15-19).

The storage of liquid methane or other liquids at low temperature can rely in part on experiences with liquid oxygen and nitrogen. Insulation becomes of prime consideration. Many new substances such as plastic foams and glass fibers compete with the more conventional cork blocks or granules. The need for sealing the insulation to prevent moisture from the air from entering the pores is apparent. When a vessel is cooled from room temperature to −250°F, considerable shrinkage in size takes place. This shrinkage must be taken into account in the design of both the vessel and the pipe connections.

Heat entering a tank of liquefied gas will create a positive pressure. When a tank used for storing liquid methane no longer contains any liquid, the temperature rise on the vapor due to heat absorption will cause some positive pressure as the tank warms. It was suggested that dry ice be used to blanket an empty tank with carbon dioxide gas (15-2). This suggestion neglects the fact that dry ice is soluble to the extent of 0.2 mole % in liquid methane and the low vapor pressure of the dry ice at −258°F (0.001 mm Hg). Dry ice requires a temperature of −108°F to have a vapor pressure of 1 atm.

Safety practices for a liquefaction plant should be more stringent than for a normal processing plant; the need is demonstrated by the Cleveland accident. Diking of all tankage, sufficient to hold the liquefied gas, is imperative. Ruhemann (15-28) describes control processes for gas-separation plants. Pressure-relieving systems (15-32) which have assurance of operation in case of overpressure are normally required, but problems of making sure that relief valves are operable at all times may arise. Depressuring systems may be needed in case a fire accidentally starts, to prevent rupture of the vessel (15-33).

In regasification equipment (Fig. 15-23) pumps take the liquid methane to discharge it to steam-heated exchangers. Provision must be made for possible leakage of vapor at packing glands.

Transportation by Boat

The best method of transporting liquid methane is

in moderate-sized tanks operating just above atmospheric pressure. The use of barges or boats to move these tanks appears to have many advantages, including low cost (15-2, 15-13). Figure 15-28 shows a proposed partial conversion of a T-2 tanker to the transportation of liquid methane along with crude oil. For offshore fields, barges would have the advantage of transporting the liquefied gas directly from the field, without requiring the laying of a pipeline.

HELIUM PRODUCTION

The United States government has maintained since 1917 one or more plants for extracting helium from natural gas (15-29, 15-35, 15-1, 15-24). The plants are operated by the Bureau of Mines. The plant at Amarillo, Tex., started in 1929, processes gas containing nearly 1.8 per cent helium, 0.4 per cent carbon dioxide, and 25 per cent nitrogen, the remainder being primarily methane with some of the heavier hydrocarbons. The Navajo plant in New Mexico processes gas containing 7.8 per cent helium, 1.7 per cent carbon dioxide, 76 per cent nitrogen and the remainder (14.5 per cent) hydrocarbon gases. Many gases from the Texas Panhandle and Kansas contain 0.3 to 0.4 per cent helium, but such gases usually also contain nitrogen at some ten times the helium concentration.

The Amarillo helium plant originally scrubbed out carbon dioxide with caustic soda solution; the newer plants use monoethanolamine and diethylene glycol to remove both carbon dioxide and water. Alumina dryers are used to reduce the moisture content to the final level.

The helium-extraction process is described by

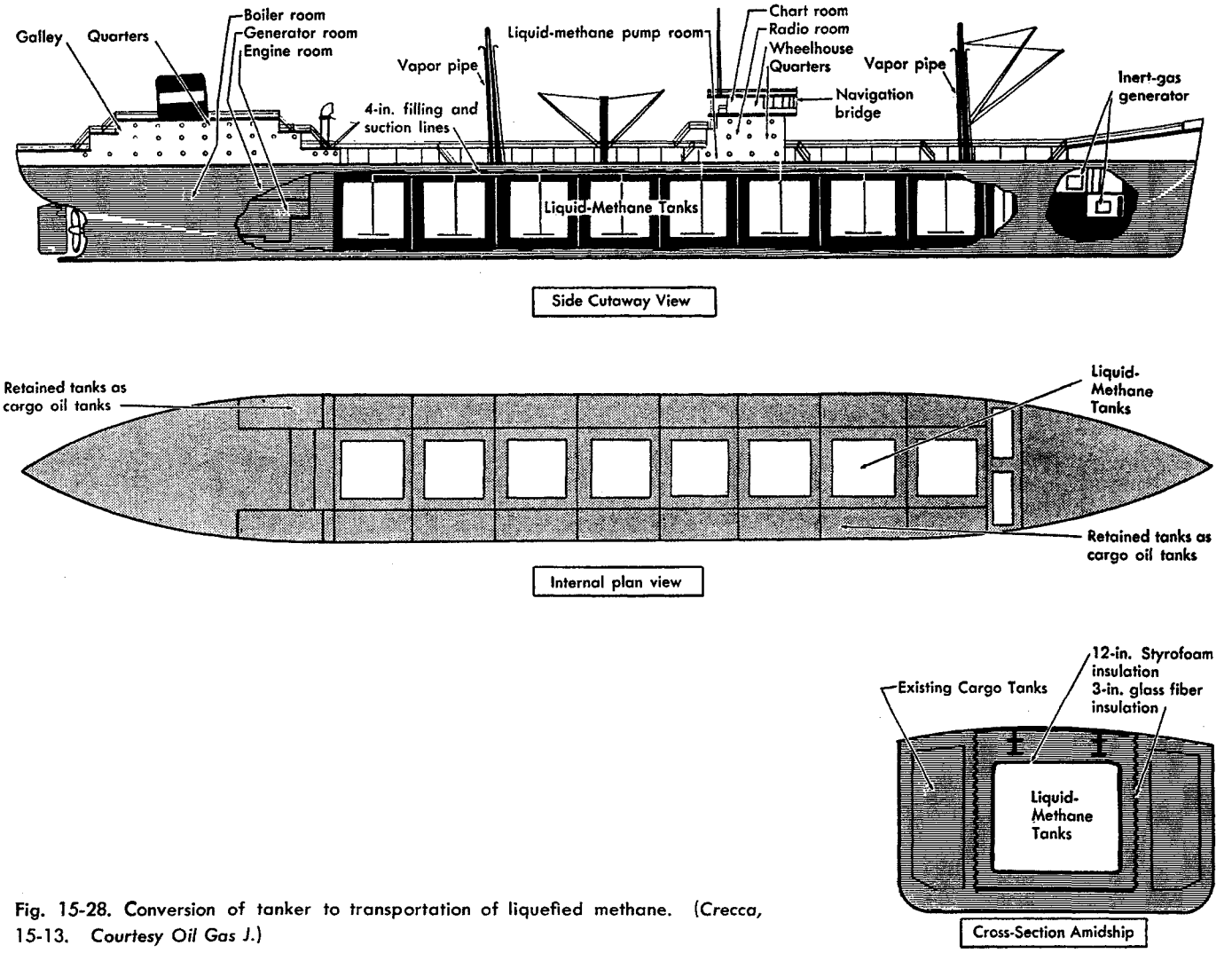

Fig. 15-28. Conversion of tanker to transportation of liquefied methane. (Crecca, 15-13. *Courtesy Oil Gas J.*)

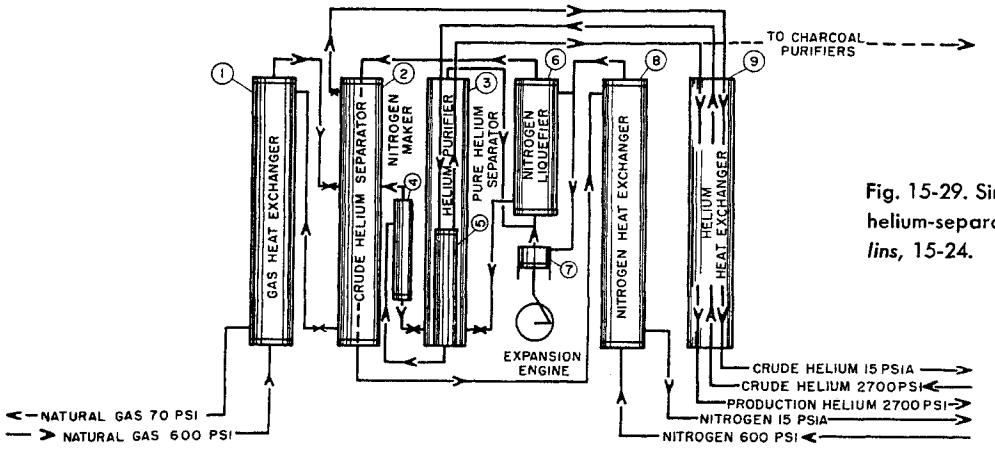

Fig. 15-29. Simplified diagram of Bureau of Mines helium-separation and purification cycles. (*Mullins*, 15-24. *Courtesy AIChE.*)

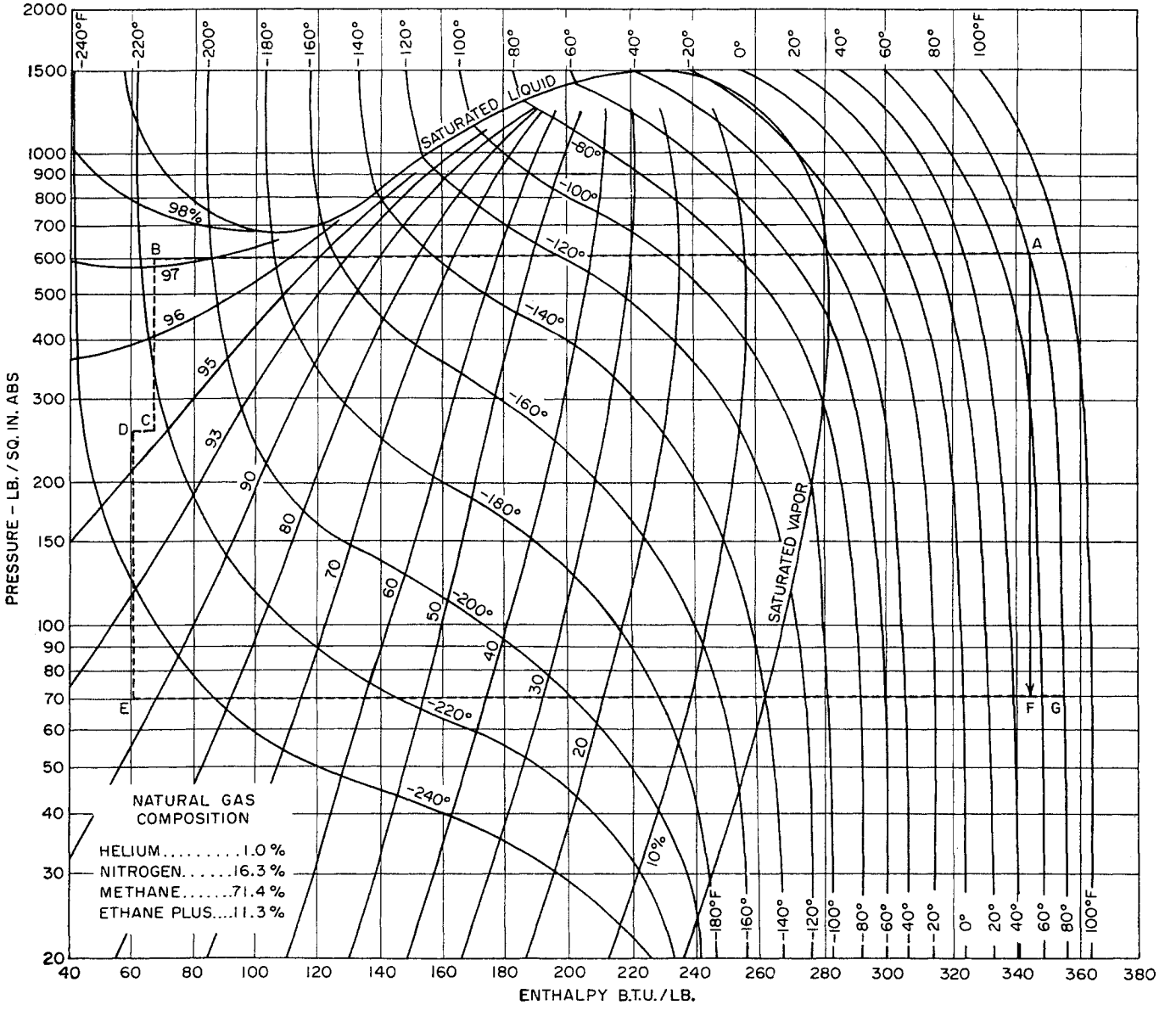

Fig. 15-30. Crude-helium separation cycle on pressure-enthalpy diagram. (*Mullins*, 15-24. *Courtesy AIChE.*)

Mullins (15-24) and shown in Fig. 15-29. Crude helium containing appreciable nitrogen is separated at low temperature from the hydrocarbons and then this crude helium-nitrogen mixture is separated to provide pure helium. Mullins describes the process as follows:

The gas passes through heat exchanger (1) for precooling and virtually complete liquefaction by exchange of heat to cold outgoing processed gas and then is throttled into a combination heat-exchanger and separator (2), which is operated at about 200 to 300 psi. Temperature and pressure conditions in the separator are such that the natural gas is approximately 98 per cent condensed and the gas phase contains about 60 per cent helium, 40 per cent nitrogen, and very small amounts of methane. Cold nitrogen vapors from an auxiliary refrigeration cycle, described later, pass downward through the tube pass of the combination heat exchanger-separator (2), resulting in some cooling of both phases and rectification of the gas phase, which increases the helium content or purity. Separate and controlled withdrawals of liquid and gas phases are made continuously from the separator. The gas phase withdrawn is designated as "crude helium" and is passed through heat exchanger (9) where it is warmed to near atmospheric temperature and then passed to temporary storage in a low-pressure gasholder pending further purification. The liquid phase in the separator is throttled therefrom to about 70 psi and passed back through heat exchanger (1) to cool and liquefy high-pressure incoming gas, while warming to near atmospheric temperature. Finally, this low-pressure processed gas is recompressed and returned to the original pipe-line sources.

Crude helium is purified in a cycle integrated with the crude helium cycle, as indicated in Fig. 15-29. The first step in purification is four-stage compression of crude helium from holder pressure to about 2,700 psi. This is followed by passage through lump caustic to remove water vapor and then by cooling, without pressure reduction, in heat-exchanger (9) by exchange of heat to cold outgoing helium streams, and then by passage into separator pot (5) in vessel (3). Separator (5) is immersed in a bath of liquid nitrogen provided by the auxiliary nitrogen refrigeration cycle. The liquid-nitrogen bath is at or near atmospheric pressure and reduces the temperature of the high-pressure crude helium to about −310°F, causing virtually all nitrogen in the 60-40 helium-nitrogen mixture to liquefy. The final step in purification is continuous separation of the two phases in separator (5) with passage of the gas phase—"production helium" of about 98.5 per cent purity—through heat exchanger (9) to high-pressure shipping containers or storage. The production helium may be purified further by passage through activated charcoal at −250°F to −300°F to raise the purity to 99.7 per cent or higher. Helium of this high purity has been produced for special purposes only, in the past, but the Bureau of Mines is making arrangements for its large-scale production.* In these arrangements, production helium at about −300°F from separator (5) will

* Recent developments include the production of 99.99+ per cent helium for welding.

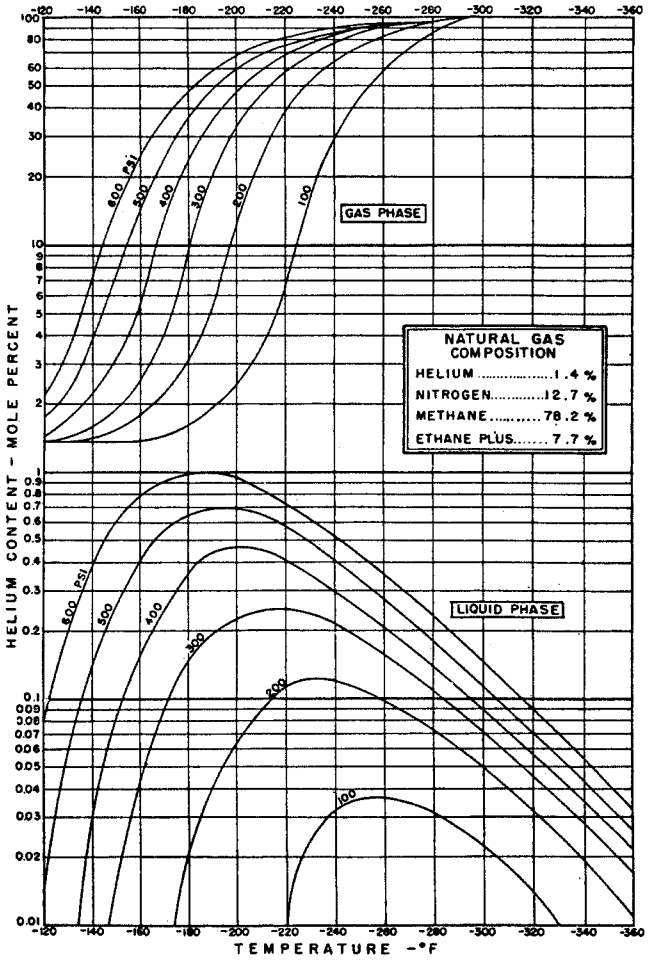

Fig. 15-31. Helium content of gas and liquid phases of typical helium-bearing natural gas. (*Mullins*, 15-24. *Courtesy AIChE.*)

be passed directly to charcoal-filled vessels, where the cold helium will provide refrigeration to the charcoal and result in adsorption of impurities, chiefly nitrogen. The charcoal purifiers will be reactivated periodically by warming and evacuation.

The liquid nitrogen in separator (5) contains appreciable amounts of helium in solution and is throttled from separator (5) to vessel (4); the latter is connected to and operated at the pressure of crude-helium separator (2), permitting release of dissolved helium by reduction in pressure on the liquids and recovery of the helium in crude-helium separator (2). Vessel (4) is termed a "nitrogen maker"; liquid nitrogen therefrom is throttled to helium purifier vessel (3), thus supplying liquid therein and "make-up nitrogen" to the auxiliary nitrogen refrigeration cycle. The make-up nitrogen contains 95 per cent or more nitrogen; the impurities are small amounts of methane and helium.

Most of the refrigeration for the over-all helium extraction process is obtained from expansion of the natural gas in the crude-helium cycle. The balance of the refrigeration, and that responsible for the lowest temperatures, is obtained from the auxiliary nitrogen refrigeration cycle. In this

cycle, nitrogen is compressed in three stages from a low-pressure holder to 500 to 600 psi, water-cooled, and then passed through heat exchanger (8) for precooling by cold outgoing nitrogen, followed by division of the stream with a portion going to nitrogen liquefier (6) and the balance being expanded to near atmospheric pressure in expansion engine (7). The cold nitrogen exhaust vapors from the engine are joined by nitrogen vapors from helium purifier (3) and directed through nitrogen liquefier (6) to cool and liquefy high-pressure nitrogen therein; then passed through crude-helium separator (2) for rectification of the crude-helium and cooling of the liquid phase therein, followed by passage through heat-exchanger (8) to cool incoming high-pressure nitrogen to the cycle. Nitrogen liquids formed in liquefier (6) at 500 to 600 psi are throttled to nearly atmospheric pressure in helium purifier (3) as needed, to maintain an adequate quantity of nitrogen liquids in the purifier at all times.

The crude-helium separation process is shown in Fig. 15-30 as *ABCDEG* on the pressure-enthalpy diagram for a helium-bearing natural gas. The helium content of the phases in the separation is given by Fig. 15-31.

The several plants operated by the Bureau of Mines process natural gas on the way to market. It may be more economical to process gas with a moderate content of helium (0.5 to 1.0 per cent) than the gases richer in helium. The increased helium content normally implies added nitrogen, which makes the residue gas worthless as fuel.

NITROGEN REMOVAL FROM NATURAL GAS

Natural gases containing 10 per cent or more of nitrogen are available in large volumes, especially in the Panhandle and Hugoton fields, where some gas has 30 to 35 per cent nitrogen. To avoid transporting large volumes of inert gas over long distances, the removal of nitrogen by low-temperature processes has been considered (15-25). The most logical process is that of liquefaction. Data on the methane-nitrogen system indicate the phase-separation conditions required. Pilot-plant and engineering studies have been made on the liquefaction process, but commercial operation has not been reported.

CHAPTER 16

The Dehydration and Sweetening of Natural Gas

Natural gas destined for the pipeline market must meet certain requirements of water-vapor content and hydrogen sulfide content. The water content is normally reduced to about 6 to 8 lb of water per MMcf of gas. The hydrogen sulfide content of sour gases is reduced to 0.1 to 0.25 grain per 100 cu ft to make them "sweet." Processes are available for treating gases to prepare them for the pipeline market and for eventual domestic or commercial consumption.

DEHYDRATION OF NATURAL GAS

The dehydration of natural gas is the removal of the water that is associated with natural gases in vapor form. The natural gas industry has recognized that dehydration is necessary to ensure smooth operation of gas-transmission lines. Dehydration prevents the formation of gas hydrates and reduces corrosion. Unless gases are dehydrated, liquid water may condense in the pipelines and accumulate at low points along the line, reducing the flow capacity of the line. Several methods have been developed to dehydrate gases on an industrial scale. Since no single process is unequivocally superior to the others, familiarity with all the methods is necessary in selecting the best and most economical method to solve a given drying problem.

The methods of dehydration in current usage are:

1. Adsorption
2. Absorption
3. Direct cooling
4. Compression followed by cooling
5. Chemical reaction

Adsorbents such as alumina, silica gel, and bauxite comprise the desiccants used in adsorption processes. The absorption processes most frequently used employ di- and triethylene glycol as desiccants. The last three methods have minor usage and will be discussed briefly.

Dehydration by Cooling

The saturated-water content of natural gas decreases with increased pressure or decreased temperature (Fig. 5-8). Thus, hot gases saturated with water vapor may be partially dehydrated by direct cooling. Gases subjected to compression are normally "aftercooled," and this cooling may well remove water from the gas. Unless the cooling process reduces the temperature to the lowest value that the gas will encounter at the prevailing pressure, cooling does not prevent further condensation of water.

The use of Joule-Thomson or expansion cooling in wellhead separators to dehydrate natural gas is discussed in Chap. 13.

Chemical Reaction

Chemical reaction between water and chemical substances may be so complete that the resulting compounds of hydration have extremely low water-vapor pressures. Chemical drying agents which produce essentially complete dehydration are available (16-2). As a natural consequence of the completeness of their reaction with water, they are difficult, if not impossible, to regenerate. This characteristic makes them unfeasible for use as commercial desiccants. They do, however, find wide application in the laboratory determination of water in gases, as explained in Chap. 5.

Gas Dehydration by Absorption of Water in a Liquid

A liquid absorbent suitable for the dehydration of natural gases must fulfill many requirements. Among the more prominent requirements are:

1. High affinity for water
2. Low cost
3. Noncorrosiveness
4. Stability toward gas components
5. Stability during regeneration
6. Ease of regeneration
7. Low or moderate viscosity
8. Low vapor pressure at contact temperature

9. Low solubility for natural gases and hydrocarbon liquids
10. Low foaming or emulsifying tendencies

Two organic compounds which fulfill all of these requirements to a satisfactory degree are diethylene glycol

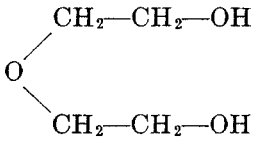

and triethylene glycol

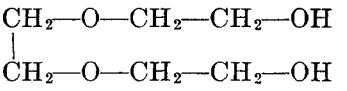

These two polyhydroxy ethers have been used most frequently in the dehydration of pipeline natural gases by absorption (16-4 to 16-9, 16-20).

Physical Properties of the Glycols

The physical properties of the glycols that constitute the basis for process design and computations

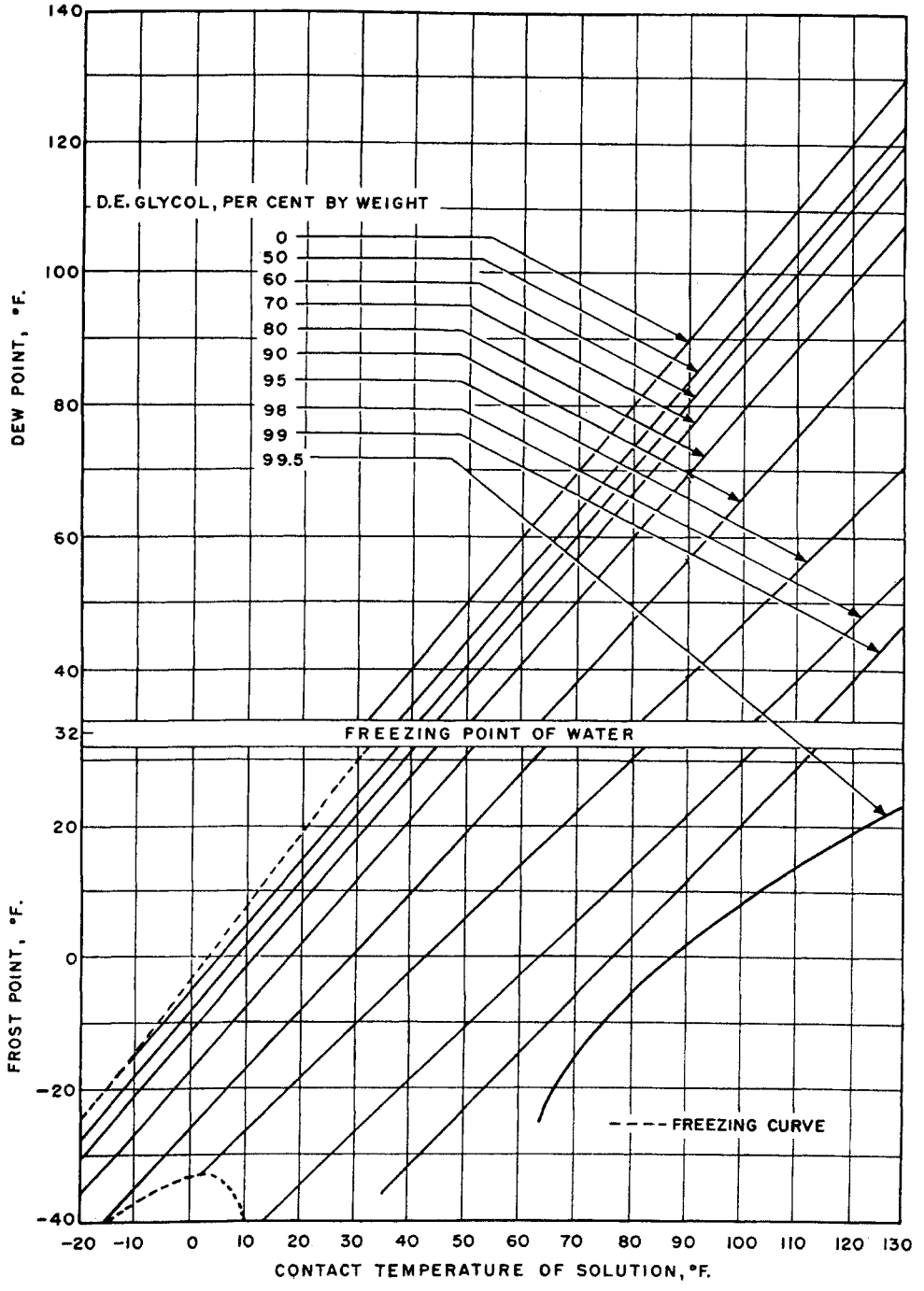

Fig. 16-1. Effect of aqueous diethylene glycol solutions on dew points at various contact temperatures at atmospheric pressure. (16-10, *Courtesy Carbide and Carbon Chemicals Co., Div. of Union Carbide Corp.*)

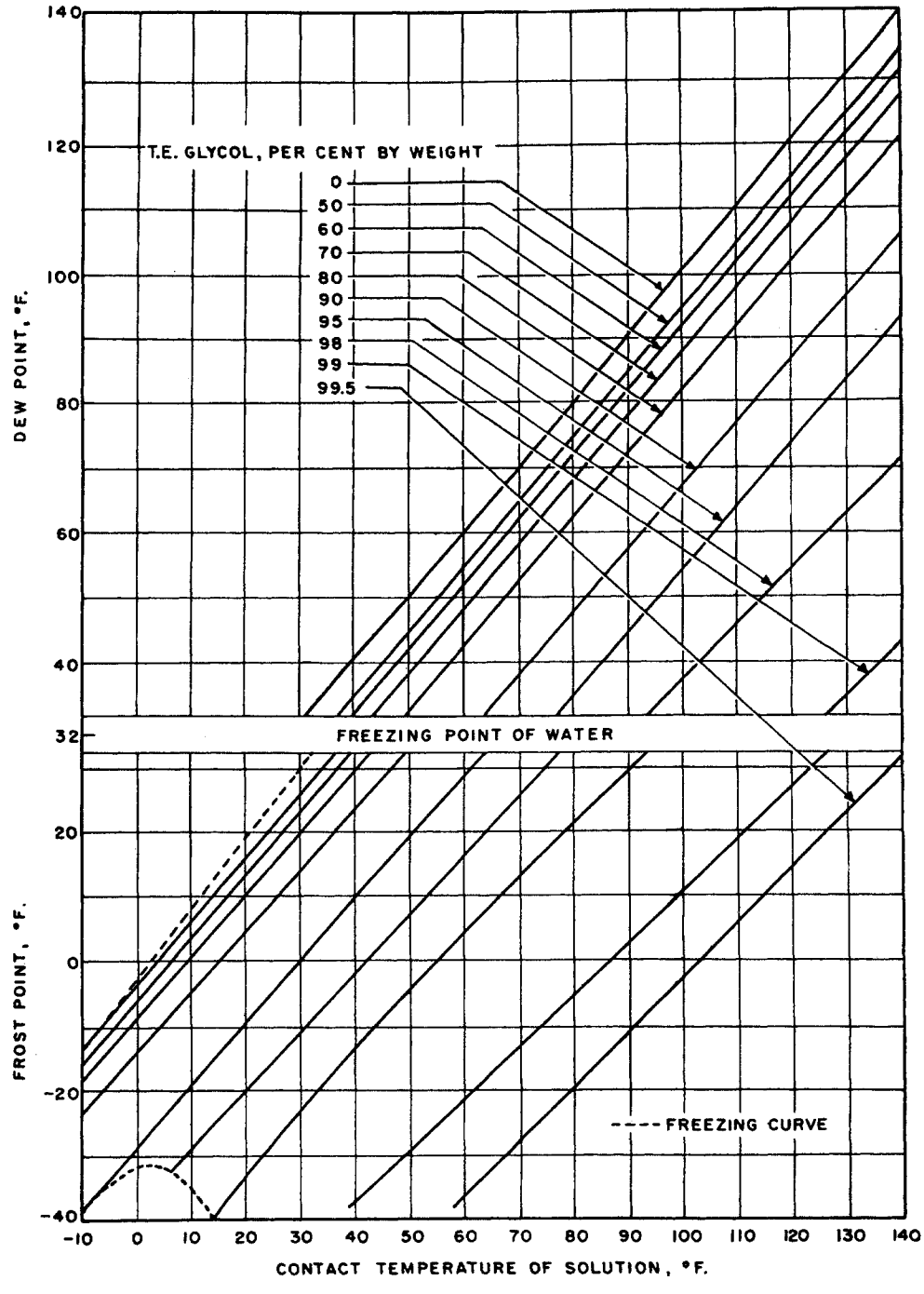

Fig. 16-2. Effect of aqueous triethylene glycol solutions on dew points at various contact temperatures. (16-10, *Courtesy Carbide and Carbon Chemicals Co., Div. of Union Carbide Corp.*)

will be discussed first. Then, the restrictions that these properties place on the choice of process conditions will be presented.

Water and the glycols show complete mutual solubility in the liquid phase. The high affinity of the glycols for water may be attributed to hydrogen-oxygen bonds which are set up between atoms of the hydroxy groups and those of water (16-15). Experimental vapor-liquid equilibrium data on glycol-water solutions indicate that concentrated glycol-water solutions exert very low water-vapor pressures. The vapor pressure of water in equilibrium with various concentrations of glycol can be presented conveniently by plotting water dew point as a function of solution or contact temperature for various glycol concentrations, since the dew points are found to be relatively independent of the total gas pressure on the system. Such plots are given in Figs. 16-1 and 16-2 (16-10). Assigning a contact temperature and glycol concentration yields a gas dew-point temperature. These

figures may be used in conjunction with a water-dew-point chart such as Fig. 5-8 to give the absolute water content of gas in equilibrium with glycol solutions. It should be noted that the frost points indicated below 32°F may be metastable dew points if the glycol does not interfere in the determination of the dew point.

The viscosity of di- and triethylene glycol, though relatively high as compared with that of other absorbents, is not excessively high until temperatures as low as 50°F are reached. Figures 16-3 and 16-4 give the effect of concentration and temperature on the viscosity of glycol-water solutions. It should be noted that pressure has a marked effect on the viscosities of di- and triethylene glycol. This effect of pressure on viscosity is partially offset in the absorber by the large effect of slightly soluble gases on the viscosity of liquids (16-22). The viscosity of diethylene glycol at 1,000 psi is reported to be 3 or 4 times the atmospheric value (16-10). Bridgman (16-3) reports similar effects of pressure on viscosity for highly branched molecules. Liquid-phase viscosity and solubility are principal variables in the correlation of over-all plate efficiencies of absorbers.

Since it is necessary to use solutions that are quite concentrated with respect to the glycols, the reconcentration of the dilute glycol-water solution must be achieved easily. Isobaric temperature-composition diagrams of the glycol-water systems, which are presented in Figs. 16-5 and 16-6, and the normal boiling point of aqueous glycol solutions indicate the ease with which the glycols can be reconcentrated. The low concentration of water in the vapor phase that is in equilibrium with 92 to 99 wt % glycol-water solution is attributed primarily to the low molecular concentration of water in such solutions and secondarily to the fact that the activity coefficient of water is less than 1. The activity coefficient at low pressures is defined as

$$\gamma_1 = \frac{Py_1}{px_1} \tag{16-1}$$

where γ_1 = activity coefficient of water
P = total pressure of system taken as sum of partial pressures of water and of glycol
y_1 = mole-fraction concentration of water in gas phase

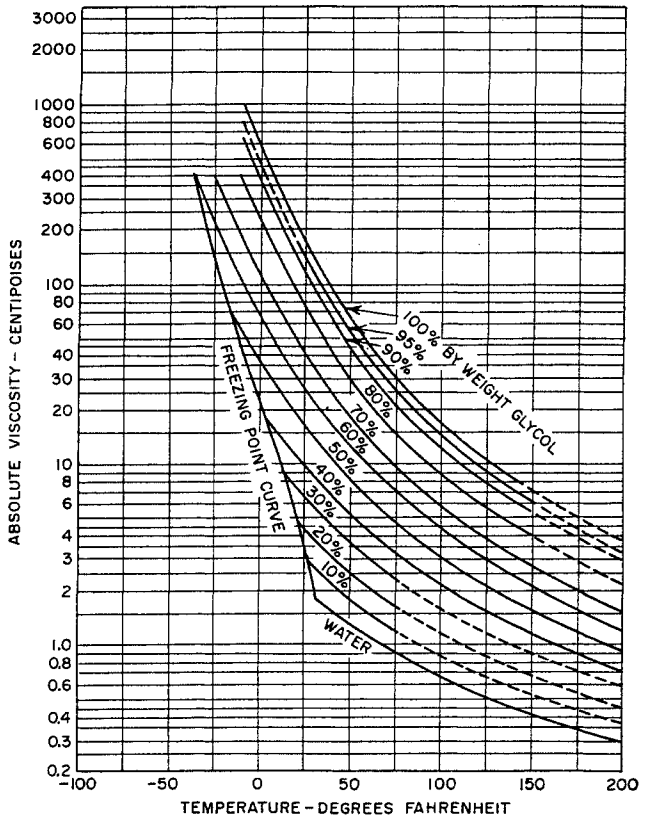

Fig. 16-3. Viscosity of aqueous diethylene glycol solutions. (16-13, Courtesy Dow Chemical Co.)

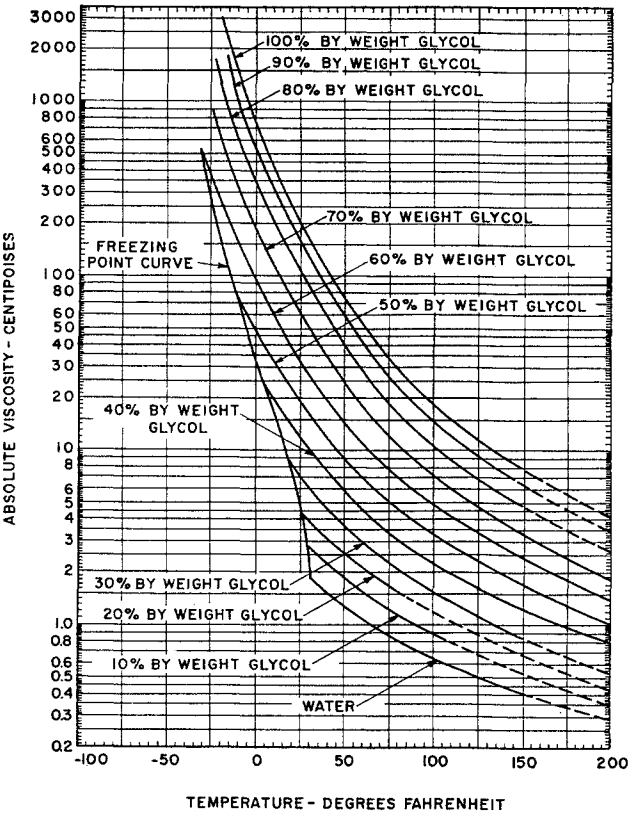

Fig. 16-4. Viscosity of aqueous triethylene glycol solutions. (16-13, Courtesy Dow Chemical Co.)

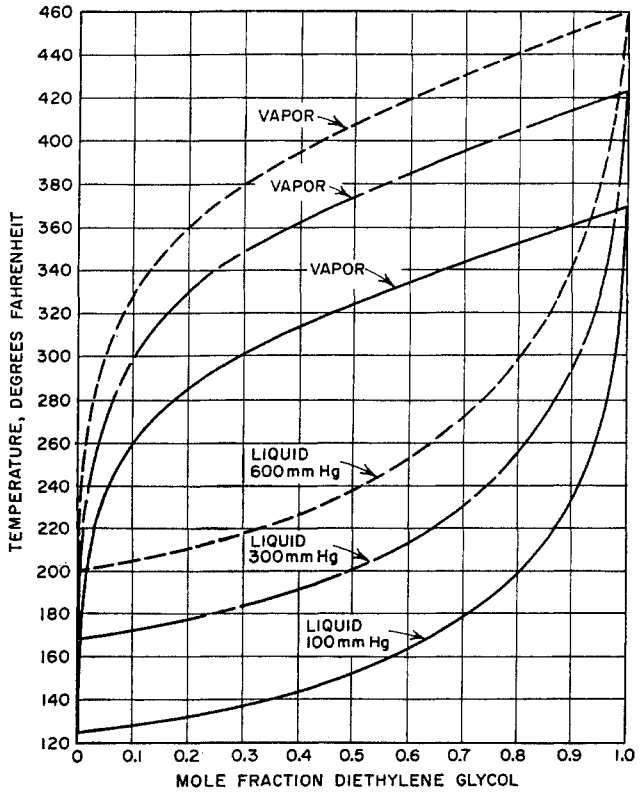

Fig. 16-5. Vapor-liquid composition curves for aqueous diethylene glycol solutions. (16-13, *Courtesy Dow Chemical Co.*)

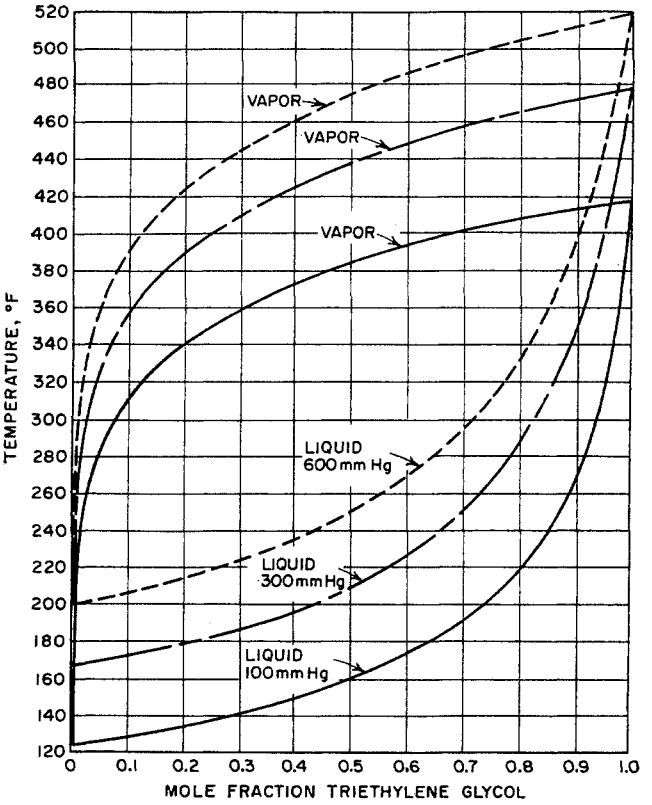

Fig. 16-6. Vapor-liquid composition curves for aqueous triethylene glycol solutions. (16-13, *Courtesy Dow Chemical Co.*)

p = vapor pressure of pure water
x_1 = mole-fraction concentration of water in liquid phase

Pollitzner et al. (16-19) report triethylene glycol losses attributable to vaporization of 0.012 gal/MMcf, which agree with total losses of 0.025 gal/MMcf reported in field practice by Campbell and Laurence (16-7). The second figure includes losses by entrainment, leakage, solubility, etc.

Another property of the glycols is their slight solubility for light hydrocarbons. Direct injection of diethylene glycol into two phase streams containing light-hydrocarbon liquids is possible as in the glycol-injection units. The solubility of the light-hydrocarbon gases and liquids is likewise very small.

The glycols exhibit occasional foaming tendencies in the presence of light hydrocarbons. Foaming is minimized by carefully prescrubbing the absorber-feed gas. Antifoam agents have been utilized successfully at times to mitigate foaming tendencies (16-7).

Additional properties of aqueous glycol solutions are presented in Figs. 16-7 to 16-15. The freezing-point locus of aqueous glycol solutions is given in Fig. 16-14.

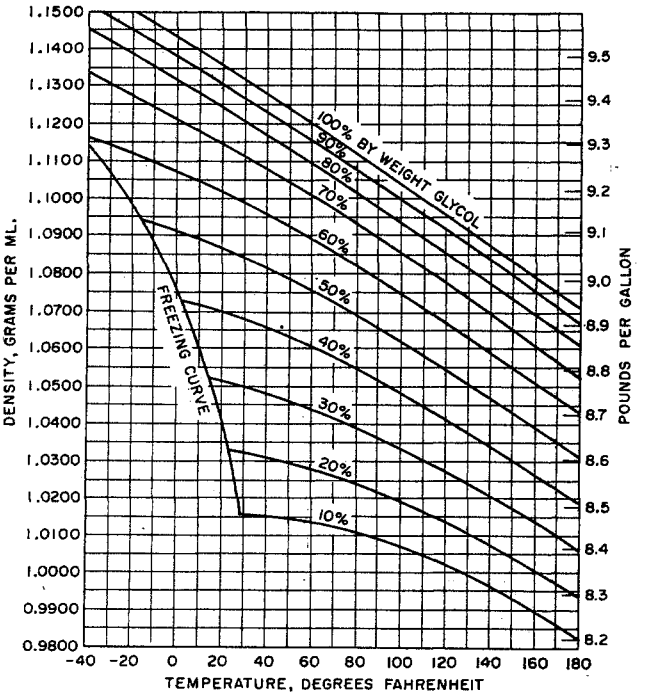

Fig. 16-7. Density of aqueous diethylene glycol solutions at various temperatures. (16-13, *Courtesy Dow Chemical Co.*)

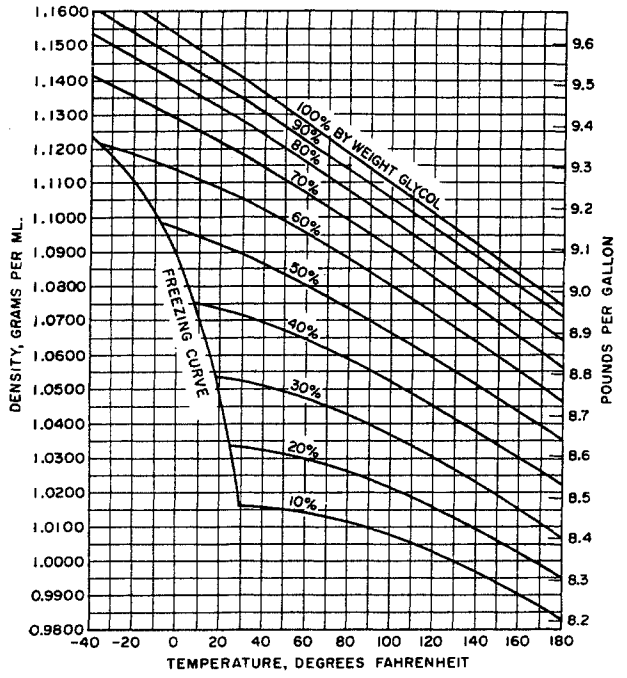

Fig. 16-8. Density of aqueous triethylene glycol solutions at various temperatures. (16-13, *Courtesy Dow Chemical* Co.)

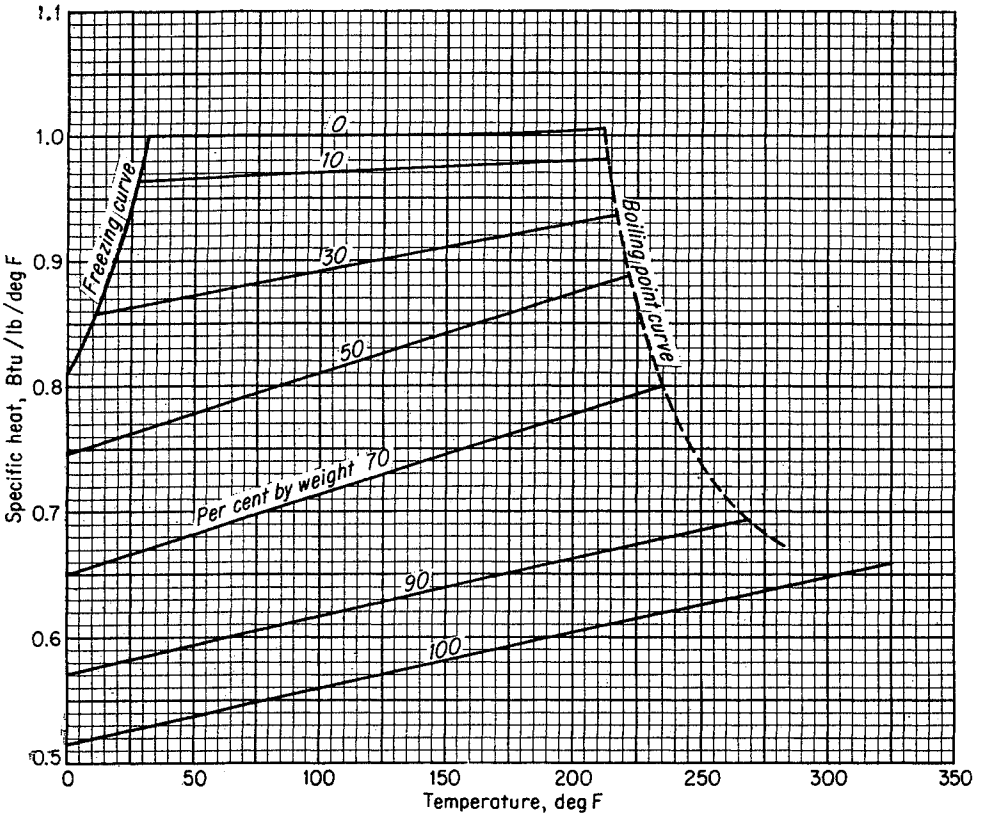

Fig. 16-9. Specific heat of aqueous diethylene glycol solutions. (16-13, *Courtesy Dow Chemical* Co.)

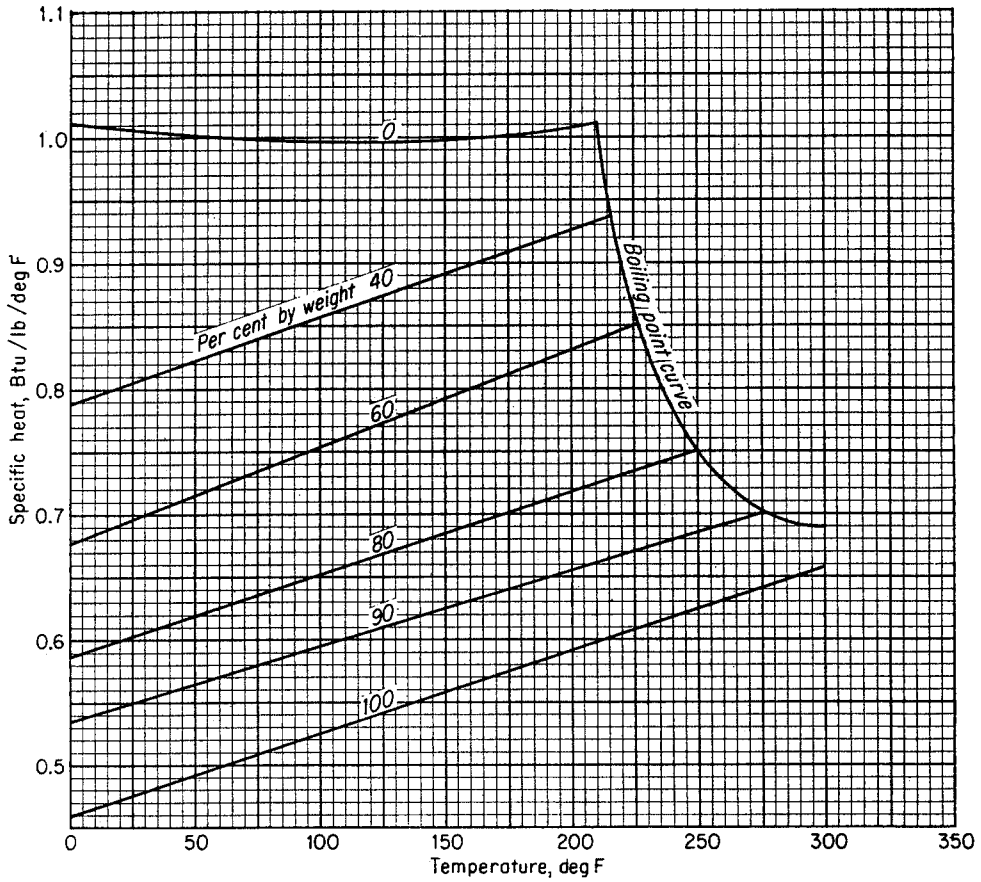

Fig. 16-10. Specific heat of aqueous triethylene glycol solutions. (16-13, *Courtesy Dow Chemical Co.*)

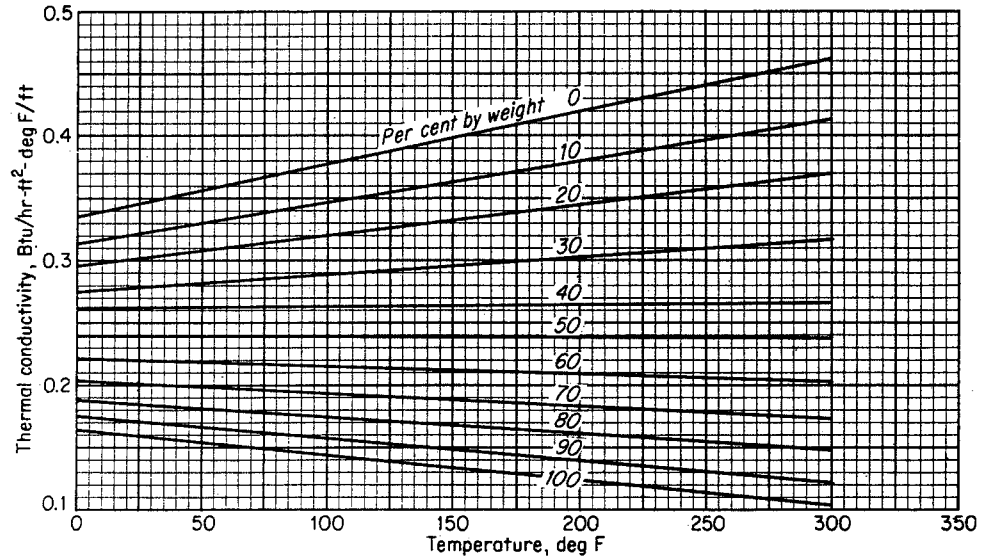

Fig. 16-11. Thermal conductivity of aqueous diethylene glycol solutions at various temperatures. (16-10, *Courtesy Carbide and Carbon Chemicals Co., Div. of Union Carbide Corp.*)

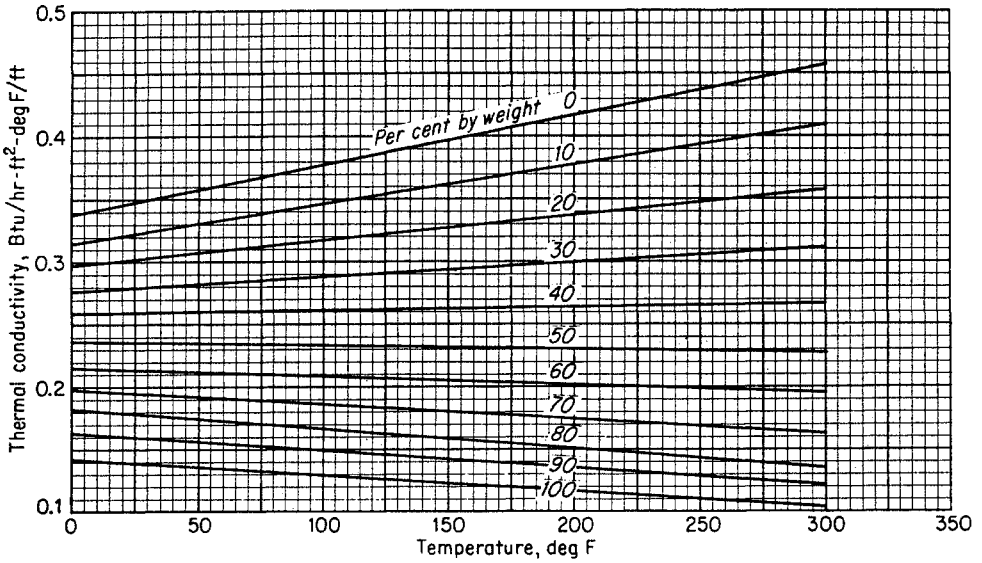

Fig. 16-12. Thermal conductivity of aqueous triethylene glycol solutions at various temperatures. (16-10, *Courtesy Carbide and Carbon Chemicals Co., Div. of Union Carbide Corp.*)

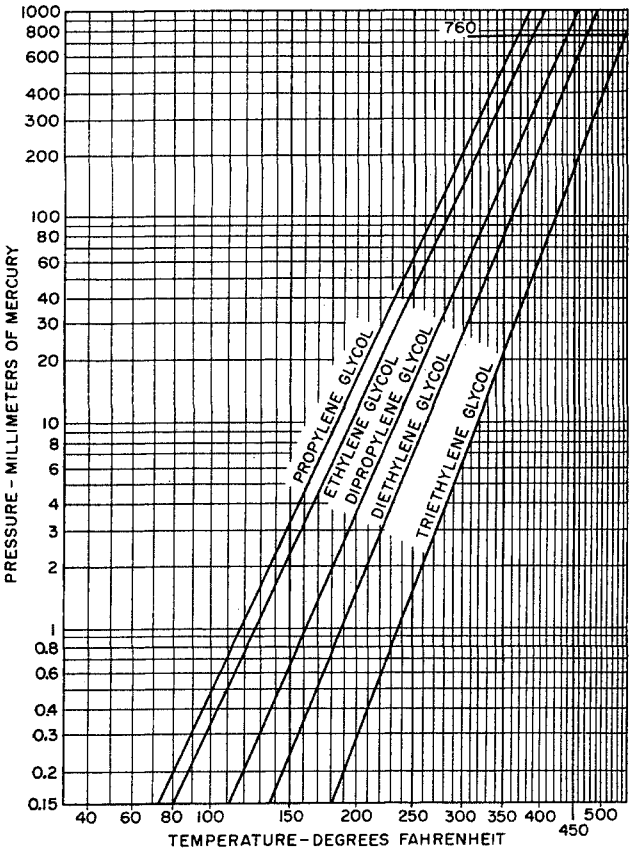

Fig. 16-13. Cox chart for glycols. (16-13, *Courtesy Dow Chemical Co.*)

Process Conditions for Glycol Dehydration Using Absorbing-Stripping Cycle

Currently, diethylene glycol, as well as triethylene glycol, is being used extensively in the dehydration of natural gas when liquid desiccants are employed. Typical flow sheets for diethylene glycol dehydration and triethylene glycol dehydration plants have been reproduced in Figs. 16-16 and 16-17, respectively (16-7). Basically the plants are of similar design. One difference to note is in the reflux arrangements.

The Absorber. The upper limit of the temperature of absorption is governed by the vaporization losses of di- or triethylene glycol that can be tolerated. A practical upper temperature limit is about 100°F. The actual temperature of the absorption is determined by the temperature to which the regenerated glycol can be cooled, the inlet gas temperature, the heat of absorption of the absorbed water, and the gas-liquid ratio. The lower limit of absorption temperature is set by the effect of viscosity on the contact efficiency for the absorption of water. A minimum operating temperature of about 50°F is generally observed, although glycol injection units are designed to operate at much lower temperatures.

Equipment-construction costs rather than phase-equilibrium relationships place limitations on the pressure at which glycol-absorption units may be operated. Triethylene glycol plants with working pressures up to 2,000 psi have been reported (Campbell and Laurence, 16-7). Earlier data showing an increase in the vaporization-equilibrium ratio with

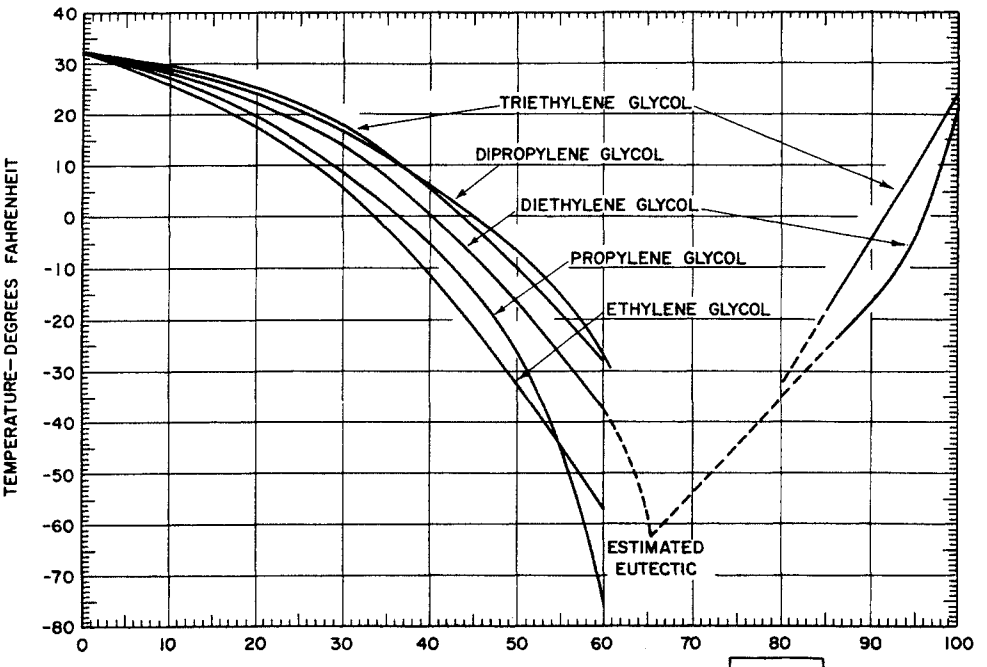

Fig. 16-14. Freezing points of aqueous diethylene and triethylene glycol solutions. (16-10; 16-13, *Courtesy Dow Chemical Co.*)

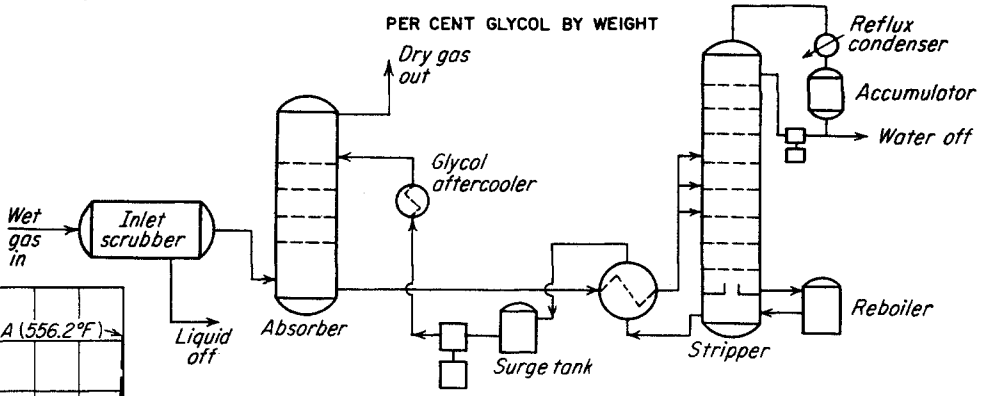

Fig. 16-16. Flow sheet for diethylene glycol dehydration plant. (Campbell and Laurence, 16-7. Courtesy Petrol. Refiner.)

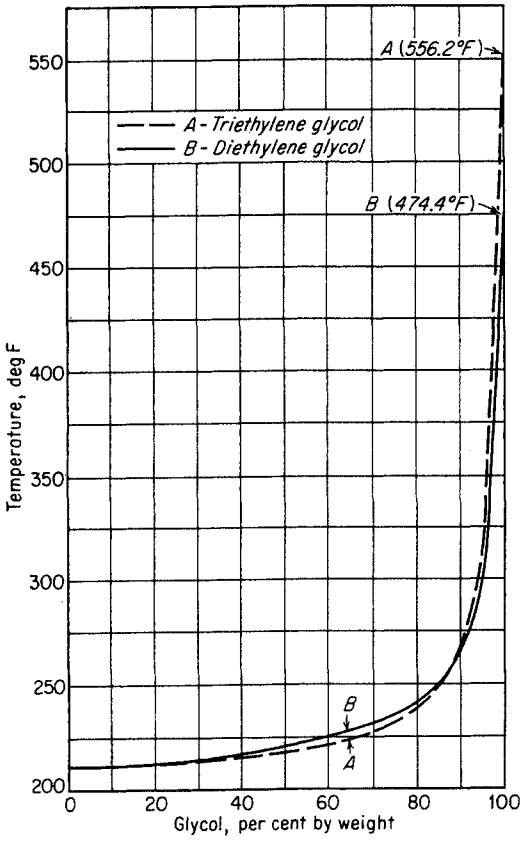

Fig. 16-15. Atmospheric boiling points of aqueous glycol solutions. (16-13, *Dow Chemical Co.*)

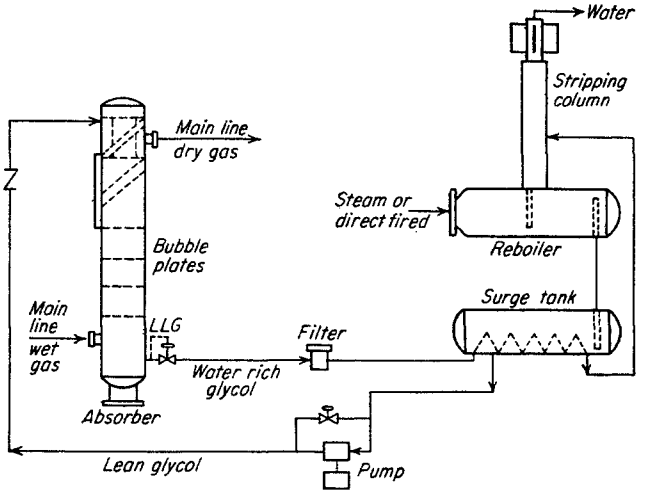

Fig. 16-17. Flow sheet for triethylene glycol dehydration plant. (Campbell and Laurence, 16-7. Courtesy Petrol. Refiner.)

pressure for water in the glycol–water–natural gas system (16-19) is supposed to be incorrect. The conclusion of Campbell and Laurence seems reasonable in view of the extremely high critical pressures one would expect for natural gas–glycol systems.

The cross-sectional area of the absorber is governed primarily by its gas-handling capacity, since the liquid rate required to dehydrate the gas is so low. Conventional methods of tower sizing for bubble-cap trays discussed in Chap. 14 may be used. Even though the liquid rates are generally low, stagewise efficiencies of the order of 70 per cent can be obtained in a properly designed tower.

The water dew point of the gas leaving the absorber is determined by the degree to which the glycol solution is regenerated and cooled, since high contact efficiencies permit dehydration to approach the equilibrium values presented in Figs. 16-1 and 16-2. Dew-point depressions in the neighborhood of 50°F corresponding to inlet diethylene glycol solutions of 95 to 96 wt % may be obtained. This corresponds to a maximum regeneration temperature of 330°F. Triethylene glycol permits dew-point depression of 60 to 75°F, corresponding to regenerated solutions containing 98 to 99 wt % glycol.

The Stripper. The temperature on the glycol side of the regenerator is an important variable because it determines the concentration of the regenerated glycol-water solution and because an excessive temperature will cause the thermal decomposition of the glycols. The maximum regenerator temperature permissible for aqueous diethylene glycol solutions is about 330°F, although occasional temperatures of 350°F are permissible. The presence of oxygen and hydrogen sulfide enhances the decomposition of glycols; hence their presence would require lower than normal regeneration temperatures. The release of dissolved gases by depressuring the spent glycol from the absorber has been recommended (16-23).

For a triethylene glycol stripper the reflux required is even lower. Sufficient reflux may be provided for the smaller units by means of a vertical tube with extended surfaces which are cooled by the atmosphere.

Gas-liquid contact in the stripper is usually made by means of bubble-cap trays for the larger units and by means of a packed section for the smaller units. A large excess of plates or packed height is usually provided, although the separation is rapid and requires but a few theoretical plates.

Accessory units for the glycol dehydration plants include pumps, heat exchangers, reboilers, filters, instrumentation, etc. These features are more suitably discussed in detailed articles (16-7, 16-20).

GAS DEHYDRATION BY ADSORPTION

Solid desiccants or adsorbents are commonly used for dehydrating gases. The use of solid adsorbents has been extended to the dehydration of liquids. Solid adsorbents have the property of removing water from the hydrocarbon stream and of releasing the water to another stream at higher temperatures in a regeneration step.

The Nature of Adsorption

Classically, adsorption has been described as chemical or physical, depending on whether the association between the adsorbed molecules and the solid surface is physical or chemical in nature. Today adsorption may be described on the basis of the forces attracting the molecules to the surface. The attraction of water to desiccants is believed due to van der Waals forces or forces due to the "dispersion effect" (16-17), which may be classified in the physical category. The equilibrium between solid and gas in van der Waals adsorption is reversible and readily adjusts to changes in temperature and pressure.

Adsorbents are characterized by extremely large surface areas which are distributed through the solid in the form of fine, nonuniform capillaries. These surface areas present a large residual field of force. Condensation on these surfaces is one possible path by which the residual forces are minimized. Condensation thus takes place in fine capillaries, producing *not* droplets of liquid but a multitude of fine convex liquid surfaces. Thermodynamic calculations show that the vapor pressure of liquids in fine wetted capillaries is appreciably lower than the vapor pressure of a flat surface of the same liquid. The vapor pressure of liquids in these capillaries is therefore in equilibrium with water vapor of much lower partial pressure than the normal saturation pressure (16-6). Another interesting characteristic showing a high degree of capillarity is that the quantity adsorbed in equilibrium with a given partial pressure of gas depends on the direction from which equilibrium is approached. This behavior, which is known as "adsorption hysteresis" (16-11), is probably, however, an unimportant phenomenon in commercial adsorption after the first few adsorption-regeneration cycles have been run.

Temperature changes and other phenomena that cause destruction of the physical structure of the adsorbent reduce the holding capacity for water. Campbell, Skinner, and Laurence (16-5) cite the following requirements for a good granular desiccant:

1. High equilibrium adsorptive capacity for water
2. Reversibility of adsorption and ease of regeneration

3. High rate of adsorption
4. Low resistance to gas flow
5. High resistance to crushing and dust formation
6. Chemical inertness
7. Low volumetric change with temperature and with saturation

Fortunately, desiccants possessing these attributes have been developed and are continually being improved. The most frequently used adsorbents today are bauxite, activated alumina, and silica gel, which are marketed under various trade names.

A discussion of the equilibrium, kinetic, chemical, and mechanical properties of some economical desiccants follows:

Because the dehydration of gases and liquids using dry desiccants is conducted in fixed beds, the process is a batch operation. However, an equilibrium relationship between the gas stream and the bed can be closely approached, so a knowledge of equilibrium relationships indicates practicable limiting capacities of a bed (16-14).

Figure 16-18 presents typical equilibrium-adsorption isotherms which relate the partial pressure of water in the gas to the adsorbed water content based on the regenerated bed (16-18). The sensitivity of the equilibrium conditions to temperature is evident.

The adsorptive capacity of commercial desiccants decreases with use because (1) some of the stronger adsorption sites are permanently inactivated, and (2) high-molecular-weight hydrocarbons that are adsorbed may be difficult to desorb. The decay in the activity of a commercial desiccant regenerated every sixteen hours is reproduced in Fig. 16-19 (16-16). Obviously, the design capacity of an adsorbent should be chosen at a value somewhat lower than the "asymptotic value" of the capacity curve for the service in question. The useful capacity of an adsorption bed is sensitive to the rate of gas flow, which is frequently expressed as contact time. Figure 16-20 shows, however, that the adsorptive capacity may become rate-independent for reasonably short contact times (16-2); a 36-in. column of 4/8 mesh Florite activated at 350°F was used in the test. Sufficient contact time is provided for most beds if the superficial gas velocity is held below 1 ft/sec.

Eagleton and Bliss have studied the rate of drying of air in fixed beds of activated alumina, Florite, and silica (16-14). Effluent concentrations of water were measured at several values of inlet concentration, bed length, flow rate, and temperature. Their measurements lead to the conclusion that the rate is governed by diffusion both through the air film and within the solid particle. Typical breakthrough

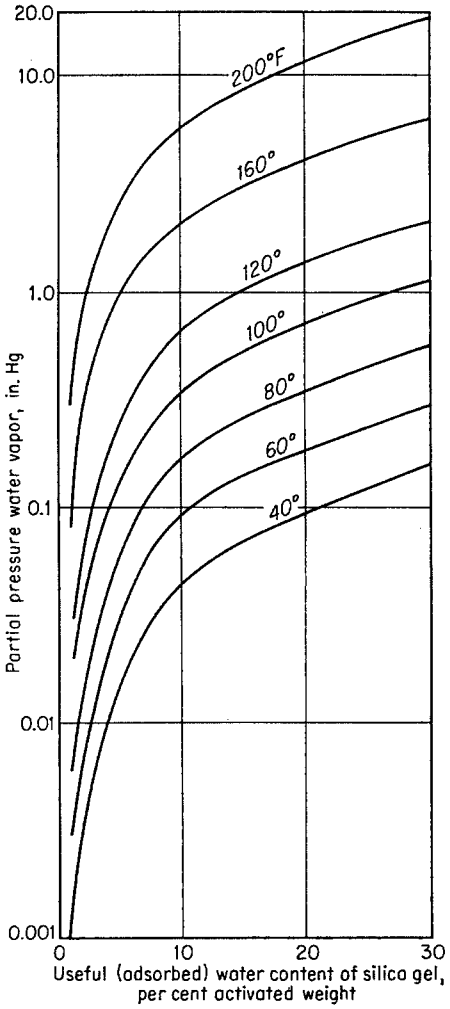

Fig. 16-18. Absorption isotherms for water on silica gel.

curves showing ratio of exit water concentration to inlet water concentration as a function of time are plotted in Fig. 16-21. It is felt that, for commercial-size beds, the width of the breakthrough curves is sufficiently small so that 95 per cent of the bed thickness can be utilized to produce equilibrium effluent gas.

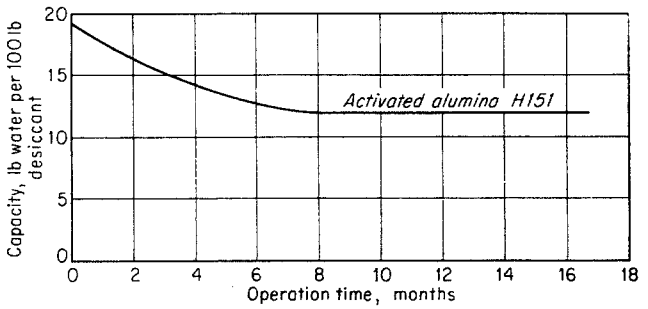

Fig. 16-19. Effect of operation time on absorbent capacity. (*Getty, Lamb, and Montgomery*, 16-16. *Courtesy Petrol. Engr.*)

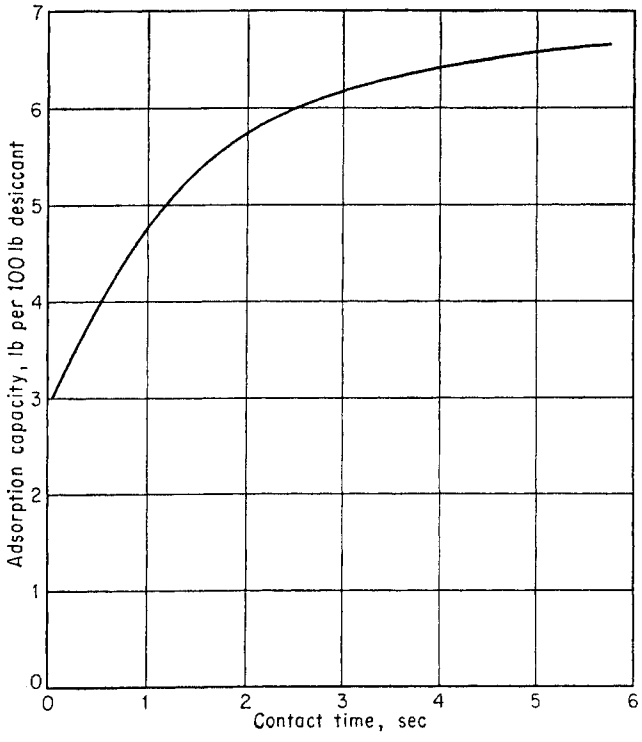

Fig. 16-20. Effect of contact time on desiccant capacity for bauxite, Florite. (*Amero, Moore, and Capell*, 16-2. *Courtesy AIChE.*)

The distribution of water in the bed and in the gas stream is shown in Fig. 16-22 for the beginning of a drying period; an intermediate time (30 per cent); and the conclusion of the drying period just prior to breakthrough. The regeneration period should start just before breakthrough of the nondehydrated gas to obtain maximum capacity for each regeneration. The breakthrough curve of Fig. 16-21 is related to the shape of the moisture-gradient curves and the portion of the bed not completely saturated with water.

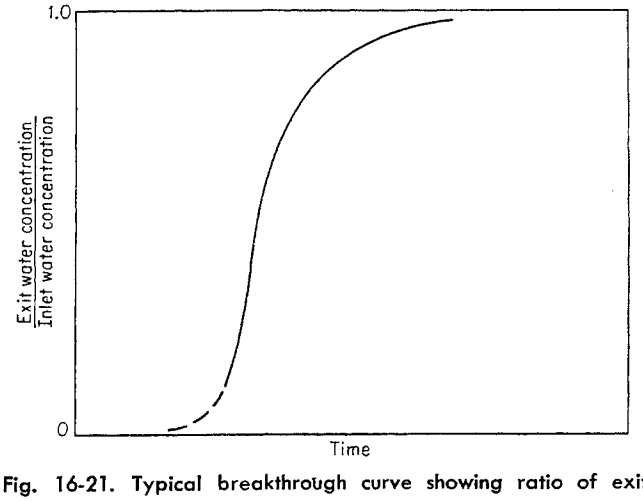

Fig. 16-21. Typical breakthrough curve showing ratio of exit water concentration to inlet water concentration as a function of time. (*Eagleton and Bliss*, 16-14. *Courtesy AIChE.*)

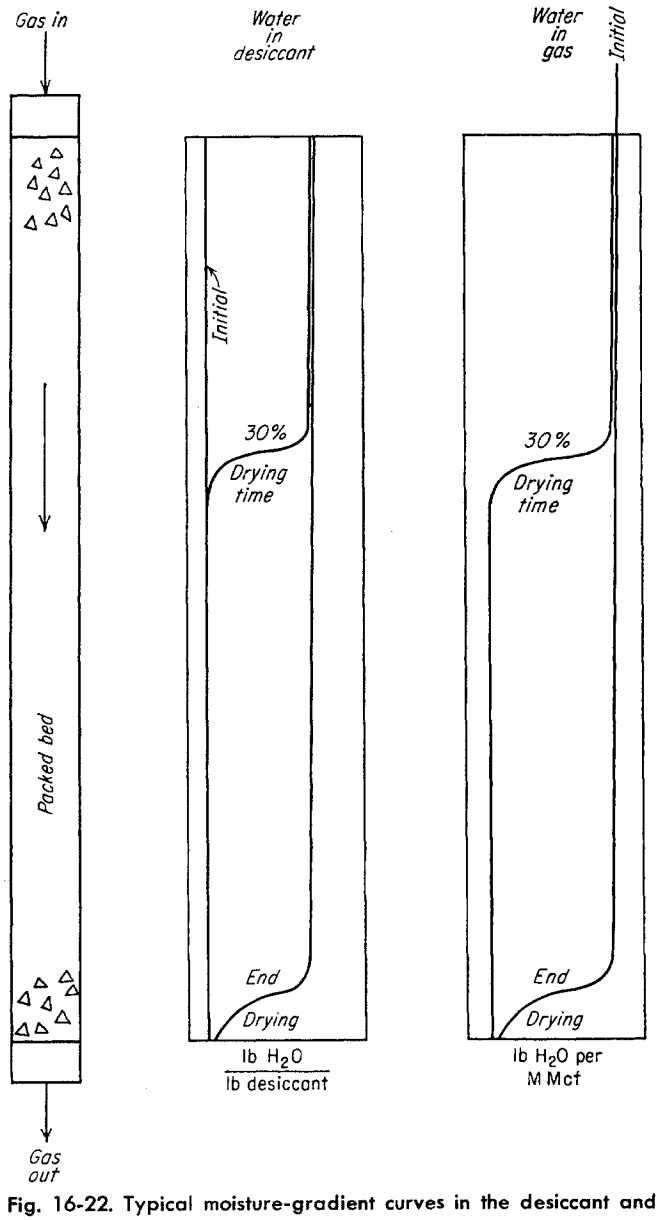

Fig. 16-22. Typical moisture-gradient curves in the desiccant and in the gas phase during absorption periods.

Recovery of Hydrocarbon and Regeneration of Desiccant

Hydrocarbons are adsorbed on desiccants just as water is but less preferentially. That portion of the bed at a given time which is not dehydrating gas is retaining hydrocarbons. The heavier hydrocarbons are retained preferentially over the light hydrocarbons. When dehydration stops short of the breakthrough point, the portion of the bed not used for dehydration will have retained hydrocarbons. Many dehydration units produce hydrocarbon liquid in the regeneration condensate. In some cases, solid desiccants can be used for both dehydration and removal of heavier hydrocarbons to prepare a satisfactory pipeline gas. The carrying capacity of Sovabead for hydrocarbons

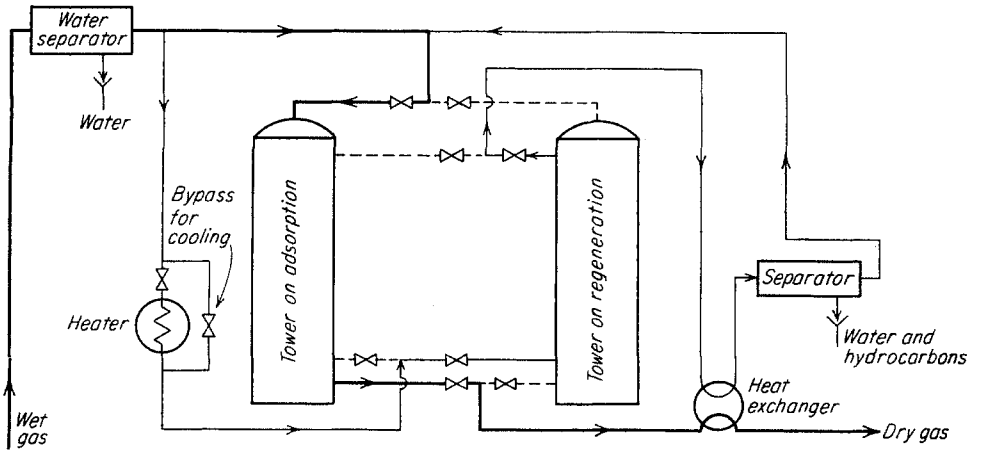

Fig. 16-23. Flow diagram for solid-desiccant dehydration.

at 700 psi and 60°F was observed to be 0.020 to 0.025 gal of recovered natural gasoline per pound of Sovabead for each regeneration. Seale (16-24) reports 3 gal of hydrocarbons recovered per 100 lb of adsorbent at 800 psi. The plant recovered 23 bbl of distillate and 2 bbl of water per day when processing 23 MMcf of gas on a 72-min adsorption-regeneration cycle.

The Regeneration of large, commercial solid-desiccant dryers is usually carried out by passing natural gas which has been heated to a temperature of from 350 to 450°F through the desiccant bed (Fig. 16-23). Higher regeneration temperatures lead to shorter desiccant life, and lower regeneration temperatures lead to insufficient dehydration capacities.

The resistance of beds of granular adsorbents to the flow of gases and liquids has been studied by Allen (16-1) and later extended by Amero et al. (16-2). The final curves developed by Amero are reproduced in Fig. 16-24. Table 16-1 may be used to convert from mesh size to average particle diameter. Not

Table 16-1. Conversion of Mesh to Particle Diameter

Mesh size	*Effective particle diameter, ft*
2/4	0.013
4/8	0.0091
8/16	0.0037

SOURCE: (16-2).

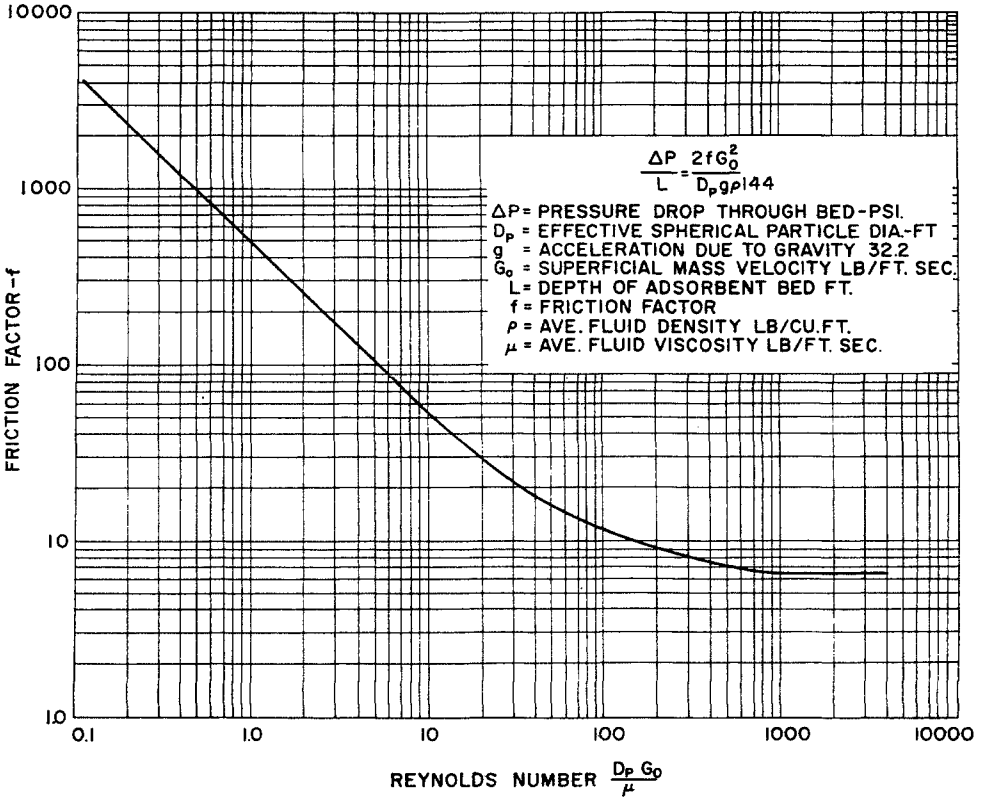

Fig. 16-24. Pressure drop through beds of granular adsorbents. (*Amero, Moore, and Capell*, 16-2. Courtesy AIChE.)

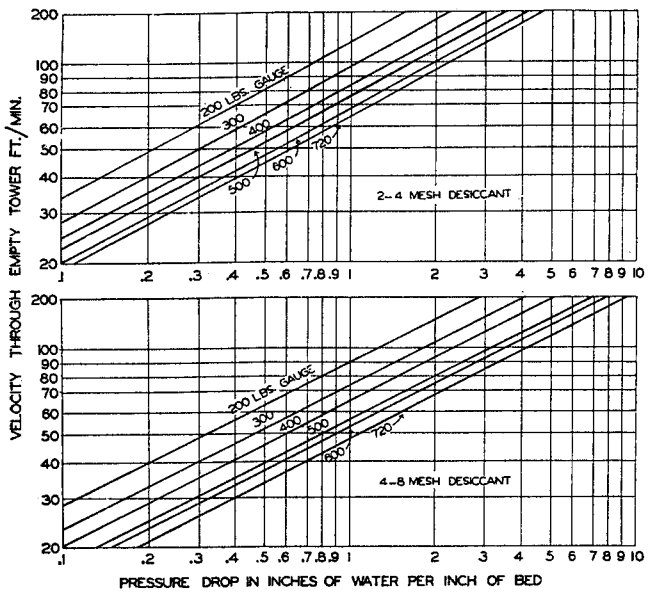

Fig. 16-25. Pressure drop through adsorbent beds for 0.677 gravity gas. (*Amero, Moore, and Capell*, 16-2. *Courtesy AIChE.*)

all desiccants have the same roughness factor, but the friction factor will be little displaced from desiccant to desiccant (16-5). Figure 16-25 gives the pressure drop for a 0.677 gravity gas with two sizes of desiccant (16-2).

In vertical towers, it is customary to pass gas downward to prevent lifting of the desiccant with pressure surges in the system.

The adsorbent must be chemically inert to natural gas constituents in order that it may remain active for the adsorption of water. Volumetric changes of the desiccant with temperature and saturation should be low to avoid movement of the bed once it is charged to the dryer. Periodic expansion and contraction tend to promote fracturing of the desiccant particles.

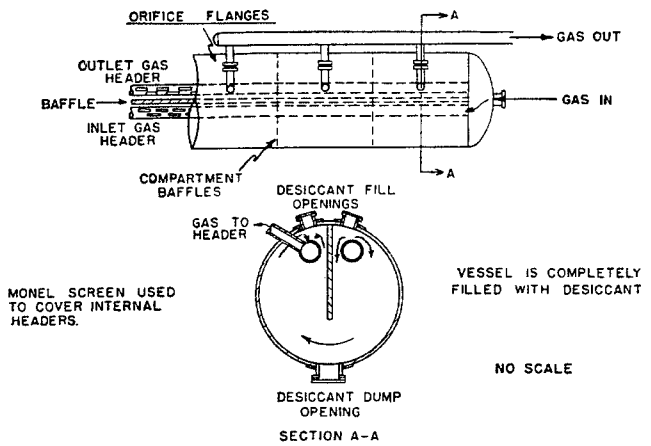

Fig. 16-26. Diagram of horizontal sorber. (*Campbell and Laurence*, 16-7. *Courtesy Petrol. Refiner.*)

The desiccant is replaced in from two to five years, with more frequent changes needed when oil or foreign material is deposited at the entrance to a tower.

Process Conditions for Dry-desiccant Dehydration

The process conditions for the design of dry-desiccant dehydration are determined by the limitations imposed by the properties of dry desiccants discussed in the previous section and by mechanical costs.

The horizontal sorbers with transverse gas flow around a baffle, as pictured in Fig. 16-26 (16-7), have largely superseded vertical towers where space requirements are not a primary consideration. Pressure drop through the bed is thus reduced, and added flexibility is gained by building the bed in compartments that can be isolated from one another. An asymptotic adsorption capacity for water of 5 to 7 per cent is used for commercial adsorption, although a new desiccant capable of adsorbing 12 wt % of water has been reported (16-16).

Some adjustment of the capacity for the activated aluminas is necessary when the contact temperature exceeds 90°F. The temperature to the dehydrator inlet ranges from 2 to 5°F higher than the main-stream temperature because of reinjected gas which has been used for reactivation purposes. This is to be expected since 5 to 15 per cent of the total gas is used for regeneration. About two-thirds of the heat is used in heating up the drying vessel and its desiccant contents. A typical temperature record of a single regeneration cycle has been reproduced in Fig. 16-27. When hot natural gas is used for regeneration the heat load is the sum of the following quantities:

1. Sensible heat of drying vessel and solid desiccant
2. Sensible heat of regenerator gas
3. Heat of desorption of water
4. Heat losses to surroundings

During the heating cycle, if natural gas is used as the regenerating medium, the rate of heat transfer is

$$\frac{Q}{t} = \frac{1}{t}[M_v C_{p,v}(T_2 - T_1) + M_d C_{p,d}(T_2 - T_1) + M_g(C_{p,g})(T_2 - T_1) + M_w \Delta H + \text{heat losses}] \quad (16\text{-}2)$$

where Q/t = rate of heat transfer, Btu/hr
t = length of heating cycle, hr
M_v = mass of vessel, lb
$C_{p,v}$ = specific heat of vessel material, Btu/(lb)(°F)
T_2 = temperature of vessel at regenerator conditions, °F
T_1 = temperature of vessel at beginning of cycle, °F

M_d = mass of desiccant, lb
$C_{p,d}$ = specific heat of desiccant, Btu/(lb)(°F)
M_g = mass of gas used in heating portion of regeneration cycle, lb
$C_{p,g}$ = specific heat of natural gas, Btu/(lb)(°F)
M_w = mass of water absorbed during cycle, lb
ΔH = heat of desorption of water, estimated as 1100 Btu/lb
heat losses = total for regeneration cycle, Btu

For insulated vessels, the heat loss should not exceed 10 per cent of the adiabatic heat requirements.

In sizing the dry-gas regenerator and gas heat exchanger in Fig. 16-23, it is important to recognize that the bulk of the water is desorbed in about one hour rather than over the entire heating portion of the regeneration cycle. The average temperature of the regenerator exit gas is conservatively estimated as 250°F, or somewhat lower than the maximum regeneration temperature.

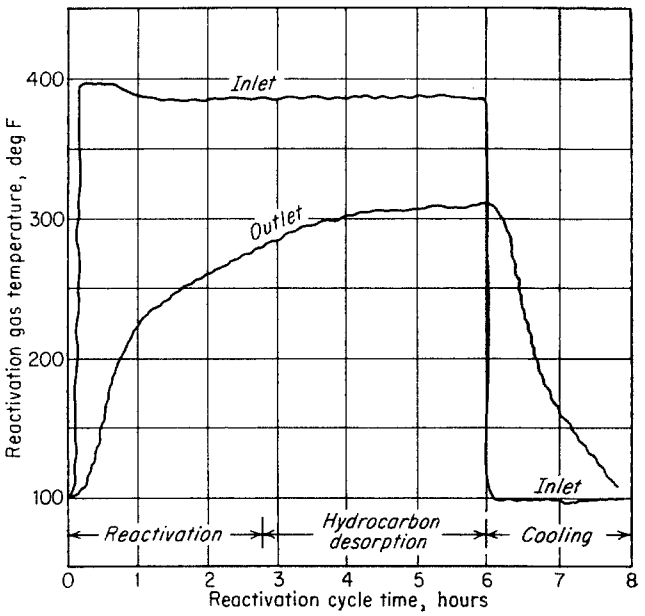

Fig. 16-27. Temperature record of a regeneration cycle.

DEHYDRATION OF LIQUIDS

The reasons for the dehydration of liquids parallel the reasons for the dehydration of gases. The techniques used for commercial dehydration of liquids are sufficiently different from those used for gases to warrant separate treatment. The two most common procedures used for the dehydration of light-hydrocarbon liquids are adsorption and distillation. The variability of water content in light-hydrocarbon products leads to more frequent use of adsorption processes for the conditioning of liquid pipeline products.

Adsorption Drying Processes

Campbell and Laurence (16-6) classify adsorption dehydration according to the manner in which the spent-desiccant bed is regenerated, as follows:

1. Closed vapor systems
2. Closed steam systems
3. Open vapor systems
4. Open steam systems

The "closed systems" are those in which the heating medium *is not* in direct contact with the adsorbent. During the regeneration period the hold-up stock that remains after the liquid hydrocarbons are drained from the bed provides the main source of regeneration gas. Open "vapor systems" use as heat source either highly superheated steam or, preferably, hot gases in direct contact with the bed.

A step preliminary to any dehydration process is the removal of the free water from the feed stream. Even a properly designed separator may not remove all the free water from the liquid. An average of 20 per cent of the total water is apt to be free water.

In the preparation of light hydrocarbons for transmission of liquids through product pipeline, the general practice is to reduce the water content to a value of less than the saturated-water content at the lowest line temperature. The specification for dehydrated propane is usually set in the range from 17 to 30 ppm.

The weight of desiccant required for an adsorption unit is based on the adsorption capacity of the desiccant in the presence of light hydrocarbons; the desiccant is required to dehydrate the feed completely. It is preferable to calculate the water content of the feed on the basis of a measured value. The saturated-water content of light hydrocarbons, as predicted from Fig. 5-18 or 5-19, times a factor of 1.25 to correct for entrained water, is suggested as such a base value; this is the estimated water content of the feed stream leaving the water-knockout vessel. Contact times of the order of 2 to 3 min are used, although contact times of 3 sec for drying gasoline on a laboratory scale have been shown to be sufficient (16-12).

Liquid Dehydration by Distillation

Systems which exhibit limited miscibility with water in the liquid–liquid gas region may be dehydrated by distillation provided the feed concentration is less than or in the neighborhood of the saturation conditions for the light hydrocarbon. For example, distillation carried out in the area L_2-V of Fig. 5-1

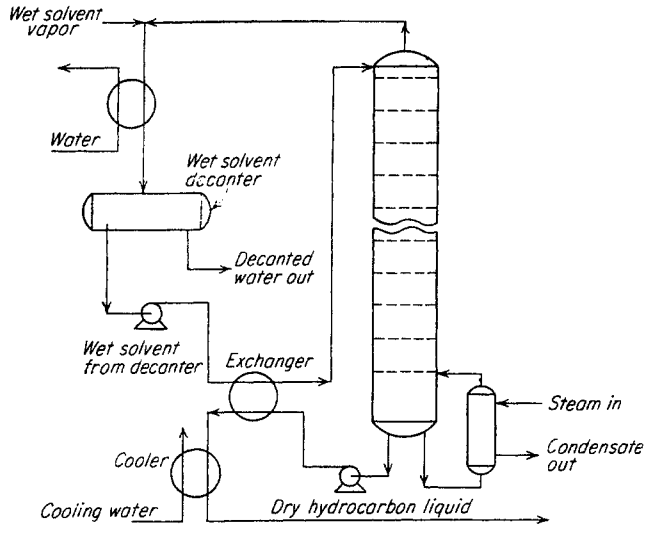

Fig. 16-28. Process for dehydration of hydrocarbon liquids by distillation. (Gester, 5-30. Courtesy AIChE.)

will concentrate the liquid with respect to hydrocarbon and reject water in the vapor. Figure 16-28 gives a flow diagram of a distillation dryer in which water is rejected overhead and dehydrated hydrocarbons are produced as bottoms product. Calculated or experimental equilibrium-vaporization ratios for water in light hydrocarbons may be used to calculate the ideal stages required to effect the desired dehydration. However, the utility of the equilibrium-stage approach is diminished by the observation (5-30) that the overall plate efficiencies will probably be of the order of 4 to 8 per cent. The theoretical plates may number 1 or 2, whereas the actual trays required may be as high as 30.

The distillation is essentially a stripping operation, since the feed is introduced near the very top of the column. A stripping ratio of from 0.16 to 0.24 lb of rising vapor per pound of descending liquid has been reported by Gester (5-30) for drying of hexanes.

ECONOMICS OF NATURAL GAS DEHYDRATION

The economics of dehydration can best be determined by calculating costs for a specific unit. However, the relative initial equipment cost and operating costs fall heavily in favor of glycol dehydration (16-8, Figs. 16-29 and 16-30). Campbell gave, in 1952, operating costs in dollars per MMcf as 0.20 to 0.40 for triethylene glycol and 0.60 to 1.20 for dry desiccant. However, because of greater ease of operation, especially for systems that have frequent changes in flow rates, the adsorption units are frequently chosen even at the higher cost. The flexibility of operation and assurance that processed gas will be free of liquid are factors to be considered.

Dehydration for very low moisture contents such as are required for processes at temperatures below −50°F always employs solid desiccants, at least for the final moisture removal. Hydrocarbon recovery at the wellhead requires glycol to permit the combination of dehydration and hydrocarbon recovery when the pressure drop is limited. In general, dry desiccants can handle gases at higher temperatures than glycol solutions.

THE SWEETENING OF NATURAL GASES

Many natural gases contain hydrogen sulfide (H_2S) in concentrations ranging from barely detectable quantities to over 30 mole %. Gases containing H_2S are classified as "sour" and gases free from H_2S are called "sweet." Natural gas that is transported to the fuel market must meet legal requirements,

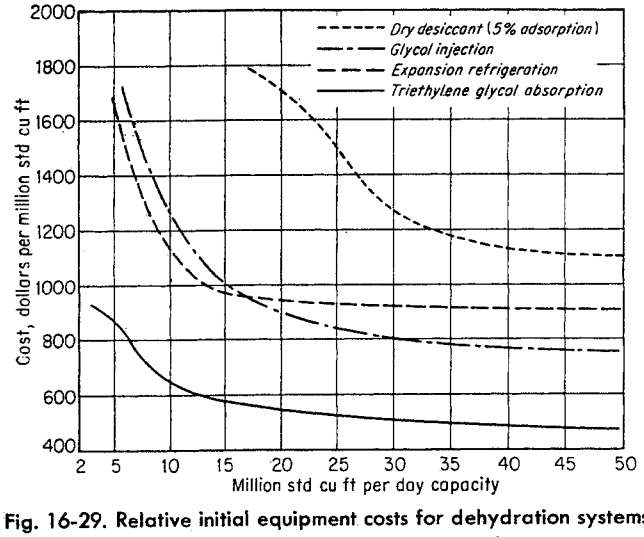

Fig. 16-29. Relative initial equipment costs for dehydration systems at 1,000 psig. (Campbell, 16-8. Courtesy AIChE.)

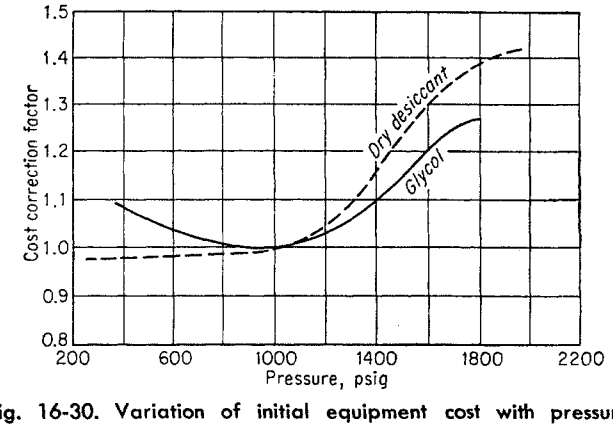

Fig. 16-30. Variation of initial equipment cost with pressure. (Campbell, 16-8. Courtesy AIChE.)

which specify a maximum H_2S content in the range of 0.1 to 0.25 grain per 100 std cu ft. These requirements are justified since H_2S is a toxic gas and since its combustion products are sulfur dioxide or trioxide.

The removal of H_2S from natural gas is accompanied by the removal of carbon dioxide (CO_2), if present, since CO_2 has similar acid characteristics. Corollary benefits obtained from the removal of both acid gases from a pipeline stream include decrease in corrosive effects, especially when liquid water is present.

Requirements of Sweetening Process

An economical sweetening process applicable to the natural gas industry must provide for (1) substantially complete removal of H_2S, (2) handling of large volumes of gas, and (3) high-pressure operation.

At first glance, a large number of processes appear to be available for consideration. Indeed, the applicability of these processes to some portion of the chemical and gas-processing industry has encouraged their discovery and development. The processes available for consideration may be classified as regenerative or nonregenerative processes, according to whether the agent that removes the acid gases can be returned to its original form for reuse.

Nonregenerative processes are inapplicable to the removal of large quantities of acid gases. Under special circumstances, nonregenerative processes, such as the lime-slurry process [$Ca(OH)_2$ suspension], or absorption by caustic soda (NaOH) solution, potassium permanganate solution, or a buffered solution of sodium bichromate and zinc sulfate, may find use in "cleaning up" residual quantities of H_2S that remain after the bulk of the H_2S has been removed by other processes. These processes permit the reduction of H_2S concentration to values unattainable by the regenerative processes.

Foremost among the regenerative processes used in the removal of acid gases is the Girbotol process, which uses aqueous organic amines as the absorbing medium (16-29, 16-43, 16-58). Modifications of the Girbotol process to dehydrate and sweeten the gas simultaneously (16-32) and to absorb H_2S selectively from gases containing CO_2 have been conceived (16-40). Other regenerative processes which warrant consideration under special conditions employ:

1. Water
2. Aqueous sodium carbonate solution (Seabord process, 16-64)
3. Iron oxide, dry box (16-62)
4. Aqueous sodium or ammonium thioarsenate solution (Thylox process, 16-53)
5. Aqueous tripotassium phosphate solution (Shell process, 16-45)
6. Aqueous sodium phenolate solution (phenolate process, 16-63)
7. Aqueous sodium carbonate–iron oxide solution (16-45)
8. Hot, aqueous potassium carbonate solution (16-27)

Most of these processes have not been chosen over the Girbotol processes except for special cases. The hot aqueous potassium carbonate shows advantages in the treatment of natural gas with high acid concentrations. A new process in which SO_2 is reacted with H_2S to form elemental sulfur in the presence of a glycol solution shows promise of becoming the most economical (16-58a).

Although this section will be devoted mainly to the treatment of natural gas sweetening by aqueous organic-amine solutions, the general theories on simultaneous absorption and chemical reaction, which will be discussed briefly, apply to many of the noncompetitive processes listed above. Figure 16-31 gives one version of the amine process for the sweetening of natural gases.

Equilibrium Relationships and Physical Properties of Aqueous Amine Solutions

Systems of acid gases with aqueous ethanolamines exhibit phase-equilibrium and kinetic properties that permit substantially complete removal of acid gases from inert gases in stagewise contacting devices. The phase distribution of acid gases in aqueous amine solutions is such that the solution has a high capacity for absorbing the acid gases through chemical reactions while exerting a very low equilibrium vapor pressure on the gases. Another requirement fulfilled is that equilibrium of the phase reaction be reversible at some higher temperature, in order to permit regeneration and reuse of the original solution.

The organic ethanolamines represents a class of compounds that can be used for substantially com-

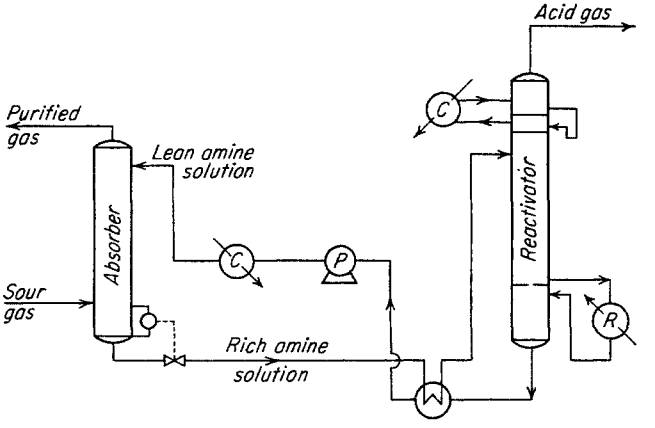

Fig. 16-31. Flow diagram of amine treating process for CO_2 and H_2S removal.

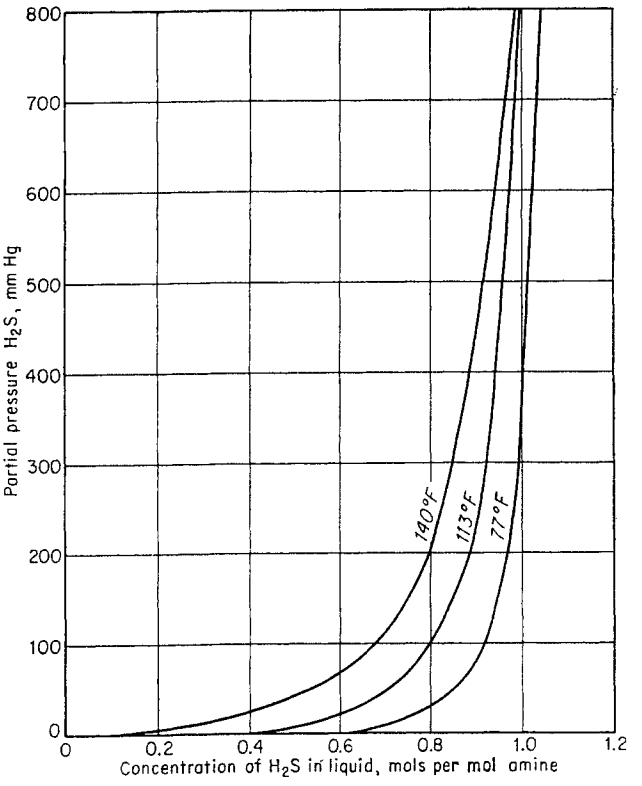

Fig. 16-32. Equilibrium pressure of H_2S from 10.9 wt %, 2 *M* monoethanolamine solution. (*Data from Riegger et al.*, 16-59.)

plete removal of H_2S and CO_2 from "inert gases" such as natural gases. Table 16-2 gives the physical properties and Table 16-3 (16-30) gives the chemical formulas and some physical properties of mono-, di-, and triethanolamine, three amines which are finding current application. Table 16-3 gives a summary of available equilibrium data for various systems involving the acid gases, organic amines, and water. The data are predominantly for aqueous carbon dioxide–amine systems, although some data are available on systems containing H_2S. A superficial glance at the table indicates also the dearth of high-temperature equilibrium data on acid gas–aqueous amine systems. Stripping calculations are hampered by this lack of equilibrium, rate, and thermal data. The data of Riegger et al. on the solubility of H_2S in aqueous monoethanolamine solutions at several values of H_2S partial pressure, temperature, and concentration are reproduced in Table 16-4 (16-59) and in Figs. 16-32 to 16-34. Figures 16-35 to 16-37 (16-52) show equilibrium isotherms for CO_2 in an aqueous solution containing 12.3 to 20 wt % amine solutions. The positions of the isotherms representing the solubility of CO_2 at various partial pressures of CO_2 vary considerably with temperature. For a given isotherm, large variations of the liquid-phase concentration are confined to the region of low CO_2 partial pressures.

Table 16-2. Physical Properties of Amines*

Property	MEA	DEA	TEA
Molecular weight	61.08	105.14	149.19
Apparent specific gravity, 68/68°F	1.0179	1.0919	1.1258
Δ specific gravity/ΔT	0.00078	0.00064	0.00054
Boiling point, °F:			
At 760 mm Hg	339	Decomp.	680
At 50 mm Hg	212	369	471
At 10 mm Hg	156	302	406
Vapor pressure at 68°F, mm Hg	0.4	0.01	0.01
Freezing point, °F	50.9	82.4	70.2
Solubility at 68°F, wt %:			
In H_2O	Complete	96.4	Complete
Of H_2O in	Complete	.....	Complete
Absolute viscosity at 68°F, centipoises	24.1	380	1,013
Refractive index N_D at 68°F	1.4544	1.4747	1.4852
Heat of vaporization, Btu/lb	355	284	230

* Designations: MEA = monoethanolamine
DEA = diethanolamine
TEA = triethanolamine

SOURCE: (16-30).

Table 16-3. Sources of Equilibrium Data on Solubility of Acid Gases in Amines

System*	Temperature range, °C	Partial pressure range of acid gas	Reference
CO_2-DEA-H_2O	25–55	0–760 mm Hg	16-29
CO_2-TEA-H_2O	25–55	0–760 mm Hg	16-29
CO_2-MEA-H_2O	0–75	1–760 mm Hg	16-52
CO_2-DEA-H_2O	0–75	10–760 mm Hg	16-52
CO_2-TEA-H_2O	0–75	1–760 mm Hg	16-52
H_2S-MEA-H_2O	25–60	25–700 mm Hg	16-59
CO_2-MEA-H_2O	25–75	2.5–41 atm	16-51
CO_2-DEA-H_2O	25–75	2.5–41 atm	16-51
CO_2-H_2S-MEA-H_2O	15–50	0.050–66 mm Hg	16-48
CO_2-H_2S-DEA-H_2O	15–50	0.30–312 mm Hg	16-48
CO_2-MEA	25–70	2–42 atm	16-26
CO_2-MEA	60–140	.....	16-41
CO_2-MEA	100–140	1.5–15 atm	13-37
CO_2-H_2S-MEA	25–100	0–1 atm	16-52a

* Designations: MEA = monoethanolamine
DEA = diethanolamine
TEA = triethanolamine

The postulated over-all reactions for the acid gases and monoethanolamine are as follows:

For CO_2:

$$2HOCH_2CH_2NH_2 + H_2O + CO_2 \rightleftharpoons (HOCH_2CH_2NH_3)_2CO_3 \quad (16\text{-}3)$$

$$(HOCH_2CH_2NH_3)_2CO_3 + H_2O + CO_2 \rightleftharpoons 2HOCH_2CH_2NH_3HCO_3 \quad (16\text{-}4)$$

For H_2S:

$$2HOCH_2CH_2NH_2 + H_2S \rightleftharpoons (HOCH_2CH_2NH_3)_2S \quad (16\text{-}5)$$

$$(HOCH_2CH_2NH_3)_2S + H_2S \rightleftharpoons 2HOCH_2CH_2NH_3HS \quad (16\text{-}6)$$

It is supposed that the ratio of the bicarbonate to the carbonate form increases as the equilibrium partial pressure of CO_2 increases at a given temperature and amine concentration. Similarly, high partial pres-

Table 16-4. Equilibrium Data, Hydrogen Sulfide–Monoethanolamine–Water System

Moles of hydrogen sulfide per mole of amine, for monoethanolamine solutions corrected to identical values of amine molality

Partial pressure of H_2S, mm Hg	Molality of amine						
	0.6	1.0	1.5	2.0	3.0	4.0	5.0
At 77°F:							
700	1.148	1.086	1.050	1.033	1.011	0.998	0.991
600	1.126	1.072	1.041	1.025	1.004	0.991	0.984
500	1.101	1.058	1.032	1.016	0.996	0.980	0.974
400	1.080	1.042	1.020	1.006	0.985	0.971	0.963
300	1.053	1.022	1.002	0.990	0.970	0.955	0.945
200	1.027	0.998	0.979	0.966	0.946	0.931	0.918
100	0.986	0.956	0.934	0.919	0.893	0.870	0.852
50	0.934	0.902	0.876	0.856	0.819	0.784	0.758
25	0.866	0.833	0.802	0.777	0.730	0.687	0.643
At 113°F:							
700	1.124	1.051	1.011	0.988	0.958	0.940	0.927
600	1.097	1.033	0.996	0.975	0.948	0.928	0.914
500	1.070	1.012	0.980	0.960	0.934	0.913	0.899
400	1.045	0.993	0.961	0.943	0.918	0.897	0.880
300	1.011	0.967	0.939	0.921	0.891	0.869	0.850
200	0.971	0.929	0.900	0.880	0.846	0.819	0.800
100	0.908	0.864	0.826	0.795	0.748	0.714	0.684
50	0.826	0.782	0.742	0.706	0.648	0.601	0.564
25	0.731	0.686	0.631	0.601	0.533	0.487	0.453
At 140°F:							
700	1.083	1.040	0.998	0.968	0.934	0.909	0.891
600	1.056	1.011	0.970	0.944	0.910	0.884	0.865
500	1.027	0.984	0.945	0.916	0.880	0.858	0.837
400	0.995	0.952	0.912	0.885	0.848	0.821	0.801
300	0.960	0.916	0.876	0.847	0.810	0.778	0.753
200	0.908	0.863	0.822	0.793	0.751	0.714	0.683
100	0.811	0.757	0.708	0.674	0.624	0.581	0.547
50	0.694	0.634	0.576	0.532	0.474	0.425	0.386
25	0.551	0.490	0.433	0.388	0.331	0.291	0.285

SOURCE: (16-59).

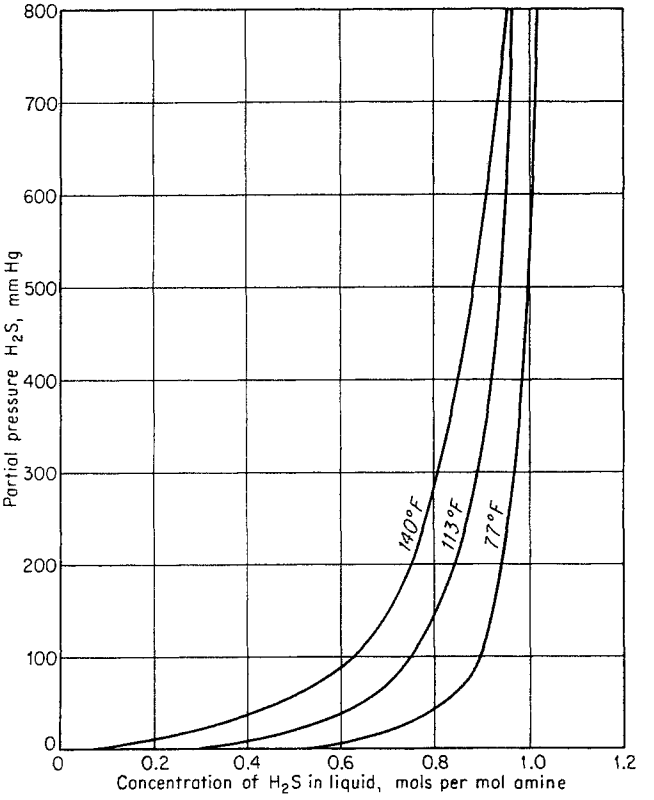

Fig. 16-33. Equilibrium pressure of H_2S from 15.5 wt %, 3 *M* monoethanolamine solution. (*Data from Riegger et al.*, 16-59.)

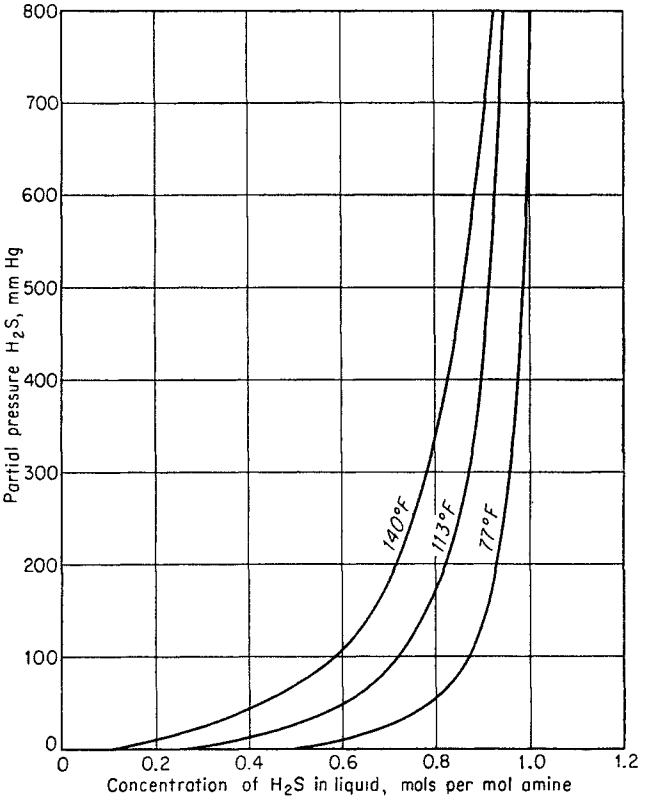

Fig. 16-34. Equilibrium pressure of H_2S from 19.7 wt %, 4 *M* monoethanolamine solution. (*Data from Riegger et al.*, 16-59.)

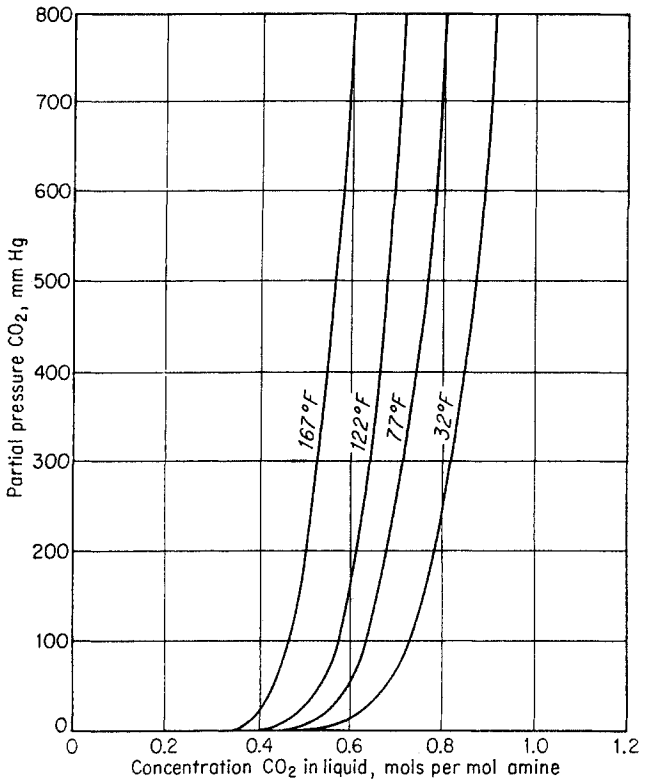

Fig. 16-35. Equilibrium pressure of CO_2 from 12.3 wt %, 2 M monoethanolamine solution. (*Mason and Dodge*, 16-52. *Courtesy AIChE.*)

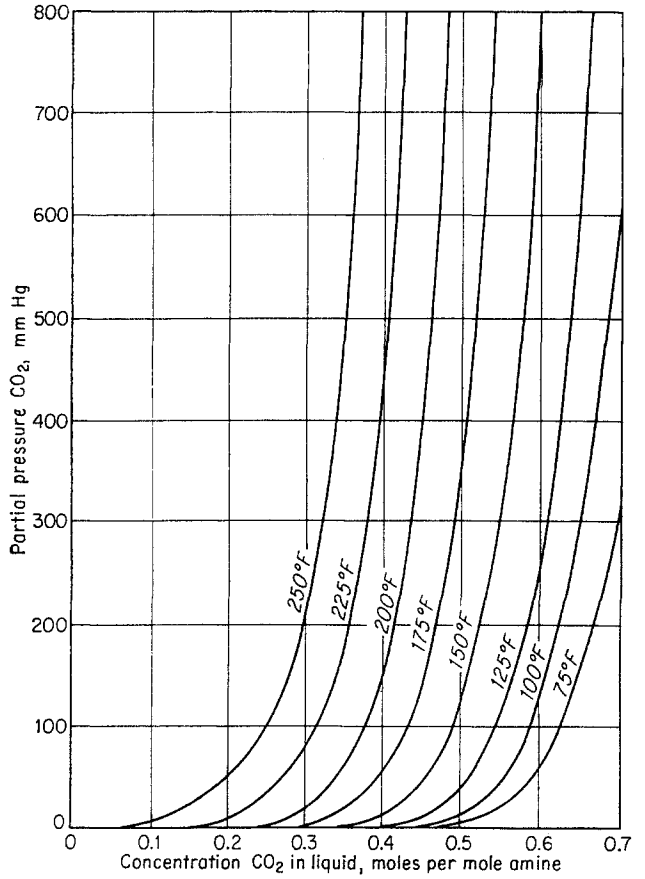

Fig. 16-36. Equilibrium pressure of CO_2 from 15 wt % monoethanolamine solution. (*Kohl*, 16-45; *Mason and Dodge*, 16-52. *Courtesy AIChE.*)

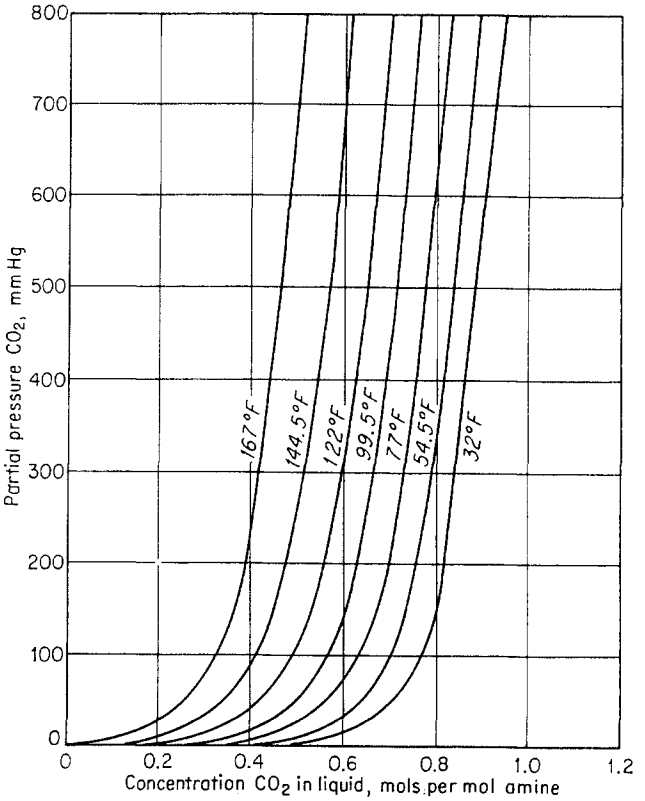

Fig. 16-37. Equilibrium pressure of CO_2 from 20.6 wt %, 2 M diethanolamine solution. (*Mason and Dodge*, 16-52. *Courtesy AIChE.*)

sures of H_2S increase the concentration of the amine hydrosulfide. The stoichiometric value representing complete chemical conversion of the amines may be exceeded at high partial pressures of the acid gases as a result of "physical" solution in addition to chemical reaction (16-26, 16-51).

The solubility data for mixtures of CO_2 and H_2S have been studied by Leibush and Shneerson (16-48). The total solubility of H_2S and CO_2 for the mixture was depressed slightly below that for either gas at low partial pressures of acid gas.

Figures 16-38 and 16-39 provide phase-equilibrium data for the water-amine systems which are applicable to calculations involving the separation of water from the amine in the reflux section of the stripper.

Density data on aqueous amine solutions are reproduced in Figs. 16-40 and 16-41, and the transport properties (viscosity and thermal conductivity) are presented in Figs. 16-42 to 16-44. In considering the possible application of pure monoethanolamine for the removal of CO_2 from inert gases, Chambers and Wall (13-8) have found that the reaction products of CO_2 and monoethanolamine produce highly viscous fluids whose viscosities show wide variation with temperature and with CO_2 concentration.

Thermal Properties

The thermal properties are required for rate calculations as well as for heat-and material-balance calcu-

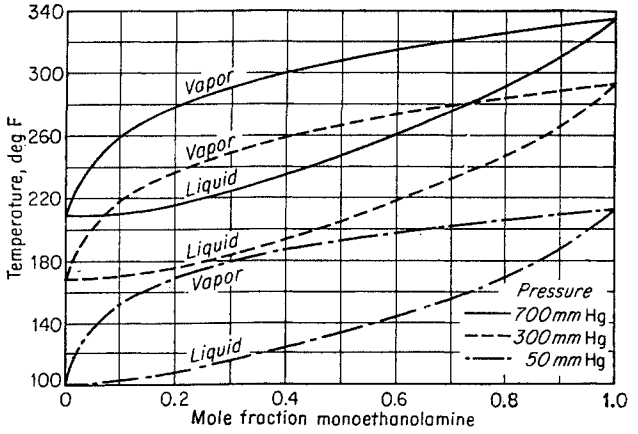

Fig. 16-38. Vapor-liquid compositions for aqueous monoethanolamine solutions. (16-38, *Courtesy Dow Chemical* Co.)

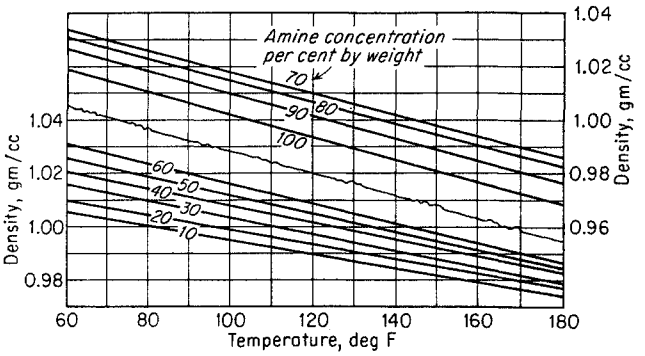

Fig. 16-40. Density of aqueous monoethanolamine solutions. (16-38, *Courtesy Dow Chemical* Co.)

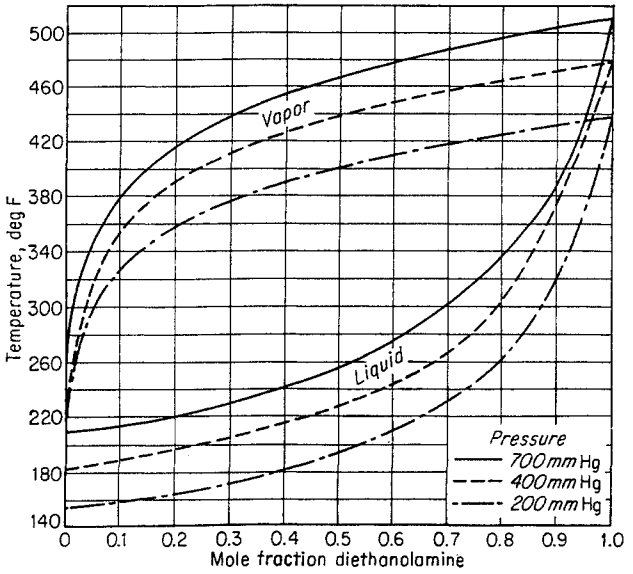

Fig. 16-39. Vapor-liquid compositions for aqueous diethanolamine solutions. (16-38, *Courtesy Dow Chemical* Co.)

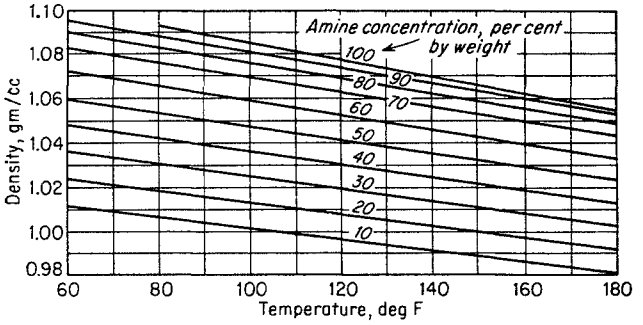

Fig. 16-41. Density of aqueous diethanolamine solutions. (16-38, *Courtesy Dow Chemical* Co.)

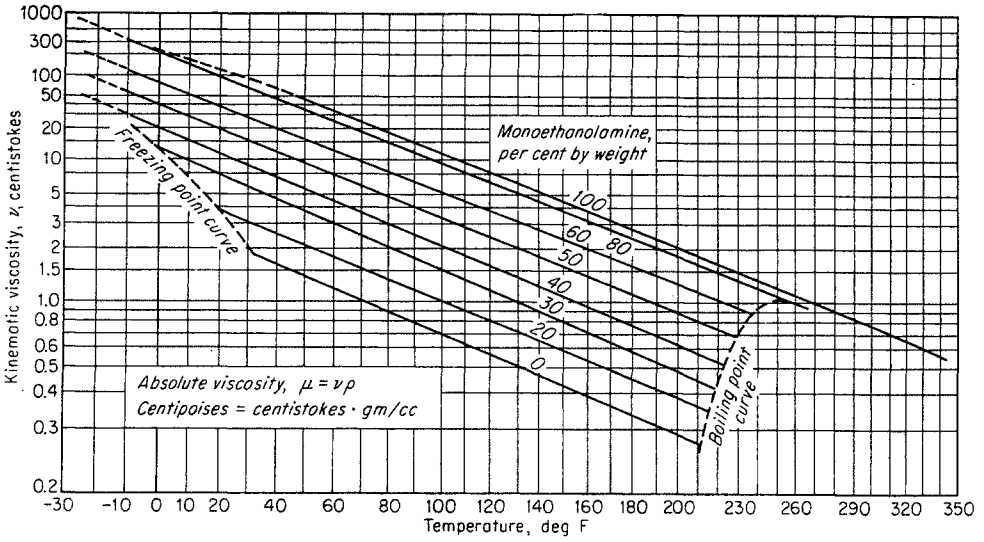

Fig. 16-42. Viscosity of aqueous monoethanolamine solutions. (16-30, *Carbide and Carbon Chemicals Co., Div. of Union Carbide Corp.*)

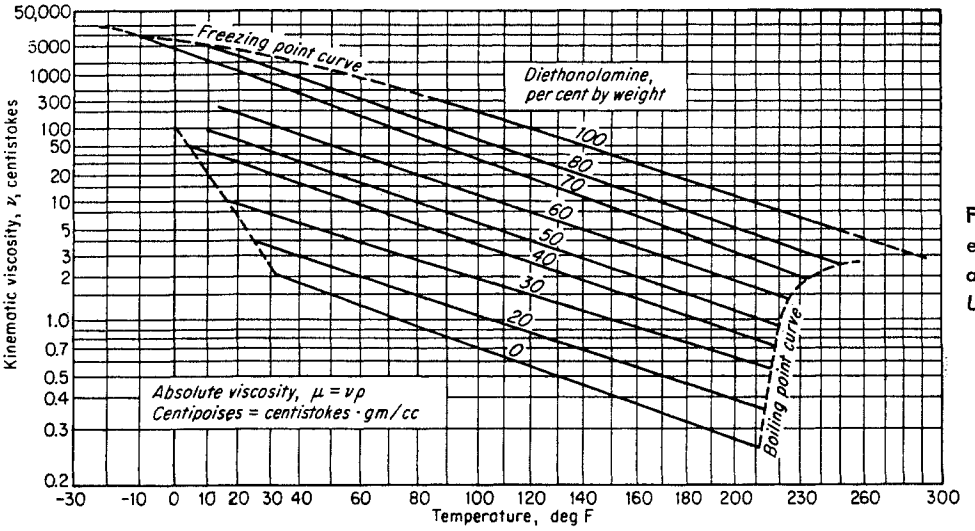

Fig. 16-43. Viscosity of aqueous diethanolamine solutions. (16-30, *Carbide and Carbon Chemicals Co., Div. of Union Carbide Corp.*)

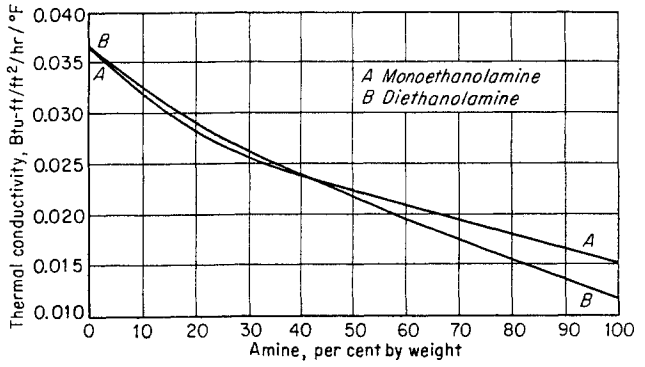

Fig. 16-44. Thermal conductivity of aqueous mono- and diethanolamine solutions at 35°C. (16-30, *Courtesy Carbide and Carbon Chemicals Co., Div. of Union Carbide Corp.*)

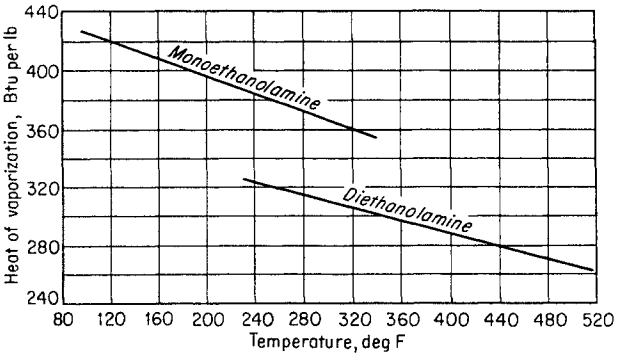

Fig. 16-45. Latent heats of vaporization of mono- and diethanolamine as pure substances (calculated—100 per cent material). (16-38, *Courtesy Dow Chemical Co.*)

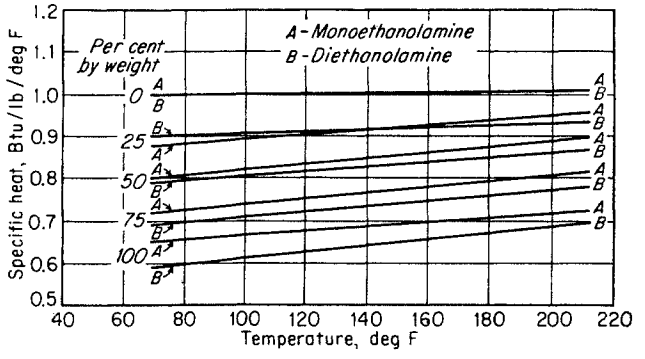

Fig. 16-46. Specific heat of aqueous mono- and diethanolamine solutions. (16-30, *Courtesy Carbide and Carbon Chemicals Co., Div. of Union Carbide Corp.*)

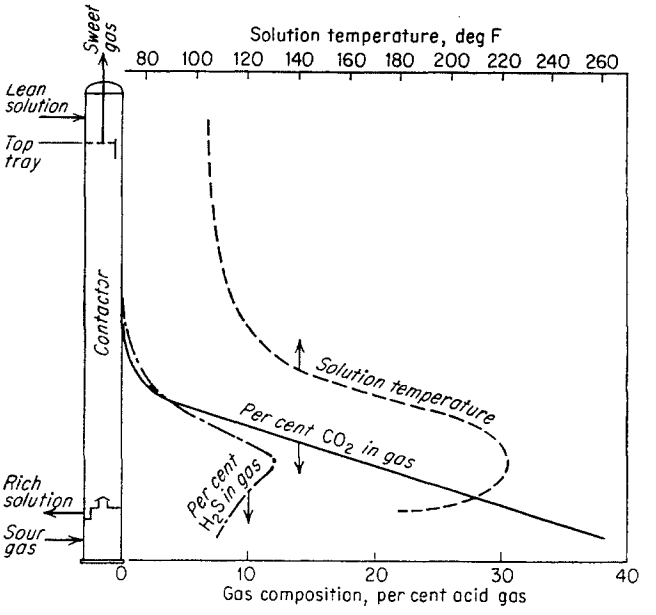

Fig. 16-47. Gas composition and temperature profile of contactor during run A-4. (*Kohl and Blohm, 16-44. Courtesy Petrol. Engr.*)

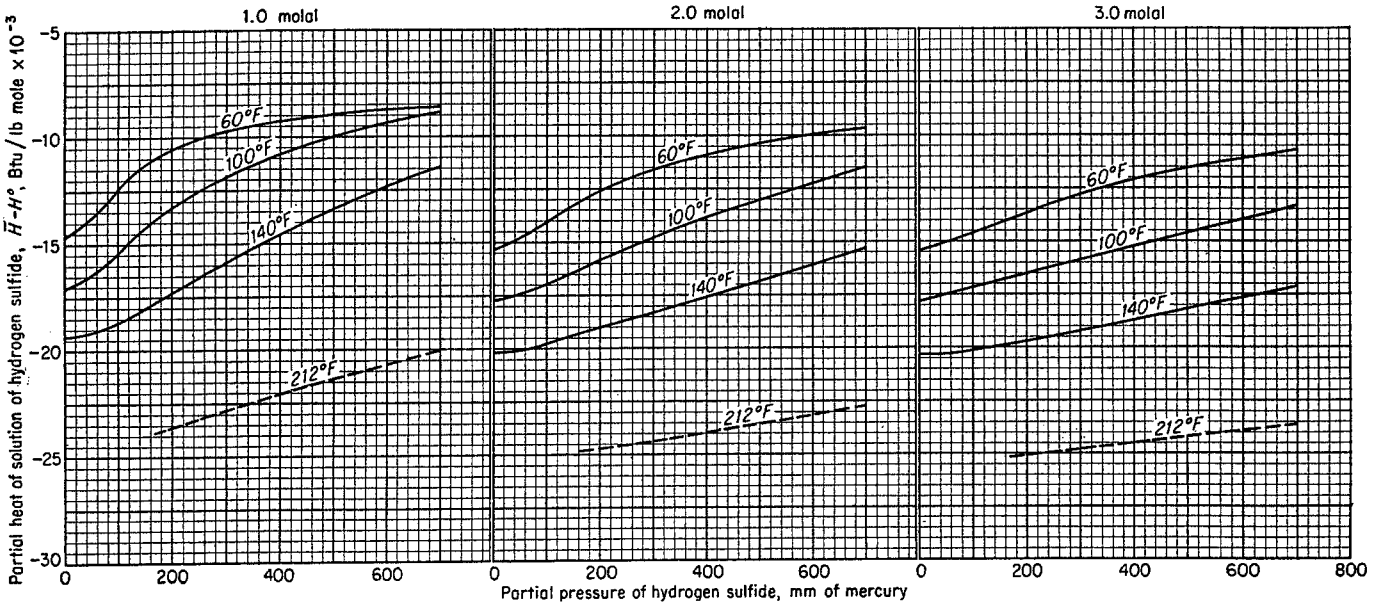

Fig. 16-48. Heat of solution of H_2S in monoethanolamine solutions. (*Yorizane*, 16-66.)

lations. The heats of vaporization of mono- and diethanolamine solutions are given in Fig. 16-45 (16-38) and the specific heats of their aqueous solutions are given in Fig. 16-46 (16-30).

Scant heat-of-absorption data for CO_2 and H_2S have been reported in the literature (16-28). Calculations based on these data and temperature profiles (Fig. 16-47) for the absorption of acid gases in monoethanolamine–diethylene glycol–water solutions (16-44) indicate that the heat of absorption imposes a severe limitation on the permissible concentration of monoethanolamine in the lean solution. Using high amine concentrations, the heat liberated by the chemical reaction may produce stripping of the acid gases on some intermediate trays in the absorber. Lyudkovskaya and Leibush (16-51) calculated the partial heats of solution of CO_2 in aqueous mono- and triethanolamine solutions and found them to be functions of amine concentration. Later, Yorizane (16-66) made a detailed thermodynamic analysis of the hydrogen sulfide–monoethanolamine system to compute the partial heat of solution of H_2S in aqueous monoethanolamine solutions. Although the validity of these data have not been checked experimentally, calculations show that the partial heat of solution of H_2S in monoethanolamine is a pronounced function of temperature, amine concentration, and the partial pressure of H_2S in the gas phase. The calculated heats of solution as functions of these variables are presented in Figs. 16-48 to 16-50. Since equilibrium conditions are far from being attained in a normal amine-contacting unit because of the limitations imposed by rate effects, the partial heat of solution

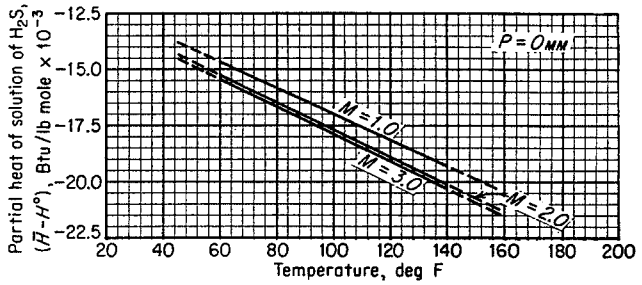

Fig. 16-49. Heat of solution of H_2S in monoethanolamine solutions for partial pressure of H_2S = 0 mm. (*Yorizane*, 16-66.)

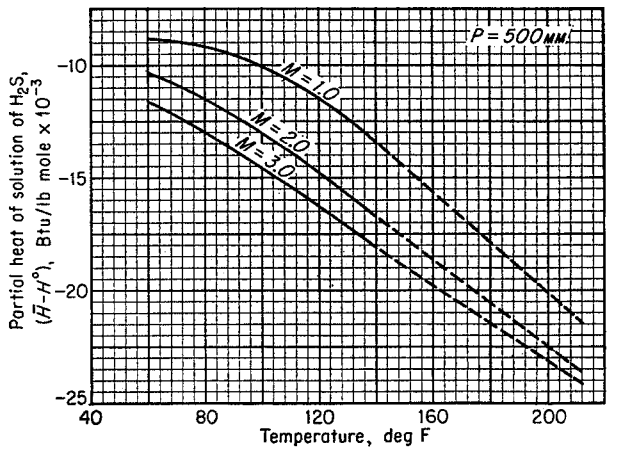

Fig. 16-50. Heat of solution of H_2S in monoethanolamine solutions for partial pressure of H_2S = 500 mm. (*Yorizane*, 16-66.)

of H_2S that is recommended for process calculations is the intercept value at zero partial pressure of H_2S at the temperature and amine concentration in question. A single experimental value for the partial heat of solution of CO_2 in monoethanolamine is given by Gregory and Scharmann (16-43); this value is 720 Btu per pound of CO_2 absorbed. Bottoms (16-28) reports heats of solution of 650 Btu per pound of CO_2 absorbed and 511 Btu per pound of H_2S absorbed for normal absorber conditions.

Absorption Calculations

Typical equilibrium relationships have been presented for systems comprised of acid gases, organic amines, and water. The formal design of absorbers, whether packed or plate columns, needs to take into account the rate of absorption. A net CO_2 removal of 0.12 to 0.20 std cu ft/gal per weight per cent of monoethanolamine is reported for monoethanolamine units. The net removal is obtained from the difference between CO_2 entering and leaving the absorber. The concentration of amine is generally taken between 10 and 30 wt % in order to maintain favorable viscosity characteristics, to minimize corrosion, and to provide sufficient heat capacity to absorb the effects of the high heats of solution of acid gases in the amine solution. Absorbers usually contain from 15 to 30 trays or an equivalent amount of tower packings. Conservative liquid flow rates in columns and piping and low generation temperatures have been recommended to reduce corrosion problems (16-39, 16-60).

Diameters of towers using plates with bubble caps may be sized according to conventional procedures. Packed-column design has been outlined by several authors (16-49, 16-58). Mass-transfer rates for the absorption of CO_2 in aqueous mono- and diethanolamine solutions in packed columns are available (16-34, 16-47).

The effect of type of amine on the over-all absorption coefficient for a 1-in. packed column is presented in Table 16-5. It should be noted that the low transfer coefficient for triethanolamine solutions prevents their use in conventional contacting equipment.

Table 16-5. Relative Effect of Type of Amine on the Over-all Absorption Coefficient for Packed Column

Liquid rate = 695 lb/(hr)(sq ft)
3–5 mole % CO_2 in gas
5% of amine converted to carbonate
Temperature of operation = 122°F

Amine	$K_g a$, *lb-moles/(hr)(cu ft)(atm)*
2 *M* monoethanolamine	6.89
2 *M* diethanolamine	2.83
3 *M* triethanolamine	0.295

SOURCE: (16-47, 13-37).

A publication by Kohl (16-46) permits a plate-to-plate calculation for the absorption of CO_2 in aqueous monoethanolamine solutions. His procedure will be presented in anticipation of similar procedures which may follow for calculating the absorption of H_2S and mixtures of acid gases from natural gases as soon as experimental tray-efficiency data are made available. The absorption of acid gases in organic solutions involves mass-transfer operations in which the absorption and the chemical reaction must be considered simultaneously. Equilibrium relationships that show low equilibrium partial pressure of the reacting gas provide maximum possible driving forces and, therefore, promote rapid over-all absorption rates. In addition to having the maximum possible gas-phase driving force, rapid removal of acid gases from the gas-liquid interface by chemical reaction tends to ensure high mass-transfer rates (16-55). The result is over-all mass-transfer rates much higher than those obtained in the solution of CO_2 in water (16-65), for example. However, CO_2 and H_2S do not dissolve readily in aqueous solutions, and, despite a rapid chemical reaction at the gas-liquid interface, the over-all tray efficiencies are low [9 to 23 per cent (16-55)]. It is estimated that the liquid-film resistance is 85 to 95 per cent of the total resistance for efficiencies typically encountered in CO_2 absorption units. Low tray efficiencies and an equilibrium line which coincides with the zero-partial-pressure line render calculations by equilibrium stages meaningless. Therefore, Kohl resorts to the use of actual tray efficiency expressed as the Murphree vapor efficiency for the entire plate, which is given by

$$E_{Mv} = \frac{y_{n+1} - y_n}{y_{n+1}} \tag{16-7}$$

where E_{Mv} = Murphree vapor efficiency for entire plate
y_{n+1} = mole fraction of acid gas entering tray n (leaving $n + 1$)
y_n = mole fraction of acid gas leaving tray n

It should be noted that the Murphree vapor efficiency taken at a point is numerically equal to the Murphree vapor efficiency over the whole plate, since the gas composition in equilibrium with the solution leaving each tray is essentially the same as it is with respect to the solution at any point on the tray, i.e., zero CO_2 or H_2S.

The individual tray efficiencies for the absorption of CO_2 in aqueous monoethanolamine solutions have been correlated by Kohl (16-46), using the following assumptions:

1. That the vapor pressure of CO_2 in equilibrium with the monoethanolamine is zero

2. That the liquid-film resistance controls the rate of absorption even though the chemical reaction is rapid and of second order

3. That the product of the interfacial-contact area and the over-all gas-film coefficients varies directly with the amine concentration and with the difference between the concentration of CO_2 in solution and its equilibrium value in the solution, inversely with the viscosity to the 0.68 power

4. That the dependence of the gas-film coefficient upon temperature and partial pressure can be expressed as simple exponential functions

5. That the interfacial-contact area for a given gas is a function solely of the gas velocity through the slots

In determining the empirical coefficients for the effect of partial pressure and temperature, and the viscosity exponents, reliance was placed on the data of Leibush and Shneerson (16-47). The final correlation is given in Fig. 16-51 and the correlation for the interface-contact area in Fig. 16-52. The key to the definition of terms in Fig. 16-51 is as follows:

K_g = over-all gas-film coefficient, lb moles/(hr)(sq ft)(atm)
μ = viscosity, centipoises
C = concentration of CO_2 in solution, moles per mole of monoethanolamine
A = contact area, sq ft per square foot of tray
M = amine concentration of solution, gram moles/liter
T = temperature, °F
p = partial pressure of acid gas, atm
V = actual gas volume, cu ft/hr per square foot of tray

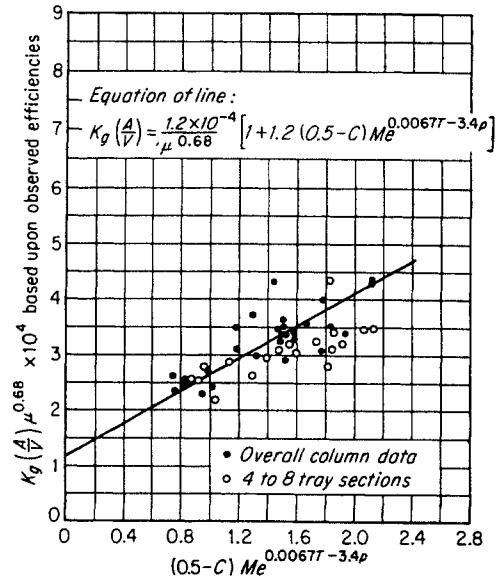

Fig. 16-51. Determination of $K_g(A/V)$ equation for CO_2 absorption in plate columns. (Kohl, 16-46. Courtesy AIChE.)

The Murphree vapor efficiency is then related to the over-all gas-film coefficient by the relation

$$E_{Mv} = 1 - e^{-K_g(A/V)RT_a} \qquad (16\text{-}8)$$

where A/V is obtained from Fig. 16-52

R = gas constant = 0.729 cu ft-atm/(lb mole)(°R)
V = actual gas volume, cu ft/hr per square foot of tray
T_a = absolute temperature, °R

The calculated values of the Murphree vapor efficiency E_{Mv} may be applied to determine the relations among

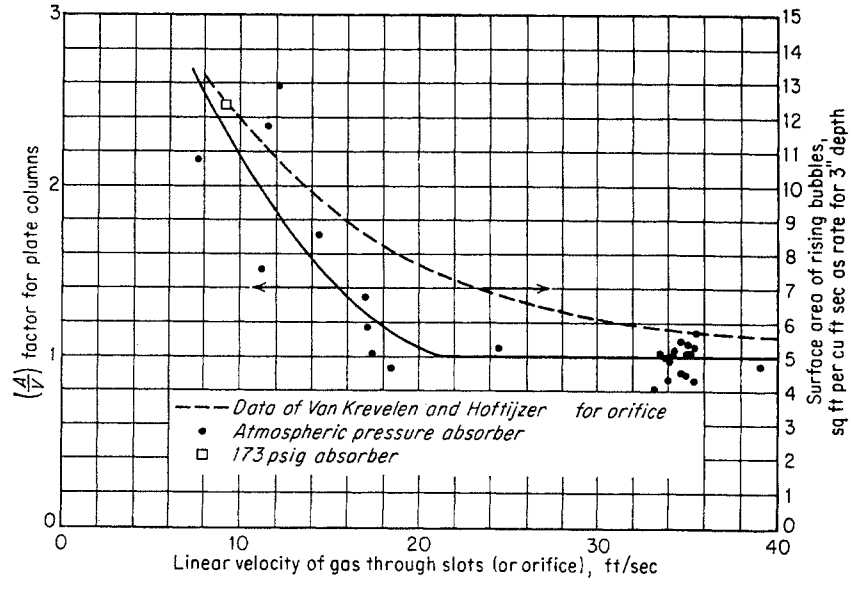

Fig. 16-52. Effect of gas velocity through slots on the interfacial area in bubble-plate columns. (Kohl, 16-46. Courtesy AIChE.)

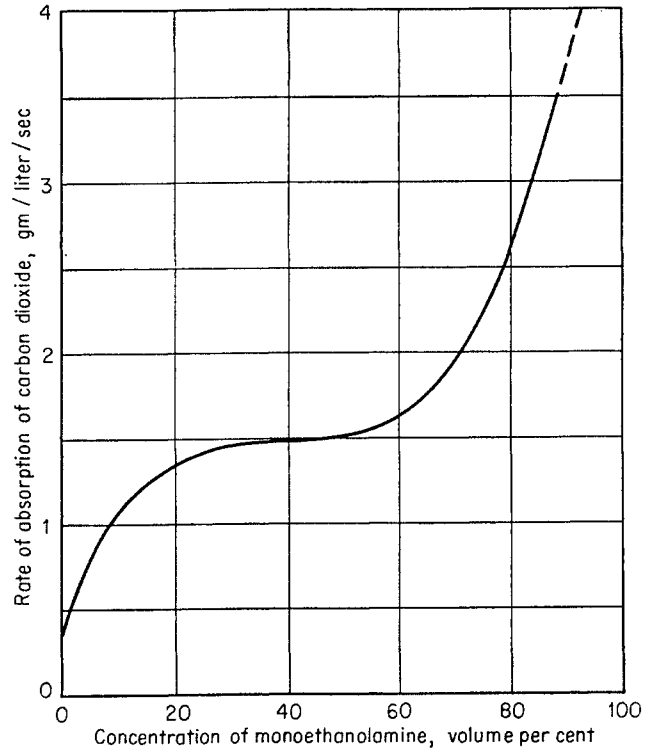

Fig. 16-53. Influence of the concentration of monoethanolamine on the rate of absorption. (*Dixon*, 16-36. *Courtesy Carbide and Carbon Chemicals Co., Div. of Union Carbide Corp.*)

the gas concentration, the solution concentration, and the number of theoretical trays. It should be noted that the graphical solution does not specify the ratio of gas rate to liquid rate. This follows from the fact that the slope of the equilibrium line is, in fact, equal to zero (13-37).

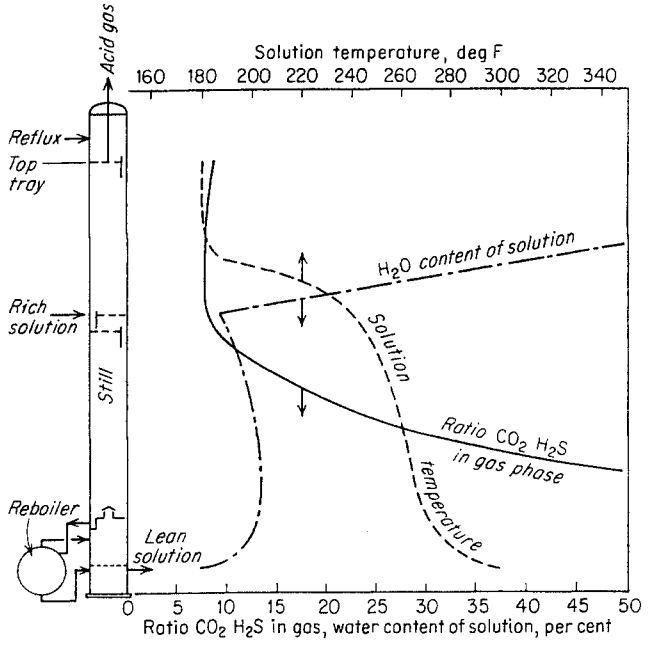

Fig. 16-54. Composition and temperature profile on still and reboiler during run A-2. (*Kohl and Blohm*, 16-44. *Courtesy Petrol. Engr.*)

The problem of increasing the rate of absorption of CO_2 in pure monoethanolamine has attracted considerable attention in England (16-31, 16-36). It has been observed that there is a rapid increase in the rate of absorption of CO_2 during drop formation as the amine concentration increases beyond 60 vol % of monoethanolamine in water. The relative rate of absorption of CO_2 over a considerable amine-concentration range during drop formation is depicted in Fig. 16-53 (16-36). Concentrated amine solutions would lead, also, to high absorption capacities.

Recourse to centrifugal absorbers (16-31, 16-36) is based on the observation that the rate of gas absorption during the period of formation of a drop (or bubble) is very high because of the turbulence produced within the drop during its formation (16-37). Thus, the repeated formation of new interfacial surfaces, as in a centrifugal absorber (16-36), will lead to high contact efficiencies. Whether these studies will lead to results that are applicable to large-scale gas purification is not known at the present time. The centrifugal absorber solves problems that arise from high liquid viscosities, but those resulting from high heats of absorption remain unsolved.

Stripping Column

The absence of tray-efficiency and thermal data does not permit rigorous stripper calculations. Instead, reliance is placed on heat-and-material-balance calculations which are based on workable exit- and inlet-stream conditions.

Figure 16-54 gives the temperature and composition profiles of still and reboiler for a plant using a glycol-amine-water solution. The water content of the solution rises rapidly above the feed tray and approaches 100 per cent at the top tray.

Top-plate temperatures ranging from 150 to 190°F are sufficient to maintain negligible amine losses overhead. Figure 16-55 gives the volatility of amines from solutions. Under these conditions the feed is preheated to temperatures slightly in excess of 200°F. Reflux ratios of 0.007 to 0.009 gal of water per standard cubic foot of acid-gas product are reported for glycol-amine strippers (16-44). Complete regeneration of the lean solution is not possible at temperatures that are reasonable from the standpoint of corrosion. For a 23.2 mole % monoethanolamine concentration using a regeneration temperature of 278°F, a lean-solution concentration of 0.039 std cu ft/gal per per cent of monoethanolamine is reported (13-37). Considerably lower CO_2 concentrations are reported for lean solutions from glycol-amine strippers operating with reboil temperatures of 300°F (16-44).

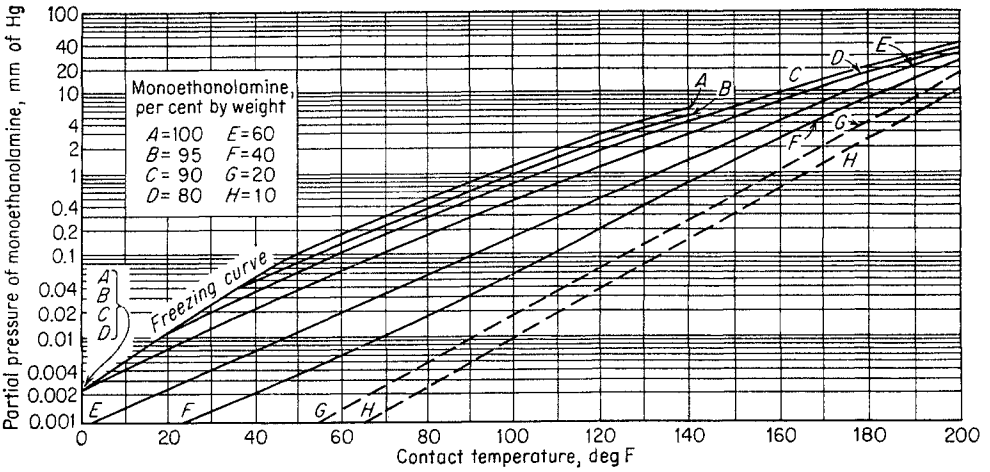

Fig. 16-55. Volatility of aqueous monoethanolamine solutions. (16-30, *Courtesy Carbide and Carbon Chemicals Co., Div. of Union Carbide Corp.*)

Reboiler steam requirements vary from 0.5 to 1.2 lb per gallon of solution, depending on the effectiveness of the feed preheater and the stripping temperature.

The overhead-condenser duty may be computed by assigning values for the top-plate temperature, the reflux ratio, and the acid gas leaving the regenerator overhead. It follows that the amount of water leaving the top plate may be computed from the relation

$$\frac{W}{G} = \frac{p_w}{P - p_w} \qquad (16\text{-}9)$$

where W = moles of water in vapor leaving top plate
G = moles of acid gas leaving top plate
p_w = vapor pressure of water at top-plate temperature
P = total pressure at top plate

Then the heat duty of the condenser is essentially the heat duty required to cool the acid gas and condense the water.

The heat duty of the reboiler follows from a material-and-heat balance around the whole tower. Allowance should be made for the heat of decomposition of the amine salts during the stripping operation.

Corrosion in Gas-sweetening Plants

An important consideration in the design and operation of gas-sweetening plants is the corrosion of the component parts. One company lists the operational problems of gas-sweetening plants in the following order of importance: corrosion, amine losses, and frequency of operational upsets caused by foaming, loss of sweetening specifications, etc. (16-39). On the basis of field observations and research work, solutions have been recommended, some tentatively, to minimize corrosion problems (16-33, 16-39). Paredes (16-54) has shown that reclaiming of the amine solution reduces corrosion.

The term "stress corrosion" refers to the increased susceptibility of materials to corrosive attack when under a state of stress (16-57), either imposed or residual. In amine plants stress corrosion is associated with residual stresses which are due to localized heating, as in welds. One characteristic of stress corrosion is the intergranular nature of the cracking. Several cases of stress-corrosion cracking have been reported in various components of amine gas-treating plants [Fig. 16-56 (16-42)]. The cracking was con-

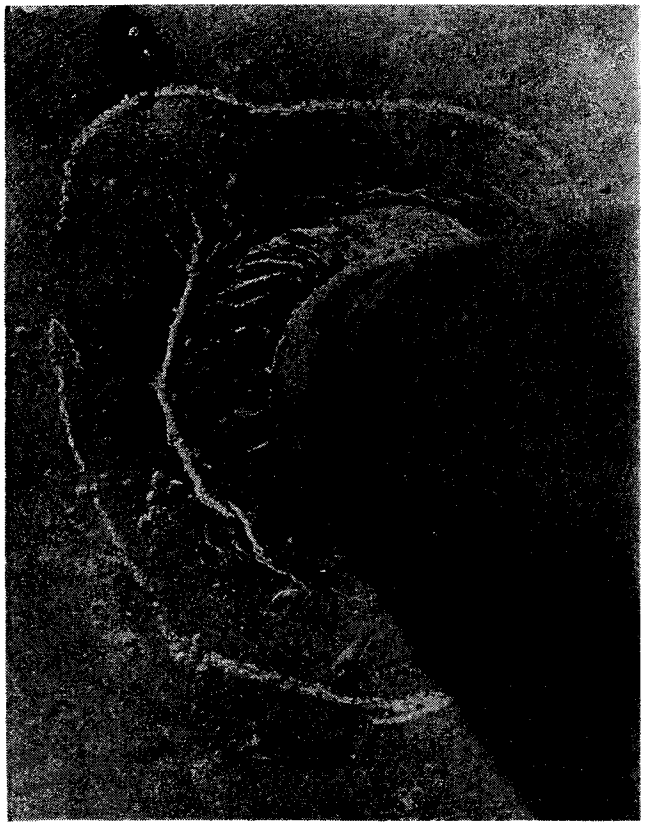

Fig. 16-56. Magnetic-particle indications revealing stress-corrosion cracks adjacent to weld joining 2-in. drain nozzle to bottom head of absorber. (*Garwood*, 16-42. *Courtesy Phillips Petroleum Co. and NGAA.*)

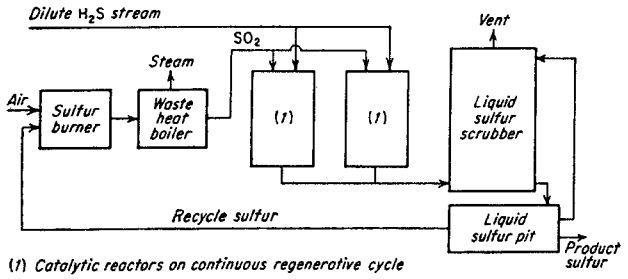

Fig. 16-57. Desulfurization of and sulfur recovery from dilute hydrogen sulfide gases. (*Gamson and Elkins*, 16-40a. *Courtesy AIChE.*)

fined to the vicinity of welds in absorbers, strippers, and even along piping. Stress corrosion may be averted by stress-relieving, by thermal means, all major equipment in contact with corrosive gases and solutions (16-33, 16-42).

Other types of corrosion in gas-treating plants have been attributed to:

1. Decomposition products of amines
2. Oxidation products of amines
3. Acid gases in the presence of condensed water

At regeneration temperatures, mono- and diethanolamine decompose to form corrosive compounds. Simultaneous analyses of monoethanolamine before and after prolonged heating for primary amine strength, alkalinity, and total nitrogen show that considerable rearrangement takes place as a result of the heating (16-39, 16-56). One change that takes place is increase, with use, in the power of the amines to dissolve powdered iron. The corrosiveness of used amine solutions, however, may be appreciably reduced by redistilling a fraction of the recycled stream in a "reclaimer" (16-54).

The corrosive nature of acid gases in the presence of condensed water has long been known. In stripping columns using glycol-amine-water solutions, the corrosion of steel has been found to be most severe where vapor condensate appears as a result of falling temperatures. High corrosion rates have been observed in oil-amine exchangers where temperatures in the neighborhood of 500°F have been used. Under certain conditions aluminum alloys have been found to be superior to steel (16-61).

General recommendations to mitigate corrosion in amine plants, outlined by Feagan et al. (16-39), are:

1. Use of low reboiler heating-medium temperatures (preferably less than 400°F)
2. Use of low amine concentrations (from 10 to 20 wt % amine)
3. Use of an amine-distillation purifier or "reclaimer"
4. Use of an effective filter for the recirculated solution
5. Stress relieving of major equipment
6. Use of low reactivator pressure
7. Avoiding the use of dissimilar metals

In addition, it is recommended that consideration be given to the use of packed towers with cemented tower lining.

Conversion of H_2S to Sulfur

The H_2S recovered from sour natural gases may be converted into elemental sulfur. A review of the literature and processes used is given by Gamson and Elkins (16-40a). The processes depend upon the partial vapor-phase oxidation of H_2S to S, as in Eq. (16-10).

$$H_2S + \tfrac{1}{2}O_2 \rightarrow H_2O + S \qquad (16\text{-}10)$$

The process problems are to control the temperature resulting from the exothermic reaction and to recover the sulfur as a liquid after it passes through a catalytic converter. Figure 16-57 presents the Jefferson Lake process.

Several commercial plants are producing sulfur from H_2S recovered from natural gas.

CHAPTER 17

Transmission to Market

Natural gas is transported to market by long-distance pipelines (Fig. 1-1). The design and construction of these pipelines is of interest, as well as of the compressor stations which provide the motive power. Protection from corrosion is an important aspect in completing a project. Once the gas has reached the market area, it is often sold to a distributor through a city gate station. Pressure regulation, metering, and odorization normally take place at this point. Gas flows through low-pressure distribution systems to the domestic and commercial market.

DESIGN OF PIPELINES

With the tremendous expansion of markets for natural gas in the past few years, the concept of pipeline design has changed considerably. Formerly, a pipeline to supply a specific market was designed to handle its present load plus a moderate growth of perhaps 15 to 30 per cent. Today, a pipeline is designed at maximum diameter, with a minimum number of compression stations in order not to exceed a reasonable unit transportation cost at the present market demand. The thought is that expansion to meet an expanded future market demand will soon be required, and that this can be accomplished by adding compressor stations. The market expansion will lower the unit transportation cost.

Table 17-1 shows the steps in order in completing a pipeline project.

Tab e 17-1. Steps in a Pipeline Project

1. Market survey—immediate and prospects for growth
2. Pipe size and working pressure
3. Pipe specifications
4. Map of tentative route
5. Bill of materials
6. Total cost estimate
7. Certificate of convenience and necessity
8. Right of way
9. Construction survey
10. Construction contract
11. Construction
12. Testing
13. Putting in service

Use of Flow Formulas

The various flow formulas are developed and discussed in detail in Chap. 7, Flow and Compression Calculations. The Panhandle formula or slight modifications of it are in most common use in the natural gas industry for design of cross-country pipelines. The Panhandle formula, given earlier as Eq. (7-33), may be written as follows:

$$Q = 435.87E \left(\frac{T_0}{P_0}\right)^{1.07881} \left(\frac{P_1^2 - P_2^2}{G^{0.8539} TL}\right)^{0.5394} d^{2.6182} \tag{17-1}$$

where Q = flow rate measured at T_0 and P_0, cu ft/day
E = pipeline efficiency
T_0 = temperature base, °R
P_0 = pressure base, psia
P_1 = inlet pipeline pressure, psia
P_2 = outlet pipeline pressure, psia
G = gravity of gas
T = mean flowing temperature, °R
L = length of pipe, miles
d = internal pipe diameter, in.

Fig. 17-1. Chain saw for clearing right of way. (*Courtesy H. C. Price Company.*)

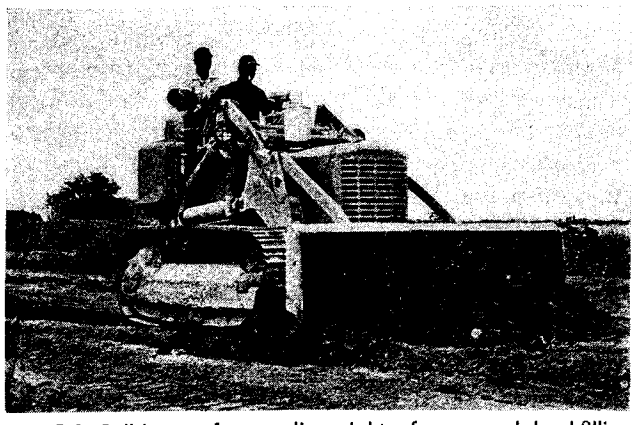

Fig. 17-2. Bulldozers for grading right of way and backfilling.

Substituting

$$T_0 = 60°\text{F} + 460 = 520°\text{R}$$
$$P_0 = 14.735 \text{ psia}$$
$$T = 60°\text{F} + 460 = 520°\text{R}$$
$$G = 0.600$$

the equation becomes

$$Q = 883E\left(\frac{P_1^2 - P_2^2}{L}\right)^{0.5394} d^{2.6182} \qquad (17\text{-}2)$$

The pipeline efficiency can vary between 85 and 95 per cent, and an average value of 92 per cent is often used. If the inside walls of the pipe were clean and smooth and if the pipeline were in perfect condition, an efficiency of 100 per cent could be attained. Slide rules have been developed using this formula, for example, the Grizzle gas-pipeline slide rule (7-19) and the Hutchison calculator (17-16a). With the Hutchison calculator, flow calculations can be made from the Panhandle, Weymouth, or Spitzglass formulas. The Spitzglass formula is used for design of distribution systems and will be discussed under that section of this chapter. With these slide rules one can make gas-flow computations quickly and efficiently.

Ford, Bacon, and Davis, Inc., Engineers (17-12), have developed a flow formula for design of pipelines. Their formula, Eq. (7-34), is similar to the Panhandle formula and may be expressed as follows:

$$Q = 840EMN\left(\frac{P_1^2 - P_2^2}{L}\right)^{0.541} d^{2.625} \qquad (17\text{-}3)$$

where M = measurement-base adjustment factor

$$= \frac{14.735}{P_0}\,\frac{T_0}{520}$$

N = gas-characteristic adjustment factor

$$= B^{0.54}\left(\frac{0.6}{G}\right)^{0.46}\left(\frac{7.0}{\mu}\right)^{0.08}\left(\frac{520}{T}\right)^{0.54}$$

where B = 1 + deviation from Boyle's law at average pressure = $1/z$

z = compressibility factor

μ = viscosity, English absolute units $\times 10^6$, or centipoises $\times$ 672

and where $Q, E, P_0, T_0, G, T, d, P_1, P_2, L$ are the same as in the Panhandle formula.

Fig. 17-3. Truck with pipe trailer for stringing pipe. (*Courtesy H. C. Price Company.*)

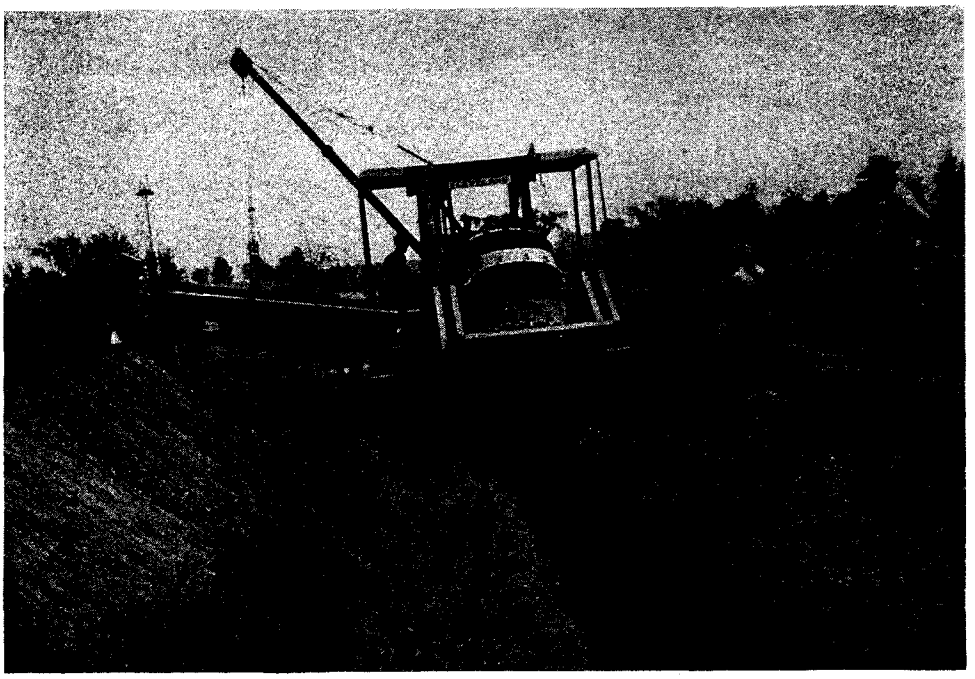

Fig. 17-4. Ditching machine.

Substituting

$T_0 = 60°F + 460 = 520°R$
$P_0 = 14.735$ psia
$B = 1.75$ per cent per 100 psi
$= 1 + 0.0175(750/100)$
$= 1.1313$ (average line pressure = 750 psia; alternatively $1/z = 1/0.884 = 1.1313$)
$G = 0.600$
$\mu = 7.0$ English absolute units $\times 10^6(0.0104 \times 672 = 7.0)$
$T = 60°F + 460 = 520°R$

the equation becomes

$$Q = 898E\left(\frac{P_1^2 - P_2^2}{L}\right)^{0.541} d^{2.625} \qquad (17\text{-}4)$$

Illustrative Problem

Given a market area with a present peak-day demand of 60 MMcf located 50 miles from an underground storage field. A pressure of 200 psig is needed at the city gate station to distribute the gas. Compression is installed at the storage field and a maximum pressure of 1,000 psig is available. Prospects for growth in the market area are to a peak-day demand of 80 MMcf in 5 years and 100 MMcf in 10 years. What diameter pipeline should be constructed?

Solution

Substituting in the Panhandle formula,

$$60{,}000{,}000 = 883 \times 0.92\left(\frac{1{,}015^2 - 215^2}{50}\right)^{0.5394} d^{2.6182} \qquad (17\text{-}5)$$

$d = 9.4$ in.

It is calculated that a pipeline with an ID of 9.4 in. would supply this present market. Since standard pipe can be purchased only in even-numbered diameters it would be necessary to construct a 10-in. pipeline. When the future is considered, it is seen that 10 years hence a pipeline with an internal diameter of 11.5 in. would be needed. At least a 12-in. pipeline should be constructed, and it might be advisable to go to a 16-in. line (14-in. pipe is not readily available) if the future prospects for growth were especially good. A 12-in. pipeline could deliver 113 MMcf/day and a 16-in. line (15.25 in. ID), 211 MMcf/day. Horsepower requirements at the storage field might make it advisable to operate at a lower inlet pressure, which would make a 16-in. line more desirable. Normal procedure would be to establish a pipe diameter large enough to supply the present market peak-day load with a minimum of compression. Future growth in the market or markets can then be handled by the addition of horsepower.

Long-distance (1,000 miles or more) pipelines are usually designed in the same manner with a minimum of horsepower for the initial capacity. These lines can be designed to handle annual market requirements and not peak-day demands, provided that sufficient storage is available at the market end of the line.

Engineering Design and Specifications

Coupled with the selection of a pipeline diameter is the establishment of the maximum working pressure on the pipeline. The American Society of Mechanical Engineers (ASME) has published a code (17-4) which states in detail the limitations on design pressures, dependent upon steel specifications, type of weld, and type of construction—cross-country or in heavily

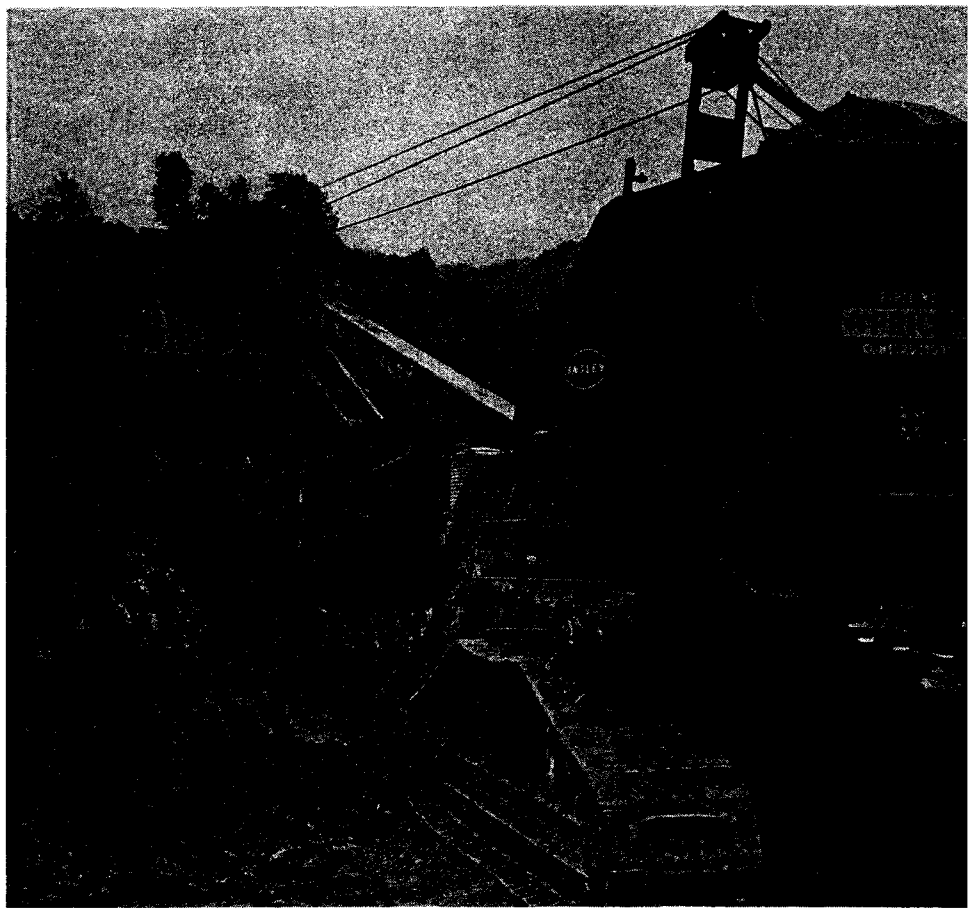

Fig. 17-5. Backhoe crane. (*Courtesy H. C. Price Company.*)

populated areas. The code is commonly called the ASA B31.1 code.* It is accepted in the natural gas industry, although some states have placed added restrictions upon pipeline construction within their boundaries and these must be obtained from the individual states.

The code (17-4) presents the following steel-pipe-design formula for gas transmission and distribution:

$$P = \frac{2St}{D} FET \qquad (17\text{-}6)$$

where P = design pressure, psig
S = specified minimum yield strength of pipe, psi
D = nominal outside diameter of pipe, in.
t = nominal wall thickness, in.
F = construction-type design factor
E = longitudinal-joint factor
T = temperature-derating factor

* Tables 17-3 to 17-7 and 17-11 to 17-14 are extracted from American Standard Gas Transmission and Distribution Piping Systems (ASA B31.1.8–1955, Section 8 of "American Standard Code for Pressure Piping," ASA B31.1–1955), with the permission of the publisher, The American Society of Mechanical Engineers, 29 West 39th St., New York 18, N.Y.

The American Petroleum Institute (API) has published specifications (17-2, 17-3) for high-test line pipe. Most steel companies manufacture pipe according to these specifications. The standard grades of pipe that can be purchased and the specified minimum yield strength of the various grades are given in Table 17-2. Table 17-3 gives the values of design factor F for various types of construction.

A description of where each construction type, A, B, C, or D, may be used is given in Table 17-4.

Table 17-2. American Petroleum Institute Grades of Pipe and Minimum Yield Strength

Grade	*Minimum yield strength, psi*
A	30,000
B	35,000
X42	42,000
X46	46,000
X52	52,000

Table 17-3. Values of Design Factor F

Construction type	*Design factor F*
A	0.72
B	0.60
C	0.50
D	0.40

SOURCE: ASA B31.1 code (17-4).

Many railroads and state and county highway departments require a casing around the pipeline underneath the railroads and highways. The class of location referred to in Table 17-4 has to do mainly with population density and is described in Table 17-5.

The 1-mile population-density index is the number of buildings intended for human occupancy in 1 sq mile of land with the pipeline crossing the center of it. The 10-mile population-density index is the average 1-mile index over a length of 10 consecutive miles where any 1-mile index exceeding 20 is averaged at 20.

Table 17-6 gives values of the longitudinal-joint factor E for various types of welding and steel specifications. It can be observed from this table that the American Society for Testing Materials (ASTM) has

Table 17-4. Classification of Steel-pipe Construction

Four types of steel-pipe construction are prescribed in this code. The distinguishing characteristics of each type and the locations in which each type shall be used are as follows:

A. Characteristics.....	Type A construction	Type B construction	Type C construction	Type D construction
1. Design factor F....	0.72	0.60	0.50	0.40
B. Locations where type of construction shall be used	*a.* On private rights of way in class 1 locations *b.* Parallel encroachments on: Privately owned roads in class 1 locations Unimproved roads in class 1 locations *c.* Crossings without casings of privately owned roads in class 1 locations *d.* Crossings in casings of unimproved public roads, hard-surfaced roads, highways or public streets, and railroads in class 1 locations	*a.* On private rights of way in class 2 locations *b.* Parallel encroachments on: Privately owned roads in class 2 locations Unimproved public roads in class 2 locations Hard-surfaced roads, highways or public streets, and railroads in class 1 locations *c.* Crossings without casings of: Privately owned roads in class 2 locations Unimproved public roads in class 2 locations Hard-surfaced roads, highways or public streets, and railroads in class 1 and class 2 locations *d.* Crossings in casings of: Hard-surfaced roads, highways or public streets, and railroads in class 2 locations *e.* On bridges in class 1 and class 2 locations *f.* Fabricated assemblies in pipelines in location classes 1 and 2	*a.* On private rights of way in class 3 locations *b.* Parallel encroachments on: Privately owned roads in class 3 locations Unimproved public roads in class 3 locations Hard-surfaced roads, highways or public streets, and railroads in class 3 locations *c.* Crossings without casings of: Privately owned roads in class 3 locations Unimproved public roads in class 3 locations Hard-surfaced roads, highways or public streets, and railroads in class 2 and 3 locations *d.* Compressor-station piping	*a.* In all locations in location class 4

It is necessary to distinguish between construction types, as defined by Section A of this table, and location classes, to avoid confusion. If pipelines or mains are located in private rights of way, the code prescribes that type A construction be used in class 1 locations, type B construction in class 2 locations, type C construction in class 3 locations, and type D construction in class 4 locations. There are many exceptions to this association of class 1 with type A, etc., however, as this table shows, most of which are cases where pipelines or mains are located in highways or on bridges, etc.

SOURCE: ASA B31.1 code (17-4).

Table 17-5. Classifications of Locations

Class	*Description*
1	Waste lands, deserts, rugged mountains, grazing land, and farm land, provided that 10-mile population-density index is 12 or less
2	Fringe areas around cities and towns and farm or industrial areas where 1-mile density index exceeds 20 or 10-mile density index exceeds 12
3	Area subdivided for residential or commercial purposes where, at time of construction, less than 10 per cent of lots abutting on street or right of way are built upon and where a class 4 classification is not called for
4	Areas where multistory (four or more floors above ground including ground floor) buildings are prevalent, and where traffic is heavy or dense, and where there may be numerous other utilities underground

SOURCE: ASA B31.1 code (17-4).

Table 17-6. Longitudinal Joint Factor E

Spec. no.	Pipe type	E factor
ASTM A53	Seamless	1.00
	Electric resistance welded	1.00
	Furnace lap welded	0.80
	Furnace butt welded	0.60
ASTM A106	Seamless	1.00
ASTM A134	Electric fusion welded	0.80
ASTM A135	Electric resistance welded	1.00
ASTM A139	Electric fusion welded	0.80
ASTM A155	Electric fusion welded	1.00
API 5L	Seamless	1.00
	Electric resistance welded	1.00
	Electric flash welded	1.00
	Furnace lap welded	0.80
	Furnace butt welded	0.60
API 5LX	Seamless	1.00
	Electric resistance welded	1.00
	Electric flash welded	1.00
	Submerged arc welded	1.00

SOURCE: ASA B31.1 code (17-4).

Table 17-7. Temperature-derating Factor T for Steel Pipe

Temperature, °F	*Temperature-derating factor T**
250 or less	1.000
300	0.967
350	0.933
400	0.900
450	0.867

* For intermediate temperatures, interpolate for derating factor.

SOURCE: ASA B31.1 code (17-4).

several steel specifications also. The API specifications 5L and 5LX (17-2, 17-3) are in more common use in the natural gas industry.

Table 17-7 gives values of the temperature-derating factor T for various maximum pipeline flowing temperatures.

All normal pipeline operation is at temperatures under 250°F, so the temperature derating factor would be 1.000.

Illustrative Problem

What would be the extra cost of purchasing 1 mile of 24-in. API, 5LX42 pipe for a design pressure of 1,000 psig, as compared with a design pressure of 800 psig, at a steel cost of $100 per ton? The pipe is electric-resistance-welded, will be constructed under type A construction, and will operate under 250°F.

Solution

Substituting in Eq. (17-6),

$$800 = \frac{2 \times 42{,}000t}{24} 0.72 \times 1.00 \times 1.00$$

$t = 0.3175$ in. for 800 psig design pressure
$t = 0.3968$ in. for 1,000 psig design pressure

Standard 24-in. pipe can be purchased with wall thicknesses of 0.250, 0.281, 0.312, 0.344, 0.375, 0.406, 0.438, and 0.500. It would be necessary to use pipe with a wall thickness of 0.344 weighing 86.85 lb/ft for an 800-psig design pressure and a wall thickness of 0.406 weighing 102.37 lb/ft for a design pressure of 1,000 psig. The costs would then be

$$\text{1,000 psig} \quad \frac{102.37 \times 5{,}280}{2{,}000} \times \$100 = \$27{,}025.68$$

$$\text{800 psig} \quad \frac{86.25 \times 5{,}280}{2{,}000} \times \$100 = 22{,}928.40$$

Extra cost for 1,000 psig design pressure = $ 4,097.28

The design pressure P in Eq. (17-6) shall not exceed 60 per cent of the mill-test pressure for furnace-butt-welded pipe or 85 per cent of the mill-test pressure for all other types of welded pipe, according to the ASA B31.1 code (17-4). Mill-test pressures are given in table form for all standard diameters and wall thicknesses in the API specifications 5L and 5LX (17-2, 17-3). These mill-test requirements may be calculated from the following formula, which is given in the specifications.

$$P' = \frac{2S't}{D} \text{ or } 3{,}000, \text{ whichever is smaller} \quad (17\text{-}7)$$

where P' = hydrostatic-test pressure, psig
S' = fiber stress, psi
= 75 per cent of specified minimum yield strength for $8\frac{5}{8}$-in. pipe and smaller
= 85 per cent for $10\frac{3}{4}$-in. pipe and larger
t = nominal wall thickness, in.
D = nominal outside diameter of pipe, in.

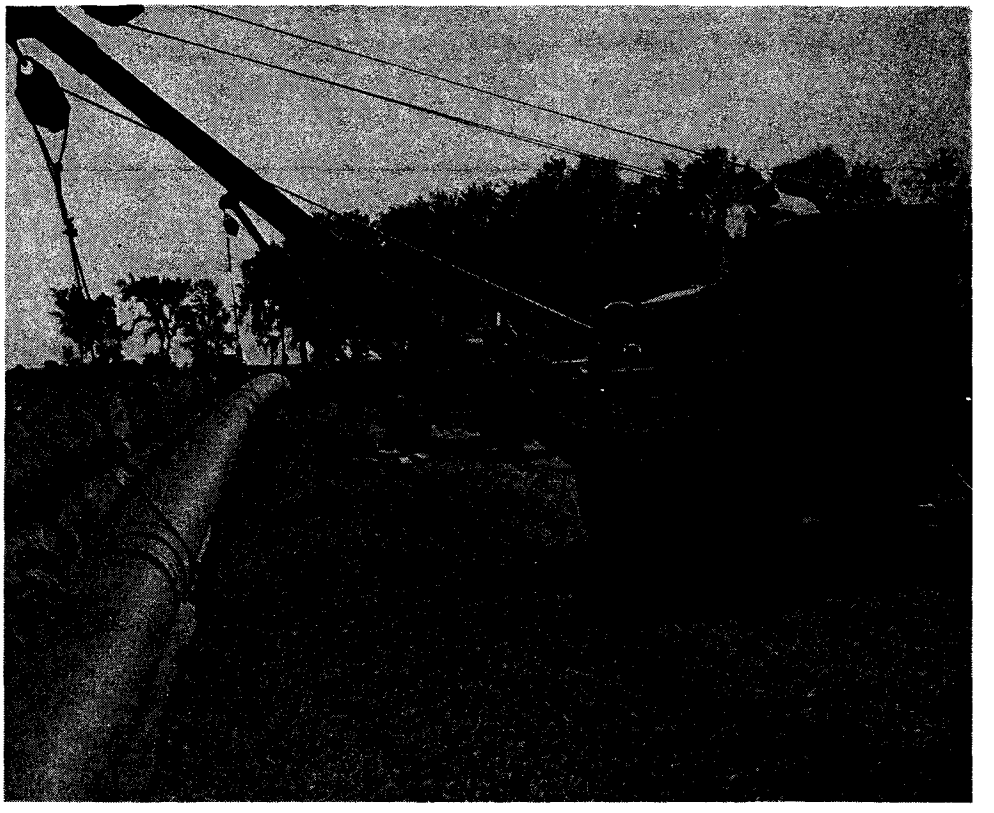

Fig. 17-6. Sideboom caterpillars for lifting, holding, and lowering pipe.

Fig. 17-7. Electric welding equipment. (*Courtesy American Louisiana Pipe Line Company.*)

(a)

(b)

Fig. 17-8. X-ray machine. (a) Working on pipeline. (b) Inserting device in pipe. (Courtesy *Industrial X-Ray, Inc.*)

Total Cost Estimate

It is difficult to make a general statement regarding total costs. Steel costs are increasing periodically. Aerial surveying costs depend upon how detailed the plans must be. The extent of X ray of field welds will affect the cost. Construction costs will be affected by soil conditions, prevailing weather conditions, and competitive conditions. A rule of thumb for approximate total costs would be 50 to 60 cents per inch diameter per foot length of pipeline, or $2,640 to $3,168 per inch diameter per mile. A bill of materials and detailed cost estimates are necessary in making applications for certificates.

Certificate of Convenience and Necessity

The Natural Gas Act passed in 1938 gives the Federal government the power to regulate the transportation and sale of natural gas in interstate commerce (19-1). This act is administered by the Federal Power Commission (FPC). The steps in obtaining a certificate of convenience and necessity from the FPC are explained in Chap. 19.

Natural gas pipelines constructed wholly within one state are usually subject to a public service commission within that state. Certificates are necessary for all projects since the state is responsible for the public safety of any pipeline. If the company desires to make use of state condemnation laws to complete the acquisition of right of way, the courts normally will require a certificate.

Pipeline Routes

There are many ways of selecting the route of the pipeline right of way. One method of low cost would be to establish the route from state highway maps, county road maps, county plat books, and state conservation department county maps.

The U.S. Department of Agriculture has aerial photographs available of much of the United States. These can be ordered from the Performance and Aerial Photography Division, Commodity Stabilization Service, U.S. Department of Agriculture, at the Eastern Laboratory, Washington 25, D.C., for any part of the United States east of and including Texas, Oklahoma, Nebraska, and South Dakota, or at the Western Laboratory on 167 West Second South, Salt Lake City 1, Utah, for any part of the United States west of and including Kansas and North Dakota. Contact prints, photoindexes, and enlargements can be purchased in scales ranging from 1 in. = 1 mile for photoindexes to 1 in. = 400 ft for enlargements. Costs range from 65 cents for a contact print 10 by 10 in. at a scale of 1 in. = 1,667 ft to $5.10 for an enlargement 40 by 40 in. at a scale of 1 in. = 400 ft.

The Geological Survey Division of the U.S. Department of the Interior has quadrangle topographic maps available for parts of the United States. These maps show lakes, rivers, swamps, surface contours, roads, railroads, and location of houses. The maps are of nearly uniform size (about 16.5 by 20 in.) but are of varying scales from 1 in. = ½ mile to 1 in. = 2 miles. They cost 20 cents each, with a discount of 20 per cent on orders of $10 or more.

Aerial survey corporations are available and will make aerial surveys of tentative pipeline routes on a contract basis. The cost of this service is relatively high and depends upon the extent of the service that is to be performed. They will make just the aerial survey and supply contact prints or enlargements for layout of the pipeline route or they will follow through and make completion drawings of the pipeline showing

Fig. 17-9. Coating and wrapping machine. (*Courtesy American Louisiana Pipe Line Company.*)

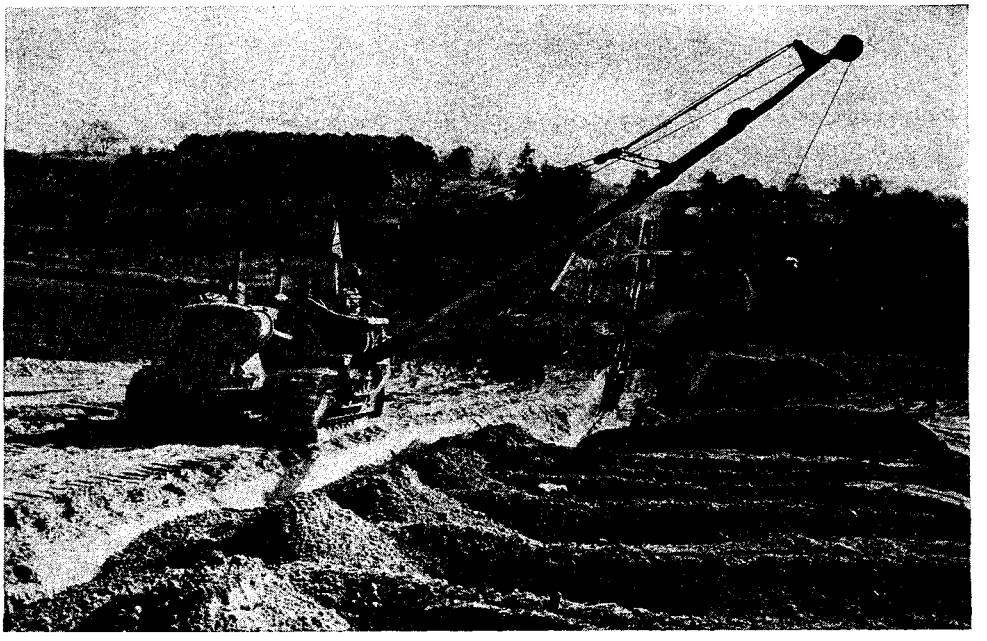

Fig. 17-10. Dragline caterpillar for backfilling. (*Courtesy American Louisiana Pipe Line Company.*)

all construction, topographical, and right-of-way information.

In laying out a pipeline route, a study should be made of the type of soil or rock to be traversed and how it is being used, of the groundwater levels, of major river crossings, of highway and railroad crossings, and of population indices. All these factors can have a significant effect upon construction costs.

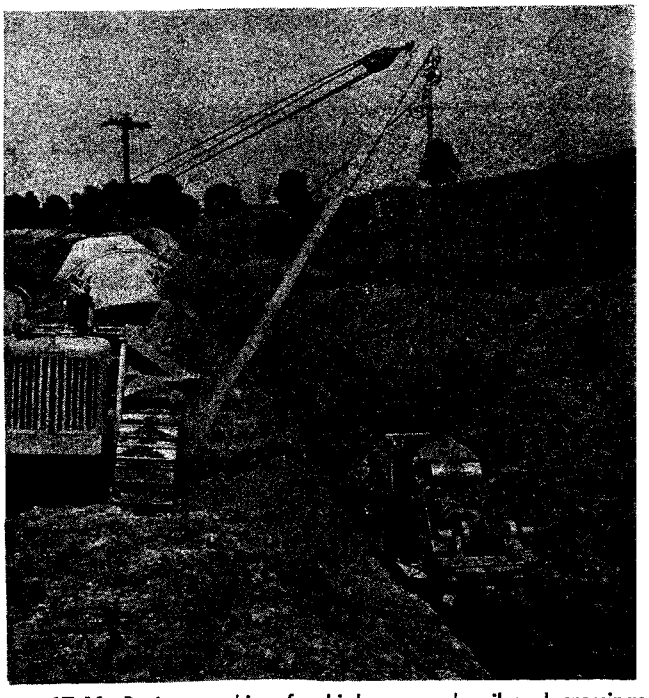

Fig. 17-11. Boring machine for highway and railroad crossings. (*Courtesy H. C. Price Company.*)

After the pipeline route is tentatively laid out on maps, it is necessary to go out and obtain the right of way. It will normally be necessary to send out simultaneously a surveying crew to stake out the actual route of the pipeline. Title searches must be made and documents prepared for acquiring the right of way. Payments per rod for right of way must be established and damage settlements considered. Timing of these operations can be critical. Initial contact with the landowners must be made to obtain permission for the survey crew to cross the land. Often landowners will not sign right-of-way agreements until they know the staked-out route of the pipeline. Nominal figures of 50 cents to $5.00 per rod are usually established as payments for right of way. Damage settlements then become the major point of contention in getting signatures on right-of-way documents. Some companies are making damage settlements in advance so as essentially to complete the transaction with the landowner at the time the document is signed. Some landowners insist upon this because they realize that their bargaining position is weak once the pipeline has been constructed and is in operation. Damage payments have gone as high as $75 per rod in areas around large cities where land values have skyrocketed. These damage payments will include immediate damage to crops, timber, etc., as well as any long-range damage to property values in suburban areas.

Most states have condemnation laws for pipeline right of way similar to those for highway construction.

It is not possible then for a single individual to hold up a project that is in the public interest. A fair value to be paid for right of way obtained under condemnation proceedings is usually established by a board of commissioners appointed by the court. It is not the purpose of this discussion to go into the details of condemnation laws, for these vary from state to state.

There is an American Right-of-Way Association with offices in Sacramento, Calif. Its membership includes those interested in highway as well as pipeline right of way.

Contracts for Pipeline Construction

Almost all major pipeline construction is done on a contract basis, with contracts usually awarded by competitive bidding. These contracts are usually lengthy documents even for minor construction jobs. They are often divided into five or more sections on agreement, general conditions, specifications, drawings, and maps. Table 17-8 is a list of the subjects that might be covered in the general-conditions section of a contract document. Table 17-9 is an outline for a specifications section. The sections for drawings and maps might include drawings of line-valve and blowdown-valve assembly, highway-crossing detail,

Table 17-8. General Conditions for Pipeline Construction

Articles	*Subject*
1	Definitions
2	Method and manner of performance
3	Work to be performed
4	Material and equipment
5	Changes
6	Extra work
7	Right of way
8	Adjacent pipelines
9	Delays
10	Inspection
11	Workmanship
12	Superintendence by contractor
13	Subcontracts
14	Permits and licenses
15	Patents and royalties
16	Social security and unemployment compensation
17	Injuries and damages
18	Insurance
19	Liens
20	Bond
21	Title
22	Indemnity and compliance with laws
23	Nonwaiver of defaults
24	*Force majeure*
25	Termination
26	Records
27	Notices
28	Conflicts
29	Interpretation
30	Authorized representatives

Table 17-9. Specifications for Pipeline Construction

A. General
1. Work to be performed
2. Design pressure
3. Maximum allowable operating pressure
4. Approval of working drawings
5. Deviations
6. Right of way
7. Material to be furnished by company
8. Items to be furnished by contractor
9. Inspection of materials
10. Supervision of work
11. Clearing right of way, including installation and maintenance of fences and gates
12. Grading right of way, including grubbing
13. Unloading, hauling, and stringing all materials
14. Trenching
15. Rock excavation
16. Welding
17. Bending, laying, and lowering in
18. Backfilling and cleanup, including necessary breakers and terraces
19. River clamps or weights
20. Railroad and highway crossings
21. Drainage tile
22. Pigging, purging, blowing, and testing
23. Sectionalizing valve assemblies
24. Pipeline markers
25. Intent of specifications

B. Material specifications
1. Pipe
2. Valves
3. Butt-welding fittings
4. Other material and equipment

C. Installation procedures and fabrication details
1. Joints
2. Bends
3. Branch connections
4. Reducers
5. Railroad and highway crossings

D. Welding procedure
1. Standard
2. Equipment and nature of electric current
3. Filler metal
4. Preparation of welding edges
5. Welding technique
6. Test of welds

E. Coating and wrapping pipe
1. Coating and wrapping
2. Handling coated and wrapped pipe

F. Corrosion control
1. Tests for coating defects and electrical contacts
2. Test wire stations

railroad-crossing detail, stream- or river-crossing detail, cathodic-protection detail, and a strip map or maps showing line location, roads, streams, railroads, right-of-way parcel ownership, land use, houses, etc.

Contracts for pipeline construction may be bid for on a total-project basis or on a unit-cost basis. Bidding on a unit-cost basis has some advantage since at the time the contract is let the exact footage of pipe or exact number of valve assemblies may not be known. The contractor can then be paid at his bid cost per foot times the total footage actually installed.

CONSTRUCTION OF PIPELINES

Equipment Required

Figures 17-1 to 17-11 are photographs of the types of equipment used in laying a pipeline.

Laying the Line

Table 17-10 is an ordered list of the operations that must be accomplished in laying a pipeline. Two of these operations, X ray of welds and test of coating for hollidays (Fig. 17-12), would be done by company personnel or by separate contractors, since these, in effect, are a check on the workmanship of the construction contractor.

Road and River Crossings

Tables 17-11 and 17-12 show the construction type required for pipelines paralleling and crossing roads and railroads. These tables must be used in conjunction with Tables 17-4 and 17-5 to determine the type and class of construction and thereby the design factor F in designing the pipeline. Many railroads and highway departments will require that all improved roads and railroads be cased and that this casing be insulated from the main pipeline. Figure 17-13 is a sketch of a typical cased highway or railroad crossing. It will also be necessary in most instances to bore these crossings. Figure 17-11 is a photograph of a boring machine in operation.

Table 17-10. Operations in Laying a Pipeline

1. Clearing right of way
2. Grading right of way
3. Stringing pipe along right of way
4. Digging the trench
5. Lining up and welding pipe
6. X ray of welds
7. Cleaning, coating, and wrapping pipe
8. Lowering into trench
9. Backfilling the trench and cleanup of right of way
10. Test of coating for hollidays
11. Pigging, purging, and blowing
12. Sectionalizing valve installation

Table 17-11. Construction Types Required for Parallel Encroachment of Pipelines and Mains on Roads and Railroads

Kind of thoroughfare	Construction type required for location class			
	1	2	3	4
a. Privately owned roads.....	A	B	C	D
b. Unimproved public roads.....	A	B	C	D
c. Hard-surface roads, highways or public streets, and railroads	B	B	C	D

SOURCE: ASA B31.1 code (17-4).

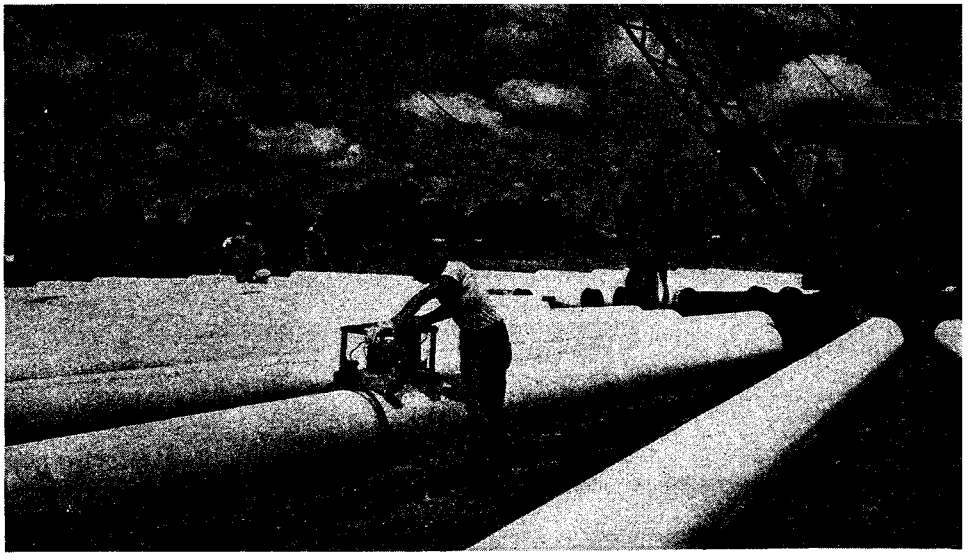

Fig. 17-12. Holliday detector. (*Courtesy H. C. Price Company.*)

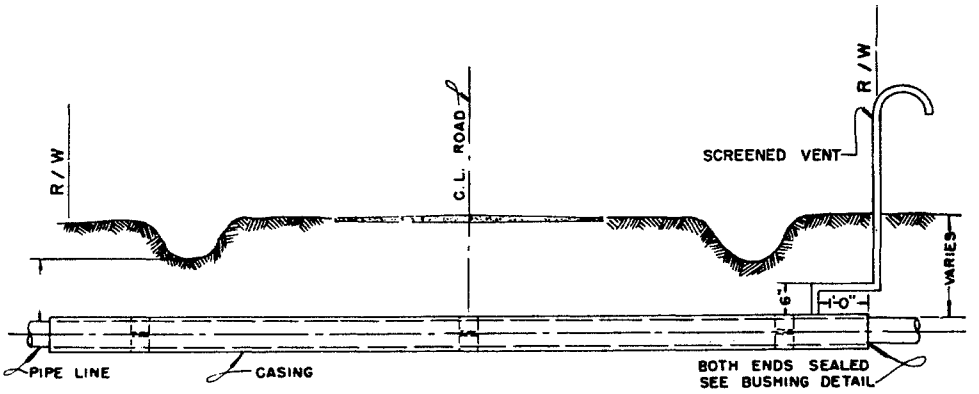

Fig. 17-13. Typical highway crossing.

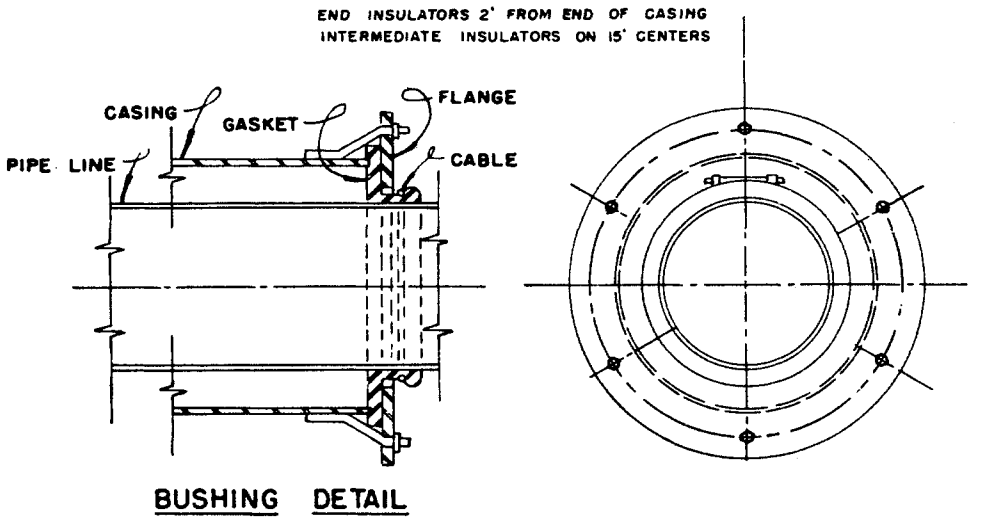

River crossings require special techniques. With a main transmission line where uninterrupted service is essential, twin river crossings are usually made. The pipe is welded, coated, and wrapped, given a coating of concrete for added protection on shore, and floated into position over a ditch dug out of the river bottom. The 50-gal drums often used to float the pipe are cut loose, and the pipe sinks into the ditch. The current of the river will soon backfill the ditch and cover the pipe. Figure 17-14 shows a river crossing under construction. Highway and river crossings are normally laid by a special crew, with the regular crew doing just cross-country pipelining.

Swamp or bayou and open-water pipelining is done from barges. In bayou country an open canal must first be cleared. A coating of concrete on pipe is also used in this type of construction.

Valves

Valves, often called sectionalizing valves, are normally installed every 10 to 30 miles along a pipeline.

Table 17-12. Construction Types Required for Pipelines and Mains Crossing Roads and Railroads

Kind of thoroughfare	Construction type required for location class			
	1	2	3	4
a. Privately owned roads	A without casing	B without casing	C without casing	D without casing
b. Unimproved public roads	A with casing, B without casing	B without casing	C without casing	D without casing
c. Hard-surface roads, highways or public streets, and railroads	A with casing, B without casing	B with casing, C without casing	C without casing	D without casing

SOURCE: ASA B31.1 code (17-4).

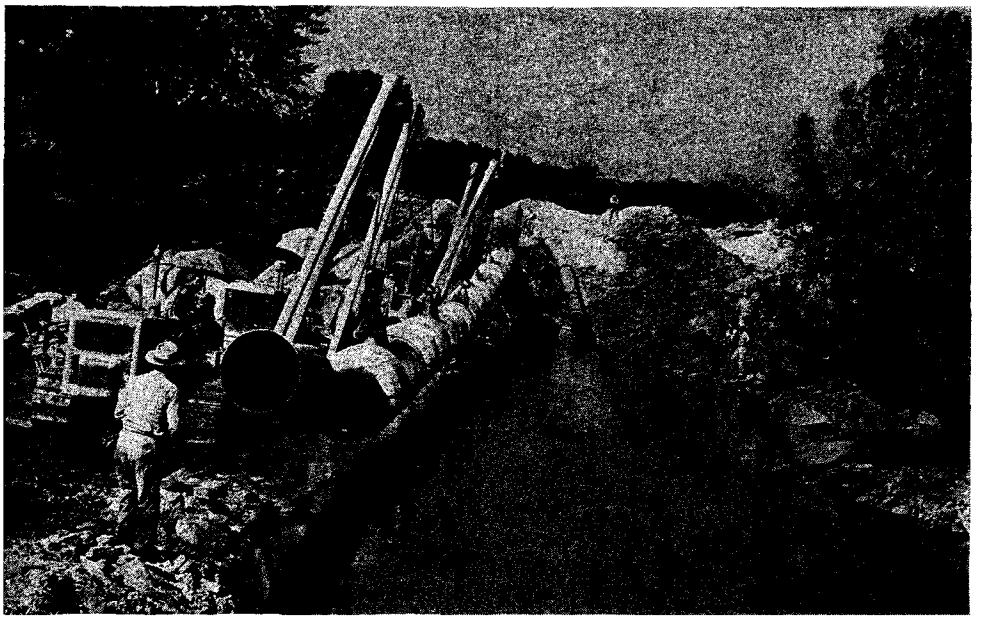

Fig. 17-14. Stream or river crossing. (*Courtesy H. C. Price Company.*)

These valves should not be installed until the pipeline has been thoroughly purged, blown, and cleaned. Figure 17-15 is a drawing of a typical line-valve and blowoff-valve assembly. There is a trend toward the installation of full-opening line valves so that, periodically over the years, the inside walls of the line can be cleaned by pigging. This will keep the pipeline efficiency at a high value (17-17). Figure 17-16 is a photograph of the instrument used for internal cleaning of line pipe, commonly called a pig.

Sectionalizing valves are often equipped with automatic closing devices. These are of different types, but the principle is the same. The device will automatically close the valve with any rapid large drop in pressure. Closure is accomplished with the use of a pressure tank connected to the pipeline through a small-diameter pipe with an orifice. A small gradual change in line pressure will cause gas to flow through the orifice and equalize the line pressure with the tank pressure. A rapid change in line pressure will set up a pressure differential between the pressure tank and transmission line due to the limited flow capacity of the connecting small-diameter pipe and orifice. This pressure differential will actuate

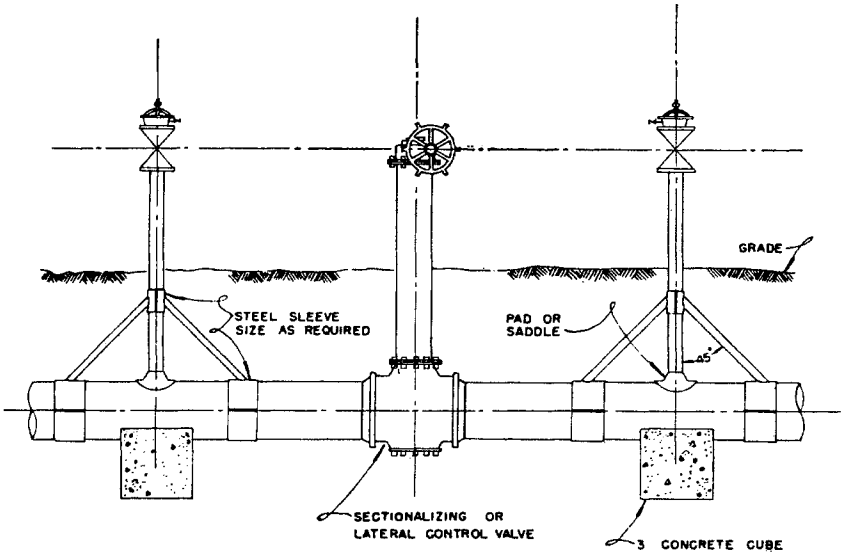

Fig. 17-15. Typical line-valve and blowoff-valve assembly.

and close the valve. The rate of pressure drop in the line that will cause the valve to close can be regulated by the size of the orifice.

Pressure Test

Table 17-13 lists the prescribed test pressure and permissible test fluid for all transmission lines in location classes 1, 2, 3, or 4 that will operate at hoop stresses greater than 30 per cent of the minimum yield strength of the pipe. Under normal conditions, almost all transmission lines will operate at hoop stresses greater than 30 per cent of the minimum yield strength of the pipe. Hoop stresses can be calculated from the following formula:

$$P'' = \frac{2S''t}{D} \qquad (17\text{-}8)$$

Table 17-13. Test Requirements for Pipelines and Mains to Operate at Hoop Stresses of 30 Per Cent or More of the Specified Minimum Yield Strength of the Pipe*

Location class	Permissible test fluid	Prescribed test pressure		Maximum allowable operating pressure, the lesser of
		Minimum	Maximum	
(1)	(2)	(3)	(4)	(5)
1	Water	1.1 × MOP†	None	TP/1.1
	Air	1.1 × MOP	1.1 × DP	or
	Gas	1.1 × MOP	1.1 × DP	DP
2	Water	1.25 × MOP	None	TP/1.25
	Air	1.25 × MOP	1.25 × DP	or DP
3	Water	1.40 × MOP	None	TP/1.40 or DP
4	Water	1.40 × MOP	None	TP/1.40 or DP

* This table brings out the relationships between test pressures and maximum allowable operating pressures subsequent to the test. If an operating company decides that the maximum operating pressure will be less than the design pressure, a corresponding reduction in prescribed test pressure may be made as indicated in column 3. However, if this reduced test pressure is used, the maximum operating pressure cannot later be raised to the design pressure without retesting the line to the test pressure prescribed in column 4.

† MOP = maximum operating pressure (not necessarily the maximum allowable operating pressure)
DP = design pressure
TP = test pressure

SOURCE: ASA B31.1 code (17-4).

where P'' = maximum operating pressure, psig
S'' = hoop stress, psi
t = nominal wall thickness, in.
D = nominal OD of pipe, in.

By comparing Eqs. (17-6) and (17-8), it can be seen that any pipeline operating at its design pressure will be operating at a hoop stress greater than 30 per cent of the minimum yield strength of the pipe. Test pressures for pipelines that will operate at a hoop stress always less than 30 per cent of minimum yield strength can be found in the ASA B31.1 code, page 50 (17-4).

Test pressures are maintained for 4 hr or more to determine if the line is gastight.

CORROSION AND CATHODIC PROTECTION

Principles of Corrosion

Corrosion may be defined as the destruction of metal by electrochemical action, and it cannot take place unless an electrolyte is present. Corrosion occurs when d-c electricity flows from a metal surface to a surrounding electrolyte and results in a loss of metal depending upon the magnitude and duration of cur-

Fig. 17-16. Pig for cleaning pipeline.

rent flow. Steel, for instance, can lose a theoretical maximum of 20 lb in weight per ampere discharged per year. When these iron ions are free they can combine with oxygen to form iron oxide or rust. This action continues as long as current flows, and after a time a definite pit will be formed in the pipe. The formation of iron oxide can have three possible effects upon the rate of corrosion: (1) It may remove the iron ions from solution, permitting the formation of additional iron ions from the metal. (2) The rust may form a somewhat protective coating on the iron surface. (3) The oxygen supply may be removed by combination with iron and thus retard further corrosion.

The rate of corrosion of the pipe depends upon the condition of the protective coating on the metal, if any; the characteristics of the soil in which the pipe is buried; and the presence of foreign materials or stray currents. The use of coating materials is to prevent moisture, which serves as the electrolyte, from reaching the metallic surface. In general, soil increases in corrosiveness with poor drainage, heavy texture, organic-matter content, acidity, and content of soluble salts. Foreign materials such as cinders, scraps of metal, or organic materials tend to act as a cathode and set up differences in potential.

Methods of Protection

It is essential to know in detail the characteristics of the soil in which the pipe is to be buried. Soil testing and analysis will be of assistance. Leak surveys of older pipelines in similar soils should be studied. These factors and perhaps others will help to determine whether it is economical to use protective methods against corrosion on a given pipeline.

The most universally used method of protecting pipe is by coating and wrapping. Today, almost all newly constructed natural gas pipelines are coated and wrapped. Coal-tar, asphalt-enamel, or hot-wax coatings shielded by wrappers are most often used.

Cathodic protection is often used in addition to coating and wrapping of the pipe. Cathodic protection is the application of direct current, supplied by an external source, to oppose the flow of current from a metal surface to an electrolyte. The current requirements for cathodic protection of steel will vary over wide limits, depending upon soil characteristics, condition of metal surface, and type and condition of coatings. The current for cathodic protection may be generated by use of a sacrificial galvanic anode such as magnesium or zinc or by use of rectifiers where electric power is available.

Table 17-15 is a list of the galvanic series of metals. McKay and Worthington (17-22) state:

This series is built upon actual experience with corrosion and laboratory measurement. Metals grouped together have no strong tendency to produce galvanic corrosion on each other; connecting two metals distant on the list from each other tends to corrode the one higher in the list. Voltage figures are not given because they vary with every new corrosive condition. Relative positions of metals change in many cases but it is unusual for changes to occur across the spaces left blank. The chromium-irons and chromium-nickel-irons change position as indicated depending on oxidizing conditions, acidity, and chloride in solution. The series as it stands is correct for many common dilute water solutions such as sea water, weak acids and alkalies.

When two dissimilar metals not in the same grouping on the list are placed in an electrolyte and connected with a wire, a current will flow through the wire, corroding the metal nearest the top or anodic end of the galvanic series and protecting the other metal. This, then, is the principle of cathodic protection by use of galvanic anodes. As can be seen from Table 17-15, the common metals above iron in the galvanic series are magnesium, aluminum, and zinc. Aluminum has not been used extensively as a galvanic anode. Magnesium anodes have a greater driving potential than anodes of other common metals and also a larger storage capacity for electricity, theoretically 1,000 amp-hr/lb. Magnesium or zinc anodes are buried in the soil, often surrounded by a suitable low-resistance backfill, and connected to the pipeline by means of an insulated copper wire. On newly coated and wrapped pipelines, these expendable anodes may be spaced as widely as 1 or 2 to the mile, depending on local conditions of soil. Various-sized anodes are available, and they should be selected according to current requirements and life expectancy. Current requirements should be determined by test for each installation. A rule of thumb used is that the average current density needed to protect bare pipe varies from 1 to 3 milliamperes/sq ft and, for coated and wrapped pipe, from 0.005 to 0.025 milliampere/sq ft. As coating deteriorates, the current necessary for protection will increase until it approaches that for bare pipe. Galvanic anodes are preferred over rectifiers or other high-capacity current sources for use where current requirements are small or where it is desired to distribute the current in small increments along a pipeline. The advantage is largely economic, since small currents can often be generated more cheaply with galvanic anodes.

Rectifiers are used as a source of cathodic protection current where the magnitude of current required is high and where soil resistivity is high. High driving voltages are available from rectifiers, as compared with galvanic anodes. Extremely wide spacing of

rectifiers is possible when a pipeline has a good coating, but this can result in high negative potentials in the vicinity of the rectifier, with consequent damage to the coating and eventual increase in current requirement. Rectifiers using outside sources of power are subject to off time due to power interruption and equipment maintenance. Equipment maintenance is also an added operating expense with rectifiers, especially in remote locations.

COMPRESSOR STATIONS

Design and Layout of Manifold

The design formula used for steel pipelines, Eq. (17-6), is also applicable for compressor-station piping. From Table 17-4, it can be observed that compressor-station piping is considered type C construction with a design factor F of 0.50. There are minimum wall thicknesses of pipe specified for compressor-station piping which vary with the pipe size. These are given in Table 17-14, which also gives minimum wall thicknesses for pipelines constructed in location classes 1, 2, 3, and 4. Gas piping in compressor stations must be tested hydrostatically after installation to at least 1.4 times the maximum operating pressure.

Piping around compressor stations, including outside headers and lead-in and lead-out lines, should not be sized by the usual mathematical formula, Eq. (17-1), relating to normal pipe flow. It has been standard practice to make lead-in and lead-out lines the same size. If the discharge lines are designed for low linear gas velocities to help overcome more severe pulsations present in them, intake lines of the same diameter will almost always have permissible velocities. A limiting maximum velocity of 60 ft/sec in compressor lead-out or discharge lines will give good operating results.

Calculation of the size of outside headers connecting

Table 17-14. Least Nominal Wall Thicknesses

	Nominal diameter, in.	Location classes*		Compressor stations
		1	2–4	
Threaded or plain end	⅛	0.068	0.068	0.095
	¼	0.088	0.088	0.119
	⅜	0.091	0.091	0.126
	½	0.109	0.109	0.147
	¾	0.113	0.113	0.154
	1	0.133	0.133	0.179
	1¼	0.140	0.140	0.191
	1½	0.145	0.145	0.200
	2	0.154	0.154	0.218
Plain end only	2½	0.103	†0.125	0.203
	3	0.104	†0.125	0.216
	3½	0.104	†0.125	0.226
	4	0.104	†0.125	0.237
	5	0.104	†0.125	0.250
	6	0.104	0.156	0.250
	8	0.104	0.172	0.250
	10	0.104	0.188	0.250
	12	0.104	0.203	0.250
	14	0.134	0.210	0.250
	16	0.134	0.219	0.250
	18	0.134	0.250	0.250
	20	0.134	0.250	0.250
	22, 24, 26	0.164	0.250	0.250
	28, 30	0.164	0.281	0.281
	32, 34, 36	0.164	0.312	0.312

* If threaded pipe is to be used in those sizes for which least nominal wall thicknesses are given for "plain-end pipe only," those sizes marked by † shall be increased as follows: 2½ in. to 0.203, 3 in. to 0.216, 3½ in. to 0.226, 4 in. to 0.237, 5 in. to 0.258, and 0.100 in. shall be added to all other wall thicknesses given in this table.

SOURCE: ASA B31.1 code (17-4).

Table 17-15. Galvanic Series of the Metals

Corroding end (anodic)

Magnesium
Aluminum
Duralumin

Zinc
Cadmium

Iron
Chromium iron (active)
Chromium-nickel
Iron (active)

Soft solder
Tin
Lead

Nickel
Brasses
Bronzes
Nickel-copper alloys
Copper

Chromium-iron (passive)
Chromium-nickel-iron (passive)

Silver solder

Silver
Gold
Platinum

Protected end (cathodic)

SOURCE: McKay and Worthington (17-22). Courtesy Reinhold Publishing Corporation.

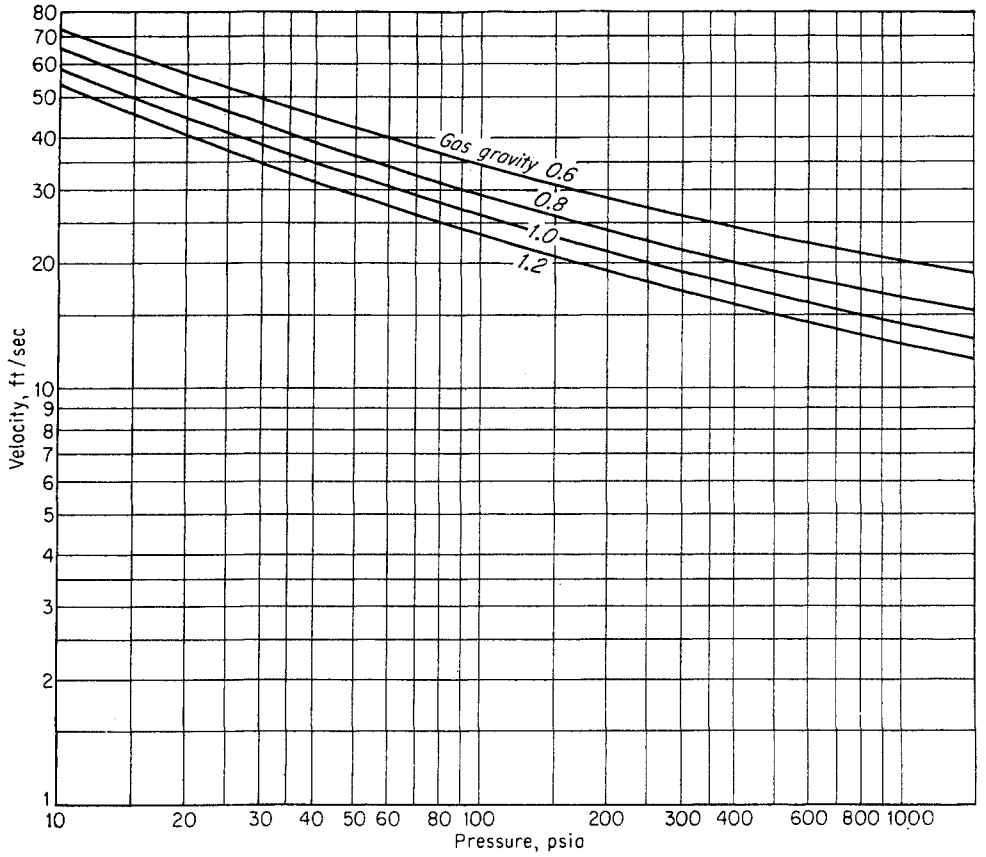

Fig. 17-17. Maximum allowable velocity in compressor-station piping. (*Flaherty*, 17-14a.)

a group of machines should also be based upon maximum allowable linear velocities. Figure 17-17 is a plot of these maximum allowable velocities for gases of different gravity. For compressor stations containing a large number of machines, the diameter of the outside headers can be reduced by placing the inlet and outlet connections at central points, as shown in Fig. 17-18. This figure also shows the lead-in and lead-out lines and a typical way to connect the compressor station into the main pipeline. With this hookup, the main pipeline could remain in service even though the compressor station was not operating. The throughput of the line would be reduced but some of the slack could be picked up by adjoining compressor stations.

If there is any possibility that gas may ever flow in the opposite direction through the main line, the station should be connected accordingly. Figure 17-18 shows a possible hookup in which the compressor station can be used to pump gas in either direction.

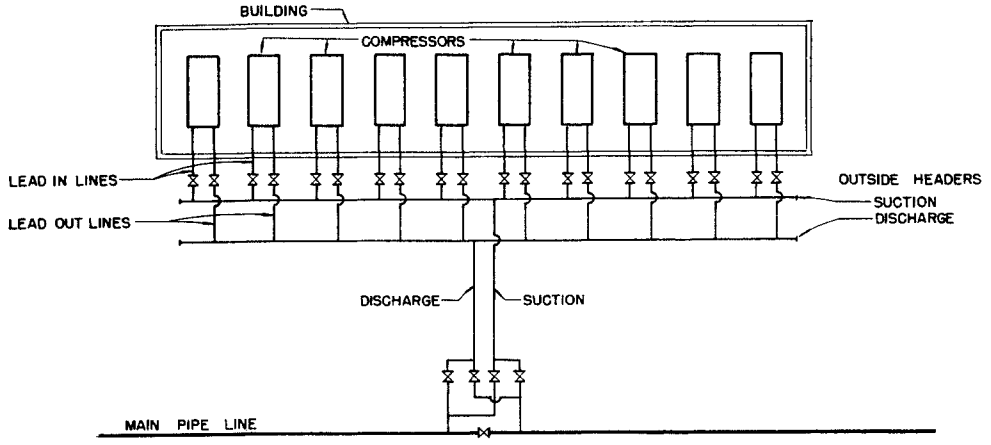

Fig. 17-18. Compressor-station layout.

This can occur in a pipeline with large natural gas reserves at one end of the line and underground storage at the other.

Compressors

The formulas for calculating the theoretical work or horsepower required to compress natural gas are developed and discussed in Chap. 7. Ford, Bacon, and Davis, Inc., Engineers (17-12), have adapted the adiabatic compression formula [Eq. (7-71)] for computing the power to compress natural gas for common use in the gas industry. This formula may be expressed as follows:

$$\text{hp} = \frac{T_s}{T_0}\frac{3.03P_0}{E_m}\frac{k}{k-1}(R^{(k-1)/k} - 1) + 3.5 \quad (17\text{-}9)$$

where hp = brake horsepower per MMcf per day of gas compressed
P_0 = pressure base, psia
T_0 = temperature base, °R
T_s = suction temperature, °R
k = specific-heat ratio
R = compression ratio
E_m = mechanical efficiency
valve losses = 3.5

Substituting

$$P_0 = 14.735 \text{ psia}$$
$$T_0 = 60°\text{F} + 460 = 520°\text{R}$$
$$T_s = 60°\text{F} + 460 = 520°\text{R}$$
$$k = 1.3$$
$$E_m = 0.92$$

the equation becomes

$$\text{hp} = 210.2(R^{0.231} - 1) + 3.5 \quad (17\text{-}10)$$

This formula and others similar to it have been used to prepare charts from which the brake horsepower per MMcf per day can be read, given the ratio of specific heats and compression ratio (CR). One such set of charts has been published in an engineering data book (5-1). Figure 17-19 is a chart of Eq. (17-10) for various values of specific-heat ratio k.

The capacity of any specific engine and compressor unit at various inlet pressures and CR's will depend upon its individual design. Compressor manufacturers will furnish charts and tables giving operating characteristics of any of their units. Figure 17-20 is a performance chart for a 2,000-hp Ingersoll-Rand Company turbocharged gas-engine-driven reciprocating compressor designed to handle natural gas intake pressures varying from 200 to 600 psig and discharge pressures from 600 to 975 psig. This installation is located at an underground storage field. Line engines and compressors designed to operate at fairly constant intake pressures and discharge pressures often do not have or need the flexibility of this unit.

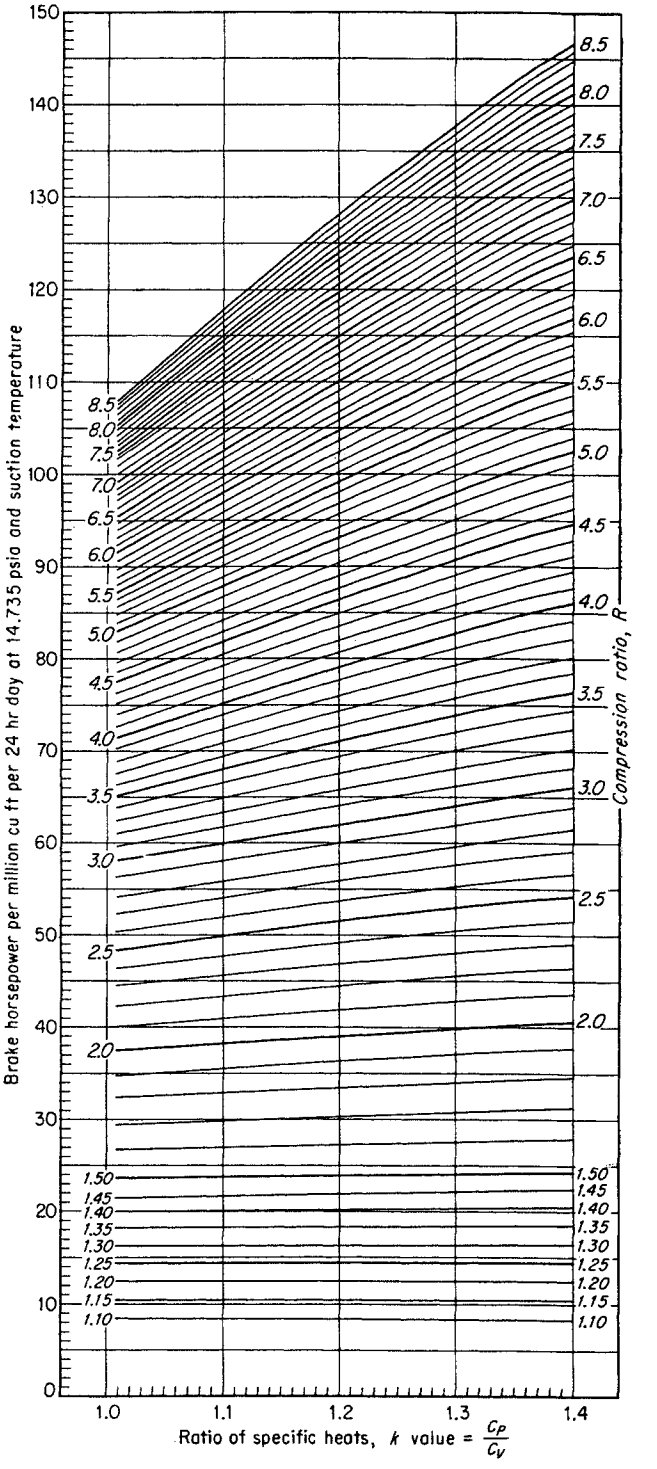

Fig. 17-19. Brake horsepower required for compression. Mechanical efficiency of compressor cylinder = 92 per cent.

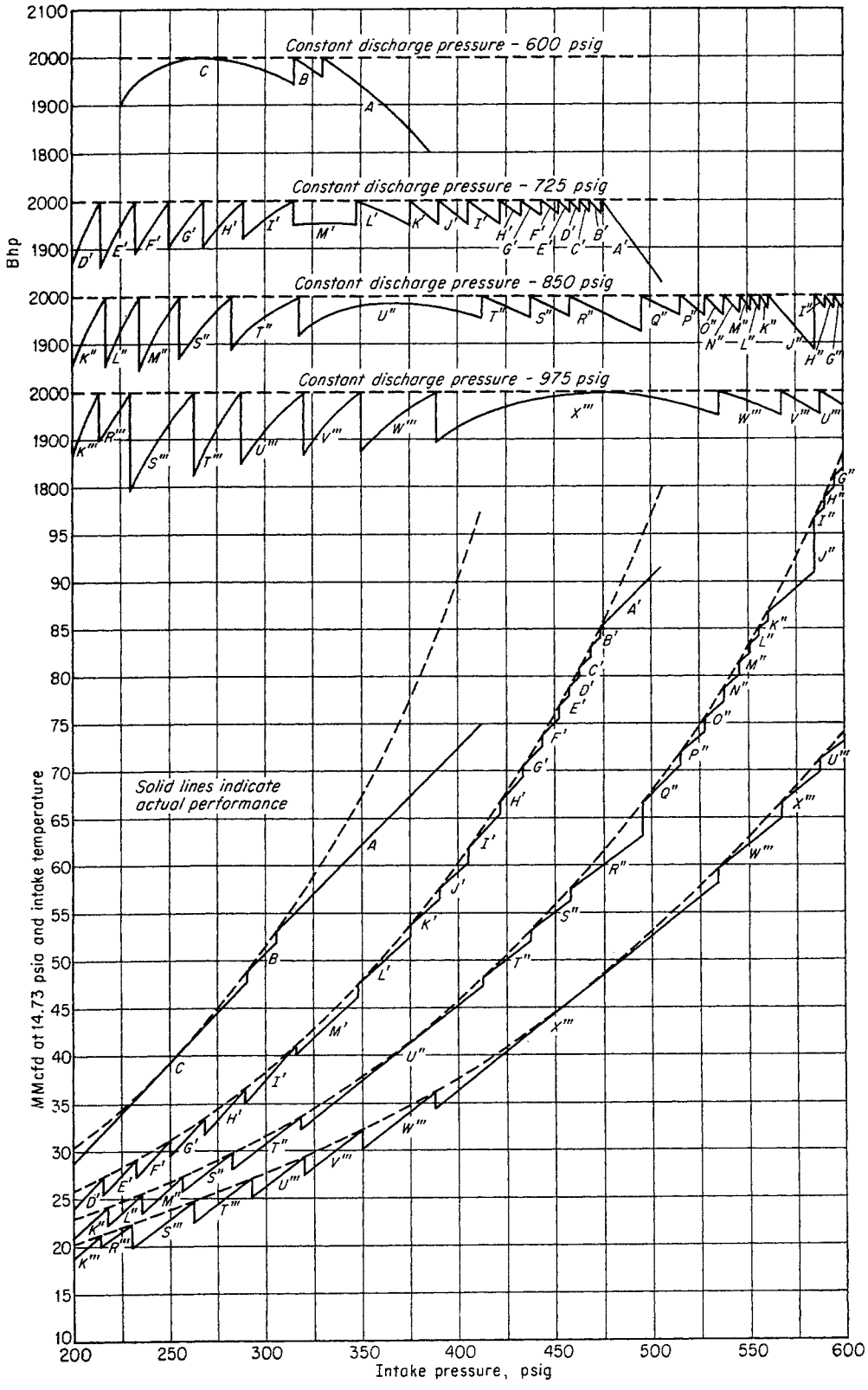

Fig. 17-20. Performance characteristics of an Ingersoll-Rand Company 2,000-hp 10¾ and 10¾ and 10¾ and 10¾ × 15–412 KVS compressor unit handling natural gas; k value, 1.30; 330 rpm; piston displacement, 1,968 cfm (with one outer end unloaded, 1,708 cfm; with two outer ends unloaded, 1,448 cfm); rated brake horsepower, 2,000; altitude 600 ft. *A*, 0 pockets open; *B*, 1 pocket open; C, 2 pockets open. *A′*, 0 pockets open; *B′*, 1 pocket open; C′, 2 pockets open; *D′*, 3 pockets open; *E′*, 4 pockets open; *F′*, 5 pockets open; *G′*, 6 pockets open; *H′*, 7 pockets open; *I′*, 8 pockets open; *J′*, 1 outer end unloaded, 0 pockets open; *K′*, 1 outer end unloaded, 1 pocket open; *L′*, 1 outer end unloaded, 2 pockets open; *M′*, 1 outer end unloaded, 3 pockets open. *G″*, 6 pockets open; *H″*, 7 pockets open; *I″*, 8 pockets open; *J″*, 1 outer end unloaded, 0 pockets open; *K″*, 1 outer end unloaded, 1 pocket open; *L″*, 1 outer end unloaded, 2 pockets open; *M″*, 1 outer end unloaded, 3 pockets open; *N″*, 1 outer end unloaded, 4 pockets open; *O″*, 1 outer end unloaded, 5 pockets open; *P″*, 1 outer end unloaded, 6 pockets open; *Q″*, 1 outer end unloaded, 7 pockets open; *R″*, 2 outer ends unloaded, 0 pockets open; *S″*, 2 outer ends unloaded, 1 pocket open; *T″*, 2 outer ends unloaded, 2 pockets open; *U″*, 2 outer ends unloaded, 3 pockets open. *K‴*, 1 outer end unloaded, 0 pockets open; *R‴*, 2 outer ends unloaded, 0 pockets open; *S‴*, 2 outer ends unloaded, 1 pocket open; *T‴*, 2 outer ends unloaded, 2 pockets open; *U‴*, 2 outer ends unloaded, 3 pockets open; *V‴*, 2 outer ends unloaded, 4 pockets open; W‴, 2 outer ends unloaded, 5 pockets open; *X‴*, 2 outer ends unloaded, 6 pockets open. (*Redrawn from operating charts supplied with the unit. Courtesy Ingersoll-Rand Company.*)

Most new reciprocating gas engines are turbocharged units, and many pipeline companies are rapidly turbocharging presently installed engines so as to obtain additional brake horsepower from the existing engines. Intake-air heat exchangers using the heat in exhaust gases are being used to increase engine efficiency. Daugherty (17-10) has made a comparison of the design and operating characteristics of the 2,000-hp compressor units of the four leading manufacturers of reciprocating compressors. Figure 17-21 is a photograph of a 1,500 brake horsepower turbocharged reciprocating gas-engine-driven compressor.

A total of 270,000 hp of gas-turbine-driven centrifugal compressors (17-26) have been installed by the natural gas industry in the three years from 1952 to 1955. The turbine-driven centrifugals installed to date have been essentially units developing 5,000 hp or more each. Maximum CR's per stage have increased to 1.45. Multistage compressors on a single gas turbine have made possible higher compression ratios on an individual unit. The advantages of gas-turbine-driven centrifugal compressors are absence of vibration; installed cost lower by as much as $50 per brake horsepower, in part because of simpler foundations; and lower operating costs, because of smaller maintenance and operating-personnel requirements. The lower installation and operating costs are offset, at least in part, by increased fuel consumption and by the added brake horsepower needed to perform the same volume of compression at CR's requiring more than one stage of centrifugal compression. Gas turbines can be started from cold to full load in fifteen minutes. Gas turbines are capable of putting out additional horsepower at low ambient temperatures in wintertime when demands for gas are high. The turbines appear to be economical only in large units of 5,000 hp or more, which limits somewhat the flexibility of a compressor station and its ability to continue operations at close to capacity with one unit shut down. A 10,000-hp compressor station, for

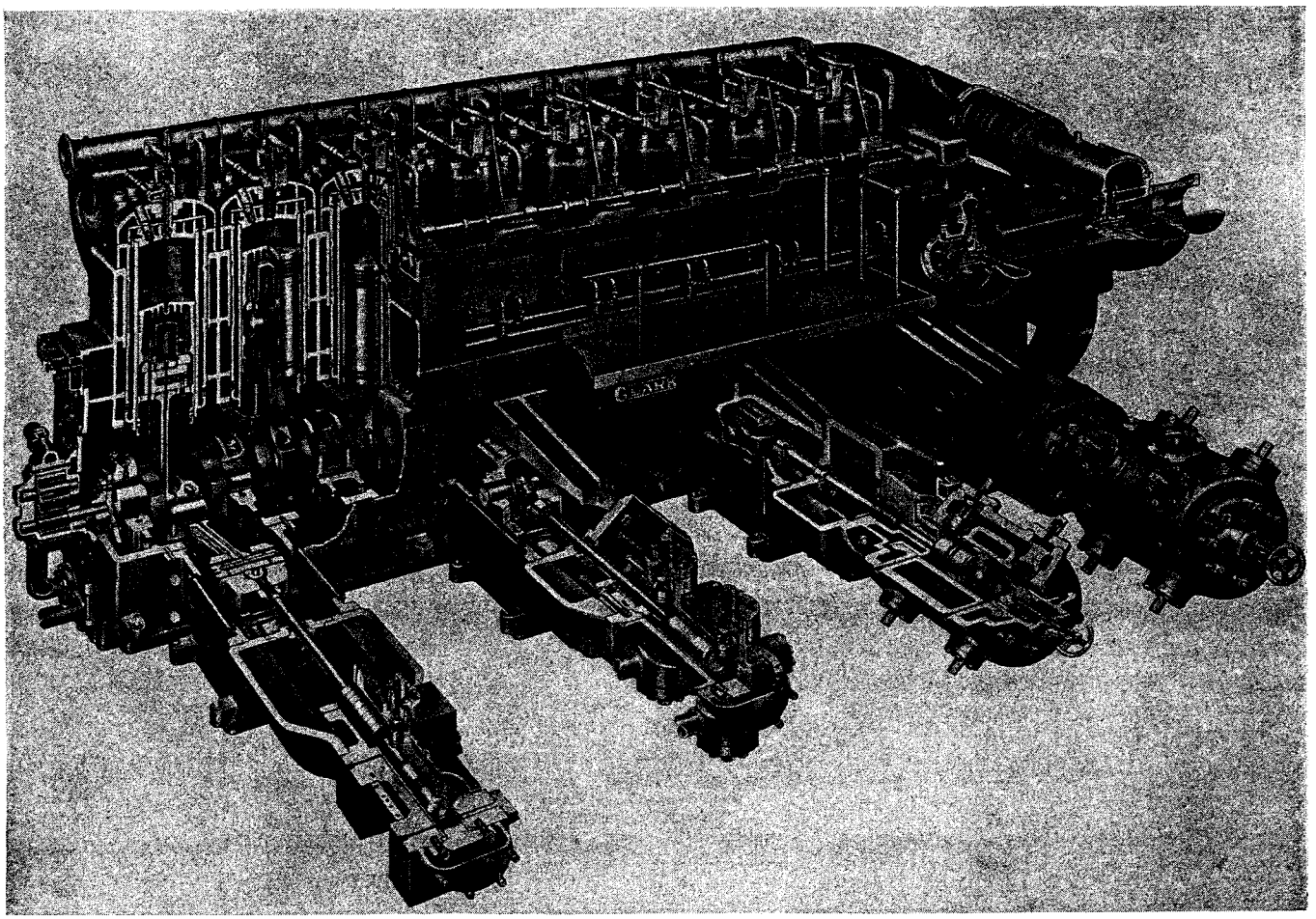

Fig. 17-21. *Turbocharged reciprocating engine-driven compressor, 1,500 brake horsepower. (Courtesy Clark Brothers Company, Div. of Dresser Industries, Inc.)*

instance, containing two 5,000-hp turbines, as compared with a station containing five 2,000-hp reciprocating engines, would have greater difficulty with one unit shut down. The perennial need for a spare unit at compressor stations means that a lot of horsepower must be installed for only intermittent use. Limiting maximum CR's on turbine-driven centrifugals could cause serious difficulty in an emergency, when the required CR at a station might be increased by 50 per cent or even doubled if another station on the same pipeline is completely shut down. On a pipeline serving natural gas to public utilities where continuous operation at market-demand rates is essential, it appears that the place where gas-turbine-driven centrifugals can be most advantageously used is in intermediate booster stations flanked by stations containing reciprocating-engine-driven compressors. Figure 17-22 is a photograph of 10 gas-turbine-driven centrifugal compressors of 6,000 hp each, installed on a platform over Lake Maracaibo in Venezuela and used to compress 137 MMcf/day of gas from 25 psia to 1,950 psia for pressure maintenance in the oil reservoir.

Auxiliaries

Any compressor station must of necessity contain several auxiliaries in order to be an independent plant free of outside utility services, which often are not available. The plant must contain a means of cooling the gas and the compressors. Compressor cylinders are water-jacketed for cooling, since compression becomes more efficient as it approaches the isothermal. Aftercoolers for the compressed gas are also an integral part of any compressor station, and intercoolers are provided between stages in multistage compression. Water is almost universally used as the cooling medium. The water supply is provided if possible from a well, although in some locations it may be necessary to truck in the water. The cooling-water system is normally a closed system, with the heated

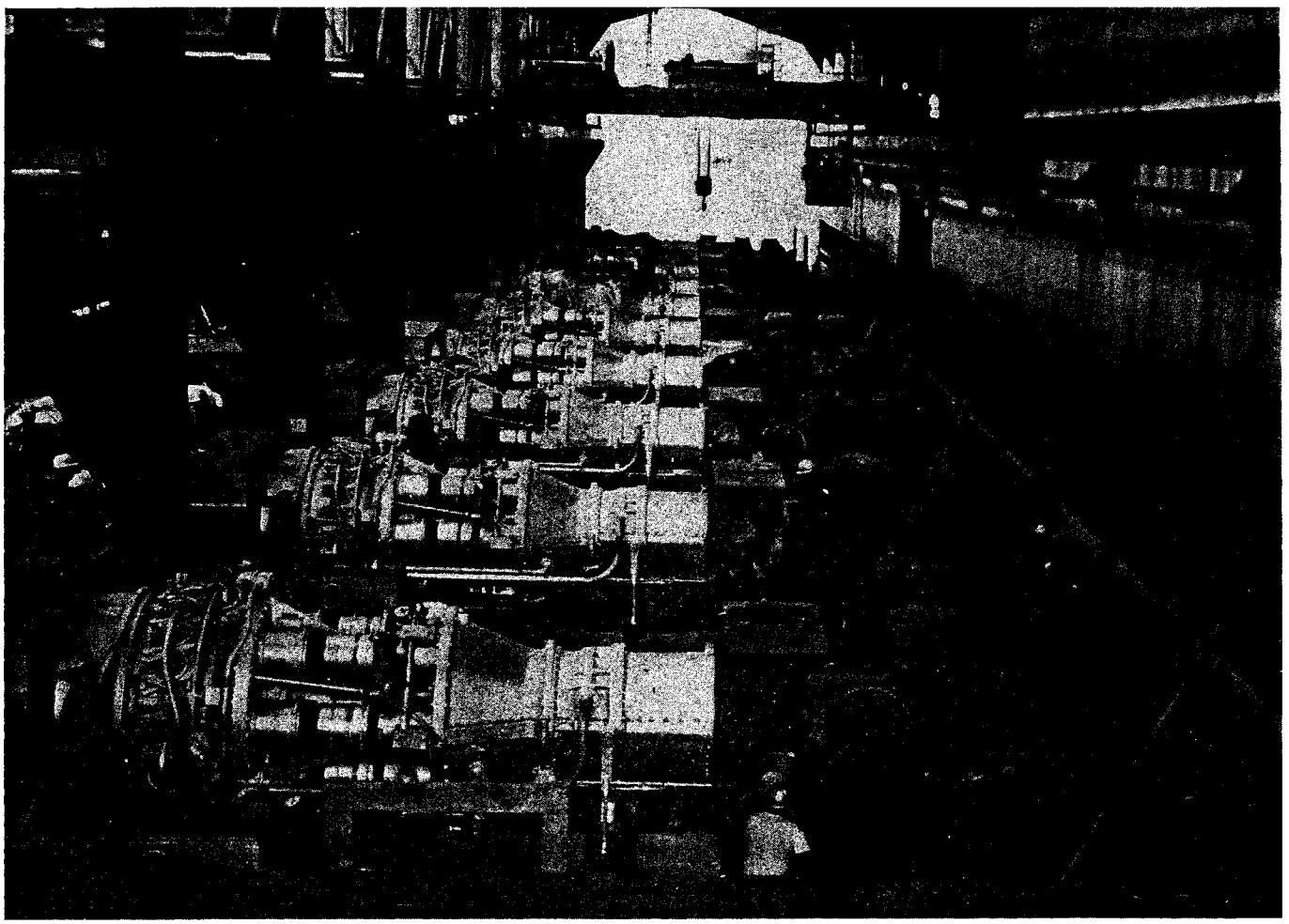

Fig. 17-22. Gas-turbine-driven centrifugal compressors. Ten gas turbines, 6,000 hp each, at Lake Maracaibo. (*Courtesy General Electric Company.*)

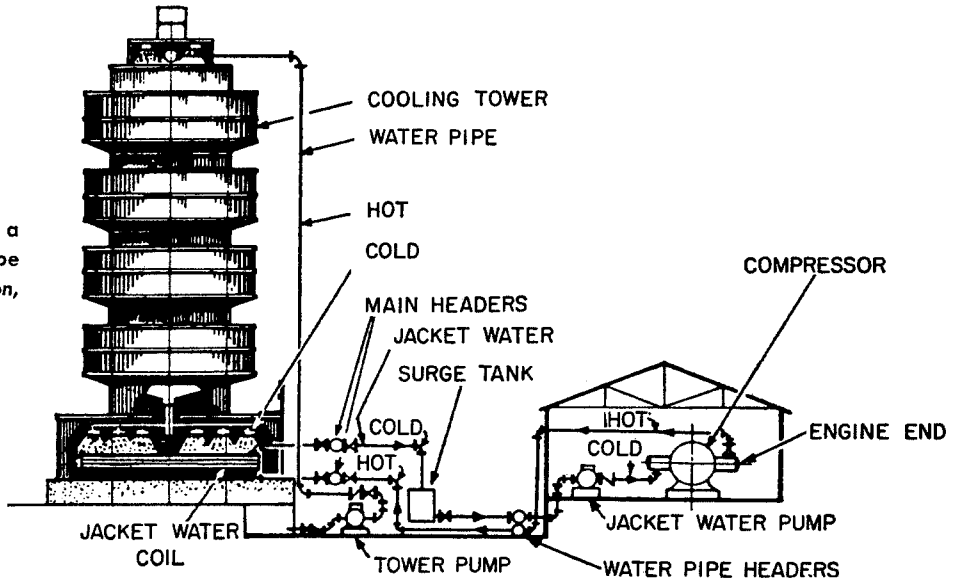

Fig. 17-23. Typical flow diagram for a closed cooling system utilizing the coil type of atmospheric cooling tower. (*De Flon*, 17-10a. *Courtesy Petrol. Refiner.*)

water recirculated over an aerated cooling tower and back to the compressors. Make-up water is provided from a storage tank.

Cooling towers are an important part of most compression or processing plants. They may be of the natural-draft or of the induced-draft type. Water is circulated over the tower by pumps which provide enough pressure to distribute the water as a spray in the tower to provide intimate contact with the air. Figure 17-23 shows a cooling-tower cooling-engine jacket water in a closed system. The variables in cooling-tower design and operation are (1) the approach of cooled-water temperature to wet-bulb temperature, (2) cooling range on water, (3) wind velocity, and (4) tower height.

Finned-tube cooling units are used to cool engine water in closed systems, in place of cooling towers with fans blowing the air over the tubes to increase the heat transfer.

A pressure lubrication system supplies oil under pressure to all main bearings, to connecting-rod bearings, to other bearings, and to many other moving parts in the gas engine and compressor that need lubrication.

The engines are started by compressed air at pressures not exceeding approximately 250 psi. An auxiliary air compressor must be used that is capable of pumping air up to 250 psi. An air receiver or tank of adequate capacity is used to store compressed air.

Gas-engine-driven generators are an integral part of compressor-station auxiliaries; they provide the complete electrical requirements for lighting, small electric motors, controls, pumps, etc.

With the gas-turbine-driven centrifugal compressors, a small expansion-gas turbine expanding natural gas to atmosphere or an internal-combustion engine can be used for cranking or starting.

OPERATION OF PIPELINES—DISPATCHING AND MAINTENANCE

Dispatching of natural gas must be done from the marketing end of a pipeline by the dispatcher's office, which is set up to predict weather conditions and industrial and commercial loads. These predictions must be translated into hourly rates of natural gas to be delivered to the market area. The dispatcher can send out these orders in the form of pressures to be maintained at the upstream end of the pipeline, or as engines to be put on stream at the compressor station, or as volumes of gas to put into the line at the upstream end. It is probably preferable just to leave orders that certain minimum pressures or pressure ranges be maintained on the pipeline. The compressor-station operators or storage-field operators at the source of gas for the pipeline are closer to the operations and in the best position to know what to do in order to establish and maintain the required pressures. It is very difficult to increase line pressures at a time when throughput is high; it usually requires all the horsepower available to do so and perhaps excessive withdrawal from a storage field or storage fields. It is necessary, then, to anticipate heavy loads as far in advance as possible and to increase the line pressure before the load comes on. Line pressures should not be maintained higher than necessary either, for this involves excessive compression.

Maintenance on any pipeline system is a constant vigil. Emergency crews must be trained and must be immediately available to repair line breaks. Leak

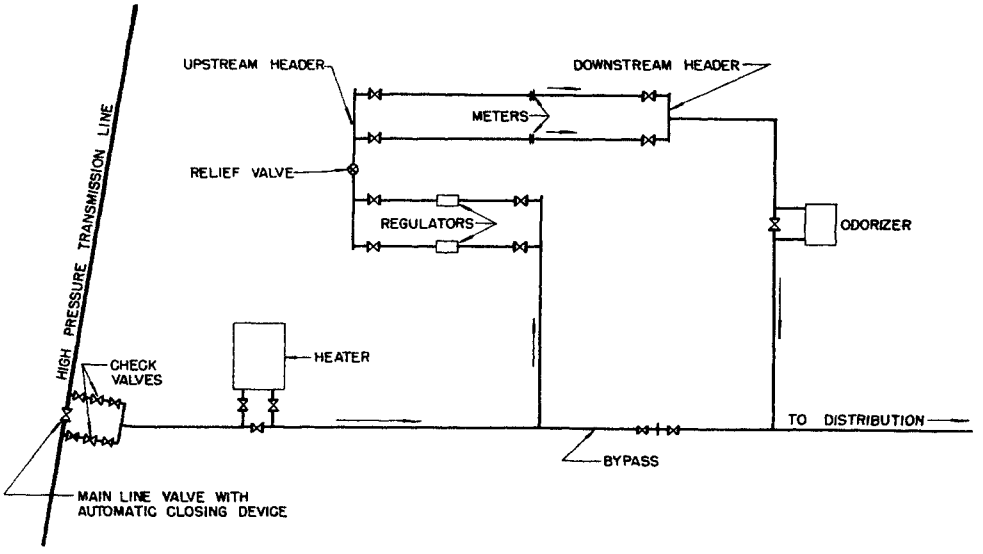

Fig. 17-24. Typical city gate station.

clamps, sections of pipe, and all other necessary repair parts must be available in accessible points at intervals along a pipeline route. Pipeline routes must be walked regularly or inspected by low-level flying. Walking a cross-country pipeline can be done by two men and an automobile. The first man starts walking the pipeline route while the second man drives the automobile around to the next road crossing. He leaves the automobile there and starts walking. When the first man arrives at this road crossing he takes the automobile around to the next road crossing and starts walking. This is repeated until the pipeline is completely walked. Pin-hole leaks and other small leaks will be discovered by this walking or by low-level flying, because vegetation will have turned brown. Walking the pipeline may find some small leaks that might not be observed through flying. These leaks can then be repaired before they become serious and cause an interruption of service. Pipeline valves must be lubricated periodically, and all aboveground piping must be protected from the weather by painting. Maintenance work is a continuing activity around compressor stations. Engines must be overhauled, repairs made, valves and other parts lubricated, buildings and equipment kept clean and painted, etc.

CITY GATE STATIONS

The purpose of a city gate station is to meter gas volumes delivered, control pressures by regulation, and introduce the proper quantity of odorant into the gas stream. Proper selection of the number, capacity, and location of city gate stations depends upon the over-all transmission, storage, and distribution-system design. In general, large distribution systems should be supplied from two or more stations, so that the outage of one station can be offset by the operation of emergency capacity in the other stations. High-pressure transmission mains within populated areas must meet extra and costly material specifications under the 1955 ASA B31.1 code (17-4) for pressure piping. Accordingly, location of terminal points of high-pressure transmission mains at city gate stations must consider present and future real estate development. Location must also be considered for availability of electricity and telephone and year-round accessibility by adequate roads. The location and capacity of the city gate station, coupled with the network of supply mains from the station into the city, can be called the heart of the local distribution system. Their proper design will allow greatly fluctuating loads to be supplied with a minimum of expense, to meet changing and expanding community needs.

A city gate station must be designed carefully. It is the source of supply to the distribution system and the cash register for the local utilities' gas purchase. The contract under which the gas is purchased should set forth the conditions of gas delivery and measurement, which in turn will determine the design of the station. Specifications under the purchase contract should state whether seller or buyer shall install, maintain, and operate at his own expense pressure-regulating, heating, metering, and odorizing equipment. If it is assumed that the seller is so obligated under the contract, the contract should state the delivery pressure and the volume capacity that the seller agrees to furnish to the buyer at the station outlet. In other instances, the seller may only agree to meter the gas at delivery pressures ranging from an agreed minimum to an agreed maximum, the vol-

ume capacity depending upon whether the contract is a full, partial, or limited-requirement contract. Variations in the terms and specifications of the gas-purchase contract will affect the design of the station or stations constructed and operated by the buyer and seller.

Figure 17-24 shows a schematic drawing of the components required in a city gate station, assuming all functions are to be performed in one station. Briefly, the drawing shows a lateral pipe connection to the high-pressure transmission main. Where possible a double connection is made upstream and downstream of an automatic-closing-type main-line block valve. Check valves are usually installed in these connections so that in cases of emergency, when the block valve closes, the connection will not act as a bypass around the block valve. This design is followed to prevent reduction or complete loss of gas supply from a main pipeline break above or below the take-off to the city gate station. Whether such a provision is desirable in any specific instance is a matter of over-all pipeline-system design and operation.

Off the lateral immediately upstream of regulation, a take-off is provided through an indirect gas heater in which the temperature of all or part of the gas may be increased prior to regulation. The need for and capacity of a gas-heating device depends upon the temperature of the gas being delivered, its water-vapor content, and the amount of gas-temperature reduction that will be caused by the adiabatic expansion of the gas in reducing its pressure through the regulators. In this regard, although a gas may be sufficiently dry to prevent hydrate formation and so require no heating for hydrate prevention, care must still be taken to keep gas temperatures above 32°F, or the freezing temperature of water. Serious damage has occurred where groundwater or moisture has frozen around and above gas piping and has resulted in ground swelling and in breakage of piping, structural foundations, and concrete roadbeds.

Regulation of gas pressure can be accomplished with spring-, weight-, or pilot-operated regulators. Figure 17-25 is a cross section of a spring-operated regulator. The top of the diaphragm would be connected directly to the pipe downstream of the regulator. In the spring-operated regulator, downstream gas pressure is against one side of the diaphragm, and a spring set at the pressure to be maintained downstream is on the other side of the diaphragm. When the downstream pressure drops below the spring setting, the spring moves the diaphragm, which is directly connected to the regulator valve, causing the valve to open and allow gas to flow, thus increasing the downstream pressure. When the downstream pressure builds up above the spring setting, the diaphragm moves in the other direction and closes the valve. Pilot-operated regulators hold a minimum pressure variation in the outlet pressure setting and

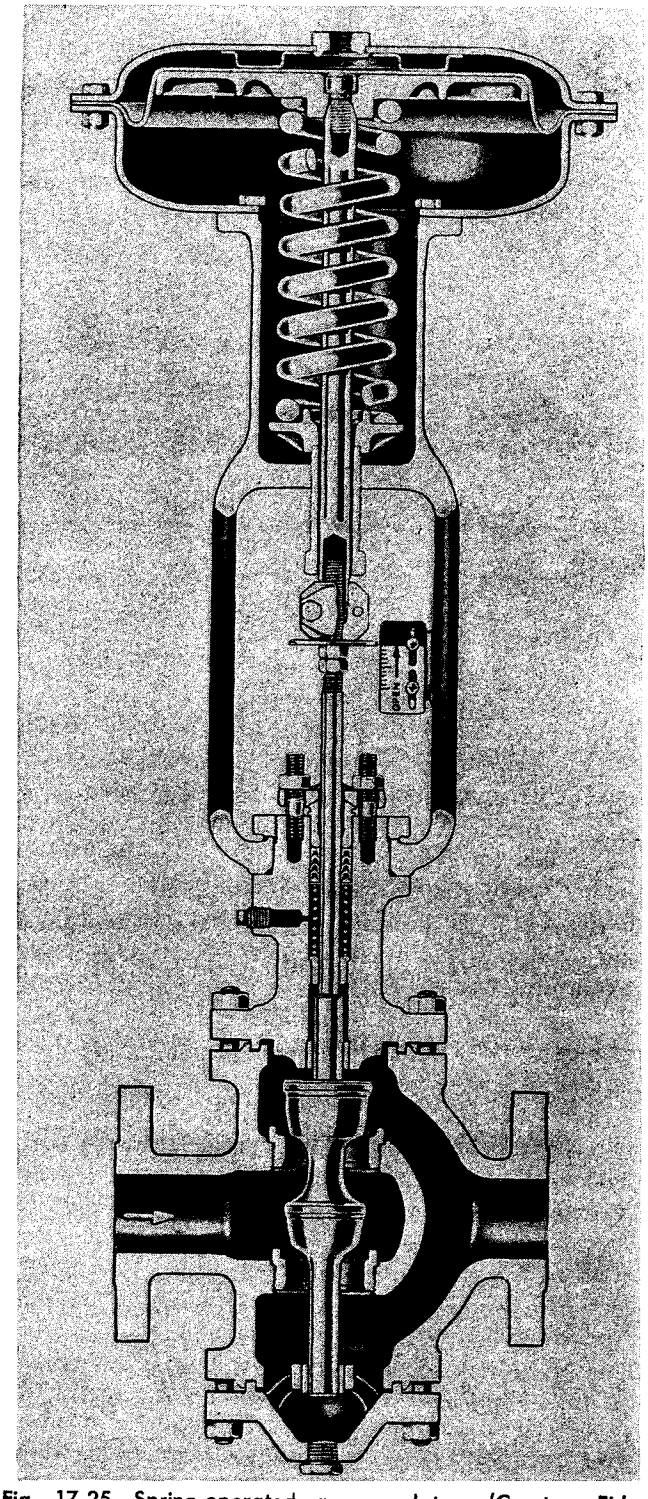

Fig. 17-25. Spring-operated gas regulator. (*Courtesy Fisher Governor Company.*)

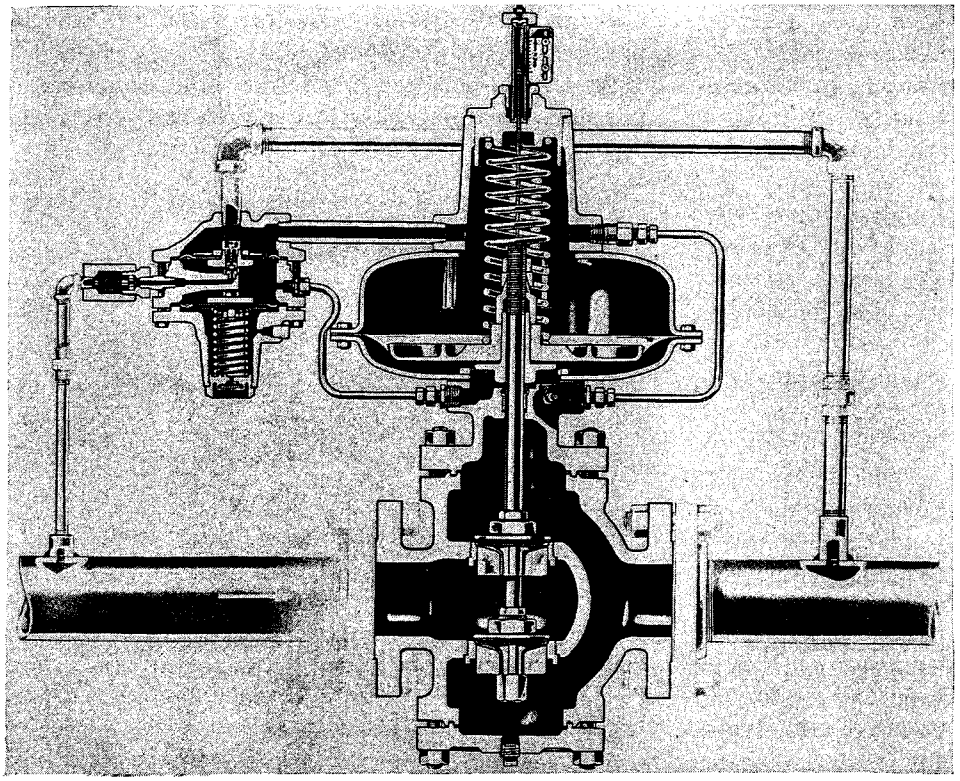

Fig. 17-26. Pilot-operated gas regulator. (*Courtesy Fisher Governor Company.*)

thus ensure more accurate metering. Figure 17-26 shows a cross section of a pilot-operated regulator. With this regulator the downstream gas pressure is against one side of the pilot diaphragm, and opens and closes the pilot valve. When the pilot valve is open it puts upstream gas pressure against one side of the main diaphragm, thus moving the diaphragm and opening the main regulator valve. Sizing of regulators should take into account the desirability of using either more than one regulator or a bypass arrangement so that failure of one regulator will not incapacitate the station.

From the regulators, the gas flows to the upstream metering header. The relative location of this header, its capacity, and its design materially affect the accuracy of the meters. The header acts to cushion the expanded gas leaving the regulators, eliminating pulsation directly from any one regulator into any one meter run. Overpressure safety relief valves are installed on the above-described header. Their function is to protect the meters and downstream piping against excessive pressures in any instance of regulator malfunction or total failure. Generally, the relief system, including piping and valves, is designed to vent gas to the atmosphere at a volume rate adequate to hold a minimum gas pressure on the upstream of the station meters, avoiding complete loss of supply to the distribution system. Figure 17-27 shows a cross section of a safety relief valve. When the pressure setting of the spring is exceeded, the valve opens and vents gas into the atmosphere. Where either of two or more city gate stations is adequate to supply the distribution system, positive shutoff overpressure devices can be used in place of atmospheric-vent pressure relief valves.

Either orifice or positive-type meters are used, depending upon the volumes to be metered. Orifice meters are discussed in detail in Chap. 8. Following the meter runs, the gas is discharged into a downstream header which is similar to the upstream meter header and which acts to cushion the gas stream and eliminate pulsation or surging. Gas odorant is generally introduced at or beyond the downstream meter header. Instrumentation, including calorimeters, gravitometers, recording thermometers, and telemetric pressure equipment, is generally installed in an adjacent auxiliary building.

Specific design and sizing of piping, meters, valves, and regulators for a city gate station can be accomplished by reference to manufacturers' equipment tables, or to the "American Gas Journal Handbook" (17-1) published annually by the American Gas

Journal. Structural design and layout should provide adequate space, ventilation, explosionproof electrical systems, and protection against extreme heat and cold. It may be advantageous to extend the meter-pipe leads and locate the orifice-meter instrumentation in a separate, well-insulated, and heat-controlled auxiliary building. Meter-chart changing, meter calibration, and adjustment are best accomplished where personnel can comfortably and effectively do work of an exacting nature.

Odorization

Natural gases that are free of compounds containing sulfur have practically no odor. It is desirable that the presence of a commodity with such widespread use be detectable by the casual observer. Gas odor

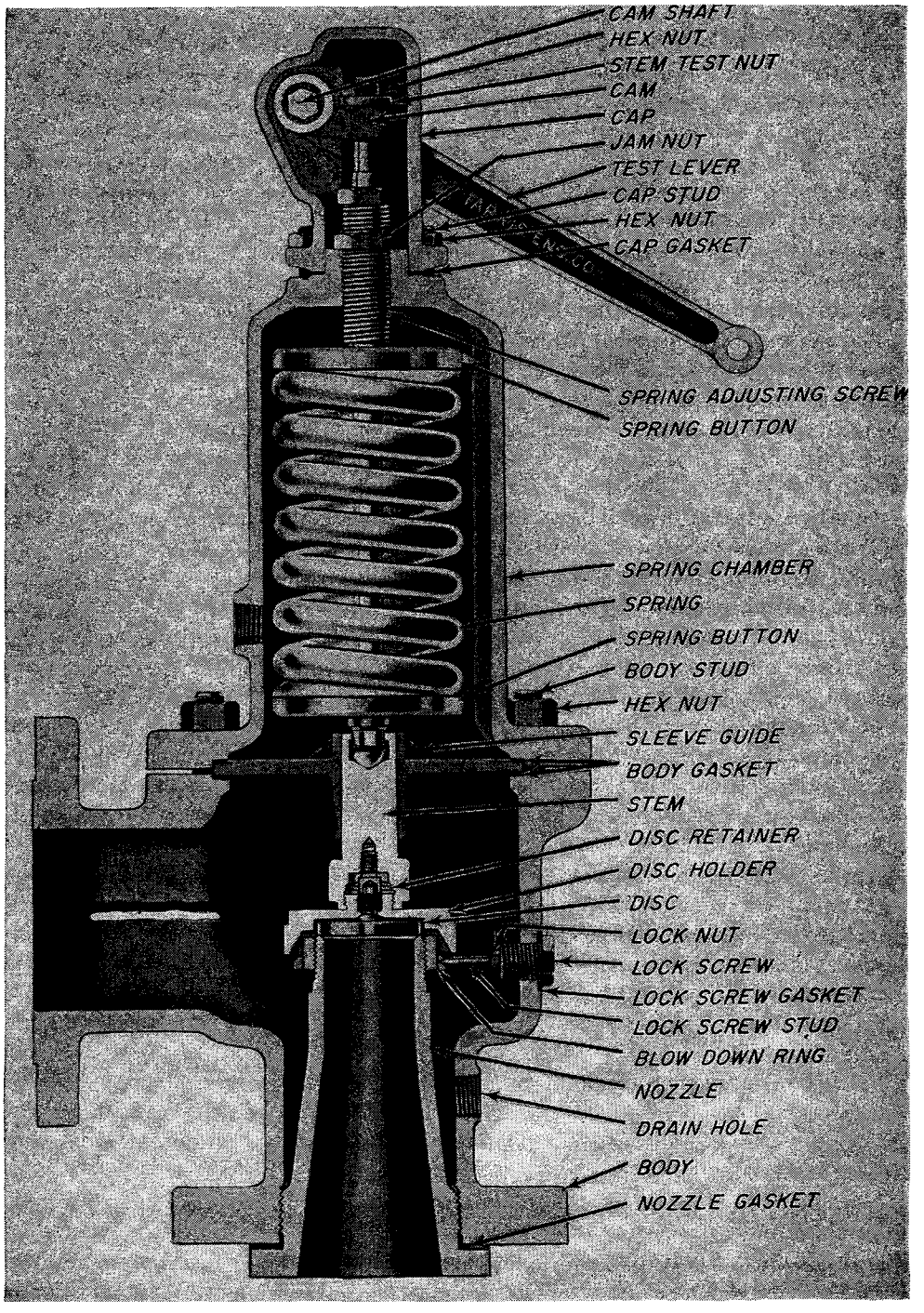

Fig. 17-27. Safety relief valve. (*Courtesy Farris Engineering Corporation.*)

serves as an immediate warning of the presence of gas and as an aid in locating gas leaks. In order to impart to natural gases a characteristic odor similar to the odor of manufactured gases, sulfur-containing compounds are added to the natural gas in trace quantities.

Fuel gases manufactured from sulfur-bearing coals possess a characteristic odor which provides ample evidence of their presence. The odor of manufactured gases derives from unsaturated compounds and sulfur compounds in the coal. The initial search for an odorant aimed to duplicate economically the characteristic odor of manufactured gases.

Early work on gas odorization was carried out by the Bureau of Mines (17-20) in connection with mine safety. Comprehensive studies on the various possible odorants were published in the form of a monograph (17-14). Articles and patents on the subject of gas odorization, abstracted up to 1951 by the Institute of Gas Technology (17-19), indicate the interest and significance of gas odorizing.

The properties of an ideal odorant and of available odorants are listed and discussed below. Contemporary techniques used to odorize natural gas streams are treated briefly.

Properties of Odorants

An ideal odorant would have the following characteristics when mixed with natural gas and exposed to the environments of transmission, distribution, and utilization systems:

1. Chemical stability
2. High odor intensity below condensation concentrations at all pressure-temperature conditions
3. A distinct odor
4. Nontoxic, nonirritating properties
5. Nontoxic, nonodorous combustion products
6. Economical price and low dispensing cost

A list of important properties of some commercial odorants for gases and liquefied petroleum gases have been compiled by Henderson (17-16). Commercial odorants are organic compounds containing sulfur; they may be listed in order of increasing odor strength, as follows:

1. Disulfides
2. Thioethers
3. Carbon-sulfur ring compounds
4. Mercaptans

The odor strength of each class of compounds varies with sulfur-carbon ratio.

The chemical stability of these compounds to environmental conditions provided by gas-transmission systems is also important. The compounds may be listed in order of increasing stability, as follows:

1. Mercaptans
2. Disulfides
3. Thioethers
4. Carbon-sulfur ring compounds

Mercaptans react readily with very low concentrations of oxygen to form disulfides (17-24). The rate of disappearance of the mercaptan is determined by the oxygen concentration, the catalytic activity of the pipeline, and the residence time. Oxygen is not produced from petroleum reservoirs, but is introduced from time to time during some stage of transmission. The trace quantities of oxygen, together with the catalytic effect of the iron oxide coating on pipes, lead to the formation of the more stable, but less odorous disulfides. The disulfides, thioethers, and carbon-sulfur ring compounds are chemically inactive under usual pipeline conditions.

The sorptive properties of different soils to various gas odorants have been studied (17-6). Detection by sense of smell of the emergence of gas from buried lines may be delayed significantly by the adsorptive properties of soils.

Odorants must be effective at concentrations substantially lower than the solubility of the odorant in the gas at the pressures and temperatures encountered while the gas is in transit. An approximate concentration of odorizing material in the gas phase may be predicted from the relationship

$$y = \frac{p}{P} \tag{17-11}$$

where y = mole fraction of odorant in vapor
p = vapor pressure of odorant at the temperature
P = total pressure of system

Equation (17-11) assumes that natural gas is insoluble in the odorant and that there is no effect of total pressure on the vapor pressure of the odorant.

An effective odorant must have a smell sufficiently distinct from other ambient odors to avoid confusion. The sulfur compounds listed above are nontoxic at effective concentration levels. Upon combustion of odorants, sulfur dioxide and sulfur trioxide are produced, but in sufficiently low concentration to be physiologically harmless (17-25).

Although trace amounts of odorants are used in natural gases, the cost of the odorant comprises a major portion of the cost required to install and operate an odorizing station (17-11). The large-scale production of odorants for various services has reduced the price of odorants to an economical level.

Since the purpose of the odorant is to alarm human beings, the sense of smell provides the ultimate measure of odorant effectiveness. This is not to say that

human detection cannot profitably be correlated with analytical procedures capable of detecting trace quantities of sulfur (17-5, 17-15, 17-18). The human sense of smell varies from individual to individual and for the same individual with time. Also, human beings become acclimated or insensitive to odors at concentration levels that would normally be effective, if the concentration is gradually raised from a low level (17-25).

The explosive limit of natural gases in air is approximately 5 vol %. This provides the basis for the legal requirement that the concentration of the odorant be fixed at a value that can be detected by a "normal" individual at a gas concentration in air of 1 vol %. Excessive odorization at domestic outlets is to be avoided, since this would lead to an abnormal number of leak reports (17-8).

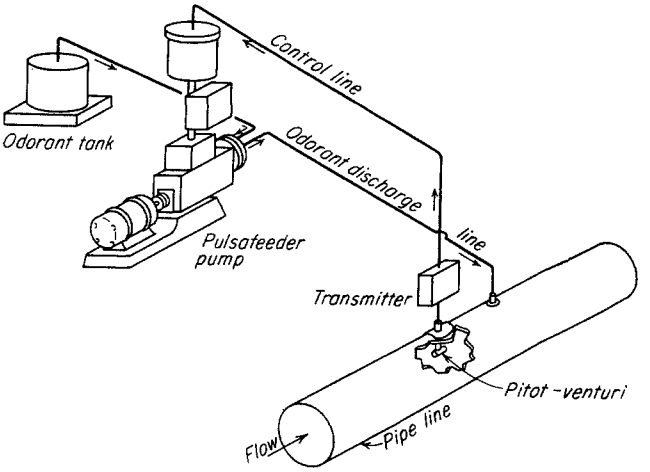

Fig. 17-28. Principal equipment, automatic odorization plant. (Cline, 17-7. Courtesy Petrol. Engr.)

Gas Odorizers

Gas odorizers may be classified according to the method by which the odorant is introduced into the gas. Common methods employ direct injection or mass transfer from a surface wetted by the odorant to a bypassed gas stream. The latter type is frequently called the "absorption odorizer."

An essential feature of all odorizers is that the amount of odorant injected must be proportional to the gas flow rate. Figure 17-28 gives a schematic diagram of a direct-injection odorizer (17-7). The rate of injection is controlled by transmitting a signal from the pitot-venturi tube to a controlled-volume pump. Factors to be considered in the design of odorizer installations are discussed in detail by Manfred (17-23).

DISTRIBUTION SYSTEMS

Mains, services, and meters required to distribute gas to the ultimate consumers constitute the gas-distribution system. The design of new systems and additions to and renewals of existing systems is a branch of gas engineering in itself. The primary objective of good design is to be able to supply the market demand of any customer in the system with a minimum capital investment consistent with sound safety practices. A public utility, being a monopoly, accepts the responsibility of supplying the demand of each and every customer within its service area without discrimination, provided any specific main or service extension is economically feasible in view of the capital outlay versus the gas revenue involved. The ultimate in successful design is to be able to offer adequate gas service economically to any customer within the service or "franchised" area. The degree to which a distribution system fails to provide such service reflects upon the engineering-design practices of the utility involved. Considering the rapid growth of communities, the demand for large gas volumes for residential and commercial space heating, and the increasing needs of commercial and industrial customers, the distribution-design policies become the major engineering and investment problem for the natural gas–distributing utility.

Natural gas is seldom introduced into a community where a manufactured-gas distribution system does not already exist. For the most part, these old systems were designed for relatively small gas-volume throughput where ¼-psig distribution pressures in nominally-sized-diameter mains were adequate. In larger systems, intermediate system-supply mains at higher pressures were used to feed the ¼-psig system at strategic points located some distance from the gas-manufacturing plant. Construction of these older systems started fifty and more years ago and, through the years, they have served the industry very well. Engineering knowledge, construction, and maintenance techniques have made it possible to repair, renew, replace, and extend these older systems to distribute natural gas as required. Specifically, when and where to repair and when and where to replace these older systems in whole or in part are problems for the distribution-design engineer. With a new system and with the new techniques available for welding steel pipe, X-ray examination, cathodic protection, compression fittings for cast-iron mains, pressure testing of facilities, regulator safety overpressure devices, and so forth, the engineer knows that considerably higher distribution-system pressures

can be utilized today with less risk and greater safety than was ever possible with the old ¼-psig-pressure manufactured-gas distribution systems. Accordingly, every engineering and construction-technique advantage must be exploited to result in the safest, most flexible-capacity distribution system per dollar invested. This directly relates to distribution-design policy, which determines whether a system is to be designed to function ultimately at ¼, 2, 10, 25 psig, or higher maximum distribution pressure. Considering the ultimate demand on the system, this is usually determined on the basis of integration with the old system and estimation of the maximum pressure the old system can be graded up to by compression clamping of bell joints, renewal of poor pipe, etc. In many instances, a distribution system is divided into pressure-design areas, with the boundaries of each area dictated by the economics in establishing proper distribution pressures. Total replacement of a system or a portion thereof may be warranted, and the new system designed for 15 to 25 psig ultimate maximum distribution pressure.

Natural gas is generally delivered to the distribution system at one or more city gate stations at pressures not less than 150 psig and up to 500 psig or higher. The delivery pressure may be determined by the transmission-main operating pressure in the area or may be a matter of contractual obligation. System supply mains from the city gate stations into the distribution system are designed to take full advantage of the city gate delivery pressure. The higher the pressure, the greater the number of smaller-size supply mains that can be constructed to all parts in and around the system to give the most flexibility in design.

In designing the various street mains in a distribution system to serve individual residential or commercial customers, it is first necessary to establish a maximum pressure at which the system will operate. This pressure could vary anywhere from ¼ to 25 psig. If street-main pressures are maintained much above ¼ psig it will be necessary to install individual house or service regulators. The next step is to establish the volumes of gas that these mains will be expected to deliver. Average residential and commercial space-heating consumption factors per customer may be used. These consumption factors are explained in Chap. 18, Underground Storage of Natural Gas. It may be advisable to go to each customer or prospective customer and attempt to determine the input capacity of each of his present or prospective appliances and other gas-burning equipment.

It will be necessary to establish a pressure setting for all individual house regulators, usually 5 to 8 in. of water column. Permissible pressure drop and sizing of service from the street main to the service regulator must be established, usually a minimum size of 1 in. for 2-psig mains or ¾ in. for 10-psig mains.

The area to be served by the specific street-main system under consideration must be delineated, and points must be selected at which street regulators supply high-pressure gas to the system.

Large-volume commercial and industrial customers using more than 2,500 cu ft/hr are usually considered separately, and mains are designed to serve them individually and directly from or with high-pressure gas.

Sizing of street mains is accomplished with special low-pressure design formulas. One such formula used widely in the natural gas industry is the Spitzglass formula. For pressures not exceeding 1 psig the formula may be stated as follows:

$$Q = 3{,}550K\left(\frac{h}{GL}\right)^{1/2} \qquad (17\text{-}12)$$

where Q = flow at 14.73 psia and 60°F, cu ft/hr
h = pressure drop, in. of water column
G = specific gravity of gas
L = length of pipe, ft
$K = \left(\dfrac{d^5}{1 + 3.6/d + 0.03d}\right)^{1/2}$
d = ID of pipe, in.

For pressures exceeding 1 psig, the formula becomes

$$Q = 4{,}830K\left(\frac{Pa}{GL}\right)^{1/2} \qquad (17\text{-}13)$$

where Q, G, L, K, d are used as above
P = pressure drop, psi
a = average pressure in pipeline, psia

Other formulas that have been used for sizing of low-pressure street mains are the Pole formula and the Fritzsche formula. The Fritzsche formula is used for main pressures of 15 psig or less and sizes of 8 in. or smaller. These formulas are discussed by Stephens and Spencer (7-40), and examples of factors to apply to the Spitzglass formula for specific applications are given in the "American Gas Journal Handbook" (17-1).

The design formula, Eq. (17-6), discussed earlier in this chapter is also applicable to distribution-system piping. The location class for distribution mains would always be class 4.

Cathodic protection for distribution mains is just as essential as it is for transmission mains. Cathodic protection in distribution systems must usually be planned in conjunction with other utilities that have underground facilities. Stray currents are more prevalent in cities than they are cross-country, and they must be considered and counteracted when cathodic-protection systems are planned.

CHAPTER 18

Underground Storage of Natural Gas

Underground gas storage may be defined as the storage in reservoirs of porous rock at various depths beneath the surface of the earth of large quantities of natural gas not native to these reservoirs. The gas is stored in the pore spaces within the rock that originally contained gas, oil, or water. Reservoirs that produced gas or oil before their use for storage have exhibited their ability to hold gas under pressure. Gas is being stored in water-bearing formations, "aquifer storage," in a few cases where there are no depleted petroleum reservoirs near the market area.

The importance of underground storage to the natural gas industry may be seen from Table 18-1, which shows its growth since 1944.

Before planning storage-field capacity and deliverability, one must have a knowledge of the market requirements. The influence of the weather on sales of gas for space heating of buildings is important. When the annual storage volumes and daily delivery rates are developed for a distribution system, the facilities for storage fields may be designed to meet the need. The use of partially depleted gas fields, partially depleted oil fields, and aquifers will be described.

Trend to Full Pipeline Loads

The highly industrialized northeast and north central areas of the United States and eastern Canada are the "have-nots" with respect to natural gas reserves. The natural gas fuel supplies must be brought in by long-distance pipelines, as long as 2,000 miles, from the southwestern part of the United States and western Canada. The goal of the companies operating long-distance pipelines is operation at 100 per cent of capacity every day the year round. This type of operation permits the lowest possible transportation cost. It allows distribution of all costs—operation, maintenance, depreciation, general administration, and tax—over the largest quantity of product, thereby reducing the cost per unit quantity of product. Operation at 100 per cent of annual capacity is termed 100 per cent "load factor." The total annual actual deliveries divided by the total annual delivery capacity is termed the "percentage load factor" of operation of a pipeline.

The trend is toward pipeline operation at higher and higher load factors. This is accomplished in many instances by making off-peak or interruptible industrial sales at lower rates. In other cases, the utilization of underground gas storage located at or near the marketing areas makes possible high-load-factor operation of long-distance pipelines.

LOAD FACTORS IN GAS DISTRIBUTION

All types of natural gas sales, whether domestic, commercial, industrial, or space-heating, present variable load factors. Probably the most difficult load for the distributor to meet is the space-heating load. It varies from a minimum of zero in the summertime to a maximum that can occur any time during the cold winter months. Natural gas is generally accepted as a premium fuel for domestic space heating, and it can command a higher price and still compete with other fuels. Probably the largest remaining potential market for the natural gas distributor is residential space heating. The problem of the distributor, then, is to find efficient and economical

Table 18-1. Growth of Underground Storage of Natural Gas in the United States*

Year	Number of pools	Number of states	Output from storage,† MMMcf	Estimated ultimate capacity, MMMcf
1944	50	11	...	135
1947	70	11	...	250
1949	80	11	...	497
1950	125	15	143	774
1951	142	15	200	916
1952	151	16	235	1,292
1953	167	17	233	1,735
1954	172	17	304	1,859
1955	178	18	352	2,096
1956	188	20	492	3,402

* Data as of Dec. 31, 1956, from the 6th Annual Report on Statistics, AGA committee on underground storage.

† Computed on year ending Oct. 31.

methods of handling the load-factor problem in distribution of space-heating gas.

Space-heating Load

Let us take a look at the magnitude of variation of the space-heating load. Space-heating loads are usually correlated with degree-day deficiencies in atmospheric temperatures obtained by the U.S. Weather Bureau. An atmospheric temperature of 65°F is taken as the base temperature at which no space heat is required. A mean atmospheric temperature of 64°F for a day would amount to 1 degree-day deficiency. A mean temperature of 0°F for a day is equivalent to 65 degree-days. A normal heating season in Detroit, for instance, totals 6,404 degree-days. This is a 30-year average (1921–1950) based upon U.S. Weather Bureau records. Table 18-2 lists the 30-year average degree-days by months for twenty-four cities scattered across the United States and one city in Canada. As can be seen from Table 18-2, approximately 70 per cent of the total heating load occurs during the four months of December, January, February, and March, whereas less than 5 per cent occurs during the four months of June, July, August, and September. Minimum weather variations throughout the year in the United States are found on the West Coast.

A distributing company with annual sales of 200 MMMcf of natural gas of which 50 per cent was space-heating load, the remaining sales being made at 100 per cent load factor, would need storage capacity of between 35 and 40 per cent of its space-heating load, in this instance 35 to 40 MMMcf, in order to be able to purchase gas from a long-distance pipeline at 100 per cent load factor. This is a tremendous amount of storage, and can be achieved economically only by use of large underground storage fields.

Figure 18-1 is a plot of the degree-day normals in Detroit, Mich., by days for a complete year. It shows clearly the variation in space-heating load within a year, based upon 30-year average normals. To show the complete picture, however, the individual yearly variation from normal in total degree-days and the daily variation from normal within any specific year must be shown. Figure 18-2 shows the variation in total annual degree-days by years from 1900 to 1953 for eight typical cities. Figure 18-2 shows clearly that variations in the total number of degree-days for Detroit since 1900 have been as much as 18 per cent colder and 15 per cent warmer than normal. This means that the space-heating load can vary considerably from year to year; it poses another problem for the pipeline companies, especially for the ones whose purchase contracts with producers call for

Table 18-2. Average Degree-days by Months

City	Jan.	Feb.	Mar.	Apr.	May	June	July	Aug.	Sept.	Oct.	Nov.	Dec.	Annual
Detroit	1,203	1,072	927	558	251	60	0	8	96	381	747	1,101	6,404
Chicago	1,243	1,053	868	507	229	58	0	0	90	350	765	1,147	6,310
New York	1,001	910	747	435	130	7	0	0	31	250	552	902	4,965
Minneapolis	1,562	1,310	1,057	570	259	80	8	17	157	459	960	1,414	7,853
Omaha	1,302	1,058	831	389	175	32	0	5	88	331	783	1,166	6,160
Denver	1,125	924	843	525	286	65	5	11	120	425	771	1,032	6,132
Seattle	862	675	636	477	307	155	75	70	192	412	633	781	5,275
San Francisco	530	398	378	327	264	164	144	136	101	174	318	487	3,421
Los Angeles	378	305	273	185	121	56	31	22	56	87	200	301	2,015
Salt Lake City	1,194	885	741	453	233	81	0	0	88	381	771	1,039	5,866
Houston	394	265	184	36	0	0	0	0	0	7	181	321	1,388
Louisville	933	778	611	285	94	5	0	0	51	232	579	871	4,439
St. Louis	1,017	820	648	297	101	11	0	0	45	233	600	927	4,699
Washington, D.C.	893	781	619	323	87	0	0	0	37	237	519	837	4,333
Memphis	725	574	427	139	24	0	0	0	17	126	432	673	3,137
Atlanta	632	512	404	133	20	0	0	0	8	110	393	614	2,826
Tampa	201	148	102	0	0	0	0	0	0	0	60	163	674
Phoenix	921	717	626	368	164	17	0	0	34	261	582	843	4,533
Albuquerque	970	714	589	289	70	0	0	0	10	218	630	899	4,389
Oklahoma City	865	650	490	182	40	0	0	0	14	154	480	769	3,644
Portland (Maine)	1,373	1,218	1,039	693	394	117	15	56	199	515	825	1,237	7,681
Winnipeg (Canada)	2,027	1,686	1,445	725	397	214	42	96	396	781	1,305	1,767	10,881
Helena	1,469	1,165	1,017	654	399	197	36	66	320	617	999	1,311	8,250
Bismarck	1,730	1,464	1,187	657	355	116	29	37	227	598	1,098	1,535	9,033
New Orleans	364	248	190	31	0	0	0	0	0	7	169	308	1,317

SOURCE: U.S. Weather Bureau records, 30-year average, 1921–1950.

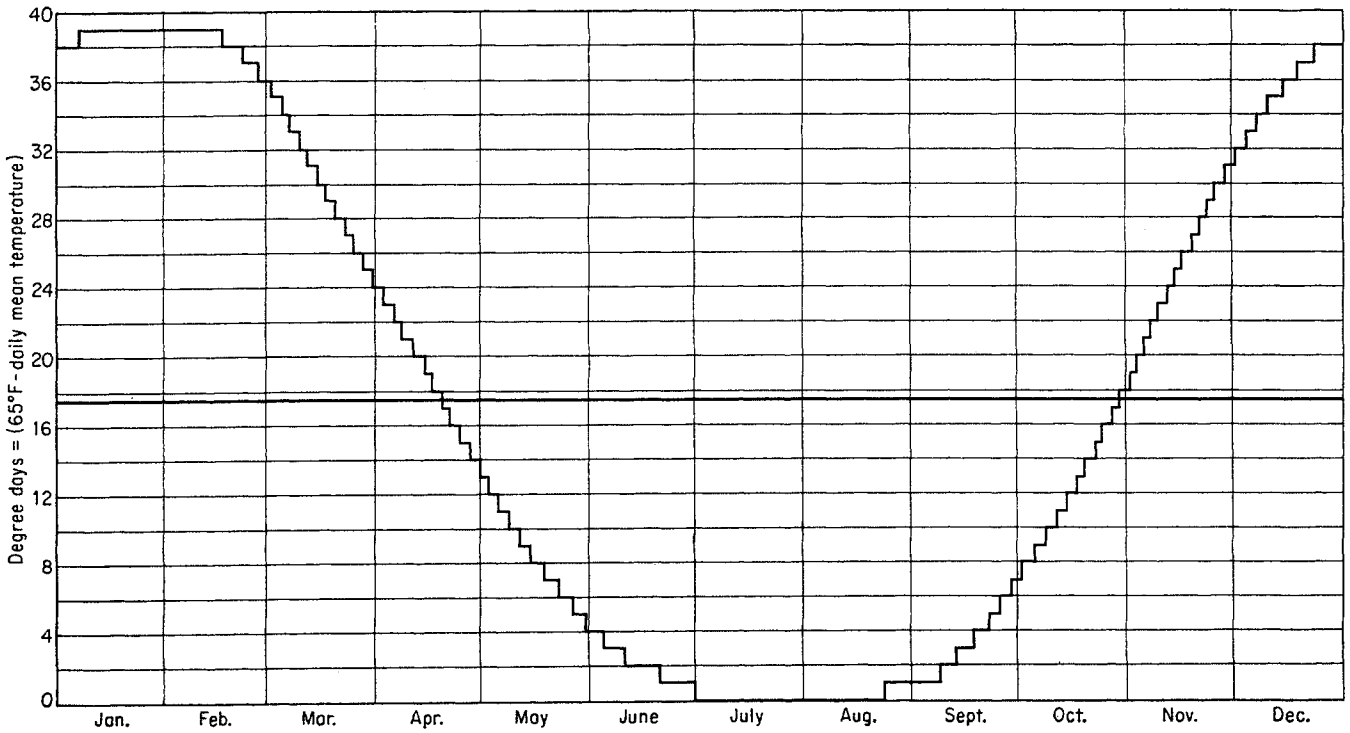

Fig. 18-1. Degree-day normals: Detroit, Mich.

fixed quantities of natural gas with penalties to be paid for annual purchases lower than the fixed quantity. The problem is where to find additional supplies of gas, how much additional pipeline capacity to install against colder than normal winter seasons, and how to dispose of excess quantities of gas in warmer than normal seasons. Interruptible industrial sales are, then, essential even for companies that have underground storage, in order to dispose of excess quantities of gas accruing from warmer than normal weather conditions for a season.

Figure 18-3 shows the daily variation in degree-days for New York City and Detroit, for winter seasons 1941–1942 to 1953–1954. It can be seen from the charts that during this period the winter-season peak day in New York City occurred as early as December 15 and as late as February 21. The second coldest day in the winter of 1948–1949 occurred on March 19. In Detroit during the same period, the winter-season peak day occurred as early as December 14 and as late as February 20. Peak days occurring late in the winter season are much more critical than those occurring early. Late in the season, supplies of storage gas are approaching depletion, there is less pressure to cause gas flow from wells, and compression horsepower requirements are larger.

There is also considerable hourly variation in temperature throughout a 24-hr day. A clear winter day can mean a much greater spread between the maximum and minimum temperatures than a cloudy day. Figure 18-4 shows hourly temperature variations for several typical winter days.

Wind velocity is another factor that affects fuel consumption considerably: a high wind velocity causes higher fuel consumption. Distributing companies normally do not include wind velocity as a separate factor in estimating maximum-day fuel consumption. Wind velocities are related more to geographic location than to any other one factor, and so would be compensated for in an over-all consumption factor for any specific locality.

Other Loads

Industrial sales may be defined as those made to manufacturing companies that do not deal directly with the consumer. They are probably the largest annual sales for most gas companies, except for space-heating sales. These sales are primarily an 8 A.M.–to–5 P.M., Monday-to-Friday load. Holidays also have a significant effect upon industrial sales. Commercial sales, though appreciably smaller for most companies, exhibit the same load characteristics as industrial sales. Commercial sales are those made to business establishments selling directly to the consumer. Domestic sales, which include cooking, refrigeration, water heating, clothes drying, and in-

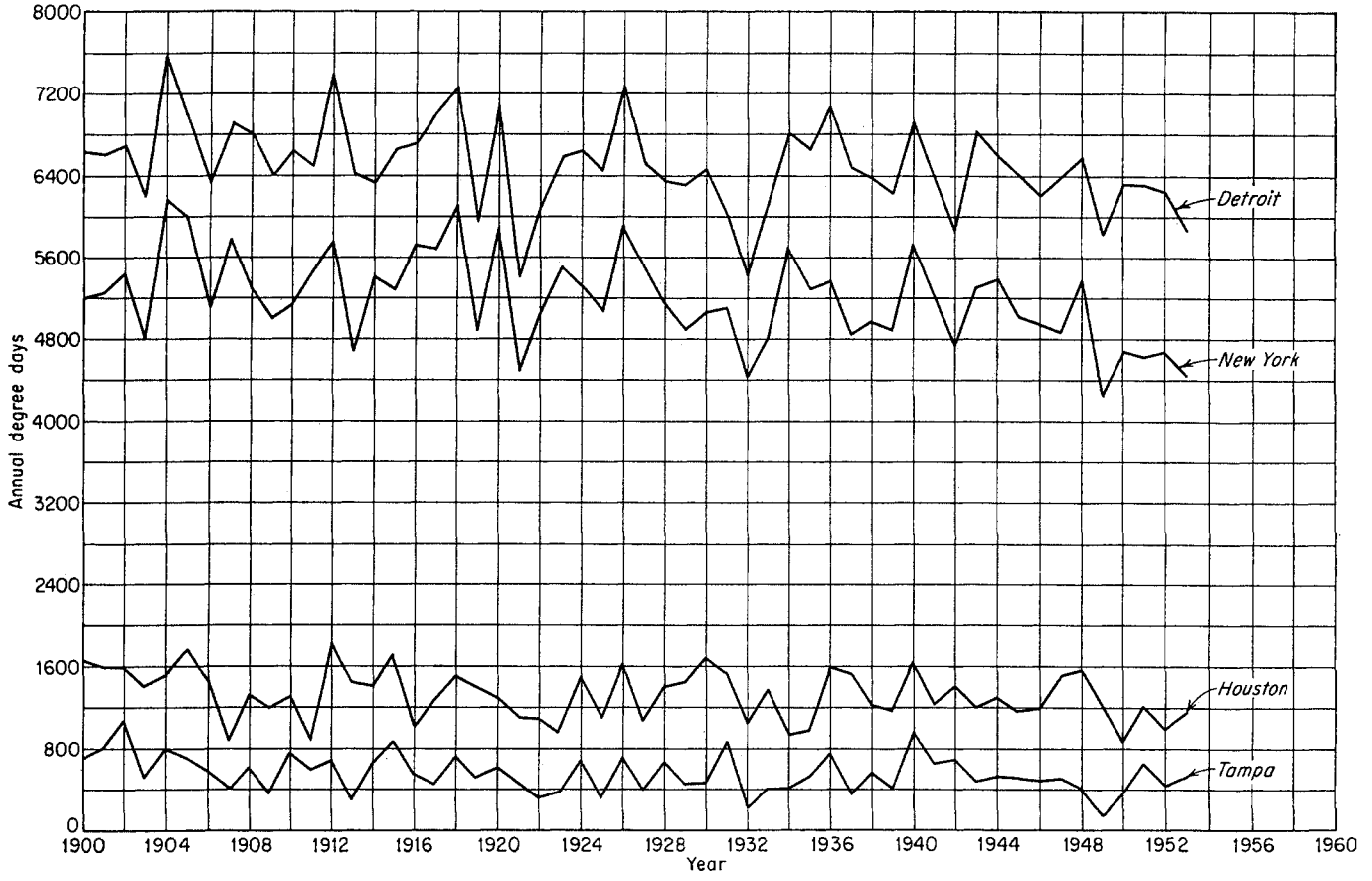

Fig. 18-2. (*Above and opposite*) Annual degree-days by years.

cineration, present a Monday morning water-heating and clothes-drying peak load, a 4 P.M.–to–6 P.M. cooking peak load, and a summertime refrigeration peak load. The air-conditioning load, a summertime load, is growing fast and is of especial significance in the warmer areas of the United States.

DISTRIBUTION-SYSTEM LOAD FACTORS

The over-all load factor for any distribution system depends upon the relative volumes of the types of sales listed above. Figure 18-5 illustrates the daily sendouts for a period of 1 year for five cities in the north central area of the United States. Curve *A* is for a small resort town with about 1,800 meters serving 800-Btu propane-air. It has no space-heating load; and its peak sendout occurs during the summertime, when many tourists are in the area. Curve *B* is for a larger town of approximately 19,400 meters with small industrial sales, only 9 per cent of its total sales, and with a heating saturation of 35 per cent. "Space-heating saturation" is a term used frequently in the natural gas industry. Although there are variations in definition within the industry, the term is used here to mean the percentage of the total number of residential and commercial meters (excluding industrial meters) that use gas for space heating. Curve *C* is for a city of approximately 77,000 meters with small industrial sales, about 14 per cent of the total sales, and a heating saturation of 46 per cent. Curve *D* is for a small town of 2,800 meters with a high heating saturation of 82 per cent and small industrial sales. Curve *E* is for a city of 26,700 meters with high industrial sales, about 35 per cent of total sales, and a heating saturation of 41 per cent.

Notice the decreasing load factor as space-heating saturation increases. Observe the larger fluctuations on weekends during the summertime for curve *E*, the city with high industrial sales. The curves also point

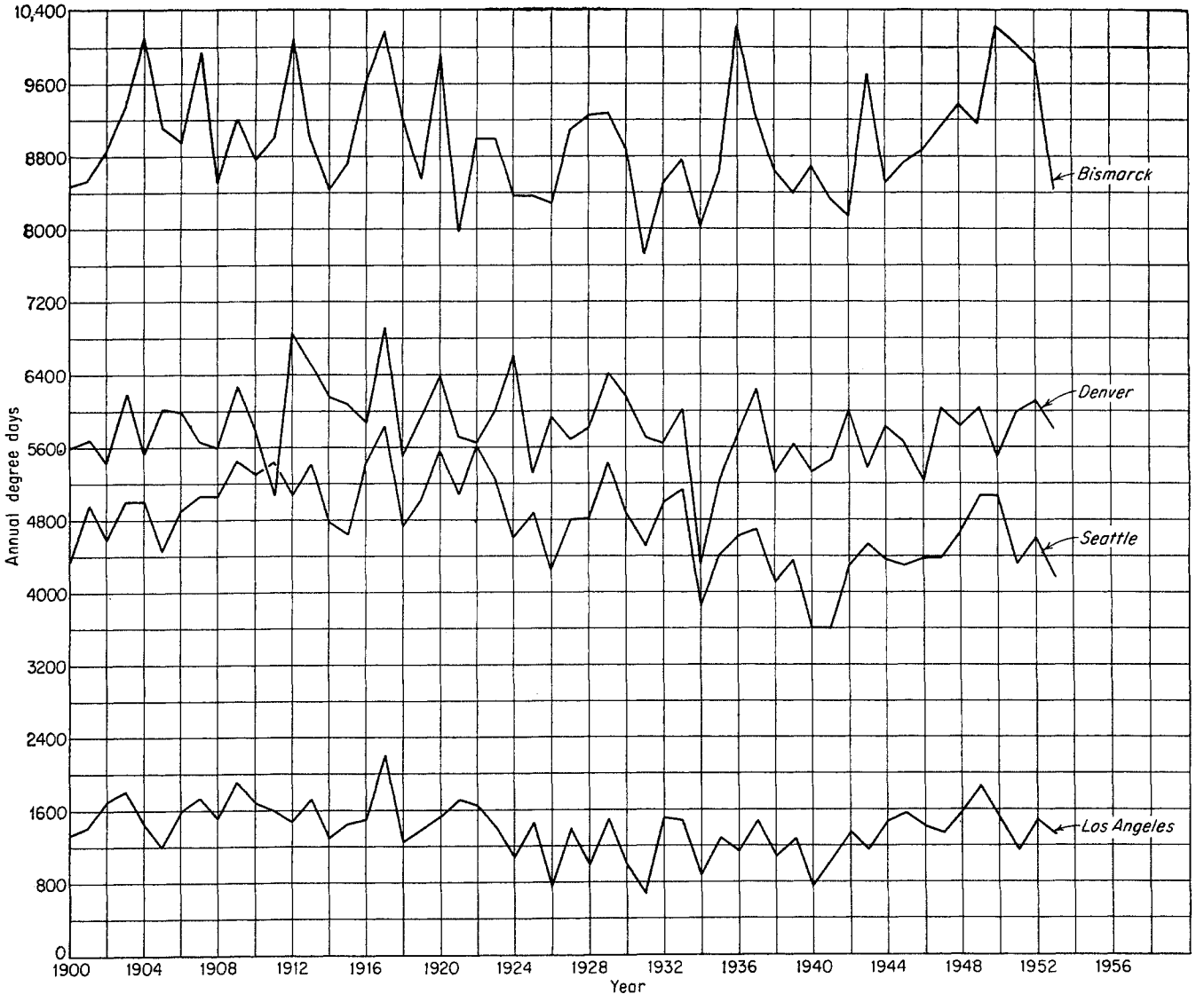

up vividly the fact that where space-heating saturation is significant the fluctuating character of other types of loads is not noticeable during the heating season.

Figure 18-6 is a plot of hourly load variations for typical winter and summer days for the same city as curve *C* in Fig. 18-5. The maximum sendout occurs consistently both winter and summer at approximately 9 A.M. and the minimum from midnight to 4 A.M. During the summertime an increased sendout from 4 P.M. to 6 P.M. reflects the cooking load, whereas, during the wintertime, the space-heating load almost completely masks the cooking load.

PREDICTING FUTURE SENDOUT

The problem of predicting future sendout is an important one, and predictions must be made a year or more in advance in order to ensure adequate supplies of natural gas and facilities to handle the predicted sendouts. Sendouts, and especially peak-day sendouts, must be estimated for all classes of service and then combined into a total peak-day and peak-hour sendout. The problem becomes more difficult in a new area where there is no previous consumption experience.

Consumption Factors

A reasonable range in consumption factors per customer for various classes of service is shown in Table 18-3.

The annual consumption factor per residential customer depends largely upon the number of domestic appliances installed in each customer's home, such as water heaters, ranges, refrigerators, clothes dryers, incinerators, etc. In general, in any market area where the distributing company maintains an aggressive sales policy, the residential consumption factor

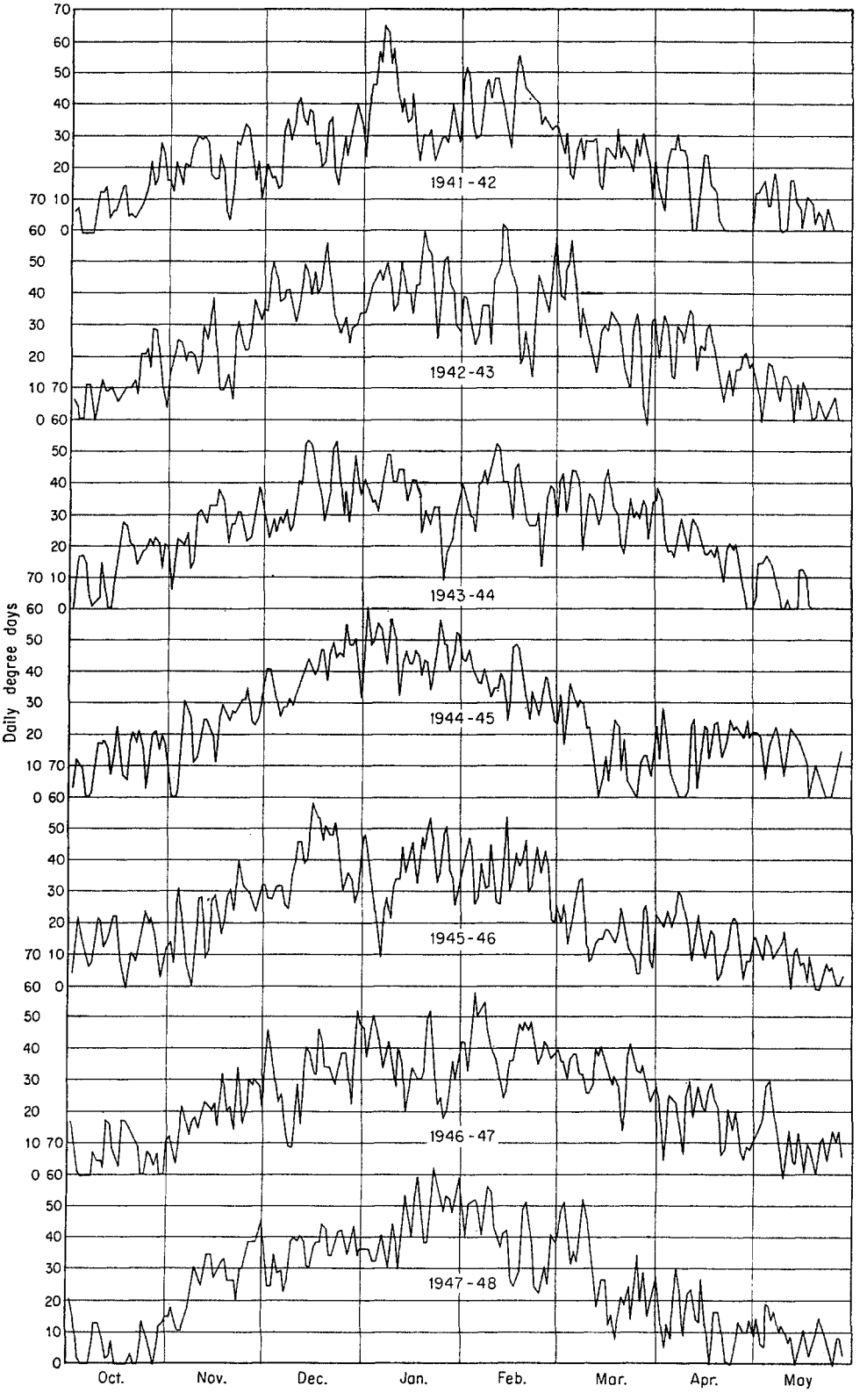
Daily degree days
1941-42
1942-43
1943-44
1944-45
1945-46
1946-47
1947-48
Oct.
Nov.
Dec.
Jan.
Feb.
Mar.
Apr.
May

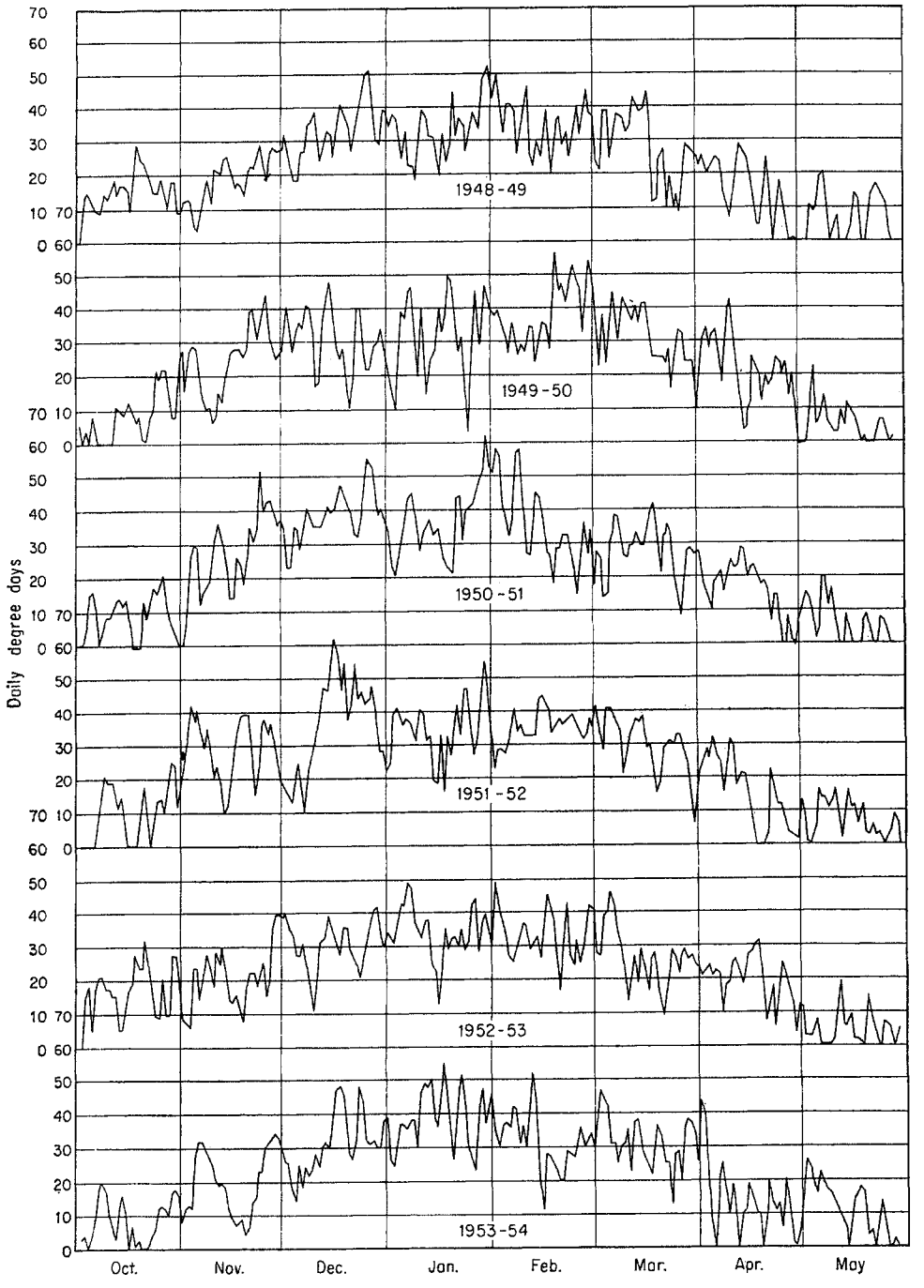

Fig. 18-3a. (*Opposite and above*) **Daily degree-days, Detroit, Mich.**

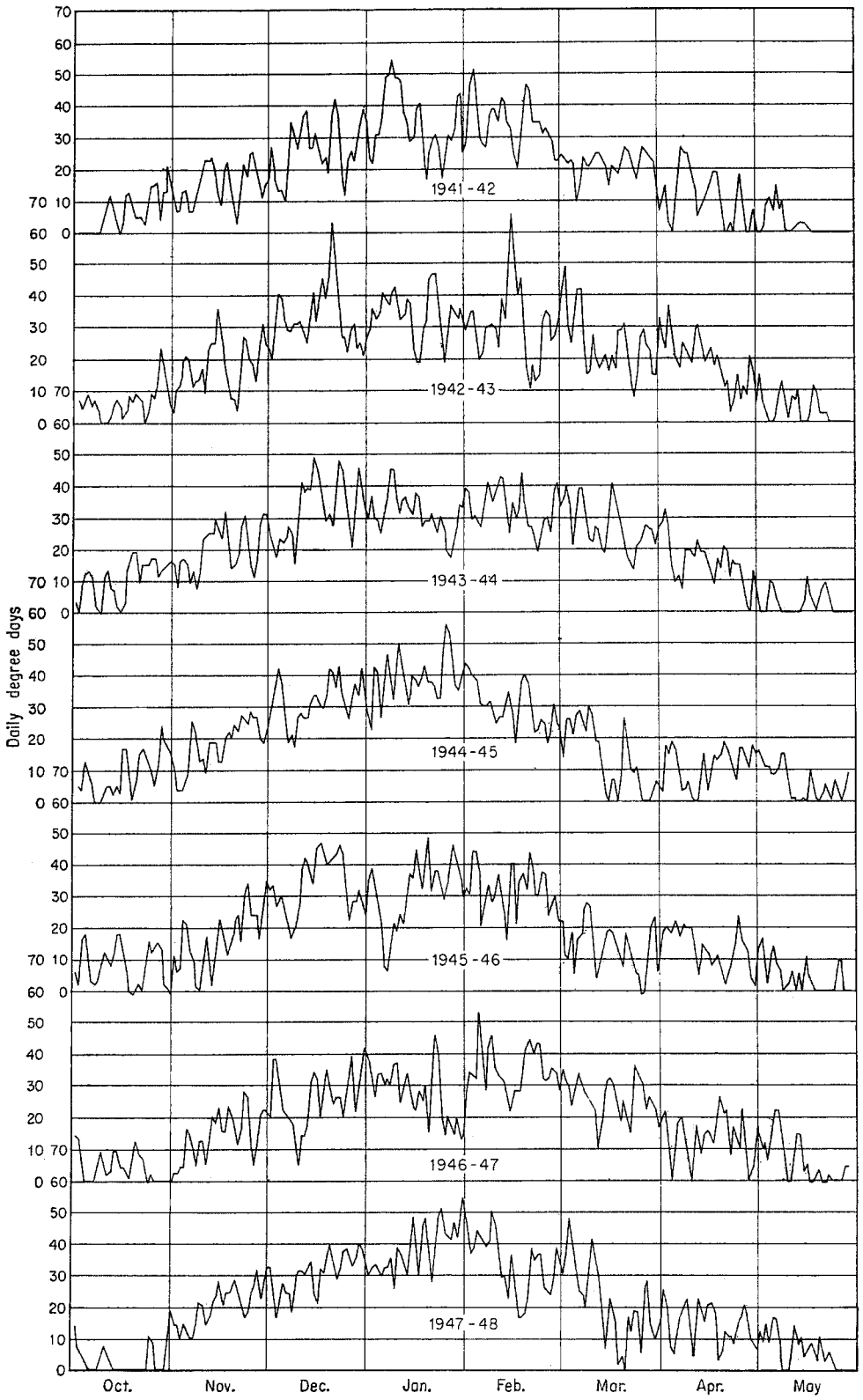
Daily degree days
1941-42
1942-43
1943-44
1944-45
1945-46
1946-47
1947-48
Oct.
Nov.
Dec.
Jan.
Feb.
Mar.
Apr.
May

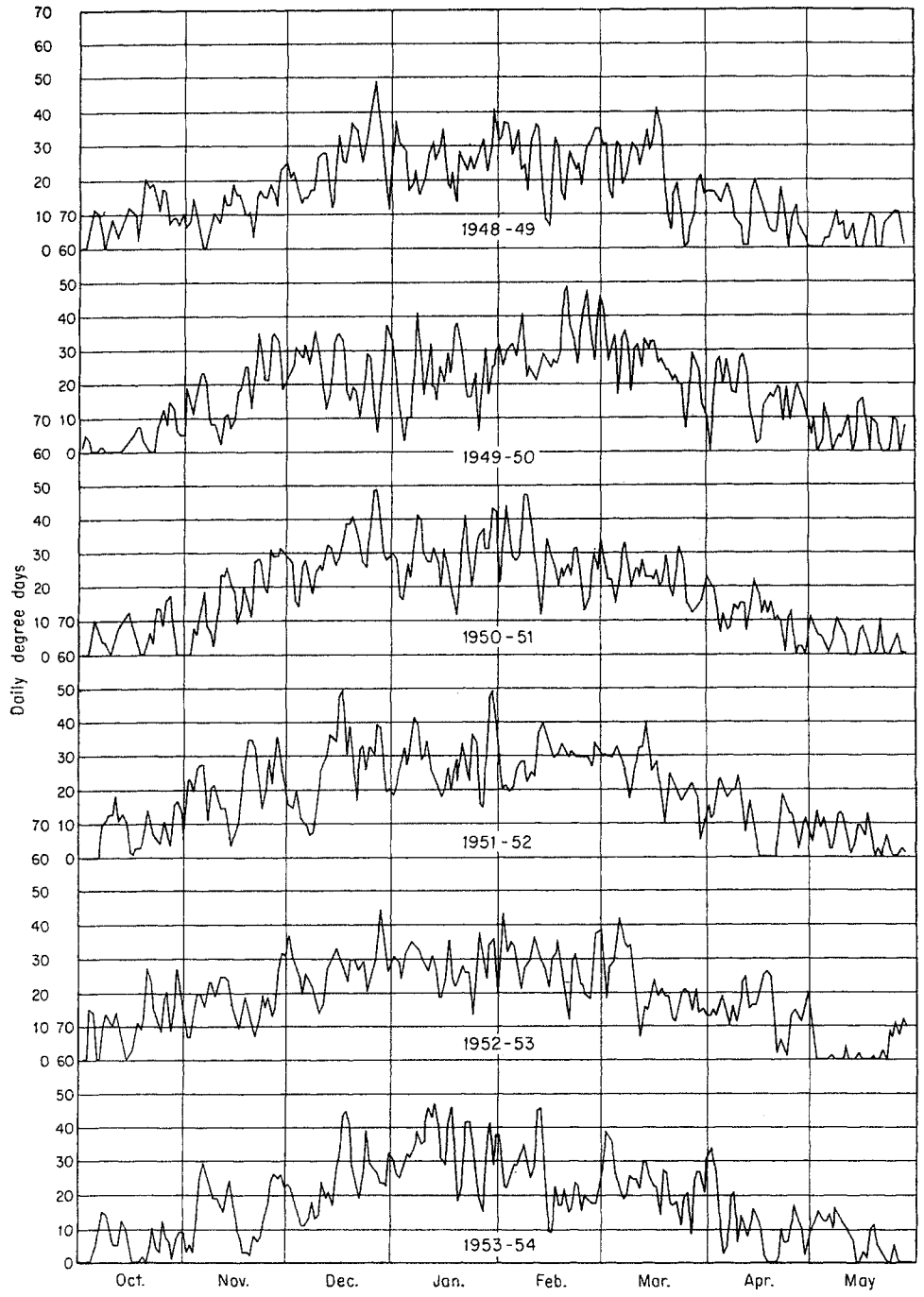

Fig. 18-3b. (*Opposite and above*) Daily degree-days, New York.

Table 18-3. Consumption Factors per Customer

Residential	20–35 Mcf/year
Commercial	75–175 Mcf/year
Residential space heating	0.02–0.035 Mcf/DDD*
Commercial space heating	0.05–0.10 Mcf/DDD

* DDD = degree-day deficiency.

Table 18-4. Load Factors for Various Classes of Sales

Class of sale	%
Residential and commercial	75–85
Firm industrial	55–75
Company use and unaccounted for	90–100

will gradually increase. Residential-space-heating consumption factors per degree-day deficiency depend on the average size and methods of construction of homes in any specific locality. Insulation of homes will decrease the consumption factor appreciably. In colder climates, where the cost of fuel for heating a home is a major consideration, methods of construction will tend toward a minimum of heat loss from the home. Commercial consumption factors, both general and space-heating, depend upon the size of the establishment. The commercial general factor is dependent also upon the type of gas use: for restaurants, dry cleaners, bakeries, dairies, etc.

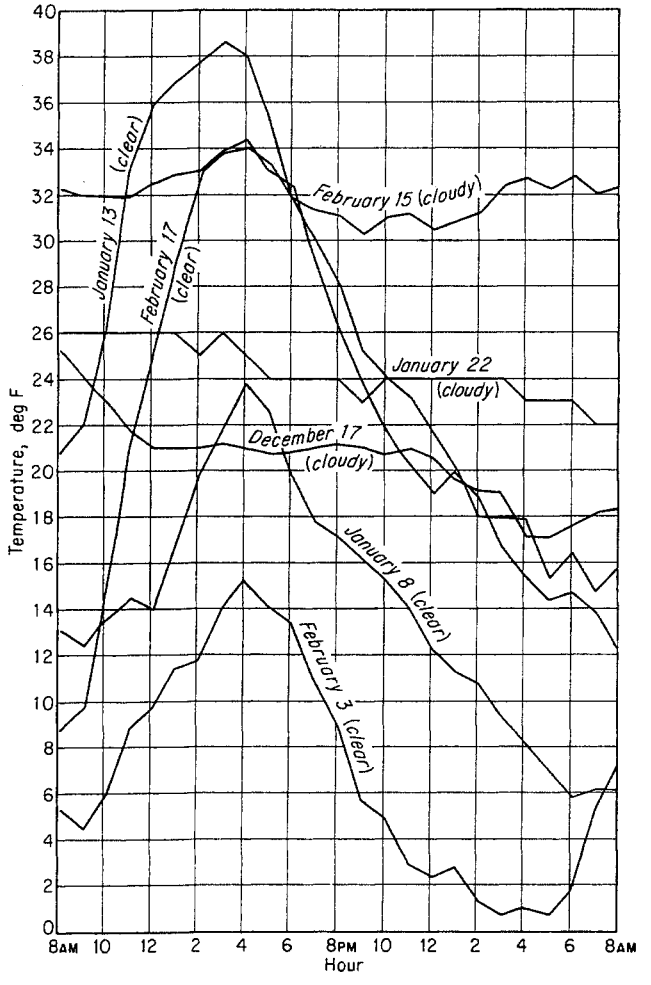

Fig. 18-4. Hourly temperature variations for typical winter days.

Load Factors

Table 18-4 lists the range of load factors for the various classes of service.

The load factor for space heating depends upon the relationship between the coldest winter day and the total number of degree-days in a winter, and may be calculated in the following manner. For instance, from Fig. 18-3 it can be seen that the season peak day in Detroit from 1941 to 1950 varied between −1°F in 1941–1942 and +12°F in 1948–1949 with an average for this period of +5°F or 60 degree-days. The 30-year-average annual degree-days in Detroit from Table 18-2 is 6,404. The load factor for space heating is then

$$\frac{6{,}404}{60 \times 365} \times 100 = 29.2 \text{ per cent}$$

Annual Sales and Peak-day Requirements

Table 18-5 is an illustration of how the annual sales and peak-day requirements for the various classes of service can be combined into an estimated system annual-sales capacity and peak-day sendout. This hypothetical market has a space-heating saturation of 60 per cent, which means that 60 per cent of the residential and commercial customers use gas for space heating.

The annual sales for residential and commercial customers are found by a simple multiplication of consumption factor by number of customers. For residential and commercial space heating, the annual sales are found by multiplication of consumption factor, number of customers, and annual degree-days. The average day is obtained by dividing the annual sales by 365, and the maximum day by dividing the average day by the load factor. The total maximum day is multiplied by 0.9, which is known as a "diversity factor." The diversity factor is an experience factor, and reflects the fact that during any one day only a portion of the total of all classes of customers would be using gas at maximum day capacity. The diversity factor could range as low as 0.7 and as high as 1.0.

To supply this market, a pipeline with a capacity of 117.4 MMcf/day would have to operate at 53.7 divided by 117.4 times 100 or 45.7 per cent load factor. The 30-year-average annual degree-days in Detroit from Table 18-2 is 6,404. If this were spread out evenly over the entire year of 365 days it would

Table 18-5. Annual Sales and Peak-day Requirements

Class	No. of customers	Consumption factor, Mcf	Annual degree-days	Annual sales, MMcf	Load factor, %	Av day, MMcf	Max day, MMcf
Residential	100,000	30	.....	3,000	80	8.2	10.3
Commercial	5,000	100	.....	500	80	1.4	1.8
Residential space heating	60,000	0.025	6,400	9,600	29	26.3	90.7
Commercial space heating	3,000	0.075	6,400	1,440	29	3.9	13.4
Firm industrial	.....	.....	.....	3,000	65	8.2	12.6
Interruptible industrial	.....	.....	.....	1,500	...	4.1	
Company use and unaccounted for	.....	.....	.....	600	100	1.6	1.6
Total	.....	.....	.....	19,640	...	53.7	130.4*

* 130.4 × 0.9 = 117.4.

amount to 6,404 divided by 365, or 17.5 degree-days each day of the year. This is shown as a heavy horizontal line in Fig. 18-1. From Fig. 18-1, the number of degree-days above this yearly average can be determined to be 2,470. This amounts to 2,470 divided by 6,404 times 100, or 38.6 per cent of the annual space-heating load. If the market under discussion were to be supplied from a pipeline at 100 per cent load factor, it would be necessary to provide storage capacity for 38.6 per cent of the space-heating load. This would amount to 9,600 plus 1,440, or 11,040, times 0.386, which equals 4,260 MMcf. This storage capacity would need a maximum daily delivery of 117.4 minus 53.7, or 63.7 MMcf.

The maximum-hour delivery is usually set up as a certain percentage of the maximum-day delivery. At equal hourly deliveries for an entire day, this percentage would be 4.2. It can go as high as 6 or 6.5 per cent, and facilities must be available to handle these peak hourly rates.

PREPARATION OF STORAGE SCHEDULE

By referring again to the market under discussion, the annual sales can be broken down by months and by classes of service. Let us assume further that the supply to this market is by long-distance pipeline operating at 100 per cent load factor. Table 18-6 illustrates the procedure for setting up a storage schedule by months for this market. In all classes of sales except space heating, the monthly sales are obtained by dividing the annual sales by 12. For space-heating sales, the consumption factor from Table 18-5 is multiplied by the monthly degree-day deficiencies for Detroit from Table 18-2. The pipeline supply is merely the product of the total average daily requirement, 53.7 MMcf (from Table 18-5), by the number of days in the month. The storage requirements are the difference between the total sales and the pipeline supply. It should be noticed that the maximum monthly requirement into or out of

Table 18-6. Market Requirements, Supply and Storage Schedule
All volumes in millions of cubic feet (MMcf)

Month	Residential	Commercial	Space heating		Industrial		Company use and unaccounted for	Total	Pipeline supply	Storage requirements	
			Residential	Commercial	Firm	Interruptible				Input	Withdrawal
January	250	42	1,805	271	250	125	50	2,793	1,670	.....	1,123
February	250	42	1,608	241	250	125	50	2,566	1,510	.....	1,056
March	250	42	1,390	209	250	125	50	2,316	1,670	.....	646
April	250	42	837	125	250	125	50	1,679	1,610	.....	69
May	250	41	377	56	250	125	50	1,150	1,670	520	
June	250	41	90	14	250	125	50	821	1,610	789	
July	250	41	.....	.....	250	125	50	717	1,670	953	
August	250	41	12	2	250	125	50	731	1,670	939	
September	250	42	144	22	250	125	50	882	1,610	728	
October	250	42	571	85	250	125	50	1,372	1,670	298	
November	250	42	1,121	168	250	125	50	2,005	1,610	.....	395
December	250	42	1,645	247	250	125	50	2,608	1,670	.....	938
Total	3,000	500	9,600	1,440	3,000	1,500	600	19,640	19,640	4,227	4,227

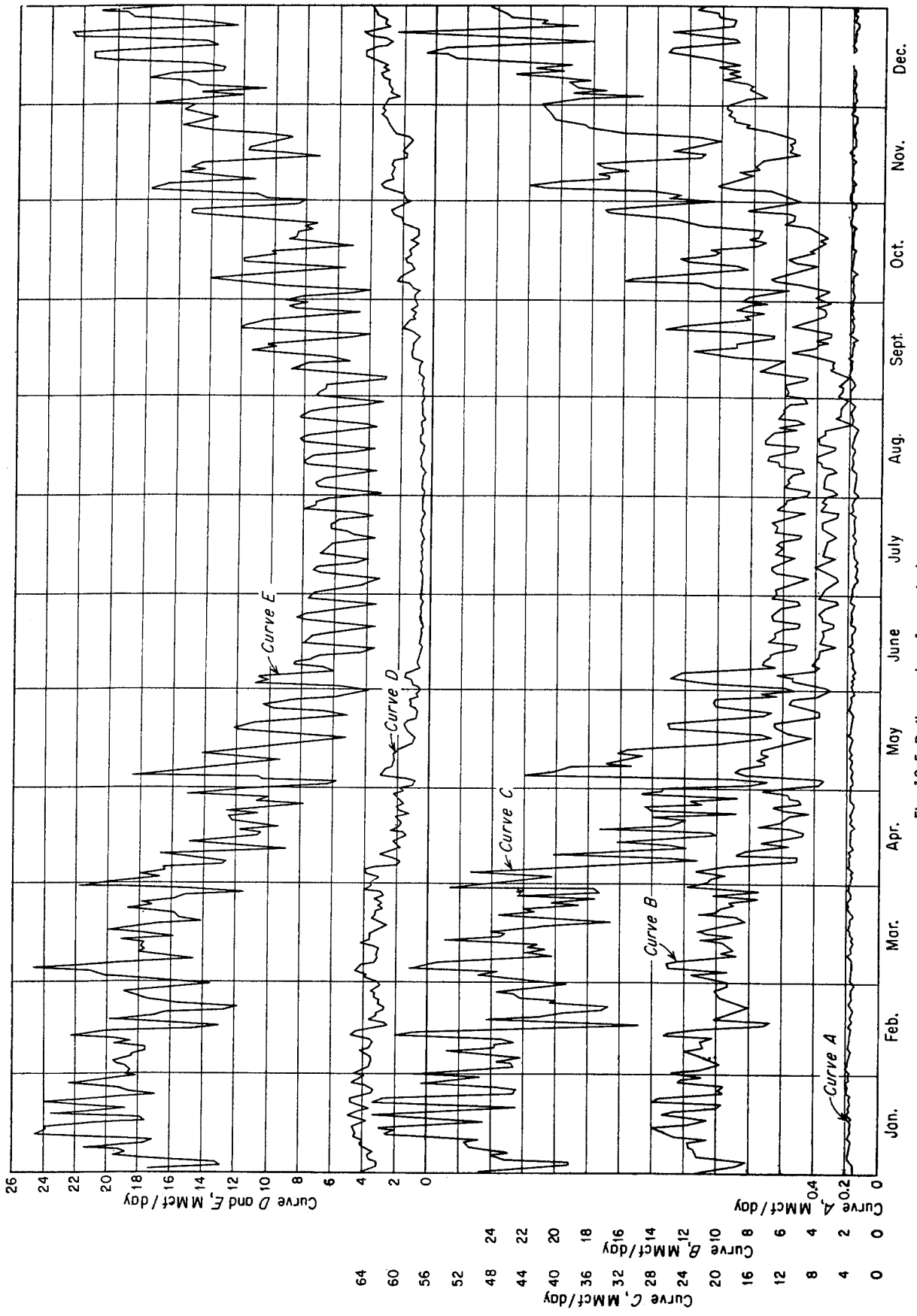

Fig. 18-5. Daily sendout for typical systems.

storage occurs during January. In designing facilities for storage it is usually necessary to design for the maximum winter day; summertime volumes into storage can normally be handled easily with those facilities. An exception to this rule occurs when the storage is very-high-pressure storage, considerably above pipeline pressures. In this case a substantial amount of horsepower is needed to compress the gas for injection into storage.

It should be remembered that this is an idealized situation in which annual pipeline supply exactly equals annual sales; this almost never occurs in actual operations. Business conditions, strikes, abnormal winters, etc., all affect this situation. There is always an indeterminate delay in connecting or disconnecting interruptible industrial customers. Storage capacity somewhat in excess of that needed for a normal winter season is essential to provide for these unpredictable factors in the natural gas business.

STORAGE FIELD DEVELOPMENT

The use of partially depleted oil and gas fields will be treated first, followed by the development of storage in water sands.

Use of Depleted Gas or Oil Fields

If depleted or partially depleted gas fields are available within a reasonable distance of marketing centers, they will almost invariably make the best and most economical storage fields. Depleted oil fields are also usually satisfactory, although they do create some problems not present in gas fields. The added factors to be considered in depleted oil fields will be discussed later. A common problem is: how far from a marketing center can one go to look for suitable underground storage fields? There is no specific answer to this question. It is a matter of economics. One can go to the point at which it becomes cheaper to use other types of storage or to expand the pipeline facilities from areas of large gas reserves. Each geographic location would present a different answer to this question.

Table 18-7 lists by states the number of storage reservoirs; whether they were originally dry gas, oil and gas, oil, or water reservoirs; and their cushion gas, active working gas, and total reservoir capacities. This table shows the magnitude of underground storage facilities. At the end of 1955 more than 375 million dollars have been invested in physical properties and cushion gas (inactive base gas) in storage fields.

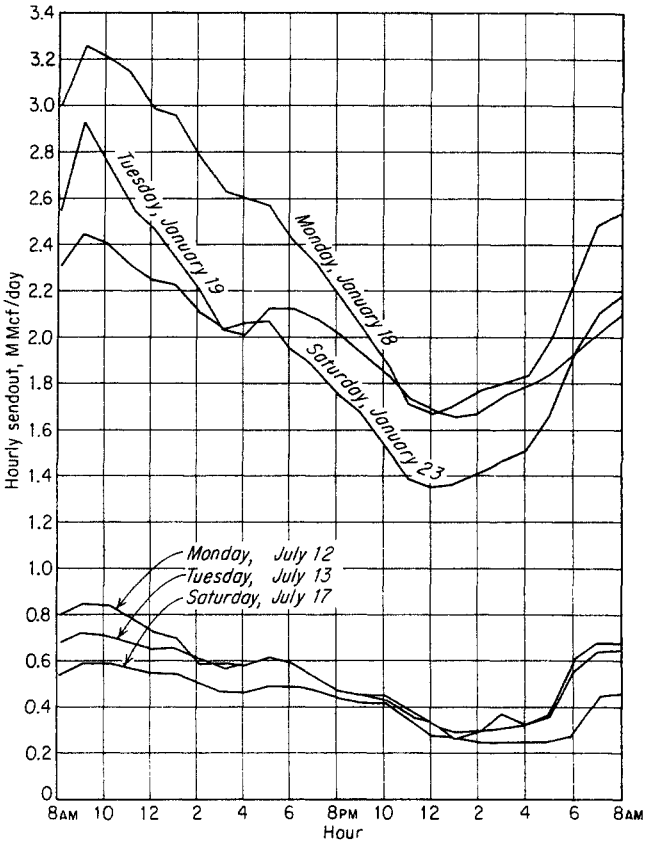

Fig. 18-6. Hourly sendout for typical winter and summer days.

Geological and Engineering Data

Before any decision can be made on acquiring a depleted field for storage, it is necessary to make a thorough study of all geological and engineering data available about the field. Such data can be obtained from state conservation departments, state regulatory bodies, field operators, drillers, company scouting records, and people living in the area.

Table 18-8 is an example of a scout ticket, Table 18-9 an example of a well log filed with the Illinois Geological Survey, and Table 18-10 is an example of a well-plugging report filed with the Michigan Conservation Department. Production and pressure history of the individual gas wells should also be obtained. Any core data showing porosity, permeability, and laboratory determinations of interstitial water are valuable. These data, combined with geological data, are necessary to determine the size of the reservoir. Back-pressure or any other type of individual-well performance tests must be studied to determine the deliverability of a reservoir and, from this, the estimated number of storage wells necessary to meet market requirements.

Table 18-7. Underground Storage Reservoirs by States

State	Original reservoirs*					Ultimate capacity of existing reservoirs,† Mcf		
	Dry gas	Oil and gas	Oil	Water	Total	Cushion gas	Active working gas	Total reservoir capacity
Arkansas	2	...	...	...	2	4,481,375	1,730,615	6,211,991
California	1	2	...	...	3	42,385,198	19,003,208	61,388,406
Illinois	...	...	...	2	2	19,795,222	19,795,222	39,590,444
Indiana	4	...	...	...	4	5,008,767	3,196,152	8,205,919
Iowa	...	...	...	1	1	25,136,519	25,136,519	50,273,038
Kansas	15	...	...	...	15	35,746,296	27,195,900	62,942,216
Kentucky	4	...	...	1	5	14,161,654	5,923,933	24,861,525
Michigan	12	...	...	...	12	146,826,227	158,035,304	304,861,531
Mississippi	1	...	...	...	1	323,555	698,785	1,022,340
Montana	1	...	...	1	2	16,428,017	65,722,324	82,150,341
New Mexico	4	...	...	...	4	54,299,462	65,135,683	119,435,145
New York	12	...	...	...	12	30,314,915	25,463,429	56,250,911
Ohio	14	...	...	...	14	160,569,048	167,407,029	327,976,077
Oklahoma	7	...	...	...	7	56,352,156	138,752,115	195,144,771
Pennsylvania	48	4	...	...	52	209,734,037	204,378,916	418,811,105
Texas	1	1	1	...	3	5,099,984	10,902,016	16,000,000
West Virginia	27	3	...	...	30	110,027,074	147,689,632	257,716,706
Wyoming	2	...	...	...	2	6,973,036	55,998,636	62,971,673
Total	155	10	1	5	171	943,662,542	1,142,165,418	2,095,814,139

* All companies did not report types of original reservoirs.

† All companies did not report ultimate capacity.

SOURCE: Data as of December 31, 1955, from the 5th Annual Report on Statistics, AGA committee on underground storage.

Casing and cement records of the original gas or oil wells and well-plugging records must be studied carefully to evaluate the possibility of reservoir leakage through improperly plugged wells or behind the casing of remaining active wells with poor cement jobs or insufficient cement. A study must be made of all wells drilled within the field limits that have penetrated the storage formation. It may be necessary to go back in and permanently plug certain old wells or set new casing on some wells. Examples of this practice are frequent in the industry. The results of such a study and report will determine whether it is advisable to proceed with the acquisition for storage of a given depleted or partially depleted gas or oil field.

Acquisition

Acquisition of the right to use a formation for storage is accomplished with different procedures by various companies. The type, form, and payments made in acquiring storage rights from the mineral and the surface owner or owners are governed by state laws and regulations, the value of the surface area, and the question of whether operations in the area are limited to gas storage or include production or possible future exploration for oil and gas in other formations. In many instances, a special form of gas-storage lease is obtained which provides for a payment of $1 to $2 per acre per year for unoperated leases (no wells) and a flat payment of $200 to $400 per well per year for operated leases. Generally, these leases allow storage in any and all formations and drilling for and producing oil and native gas. The lessor usually retains his mineral interest in any present oil production or possible future oil discoveries. No payment for possible future gas production from other formations is made other than the $200 to $400 per well per year payment. Such oil-and-gas-storage leases give complete control of an area for exploratory and producing operations and utilization of any formation for storage. Where minerals are owned independent of the surface, additional rights for storage operations are obtained from the surface-fee owner.

In other instances, where in a specific formation storage only is involved, warranty deeds to the formation desired for storage are obtained from the landowner along with rights to drill wells, construct gathering and well lines, and otherwise conduct storage operations. The usual payments are made for damages to crops, timber, fences, etc. Any remaining native gas is paid for in toto, and assignment

of minerals is obtained limited to the formation being used. Depending upon the surface value, $5 to $50 per acre is paid for the formation storage rights. Where surface values are low, fee ownership can be purchased in toto for the same or for slightly higher cost per acre than would be paid for warranty deeds to a specific formation.

Whether a gas-storage lease or a warranty deed to a specific formation is obtained, free gas is usually given for use in the principal dwelling upon the farm, sometimes with a limit of 200,000 cu ft/year. There are certain advantages in giving free gas for use in the principal dwelling. Most of these homes have had free gas during the producing life of the gas field. Knowing that this is to be continued for many years to come encourages these people to sign storage agreements. This is the only form of annual rental that is paid directly to the persons living on the premises. One of the main purposes of an annual rental is to reimburse the people involved for any inconveniences caused them by day-to-day storage operations. Payment of an annual rental per acre per well to the landowner who often does not live on the premises does not accomplish this purpose.

Where gas storage is contemplated in depleted or semidepleted oil reservoirs, acquisition and use of such reservoirs are complicated by the presence of oil. Primary recovery of oil will vary from 15 to 60 per cent of the oil in place depending upon the reservoir depletion mechanism. Accordingly, injec-

Table 18-8

Permit No. 19496	DP No. 1041	Depth 4500' FW-WC
Operator WOODSON OIL CO.		
Name & No. DETROIT HOUSE OF CORR. #3		
Loc. SW NE SE	Sec. 17	T 1 S R 8 E
NL 1084 SL	EL 990 WL	
Elev. 900.4 / 899.4 (NORTHVILLE)	WAYNE	County
Spud 3-4-55	Comp. 4-22-55	Contr. SCOTT DRLG.
Casing: 14" 10"	8" 469 6"	5" 4,350
GRND: 7.0	(200)	(140)

Formation	Datum	Drilling Data
Drift 311		MAR. 20 ϕ 3280
Bm Dolo		MAR. 28 ϕ 4113
Stray Stray		
Stray Dolo		DST: 3867-4035
Stray Sand		0: 2 HRS.
Pay		R: 120' MUD & ODOR GAS
Pay		FLO.P: 72#
Wtr		SIP: 160# ½ HR.
Mar.		APR. 4 ϕ 4618
L. Mar.		
Wtr.		DST: 4035-4200
CwLs.		0: 1½ HRS.
CwRR		R: GAS 15 MIN. (25MCF)
		BHP: 1380# ½ HR.
Sun.		
Berea		DST: 4200-4423
		0: 1½ HRS.
Wtr		R: 50' MUD
L. Ant.		BHP: 50# ½ HR.
Ant. 311[S]		
Tt.		APR. 11 ϕ 5110
TvLs. 454[S]		
"Alp.		DP # 1041 4/5/55
		DPN. 1300' TP ABOUT 6000'
Pay		APR. 18 ϕ 5375
Pay		APR. 25 TO TEST TRENTON GAS
Wtr		MAY 2 WOC
		MAY 9 ✓ MAY 16✓
Bell Sh.		MAY 23✓ MAY 31 TTT
Dun. 664[S]		JUNE 6 RETREAT
		B SALT 2335
Pay		A[2] DOLO 2665
Pay		SALT 2880-89
Wtr		A' DOLO 2889

Formation	Datum	Drilling Data
Mon. DOLO 797		DST 5453-83
		0: 2 HRS.
1st Salt		R: 1320' SW
Salt		FLO.P: 110# TP 745#
		BHP: 2443# ½ HR.
Mass Anhy		
Big Anhy		MAY 29 SHOT 80 @ 4176-96
Blk Lmst.		500 MUD ACID
Sylv. 1103		NO RESULTS
Bois Blanc 1302[S]		
Bass Isle 1333[S]		SET PLUG 4110
Salina 1686[S]		
Niag-brn. 2993[S]		CAL SEAL TO 4092
Niag-wht.		
		MAY 31 SHOT 120 @ 4028-58
Clinton 3120		JUNE 1 5000 ACID
Cab. Hd.		JUNE 2 SWB. DRY
Maint.		10000 ACID
Cinn.		EST: 4,000 MCF GAS
Trent. 3866	-2966	SET BP @ 3930
		SHOT 52 @ 2904-17
BLACK RIVER 4282		500 MUD ACID
St. P.		5000 ACID
Pay		JUNE 13 SHOT 2841-2929
Pay 4028-58		SQZ. CMT.
Pay		CO TO 4350
Pay		TUBE ON PK B @ 4015
		TP: 1150#
		SHUT IN GASS WELL
T.D. 5483		
P.B.-T.D. 4350		JUNE 20 EST. 10,000 MCF
N.I.P.		JUNE 27 SHUT IN
		JULY 6 ✓ JULY 11 ✓
		JULY 18 ✓
Acid 5000		
10,000		SEPT. 12
		PSC GAUGE 7400 MCF
A.I.P. PSC GAUGE 7400 MCF		SIP: 1613#
		BHP: 1882# @ 4270

Table 18-9

ILLINOIS GEOLOGICAL SURVEY, URBANA

Page 1

Strata	Thickness	Top	Bottom
GAS INPUT			
Company sample log summary:			
PLEISTOCENE			
Sand, fine to medium grained; quartz rounded		40	60
Gravel, quartz, limestone, etc., below pea size		60	114
PENNSYLVANIAN			
Shale, gray; gravel, above pea size		114	150
Sand, fine to medium grained loose; limestone, gray; shale, gray		150	170
Shale, gray clay		170	190
Shale, medium light gray, micaceous, pyritic		190	230
Shale, medium grained, clay		230	250
Shale, medium light gray pyritic; shale, dark gray and coal		250	260
Shale, medium light gray; limestone, brown and coal		260	280
Shale, medium light gray; dolomite brown finely crystalline and coal		280	290
Shale, gray, arenaceous; limestone brown		290	320
Sandstone, medium light gray, very fine to fine, clusters, kaolin matrix		320	340
Shale, gray and medium light gray, clay		340	360
Shale, dark gray		360	380
Shale, dark gray and shale, medium light gray arenaceous, limestone, gray		380	400

COMPANY	Panhandle Eastern Pipe Line Co.
FARM	Davidson NO. 1
DATE DRILLED	May 1954 COUNTY NO.
AUTHORITY	Panhandle Eastern Pipe Line Co.
ELEVATION	617" RB-Co.
LOCATION	324" S line, 30' E line of NW NW
COUNTY	MORGAN 23-13N-8W

ILLINOIS GEOLOGICAL SURVEY, URBANA

Page 2

Strata	Thickness	Top	Bottom
Shale, medium light gray, clay, pyritic; shale, medium gray clay, limestone, gray brown		400	420
Shale, medium dark gray		420	480
Sandstone, fine grained loose quartz, medium light gray		480	540
MISSISSIPPIAN			
Warsaw			
Shale gray to medium light gray, quartz and chert pebbles		540	590
Keokuk-Burlington			
Limestone, light gray and chert bluish white		590	650
Limestone, light gray dense and chert		650	690
Limestone, fine-medium, light to very light gray very cherty		700	760
Limestone, fine-medium, light to very light gray very cherty, glauconitic spots in part		760	800
Kinderhook			
Hannibal			
Dolomite, silty, gray fine, argillaceous		800	820
Shale, medium gray, silty		820	840
Shale, medium gray		840	950
Grassy Creek			
Shale, gray and gray brown		950	970
Shale brown		970	1016
DEVONIAN			
Dolomite, brown fine crystalline		1016	1035
Limestone, gray, dense		1037	1040
Limestone, light gray finely crystalline		1040	1070
Limestone, light gray, dense, slightly dolomitic		1070	1082
SILURIAN			
Show of oil		1094	1190

Panhandle Co. Davidson #1
COUNTY MORGAN 23-13N-8W

Table 18-9 (*Continued*)

ILLINOIS GEOLOGICAL SURVEY, URBANA

Page 3

Strata	Thickness	Top	Bottom
Dolomite, brown finely crystalline, poor show of oil; limestone, light gray dense dolomite; dolomite, light gray finely crystalline		1082	1100
Dolomite, light gray finely crystalline		1100	1110
Limestone, light gray dense very slightly dolomitic		1110	1130
Dolomite, light gray fine; and limestone, light gray dense		1130	1150
Limestone, light gray dense cherty; dolomite light gray finely crystalline		1150	1170
Limestone, light gray, dense cherty		1170	1180
Limestone, light gray dense		1180	1200
Limestone, light gray dense; dolomite brown		1200	1230
Dolomite, brown finely crystalline		1230	1250
Dolomite, brown finely crystalline; shale, gray		1250	1260
Dolomite, brown finely crystalline; limestone light gray cherty; shale gray-green		1260	1280
ORDOVICIAN			
Maquoketa			
Shale gray-green; dolomite brown finely crystalline and limestone, light gray		1280	1300
Shale gray		1300	1310
Shale gray and red-brown		1310	1340
Shale, gray pyritic		1340	1400
Shale gray		1400	1436
Trenton			
Show of oil		1448	1546
Galena			
Limestone, gray fragments, show oil staining		1436	1500

Panhandle Co. Davidson #1
COUNTY MORGAN 23-13N-8W

ILLINOIS GEOLOGICAL SURVEY, URBANA

Page 4

Strata	Thickness	Top	Bottom
Limestone, gray, fragments, show oil staining pyrite		1500	1550
Platteville			
Limestone, brown, fine, dolomite; limestone, gray fragments		1550	1590
Limestone, gray fragments		1590	1600
Limestone, gray fragments; limestone, gray brown dense		1600	1640
Limestone, gray-brown, dense, brown chert; dolomite brown		1640	1670
Limestone, gray fragments to dense		1670	1680
Limestone, medium gray dense		1680	1740
Limestone, medium gray dense; dolomite brown finely crystalline		1740	1750
Limestone, brown dense; limestone medium gray dense		1750	1758
Joachim			
Dolomite, brown finely crystalline		1758	1772
Core #2 1792-1796			
Cut and recovered 24'			
Limestone, dense, shaly, brown slightly dolomitic		1772	1772½
Dolomite, finely crystalline, brown, with visible porosity		1772½	1780
Limestone, gray-brown fine, dolomite, carbonaceous streaks, no visible porosity		1780	1780½
Dolomite, brown finely crystalline, visible porosity		1780½	1784
Limestone, gray-brown, fine, dolomite, no visible porosity, mottled		1784	1785
Dolomite, brown, finely crystalline, mottled with dark gray argillaceous		1785	1788
Dolomite, gray, dense, with shale streaks		1788	1789
Dolomite, brown finely crystalline		1789	1790
Dolomite, gray finely crystalline		1790	1791

Panhandle Co. Davidson #1
COUNTY MORGAN 23-13N-8W

Table 18-9 (*Continued*)

ILLINOIS GEOLOGICAL SURVEY, URBANA

Page 5

Strata	Thickness	Top	Bottom
Dolomite, brown, dense to finely crystalline, shale streaks		1791	1792
Dolomite, gray finely crystalline		1792	1794
Dolomite, gray finely crystalline with dark gray shale streaks		1794	1795
Dolomite, brown finely crystalline shaly		1795	1796
Core #3 1796-1820 19-3/4 /24			
0-½ dolomite, brown shaly			
½-1½ dolomite, brown, porous			
1½-2 dolomite, brown, dense, shaly			
2-2½ dolomite, brown, porous			
2½-4 dolomite, brown, shaly			
4-4½ dolomite, brown, porous			
4½-6 dolomite, brown, argillaceous, shaly			
6-6½ same with visible pore			
6½-8 dolomite, brown, dense, very soft			
8-9½ dolomite, brown, porous			
9½-11 dolomite, brown, shaly			
11-13 dolomite, brown, shaly with black shale layers to 2" thick			
13-14½ dolomite, brown, porous			
14½-16½ dolomite, brown and shale, black interbedded in Laminae to 2" layers			
16½-17 dolomite, dark gray, arenaceous			
17-17½ dolomite, brown, shaly			
17½-18 shale, dark gray			
18-18½ dolomite, brown			
18½-19 sandstone, gray, fine-medium grained, dolomite.			
19-19½ laminated shale and shaly dolomite			
19½-19-3/4 sandstone, gray, fine-			

Panhandle Co.
COUNTY MORGAN

Davidson #1
23-13N-8W

ILLINOIS GEOLOGICAL SURVEY, URBANA

Page 6

Strata	Thickness	Top	Bottom
medium grained with rounded dolomitic			
Sandstone, gray, fine-medium grained with rounded		1820	1822
Shows of oil occurred in the following zones Silurian 1084-1190 Trenton 1448-1546 1612-1632			
None of these zones are commercial. Coring was attemped in the Devonian with no recovery, but was successful in the Joachim with full recovery. Recovery of the lower Joachim and upper St. Peter was 83%. Core recovery was inadequate to use for the St. Peter top and drilling time had to be used, placing the St. Peter at 1817½ (-1200½)			
At -1200, the total depth recommended by the storage engineer, the St. Peter had not been penetrated and it was necessary to cut five more feet in order to have the desired St. Peter penetration, making total depth -1205 driller.			
Casing was set to 1765 in the Joachim in order to leave the Joachim porosity open.			
Total depth			1822
Drilling-Time Log filed			
Sample Set No. 24529			
Radioactivity Log filed.			

Panhandle Co.
COUNTY MORGAN

Davidson #1
23-13N-8W

Table 18-10

STATE OF MICHIGAN
DEPARTMENT OF CONSERVATION

WELL PLUGGING RECORD

TO BE FILED WITHIN THIRTY DAYS AFTER FINAL ABANDONMENT

Permit No. 11142 Date September 30, 1951

Owner or operator Sohio Petroleum Co. Address Mt. Pleasant, Michigan

Well No. 1, Farm George H. Coe, Sec. 33, T. 16, N. S., R. 6, E. W.

Township Coldwater County Isabella

Located 1330 feet from the { N / S } line of quarter Sec. and 1330 feet from the { E / W } line of quarter Sec.

Type of well Oil (Oil, Gas, or Dry Hole) Name of producing sand Dundee

Top sand Bottom sand Total depth 3752'

Date plugging began September 4, 1951 Date plugging completed September 12, 1951

Was permission of Department of Conservation secured before plugging began? Yes

Name of representative of Department who supervised plugging

OIL, GAS AND WATER SANDS

Name	Content	From	To
Michigan Stray	Gas	1412'	1467'

CASING RECORD

Size Casing	Amount Casing Pulled
5"	3705.35'
7"	804.34'

Describe in detail how well was plugged Filled the hole with mud from the td. to approximately 2900'. Ripped the 5" casing at top of cement and filled hole with mud to base of 7" casing thru the 5" casing as it was pulled. Ripped the 7" casing at top of cement and set bridge at top of pipe left to hole. Filled the hole with mud from bridge to base of 10" thru the 7" casing as it was pulled. All oil, gas and water confined to formation as encountered. 10" casing abandoned with the hole. 10" capped when completed.

Names of workmen present when well was plugged T. Grisdale, A. Grisdale, F. Scholl

Signed Scholl and Ullom By S / Fred D. Scholl

Address Mt. Pleasant, Michigan, Partner (Title)

State of Michigan, County of Isabella ss:

I, Fred Scholl, do hereby swear that the above statements are true and correct to the best of my knowledge and belief.

S / Fred D. Scholl

Subscribed and sworn to before me this 30th day of September 19 51.

My commission expires 4-26-54 S / A. P. McPheron (Notary Public)

O. K. by Department representative

tion of gas may activate a secondary oil-recovery operation in varying degrees depending upon the primary reservoir-depletion mechanism. The storage company obtains working agreements with the oil producers, and the field is unitized and operated initially as a secondary recovery project. Obtaining working agreements with the oil producers and unitization of the field are the major items in converting an oil field to storage. Once these are brought under control, it is possible to obtain storage rights, or oil-and-gas-storage leases, as outlined for dry-gas field-storage acquisition.

It is not the purpose of this discussion to go into the legal aspects of storage acquisition. Typical forms, deeds, and legal documents used in acquiring underground storage rights have been compiled in book form, and copies are on file in the AGA library at 420 Lexington Avenue in New York City. Nearly one hundred different forms are included in the compilation.

Reconditioning of Wells

One of the major projects in the initial stage of storage-field development can be the reconditioning of all remaining gas wells. It may be necessary to recase many of the remaining wells because of the use of insufficient cement in the setting of the original casing. The original casing may have been of substandard grade. It may be badly corroded, especially near the surface, and need replacement. It has been the practice in one field to replace the upper 6 to 8 ft of the producing casing by digging down to this depth and welding on a new section of casing. Generally, it will not be possible to pull the old production casing, especially if it is cemented in the hole. To recase the well it will then be necessary to run and set the next smaller size of casing that will fit into the hole. It will usually be advisable to pressure-test each of the remaining wells by setting a bottom-hole plug in the top of the storage formation or bottom joint of casing and test with natural gas or air somewhat above the maximum contemplated storage pressure.

Often, an even larger and more extensive project is the redrilling of all the plugged and abandoned wells. At the time these wells became unable to produce and were plugged and abandoned, no one had conceived of the idea that eventually the field might be used for storage. The plugging of these wells was done primarily to prevent the intermixing of different formation waters, and in many cases was supervised by state conservation departments. The persons plugging the well were interested in recovering as much casing as possible, and it was usually shot off at the top of the original cement behind the casing and pulled. Drilling mud, sand, gravel, clay, brush, or anything available at the well site would be used to fill up the hole after a few sacks of cement or drilling mud were spotted at the bottom of the hole. Such plugging operations were adequate for the purposes for which they were intended, but are not adequate for storage operations. It becomes necessary to go back into each one of these wells to ensure that there will be no gas leakage through any of them. Many of the wells are difficult to find at the surface, especially if they have been plugged for many years and if the original well records were not too accurate, which is often the case for wells more than 20 or 30 years old. Buried sections of old gathering line, cellar box for original drilling, or discoloration of the soil after the surface has been bulldozed off may disclose the location of the well. Pipe locators may be of considerable assistance.

The problem of drilling out the old hole down to the storage formation can be very difficult. In most instances, the goal will be to clean out the old hole effectively so that new casing can be run and set with cement and a storage well completed. If this is not possible, it will be necessary to plug the well permanently. It may be difficult to get into the old casing, especially if it has been ripped off. Special bits may have to be devised. Cavings and fresh-water sands may complicate matters. As with most storage wells, it will probably be advisable to run a surface casing and thereby case off surface water and cavings. Figure 18-7 illustrates this clearly. Sometimes it will be possible to drill right to bottom without any difficulties; in other wells the drilling can be full of trouble all the way to the total depth.

Drilling New Wells—Delimitation, Peak Day, Drainage

It is wise to define carefully the field limits in any storage project so as not to acquire storage rights on acreage that will eventually prove to be well outside the field limits. If the original field was not well delimited when it was being developed, it may be necessary to drill several delimitation wells before major storage operations commence. These wells will be drilled primarily for structural information. It is definitely advisable to set casing in these wells and retain them for observation purposes. If they are completed below the water level in the storage formation they can be used to observe fluctuations in the water pressure as the pressure in the storage field goes up and down each year. They will also enable one to detect any storage gas that has migrated out to these wells. In storage fields with active water drive, where the water level changes continuously, these observation wells will enable one to tell when the water level reaches the point where the observation well penetrates the formation. By means of a float, water levels can be continuously measured at such wells.

In nearly all depleted gas fields that are being developed for storage, it will be necessary to drill additional wells for peak-day deliverability. The number will depend upon the thickness and permeability of the formation, the maximum safe daily production rate per well, the maximum wellhead pressure drawdown during withdrawal, etc. Wells producing at high linear gas velocities will carry particles of the formation in the gas stream. These particles will be thrown against the wall of the pipe at any point of abrupt change in direction of flow, such as at wellhead tees and elbows. This action can cut metal severely and even cause rupture. Maximum production rates per well should be set so that there are no formation particles in the gas stream.*

* Flow rates of 35 MMcf/day in 8-in. casing at wellhead pressures of 600 psia are near the border where gas will carry loose sand out of the well.

Excessive wellhead pressure drawdown during withdrawal can cause water to enter wells and seriously impair the well's productivity. The maximum pressure drawdown will be different for each field and even different for individual wells within a field. It is the practice of one company to throttle certain wells at low field pressures to prevent water from coming into them.

Wells drilled for deliverability purposes will be drilled at locations that will give the highest well capacity, normally at the top of the structure. The concentration of high-capacity wells at the top of the structure may set up significant pressure gradients within the reservoir during sustained periods of withdrawal or input. It will probably not be possible to equalize completely the pressure within the reservoir, but the drilling of drainage wells around the periphery of the field will be a step in this direction. The advantage of nearly uniform pressures across the reservoir is that, for any given content of gas in the field and withdrawal rate, the flowing pressure will be higher. This advantage becomes a real one when it becomes necessary to add horsepower because of the low flowing pressure from the storage field.

The development of a storage field is similar to that of a primary gas field in many respects, but different in others. The major difference is in the rate of production. Enough gas may be withdrawn from storage fields to lower the reservoir pressure as much as 30 psi/day, whereas in primary production such a pressure drop might occur over a year or two. Accordingly, the number, spacing pattern, and penetration of wells in a storage field may require careful consideration.

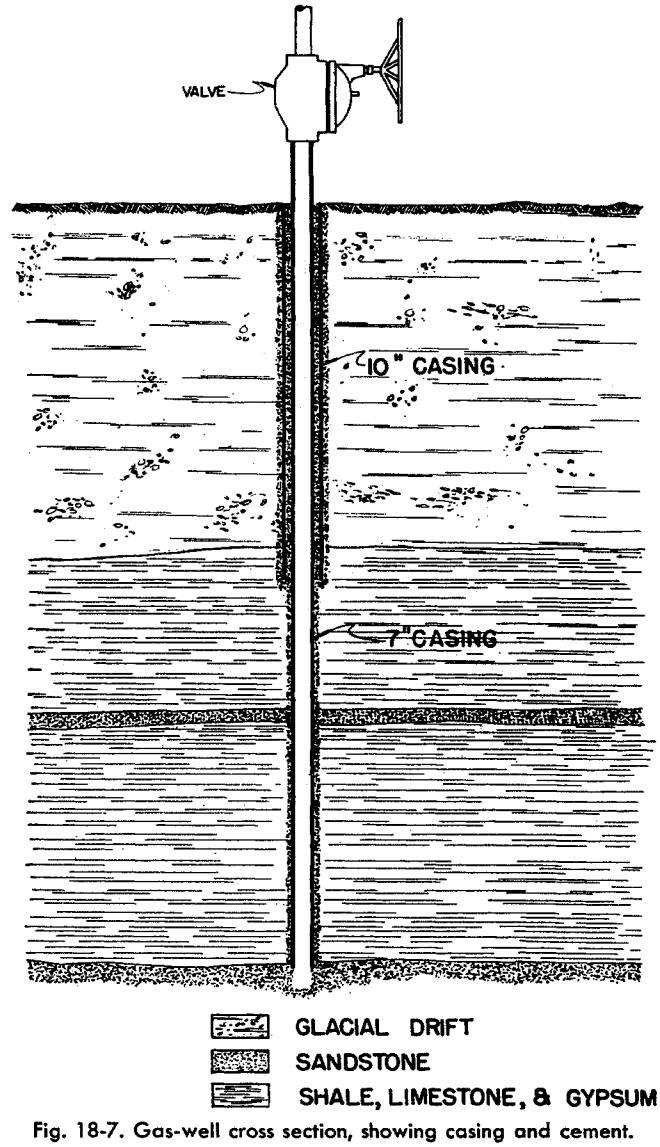

Fig. 18-7. Gas-well cross section, showing casing and cement.

Wellhead Structures

There are as many different types of wellhead structures in storage fields as there are companies that have storage fields. The wellhead structure should contain sufficient equipment to enable the operator to test and service the well in normal operations without special equipment or delay. It should contain a pressure tap so situated that wellhead shut-in pressures can be taken with a deadweight gauge. A good wellhead structure should include a horizontal meter run with orifice fittings, a valve at the gathering-system end of the meter run for controlling flow rate to or from the well, and a meter or a manometer for measuring the differential across the orifice plate. These facilities will allow periodic testing of the well's deliverability without having to blow any gas to the atmosphere. Daily check of the manometer differential will make it possible for the field operator to know immediately if a well is frozen off or not producing for some other reason. A blowoff valve for cleaning the well and for running instruments into the well is an integral part of a wellhead structure. A well house to enclose and protect wellhead equipment from the weather is advisable. In some areas, depending on the depth of the storage reservoir, reservoir temperature, and surface weather conditions, it may be necessary to install a heater at the wellhead to prevent hydrate formation and freezing off of the gathering lines. Individual wellhead gas dehydrators can be used in some instances. Figure 18-8 is a photograph of a storage-field well house. Figure 18-9 is a photograph of a wellhead structure with the well house removed, which incorporates most of the items just discussed.

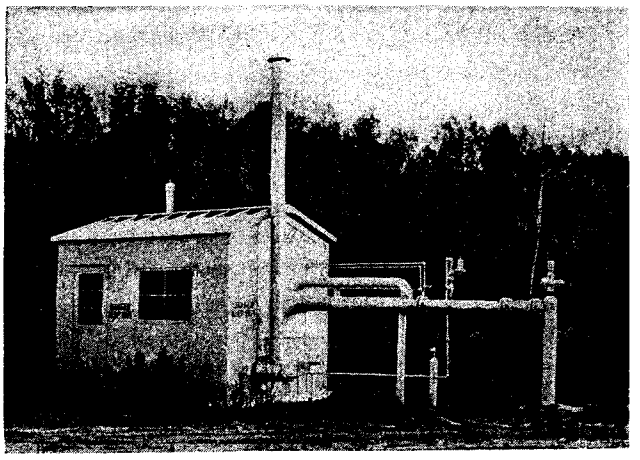

Fig. 18-8. Storage-field well house.

Gathering System

Gathering systems are sized with the aid of the usual pipeline formulas. They must be sized to handle peak-day wintertime loads. Consideration is often given to oversizing individual well lines to prevent freeze-off due to hydrate formation. In one storage project all individual-well lines will be constructed with 12-in. pipe. Another company does not install any well lines with smaller than 4-in. pipe. In laying out the system, consideration must be given to the location and capacity of present wells as well as to the location and potential capacity of wells to be drilled in the future. The gathering system is often designed for an over-all pressure drop at maximum flow rates not to exceed 25 psi. Figure 18-10 shows the gathering-system layout and pipe sizes for field A, a typical storage field.

Dehydration Plant

Many storage fields require dehydration of the gas withdrawn from storage. Even though dry gas is injected into the field, it picks up water in the reservoir and approaches saturation upon withdrawal. This requires dehydration to prevent freezing at high pressures in transmission mains. Occasionally, wellhead dehydrators are installed, although usually it is more economical to dehydrate the gas at one central location at the outlet of the gathering system. In such cases, gas hydrates may accumulate in the field-gathering system during the winter. The observation that the water separator yields large volumes of liquid in the springtime, when one would expect the hydrates to melt, substantiates the belief that field lines partially dehydrate the gas by retaining hydrate. For this reason, gathering lines should have greater volumetric capacity than needed for flow when clean. There are two main types of dehydration processes: the liquid (glycol) and the solid-absorbent types (Chap. 16). Suffice it to say here that the use of solid desiccants will make it possible to attain a higher dew-point depression and thereby a drier gas. If this is critical at any installation, the solid type should be strongly considered. The initial installation cost of a solid-type plant may be as high as 50 per cent above that of the glycol type.

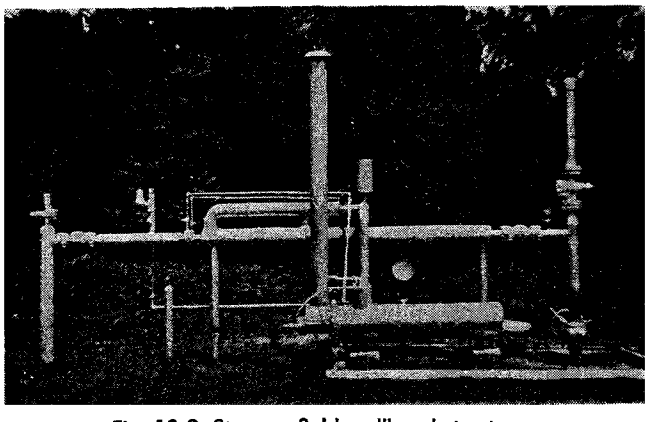

Fig. 18-9. Storage-field wellhead structure.

Much consideration has been given to the location of the dehydration plant: whether dehydration should take place before or after compression. There are advantages and disadvantages to both locations, and there is no general agreement on the question. Dehydration following compression permits the use of smaller-sized vessels, but the specifications of the vessels must allow a higher maximum working pressure. When dehydration following compression takes place beyond the coolers, care must be exercised not to overcool, for gas hydrates might freeze up the coolers. With glycol dehydration, it is possible to inject glycol ahead of the coolers and dehydrate the gas after it is cooled without its freezing in the coolers. Entrained oil from the compressors can render some types of solid desiccants ineffective for dehydrating; this would disqualify these desiccants for use after compression, unless some means are found to remove the oil before the gas reaches the dehydration towers.

Dehydration before compression requires the use of larger vessels, but with specifications for a lower maximum working pressure. For the solid type of desiccant there seems to be no noticeable cost advantage one way or the other. High gas velocities through some of the solid-desiccant beds may cause carry-over of small dust particles of the desiccant, which would cause increased wear on pistons, piston rings, cylinders, valves, valve seats, packing, etc., in the compressors. Where centralized gas-metering facilities into and out of storage are located at the

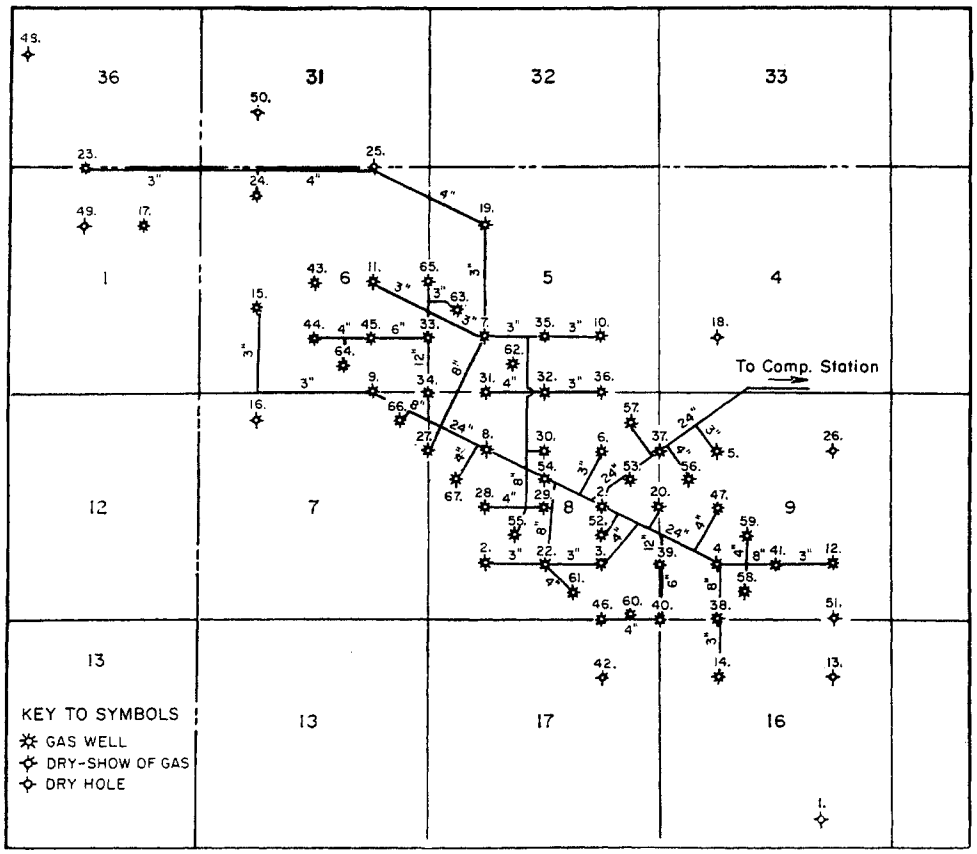

Fig. 18-10. Storage-field gathering system, field A.

site of the dehydration and compressor-station plant, it may be advisable to dehydrate the gas ahead of the meters upon withdrawal from storage. Thus, both on injection and on withdrawal, dry gas will be metered, and it will not be necessary to make metering corrections for water content on gas being withdrawn from storage.

In many installations it may be impossible to locate a glycol dehydration plant ahead of compression, especially if the compression ratio (CR) is high. It is probably not possible, with a glycol plant during normal operations, to maintain a dew-point depression greater than 50 to 60°F. Storage-field gas saturated with water at 60°F and 200 psia could have its dew point depressed to 0°F in a glycol plant. Compressing this gas to 1,000 psia would raise its dew point to approximately 32°F. This high dew point could cause water condensation, hydrate formation, and freezing in many pipelines during the wintertime.

Figure 18-11 is a photograph of a dehydration plant in Michigan using solid desiccant, and Fig. 18-11*a* shows a glycol-type plant.

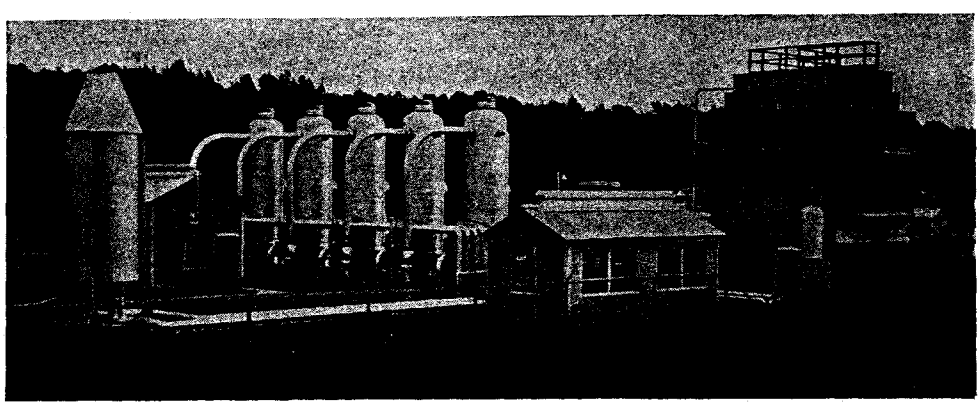

Fig. 18-11. Dehydration plant: solid desiccant; capacity, 240 MMcf/day; operating pressure, 650 psig.

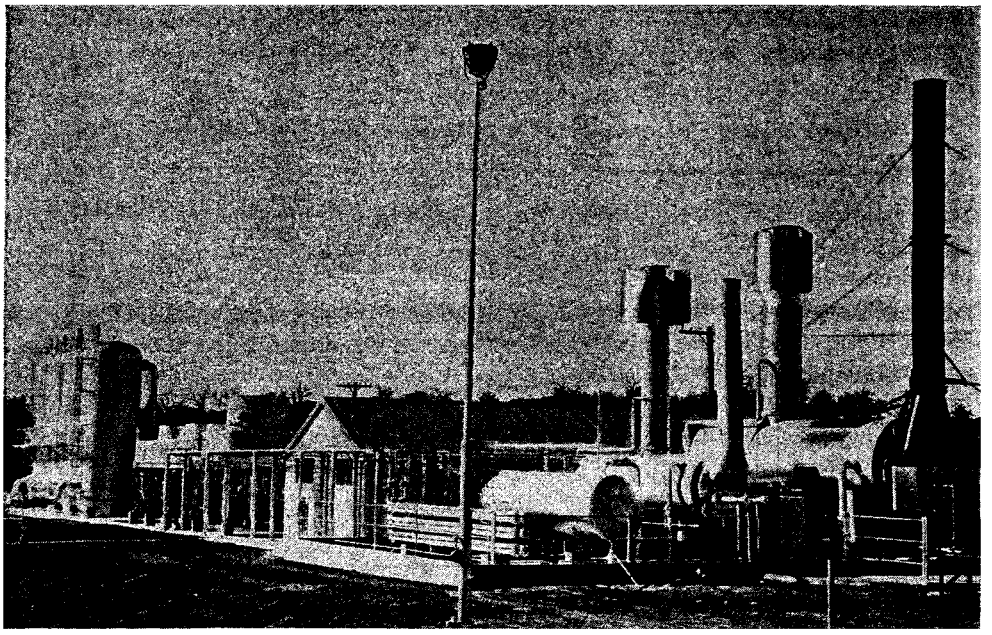

Fig. 18-11a. Glycol dehydration plant: capacity, 560 MMcf/day; operating pressure, 800 psig. (Courtesy Black, Sivalls, and Bryson, Inc.)

Metering

Orifice meters are constructed and installed at storage fields in accordance with specifications set forth in the AGA gas measurement committee report 3 (8-2), as was discussed in Chap. 8. Storage-field gas metering can be accomplished for the whole field at one centralized location, usually at the convergence of the gathering system, or at the individual wells, or at various points in the field for groups of wells. There are advantages to metering at one central location. The labor necessary to calibrate, maintain, change charts, change plates, and adjust the meters is held to a minimum. The number of charts from which gas flow is computed is held to a minimum. Severe weather and bad road conditions will not prevent careful servicing of the meters. The tendency to neglect certain meters because they are located way back in the field somewhere is not present. Control of the rate of flow from a field and the possibility of turning the field on or off from one central point are necessary for quick response to load changes. Under this centralized system all storage wells would always be open to the gathering system.

Such a central system of field measurement does not allow a day-by-day accurate check on how individual wells or groups of wells are performing. A daily record of manometer differentials at each well does afford a qualitative check on the performance of individual wells at the instant the manometer reading is taken. This requires a daily trip to each storage well. Figure 18-12 is a photograph of centralized metering facilities for a storage field.

Compression

Compression will be needed to serve almost every storage project. At high-pressure storage fields where the range of storage pressures is above the pipeline pressure, compression will be needed during the summertime to inject gas into storage. If at any point in the storage cycle the field pressure is lower than the pipeline pressure required to deliver the gas to market, compression will be needed upon with-

Fig. 18-12. Storage-field metering facilities.

drawal. In many storage projects where field pressures are low in the spring and high in the fall of the year, compression will be needed for injection as soon as field pressures build up to a certain point in early summer and will be needed for withdrawal as soon as field pressures are pulled down to a certain level in early winter. Compression needs will fluctuate much more rapidly in wintertime, as weather conditions change the market demands from storage. For most storage fields, it will be necessary to design the compressor station for peak-day wintertime loads. Summer loads into storage are steadier and usually at lower average and maximum rates than wintertime loads from storage. The summer loads, then, require less horsepower for compression. These statements, of course, do not apply to high-pressure storage projects, where very little or no compression is needed upon withdrawal.

Because of the wide range of compression ratios (CR), pressure levels, and loads required from a storage-field compressor station, it is necessary to select compressor units with care. It is usually advisable to have compressor units with at least two different horsepower ratings, for example, 1,000- and 2,000-hp units. There is an advantage to having some smaller units rather than only a few really large units. As loads and CR's fluctuate, it is possible to set up workable and efficient combinations of smaller and larger units for almost all conditions. This is not always possible with a few large units. It may be advisable to equip a few of the smaller units with larger compression cylinders to handle the gas when field pressures are low. Figure 18-13 shows a storage-field compressor station with about 20,000 hp.

OPERATION OF STORAGE FACILITIES

There are several facets to the operation of storage fields. First, there is the matter of storage capacity for a given season. The prediction of the field deliverability requires careful analysis of the data and field experience. An inventory of gas remaining in storage is required annually in normal business procedures.

Storage Capacity and Pressure Limits

In the gas-expansion type of storage field where there is no active water drive to maintain pressures, the storage capacity is set by the upper and lower pressure limits. There are several factors that must be considered in selecting these pressure limits. To how low a pressure was the field taken during its producing history? Was there any serious deterioration in well performance at this pressure due to water coning or other factors? If so, at what field pressure did this deterioration begin? How many of the edge wells have been abandoned at these low pressures during the production of primary gas? At what field pressure did the operator of the producing field start abandoning these wells? To evaluate these questions properly, a good record of the producing history of the field must be available. Back-pressure tests on the wells at various times in the field's producing history are very helpful. The economics of cushion-gas cost versus compression costs must also be considered. An evaluation of all the above factors will lead to the tentative selection of a minimum storage pressure, the storage-field base pressure. The selection of this pressure will establish a certain volume of

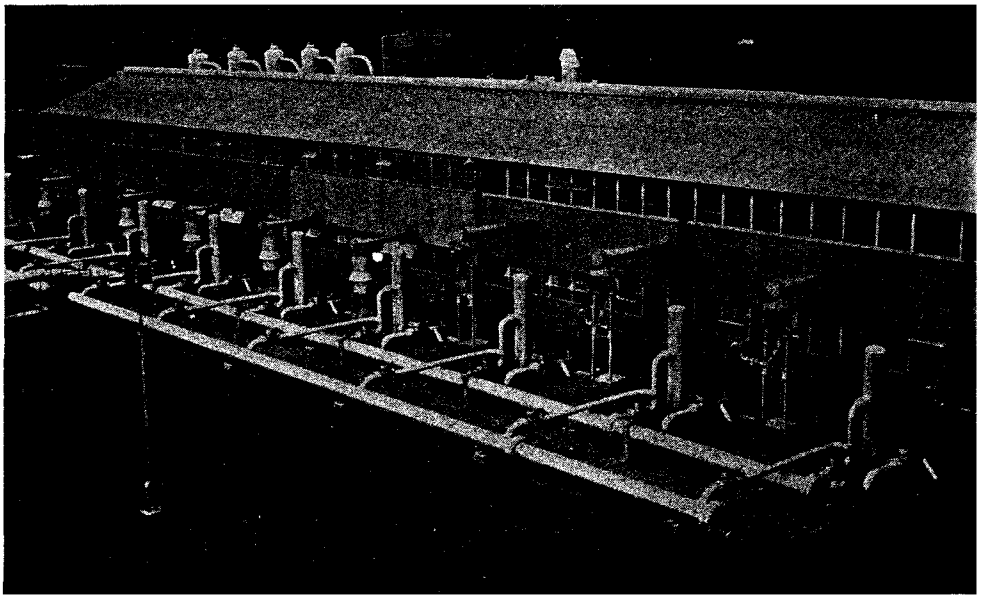

Fig. 18-13. Storage-field compressor station.

cushion gas. If the native gas remaining in the field is less than this cushion-gas volume, the difference must be injected and allowed to remain in the field. Normal storage operations can withdraw all the gas down to this cushion-gas volume, but will not dip into it. This does not mean that, in an emergency, some of this cushion gas cannot be withdrawn and transmitted to market. Figure 18-14 is a diagrammatic sketch showing the names applied to various gas quantities in storage fields.

The following is an example of how the base pressure was established in one field where good records and individual-well back-pressure-test data were available. All of the active wells in the field were back-pressure-tested five times for proration purposes during the field's producing history. Figure 18-15 shows the field-performance curves for each one of these tests. The field curve is obtained by adding together the open-flow measurements of all the wells tested and plotting this total against the square of the average absolute formation pressure. The average wellhead shut-in pressure at the time of the tests and the number of wells tested are noted on the chart at each point. The field curve is then drawn through this point at a reciprocal slope or n value of 0.85, which is the average slope of the individual-well (three-point) back-pressure tests. As long as these points fall on the same curve or approximately so—as the 1936, 1937, and 1939 tests do in Fig. 18-15—there is no deterioration in field performance. The 1943 tests show a deterioration of 26 per cent, and the 1945 tests a deterioration of 67 per cent. By 1943 and 1945 many of the wells had deteriorated to the point where they were unable to produce and had been plugged and abandoned. The deterioration was due mainly to water encroachment and finally to the drowning out of the well.

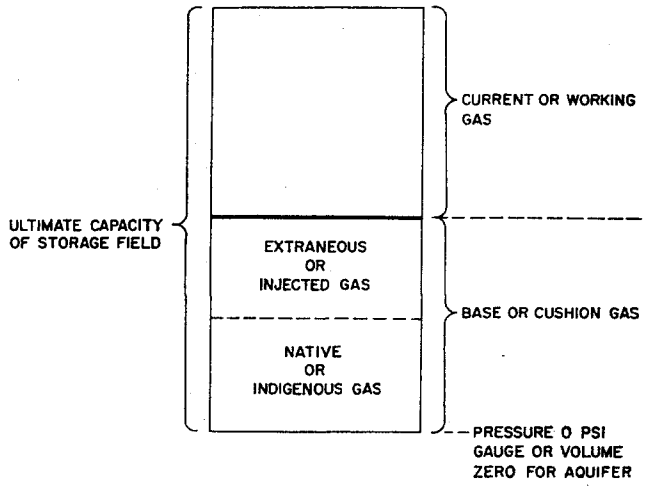

Fig. 18-14. Diagrammatic sketch of breakdown of gas in storage fields.

Ten wells were plugged and abandoned in this field between the field pressures of 400 and 300 psig, twenty-seven wells between 300 and 200 psig, and forty-one wells between 200 and 100 psig. An evaluation of these factors and of comparative cost factors of cushion gas and compression would determine the selection of the base pressure for this field—probably somewhere between 175 and 300 psig wellhead.

Maximum daily market demands from storage near the end of the heating season, when the fields are near base pressure, might be a factor in selecting the base pressure. This problem of end-of-season demand can be alleviated by drilling additional wells. It is then a question of the cost of drilling additional wells versus the cost of cushion gas.

In storage fields that contain no bottom or edge water—there are many such in the Appalachian region—low pressures cannot lead to danger of well injury from water. The criterion for establishing the field base pressure would then be field deliverability near base pressure plus compression needs versus availability and cost of cushion gas.

There are several factors that must be considered in establishing maximum storage-field pressures. The maximum allowable working pressure of the physical equipment in the field, such as well casing, line pipe, valves, etc., cannot be exceeded. Section 8 of the American Standard code for pressure piping (ASA B31.1, 17-4), published by the American Society of Mechanical Engineers (ASME), sets forth limitations on maximum working pressures; and the code is recognized by regulatory bodies and by the industry in general.

In several storage fields the operators are not willing to store gas at pressures appreciably above the field-discovery pressure prior to any gas or oil production. In these fields, then, the field-discovery pressure is considered the maximum storage-field pressure.

In relatively shallow storage fields with reservoir temperatures under 70°F, maximum pressure may be limited by hydrate-formation conditions. Chapter 5 contains a detailed discussion of gas hydrates. Liquid water must be present to form solid hydrates. Most underground storage reservoirs have liquid water in them as connate water or as bottom or edge water. The salinity of this water affects the hydrate-formation temperature and pressure. Increasing brine concentrations reduce the temperature and increase the pressure at which hydrates will form. Highly concentrated brines as formation waters practically remove the possibility of hydrate formation at present storage pressures unless, somewhere in the flow of gas from the reservoir, there is a sharp reduction in flowing-gas temperature causing the condensa-

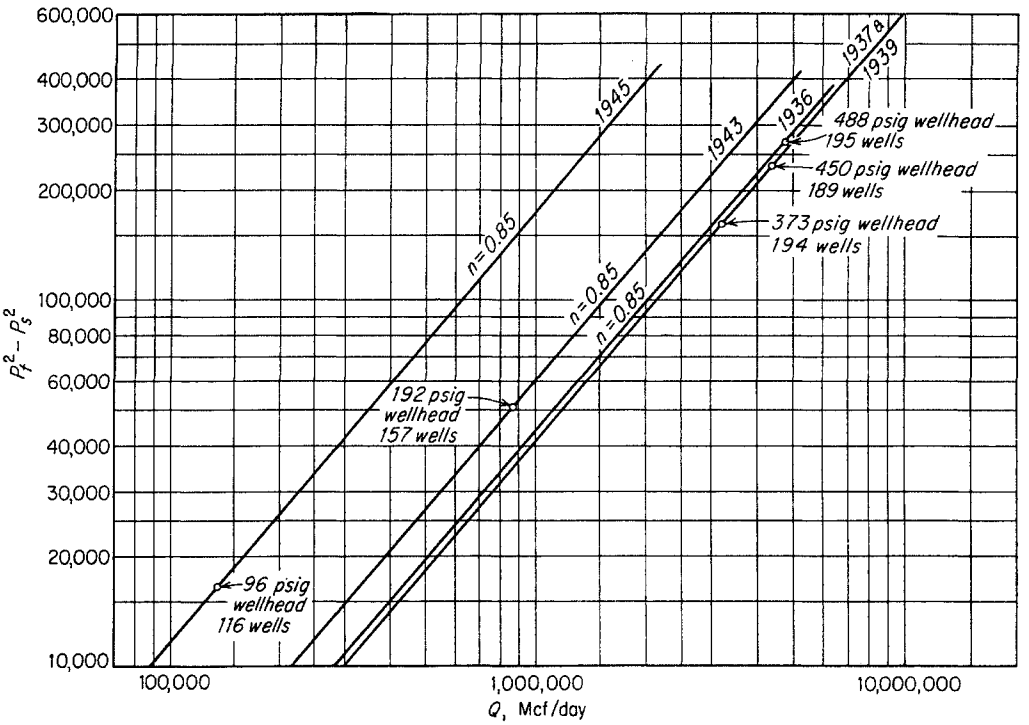

Fig. 18-15. Field-performance curves at various field pressures.

tion of fresh water from the gas. Kobayashi, Withrow, Williams, and Katz (5-43) have presented laboratory data showing the effect of brine concentration upon hydrate-formation conditions.

Maximum pressures in storage fields may also be limited by formation breakdown pressures or by hydraulic-fracturing pressures. Yuster and Calhoun (9-67a) have determined the formation-breakdown factor for several wells in the Bradford-Allegheny area. The formation-breakdown factor is the bottom-hole pressure, in pounds per square inch absolute, at which fracturing takes place, divided by the depth of the formation in feet. The factors reported by Yuster and Calhoun vary from 0.47 to 1.43 psi/ft, with most wells showing 1.0 psi/ft or more.

In storage fields where there is bottom or edge water in contact with the storage gas, there is a definite tendency toward increasing the gas-reservoir volume when gas pressures are maintained higher than field-discovery pressure. This is accomplished by movement and compressibility of the underlying water. As this process continues there is a point at which the gas will reach a spill point in the structure and spill over into adjoining structures. This is undesirable in storage operations, since the gas will be recoverable only by drilling of additional wells into the adjoining structures. This gas may spread out so far or collect in such small pockets that it would be uneconomical to try to recover any of it. The converse of the above is also true: if storage pressures are maintained below field-discovery pressure, water will tend to move into the storage reservoir, thereby decreasing its volume. It is possible to calculate the magnitude of these reservoir-volume changes by using the unsteady-state equations of fluid flow and solutions developed by Van Everdingen and Hurst (10-27) for flow of fluids through porous media.

Pressure Observations and Pressure History

Pressure-observation wells are an important part of storage operations. Approximately 4 per cent of all storage wells are used for pressure observation. These wells remain shut in continuously, and wellhead pressures are gauged, usually with a deadweight gauge, as often as once a day. These pressures can be correlated with net cumulative metered volumes of working-storage gas to establish a curve showing average or individual-observation well pressure versus content of working-storage gas. Figure 18-16 is a plot of observation-well pressure versus working-storage-gas content. It is easy to observe the repeated cycles with a gradual shifting toward higher storage-gas contents at any given pressure. This shifting is an indication of increasing reservoir volumes, which in turn are the result of recent pressure history, averaging out considerably above field-discovery pressure. Figure 18-17 shows the magnitude of the change in reservoir volume year by year corresponding to the shifting pressure-volume curve in Fig. 18-16.

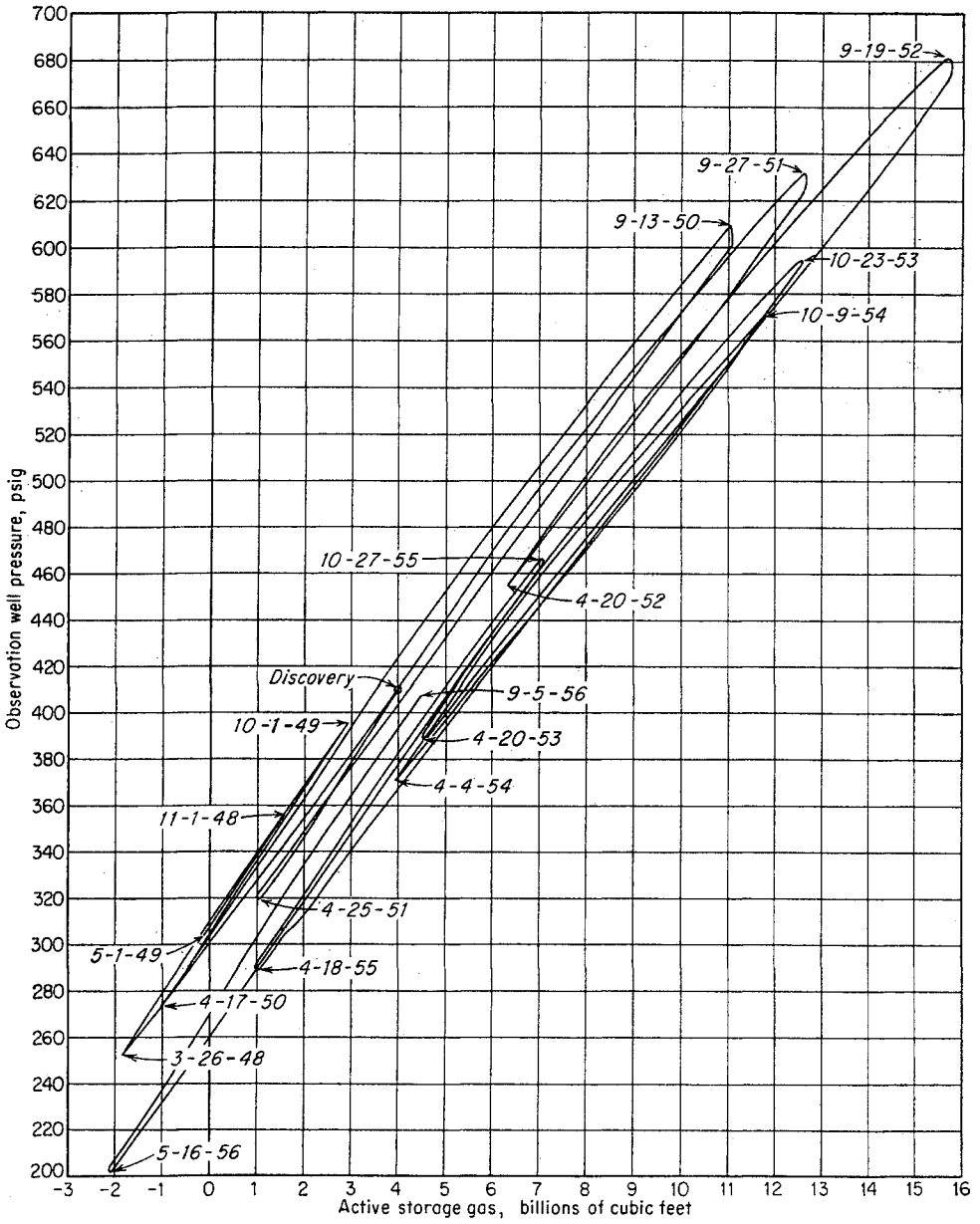

Fig. 18-16. Field A, pressure vs. volume from discovery to date.

Cycling around Discovery Pressure

Referring again to Fig. 18-16, it becomes desirable over a period of several years of storage operations to prevent this curve from shifting either to the left or to the right. A curve shifting to the left means smaller reservoir volume and water movement into the edge or bottom of the reservoir. As soon as this water reaches any of the wells it causes a reduced field deliverability. A curve shifting to the right means larger reservoir volume and movement of gas into the underlying water reservoir. This will require larger volumes of cushion gas to maintain the minimum or base storage pressure. Cycling around discovery pressure, so that the average field pressure for the year or cycle is at or close to the field-discovery pressure, should keep the curve of Fig. 18-16 retracing itself from cycle to cycle.

In some instances it may be desirable to maintain field pressures above field-discovery pressure purposely, in order to enlarge the size of the reservoir and, thereby, its storage capacity. Good structural control must be achieved all around the field, and the spill point must be known to be well below the original water level, before this procedure should be attempted.

Field Deliverability

Storage-field deliverability is generally taken as a summation of individual-well deliverability for all

active storage wells in the field. This is invariably the limiting factor in field deliverability, for surface facilities such as gathering lines, dehydration plants, and compressor stations are normally designed to handle all the gas that the wells will deliver. The answer, then, to increased field-delivery capacity is either to increase the delivery capacity of present wells or to drill additional wells.

Individual-well Back-pressure Tests

Back-pressure tests measure the ability of a well to take or produce gas. These tests are discussed in Chaps. 9 and 11. In storage fields, we are interested in stabilized back-pressure curves, which show the ability of a well to produce for sustained periods of time. The procedures necessary to obtain stabilized curves will vary from field to field, depending mainly upon the permeability of the reservoir rock. Vary, Elenbaas, and Withrow (11-30) state that, in the storage fields in Michigan, it is possible to obtain a stabilized flow point from a well in from 20 min to 1 hr. In the Hugoton field in Kansas, Oklahoma, and Texas it may take as long as 10 days of flow to obtain a stabilized flow point. Isochronal methods of well testing have been developed which cut down considerably the time necessary to test a slow-stabilizing well, and these should be used in such cases.

Experience in storage operations has shown that individual-well performance fluctuates from year to year. This change in the back-pressure curve is due to a change in the condition of the sand face in the well. It can be caused by water encroachment, cavings, salt deposition, compressor lubricating-oil deposition, and possibly other factors. Periodic back-pressure testing is essential in order to determine individual-well and over-all field performance. A gradual deterioration in well capacity cannot be detected during normal field operations. Annual well tests are recommended when they can be made economically on a large scale, possibly with some additional checks on troublesome wells. Vary, Elenbaas, and Withrow have presented a procedure for testing large numbers of wells, with injection during the summertime, when there are relatively small demands upon personnel and equipment (11-30). Figure

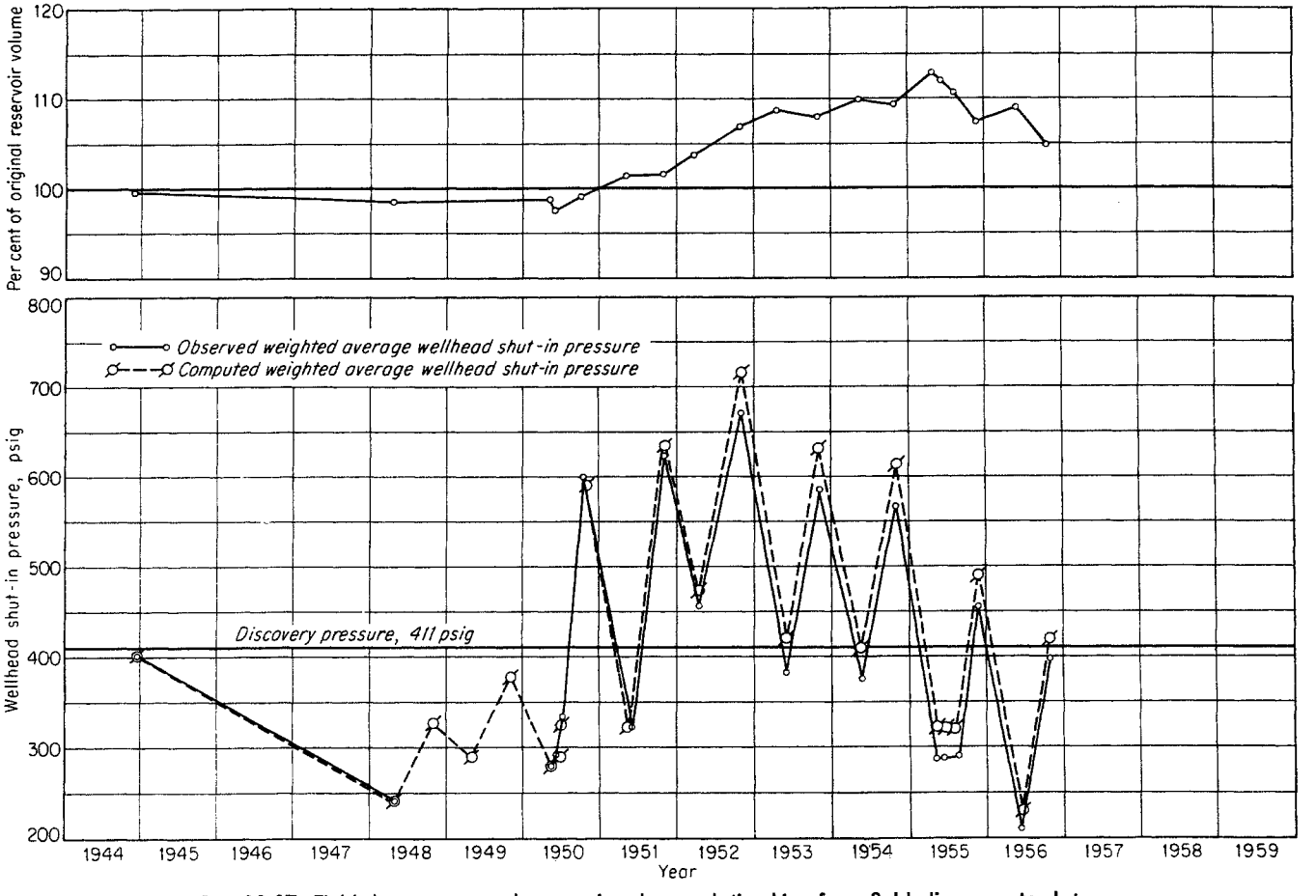

Fig. 18-17. Field A, pressure and reservoir-volume relationships from field discovery to date.

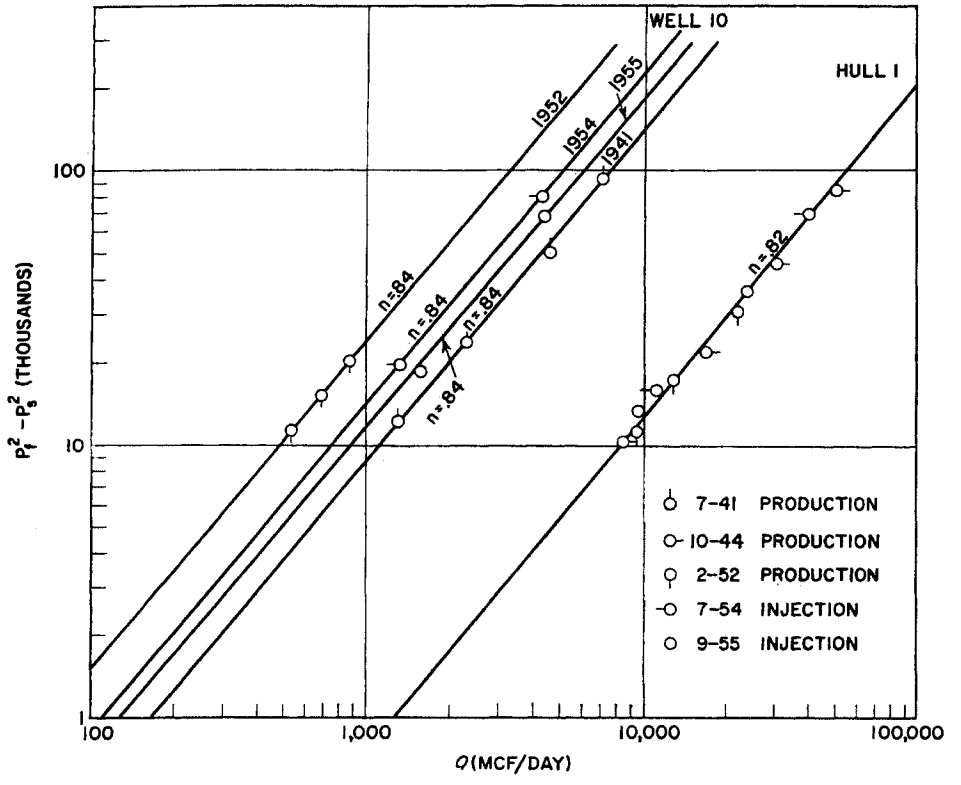

Fig. 18-18. Back-pressure curves.

18-18 shows the results of back-pressure tests made on two wells over a period of from 10 to 14 years. All the test points on the Hull 1 well fall on the same curve, indicating continuous, constant well performance. Tests on well 10 show fluctuating performance. This well was probably at some time prior to storage operations affected by water encroachment and salt deposition in and near the well bore. This well has been cleaned each year, and its performance has continued to improve, although not yet to its original curve.

It is significant to note that the slope of the back-pressure curve of well 10 (Fig. 18-18) has not been affected by the shifting of the curve. The slope appears to be a characteristic of the well. This relation has been found in testing many other wells.

The results of annual back-pressure tests on storage wells show the need for remedial procedures to maintain field performance. Some wells can be improved by periodic blowing to the atmosphere to remove cavings. When shale is present below the casing, liners can be set to prevent cavings. Chemical treatment to clean the sand face may help some wells. In some instances underreaming may be necessary to clean the well. Open-hole perforations into the reservoir rock should improve capacity. All these procedures would in any case be more economical than drilling an additional well to make up the lost deliverability.

Field-deliverability Curve

A field-deliverability curve is obtained by adding together in some manner the individual-well back-pressure curves. This can be accomplished by reading each of the individual-well curves at three different values of the function $P_f^2 - P_s^2$ (Fig. 18-18), which is the shut-in formation pressure squared minus the sandface flowing pressure squared; adding the respective values of flow Q that are obtained; plotting these totals at their respective values of $P_f^2 - P_s^2$; and drawing a field curve through these three points.

The above method will result in a field curve with a weighted average slope. If there is any performance interference between wells while all wells are flowing, the field curve will be too high. Performance interference would be the result of intersecting pressure gradients in the formation back away from the wells. This would mean that the wells would be producing from some pressure lower than the shut-in formation pressure. Vary, Elenbaas, and Withrow (11-30) state that they are unable to observe any performance interference among wells located as close together as 660 ft in a sandstone reservoir with permeability averaging about 300 millidarcys.

Maximum Withdrawal Rates

There are several factors that will influence the maximum withdrawal rate from a well or field. One

of the most significant is water encroachment. A high-pressure drawdown during a withdrawal will create a high differential in pressure at the bottom of the well between the gas and the underlying water. This will cause the water to encroach into the bottom of the well. The minute it reaches the well there will be a reduction in the deliverability of the well. This is undesirable in storage operations. The pressure drawdown, during withdrawal, that will cause water to reach the well will vary from well to well and from field to field. It must be determined by experience, and depends upon the pressure level in the field at the time of withdrawal, the thickness of the reservoir gas sand between the total depth of the well and the underlying water, and the permeability of this thickness of sand plus any permeability barrier between the gas reservoir and underlying water reservoir. In one area, pressure drawdown (difference between wellhead shut-in and flowing pressures) has been limited to approximately 60 psi for field pressures up to 700 psig.

In fields where there are no water problems, maximum withdrawal rates may be limited by the transmission-line pressure against which the field must feed, or by the installed horsepower at the compressor station which must compress the gas into the transmission line.

As stated previously, maximum withdrawal rates should be set low enough to prevent the breakoff and flow of small particles of reservoir rock, because of the severe cutting effect of such particles on metal, possibly leading to rupture.

Figure 18-19 shows the maximum withdrawal rate for field A at various field pressures. The discovery pressure in this field was 411 psig at the wellhead. Wellhead-pressure drawdown was limited to 50 psi at all pressures above the discovery pressure and was reduced gradually as the field pressure went below discovery pressure. These limits were set to avoid water encroachment and were established from field experience.

Predicting Field Performance

It is important to be able to predict, months and even years in advance, what field outlet pressures will be at various rates of storage-field withdrawal with various quantities of stored gas in the field. Figure 18-20 is a chart which has been developed to supply this information for field A. The chart has been set up for an actual facility where it is desirable to know the compressor-station inlet pressure for a compressor station located about twelve miles away from the storage field. The chart is a combination of a field-performance curve and a gathering-system, dehydration-plant, and transmission-line pressure drop. This chart is plotted with observation-well pressure as a parameter. The observation-well pressure can be converted to the volume of active stored gas in the field by use of Fig. 18-16, on the withdrawal portion of the cycle. To estimate future operations, this curve on Fig. 18-16 must be projected into the future as far as is necessary. After a few years of storage history and with knowledge of maximum and minimum storage volumes, this can be accomplished quite accurately.

By use of Figs. 18-16 and 18-20 it is possible to calculate the volume of stored gas that must remain in the field to meet stipulated peak market demands from storage, months and even years in advance. Conversely, with known volumes of stored gas in the field it is possible to determine the maximum withdrawal rates from the field and to estimate the facilities necessary in the way of wells, gathering system, and horsepower to make it feasible to withdraw at even higher rates of flow.

Table 18-11 shows a series of actual observation-well

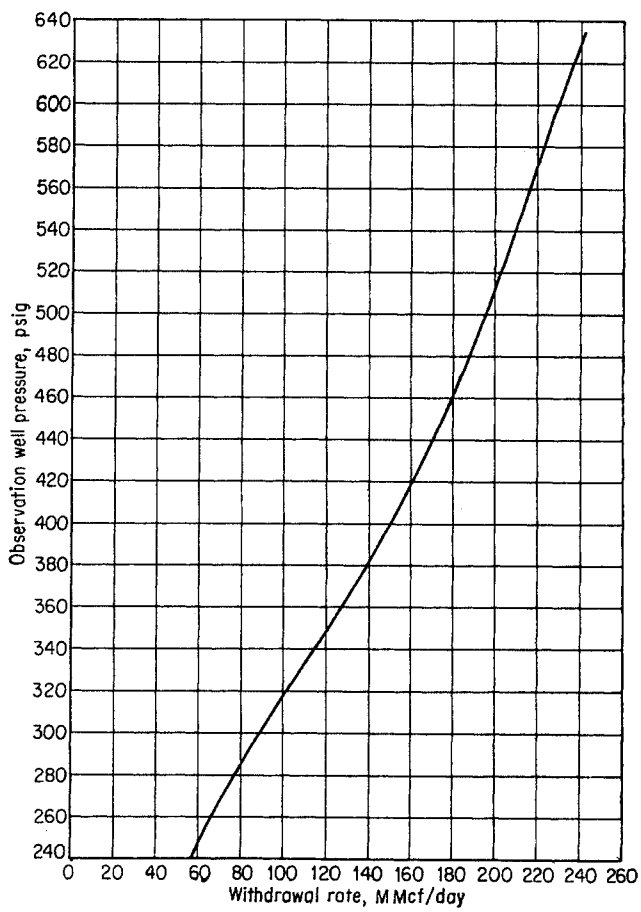

Fig. 18-19. Field A, maximum withdrawal rate.

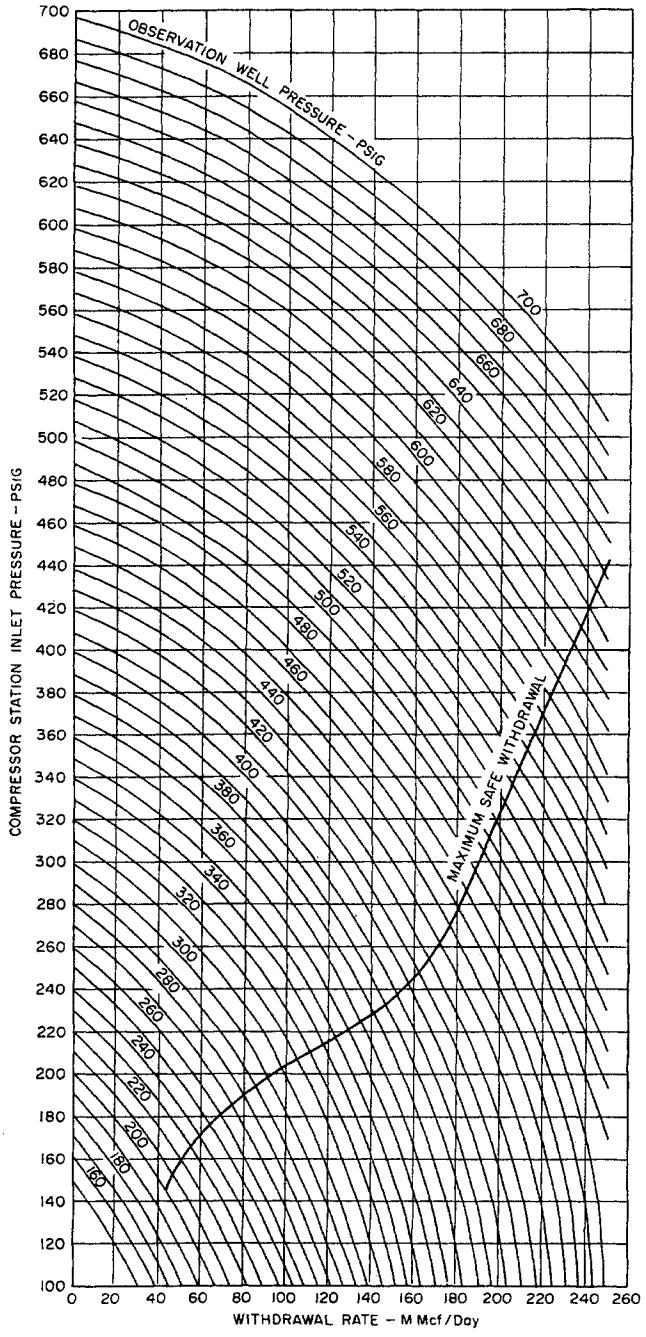

Fig. 18-20. Field A, rate–terminal pressure relationship chart.

pressures, withdrawal rates, and station inlet pressures of field A, taken to check Fig. 18-20. The computed station inlet pressures from Fig. 18-20 are compared with actual pressures, and the differences are shown. The differences on this table vary from +8 to −4 psi. Many more such comparisons have been made, and the maximum differences have been from +10 to −10 psi. This is considered reasonably accurate. The withdrawal rates are not held constant for a whole day, but 4- to 6-hr constant withdrawal rates are converted to daily rates. The actual station inlet pressures may then be affected slightly by the different rate of withdrawal prior to the 4- to 6-hr period. Also, although observation-well pressures are taken with a deadweight gauge to the nearest 0.1 psi, the actual station inlet pressures are obtained from the static pressure element on an orifice-meter chart. These charts are graduated only every 20 psi and probably cannot be read within 2 to 3 psi.

Table 18-11. Field A, Comparison of Actual versus Calculated Compressor-station Inlet Pressures

Date	Observation-well pressure, psig	Withdrawal rate, MMcf/day	Station inlet pressure, psig		
			Computed	Actual	Diff.
Dec. 1, 1952.....	637.7	100.6	592	590	+2
Dec. 13, 1952....	623.3	62.3	601	600	+1
Dec. 21, 1952....	610.5	22.0	605	600	+5
Dec. 31, 1952....	594.8	79.7	559	560	−1
Jan. 6, 1953.....	582.9	152.2	481	485	−4
Jan. 12, 1953....	567.0	104.8	510	510	0
Jan. 20, 1953....	549.2	120.4	476	480	−4
Jan. 27, 1953....	530.8	137.2	437	438	−1
Feb. 10, 1953....	489.8	126.6	400	400	0
Feb. 27, 1953....	439.5	126.7	338	335	+3
Feb. 5, 1954.....	416.3	59.5	384	380	+4
Feb. 20, 1954....	400.8	20.9	391	393	−2
Mar. 19, 1954 . . .	380.3	38.0	359	358	+1
Feb. 14, 1955....	359.5	87.1	288	280	+8
Mar. 2, 1955	322.4	52.3	283	277	+6
Mar. 19, 1955 . . .	308.6	48.6	270	270	0
Mar. 27, 1955 . . .	301.3	29.8	279	280	−1

Figure 18-20 can also be used in reverse to determine the compressor-station outlet pressure necessary to inject various quantities of gas into the field. Since gas being injected into the field is not dehydrated, the dehydration-plant pressure drop incorporated in Fig. 18-20 must be subtracted out. Also, the observation-well pressure would be read along the ordinate and the compressor-station outlet pressure as the parameter.

Daily Operations

Gas dispatching is an important phase of the operations of a natural gas utility (18-23). The gas dispatcher, usually located at the major market area of the utility, must gather weather data and forecasts and must correlate hourly demands for gas with weather, industrial activity, commercial activity, and residential-appliance needs. He must predict loads hour by hour and relay this information to the center of storage operations. Since long-distance transmission lines operate or at least attempt to operate at fairly constant daily and hourly rates, all fluctuations in load must be handled from underground storage.

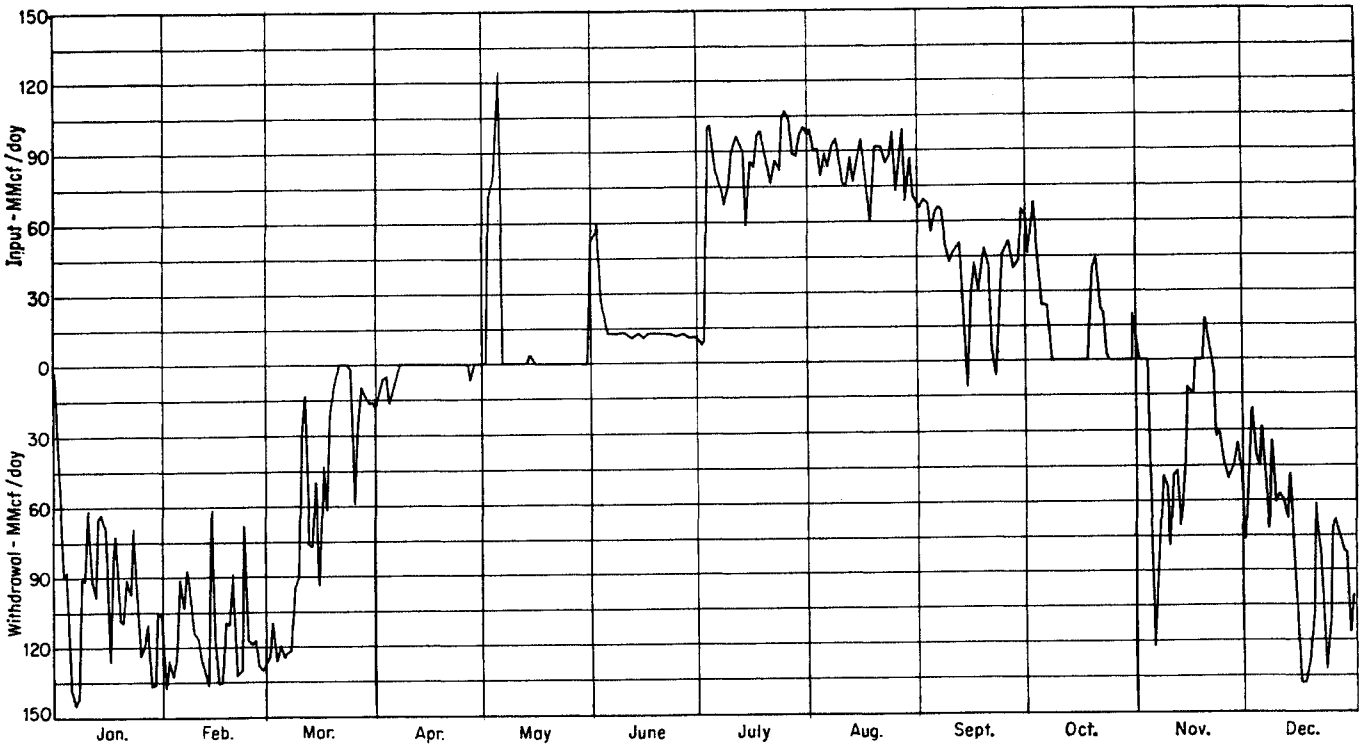

Fig. 18-21. Field A, daily withdrawal and injection rates.

The gas dispatcher will relay to the storage center the rates necessary to supply each market area. This may be done in the form of hourly rates or in the form of pressures to be maintained on each of the transmission lines or both. The control center for storage operations will translate this information into rates from each of the storage fields and engine needs at each one of the storage-field compressor stations.

To increase the rate of withdrawal from a storage field with all active wells open to the gathering system, it is only necessary to lower the pressure at the outlet of the gathering system or at the inlet to the compressor station. Orifice metering facilities must also be changed to meter accurately the increased volume of gas. It may be necessary to turn in another meter run or to increase the size of the orifice plate or plates in the operational meter runs. It may be necessary to change the time cycle in the dehydration plant, although the time cycles are usually set for maximum flow rates so that any lower rate can easily be handled with no change in operations. Figure 18-21 shows the daily withdrawal and injection rates for field A for the year 1953. Figure 18-22 shows the hourly withdrawal and injection rates for field B for typical winter and summer days.

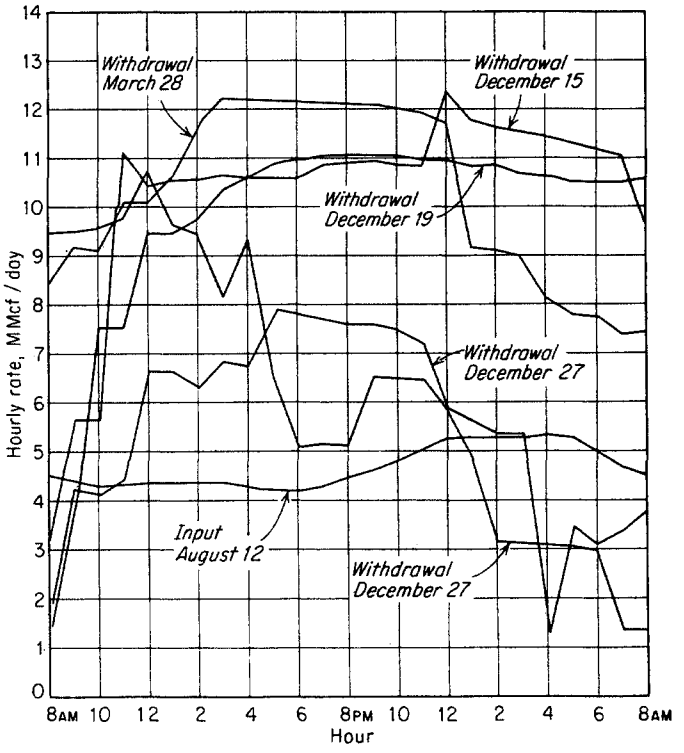

Fig. 18-22. Field B, hourly withdrawal and injection rates.

The increased rate of withdrawal from storage will require additional compressor horsepower. This may involve starting additional engines or just manipulating cylinder pockets and loading or unloading one or more outer cylinder ends. In some stations with high CR it may be necessary to change over to double-staging the gas.

Reversal of flow in a storage field from injection to withdrawal is accomplished simply by reversing leads at the centralized orifice meters; properly sizing orifice plates; starting and putting on stream the dehydration plant that is normally not used during injection; and lowering the pressure at the inlet to the compressor station or transmission line enough to cause the gas to flow out of the field. In some storage fields that contain individual wellhead heaters it may be necessary to light the pilots on these heaters. Normally these pilots would remain lit throughout all the months of the year when gas might be required from storage.

During withdrawal periods from storage each active gas well should be visited frequently. This may be done once every day; in some fields it is done once every 8-hr shift during the day and night. Well flowing pressures and manometer differentials are recorded. The well heater is checked. These frequent visits and continuous records make it possible for the field operator to know almost immediately when a well is not performing up to its capacity. During periods of injection trips to each of the wells are not so essential and are often made only once or twice a week. Key pressure-observation wells should be checked once a day the year round and pressures should be taken with a deadweight gauge. Other observation wells can be checked periodically.

Inventory of Stored Gas—Shut-in Period for Pressure Observation

There are periods during the spring and fall of the year when market requirements will balance very closely the pipeline supply of gas. During these periods the storage fields can be shut in one or more at a time. With each well shut in, deadweight-gauge pressures can be taken on all of the individual wells daily or every other day for a period of from 7 to 15 days. This will allow sufficient time for a substantial pressure equalization between wells and for removal of most of the pressure-drawdown gradient set up during production from the wells. Taking pressures daily on all of the wells should make possible the charting of underground gas migration within the reservoir during the shut-in period.

Computation of Average Field Pressure

Pressures taken on the final day of shut-in must be averaged in some manner to obtain an average field pressure. The most accurate method of doing this would be to determine the portion of the total reservoir volume that each well pressure represents and weight that pressure by its corresponding portion of the total reservoir volume. To do this, an isopachous map of the reservoir must be constructed, and the distribution of porosity and residual water-saturation values must be known or averages used. If the well spacing in the reservoir is such that all portions of the reservoir are not represented by wells, it may be necessary to draw an isopeistic map and, with the aid of a planimeter, determine the average pressure for each portion of reservoir volume. When reservoirs are rather tight or when the closed-in pressure measurements can be taken for only 2 or 3 days, the methods of obtaining equalized reservoir pressures described in Chaps. 10 and 11 may be used. Then, weight each pressure by its corresponding reservoir volume and determine the average field pressure. Given this pressure and the known volume of gas metered into the field, the volume of the reservoir can be calculated. Repeated similar calculations for different dates can be plotted (see the upper curve in Fig. 18-17). If any of these calculations gives an answer that shows a much larger than normal reservoir volume, there is reason to suspect that some gas may have escaped from the reservoir.

Todd (18-21) presents a table showing a very good check on storage inventory for the La Goleta storage field in California. Pacific Lighting Gas Supply Company has been able to operate this storage project over a period of several years at annual-average reservoir pressures approximately equal to the original reservoir pressure. Such an operation would tend to hold a constant reservoir volume.

Lost and Unaccounted-for Gas Volumes

All pipeline transmission and distribution systems operate with some lost and unaccounted-for gas volume, even after accounting for all company use. This is usually expressed as a certain percentage of the gas purchased or of input to the system. The volume is due to leakage around compressor piston rods, leakage through screwed joints, leakage through packing glands around valve stems, through blowdown valves, and through tiny holes in the pipe surface. When any of these leaks becomes large enough it is detected and repaired. While the leaks are developing, however, small volumes of gas are lost.

Since the same facilities are present in storage fields as in pipeline systems, there is every reason to believe that equivalent losses exist in storage operations. The difficulty is that it is not possible to determine with high accuracy the volume of gas in a storage reservoir. The amount of loss in a storage system, then, is not detectable until it has accumulated over a period of years and has become a sizable volume. Ideally, these losses should be accounted for as they occur from month to month.

One solution would be to set up loss figures similar to those of known volumes in transmission systems. The relative amounts of valves, piston rods, screwed joints, and pipe surfaces in transmission lines and storage fields could be determined. Since these losses are proportional to the pressure in the system and not to the throughput, they should be correlated with pressures. When storage-field pressures are high in the fall of the year, losses will be at a maximum but throughput may be at a minimum, because distribution-system loads will balance closely against pipeline deliveries. The situation is different in transmission lines, for pressures are held fairly constant the year round and throughputs do not fluctuate widely, especially where pipelines are operated in conjunction with underground storage fields.

The Bureau of Mines (18-19) made a careful study of gas losses from screwed-joint and welded pipelines in 1928. Facilities constructed in recent years will have less losses than those constructed prior to 1928. A figure of 0.0002 Mcf/(yr)(psi) per square foot of pipe surface appears to be of the right order of magnitude for losses from storage-field systems.

Gas Analysis for Studying Gas Movement

Gas analysis may be a useful tool for studying underground gas movement, mixing within a storage reservoir, and possible gas migration to nearby reservoirs. Foreign gases injected into a storage reservoir often have distinctive amounts of certain components by which they can be distinguished from native field gases. Hugoton field gas, for instance, has a high nitrogen content and a distinctive helium content. Gulf Coast gas often contains significant amounts of carbon dioxide.

Gas mixing within a reservoir may not take place nearly so completely as is sometimes assumed. Mertz and Huntington studied gas mixing in pilot operations (18-15). In the Michigan storage fields, 50 per cent of dry gas injected during the summertime can be withdrawn before the dew point of the gas begins to climb. By the end of the withdrawal period the gas is saturated. In one storage field a top structural well has been shut in for pressure observation continuously since storage operations commenced. After injecting foreign gas containing 15.5 per cent nitrogen for five consecutive summers, gas samples taken from this well show by mass-spectrometer analysis a maximum of 10.1 per cent nitrogen. The native gas in this field contained 8.0 per cent nitrogen.

Small gas reservoirs frequently exist adjacent to large storage reservoirs. It may not be possible to determine structurally whether these reservoirs are connected, without drilling several wells at a considerable cost. Pressure changes in these small reservoirs because of gas-storage operations may be due entirely to pressure transmission through underlying continuous brine aquifers. Periodic sampling and analysis of gas produced from wells in the small reservoirs will give evidence of gas migration from the storage reservoir if it exists, provided that stored gas can be distinguished from native field gas.

Two adjacent producing fields in Michigan were shut in for storage in 1950 at pressures of 200 to 250 psig. One of the fields was developed immediately, and has been since 1951 an active storage field with pressures ranging up to 700 psig every fall. The other field has been dormant; the pressure on the wells, however, has gradually built up to 400 psig in the center of the field. The pressure on the dormant well nearest the active storage field does cycle up and down to a limited degree with the storage-field pressure. All structural information would indicate that the fields are connected. Gas analysis of samples taken from the dormant wells shows no concrete evidence as yet that storage gas has migrated into the adjacent field.

The methods of gas analysis mentioned in Chap. 6 may be considered for detecting the key components used to differentiate between gases. The mass-spectrometer and gas-chromatography analyses are likely to be most useful. Since instrument calibration is so important for accurate gas analysis, it is suggested that a reference sample be included with each group of samples to be analyzed.

STORAGE OF GAS IN DEPLETED OIL FIELDS

A partially depleted oil field has many characteristics of a partially depleted gas field; and the same procedures of development and operation apply. There are also characteristics of oil fields that need special mention when oil fields are considered for use as gas-storage reservoirs. The flow capacity for oil indicates the capacity of wells for gas. Oil and gas production indicate the space available for gas

storage. The injection of gas into the oil field can become a project for secondary recovery of crude oil (18-2, 18-5 to 18-7, 18-11, 18-20).

The first prerequisite in considering a depleted oil field for gas storage and secondary recovery of oil is knowledge of the field history. The reservoir mechanism of oil production is important: whether it was by water drive, solution-gas drive, or gas-cap drive, and to what degree by gravity drainage. The initial capacity of the wells to produce oil indicates their capacity for gas injection and gas production. The accumulated production of crude oil and natural gas will permit computation of the space available for gas storage. The reservoir pressure history is related to the mechanism of the reservoir and will assist in determining the pressure range to be used for the storage cycle.

The conversion of three oil fields to gas storage has been reported: Playa del Rey near Los Angeles, Calif. (18-20, 18-11), the New York City field (18-6, 18-5, 19-5, 19-6) in Clay County, Tex., and the Monte Bello field in California. Data on these fields are given in Table 18-12.

The Playa del Rey field was developed by the U.S. government to provide fuel for defense plants. It was later sold to the local gas company. Gas was injected in the structurally high wells, with intermediate wells flowing oil and water and downstructure wells pumping. Oil production in 1956 was about 1,000 bbl/day. The oil is of low gravity and is relatively viscous. Difficulties with emulsions occurred when the same well was used for injection and for production. The field is used for peak-load shaving in the early morning of the colder days. The reservoir may be recharged the equivalent of three times during a single heating season.

Table 18-12. Data on Oil Fields Used for Gas Storage

Field	Playa del Rey	New York City	Monte Bello
Year first drilled	1931	1941	1938
Year storage started	1942	1952	1956
Depth, ft	6,500	6,100	7,500
Initial reservoir pressure, psi	2,600	3,134	3,300
Reservoir temperature, °F	230	164	210
Oil gravity, °API	14–22	47	34
Accum. oil production, MM bbl	8.3	8.25	8.48
Accum. gas production, MMMcf	.....	3.74	38.8
Gas storage, MMMcf:			
Ultimate working	2.0	4.0	12.5
Cushion	4.0	2.0	26
Wellhead pressure range, psi:			
Low	900	1,000	2,000
High	1,300	3,200	3,000
Formation	Sand	Limestone	Conglomerate
Area, acres	240+	400	540
Thickness, ft	150	300	62
Porosity, per cent	17–24	.....	22
Permeability, md	62–950	.....	77
Reservoir mechanism	Solution gas	Solution gas	Solution gas
Deliverability of gas, MMcf/day	450	60	200
Station horsepower	6,220	2,640	8,100

The New York City field is a reef structure. The field contained a volatile oil, undersaturated with gas at 2,300 psi. The formation volume factor of the reservoir oil was 1.66, and 960 cu ft/bbl of gas was dissolved in the oil. The gas-oil ratios rose during primary production and were up to about 160,000 cu ft/bbl when the reservoir was abandoned for oil at a reservoir pressure of 130 psig. The low recovery of about 18 per cent of the oil present was due in part to the high shrinkage of the oil, which led to high gas-oil ratios. Two high wells were used initially for gas injection and withdrawal, with four lower wells producing oil and cycled gas. Accumulated secondary oil at the end of 1955 was 145,000 bbl.

The Monte Bello storage field is the eighth zone in a multizoned field. Its oil production rate was down to 350 bbl/day when gas was injected. Initially six injection wells and eleven producing wells were used. It is expected that new wells will eventually be whipstocked from a neighboring site to the reservoir, since the surface is being plotted for subdividing.

Storage Capacity

The production of oil and gas is evidence that space is available for gas storage. The shrinkage that takes place when reservoir oil is produced should be noted–also, for pressure-depletion fields, the shrinkage of oil still in the reservoir when natural gas was produced in excess of that dissolved in the produced crude oil. When material-balance calculations have been made on a reservoir, the gas phase is obtained directly.

The capacity of a depleted oil reservoir for gas may be found from the following equation.

Let ΔN = oil produced, bbl
B_0 = formation volume factor
V = volume of gas to replace oil produced, Mcf
P = reservoir pressure, psia
T = reservoir temperature, °R
z = compressibility factor for gas

Then

$$V = \frac{5.61\,\Delta N\,B_0}{1{,}000}\,\frac{P}{14.65}\,\frac{520}{Tz} = 0.199\,\frac{\Delta N\,PB_0}{Tz} \qquad (18\text{-}1)$$

The space vacated by solution gas from oil still unrecovered can be computed when the recovery is known. However, the problem remains to determine whether injected gas will go into solution when the reservoir is repressured. After several cycles of storage and

secondary-oil recovery are completed, then some storage capacity will be available as a result of this shrinkage.

Computation of the quantity of gas in working storage requires a determination of the pressure cycle as well as of the reservoir volume. The pressure cycle will depend upon the permeability of the reservoir, depth, and other circumstances. Reservoirs are normally found at the hydraulic-pressure gradient corresponding to the depth (Fig. 1-37). It has been found that pressures higher than discovery may be used when a good cap rock is present. In case underlying water is present, whether or not it provides an active water drive, the volume of the gas space may vary with the pressure due to water movement. It is believed that a pressure cycle which goes as many pounds above the discovery in summer as it goes below this pressure at the end of the withdrawal season will cause a minimum of water movement. The maximum pressure depends upon the nature of the cap rock and probably should not exceed 0.6 psi per foot of depth.

Figure 18-23 has been prepared to find an approximate storage capacity for 0.6 gravity gas in a depleted oil reservoir. The earth-temperature gradient is taken as 55 to 200°F for 0 to 10,000 ft. The formation volume factor is taken corresponding to 40°API oil, that is, 1.75 at 4,300 psi. The chart gives the total storage capacity for gas per million barrels of oil produced. It does not take into account the reservoir space voided by gas produced from crude oil still in the reservoir. For example, at 200 psia pressure with a 40 per cent oil recovery in a solution-gas-drive reservoir, an extra 40 per cent of gas could be stored in the reservoir because of the space created by vaporization of gas from the unrecovered oil. Some gas would go into solution in the oil but, when secondary oil recovery ceases, this could become advantageous, since, at pressures under about 3,000 psi, the gas in solution occupies less space than it would in the gas phase.

The proportion of total storage gas that becomes working storage depends upon the pressure cycle. It may range from 40 to 70 per cent of the total gas in the reservoir.

The capacity for gas of an oil field that produced oil by water drive depends upon the ability to remove the water. Water-drive oil fields produce much water along with the oil, and often return the water to the producing horizon through edge wells. Much of the water can be pumped from the reservoir and not returned to the producing horizon. Gas pressure exceeding the reservoir discovery pressure should return the encroached water to the aquifer from which

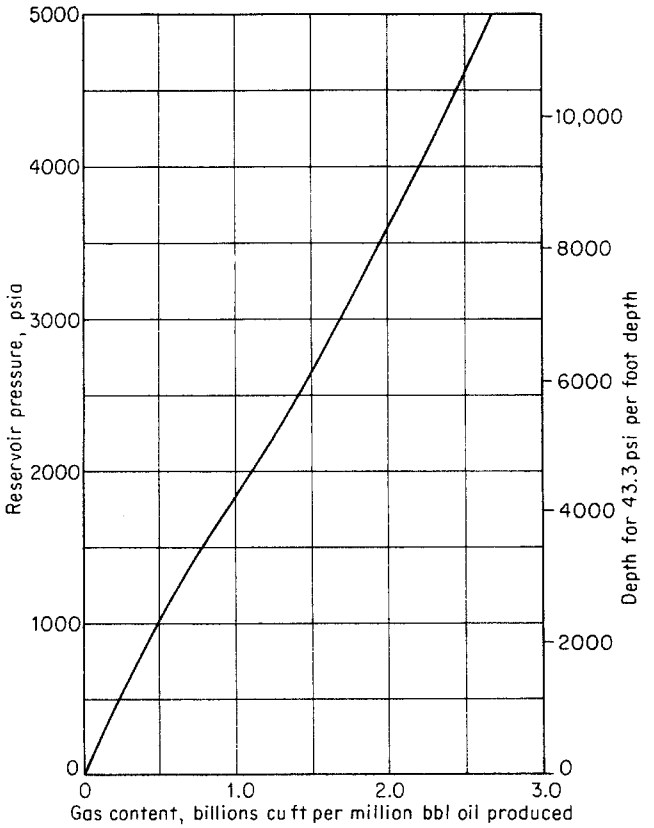

Fig. 18-23. Storage capacity for gas of depleted oil reservoirs, based on produced oil only, 0.6 gravity gas.

it came. The ability of water to drain out of a porous medium is not known, but one would expect that most of the encroached water could be removed in a few years of gas storage.

Flow Capacity of Oil Wells for Gas

In predicting the capacity of oil wells for gas injection or production, the flow rate and flowing bottom-hole pressure on the oil well are desired. The flow equations for oil and gas can be combined as follows. For oil flow, Eq. (10-3), rearranged, becomes

$$\frac{hK}{\ln (r_2/r_1)} = \frac{Q_o B \mu_o}{0.00708(P_1 - P_2)} \qquad (18\text{-}2)$$

where Q_o = oil flow rate, bbl/day (of stock-tank oil)
B = formation volume factor
μ_o = oil viscosity, centipoises
P_1 = reservoir pressure, psia
P_2 = flowing bottom-hole pressure, psia
hK = thickness-permeability product, millidarcy-ft
r = radius, ft
subscript 2 indicates well bore
subscript 1 indicates reservoir

Likewise, for laminar flow of gas, Eq. (10-2) applies.

$$\frac{hK}{\ln (r_2/r_1)} = \frac{Q_z T \mu_g}{0.000703(P_1^2 - P_2^2)} \qquad (18\text{-}3)$$

where Q = gas flow rate, Mcf/day
z = compressibility factor at average reservoir conditions
T = reservoir temperature, °R
μ_g = gas viscosity, centipoises

Combining the equations and rearranging,

$$Q = \frac{0.0993 Q_o B \mu_o (P_1^2 - P_2^2)_g}{z T \mu_g (P_1 - P_2)_o} \qquad (18\text{-}4)$$

The laminar-flow equation for gas can be solved when the following are known: the oil-well flow rate Q_o for a given pressure drop $(P_1 - P_2)_o$, the formation volume factor B, the oil viscosity μ_o, the gas viscosity μ_g, the reservoir temperature T, and the gas compressibility z. Equation (18-4) neglects any extraneous gas produced with the oil and the effect of vaporization upon flow. The equivalent equation which includes the turbulent flow of gas can be derived. Core analyses giving the millidarcy-feet can be used with Eqs. (10-2) and (10-5) to predict flow capacity, or Fig. 11-5 may be used.

Secondary Recovery of Oil

There are three aspects of secondary recovery that are worthy of note. First, the recovery of oil can be of considerable economic benefit, both from the value of the oil produced and from the extra gas space created by oil production (18-6, 18-7). Second, the time table for developing a partially depleted oil field for gas storage may be controlled to a large degree by secondary recovery processes. Third, oil recovery may be necessary to develop the full flow capacity of wells for gas. Oil-production processes described in Chap. 12 and references on secondary recovery mentioned may be helpful.

In the developing of a partially depleted oil field for gas storage, wells can be drilled so as to facilitate oil production resulting from gravity drainage. Structurally low wells are required to remove from the reservoir liquid caused by swelling of the residual oil as a result of repressuring. The removal of any mobile liquid phase that is present is necessary to provide a dry porous medium capable of transmitting gas. It may be wise to proceed with secondary recovery processes whether or not the expected oil recovery justifies the operation, since successful gas-storage operations may depend upon removing any mobile crude oil in the reservoir.

STORAGE OF GAS IN WATER RESERVOIRS

Table 18-7 shows that, in four different states as of January 1, 1956, there were five underground storage reservoirs that originally contained water. These reservoirs have an active working-storage capacity of approximately 50 MMMcf, or less than 5 per cent of the total underground storage capacity in the United States.

Determination of Structure

In the search for an underground storage reservoir of this type it is first necessary to find an underground anticlinical structure. Occasionally a structure can be found by surface geology or core drilling. More often it will be necessary to use geophysical methods. It may be necessary to drill "slim" holes to a marker bed in order to find a structure. A study of a generalized geological column of the area will indicate the formations that have storage possibilities. A standard-sized well must be drilled on top of the structure and cored in order to test possible porous and permeable water-bearing sandstone, dolomite, or limestone formations and to determine whether an impermeable cap rock of shale or limestone lies immediately on top of the porous and permeable formation. Once a formation has been selected, additional test wells must be drilled to the formation to delineate the structure. Storage rights must be acquired.

Probably the most important requirement of a storage field in an aquifer is that it have an impermeable continuous cap rock. Coring and laboratory testing of the cores for permeability will give an indication of the tightness of the cap rock. How low this permeability must be or how thick the cap rock must be or what combination of the two makes an effective seal to gas movement has not been determined. The permeability must be low enough (10^{-5} millidarcy or below) to prevent displacement of water from the pores. Any solution cavities or fractures in cores from limestone cap rock should be noted. In most cases it will be necessary actually to test the formation by injecting gas into it and by observing over a period of time whether the gas remains in the formation or seeps through the cap rock to shallower formations. It may be possible to tolerate a small amount of seepage and still make an efficient and economical storage field by collecting and recycling the gas from a shallow zone.

Aquifer Behavior

A blanket water-bearing sand with impermeable top and bottom that extends over many miles is often

described as an "aquifer." When wells are drilled into an aquifer and water is produced, the water in the sand flows to the well because of the pressure reduction. It may take years for water production to lower the pressure significantly some 10 miles from the well, since the capacity of the sand is large and the expansibility of the water and porous medium in the area around the well provides the water.

When gas is stored in an aquifer, gas pressure in the reservoir must be maintained higher than the original water pressure to force any water out into the aquifer. During the initial injection of gas into a water well, pressures from 100 to 300 psi above the water reservoir may be required to start gas entering the porous rock. Once gas has started flowing, the usual flow considerations for gas apply. The rate at which gas can be injected at some fixed gas-bubble pressure is determined by the aquifer behavior in the unsteady-state process.

The solutions to the unsteady-state flow equation provided by Van Everdingen and Hurst (10-27) are useful at this point. Equation (10-28) may be converted to field units for aquifers:

$$q = 6.283\phi C_w R_g^2 h(P_g - P_f)Q_t \qquad (18\text{-}5)$$

where q = water movement from gas bubble, cu ft
ϕ = fractional porosity of formation
C_w = compressibility of water including formation, volumes/(volume)(psi)
R_g = radius of gas bubble, ft
h = formation thickness, ft
P_g = pressure on gas bubble, psia
P_f = initial water pressure, psia
Q_t = a function of dimensionless time t_D obtained from Tables 10-4 to 10-8

$$t_D = \text{dimensionless time} = \frac{0.00632Kt}{\phi\mu C_w R_g^2} \qquad (18\text{-}6)$$

K = permeability of formation, millidarcys
t = time from beginning of pressure maintenance, days
μ = water viscosity, centipoises

To use the equations, the compressibility of water (Fig. 18-24) and the reduction in pore volume with pressure decrease (Fig. 2-28) are needed. Solution gas increases the compressibility of water by 20 per cent for each 20 cu ft/bbl dissolved in the water.

Illustrative Problem

A gas bubble 1,000 ft in radius has been developed on an anticline in a blanket fresh-water sand 50 ft thick. The permeability of the sand is 300 millidarcys and the porosity 20 per cent. The temperature of the reservoir is 68°F and the pressure is 1,000 psia. How much gas can be injected over a period of 1 year by maintaining the gas bubble at 100 psi above the original aquifer pressure and pushing water out into the surrounding area? The stored gas has a gravity of 0.6.

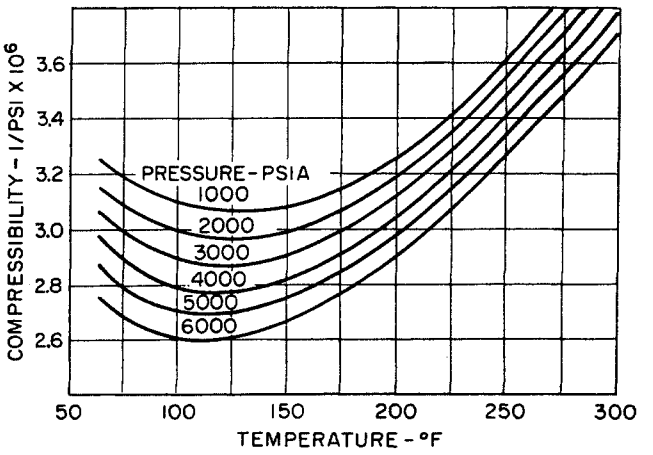

Fig. 18-24. Compressibility of pure water. (*Dodson and Standing, 5-25. Courtesy API.*)

Solution

The compressibility of water and formation are taken as 3.2×10^{-6} from Fig. 18-24 and 3.6×10^{-6} from Fig. 2-28, respectively, for a total of 6.8×10^{-6} vol/(vol)(psi).

$$q = 6.283 \times 0.20 \times 6.8 \times 10^{-6} \times 1{,}000^2 \times 50 \times 100Q_t$$
$$= 42{,}700Q_t$$

$$t_D = \frac{0.00632 \times 300 \times 365}{0.20 \times 1.0 \times 6.8 \times 10^{-6} \times 1{,}000^2}$$
$$= 509$$

From Table 10-4, at $t_D = 509$, $Q_t = 165.1$. Therefore,

$$q = 42{,}700 \times 165.1 = 7{,}050{,}000 \text{ cu ft of water}$$

At 1,100 psia, the 7,050,000 cu ft of space would hold 7,050,000 × 93 (from Fig. 11-30) or 655,000,000 cu ft of gas, which would be injected at constant pressure as a result of water moving out from the bubble.

If it is essential that the storage space be expanded more rapidly, water can be pumped out near the edge of the bubble, or a higher gas-bubble pressure may be used.

Calculations similar to this can be made for storage fields which were originally gas or oil fields with underlying or edge-water contact. The average differential between the gas pressure in the storage field and the aquifer pressure can be used to calculate the change in reservoir volume for any specific period of time. It appears that the restriction of water movement into or out of a reservoir is in the horizontal flow of water at the periphery of the reservoir, even though underlying water is present.

The Van Everdingen and Hurst equation for computing cumulative pressure increase at the field radius for constant rates of water flow is as follows:

$$P_g - P_f = \frac{25.2q\mu P_t}{Kh} \qquad (18\text{-}7)$$

where q = water flow rate, cu ft/day

P_t = function of t_D from Tables 10-4 to 10-8

It is possible to handle cases in which neither constant pressure nor constant rate applies, by using the principle of superposition. A series of flow rates are taken, starting at different times, and the results are added together.

Figure 18-25 shows the nature of the pressure behavior at constant flow rate or of the flow rate at constant pressure, for an aquifer following these relationships.

ECONOMICS OF STORAGE

Several items enter into the total investment necessary to put an underground storage field into operation. These items include cost of acquisition, development, cushion gas, dehydration, compression, and transmission.

Acquisition cost will involve purchase of all physical equipment in the field including remaining gas or oil wells, gathering lines, process equipment, compressor station, etc. It will be necessary to purchase the remaining recoverable gas or oil in the formation and the right to use the formation for storage. Physical equipment can often be purchased for its depreciated value. Remaining minerals can usually be acquired at the same rate as the rate paid during production.

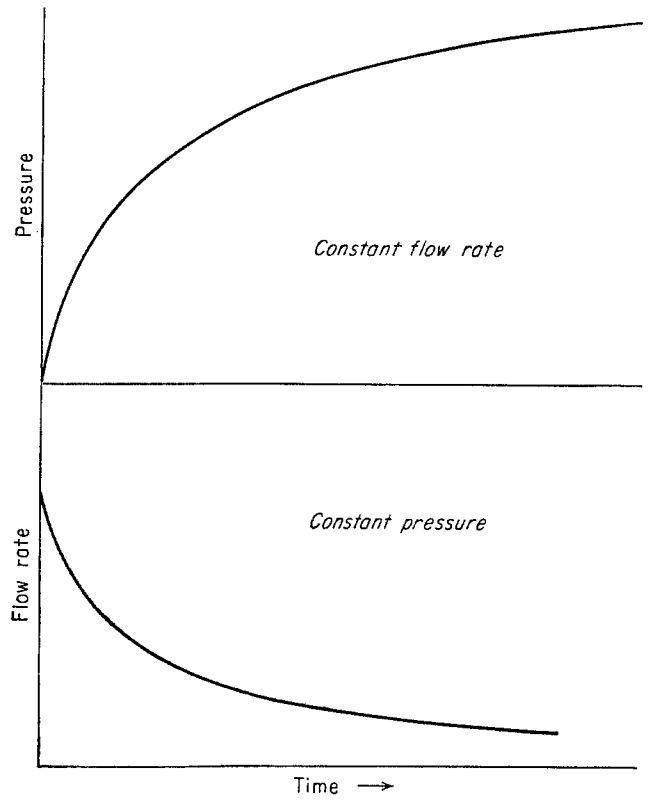

Fig. 18-25. Nature of pressures and flow rates in aquifers

Development cost includes cost of drilling storage wells, observation wells, and structure-control wells and cost of wellhead structures and gathering system. Complete drilling costs—including drilling, well casing, cement, logging, coring, and testing—could vary from $5 to $100 per foot, depending upon the depth and amount of logging, coring, and testing that is done. A shallow storage well less than 2,000 ft in depth could be drilled and completed for no more than $10 per foot. Wellhead structures might cost up to $5,000 per well. Gathering-system costs will depend upon the capacity of the wells and well-spacing patterns, but should not cost more than $10,000 per well. Another significant cost in some fields might be the money necessary to redrill and activate or permanently plug and abandon all old gas or oil wells abandoned during the producing history of the field. This item could amount to a larger figure per well than the cost of drilling new wells.

In the average underground storage field, the total reservoir capacity is divided approximately into 50 per cent cushion gas and 50 per cent working gas. The cost of cushion gas could fluctuate from 25 to 50 cents per Mcf, depending upon the locality. In any instance it should be equal to the pipeline company's off-peak or interruptible sales price.

Compression, transmission, dehydration, and other gas-treating costs are entirely dependent upon individual situations. Compressor stations can be built for $250 to $300 per installed horsepower. Transmission-line costs vary widely. A rule of thumb that would prove satisfactory for approximate costs would be 50 to 60 cents per inch of diameter per foot of length of transmission line. Gas-treating costs would depend upon what treatment is necessary. Separators and gas cleaners would be included in the compressor-station costs.

Douglas Ball (18-3) states that so far the highest investment cost for underground storage capacity has been slightly under $1 per Mcf of working storage capacity. The underground storage committee of the AGA (18-1) reports, as of December 31, 1955, a total capital investment in underground storage of approximately 377 million dollars. This figure includes cost of cushion gas and of such physical properties as wells, gathering lines, compressor stations, etc. The same report shows a total ultimate working storage ca-

pacity of 1,142 MMMcf. This is equivalent to an investment cost of 33 cents per Mcf. This amount is probably somewhat low, because not all the storage fields have sufficient physical facilities to utilize their ultimate storage capacity. One company with a total working storage capacity of over 100 MMMcf has experienced a capital investment cost of 40 cents per Mcf.

Ball also states that operating cost for underground storage is about 5 cents or less per Mcf delivered, depending on how fast the field investment is depreciated. Since not over 25 per cent of total sales would normally come from underground storage, the 5 cents would be equivalent to not more than 1.25 cents per Mcf of total sales. The experience of one company making deliveries from storage during the 1955–1956 winter season of over 50 MMMcf was an operating cost of about 3.5 cents per Mcf delivered, including depreciation at an annual rate of 3 per cent.

Costs of Other Methods of Storing Gas

Other methods of storage cost considerably more. According to Ball, low-pressure steel holders cost hundreds of dollars per Mcf and high-pressure pipe batteries or pipe bottles cost tens of dollars per Mcf. Ball also states that low-temperature liquefaction and storage may cost \$5 to \$10 per Mcf of capacity, perhaps considerably less for very large capacities. Kroeger (18-12) calculates the capital cost of storage in a sphere as \$227 per Mcf, in a gas holder as \$156 per Mcf, in steel pipe as \$48 per Mcf, and by liquefaction as \$13 per Mcf.

At this date there are no active natural gas storage projects in mined caverns, although this method of storage is under study. For at least 5 years, liquid hydrocarbons, especially liquefied petroleum (LP) gas, have been stored in mined caverns and in caverns dissolved from salt (18-4, 18-12 to 18-14, 18-16, 18-17). Storage costs for mined caverns are in the neighborhood of \$4 to \$5 per Mcf of capacity, and half that for caverns dissolved in salt (Ball, 18-3). Kroeger calculates the capital cost of plant and storage for storing LP gases as liquids, gasifying them, and diluting them with air to 1000 Btu/cu ft for distribution; his calculations give \$5.50 to \$6.45 per Mcf of capacity for cavern storage and \$4.20 to \$4.30 per Mcf for dissolved-salt storage.

Winter-peak Shaving with Natural Gas Substitutes

Manufactured oil gas or LP gas–air can be used to shave wintertime peaks. According to Henry (18-10) the investment cost for new high-Btu oil-gas plants varies from \$262 to \$170 per Mcf of daily production capacity, with higher-capacity plants in the lower cost range. Henry also shows that investment cost for LP gas–air plants with cavern storage for a 20-day LP supply can be \$20.70 per Mcf of daily production capacity or lower if capacity is 15,000 Mcf/day or more.

The cost of propane is the major item in the cost of producing propane-air for wintertime-peak shaving. Propane at 10 cents per gallon, when diluted with air to 1000 Btu, has an equivalent cost of \$1.10 per Mcf. Processing costs can be as low as 2 cents per Mcf (Henry, 18-10). Depreciation costs for plant and storage depend entirely upon how much propane-air is produced annually, over which to spread the depreciation dollars.

There are different processes for manufacturing high-Btu oil gas. The raw-material and operating costs do not vary significantly among processes. Again, cost of raw material is a large portion of total cost. According to Henry, it takes approximately fifteen to sixteen gallons of bunker C oil to make an Mcf of 1000-Btu gas. Oil at 7 cents per gallon would be equivalent to gas at \$1.05 to \$1.12 per Mcf. According to Henry's figures, sale of by-products—tar and light oil—and installation of a waste heat boiler might reduce the cost by as much as 50 cents per Mcf. Processing and maintenance costs appear to be around 20 cents per Mcf. Depreciation costs would again depend upon the volume of gas manufactured annually. It is clear, however, that depreciation costs for manufactured oil gas would be more than ten times the depreciation cost for propane-air with the same volume of annual production.

Summarizing, then, it seems evident that underground storage of gas in depleted gas, oil, or water reservoirs is more economical than other known means of storage or substitute gas-manufacturing facilities. Investment costs are not more than \$1 per Mcf of storage capacity, and operating costs including depreciation are not more than 5 cents per Mcf delivered. It appears that shaving extreme winter peaks that occur only two or three times a year can be accomplished with other types of storage or by manufacturing natural gas substitutes.

CHAPTER 19

Conservation and Governmental Regulation

In the early days of the industry, companies or individuals would drill for oil and gas, produce any oil or gas found as rapidly as possible, and sell the products. The common law of capture, which prevailed in the oil and gas industry, provided that any oil or gas that came to a well belonged to the owner of the well. This law grew out of laws concerning water rights and game, which in effect provided for the right to capture what one could of the game or fluid at hand. Once the nature of oil and gas reservoirs and the ability of one well owner to produce the products from under another's land were fully appreciated, the concept of ownership of oil and gas in place gained favor. The state laws enacted concerning ownership of oil and gas often recognize both the quantity of fluids in place and the ability of wells to capture them.

Under the law of capture, the waste of natural gas in some fields was great, especially when the gas was produced with crude oil or naphtha. In the early 1930s, an excess in the supply of crude oil over the market demand, coupled with prolific deeper production like East Texas, made it necessary to enact state conservation laws. These laws give to state conservation agencies the power to regulate the rate of production of oil and gas from individual wells. These laws are often called proration laws inasmuch as the market demand for products is prorated to the wells according to a given formula or set of rules. During the past ten years there has been little waste of natural gas, unless it was produced with crude oil at low rates and at isolated locations.

Coincident with the proration of oil and gas was the development of reservoir engineering. Now that wells were closed in for part of the time, pressures at the wellhead and at the bottom of the well were measured. Methods of estimating oil recoveries other than by extrapolation of production-decline curves were inaugurated. The concept of unit operation of the entire reservoir was developed (19-9).

The Interstate Oil Compact Commission* was organized under an act of Congress to coordinate and improve conservation practices. This body has representatives from all the oil-producing states. The conservation and regulation agencies of the member states are listed in Table 19-1. This Interstate Oil Compact Commission holds meetings for the discussion of conservation practice and governmental regulation. It has committees devoted to legal, engineer-

Table 19-1. Conservation Agencies of States Administering *Oil and Gas Production Law*

Alabama	Oil and Gas Board, Montgomery
Arizona	Oil and Gas Conservation Law, Phoenix
Arkansas	Oil and Gas Commission, Little Rock
Colorado	Oil and Gas Conservation Commission, Denver
Florida	Board of Conservation, Tallahassee
Illinois	Department of Mines and Minerals, Springfield
Indiana	Department of Conservation, Indianapolis
Kansas	Corporation Commission, Topeka
Kentucky	Department of Mines and Minerals, Frankfort
Louisiana	Department of Conservation, Baton Rouge
Michigan	Department of Conservation, Lansing
Mississippi	Oil and Gas Board, Jackson
Montana	Oil and Gas Conservation Commission, Helena
Nebraska	Conservation and Survey Division, Lincoln
Nevada	Oil and Gas Conservation Commission, Carson City
New Mexico	Oil Conservation Commission, Santa Fe
New York	State Science Service, Albany
North Dakota	State Industrial Commission, Bismarck
Ohio	Department of Industrial Relations, Columbus
Oklahoma	Corporation Commission, Oklahoma City
Pennsylvania	Department of Internal Affairs, Harrisburg
South Dakota	Oil and Gas Board, Pierre
Tennessee	Department of Conservation, Nashville
Texas	Railroad Commission, Austin
West Virginia	Department of Mines, Charleston
Wyoming	Oil and Gas Conservation Commission, Cheyenne

* Office, 900 Northeast 23d Street, P. O. Box 3127, Oklahoma City 5, Okla.

ing, and regulatory-practice problems. It has prepared a book on "Oil and Gas Production" (1-4), and publishes its proceedings in the *Oil and Gas Compact Bulletin*.

The Doherty memorial volume "Petroleum Conservation" was prepared by a group of men headed by S. E. Buckley (19-5).

Public utilities within states are regulated by state utility commissions. The list of these commissions is given in Table 19-2. These commissions fix rates

Table 19-2. State Utility Regulatory Commissions

Alabama	Public Service Commission, Montgomery 1
Arizona	Corporation Commission, Phoenix
Arkansas	Public Service Commission, Little Rock
California	Public Utilities Commission, San Francisco 2
Colorado	Public Utilities Commission, Denver 2
Connecticut	Public Utilities Commission, Hartford
Delaware	Public Service Commission, Dover
District of Columbia	Public Utilities Commission, Washington 4
Florida	Railroad and Public Utilities Commission, Tallahassee
Georgia	Public Service Commission, Atlanta 3
Hawaii, Territory of	Public Utilities Commission, Honolulu 13
Idaho	Public Utilities Commission, Boise
Illinois	Commerce Commission, Chicago 1
Indiana	Public Service Commission, Indianapolis 4
Iowa	State Commerce Commission, Des Moines 19*
Kansas	State Corporation Commission, Topeka
Kentucky	Public Service Commission, Department of Motor Transportation, Railroad Commission, Frankfort
Louisiana	Public Service Commission, Baton Rouge 4
Maine	Public Utilities Commission, Augusta
Maryland	Public Service Commission, Baltimore 2
Massachusetts	Department of Public Utilities, Boston 33
Michigan	Public Service Commission, Lansing 13
Minnesota	Railroad and Warehouse Commission, St. Paul 1†
Mississippi	Public Service Commission, Jackson 44†
Missouri	Public Service Commission, Jefferson City
Montana	Board of Railroad Commissioners, Helena
Nebraska	State Railway Commission, Lincoln 9*
Nevada	Public Service Commission, Carson City
New Hampshire	Public Utilities Commission, Concord
New Jersey	Board of Public Utility Commissioners, Trenton 7
New Mexico	Public Service Commission, Corporation Commission, Santa Fe
New York	Public Service Commission, Albany 1
North Carolina	Utilities Commission, Raleigh
North Dakota	Public Service Commission, Bismarck
Ohio	Public Utilities Commission, Columbus 15
Oklahoma	Corporation Commission, Oklahoma City 5
Oregon	Public Utilities Commissioner, Salem
Pennsylvania	Public Utility Commission, Harrisburg
Puerto Rico, Government of	Public Service Commission, San Juan 4
Rhode Island	Department of Business Regulation, Providence 2
South Carolina	Public Service Commission, Columbia 1
South Dakota	Public Utilities Commission, Pierre†
Tennessee	Railroad and Public Utilities Commission, Nashville 3
Texas	Railroad Commission, Austin 11‡
Utah	Public Service Commission, Salt Lake City 1
Vermont	Public Service Commission, Montpelier
Virginia	State Corporation Commission, Richmond 9
Washington	Public Service Commission, Olympia
West Virginia	Public Service Commission, Charleston 5
Wisconsin	Public Service Commission, Madison 2
Wyoming	Public Service Commission, Cheyenne

* Limited regulation of electric and gas utilities. † No regulation of electric and gas utilities. ‡ No regulation of electric utilities. SOURCE: (19-4).

of electric and gas utilities and make regulations for the construction of new facilities.

The growth of natural gas pipelines and of distribution companies has been accompanied by Federal laws intended to protect the consumer and the national public interest. The economic depression of the early thirties, with the collapse of industrial empires, was the occasion for enactment of laws administered by the Securities and Exchange Commission (SEC) with regard to the marketing of securities. The Natural Gas Act was passed in 1938 (19-1) to regulate the pipeline industry under the supervision of the Federal Power Commission (FPC). The Supreme Court decision in 1954 in the Phillips case had the effect of bringing all producers of natural gas for interstate commerce under the Natural Gas Act (19-3, 19-8).

Conservation practices by the states and Federal regulation of interstate commerce have been concerned with engineering phases of oil and gas production, reserves, gas transportation, and underground storage. Accordingly, the occasion for much engineering work needed for operation of gas fields and design of pipelines is the application to some regulatory body for a certificate of convenience and necessity. A brief review of some regulations intended to foster conservation or to serve the consumer and public interest will be given, and the role that the engineer is expected to fill will be presented.

In conservation and regulatory cases the engineer works closely with lawyers and laymen. Clear exposition of technical material in nontechnical terms becomes of paramount importance.

OWNERSHIP OF OIL AND GAS IN PLACE

The title to oil and gas under a given piece of ground is often referred to as "mineral rights," since oil and gas are included with the other minerals. The title to the minerals may be separated from the title to the surface, along with the right of ingress to drill and operate wells. The owner of the mineral rights leases the property to an operator who agrees to drill for oil or gas. The mineral owner normally reserves a royalty of one-eighth of the production as his share of the minerals. Thus, in a modern oil or gas field there may be three parties of concern on a given property or lease: the surface owner, the mineral or royalty owner, and the operator of the wells. The operator or lessee is the person concerned directly with state regulation, although the royalty owner also has an interest in proration or unitization practices since they may affect the royalty income from a given piece of property. The surface owner may be involved with regard to damage to crops from the drilling of wells.

STATE REGULATORY COMMISSIONS

The two functions of petroleum conservation and public utility regulation may be vested in the same state agency or in separate state agencies, as shown in Tables 19-1 and 19-2.

One function of a conservation agency is to keep records of well information. Well permits are obtained for drilling wells with the requirement that certain information be provided at the completion of drilling. Casing programs may be stipulated to provide safe drilling through known oil and gas horizons. Regulations provide procedures for plugging and abandoning of wells. To safeguard water supplies, approval is required for returning oil-field waters to underground zones.

State conservation laws vary, but all states with significant production, except California and Illinois, provide for some form of compulsory proration of oil and gas. Provisions for compulsory unitization of reservoirs are given in some states once some 75 to 90 per cent of the interests in a reservoir have joined. Oil proration or restriction is relatively severe in some states. For example, many wells capable of producing several thousand barrels per day are allotted 20 bbl/day. The proration to market demand reduces "economic waste" and stabilizes the industry. The maximum efficient rate (MER) for a reservoir is the rate that will result in the maximum ultimate recovery and that will eliminate underground waste.

The individual states have specific laws governing the "rate of take" for gas from wells. In some instances, this rate is limited to 25 per cent of the computed absolute open flow for the well. Some flow-test data and/or information on closed-in pressures and acreage allotment per well constitute the basic information required for proration formulas.

Current problems in Louisiana and Texas were reported at the Miami Beach meeting of the Interstate Oil Compact Commission (19-6, 19-7).

John B. Hussey, Louisiana Commissioner of Conservation, in his paper on "Ratable Take," made the following statement (19-7):

> As early as 1900 the United States Supreme Court enunciated the principle of law that all owners of lands, minerals or leases overlaying an oil or gas reservoir have the common right to take oil or gas from the reservoir. The Court also held that oil or gas taken from the reservoir should not be wasted and no owner should take an undue proportion.
>
> Some states recognize the theory of ownership of minerals in place and other states recognize only the right of land, mineral and lease owners to reduce the minerals to possession. However, in all states, including those which recognize the Law of Capture, no land, lease or mineral owner is entitled to take an undue proportion of the minerals

from the common source of supply, but each owner should be afforded the opportunity of taking his proportionate share.

That is the basis of proration, and proration is designed to give each owner the opportunity to take his proportionate share of the minerals from the reservoir.

However, the mere opportunity of an owner to take his share of the minerals from a common source of supply does not provide complete protection of his property rights in the minerals. If others produce and market, he must also produce and market or lose much of his share through drainage and through exhaustion of the reservoir energy. He cannot produce and market unless a market outlet is available, and he cannot produce and market his share of the minerals from the common supply unless the purchaser takes his full or ratable share.

Where there is a single market outlet in a field, the problem of ratable take from the standpoint of a regulatory body is comparatively simple but where there is more than one pipeline purchasing gas from a field with each purchaser satisfying a different market, the problem of ratable take becomes complex indeed.

Most gas purchasers have their pipelines connected to more than one field and we have the problem of ratable take between fields as well as the problem of ratable take among wells within a single field.

The first step in accomplishing ratable take is to require a market outlet for every producing well. The predicate for such action is a Common Purchaser Statute. Such statutes declare any gas pipeline purchasing gas within a state to be a "Common Purchaser" of gas and such pipeline is required to purchase gas from all producers who bring their gas to the purchaser's gathering or transmission lines. These statutes also usually provide that the purchasers must take gas from this producer ratably in proportion to its takes from the other producers from which it purchases.

Where we have a single purchaser of gas in a single field and we have a common purchaser statute, enforcement of ratable take is no great problem. If a producer has no outlet for his gas, he can, by building a line to the purchaser's gathering or transmission system, secure an order from the conservation regulatory agency requiring the pipeline to take his gas. If the pipeline takes more gas from his neighbor than from him, the producer can secure an order requiring the purchaser to take ratably.

In such instances the proper questions are (1) what is the producer's ratable share and (2) what price is to be paid for the gas to be taken? Where we have proration and allowable orders for the field, the producer's share in volume will be his proportion of the total take that his wells allowable bears to the total allowables from all wells producing from the reservoir. The proration orders may be based on percentage of open flow rates, on a percentage of reserves, a so-called maximum efficient rate or other engineering formulae, or it may be a percentage of market, either on a per well or surface acreage basis. But regardless of the method of establishing the allowable, the producer's ratable share would be his proportion of that allowable. If there is no proration or allowable order in effect, his share would be open for determination by the conservation regulatory body.

The second problem involved is that of price. Ratable takes mean ratable take as to volume only; it does not mean identical price. Price is a matter of contract, or, in the absence of contract should be market value at the point of delivery. Market value varies with location, reserves committed, minimum and maximum takes, etc. We will not go into at this time the question as to whether that market price is properly determinable in a ratable take hearing by state regulatory authorities, by the courts or by other regulatory bodies who might be compelled to invade that field against their better judgment.

Where we have more than one purchaser or more than one market outlet in a field or fields, each serving different and varying markets, the problem of ratable take becomes more complex.

The first step in accomplishing ratable take among gas wells in a single field with multiple market outlets, is, of course, a proper proration order which establishes the proper share of each well and gives the producer an opportunity to produce this proportionate share. The second step is to provide flexible operation through carry-over and carry-back of over- and underproduction by balancing out arrangements and periods which allow the producer and purchaser to satisfy fluctuating and changing gas markets and still maintain an over-all ratable average take. . . .

It is standard procedure for gas pipeline producers to base their takes on reserves. This should tend to accomplish ratable takes and probably would do a reasonable job if the reserves were calculated well by well and the percentage of take was distributed well by well.

John S. Cameron, Jr., Railroad Commission of Texas, in his paper on "How Texas Prorates Gas," made the following statement (19-6):

This paper is to be a discussion of the present methods of prorating gas in Texas, followed by a brief discussion of the more recent new orders the Texas Railroad Commission has issued to obtain ratable take in the Henze, Blue Basin, Alco-Mag and Puckett-Ellenburger gas fields.

The Commission's basic duty in gas proration in Texas is to determine the market demand for gas from a field and to grant that demand as the field allowable in such manner as to allow each well its ratable share. The present basic method used to determine the market demand in Texas is based upon receiving monthly nominations from all the producers in a field. In Texas each reservoir is prorated separately and nominations are required from the producers in that reservoir. However, experience has shown that the nominations do not always accurately reflect the true market demand in a field, so adjustments comparing the nominations with the actual reported production are necessary to maintain the field in proper balance. The nominations from every producer in a reservoir are totalled to determine the current market demand and then this nomination is adjusted by the difference between the total nomination and the actual production from that reservoir for the third previous month. The nominations and production for the

third previous month must be used because our monthly gas reports are not required until the last day of the month following the month for which the report is made. Therefore, in the preparation of the monthly gas schedules for December the difference between the September nominations and September production is calculated and applied to the December nominations to obtain the December allowable for a field. Attachment 1 is the latest memorandum issued by the Commission explaining and adopting this basic method. A monthly gas proration schedule is issued in Texas on the first of the month showing the allowable of every prorated gas well for that month.

In all of our prorated gas fields the Commission requires semi-annual flow tests on each well to determine that well's ability to produce into the pipeline. In this manner a well is not assigned more allowable than it can produce if accurate tests are submitted. Special flow tests may be filed at any time that conditions may warrant such a retest but regular test periods are assigned for each field and each well must be tested to get an allowable.

Very early in gas proration in Texas it became apparent that the variance in seasonal demand in the summer and winter periods could not adequately be handled by nominations alone. The demand for Texas gas in the winter time is at best very hard to anticipate so that some method whereby gas wells could produce in excess of their allowable during a period of high demand and make up this overproduction during the summer months of minimum demand became very necessary to meet the demand when necessary. This problem was most critical in the early days of proration when most of Texas' gas was distributed to local consumers who needed a lot of gas in winter and very little gas in summer. The development and growth of the major transmission companies has done much to stabilize Texas gas production between winter and summer to the point that there was only a 17 per cent difference between summer and winter demand in Texas in 1955. To alleviate this problem the Texas Legislature enacted a statute setting up two six-month balancing periods in all prorated gas fields in Texas. This statute is our Statewide Rule 24(b) which provides for two six-month periods from 7:00 A.M., March 1, to 7:00 A.M. September 1 as a separate period and 7:00 A.M., September 1, to 7:00 A.M., March 1, as another separate period. This rule was first applied to the big Carthage gas field, Panola County, Texas, in September, 1947. This rule provides for the overproduction and underproduction of gas wells within these specified periods by stating: (1) that any well that overproduces through two consecutive balancing periods without making up its overproduction as of the beginning of the first period must be shut in until all its overproduction as of the last balancing date is made up, (2) that any well that is underproduced through two balancing periods and does not make up the underproduction as of the first balancing date before the end of the next period will have that underproduction cancelled.

Therefore, the balance or status of every well is determined on March 1 and September 1 of every year and these individual well balances are added to determine the reservoir balance as of each balancing date. Then each reservoir is balanced in May when the March 1 balance is calculated and in November when the September 1 balance is known. The status or balance of each well is determined by subtracting the monthly allowable from the monthly production and adding the differences each month for the six month periods. In this manner every prorated gas reservoir in Texas is put in balance twice each year and gas wells have the necessary flexibility to meet the seasonal demands.

From the foregoing discussion of the basic gas proration system used in Texas, it is apparent that accurate nominations and good flow tests are vital to the proper operation of this method. There are now approximately 7,000 Texas gas wells in 400 gas fields prorated under this system and in most of these fields this system is working satisfactorily. However, unrealistic nominations and tests can completely disrupt this method, but this method can work to allow ratable take if all parties involved cooperate, and produce their assigned allowables.

The following exerpts are taken from the Basic Proration Order for the Hugoton Gas Field, 1951, to illustrate the proration rules for gas fields:

g. That one well completed in the said formation can adequately and sufficiently drain 640 acres without causing waste and, considering the cost of drilling, equipping and operating one well in comparison with the estimated recovery per acre and the slow rate at which the production for said field can be ratably and nonwastefully marketed, the Commission finds that the basic acreage unit to be used in the proration formula hereinafter prescribed should be 640 acres, and that in no instance shall more than 640 acres be attributable to a well for the purpose of calculating the acreage factor except by specific order of the Commission as hereinafter provided. The acreage factor of a well shall equal the number of acres held by production from said well divided by 640. Expressed in a mathematical formula, said acreage factor may be set forth as follows:

$$\text{Acreage Factor} = \frac{\text{No. of acres attributable}}{640}$$

j. The adoption of a formula that will enable each well to currently produce its allowable and ultimately produce approximately the amount of gas underlying the lease upon which it is located is the object sought to be accomplished by this order. The testimony at the numerous hearings held by the Commission indicates that there are many factors which should be considered in connection with the formula, such as, acreage, pressures, open-flow, porosity and thickness of the pay. It is conceded by practically all of the witnesses that acreage is one of the most important of these factors and should be one of the factors included in the formula. It is also the opinion of many of the expert witnesses that the other factors above enumerated, namely, pressures, open-flow, porosity and thickness of pay, are all taken into consideration and given their proper weight when the deliverability of the well to put gas into a pipeline against pipeline pressure is taken into account. Therefore, a formula that considers acreage and deliverability and gives

due value to both should result in the establishment of well allowables that will permit each well to currently produce its allowable and to ultimately produce approximately the amount of gas which underlies the lease upon which it is located. Since the pipeline pressures in the Hugoton Field are maintained at approximately eighty per cent of the average field pressure, this fact should be taken into consideration in determining the deliverability factor. Hence, the Commission finds that the formula to be used in fixing well quotas for the Hugoton Field should include the factors of acreage and deliverability. The acreage factor shall be determined as set forth in paragraph "*g*" of this order. Deliverability shall be deemed to be the ability of said well to produce gas against eighty percent of the average field pressure.

k. The deliverability of each connected well in the Hugoton Field shall be determined as follows: The well shall be produced into the pipeline for approximately seventy-two hours, during which time the working pressure at the wellhead shall be maintained at eighty per cent of the average shut-in wellhead pressure of the field, expressed in pounds per square inch gauge and designated herein as the deliverability standard pressure, or as closely thereto as operating conditions in the field will permit. In no case shall the working wellhead pressure be more than ninety per cent or less than seventy per cent of the shut-in wellhead pressure of the well being tested unless, in the judgment of the Commission's representative, it is impractical to maintain the pressure within the above-described limits. If it is impossible or impractical to reduce the working pressure to ninety per cent of the shut-in pressure, the deliverability shall be calculated by substituting ninety per cent of the shut-in wellhead pressure of the well for P_w in the formula hereinafter set forth. Flow shall be measured by approved meter throughout the seventy-two hour test period, and the wellhead pressure shall be measured by dead weight gauge at the close of the test period. The rate at which the well is producing at the end of seventy-two hours shall be considered the stabilized producing rate corresponding to the working wellhead pressure existing at that time, provided such rate is not greater than the average producing rate for the entire seventy-two hour period. If the working wellhead pressure at the close of the test is exactly equal to the deliverability standard pressure, then the corresponding stabilized producing rate, expressed in Mcf per day at a base temperature of sixty degrees Fahrenheit and a base pressure of 14.65 psia, shall constitute the well's deliverability. If the wellhead pressure at the end of the test is either greater than or less than the deliverability standard pressure, the observed stabilized producing rate shall be converted to deliverability by use of the following formula:

$$D = R \times \left[\frac{P^2 - P_d^2}{P^2 - P_w^2}\right]^{.85}$$

where D = deliverability
R = observed producing rate
P = shut-in pressure of the well, psia
P_d = deliverability standard pressure, converted to pounds absolute
P_w = working wellhead pressure at rate R, psia

The term "working wellhead pressure," as used in this paragraph, refers to pressure at the casing-head, except in cases where the casing-head is not in open communication with the producing formation because of the presence of a packer or other obstruction in the annular space between casing and tubing. In such cases, the working wellhead pressure shall be calculated by adjusting the tubing pressure for the increased effect of friction caused by flow through the tubing.

Shut-in wellhead pressure shall be measured by deadweight gauge after the well has been shut in for approximately seventy-two hours. In no case shall the well have been shut in for less than sixty-six hours nor more than seventy-eight hours at the time the shut-in pressure is taken. If the representative of the Commission should for any reason believe that the shut-in pressure taken upon a well is incorrect, he may require that such well be blown to clean fluids from the well bore, or take any such other reasonable steps that may be necessary to get a true pressure upon the well. In the event that more than one shut-in pressure is taken upon a well during the test period, the highest such shut-in pressure obtained will be used in figuring the deliverability of such well. . . .

l. To determine a well's quota for a given proration period, determine first the proration factor for the field by dividing the total field allowable for such period by the sum of the products of deliverability times the acreage factors of all the wells in the pool, then multiply the field proration factor by the product of the deliverability times acreage factor for the well. The result reached by this calculation shall constitute the well's allowable, in cubic feet, which it may produce for such proration period. . . .

n. That there shall be held two market demand hearings for each year. The first hearing shall cover the period from October 1 to March 31, both inclusive, and the second shall cover the period from April 1 to September 30, both inclusive. The allowable period established shall be a calendar month. The Commission shall issue its orders covering each allowable period, and such orders shall be issued on, or near, the first day of the month for which such order is issued.

o. At such time and place as the Commission shall fix, the Commission will, after notice, conduct a hearing to determine the market demand for natural gas from said field for the next six succeeding proration periods, or for such other period of time as the Commission shall prescribe, and at said hearing may determine any other questions which may properly and legally come before the Commission for consideration thereat, and a new schedule of production allowables for the wells in said field, based upon the determination made as a result of such hearing, shall be prepared and promulgated for the ensuing proration periods.

p. Operators of wells and purchasers, or others taking gas from any well, shall endeavor to limit their takes of gas to the quantities fixed in the schedule as the allowable production for such well, provided that, if, during the period covered by any schedule there should develop a substantial increase in the amount of the market demand for gas from said field, the Director may permit production to be increased ratably from all the wells in the field to meet such

emergency increased demand and the facts respecting same shall be reported to the Commission at or before the next periodic market demand hearing for such action thereon as may be proper. If, at the end of any proration period, there is an overage or underage in production for any well during such period, same shall be carried forward as a charge against or credit in favor of such well and subtracted from or added to, as the case may be, the allowable for such well for the next proration period. Any overage in production from any well during any proration period which is not equalized by ratable overages from all other wells in the field or which is not compensated for in the allowables fixed for other wells in the field for the next succeeding proration period or not otherwise made up within one year after the proration period in which it occurred, shall constitute illegal overproduction from such well and such well shall be shut in until such overage is thereby fully made up. All wells with an overproduction of three times the amount of their current month's allowable shall be shut in by the operator or producer and not permitted to produce any gas until such overproduction has been fully absorbed by deductions from such overproduction made by current allowables. When any connected well has accumulated an underage in excess of three times its allowable for the current month, such excess shall thereupon be canceled and the amount so canceled shall be spread among all the wells of the field. Any underage so canceled shall not be considered in the determining of the future production of any such well, unless, upon notice and hearing, the Commission shall otherwise determine: *Provided, however*, that in no event shall any underproduction of an unconnected well be canceled.

When rules relating to unitization (19-9) of oil and gas fields are enacted, they are administered by conservation commissions. Unitization is the pooling of all interests into one operation with a sharing of the income from the property. Once the nature of oil and gas fields was understood, the advantages of handling the entire reservoir as a unit became obvious, for oil fields and gas-condensate fields. Unitization is required for cycling and for repressuring projects, since fluid migration would interfere with the normal recovery obtained from a given well. Under unitization, the sharing in the income no longer depends upon the particular well from which the product comes. Most unitization agreements are made on the basis of shares in the income in proportion to the recoverable oil or gas in place. Many states have laws requiring compulsory unitization of an oil or gas-condensate reservoir once some 75 to 90 per cent of ownership has been pooled voluntarily. It is necessary to include the royalty interests as well as the working interests in unitization agreements.

The second type of state regulation relates to distribution of natural gas at the retail level. Natural gas companies, which are utilities holding the only pipelines to the consumer, have each an exclusive franchise or service area. Their rates are set by a governmental agency, usually at a level expected to yield sufficient moneys on the depreciated investment (normally referred to as "rate base") to give an earning after taxes of 6 to 7 per cent. Table 19-2 lists the regulatory bodies for this function.

In addition to rates, state commissions regulate service standards, extensions of facilities, and financial operations. They grant certificates, licenses, or permits for construction of facilities. Commissions require the submission of accounting and report forms. Since the engineer is responsible for the design of new facilities, he must be familiar with the codes and standards of his state commission. He may be called upon to prepare the information required in order to obtain permits for construction of facilities. Safety practices in design and operation are set forth by the commission for companies to observe. Rules concerning odorization of gas, domestic installations, and numerous other items may be established for companies to follow. Occasionally the engineer may find it necessary to study proposed changes in the laws and to testify at hearings held to learn the effects of changes on company operations as well as to find the public interest.

FEDERAL POWER COMMISSION (FPC)

The Natural Gas Act passed in 1938 provides for the regulation of natural gas companies engaged in the transportation and sale of natural gas in interstate commerce. Under this act the FPC is required to regulate rates, to certify facilities and service, to provide for and to enforce a uniform system of accounts, and to perform certain other related functions. The necessity for this regulation was recognized and is stated in the act as follows:

> It is hereby declared that the business of transporting and selling natural gas for ultimate distribution to the public is affected with a public interest, and that Federal regulation in matters relating to the transportation of natural gas and the sale thereof in interstate and foreign commerce is necessary in the public interest.

Before any facilities to be used in the transportation and sale of natural gas in interstate commerce can be constructed, it is necessary to obtain a certificate of public convenience and necessity from the FPC. Any application to the FPC for a certificate must contain the exhibits listed in Table 19-3.

An engineer would most likely be asked to prepare or help prepare exhibits G, H, I, J, and K.

Exhibit G, Flow Diagram, must include daily design capacity of proposed facilities; diameter, wall thickness, and length of pipe to be installed; size,

Table 19-3. Exhibits to Be Attached to Each Application to the FPC for a Certificate of Convenience and Necessity

Exhibit	*Title*
A	Articles of incorporation and bylaws
B	State authorization
C	Company officials
D	Subsidiaries and affiliation
E	Corporate authorization
F	Location of facilities
G	Flow diagram showing daily design capacity and reflecting operation with proposed facilities added
H	Total gas-supply data
I	Market data
J	Conversion to natural gas
K	Cost of facilities
L	Financing
M	Construction, operation, and management
N	Revenues, expenses, income
O	Depreciation and depletion
P	Tariff

number, and type of compressor units, horsepower required, horsepower to be installed, volume of gas to be used as fuel, suction and discharge pressures, and compression ratio in each proposed and existing compressor station; formulas and methods used in development of flow diagram; and type, capacity, and location of each storage field, dehydration plant, hydrocarbon extraction, or other similar plant connected to applicant's system.

Exhibit H, Total Gas-supply Data, must include the estimated total volume of proved reserves in place for each reservoir in each field from which applicant takes or proposes to take natural gas; the estimated share of these total reserves contracted to applicant; the effective dates, remaining terms in years, and estimated volumes of gas reserves available under each contract; a deliverability study showing the daily volumes of natural gas estimated to be available each year from each source of supply; a confirmed copy of each gas-purchase contract; an estimate of the Btu content of the gas; maps of each gas field showing proved limits and acreage committed to applicant; a study of each proposed gas-storage field showing location, geology, original and present reserves, original and present pressure, proposed top- and base-storage pressures, proposed top- and base-gas volumes to be stored; a deliverability study including daily and annual injection and withdrawal rates and pressures, maximum daily deliverability, and maximum storage capacity under proposed plan of development.

Exhibit I, Market Data, must include a system-wide estimate of volumes of gas to be delivered during each of the first three full years of operation of proposed facilities and actual data for each of the last three years of actual operation; names and locations of customer companies and municipalities showing number of residential, commercial, firm-industrial, interruptible-industrial, residential-space-heating, commercial-space-heating, and other types of customers; applicant's total annual and peak-day gas requirements for each service classification; explanation of basic factors used in estimating future requirements, including peak-day and annual degree-day deficiencies, annual load factors, annual consumption factors for each class of customers, forecast of space-heating saturation, and full detail on all other sources of gas supply available to applicant and to each of its customers including manufacturing facilities and LP gas.

Exhibit J, Conversion to Natural Gas, must include a description of existing gas-manufacturing facilities and their physical condition including type, size, daily output capacity of each gas-generating unit, daily sendout capacity of plant, and capacity of storage holders; estimated cost of converting gas-manufacturing facilities to high-Btu gas production if proposed; estimated cost of converting consumers' appliances to natural gas, estimated cost of new facilities to be constructed to receive and distribute natural gas; and a study showing estimated savings during each of first three full years of proposed natural gas operation.

Exhibit K, Cost of Facilities, must include a detailed estimate of total capital cost of proposed facilities for which application is made, showing cost of construction by operating units such as compressor stations, main pipelines, laterals, and measuring and regulating stations, and stating separately the costs of rights of way, damages, surveys, materials, labor, engineering and inspection, administrative overhead, fees for legal and other services, interest during construction, and contingencies.

After all these data are compiled and the application filed, the FPC will accept the application or reject it if it is improperly filed, and, when it is accepted, set a date for a hearing. This notice of a date for a hearing will be adequately publicized, and anyone affected by the proposed application may file a notice to intervene in the hearing. The commission will permit or not permit the intervention or limit it to certain phases of the hearing, depending upon whether or not the intervenor will legitimately be affected by granting of the application. The commission normally leans over backward to be sure that everyone is given an opportunity to be heard. At the hearing the applicant must produce witnesses to sponsor and be responsible for all exhibits presented in the application. These witnesses must be qualified as experts in their fields; qualification is established through questions by the applicant's attorney about their education and

experience. Each witness must explain on the record each exhibit for which he is responsible, usually on questioning by applicant's attorney. The commission will appoint an examiner to hear the case, and he will preside over the hearing. The FPC maintains a staff of engineers, accountants, and specialists of all kinds to study applications. These staff specialists will be present at the hearing and will be represented by a staff attorney. Each witness will normally spend some time outside the hearing room with the staff experts, explaining his exhibits and providing all working papers used in preparing the exhibits. At the hearing each witness, after presenting his direct testimony, will be made available for cross examination by each "intervenor" and by the FPC staff attorney. Opportunity for rebuttal testimony will also be available. Any intervenor or the FPC staff may provide witnesses and put in exhibits and direct testimony on any phase of the hearing in support of or against the applicant. These witnesses will also be made available for cross examination. At the conclusion of the public hearing, the attorney for applicant, the attorney for each intervenor, and the attorney for the FPC staff will each present a written brief summarizing his case. A date for oral argument may be set; and here each attorney may argue his case orally in limited time before the Commissioners, who are not ordinarily present at any of the public hearings. The Commissioners, five in number, are appointed by the President of the United States and must be confirmed by the United States Senate for terms of eight years. One of the commissioners is appointed chairman by the President, also approved by the Senate. These commissioners, after hearing oral argument and the recommendations of the trial examiner and after studying the record presented in the public hearing and the briefs, will decide the case. The commission secretary will then issue an order granting or rejecting certificates and approving or disapproving rates.

All exhibits filed with the FPC in connection with an application for pipeline facilities may be examined by any one in the reference room of the Commission in Washington. Annual reports filed by each operating company (form 2) are also available.

SECURITIES AND EXCHANGE COMMISSION

The Securities and Exchange Commission (SEC) administers the Public Utilities Holding Company Act of 1935 (19-2), the Securities Act of 1933, the Securities Exchange Act of 1934, and other laws with regard to the financing of utility companies. Utility companies are companies that distribute gas or generate and distribute electricity. The Commission is composed of five members appointed by the President and confirmed by the Senate for a term of five years. The Commission is organized into divisions, such as the Registration Division, the Public Utilities Division, the Trading and Exchange Division, and the Legal Division.

The Registration Division receives and examines registrations under the Securities Act and the Securities Exchange Act. The Securities Act requires that a full and fair disclosure be made to investors of material facts regarding securities publicly offered and sold in interstate commerce or through the mails. The Act is intended to prevent fraud in the sale of securities. Registration statements covering securities to be sold are filed in a manner required by the Commission. The statements are required to contain specified information, exhibits, and the form of the prospectus proposed for use in selling the securities. For a natural gas pipeline or distribution company, the information may include such items as dedicated gas reserves, financial statements, etc.

The Public Utility Holding Company Act applies to electric and gas utility systems. A holding company, under the act, is "any company which directly or indirectly owns, controls, or holds with power to vote, 10 per centum or more of the outstanding voting securities of a public utility company. . . . " unless the Commission by order declares such a company not to be a holding company. A holding company system is the holding company along with its subsidiary companies. Gas-transmission pipeline companies not in retail sales are exempt from the Holding Company Act as such, since they are not classed as gas utilities. Whenever pipeline companies are held by a company also owning gas-distributing companies, they become a member of a holding company system and come under the Utility Holding Company Act.

The statute cites the necessity for control of holding companies in the national public interest as follows:

1. Their securities are sold through the mails and in interstate commerce.
2. Their service, sales, construction, and contracts are often made through the mails and in interstate commerce.
3. Their subsidiary public utility companies often sell and transport gas in interstate commerce.
4. Their financial activities, extending over many states, are not susceptible to effective control by any state.

The act is intended to protect investors in utility holding companies and consumers of gas and electricity.

Holding companies must file a registration statement with the Public Utilities Division of the SEC.

The statement includes the organization and financial structure of the company, arrangements concerning the various securities, balance sheets, and profit-and-loss statements for a 5-year period. An annual supplement to the registration statement is also required to be filed.

Much of the Holding Company Act has to do with rules for financing and accounting. The engineer may be asked to provide information relative to evaluation of existing properties, costs of construction of proposed facilities, capacities of physical facilities, or other information available to him pertinent to the financing or transfer of properties. Such information would be summarized in exhibits provided to the SEC with a filing. The engineer would be expected to present the exhibits before an examiner at a public hearing and be subject to cross examination concerning the validity of his work.